

Sunday Afternoon, November 6, 2016

Biomaterials Plenary Session

Room 101A - Session BP-SuA

Biomaterials Plenary

Moderator: Stephanie Allen, The University of Nottingham, UK

3:00pm BP-SuA1 Common Principles in Synthetic Mechanophores and Mechanoresponsive Biomolecules, Kerstin Blank, Max Planck Institute of Colloids and Interfaces, Germany **INVITED**

Much effort is currently invested in the development of (bio)materials with well-defined mechanical properties. This is motivated by the desire to measure cell generated forces *in situ* at the molecular level and to direct cellular behaviour using controlled mechanical stimuli. In parallel, materials scientists aim at the development of self-reporting and self-healing materials that respond to mechanical force in a predefined way. Key to all these efforts are mechanosensitive molecular building blocks, such as synthetic small molecule mechanophores and mechanoresponsive biomolecules.

Focussing on common principles that guide the design of mechanosensitive molecules, I will introduce our current set of synthetic and biological mechanical building blocks. Following a mechanical calibration at the single molecule level, these building blocks are equipped with a fluorescent reporter system that reports on the mechanical state of the molecule. This allows us to directly correlate the force acting on an individual molecule with a fluorescence readout so that a molecular force sensor is obtained. Considering the above applications, such sensors report on mechanical material deformation in a highly sensitive manner down to the single molecule level. Our approach further opens up new routes towards correlating the bulk and molecular mechanical properties of a material.

3:40pm BP-SuA3 Formation of Stacked Lipid Lamellae and Development of Myelin-like Structures Is Promoted by a Surfactant Protein B Analog: A Micropipette Study of Lung Surfactants at Microscopic interfaces, David Needham, Duke University; E. Parra, K. Konoshita, University Southern Denmark, Denmark **INVITED**

The present study is a microscopic interfacial characterization of a series of lung surfactant materials performed with the micropipette technique. We measured the equilibrium and dynamic surface tensions for a series of animal-derived and synthetic lung surfactant formulations, including a Super Mini-B (SMB)-containing formulation. Somewhat surprisingly interfacial structures were found to occur at these microscopic air-water interfaces (see Figure below) for the SMB-containing formulation over time and during area compression at the microscopic air-water interface. We compared the results to other lung surfactants, including: native surfactant obtained from porcine lungs (NS) and the commercial, animal-derived formulations Curosurf, Infasurf and Surfacta. The presence of SMB promoted vesicle condensation as thick membrane multilayers beneath the interface, the nucleation and growth of microtubes emanating from these lamellae and their subsequent transformation into helices. The dimensions of these tubes (2-15 μm diameter) and their linear (2-3 $\mu\text{m/s}$) and volumetric growth rates (20-30 $\mu\text{m}^3/\text{s}$) were quantified, and no specific effects were found on them for increasing SMB concentrations from 0.1 to 4%. Nevertheless, we found a direct correlation between the number of tubes and SMB contents, which suggests that SMB molecules are the promoters of tube nucleation in these membranes. Microtube formation was also observed in Infasurf, and in NS only after subsequent expansion and compression, but neither in the other clinical surfactants nor in protein-free preparations. The connection between this data and the observations from the lung surfactant literature concerning the widely reported “near-zero surface tension” for lung surfactant films and intact alveolar surfaces will also be discussed.

4:20pm BP-SuA5 Stem Cell Biophysics: From 3D Tissue Analyses to Gels of Controlled Flexibility, Heterogeneity, and Thickness, Dennis Discher, University of Pennsylvania **INVITED**

Scarring is a long-lasting problem in higher animals, and reductionist approaches that include studies of stem cells could aid in regenerative treatments. Following our early studies showing homogeneous matrix elasticity can direct stem cell lineages *in vitro* [Engler et al. Cell 2006], our latest studies involve a new platform wherein copolymerization of collagen I with polyacrylamide produces minimal matrix models of scars (MMMS) in which fractal-fibre bundles segregate heterogeneously to the hydrogel subsurface [Dingal et al. Nature Materials 2015]. Matrix stiffens locally—as in scars—while allowing separate control over adhesive-ligand density. Based on expression analyses of injured mesenchymal tissue, detailed analyses of key pathways focus on scar-like phenotypes of mesenchymal

stem cells (MSCs). These cells spread and polarize quickly, increasing nucleoskeletal lamin-A while also slowly up-regulating the ‘scar marker’ smooth muscle actin (SMA). Surprisingly, expression responses to MMMS exhibit less cell-to-cell noise than homogeneously stiff gels. Such differences from bulk-average responses arise because a strong SMA repressor, NKX2.5, slowly exits the nucleus on rigid matrices. NKX2.5 overexpression overrides rigid phenotypes, inhibiting SMA and cell spreading, whereas cytoplasm localized NKX2.5 mutants degrade in well-spread cells. MSCs thus form a ‘mechanical memory’ of rigidity by progressively suppressing NKX2.5, thereby elevating SMA in a scar-like state.

2D Materials Focus Topic

Room 103B - Session 2D+MI+SA-MoM

2D Materials Characterization including Microscopy and Spectroscopy

Moderator: Matthias Batzill, University of South Florida

8:20am **2D+MI+SA-MoM1 Scanning Tunneling Microscopy and Spectroscopy of Air Exposure Effects on Molecular Beam Epitaxy Grown WSe₂ Monolayers and Bilayers**, *J.H. Park*, Univeristy of California, San Diego; *S. Vishwanath*, Cornell University; *X. Liu*, University of Notre Dame; *H. Zhou*, Cornell University; *S.M. Eichfeld*, Pennsylvania State University; *S.K. Fullerton-Shirey*, University of Pittsburgh; *J.A. Robinson*, Pennsylvania State University; *R. Feenstra*, Carnegie Mellon University; *J. Furdyna*, University of Notre Dame; *D. Jena*, *H.G. Xing*, Cornell University; **Andrew Kummel**, University of California, San Diego

The effect of air exposure on 2H-WSe₂/HOPG was determined *via* scanning tunneling microscopy. WSe₂ was grown by molecular beam epitaxy on highly oriented pyrolytic graphite (HOPG), and afterwards, a Se adlayer was deposited *in-situ* on WSe₂/HOPG to prevent unintentional oxidation during transferring from the growth chamber to the STM chamber. After annealing at 773 K to remove the Se adlayer, STM images show that WSe₂ layers nucleate at both step edges and terraces of the HOPG. The grain boundaries and the step edges of WSe₂ ML have a bias dependence in STM imaging, consistent with difference electronic states with the defect-free terraces. After exposure air for 1 day, although the edge of WSe₂ is partially oxidized, the grain boundaries still maintain a defective electronic structure. Exposure to air for 1 week and 9 weeks caused air-induced adsorbates to be deposited on the WSe₂ surface; however, as shown for localized electronic structure measurement using scanning tunneling spectroscopy (STS), the bandgap of the terraces remained unaffected and nearly identical to those on de-capped WSe₂. The air-induced adsorbates can be removed by annealing at 523 K. In contrast to WSe₂ terraces, air exposure caused the edges of the WSe₂ to oxidize and form protrusions, resulting in a larger STS bandgap compared to the terraces of air exposed WSe₂ monolayers. The preferential oxidation at the WSe₂ edges compared to the terraces is likely the result of dangling bonds at step edges. In the absence of air exposure, the dangling edge bonds have a smaller band gap compared to the terraces and a shift of about 0.73 eV in the Fermi level towards the valence band. However, after air exposure, the band gap of the oxidized WSe₂ edges became larger about 1.08 eV that of the WSe₂ terraces, resulting in the electronic passivation of the WSe₂.

8:40am **2D+MI+SA-MoM2 Tuning the Trion Photoluminescence Polarization in Monolayer WS₂**, *Aubrey Hanbicki*, *K.M. McCreary*, *M. Currie*, Naval Research Laboratory; *G. Kioseoglou*, University of Crete; *C.S. Hellberg*, *A.L. Friedman*, *B.T. Jonker*, Naval Research Laboratory
Monolayer transition metal dichalcogenides (TMDs) such as MoS₂ or WS₂ are semiconductors with degenerate, yet inequivalent *k*-points labeled *K* and *K'* that define the direct bandgap. The valence band maximum in each valley has only one spin state in which the spins are opposite for *K* and *K'*. Consequently, one can selectively populate each valley independently with circularly polarized light and determine the valley populations via the polarization of emitted light. Monitoring changes in emitted polarization, therefore provide insights into the fundamental processes of intervalley scattering. We prepare single-layer WS₂ films such that the photoluminescence is from either the neutral exciton or the negatively charged trion [1,2]. In most TMDs, the optical polarization is small at room temperature, and we find that the neutral exciton emission indeed has zero polarization at room temperature. However, we observe a room temperature optical polarization in excess of 40% for the trion. The trion polarization always exceeds that of the exciton and exhibits a pronounced, non-monotonic temperature dependence – the polarization nearly doubles as the temperature increases from 125 K to 175 K. The observed increase in optical polarization directly correlates with a decrease in emission intensity between 125-175 K indicating that this effect is a consequence of the onset of nonradiative processes. Because this dependence involves trion systems, one can use gate voltages to modulate the polarization or intensity emitted from TMD structures. Using an applied gate voltage, we can modulate the electron density and subsequently the polarization of WS₂ trions continuously from 20-40%. Both the polarization and the emission energy monotonically track the gate voltage with the emission energy increasing by 45 meV. We discuss the role electron capture of the trion has on suppressing the intervalley scattering process. This work was supported by

core programs at NRL and the NRL Nanoscience Institute, and by the Air Force Office of Scientific Research #AOARD 14IOA018-134141.

[1] M. Currie, A.T. Hanbicki, G. Kioseoglou, and B.T. Jonker, *Appl. Phys. Lett.* **106**, 201907 (2015).

[2] A.T. Hanbicki, G. Kioseoglou, M. Currie, C.S. Hellberg, K.M. McCreary, A.L. Friedman, and B.T. Jonker, *Sci. Rep.* **6**, 18885 (2016).

9:00am **2D+MI+SA-MoM3 Quantum Hall Effect in Graphene Visualized through Scanning Tunneling Microscopy and Spectroscopy**, *Adina Luican-Mayer*, University of Ottawa, Canada **INVITED**

The ability to controllably layer atomically thin crystals into custom-made materials holds promise for realizing physical systems with distinct properties, previously inaccessible. The experimental results described in this talk seek to uncover the unique nature of the charge carriers in such few-atoms-thick materials as well as effects that interlayer coupling and disorder have on their properties. To that end we use scanning tunneling microscopy (STM) and spectroscopy (STS) experiments performed on graphene systems at low temperatures and in magnetic field. We study Landau quantization in graphene and by performing spatially resolved STM/STS we demonstrate the true discrete quantum mechanical electronic spectrum within the Landau level band near charged impurities in graphene in the quantum Hall regime.

9:40am **2D+MI+SA-MoM5 Enhancing the Electrical Conductivity of VUV-reduced Graphene Oxide by Multilayered Stacking**, *Yudi Tu*, *T. Utsunomiya*, *T. Ichii*, *H. Sugimura*, Kyoto University, Japan

Reducing graphene oxide (GO), a highly oxidized graphene derivatives, by utilizing light irradiation has drawn great attention, due to its flexibility to locally fabricating conductive patterns and tuning the electrical property. We have demonstrated the reduction of GO under the 172 nm vacuum-ultraviolet (VUV) irradiation under high vacuum and combined it with mask photolithography to make reduced graphene oxide (rGO) conductive pattern at sub- μm scale.^{1,2} The recovery of electrical conductivity at the reduced regions was confirmed by conductive-probe atomic force microscope (CAFM). However, further researches by applying micro Raman spectroscopy (μRS), scanning tunneling microscopy (STM) and CAFM have revealed that the pristine defects induced by the harsh oxidative synthesis of GO is unable to be repaired. On purpose to enhance the electrical conductivity of rGO pattern, generating more conductive paths for the carriers' transportation is of great importance. In this presentation, we will demonstrate the enhanced electrical conductivity in multilayered rGO sheets. The nanoscale conductive sp^2 domains in rGO are connected to construct 3-dimensional conductive paths between the multilayered sheets.

The GO-coated Si substrate was irradiated by the VUV light in the high vacuum ($< 10^{-3}$ Pa) chamber. The CAFM current mapping revealed that GO and the derived rGO were heterogeneous hybrids of both conductive and insulating domains. Interestingly, besides the nanoscale domains distribution revealed by the previous μRS and STM results, the microscale domains distribution was also observed within the sheets, which was attributed to the uncertainly harsh oxidation synthesis. The CAFM current mapping showed obvious enhancement on the electrical conductivity of bi-layered rGO comparing with the single-layered rGO. A triangle approximate model was applied to estimate the lateral electrical conductivity of rGO sheets. It was found that the tip contact area showed no clear influence on the lateral electrical conductivity. By further measuring the current signals from both bi-layered and single-layered rGO sheets, it was found that the enhancement was not due to the parallel-connection of two rGO sheets but originated from the newly constructed 3-dimensional conductive paths between them.

(1) Tu, Y.; Ichii, T.; Utsunomiya, T.; Sugimura, H. *Appl. Phys. Lett.* **2015**, *106*, 133105.

(2) Tu, Y.; Ichii, T.; Khatri, O. P.; Sugimura, H. *Appl. Phys. Express* **2014**, *7*, 75101.

10:00am **2D+MI+SA-MoM6 Silicene-like Reconstruction via Surface Relaxation of Hexagonal-MoS₂ Crystallites**, *Cameron Volders*, *P. Reinke*, *G. Ramalingam*, *E. Monzami*, University of Virginia

The exciting properties of 2D materials have intrigued scientists and engineers for over a decade. A new wave of 2D materials are being explored in the scientific community, specifically, Silicene has garnered much attention for its potential in device integration. The current Silicene literature has accepted a synthetic method of depositing monolayer (ML) amounts of Si atoms onto a heated Ag (111) substrate to produce the 2D

layer. Alternative substrates such as Ir (111) have been explored to obtain silicene, however, the validity of these results are still being debated.

The current work will address an approach, which is a potential alternative route for growing a silicene layer, based on the observation of a Silicene-like reconstruction (SLR) on the surface of nanometer-scale hexagonal MoSi₂ crystallites terminated by the (0001) plane. The bulk (0001) MoSi₂ surface is comprised of Si hexagons with a Mo atom in the center. The honeycomb pattern exhibited by the SLR is formed via relaxation of the (0001) plane where the Si atoms decouple from the underlying h-MoSi₂ crystallites. Signatures of a 'graphite-like' Si structure have been reported in literature, but have not yet been pursued in 2D materials studies. We will present an extensive study of the SLR based on Scanning Tunneling Microscopy and Spectroscopy data.

Initially, this work will describe a parameter space in which the SLR can be confidently reproduced. Mo atoms are deposited onto a Si (001) surface and annealed to grow the h-MoSi₂ crystallites, which is where the SLR resides. Our experimental data supports an optimal growth regime of approximately 750°C and 3-5 ML's of Mo. The focus will then switch to demonstrating the geometrical parameters of our SLR are strikingly similar with that of the current Silicene literature. Our experimental results indicate the honeycomb pattern of the SLR corresponds to a superstructure. When comparing the lattice constant and Si-Si distance in our structure with that of silicene literature, the results strongly suggest we are observing a low-buckled silicene layer. Also included, will be a statistical treatment contributing to the validity that a surface relaxation process is the pathway by which the layer is grown. Specific features are always observed, including a well-defined 'rim' structure and defect motif, when the SLR is observed.

The final stage of this presentation will focus on addressing the electronic structure of the SLR based on STS data. A few studies have provided STS measurements indicating the observation of a Dirac-point (DP) near 0.5 eV. Our experimental results contain an intriguing feature in the same region, which will be discussed.

10:40am **2D+MI+SA-MoM8 Electron Dynamics in Two-Dimensional Materials, Philip Hofmann**, Aarhus University, Denmark **INVITED**

Changing the dimensionality of a material results in significant modifications of its electronic properties. This is even the case if the parent material already has a layered structure with little interaction between the layers, as in the case of graphene, bilayer graphene and single-layer transition metal chalcogenides.

While the static electronic properties of novel two-dimensional materials can be studied by standard angle-resolved photoemission spectroscopy (ARPES), investigations of the ultrafast carrier dynamics require both time- and angular resolution and thus time-resolved (TR)-ARPES. There is, moreover, the technical requirement of high photon energies since the interesting part of the aforementioned materials' electronic structure (i.e. the (gapped) Dirac cone) is placed at the two-dimensional Brillouin zone boundary. Recently, it has become possible to probe states at such high k by TR-ARPES, thanks to the arrival of ultrafast high harmonic laser sources.

Here we characterize the dynamic processes around the Dirac point in epitaxial graphene [1,2], as well as around the band gap of single layer MoS₂ [3,4] using TR-ARPES. In the graphene, we can determine and control the timescales of hot carrier scattering processes. For single layer MoS₂, we can directly measure the size of the direct band gap by pumping electrons into the conduction band minimum. We find that this band gap can be strongly renormalized, both by a static interaction with the substrate and by a dynamic screening due to a high density of excited free carriers.

References

- [1] J.C. Johansson et al., Physical Review Letters 111, 027403 (2013).
- [2] S. Ulstrup et al., Physical Review Letters 112, 257401 (2014)
- [3] J. Miwa et al., Physical Review Letters 114, 046802 (2015).
- [4] A. Grubisic Cabo et al., Nano Letters, 15, 5883 (2015).

11:20am **2D+MI+SA-MoM10 Novel Characterization Techniques for 2D Materials: Visualizing Inherent and External Defects, Rudresh Ghosh, S.K. Banerjee, D. Akinwande**, University of Texas at Austin

Over the last decade, since the demonstration of exceptional physical, chemical and electrical properties of graphene, there has been a lot of interest in two-dimensional materials. Of these new materials significant effort has been focused on transition metal dichalcogenides (TMDs) due to their various possible applications. Initial work on TMDs, similar to that of graphene, has depended on exfoliated samples. In this work we present

controlled large-area synthesis of highly crystalline few to monolayers of various TMDs (MoS₂, WS₂, WSe₂) using both solid and gas precursors. Characterization of the TMDs are done using a combination of conventional techniques such as Raman and Photoluminescence spectroscopy, Atomic force microscopy, scanning and transmission electron microscopy. Shifts in Raman and PL spectra as a function of strain shows obvious differences between exfoliated and CVD grown material. New characterization tools with the capability of localized dielectric mapping (Microwave impedance microscopy) also show us a way to analyze defects that are inherent during CVD growth processes. Elemental identification of individual layers and their interfaces (using Time of Flight SIMS) are demonstrated as extremely useful for studying these 2d heterostructures. Electrical device characterization and paths of optimization are also presented. Electrical characterization of the devices on various substrates is also presented.

11:40am **2D+MI+SA-MoM11 Anomalous Dynamical Behavior of Freestanding Graphene, Paul Thibado, M. Ackerman, P. Kumar, S. Singh**, University of Arkansas; *M. Neek-Amal, F. Peeters*, University of Antwerp, Belgium

Local, long-time evolution measurements of the height fluctuations of a 2D membrane allows examination of the fundamental foundations of statistical mechanics in soft condensed matter. However, such measurements have proved elusive, thereby forcing critical theoretical assumptions in our best models. We report sub-nanometer, high-bandwidth height measurements of freestanding graphene using constant-current, point-mode scanning tunneling microscopy, as a follow-up to our previous related works [1-2]. By tracking atoms directly, the ability to measure dynamic events is increased by a factor of 1000 over the present state-of-the-art membrane imaging technology. Surprisingly, the membrane velocities follow the Cauchy-Lorentz distribution consistent with a Lévy process, rather than the expected Maxwell-Boltzmann distribution. We also present molecular dynamics simulations, which illustrate spontaneous mirror buckling events that give rise to the long excursions.

Acknowledgements:

This work was supported in part by Office of Naval Research (USA) under Grant No. N00014-10-1-0181 and National Science Foundation (USA) under Grant No. DMR- 0855358.

References:

- [1] P. Xu, M. Neek-Amal, S.D. Barber, J.K. Schoelz, M.L. Ackerman, P.M. Thibado, A. Sadeghi, and F.M. Peeters, Nature Comm. **5**, 3720 (2014).
- [2] M. Neek-Amal, P. Xu, J.K. Schoelz, M.L. Ackerman, S.D. Barber, P.M. Thibado, A. Sadeghi, and F.M. Peeters, Nature Comm. **5**, 4962 (2014).

Applied Surface Science

Room 101B - Session AS-MoM

Quantitative Surface Analysis: New Ways to Perform Old Tricks

Moderators: Tony Ohlhausen, Sandia National Laboratory, Carl Ventrice, Jr., SUNY Polytechnic Institute

8:20am **AS-MoM1 Quantitative Analysis of Dendrimer-Encapsulated Nanoparticles, P. Bhattacharya**, University of Dayton Research Institute; *M.H. Engelhard, L. Kovarik, L. Estevez*, Pacific Northwest National Laboratory; *Y.-C. Wang*, University of Washington; *D.R. Baer*, Pacific Northwest National Laboratory; *D.G. Castner*, University of Washington; **Daniel Gaspar**, Pacific Northwest National Laboratory **INVITED**

At the nanoscale, quantitatively and accurately measuring material physical and chemical structure remains a fundamental challenge. Many processes essential to energy production or storage, such as catalysis and battery electrochemistry, rely on nanoscale materials with complex three-dimensional structure. In this work, we describe the characterization of ruthenium oxide polyamidoamide (RuO_x-PAMAM) dendrimer-encapsulated nanoparticles (DEN) that have been developed as catalysts for lithium-air batteries. In a lithium-air battery, the RuO_x-PAMAM DENs catalyze the oxygen evolution reaction during charging. The composition and chemical state of the core nanoparticle, and the three-dimensional structure of the DEN are of great interest in understanding and tuning the performance of these materials in Li-air electrochemical cells. X-ray photoelectron spectroscopy (XPS) has become one of the most widely used tools for surface characterization, including quantitative determination of composition. Accurate XPS quantitation requires accurate understanding of

electron escape depth, but this information can, in turn, be used for a more detailed understanding of the distribution of elements with depth in a sample. Rudimentary estimates of the electron escape depth in elemental solids have been supplanted by more accurate methods of accounting for chemical differences in electron escape depth. One such tool is the database developed by Powell, et al., called the NIST Database for Simulation of Electron Spectra for Surface Analysis (SESSA), which allows a user to automatically retrieve data needed for a specific practical application and simulate AES and XPS spectra for a multi-layered thin-film or nanoparticle for measurement conditions specified by the user. This database contains extensive sets of data for the physical quantities relevant to AES and XPS. The internal databases are linked to a user interface via a small expert system that allows a user to automatically retrieve data needed for a specific practical application. SESSA can simulate AES and XPS spectra for a multi-layered thin-film sample for measurement conditions specified by the user. In this work, we have used SESSA to help determine the depth distribution of RuO_x and compare to electron microscopy measurements of DEN structure. We have compared the computed model of XPS signal intensity with the experimental measurements.

9:00am **AS-MoM3 Developing a Straightforward Method to Calculate Shell Thicknesses for Core-Shell-Shell Nanoparticles from XPS Data, David Cant**, National Physical Laboratory, UK; Y.C. Wang, D.G. Castner, University of Washington; A.G. Shard, National Physical Laboratory, UK

There is currently great interest in the study of core-shell and core-multi-shell nanoparticles. XPS, as a highly surface sensitive and quantitative analysis method, is potentially of great use in the characterisation of these nanoparticle systems. In particular, understanding the chemical composition and thickness of nanoparticle shells is of great importance for understanding how a given nanoparticle system may interact with its environment. More complicated structures, such as core-shell-shell systems are now commonly studied, whether in the context of core-shell systems affected by adventitious carbon contamination or systems with a core-shell-shell structure by design, and as such there is a need for analysis methods capable of providing quantitative information on the structures of such systems.

Straightforward methods for the characterisation of planar overlayers via the use of XPS have been available for some time¹, however such planar analysis techniques are clearly unsuited to providing reasonable estimates of nanoparticle shell thicknesses. Several methods exist for the quantitative analysis of shells in core-shell nanoparticle systems via XPS, including by comparison to simulated data^{2,3} or by direct calculation from empirical formulae⁴. While comparison to simulation can also be used to characterise core-shell-shell nanoparticles, such methods typically require specialist software or expertise, and are not necessarily easily applicable by the general practitioner of XPS. As such, it is important to consider whether a simpler technique for core-shell-shell systems, accessible to any analyst, can be conceived. While not as straightforward as for the core-shell case, an empirical formula for the calculation of core-shell-shell nanoparticle shell thicknesses has been developed⁵ as an extension to the T_{NP} formula⁴ for core-shell nanoparticles. This technique requires no specialist knowledge or software, and with a few iterations converges rapidly upon estimates of shell thickness with a deviation typically lower than the error expected in the estimation of the required electron attenuation lengths.

1. Cumpson, P. J. *-Surf. Interface Anal.* **29**, 403–406 (2000).
2. Smekal, W., Werner, W. S. M. & Powell, C. J. *-Surf. Interface Anal.* **37**, 1059–1067 (2005).
3. Mukherjee, S., Hazarika, A., Santra, P. K., Abdelhady, A. L., Malik, M. A., Gorgoi, M., O'Brien, P., Karis, O. & Sarma, D. D. *-J. Phys. Chem. C* **118**, 15534–15540 (2014).
4. Shard, A. G. *-J. Phys. Chem. C* **116**, 16806–16813 (2012).
5. Cant, D. J. H., Wang, Y.-C., Castner, D. G. & Shard, A. G. *-Surf. Interface Anal.* **48**, 274–282 (2016).

9:20am **AS-MoM4 Double-Lorentzian Asymmetric Line-shape as a Practical Tool for Peak-fitting Multiplet Structures in XPS Data, Alberto Herrera-Gomez**, D. Cabrera-German, CINVESTAV-Queretaro, Mexico; J.A. Huerta-Ruelas, CICATA-Unidad Queretaro, Mexico; M. Bravo-Sanchez, IPICT, Mexico

The peak-asymmetry commonly found in core level photoemission spectra, especially from transition metals and their oxides, has been described in a number of ways. Doniach and Sunjic (DS) [1] proposed that the asymmetry is due to a “combination of the Kondo effect and a transient and singular

re-adjustment of the ground state of the entire Fermi gas to the presence of the effective potential of the hole.” The argument was done for metals since the phenomenon requires occupation at the Fermi level. The proposed line-shape, which is extensively employed for peak-fitting, has important shortcomings. The form is not integrable (the area under it is infinite) for any possible value of the associated asymmetry parameter. Since integrability is paramount for composition analysis, the DS line-shape can only be employed in qualitative studies. Another proposed source is the divergence of the energy loss function at zero-loss [2]. Although this argument could apply to both metals and insulators, the divergence in turn causes a divergence in the calculated spectrum, forcing the near-zero loss region to be cut during integration.

A very extended view is that the skewedness is caused by the multiplet structure. Each multiplet component is considered as symmetric and the apparent asymmetry is due to the presence of components of different intensities near each other. In this way it has been possible to qualitatively reproduce the main features (satellites) of a number of materials. An excellent example is the work of Fujii et al. [3] for the Fe 2p spectrum for iron in Fe₂O₃ and in Fe₃O₄. As shown in their Fig. 3 and 10, the components are many and distributed with no apparent order. Since the intrinsic width of each component is much larger than the separation among them, it is impossible to experimentally resolve them. In addition, it would not make sense to try to construct a “fundamental” asymmetric line-shape.

Thereupon, we present a practical asymmetric line-shape, the double-Lorentzian (DL) [4], that minimizes the number of parameters employed for fitting complex spectra with apparent peak-asymmetries. The fits are clearly superior than those employing DS and also lacks for the integrability problem. Through DL it is possible to fit theoretical spectra, allowing for the quantitative comparison between the predicted and the experimental data.

1. S. Doniach and M. Sunjic, *J. Phys. C* **3**, 285 (1970).
2. A.C. Simonsen, F. Yubero, S. Tougaard. *Phys. Rev. B* **56**, p. 1612 (1997).
3. T. Fujii, F.M.F. de Groot, G. a Sawatzky, F.C. Voogt, T. Hibma, K. Okada. *Phys. Rev. B* **59** (1999) 3195–3202.
4. <http://www.gro.cinvestav.mx/~aherrera/reportesInternos/doubleLorentzia.n.pdf>.

9:40am **AS-MoM5 Quantitative Evaluation of the Carbon Hybridization State by Near Edge X-Ray Absorption Fine Structure Spectroscopy, Filippo Mangolini**, University of Leeds, United Kingdom of Great Britain and Northern Ireland; J.B. McClimon, R.W. Carpick, University of Pennsylvania

We present a method to determine the carbon hybridization state of carbon-based material using near edge X-ray absorption fine structure (NEXAFS) spectroscopy. Carbon-based materials are of interest due to their exceptional physical and mechanical properties. Characterizing their structure is challenging, but of paramount importance for a wide range of applications.

Of the analytical methods used to characterize the near-surface region of carbon-based materials, carbon 1s NEXAFS spectroscopy is one of the most powerful. However, a critical assessment of the methodology for quantifying the local carbon bonding configuration using NEXAFS data, which is based on the analysis of the sample of interest and of a highly ordered pyrolytic graphite (HOPG) reference sample, is lacking.

In this study [1], the methodology is critically reviewed. Inconsistencies applying this method are found in the literature. A derivation for the correct experimental conditions to be used for acquiring HOPG reference spectra is presented along with the potential sources of uncertainty. Using this, we present a specific method for determining the distribution of carbon hybridization state in a carbon-based material using carbon 1s NEXAFS spectroscopy. As an example, a hydrogenated amorphous carbon film was analyzed. NEXAFS results were compared with results from X-ray photoelectron spectroscopy and Raman spectroscopy. Good agreement was seen, validating our method. This work can assist surface scientists in accurately characterizing the bonding state in carbon-based materials.

1. F. Mangolini, J.B. McClimon, R.W. Carpick, *Anal. Chem.*, **88** (5), 2817, 2016.

10:00am **AS-MoM6 Simultaneous XPS-UPS Depth Profiling of Thin Films, Jon Treacy**, C. Deeks, P. Mack, T.S. Nunnery, Thermo Fisher Scientific, UK
Thin films have found use in the fields of microelectronics, coatings and photovoltaics, amongst others and continued research is of vital importance in order to improve their performance in these applications. X-

Monday Morning, November 7, 2016

ray Photoelectron Spectroscopy (XPS) is a long established technique for analysing these types of samples due to its chemical specificity and surface sensitivity. The closely related technique, Ultraviolet Photoelectron Spectroscopy (UPS), has also been widely utilised to provide detailed valence electronic information with greater surface specificity than XPS, due to the incident radiation being of lower energy.

While useful information is acquired from XPS and UPS in isolation, a more powerful insight into the structure of a material comes from using these two techniques in conjunction, allowing a more complete material characterisation to be performed. Previously, switching between techniques throughout the course of an experiment has been an involved and often laborious process, discouraging more widespread use. Recently the automation of UPS has allowed concurrent acquisition of XPS and UPS data during depth profiling, providing a much sought after insight into the correlation between chemical and electronic structure at within a substrate at various depths.

Of particular interest is the ability to access the valence electronic structure at mixed oxide interfaces using small argon ion gas clusters, which was not previously possible due to the loss of electronic structure in semiconductors or organic materials on exposure to monatomic argon ion beams. This presentation demonstrates the wealth of information that can be acquired by performing XPS-UPS depth profiles and the ease with which this information can be acquired and processed, due to recent instrumentation and software developments.

11:00am AS-MoM9 Quantification of the Layer Thickness of Thin Organic Layers by Secondary Ion Mass Spectrometry Depth Profiling. *M.P. Seah, Rasmus Havelund, I.S. Gilmore*, National Physical Laboratory, UK

Secondary ion mass spectrometry depth profiling using argon gas cluster sputtering is increasingly applied for the analysis of organic materials including layer stacks used in organic electronic devices. The depth profiles provide valuable information about layer diffusion, segregation, chemical degradation and contaminants in the stack but are generally not quantitative.

We report a study of the quantification of the amount of matter by secondary ion mass spectrometry (SIMS) when depth profiling a nominally 3.1 nm delta layer of fmoc-pentafluoro-L-phenylalanine in Irganox 1010. The depth profiles are made using 5 keV Ar₂₃₀₀⁺ sputtering with analysis by 25 keV ions. Data for 89 negative secondary ions shows profiles whose integrated areas, when normalized to the intensity for the pure material, vary over a factor of 12. This variation mainly arises from matrix effects that are measured here using separate samples with mixed layers of 3 intermediate compositions of the two materials. Strong effects can cause the delta layer signal to show structure that may be misinterpreted. The compositional profile is established by using trial profiles, representing the composition, which are then enhanced or reduced according to the measured matrix effect and the result is fitted to the normalized intensity data. It is critical to include the roughening caused by the ion beam. When this is included, the amount of matter is found to be equivalent to 3.25 ± 0.05 nm.

It is concluded that the matrix terms used are a good description of the phenomenon and that SIMS profiles may be made quantitative if suitable secondary ions are available and the matrix terms measured.

11:20am AS-MoM10 Spectromicroscopy and Vector Analysis of Carbon Materials, *Adam Roberts*, Kratos Analytical Limited, UK; *N. Fairley*, Casa Software Ltd, UK; *J.D.P. Counsell, C.J. Blomfield*, Kratos Analytical Limited, UK

Material characterisation by photoelectron spectroscopy is an established technique with a wealth of published data. With the improvement in spectrometer performance spectra are routinely acquired from areas with diameters in the tens of microns, although most routine analysis is performed at much larger areas. Spectra averaged over an analysed area assume a material is homogeneous over this probed area although this might not be true [1,2]. Information from lateral and in-depth distributions [3] for elemental and chemical states on a surface can be probed using XPS imaging either at a single binding (kinetic) energy or over a narrow energy range corresponding to a core-level photoemission peak.

A relatively new and under exploited approach for materials surface characterisation is multispectral XPS imaging, also referred to as spectromicroscopy, where a series of images incremented in energy such that each pixel contains a spectrum. A great advantage of this approach is that spectral information can be reconstructed from defined areas which are smaller than those possible with focused x-ray or virtual probe selected

area XPS. Furthermore intensity may be classified by pixel location and binding energy, and summed to reveal multiple spectral forms from a measurement. These spectral forms are ideal for a novel vector method used to identify spectral components characteristic of a material [4,5]. Analysis of the spectra-from-images where the reconstructed spectra are no longer averaged over the total area from which the image is acquired is central to the success of the vector analysis approach. This allows both sample and instrument dependent differences to be 'removed' from the data.

Development of data processing to support spectromicroscopy data reduction has been necessary and a number of approaches have been successfully applied in the characterisation of model and real-world samples[6,7]. This approach has been extended to the interpretation of C 1s spectra for carbon based materials from purely sp² graphite and a small number of polymeric materials. As part of this study the influence of sputter cleaning such materials using Ar⁺ ion gas clusters is also presented.

[1] S. Béchu *et.al* Surf. Interface Anal., 2016,48,301-309

[2] E.F. Smith *et.al* Surf. Interface Anal. 2005, 38, 69-75

[3] J. Walton, *et.al* Surf. Interface Anal. 2016, 48, 164-172

[4] J. Baltrusaitis, *et.al*, Applied Surface Science 326 (2015) 151-161

[5] M. d'Halluin, *et.al*, 2015 Carbon, 93, 974 -983

[6] J. Walton, *et.al*, Surf. Interface Anal. 2008, 40, 478 - 481

[7] A.J. Barlow *et.al*, Surf. Interface Anal. 2015, 47, 173-175

11:40am AS-MoM11 Angular Broadening in Core Electron Spectroscopy, *H. Cohen*, Weizmann Institute of Science, Israel; *Alon Givon*, Tel Aviv University, Israel

Using an analytic approach, the role of angular broadening in quantitative core-electron spectroscopy is investigated. It is shown why, practically, the broadening effect remains relatively small for a broad range of parameters, including detection angular openings of nearly ± 30 degrees. Based on the analytic expression, a correction factor can be derived, suggesting that the replacement of inelastic-mean-free-path by an effective attenuation-length parameter is not necessarily an optimal choice. The derived expression further proposes useful insight on the contribution of leading experimental parameters and, in particular, on the sharp increase of elastic-scattering corrections above a (depth dependent) critical angle.

Biomaterial Interfaces

Room 101A - Session BI+AS-MoM

Biomolecules and Cells at Interfaces

Moderator: Joe Baio, Oregon State University

8:20am BI+AS-MoM1 Probing the Selectivity of Antimicrobial Peptides to Cell Membranes by Sum Frequency Generation Spectroscopy, *Thaddeus Golbek*, Oregon State University; *J. Franz*, Department of Molecular Spectroscopy, Max Planck Institute for Polymer Research, Mainz, Germany; *J.E. Fowler, K.F. Schilke*, Oregon State University; *T. Weidner*, Department of Molecular Spectroscopy, Max Planck Institute for Polymer Research, Mainz, Germany; *J.E. Baio*, Oregon State University

Cationic amphiphilic peptides have been engineered to target both Gram-positive and Gram-negative bacteria while avoiding lysis of other cell types. However, the exact mechanism of how these peptides target, bind, and disrupt bacterial cell membranes is not understood. One specific peptide that has been shown to selectively capture bacteria is WLBU2 (sequence RRWVRRVRRWVRRVRRVRRVRRVRR). It has been suggested that WLBU2 activity stems from the fact that when interacting with bacterial cell membranes the peptide assumes an α -helical structure and inserts itself into the membrane. To test this hypothesis, we applied sum frequency generation (SFG) spectroscopy and surface tensiometry to probe the peptide-lipid-air interface and identify the structure and monitor the interaction of WLBU2 with two model lipid monolayers that mimic mammalian and bacterial cell membranes. Model mammalian cell membranes were built upon zwitterionic 1,2-dipalmitoyl-*sn*-glycero-3-phosphocholine (DPPC) lipids while bacterial cell membranes were constructed with negatively charged 1,2-dimyristoyl-*sn*-glycero-3-phospho-(1'-*rac*-glycerol) (DMPG) lipids. The rate at which the surface pressure reaches equilibrium is 4.3 times faster for WLBU2 interacting with the negatively charged DMPG lipid monolayer than with the zwitterionic DPPC lipid monolayer. This observed WLBU2 binding affinity preference to negatively charged membranes is likely due to electrostatic interactions

between positively charged amino acids within the peptide and negatively charged lipids. SFG studies at the peptide-lipid-air interface demonstrate that binding of WLBU2 induces increased lipid monolayer order. A larger increase in acyl chain order from 2.2 to 3.4 determined by the ratio of the CD₃ symmetric (2075 cm⁻¹) and CD₂ symmetric (2100 cm⁻¹) peak amplitudes suggest that WLBU2 is found at the surface of the zwitterionic phospholipid monolayer and not inserted. The amide I region SFG spectrum of WLBU2 interacting with the zwitterionic lipid monolayer shows two peaks near 1642 cm⁻¹ and 1678 cm⁻¹ indicative of an inactive β -sheet structure. A peak near 1651 cm⁻¹ for WLBU2 interacting with negatively charged lipids is assigned to an active α -helix structure. Altogether, we demonstrate that WLBU2 shows a higher binding affinity to bacterial cell membranes and is in an active α -helix structure, alternatively in the presence of mammalian cell membranes in an inert β -sheet structure.

8:40am BI+AS-MoM2 Bacterial Adhesion to Immobilized Liquid Layers under Dynamic Conditions, Caitlin Howell, University of Maine; Y. Kovalenko, I. Sotiri, Harvard University; J. Overton, University of Maine; J. Aizenberg, Harvard University

Immobilized liquid (IL) layers are an emerging technology shown to prevent bacterial biofouling of surfaces. In this work, we show how in one class of IL-coated materials, infused polymers, bacterial adhesion can be strongly dependent on growth conditions. Samples grown with *Escherichia coli* under more relevant dynamic conditions showed significantly increased colony-forming unit counts compared to the same system grown under static conditions. Direct visualization of the surfaces suggested that this was due to a disturbance of the IL layer when exposed to shaking conditions, which allowed more bacteria to remain on the surface after an initial rinse. However, no incorporation of the bacteria into the oil layer was detected. To further investigate the extent of this adhesion, we used sequential removal cycles to gauge the relative adhesion strength of the remaining surface-bound *E. coli*. Through this method, we found that despite no initial difference in adherent CFUs compared to control samples with no IL layers, IL samples did reduce overall adhesion of the bacteria even after incubation under dynamic conditions. Further tests on a flagella-deficient strain of *E. coli* revealed that while flagella play a significant role in adhesion to IL layers, they are not the sole adhesion mechanism for this species. Finally, tests on two other clinically-relevant species of bacteria, *Staphylococcus aureus* and *Pseudomonas aeruginosa*, using similar methods revealed clear species-dependent differences in adhesion after growth under dynamic conditions. These results shed new light on the interaction of bacteria with IL layers, and demonstrate the importance of both relevant growth conditions and thorough analysis to obtaining clear results in these systems.

9:00am BI+AS-MoM3 Nitric Oxide Materials—An Approach to Creating More Hemocompatible Medical Device Coatings, Hitesh Handa, University of Georgia

Blood/material interaction is critical to the success of implantable medical devices, ranging from simple catheters, stents and grafts, to complex extracorporeal artificial organs which are used in thousands of patients every day. There are two major limiting factors to clinical application of blood contacting materials: 1) platelet activation leading to thrombosis, and 2) infection. Despite a thorough understanding of the mechanisms of blood-surface interactions, and decades of bioengineering research effort, the ideal non-thrombogenic prosthetic surface remains an unsolved problem. One approach to improving the hemocompatibility of blood-contacting devices is to develop materials that release nitric oxide (NO), a known potent inhibitor of platelet adhesion/activation and also an antimicrobial agent. Healthy endothelial cells exhibit a NO flux of 0.5-4x10⁻¹⁰ mol cm⁻² min⁻¹, and materials that mimic this NO release are expected to have similar anti-thrombotic properties. I will discuss the potential of incorporating NO donor molecules such as diazeniumdiolates or S-nitrosothiols (RSNOs) into various polymers, and their hemocompatibility and antibacterial properties in short-term (4 h) and long-term (7 d) animal models.

9:40am BI+AS-MoM5 Why do Bacteria Stick to Some Surfaces and Not Others? Characterisation of the Behaviour of Motile Bacteria at and Above the Surface of Materials, A.L. Hook, A. Carabelli, N.A. Russell, P. Williams, Morgan Alexander, The University of Nottingham, UK

High throughput screening has been used to discover a novel class of polymers with resistance to bacterial attachment and subsequent biofilm formation.[1,2] Physicochemical descriptions of the surfaces have to date been found insufficient to predict the wide range of bacterial attachment across these diverse polymer libraries, and cannot offer an explanation of

the controlling phenomena. Whilst perhaps disappointing for the physical sciences, the life sciences are replete with information on how bacteria respond to their local environment, with chemotaxis being one of the most readily observed processes. Unsurprisingly, microorganisms cannot be approximated to inert spheres and rods as they possess surface responsive appendages such as flagella, which enable them to swim, pili that confer twitching motility and fimbriae that mediate surface attachment. These in turn are coupled to sophisticated signal transduction mechanisms that facilitate integration of multiple local environmental parameters at both single cell and population levels. Many of these sensory systems are postulated to contribute to surface sensing. As an example of the complexity of these processes, the opportunistic pathogen *Pseudomonas aeruginosa* has over 60 two-component sensor kinase response regulator systems involved in environmental adaptation.

We believe that bacterial decision-making is key to determining whether a surface is colonised or not. I will present the early results from our optical microscopy investigations of how individual bacterial cells respond to surfaces. We have developed a novel microscope that collects temporal 3D information on cell position using both holography and remote scanning microscopy. [3] Simultaneously surface tracking can be achieved using DIC, TIRF and TIR microscopy. This allows us to track not only the motion of single cells at the surface, but also their approach to and behaviour after contact with the surface.

We will combine these findings with our existing understanding of the surface chemistry-attachment relationships achieved for certain subsets of materials and attachment regimes,[4,5] with chemical analysis of the in situ surface to build a complete description of this complex biointerface and the response of bacteria to it. This information is crucial in determining how bacteria behave with respect to defined surfaces and has important implications for the prevention of device centred infections.

1. Hook et al. Nature Biotechnology 2012
2. Hook et al. Advanced Materials 2013
3. Botcherby et al. Circulation Research 2013
4. Epa et al. Advanced Functional Materials 2014
5. Sanni et al. Advanced Healthcare Materials 2015

10:00am BI+AS-MoM6 Probing Adhesion of Marine Biofilm Formers by Microfluidics, K. Nolte, Ruhr-University Bochum, Germany; M. Alles, M.P. Arpa-Sancet, C. Christophis, University of Heidelberg, Germany; Axel Rosenhahn, Ruhr-University Bochum, Germany

When new Materials are developed to control and influence Biofilm growth, the ability of biofilm formers to firmly adhere to the coatings is one key property. Several techniques have been developed in the past to probe attachment strength of cells [1]. Especially microfluidic test systems [2] offer several advantages, such as small sample area, small amounts of target species, and high throughput. We developed microfluidic assays that allow to test bacterial and diatom adhesion on coatings [3,4]. Cells are driven through a microchannel at a precisely controlled flow rate and at a constant concentration and both, accumulation and detachment can be monitored by video microscopy. Using self-assembled monolayers as model surfaces we were able to show that the adhesion strength correlates with the accumulation dynamics if an appropriate shear stress is applied. Based on this finding, a parallelized microfluidic system has been developed that allows simultaneous, comparative testing of materials. Due to the modular assembly of the setup, not only model surfaces and thin organic films, but also practical coatings can be analyzed.

- [1] L. Marcotte, M. Tabrizian, ITBM-RBM 2008, 29, 77
- [2] D.P. Bakker, A. van der Plaats, G.J. Verkerke, H.J. Busscher, H.C. van der Mei, Appl. Envir. Microbiol. 2003, 69(10), 6280
- [3] M. Arpa-Sancet, C. Christophis, A. Rosenhahn, Biointerphases 2012, 7, 2
- [4] M. Alles, A. Rosenhahn, Biofouling. 2015, 31, 469–480.

10:40am BI+AS-MoM8 Protein Control of Materials Nucleation Probed by Sum Frequency Generation, Tobias Weidner, Max Planck Institute for Polymer Research, Mainz, Germany

Proteins can act as Nature's engineers at interfaces and manipulate both hard and soft tissue – they shape biominerals, manipulate cell membranes and nucleate materials. Despite the apparent importance for engineers working in the fields of surface engineering, drug delivery, or diagnostics, the molecular mechanisms dictating interfacial protein action have remained largely elusive. Our goal is to probe the structure and structural dynamics of such active proteins – in action at the surface.

Mineral proteins have the ability to control and steer the growth of hard tissue by binding specific mineral facets and precipitating silica and phosphates. They control the intricate mineral morphologies found in diatom cell walls, mollusk nacre, but also human teeth and bone. Inspired by diatom silification we used amphiphilic peptides consisting of leucine and lysine (LK peptides) to investigate biomineralization at surfaces. These peptides can adopt helical or beta sheet structures at the air-water interface. Upon addition of a silica precursor we obtained freestanding peptide-silica hybrid sheets with thicknesses of ~4 nm. We have followed the biomineral composition and interactions between peptides and silica at different early stages of biomineralization using a combination of surface spectroscopies and microscopies. Our experimental findings were complemented with molecular dynamics simulations. Our data shows that the peptide surface folding dictates the nanometer scale morphology of the prepared silica film.[1]

A particularly fascinating example of protein driven nucleation and phase transitions are ice-nucleating proteins. These proteins are used by specific bacteria to attack plants and cause frost damage by growing ice crystals at temperatures that would otherwise not allow ice formation. A recent survey by the NASA found large amounts of biological ice nucleators in the troposphere where they may affect global precipitation patterns. We have followed the interaction of freeze proteins with surrounding water molecules – how specialized protein sites lock water molecules in place and manipulate the flow of energy within the surrounding layers of water.[2]

1 H. Lutz, V. Jaeger, R. Berger, M. Bonn, J. Pfaendtner, T. Weidner

Biomimetic growth of ultrathin silica sheets using artificial amphiphilic peptides

Advanced Materials Interfaces, 1500282 (2015).

2 R. Pandey, K. Usui, R. A. Livingstone, S. A. Fischer, J. Pfaendtner, E. H. G. Backus, Y. Nagata, J. Fröhlich-Nowoisky, L. Schmüser, S. Mauri, J. F. Scheel, D. A. Knopf, U. Pöschl, M. Bonn, T. Weidner

Ice-nucleating bacteria control the order and dynamics of interfacial water

Science Advances, 2 (2016).

11:20am **BI-AS-MoM10 Regulation of Cell Surface Access and Mechanics at the Interface**, *Jennifer Curtis, P. Chang, W. Wei, L.T. McLane*, Georgia Institute of Technology; *J. Scrimgeour*, Clarkson University **INVITED**

A polymer brush-like structure decorates the cell surface of many cell types ranging from fibroblasts to mesenchymal stem cells to cancer cells. This sugar-rich pericellular matrix (PCM) plays physical and chemical roles in biological processes ranging from brain plasticity, to adhesion dependent processes like cell migration, to the onset of cancer. Here I will report on biophysical and mechanical assays that characterize the structure of the pericellular matrix and its impact on the transport of nanoparticles and molecules to the cell surface. Further, I will present compelling quantitative evidence that hyaluronan polymer expression at the cell-substrate interface tunes cell adhesion strength, working in concert with focal adhesions.

Electronic Materials and Photonics

Room 102A - Session EM+NS+PS+SS+TF-MoM

Growth and Devices Technology of Group III-Nitrides

Moderators: Nikolaus Dietz, Georgia State University, Shalini Gupta, Northrop Grumman ES

8:20am **EM+NS+PS+SS+TF-MoM1 Development of AlGaIn based UV Laser Diodes**, *Ronny Kirste*, Adroit Materials; *B. Sakar, A. Franke*, NCSU; *J. Tweedie*, Adroit Materials; *Z. Bryan, I. Bryan*, NCSU; *S. Mita*, Adroit Materials; *R. Collazo, Z. Sitar*, NCSU **INVITED**

UV laser diodes are widely desired for many important applications such as chemical and biological sensing, non-line of sight communications, and DNA tagging. Design and fabrication of AlGaIn based laser diodes is the most promising pathway for next generation UV lasers but challenges for these devices are many including low n- and p-conductivity, absorbing injection layers, and non-ohmic contacts. Here, we present recent advances in the growth and fabrications of UV laser diodes. The presentation will cover the most important steps that are necessary to achieve electrically injected UV laser diodes. These include: AlGaIn epitaxy, doping, fabrication, and design.

As an advancement over most existing approaches, we pursue the growth of our device structures on single crystalline AlN substrates which allows

for low dislocation densities $< 10^4 \text{ cm}^{-2}$. Any such device fabrication is started with the growth of an AlN homoepitaxial layer. It is demonstrated that this epitaxial layer can be grown with a dislocation density that follows that of the substrate and no interface between layer and substrate is observed in TEM, which indicates true homoepitaxy. Subsequent growth of AlGaIn layers with Al content ranging 50-85% is shown to be pseudomorphic. An excellent control of the AlGaIn surface morphology is demonstrated using a supersaturation scheme and bilayer steps as needed for highly efficient MQWs are achieved. MQWs for emission at wavelengths ranging 240-280 nm are discussed and optically pumped lasing in this region is demonstrated. The chosen approach to grow on AlN is validated by realizing MQWs with an IQE exceeding 90%. In order to achieve electrically injected UV lasing, Al-rich AlGaIn is doped and free electron concentrations for the n-cladding with 80% Al-content is shown to be around $8 \times 10^{18} \text{ cm}^{-3}$. In contrast, p-doping of AlGaIn is much more challenging because of the high activation energy of the Mg acceptor. Consequently, achievable free hole concentration and conductivity of the p-cladding are low. We discuss how these epitaxial layers can be used for realizing laser diodes. Experimental work is supported by simulations and used to direct the UV laser design. Finally, we present electrical data and electroluminescence spectra from fully fabricated diodes and discuss the future challenges that need to be addressed to demonstrate the first electrically injected UV laser diode.

9:00am **EM+NS+PS+SS+TF-MoM3 Low-Temperature PA-ALD Growth Technology for Group III-Nitride Nano-heterostructures and their (Opto)Electronic Device Applications**, *Necmi Biyikli, A. Haider, S. Kizir, P. Deminskyi, M. Yilmaz, S. Bolat, A. Celebioglu, A.K. Okyay, T. Uyar*, Bilkent University, Turkey; *F. Buyukserin, S. Altuntas*, TOBB University of Economics and Technology, Turkey; *I. Yilmaz, K. Khaled*, Turgut Ozal University, Turkey **INVITED**

Being initially developed for an entire different area of use, atomic layer deposition (ALD) became a widespread tool to grow functional films and conformal ultra-thin coatings for numerous applications. Based on self-limiting surface reactions, ALD enabled the low-temperature growth of various materials including dielectrics, semiconductors, and metals. Featuring the capability to deposit wafer-scale uniform semiconductor films at relatively low-temperatures with sub-monolayer thickness control and ultimate conformality makes ALD attractive for the semiconductor community. Towards this end, precursors and growth recipes are developed to deposit crystalline thin films for compound and elemental semiconductors. Conventional thermal ALD techniques as well as plasma-assisted and radical-enhanced ALD techniques have been exploited to achieve decent film quality compatible with device applications.

In this presentation, we give an overview of our research efforts on plasma-assisted ALD-based nanoscale semiconductor research focusing on III-nitrides. We have combined our low-temperature thin-film growth recipes with various nanoscale templates and exploited the conformality feature of ALD technique to fabricate nitride nanostructures. Electrospun polymeric nanofibers have been used to produce flexible polymer/III-nitride core-shell structures which might be used for flexible optoelectronics. In addition, hollow-core multi-shell III-nitride nano-heterostructures are demonstrated as well. Anodized alumina (AAO) templates were utilized to fabricate large-area ordered III-nitride nanostructures including radial heterostructures. Extensive growth and fabrication recipe development and materials characterization details will be presented.

The synthesized III-nitride nanoscale semiconductor materials might find applications in a vast amount of applications including physical and chemical sensing, piezo-electric energy harvesting, photocatalysis, nanoscale and flexible (opto)electronics. As proof-of-principle device demonstrations, we have shown nanofibrous GaN/InN-based photocatalysis, GaN/InN-based chemical (gas) sensing, and nanoscale GaN-based UV photodetectors.

9:40am **EM+NS+PS+SS+TF-MoM5 Structural Qualities of GaN Grown on AlN Buffer Layer by MEPA-MOCVD**, *Daniel Seidlitz, I. Senevirathna, A. Fali, Y. Abate, N. Dietz*, Georgia State University; *A. Hoffmann*, Technical University Berlin, Germany

This study focusses on the influence of Aluminum nitride (AlN) buffer layers on the structural and optoelectronic properties of subsequent overgrown Gallium nitride (GaN) layers, using Migration Enhanced Plasma-Assisted Metal Organic Chemical Vapor Deposition (MEPA-MOCVD).

One challenge in group-III nitride growth is the lattice mismatch between the substrate (e.g. sapphire (Al_2O_3), silicon or silicon carbide) and the group III-Nitride layer as for example GaN. Lattice mismatch imposes compressive

strain/stress and influences the crystal quality of subsequent grown group-III nitrides. Inserting an AlN interlayer between the sapphire substrate and the GaN epilayer, transitions the oxygen surface chemistry to a nitrogen surface chemistry, separating surface chemistry related defects from lattice mismatch induced defects, which leads to an improved crystalline quality of the overgrowing GaN layer.

All group III-Nitride layers are grown on sapphire substrates using MEPA-MOCVD. The system design allows the growth of GaN at lower temperatures by using plasma activated nitrogen species ($N^*/NH^*/NH_x^*$) as nitrogen precursor, which are generated by a radio-frequency hollow cathode plasma source (MEAgrow™) scalable from 20W up to 600W. The tunable nitrogen plasma source enables to control the kinetic energies of the active nitrogen species in the afterglow region to be directed at the growth surface, where they interact with metalorganic (MO) precursors. The growth process parameter set includes: reactor pressure, growth temperature, pulsed injection of MO- and nitrogen plasma fluxes, plasma species and their energies.

The structural properties of the AlN buffer layers (e.g. local ordering, grain size, surface topography) are analyzed by Atomic Force Microscopy (AFM) and Raman spectroscopy. The film thickness and optoelectronic properties of the AlN and GaN layers are studied Fourier Transform infrared (FTIR) and reflectance spectroscopy. Results are presented on the structural and optoelectronic properties of the GaN layers as function of the process parameters and the properties of the underlying AlN buffer layer.

10:00am EM+NS+PS+SS+TF-MoM6 Optical and Electrical Characteristics of Gamma-ray Irradiated AlGaIn/GaN Heterostructures, MinPrasad Khanal, B. Ozden, K. Kim, S. Uprety, V. Mirkhani, L. Shen, K. Yapabandara, A.C. Ahyi, M. Park, Auburn University

AlGaIn/GaN high electron mobility transistors (HEMTs) show their potential immunity toward high energy radiation related damages, making them promising candidates for the radiation hard electronics. The degradation in performance of these devices under radiation exposed environment might be due to different possible effects in the device structure such as strain/stress, generation of dislocation, carrier removal and reduction in two-dimensional-electron-gas (2DEG) concentration. The AlGaIn/GaN epi structures grown on 6 inch Si wafer were used and irradiated with 120 MRad doses of gamma-ray produced from ^{60}Co source. The semi-transparent (with 10-15 nm thickness) Ni Schottky diodes and circular HEMT devices were fabricated using un-irradiated and gamma-ray irradiated AlGaIn/GaN epi structures. In the case of HEMT devices, Ti/Al/Ni (30/180/40 nm thickness) for the ohmic contact and Ir (15 nm thickness) for the gate contact formation were deposited using dc magnetron sputtering system. Spectroscopic photo current-voltage (IV) measurements both with sub-band gap and above band-gap illumination, micro-Raman/photoluminescence spectroscopy, and transistor characterizations were performed. The spectroscopic photo IV measurements were carried out by applying the variable wavelength ultra-violet (UV) and visible light from Xenon lamp source under reverse bias condition. Sub-bandgap illumination (800 nm-400 nm) provided the information about sub-bandgap energy levels of defects by relating the change in photocurrent level in response to the applied light spectrum. On the other hand, above bandgap illumination (280 nm-400 nm) utilizes the fact that the penetration depth of a light varies as a function of wavelength. The result showed reduction in photocurrent on the gamma-ray irradiated samples in comparison to the un-irradiated samples, revealing the possibility of creation of extra defects, and hence, decreasing the carrier concentration in the 2DEG. Micro-Raman and photoluminescence (PL) spectroscopic analysis on both the samples were also performed and the results show no substantial change in their spectra, supporting the conclusion from previous scientific reports of radiation resistance of the HEMTs on their bulk structure level. Decrease in drain current and transconductance were observed from the transistor IV measurements, indicating a possible reduction in carrier concentration. It can be concluded that the reduction on photocurrent, drain current level and transconductance after the gamma-ray irradiation are due to the possible creation of some extra defects and decrease of carrier concentration on 2DEG channel.

10:40am EM+NS+PS+SS+TF-MoM8 Seeded Regrowth for Production of AlN and GaN Substrates by HVPE, Jacob Leach, K. Udawary, G. Dodson, K. Gentry, P. Quayle, T. Schneider, H. Splawn, K. Evans, Kyma Technologies, Inc. INVITED

Freestanding GaN and freestanding AlN remain the substrates of choice for the highest performing vertical high voltage switching devices (>1200V) and UV optoelectronics, respectively. However, the cost of these substrates

remains high, availability remains low, and the crystalline quality of these substrates varies depending on the growth technique employed. In particular, the electrical quality of GaN substrates and the UV transparency of AlN substrates depend on the specific growth conditions utilized and it remains a challenge to maintain high crystalline quality while simultaneously realizing high electrical quality or UV transparency. We proposed the use of hydride vapor phase epitaxy (HVPE) as a cloning technique to replicate the high crystalline quality of existing solvothermally grown GaN or physical vapor transport (PVT) grown AlN substrates while maintaining high electrical and optical quality. In this talk, we report Kyma's recent results in the use of the HVPE replication technique for realizing both AlN and GaN substrates.

Electronic Materials and Photonics Room 102B - Session EM-MoM

Advances in Photonics

Moderators: Michael Filler, Georgia Institute of Technology, Daniel Wasserman, University of Texas at Austin

8:20am EM-MoM1 Optical Materials for Far-IR Reststrahlen Optics, Daniel Wasserman, University of Texas at Austin INVITED

The mid-infrared (mid-IR) spectral range (3-15 μm) has become a burgeoning and dynamic field of research both for fundamental exploration as well as for more applied research in health and the environment, security and defense, communication, and sensing. New optoelectronic devices, in particular sources and detectors, have allowed for the rapid growth of the mid-IR, and the development of a range of optical systems for a variety of applications. At the same time, the areas of plasmonics and metamaterials have experienced explosive growth over the past decade, fueled in part by rapid developments in fabrication, characterization, computational science, and theory. These have become increasingly important in the mid-IR, where sub-wavelength confinement and manipulation of light offer the potential for new types of optical materials and structures for integration with the ever-improving mid-IR optoelectronic devices. Yet all of the above developments are, in some ways, spectrally limited to wavelengths <20 μm , due largely to the strong absorption of light in semiconductors at, or near, to optical phonon energies. The strong absorption of optical phonons results in a far-IR wavelength band, which for simplicity sake we refer to as the Reststrahlen region, from 20-60 μm where little to no optical and optoelectronic infrastructure exists.

In this talk, I will discuss our group's recent work developing novel optoelectronic, plasmonic, and phononic devices and structures for far-IR applications. I will present far-IR perfect absorber structures and discuss the potential and limitations of selective thermal emitters in the far-IR. In addition, I will demonstrate how phononic materials can behave similarly to plasmonic materials in a limited spectral band near the longitudinal optical (LO) phonon, showing coupling to both propagating and localized surface phonon modes. I will also show how careful control of doping in semiconductor epilayers offers some wavelength flexibility in designing materials capable of supporting hybrid plasmonic/phononic modes. Finally, I will discuss the opportunities for development of far-IR optoelectronic devices capable of serving as light sources at far-IR wavelengths. In all, I hope to present a picture of the far-IR as a new optical frontier where we can not only apply the lessons from shorter wavelength photonic structures, but also explore exciting new approaches to the development of Reststrahlen band optical infrastructure.

9:00am EM-MoM3 Mid-IR to THz Nanophotonics: Realizing Alternative Polaritonic Materials, Joshua Caldwell, US Naval Research Laboratory INVITED

The field of nanophotonics is based on the ability to confine light to sub-diffractive dimensions. Up until recently, research in this field has been primarily focused on the use of plasmonic metals. However, the high optical losses inherent in such metal-based surface plasmon materials has led to an ever-expanding effort to identify, low-loss alternative materials capable of supporting sub-diffractive confinement. Beyond this, the limited availability of high efficiency optical sources, refractive and compact optics in the mid-infrared to THz spectral regions make nanophotonic advancements imperative. One highly promising alternative are polar dielectric crystals whereby sub-diffraction confinement of light can be achieved through the stimulation of surface *phonon* polaritons within an all-dielectric, and thus low loss material system. Due to the wide

Monday Morning, November 7, 2016

array of high quality crystalline species and varied crystal structures, a wealth of unanticipated optical properties have recently been reported. However, these materials also have some limitations, primarily in the limited spectral bandwidth of operation for any given material. This talk will discuss recent advancements to improve the material lifetime and to induce additional functionality through isotopic enrichment and hybridization of polaritonic modes for realizing low-loss, actively tunable/modulated nanophotonic materials.

9:40am **EM-MoM5 Time-Resolved Optical Studies on Reflection and Transmission of Niobium Dioxide Thin Films**, *Melissa Beebe**, College of William and Mary; *J.M. Klopff*, Helmholtz-Zentrum Dresden-Rossendorf, Germany; *D. Lahnehan*, *Z. Xing*, *M.M. Qazilbash*, College of William and Mary; *Y. Wang*, *S. Kittiwatanakul*, *J. Lu*, *S.A. Wolf*, University of Virginia; *R.A. Lukaszew*, College of William and Mary

Niobium dioxide (NbO_2) is a highly correlated material that, like vanadium dioxide (VO_2), exhibits a first-order insulator-to-metal transition (IMT) at a material-dependent critical temperature, accompanied by a structural transformation from monoclinic to rutile. The nature of the IMT in VO_2 has been discussed at length, while fewer studies have been carried out on NbO_2 . Here, we present ultrafast pump-probe studies comparing reflection measurements to the first ultrafast transient transmission measurements of this optically-induced transition in NbO_2 thin films, as well as compare these studies to similar ones carried out on VO_2 thin films.

10:00am **EM-MoM6 Fabrication of Nanosphere-Based Disordered Coatings for Radiative Cooling under Direct Sunlight**, *Sarun Atiganyanun*, *S.E. Han*, *S.M. Han*, University of New Mexico

In this study, we investigate a facile fabrication of coatings made of silica nanosphere-based disordered structures via evaporation coating and air atomization coating. In both methods, silica nanospheres with a diameter of ~900 nm are dispersed in a water or methanol solution, where the sphere size can be further tuned. The colloidal stability is then disrupted by dissolving salt in the solution. In the evaporation coating, the bulk solution is confined in a substrate and is let to evaporate. In the atomization coating, the solution is atomized by a spray nozzle, and resulting droplets are deposited onto a substrate. Scanning electron microscopy images and subsequent autocorrelation analyses show that the resulting structures are disordered without short- or long-range order. Transmission measurement also indicates that the structures have a short transport photon mean free path of approximately 4-8 μm . These results suggest strong photon scattering properties in the visible region, while providing a strong emission window in 8 to 13 μm range. Such films would enable potential applications in radiative cooling. To investigate this aspect, a computational model is used to calculate the cooling power of the coatings under direct sunlight. The model predicts that the disordered coating with 200 μm thickness has a cooling power of ~250 W/m^2 at 27°C and could reduce the temperature of the sample under a direct sunlight by approximately 37°C below the ambient temperature. We will further discuss our experimental measurements in this presentation.

10:40am **EM-MoM8 Symmetry-Breaking Nanostructures for Light Trapping in Thin Crystalline Silicon Solar Cells**, *Seok Jun Han*, *S. Ghosh*, *O.K. Abudayyeh*, *B.R. Hoard*, *E.C. Culler*, *J.E. Bonilla*, *S.M. Han*, *S.E. Han*, University of New Mexico

While various materials have been investigated for photovoltaics, solar cells based on crystalline silicon (c-Si) dominate the current photovoltaics market. To reduce the cost of c-Si cells, wafer manufacturing companies have produced competitively priced thin c-Si films, ranging from a few microns to tens of microns, using a kerfless process. In such thin-film c-Si cells, light absorption becomes poorer than in thick films and light trapping is crucial to increase the photovoltaic efficiency. Han *et al.* have demonstrated that, among various light-trapping schemes, symmetry breaking in photonic nanostructures can approach the Lambertian light-trapping limit very closely. However, fabricating symmetry-breaking nanostructures in a scalable, cost-effective, manufacturable manner remains elusive. Here, we introduce a new approach to systematically break the symmetry in photonic nanostructures on c-Si surface. Using our approach, we fabricate low-symmetry inverted nanopyramid structures. Our method makes use of low-cost, manufacturable wet etching steps on c-Si(100) wafers without relying on expensive off-cut wafers. Our experiment and computational modeling demonstrate that the symmetry breaking can increase the Shockley-Queisser efficiency from 27.0 to 27.9% for a 10-micron-thick c-Si film. Further, our computation reveals that this

improvement would increase from 28.1 to 30.0% with over-etching for a 20-micron-thick c-Si film.

11:00am **EM-MoM9 Non-thermal Plasma Synthesis of *In Situ* Graphene Shells on Silicon Carbide Nanoparticles**, *Devin Coleman*, *L. Mangolini*, University of California - Riverside

The synthesis of beta-phase silicon carbide nanoparticles exhibiting a hollow core-shell morphology is demonstrated by means of a two-step non-thermal plasma method.[1] Crystalline silicon nanoparticles are nucleated from silane precursor gas in a non-thermal plasma reactor similar to the one described in [2] and injected into a secondary methane-containing plasma reactor, where they are carbonized to form beta-phase silicon carbide nanoshells. Furthermore, at sufficiently high input power in the second plasma, a single-layer graphene coating forms around the silicon carbide particles. These findings are consistent with XRD and Raman spectra. An analytical solution of the 1D diffusion equation in spherical coordinates, as well as the lattice volume expansion from silicon to silicon carbide are used to explain the formation of the interior void. This provides an alternative to previously reported results, which invoke the nanoscale Kirkendall effect to explain the void formation by means of fast out-diffusion of the core element.[3] Further consideration of the system kinetics indicates interactions with the ionized gas leads to particle superheating, allowing for the diffusion of carbon into the silicon matrix and nucleation of beta-phase silicon carbide to occur during the short residence time of the particles in the system. This work expands upon the materials achievable by non-thermal plasma synthesis and suggests that such systems offer the capability to engineer particle morphology, as well as grow conformal 2D materials on freestanding nanoparticles.

References:

[1] Hollow silicon carbide nanoparticles from a non-thermal plasma process. D. Coleman, T. Lopez, O. Yasar-Inceoglu, and L. Mangolini. J. Appl. Phys. In press (2015).

[2] Silicon nanocrystal production through non-thermal plasma synthesis: a comparative study between silicon tetrachloride and silane precursors. O. Yasar-Inceoglu, T. Lopez, E. Farshihagro, and L. Mangolini, Nanotechnology 23, 255604 (2012).

[3] Formation of Hollow Nanocrystals Through the Nanoscale Kirkendall Effect. Y. Yin, R. M. Rioux, C. K. Erdonmez, S. Hughes, G. A. Somorjai, and A. P. Alivisatos, Science 304, 711 (2004).

11:20am **EM-MoM10 Size and Structure Dependence of Electronic Transport Properties at Nanosized Interfaces**, *Dawn Bonnell*, *J. Hou*, The University of Pennsylvania

It is an accepted truism that the behavior of surfaces and interfaces is dictated by the interactions of atoms. Consequently, understanding atomic interactions at surfaces and interfaces is the foundational basis for predicting, controlling, and designing devices and processes. This is particularly relevant to devices for memory storage, sensing, and photonics in which electrical contacts must be made at very small scales. We use an ideal system to examine the size and structure dependence of interfaces.

We report that the size dependence of electronic properties at nanosized metal-semiconducting oxide (Au nanoparticle/ SrTiO_3) interfaces is significantly affected by the interface atomic structure. The properties of interfaces with two orientations are compared over size range of 20–200 nm. Three different mechanisms of size dependence occur at various size regimes. The difference in interface atomic structure leads to electronic structure differences that alter electron transfer paths. Specifically, interfaces with a higher concentration of undercoordinated Ti result in enhanced tunneling due to the presence of defect states or locally reduced tunnel barrier widths.

In the case of materials which exhibit resistive switching the observed “eight-wise” bipolar resistive hysteresis loop is modulated by trap/detrapping process. The size-dependent high resistance state is consistent with changes in both the interfacial area and Schottky properties. The low resistance state exhibits size independent resistance through the dominant fast conductive path. Detrapping requires more work for smaller interfaces due to the associated larger built-in electric field.

Monday Morning, November 7, 2016

11:40am **EM-MoM11 Metal Nanoparticles formed in Organic Molecular Crystals: HR-TEM and HR-PES Characterisation**, *Olga Molodtsova*, DESY, Hamburg, Germany; *I.M. Aristova*, ISSP RAS, Chernogolovka, Russia; *S.V. Babenkov*, DESY, Hamburg, Germany; *V.Y. Aristov*, ISSP RAS, Chernogolovka, Russia

The evolution of the morphology and the electronic properties of the hybrid organic-inorganic systems composed of metallic nanoparticles distributed in semiconductor organic matrix (FxCuPc, x=0,4,16), as a function of nominal metal content was studied by high-resolution transmission electron microscopy and by surface- and bulk sensitive high-resolution photoelectron spectroscopy performed at different Synchrotron Radiation facilities. Using HR-TEM the images of metal nanoparticles with direct resolving of atomic planes were obtained (see Figure). In particular, by this method for some coatings the coalescence processes of nanoparticles depending on the initial mutual orientation of the nanoparticles was observed. This work supported by the RFBR Grant No. 13-02-00818 and the BMBF-Project No. 05K12GU2, PSP-Element No. U4606BMB1211

Magnetic Interfaces and Nanostructures

Room 101C - Session MI+2D+AC-MoM

Chiral Magnetism (8:20-10:20 am)/Magnetism and Spin Orbit Effects at Interfaces and Surfaces: Recent Experimental and Theoretical Advances (10:40 am - 12:00 pm)

Moderators: Markus Donath, Westfälische Wilhelms-Universität Münster, Germany, Hendrik Ohldag, SLAC National Accelerator Laboratory

8:20am **MI+2D+AC-MoM1 Manipulation of Magnetic Skyrmions with STM**, *Kirsten von Bergmann*, University of Hamburg, Germany **INVITED** Magnetic skyrmions are topologically distinct from their ferromagnetic environment. They may form in an inversion asymmetric environment and are induced by a competition between magnetic exchange, Dzyaloshinsky-Moriya interaction, and typically the Zeeman energy. Scanning tunneling microscopy (STM) is a valuable tool to study the properties of nanometer-scale skyrmions [1]. In addition to measurements with spin-polarized STM tips skyrmions can also be detected with unpolarized electrodes due to spin-mixing effects in the non-collinear spin texture. We employ spatially resolved magnetic field dependent tunneling spectroscopy to identify this effect of non-collinear magnetoresistance and find that it scales with the angle between nearest neighbors [2]. With a non-magnetic STM tip it is also possible to locally switch the topology of a thin magnetic layer via the sign of the electric field between tip and sample [3]. The combination of these two phenomena –electrical detection and electric field switching of topologically distinct states– could lead to a robust non-magnetic read- and write-head for future skyrmion racetracktype devices.

[1] K. von Bergmann et al., *J. Phys.: Cond. Mat.* **26**, 394002 (2014).

[2] C. Hanneken et al., *Nature Nanotechn.* **10**, 1039 (2015).

[3] P.-J. Hsu et al., arXiv:1601.02935.

9:00am **MI+2D+AC-MoM3 Skyrmion Hall Effect**, *W. Jiang*, Argonne National Laboratory; *X. Zhang*, The University of Hong Kong, Hong Kong Special Administrative Region of China; *G. Yu*, University of California Los Angeles; *M.B. Jungfleisch*, *J.E. Pearson*, *O. Heinonen*, Argonne National Laboratory; *K.L. Wang*, University of California Los Angeles; *Y. Zhou*, The University of Hong Kong, Hong Kong Special Administrative Region of China; *S.G.E. te Velthuis*, *Axel Hoffmann*, Argonne National Laboratory

Magnetic skyrmions are a perfect example for the ensuing complexity of mesoscale magnetism stemming from competitions between interactions crossing many length scales [1]. The interplay between applied magnetic fields, magnetic anisotropies, as well as symmetric and antisymmetric exchange interactions, can stabilize topologically distinct spin textures known as magnetic skyrmions. Due to their topology magnetic skyrmions can be stable with quasi-particle like behavior, and can be manipulated with very low electric currents. This makes them interesting for extreme low-power information technologies [2,3], where data is envisioned to be encoded in topological charges, instead of electronic charges as in conventional semiconducting devices. Recently, we demonstrated the ability of generating and stabilizing magnetic skyrmions at room temperature in Ta/CoFeB/TaOx trilayers, where the broken inversion symmetry gives rise to a net chiral exchange interaction [4,5]. Using spin Hall effects [6] from the Ta layer it is possible to efficiently move these

skyrmions with electric currents. Theoretically it is expected that the motion of the skyrmions have a significant transverse component, the skyrmion Hall effect, which is directly related to the topological charge resulting in a net gyrotropic force. Here we demonstrate the direct observation of this transverse motion [7] using magneto-optic Kerr effect imaging. We observe that the skyrmion Hall angle varies continuously from zero just above the depinning threshold until 15° for current densities up to 107 A/cm². This gradual variation of the skyrmion Hall angle indicates the changing competition between pinning and gyrotropic forces as the skyrmion motion transitions from the creep to the flow regime. The maximum observed Hall angle is in good agreement with theoretical expectations.

This work was supported by the U.S. Department of Energy, Office of Science, Materials Sciences and Engineering Division. Lithographic patterning was carried out at the Center for Nanoscale Materials, which is supported by DOE, Office of Science, BES (#DE-AC02-06CH11357).

References

1. A. Hoffmann and H. Schultheiß, *Curr. Opin. Solid State Mater. Sci.* **19**, 253 (2015)

2. A. Hoffmann and S. D. Bader, *Phys. Rev. Appl.* **4**, 047001 (2015).

3. W. Jiang, et al., *AIP Adv.* **6**, 055602 (2016).

4. W. Jiang, et al., *Science* **349**, 283 (2015).

5. O. Heinonen, et al., *Phys. Rev. B* **93**, 094407 (2016).

6. A. Hoffmann, *IEEE Trans. Magn.* **49**, 5172 (2013).

7. W. Jiang, et al., arXiv:1603.07393.

9:20am **MI+2D+AC-MoM4 Microscopic Magnetic Structures in Dy/Y Superlattices Measured by Polarized Neutron Reflectometry with Off-specular Scattering**, *Gary Mankey*, *J. Yu*, *P. LeClair*, University of Alabama; *R. Fishman*, *J.L. Robertson*, *H. Ambaye*, *V. Lauter*, *H. Lauter*, Oak Ridge National Laboratory

Epitaxial Dy/Y superlattices with vertically-oriented c-axes, nanometer-scale layer thicknesses and 8-80 repeats were fabricated by magnetron sputtering on a-sapphire substrates with Nb buffer layers. The samples are designed to study how helical magnetic structures in Dy are modified by coupling through non-magnetic Y layers. X-ray characterization was used to evaluate the crystallographic orientations and interface widths of the superlattices. The macroscopic magnetic properties were characterized by low-temperature magnetometry that shows cooling in a 1 T in-plane field results in significant ferromagnetically-aligned moments below magnetic transition temperatures of approximately 150 K. The microscopic magnetic structures were investigated by polarized neutron reflectometry with off-specular scattering (PNROS) with variable magnetic fields in a temperature range from 300K down to 5K. PNROS confirms the magnetic transition and shows how the microscopic magnetic structures of the multilayered samples change with temperature. The ordering of the helical modulation is sensitive to the interfacial roughness of the multilayers as well as the magnetic and temperature history of the samples. The turn angles of the helical magnetic moment can be extracted from fitting the data. When the samples are cooled from room temperature to 5 K in a 10 mT in-plane applied magnetic field, the helical magnetic structures appear to decompose into lateral domains of opposite chirality, as evidenced by strong off-specular Bragg sheets. The Bragg sheets originate from the magnetic peaks associated with the helical magnetic ordering. The strength of the scattering from these sheets varies from sample to sample, suggesting that some samples may have a preferred chirality, due to differences in the microscopic film structure.

The authors gratefully acknowledge financial support from DOE award DE-FG02-08ER46499. A portion of this research used resources at the Spallation Neutron Source, a DOE Office of Science User Facility operated by the Oak Ridge National Laboratory.

9:40am **MI+2D+AC-MoM5 Chirality Effects in Rare Earth based Thin Films and Multilayers**, *Dieter Lott*, Helmholtz Zentrum Geesthacht, Germany; *K. Chen*, Universität Köln, Germany; *V. Tarnavich*, Petersburg Nuclear Physics Institute, Russian Federation **INVITED**

Films consisting of rare-earth elements became recently in the focus of attention due there rich variety of magnetic effects owed to the complex interplay between their spin and orbital magnetic moments. On the search of novel types of magnetic sensors and other spintronic devices they offer a path for creating complex magnetic spin structures that have the potential for being used in future applications in the field of information technology. In this presentation the focus is on the phenomena of

Monday Morning, November 7, 2016

magnetic chirality that was lately found in Rare-Earth multilayers. In the first part the chirality effects will be discussed for Dy/Y and Ho/Y multilayer where the symmetry of left- and right handed helical spirals formed by the RKKY interaction can be broken by the application of a magnetic field leading to a chiral state [1-3]. Here, different theoretical models are applied to explain the observed phenomena and will be discussed here. In the second part it will be shown how chirality in a thin film system consisting of alloys of rare-earth elements and 3d transition metals may be utilized for creating an exchange bias effect that differs fundamental from the one formed by conventional antiferromagnetic/ferromagnetic film systems. Furthermore, an outlook on the highly promising rare-earth elements / 3d transition metals alloys will be given [4]. For the exploration of the chirality effects in the here given examples, the application of polarized neutrons were essential enabling one to identify the magnetic states of the samples and the investigation of the intriguing phenomena of chirality.

[1] S.V.Grigoirev, Yu.O. Chetverikov, D.Lott, A. Schreyer, Phys. Rev. Lett. 100, 197203. (2008)

[2] S.V.Grigoirev, D. Lott, 2 Yu. O. Chetverikov, 1 A. T. D. Grünwald, R. C. C. Ward, and A. Schreyer, Phys. Rev. B 82, 195432 (2010)

[3] V. V. Tarnavich, D. Lott, S. Mattauch, A. Oleshevych, V. Kapaklis, and S. V. Grigoirev, Phys. Rev. B 89, 054406 (2014)

[4] K. Chen, D. Lott, F. Radu, F. Choueikani, E. Otero, P. Ohresser, Scientific Reports 5, 18377 (2015)

10:40am MI+2D+AC-MoM8 Is the High T_c Superconductivity in Cuprates an Interface Problem?, *Qi-Kun Xue*, Tsinghua University, China **INVITED**

We investigate the pairing mechanism of high T_c superconductivity in cuprates by using state-of-the-art molecular beam epitaxy (MBE)-scanning tunneling microscopy (STM) in ultra-high vacuum conditions. By two different approaches in sample preparation, namely Ar⁺ ion bombardment and ozone-assisted MBE growth, we are able to study the gap structure of superconducting copper oxide planes in unprecedented way. We show that the Cooper pairing in cuprates is rather conventional and the unique interfacial structure plays a crucial role in the high temperature superconductivity.

11:20am MI+2D+AC-MoM10 How to do Depth-Dependent Measurements on Magnetic or Magnetoelectric Thin Films, *Mikel Holcomb, R. Trappen, J. Zhou, C-Y. Huang, G. Cabrera*, West Virginia University; *S. Dong*, Southeast University; *Y-H. Chu*, National Chiao Tung University, Taiwan

Analysis of depth-dependent measurements can provide useful information on how material properties change near surfaces or interfaces with other materials. For example, this deviation commonly occurs in magnetic thin films and the variation of these properties can strongly influence how different materials couple with one another. We have recently utilized a combined approach of bulk and surface sensitive x-ray absorption techniques to nondestructively map out depth-dependent atomic valence and magnetization across magnetic La_{0.7}Sr_{0.3}MnO₃ and magnetoelectric La_{0.7}Sr_{0.3}MnO₃/PbZr_{0.2}Ti_{0.8}O₃ thin films. We have combined measurements on multiple sample thicknesses with theoretical approaches to map out the layer-by-layer atomic valences and how they vary with film thickness. Such efforts may play a critical role in understanding how to build future generations of devices that rely on enhanced surface and interface properties.

11:40am MI+2D+AC-MoM11 Nano-Pico-Mikro - Dynamic Soft X-ray Microscopy of Magnetic Materials with High Sensitivity, *Hendrik Ohldag*, SLAC National Accelerator Laboratory

Understanding magnetic properties at ultrafast timescales is crucial for the development of new magnetic devices. Such devices will employ the spin torque or spin Hall effect, whose manifestation at the nanoscale is not yet sufficiently understood. The samples of interest are often thin film magnetic multilayers with thicknesses in the range of a atomic layers. This fact alone presents a sensitivity challenge in STXM microscopy, which is more suited toward studying thicker samples. In addition the relevant time scale is of the order of 10 ps, which is well below the typical x-ray pulse length of 50 – 100 ps. The SSRL STXM is equipped with a single photon counting electronics that effectively allows using a double lock-in detection at 476MHz (the x-ray pulse frequency) and 1.28MHz (the synchrotron revelation frequency). The pulsed or continuous sample excitation source is synchronized with the synchrotron source with a few picosecond drift over 24 hours.

In the first year of operation the excellent spatial resolution, temporal stability and sensitivity of the detection electronics of this microscope has
Monday Morning, November 7, 2016

enabled researchers to acquire time resolved images of standing as well as traveling spin waves in a spin torque oscillator in real space as well as detect the real time spin accumulation in a non-metal in contact with a ferromagnet.

Manufacturing Science and Technology

Room 103A - Session MS-MoM

Manufacturing for Next-Generation Energy Solutions

Moderator: Erik B. Svedberg, The National Academies

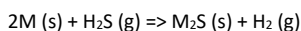
9:00am MS-MoM3 Manufacturing Challenges in Batteries: Lessons from Current Technology for Future Energy Storage Developments, *Yet-Ming Chiang*, MIT **INVITED**

The evolution of today's highly successful lithium ion battery manufacturing technology over 25 years provides many useful lessons, pro and con, for future storage technologies. Along with the development of higher performance/lower cost cathodes, anodes, electrolytes or other cell components, efficient cell designs and low cost/highly scalable manufacturing techniques are needed for any new technology to succeed. This talk will discuss prevailing Li-ion cell design and manufacturing methods which, despite evident success, have inherent inefficiencies which in the author's view have prevented the full exploitation of Li-ion chemistry. A "clean sheet" redesign developed at MIT and 24M Technologies will be discussed, based on a new semi-solid electrode form that enables manufacturing of high performance Li-ion cells by radically simpler and lower-cost methods. Concepts from this case study that may be transferable to new storage technologies include the need to minimize of non-energy-storing materials content in any device design; the benefits of reducing the tortuosity of ion transport pathways; how multiple functions can be served by a single component, and the importance of developing manufacturing processes that are cost-effective at small production scale, yet can be readily scaled to GWh volumes.

Support for this work by the U.S. Department of Energy through the ARPA-E program, the Vehicle Technologies Office of EERE, and the Advanced Battery Materials Research (BMR) program is gratefully acknowledged.

9:40am MS-MoM5 Efficient Manufacturing of Nano-structured Lithium Sulfide for Next Generation Batteries, *X. Li, Y. Yang, Colin Wolden*, Colorado School of Mines

Lithium ion batteries (LIBs) currently dominate the market and are expected to for another decade due to incremental improvements. However, with performance approaching intrinsic material limits, LIBs cannot meet the increasing demands of electric vehicles and stationary storage. In the next decade both solid state and lithium-sulfur (Li-S) batteries will begin displacing LIBs. Central to both technologies is Li₂S, which serves as the active cathode material in Li-S batteries and is the key precursor and cost driver for leading solid-state electrolytes. In both applications Li₂S has demonstrated excellent performance when used in nanoparticle (NP) form. However, Li₂S is very costly and commercially available only as micropowders with impurities being a major concern, reflecting the energy-intensive carbothermal reduction processes currently used for synthesis. In this paper we describe a green chemistry-inspired approach for synthesizing alkali sulfide (M₂S, M = Li and Na) NPs through the reaction of hydrogen sulfide (H₂S) gas with alkali metal-organic (M-R) complexes dissolved in solution. This thermodynamically favorable reaction occurs spontaneously and proceeds rapidly to completion with near 100% atom efficiency at ambient temperature, forming phase-pure, anhydrous M₂S nanopowders that are readily separated from solution. H₂S, a major industrial waste, is completely abated and the valuable hydrogen stored therein may be fully recovered as H₂. The overall stoichiometry of the two step process is:



As such, this innovative synthetic approach is expected to be scalable, energy-efficient, and cost-effective. In this presentation we describe the process chemistry, focusing on the role of the complexing agent (R) and solvent to control the yield, size, and morphology of the resulting M₂S NPs.

Monday Morning, November 7, 2016

10:00am **MS-MoM6 Anode Protection for Advanced Energy Storage Systems via Atomic Layer Deposition**, *Chuan-Fu Lin, M. Noked*, Institute for System Research, University of Maryland; *A.C. Kozen*, Naval Research Laboratory; *A.J. Pearse*, University of Maryland, College Park; *K. Gregorczyk*, Institute for System Research, University of Maryland; *S.B. Lee*, University of Maryland College Park; *G. Rubloff*, Institute for System Research, University of Maryland

To meet the demand for higher capacity longer life batteries in a “next-generation batteries” technology, anodes with substantially higher energy density than current graphite are needed. One class - metal anodes (particularly Li) - offers far higher energy density, but to date their utilization has been impeded by their high surface reactivity (especially to the organic electrolyte) and tendency to form dendritic Li (a shorting and safety hazard). Another category - conversion materials, also high energy density - involves complex material reactions as part of lithiation/delithiation, degrading the material during cycling.

We have used atomic layer deposition (ALD) to create highly controlled, thin protective layers on Li metal anodes and on RuO₂ conversion anodes, testing their efficacy by cycling in batteries. ALD protection layers, including Al₂O₃ and the solid electrolyte LiPON (lithium phosphorus oxynitride), were directly deposited on the anodes in controlled inert ambient conditions. For Li metal anode protection, both Al₂O₃ and LiPON markedly suppress corrosion and degradation, as evaluated in Li-S cells by charge/discharge cycling and a variety of other characterization methods, with considerably higher capacity for the LiPON. The ALD films also stabilize the Li metal surface, preventing Li dendrite formation upon repeated cycling above the threshold current density for dendrite formation. For the conversion anode, the ALD coatings suppress electrolyte decomposition, thereby enhancing capacity retention during cycling, and lowering overpotentials required for delithiation, effects attributed to the layers mechanically constraining the RuO₂ the lithiation products Li₂O and Ru, preserving structural integrity.

These results demonstrate promise for achieving high energy density anodes with significantly enhanced chemical stability, electrochemical cyclability, and dendrite protection as needed for a viable beyond Li ion battery technology.

10:40am **MS-MoM8 Controlling Nanomaterial Assembly to Improve Material Performance in Energy Storage Electrodes using Electrophoretic Deposition**, *Landon Oakes, R.E. Carter, A.P. Cohn, C.L. Pint*, Vanderbilt University

Electrophoretic deposition (EPD) provides a promising tool for large-scale manufacture of nanomaterial systems using conventional liquid processing techniques. One major roadblock to commercially viable applications of nanomaterials, such as in energy storage devices, is the ability to cost-effectively manufacture electrode-scale films while still maintaining precise control over the nanoscale and microscale morphology. We emphasize the ability of EPD to control nanoscale assembly for high throughput battery manufacturing through the design of a benchtop roll-to-roll platform. Using this approach, we fabricate electrodes for a range of battery technologies, such as lithium-ion batteries, lithium-sulfur batteries, and lithium-oxygen batteries. This makes possible the development of binder-free, electrode assemblies with uniformity and control that enables improved performance across all of these battery platforms. Specifically, for lithium-sulfur batteries, we fabricate binder-free electrodes that achieve over 75% sulfur loading with a capacity greater than 1,200 mAh/g that retains more than 80% of the initial capacity after 100 cycles. For lithium-oxygen batteries, we demonstrate electrodes with improved overpotential of 50 mV during oxygen reduction and 130 mV during oxygen evolution in addition to a nearly 2X improvement in durability compared with conventional assembly methods. Overall, as battery manufacturing remains a critical barrier separating state-of-the-art research efforts from practical commercial energy storage innovations, we emphasize EPD as a versatile process able to provide the scalability, high throughput, and nanoscale control that are necessary to advance battery systems manufacturing.

11:00am **MS-MoM9 3D Architectures for Thin Film Batteries – from Science to Manufacturing**, *Gary Rubloff, C. Liu, E. Hitz, S.B. Lee*, University of Maryland College Park; *K. Gregorczyk*, University of Maryland, College Park

Recent research has elucidated several guidelines for energy storage approaches to achieve higher power at high energy density along with good capacity retention during cycling. These guidelines address electrode surface areas and active storage layer thicknesses, integration of current collecting features with active layers, and overall structure of 3D electrode

features at the micro or nano scale. Here we consider solid state thin film battery architectures fabricated by thin film processes, where the solid electrolyte enables complex interdigitated electrode arrangements. We report projected performance in power and energy density for several configurations as a function of design parameters, including scaling of nanopore batteries already achieved experimentally. Finally, we consider manufacturability aspects in terms of (1) process sequence complexity and (2) comparison to that of other existing technologies based on thin film processing.

11:20am **MS-MoM10 Advanced Manufacturing R&D for Clean Energy in the US Department of Energy**, *Mark Johnson*, Advanced Manufacturing Office, U.S. Department of Energy

INVITED

Manufacturing is a critical component of the U.S. economy, responsible for 12.5% [1] of GDP, direct employment for over 12 million people [1], and close to 75% [2] of U.S. exports of goods. The U.S. manufacturing sector, while it produces 17% [3] of the world's manufacturing output, also represents a quarter of the country's energy consumption [4]. On the R&D side, it is responsible for 70% of all business R&D performed (in 2010 and 2011) and nearly 60% of patent applications [5]. As such, DOE has a vested interest in broadly applicable energy efficiency technologies for use in energy intensive manufacturing, as well as platform materials and processes for use in the manufacturing of clean energy technologies.

This talk will review the Advanced Manufacturing Offices work towards making the U.S. manufacturing sector more energy productive—and the U.S. clean energy manufacturing sector more competitive—through targeted R&D and partnerships with industry, academia, technology incubators and other stakeholders.

Nanometer-scale Science and Technology

Room 101D - Session NS-MoM

Nanopatterning and Nanofabrication + 3D

Moderators: Keith Brown, Boston University, Indira Seshadri, IBM Research Division, Albany, NY

8:20am **NS-MoM1 Fabrication and Characterization of Carbon Nanotube-Based Electronic Devices**, *Zhigang Xiao, S. Budak, A. Kassu, X. Crutcher, T. Strong, J. Johnson, R. Hammond, J. Gray, A. Reynolds, R. Moten*, Alabama A&M University

Single-walled carbon nanotubes (SWCNTs) are used widely in fabricating nanoelectronic devices because of their unique electrical properties. We report the fabrication of carbon nanotube field-effect transistors (CNTFETs)-based inverter and ring oscillator electronic circuits using the dielectrophoresis (DEP)-aligned single-walled carbon nanotube mesh networks. The electrical property of the fabricated CNTFET-based devices was measured. The CNTFET-based inverter shown excellent electrical transfer characteristics, while the CNTFET-based ring oscillator demonstrated oscillation characteristics, denoting that the CNTFET-based circuits can function well for the application of electronic circuits. The DEP-based fabrication of carbon nanotube electronic circuits is wafer-scale, and compatible with the integrated circuit (IC) fabrication.

8:40am **NS-MoM2 Multi-Material Two Photon and Direct Write Lithography for Photonics, Phononics and Mechanics**, *Steven Kooi*, Massachusetts Institute of Technology

A combination of two-photon (2PL), holographic and direct write lithography, in positive and negative tone photoresists as well as photopatternable hydrogel materials, is used to produce nano and microscale structures for photonic, phononic and mechanical applications. The lithographic processes are described as well as the conversion of the 3D structures into higher index of refraction materials (Si, Ge and metals) for photonic applications and engineered modulus materials for phononic and mechanical applications by atomic layer deposition, chemical vapor deposition, chemical etching and ion etching techniques. Standard piezo stage scanning two-photon lithography is used to produce 3D structures as well as an upgraded design that incorporates galvo-scanning mirrors that greatly increase the writing speed and area.

The conversion of polymeric structures to higher index materials allows us to access more interesting and measurable optical properties in the visible wavelength range. Optical measurements include reflectivity to characterize optical bandgaps and to evaluate structural uniformity and quality. In addition, near field scanning optical microscopy (NSOM) techniques are used to follow light propagation through engineered

Monday Morning, November 7, 2016

photonic structures. These results are compared to theoretical predictions of optical properties and are used to evaluate not only the defect density in the printed structures, but also the quality of the multi-step conversion process. The 3D structures are also characterized by serial focused ion beam (FIB) milling and imaging.

Phononic and mechanical 3D structures are also produced by the same lithographic techniques. These materials are tested by light scattering techniques to evaluate phononic properties as well as static and dynamic mechanical measurements to investigate size and structure dependent mechanical properties. 2PL is also used to produce periodic structures that are used in laser-induced shock wave imaging experiments. These experiments are designed to study the influence of the periodic structures on the propagation and/or mitigation of shock waves.

9:00am NS-MoM3 Applications of 2-photon 3D Stereolithography to Aerial Microrobots and Air-Microfluidics, Igor Paprotny, University of Illinois at Chicago

INVITED

Additive manufacturing, commonly called 3D printing, is currently revolutionizing manufacturing worldwide. Two-photon polymerization has in the last decade been used as a novel 3D stereolithography method that enables the fabrication of microscale structures with a resolution on the order of 100s nanometers. The ability to 3D print microscale structures enables development of novel microelectromechanical systems (MEMS) that transcend traditional top-down micromachining processes. This talk will review the theory of 2-photon polymerization and the applications of this method to microstereolithography. I will also review two novel applications of this technique to MEMS devices fabricated in the Micromechatronic Systems Laboratory at the University of Illinois at Chicago. One application is the investigation of microscale flight, where two-photon stereolithography is used to develop test structures and devices that hover upon application of a localized thermal gradient. New results, enabled by our ability to 3D print 'microflier' designs with varying geometry, show similarity to flight performance observed in microscale flying insects. This talk will also describe the application of two-photon microstereolithography to air-microfluidics, where the creation of microfluidic channels with complex geometries have tremendous applications to the development of lab-on-a-chip sensors for air quality and gas measurements. Several examples of such air-microfluidics circuits are presented and discussed.

9:40am NS-MoM5 Elucidating Proximity Effects during Direct-Write Synthesis of Complex 3D Nanostructures, Brett Lewis, University of Tennessee; J.D. Fowlkes, Oak Ridge National Lab; R. Winkler, Graz Centre for Electron Microscopy, Austria; H. Plank, Graz University of Technology, Austria; P.D. Rack, University of Tennessee

Cutting edge 3-dimensional nanofabrication techniques are essential for the future technological advancement in many fields and applications ranging from metamaterials to memory devices. One technique to realize truly flexible 3D nanoprinting is focused electron beam induced deposition (EBID), which uses a focused scanning electron beam to decompose precursor molecules adsorbed onto a substrate surface. The electron/precursor/solid intersection generates a deposit composed of the desired material and shape dictated by the prescribed scanning parameters. EBID has the advantage of being compatible with a wide range of materials, substrates and complex geometries at the nanoscale.

In this work, we will overview the relevant electron/precursor/solid interactions and present a systematic study of the geometric dependence of unwanted proximity effects that occur during the deposition process. Notably, we present a solution designed to minimize proximal deposition by appropriately adjusting the scanning parameters and beam conditions dependent on the desired final geometry. Specifically, we have developed a computer aided design (CAD) program that automatically calibrates the scanning pattern by calculating the predicted contribution from nearest neighbor elements. Our program has been demonstrated for use with platinum and gold structures grown from the organometallic precursors *MeCpPt(IV)Me₃* and *Me₂Au(acac)* and the principles can easily be adapted to other material systems. Furthermore, we will demonstrate a laser-assisted process which significantly reduces contamination in the nanoscale deposits.

10:00am NS-MoM6 Surface Textures with Asymmetric Wetting and Optical Properties Enabled by Two-Photon Direct Laser Writing, Nick Laurik, Oak Ridge National Laboratory; C. McKown, UT/ORNL Breddesen Center

Over the last decade, advances in direct laser writing (DLW) using two-photon polymerization have led to development and proliferation of user friendly commercially available tools that extend the concept of additive manufacturing into the nanoscale and enable a researcher with facile and flexible means of fabricating arbitrary complex 3D elements with submicron fidelity. Using one of such recently emerged tools, namely a Photonic Professional GT system (Nanoscribe GmbH), we have explored various asymmetric motifs with the purpose of creating surface textures with unique wetting and optical properties. Starting with simple bio-inspired elements, such as arrays of deformed pillars and fish scale elements, we design and create surface textures that exhibit asymmetric contact angle hysteresis as well as strongly anisotropic reflectivity.

The unique flexibility in creating intricate 3D elements offered by two-photon DLW allows us to elucidate relationships between the subtle variations in the surface topology and changes in the targeted functionalities. Examples of model systems based on asymmetric textures with characteristics promising for a number of applications will be discussed. This talk will also discuss how two-photon DLW can be integrated with and augmented by more conventional wafer scale processing and thin film technologies. Of our particular attention are fabrication sequences that combine two-photon DLW with ALD and thermal post-processing with the goal of creating asymmetric textures represented by more diverse classes of materials beyond crosslinked photopolymers.

10:40am NS-MoM8 New 3D Structuring Process, by Ion Implantation and Selective Wet Etching, Lamia Nouri, N.P. Posseme, S.L. LANDIS, F.G. GAILLARD, F.M. MILESI, CEA, LETI, MINATEC Campus, France

Silicon patterning is a one of the most important steps in nano/micro fabrication, especially for micro/nano electro-mechanical systems (MEMS/NEMS), optoelectronic devices etc ... The fabrication schemes that microelectronics had boosted for decades for the production of integrated circuits, (based essentially on layering and planar patterning stacks of semiconductors, metals, and dielectrics) do not meet the new structuration's requirements. Indeed, for the new emerging fields which may involve complex 3D patterns, the structuration becomes more challenging and requires several complex and expensive patterning processes such as gray-scale electron beam lithography, laser ablation, focused ion beam lithography, two photon polymerization and dry etching techniques.

In this work, we propose a straightforward technique for realizing 3D structuration intended for silicon based materials (Si, SiN, SiOCH ...). This structuration technique is based on ion implantation and selective wet etching.

In a first step a pattern is performed by lithography on a substrate, then ion implantation is performed through the resist mask in order to create localized modifications in the material, thus the pattern is transferred into the subjacent layer. Finally, after the resist stripping, a selective wet etching is carried out to remove selectively the modified material regarding the non-modified one. The type of implanted ions and wet etching baths depend on the morphology of the substrate.

In this study we have demonstrated the feasibility of this new 3D structuration process on Silicon and SiOCH. The mechanisms understanding involved during both implantation and wet etching processes will be presented through characterizations by photoluminescence spectroscopy, Raman spectroscopy and Secondary Ion Mass Spectrometry (SIMS) for silicon samples, and ellipso-porosity, Fourier Transform InfraRed spectroscopy (FTIR) for SiOCH samples.

11:00am NS-MoM9 Design and Realization of 3D Printed AFM Probes, N. Alsharif, A. Burkatovsky, C. Lissandrello, A.E. White, Keith Brown, Boston University

Atomic force microscopy (AFM) is an enabling tool for nanoscience due to its ability to image surfaces with sub-nanometer resolution. One drawback, however, is that the AFM probe must be chosen to complement the material properties of the system of interest – e.g. stiff probes are ideal for imaging hard surfaces while soft probes are needed for softer biological materials. Furthermore, the conventional lithography techniques that are used to fabricate AFM probes can only generate limited architectures from a narrow subset of materials. In analogy to the impact rapid prototyping

has made on macroscopic manufacturing, nanoscale 3D printing can in principle be used to construct AFM probes in a manner that allows important properties such as spring constant and vibrational resonance frequency to be rationally chosen. Moreover, since it is possible to fully control the 3D structure of a probe, additional properties such as higher harmonic resonance frequencies and deflection sensitivity can be independently adjusted. Here, we demonstrate that functioning AFM cantilevers that are compatible with commercial AFM systems can be 3D printed and used for imaging. In particular, a series of bisegmented probes with consistent spring constants but different resonance frequencies were designed, printed, and evaluated using an AFM. Their properties were found to be consistent with finite element mechanical simulations and comparable to commercially available probes. In addition, we found that the second harmonic mode could be tuned to an integer multiple of the principle harmonic, in a manner that could provide multimode imaging with resonance enhancement. This work opens the door for complex non-rectilinear cantilevers that provide uniquely tuned force-distance relationships or harmonic behavior.

11:20am NS-MoM10 Evaluating the Reproducibility of Atomically Precise Dopant Structures, J. Koepke, D. Scrymgeour, R.J. Simonson, M. Marshall, Sandia National Laboratories; J. Owen, Zyvex Labs; D. Ward, R. Muller, M. Carroll, S. Misra, **Ezra Bussmann**, Sandia National Laboratories

Moore's law extrapolates to microelectronic devices with atomic size features around 2020 [1]. Anticipating engineering of nanoelectronics at this scale, techniques to tune dopant profiles in silicon have evolved to the ultimate limit of single-atom control. A single atom transistor [2], a device with just one P dopant atom placed in the channel with atomic selectivity, was recently fabricated via hydrogen resist scanning tunneling microscopy (STM) lithography. Despite the promise of atomically precise dopant placement, there are significant challenges to fabrication based on STM lithography such as scale-up, robustness, yield, and reproducibility.

This talk describes techniques to evaluate and optimize the yield and reproducibility of patterning and incorporation for single dopant placement. The hydrogen resist STM lithography method uses electrons from the STM tip to selectively desorb hydrogen atoms from the Si(100) – 2x1:H surface. Dosing the sample with PH₃ and annealing selectively incorporates P dopants into the regions patterned with the STM tip. The key challenges for fabricating the dopant arrays are alignment of the STM tip to the dimer rows of the Si(100) surface, choice of lithographic window size and patterning conditions, and identification of the incorporated dopant after dosing and annealing the sample. Scaling the arrays to larger sizes requires reproducible STM tips that pattern consistently and very low alignment error. Using the precise alignment of the STM tip to the dimer rows of Si(100) surface, we have improved lithography yield for patterning windows for single dopant incorporation from 10% to 40%. We have developed image analysis capability to rapidly identify the dopant atoms in order to verify the results of the array fabrication and provide feedback to the lithography and dosing conditions for process optimization. Comparing results of dopant incorporation with modeling enables fine tuning of the PH₃ dosing and incorporation conditions to improve the single dopant yield.

This work was performed, in part, at the Center for Integrated Nanotechnologies, an Office of Science User Facility operated for the U.S. Department of Energy (DOE) Office of Science. Sandia National Laboratories is a multi-program laboratory managed and operated by Sandia Corporation, a wholly owned subsidiary of Lockheed Martin Corporation, for the U.S. Department of Energy's National Nuclear Security Administration under contract DE-AC04-94AL85000. Data collected using a ZyVector™ STM Lithography Control System from Zyvex Labs.

[1] International Technology Roadmap for Semiconductors, <http://www.itrs2.net/>.

[2] Fueschle, et al., *Nat. Nano.* **7**(4), 242 (2012).

Plasma Science and Technology Room 104D - Session PS+SE-MoM

Atmospheric Pressure Plasma Processing

Moderator: Lorenzo Mangolini, University of California Riverside

9:00am PS+SE-MoM3 Fundamental Characterization of a Low Frequency, Ambient Air, Plasma Jet Discharge, **Vladimir Milosavljevic**, Dublin Institute of Technology, Ireland; L. Scally, J. Lalor, P.J. Cullen, Dublin Institute of Technology

Plasma discharge in open air has charged species, energetic photons, active radicals, and also a low degree of ionization gas. Interaction of such plasma with surfaces has been a subject of intense study for many decades. In particular, an atmospheric jet plasma system used to solve surface preparation problems. The biggest advantages of such a system are: high density plasma in contrast to corona discharge, no electrical current or filamentary streamers in the plasma jet, broad material application capability, simple host automation integration, low environmental impact, and low thermal load allows low melting point polymers to be treated. Despite the widespread usage of plasma jet technology, it remains largely unknown whether atmospheric plasma maintains similar characteristics, such as gas temperatures and particle flux, when they breakdown while arcing or whether they possess different operating modes. In this work optical spectroscopy was used as a diagnostic method due to its non-intrusive nature. In addition to this, surface metrology based on a measurement of the water contact angle (WCA) and surface energy was also engaged.

In this study a high pressure (6 bar) atmospheric plasma jet system, which operates with ambient air chemistry, was employed. The plasma jet operated at a frequency of 60 Hz and used a pencil type beam applicator. The low operation frequency makes this system significantly different from a vast majority of other plasma jets. Namely, at low frequencies (<50 kHz) ions and electrons both oscillate and therefore both contributed in interaction with surfaces. At high frequencies (>50 kHz) heavy ions cannot follow switching fields and therefore only electrons oscillate while ions are relatively stationary which has a huge impact on the plasma sheath dynamics.

The polymer used in this work was polyethylene terephthalate (PET) and was widely used in a variety of industries from food packaging to the electrical, electronics, and biomedical industries. PET could be easily thermally damaged at relatively low temperatures and so a delicate balance must be reached where surface activation of the polymer was maximised, while thermal damage was prevented. The level of polymer surface activation was evaluated based on changes to the WCA of PET samples after plasma treatment. A direct correlation was obtained between the polymer WCA changes and the OES measurement. This correlation may indicate that OES peak intensities can be used as an indicator of the treated polymer WCA, without the need for conventional off-line metrology.

This work was a funded by SFI under the PlasmaGrain project.

9:20am PS+SE-MoM4 CO₂ Splitting by Dielectric Barrier Discharge at Atmospheric Pressure: Understanding the Influence of Electrical Regimes and Electrical Configurations, **Alp Ozkan**, T. Dufour, Université Libre de Bruxelles, Belgium; A. Bogaerts, University of Antwerp, Research group PLASMANT, Belgium; F. Reniers, Université Libre de Bruxelles, Belgium

Dielectric barrier discharges (DBDs) are commonly used to generate cold plasmas at atmospheric pressure. In this experimental work, a flowing tubular DBD is used for the CO₂ splitting into O₂ and CO. The influence of the frequency (from 16 to 28 kHz), the power (from 30 to 100 W), the role of the barrier thickness (2.0, 2.4 and 2.8 mm), the kind of dielectric material (alumina, mullite, pyrex, quartz), and the effect of a pulsed AC discharge (so-called burst mode) are investigated on the filamentary behavior of the plasma and on the CO₂ conversion, by means of mass spectrometry measurements correlated with electrical diagnostics. Their influence on the gas and electrode temperature is also evidenced through optical emission spectroscopy and infrared imaging. A new methodology is developed to investigate the microdischarge properties. For this purpose, electrical measurements, based on a numerical method, are carried out to explain the conversion trends and to characterize the microdischarges through their number (N_{md}), their lifetime (L_{md}), their intensity (i_{pl}) and the induced electrical charge (Q_{pl}) for a given analysis time. These extracted data are usually underestimated or poorly described in literature.

It is shown that, when the applied power is modified, the conversion depends mostly on the Q_{pl} and not on the effective plasma voltage (V_{pl,eff}).

Similarly, a better conversion is observed at low frequencies, where a more diffuse discharge with a higher $V_{pl,eff}$ than at higher frequency is obtained. Moreover, increasing the barrier thickness decreases the capacitance while preserving the electrical charge. As a result, the voltage over the dielectric (V_{die}) increases and a larger N_{md} is generated, which enhances the CO_2 conversion. Furthermore, changing the dielectric material of the barrier, while keeping the same dimensions, also affects the conversion. The highest CO_2 conversion and energy efficiency are obtained for quartz and alumina. From the electrical characterization, we clearly demonstrate that the most important parameters are the somewhat higher $V_{pl,eff}$ (yielding a higher electric field and electron energy involved in CO_2 dissociation) for quartz, as well as the higher plasma current (thus larger electron density) and the larger N_{md} (mainly for alumina due to its higher roughness, but also for quartz due to its higher V_{die}). Finally, a comparison between DBD ignited in burst mode and pure AC mode is achieved. Decreasing the duty cycle from 100% (pure AC mode) to 40% leads to a rise in the conversion due to a larger N_{md} and a higher voltage.

9:40am **PS+SE-MoM5 Effect of Structural Variations of the Monomer on the Fast Synthesis of Highly Oxygenated Coatings in an Argon DBD**, *Jérémy Mertens, F. Reniers*, Université Libre de Bruxelles, Belgium

The use of atmospheric plasma DBD for the synthesis of organic coatings has recently become more and more popular. Their unconventional polymerization pathways allow the synthesis of brand new polymers with specific properties which are strongly dependent on the chemical structure of the injected monomer^{1,2}.

The goal of this research is the development of an intermediate coating presenting a high surface energy with an important deposition rate in order to improve the adhesion of a resin on aluminum by DBD. Because of their initial structure, anhydrides are seen as ideal candidates for the synthesis of such films. We here present how small variations in their chemical structure can affect their behavior in the discharge and the chemical properties of the coatings. Firstly, the influence of the C/O ratio in the injected monomer is investigated by the use of acetic, propionic and butyric anhydride. The addition of double bonds in the initial structure of the precursor is then studied using isobutyric and methacrylate anhydride. Surface analyses such as infrared spectroscopy (IRRAS), X-Ray Photoelectron spectroscopy (XPS) and stylus profilometry showed that highly oxygenated coatings could be synthesized when the C/O ratio of the injected monomer was decreased. Nevertheless, high deposition rates could only be reached with the addition of double bonds in the structure of the monomer. By combining these observations with oscilloscope and mass spectrometry measurements of the discharge, a fragmentation/recombination polymerization is suggested for the non-conventionally polymerizable monomers. On the contrary, a mainly radical propagation through the double bonds is proposed for the methacrylate anhydride. The amount of carboxylic components on the surface can be tuned by the addition of an Ar-O₂ post-treatment but is limited by the degradation of the films that leads to the formation of oxidized volatile compounds.

This work was financially supported by the Walloon Region (FLYCOAT project n°131847) and by the Belgian Federal Government (Interuniversity Attraction Belgian Science Policy IAP research project P7/34 – Physical Chemistry of plasma surface interactions).

¹ J. Hubert & al., *Journal of Materials Research*, **2015**, 30, 21, 3177-3176

² A. Batan & al., *Plasma Processes and Polymers*, **2013**, 10, 857-863

10:00am **PS+SE-MoM6 Quantitative Study of Plasma Electrochemical Reduction of Aqueous Metal Salts**, *S. Ghosh, A. Aube, R. O'Toole, R. Hawtof, R. Mohan Sankaran*, Case Western Reserve University

The possibility of combining ionized gases and ionic solutions to initiate electrochemical reactions in solution with a plasma electrode has been explored for over 100 years. Recently, this idea has been the basis of numerous reports of metal nanoparticle formation when aqueous solutions of metal salts are exposed to a plasma. While this approach has been successfully demonstrated by a range of plasma sources and experimental conditions, the chemistry behind the reactions between plasma and solution species is highly complex and remains poorly understood.

Here, we report quantitative studies of the reduction of aqueous metal salts by a plasma electrode to better understand the reaction kinetics and thermodynamics, analogous to conventional electrochemistry. Kinetic studies were performed by measuring the rate and efficiency of the reduction of a metal salt, silver nitrate. Analogous to weight measurements in electrodeposition of metal thin films, we developed a methodology to

measure the mass of the final product, silver (Ag) nanoparticles, by separating the agglomerated particle powder. The reduction efficiency was defined as the actual amount of reduced Ag compared to that predicted by Faraday's law based on the plasma current. We find that in ambient air, the faradaic efficiency for silver nitrate reduction is approximately 80%, and, curiously, the efficiency increases to >100% in a closed reactor cell with an Ar ambient. We interpret these results as follows. Assuming that the chemistry in solution is driven by electrons from the plasma which are directed into solution and can solvate, in ambient air, there is a decrease in the electron flux to the solution because of electron attachment processes involving O₂ gas. Removing air with ambient Ar increases the electron flux and, thus, increases the faradaic efficiency. The surprising efficiency of more than 100% most probably results from an autocatalytic effect whereby reduced Ag (Ag⁰) also reduces Ag⁺, a mechanism that has been previously reported in radiolytic synthesis of Ag nanoparticles. The thermodynamics of the reduction process was probed by studying a series of metals which have different reduction potentials including copper, iron, and zinc. Successful reduction of the corresponding metal salts for these metals suggests that solvated electrons, which are one of the strongest reducing species, are involved. We will also discuss the respective reduction rates and efficiencies of these metals as compared to Ag.

10:40am **PS+SE-MoM8 LDPE Modified by an Ar/H₂O Dielectric Barrier Discharge: Correlation between Texturization, Wettability and Grafting of Oxygen**, *Stéphanie Collette*, Université Libre de Bruxelles, Belgium; *P. Viville*, Université de Mons, Belgium; *F. Reniers*, Université Libre de Bruxelles, Belgium

In the literature, some studies focus on the use of H₂O in plasma discharges because of its potential high reactivity. However, it is also known to destabilize plasmas. In this study, the reactivity of water at the interface between the plasma and the surface of the low density polyethylene (LDPE) was investigated. LDPE is chosen as polymer because of its high capacity to be functionalized.

In the first part of this project, we study the water reactivity in atmospheric plasma by injecting H₂O vapor in the discharge of a dielectric barrier discharge, supplied with Ar as carrier gas. OES evidenced the production and the consumption of Ar, O, OH, and N₂ species. They can be quantified as a function of the H₂O flow rate and the treatment time in order to have a better understanding of the reactivity. Some chemical reactions occurring within the discharge can be highlighted. To characterize the discharge itself, current measurements are performed and a high speed camera is used to observe the changes of the discharge (number and size of the streamers).

In the second part of this research, LDPE surfaces exposed to water-containing plasma are characterized by XPS. The measurements of the O 1s peak reveal a strong increase of oxygen from 0% to 16%. XPS Depth profiles evidence the diffusion of O in the subsurface. These results have been compared with WCA measurements expressed as a function of time. Between 0 and 30 s, a strong decrease in the WCA is observed (from 100° to 63°) and can be linked to the rise of the O% (from 0% to 13%). After 30 s, the WCA rapidly decreases to 43° which seems inconsistent with the very slow increase of the O% (almost no rise) observed by XPS. In parallel, AFM measurements show a texturization of the treated LDPE, as the surface roughness increases from 27 nm to 75 nm. The effect observed after 30 s of treatment can be explained by the Wenzel equation:

$$\cos \Theta_{app} = r \cos \Theta$$

Indeed, the "r" factor in the Wenzel corresponds to the roughness ratio defined as the ratio of true area of the solid surface to the apparent area. $\cos \Theta$ can be linked to the polar component of the surface energy and therefore to the oxygen concentration at the surface. The roughness and the oxygen content increase simultaneously with time and the combination of these two factors lead to obtain a higher $\cos \Theta_{app}$. Indeed, the texturization and the grafting of oxygen are correlated by the use of the Wenzel equation thereby allow the understanding of the large decrease of WCA.

This work is supported by the Belgian Federal Government (Interuniversity Attraction Belgian Science Policy IAP research project P7/34 – Physical Chemistry of plasma surface interactions).

Monday Morning, November 7, 2016

11:00am **PS+SE-MoM9 Particle-free Fabrication of Stretchable, Electrically Conductive Features by Atmospheric-Pressure Plasma Reduction of Metal-Ion-Containing Polymer Films**, *Souvik Ghosh**, P.X.-L. Feng, C.A. Zorman, R.M. Sankaran, Case Western Reserve University

Stretchable electrically conductive patterns are an importance class of materials for emerging electronic applications. A relatively well-established approach for their fabrication is printing metal nanoparticle inks on elastomeric polymers to combine the high electrical conductivity of metals with the large mechanical deformability of polymers. However, nanoparticle-based inks have organic-based solvents and contain organic capping molecules to stabilize the nanoparticles, limiting the conductivity of as-printed features and requiring high temperature sintering (>200 °C) to remove the organics, which is not compatible with most polymers. Moreover, the printed metal nanoparticle film may not be well-integrated with the polymer, compromising conductivity at large deformation.

Here, we report a plasma-based approach to producing electrically-conductive metallic features at the surface of polymer films that eliminates the need for nanoparticle inks and has the potential to better integrate metals and polymer. In general, metal salts are initially mixed with a polymer and cast as a thin film. The films are then exposed to a plasma which results in reduction of the metal ions to metal nanoparticles. By using an atmospheric-pressure microplasma jet and rastering the metal-ion-containing polymer film, the reduction is localized and two-dimensional patterns of metal nanoparticles are fabricated.

We initially focused our study on films prepared from silver nitrate (AgNO₃) and polyacrylic acid (PAA) which is known to cross-link with metal cations. After exposure to the microplasma, films were characterized by X-ray diffraction (XRD) which confirmed crystallinity from the presence of peaks corresponding to face-centered cubic silver (Ag). Further materials analysis by scanning electron microscopy (SEM) and energy dispersive spectroscopy (EDX) revealed that microplasma reduction leads to nanoparticle formation only at the surface of the film. The bulk resistivity of the patterned features was determined by two-point probe measurements and reached values as small as ~1 mΩ-cm.

To obtain stretchable films, two approaches were explored. First, PAA-Ag thin films were cast on top of polydimethylsiloxane (PDMS) - an elastomer, and reduced by the microplasma. Second, we extended our process to a rubber polymer (styrene-isoprene-styrene) (SIS) which could be mixed with silver trifluoroacetate to be reduced and form Ag in a single polymer layer. Results for the resistivity as a function of the strain in the various material systems will be presented, as well as a working model for the role of the plasma in the reduction of the metal in the polymer and its final morphology.

11:20am **PS+SE-MoM10 Plasma Polymerised 4-vinyl Pyridine Films with High Charge Density Synthesised in Atmospheric Roll-to-Roll System**, *Hindrik de Vries*, FOM institute DIFFER, Netherlands; *W. van Baak*, S.A. Starostin, FUJIFILM Manufacturing Europe B.V., Netherlands; *M.C.M. van de Sanden*, FOM institute DIFFER, Netherlands

Nowadays plasma polymerisation is considered as an attractive tool to synthesise ultra-thin organic functional coatings. In this contribution we report for the first time the synthesis of PP thin 4-vinylpyridine containing films synthesised in a roll-to-roll set-up in an atmospheric pressure plasma enhance chemical vapour deposition (AP-PECVD) reactor using low cost nitrogen gas. The general details of the reactor and plasma parameters were described elsewhere [1]. Specific of the present work is the use of a variable short pulse trains. Nitrogen was used as a carrier gas admixed with a variable flow of argon to control the vaporisation rate of 2 monomers: 4-vinylpyridine (4-VP) and divinylbenzene (DVB) to enable copolymerisation reaction. The film properties were tuned by varying the power per injected precursor molecule and the mixing ratio of the 2 monomers. The films were characterized on thickness (spectroscopic ellipsometry), adhesion (tape test), roughness (interferometric microscopy), and wettability (water contact angle). The microstructure of the 4-VP films was assessed by Attenuated Total Reflection Fourier Transform Infrared (ATR-FTIR) and X-ray Photoelectron Spectroscopy (XPS). The fixed charge was characterised by zeta potential measurements. Film analysis showed that the main feature (pyridine group) was preserved although newly formed peaks in the ATR-FTIR spectrum indicate partial dissociation of the 4-VP. Pulse parameters as well as the DVB [2] flow were studied to improve cross-linking of the film. Zeta potential measurements confirmed the presence of positive charge at the surface. Subsequently, the films were quaternized

leading to a further enhancement of the fixed charge on the surface. Recent results will be highlighted and recommendations for further improvement of the atmospheric plasma processing will be discussed.

[1] S.A. Starostin et al. *Plasma Process. and Polym.* 12, no. 6 (2015): 545–54.

[2] R. Yang et al. *Advanced Materials* 26, no. 11 (2014): 1711–18.

11:40am **PS+SE-MoM11 Plasma-Surface Interactions in Atmospheric Pressure Plasmas: In Situ Measurements of Local Excitations in Thin Films**, *Scott Walton*, Naval Research Laboratory; *B.M. Foley*, University of Virginia; *D.R. Boris*, *E.D. Gillman*, *S.C. Hernández*, Naval Research Laboratory; *A. Giri*, University of Virginia; *Tz.B. Petrova*, *G.M. Petrov*, Naval Research Laboratory; *P.E. Hopkins*, University of Virginia

The energy flux to a surface during plasma exposure and the associated surface heating are of long standing interest as they contribute to the physicochemical changes associated plasma-based materials processing. The unique feature of plasmas compared to other methods of materials synthesis and processing is that the energy flux is delivered and absorbed at or very near the surface over short time scales, and thus requires fast, surface-sensitive techniques to fully appreciate the dynamics of the plasma-surface interface. To achieve this, we employ pump-probe Time-Domain Thermoreflectance (TDTR) to measure the electron and phonon excitation and energy transport dynamics in thin metal films during exposure to an atmospheric pressure plasma jet. The results show the energy delivered by the plasma jet causes a localized thermal spike that is dissipated radially from the point of contact. More specifically, energy delivered via the flux of particles and photons causes the kinetic energy of the electrons within the material to increase over an area commensurate with the plasma jet radius. That energy is then dissipated through electron-electron collisions and electron-phonon interactions as the excited electrons propagate radially from the point of contact. These results, in conjunction with plasma characterization, will be discussed in an effort to develop a first order understanding of energy transfer and relevant kinetics during plasma jet-surface interactions. This work is partially supported by the Naval Research Laboratory base program.

Plasma Science and Technology

Room 104B - Session PS-MoM

Advanced FEOL/Gate Etching

Moderator: Ankur Agarwal, Applied Materials, Inc.

8:20am **PS-MoM1 Novel Etch Strategies for Sidewall Image Transfer**, *Sonam Sherpa*, *P. Chan*, *A. Ranjan*, Tokyo Electron Ltd.

Sidewall image transfer (SIT) is an indirect patterning method that involves the deposition and etching of silicon nitride spacer to achieve sub-lithographic linewidths. Current approaches to etch silicon nitride spacer face two main challenges --- footing and corner rounding. Solution to these problems requires a non-polymerizing chemistry that must be anisotropic and yet avoids the adverse impact of ion-bombardment. To this end, an alternative etching process based on the modification of silicon nitride by light ions followed by the selective removal of the modified layers by DHF has already been reported [1]. However, this process uses non-compatible etch techniques (dry and wet etch). To overcome this challenge, we have developed a plasma-based alternative to DHF. After the spacer etch, isotropic etching of silicon with infinite selectivity to the nitride spacer and underlying oxide is required for mandrel pull. Current methods used to etch silicon involve the redeposition of etch by-products and bombardment by energetic ions. Therefore, these processes are not isotropic and result in footing and significant damage to the underlying material.

In this presentation, we will demonstrate the feasibility of our approach to etch silicon nitride spacer without any footing and corner rounding. In addition, damage to the underlying oxide is negligible. We will also discuss the effects of non-idealities such as scattering and deflection of ions during the hydrogen plasma treatment and the incoming topographical defect on the etch profile. In addition, we will demonstrate the feasibility of novel strategies for isotropic etching of silicon with infinite selectivity to oxide, nitride, and other materials. These processes are by-product free and we do observe any footing. In addition, damage to the underlying material is negligible.

1. N. Posseme, O. Pollet, and S. Barnola, *Appl. Phys. Lett.*, **105**, 051605 (2014).

Monday Morning, November 7, 2016

8:40am **PS-MoM2 Enhancing Fin Retention in Low-K Spacer Etch Processes Using a Highly Selective Etch Chemistry**, *N.P. Marchack*, IBM Research Division, T.J. Watson Research Center; *E. Miller*, IBM Research at Albany Nanotech; *R.L. Bruce*, *H. Miyazoe*, *E.M. Sikorski*, **Sebastian Engelmann**, *E.A. Joseph*, IBM Research Division, T.J. Watson Research Center; *S. Kanakasabapathy*, IBM Research at Albany Nanotech

Low-k spacer materials such as SiBCN have garnered attention recently for advanced technology nodes due to their controllable electrical conductivity, low thermal expansion coefficient and potential for reducing loading capacitance. [1] Of particular concern in a spacer etch process is reducing the damage caused to materials such as the bottom oxide (BOX) and the underlying fins in FinFET systems. This is often a difficult challenge owing to the tight pitches and widely disparate critical dimensions (CDs) between the fin and gate geometries.

We present a spacer etch process using a novel high-selectivity gas chemistry that shows minimal damage in a FinFET system with SiBCN spacer deposited over SiGe fins. In addition to reduced damage compared to a conventional $\text{CH}_3\text{F}/\text{O}_2$ plasma chemistry, we also demonstrate greatly improved throughput even at low duty cycles by taking advantage of the unique chemical properties of the gas. We show <5nm SiGe fin loss for long overetch values, with minimal box loss as measured by high-resolution transmission electron microscopy (TEM).

The effect of pulsed plasma parameters are analyzed via optical emission spectroscopy (OES) in an attempt to define the etching mechanisms, as well as explain the difference between blanket etch conditions and patterned features. We focus on the effect of He dilution within the plasma as well as the effect of phase difference between source and bias for synchronous pulsing cases.

References:

[1] R.G. Southwick et al., IEEE International Reliability Physics Symposium pp. BD.2.1-2.4, 2014

9:00am **PS-MoM3 Effect of the Amount of Hydrogen During SiN etching on Etching Properties**, *Nobuyuki Kuboi*, *H. Minari*, *M. Fukasawa*, *Y. Zaizen*, *J. Komachi*, *T. Kawamura*, *T. Tatsumi*, Sony Corporation, Japan

Silicon nitride (SiN) is an essential film in complementary metal oxide semiconductor devices. The amount of hydrogen contained in SiN films depends on the process conditions used in chemical vapor deposition (CVD), and strongly affects the etching properties of etching rate (ER), C-F polymer thickness ($T_{\text{C-F}}$), and damage. Therefore, revealing the mechanism of how hydrogen influences etching is very important to predict and control damage distribution considering the etching profile, and to develop etching processes with high selectivity for SiN over SiO_2 .

To model SiN etching under the effect of hydrogen, we performed experiments using a dual-frequency capacitively coupled plasma system. We prepared three kinds of SiN_xH_y films with $y = 2.6\%$, 16.8% , and 21.9% (denoted as LP-SiN, Low-H SiN, and High-H SiN, respectively) on Si substrates using different CVD processes. The films were treated with $\text{CH}_2\text{F}_2/\text{O}_2/\text{Ar}$ plasma under a gas pressure of 20 mTorr and V_{pp} of 350 V, for which we measured ER and $T_{\text{C-F}}$ values. We also measured plasma and surface conditions using various monitoring techniques. We analyzed the results through a first-principles calculation with VASP [1].

We found that for the low $\text{CH}_2\text{F}_2/(\text{CH}_2\text{F}_2+\text{O}_2)$ ratio where few C-F polymer layers existed, the ER values of High-H SiN were 20%–40% smaller than those of LP-SiN and Low-H SiN. In contrast, inverse behavior was observed in the case of a high $\text{CH}_2\text{F}_2/(\text{CH}_2\text{F}_2+\text{O}_2)$ ratio. Considering variation of OES data and reactivity estimated by the VASP calculation, under the assumption that the etching front consisted of two layers (C-F polymer layer and reactive layer) [2], not only reaction between the outflux of H from the reactive layer and F from plasma but also termination of Si dangling bonds by H seems to cause variation of the ER value when the $\text{CH}_2\text{F}_2/(\text{CH}_2\text{F}_2+\text{O}_2)$ ratio is low. Because a C-F polymer layer of moderate thickness existed over the reactive layer at high $\text{CH}_2\text{F}_2/(\text{CH}_2\text{F}_2+\text{O}_2)$ ratio, some H was consumed by reaction with C in the polymer layer, which weakened the effects of H such as deactivation of F and termination of Si dangling bonds. This seems to lead to the inverse behavior observed at high $\text{CH}_2\text{F}_2/(\text{CH}_2\text{F}_2+\text{O}_2)$ ratio.

We formulate the above effect of H and include it in our SiN surface reaction model using the 3D voxel-slab method [3], reproducing ER and $T_{\text{C-F}}$ values. We also demonstrate SiN side-wall etching of fin-type field-effect transistors and discuss how to control etching profile and damage distribution.

[1] G. Kresse and J. Furthmüller, Phys. Rev. B **54**, 11169 (1996).

[2] M. Matsui et al., J. Vac. Sci. Technol. A **19**, 2089 (2001).

[3] N. Kuboi et al., J. Vac. Sci. Technol. A **33**, 061308 (2015).

9:20am **PS-MoM4 Dual Channel Si/SiGe Fin patterning for 10nm Node and Beyond**, *Fee Li Lie*, *E. Miller*, *P. Xu*, *S. Sieg*, *M. Sankarapandian*, IBM Research; *S. Schmitz*, *P. Friddle*, Lam Research Corporation; *G. Karve*, *J. Strane*, IBM Research; *K.Y. Lim*, *K. Akarvardar*, *M.G. Sung*, GLOBALFOUNDRIES, Inc.; *S. Kanakasabapathy*, IBM Research

As geometric scaling of silicon CMOS technology reaches its limits, continued device performance enhancement requires innovative approaches such as alternative channel materials. Owing to its relatively high hole mobility, much attention has been given to SiGe as a candidate for PFET channel material. The introduction of Ge in the material system affects the vertical and lateral etch behavior of the system depending on the Ge%. Typical balancing act of sidewall passivation and etch to yield vertical and on-target critical dimension (CD) fins now needs to be done on both Si and SiGe simultaneously. Furthermore, subsequent dry/wet clean processes, which generally does not impact Si fins, also interacts with SiGe fin and affects the final fin profile and CD. In this paper, we will present key challenges and approaches pertaining to etching dual channel Si/SiGe fin and subsequent dry/wet clean processes.

9:40am **PS-MoM5 Computational Patterning and Process Emulation: Linchpins to Enable Continued Scaling through Design Technology Co-optimization for Advanced Nodes**, *Derren Dunn*, IBM Corporation **INVITED**

Enabling continued scaling at a pace that meets market demands will require new paradigms to define and evaluate early hardware design guidelines. Increasingly, patterning process implementations will be key factors in defining the boundaries of design spaces available for nodes beyond 10 nm. Self aligned patterning approaches will enable design spaces with significantly different entitlements than direct print patterning strategies due to process control dependencies, complexity, and physical process limitations. Identifying early design guidelines through process simulation and emulation that incorporate a full range of patterning processes required for a given front end of line (FEOL) approach will be key to delivering nodes on time. These processes will undoubtedly include lithography, reactive ion etch, spacer deposition, and wet clean processes. In addition, EUV solutions will require accurate estimates of line width variation, line end pull-back, and new materials challenges that will influence early design decisions. In this talk, we will demonstrate how coupling advanced process simulation with process emulation can be used to evaluate early FEOL design guidelines and establish criteria for equipment and materials vendors. We will also suggest approaches to establishing design entitlement metrics for typical FEOL self aligned patterning processes and EUV direct print approaches that might be used in future gate and fin process modules.

10:40am **PS-MoM8 Overcoming Challenges of sub-10NM FinFET Gate Etching in Halogenated Plasmas**, *Sergey Voronin*, TEL Technology Center, America, LLC; *J.R. Sporre*, *S. Kanakasabapathy*, International Business Machines – Research Division; *A. Ranjan*, TEL Technology Center, America, LLC

Moore's law extension in the semiconductor industry requires processing of features at nanometer scale. Approaching sub-10NM technological fabrication we face more stringent requirements to the etch process (high anisotropy and high selectivity to the mask films).

We present peculiarities and new challenges of 3D gate etch processing in halogen-based plasmas. These include by-product -free etching of narrow features, "FIN-Gate" corner residue removal, prevention of merging of the neighboring gates and advanced selectivity control to the FIN oxide. To combine all these in one process, we need multiple unique steps responsible for certain stages of etching. The etching mechanisms and dependence of the etching properties (selectivity, anisotropy and etch rate) on the plasma discharge parameters (electron temperature, ion and radical densities, ion energy) will be described for each step. We have successfully approached the 7NM technological node at aspect ratios and, etch depths up to 6:1 and 160 nm, respectively, with a potential for the next technological generation.

An additional subject of discussion is related to surface-plasma interactions between charged and neutral species in HBr plasmas. Formation and deposition of non-volatile bromine-containing by-products SiBr_x ($x=1,2$) and

Monday Morning, November 7, 2016

SiBr_xO_y can result in clogging of narrow features, etch profile distortion, limited etching depth and residual Si at high aspect ratios. These non-volatile species are accumulated on the process chamber wall, desorb to the gas phase and can re-deposit on the processed wafer for long times – well after the main etch process is over. We demonstrate the importance of the chamber wall chemistry condition and plasma discharge parameters in formation and re-deposition of these species. Chamber wall surface cleaning by fluorine-containing plasmas and lowering the source power resulted in significantly smaller amounts of by-product and can be used as profile control knobs in the process.

11:00am PS-MoM9 Gate Etch Challenges Introduced by FinFET Gate Pitch Scaling, John Sporre, IBM Research Division; *X. Liu*, IBM Research Division, T.J. Watson Research Center; *S. Seo*, IBM Research Division; *C. Prindle*, GLOBALFOUNDRIES, Inc.; *P. Montanini*, IBM Research Division; *R. Xie*, GLOBALFOUNDRIES, Inc.; *M. Sankarapandian*, *S. Mehta*, *M. Breton*, *S. McDermott*, *S. Kanakasabapathy*, IBM Research Division; *B. Haran*, IBM Research

Continued scaling of FinFET technology introduces unique challenges with respect to patterning high aspect ratio structures. In addition to the traditional challenge of etching a gate with uniform sidewall and cross wafer uniformity, new challenges are introduced as a result of the reduction of inter-gate spacing. Maintaining selectivity to dielectrics during Si etch can result in profile degradation due to etch polymer by-product pinch-off. Low polymer producing chemistries can prevent this pinch-off, but with the cost of unacceptable Fin erosion. Furthermore, gate profile and pitch control can have significant impact on down stream process stability and may result in downstream gate bending. In this paper, the unique challenges caused by gate pitch scaling will be explored with respect to not only their impact on downstream functionality, but also to the gate etch itself.

11:20am PS-MoM10 Hybrid Fin reveal for tight Fin Pitch Technologies, Peng Xu, IBM Research Division; *P. Wang*, Lam Research Corporation; *Z.X. Bi*, IBM Semiconductor Technology Research; *T. Devarajan*, IBM Research Division; *B. Nagabhirava*, *A. Basavalingappa*, Lam Research Corporation; *F.L. Lie*, *J. Strane*, *M. Sankarapandian*, *S. Mehta*, *R. Conti*, IBM Research Division; *M. Goss*, LAM Research Corporation; *D. Canaperi*, *D. Guo*, *S. Kanakasabapathy*, IBM Research Division

FinFET based CMOS technologies continue scaling down in Fin Pitch1-3. Self-aligned double patterning (SADP) and Self-aligned quadruple patterning (SAQP) have been used to form tight Fin pitch structure. Device requirements and layout constraints can result in the need to cut different numbers of fins, which form variable spaces between fins, but a consistent Fin height must be maintained. In addition to the space variability, gap fill oxide density variations are observed depending on local feature density. A key process for defining the height of the active fin for Bulk Substrates is the Fin reveal process

Such space and film density variations between Fins introduce significant challenges for the Fin reveal process, especially in the sub 40nm Fin pitch range. In this paper, we show initial results from a hybrid Fin reveal process, that combines anisotropic etching with reactive clean techniques. We show the ability to maintain fin reveal depth uniform across feature densities and quality.

1.Chang *et al.*, "Extremely scaled silicon nano-CMOS devices," in *Proceedings of the IEEE*, vol. 91, no. 11, pp. 1860-1873, Nov 2003.

2.K. I. Seo *et al.*, "A 10nm platform technology for low power and high performance application featuring FINFET devices with multi workfunction gate stack on bulk and SOI," *VLSI Technology (VLSI-Technology): Digest of Technical Papers, 2014 Symposium on*, Honolulu, HI, 2014, pp. 1-2. Saurabh Sinha, Greg Yeric, Vikas Chandra, Brian Cline, and Yu Cao. 2012. Exploring sub-20nm FinFET design with predictive technology models. In *Proceedings of the 49th Annual Design Automation Conference (DAC '12)*. ACM, New York, NY, USA, 283-288.

11:40am PS-MoM11 Damage Free Plasma Etching Processes for the Patterning of InGaAs fin for the sub-10nm Technological Node, Maxime Bizouerne, *E. Pargon*, LTM, Univ. Grenoble Alpes, CEA-LETI, France; *P. Burtin*, CEA, LETI, MINATEC Campus, France; *C. Petit-Etienne*, *E. Latu-Romain*, *S. Labau*, *M. Martin*, LTM, Univ. Grenoble Alpes, CEA-LETI, France
The conventional Si CMOS technology recently encounters difficulties to maintain its dimensional scaling owing to the high power consumption of logic chips. The planar MOSFET has already evolved to a FinFET, a three dimensional device architecture which provides lower leakage current.

New channel materials are now therefore considered to continue the transistor scaling and enable higher device densities with faster logic switching and lower power consumption. The III-V semiconductors which present electron velocities ten times higher than the silicon, are seriously considered as N-channel materials in a FinFET architecture for the sub-10nm technological node. To complete this integration, the development of plasma etching processes dedicated to the III-V fin patterning is necessary. The major challenge for nanometer-scale III-V finFET definition by plasma etching is the realization of vertical sidewalls with a high quality surface.

In this work, we address this challenge by undertaking a systematic investigation of dry etch processing for InGaAs fin formation, with the aim of obtaining high resolution fins with vertical sidewalls and clean etch surfaces. The InGaAs layers have been grown by MOCVD on 200mm Si wafer and photoresist lines with dimensions ranging from 20 to 100nm have been patterned by ebeam lithography. The plasma etching experiments are carried out on a 200mm etching platform from AMAT composed of two inductive coupled plasma reactors, whose one is equipped with a hot cathode. The performance of Cl₂ and CH₄ based plasma processes at 50°C and 200°C have been evaluated and compared in terms of anisotropy, surface roughness and plasma induced chemical damages. A particular attention is paid on the chemical and physical damages induced on the pattern sidewalls. The pattern profiles are characterized by electron microscopies. The sidewalls roughness is measured by AFM using a homemade setup where the sample is tilted to allow the tip to scan the sidewalls. The sidewalls chemical composition and stoichiometry after etching is analyzed by nanoauger spectroscopy. We also investigate restoring processes to mitigate the etch-induced sidewalls damages by combining oxidation and wet removal steps. Finally, we propose a new method to pattern the III-V fins without generating etching damages. It consists of a two-step process, starting with a surface modification by a He or H₂ plasma implantation followed by a wet cleaning to remove the modified surface without damaging the non-modified one. This method appears promising to etch the III-V fin without damaging the fin sidewalls and will be benchmarked to conventional plasma technique.

Novel Trends in Synchrotron and FEL-Based Analysis Focus Topic

Room 103C - Session SA+AS+MI-MoM

Advances in High-Resolution Imaging Techniques (8:20-10:20 am)/Pushing the Limits with X-Ray Spectroscopy (10:40 am-12:00 pm)

Moderators: Maya Kiskinova, Elettra-Sincrotrone Trieste, Italy, Claus Michael Schneider, Forschungszentrum Juelich GmbH, Germany

9:00am SA+AS+MI-MoM3 Applications of Novel Hard X-ray Nanoprobe in Nanoscience, Gema Martinez-Criado, Madrid Materials Science Institute, CSIC, Spain

INVITED

Owing to the spatial resolution and sensitivity (i.e., signal to background ratio), nano and micro X-ray beams are emerging tools with a strong impact in nanoscience. Although the optical quality of the X-ray focusing devices has limited the progress of hard X-ray nanoprobe, recent advances in fabrication techniques have pushed the spatial resolution towards the diffraction limit. As a result, the use of nano and micro X-ray beams has begun to extend towards the atomic domain, with concomitant and continuous developments of multiple analytical tools. The study of micro/nanoscale objects, small embedded nanodomains with weak signals and/or heterogeneous structures at the nanometer scales has required the use of intense X-ray pencil beams. Additionally, stimulated by the great brilliance with reduced emittance of current third generation synchrotron sources, and new developments in X-ray detector technology, today intense nano-X-ray beams are available with a variety of focusing devices. Finally, thanks to the multiple interactions of X-rays with matter these X-ray probes can be used for manifold purposes, such as ultra-sensitive elemental/chemical detection using X-ray fluorescence/X-ray absorption, or for identification of minority phases, and/or strain fields by X-ray diffraction with nanometer resolution. In the present talk I describe how hard X-ray nanobeams are produced and exploited today for space-resolved determination of structural and electronic properties, as well as for chemical speciation of nanosized materials. Selected recent examples will range from phase separation in single nanowires to visualization of

Monday Morning, November 7, 2016

dislocations and buried interfacial defects, to domain distortions and quantum confinement effects.

10:40am **SA+AS+MI-MoM8 Extreme X-ray Flux to Probe Picosecond Dynamics, Alfred Baron**, RIKEN SPring-8, Japan **INVITED**

Inelastic x-ray scattering (IXS), *in principle*, provides a nearly ideal opportunity to probe dynamics on ps and sub-ps time scales via direct measurement of the dynamic structure factor, $S(Q, \omega)$. Such measurements are interesting in many areas of science, including fundamental understanding of liquid behavior, investigations of phonons in complex materials such as superconductors and ferroelectrics, and even to help determine the composition of the earth's interior. However, high-resolution non-resonant IXS measurements are *severely flux limited*.

Over the last 18 years, the author has spearheaded a program to increase the world capability for high-resolution IXS measurements through work at SPring-8 in Japan. This began with designing and constructing a beamline based on a standard insertion device [1] then progressed to a second beamline using 3x5m tandem small-gap insertion devices (IDs) [2], while in parallel, upgrading the earlier facility to a optimized small-gap ID. *This has successfully led to world-leading flux at workhorse spectrometers with ~1.25 meV resolution and 30 GHz onto the sample at 21.7 keV*, and up to 30 momentum transfers collected in parallel. Resolution as good as 0.75 meV [3] can be achieved at higher (25.7 keV) energy while medium resolution spectrometer provides in excess of 2 THz onto a sample with 27 meV resolution for measuring electronic dynamics.

The presentation will discuss aspects of the instrumentation for IXS, and recent sample science. On the instrumentation side, on top of "straightforward" issues such as sub-mK temperature control over >50 channels, installation of more than 30 tons of spectrometer, there were unique and new issues related to operating 3x5m tandem small- (6mm-) gap insertion devices [4]. On the sample side, the talk will highlight recent efforts in geoscience, where measurements at record pressures and temperatures have allowed us to constrain to composition of the Earth's core - both the outer liquid core [5] and the inner solid core. This will be complemented by a short discussion of a surprising phonon anomaly in YBa₂Cu₃O_{7-d}, where phonon line-widths undergo a remarkable increase below the superconducting transition temperature [7] in what is perhaps the largest phonon anomaly observed to date in the absence of a structural phase transition.

[1] Baron, *et al.*, J. Phys. Chem. Solids **61**, 461 (2000).

[2] Baron, SPring-8 Inf. Newsl. **15**, 14 (2010).

[3] Ishikawa, *et al.*, J. Synch. Rad. **22**, (2015).

[4] Baron, *et al.*, AIP Conf. Proc. **SRI2015** (Accepted).

[5] Nakajima, *et al.*, Nat Commun. **6**, (2015).

[6] Sakamaki, *et al.*, Sci. Adv. **2**, (2016).

[7] Baron, *et al.*, in preparation.

11:20am **SA+AS+MI-MoM10 Beating Complexity through Selectivity: Anti-Stokes Resonant Inelastic X-ray Scattering for Excited State Dynamics, Alexander Föhlisch**, University of Potsdam, Germany **INVITED**

Ultrafast electronic and structural dynamics of matter govern rate and selectivity of chemical reactions, as well as phase transitions and efficient switching in functional materials. Since X-rays determine electronic and structural properties with elemental, chemical, orbital and magnetic selectivity, short pulse X-ray sources have become central enablers of ultrafast science. Despite of these strengths, ultrafast X-rays have been poor at picking up excited state moieties from the unexcited ones. With time-resolved Anti-Stokes Resonant X-ray Raman Scattering background free excited state selectivity in addition to the elemental, chemical, orbital and magnetic selectivity of X-rays can be achieved. For low symmetry systems energetically off-set signatures dominate, and for inversion symmetric systems a clear separation between ground and excited states occurs. This unparalleled selectivity extracts low concentration excited state species along ultrafast dynamic pathways. These approaches will benefit from recent advances towards non-linear X-ray matter interaction and an outlook is given how future fourier limited X-ray laser pulses will explore ultrafast dynamics.

Scanning Probe Microscopy Focus Topic

Room 104A - Session SP+AS+MI+NS+SS-MoM

Advances in Scanning Probe Microscopy

Moderators: Saban Hus, Oak Ridge National Laboratory, Chanmin Su, Bruker Nano

8:20am **SP+AS+MI+NS+SS-MoM1 Ultrafast Imaging of Polarization Switching in Ferroelectrics via Complete Information Acquisition in SPM, Suhaz Somnath, A. Belianinov, S.V. Kalinin, S. Jesse**, Oak Ridge National Laboratory

SPM imaging can be represented as an information channel between the dynamic processes at the tip-surface junction and the observer. Current SPM techniques use heterodyne detection methods such as lock-in amplifiers which result in significant loss in vital information such as information from higher eigenmodes, mode-mixing, and other non-linear phenomena in the tip-surface interaction. We present a new technique called General-mode (G-mode) where we capture the complete broadband response of the cantilever at sampling rates of 1-100 MHz. The availability of the complete cantilever response facilitates the application of various physical models as well as multivariate statistical methods to extract information that has been unavailable from current SPM techniques. Polarization switching in ferroelectric and multiferroic materials underpins the next generation of electronic devices such as tunneling devices, field effect transistors, and race-track memories. The switching mechanisms in these materials are highly sensitive to the local defects and structural imperfections at the micro and nanometer scale, which have undesirable effects on ferroelectric domains. These considerations necessitated the development of Piezoresponse Force Microscopy (PFM) imaging and spectroscopy techniques to measure and manipulate local polarization states. However, the current state-of-art PFM spectroscopy techniques suffer from serious compromises in the measurement rate, measurement area, voltage and spatial resolutions since they require the combination of a slow (~1 sec) switching signal and a fast (~1 – 10 msec) measurement signal. Furthermore, these techniques only capture the narrow-band cantilever response. We report on a fundamentally new approach that combines the full cantilever response from G-mode with intelligent signal filtering techniques to directly measure material strain in response to the probing bias. Our technique enables precise spectroscopic imaging of the polarization switching phenomena 3,500 times faster than currently reported methods. The improved measurement speed enables dense 2D maps of material response with minimal drift in the tip position.

This research was conducted at the Center for Nanophase Materials Sciences, which is sponsored at Oak Ridge National Laboratory by the Scientific User Facilities Division, Office of Basic Energy Sciences, U.S. Department of Energy.

8:40am **SP+AS+MI+NS+SS-MoM2 Development of Synchrotron X-ray Scanning Tunneling Microscopy, Nozomi Shirato**, Center for Nanoscale Materials at Argonne National Laboratory; H. Chang, Ohio University; M. Cummings, Advanced Photon Source at Argonne National Laboratory; S.W. Hla, Center for Nanoscale Materials at Argonne National Laboratory; V. Rose, Advanced Photon Source at Argonne National Laboratory

Advancements of scanning probe microscopy have been contributing to broaden fundamental understating of surface physics. By combining high intense X-ray beam as a probe and a functionalized tip as a detector, synchrotron X-ray scanning tunneling microscopy has been developed in Advanced Photon Source at Argonne National Laboratory. The recent studies demonstrated the technique has capabilities to extract chemical information with sensitivity at the atomic limit [1] and localized magnetic contrast by utilizing polarized beams [2]. Furthermore, at Argonne, in order to fully exploit potentials of the microscope, a dedicated beamline is under construction. The soft X-ray beamline has the energy range of 400 to 1600 eV and is equipped with a polarizer and focusing optics. The capabilities of the beamline will benefit the communities to explore chemical, magnetic and electronic properties of materials at atomic resolution.

References

[1] N. Shirato *et al.*, Nano Letters **14**, 6499 (2014).

[2] A. DiLullo *et al.*, J. Synchrotron Rad. **23**, 574 (2016).

Monday Morning, November 7, 2016

9:00am **SP+AS+MI+NS+SS-MoM3 Development and Integration of a Universal SPM head: Design Criteria and Challenges**, B. Guenther, Sigma Surface Science GmbH, Germany; J. Hilton, Mantis Deposition; A. Feltz, Sigma Surface Science GmbH; **Andreas Bettac**, Sigma Surface Science GmbH, Germany

Recently we have developed an SPM microscope head that merges the needs for high resolution STM/QPlus¹-AFM and at the same time satisfies the requirements for integration into different cryogen environments including tip and sample handling.

The new SPM head was integrated into different platforms, e.g. in a UHV Helium Flow Cryostat system for temperatures <10K and in a ³He Magnet Cryostat UHV system for high magnetic fields (± 12 T) and temperatures <400mK.

This contribution focuses on design aspects and challenges for the new SPM head with respect to spatial restrictions, sample sizes/standards, QPlus and STM signal shielding as well as on first results (STM, STS and QPlus) obtained with the different instrumental setups.

[1] F. J. Giessibl, Applied Physics Letters 73 (1998) 3956

9:20am **SP+AS+MI+NS+SS-MoM4 How Soft Is a Protein? Stress-Strain Curve of Antibody Pentamers with 5 pN and 50 pm Resolutions**, **Alma Perrino**^{*}, Instituto de Ciencia de Materiales de Madrid, CSIC, c/ Sor Juana Ines de la Cruz 3, 28049 Madrid, Spain; R. Garcia, Instituto de Ciencia de Materiales de Madrid, CSIC, Spain

Understanding the mechanical functionalities of complex biological systems requires the measurement of the mechanical compliance of their smallest components. Here, we develop a force microscopy method to quantify the softness of a single antibody pentamer by measuring the stress-strain curve with force and deformation resolutions, respectively, of 5 pN and 50 pm [1]. The curve shows three distinctive regions. For ultrasmall compressive forces (5-75 pN), the protein's central region shows that the strain and stress are proportional (elastic regime). This region has an average Young modulus of 2.5 MPa. For forces between 80 and 220 pN, the stress is roughly proportional to the strain with a Young modulus of 9 MPa. Higher forces lead to irreversible deformations (plastic regime). Full elastic recovery could reach deformations amounting 40% of the protein height. The existence of two different elastic regions is explained in terms of the structure of the antibody central region. The stress-strain curve explains the capability of the antibody to sustain multiple collisions without any loss of biological functionality.

[1] Alma P. Perrino and R. Garcia. How soft is a protein? Stress-Strain curve of antibody pentamers with 5 pN and 50 pm resolutions. *Nanoscale*, 10.1039/C5NR07957H (2016)

9:40am **SP+AS+MI+NS+SS-MoM5 AVS Medard W. Welch Award Talk: Action Spectroscopy: Characterizing Molecules at Surfaces and its Dynamics**, **Maki Kawai**[†], Institute for Molecular Science, Japan; Y. Kim, RIKEN Surface and Interface Science Laboratory, Wako, Saitama, Japan; K. Motobayashi, Nagoya Institute of Technology, Japan; H. Ueba, Toyama University, Japan

INVITED

STM is a useful tool for spectroscopy utilizing its ultimate spatial resolution. Electronic and vibrational information that STS and inelastic electron tunneling spectroscopy (IETS) carries is not only the reflection of the static spectroscopic information but also related to dynamical phenomena as motion or reaction of molecules induced by the excitation of molecular states. Action spectroscopy is the method to related the action of molecules induced and is utilized to identify the quantum states of the molecules. Dynamical information includes as how molecular vibrations can couple with the relevant dynamical processes [1,2]. I will present typical examples of how the fundamental excitation of vibration modes is coupled with chemical reactions at surfaces.

References:

[1] Y. Kim, K. Motobayashi, T. Frederiksen, H. Ueba and Maki Kawai, *Proffress in Surface Science* 90 (2015) 85-143, and the references within.

[2] K. Motobayashi, Y. Kim, M. Ohara, H. Ueba and Maki Kawai, *Surf. Sci.* 634 (2016) 18-22.

10:40am **SP+AS+MI+NS+SS-MoM8 Near-Field Spectroscopy and Imaging of Single Nanoparticles**, **Yohannes Abate**, D. Seidlitz, A. Fali, S. Gamage, V.E. Babicheva, V.S. Yakovlev, M.I. Stockman, Georgia State University; R. Collazo, D. Alden, North Carolina State University; N. Deitz, Georgia State University

INVITED

We investigate nanoscale phase separation on single InGaN QDs and nanostructures by using high-resolution s-SNIN (scattering type scanning near-field infrared nanoscopy) technique in the mid-IR spectral region. We fabricated patterned nanolayers down to few atomic layers thick that allow determination of the near-field infrared response of InGaN/InN/GaN heterostructures quantitatively. We first calibrate the near-field IR amplitude contrast as a function of composition and thickness of the semiconductor nanolayers and QDs. We then use this quantitative leads to identify phase separation in single QDs. An advanced theoretical model is developed to guide the experimental results. Unlike previous models that consider the probe conical tip as approximate point dipoles or spheroids, our model considers the full geometry of the tip and all the sample and substrate layers.

11:20am **SP+AS+MI+NS+SS-MoM10 Atomically-resolved Three-dimensional Structures of Electrolyte Aqueous Solutions near a Solid Surface**, **Daniel Martin-Jimenez**, E. Chacon, Instituto de Ciencia de Materiales de Madrid, CSIC, Spain; P. Trazona, IFIMAC Condensed Matter Physics Center, UAM, Spain; R. Garcia, Instituto de Ciencia de Materiales de Madrid, CSIC, Spain

Atomic-resolution three-dimensional images of electrolyte solutions near a mica surface demonstrate the existence of three types of interfacial structures [1-3]. At low concentrations (0.01-1 M), cations are adsorbed onto the mica until charge neutrality is reached. The cation layer is topped by a few hydration layers while anions are excluded from the mica surface [4]. At higher concentrations, the interfacial layer extends several nanometers into the liquid. It involves the alternation of cation and anion planes. Classical Fluid Density Functional calculations show that water molecules are a critical factor for stabilizing the structure of the ordered interfacial layer. The interfacial layer compatibilizes a crystal-like structure with liquid-like ion and solvent mobilities. At saturation, some ions precipitate and small ionic crystals are formed on the mica. The three-dimensional images have been acquired at 300 K.

[1] E. T. Herruzo, H. Asakawa, T. Fukuma, and R. Garcia, *Nanoscale* **5**, 2678-2685 (2013).

[2] K. Kobayashi *et al.* *The Journal of Chemical Physics* **138**, 184704 (2013)

[3] T. Fukuma *et al.* *Physical Review B* **92**, 7 (2015).

[4] M. Ricci, P. Spijker and K. Voitchovsky *Nat. Commun.* **5**, 4400 (2014).

11:40am **SP+AS+MI+NS+SS-MoM11 Super-resolution Optical and Chemical Imaging of Organic Thin Films using Tip-enhanced Near-Field Optical Microscopy**, A.L. Heilman, R. Hermann, **Michael Gordon**, University of California at Santa Barbara

Sub-diffraction-limited (super-resolution) optical and chemical characterization of organic surfaces using a custom-built tip-enhanced near-field optical microscope with side-on and attenuated total reflectance (ATR) excitation and collection will be discussed. ATR illumination is combined with an Au optical antenna tip to show that (i) the tip can quantitatively transduce the optical near-field (evanescent waves) above the surface by scattering photons into the far-field, (ii) the ATR geometry enables excitation and characterization of surface plasmon polaritons (SPPs), whose associated optical fields can enhance Raman scattering from coumarin-6 (C6) and copper phthalocyanine (CuPc) films, and (iii) SPPs can be used to plasmonically excite the tip for super-resolution chemical imaging of patterned C6 and CuPc via tip-enhanced Raman spectroscopy (TERS). ATR-illumination TERS is quantitatively compared with the more conventional side-on illumination scheme using both experiment and FDTD optical simulations. In both cases, spatial resolution was better than 40 nm and tip on/tip off Raman enhancement factors were >6500. ATR illumination was shown to provide similar Raman signal levels at lower 'effective' pump powers due to additional optical energy delivered by SPPs to the active region in the tip-surface gap. Additional observations, such as the distance scaling of Raman enhancement and inelastic scattering generated by the plasmonic tip, as well as tip-enhanced photoluminescence imaging of patterned phthalocyanine films at spatial resolutions better than 20-30 nm, will be presented.

^{*} NSTD Student Award Finalist

[†] Medard W. Welch Award Winner

Surface Science

Room 104E - Session SS+AS+HC-MoM

Mechanistic Insights on Surface Reactions in Catalysis and at Novel Interfaces

Moderator: Bruce D. Kay, Pacific Northwest National Laboratory

8:20am **SS+AS+HC-MoM1 Study of Metal-Organic Complexation at Metal and Metal Oxide Surfaces by HREELS, Miao Wang, C. Williams, S.L. Tait, Indiana University**

The ordering of organic molecules at surfaces and the formation of ordered metal nanostructures at surfaces have been extensively studied for the advancement of organic photovoltaics, nanoscale molecular electronics, and catalysts. There are many chemical systems that benefit from the combination of organic ligands with single-site metal centers to design and tune specific chemistries, but metal-organic complexation at surfaces has not yet been significantly studied. Molecular ligands on a surface with specific binding pockets can bind metal centers to achieve uniform oxidation states, as has been shown in prior studies by our group and by other groups. The goal of these studies is to improve selectivity in heterogeneous catalysts and to develop other novel surface chemistries. With that end in mind, we present new experiments with metal-organic coordination on oxide support surfaces. Most of the metal-organic surfaces studies have been done on metal surfaces to facilitate surface analysis. We have studied the redox assembly of 3,6-Di-2-pyridyl-1,2,4,5-tetrazine (DPTZ) and Pt on oxide surfaces, including rutile $\text{TiO}_2(110)$ using High Resolution Electron Energy Loss Spectroscopy (HREELS), Auger Electron Spectroscopy (AES) and Low Energy Electron Diffraction (LEED). HREELS characterizes vibrational modes, which can provide key information about adsorbate interactions and metal-organic interactions at surfaces. DPTZ and Pt were sublimated onto the surface from a Knudsen-type evaporator. Submonolayer DPTZ vibrational modes were observed on $\text{Ag}(111)$ (C-H bending modes at 400 cm^{-1} , 618 cm^{-1} and 772 cm^{-1} ; ring deformation modes at 966 cm^{-1} , 1145 cm^{-1} and 1354 cm^{-1}) and on $\text{TiO}_2(110)$ (a ring deformation mode at 1580 cm^{-1} and a C-H stretching mode at 3060 cm^{-1}). To see the vibrational modes of adsorbates on TiO_2 , a Fourier deconvolution technique was applied to remove multiple excitations of surface phonon. Annealing DPTZ on $\text{Ag}(111)$ at 170°C caused significant changes to the HREEL spectra (C-H bending modes at 400 cm^{-1} and 740 cm^{-1} , ring deformation modes at 1100 cm^{-1} , 1445 cm^{-1} , 1574 cm^{-1} , a C-H stretching mode at 3080 cm^{-1}), but no observable changes were seen for DPTZ on $\text{TiO}_2(110)$ until the sample was annealed at 290°C . Adding equimolar Pt onto submonolayer DPTZ on $\text{Ag}(111)$ caused similar vibrational changes to be observed, but at a lower temperature of 140°C . HREELS studies of the Pt-DPTZ complex on $\text{TiO}_2(110)$, $\text{Au}(100)$, and other surfaces are ongoing. By studying the redox assembly of metal-organic complexes on these surfaces, strategies can be developed to customize and tune the reactivity of novel surface catalysts.

8:40am **SS+AS+HC-MoM2 Studies of Single-site Catalysts on Powdered Oxide Support through Redox Assembly, Linxiao Chen, J.P. McCann, S.L. Tait, Indiana University**

High levels of reaction selectivity for selective alkane functionalization are generally difficult to achieve with metal nanoparticle heterogeneous catalysts, due to the variety of metal binding sites available. Motivated by the desire towards the development of uniform single-site metal centers at surfaces, our group has been working on the redox assembly of metal-organic systems at surfaces. On a single crystal gold surface, electrons are transferred from platinum to the ligand 3,6-Di-2-pyridyl-1,2,4,5-tetrazine (DPTZ). Utilizing this unique redox chemistry, long-range ordered 1D chains with an alternating metal-ligand structure were assembled at deposition of DPTZ with pre-adsorbed metallic platinum. All platinum sites are oxidized into Pt(II) , and stabilized in the binding pocket between two DPTZ with identical chemical environment. Here, aiming at practical applications in catalysis, a novel solution-phase synthetic strategy was developed based on wet impregnation approach, in attempt to reproduce the similar metal-ligand structure on high-surface-area powdered oxide catalyst supports. X-ray photoelectron spectroscopy verified that the redox chemistry is applicable to real supports, and is crucial in the successful deposition of DPTZ despite a weak ligand-support interaction. The surface structure is further elucidated by X-ray diffraction and surface titration. It was concluded that the mobility of the metal and ligand on a rough support surface, and the existence of residual Cl from Pt precursors represent major challenges. This metal-ligand structure can be manipulated by tuning strength of interaction between the supports, metal and ligand. Initial

catalytic tests with the methane oxidation reaction exhibited C-H activation ability and selectivity similar to traditional highly-dispersed Pt catalysts. We have compared these catalysts and explored the limitations of single-site metal-organic complexes at oxide supports. Though being significantly stabilized by the favored coordination geometry and the redox chemistry, the thermal stability of the metal-ligand structure needs to be further enhanced.

9:00am **SS+AS+HC-MoM3 Controlled Reactions of Coordination Complexes on Oxide Surfaces, Susannah Scott, University of California at Santa Barbara**

INVITED

The reactions of coordination complexes with functional groups on oxide surfaces (acidic and basic hydroxyl groups, Lewis acidic cations and Lewis basic oxide anions) can lead to anchored metal complexes with a high degree of uniformity when conducted under carefully controlled conditions (low-to-moderate temperatures, absence of moisture and/or O_2). Detailed characterization of these sites using spectroscopic methods, elemental analysis and reactivity studies leads to information about their structure and insight into the underlying structure of the oxide surface. Experiments with gold and silver complexes such as $\text{Me}_2\text{Au}(\text{acac})$ and $\text{Ag}(\text{acac})$ reveal that interactions with surface hydroxyls involving strong H-bonding to ligand donor atoms are primarily responsible for their dispersion as isolated metal sites. By modulating the hydroxyl density via thermal pretreatment, it is possible to control not only the surface density of metal atoms, but also their subsequent mobility. In the case of nucleation and subsequent autocatalytic growth of metal nanoparticles, it is possible to exert control over particle size via the initial metal complex-oxide surface interaction.

9:40am **SS+AS+HC-MoM5 Adsorption and Activation of CO_2 on $\text{Cu}(997)$ at Low Temperature, Jun Yoshinobu, The University of Tokyo, Japan**

Adsorption and activation of carbon dioxide on $\text{Cu}(997)$ were investigated by infrared reflection absorption spectroscopy (IRAS), temperature programmed desorption (TPD), and X-ray photoelectron spectroscopy (XPS). CO_2 molecules are physisorbed on $\text{Cu}(997)$ at temperatures below 70 K. However, the vibrational spectra of adsorbed CO_2 depend significantly on the substrate temperature; IR spectra of CO_2 vibrational modes at 70 K show asymmetric Fano line shapes. On the other hand, at 85 K, the dissociation of CO_2 into CO was observed on $\text{Cu}(997)$ by IRAS and XPS, but not on $\text{Cu}(111)$. In addition, the reaction of CO_2 on $\text{Cu}(997)$ surface at 340 K under CO_2 gas pressure of 0.8 mbar was investigated by ambient pressure XPS. A main reaction product on the surface was identified as carbonate (CO_3), based on estimation of the composition ratio of oxygen to carbon. CO_3 was produced on the surface through the reaction of CO_2 with atomic oxygen formed from CO_2 dissociation.

10:00am **SS+AS+HC-MoM6 D_2O Interaction with Planar $\text{ZnO}(0001)$ Bilayer Supported on $\text{Au}(111)$: Structures, Energetics and Influence of Hydroxyls, Xingyi Deng, D.C. Sorescu, J. Lee, National Energy Technology Laboratory**

Ultrathin oxides with single or few atomic layers are considered new types of due to the emergence of film-specific structures with properties distinct from their bulk counterparts. $\text{ZnO}(0001)$ bilayer grown on $\text{Au}(111)$ adopts a planar, graphite-like structure via an intralayer relaxation from the bulk wurtzite structure. In this work, we investigate the interaction between D_2O and the planar $\text{ZnO}(0001)$ bilayer grown on $\text{Au}(111)$ with temperature programmed desorption (TPD), low energy electron diffraction (LEED), X-ray photoelectron spectroscopy (XPS), and density functional theory (DFT) calculations. D_2O molecules adsorbed on this planar surface form two ordered overlayers, a (3×3) and a $(\sqrt{3} \times \sqrt{3})R30^\circ$, not seen before on any of the bulk ZnO single crystal surfaces. The apparent activation energies of desorption (E_d) estimated from TPD peaks agree well with the adsorption energy values calculated from DFT. The DFT calculations also reveal that both overlayers are mediated by extensive hydrogen bonding among the molecules but with different packing densities. The hydroxyl groups, accumulating very slowly on the $\text{ZnO}(0001)$ bilayer surface under the standard ultrahigh vacuum (UHV) environment, strongly suppress the formation of the $(\sqrt{3} \times \sqrt{3})R30^\circ$ overlayer but have less impact on the (3×3) overlayer. We suggest that the difference in packing densities of the overlayers leads to these findings such that only the (3×3) overlayer with a more open structure can accommodate small amounts of the adsorbed hydroxyls.

Monday Morning, November 7, 2016

10:40am **SS+AS+HC-MoM8 Nanoscale Silicon as a Catalyst for Graphene Growth: Mechanistic Insight from In-Situ Raman Spectroscopy**, **Keith Share**, R.E. Carter, Vanderbilt University; P. Nikolaev, D. Hooper, Air Force Research Laboratory; L. Oakes, A.P. Cohn, Vanderbilt University; R. Rao, Air Force Research Laboratory; A.A. Puzetzy, Oak Ridge National Lab; D.B. Geohegan, B. Maruyama, Air Force Research Laboratory; C.L. Pint, Vanderbilt University

Nanoscale carbons are typically synthesized by thermal decomposition of a hydrocarbon at the surface of a metal catalyst. Whereas the use of silicon as an alternative to metal catalyst could unlock new techniques to seamlessly couple carbon nanostructures and semiconductor materials, stable carbide formation in bulk silicon prevents the precipitation and growth of graphitic structures. Here, we provide evidence supported by comprehensive *in-situ* Raman experiments that indicates nanoscale grains of silicon in porous silicon (PSi) scaffolds act as catalysts for hydrocarbon decomposition and growth of few-layered graphene at temperatures as low as 700 K. Self-limiting growth kinetics of graphene with activation energies measured between 0.32 – 0.37 eV elucidates the formation of highly reactive surface-bound Si radicals that aid in the decomposition of hydrocarbons. Nucleation and growth of graphitic layers on PSi exhibits striking similarity to catalytic growth on nickel surfaces, involving temperature dependent surface and subsurface diffusion of carbon. This work elucidates how the nanoscale properties of silicon can be exploited to yield catalytic properties distinguished from bulk silicon, opening an important avenue to engineer catalytic interfaces combining the two most technologically-important materials for modern applications – silicon and nanoscale carbons.

11:00am **SS+AS+HC-MoM9 Functionalization of Graphene on Ru(0001) with Atomic Oxygen**, **Zbynek Novotny**, Pacific Northwest National Laboratory; F.P. Netzer, Karl-Franzens University, Austria; Z. Dohnálek, Pacific Northwest National Laboratory

Well-defined, monodispersed catalysts supported on oxidized carbon nanotubes are a promising class of new materials for heterogeneous catalysis. While such systems exhibit lower complexity compared to traditional catalysts, many questions, such as the reproducible preparation of carbon nanotubes and the range of functionalities used for anchoring of the clusters, make determination of their oxidation state and structure difficult. An analogous model system, graphene, can be prepared and studied under UHV conditions with great control. We employ scanning tunneling microscopy (STM) to study chemical functionalization of supported graphene on Ru(0001) with atomic oxygen. On Ru(0001) graphene forms a defect-free moiré structure with a periodicity of 3 nm, offering variety of distinct, regularly-spaced adsorption sites. Three different regions can be distinguished in STM images: bright regions (C atop of Ru) with the largest distance to the underlying Ru metal, dark hcp regions where graphene is closest to the metal, and medium-bright fcc regions where graphene is slightly further away compared to the hcp regions. Interestingly, for temperatures above 114 K, atomic oxygen (AO) is preferentially observed within the medium-bright fcc regions but in a minority of cases also in the hcp regions. The onset of AO mobility is observed at 400 K, where AO is occasionally moving inside the fcc region, or away from the less-stable hcp region towards the bordering fcc region. At higher temperatures (450-500 K), a dramatic increase in AO diffusion is observed allowing for AO transport between neighboring fcc regions through the hcp region. Upon encounter, the AO groups form stable immobile dimers and large clusters. The high-resolution time-lapsed data is used to assign the AO adsorption configuration to the on-top bonded enolate groups rather than the expected bridge-bonded epoxys. Our ongoing effort focuses on quantifying the enolate diffusion barrier and understanding their interactions with adsorbates such as H₂O, CO, and CO₂. The high thermal stability of enolate groups, and their large periodic separation (~3 nm) makes functionalized graphene/Ru(0001) an ideal model system for model studies of monodispersed catalysts.

11:20am **SS+AS+HC-MoM10 Interaction of BaO with H₂O, CO₂ and NO₂ Studied with APXPS and NEXAFS**, **Osman Karslioglu**, I. Zegkinoglou, L. Trotochaud, H. Bluhm, Lawrence Berkeley National Laboratory

Barium is a constituent of several technologically important materials such as NO_x storage and reduction (NSR) catalysts in automobiles, getters for UHV applications, perovskite catalysts for electrochemical reactions and high-temperature superconductors. Interaction of barium compounds with simple molecules such as H₂O, CO₂ and NO₂ is thus of practical importance. We studied the interaction of in-situ prepared BaO with H₂O, CO₂ and NO₂ as a function of temperature and pressure using ambient pressure X-ray photoelectron spectroscopy (APXPS) and near-edge X-ray absorption fine

structure (NEXAFS). Using in-situ preparation proved essential for preparing clean BaO, as the compound is extremely reactive even with minute amounts of H₂O and CO₂. We report the first experimental O K-edge X-ray absorption spectrum of clean BaO, for which the published spectra in the literature are more consistent with BaCO₃.

Thin Film

Room 105A - Session TF-MoM

ALD Precursors and Surface Reactions

Moderators: Robert Grubbs, Micron Technology, Erwin Kessels, Eindhoven University of Technology, Netherlands

8:20am **TF-MoM1 New Heteroleptic Precursors Enabling Industrial Scale ALD of Next Generation Metal Oxides and Metal Films**, **Nicolas Blasco**, Air Liquide, France

Thermal and Plasma Enhanced Atomic Layer Deposition (ALD & PEALD) have been major enablers to access new film systems in complex 3D architectures such as sub-14nm logics, sub 20nm DRAM architectures as well as new memory concepts. For example, new oxides film systems could be deposited in a conformal way. Similarly, Ni, Co, Ru metal (PE)ALD drew tremendous attention, with recent efforts towards selective deposition. Chemical functionalization requirements of ALD precursors have been more and more challenging, requiring creative approaches to overcome limitations of previous processes.

Leading groups in 2005-2006 opened the path to the use of “combinatorial” heteroleptic chemicals as ALD precursors. This approach consists in multi-functionalizing the molecule by combining the advantages of several ligand systems, and therefore empirically tailoring its physical and chemical properties (for instance melting point, volatility, thermal stability) - a traditional example being Air Liquide’s ZyALD™ precursor, ZrCp(NMe₂)₃. This concept has been extended to multiple ligands and elements. Beyond expected outcome (e.g. physical properties tuning), surprising effects have been observed such as synthesis yield improvement, deposited film crystallinity/stability impact, or even selective deposition.

In this work, achievements using this methodology with new ligand systems and elements will be presented. Specific emphasis will be put on necessary requirements for an industrially viable new precursor, and benchmark with standard molecules.

First, a new set of rare-earth/lanthanide (La, Lu, Sc, Y) precursors will be presented and characterized by various techniques, from a physical & chemical point of view (TGA, DSC, VP), and from deposition behavior point of view (growth rate, film composition). Those novel precursors, for instance combining amidinate (-(R¹NC(R²)NR³) and alkylcyclopentadienyl (CsRs) ligands, present unique properties which enable access to new material systems via ALD, not only ternary oxides in semiconductor field but also in other areas such as hydrophobic surfaces. This concept will be illustrated with new elements and for example new viable high yield liquid Scandium and lanthanum Oxide precursors will be introduced.

Second, recent improvements in Co, Ni metal ALD/PEALD processes will be presented, especially with the introduction of alkylsilyl ligands for Co precursors chemistry and allyl/amidinate ligands for Ni precursors chemistry. Applicability of those new precursors for advanced logics metal PEALD/ALD/CVD and their comparison with standard molecules (like dicobalt hexacarbonyl tert-butylacetylene - CCTBA) will be presented.

9:20am **TF-MoM4 Time-resolved IR Spectroscopy during ALD of La₂O₃/Al₂O₃ Nanolaminates**, **Brent Sperling**, J.E. Maslar, B. Kalanyan, National Institute of Standards and Technology (NIST)

Atomic layer deposition (ALD) of La₂O₃-containing films is of interest for high-k dielectric layers in semiconductor manufacturing. Characterization of as-deposited films is made difficult by the tendency of La₂O₃ to form lanthanum carbonates and hydroxides upon exposure to the atmosphere. Previous *in situ* studies have shown evidence for the formation of carbonates during the actual deposition process using an amidinate and water. *Ex situ* studies have found unusual growth behavior that is typically attributed to lanthanum hydroxide formation during deposition. One of the strategies often employed for establishing typical ALD-type growth in La₂O₃-containing films is the incorporation of a second oxide. Although known to be effective, the reasons why are not known. Here, we use time-resolved IR spectroscopy to study surface reactions during La₂O₃/Al₂O₃ nanolaminate formation. A laminar flow reactor using La(PrCp)₃, TMA, and H₂O as precursors is used. We show that, contrary to previous speculation,

non-ideal growth is not due to hydroxide formation. The benefits of incorporating the second oxide is unrelated to suppressing lanthanum hydroxide; alternate explanations must be considered.

9:40am TF-MoM5 Incomplete Elimination of Precursor Ligands during Atomic Layer Deposition of Metal Oxides, Adrie Mackus, Eindhoven University of Technology, Netherlands; **C. MacIsaac,** Stanford University; **V. Vandalon, W.M.M. Kessels,** Eindhoven University of Technology, Netherlands; **S.F. Bent,** Stanford University **INVITED**

Atomic layer deposition (ALD) has become an important technique for the deposition of ultrathin and conformal films for a wide variety of applications in nanoelectronics and photovoltaics. Although the reactions mechanisms of several metal oxide ALD processes have been investigated in detail, there are still some open questions regarding the understanding of their growth characteristics. ALD typically relies on two fundamental surface reactions: (i) the adsorption of a precursor molecule at specific surface groups (e.g. hydroxyl groups) in the first half-reaction, (ii) the elimination of the precursor ligands (while new functional surface groups are formed) in the second half-reactions. In this presentation, it will be shown that the elimination of precursor ligands is often not complete, which has broad implications for the growth characteristics of binary and ternary metal oxide ALD processes.

Experimental evidence for the presence of persisting ligands after the H₂O half-reaction at low temperatures (< 200 °C) will be presented for the binary ALD processes of Al₂O₃ from TMA, SnO₂ from TDMASn, and ZnO from DEZ. The data for Al₂O₃ was measured using broadband sum-frequency generation (BB-SFG) spectroscopy,¹ while the SnO₂ and ZnO processes were studied using Fourier transform infrared (FTIR) spectroscopy. The incomplete removal of precursor ligands will be explained based on previously reported density functional theory (DFT) studies on cooperative effects during the H₂O half-reaction.² In addition, we found that the elimination of precursor ligands is even less effective when ZnO ALD is carried out after SnO₂ ALD, which likely causes the nucleation delay that has been observed for ZnO during the growth of the ternary material zinc-tin-oxide (ZTO).^{3,4}

The consequences of the persisting ligands on the growth rate and temperature dependence of the binary ALD processes will be described. Moreover, it will be discussed that the incomplete removal of precursor ligands is expected to play an important role during many other ternary ALD processes, which can explain some of the deviating growth characteristics that have been reported.

1. V. Vandalon and W.M.M. Kessels, *Appl. Phys. Lett.* **108**, 011607 (2016)
2. M. Shirazi and S.D. Elliott, *Nanoscale* **7**, 6311 (2015)
3. M.N. Mullings *et al.*, *Thin Solid Films* **556**, 186 (2014)
4. C. Häggglund *et al.*, *J. Vac. Sci. Technol. A* **34**, 021516 (2016)

10:40am TF-MoM8 Surface Chemistry of Pt and Al₂O₃ ALD Studied with Vibrational Sum-Frequency Generation, Vincent Vandalon, W.M.M. Kessels, Eindhoven University of Technology, Netherlands

The surface chemistry during atomic layer deposition (ALD) of Al₂O₃ and Pt were investigated with vibrational broadband sum-frequency generation (BB-SFG) spectroscopy. These two processes represent examples of two different material classes for ALD: For metal oxides, ALD of Al₂O₃ with Al(CH₃)₃ and H₂O as reactants is the prototypical ALD process. Whereas for noble metals, ALD of Pt using MeCpPtMe₃ and O₂ as reactants can be considered as prototypical.

Vibrational BB-SFG spectroscopy is excellently suited for in-situ studies of the surface chemistry governing ALD because of its inherent interface selectivity, submonolayer sensitivity, and short acquisition times. It is a nonlinear optical technique which uses the mixing of picosecond visible and femtosecond mid-IR pulses to probe the vibrational response of surface groups. The unique nature of BB-SFG allows the *in-situ* investigation of the surface chemistry on both reflective and transparent substrate without any modifications to the setup.

For ALD of Al₂O₃, both the -CH₃ and -OH surface groups ruling the growth mechanism were monitored in-situ with BB-SFG. This study resulted in several new insights into the surface chemistry of this ALD process: Persistent -CH₃ groups were observed after the H₂O half-cycle at low temperatures and these significantly influence the growth [Vandalon and Kessels, *Appl. Phys. Lett.*, 2016, Vol. 108] Moreover, the reaction kinetics were studied as a function of temperature and reaction cross sections for both half-cycles were quantified. At low temperatures it was found that the reaction kinetics in the H₂O half-cycle showed a strong dependence on

surface coverage. Furthermore, the initial growth of Al₂O₃ on H-terminated silicon was investigated.

ALD of Pt was studied with BB-SFG by probing the C-H stretch region around 3000 cm⁻¹. After precursor exposure, the signature of the C-H stretch mode of the -CH₃ groups was clearly observed. Moreover, a spectrally broad feature was observed in the BB-SFG spectra. This contribution was assigned to unsaturated C chains such as present in the Cp ring. Dosing gas phase MeCp on a Pt and SiO₂ surfaces showed a similar broad feature, supporting this assignment. After O₂ exposure both the -CH₃ and Cp related signals disappeared. These results suggest that after precursor adsorption both -CH₃ and Cp rings (or parts of it) are present at the surface and these groups are removed in the O₂ half-cycle.

11:00am TF-MoM9 Surface Chemistry of Molybdenum Oxide Atomic Layer Deposition: Role of Precursor Chemisorption on Nucleation Delay and Initiating the ALD Process, Charith Nanayakkara, A. Vega, The University of Texas at Dallas; **G. Liu, C. Dezelah, R. Kanjolia,** SAFC Hitech; **Y.J. Chabal,** University of Texas at Dallas

Atomic layer deposition (ALD) is an attractive technique for thin film deposition due to its sequential and self-limiting surface reactions leading to conformal and controlled film growth. However, nucleation delays (incubation) can lead to non-uniform island growth, particularly for metal films, often requiring many cycles to obtain a continuous film.

Molybdenum oxide thin films are important for a number of electrical, catalytic, and optical applications. Several Mo precursor-oxidant combinations have been used. For instance, molybdenum hexacarbonyl and ozone (with ALD window between 152 and 172 °C),¹ and Bis(tert-butylimido)bis(dimethylamido) molybdenum and ozone (with an ALD window between 250 and 300 °C)² gave good film with higher nitrogen content at deposition temperatures less than 250 °C for the latter.² The use of oxygen plasma with bis(tert-butylimido)bis(dimethylamido) molybdenum has shown film growth between 50 - 350 °C with high elemental H (4 - 11%).³

Here, we introduce a new molybdenum precursor, Si(CH₃)₃CpMo(CO)₂(η³-2-methylallyl) (MOTSMA), which has a good thermal stability (>200 °C), higher volatility with increased vapor pressure (3s exposure results 0.6 Torr gas phase pressure with bubbler at 90 °C), and increased deposition rates. However, *In-situ* FTIR spectroscopy of the MOTSMA and ozone ALD process reveals that there is a ~15 cycle incubation period at 250°C on OH-terminated oxidized Si(100) surfaces. After this incubation period, i.e. once the steady state ALD process is established, the expected ligand exchange is observed, with formation of surface Si(CH₃)₃CpMo(η³-2-methylallyl) species after the precursor exposure and their removal during the ozone pulse, resulting in Mo(=O)₂ surface species. Since this nucleation delay can be reduced by raising the temperature above 300°C, the initial adsorption of the precursor on OH-terminated surfaces was examined as a function of temperature. Indeed, this initial adsorption of MOTSMA on OH-terminated surfaces was found to require higher temperatures. Therefore, we used an initial 350 °C MOTSMA grafting step in order to overcome the nucleation delay but then performed the ALD process at 250 °C and 300 °C. In this manner, steady state film growths with no nucleation delay were obtained at both temperatures, with stoichiometric composition (MoO₃) as confirmed by X-ray photoelectron spectroscopy. The current study highlights the critical role of precursor grafting on eliminating the nucleation delay for ultra-thin ALD grown film deposition.

1. *J. Mat. Chem.* **2011**, 21, 705
2. *J. Vac. Sci. & Tech. A* **2014**, 32, 01A119
3. *J. Vac. Sci. & Tech. A* **2016**, 34, 01A103

11:20am TF-MoM10 In situ FTIR Study of the Surface Reactions during Plasma-assisted Atomic Layer Deposition of SiN_x from Silicon Amides, Naomi Leick, R.A. Ovanessian, R.J. Gasvoda, P. Walker, Colorado School of Mines; **K.M. Kelchner, D.M. Hausmann,** Lam Research Corporation; **S. Agarwal,** Colorado School of Mines

Recently, atomic layer deposition (ALD) of silicon nitride (SiN_x) films has been increasingly researched for applications with stringent conformality and processing temperature (≤ 400°C) requirements, such as conformal spacer or etch stop dielectric material in 3-D transistors and air gap interconnect technologies. The necessity for a low-temperature ALD process has shifted focus toward plasma-assisted ALD, mainly using N₂ or NH₃ plasmas. While Cl-based Si precursors have been widely used in ALD of SiN_x films due to their high reactivity, these precursors also form undesirable corrosive byproducts. Silicon amide precursors can overcome these challenges while maintaining a sufficiently high reactivity for ALD.

Monday Morning, November 7, 2016

In this contribution, the focus will be on the growth mechanism of SiN_x films during ALD using H₂Si(N(C₂H₅)₂)₂ (BDEAS) and N₂ or NH₃ plasma, at substrate temperatures between 200 – 300 °C. Specifically, we have employed *in situ* attenuated total reflection Fourier transform infrared (ATR-FTIR) spectroscopy to study the film composition, surface reactions during each half-cycle, and the surface species involved in the growth process. From these measurements, we conclude that BDEAS adsorption occurs via a ligand-exchange reaction between one of the diethylamino ligands and surface H, liberating HN(C₂H₅)₂ into the gas phase as the main reaction by-product. During the N₂ plasma based ALD process, the N₂ plasma removes the remaining diethylamino ligands from the surface and restores the surface sites necessary for BDEAS chemisorption during the subsequent cycle. The hydrocarbon species on the surface during the N₂ plasma step also leads to the incorporation of C_xN_y species in the SiN_x film. In contrast to the N₂ plasma-based process, NH₃ plasmas in combination with very similar amide precursors have been reported to inhibit SiN_x growth. While our results ultimately confirm these findings, our infrared measurements show that SiN_x growth can initially be achieved with a NH₃ plasma, but attenuates rapidly after the first 5 cycles. The infrared data however suggests that the NH₃ plasma leads to complete removal of the carbon-containing species leading to C-free SiN_x films. Since the composition of SiN_x films deposited by ALD using amide precursors is affected by the nitrogen source in the plasma, a 3-step ALD process involving a NH₃ plasma (to remove C-containing species) followed by a N₂ plasma (to restore surface reactive sites) can potentially optimize the film composition and growth process.

Vacuum Technology

Room 104C - Session VT-MoM

Vacuum Measurement, Calibration, Primary and Industry Standards

Moderators: Yulin Li, Cornell Laboratory for Accelerator-Based Sciences and Education, Joe Becker, Kurt J. Lesker Company

8:20am VT-MoM1 Industry Practice for Using Primary Leak Standards to Validate Calibration Methods, *Jason Alfrey*, VACUUM TECHNOLOGY INC INVITED

Accredited metrology labs are required to maintain traceability to a primary laboratory and periodically validate measurement methods. For calibration laboratories operating multiple systems, what is a suitable process to validate measurements and prove traceability while still being economically competitive?

Vacuum Technology, Inc (VTI) utilizes two methods for gas flow measurement of Leak Standards – both primary and comparison methods. Although these are well established methods in the industry, an accredited laboratory is always interested in proving it is linked to the “chain of metrology.” The following discussion presents the methods for both inter-laboratory and intra-laboratory testing using Primary Leak Standards calibrated by NIST.

9:00am VT-MoM3 Fixed Length Optical Cavity for Photonic Realization of the Pascal, *Jay Hendricks, J. Ricker, P. Egan, J. Stone, G. Scace, G.F. Strouse*, National Institute of Standards and Technology

NIST is actively developing a new paradigm in the methodology of pressure and vacuum gauging and metrology. In a break with nearly 400 years of mercury based primary standards, NIST has developed a new standard that is based on the fundamental physics of light interacting with a gas. For the vacuum community, this represents a shift in how we think about the unit of the Pascal in that it will be directly related to the density of a gas, the temperature, the refractive index, and the Boltzmann constant. The photonic technique has now achieved important benchmarks in performance when compared to the existing primary standards based on mercury manometers: The photonic technique has a 20X smaller footprint, 100X faster sensing response time, 100X lower pressure range, and for an emerging technique has demonstrated impressive accuracy, reproducibility and hysteresis. Photonic sensing of the pascal has the potential to be further miniaturized, and has the key advantage that the light used for sensing the pressure can be transmitted over light-weight, high-speed fiber optic cables and networks. This talk will highlight the NIST efforts to replace our mercury Ultrasonic Interferometer Manometers (UIMs) with the new quantum-based, photonic technique. New data will be presented that shows that two independent Fixed Length Optical Cavities are now operating with part per million reproducibility and measurement

agreement. The optical technique has now surpassed mercury manometer performance, and a new paradigm for vacuum metrology and realization of the SI unit, the pascal has begun.

9:20am VT-MoM4 Analysis of a Quantum Based Refractometer to Replace Mercury Manometers as the Primary Standard for the United States, *Jacob Ricker, J. Hendricks, P. Egan, J. Stone*, NIST

NIST has developed a technique to measure pressure using the gas refractivity of nitrogen for pressures in the range of 1 Pa to 360 kPa. This range is critical to many application including altimetry, weather, process control, etc.; all of which require high accuracy calibration of vacuum gauges. Currently the highest claimed accuracy of a primary standard is the NIST mercury Ultrasonic Interferometer Manometers (UIMs) operating at an uncertainty of $U(P_{UIM}) = [(6 \text{ mPa})^2 + (5.2 \cdot 10^{-6} \text{ P})^2]^{1/2}$. NIST proposes replacement of these standards with an optical gas refractometer with an uncertainty of $U(P_{OGR}) = [(2.0 \text{ mPa})^2 + (8.8 \cdot 10^{-6} \text{ P})^2]^{1/2}$.

The optical refractometer has many benefits over the current UIMs, however we also need to show the feasibility of the fixed length refractometer as a primary standard. The two key requirements to define a primary standard are traceability of the standard back to the International System of Units (SI) and the ability to transfer the measurement/uncertainty to a high accuracy gauge or a transfer standard. The traceability and associated uncertainty will be discussed along with the derivation of the above stated uncertainty for the optical gas refractometer. Additionally, results of a calibration using the refractometer will be compared to that obtained using the NIST UIM. The capability and limitations of both the refractometer and UIM will be discussed and will show that the refractometer outperforms the UIM and will be slated to replace the mercury standards in the near future.

9:40am VT-MoM5 Creating Vacuum Standards in the UHV and XHV to Support Cold-Atom Physics and Other Cool Stuff, *James A. Fedchak, J. Scherschligt, M.S. Sefa, S. Eckel, D. Barker*, National Institute of Standards and Technology (NIST)

We are creating a program at NIST to develop new vacuum standards that cover the UHV and XHV. This addresses the needs of advanced manufacturing and research, including the semiconductor industry, accelerators, nanotechnology, and space science. NIST is also interested in developing metrological tools and other practical devices based on ultra-cold atoms, a technology pioneered at NIST that fundamentally operates in the UHV. Gravimeters, inertial sensing, and clocks are all examples of such devices, and any such device based on ultra-cold atoms will necessarily operate in UHV. To this end, we are presently developing a cold-atom vacuum standard (CAVS) to absolutely determine the vacuum level in the range of 10⁻⁷ torr to 10⁻¹² torr. Our CAVS will use ultra-cold atoms to sense the absolute number density of gas molecules in the vacuum, and will be an SI traceable primary realization of UHV and XHV. In addition, we're developing the Cold-Core Technology program, which seeks to create a platform enabling the miniaturization of the CAVS and other practical cold-atom devices. An active UHV and XHV program is critical and necessary for this effort. This includes traditional activities such as producing and measuring low-outgassing rate materials and building dynamic expansion chambers for generating UHV pressures, as well as new efforts like building the CAVS. This talk will be an overview of these activities in light of creating the CAVS and other devices based on ultra-cold atom technology.

10:00am VT-MoM6 Technical Challenges of the Cold Atom Vacuum Standard, *Julia Scherschligt, J.A. Fedchak, M.S. Sefa, S. Eckel, D. Barker*, National Institute of Standards and Technology (NIST)

NIST has recently launched a program combining cold-atom physics with vacuum metrology and has begun to build the Cold Atom Vacuum Standard (CAVS). Development of the cold atom vacuum standard presents a variety of technical challenges: we need a thorough understanding of the collision cross section of trapped atoms with background gas, we need to achieve excellent vacuum levels and prevent contamination of the test system with sensor alkali atoms, and we need a robust and user-friendly design if the device is ever to be practical for real-world applications. We will discuss progress that has been made in determining collision cross sections, measuring and reducing outgassing rates, as well as design considerations of the cold atom device itself.

Monday Morning, November 7, 2016

10:40am **VT-MoM8 Investigation of a Novel Cold Cathode Ionization Gauge Geometry with Wide Range from High Vacuum to Atmosphere in a Single Gauge**, *T.R. Swinney, C. Percy, Gerardo Alejandro Brucker*, Pressure & Vacuum Measurement Solutions, MKS Instruments, Inc.

Wide range vacuum gauges are in use now, however, all rely on multiple technology sensors with various mismatched pressure responses for various gases. An overview of the problems created by multiple technologies and mismatched pressure responses along with novel solutions will be presented. A new internal geometry of a cold cathode ionization gauge has been investigated and has produced a usable pressure signal from high vacuum to atmosphere, using only one gauge and only one physical electronics mechanism, namely a gaseous discharge. A redesigned electrode structure avoids mixing differences in gauge types and their responses to different gas types when using multiple gauge types over this full range. Careful choice of the anode-to-cathode spacing can sustain a gaseous discharge with the usual electric and magnetic fields. The various electrical signals used to display a pressure read-out will be presented and compared. This was accomplished during the investigation with available control circuitry.

11:00am **VT-MoM9 Advanced Manufacturing Techniques for Cold Cathode Ionization Gauges**, *Clinton Percy*, Pressure & Vacuum Measurement Solutions, MKS Instruments, Inc.

Cold cathode ionization gauges (CCIGs) have been used for decades to make high vacuum measurements on a variety of production and laboratory equipment. Interestingly, the manufacturing techniques used to produce these gauges have not appreciably changed during this same time period. Furthermore, the typical, currently marketed extended-range CCIG products involve multiple gauging technologies, which introduce additional complexity and costly design challenges. Our laboratory investigated the impact on gauge cost and performance of a variety of materials, manufacturing techniques, electronic circuit designs and sensor technologies that could be employed to produce a reduced cost CCIG that can measure an extended pressure range. The outcomes of this investigation resulted in improved design techniques which have been implemented in a prototype embodiment of a wide pressure range CCIG.

11:20am **VT-MoM10 Operation and Performance of a Wide Range Cold Cathode Ionization Gauge**, *Tim Swinney, C. Percy*, Pressure & Vacuum Measurement Solutions, MKS Instruments, Inc.

A novel wide range cold cathode ionization gauge (CCIG), capable of measuring pressures from high vacuum to atmosphere and relying on only one gauge and only one physical electronics mechanism, was recently developed in our laboratory. Many technical challenges exist in operating a CCIG above the standard 10^{-2} Torr upper limit of the current CCIGs available on the market. We will present detailed operational aspects of our new sensor technology including: (1) selection criteria for the discharge characteristics used to derive pressure measurements, (2) accuracy of the pressure measurements produced and (3) long term stability and lifetime of the technology over its wide pressure range.

11:40am **VT-MoM11 Improving Process Resistance of Capacitance Diaphragm Gauges**, *B. Andreas, C. Strietzel, Martin Wüest*, INFICON Ltd., Liechtenstein

Process industry is constantly changing. New manufacturing processes using new chemistries are developed that can also affect sensors. Yet, quality and cost pressure demand that processes are highly reliable, repeatable and need fewer maintenance interruptions. For capacitance diaphragm gauges, process stability means that process effects on the diaphragm deflection remain in the 1 nm range for a diaphragm with 30 mm diameter. To cope with this we have investigated ways to better protect the CDGs from process related influences. We will present results from experiments performed with protective layers.

2D Materials Focus Topic

Room 103B - Session 2D+MI-MoA

Dopants, Defects and Interfaces in 2D Materials

Moderators: Philip Hofmann, Aarhus University, Denmark, Adina Luican-Mayer, University of Ottawa, Canada

1:40pm 2D+MI-MoA1 High-k Dielectrics on WSe₂ by Ozone-based Atomic Layer Deposition: An In-situ XPS Study, Angelica Azcatl, R.M. Wallace, The University of Texas at Dallas

Two-dimensional tungsten diselenide (WSe₂) is a layered material that have shown a promising performance when implemented in field effect transistors, exhibiting a hole mobility up to 250 cm²/V·s. [1] Furthermore, WSe₂ possess hole and electron effective masses smaller than those of MoS₂, another widely studied transition metal dichalcogenide, making WSe₂ a promising candidate channel material for tunnel field effect transistor applications (TFETs). For the realization of WSe₂ based TFETs, a high quality ultra-thin high-k dielectric film is a key requirement. However, the integration of high-k dielectrics by a conventional atomic layer deposition (ALD) process results challenging due to the dearth of nucleation sites at the WSe₂ surfaces. Previous studies have shown that the deposition of high-k dielectrics by water-based ALD on WSe₂ leads to non-uniform dielectric films. [2]

In this work, we explore the use of an alternative ALD approach to obtain uniform dielectric films on WSe₂ through the use of ozone as oxidant precursor. The surface chemistry of WSe₂ upon ozone exposure was studied by in-situ X-ray photoelectron spectroscopy to understand the reactivity between ozone and the WSe₂ surface. Then, the ozone-based ALD process was studied for the deposition of Al₂O₃ and HfO₂ on WSe₂. It was found that the interfacial chemistry and the nucleation of the dielectric have a dependence on the deposition temperature. Based on these results, a temperature window was identified at which interfacial oxide formation is avoided while a uniform dielectric film is obtained. Furthermore, the differences in reactivity and growth rate between HfO₂ and Al₂O₃ will be discussed. This study helps to elucidate the reaction mechanism of the ozone based ALD process on WSe₂ and facilitates the implementation of the ozone based ALD approach to obtain uniform and thin dielectric films on WSe₂ for TFETs applications.

This work is supported in part the Center for Low Energy Systems Technology (LEAST), one of six centers supported by the STARnet phase of the Focus Center Research Program (FCRP), a Semiconductor Research Corporation program sponsored by MARCO and DARPA, and by the SWAN Center, a SRC center sponsored by the Nanoelectronics Research Initiative and NIST.

References

- [1] H. Fang, et al., Nano Lett. 2012, 12, 3788–3792
- [1] A. Azcatl, et al. 2D Materials, 2015, 2, 1, 014004

2:00pm 2D+MI-MoA2 A Two-step Atomic Layer Etching on MoS₂ Realized by Remote O₂ Plasma, Hui Zhu, X. Qin, L. Cheng, A. Azcatl, J. Kim, R.M. Wallace, University of Texas at Dallas

Molybdenum disulfide (MoS₂), a representative layered transition metal dichalcogenide, has obtained considerable research interest in recent years, due to its promising mechanical, electronic, and photonic properties.^{1,2} The mechanical exfoliation of MoS₂ has led to an intensive research on thin film field-effect transistors made with MoS₂ flakes.^{3,4} However, the scalable layer engineering of MoS₂ flakes is still a challenge for device fabrication. In this work, a novel MoS₂ functionalization and layer thinning process is presented by combining the surface oxidation of MoS₂ with a remote O₂ plasma to form an amorphous MoO_x layer and subsequent annealing to selectively desorb the MoO_x surface layer. Exfoliated MoS₂ is shown to chemically oxidize in a layered manner upon exposure to the remote O₂ plasma. X-ray photoelectron spectroscopy (XPS), low energy electron diffraction (LEED), and atomic force microscopy (AFM) are employed to characterize the surface chemistry, structure and topography of the oxidation process, and indicates that the oxidation mainly occurs on the topmost layer without altering the chemical composition of underlying layer. After the desorption of MoO_x by the annealing at 500 °C, a clean, flat and chemically undisturbed MoS₂ surface as evidenced from XPS, LEED, AFM and scanning tunneling microscopy (STM) characterization. This work renders promising atomic scale fabrication applications such as surface functionalization, charging engineering and atomic layer etching.

This work was supported in part by the SWAN Center, a SRC center sponsored by the Nanoelectronics Research Initiative and NIST, the Center for Low Energy Systems Technology (LEAST), one of the six SRC STARnet Centers, sponsored by MARCO and DARPA, and the US/Ireland R&D Partnership (UNITE) under the NSF award ECCS-1407765.

Reference

- ¹ T. Cao, G. Wang, W. Han, H. Ye, C. Zhu, J. Shi, Q. Niu, P. Tan, E. Wang, B. Liu, and J. Feng, Nat. Commun. **3**, 887 (2012).
- ² B. Radisavljevic, A. Radenovic, J. Brivio, V. Giacometti, and A. Kis, Nat. Nanotechnol. **6**, 147 (2011).
- ³ M.S. Fuhrer and J. Hone, Nat. Nanotechnol. **8**, 146 (2013).
- ⁴ S. Kim, A. Konar, W.-S. Hwang, J.H. Lee, J. Lee, J. Yang, C. Jung, H. Kim, J.-B. Yoo, J.-Y. Choi, Y.W. Jin, S.Y. Lee, D. Jena, W. Choi, and K. Kim, Nat. Commun. **3**, 1011 (2012).

2:20pm 2D+MI-MoA3 Engineering the Atomic Structure of 2D Transition Metal Dichalcogenides using Electron Beam: Experiments and Simulations, Arkady Krasheninnikov, Helmholtz Zentrum Dresden-Rossendorf, Germany INVITED

Following isolation of a single sheet of graphene, many other 2D systems such as hexagonal BN sheets and transition metal dichalcogenides (TMD) were manufactured. Among them, TMD sheets have received particular attention, as these materials exhibit intriguing electronic and optical properties. Moreover, the properties can further be tuned by introduction of defects and impurities. Specifically, as many in-situ transmission electron microscopy experiments indicate, electron beam irradiation can give rise to phase transitions in 2D TMDs (e.g., from H to T phase), development of line defects and domains with mirror symmetry, and other structural transformations. In my talk, I will present the results [1] of our first-principles theoretical studies of the response of 2D TMDs to electron irradiation, and dwell on the characteristics of irradiation-induced defects, their evolution and agglomeration. I will also touch upon beam-mediated phase transitions in 2D TMDs. The theoretical results to be presented were obtained in close collaboration with several experimental groups, so that a detailed comparison of the theoretical data and experimental results will be given. Finally, I will further discuss defect- and impurity-mediated engineering of the electronic structure of 2D TMDs.

[1] Nature Comm. **6** (2015) 6736; ACS Nano **9** (2015) 3274; ACS Nano (2015) ACS Nano **9** (2015) 11249; Phys. Rev. B **91** (2015) 125304; Adv. Mater. **26** (2014) 2857; Phys. Rev. X **4** (2014) 031044; see <http://users.aalto.fi/~ark/publist.html> for complete list of publications.

3:00pm 2D+MI-MoA5 New Computational Tool for Electron Localization: Application to Low-dimensional Monolayers of h-BN and MoS₂, Chinedu Ekuma, NRC/NRL Postdoctoral Fellow; V. Dobrosavljevic, Florida State University; D. Gunlycke, Naval Research Laboratory

Low-dimensional monolayer materials such as graphene, MoS₂, and hexagonal BN (h-BN) exhibit electronic degrees of freedom that produce exotic properties, which can be fine-tuned to engineer new functionalities for diverse applications. However, the performance of device applications depends strongly on the defect morphology and the quality of the sample. Herein, we explore the role of vacancy and/or Hubbard-type interactions for a spin-1/2 system in monolayer MoS₂ and h-BN. We utilize a first-principles many-body typical medium dynamical cluster formalism, which is an effective medium approach with an intrinsic order parameter for characterizing disordered and/or interacting electron systems even in the regime of insulator-metal quantum transition (IMQT). The focus is mainly on the distribution of the local density of states, which is a key fingerprint of the optoelectronic properties of disordered systems. Within our formalism, we predict an IMQT in both systems and show that IMQT in h-BN is due to a combination of electron interactions and defects. A sulfur vacancy concentration as low as 0.01% in MoS₂ is shown to lead to an IMQT in agreement with experiments.

3:20pm 2D+MI-MoA6 Effects of helium-ion beam irradiation on optoelectrical properties of multi-layers WSe₂, Anna Hoffman, P.R. Pudasaini, M.G. Stanford, P.D. Rack, D.G. Mandrus, N. Cross, J.H. Noh, M. Koehler, G. Duscher, The University of Tennessee Knoxville; A. Belianinov, A.J. Rondinone, Oak Ridge National Laboratory; I. Ivanov, T.Z. Ward, Oak Ridge National Lab

Transition metal dichalcogenides (TMD) possess interesting properties that render them attractive for opto-electronic applications. Tuning optical and electrical properties of mono and few layer TMDs, such as tungsten diselenide (WSe₂), by inducing defects is an intriguing opportunity to

fabricate the next generation opto-electronic devices. Here we report the effects of helium ion beam irradiation on optical and electrical properties of few layer WSe₂. By controlling the ion dose irradiation, we can tune the concentration of point defects present on few layer WSe₂, thereby locally tuning the electrical resistivity of the material. Semiconductor-insulator-metal like transitions have been observed with exposure to increasing helium ion beam dose, resulting in more than a seven order change in electrical resistivity. Furthermore, by selectively exposing the ion beams at the metal-WSe₂ contact area, we demonstrate reduced contact resistance of the described device, thereby reducing the Schottky barrier height. This could be particularly interesting for single layer TMD devices as the Schottky contacts, formed at metal/semiconductor interfaces, have a huge influence on the TMD device's performance.

4:00pm 2D+MI-MoA8 CO₂ Adsorption Kinetics on Nitrogen Doped Graphene and Graphite, Takahiro Kondo, R. Shibuya, D. Guo, J. Nakamura, University of Tsukuba, Japan

Nitrogen doped carbon materials are known to have CO₂ adsorption property at room temperature under atmospheric pressure. Recently, we have clarified that the CO₂ adsorption property is created by the one of the specific type of nitrogen dopants, pyridinic-N, which has two N-C bonds based on the temperature programmed desorption (TPD) measurements of CO₂ from nitrogen-doped graphene nanosheets (N-GNS) and nitrogen-doped model graphite (N-HOPG) catalysts [1]. According to our scanning tunneling microscopy and spectroscopy (STM/STS) measurements of N-HOPG, the CO₂ adsorption sites are suggested as the carbon atoms next to the pyridinic-N, where the distinct localized states are formed at near the Fermi level in the occupied region as non-bonding p_z orbital of carbon which plays a role of Lewis base site [2]. Furthermore, based on the X-ray photoelectron/absorption spectroscopy, we found that the adsorbed CO₂ is lying flat on the N-HOPG surface [3]. In this work, we reports the kinetics of CO₂ adsorption on both N-GNS and N-HOPG. From the measurements of CO₂-TPD, the desorption temperatures of CO₂ have been found to be 373 K in both N-GNS and N-HOPG, indicating that the same Lewis base sites are formed on N-GNS and N-HOPG. The adsorption energy can be roughly estimated as 100 kJ/mol from the desorption temperature. The relatively small adsorption energy can be attributed to the larger activation barrier and/or small pre-exponential (frequency) factor for CO₂ adsorption. The adsorption probability of CO₂ at 300 K has been estimated to be as 1/100 for N-HOPG. The detail kinetics as well as the selectivity for the CO₂ adsorption among many type of mixture gas will be presented.

[1] D. Guo, R. Shibuya, C. Akiba, S. Saji, T. Kondo, J. Nakamura, Science 351 (2016) 361.

[2] T. Kondo, S. Casolo, J. Nakamura et al., Phys. Rev. B 86 (2012) 035436.

[3] H. Kiuchi, R. Shibuya, T. Kondo, J. Nakamura, et al., Nano. Res. Lett. 11 (2016) 127.

4:20pm 2D+MI-MoA9 Electronic Structure of Metallic Twin Grain Boundaries in Monolayer MoSe₂, Matthias Batzill, University of South Florida

Monolayers of MoSe₂ grown by molecular beam epitaxy on van der Waals substrates (HOPG or MoS₂), may exhibit twin grain boundaries. These Se-deficient line defects have been predicted by DFT to be metallic with dispersing bands. We examine their structural and electronic properties by scanning tunneling microscopy (STM) and angle resolved photoemission spectroscopy (ARPES). A dispersing parabolic band is observed that intersects the Fermi-level indicating the metallic property of this defect. Below 235 K the line defect undergoes a Peierls, or charge density wave (CDW), transition. STM indicates a periodicity of 3 lattice constants of the CDW consistent with the Fermi-wavevector determined in ARPES. In addition, we determine that the defect behaves like an ideal one-dimensional metal. More specifically we show evidence of Tomonaga-Luttinger liquid suppression of the density of states at the Fermi-level and the splitting of the band in a 'spinon' and 'holon' band, also known as spin-charge separation.

Applied Surface Science

Room 101B - Session AS+BI-MoA

Practical Surface Analysis I: Advancing Biological Surface Analysis/Imaging Beyond 'Show and Tell'

Moderators: Ian S. Gilmore, National Physical Laboratory, UK, Jordan Lerach, The Pennsylvania State University

1:40pm AS+BI-MoA1 A Multi-technique Approach for Studying the Effect of Protein G B1 Orientation on Antibody Binding, Elisa Harrison, G. Interlandi, D.G. Castner, University of Washington

The orientation of adsorbed proteins on surfaces plays a vital role in the function and performance of biomaterials. Development of diagnostic tools such as sandwich ELISAs have focused on controlling the orientation of each protein layer. A full understanding of adsorbed proteins on surfaces, especially at the molecular level, is therefore essential. Our research addresses the challenges for characterizing protein orientation by developing new methods to study multilayer protein systems.

The aims of this study were to control and characterize the orientation of protein G B1, an IgG antibody-binding domain of protein G, on well-defined surfaces and measure the effect of its orientation on antibody binding using a variety of surface-sensitive tools and simulations. We hypothesize that binding selectivity would increase for well-ordered protein films due to higher availability of binding domains.

The surface sensitivity of time-of-flight secondary ion mass spectrometry (ToF-SIMS) enables us to distinguish between different proteins and their orientation by monitoring the changes in intensity of amino acid mass fragments. We have developed ToF-SIMS methods for analyzing the orientation of five different cysteine mutants of protein G B1 covalently attached to a maleimide surface. This technique was further extended by studying multilayer protein systems, specifically the binding of IgG antibodies to the protein G B1 films.

To study the effect of protein orientation on antibody binding, we utilized self-assembled monolayers (SAMs) to form protein G B1 films with both random and well-defined orientations. Using complementary techniques, such as X-ray photoelectron spectroscopy and quartz crystal microbalance with dissipation monitoring (QCMD), the ratio of bound IgG antibodies to protein G B1 increased from 0.06, when chemisorbed onto bare gold, to 0.2, when covalently attached to the surface. Further analysis revealed structure/orientation rearrangement of protein G B1 upon adsorption onto bare gold, which is likely responsible for decreased antibody binding.

Additionally, we developed and applied Monte Carlo (MC) simulations to predict protein orientation on a surface. The MC simulations showed that the outermost β -sheet of protein G B1 interacts most frequently with a hydrophobic surface. The predicted orientations were verified using molecular dynamics simulations, QCMD, and sum frequency generation.

The model systems explored in this study are a first step in developing methodology using state-of-the-art tools that can be applied to more complex systems and expand our knowledge and control of biomolecules on surfaces.

2:00pm AS+BI-MoA2 ME-SIMS Revisited: Attempting to Unlock the Potential using Advancements in Sample Preparation and SIMS Technology, Nina Ogrinc Potocnik, Maastricht University, The Netherlands; C.R. Anderton, L. Pasa-Tolic, Pacific Northwest National Laboratory; R.M.A. Heeren, Maastricht University, The Netherlands

This year marks the 20th anniversary of Wu and Odom first describing the application of a solid organic matrix to improve the ionization efficiency of molecular species in secondary ion mass spectrometry (SIMS) measurements. This so-called matrix enhanced-SIMS (or ME-SIMS) method overcame one of the disadvantages of SIMS analysis, providing the capability of imaging large molecules with high spatial resolution. With increased ionization efficiency and minimized fragmentation caused by the primary ion beam, the method is ideal for detection of intact bimolecular species, where detection of proteins greater than 10,000 Da is feasible. However, the combination of instrumentation limitations of resolving isobaric compounds and lateral diffusion caused by matrix application has pushed this technique into near irrelevance. Here, we reevaluate ME-SIMS with new technologies such as parallel MS/MS capabilities on the PHI nano-TOF TRIFT V, and the custom-build FTICR-SIMS capable of unmatched mass resolving power and mass accuracy. We also explore new matrix application techniques to revisit the potential of ME-SIMS and apply it to a number of different biological settings.

Monday Afternoon, November 7, 2016

Specifically, we reexamined peptide standard profiling with the addition of tandem MS on the nano-TOF TRIFT V. The ability to isolate precursor ions with a 1 Da mass window, followed by a high-energy collision-induced dissociation (CID), enables a very precise fragmentation of molecules. We observe peptide fragmentation through the amino terminus, a_m , providing us with a specific fragmentation pattern for identification of peptide species and opening doors to *de novo* peptide sequencing. Further on, we applied it for characterizing tryptically digested peptides investigating the applicability to bottom-up proteomics. We then imaged model plant and mammalian tissue sections that were subjected to a variety of different matrices *via* supplantation using a home-built sublimation chamber. Matrix sublimation produces small, homogenous crystal sizes, without the need for solvents that delocalize molecular species. Consecutive sections were analyzed by FTICR-SIMS, to accurately identify molecular species of interest, and by the nano-TOF TRIFT V for high lateral resolution images and confident identification of said species with tandem MS.

2:20pm AS+BI-MoA3 Improvements in SIMS Methods and Instrumentation in Effort to Make Measurements Biologists Can Use, Christopher R. Anderton, Pacific Northwest National Laboratory **INVITED**

The ability of mass spectrometry imaging (MSI) to visualize chemical distributions within samples has made it an increasing popular method in many biological fields, including medicine, pathology, and microbial ecology. Secondary ion mass spectrometry (SIMS) is a surface sensitive MSI technique that offers extensive versatility in its ionization and analysis modes, requires relatively minimal preparation, and can achieve the highest lateral resolution of any MSI method. Early bio-applications of SIMS routinely focused on pursuing the molecular information attainable by softer ionization methods (e.g., matrix assisted laser desorption/ionization), but with the added benefit of achieving subcellular lateral resolution. Even though primary ion beams used in SIMS measurements afford smaller probing areas than other ionization methods, their excessive energy typically causes extensive fragmentation of most biorelevant molecules. This renders identification of parent molecules from the detected secondary ions a nontrivial endeavor. Nevertheless, recent improvements in SIMS instrumentation, methods, and data analysis approaches have unlocked biochemical information that was previously unattainable. Here, I will discuss our efforts in improvements in sample preparation methods and the employment of unique mass spectrometer technology for analyzing biological material. Stable isotope probes were used to decode lipid distributions within model and cellular membranes, to reveal the intercellular delivery of drug-loaded polymeric nanoparticles, and to elucidate metabolic processes of phototrophic communities. The use of Fourier transform-based mass spectrometers, which have unparalleled mass accuracy and mass resolving power, and tandem mass spectrometry methods have allowed us to unravel the extreme spectral complexity of biological SIMS measurements, while increasing the confidence in our measurements. Lastly, we have revisited previously reported sample preparation routes that were never fully adapted by the SIMS community, in part because they were shackled by the limited ability of more commonly employed mass analyzers.

3:00pm AS+BI-MoA5 Towards Bacterial Differentiation with Quantitative SIMS, Christopher Szakal, S. Da Silva, National Institute of Standards and Technology (NIST); *N. Olson*, National Institute of Standards and Technology(NIST)

Large geometry secondary ion mass spectrometry (LG-SIMS) has been used extensively for particle analyses and geochemical analyses, owing to its ability to maintain adequate mass resolution while operating at high secondary ion transmission. Efforts will be presented that extend the knowledge acquired in these application areas to single bacterial cell analyses of elemental species. To be useful, LG-SIMS results need to be quantitative for the amounts of a given element per cell and/or in ratios of different elements within each cell. Approaching this level of detail requires the establishment of the natural variability of such data from cell-to-cell, the reproducibility of the measurement technique, and whether the data is relevant to pertinent questions about the cellular population. Progress will be shown towards achieving these aims for single bacterial cells within different known growth conditions, including analytical figures of merit for LG-SIMS elemental ratios. Prospective application areas will be presented, along with potential pitfalls of such an approach.

3:20pm AS+BI-MoA6 New Insights into the Microenvironment of Cancerous Tissue by Combined Mass Spectrometry, Microscopy and Multivariate Analysis, Tina Angerer, University of Gothenburg, Sweden; *Y. Magnusson, G. Landberg*, Sahlgrenska Cancer Center, Sweden; *J.S. Fletcher*, University of Gothenburg, Sweden

Introduction

Mass spectrometric imaging is of growing interest for the medical field, both in applied and basic research[1]. Particularly, imaging secondary ion mass spectrometry (SIMS) is becoming of increasing value to clinicians and has been used on a number of tissues samples to successfully identify and localize different chemical components to various areas of the tissue and answer disease related questions[2]. Fatty Acid Synthase (FAS) has been shown to be increased in many cancer types and is of growing interest as therapeutic target[3]. The changed lipid composition due to increased FAS activity is an ideal ToF-SIMS study target.

Methods

With the J105- 3D Chemical Imager (Ionoptika Ltd), fitted with a 40 kV gas cluster ion gun[4], we are now able to overcome some previous limitations of ToF-SIMS analysis and image large intact molecular species at high spatial and high mass resolution simultaneously. To capitalize on these improved capabilities we performed imaging SIMS on fresh frozen hydrated and freeze dried, ductal mammary breast cancer sections, followed by H&E staining of the analysed sections.

Results

SIMS enables us to distinguish between different areas of the diseased tissue. Multivariate analysis facilitates localizing and grouping the up to 10,000 different signals generated from the tissue to produce comprehensive chemical profiles assigned to different areas in the tissue revealing underlying structures. We have identified a number of molecules which can be, due to high spatial resolution, clearly assigned to the cancerous regions, characterized by conventional histological staining, in different breast cancer sections. Additionally, studying the distribution of specific single ions reveals reoccurring patterns of changes and gradients within the cancerous areas which cannot be observed in the conventionally stained image. Therefore ToF-SIMS can provide deeper insights into tumor metabolism and progression. Our results agree with findings from experiments using different methods, which confirm these molecules to be cancer markers while more importantly elucidating new information from the tissue with cellular resolution.

Conclusions

Imaging ToF-SIMS is a valuable tool for cancer research and can provide new insights into chemical changes within tumors. Further application of ToF-SIMS imaging will be used to study different modes of disease progression and treatment response.

[1] J. L. Norris et al., *Proteom Clin Appl* **2013**, 7, 733-738.

[2] A. Brunelle et al., *Curr Pharm Design* **2007**, 13, 3335-3343.

[3] P. M. Alli, et al., *Oncogene* **2004**, 24, 39-46.

[4] T. B. Angerer et al., *Int J Mass Spectrom* **2015**, 377, 591-598.

4:00pm AS+BI-MoA8 Super-resolution Mass Spectrometry Imaging of Biological Materials with the New 3D nanoSIMS, Ian S. Gilmore, M.K. Passarelli, National Physical Laboratory, UK; *A. Pirkel, R. Moellers, E. Niehuis*, ION-TOF GmbH, Germany; *A.A. Makarov*, Thermo Fisher Scientific; *H.F. Arlinghaus*, ION-TOF GmbH, Germany; *R. Havelund, P.D. Rakowska, A.M. Race, A.G. Shard*, National Physical Laboratory, UK; *A. West*, GlaxoSmithKline; *S. Horning*, Thermo Fisher Scientific; *P. Marshall*, GlaxoSmithKline; *M.R. Alexander*, The University of Nottingham, UK; *C.T. Dallery*, GlaxoSmithKline

SIMS has become an important technique for the surface analysis of biological materials. However, critical challenges have hampered the uptake into the life-science industry and biomedical discovery. To succeed in this important sector, it has to progress beyond "Show and Tell". Biological samples have complex chemistry and an extraordinarily large dynamic range of concentration. The present state-of-the-art struggles to identify unknowns owing to insufficient mass resolving power and mass accuracy of time-of-flight analysers. The situation is further complicated by sample form and vacuum compatibility.

To address this issue, we have developed a powerful new hybrid SIMS instrument combining an Orbitrap™-based Thermo Scientific™ Q Exactive™ HF instrument and a dedicated ToF-SIMS 5. The instrument is equipped with high-resolution ion beams including a new micron resolution argon cluster ion beam for biomolecular imaging and 3D analysis of

Monday Afternoon, November 7, 2016

organics and an ultra-high resolution Bi cluster focussed ion beam with < 80 nm resolution. The ToF analyser allows high-speed imaging needed for 3D analysis and the High Field Orbitrap analyser allows high mass resolution, mass accuracy and MS/MS for chemical identification. The instrument is designed for life-sciences applications including sub-cellular 3D imaging of metabolites, imaging of bacteria and biofilms and imaging of medical devices with complex topographies that confound traditional instrument designs.

We show data demonstrating the unique advantages of this novel instrument. Imaging with large argon clusters provides rich biomolecular spectra including intact lipids and metabolites. Existing state-of-the-art instruments are limited to a mass resolving power of around 6,000 which is insufficient to allow unique identification. We show images of mouse brain with a sub-cellular spatial resolution of less than 2 microns simultaneously with a mass resolving power of over 100,000 for intact lipids. We fully separate the (3'-sulfo)Gal-Cer(d18:1/24:1(2-OH)) and (3'-sulfo)Gal-Cer(d18:1/25:0) sulfatides, which reveals a difference in spatial distribution. In the low mass region, mass resolving powers of >400,000 are achieved allowing clear separation of the low abundance metabolite dopamine from other peaks. We show the ability to image the drug amiodarone with sub-cellular resolution and show that the mass spectra are not affected by sample topography. The instrument is also equipped with state-of-the-art cryogenic sample preparation specifically designed for high-resolution biological imaging.

All animal studies were ethically reviewed and carried out in accordance with Animals (Scientific Procedures) Act 1986

4:20pm **AS+BI-MoA9 High-resolution, Sub-cellular Imaging of Pharmaceutical Localization by Correlative SIMS and TEM, Paulina Rakowska**, National Physical Laboratory, UK; *H. Jiang*, University of Western Australia; *I.S. Gilmore*, National Physical Laboratory, UK

To accurately predict the pharmacological effect of potential drug candidates, there is a strong need in the pharmaceutical industry to image the disposition of drugs at the sub-cellular level and even within specific organelles. This is needed to answer long-standing questions about whether drug concentrations are sufficiently high in the right places to have a therapeutic effect, or if the medicine is lodging within cellular components and causing toxicity. If anomalies were spotted earlier, it might help to explain toxicities or lack of efficacy of a medicine and reduce costly late-stage failures.

Mass spectrometry imaging techniques are well-suited to measure drug distribution in biological samples and have the advantage of label-free analysis. The CAMECA nanoSIMS (secondary ion mass spectrometry) can provide elemental images with high lateral resolution of 50 nm. These high-resolution ion images can be correlated to electron microscopy images. This combination of techniques provides very precise and detailed information of cell morphology, subcellular processes and localization of different molecules within the cells. However, these high-performance instruments require high vacuum and complex sample preparations. Therefore, the sample handling needs careful consideration. Biological samples can suffer from ultrastructural reorganization or the loss or translocation of molecules, which can occur with dehydration under high-vacuum conditions. Chemical fixation of the samples followed by embedding in resin are common in the studies of cell biology by TEM but the solvents used for sample dehydration have a severe effect, translocating or even removing the drug from the cell all together. This has been a fundamental barrier for the use of the technique for intracellular drug localization measurement.

We present a correlative nanoSIMS and TEM imaging of a highly lipophilic drug – amiodarone within lung macrophages dosed at therapeutic concentrations. The protocol used for the fixation and resin-embedding of the cells prevented the drug from being removed from the organelles during solvent treatment. We are able to show, with unprecedented detail, the drug accumulating in lysosome organelles.

4:40pm **AS+BI-MoA10 Sub-Micron Imaging and Identification of Molecular Chemistry by TOF-SIMS Parallel Imaging MS/MS, Gregory Fisher***, Physical Electronics; *N. Ogrinc Potocnik*, *A.L. Bruinen*, Maastricht University, The Netherlands; *J.S. Hammond*, *S.R. Bryan*, Physical Electronics; *R.M.A. Heeren*, Maastricht University; *S. Iida*, *T. Miyayama*, ULVAC-PHI

INVITED

A recently introduced TOF-TOF imaging mass spectrometer allows conventional TOF-SIMS (MS^1) analysis and product ion (MS^2) analysis to be

achieved simultaneously and in parallel. Secondary ions for MS^1 and MS^2 analysis are produced from the same area of the surface by a pulsed and digitally raster-scanned primary ion nanoprobe. The sensitivity of the parallel imaging MS/MS spectrometer is high so that the analytical ion dose may be minimized; therefore, precious and one-of-a-kind samples may be probed without significant damage or degradation. Fragmentation of the molecular precursor ions, defined by a 1 Da precursor selection window, is accomplished by collision-induced dissociation (CID) at 1.5 keV in an activation cell of Ar gas at high pressure. Lateral resolutions produced in both MS^1 and MS^2 images are demonstrated to be in the range of $100\text{ nm} < \Delta l_{90/20} < 1\text{ }\mu\text{m}$. This tandem MS imaging capability has been brought to bear for straightforward identification as well as multifaceted studies involving biological, material, and polymer specimens. We will summarize here some of our ongoing biological research, revealing molecular identification at sub-micron practical lateral resolution.

One study concerns song bird ontogeny in male zebra finch (*T. guttata*). Several sulfatides, phospholipids, sterols and fatty acids have been identified as playing a role in song learning. We have employed parallel imaging MS/MS to unravel the roles of specific molecules because the shortcomings of TOF-SIMS imaging alone does not permit conclusive molecular identification and imaging. We have evidence suggesting that distinct sulfatides are active primarily within the song nuclei while cholesterol and specific fatty acids are active in signaling between the song nuclei.

In other work, we have probed the role of lipids and metabolites in disease states of zebrafish (*D. rerio*) that have been infected with *M. marinum*, a form of tuberculosis. The bacteria initiate a granulomatous inflammation, and first signs of the disease are observed in the spleen. We have observed so far that α -tocopherol is elevated in infected tissue as well as in the granuloma, but is not present in the necrotic cells. Cholesterol is elevated primarily in the granuloma. The role of phospholipids appears to differ, specific molecules being either elevated or depressed in the infected tissue. We have preliminary evidence of a metabolic source for bacterial growth. For example, we observe a phosphocholine, PC(16:0/16:0), to be elevated in the granuloma. However, in the necrotic cells surrounding the granuloma we observe elevated signals of a fatty acid, FA(16:0).

Electronic Materials and Photonics

Room 102A - Session EM-MoA

Surface and Interface Challenges in Wide Bandgap Materials

Moderators: Charles Eddy Jr., U.S. Naval Research Laboratory, Rachael Myers-Ward, Naval Research Laboratory

1:40pm **EM-MoA1 ALD Gate Dielectrics for GaN HEMTs, Andrea Corrión**, HRL Laboratories, LLC

INVITED

While most reported GaN high-electron mobility transistors (HEMTs) to-date have utilized a Schottky barrier gate, there is a significant need for high-performance insulated-gate devices. Gate dielectrics play a critical role in reducing gate leakage as well as increasing the forward-bias gate voltage swing in normally-off devices. Atomic layer deposition (ALD) gate dielectrics have recently generated significant interest for GaN HEMTs due to the wide variety of high-k materials available, highly controlled deposition rates and film quality, and low-temperature process compatibility. ALD Al_2O_3 in particular has been widely investigated and initial promising performance has been reported for both high-frequency RF and high-voltage power switch devices. However, significant challenges remain for the interface trap density, device reliability, and stability of the gate dielectric. This talk will review the status of ALD gate dielectrics for GaN HEMTs and on-going materials challenges, and will describe processes and device results for HRL's insulating-gate RF and power switching device technologies.

2:20pm **EM-MoA3 Advances in High-k Dielectric Integration with Ga-polar and N-polar GaN, Charles Eddy, Jr.**, U.S. Naval Research Laboratory; *C.R. English*, University of Wisconsin; *V.D. Wheeler*, U.S. Naval Research Laboratory; *D.I. Shahin*, University of Maryland College Park; *N.Y. Garces*, U.S. Patent & Trade Office; *A. Nath*, *J.K. Hite*, *M.A. Mastro*, *T.J. Anderson*, U.S. Naval Research Laboratory

Gallium- and nitrogen-polar GaN surfaces are subjected to a variety of pretreatments, including oxidation, before the application of high-k dielectrics by atomic layer deposition (ALD) in order to assess their ability to produce smooth, clean and electrically high-performing dielectric

* ASSD Peter Sherwood Award

semiconductor interfaces. In terms of topographical and chemical cleanliness, a pretreatment with a wet chemical piranha etch ($\text{H}_2\text{SO}_4:\text{H}_2\text{O}_2$) was found to be optimum for both surfaces and, additionally, $(\text{NH}_4)_2\text{S}$ is effective for N-polar surfaces. Both thermal and plasma oxidations were employed for controlled growth of native oxides. For Ga-polar surfaces, all native oxides were as smooth as pretreated surfaces, while for N-polar surfaces all native oxides are much rougher except for very short, high temperature oxidations. Thermal ALD high-k dielectrics, including Al_2O_3 , HfO_2 and ZrO_2 , were deposited on “optimally” treated surfaces. ALD Al_2O_3 films on Ga-polar surfaces are smoother for pre-treated surfaces than for as-received surfaces, whereas for N-polar surfaces the opposite is true. In general, ALD HfO_2 films on Ga-polar surfaces are rougher (0.8 nm rms) than Al_2O_3 films (0.1 nm rms), whereas for piranha treated N-polar surfaces HfO_2 films are smoother than Al_2O_3 films. ZrO_2 films are smoother than HfO_2 but rougher than Al_2O_3 films. For Ga-polar surface, capacitance-voltage measurements of simple Al_2O_3 (measured $k = 9$) capacitors show the smallest hysteresis for unintentionally oxidized surfaces (0.37 V), whereas simple HfO_2 (measured $k = 14$) capacitors show the smallest hysteresis for a thermal GaO_x at the interface (0.1 V). In both cases, the thicker the GaO_x at the interface the larger the negative threshold voltage shift – suggesting an electron trap. Calculated total trapped charges associated with the dielectrics range from $3.2 \times 10^{11} \text{ cm}^{-2}$ (for HfO_2 on thermally oxidized GaN) to $1 \times 10^{12} \text{ cm}^{-2}$ for Al_2O_3 on thermally oxidized GaN and HfO_2 on plasma oxidized GaN. Finally, the leakage current density for nearly all capacitors is $< 10^{-5} \text{ A-cm}^{-2}$ for up to a +8V bias. Interestingly, without additional GaN oxidation, ZrO_2 films present a significant positive threshold shift which could be beneficial for enhancement-mode transistor operation. Further details of ZrO_2 performance on “optimally” treated Ga-polar surfaces will also be presented.

2:40pm EM-MoA4 Effects of Surface Cleaning and Different Metals as Schottky Contacts to Bulk and Epitaxial $\beta\text{-Ga}_2\text{O}_3$, Yao Yao, R. Gangireddy, J. Kim, Carnegie Mellon University; T. Salagaj, N. Sbrockey, G.S. Tompa, Structured Materials Industries, Inc.; K.K. Das, JBP Materials; R.F. Davis, L.M. Porter, Carnegie Mellon University

Beta-gallium oxide ($\beta\text{-Ga}_2\text{O}_3$) has emerged over the past few years as a promising next-generation wide bandgap semiconductor. It has a bandgap of $\sim 4.8 \text{ eV}$ and a breakdown electric field of $\sim 8 \text{ MV/cm}$, giving it a superior figure-of-merit compared to traditional wide bandgap semiconductors like SiC and GaN. Moreover, it can be produced from the melt, and single-crystal (2-in diameter) substrates have recently become commercially available. Devices based on $\beta\text{-Ga}_2\text{O}_3$ that have so far been demonstrated include Schottky diodes, metal-semiconductor field effect transistors (MESFETs), metal-oxide-semiconductor field-effect transistors (MOSFETs), and ultra-violet (UV) photodiodes. However, since research on $\beta\text{-Ga}_2\text{O}_3$ as a wide bandgap semiconductor is in its very early stages, there is little understanding on how to control device-relevant interfaces to this material. In this work, we have investigated Schottky diodes fabricated on Sn-doped ($5 \times 10^{18} \text{ cm}^{-3}$) single-crystal Ga_2O_3 (-201) substrates and lightly doped ($\sim 10^{17} \text{ cm}^{-3}$) Ga_2O_3 (010) homoepilayers. A surface study was first performed to evaluate the effect of different surface cleaning techniques on contact performance. The surface cleaning methods consisted of (1) an organic solvent clean only (acetone and isopropanol), and an organic clean followed with a (2) HCl, (3) BOE, (4) HCl and H_2O_2 or (5) BOE and H_2O_2 . The corresponding Schottky barrier heights (SBHs) were calculated from the I - V and C - V behaviour of Ni Schottky diodes fabricated on bulk Ga_2O_3 (-201). SBHs were lowest for the organically cleaned sample, and highest for the sample treated in HCl and H_2O_2 . The latter also had the lowest leakage current in reverse bias and showed the most stable performance even after a period of several weeks after deposition. We have therefore established that organic clean followed by HCl and H_2O_2 treatment is the most effective of the cleaning methods tested. We have also investigated Schottky diodes fabricated using different Schottky metals. On the bulk Ga_2O_3 (-201) substrates, we calculated SBHs from the I - V behavior of Ir, Ni, Au and Sn to vary from ~ 1.0 – 0.7 eV in approximate correspondence with the metal workfunctions. On the lightly doped $\beta\text{-Ga}_2\text{O}_3$ (010) epilayer, preliminary measurements indicate a SBH $> 1.0 \text{ eV}$ for Ni. Electrical behavior of other metals on the (010) epilayer will also be investigated and reported in the presentation.

3:00pm EM-MoA5 Deep Traps in Wide Bandgap Semiconductors: From GaN to beta- Ga_2O_3 , Steven Ringel, A. Arehart, E. Farzana, Z. Zhang, The Ohio State University; E. Ahmadi, Y. Oshima, J. Speck, University of California at Santa Barbara

INVITED

Deep level defects are pervasive in wide bandgap (WBG) semiconductors such as GaN. Over the years deep levels in GaN have been extensively

studied. Several states have been directly linked with device degradation mechanisms in high electron mobility transistors and there is continued exploration of defect mitigation strategies to improve reliability. At the same time, there has been intense interest on the so-called ultra-wide bandgap (UWBG) semiconductors, whose bandgaps are $> 3.4 \text{ eV}$, driven by the desire to develop devices that can sustain even higher fields, operate at higher temperatures, while maintaining good high frequency performance. Of these UWBG materials, beta-phase gallium oxide ($\beta\text{-Ga}_2\text{O}_3$) is attracting particular interest due to its large, direct bandgap of $\sim 4.8 \text{ eV}$, the availability of n doping, the ability to create heterostructures, and the availability of native substrates to support homoepitaxial growth. This latter point is unique amongst WBG and UWBG materials.

However, compared with incumbent technologies, $\beta\text{-Ga}_2\text{O}_3$ is in its infancy, with transistors recently announced that have created excitement regarding the future of this material.[1] This presentation will build from our work on GaN and focus on basic aspects of $\beta\text{-Ga}_2\text{O}_3$: (a) the application of deep level optical and transient spectroscopy (DLOS/DLTS) to reveal traps throughout the entire material bandgap, (b) comparative DLOS/DLTS studies made on substrates and epitaxial layers grown by molecular beam epitaxy, and (c) the influence of wafer orientation on the properties of $\beta\text{-Ga}_2\text{O}_3$ Schottky diodes using various metals. DLTS and DLOS measurements revealed a spectrum of distinct bandgap states at $E_c - 0.62 \text{ eV}$, 0.82 eV , 1 eV , 2.4 eV and 4.42 eV , with a total trap concentration of $\sim \text{mid } 10^{16} \text{ cm}^{-3}$ range, dominated by the traps at $E_c - 0.82 \text{ eV}$ and $E_c - 4.42 \text{ eV}$. [2] Several traps show strong lattice-coupling effects. Regarding Schottky contacts, Ni Schottky contacts were fabricated on (010) and (-201) surfaces, revealing a change in barrier height of almost 0.5 V , as measured by both internal photoemission and C - V methods, suggesting a surface orientation dependence of Schottky barrier formation. Comparing Ni, Au, Pt and Pd contacts on (010) $\beta\text{-Ga}_2\text{O}_3$, barrier heights appear partially unpinning with barriers ranging from $\sim 1.2 \text{ eV}$ for Pd, to $\sim 1.55 \text{ eV}$ for both Ni and Pt and as high as $\sim 1.8 \text{ eV}$ for Au. In all cases, nearly ideal Schottky barrier transport characteristics were observed. This presentation will focus on the extension of trap studies from GaN to $\beta\text{-Ga}_2\text{O}_3$.

[1] M. Higashiwaki, et al., Appl. Phys. Lett. **100**, 013504 (2012)

[2] Z. Zhang, et al., Appl. Phys. Lett. **108**, 052105 (2016)

4:00pm EM-MoA8 Study of Oxygen and Moisture Effect on Device Instability of Bottom-Gate ZnO Transistors with Sol-Gel Derived Channel Layers, Kosala Yapabandara, M. Park, M.C. Hamilton, D.-J. Kim, V. Mirkhani, S. Wang, M. Sultan, B. Ozden, M.P. Khanal, S. Uprety, Y. Chung, Auburn University; M.H. Sk, Qatar University, Qatar

ZnO has been widely studied due to its promising material properties such as wide energy bandgap, optical transparency, and high carrier mobility for thin film transistor (TFT) technology. Solution-based ZnO can easily be deposited on large areas of substrates at low temperatures, which makes this material a good candidate for commercial device manufacturing. In the case of device reliability and performance, device stability under electrical stress is of imminent importance.

In this work, we report on the device instability of solution-based ZnO TFTs by studying the electrical characteristics during electrical stressing and subsequent relaxation. In order to elucidate the major source for device instability under electrical stress, the electrical characteristics of the transistors under the vacuum and ambient conditions were measured and compared. The positive shift of threshold voltage (V_T) of the device under gate stressing and negative shift under relaxation for both the vacuum and ambient conditions were observed, which suggest that the charge trapping near or at the semiconductor/dielectric interface and charge injection to dielectric layer may be main mechanisms for device instability. However, the continuous degradation of the field effect mobility with electrical bias-stressing in both environmental conditions and a full recovery of the device with a longer relaxation time provided evidence to disregard the assumption of charge injection to the dielectric layer.

Variation in sub-threshold swing (S) with biasing process indicates a new defect level creation. A negligible change in S during gate stressing and relaxation under the vacuum condition, compared to a significant change in S under ambient conditions confirmed that there is no new defect level creation in the absence of oxygen and moisture. Under ambient conditions, oxygen and moisture were adsorbed on the channel surface with the presence of a positive electric field. Upon adsorption, oxygen molecules can capture electrons from the conduction band and a depletion layer can be formed in the ZnO channel layer. Previously, it has been reported that oxygen molecules cannot diffuse into the channel layer at room temperature. However, we have suggested a plausible mechanism that

oxygen can be located closer to semiconductor/dielectric interface in thin films upon acceptor-like reaction of H_2O that diffused into the channel via voids in grain boundaries. Further confirmation of charge trapping and new defect level creation was carried out by fitting the V_T shift vs. time curve with the power law and stretched exponential functions for the vacuum and ambient conditions, respectively.

4:20pm EM-MoA9 Depth Dependent Modification of Optical Constants Arising from H^+ Implantation in n-type 4H-SiC Measured using Coherent Acoustic Phonons, Andrey Baydin, H. Krzyzanowska, Vanderbilt University; M. Dhanunjaya, S.V.S. Nageswara Rao, University of Hyderabad, India; J.L. Davidson, Vanderbilt University; L.C. Feldman, Vanderbilt University, Rutgers University; N.H. Tolk, Vanderbilt University

Silicon carbide is a promising material for new generation electronics including high power/high temperature devices and advanced optical applications such as room temperature spintronics and quantum computing. Both types of applications require the control of defects particularly those created by ion bombardment. In this work, modification of optical constants of 4H-SiC due to hydrogen implantation at 180 keV and at fluences ranging from 10^{14} to 10^{16} cm^{-2} is reported. The depth dependence of the modified optical constants was extracted from coherent acoustic phonon spectra. Implanted spectra shows a strong dependence of the 4H-SiC complex refractive index depth profile on H^+ fluence. These studies provide basic insight into the dependence of optical properties of 4H silicon carbide on defect densities created by ion implantation, which is of relevance to the fabrication of SiC-based photonic and optoelectronic devices.

4:40pm EM-MoA10 Electrical and Thermal Stability of ALD-TiN Schottky Gates for AlGaIn/GaN HEMTs, D.I. Shahin, University of Maryland College Park; Travis Anderson, V.D. Wheeler, M.J. Tadjer, A.D. Koehler, K. Hobart, C.R. Eddy, Jr., F. Kub, U.S. Naval Research Laboratory; A. Christou, University of Maryland College Park

AlGaIn/GaN high electron mobility transistors (HEMTs) are useful devices for next-generation RF and power electronics systems^{1,2}. Traditional Ni-based Schottky gates in these devices have been shown to degrade when subjected to electrical stress, thermal stress, and radiation due to Ni migration into adjacent metal or semiconductor layers^{3,4}. The instability of these Ni-based gates limits device reliability, rendering the search for replacement gate materials that are electrically- and thermally-stable a topic of tremendous importance. Of the transition metal nitrides, TiN is a particularly promising material, due to its near-metallic conductivity, suitable Schottky barrier heights and ideality factors on GaN and AlGaIn, and high temperature stability. This work investigates the performance of atomic layer deposited (ALD) TiN gates and directly compares them to traditional Ni/Au gates.

ALD TiN gates (75nm thick) were deposited on AlGaIn/GaN HEMTs in an Oxford FlexAL system at 350°C using Tetrakis(dimethylamido)titanium (TDMA-Ti) and an N_2/H_2 plasma as precursors. Devices with TiN gates exhibited improved static and dynamic on-state characteristics compared to the identical Ni/Au-gated HEMTs. Reverse bias gate stressing indicated a higher critical voltage ($V_{\text{GSTIN}} = -210\text{V}$, $V_{\text{GSNi/Au}} = -120\text{V}$) and a higher breakdown voltage ($V_{\text{BSTIN}} = -270 \pm 10 \text{ V}$, $V_{\text{BSNi/Au}} = 240 \pm 30\text{V}$) for the TiN gates. Furthermore, the TiN gates exhibited a decrease in reverse leakage current after stressing indicating enhanced stability. Gate thermal stability was assessed through sequential device annealing from 400-800°C in 100°C increments. The TiN gated devices exhibited stable DC operation up to 800°C, while the Ni/Au gates showed significant degradation after annealing above 500°C and failed above 700°C. This suggests that ALD TiN gates are a strong candidate for reliable HEMT gate metallization and other applications where increased stability is required at higher temperatures.

¹ R.S. Pengelly, et al., *IEEE Trans. Microwave Theory Tech.* **60** [6], 1764 (2012).

² S.J. Pearton, et al., *J. Vac. Sci. Technol. A* **31** [5], 050801 (2013).

³ Y.H. Choi, et al., *Mater. Res. Soc. Symp. Proc.* **1167**, 1167-005-06 (2009).

⁴ A.D. Koehler, et al., *IEEE Elect. Dev. Lett.* **35** [12], 1194 (2014).

5:00pm EM-MoA11 Spectroscopic Photo Current Voltage Measurements to Investigate Non-uniform Defect Distributions in AlGaIn/GaN HEMT Heterostructures, Burcu Ozden, M.P. Khanal, C. Yang, L. Shen, V. Mirkhani, K. Yapabandara, M. Park, Auburn University

The nature and distributions of the electrically-active sub-bandgap point defects in the heterostructures of the AlGaIn/GaN high electron mobility transistors (HEMTs) layers have been analyzed by using spectroscopic photo current voltage (SPIV) measurement. Despite the great potential, Monday Afternoon, November 7, 2016

device performance for the next generation of high power electronics is often limited by the presence of electronic traps in the AlGaIn/GaN HEMTs device structures. Therefore, the knowledge of defect distribution is critical in understanding the origin of the surface traps for mitigation in future device applications.

In this work, the AlGaIn/GaN HEMT epi-layers were grown on a 6" Si wafer by metal-organic chemical vapor deposition (MOCVD). Ni contacts with 600μm diameter and 20nm thickness were fabricated on the samples which are chosen from the three different locations of 6" wafer. The SPIV measurement was performed using a variable-wavelength light illumination from a Xe lamp. Vertical bias was applied between circular semi-transparent Ni Schottky contacts and the bottom ohmic contact.

Presence of sub-bandgap defects at different energy levels among the wafer were revealed by SPIV measurements indicating nonhomogeneous defect distribution among the wafer. It was concluded that observed defects are most probably due to either Ga vacancies in GaN or Al vacancies in AlGaIn by comparing the energy level of the defects with the formation energies of these vacancies. In conclusion, we have demonstrated the wafer quality in terms of the distribution of electrically active defects can be successfully assess by using SPIV measurements which will be useful for AlGaIn/GaN HEMT wafer vendors as a diagnostic tool.

Magnetic Interfaces and Nanostructures Room 101C - Session MI+2D+AC-MoA

Magnetism and Spin Orbit Effects at Interfaces and Surfaces: Recent Experimental and Theoretical Advances

Moderator: Valeria Lauter, Oak Ridge National Laboratory

1:40pm MI+2D+AC-MoA1 Bi₂Te₁: A New Dual Topological Insulator, Lukasz Plucinski, M. Eschbach, M. Lanius, C. Niu, E. Mlynczak, P. Gospodaric, FZ Jülich GmbH, Germany; J. Kellner, RWTH Aachen University, Germany; P. Schüffegen, M. Gehlmann, S. Döring, E. Neumann, M. Luysberg, B. Holländer, G. Mussler, FZ Jülich GmbH, Germany; M. Morgenstern, RWTH Aachen University, Germany; D. Grützmacher, G. Bihlmayer, S. Blügel, Schneider, FZ Jülich GmbH, Germany

We present, a combined theoretical and experimental study on the prediction and verification of the dual topological insulating character of the stoichiometric natural superlattice phase $\text{Bi}_2\text{Te}_1 = [\text{Bi}_2][\text{Bi}_2\text{Te}_3]_2$ [1]. We identify Bi_2Te_1 by density functional theory to exhibit a non-trivial time-reversal symmetry-driven character of $Z_2 = (0; 001)$ and additionally a mirror-symmetry induced mirror Chern number of $\nu_M = -2$, which indicates that Bi_2Te_1 is both a weak topological insulator (WTI) and a topological crystalline insulator (TCI). The coexistence of the two phenomena preordain distinct crystal planes to host topological surface states that are protected by the respective symmetries. From the analysis of time-reversal invariant momenta (TRIM-points) the surface perpendicular to the stacking direction, for instance, is found as the time-reversal symmetry *dark* surface, while hosting mirror-symmetry protected non-TRIM surface states along the surface-Gamma-M direction. We confirm the stacking sequence of our MBE-grown Bi_2Te_1 thin films by X-ray diffraction and transmission electron microscopy (STEM), and find clear indications of the TCI and WTI character in the surface electronic spin structure by spin- and angle-resolved photoemission spectroscopy.

[1] M. Eschbach et al., arXiv:1604.08886 (2016).

2:00pm MI+2D+AC-MoA2 Spin-Polarized Scanning Tunneling Microscopy of a Two-Dimensional Ferromagnetic Semiconductor at Room-Temperature, Yingqiao Ma, A.R. Smith, Ohio University; A. Barral, V. Ferrari, Centro Atómico Constituyentes, GlyA, CNEA, Argentina

Ferromagnetic semiconductors are very promising materials for the spintronic applications, as they are good spin-polarized carrier sources and easy to be integrated into semiconductor devices. The search for ferromagnetic semiconductors with Curie temperature above the room-temperature has been a long-standing goal, since the Curie temperature T_C of most ferromagnetic semiconductors are at the cryogenic level with little possibility of improvement, which hinders their future practical spintronic applications.

Here, we observed the ferromagnetic domain structure at room-temperature on a GaN-based two-dimensional MnGaN semiconducting surface alloy, using spin-polarized scanning tunneling microscopy/spectroscopy which is sensitive to the surface magnetic

nanostructures and can completely rule out the extrinsic origin of the ferromagnetism such as magnetic elements segregation by its ultimate spatial resolution. In contrast to the randomly doped dilute magnetic semiconductors, the two-dimensional surface structure has a unique and well-ordered hexagonal-like $\text{Mn } \sqrt{3} \times \sqrt{3} - R30^\circ$ symmetry. The total density of states of the $\text{Mn } \sqrt{3} \times \sqrt{3} - R30^\circ$ structure calculated by the density functional theory agree well with our normalized differential tunneling dI/dV spectroscopy, which clearly reveal the spin-polarized and spin-split Mn surface density of states peaks and prove the semiconducting nature of the surface as the normalized dI/dV goes to zero at the Fermi level. By applying a small magnetic field to the sample, the magnetic hysteresis is mapped out, which further proves its ferromagnetic nature. In conclusion, we demonstrated the room-temperature ferromagnetic nature of the two-dimensional $\text{Mn } \sqrt{3} \times \sqrt{3} - R30^\circ$ structure, which makes it a promising material for future realistic magnetic storage, field-controlled, and quantum computing nano spintronic devices.

2:20pm MI+2D+AC-MoA3 Spin-Orbit Induced Surface States of Rashba Systems and Topological Insulators, Peter Krüger, T. Förster, M. Röhlfing, P. Eickholt, A.B. Schmidt, M. Donath, Westfälische Wilhelms-Universität Münster, Germany

INVITED

The generation of spin-polarized electrons on the basis of spin-orbit coupling at the surfaces of nonmagnetic solids has attracted considerable interest in recent years. Adlayers of heavy atoms, in particular, give rise to an interesting physics of spin-split surface states going far beyond the simple Rashba model. However, only very few studies have been reported that address unoccupied states of these systems, despite their relevance for potential applications. In the first part of this contribution, we present results from ab-initio calculations as well as spin- and angle-resolved inverse photoemission (IPE) for systems showing empty bands with a giant spin splitting and a unique structure of the spin polarization. For Ti/Si(111) and Ti/Ge(111) , we identify spin-split states whose polarization vector rotates from the Rashba direction to an out-of-plane polarization when going from Gamma to K. Surprisingly, the spin splitting of the bands on Ti/Ge(111) is much smaller than on Ti/Si(111) despite the stronger surface localization and the heavier substrate. Our detailed analysis of the electronic structure shows that a remarkable interplay between spin-orbit coupling and hybridization is responsible for this unexpected result. Furthermore, we notice a distinct spin asymmetry in the intensity of the measured spectra at M, a time-invariant k-point. Our simulations of the IPE process unravel this puzzling behavior.

In the case of topological insulators, spin-orbit coupling gives rise to topologically protected surface states. We identify problems of the widely used density-functional theory (DFT) with a proper description of these states and demonstrate that they can be overcome by employing the GW self-energy operator within ab initio many-body perturbation theory. In particular we have investigated thin films of Bi_2Se_3 , Bi_2Te_3 , and Sb_2Te_3 with thicknesses from one to six quintuple layers. The quasiparticle band structures show highly improved agreement with experiments compared to DFT. In addition to a correction of the band gaps, the energetic positions and dispersions of the surface states change significantly around the Dirac point. As the wave functions are updated in our approach, the two-dimensional topological phases (quantum spin Hall or trivial) in GW can be different from the DFT result. We find the nontrivial quantum spin Hall phase, together with a sizable band gap 0.13 eV for a Bi_2Te_3 slab of 2 QL thickness.

[1] P. Eickholt et al., Phys. Rev. B **93**, 085412 (2016)

[2] T. Förster et al., Phys. Rev. B **92**, 291404 (R) (2015)

3:00pm MI+2D+AC-MoA5 Spin-Resolved Momentum Microscopy of Strongly Correlated Electron Systems and Topological Insulators, Christian Tusche, Forschungszentrum Jülich, Germany

INVITED

One of the fundamental concepts in solid state physics is the description of the degrees of freedom of the electrons in the solid by the relation of the energy E vs. the crystal momentum k in a band structure of quasi particles. Of particular importance is the spin of the electron that leads to phenomena like ferromagnetism, spin-polarized surface- and interface-states, and recently, the discovery of new material classes like topological insulators. The latter attracted wide interest by the unusual relations of electron-spin and -momentum. In addition, strong spin-orbit coupling also leads to a rich band-structure of highly polarized states beyond the well known "Dirac cone" surface state. A direct conclusion on the ground state polarization in these systems is rather complicated by the peculiar interplay between spin- and light-polarization, as directly observed in spin-resolved photoemission maps over the full surface Brillouin zone.

On the experimental side, the novel concept of momentum microscopy evolved to provide an intuitive and comprehensive insight to these band structures. A momentum microscope captures the complete 2π solid angle of emitted photoelectrons into a high resolution image of electronic states in reciprocal space [1]. With the introduction of imaging spin analyzers, the efficiency of spin-resolved measurements experienced a tremendous boost [2]. Together with modern synchrotron radiation sources, delivering photon energies from UV to soft X-rays as well as a flexible timing structure, the electron spin now becomes routinely accessible in photoemission experiments. In particular, new developments like time-of-flight momentum microscopy now provide comprehensive three-dimensional data sets of the complete valence band region within a single measurement [3]. Here, we discuss examples and prospects of spin resolved momentum microscopy, ranging from tomographic imaging of the spin-resolved Fermi surface of ferromagnets to the rapid band-structure mapping of novel materials.

[1] C. Tusche, A. Krasnyuk, J. Kirschner: Ultramicroscopy **159**, p. 520 (2015),

[2] C. Tusche, M. Ellguth, A. A. Ünal, C.-T. Chiang, A. Winkelmann, A. Krasnyuk, M. Hahn, G. Schönhense, J. Kirschner: Appl. Phys. Lett. **99**, 032505 (2011)

[3] C. Tusche, P. Goslawski, D. Kutnyakhov, M. Ellguth, K. Medjanik, H. J. Elmers, S. Chernov, R. Wallauer, D. Engel, A. Jankowiak, G. Schönhense: Appl. Phys. Lett., in press (2016)

4:00pm MI+2D+AC-MoA8 Spin-orbit-Induced Effects in the Electronic Structure of W(110) and Ta(110): Similarities and Differences, Markus Donath, K. Miyamoto, H. Wortelen, B. Engelkamp, Muenster University, Germany; H. Mirhosseini, Max Planck Institute for Microstructure Physics, Germany; T. Okuda, Hiroshima Synchrotron Radiation Center, Japan; A. Kimura, Hiroshima University, Japan; A.B. Schmidt, Muenster University, Germany; J. Henk, Martin Luther University Halle-Wittenberg, Germany

Tungsten and tantalum are direct neighbors in the periodic table and exhibit, at first glance, a very similar electronic structure. Only the bands of tantalum are less occupied due to the lack of one electron. For W(110), an exceptional surface state was discovered [1]: Resembling a topological surface state (TSS), it exhibits a linear dispersion with a helical spin texture in reciprocal space, often called Dirac-cone-like behavior. Interestingly and again reminiscent of the TSS behavior, photoemission calculations predict a spin reversal upon changing the light polarization used for excitation from p to s [2]. We verified this orbital-symmetry-selective spin texture by spin-resolved photoemission [3]. This result unveils, in which way spin-orbit interaction entangles spin and orbital degrees of freedom. "Spin control" is not restricted to topological insulators but a much more general phenomenon.

A surface state, similar to the Dirac-cone-like state on W(110), may be expected for Ta(110), yet above the Fermi level. Surprisingly, our spin-resolved inverse-photoemission results do not show this state. Instead, spin-polarized unoccupied surface bands [4] and an occupied d^2 -surface state with Rashba-like spin texture [5] were identified, which have no equivalents on W(110). These findings are explained by subtle differences in the energetic positions of the surface states relative to the bulk states for W(110) and Ta(110), which critically depend on the values for the lattice constant and the surface relaxation.

[1] K. Miyamoto et al., Phys. Rev. Lett. **108**, 066808 (2012); Phys. Rev. B **86**, 161411(R) (2012); J. Electron Spectrosc. Relat. Phenom. **201**, 53 (2015).

[2] H. Mirhosseini et al., New J. Phys. **15**, 033019 (2013).

[3] K. Miyamoto et al., Phys. Rev. B **93**, 161403(R) (2016).

[4] B. Engelkamp et al., Phys. Rev. B **92**, 085401 (2015).

[5] H. Wortelen et al., Phys. Rev. B **92**, 161408(R) (2015).

4:20pm MI+2D+AC-MoA9 Formation of a 2D Interface by Low Energy Proton Implantation in ZnO Microwires, Israel Lorite, Y. Kumar, Universität Leipzig, Germany; B. Straube, S. Perez, Universidad Nacional de Tucumán, Argentina; C. Rodriguez, Universidad Nacional de La Plata, Argentina; P. Esquinazi, Universität Leipzig, Germany

Recently we showed the possibility of obtaining room temperature magnetic order by implanting protons (H^+) at low energies (300 V) into Li-doped ZnO microwires [1]. The low energy implantation is enough to produce Zn vacancies (V_{Zn}) within 10 nm from the surface, without creating too much disorder in the ZnO lattice. The formation of a stable density of defects in the 10 nm depth region is possible since Li doping reduces the energy of stabilization of V_{Zn} . Thus, the concentration of V_{Zn} will be approximately the one of the Li doping. Along with the observation of

Monday Afternoon, November 7, 2016

magnetic order at room temperature, the ZnO microwires present an anomalous temperature dependence of the negative magnetoresistance. Such a behavior can be related to the formation of an interface at the boundary between the magnetic and non-magnetic structure produced by the implantation. In this contribution we show the observation of a photogalvanic effect related to the Rashba effect. This effect is due to the formation of a 2D electron gas at the interface of the magnetic/non-magnetic structure. In addition, an increase of this effect is observed by the application of a small external magnetic field, related to the existence of a 10 nm magnetic region produced during the proton irradiation.

[1] I.Lorite, et al; Advances in methods to obtain and characterize room temperature magnetic, Appl. Phys. Lett. 106, 082406 (2015)

4:40pm **MI+2D+AC-MoA10 Density Functional Studies of Magnetic and Spintronic Materials**, *Ruqian Wu*, University of California Irvine **INVITED**

Magnetism, one of the oldest branches of physics, is having its renaissance in recent years due to the interest in developing various nanomagnets, molecular magnets and magnetic nanojunctions for the development of innovative devices. Magnetization of surfaces and nanostructures is sensitive to the change of environment and hence the availability of ultrahigh vacuum is crucial for the exploration of various magnetic systems. Equally important is the rapid advance of density functional theory (DFT) approaches, which now can reliably predict large amount physical properties of real materials in either their ground states or excited states. In this talk, I will discuss several our recent theoretical progresses in spin-related physics, including 1) the search for giant magnetic anisotropy energy in nanostructures; 2) the design to imprint large spin orbit coupling into graphene and other two-dimensional materials for the realization of quantum spin Hall effect and quantum anomalous Hall effect; 3) the photo-spin-voltaic effect; and 4) the generation of spin-polarized two-dimensional electron gas at oxide interfaces. Most of our DFT studies are performed in close collaboration with experimental groups so some experimental results will also be discussed.

Work at UCI was supported by DOE-BES (Grant No. DE-FG02-05ER46237) and NERSC.

Manufacturing Science and Technology

Room 103A - Session MS-MoA

pb

Moderator: Gary Rubloff, Institute for System Research, University of Maryland

1:40pm **MS-MoA1 Metrology of Laser-based Powder Bed Fusion Additive Manufacturing Systems**, *John Slotwinski*, The Johns Hopkins University Applied Physics Laboratory **INVITED**

Metrology of Laser-based Powder Bed Fusion Additive Manufacturing Systems

John A. Slotwinski, Ph.D.

The Johns Hopkins University Applied Physics Laboratory

Additive Manufacturing (AM, aka 3DPrinting) is a potentially revolutionary manufacturing technology that is changing how both polymer and metal parts can be designed and fabricated. Geometrical complexity, gradient materials, and one-piece assemblies, all of which are difficult or impossible to fabricate with traditional removal processes, are all realizable with additive manufacturing. However, there are several technical challenges that are preventing more widespread adoption of additive manufacturing systems, especially for high-value, mission-critical parts. Chief among these challenges are a lack of full understanding of AM processes, especially for metal AM processes, and the factors influencing the mechanical properties of AM parts. In this talk I will give a brief overview of additive manufacturing processes, describe the technical challenges that are hindering broad adoption of AM parts for critical applications, and describe some recent efforts to measure and better understand both AM processes and AM material properties.

2:20pm **MS-MoA3 Investigation of Superconductive Heavily Doped Boron Diamond for Device Fabrication**, *Delroy Green, G.L. Harris*, Howard University; *R.D. Vispute*, Bluewave Semiconductor Inc.

Diamond has a wide bandgap of 5.47 eV at room temperature and is the hardest known naturally occurring material with a Knoop hardness of 10,400 kg/mm² or 10 on the Mohs scale. Due to the structure of the covalent bonding of its carbon atoms, diamond is extremely strong having

each carbon bonded to four neighboring carbon atoms. Although diamond is hard, its toughness, when compared to most engineering materials, is poor. However, because of its hardness, it is an efficient cutting and drilling tool. With the exception of naturally occurring blue diamonds, which are semiconductors, diamond is a good electrical insulator. However, unlike most insulators, diamond has the highest thermal conductivity of 22 W/cm-K among naturally occurring materials. Although diamond is a good electrical insulator, it also shows semiconducting properties when doped with impurities. When diamond is heavily doped with boron the resulting material possess excess electron holes and as such it is classified as a p-type material. If excess boron doping is achieved, then the resulting material is found to behave like a superconductor at very low temperatures. In this superconducting state, the doped diamond conducts electricity.

A series of boron-doped diamond films were grown by hot filament chemical vapor deposition (HFCVD) and tested to determine the optimum technique for doping diamond with boron for superconductivity. The first technique involved the insertion of boron powder (B₂O₃) around the sample holder to dope seeded poly and nano diamond during growth. The second technique involves doping with diborane gas (B₂O₆).

Various processing parameters were optimized for diamond quality, structure, morphology, and doping. A combined analysis of scanning electron microscope, Raman mapping and Hall measurements at various temperatures were conducted to ascertain the superconductive nature of the material. Preliminary results of the boron solid source doping on diamond show a superconductive transition temperature of 2.3 °Kelvin at a doping concentration of

$2.3 \times 10^{20} \text{ cm}^{-3}$.

This research is conducted under research grants CIQM NSF DMR# 1231319 and PREM NSF DMR# 0611595

2:40pm **MS-MoA4 Two-Dimensional Layered Materials For Composites Applications**, *Jorge Catalan, A. Delgado, A.B. Kaul*, University of Texas at El Paso

Composite materials provide us with an alternative route to combine the characteristic properties from two different materials into one. At the same time, this characteristic of composite materials opens up a new window for different applications such as optoelectronic sensors, strain sensors, capacitive sensor and opto-electro-mechanical sensors. Initially, the isolation of single layered graphene by mechanical exfoliation and nowadays with different methods such ion intercalation, solvent based exfoliation and chemical vapor deposition (CVD) have allowed the utilization of two-dimensional (2D) materials as reinforcement particles into different polymer matrixes for composite materials. This is because 2D materials offer interesting semiconducting properties that might be able to be captured in a polymer-based matrix that provides a ductile medium make them suitable for printable flexible electronic devices and sensors. In this work we have explored graphene, MoS₂, and WS₂ as possible reinforcement material in different polymers matrixes. The first type of composite consisted of a poly-methyl-methacrylate (PMMA) matrix with different type of fillers (graphene, MoS₂ and WS₂). The second type of composite materials that we studied consists of a poly-isoprene matrix (natural rubber band) and graphene, MoS₂, and WS₂ as reinforcement material. We have conducted strain testing on the structures we have fabricated to make strain-dependent electrical and optical properties. The PMMA/filler material composite was optically and electrically characterized under different strains with the help of different fixtures with different radius of curvature. On the other hand, the poly-isoprene composites were characterized with the help of a self-made type of clamp that allows us to strain the rubber band like composite to different degrees and measure the electrical characteristics of the compound. The opto-electro-mechanical characterization was developed with the scope of utilizing these composite materials as strain or flexible sensors for health monitoring or non-destructive evaluation.

4:00pm **MS-MoA8 AIM Photonics – Manufacturing Challenges for Photonic Integrated Circuits**, *Michael Liehr*, SUNY Polytechnic Institute **INVITED**

Abstract: The recently established American Institute for Manufacturing Photonics (AIM Photonics) is a manufacturing consortium headquartered in NY, with funding from the US Department of Defense, New York State, California and Massachusetts, and industrial partners to advance the state of the art in the design, manufacture, testing, assembly, and packaging of integrated photonic devices. Dr. Michael Liehr, CEO of AIM Photonics, will

Monday Afternoon, November 7, 2016

describe the technical goals, operational framework, near-term milestones, and opportunities for the broader photonics community.

The scope of AIM Photonics will span several industry segments, with the most prominent and near term commercial segment of Datacom applications, to analog/RF, array and sensor applications that are expected to mature at a later time. Photonic Integrated Circuits (PIC) technology enables optical systems to be miniaturized and fabricated on semiconductor chips. Just as electronic integrated circuits revolutionized electronics by miniaturizing transistor circuitry, PICs integrate lasers and other optical devices to route and process information with reduced size and power. PICs can also scale in complexity to do things that would not be possible using conventional optical design approaches. By putting these components on a single platform, PICs have the potential to advance technology in ways never before possible.

Targeted markets include:

Ultra-high-speed transmission of signals for the internet and telecommunications

New high-performance information-processing systems and computing

Compact biomedical sensor applications enabling dramatic medical advances in diagnostics and treatment

Multi-sensor applications including urban navigation, free space optical communications, and quantum information sciences

Other military applications, including electronic warfare, analog RF sensing, communications, and chemical/biological detection

4:40pm MS-MoA10 Development of III-Nitrides for Energy Harvesting Applications, B. Kucukgok, N. Lu, Purdue University; Ian T. Ferguson, Missouri University of Science and Technology

III-Nitride wide-bandgap semiconductors have recently enabled state-of-the-art technologies for energy harvesting applications, such as photovoltaics and thermoelectrics. III-Nitride materials and devices have provided tremendous advantages due to their distinguished features, including tunable bandgap, superior electrical properties, high-temperature stability, enhanced chemical stability, and mechanical strength. Furthermore, InGaN with indium compositions up to 30% (2.5 eV band gap) have been developed for photovoltaic applications by controlling defects and phase separation. Additionally, InGaN solar cell design consists of 2.9 eV InGaN p-n junction sandwiched between p- and n-GaN layers results in internal quantum efficiencies as high as 50%; while devices utilizing a novel n-GaN strained window-layer enhanced the open circuit voltage. These results establish the potential of III-Nitrides and related materials in ultra-high efficiency photovoltaics. Moreover, thermoelectrics, conversion of waste thermal energy into electrical energy, have seen pioneering developments over the past 20 years. A figure of merit ZT, used to measure the efficiency of the thermoelectric materials. Various approaches have been taken to increase the efficiency of thermoelectric materials, such as electron quantum confinement and phonon scattering to increase the power factor and decrease the lattice thermal conductivity, respectively. The objectives of this study are to highlight the use of III-Nitrides in high efficient photovoltaic and thermoelectric energy harvesting applications. Some recent measurements of the thermoelectric properties—the Seebeck coefficient, the electrical conductivity and the power factor—of GaN and InGaN thin films will also be reported.

Nanometer-scale Science and Technology

Room 101D - Session NS-MoA

Nanophotonics, Plasmonics, and Energy

Moderators: Stephane Evoy, University of Alberta, Canada, Wei Wu, University of Southern California

2:00pm NS-MoA2 The Effects of N Incorporation in GaAsSb/GaAs Core-shell Nanowires, Prithviraj Deshmukh, P. Kasanaboina, NCA&T State University; C. Reynolds Jr., Y. Liu, North Carolina State University; S. Iyer, NCA&T State University

Bandgap tuning beyond 1.3 μm in GaAsSb based nanowires by incorporation of dilute amount of N is reported, for realizing nanoscale optoelectronic devices in the telecommunication wavelength region. Vertical GaAs/GaAsSbN/GaAs core-shell configured nanowires are grown on Si (111) substrates using plasma assisted molecular beam epitaxy. Effects of N incorporation and thickness of the shell layers on the micro-photoluminescence spectral peak shifts have been studied. Annealing in N_2 ambient led to enhanced spectral intensity, which is attributed to the annihilation of defects. Shifts and changes in the spectral shapes of the Raman spectra prior to and after annealing have been used to ascertain the nature of the defects being annihilated during the growth. I-V measurements also provided further support to the annihilation of predominantly point defects on annealing. Results from the transmission electron microscopy study on the planar defects will also be presented.

2:20pm NS-MoA3 Exploitation of Microwave Interaction and Photoconductive Effects in TiO_2 Nanotube/Nanowire Arrays for Use in Light Harvesting and Sensing Devices, Karthik Shankar, University of Alberta and The National Institute for Nanotechnology, Canada; M.H. Zarifi, S. Farsinezhad, M. Daneshmand, University of Alberta, Canada INVITED

Nanostructures made of semiconducting metal oxides such as TiO_2 , ZnO, SnO_2 , WO_3 , etc. have a remarkably versatile application spectrum, serving applications in sensing, catalysis, photocatalysis and solar cells. Metal oxide nanostructures abound in electronic defects originating in their high surface area and the method of fabrication. Such defects include dangling bonds, grain boundaries and color centers which in turn may act as shallow or deep trapping sites for electrons and/or holes. These defects have been more or less uniformly viewed negatively in the literature for their deleterious effects on light harvesting and charge transport. However, a recently emerging view is that the defects also provide an opportunity to engineer sensitivity and much-needed selectivity in sensor designs, particularly with regards to the detection and quantification of small molecules.

We used highly ordered TiO_2 nanotube arrays (TNA) grown by low-cost electrochemical anodization as platforms to perform the selective sensing of alcohols without the use of external binding receptors. TNA membranes were placed in the active coupling gap of a microwave ring-type resonator [1]. By monitoring the resonator's Quality factor (Q) and resonance frequency (f_0) as a function of time following light illumination of the nanotube membrane, we were able to distinguish between the methanol, ethanol and isopropanol [2].

Our work also brings in focus a hitherto underexplored topic in nanomaterials - namely the leveraging of the interactions of microwaves and semiconductor nanostructures to build better sensors and diagnostic platforms [2]. Extension of this concept enabled us to detect a molecular monolayer by monitoring the interactions of microwaves with semiconductors, and also enabled us to use the molecular monolayer to tune the electronic interactions of the surface of wide bandgap TiO_2 with external analytes in the service of VOC sensing as well as extremely low-level photodetection.

REFERENCES

1. Zarifi MH, Mohammadpour A, Farsinezhad S, Wiltshire BD, Nosrati M, Askar AM, Daneshmand M and Shankar K, TRMC Using Planar Microwave Resonators: Application to the Study of Long-lived Charge Pairs in Photoexcited Titania Nanotube Arrays, *Journal of Physical Chemistry C*, 119 (25), 14358-14365, 2015.
2. Zarifi MH, Farsinezhad S, Abdolrazzaghi M, Daneshmand M and Shankar K, Selective microwave sensors exploiting the interaction of analytes with trap states in TiO_2 nanotube arrays, *Nanoscale*, DOI: 10.1039/c5nr06567d, 2016.

3:00pm **NS-MoA5 Next Generation Photovoltaics from Solution-processed Quantum Dot Assemblies**, *Joseph Luther*, National Renewable Energy Laboratory

INVITED

Quantum confined semiconductor nanocrystals called quantum dots (QDs), are promising materials for next-generation photovoltaic technologies and other various optoelectronic applications. QDs offer several key benefits over bulk semiconductors. Researchers are actively exploiting these benefits to produce prototypes for the next generation of photovoltaic devices. New synthetic routes that employ cation-exchange reactions to produce well-controlled and stable lead chalcogenide materials will be discussed. Similarly, the effects of metal halide treatments of PbSe QD solids will be explored in various approaches. These metal halides improve the surface properties of the QD assemblies, result in conductive QD solids, and the resulting QD solids have a significant reduction in the carbon content compared to typical QD film treatments using thiols and organic halides. Even when the QDs are coupled in arrays through the utilization of recent developments in surface ligand modification, they still exhibit quantum confinement and possess intriguing ensemble properties that can be exploited in thin films, as the active layer of solar cells. The future challenges of QDs in solar cells will be discussed in relation to device physics measurements that can probe the working principles behind state of the art devices. The method developed here produces QD solar cells that perform well even at film thicknesses approaching one micron, indicating improved carrier transport in the QD films.

4:00pm **NS-MoA8 Negative Index and Hyperbolic Metamaterials: Into the Ultra-Violet**, *Henri Lezec*, National Institute of Standards and Technology (NIST)

INVITED

Artificial metamaterials – metallo-dielectric composites tailored on deep-subwavelength scale – enable implementation of electromagnetic responses not found in nature, leading to potentially useful applications as well as yielding new insights into the fundamental nature of light. Here we show how we have leveraged ultrasubwavelength planar nanoplasmonic waveguides deposited by ion-beam-assisted sputter deposition to implement easy-to-fabricate bulk metamaterials operating at visible and near-ultraviolet wavelengths and having refractive indices ranging from highly anisotropic and positive [1] to quasi-isotropic and negative [2]. Exploiting these structures to tailor the flow of light in exotic ways, we realize devices ranging from high-contrast, near-field nanoparticle optical sensors working in the visible, to the first implementation of a Veselago flat lens [3] functioning in the near ultraviolet. Substituting Al for Ag as the constituent plasmonic metal of choice, we investigate the extension of bulk metamaterial operation into the far-ultraviolet, for lithographic applications beyond the diffraction limit.

[1] T. Xu and H.J. Lezec, Nat. Comm. 5, 4141 (2014). [2] T. Xu, A. Agrawal, M. Abashin, K.J. Chau, and H.J. Lezec, Nature 497, 470 (2013). [3] V.G. Veselago, Sov. Phys. Usp. 10, 509 (1968).

4:40pm **NS-MoA10 Probing Sub-5 nm Gap Plasmon Using Collapsible Nano-fingers**, *Boxiang Song, W. Wu*, University of Southern California

Plasmonic nanostructures are of great interests recently due to their ability to concentrate light to small volume. They have many potential applications in optical communication, disease diagnosis, and chemical sensing. Therefore it is extremely important to investigate the plasmonic hot spots both theoretically and experimentally. While it is theoretically predicted that the optimal hot spot is a sub-5 nm gap between two metallic particles, due to the difficulties in fabrication of sub-5 nm structures, most of the studies on hot spot behaviors at that scale are theoretical only. Therefore, it is essential to find a way to fabricate hot spots with sub-5 nm gap sizes deterministically and reliably as the experimental platform to probe and utilize those hot spots.

Recently, we have successfully fabricated gap plasmonic structure with precisely controlled nano-gap by using collapsible nano-fingers. First, a nano-finger array in flexible polymer (i.e. nanoimprint resist) is fabricated using nanoimprint lithography (NIL), and metallic caps, such as gold disks, are deposited on the top of each finger using electron-beam evaporation. Second, atomic-layer deposition (ALD) is used to coat a thin conformal dielectric layer. Finally, the nano-finger sample is dipped into Ethanol (water works too) and air-dried. When the Ethanol dries up, the capillary force makes the nano-fingers close together. The ALD-coated dielectric layer serves as the spacer to define the gaps between the metallic particles. If we use TiO₂ as an example, each atomic layer of TiO₂ is only about 1 Å thick, which means the gap between the metallic particles can be precisely controlled with an accuracy of 2 Å and as small as 2 Å. For the first time, we can reliably achieve such small gaps deterministically and precisely. It is the

ideal experimental platform to probe the rich sciences at the gap plasmonic hot spots.

As the polarized light shone on the dimer-like structure, it will trigger dipole-like charge distribution inside gold nanoparticle. Based on classical electromagnetic theory, field at gap center increases as the gap gets smaller. However, as gap size reduces, for sub-5 nm gap structure, electron tunneling between two gold nanoparticles becomes significant, which would cancel part of the charge in opposite sides and hence reduce the field. The competing factors result in an optimal gap size for the strongest optical field enhancement. But such a small gap structure has not been fabricated reliably until recently we demonstrated how to define and scale sub-5nm gaps by using collapsible nano-fingers

5:00pm **NS-MoA11 Strong Near-Field Coupling of Plasmonic Resonators Embedded in Si Nanowires**, *Dmitriy Boyuk, L.-W. Chou, M.A. Filler*, Georgia Institute of Technology

We show that the near-field coupling strength between neighboring infrared localized surface plasmon resonances (LSPRs) supported in Si nanowires is ~5 times stronger than reported for conventional noble metals. We specifically measure the spectral response of selectively doped Si nanowire arrays with in situ infrared spectroscopy to demonstrate this effect. Discrete dipole approximation calculations are consistent with our experimental data, revealing that this behavior arises from a synergistic combination of the nanowire's anisotropic dielectric structure and the large permittivity of intrinsic Si in the infrared. Our experiments reveal that the "universal" scaling of near-field coupling interactions (i.e., independent of material, shape, dielectric environment, etc.), which underlies the so-called "plasmon ruler" widely used to measure nanoscale distances in the chemical and biological sciences, is largely a misnomer. Rather, the plasmon ruler only yields accurate measurements in isotropic dielectric environments. Complex structures, including Si nanowires, require a more thorough exploration of their near-field coupling behavior. Our findings also demonstrate that equivalent near-field interactions are achievable with a smaller total volume and/or at increased resonator spacing, offering new opportunities to engineer plasmon-based chemical sensors, catalysts, and waveguides.

Plasma Processing for Biomedical Applications Focus Topic Room 101A - Session PB+BI+PS-MoA

Plasma Processing of Biomaterials

Moderators: Denis Dowling, University College Dublin, Deborah O'Connell, University of York, UK

2:00pm **PB+BI+PS-MoA2 Atmospheric Plasma Deposition of Antimicrobial Nano-Coatings on Biomedical Textiles**, *A. Nikiforov, I. Kuchakova, T. Coenye, C. Leys*, Ghent University, Belgium; *N. Hojnik, M. Modic, Uroš Cvelbar*, Jozef Stefan Institute, Slovenia

In this work, the antimicrobial non-woven fabrics were prepared with the use of atmospheric pressure plasma deposition. Atmospheric pressure DC jet operating in N₂ at current density of 6 mA/cm² and voltage of 15 kV is used as a source of non-thermal plasma for engineering of the antibacterial nano-composites on surface of polymeric polyethylene terephthalate (PET) meshes. Nano-particles of Ag, Cu and ZnO are tested as antimicrobial agents through incorporation in to the structure of the plasma deposited composite film. The deposition process is carried out in three steps process. The fabric is first pretreated by depositing a first layer (250 nm - 500 nm) of organosilicon thin film using an atmospheric pressure plasma system, then nano-particles are incorporated by a dipping-dry, and finally the nano-particles are covered by a second organosilicon layer of 10-50 nm thickness. Top layer in the composite coating of "sandwich-like structure" with variable thickness is used for precise control of metal ions release and so to tune antimicrobial efficiency of the material. The deposition process and surface chemistry of the coatings are studied by emission spectroscopy, and surface analysis techniques: XPS, AFM and SEM. The antimicrobial activity of the treated fabrics is also tested against *Pseudomonas aeruginosa* and *Staphylococcus aureus*. It is revealed that thickness of top (barrier) layer plays a key role in release of metal ions and negligible small antibacterial activity is observed if barrier thickness exceeds 50 nm. Tests with *S. aureus* show that the highest 98% bacterial reduction is achieved with Cu NPs whereas Ag NPs are much less effective and can provide only 79% reduction. In contrast, the fabric antibacterial efficiency against *Pseudomonas aeruginosa* is very low for both Cu and ZnO nanoparticles in spite of the load and only Ag NPs are proved to be

Monday Afternoon, November 7, 2016

effective (2 orders reduction) against of *P. Aeruginosa*. The results clearly indicate that plasma of atmospheric pressure can be used as effective tool for immobilization of nano-particles in composite coatings. Control of antibacterial activity can be achieved through variation of deposition parameters and a type of incorporate nanoparticles. The approach might present a new route to preparation of effective antimicrobial materials against of certain class of bacteria.

This work is partially supported by the M.Era-Net project "PlasmaTex".

2:20pm PB+BI+PS-MoA3 Plasma Polymers for Biomedical Applications, Farzaneh Arefi-Khonsari, l'université Pierre et Marie Curie, France; A. Baitukha, J. Pulpytel, A. Valinataj Omran, Sorbonne Universités, UPMC, France **INVITED**

In this talk, different nonequilibrium atmospheric pressure plasmas used for biomedical applications such as planar DBD, single and double barrier DBD plasma jets, and transported discharges in tubes will be discussed. Indeed in the case of the latter, deposition and surface treatment, by means of a He cold transported discharge in tubes as long as 200 cm and tube inner diameters ranging from 1 to 20 mm, can present a great potential for surface modification of polymers used as biomaterials. We have, as well as several research groups, succeeded to retain the precursor moieties to obtain PEG like polymers which present interesting antifouling properties by using planar DBD and jets. However for particular plasma applications such as making a Drug Delivery System (DDS) based on several polymer or copolymer layers, encapsulating the drug, it is more reasonable to use a low pressure plasma which can give rise to dense crosslinked barrier films. The latter are less flexible and develop microcracks due to swelling and curvature of the host biocompatible and biodegradable substrate. In order to obtain good cohesive coatings with excellent barrier and mechanical properties, it is very important to deposit layers presenting a vertical chemical gradient, where stress is gradually distributed over the rigid and flexible zones of the DDS, which is more easily deposited in low pressure plasmas. Our recent results in copolymerizing amphiphilic precursors for the use of cell adhesive or nonadhesive surfaces will be presented. Such copolymers can be also used as biodegradable multi-layer copolymers for drug delivery applications. Human ovarian carcinoma cell lines (NIH:OVCAR-3) were used for *in vitro* measurements of cell interactions with the surface of fabricated DDS. Proposed model of DDS on collagen films prevents migration, adhesion and growth of cancer cells on its surface, and by tuning the thickness of the dense barrier films, encapsulating the drug, it is possible to control the drug release kinetics and to improve the therapeutic effect. *In vivo* experiments were carried out by injecting OVCAR3 cells in mice lymph nodes to develop a tumor, followed by implantation of the DDS membranes to evaluate the feasibility of the proposed model.

3:00pm PB+BI+PS-MoA5 Plasma Coating Using Biologics: Degradation or Polymerisation?, Liam O'Neill, J. O'Donoghue, TheraDep, Ireland **INVITED**
The interaction of plasma with biomolecules is generally viewed as being a simple degradation reaction in which the plasma denatures any biologic material it encounters. Using a combination of heat, UV, free radicals, electrons and ions from the plasma, it is possible to cut, oxidise, burn and even ablate biological materials and this has established plasma sterilisation as a trusted technique in science, medicine and engineering.

However, recent research in our labs has shown that it is possible to minimise these effects and to instead use the plasma to cross-link biologic materials with retention of the biological properties of the precursor materials. Using low levels of applied plasma power, it is possible to produce low energy helium and argon plasma discharges. When biomolecules are nebulised into such a low temperature plasma, the materials are activated without losing their chemical structure. This activation can then effectively cross-link or coagulate the biomolecule without significant degradation. In addition, the plasma can activate substrates and effectively bind the biomolecules to the substrate as a thin nano-scale coating.

The result is a one-step process capable of modifying the surface of medical devices, research and diagnostic lab ware, implants and even living tissue. Tailored biological surfaces can be grown *in situ* over large areas using established equipment systems. The mechanisms used to control such reactions and to move the plasma from degradation to cross-linking modes are now being established and will be discussed. Examples of protein and polysaccharide coatings produced to date will also be presented.

4:00pm PB+BI+PS-MoA8 Low and Atmospheric Pressure Plasma Polymerization for Immunosensing and Tissue Engineering, Lenka Zajickova, A. Manakhov, E. Makhneva, J. Medalova, D. Necas, Masaryk University, Czech Republic; L. Strbkova, Brno University of Technology, Czech Republic; A. Obrusnik, M. Landova, Masaryk University, Czech Republic **INVITED**

Plasma polymerization provides a large playground for the preparation of surfaces suitable for immobilization of biomolecules and colonization by cells because chemical, structural and functional properties of plasma polymerized thin films can be tuned accordingly. The key decision for the particular application is the selection of functional chemical group that the final plasma polymer should contain. This contribution is going to discuss deposition of plasma polymers containing amine and carboxyl groups, functional groups that are typically used in biochemical applications and that are proposed to influence positively the attachment and proliferation of cells at surfaces. Amine-rich films were deposited in the low pressure pulsed radio frequency discharge using vapors of cyclopropylamine mixed with argon. The films contained primary and secondary amines and a small amount of oxygen. The structure of the films, reflected in their stability in water, could be tuned by the plasma conditions. The relationship between the amount of amine groups and the water stability was not straightforward because the films with similar amount of primary amine groups but different cross-linking could be prepared. The plasma polymers containing anhydride groups that hydrolyzed fastly at air into carboxyl groups were deposited in kHz-frequency dielectric barrier discharge at atmospheric pressure from the mixture of maleic anhydride and acetylene. The variation of the flow rate ratio was used to optimize the stability of films together with the amount of functional groups. Amine and carboxyl plasma polymers proved to be useful for the preparation of immunosensors based either on the principle of quartz crystal microbalance or surface plasmon resonance because in both these methods it is necessary to prepare a stable and reactive film on the gold surface. The amine films were also tested for the cultivation of human dermal fibroblasts and mouse myoblasts. It was identified that the water stability of the films is very important for successful experiments

4:40pm PB+BI+PS-MoA10 Low-Temperature Plasma Processing of Polymeric Materials for Biomedical Applications, Michelle Mann, M.R. Maynard, E.R. Fisher, Colorado State University

Polymeric biomaterials are widely used in medical applications such as wound healing, drug release, and blood dialysis. For example, Tygon® and similar thermoplastics are chosen for these applications because of excellent mechanical strength and flexibility but often suffer from bacterial attachment and proliferation that ultimately leads to infection and fouling of the biomedical device. Biocidal agents can be incorporated into the polymer to actively eradicate bacteria, but it is difficult to ensure that biocidal action is localized at the material-biological interface. As a result, changing the surface properties of the polymer ensures a second mechanism by which to discourage bacterial attachment and growth. Plasmas are frequently used to alter the surfaces of biomaterials, most often by surface modification or deposition of a film to discourage bacterial attachment, while retaining the bulk properties critical to device performance. Specifically, H₂O (v) plasma treatment can enhance the compatibility of biomaterials by increasing hydrophilicity and altering surface chemistry; here, we demonstrate the use of this treatment method specifically for antibacterial materials. First, we have used H₂O (v) plasmas to tune the release of an antibacterial agent (NO) from drug-releasing polymers. Composition of treated drug-releasing polymers measured via X-ray photoelectron spectroscopy demonstrates a 100% increase in oxygen content and an associated increase in wettability, as observed via water contact angle goniometry. Compared to the untreated polymer, H₂O (v) plasma treated polymers had a delayed, but equally dramatic 8-log reduction in growth of both gram-negative *Escherichia coli* and gram-positive *Staphylococcus aureus*. Second, in a related study, we utilized plasma-enhanced chemical vapor deposition to deposit a film of 1,8-cineole, an antibacterial constituent of tea tree oil. Bacterial attachment and biofilm formation assays reveal significantly reduced growth of both bacterial strains on plasma polymerized cineole films. H₂O (v) plasma treatment of these materials will also be discussed. Furthermore, optical emission spectroscopy allows correlation of gas phase excited state species in our plasmas under various plasma conditions to the resulting 1,8-cineole film surface properties, thereby allowing for fine-tuning of film surface properties for deposition onto biomedically-relevant polymer structures such as 3D polycaprolactone scaffolds. Collectively, our studies of plasma

processing of antibacterial materials demonstrate this technique is a valuable tool in the production of next generation biomedical devices.

5:00pm **PB+BI+PS-MoA11 Plasma-based Functionalization of Polystyrene Surfaces of Cell Culture Plates**, *Kazuma Nishiyama, T. Ito, S. Sugimoto, K. Gotoh, M. Isobe*, Osaka University, Japan; *M. Okamoto*, Osaka University Hospital, Japan; *A. Myoui*, Osaka University Hospital, Japan; *H. Yoshikawa, S. Hamaguchi*, Osaka University, Japan

Polystyrene is one of the most widely used cell-culture plate materials. Amino and/or carboxyl coated cell culture plates are commercially available and such surface functionalizations are known to contribute effectively to the control of growth and differentiation of various stem cells. Plasma-enhanced chemical vapor deposition (PECVD) or plasma ion implantation may be used to functionalize polystyrene surfaces of cell culture dishes. The goal of this research is to understand how such surface functionalizations are affected by plasma conditions. In this study, we have used molecular dynamics (MD) simulation to understand how incident ions and free radicals affect the formation of amines and carboxyl groups. The simulation is based on interatomic reactive potential functions developed in-house based on quantum mechanical calculations. Results of MD simulations under the conditions similar to PE-CVD by ammonia (NH₃), cyclopropylamine (CPA), or N₂/CH₃OH plasmas or ion implantation by NH₃, N₂/H₂, or N₂/CH₃OH plasmas suggest that, with energetic ion bombardment, functional groups such as primary amines are less likely to form and nitridation of the surface tends to occur. Some simulation results have been compared with experimental data obtained from parallel-plate discharges with an inverter power supply at a relatively high gas pressure of 250 - 2,500 Pa and found to be in good quantitative agreement.

Plasma Science and Technology Room 104D - Session PS+AS+SS-MoA

Plasma Surface Interactions

Moderator: Richard van de Sanden, FOM Institute DIFFER, Netherlands

1:40pm **PS+AS+SS-MoA1 Atomic-scale Analyses of Plasma Etching for Unconventional Materials in Microelectronics**, *Satoshi Hamaguchi, K. Karahashi*, Osaka University, Japan

INVITED

As the sizes of semiconductor devices continue to diminish and are now approaching atomic scales, the downsizing of transistors following Moore's law is bound to end in the near future. However, the continuing market demand for higher performance and lower energy consumption of large-scale integrated (LSI) circuits has driven invention of new device technologies such as three-dimensional (3D) device structures and devices based on non-silicon materials. Manufacturing of these non-conventional devices also poses new challenges for processing technologies. For example, magnetic materials used in magnetoresistive random-access memories (MRAMs) cannot be etched efficiently by the existing reactive ion etching (RIE) technologies, which has so far limited the level of integration of MRAM devices. The modern near-atomic-scale devices also require atomic level precision in their manufacturing processes, which has also driven new technologies such as atomic layer deposition (ALD) and atomic layer etching (ALE). In this study, we shall review our recent work on analyses of etching selectivity and surface chemical reactions for magnetic materials [1,2] metal oxides[3,4], Si-based materials [4] as well as damage formation mechanisms [6,7] due to ion bombardment during RIE processes. In our analyses, we use multi-beam injection experiments [8] and molecular dynamics (MD) simulations to emulate elementary processes of plasma-surface interactions that take place in RIE processes.

References

- [1] M. Satake, M. Yamada, H. Li, K. Karahashi, and S. Hamaguchi, J. Vac. Sci. Tech. B **33** (2015) 051810.
- [2] H. Li, Y. Muraki, K. Karahashi, and S. Hamaguchi, J. Vac. Sci. Tech. A **33** (2015) 040602.
- [3] H. Li, K. Karahashi, M. Fukasawa, K. Nagahata, T. Tatsumi, and S. Hamaguchi, J. Vac. Sci. Tech. A **33** (2015) 060606.
- [4] H. Li, K. Karahashi, M. Fukasawa, K. Nagahata, T. Tatsumi, and S. Hamaguchi, Jpn. J. Appl. Phys. **55** (2016) 021202.
- [5] K. Miyake, T. Ito, M. Isobe, K. Karahashi, M. Fukasawa, K. Nagahata, T. Tatsumi, and S. Hamaguchi, Jpn. J. Appl. Phys. **53** (2014) 03DD02.
- [6] K. Mizotani, M. Isobe, and S. Hamaguchi, J. Vac. Sci. Tech. A **33** (2015) 021313.

[7] K. Mizotani, M. Isobe, M. Fukasawa, K. Nagahata, T. Tatsumi and S. Hamaguchi, J. Phys. D: Appl. Phys. **48** (2015) 152002.

[8] K. Karahashi and S. Hamaguchi, J. Phys. D: Appl. Phys. **47** (2014) 224008.

2:20pm **PS+AS+SS-MoA3 Plasma Wall Interactions: Y₂O₃ Wall Interaction in Cl₂ Plasma Etching of Si and NF₃ Plasma Cleaning**, *Tianyu Ma, T. List, V.M. Donnelly*, University of Houston

The walls of a plasma etching chamber play a critical role in causing variability of processing metrics such as rate, profile shape and selectivity. Small changes in the nature of the chamber wall surfaces can affect radicals sticking coefficients, recombination probabilities, and other heterogeneous reactions that will cause changes in the number densities of species in the plasma, which in turn affects the process. Therefore, a stable chamber wall material is essential for plasma processes, and in particular plasma etching. Compared to traditional alumina and silica wall material, Y₂O₃ has high chemical stability and extending lifetime, making it one of the preferred wall materials in etching systems. Consequently, studies were performed in a chamber with Y₂O₃-coated walls to determine time-dependent variations in the number densities of species in inductively coupled Cl₂/Ar and NF₃/Ar plasmas. Si was etched in Cl₂ plasmas, after which, the wafer was removed and an NF₃ plasma was used to remove etching products that deposited on the walls. This etch-clean procedure was repeated many times, simulating an integrated circuit manufacturing etch process. Optical emission spectroscopy (OES) and Langmuir probe analysis were performed to characterize plasma. Y₂O₃-coated coupon pieces exposed to the plasma were examined by X-ray photoelectron spectroscopy (XPS). Number densities of Cl₂, Cl, O, and F were obtained with rare-gas actinometry during the entire etching and cleaning cycles. Emissions from Si, SiCl, SiCl₂, SiCl₃, SiF, and N₂ were also recorded. After exposure to the NF₃ plasma, Cl number densities are relatively low when no substrate bias is placed on the Si substrate. As soon as bias is initiated, Cl number density rises steeply at first and then slowly maximizes. This is attributed to then displacement of F on the walls with a SiCl_x containing layer. Apparently Cl on its own cannot remove F efficiently, but the reaction of Si-containing etching products produces SiF surface species that desorb and are observed as transient SiF emission in the first moments of etching. Cl recombination on this surface is much lower than on the fluorinated Y₂O₃ surface. Once prepared by etching Si with bias, the Cl number density remains high if bias is extinguished and etching nearly stops. The higher recombination coefficient on fluorinated surfaces is attributed to the longer residence time of physisorbed Cl, caused by the attraction to positively charged Y sites that are created when Y forms mainly ionic bonds with F.

2:40pm **PS+AS+SS-MoA4 Novel atomic order CD Control Technology by Fusion of Quasi-ALE and ALD**, *Yoshihide Kihara, T. Hisamatsu*, Tokyo Electron Miyagi Limited, Japan; *T. Oishi, S. Ogawa, H. Watanabe*, Tokyo Electron Miyagi Limited; *A. Tsuji, M. Honda*, Tokyo Electron Miyagi Limited, Japan

In the recent years continuous scaling has required the use of multiple mask patterning technologies such as double and quadruple patterning, and increasingly thin EUV mask films are being planned to be used in the near future. In the patterning process, the fabrication of multilayer films requires the precision of atomic layer level accuracy (within nm level). Some critical challenges that patterning schemes face includes thinning of mask materials, reduction of ARDE related CD-loading, and reduction of LER and LWR. This requires the realization of highly selective etch processes that can address the challenges without trade-offs in other process specifications.

One method to increase the mask selectivity to enable mask thinning, which is one of the major patterning issues, Si-ARC is etched in a depositing condition which protects the resist mask surface, utilizing the material difference between the mask material and the antireflective layer (Si-ARC). However, to enhance selectivity, extra amount of the deposition can be generated. The amount of deposition flux fluctuates depending on the pattern density, leading to CD loading. In order to solve the tradeoff between selectivity and loading, we have proposed a Quasi- Atomic Layer Etching (Quasi-ALE) which is a modification of ALE to employ thin-film adsorption and activation by low ion energy [1]. In this paper, Quasi-ALE is applied to Si-ARC etch step to address three challenges; high selectivity, pattern-independent CD-loading, and vertical etch profiles.

We have also proposed the combination of ALD with etch as CD-loading-free CD control technique [2]. By combining ALD and Quasi-ALE, excellent CD controllability was achieved to address the entire patterning process issues without tradeoffs. In the presentation, various merits of the Fusion Process, which is a combination of Quasi-ALE and ALD, in patterning

Monday Afternoon, November 7, 2016

process, will be introduced. Fusion Process has a significant potential to solve critical challenges in the patterning process of N7, N5 and beyond.

Reference

[1] A.Tsuji et al., AVS 62nd Int. Symp. (2015)

[2] T.Hisamatsu et al., AVS 62nd Int. Symp. (2015)

3:00pm PS+AS+SS-MoA5 Development of a New Analysis Technique of Nanostructures Etched by Plasmas: Quasi In-Situ TEM EDX Characterization, *Matthieu Serege*, LTM, Univ. Grenoble Alpes, CEA-LETI; *G. Cunge*, LTM, Univ. Grenoble Alpes, CEA-LETI, France; *L. Vallier*, *E. Latu-Romain*, LTM, Univ. Grenoble Alpes, CEA-LETI; *O. Joubert*, LTM, Univ. Grenoble Alpes, CEA-LETI, France

As the size of integrated circuit continues to shrink, plasma processes are more and more challenged and show limitations to etch nanometer size features in complex stacks of thin layers. The achievement of anisotropic etching relies on the formation of passivation layers on the sidewalls of the etched features which act like a protective film that prevents lateral etching by the plasma radicals. However, this layer also generate a slope in the etch profile and it's difficult to control the layer thickness. Another thin layer called "reactive layer" is also formed at the bottom of the feature where the energetic ion impact mix the material to be etched with the plasma radicals. Etch products are formed allowing a high etch rate of the silicon substrate. It starts to be realized that controlling the thickness of this reactive layer is the key to achieve very high selective processes. Indeed, accurate etch stop on an ultra-thin layer is only possible if the thickness of this stop layer is higher than the thickness of the reactive layer otherwise damages are created underneath the stop layer.

A better understanding of these layers chemical nature, thickness and deposition mechanism is mandatory, but the main problem is that the layers to be analyzed are chemically highly reactive because they contain large concentrations of halogens and they get immediately modified (oxidized) when exposed to ambient atmosphere.

In this work we develop an original, simple and extremely powerful approach to observe passivation layers quasi in-situ (i.e. without air exposure): After plasma etching, the wafer is transported *under vacuum* inside an adapted suitcase to a deposition chamber where it is encapsulated by a metallic layer (magnetron sputtering PVD). Then, the encapsulated features can be observed ex situ without chemical / thickness modification using FIB-SEM (specimen preparation) coupled with a TEM-EDX analysis: HRTEM observation provides an extremely precise measurement of the passivation layer and encapsulation morphology. In parallel, STEM-EDX is used to map the main atomic element in our specimen, supplying qualitative information on the layer chemical composition. STEM-EDX is also used in profile mode to give us more accurate quantitative analysis. We are able to estimate the (relative) quantitative atomic concentration along a line scan profile on the feature sidewalls.

The measurements relatively fast, provide accurate analysis at the nanoscale, and are highly promising to better understand plasma etching processes. Therefore, this technique will be very helpful to develop innovative processes controlled at the nanometer range.

3:20pm PS+AS+SS-MoA6 Atomistic Simulations of He Plasma Modification of Si/SiN Thin-Films for Advanced Etch Processes, *Vahagn Martirosyan*, LTM, Univ. Grenoble Alpes, CEA-LETI, France; *E. Despiou-Pujo*, CNRS - LTM, France; *O. Joubert*, LTM, Univ. Grenoble Alpes, CEA-LETI, France

Due to high ion bombardment energies and significant fragmentation rates, conventional continuous

wave (CW) plasma processes are not able to selectively etch ultra-thin films without damaging the

active layers of advanced nanoelectronic devices (e.g. FDSOs, FinFETs). In particular, silicon nitride

or low-k spacers etching must be performed with nanoscale-precision without creating defects to the

underlayer substrate, to preserve device performances and be compatible with epitaxial steps. To

solve this problem, one possible alternative is to use a recently developed etch technology, which

consists of two steps [1]. In the first step, the material to be etched is exposed to a hydrogen (H₂) or

helium (He) ICP or CCP plasma; in the second step, the modified material is chemically etched by wet

cleaning or exposure to gaseous reactants only.

Due to the complexity of plasma-material interactions, the development of such a new etch approach

requires a more detailed understanding of the fundamental mechanisms involved in the process.

Therefore, we develop Molecular Dynamics (MD) simulations to study the Si-He and Si-N-He systems

and provide an overview of the reaction processes at the atomic scale. The objective is to understand

precisely the role of ion energy in the self-limited ion implantation, and to determine the relationship

between the flux/energy of plasma species (He +) bombarding the surface and its structural/chemical

modifications.

In this work, we investigate the interaction between helium plasma species (He+ ions) and

silicon/silicon nitride via MD simulations, by studying the influence of ion energy (5-100eV) and ion

dose on the substrate modification. For He/Si interactions, simulations show an initial He implantation

followed by the formation of a stable modified layer at steady state, composed of two parts: a Si-He

mixed amorphous layer and a thin sublayer, which is crystalline but enriched in helium. According to

our results, the higher is the ion energy, the more rapid is the contamination and the thicker is the

amorphous layer. Few or no Si sputtering is observed for energies lower than 100eV, confirming that

He plasmas can modify/weaken the material on a precise depth without etching it. Amorphisation of

the material leads to the rupture of crystalline Si-Si bonds and to the creation of a less dense modified

layer, facilitating its subsequent removal by wet or dry etching. Mechanisms of helium

retention/desorption, as well as comparisons between He/Si and He/SiN interactions, will be

discussed during the presentation.

References

1. N. Posseme, O. Pollet, S. Barnola, Applied Physics Letters 105, 051605 (2014)

4:20pm PS+AS+SS-MoA9 Patterned Chromium Hard Mask Etching in a Two Reactant Gas for Bit Patterned Media Template Fabrication, *Daniel Staaks**, Molecular Foundry, Lawrence Berkeley National Lab; *X. Yang*, Seagate Technology; *S. Dallorto*, *S.D. Dhuey*, *S. Sassolini*, Molecular Foundry, Lawrence Berkeley National Lab; *K.Y. Lee*, Seagate Technology; *I.W. Rangelow*, Ilmenau University of Technology, Germany; *D.L. Olynick*, Molecular Foundry, Lawrence Berkeley National Lab

Plasma-based dry etching is one of the most important nanofabrication methods for transferring full-wafer patterns. As feature sizes approach the single digit nanometer regime, there is an urgent need to develop a comprehensive and detailed understanding of the associated etching mechanisms. Additionally, challenges in obtaining high anisotropy, high selectivity, and robust critical dimension control must be addressed.

Highly selective chromium etching masks are an area of particular interest. Chromium has a widespread utility in not only manufacturing photolithography masks, but also in fabricating high-resolution nanoimprint templates. For example, we use it as a highly selective hard mask when etching SiO₂ to achieve Bit Patterned Media templates towards sub-5nm features (7Tb/in²).

To date, there have been few investigations into patterned chromium films. The limited studies available involve micron-sized features and patterning by the erosion of polymer masks, which make extrapolation to the single-digit nano regime very difficult. In this work, we bridge the gap for nanoscale-patterned films. We etch a patterned 20nm layer of chromium in low pressure and low power Cl₂/O₂ plasmas. We investigate

* Coburn & Winters Student Award Finalist

the profile evolution of features ranging from 15nm- to 200nm in pitch. Previous work in etching blanket chromium films revealed that chromium etch rate was influenced by substrate temperature and Cl_2/O_2 flow [1]. Here, we vary percent O_2 flow (1%, 50%, 87%) and temperature (-50°C, +20°C) to explore the effects on lateral etching mechanisms, etch lag, and anisotropy. Using a highly selective HSQ mask for etching the chromium allows us to better determine the involved etching mechanisms. High-resolution micrographs of thin film cross-sections show significantly enhanced anisotropy at low temperatures.

Additionally, the unique etching chemistry of chromium must be considered when evaluating the material as a mask. Most materials form multiple volatile binary compounds during the etching process. Chromium, on the other hand, forms a single ternary compound: chromyl chloride. This enables us to study the effect of two-reactant gas chemistry on the etched feature profile. Results indicate that gas phase transport and surface mass transport of oxygen and chlorine are influential to profile shapes. Moreover, the effective local oxygen concentration inside the trench is important, and surface-dominated reactions highly affect the profile. Chlorine rich and chlorine poor chemistries promote very different surface reactions.

[1] D. Staaks, et al., Low temperature dry etching of chromium towards control at sub-5 nm dimensions, Nanotechnology 2016, submitted manuscript

4:40pm **PS+AS+SS-MoA10 Alternative Solutions for Nanometric-Precision Etching: H₂ Plasmas Modification of Si/ SiN Thin-Films**, *Emilie Despiiau-Pujo, V. Martirosyan, O. Joubert*, LTM - CNRS/Univ Grenoble Alpes/CEA, France

Consisting of several ultrathin layered materials, advanced transistors (FDSOI, FinFET) must be etched with a nanometric precision and nearly infinite selectivity to preserve the electronic properties of active layers (e.g. the silicon channel), a challenge which cannot be addressed by conventional CW plasma processes. To achieve uniform and damage-free etching of multi-layered transistors, an alternative etch approach has been recently proposed, consisting in two steps. In a first step, the film to be etched is modified in volume by exposition to a hydrogen or helium conventional CCP or ICP; in a second step, the modified layer is selectively removed by wet cleaning or exposure to gaseous reactants only. Such a two-steps process showed promising results for silicon nitride spacers etching [1]. To assist the development of this new technique, Molecular Dynamics (MD) simulations - coupled to experiments - are used to investigate the interactions between H₂ plasmas and Si/SiN films. These atomic-scale simulations aim at better understanding the relationship between the flux/energy of plasma species (H_x⁺ ions, H radicals) bombarding the surface and its structural/chemical modifications.

Although one material of interest is silicon nitride, the study of Si-H systems constitutes a first step to understand the impact of ion energy (5-100 eV) and ion dose on the substrate modification and self-limited ion implantation. Simulations of cumulative H_x⁺ (x=1-3) ion bombardment show a rapid hydrogenation of Si followed by the formation of a stable modified layer at steady state. This modified layer is composed of a thick amorphous Si-H mixed layer and a thin sublayer, quasi-crystalline but enriched in hydrogen. As hydrogen is highly chemically reactive, ion implantation leads to the rupture of crystalline Si-Si bonds and to the creation of SiH, SiH₂, SiH₃ covalent bonds in the modified material. At the bottom of the modified layer, hydrogen tends to saturate the dangling bonds of the amorphous silicon and to create SiH₃ bonds, thus fracturing the substrate into a modified hydrogenated layer weakly bound to the underlying crystalline material (Smartcut-like mechanism). The influence of ion dose, ion energy and ion type on the modified layer thickness (and thus on the subsequent etch precision) are discussed. Comparisons between pure ion implantation and exposition to various H₂ plasma conditions (simulated by bombarding the Si/SiN substrates with both H_x⁺ ions and H radicals) are also presented. [1] N. Posseme, O. Pollet, S. Barnola, Applied Physics Letters 105, 051605 (2014)

5:00pm **PS+AS+SS-MoA11 Plasma Dynamics at the Surface Interface in Low Pressure Capacitively and Inductively Coupled Plasmas**, *Martin Blake, D. O'Connell*, University of York, UK; *A.R. Gibson*, LPP, CNRS, Ecole Polytechnique, Université Paris-Saclay, France; *T. Gans*, University of York, UK

The plasma-surface interface in low temperature, low pressure plasmas used for industrial

wafer processing is difficult to characterise. However, understanding the plasma dynamics

at this interface is key for further optimisation of industrial plasma processes. Of particular

relevance are the densities of reactive species, such as atomic oxygen, in this region. In this

work a methodology has been developed based on newly augmented fast optical

techniques which can probe reactive species densities in the wafer region without the need

for expensive laser equipment. This technique, known as energy resolved actinometry

(ERA)[1], utilises phase resolved optical emission spectroscopy (PROES) measurements of the

direct and dissociative electron-impact excitation dynamics of three distinct emission lines,

750.4 nm (argon, added in small concentrations as a tracer gas) and 777.4 nm, 844.6 nm

(atomic oxygen). Through the ratio of the excitation functions and their energy dependence

we determine both the atomic oxygen density and the mean electron energy above the

electrode surface.

In this work ERA has been applied to measure atomic oxygen densities and local mean

electron energies in a low pressure (1 – 100 Pa) oxygen plasma produced in a GEC reference

cell system [2], operated at 13.56 MHz in both capacitive and inductive modes at power

inputs ranging from 50 – 500 W. Additional characterisation of the plasma-surface interface

is carried out through the use of a retarding field energy analyser (RFEA) to measure the ion

energy distribution at the surface. The combination of both approaches allows for

information on the neutral and ion dynamics in the surface region, both of which are known

to be important for process outcomes.

A two-dimensional hybrid plasma simulation code is used to simulate the same conditions in

order to improve understanding of the experimental results.

Acknowledgements:

This work has been supported through the UK Engineering and Physical Sciences Research

Council (EPSRC) manufacturing grant EP/K018388/1 and the authors would also like to thank

Intel Ireland, Ltd. for financial support.

References:

[1] Greb, A., Niemi, K., O'Connell, D., Gans, T. 2014; Energy resolved actinometry for

simultaneous measurement of atomic oxygen densities and local mean electron energies in

radio-frequency driven plasmas, Appl. Phys. Lett. 105 234105

[2] P. J. Hargis Jr et al (1994); The Gaseous Electronics Conference radio-frequency reference

cell: A defined parallel-plate radio-frequency system for experimental and theoretical

studies of plasma-processing discharges, Rev. Sci. Instrum. 65, 140

Plasma Science and Technology

Room 104B - Session PS-MoA

Advanced BEOL/Interconnect Etching

Moderator: Hisataka Hayashi, Toshiba, Japan

1:40pm PS-MoA1 The Search for New Multi-Pattern Etch Colors: Usual (SiO_2 , SiN , SiC) and Unusual (hi-k, BN, BC:H) Suspects, Michelle Paquette, S. Dhungana, B.J. Nordell, A.N. Caruso, University of Missouri-Kansas City; W.A. Lanford, University at Albany; G. Chollon, C. Pallier, F. Teyssandier, Universite de Bordeaux, France; K. Scharfenberger, D. Jacob, S.W. King, Intel Corporation

To continue the aggressive scaling of integrated circuit feature size demanded by current and future technology nodes, the microelectronics industry has turned to multiple patterning techniques to overcome lithography limitations. These techniques use a series of lithography and etch pattern transfer steps that require a variety of photoresist, hardmask, spacer, etch stop, and other specialized layers. These various pattern transfer materials can be categorized into 'colors,' where each color can be uniquely processed. As multiple patterning designs become increasingly complex, a number of different patterning materials with near-perfect etch selectivity will be needed, for which the current selection of materials will not suffice. Many previous etch studies have investigated the effects of plasma conditions on etch rates for common classes of metal and dielectric materials, but fewer have looked at the dependence of etch rates on material composition within a given class, and fewer still have analyzed the relative etch rates of multiple material classes and compositions under identical treatment conditions. We have surveyed etch rates for a wide range (>300) of samples using two common fluorinated etches traditionally used to pattern silicon-oxide-based (CHF_3) and silicon-nitride-based dielectrics (CF_4/O_2). These samples were drawn from material classes falling within the common Si-C-O-N-H composition space (e.g., SiO_xH , $\text{SiO}_x\text{C}_y\text{H}$, $\text{SiN}_x\text{C}_y\text{H}$), as well as classes not traditionally considered for patterning applications including hi-k dielectrics (e.g., Al_2O_3 , HfO_2) and boron-rich solids (e.g., BN:H, BP:H, BC:H). Surveying such a wide range of materials with varying densities and chemical stoichiometries has allowed us to look at both the effect of composition on etch rates as well as the relative etch rates between classes. From this information, we are able to propose materials that may serve as additional etch colors, drawn from within the classes studied, and by extrapolating the observed trends to different composition spaces.

2:00pm PS-MoA2 An Investigation into the Mechanism of High Selectivity SiO_x and SiN_x Dielectric Etching, Robert Bruce, H. Miyazoe, N.P. Marchack, IBM Research Division, T.J. Watson Research Center; J. Lee, J.C. Shearer, IBM Research, Albany, NY; J.M. Papalia, S.U. Engelmann, E.A. Joseph, IBM Research Division, T.J. Watson Research Center; J.C. Arnold, IBM Research, Albany, NY

As the semiconductor industry drives critical dimensions smaller for 7nm technology node and beyond, the challenges to dielectric etch for logic and memory chip manufacturing become ever greater. The established method of high performance dielectric etching is to employ a plasma process using a fluorocarbon (FC) gas that provides material-dependent selective deposition and sidewall passivation as the etch proceeds. Depending on the FC gas chemistry, SiO_x will etch selectively over SiN_x or vice versa. We investigate dielectric etch process parameters that influence dielectric material selectivity ($\text{SiO}_x/\text{SiN}_x$ or $\text{SiN}_x/\text{SiO}_x$) and pattern fidelity, including gas type and wafer temperature. We also study the possibility of improving selectivity by separating the FC deposition and etching steps (i.e. atomic layer etching).

2:20pm PS-MoA3 The Impact of Highly Selective Dielectric Etches on Etch Stop Layers, Andre Labonte, GLOBALFOUNDRIES; A. Carr, IBM; J.M. Dechene, GLOBALFOUNDRIES; J.C. Shearer, IBM; J.M. Lucas, B. Messer, A. Metz, Tokyo Electron America

As the semiconductor industry drives to sub 50nm gate and interconnect pitches, aspect ratios of contact and via structures are increasing. Subsequently, dielectric and etch stop layers are being thinned to mitigate the increase in aspect ratios. Likewise, the ongoing pursuit of scaling, without proportional changes in overlay, are driving the need for ever more selective Self-Aligned Contact (SAC) dry etch processes. As with any plasma, there is the potential to cause plasma damage to exposed surfaces and stop layers. The plasma damaged materials may in turn be susceptible to significant changes in their properties which may enhance or inhibit future removal of the stop layer. Finally, due to the thinner stop layers being used, this change of material properties in a plasma damaged layer

may not be limited to the surface of the layer, but may in fact convert the entire film.

In this paper, we discuss an example where a dielectric system, etched with a SAC process, exhibited an unexpected change in the material properties of the underlying etch stop layer. Process partitioning and materials analysis were used to confirm the unexpected result and develop a theory for observed changes.

2:40pm PS-MoA4 Plasma Etching of High Aspect Ratio Contacts in SiO_2 using $\text{Ar}/\text{C}_4\text{F}_8/\text{O}_2$ Mixtures: A Computational Investigation, Shuo Huang, C.M. Huard, University of Michigan; S. Shim, S. Lee, I.-C. Song, S. Lu, Samsung Electronics Co., Ltd.; M.J. Kushner, University of Michigan

As feature sizes continue to shrink and aspect ratios continue to increase in semiconductor processing, maintaining critical dimensions (CDs) of the features becomes more challenging. This is particularly the case for dielectric etch of high aspect ratio (AR) contacts (HARC), in which aspect ratios of 50-100 are desired. Our interests in this investigation are two challenges in the reactive ion etching of HARC in SiO_2 using $\text{Ar}/\text{C}_4\text{F}_8/\text{O}_2$ mixtures. The first is aspect ratio dependent etching (ARDE) where etch rates generally decrease as AR increases. The second is the origin of non-circular vias from nominally initially circular mask openings.

We report on results from a computational investigation of etching of HARCs in SiO_2 using $\text{Ar}/\text{C}_4\text{F}_8/\text{O}_2$ mixtures in a tri-frequency capacitively coupled plasma. Modeling of reactor scale and surface chemistry was performed using the Hybrid Plasma Equipment Model (HPEM). The feature scale modeling was performed using a 3-dimensional implementation of the Monte Carlo Feature Profile Model (MCFPM). The reactor utilizes 3 frequencies, two lower frequencies generally less than 10 MHz and 1 higher frequency of 50-100 MHz. For total powers approaching and exceeding 10 kW, radical fluxes to the wafer are dominated by CF_x , O and F due to there being significant dissociation of feedstock gas. Ion fluxes are dominated by Ar^+ and C_nF_x^+ .

The general trend of ARDE is observed - etch rates decrease with etch depth within a feature and features simultaneously etched show lower etch rates in smaller features. However, peaks in the instantaneous etch rate may occur when the profile becomes tapered, which funnels hot neutrals to the etch front. Factors contributing to ARDE such as molecular transport of neutral species, shading of ions with non-normal incidence and etch front geometry will be discussed. The origin of non-circular vias is likely due to small asymmetries and imperfections in the mask, which are reinforced during the etch process.

Work was supported by Samsung Electronics Ltd., Department of Energy Office of Fusion Energy Science and the National Science Foundation.

3:00pm PS-MoA5 BEOL & Interconnect Challenges in Memory Scaling, Mark Kiehlbauch, Micron Technology

INVITED

Interconnect challenges in memory are driven by scaling, novel architectures, and novel memories.

As NAND and DRAM scale, the pitch of the lower levels of metal routing shrink concurrently. With the delay in EUV lithography, 193 immersion together with complex pitch multiplication and multipatterning schemes have been implemented. These have etch challenges with regard to LWR, selectivity, and feature scale CDU.

The implementation of so-called More than Moore in memory is primarily TSV and 3D packaging to deliver multichip memory packages with extremely high bandwidth and also memory plus logic packages. Over the past several years, the integration of these technologies into high performance and cost effective packages has driven a continuous refinement of etch requirements.

Finally, new memory technologies have resulted in aggressive scaling of interconnects with unique profile and CDU requirements.

In each case, the process, hardware, and integration approaches to address these problems will be discussed.

4:00pm PS-MoA8 Control of Uniformity and Ion Energy Distributions in Tri-frequency Capacitively Coupled Plasmas Accounting for Finite Wavelength Effects, Peng Tian, S. Huang, University of Michigan; S. Shim, S. Lee, I.-C. Song, S. Lu, Samsung Electronics Co., Ltd.; M.J. Kushner, University of Michigan

To provide additional means of control of capacitively coupled plasmas (CCPs) for semiconductor processing, multi-frequency systems are being investigated. Current plasma tools now have up to 3 frequencies. The source is typically a high frequency (50-150 MHz) intended to control ionization. The biases, typically low frequencies of a few to 10 MHz, are

Monday Afternoon, November 7, 2016

used to control ion energy distributions. At sufficiently high frequencies, the applied power takes on electromagnetic properties (as opposed to electrostatic) in which the electric field is wave-guided by the plasma sheath, causing constructive and destructive interference over the wafer. In extreme cases, a center-high electric field is produced along with a non-uniform center-high plasma density. The mixing of frequencies in tri-frequency systems (TF-CCPs) has the potential to mitigate finite wavelength effects while also providing opportunities to control IEDs.

In this work, TF-CCPs were investigated using a 2-dimensional hydrodynamic model with a full-wave FDTD (finite-difference-time-domain) solution of Maxwell's equations. Results will be discussed for plasma uniformity and IEDs for Ar and Ar/C₄F₈/O₂ gas mixtures at 10s of mTorr, with frequencies of a few MHz, 10 MHz and up to 150 MHz with collective powers of up to 10-15 kW. We found that at these elevated powers, the ability to separately control ion fluxes and IEDs is at best difficult. For these conditions, the system should be viewed as a collective set of 3-frequencies that have symbiotic contributions, as opposed to separate contributions that can be uniquely controlled.

Work was supported by Samsung Electronics Ltd., Department of Energy Office of Fusion Energy Science and the National Science Foundation.

4:20pm PS-MoA9 Metal Etch Mechanisms Using NH_x and CN-based Chemistry, Nathan Marchack, IBM Research Division, T.J. Watson Research Center; *M. Yamazaki, Q. Yang, N. Joy*, TEL Technology Center, America, LLC; *S.U. Engelmann, E.A. Joseph*, IBM Research Division, T.J. Watson Research Center; *A. Ranjan*, TEL Technology Center, America, LLC

While numerous processes for generating volatile metal etch products have been established in the field of plasma processing, there remain certain families of elements, e.g. ferromagnetic transition metals and their alloys, which have yet to display similar etch mechanisms. These and similar elements are finding increasing utility in novel memory technologies and thus their patterning at shrinking length scales poses an interesting problem for future technology nodes.

The existence of gas phase organo-metallic precursors such as M[(CO)]_x (where M = Ni, Fe, Co, etc.) has piqued curiosity in seeking pathways to generate such species using NH₃/CO chemistry in the literature[1], however experimental observation of such byproducts in the gas or plasma phase through techniques such as mass spectrometry has not been reported[2]. Older literature may suggest alternative mechanisms involving the reaction of such metals in the gas phase with linear nitriles[3] and amines[4]. We explore potential reactions of such organic species generated in a variety of high density plasma sources, with a focus on defining how parameters such as source power, type, and gas ratio affect the discharge properties.

The results of this study will then be applied to patterned film stacks of commonly reported metal elements (e.g. Ni, Fe, Co) demonstrating a potential means for etching these materials at tighter pitches (<200nm) for line/space and pillar geometry with reduced sidewall residue and minimal hard mask loss.

References:

- [1]: Kubota et al., Journal of Magnetism and Magnetic Materials, 272-276, 2004.
- [2]: Jeon et al., Journal of Vacuum Science and Technology A, 33, 061304, 2015.
- [3]: Lebrilla et al., Journal of American Chemical Society, 109, 5639-5644, 1987.
- [4]: Radecki and Allison, Journal of American Chemical Society, 106, 946-952, 1984.

4:40pm PS-MoA10 The Impact of Gate Overlap on Self-Aligned Contact (SAC) Etching, Jeffrey Shearer, IBM Research Division, Albany; *A.P. Labonte*, GLOBALFOUNDRIES; *J.M. Lucas, A. Metz*, Tokyo Electron - TTCA; *J.C. Arnold*, IBM Research Division, Albany

In order to maintain aggressive scaling trends, gate and contact pitches have been reduced to a level requiring robust contact-to-gate self-alignment in order to mitigate gate-to-contact short concerns. Developing novel reactive ion etch (RIE) chemistries to achieve the necessary etch selectivity to the gate cap is one of the more critical challenges in integrated circuit (IC) process development and manufacturing. Further complicating the process space is that selectivity is impacted by the contact-to-gate overlap. This overlap can be intentionally modulated by pitch demands, mask design, and contact critical dimension (CD) or unintentionally modulated by contact-to-gate overlay shifts. Data will show a substantial difference in selectivity between one-sided (borderless) and

two-sided ("true SAC") contact-to-gate overlaps. As both situations could exist on-wafer, it is increasingly difficult to develop robust processes that can accommodate a variety of different contact designs at the same time. The data will show how process optimization can minimize some of the challenges in developing a robust process space and will explore the parameter space that can maximize the SAC selectivity process window across multiple overlap regimes. Lastly, it will be shown how overetch impacts the selectivity of the gate cap in terms of the contact-to-gate overlap. This work was performed by the Research Alliance Teams at various IBM Research and Development Facilities.

5:00pm PS-MoA11 Dynamic Plasma Etching of EUV Photoresist for Contact Profile Control and PR Selectivity Improvement, Hongyun Cottle, I. Saraf, A. Metz, P. Biolsi, TEL Technology Center, America, LLC

Continued pitch scaling of semiconductor devices to 7nm node and beyond dimensions utilizing conventional 193i based multiple patterning techniques is rapidly driving up cost, complexity, and variability control. EUV patterning can be used to mitigate or delay the challenges of pitch scaling through multiple patterning, but introduces new challenges of its own. EUV lithography introduces new types of resists that are thinner and less etch resistant compared to conventional 193nm resists. Interactions of polymers with plasma etch environments can lead to large changes of the polymer material properties and the three-dimensional nanostructures they pattern. Mask deformation during such etch process can lead to changes in nanoscale topography of device features, often with undesirable consequences, such as increased LER and LWR, tip-to-tip degradation, and line wiggling. Plasma etch faces a significant challenge to optimize its process window to enable high yields with EUV patterning.

This paper presents a unique etch process employing a dynamic etch during softmask open to improve EUV photoresist etch selectivity by greater than two fold while maintaining critical feature dimensions, such as elliptical contact minor vs major axis CD ratio. By carefully controlling the polymer deposition vs. polymer assisted etching temporal cycle, a very thin layer of conformal polymer can be used to precisely etch and transfer the desired pattern. By utilizing a direct current superposition (DCS) technology, EUV photoresist can be treated to improve not only its etch resistant, but also LER and LWR. After the in-situ photoresist treatment, the dynamic etch process initiates and defines the pattern transfer into softmask, followed by etch steps to anisotropically complete the pattern transfer. Reported is the structural characterization pre and post-etch detailing LER and LWR improvement, and shrink ratio control. In addition, a mechanistic model will be proposed based on optical emission spectroscopy (OES) and thin film compositional analysis.

Novel Trends in Synchrotron and FEL-Based Analysis Focus Topic

Room 103C - Session SA+AS-MoA

Frontiers of Photoemission with Synchrotron and XFEL Radiation/Advances in High-resolution Imaging Techniques

Moderators: Maya Kiskinova, Elettra-Sincrotrone Trieste, Italy, Olivier Renault, CEA-University Grenoble Alps, France

1:40pm SA+AS-MoA1 Photoemission with Soft and Hard X-Rays: Past, Present, and Future, Charles Fadley

University of California, Davis INVITED

In this talk, I will begin by briefly reviewing some of the key early developments in soft x-ray photoelectron spectroscopy (XPS), angle-resolved XPS (ARXPS), x-ray photoelectron diffraction (XPD), and soft x-ray angle-resolved photoemission (ARPES). I will then consider combining these well-established methods with more recent techniques involving the tailoring of the x-ray wavefield through standing-wave (SW) excitation or total-reflection (TRXPS) to provide enhanced depth resolution and the use of hard x-ray excitation in the multi-keV regime (HXPS, HAXPES) to study bulk materials and buried layers and interfaces [1-5]. Applications to semiconductor- [1], oxide- [2,4,5], and magnetic- [2] heterostructures, as well as liquid/solid interfaces [3] will be considered. Future possibilities combining these approaches with variable polarization, as well as spin-, space-, and time- resolution will also be discussed.

Acknowledgements:

This work was supported by the U.S. Department of Energy, Contracts DE-AC02-05CH11231 at LBNL and DE-SC0014697 at UC Davis, and through the LDRD Program of LBNL.

References:

[1] "Bulk Electronic Structure of the Dilute Near-Ferromagnetic Semiconductor $\text{Ga}_{1-x}\text{Mn}_x\text{As}$ via Hard X-Ray Angle-Resolved Photoemission" A. X. Gray, J. Minar, S. Ueda, P. R. Stone, Y. Yamashita, J. Fujii, J. Braun, L. Plucinski, C. M. Schneider, G. Panaccione, H. Ebert, O. D. Dubon, K. Kobayashi, and C. S. Fadley, *Nature Materials* **11**, 957 (2012).

[2] "Interface properties of magnetic tunnel junction $\text{La}_{0.7}\text{Sr}_{0.3}\text{MnO}_3/\text{SrTiO}_3$ superlattices studied by standing-wave excited photoemission spectroscopy", A. X. Gray et al., *Phys. Rev. B* **82**, 205116 (2010); "Momentum-resolved electronic structure at a buried interface from soft X-ray standing-wave angle-resolved photoemission", A. X. Gray et al., *Europhysics Letters* **104**, 17004 (2013).

[3] "Chemical-state resolved concentration profiles with sub-nm accuracy at solid/gas and solid/liquid interfaces using standing-wave ambient-pressure photoemission (SWAPPS)", S. Nemsak et al., *Nature Communications* **5**, 5441 (2014).

[4] "Depth profiling charge accumulation from a ferroelectric into a doped Mott insulator", M. Marinova, J. E. Rault, et al., *Nano Letters* **15**, 2533–2541 (2015).

[5] "Energetic, spatial and momentum character of a two-dimensional electron gas at the buried interface between GdTiO_3 and SrTiO_3 ", S. Nemšák et al., *Phys. Rev. B*, to appear, <http://arxiv.org/abs/1508.01832>.

2:20pm SA+AS-MoA3 Honorary Session for Prof. Charles Fadley, O.J. Renault, CEA-University Grenoble Alps, France; Julien Rault, Synchrotron SOLEIL, France

This contribution is intended to honor Prof. Charles Fadley for his unvaluable work in the field of photoemission over the past 50 years and will celebrate his 75th birthday. It will immediately follow his invited talk and will take the form of 3 short talks given by some of his former students.

2:40pm SA+AS-MoA4 Ultrafast Magnetization Relaxation Dynamics in $\text{La}_{0.66}\text{Sr}_{0.33}\text{MnO}_3$ Films, Tommaso Pincelli, Università di Milano, Italy; A.Yu. Petrov, G. Panaccione, Laboratorio TASC, IOM-CNR, Italy; M. Oura, RIKEN SPring-8, Japan; T.L. Lee, Diamond Light Source Ltd., UK; G. Rossi, Università di Milano, Italy

Hole-doped rare-earth manganites, like $\text{La}_{0.66}\text{Sr}_{0.33}\text{MnO}_3$ (LSMO), display exotic phenomena such as concurrent colossal magnetoresistance and half-metallicity which originate from the interplay of charge, spin, and orbital degrees of freedom [1]. The peculiar transport properties of LSMO thin films combined with the ferromagnetic order that persists up to about 350 K [2] render such system a most technologically attractive material for spin injection: the spin polarization at the Fermi level reaches about 100% for $T < T_{\text{Curie}}$ [3].

The ultrafast manipulation of spin states in LSMO can be tested by state-of-the-art time-resolved pump-probe techniques. Previous studies by optical pump-probe spectroscopy have given evidence of photoinduced effects in ferromagnetic manganites [4].

Photo-Electron Spectroscopy (PES) allows a direct measurement of the electronic structure; time-resolved PES is able to disentangle the delicate out-of-equilibrium interplay between electronic, spin and lattice degrees of freedom [5], an essential feature in the case of highly correlated materials. HARd X-ray PhotoElectron Spectroscopy (HAXPES) extends the probing depth of PES to the bulk of the solid (tens of nm), and therefore does not suffer of the modification induced by the surface.

We present here a pump-probe HAXPES study of the relaxation dynamics of LSMO thin films. We study the structure of the Mn 2p core level and, in particular, the bulk-only screening channel proportional to the metallic and ferromagnetic state in LSMO. We observe a large and 'slow' reduced lineshape change up to 200 picoseconds after the IR pumping. By comparison with all-optical techniques (Time-Resolved Magneto-Optical Kerr effect, TR-MOKE) we are able to attribute the observed quenching to a collapse of magnetic order. The sudden demagnetization reduces the mobility of electrons in the solid, inducing a localization similar to a metal-insulator transition.

Since LSMO is half-metallic, the direct exchange of energy between the optically excited electrons and the magnetic order is inhibited by the absence of final states for spin-flip scattering [3]. So we can follow the relaxation dynamics as the energy is first dissipated in the lattice and then in a reduction of the magnetic order.

References

- [1] Y. Tokura et al. *J. Magn. & Magn. Mater.* **200**, 1 (1999).
- [2] K. Horiba et al. *Phys. Rev. B* **71**, 155420 (2005).

[3] G.M. Müller et al. *Nat. Mat.* **8**, 56 (2009); J.-H. Park, et al. *Nature*, **392**, 794 (1998).

[4] A.I. Lobad et al. *Appl. Phys. Lett.* **77**, 4025 (2000); K. Matsuda et al. *Phys. Rev. B* **58**, 4203 (1998).

[5] B. Frietsch et al. *Nature Communications*, **6**, 8262 (2015).

3:00pm SA+AS-MoA5 Inelastic Background Analysis of Haxpes Spectra for Device Technology: A Non-Destructive Tool for Accessing Deeply Buried Interfaces, Charlotte Zborowski, O.J. Renault, E. Martinez, A. Torres, CEA, LETI, MINATEC Campus, France; Y. Yamashita, NIMS, Japan; G. Grenet, Inl, Ecl, France; S. Tougaard, SDU, Denmark

Recently, the advent of Hard X-ray Photoelectron Spectroscopy (HAXPES) has enabled to study deeply buried interfaces [1]. It was shown that by combining HAXPES with inelastic background analysis [2], structures at a depth >50 nm can be studied. Here, we present a study on technologically relevant High Electron Mobility power Transistors Ta/Al.

The study was performed on stacks of two metal layers of aluminum and tantalum with different thicknesses deposited on an $\text{Al}_{0.25}\text{Ga}_{0.75}\text{N}/\text{AlN}/\text{GaN}$ heterostructure [Fig. 1a]. We have used the technique to non-destructively study the activation annealing. HAXPES was performed at the Spring-8 synchrotron (Japan) using 8 keV photons.

The figure shows spectra measured around Al, Ga and Ta peaks for an as deposited sample [Fig. 1b]. The calculation of inelastic background was performed using two input parameters; the IMFP, calculated using the TPP-2M formula [3] and as the spectra present marked plasmons, after the elastic peaks, we used an average of individual inelastic cross-sections, σ , which can be determined from reflection electron energy-loss spectra. The calculation of this cross-sections' average has been made according to a mixtures rule, involving the different crossed layers, which consists in a relevant way to analyze deeply buried layers. The figure shows how the modelling of the inelastic background is used to determine the in-depth distributions, which are found in good agreement with the TEM results. We have also successfully used this technique to study the effect of annealing on the diffusion of the elements at the interfaces.

Bibliography

[1] P. Risterucci et al., *Applied Physics Letters* **104**, (2014).

[2] S. Tougaard, *Journal of Electron Spectroscopy and Related Phenomena*, **178–179** (2010).

[3] H. Shinotsuka et al., *Surface and Interface Analysis* **47**, 871–888 (2015).

Part of this work was performed at the Nanocharacterization Platform of CEA-MINATEC (PFNC).

NIMS and Spring-8 is acknowledged for providing beamtime and the staff of the BL15-XU beamline for their assistance during the experiment. Cyril Guedj is acknowledged for providing TEM analysis and expertise.

3:20pm SA+AS-MoA6 Soft X-ray ARPES Investigation of the Spin-polarized n-BaTiO₃/SrRuO₃ Buried interface, Julien Rault, P. Le Fèvre, F. Bertran, J. Rebellato, Synchrotron SOLEIL, France; T. Maroutian, P. Lecoeur, Université Paris-Sud - CNRS, France

The electric field control of functional properties such as spin injection is a crucial goal in oxide-based electronics. Non-volatile switching between different electron and spin transport in a tunnel junction channel can be achieved through charge accumulation or depletion at the interfaces [1, 2]. It has been recently suggested [3] that polarization-dependent spin-injection is expected at the interface between ferromagnetic SrRuO_3 (SRO) and semiconducting, ferroelectric n-BaTiO₃ (n-BTO), paving the way for adjustable spin-injection in full-oxide devices. This fascinating effect is due to the matching of the spin-dependent Fermi surface of SRO with n-doped BTO tube-like Fermi-surface [2, 3].

To investigate this phenomenon experimentally, we use angle-resolved photoemission spectroscopy (ARPES) to access the band structure of a buried n-BTO/SRO interface. A well-known limitation of ARPES comes from its very low probing depth (< 2 nm) due to the very low electron inelastic mean free path in the usual photon range of ARPES (1-100 eV). To overcome this limitation, we use soft x-ray photons and are able to access the interface Fermi surface below a 2-nm, upward polarized BTO thin film deposited on SRO.

Using 600 eV linearly-polarized photons, we measure the band dispersion of the interface SRO through the BTO band gap along with BTO bands for higher binding energies (see Fig. 1). The SRO-related bands were not visible at lower probing depth (photon energy ca. 250 eV) showing they actually come from the interface. Clear light-polarization dependence on the

energy-momentum cuts along Γ X high-symmetry direction is shown in Figure 1. This is used to assign some parts of the Brillouin zone to specific orbitals with different spin-polarization. The in-plane Fermi surface of the interface SRO for $k_z = Z$ was also acquired and showed some clear feature fitting well the calculated band structure from Liu *et al.*, see Figure 2.

These set of results is indicative of how soft x-ray ARPES is a technique of choice to probe the band structure of functional oxide interfaces. Combined with spin-resolved photoemission, which is available at our laboratory, it will help to better understand the spin polarization predicted in ferromagnetic/ferroelectric heterostructures.

[1] Marinova, M. *et al.*, *Nano Letters* **15**, 2533–2541 (2015)

[2] Liu, X., Burton, J. D., Zhuravlev, M. Y. & Tsymbal, E. Y., *Physical Review Letters* **114**, 46601 (2015)

[3] Liu, X., Wang, Y., Burton, J. D. & Tsymbal, E. Y., *Physical Review B* **88**, 165139 (2013)

4:00pm **SA+AS-MoA8 Progress and Perspectives in Photoemission using XFEL Radiation**, *Serguei Molodtsov*, European XFEL GmbH, Germany
INVITED

Photoemission is today one of the most powerful techniques for investigating low-energy properties of matter from the aerosol and adsorbate nanoparticles and molecules to the surface and bulk of solid state matter with many dedicated and specialized beamlines at synchrotron radiation facilities. The upcoming ultra-brilliant FEL sources, giving access to ultrashort timescales in the fs range, in combination with the outstanding peak brilliance achieved, set the stage for novel science. Experiments on X-ray FEL sources are being pioneered and planned at low repetition rate facilities (FLASH, LCLS, SACLA, FERMI). The European XFEL that will come in early user operation already in 2017 will be characterized by laser action from 260 eV to 25 keV photon energy and above. The facility will also yield an extremely high mean brilliance with a repetition rate suitable for different modes of photoemission detection. Together with the planned for 2021 source LCLS II this will make the European XFEL unique FEL facility for photoemission studies worldwide.

In this presentation an overview of time-resolved photoemission experiments on solids that were done at XFELs so far will be given and perspectives related to high repetition rate XFEL facilities, particularly European XFEL, will be provided.

4:40pm **SA+AS-MoA10 Revealing the Origins of Non-Joulian Magnetism with High-Resolution Photoemission Microscopy**, *Alexander Gray, R.U. Chandrasena*, Department of Physics, Temple University; *H.D. Chopra*, Department of Mechanical Engineering, Temple University
INVITED

All magnets elongate and contract anisotropically when placed in a magnetic field, an effect referred to as Joule magnetostriction. The hallmark of Joule magnetostriction is volume conservation, which is a broader definition applicable to self-accommodation of ferromagnetic, ferroelectric or ferroelastic domains in all functional materials. Recently, a new class of single-crystalline magnets exhibiting a 'giant' non-volume-conserving or non-Joulian magnetostriction was discovered [1]. In this talk I will discuss the results of our recent investigations of non-Joulian Fe_3Ga alloys using high-resolution polarization-dependent photoelectron microscopy. Our results suggest that non-Joulian magnetism arises from an unusual nearly-equipartition of the crystal into nm-scale lamellar domains and domain walls within highly periodic magnetic micro-cells. We suggest that this high-energy configuration is stabilized by the strain gradients arising from CDW that offsets electronic energy by a greater amount. High-resolution x-ray magnetic circular dichroism measurements at the Fe and Ga L absorption edges further provide evidence of weak iron-induced magnetism on gallium atoms via negative exchange. The results are in excellent agreement with the state-of-the-art theoretical electronic-structure calculations. Our findings open up new ways for the design of alloy systems having functional magnetic properties similar to Fe_3Ga where non-Joulian magnetostriction was first reported.

[1] H. D. Chopra and M. Wuttig, Non-Joulian magnetostriction, *Nature* **521**, 340 (2015).

Scanning Probe Microscopy Focus Topic

Room 104A - Session SP+2D+AS+NS+SS-MoA

Probing Topological States And Superconductivity

Moderators: An-Ping Li, Oak Ridge National Laboratory, Chuanxu Ma, Oak Ridge National Laboratory

1:40pm **SP+2D+AS+NS+SS-MoA1 Tuning Dirac States by Strain in Topological Insulators**, *Lian Li*, University of Wisconsin-Milwaukee **INVITED**
Topological insulators (TIs) are distinguished by their metallic boundary states populated by massless Dirac fermions and bulk topological Z_2 index. Changes in the band topology induced by external variables such as strain, electrical field, and composition thus provide a means to tune the boundary states. As a large spin-orbit coupling is necessary to produce an inverted band gap, most TIs discovered to date are narrow gap semiconductors consisting of heavy elements. These materials typically exhibit layered crystal structure with anisotropic bonding characteristic: strong covalent bonding in-plane and weak van der Waals (vdW) bonding out-of-plane, which has been predicted to facilitate effective strain engineering of their bulk band topology.

In this talk, I will first give an overview of the opportunities and challenges in the epitaxial growth of layered TIs. Using the prototypical 3D TI Bi_2Se_3 as an example, I will show that the characteristic anisotropic bonding facilitates a spiral growth mode on virtually any substrates by molecular beam epitaxy. The coalescence of these spirals results in a high density of grain boundaries that consist of alternating edge dislocation pairs, leading to periodic in-plane stretching and compression. Using scanning tunneling spectroscopy, I will show that this local strain field strongly modifies the Dirac surface states, where in-plane compression expands the vdW gap and destroys the Dirac states.

Next, I will show our recent work on the strain engineering of Dirac edge states of epitaxial Bi bilayer films grown on three different substrates: the (111) surface of 3D TIs Bi_2Se_3 , Sb_2Te_3 , and Bi_2Te_3 . Using scanning tunneling microscopy/spectroscopy, I will show that for moderately strained (<6%) single Bi bilayer on Sb_2Te_3 and Bi_2Te_3 , edge states are observed; while on highly compressed single Bi bilayer on Bi_2Se_3 (>8%), edge states are suppressed. These findings, supported by density functional theory calculations, demonstrate the uniform control of edge states in 2D topological insulators by strain.

2:20pm **SP+2D+AS+NS+SS-MoA3 Detection of Current Induced Spin Polarization in Topological Insulators via Four-Probe Spectroscopy**, *Saban Hus*, Oak Ridge National Laboratory; *Y. Chen*, Purdue University; *A.-P. Li*, Oak Ridge National Laboratory

Charge currents carried by the nontrivial surface states of topological insulators (TIs) exhibit a net spin polarization due to spin-momentum locking. Electrical detection of such a spin polarization is crucial for technological applications. However, in 3D TI materials the existence of a bulk conduction channel makes it difficult to quantify the density and the spin polarization of the current carried by the surface states. Here we report in-situ, spin sensitive four-probe spectroscopy measurements on $\text{Bi}_2\text{Te}_2\text{Se}$ single crystals. A ferromagnetic probe detects the net spin accumulation on the surface states while a set of four-probe spectroscopy measurement is used for a quantitative separation of 2D and 3D conduction. We also examine the effect of surface doping by residual gas molecules on the current induced spin polarization. Even though, the additional carriers by dopants enhance the 2D conductance in TIs they reduce the net spin polarization of current carried by topological surface states.

This research was conducted at the Center for Nanophase Materials Sciences, which is a DOE Office of Science User Facility.

2:40pm **SP+2D+AS+NS+SS-MoA4 Switching Handedness of Chiral Solitons Under Z_4 Topology**, *Tae-Hwan Kim*, Pohang University of Science and Technology, Republic of Korea; *S. Cheon*, *H.W. Yeom*, Institute for Basic Science (IBS), Republic of Korea

Chirality is a ubiquitous and interesting property of asymmetry in many fields ranging from biology, chemistry to physics. Because of its topologically distinct nature, such chiral objects in condensed matter are often topologically excited states, which are protected by system's topology and can be used to carry information robustly against external perturbations. For instance, nanoscale magnetic skyrmions, spatially localized chiral spin texture with particle-like properties in ferromagnets, have been investigated intensively as topological information carriers for next generation spintronic devices. However, logic operations using

topological excitations such as skyrmions are only conceptually proposed. On the other hand, chiral solitons are recently discovered as the topologically protected edge states of one-dimensional Z_4 topological insulators [1,2], which can be exploited as topological information carriers in electronic system. In this talk, I show experimentally and directly that switching between solitons with different chirality is possible by merging them with achiral solitons [3]. I will also show that this chiral switching corresponds to the realization of topological addition of the Z_4 topological number or chirality. With their distinct topologically protected chirality, chiral solitons could uniquely be applied for robust multilevel information storage and logic operation by storing, carrying, and switching three differently topological bits of information.

[1] T.-H. Kim and H. W. Yeom, Phys. Rev. Lett. **109**, 246802 (2012).

[2] S. Cheon, T.-H. Kim, S.-H. Lee, and H. W. Yeom, Science **350**, 182 (2015).

[3] T.-H. Kim, S. Cheon, and H. W. Yeom, submitted (2016).

3:00pm SP+2D+AS+NS+SS-MoA5 Spectroscopic-imaging STM Studies on Dirac-Landau Levels in the Topological Surface State, Tetsuo Hanaguri, RIKEN Center for Emergent Matter Science, Japan

INVITED

We show that spectroscopic-imaging scanning tunneling microscopy (SI-STM) is a powerful tool to investigate unique electronic features of massless Dirac electrons in a magnetic field.

In contrast to the conventional massive electron that is described by a single-component wave function, the massless counterpart demands the two-component wave function. In the case of the surface state of topological insulators, these two components are associated with the spin degrees of freedom, thereby governing the magnetic properties. Thus, it is highly desirable for spintronics applications to elucidate where and how the two-component nature emerges. We found that the two-component nature manifests itself in the internal structures of Landau orbits. We visualized the local density-of-states (LDOS) distributions associated with the Landau orbits in the topological surface state of Bi_2Se_3 using SI-STM. In the presence of the potential variation, Landau orbits drift along the equipotential lines, forming ring-like patterns in the LDOS images. The observed internal structures of the rings are qualitatively different from those of conventional massive electrons but are well reproduced by the calculation based on a two-component model Dirac Hamiltonian. Our model further predicts non-trivial energy-dependent spin-magnetization textures around the potential minimum. This is originated from the interplay between the two components and may provide a clue to manipulate spins in the topological surface state.

In addition to the Landau orbits, we succeeded in observing the Zeeman shift of the lowest Landau level from which precise g factor of the massless Dirac electron can be estimated. We performed experiments on two topological insulators, Bi_2Se_3 and $\text{Sb}_2\text{Te}_2\text{Se}$, and determined the surface g factors of them to be 18 and -6, respectively. Such remarkable material dependence suggests that the Zeeman effect is tunable by controlling the chemical composition, providing a new knob in manipulating the spins in the topological surface state.

4:00pm SP+2D+AS+NS+SS-MoA8 The Rashba and Quantum Size Effects in Ultrathin Bi films, Toru Hirahara, Tokyo Institute of Technology, Japan

INVITED

Precise characterization of physical properties in nanometer-scale materials is interesting not only in terms of low-dimensional physics but also in application to devices. Due to the reduced dimensionality and symmetry, these systems possess various interesting properties that cannot be found in the bulk. In this presentation, focusing on epitaxial ultrathin bismuth films formed on a silicon substrate, we introduce an intriguing interplay of the quantum size and Rashba effects in reciprocal space. Utilizing spin- and angle-resolved photoemission spectroscopy, we observed clear Rashba-split nature of the surface-state bands in these Bi films. However, the band dispersion did not follow the simple Rashba picture and the spin-splitting was lost where they overlapped with the bulk projection. From first-principles calculations, this was explained as a change in the nature of the band-splitting into an even-odd splitting induced by the quantum size effect [1]. Furthermore, we show that the interplay of the quantum size effect and the presence of the surface state induces a complicated change in the Fermi level position of the bulk states in bismuth, which is critical in discussing the surface-state contribution in the film properties [2,3].

[1] T. Hirahara, Journal of Electron Spectroscopy and Related Phenomena **201**, 98 (2015).

[2] T. Hirahara, T. Shirai, T. Hajiri, M. Matsunami, K. Tanaka, S. Kimura, S. Hasegawa, and K. Kobayashi, Physical Review Letters **115**, 106803 (2015).

[3] M. Aitani, T. Hirahara, S. Ichinokura, M. Hanaduka, D. Shin, and S. Hasegawa, Physical Review Letters **113**, 206802 (2014).

4:40pm SP+2D+AS+NS+SS-MoA10 Understanding the Microscopic Effects of Annealing in $\text{Ba}(\text{Fe}_{1-x}\text{Co}_x)_2\text{As}_2$ Superconductor, Qiang Zou, Z. Wu, Q. Zheng, S. Rajput, D.S. Parker, A.S. Sefat, Z. Gai, Oak Ridge National Laboratory

By hole or electron doping of the parent iron-based BaFe_2As_2 compound, the high-transition temperature superconductivity emerges from the suppression of the antiferromagnetic order.¹ It was widely reported that thermal-annealing significantly improves some superconducting characteristics in $\text{Ba}(\text{Fe}_{1-x}\text{Co}_x)_2\text{As}_2$, including T_c .² The microscopic origin of such effect is still an open question. To make a connection between the global and the microscopic behavior of the materials, we did a comparison measurement on the pair of well-characterized x , we call 'as-grown' vs 'annealed' $\text{Ba}(\text{Fe}_{1-x}\text{Co}_x)_2\text{As}_2$ crystals, and using low temperature scanning tunneling microscopy and spectroscopy (STM/S). The superconducting gap maps deduced from the dI/dV maps were compared. The gap width distribution of the as-grown sample are obviously narrower than that of the annealed one. The coherent peak position also shifted to higher value for the annealed sample. The corresponding reduced-gaps of $2\Delta/k_B T_{c1}$ are about 2.3 and 5.4 for the as-grown and annealed crystals, respectively. The difference of the reduced-gaps indicates that the pairing strength of the annealed crystal is stronger than the as-grown one.

This research was supported by the U.S. Department of Energy, Office of Science, Basic Energy Sciences, Materials Science and Engineering Division. A portion of this research was conducted at the Center for Nanophase Materials Sciences, which is a DOE Office of Science User Facility.

Reference

1. Stewart, G. R. (2011). "Superconductivity in iron compounds", *Reviews of Modern Physics*, **83**(4), 1589.

2. Gofryk, K., et al. "Effect of annealing on the specific heat of $\text{Ba}(\text{Fe}_{1-x}\text{Co}_x)_2\text{As}_2$ " *Physical Review B*, **83**(6), 064513

5:00pm SP+2D+AS+NS+SS-MoA11 Annealing Effect on the Properties of Superconducting Parent BaFe_2As_2 Crystal, Shivani Rajput, Q. Zou, A.S. Sefat, Z. Gai, Oak Ridge National Laboratory

Understanding of electronic interactions in a parent phase of a superconducting crystal is crucial in determining the mechanism behind high T_c superconductivity. Bulk measurements show that annealing of parent BaFe_2As_2 crystal at 700 °C for 30 days causes a 5 K shift in magnetic transition temperature (T_N) compared to as grown crystal. To understand the effect of annealing and details of magnetic phase transition, we investigate as-grown and annealed BaFe_2As_2 crystals at atomic scale using a variable temperature scanning tunneling microscopy/ spectroscopy at various temperature points across T_N . Tunneling spectroscopy exhibit a ~ 0.53 eV gap type feature above T_N , while V-shape dI/dV spectra below T_N . The dI/dV mapping measurements show that as-grown BaFe_2As_2 crystals are electronically inhomogeneous, and averaging the differential conductance spectra over a large area does not truly represent the electronic properties of the sample at local scale, whereas annealed sample is comparatively electronically homogeneous.

This research was supported by the U.S. Department of Energy, Office of Science, Basic Energy Sciences, Materials Science and Engineering Division. A portion of this research was conducted at the Center for Nanophase Materials Sciences, which is a DOE Office of Science User Facility.

Surface Science

Room 104E - Session SS+AS+HC-MoA

Metals, Alloys, and Oxides: Reactivity and Catalysis

Moderator: David Mullins, Oak Ridge National Laboratory

1:40pm SS+AS+HC-MoA1 Scanning Tunneling Microscopy Studies of Hydrogen adsorption on the RuO₂(110) Surface, Arjun Dahal, R. Mu, Z. Dohnálek, I. Lyubinetsky, Pacific Northwest National Laboratory

Understanding of hydrogen/oxide interactions is important for a variety of fundamental and applied processes. By using high resolution scanning tunneling microscopy (STM), we probed the adsorption of H₂ (or D₂) on model catalyst RuO₂(110) surface, which has wide range of applications in heterogeneous catalysis, hydrogen storage, and many other energy related areas. Well-defined RuO₂(110) surface exposes alternating rows of bridge-bonded oxygen atoms (O_b) and five-fold-coordinated Ru atoms (Ru_{cus}). STM data indicate that hydrogen molecule dissociates even at 5 K, whereas one hydrogen adatom adsorbs on top of the Ru_{cus} site (producing a hydrate, H-Ru_{cus}, species) and the second on top of the adjacent O_b site (forming a bridging hydroxyl, H-O_b, species), generating an H-Ru_{cus}/H-O_b pair. For the low hydrogen coverage, the dissociated H-Ru_{cus}/H-O_b pairs adsorb on every alternate Ru_{cus}/O_b sites adopting a (2x1) registration. When RuO₂(110) surface adopts a such registration of the H-Ru_{cus}/H-O_b pairs locally, hydrogen starts to adsorb molecularly on top of the Ru_{cus} sites in between the adjacent dissociated hydrogen-pairs. With further increase of hydrogen coverage, linear arrays of H₂ molecules are formed along Ru_{cus} rows. The saturation coverage of the hydrogen on the RuO₂(110) surface is observed to be ~0.75 ML, where 1 ML is designated as the Ru_{cus} site density on the stoichiometric RuO₂(110) surface (5.06x10¹⁴ cm⁻²). Upon annealing the hydrogen-covered RuO₂(110) surface, H₂ molecules from the linear array desorb around 110 K. On the other hand, the H-Ru_{cus} species of H-Ru_{cus}/H-O_b pair transforms (via a proton transfer) into another H-O_b group, across-row from original H-O_b group, producing crosswise H-O_b/H-O_b pair at temperatures above ~250 K.

2:00pm SS+AS+HC-MoA2 Metal Vapor Adsorption Calorimetry on Layered Ca Niobate Nanosheets: Energetics and Adsorbate Structure, Wei Zhang, J. Lownsbury, University of Washington; R. Uppuluri, T.E. Mallouk, The Pennsylvania State University; C.T. Campbell, University of Washington

The metal/oxide interface is essential to many current and prospective technologies, including oxide-supported metal catalysts, fuel cells, photocatalysis, and nanoscale electronic contacts, so understanding the strength of metal – oxide bonding at such interfaces is of great interest. These strengths have been measured on single crystal oxide surfaces by single crystal adsorption calorimetry (SCAC) of metal atom adsorption in ultrahigh vacuum (UHV)¹ and on niobate and tantalate nanosheets by solution-based isothermal titration calorimetry during the deposition of transition metal oxide (or hydroxide) nanoparticles from their aqueous salt solutions^{2,3}. These niobate nanosheets are very interesting since they are highly ordered and essentially like single crystal surfaces in that the ratio of terrace sites to defect and edge sites is huge. Furthermore, when used as supports for transition metal oxide nanoparticles, they have been shown to display unusual stability against sintering.^{2,3} Here, we directly measure the adsorption energies of metal vapor on such niobate nanosheets using SCAC in UHV. Specifically, we study the adsorption of Ca and Ag vapor onto calcium niobate films that are 4 nanosheets thick (~4 nm total). Calcium atoms show a sticking probability near unity and an initial heat of adsorption of ~660 kJ/mol, much higher than the heat of bulk Ca(s) sublimation (178 kJ/mol). Low-energy ion scattering spectroscopy (LEIS), which is element-specific and probes only the topmost atomic layer, is used to investigate the resulting metal particle/film morphology. The possible chemical reactions between the metal vapor and the calcium niobate during adsorption are elucidated using X-ray photoelectron spectroscopy (XPS).

[1] Campbell, C. T.; Sellers, J. R. V. *Faraday Discussions* **2013**, 162, 9.

[2] Strayer, M. E.; Binz, J. M.; Tanase, M.; Shahri, S. M. K.; Sharma, R.; Rioux, R. M.; Mallouk, T. E. *J. Am. Chem. Soc.* **2014**, 136, 5687.

[3] Strayer, M. E.; Senftle, T. P.; Winterstein, J. P.; Vargas-Barbosa, N. M.; Sharma, R.; Rioux, R. M.; Janik, M. J.; Mallouk, T. E. *J. Am. Chem. Soc.* **2015**, 137, 16216.

2:20pm SS+AS+HC-MoA3 Structure and Reactivity of Model Iron Oxide Surfaces, Gareth Parkinson, TU Wien, Austria INVITED

Iron oxides are abundant in nature and extensively utilized in modern technologies including heterogeneous catalysis [1]. Magnetite (Fe₃O₄), for

example, is the active phase of the industrial water-gas shift catalyst, while hematite (Fe₂O₃) is used as the photoanode for photoelectrochemical water splitting. In this talk I will discuss our recent investigations of the Fe₃O₄(100) and Fe₂O₃(1-102) surfaces using a combined experiment/theory approach. The Fe₃O₄(100) surface forms a reconstruction based on an ordered array of subsurface cation vacancies that contains exclusively Fe³⁺, and is relatively inert [2]. Although formic acid adsorbs dissociatively at regular lattice sites [3], methanol adsorption is restricted to defects containing Fe²⁺ [4]. The bulk of the talk will focus on a detailed study of water adsorption on Fe₃O₄(100) by TPD, STM, XPS, UPS, DFT+U and molecular dynamics calculations. In the remaining time I will demonstrate that a bulk terminated Fe₂O₃(1-102) surface can be prepared by annealing in 10⁻⁶ mbar O₂, and a reduced (2x1) surface forms rapidly when heating in UHV. The structure of the (2x1) reconstruction and its reactivity toward water will be discussed.

[1] G.S. Parkinson, Iron oxide surfaces, *Surface Science Reports* (2016), <http://dx.doi.org/10.1016/j.surfrep.2016.02.001>

[2] R. Bliem, E. McDermott, P. Ferstl, M. Setvin, O. Gamba, J. Pavelec, M.A. Schneider, M. Schmid, U. Diebold, P. Blaha, L. Hammer, G.S. Parkinson, Subsurface Cation Vacancy Stabilization of the Magnetite (001) Surface, *Science* **346** (2014) 1215-1218.

[3] O. Gamba, H. Noei, J. Pavelec, R. Bliem, M. Schmid, U. Diebold, A. Stierle, G.S. Parkinson, Adsorption of Formic Acid on the Fe₃O₄(001) Surface, *The Journal of Physical Chemistry C* **119** (2015) 20459-20465.

[4] O. Gamba, J. Hulva, J. Pavelec, R. Bliem, M. Schmid, U. Diebold, G.S. Parkinson, The role of surface defects in the adsorption of methanol on Fe₃O₄(001), *Topics in Catalysis* submitted (2016).

3:00pm SS+AS+HC-MoA5 Structure and Ethanol Reactivity of Ti-modified CeO₂(111) Mixed Oxide Surfaces, E.W. Peterson, Jing Zhou, University of Wyoming

Ceria has been widely studied as an oxidation-reduction catalyst due to its unique redox properties and oxygen storage capacity. There has been an interest to incorporate additional metal dopants such as Ti into ceria to potentially enhance the thermal stability as well as improve the redox properties for practical applications in catalysis. This paper focuses on the fundamental mechanistic understanding of the effect of Ti dopant on the structure and reactivity of ceria using scanning tunneling microscopy, X-ray photoelectron spectroscopy, infrared spectroscopy and temperature programmed desorption techniques. In the study, submonolayer coverage of Ti was deposited on well-ordered CeO₂(111) (1.5<x<2) thin films at room temperature. XPS studies show that Ti is oxidized to Ti⁴⁺ at the cost of Ce⁴⁺ reduction. Observation of CO IR band at 2173 cm⁻¹ further confirms the presence of titania on the ceria surface. At 300 K, small atomic-like features of Ti-O-Ce linkages are present on ceria, which can coalesce into chain structures after heating to 700 K. Upon ethanol adsorption at 300 K, ethoxy was the surface intermediate observed on both oxidized and partially reduced ceria surface. With heating, it can go through the dehydration or dehydrogenation process to form acetaldehyde, ethylene, water and hydrogen products. Our studies have demonstrated that addition of Ti in ceria can affect the dehydration and dehydrogenation selectivity. Furthermore, the nature of ceria supports associated with oxygen vacancies and Ti dopants can have a promotional effect in the stability of deposited metal nanoparticles, such as Ni, and the chemical behavior toward the adsorption and reaction of ethanol. The research is sponsored by the National Science Foundation Career Grant (Award Number: CHE1151846) and the Wyoming NASA EPSCoR (NASA Grant: NNX13AB13A).

3:20pm SS+AS+HC-MoA6 New Insights into the Coverage-Dependent Structure and Desorption Kinetics of CO on Palladium(111), Pan Xu, Stony Brook University; S.-Y. Hong, Brookhaven National Laboratory; S. Liu, Stony Brook University; N.R. Camillone, M.G. White, N. Camillone, Brookhaven National Laboratory

Carbon monoxide adlayers on palladium surfaces have, since the early days of ultrahigh-vacuum surface science, served as model systems for the study of molecule–surface interactions, structure and dynamics. As part of a recent study of the dynamics of ultrafast molecule–surface energy transfer we have revisited the CO/Pd(111) system and found that it continues to teach us about the complexities of molecule–surface interactions. Specifically, it has long been known that CO adlayers assume a wide range of ordered structures on Pd(111) at low temperature (~80 K). In fact, between the (√3×√3)R30° 0.33-ML and (2×2) 0.75-ML (saturation) structures, at least 17 well-ordered structures have been identified. Until now, however, a comprehensive correlation between these structures and the thermal desorption kinetics has not been reported. In this talk we

detail a systematic investigation that correlates individual temperature-programmed desorption (TPD) features with specific adlayer structural phase transitions. We report that in addition to the spectrum of previously-observed structures we have observed for the first time, to the best of our knowledge, a well-developed, ordered domain-boundary structure at a coverage just below saturation. We have assigned this structure as a $c(16 \times 2)$ adlayer comprised of stripes with local (2×2) structure and used density functional theory to investigate the adsorption site preferences within the adlayer. We show how our results, in combination with existing data, can be interpreted in terms of a compromise between the energy minimization that accompanies binding at high-symmetry sites and lateral repulsive interactions. Furthermore, we describe how quantifying the coverage using the integrated desorption yield areas is problematic due to difficulties in growing a fully-saturated adlayer. We attribute these difficulties to a kinetic limitation of the structural phase transitions at high coverage, and show that this limitation is easily addressed by preparing the adlayer at a somewhat elevated temperature. We also detail use of the inversion-optimization method to extract the coverage dependence of the desorption activation energy from the TPD measurements. We compare the resultant simulated TPD line shapes with those derived using the "leading-edge" analysis method.

4:00pm SS+AS+HC-MoA8 Combined Experimental and Computational Study of Water on Fe_3O_4 (001), Jan Hulva, Vienna University of Technology, Austria; **M. Meier,** Universität Wien, Austria; **J. Pavelec,** S. Maaß, R. Bliem, M. Schmid, U. Diebold, Vienna University of Technology, Austria; **C. Franchini,** Universität Wien, Austria; **G.S. Parkinson,** Vienna University of Technology, Austria

The interaction of water with metal-oxide surfaces is an important topic for a wide range of technological and environmental applications. This is particularly true for the iron oxides because of their abundance in nature and their use in chemical processes where water is involved e.g. the water-gas shift reaction [1]. Recent studies of water on iron oxide surfaces have found significant complexity, with evidence for pressure dependent adsorption, mixed-mode adsorption and coverage dependent hydrogen bonding [2-4]. Here we use a multi-technique experimental approach combined with ab-initio calculations including molecular dynamics to disentangle the coverage and temperature dependent behavior of water on the reconstructed $\text{Fe}_3\text{O}_4(001)-(\sqrt{2} \times \sqrt{2}) R45^\circ$ surface [5].

Temperature programmed desorption shows that the first monolayer of water desorbs from the surface in four distinct peaks between 150 K and 250 K. Based on XPS, STM images and ab-initio calculations, we conclude that the first three peaks originate from molecular water desorbing from a coverage-dependent hydrogen-bonded network, while the last peak results from recombinative desorption from a partially dissociated water trimer species. Two additional desorption states at 340 K and 520 K are ascribed to desorption from surface defects and recombinative desorption of the surface surface hydroxyl groups, respectively.

- [1] Parkinson, G.S., "Iron oxide surfaces", *Surface Science Reports* (2016)
- [2] Dementyev, P., et al. "Water Interaction with Iron Oxides." *Angew.Chem. Int. Ed.* 54 (2015): 13942
- [3] Mulakaluri, N., et al. "Partial dissociation of water on Fe_3O_4 (001): Adsorbate induced charge and orbital order." *Phys. Rev. Lett.* 103 (2009): 176102.
- [4] Kendelewicz, T., et al. "X-ray photoemission and density functional theory study of the interaction of water vapor with the Fe_3O_4 (001) surface at near-ambient conditions." *J. Phys. Chem C* 117 (2013): 2719-2733.
- [5] Bliem, R., et al. "Subsurface cation vacancy stabilization of the magnetite (001) surface." *Science* 346 (2014): 1215-1218.

4:20pm SS+AS+HC-MoA9 Water Desorption from Sulfur-Doped Oxide Thin Films on W (100), Anthony Babore, J.C. Hemminger, University of California Irvine

Recent first principle calculations by Pacchioni and coworkers¹ suggest that sulfur dopants incorporated into the WO_3 lattice could favorably shift the band gap for enhanced visible light absorption. The present study aims to gain fundamental insight into the reactivity of a simple sulfur doped tungsten oxide system by using temperature programmed desorption (TPD) and water (D_2O) as a probe molecule. Furthermore, water desorption spectra were also obtained for pure oxide and pure sulfide films on W (100) for comparison. Auger electron spectroscopy (AES) was used to confirm the presence and relative amounts of sulfur and oxygen on the surface. TPD was then used to monitor the m/z 20, 19, and 18 signal intensity as a function of the temperature. To quantify the reactivity of water on the

surface, activation energies of desorption were obtained. The results indicate distinct differences in the desorption spectra and desorption energies that exemplify the reactivity of each of the surfaces.

1. Wang F, Di Valentin C, Pacchioni G (2012) *J Phys Chem C* 116:8901–8909

4:40pm SS+AS+HC-MoA10 Adsorption and Decomposition of Dimethyl Methylphosphonate on Metal Oxide Surfaces Under Atmospheric Conditions, Ashley Head, L. Trotochaud, Lawrence Berkeley National Laboratory (LBNL); **R. Tsyshevsky,** University of Maryland College Park; **O. Karslioglu,** Lawrence Berkeley National Laboratory (LBNL); **M.M. Kuklja,** University of Maryland College Park; **H. Bluhm,** Lawrence Berkeley National Laboratory (LBNL)

Organophosphonates are used as corrosion inhibitors, pesticides, insecticides, and chemical warfare agents. This class of molecules has a range of acute toxicity, so dimethyl methylphosphonate is commonly used as a proxy for more toxic molecules. Metal oxides are used in applications for binding and decomposing organophosphonates despite little understanding of the chemistry and reactivity, especially in the presence of atmospheric molecules. With the ability to collect photoemission spectra at pressures up to about 25 Torr, ambient pressure XPS is well-suited to investigate the adsorption of DMMP in the presence of other molecules that have relevance to applications. Using MoO_x and CuO_x foils as model systems for chemical filtration materials, we have studied the adsorption and decomposition behavior of DMMP and how this behavior changes in the presence of atmospherically relevant molecules, including water, hydrocarbons, and NO_x . The effect of the small molecules on the substrate and the subsequent effects on DMMP binding, coverage, and decomposition will be discussed. APXPS results are interpreted with the aid of density functional theory calculations, which model DMMP adsorption, decomposition products, and reaction energies.

5:00pm SS+AS+HC-MoA11 Oxygen Chemisorption and Thermal Oxidation of TiAlN High Power Pulsed Magnetron Sputtering Hard Coatings, Martin Wiesing, T. de los Arcos, G. Grundmeier, University of Paderborn, Germany

The thermal oxidation of $\text{Ti}_{0.5}\text{Al}_{0.5}\text{N}$ hard coatings as deposited by High Power Pulsed Magnetron Sputtering was investigated at reduced oxygen partial pressures of 10^{-6} and 10^{-2} Pa in a temperature range from 298 to 800 K. Quasi in-situ X-ray Photoelectron Spectroscopy and Low Energy Ion Scattering studies revealed oxygen to bind selectively to Ti-sites on the surface [1] and oxygen migration into the near-surface region. Three dimensional oxidation leads to the formation of a double layered surface oxide including a $\text{TiAl}(\text{O},\text{N})$ growth region [2] terminated with a Ti^{IV} containing surface oxide [3]. Based on Wagner plot analysis, the surface oxide layer formed at 800 K can be described by a mixed $\text{Ti}^{\text{IV}}\text{Al}^{\text{III}}\text{O}_x$ phase while a separated $(\text{Ti}^{\text{IV}}\text{O}_2)(\text{Al}^{\text{III}}_2\text{O}_3)$ phase preferentially forms at 298 K. Complementary Ultraviolet Photoelectron Spectroscopy revealed a high degree of nitrogen doping in both cases.

The results are of importance for the design of multi-layered nitridic hard coatings and for a thorough understanding of the high-temperature oxidation resistance of such coatings.

Acknowledgement: The authors gratefully acknowledge the German Research Foundation (DFG) for financial support (SFB–TR 87). We thank Prof. Dr. J. Schneider and Holger Rueß for providing the coated specimen.

References:

- [1] C. Kunze, D. Music, M. to Baben, J.M. Schneider, G. Grundmeier, Temporal evolution of oxygen chemisorption on TiAlN, *Appl. Surf. Sci.* 290 (2014) 504–508. doi:10.1016/j.apsusc.2013.11.091.
- [2] S. Hofmann, Formation and diffusion properties of oxide films on metals and on nitride coatings studied with Auger electron spectroscopy and X-ray photoelectron spectroscopy, *Thin Solid Films.* 193–194, Part 2 (1990) 648–664. doi:10.1016/0040-6090(90)90216-Z.
- [3] C. Gnath, C. Kunze, M. Hans, M. to Baben, J. Emmerlich, J.M. Schneider, G. Grundmeier, Surface chemistry of TiAlN and TiAlNO coatings deposited by means of high power pulsed magnetron sputtering, *J. Phys. Appl. Phys.* 46 (2013) 084003. doi:10.1088/0022-3727/46/8/084003.

Thin Film

Room 105A - Session TF+EM-MoA

ALD for Energy Conversion and Storage

Moderators: Virginia Wheeler, U.S. Naval Research Laboratory, Angel Yanguas-Gil, Argonne National Laboratory

1:40pm TF+EM-MoA1 Fabrication of Nano-power Generators using Thin Atomic Layer Deposited Films, Giovanna Scarel, H.S. Mann, B.N. Lang, James Madison University; **V.D. Wheeler,** Naval Research Laboratory; **B.C. Utter,** Bucknell University

Infrared power generation is emerging as a useful method to harvest infrared (IR) light and transform it into usable energy available day and night. So far, this method is implemented using bulk power generator (PG) devices, neglecting any effort to improve the materials employed as their active element. Here we initiate this effort by fabricating thin thermoelectric TiO_2/TiN multilayer films via atomic layer deposition (ALD) and focusing on the exploration of the effects of film resistance on the voltage produced by nano-PG devices with these films as their active elements. By changing the number and thickness of the TiO_2/TiN layers, we control the sheet resistance (W/\square) over three orders of magnitude. We observe that the voltage produced by nano-PG devices linearly increases with the thin multilayer films resistance, especially in the $\text{k-W}/\square$ range. On the contrary, we measure an almost constant voltage jump versus film resistance when we excite the nano-PG device through Joule heating. The observed behavior suggests that the nano-PG device works effectively when mimicking the mechanism of a capacitor, similar to the case of a bulk device. Our studies pave the way to improving the properties of nano-PG devices by improving the properties of the active materials in the form of thin films fabricated via ALD.

2:00pm TF+EM-MoA2 Ultrafast Triggered Transient Energy Storage by Atomic Layer Deposition Into Porous Silicon for Integrated Transient Electronics, Anna Douglas, N. Muralidharan, R.E. Carter, K. Share, C.L. Pint, Vanderbilt University

We demonstrate the first on-chip silicon-integrated rechargeable transient power source based on atomic layer deposition (ALD) coating of vanadium oxide (VO_x) into porous silicon. A stable specific capacitance above 20 F g^{-1} is achieved until the device is triggered with alkaline solutions. Due to the rational design of the active VO_x coating enabled by ALD, transience occurs through a rapid disabling step that occurs within seconds, followed by full dissolution of all active materials within 30 minutes of the initial trigger. This work demonstrates how engineered materials for energy storage can provide a basis for next-generation transient systems and highlights porous silicon as a versatile scaffold to integrate transient energy storage into transient electronics.

2:20pm TF+EM-MoA3 Refractory Solar Selective Coatings Synthesized by Atomic Layer Deposition, Jeffrey Elam, A. Mane, A. Yanguas-Gil, J.A. Libera, J.R. Avila, Argonne National Laboratory

One of the most economically viable methods for solar power uses an array of mirrors to concentrate sunlight onto a central receiver tower. The receiver surface heats up, and this heat is used to drive turbines that generate electricity. To improve the efficiency of these "power tower" facilities, the receiver must operate at higher temperatures and this requires developing high performance coatings. These coatings must be spectrally selective in order to absorb all of the visible light while emitting as little infrared radiation as possible (low emissivity). In addition, these coatings must be refractory to endure decades of high temperature operation under ambient conditions. We are pursuing a novel strategy to develop refractory solar selective coatings using ALD. Our strategy uses thin film nanocomposites composed of conducting metallic nanoparticles in a dielectric matrix. These films are prepared by combining the ALD processes for a metal (e.g. W using $\text{Si}_2\text{H}_6/\text{WF}_6$) with that of an oxide (e.g. Al_2O_3 using $\text{TMA}/\text{H}_2\text{O}$). The resulting nanocomposites have tunable optical properties that can be adjusted to achieve a high solar selectivity. In addition, we use these ALD coatings to infiltrate inverse opal scaffolds which serve as photonic crystals to further enhance the spectral selectivity. In this presentation I will discuss our ongoing work synthesizing and characterizing these refractory solar selective coatings. In particular, I will describe in situ quartz crystal microbalance, mass spectrometry, and infrared spectroscopy measurements performed to elucidate the unusual surface chemistry for these ALD nanocomposites, and discuss the relationships between the composition and the optical/electrical properties of these films. I will also describe the results of finite difference time domain modeling to understand how the photonic scaffold modulates the

spectral selectivity, and finally I will report on the high temperature performance of these coatings.

2:40pm TF+EM-MoA4 Sequential Infiltration Synthesis of Doped Polymer Films with Tunable Electrical Properties for Efficient Triboelectric Nanogenerator Development, Yanhao Yu*, X.D. Wang, University of Wisconsin-Madison

Triboelectric nanogenerator (TENG) is rising as a promising technology for converting mechanical energy into electricity with merits of high output, simple design and low cost. The working principle of TENG is based on the combined effect triboelectrification and electrostatic induction. According to this mechanism, controlling the charge density on the triboelectric surface is the most fundamental strategy for improving the performance of TENG. Nowadays, surface modification of triboelectric polymer is the predominate approach to regulate the charge density. However, operation of TENGs requires intimate contact and sometimes friction between triboelectric materials, which inevitably induces wearing of surface. In this regard, surface modification/engineering yields little contributions toward the performance gain in long-term operation. Therefore, one essential solution is to extend the property engineering from mere surface to the bulk of material.

Atomic layer deposition (ALD) is a powerful thin film growth technique on the basis of sequential self-limiting surface reactions. When implemented to certain polymers, the large permittivity of metalorganic precursors allows deep infiltration of inorganic compounds during ALD process, leading to inorganic/organic hybrid materials. This process is known as sequential infiltration synthesis (SIS). It has been successfully used to convert block co-polymer nanopatterns into more durable inorganic patterns and to improve the polymeric lithography resistance to subsequent etching. Inspired by these developments, we expect SIS could effectively tailor the internal composition and electrical properties of polymer films, which may provide an ultimate solution for triboelectric material design in the development of high-performance TENGs. Here, we report an internal AlO_x doping of several polymers via SIS, including polydimethylsiloxane (PDMS), polyimide (Kapton) and poly(methyl methacrylate) (PMMA).[1,2] We showed that SIS can introduce AlO_x molecules $\sim 3 \mu\text{m}$ deep into these polymers, which effectively tuned the bulk electrical property of the film. TENG devices using the modified polymer films exhibited enhanced power output; and this enhancement remained effective after the surface of polymer film was polished off for more than $2 \mu\text{m}$. This polymer doping approach opens a new route to bulk electrical property modification of polymer films, demonstrating a promising strategy for improving the performance of functional polymer based devices, such as TENGs.

Reference

1. Y. Yu, Z. Li, Y. Wang, S. Gong, X. Wang. *Adv. Mater.*, 27, 4938-4944, 2015.
2. Y. Yu, X. Wang. *Extreme Mech. Lett.*, doi:10.1016/j.eml.2016.02.019, 2016.

3:00pm TF+EM-MoA5 ALD for Interfacial Engineering of Energy Conversion Devices, Neil P. Dasgupta†, University of Michigan, Ann Arbor

INVITED

Recently, there has been a dramatic increase in research of nanoscale materials for energy conversion and storage applications due to several advantageous features such as high surface areas, short transport distances, novel optical phenomena, and tunable material properties. However, with these benefits come challenges. In particular, the ability to precisely control the properties of surfaces and heterogeneous interfaces at the nanoscale limits the performance of many of these devices, and requires novel approaches. This problem becomes increasingly important as dimensions decrease, as the surface-to-volume ratios continually increase with decreasing feature size.

One technique that has been increasingly explored for surface and interfacial engineering of nanostructured energy conversion and storage devices is Atomic Layer Deposition (ALD). This gas-phase process allows for highly conformal deposition of a wide variety of materials with sub-nm precision in material thickness and tunable chemical composition. A wide range of materials, including oxides, sulfides, and metals can be deposited by ALD. The combination of conformality and thickness control of ALD facilitates precise tuning of the electronic, optical, thermal, and chemical properties to optimize their interfaces in energy conversion devices.

* TFD James Harper Award Finalist

† Paul Holloway Award Winner

This talk will present several examples of using ALD to fabricate highly-controlled interfaces for energy conversion and storage devices. Examples include batteries [1], photovoltaics [2-3], and photoelectrochemical cells [4-5]. The key theme linking these studies is that through deterministic control of interfacial layer composition, thickness, crystallinity, and morphology, we can “program” properties such as charge transfer resistance, catalytic activity, and chemical stability. This control enables interfacial materials engineering to optimize both device efficiency and lifetime. The importance of fully understanding ALD surface chemistry will be discussed from a theoretical and experimental perspective. The talk will conclude with a perspective on future directions and challenges for widespread commercial adaption of these technologies.

- [1] E. Kazyak, K. N. Wood and N. P. Dasgupta, *Chem. Mater.* **27**, 6457 (2015)
- [2] A. B. Wong, S. Brittman, Y. Yu, N. P. Dasgupta and P. Yang, *Nano Lett.* **15**, 4096 (2015).
- [3] S. Brittman, Y. Yoo, N. P. Dasgupta, S.-I. Kim, B. Kim and P. Yang, *Nano Lett.* **14**, 4665 (2014).
- [4] N. P. Dasgupta, C. Liu, S. Andrews, F. B. Prinz and P. Yang, *J. Am. Chem. Soc.* **135**, 12932 (2013).
- [5] J. Resasco, N. P. Dasgupta, J. Rosell, J. Guo and P. Yang, *J. Am. Chem. Soc.* **136**, 10521 (2014).

4:00pm **TF+EM-MoA8 Anchoring Down Soluble Polysulfides for Lithium and Sodium Sulfur Battery Cathodes using Atomic Layer Deposition**, *Rachel Carter*, A.P. Cohn, L. Oakes, N. Miralidharan, A.E. Douglas, K. Share, C.L. Pint, Vanderbilt University

Among the most significant challenges for practical lithium or sodium sulfur batteries is polysulfide shuttling, where intermediate discharge products (M_2S_8 , M_2S_6 and M_2S_4) dissolve into the electrolyte lowering active sulfur mass and fouling the metal anode. To overcome this, we demonstrate the use of atomic layer deposition (ALD) to produce thin oxide coatings on cathode materials to stabilize these soluble polysulfides and mitigate active material loss. We specifically focus on V_2O_5 (vanadium pentoxide) due to its demonstration in recent theoretical studies to exhibit strong polar interaction with soluble polysulfides that exceeds other oxide materials. With the application of the V_2O_5 binding interlayer the initial discharge capacity of the sulfur cathodes is enhanced by 20%, which is a direct result of anchoring the soluble species for optimal complete discharge of the sulfur. The capacity retention of the sulfur cathode is enhanced to 87% capacity retention over 100 cycles, in comparison to less than 50% retention without ALD binding layer. The binding effect was also probed using UV-Vis analysis, since there are distinct absorption peaks for the soluble S_6^{2-} state in the electrolyte. Solutions of Li_2S_6 and Na_2S_6 we studied before and after exposure to ALD binding layers with dramatic decrease in the S_6^{2-} signature in solution observed proving the binding interactions between the polysulfides and V_2O_5 binding interlayer. Overall, our work shows how ALD is a versatile tool to atomically engineer surfaces to sustain excellent performance without compromising the gravimetric performance needed for practical battery applications.

4:20pm **TF+EM-MoA9 Hybrid Inorganic-Organic Thin Films by ALD/MLD for Emerging Energy Technologies**, *Maarit Karppinen*, Aalto University, Finland **INVITED**

For hybrid inorganic-organic materials it is in principle possible to realize properties not seen for conventional materials. An elegant, yet industrially feasible way to link the inorganic and organic entities *via* strong chemical bonds to form coherent multi-layered hybrid materials is to combine the ALD (*Atomic Layer Deposition*) technique originally developed to deposit high-quality thin films of simple inorganic materials with MLD (*Molecular Layer Deposition*) cycles based on organic precursors. This enables the atomic/molecular layer-by-layer production of inorganic-organic hybrid thin films through sequential self-limiting gas-surface reactions with high precision for the film thickness and composition.

In this talk I will discuss our recent efforts towards synthesizing new functional materials by the combined ALD/MLD technique.¹ In particular, we have fabricated oxide-organic thin-film superlattices in which the periodically introduced single/thin organic layers between oxide layers are *e.g.* shown to hinder phonon transport and substantially enhance the thermoelectric properties of $(Zn,Al)O^{2,3}$ and $(Ti,Nb)O_2^{4,5}$ films. Other exciting application areas foreseen for the ALD/MLD hybrid thin films include the flexible and transparent Li-ion microbattery materials^{5,6} and so-called metal organic framework (MOF) materials.⁷

1. P. Sundberg & M. Karppinen, Organic and inorganic-organic thin film structures by molecular layer deposition: A review, *Beilstein J. Nanotechnol.* **5**, 1104 (2014).
2. T. Tynell, I. Terasaki, H. Yamauchi & M. Karppinen, Thermoelectric characteristics of $(Zn,Al)O$ / hydroquinone superlattices, *J. Mater. Chem. A* **1**, 13619 (2013).
3. T. Tynell, A. Giri, J. Gaskins, P.E. Hopkins, P. Mele, K. Miyazaki & M. Karppinen, Efficiently suppressed thermal conductivity in ZnO thin films via periodic introduction of organic layers, *J. Mater. Chem. A* **2**, 12150 (2014).
4. J.-P. Niemelä, A. Giri, P.E. Hopkins & M. Karppinen, Ultra-low thermal conductivity in $TiO_2:C$ superlattices, *J. Mater. Chem. A* **3**, 11527 (2015).
5. M. Nisula, Y. Shindo, H. Koga & M. Karppinen, Atomic layer deposition of lithium phosphorous oxynitride, *Chem. Mater.* **27**, 6987 (2015).
6. M. Nisula & M. Karppinen, Atomic/molecular layer deposition of lithium terephthalate thin films as high rate capability Li-ion battery anodes, *Nano Lett.* **16**, 1276 (2016).
7. E. Ahvenniemi & M. Karppinen, Atomic/molecular layer deposition: a direct gas-phase route to crystalline metal-organic framework thin films, *Chem. Commun.* **52**, 1139 (2016).

Thin Film

Room 102B - Session TF+PS+SE-MoA

Plasma-based Deposition Techniques and Film Characterization

Moderators: Jim Fitz-Gerald, University of Virginia, Tansel Karabacak, University of Arkansas at Little Rock

1:40pm **TF+PS+SE-MoA1 Microcrystalline Silicon Thin Film Deposited by Tailored Voltage Waveform Plasmas using an $SiF_4/H_2/Ar$ Chemistry and its Application to Photovoltaics**, *Junkang Wang*, LPICM, CNRS, École Polytechnique, Université Paris Saclay, France; *M. Elyakoubi*, TFSC-Instrument, Palaiseau, France; *E.V. Johnson*, LPICM, CNRS, École Polytechnique, Université Paris Saclay, France

For the growth of hydrogenated microcrystalline silicon ($\mu c-Si:H$) thin film by low temperature plasma-enhanced chemical vapor deposition (PECVD), silicon tetrafluoride (SiF_4) has recently attracted interest as a precursor due to the resilient optoelectronic performance of the resulting material and solar cell device. However, many questions remain concerning the critical factors determining the quality of the PECVD-deposited film.

Tailored voltage waveforms (TVWs), non-sinusoidal voltage waveforms used to excite radio-frequency capacitively coupled plasma (RF-CCP) processes, has recently been shown to be effective to separately control the maximum ion bombardment energy (IBE) and the ion flux on each electrode. Due to this unique feature, TVWs have attracted considerable research interest in a very short time. When applied to the growth of $\mu c-Si:H$ film by PECVD, it can provide an elegant approach for one to gain more insight into the physical principles governing film growth and the optimization of process parameters.

To advance knowledge on this subject, we present studies looking at the deposition of $\mu c-Si:H$ film from SiF_4 using TVWs, particularly focusing on the material's optoelectronic properties and its resulting PIN solar cell device. We underline recently obtained results concerning critical experimental findings: (1) the significant impact of the maximum IBE to the crystalline grains sizes of the deposited films, (2) the considerable difference in films' properties resulting from two types of “sawtooth” waveforms, i.e. “sawtooth-up” and “sawtooth-down”, which give similar films deposition rates and the maximum IBE but opposite plasma sheath dynamics during processing. The films generated in these studies have furthermore been characterized using the steady-state photoconductivity and steady-state photocarrier grating techniques, analyzing the coplanar electronic transport properties of the material. The modulated photoconductivity method is also utilized to reveal more specific details about the materials' sub-gap density of states. These studies - along with residual gas analysis studies and Fourier transform infrared absorption results - allow us to optimize the appropriate process parameters of such film and its resulting PIN solar cell device using SiF_4 as the precursor.

2:00pm **TF+PS+SE-MoA2 Boron Carbide-Aromatic Composite Films by PECVD: A Novel Approach to Electron-hole Separation**, *B. Dong, A. Oyelade*, University of North Texas; *E.M. Echeverria*, University of Nebraska-Lincoln; *Y-S. Jun, G.D. Stucky*, University of California at Santa Barbara; *P.A. Dowben*, University of Nebraska-Lincoln; *Jeffrey Kelber*, University of North Texas

Many photovoltaic and photocatalytic systems employ band-bending at surfaces or interfaces to achieve electron-hole separation and functionality. Boron carbide-aromatic composites, formed by plasma-enhanced co-deposition of carboranes and aromatic precursors, present an alternative approach where such separation is achieved by aromatic coordination to the carborane icosahedra. Photoemission, density functional theory calculations, and variable angle spectroscopic ellipsometry demonstrate that for orthocarborane/pyridine and orthocarborane/aniline films, with controlled aromatic/orthocarborane ratios between 1:1 and 10: 1, states near the valence band maximum are aromatic in character, while states near the conduction band minimum include those of either carborane or aromatic character. Thus, excitation across the band gap results in electrons and holes on carboranes and aromatics, respectively. Further such aromatic-carborane interaction dramatically shrinks the indirect band gap from 3 eV (PECVD orthocarborane) to ~ 1.6 eV (PECVD orthocarborane/pyridine) to ~1.0 eV (PECVD orthocarborane/aniline), with little variation in such properties with aromatic/orthocarborane stoichiometry. Recent photoabsorbance measurements show that in orthocarborane/pyridine films, the indirect band gap energy is significantly less than the exciton formation energy of 2.1 eV, allowing facile exciton elimination by phonon scattering of electrons into the conduction band at room temperature. The opposite is true for the PECVD orthocarborane film, where the exciton formation energy (2.4 eV) is less than the indirect band gap, inhibiting exciton elimination by electron-hole separation. The enhanced electron-hole separation, narrowed band gap, and significantly increased carrier lifetimes (350 μ sec for PECVD orthocarborane/pyridine vs 35 μ sec for PECVD orthocarborane), indicate the potential for greatly enhanced charge generation, as confirmed by zero-bias neutron voltaic studies. Those results--an 850% increase in charge generation per B atom for the PECVD pyridine/orthocarborane film relative to the PECVD orthocarborane film--indicate that the enhanced electron-hole separation and band gap narrowing observed for aromatic/orthocarborane films relative to PECVD orthocarborane, have significant potential for a range of applications, including neutron detection, photovoltaics, and photocatalysis.

Acknowledgements: This work was supported by the Defense Threat Reduction Agency (Grant No. HDTRA1-14-1-0041). The authors would like to thank Shireen Adenwalla for technical assistance and discussion. James Hilfiker is also gratefully acknowledged for stimulating discussions.

2:20pm **TF+PS+SE-MoA3 Impact of Pulsing the rf Power and the Precursor Injection on the Structure and Optical Properties of TiO₂ and TiSiO Thin Films Deposited by PECVD**, *Agnes Granier, S. Elisabeth, R. Michaud, N. Gautier, M. Richard Plouet*, IMN, University of Nantes CNRS, France; *M. Carette*, IEMN CNRS/Université Lille 1, France; *A. Goullet*, IMN, University of Nantes CNRS, France

TiO₂ thin films are good candidates for the development of passive optical components due to high optical refractive index ($1.8 < n < 2.7$ at 633 nm) combined with high transparency in the visible range. They are compatible with semiconductor technologies and can be synthesized at low temperature by plasma enhanced chemical vapor deposition (PECVD). PECVD is known for its ability to prepare amorphous or partially crystallized films at low temperature and to tune the film composition and optical properties. In the case of TiO₂, columnar polycrystalline anatase films can be prepared by PECVD at substrate temperature less than 150°C. Whereas these TiO₂ films are very attractive for photocatalysis, their columnar structure and low optical gap (3.2 eV) appear to be drawbacks for optical applications. Adding a small amount of silicon to TiO₂ allows both obtaining amorphous films and increasing the optical gap, which is highly suitable for optical applications.

In this study, TiO₂ and Ti-Si-O films were deposited in a low pressure rf inductively coupled plasma (ICP) from titanium tetraisopropoxide (TTIP - Ti(OC₃H₇)₄) and hexamethyldisiloxane (HMDSO - SiO₂(CH₃)₆) vapors mixed with oxygen. The structure and chemical composition of the films were investigated by X-ray diffraction, photoelectron spectroscopy, Fourier transform infrared spectroscopy and Raman spectroscopy. The morphology of the thin films was characterized by scanning and transmission electron microscopies. The optical properties were investigated by UV -Visible spectroscopic ellipsometry and absorption spectroscopy. When deposited

at the floating potential, the TiO₂ films deposited in the continuous mode in oxygen rich O₂/TTIP ICP plasmas were previously shown to be columnar and highly crystallized in the anatase form. As silicon is added to titanium, the films become amorphous. Their refractive index decreases and their optical gap increases [1].

Here, we investigate the effects of pulsing both the rf power and the precursor injection on the film structure and optical properties.

On the one hand, in the case of TiO₂ and Ti-O-Si films, the pulse frequency was fixed at 1 kHz and the duty cycle was varied from 100 to 10%. Pulsing the power allows to decrease the deposition temperature (down to about 50°C) while conserving the anatase structure in the case of TiO₂ films, so that anatase and amorphous high refractive index Ti-Si-O films can be deposited on polymer substrates.

On the other hand, TTIP and HMDSO flow rates have been pulsed, either to get benefit from oxygen plasma treatment following oxide deposition or to deposit TiO₂/SiO₂ stacks.

[1] D. Li et al, Plasma Processes and Polymers, 2016

2:40pm **TF+PS+SE-MoA4 Plasma CVD of Boron-Carbon Thin Films from Organoboron Precursors for Next Generation Neutron Detectors**, *Mewlud(Maiwulidan) Imam (Yimamu)*, Linköping University, Sweden; *C. Höglund*, Linköping University and European Spallation Source ERIC, Sweden; *R. Hall-Wilton*, European Spallation Source ERIC, Sweden; *J. Jensen*, Linköping University, Sweden; *S. Schmidt*, Linköping University and European Spallation Source ERIC, Sweden; *I.G. Ivanov, J. Birch, H. Pedersen*, Linköping University, Sweden

A novel design for neutron detectors based on thin films that are rich in the ¹⁰B isotope has been suggested for the European Spallation Source (ESS), in order to overcome the very limited availability of ³He. The detector design uses ¹⁰B₄C films deposited onto both sides of neutron transparent substrates, e.g., Al blades [1]. The use of aluminum (melting point at 660 °C) limits the deposition temperature for CVD processes and the use of chlorinated precursors due to etching of Al by HCl. Therefore, reactive organoborons are evaluated as precursors for these films using both thermal CVD [2, 3] and plasma CVD.

Plasma CVD of B_xC thin films has been studied by introducing the organoborons trimethylboron B(CH₃)₃ (TMB) or triethylboron B(C₂H₅)₃ (TEB) into a microwave-induced Ar plasma without using any intentional substrate heating. The effect of plasma power, TMB or TEB to Ar ratio and total pressure on the film composition, morphology, density, chemical structure and internal stress were investigated by means of ToF-ERDA, SEM, XRR, XPS and HRXRD, respectively. ToF-ERDA results showed that the highest B/C ratio of 2 was achieved when using TMB at high plasma power. Densification of the films was accompanied by decreasing the total pressure below 0.4 mbar, resulting in a columnar film with densities of 2.16 ± 0.01 g/cm³. The H content in the films was high (15±5 at. %) due to the low substrate temperature (~300 °C). XPS revealed that films deposited using TMB mainly contained B-C bonds and small contribution from C-C/CH bonds, that was evidenced by the observed amorphous carbon phases in the films by Raman spectroscopy. The internal compressive stresses in the films were increased with the Ar gas flow causing film delamination, while a low flow of Ar showed good adhesion and stress level is less than 300 MPa. In addition, the plasma composition studied by optical emission spectroscopy (OES) showed that BH, CH, C₂ and H lines were the most intensive lines in the spectrum. Considering the high H content in the films, we propose that BH and CH are the most likely species to contribute to the film formation.

[1] R. Hall-Wilton et al. *IEEE NSS/MIC conference record*, **2012**, 4283

[2] H. Pedersen et al. *Chem. Vap. Deposition***2012**, *18*, 221

[3] M. Imam et al. *J. Mater. Chem. C***2015**, *3*, 10898

3:00pm **TF+PS+SE-MoA5 Plasma Enhanced Atomic Layer Deposition of Superconducting Nb_xTi_yN Films**, *Mark Sowa*, Ultratech/CNT; *Y. Yemane, J. Provine*, Stanford University; *E.W. Deguns*, Ultratech/CNT; *F. Prinz*, Stanford University

NbN, TiN, and their mixtures have been studied for their use in superconducting applications. These materials are commonly deposited via sputtering techniques, but a lack of thickness control limits this technique from applying thin, uniform films. Atomic Layer Deposition (ALD) has been widely recognized for its ability to coat substrates with uniform film thicknesses ranging from a few Ångströms to 100's of nanometers. Plasma Enhanced ALD (PEALD) extends the capabilities of the ALD technique, improving the properties of certain films, particularly nitrides deposited at

low temperatures. PEALD of NbTiN has previously demonstrated superconducting properties¹ and PEALD NbN has been previously reported with a critical temperature of 10.4K².

In this work, Nb_xTi_yN (0 ≤ x, y ≤ 1) has been deposited using PEALD in an Ultratech/CNT Fiji system at substrate temperatures between 100 and 300°C. Stoichiometry was controlled by adjusting the ratio of NbN:TiN cycles during the film deposition. Precursors utilized for this study were (t-butylimido) tris(diethylamido) niobium (TBDEN) and tetrakis(dimethylamido) titanium (TDMAT). A mixture of N₂ and H₂ was used as the plasma gas for the NbN cycles while TiN was deposited with an N₂ plasma. Films were analyzed for thickness and optical properties through spectroscopic ellipsometry. Room temperature resistivity was derived from four point probe measurements. Samples were analyzed with X-ray photoelectron spectroscopy to determine stoichiometry and impurity levels. Superconductivity characteristics of the films will also be presented.

A 20nm, 300°C deposition of NbN, which had a room temperature resistivity of 282μΩ-cm, was shown to have a critical temperature of 12.4K and a critical field greater than 12 Tesla.

[1] E. F. C. Driessen, et al., "Strongly Disordered TiN and NbTiN s-Wave Superconductors Probed by Microwave Electrodynamics," Phys. Rev. Lett. 109, 107003, 2012.

[2] M. Ziegler, et al., "Superconducting niobium nitride thin films deposited by metal organic plasma-enhanced atomic layer deposition," Supercond. Sci. Technol. 26 (2013) 025008.

3:20pm TF+PS+SE-MoA6 Mechanical Reliability of PECVD Barrier Films for Flexible Electronics, Kyungjin Kim, A. Singh, H. Luo, T. Zhu, O. Pierron, S. Graham, Georgia Institute of Technology

The development of PECVD and ALD barrier films have proven to be viable approaches to create barrier films for flexible electronic applications. While much research has focused on the water vapor transport properties of these films, the mechanical reliability during flexural deformation is critical to the performance and durability of these coatings. Overall, the use of the critical onset strain is limiting in trying to define the limits of performance since it ignores time-dependent processes that can occur during mechanical deformation. In this work, we investigate the time-dependent channel crack growth behavior of silicon nitride and ALD barrier films on polyethylene substrates in humid and dry air. The evaluation of the cracking process versus applied strain and load was measuring in-situ using optical and laser scanning confocal microscopy. The results show that crack growth can occur at strains that are much lower than the standard measured onset critical strains. The results of the work show that both polymer relaxation of the PET substrate as well as environmentally assisted crack growth occurs in the films, both in a time dependent manner. Tests in dry air versus tests in humid air show crack growth rates increasing from 100 nm/s to 10 μm/s for an applied stress intensity factor of 1.6 MPa.m^{0.5}. In addition to the dramatic changes in crack growth rates with environmental conditions, larger crack densities were observed in humid environments. This suggests an easier initiation and growth of crack in humidity versus dry air. Overall, the results presented will show the strong link between environment, temperature, and the rate at which cracks grow in barrier films. Finally, the energetics of the crack growth process will be presented as a better metric than onset crack strain to evaluate the mechanical reliability of the barriers for a given application.

4:00pm TF+PS+SE-MoA8 Origin of Stress in Sputtered CdTe and ZnS Films: Influence of Sputter Ion Mass on Mechanical and Chemical Layer Properties, Ségolène Liénard, Univ. Grenoble Alpes, LTM CNRS, 38000 Grenoble, France; D. Sam-Giao, A. Kerlain, Sofradir, BP 21-38113, Veurey-Voroize, France; F. Boulard, C. Vallée, Univ. Grenoble Alpes, France
Physical vapor deposition is a mature, well understood and established technology in integrated circuit fabrication. CdTe and ZnS binary II-VI compounds materials are commonly used in photovoltaic solar cells or infrared optics. However, sputtering deposition of these materials still suffer from a lack of comprehensive study to optimize process integration.

Our study is focused on the influence of projectile ions mass on properties of sputtered deposition CdTe and ZnS films. We compare physico-chemical, mechanical and electrical properties of CdTe and ZnS films deposited with

Ar and Xe ions as sputter gas. Ar and Xe concentration in these films are characterized by Time of Flight Secondary Ions Mass Spectrometry (TOF-SIMS). Dedicated implanted reference samples are used to quantify the absolute concentration. Layers microstructures are characterized by Scanning Tunneling Electron Microscopy (STEM) and dielectric constant by capacitance-voltage measurements. We use the curvature method based on the well known Stoney concept [1] to calculate film stress while density is estimated by differential weighing.

With Ar ion deposition process (low sputter on target mass ratio), we observe Ar and cavities inside the CdTe layer. The density as well as the dielectric constant are below bulk values. A good agreement is found between the cavity density and the effective dielectric constant determined by the Bruggeman model [2-3]. on the contrary, Xe ion target sputtering (high sputter on target mass ratio) leads to denser films, without Xe inside the layers, and close to theory density and dielectric constant values. We discuss these observations in terms of backscattered ions incorporation. Moreover, the effect of thermal annealing time on stress evolution is discussed in regards of Ar or Xe incorporation and outgasing.

[1] G.G. Stoney, Proc. Soc. London, A82, 1909, 172

[2] Aspnes D. E., Thin Solid Films 89 (1982) 249.

[3] Othman M.T., PhD "Spectroscopic Ellipsometry Analysis of Nanoporous Low Dielectric Constant films Processed via Supercritical CO2 for Next-generation Microelectronic Devices", University of Missouri-Columbia, 2007

4:20pm TF+PS+SE-MoA9 Synthesis and Characterisation of MoB_{2-x} and Mo-B-C Thin Films by Non-Reactive DC Magnetron Sputtering, Paulius Malinovskis, Uppsala University, Sweden; J.P. Palisaitis, Linköping University, Sweden; P.O.A. Persson, Linköping University, Sweden; E.L. Lewin, U.J. Jansson, Uppsala University, Sweden

Transition metal diborides (MeB₂) with the AlB₂-type structure have many unique properties such as high hardness, high conductivity and oxidation resistance. One of the most studied diboride compounds is TiB₂ but also other transition metals like Cr, Nb and Mo can form the simple AlB₂ type structure.

Non-reactive magnetron sputtering is an excellent technique to deposit thin films of different MeB₂ phases. It is well-known that phases with rather simple crystal structures are preferably formed in magnetron sputtering where the quenching rates of the incoming atoms are high. Such metastable MeB₂ films may be chemically more reactive in a tribocontact and form a lubricating tribofilm of metal oxides and layered BO_x. Some metal oxides such as MoO₃ and boric acid (forming in humid atmosphere from BO_x) have been predicted to exhibit low friction coefficients. Consequently, it is possible that metastable MeB₂ films with the AlB₂-structure may exhibit excellent low friction properties. Another way to tailor metal diboride properties is to alloy it with third element, e.g. carbon.

In this study we have investigated the microstructure, mechanical and tribological properties of DC magnetron sputtered MoB_{2-x} and Mo-B-C thin films from Mo/B and graphite carbon target. The films were characterized with XRD, XPS, TEM, nanoindentation and tribological ball-on-disk method. All films exhibited the AlB₂-type structure with substoichiometric MeB_{2-x} grains surrounded by a tissue phase of a-B and a-BC. The MoB_{2-x} films were substoichiometric with respect to boron and exhibited a much higher hardness compared to bulk samples, which could be attributed to a hardening effect of the tissue phase. Friction measurements confirmed the hypothesis that a significant tribofilm formation is present on the metastable MoB_{2-x} films. However, a reduced friction coefficient could not be observed. Addition of carbon resulted in a change in the composition of the tissue phase. This caused a reduction in hardness and a reduction of the friction coefficient. General trends in the phase formation and properties of Mo-B-C films will be explained in detail and compared with other Me-B-C systems (Me= Ti, Cr, Nb).

4:40pm TF+PS+SE-MoA10 Molybdenum Back Contacts Deposited by High Power Impulse Magnetron Sputtering, D.A. Loch, Arutun Eghasarian, Sheffield Hallam University, UK

Molybdenum thin films used in chalcopyrite solar cells can influence the Na diffusion rates and the texture of the Cu(InGa)Se₂ absorber according to the microstructure and morphology. The lowest resistivity films are achieved at low working pressure and are accompanied by high residual stress and poor adhesion due to the resulting high energy of the deposited flux. High Power Impulse Magnetron Sputtering was employed to ionise the sputtered flux, achieve high adatom mobility at low energy and

influence the growth of Mo back contacts. Pulse durations in the range 60 to 1000 μ s, sputtering voltages between 800 and 1500 V and deposition pressures of 2×10^{-3} mbar and 4×10^{-3} mbar resulted in ten-fold variations in the flux ratios of $\text{Mo}^{1+}/\text{Mo}^0$, $\text{Mo}^{2+}/\text{Mo}^{1+}$, $\text{Ar}^{2+}/\text{Ar}^{1+}$ and $\text{Mo}^{1+}/\text{Ar}^{1+}$ as determined by optical emission spectroscopy and time-resolved plasma-sampling energy-resolved mass spectroscopy. The energy of metal and gas double and single-charged ions reduced with pulse duration and increased with voltage. The microstructure of the films varied from open columnar with faceted tops to fully dense as observed by secondary electron microscopy. The reflectivity of the films improved by 20% compared to industry-standard materials. The lowest resistivity was in the range of 12 $\mu\Omega\text{-cm}$ as observed by four-point probe measurements of 570 nm thick films. The correlation between resistivity, microstructure, crystallographic texture, stress and deposition flux characteristics is discussed.

5:00pm TF+PS+SE-MoA11 Plasma Characterization of Al and Cu with HIPIMS, Jason Hrebik, Kurt J. Lesker Company; *R. Bandorf, H. Gerdes, D. Spreemann*, Fraunhofer Institute for Surface Engineering and Thin Films IST, Germany

High power impulse magnetron sputtering (HIPIMS) is a well-known technique for tailoring the coating properties in comparison to DC. In many cases the thin films were developed in smaller scale R&D facilities and afterwards transferred to industrial scaled machines. But the source configuration, magnetic field, and overall mechanical layout differs for the larger sputtering plant, and therefore a direct upscaling of the process is quite difficult. Since often the thin film properties are correlating with the plasma properties, plasma characterization is very useful tool for determining the main important parameters for a process transfer.

This investigation is focused on the plasma characterization of Al and Cu on a small circular target (3 inch) and will give a short comparison to a rectangular target (10 inch by 15 inch). As plasma properties the ion density and the optical emission was measured. The measurements were carried out in a time resolved mode and can be correlated to target voltage and current.

Vacuum Technology Room 104C - Session VT-MoA

Gas Dynamics, Simulation and Partial Pressure Analysis

Moderators: Steve Borichevsky, Applied Materials, Varian Semiconductor Equipment, Ted Martinez, SLAC National Accelerator Laboratory

1:40pm VT-MoA1 Vacuum System Analysis of a Next Generation Light Source with Synrad and MolFlow+, Jason Carter, Argonne National Laboratory

INVITED

CERN's SynRad and MolFlow+ vacuum analysis programs continue to be valuable tools for accelerators as vacuum system design challenges increase. The trends for future accelerator vacuum systems, including the APS-Upgrade project, are towards narrower, conductance-limited vacuum chambers which allow for stronger magnets and lower beam impedances but restrict effective pumping and photon shielding. UHV pressure requirements remain fixed or become tighter to increase beam lifetimes and user access which leads to the need for a more thorough vacuum analysis to ensure designs are suitable to many needs. SynRad and MolFlow+ are catered to addressing these challenges and both ease of use and the understanding of their capabilities continues to grow.

SynRad/MolFlow+ users may have been limited in the past by their 3D CAD abilities, however recent improvements to mainstream CAD software such as 'direct modeling' methods have made it easier and faster to build or reverse engineer models with high complexity and precision. This allows for better understanding of complex conductance and quicker iterations on ray tracing schematics. Some examples from the APS will be discussed.

The APS-Upgrade uses SynRad and MolFlow+ extensively for vacuum system calculations and has been digging further into the programs' inputs to build confidence in their predictions. The two programs share a coupling function which predicts dynamic photon stimulated desorption (PSD) outgassing and allows for calculations of dynamic pressures and beam conditioning times. The APS-U is studying this coupling in order to build confidence that their vacuum system design will reach low pressures with reasonable conditioning. Work for this includes studying the sensitivity of the program's inputs and applying the work to existing APS vacuum systems.

2:20pm VT-MoA3 Simulations of Vacuum Pumping and Beam Conditioning for CHESS-U Vacuum System, Yulin Li, X. Liu, Cornell Laboratory for Accelerator-Based Sciences and Education; *J.S. Mershon*, The College of Wooster

A major upgrade project (dubbed CHESS-U) is planned to elevate performance of Cornell High Energy Synchrotron Source (CHESS) to the state-of-art 3rd generation light sources. As a critical part of the CHESS-U project, about 80-m of Cornell Electron Storage Ring (CESR) is to be replaced with double-bend achromat (DBA) lattice to significantly reduce electron beam emittance. In this presentation, we will describe the conceptual design of the CHESS-U vacuum system, with emphasis on the vacuum pumping design and considerations. In the DBA lattice, multifunction dipole magnets with complex magnet poles prevent use of distributed ion pumps as in current CESR vacuum system. Instead, non-evaporable getter (NEG) strips are used to provide distributed vacuum pumping in the dipole vacuum chambers, as well as in the undulator vacuum chambers. Discrete pumps are used in the straights at available spaces between quadrupole and steering magnets. A test-particle Monte-Carlo simulation program, MolFlow+, is employed to evaluate pumping performances of the CHESS-U vacuum system in two aspects. First, we demonstrate that the planned vacuum pumping system can achieve and sustain required ultra-high vacuum level in CHESS-U operations. In addition, we will explore beam commissioning processes of the new vacuum chambers, and simulate the saturations of the NEG strips during the commissioning. These simulations will aid continuing design optimization for the CHESS-U vacuum system.

2:40pm VT-MoA4 MFIG, A New Vacuum Sensor for Yield Enhancement, N.B. Koster, F. de Graaf, Michel van Putten, P.M. Muilwijk, E. Nieuwkoop, O. Kievit, D.J. Maas, TNO Technical Sciences, Netherlands

This contribution addresses the introduction of a new type of sensor that can disruptively enhance the yield of manufacturing and inspection tools where ultraclean vacuum and control is needed. This includes tools working with high energy photons, ions or electrons.

In 2007, the development of TNO's mass-filtered-ion-gauge (MFIG) started when experts realized that IC manufacturing with EUV needs extremely clean vacuum, while existing sensors are either too slow, expensive or insensitive for real-time monitoring of vacuum cleanliness. The promising results of a "quick-and-clean" test were well-received at the AVS meeting in 2008. Hence TNO incubated the concept in an EU project, in which both instrumentation was improved and application requirements were clarified by interacting with the consortium partners. In 2015 TNO has been awarded a NanoNextNL valorization grant to further mature the instrumentation and prepare for MFIG's market introduction in 2017.

This presentation will update the audience on MFIG's latest performance in laboratory and field tests as well as tell the story how an idea advanced into a product. A short explanation of the technology and new design will be part of the presentation.

3:00pm VT-MoA5 Dynamic Process Modeling on a Condensation-based Depressurization System, Bo Zhang, G. Guo, C. Zhu, Z. Ji, New Jersey Institute of Technology

A near-vacuum state in an enclosed chamber can be achieved by vapor condensation on a cooling surface. This near-vacuum chamber can function as a vacuum sink for a sustained operation of application that requires depressurization in an open flow environment. To realize such a sustained operation of gas extraction, a complete cycle of regenerating vacuum in the chamber may consist of multiple stages, including a vapor filling process, the vacuum generation by cooling-controlled condensation, a process of gas extraction from depressurization-required application, and a process of flushing non-condensable gas out of the condensation chamber. A dynamic process model is established to describe the thermodynamic characteristics of the entire cycle. The transient and non-equilibrium characteristics in the condensation-induced vacuum generating process is reasonably captured by our computational fluid dynamics (CFD) model, with modified boundary conditions accounting for the complicated coupling mechanisms of heat and mass transfer during the condensation. The CFD simulations for the entire processes are obtained using FLUENT with user-defined functions. In addition, a pseudo-equilibrium-based parametric model is further developed to evaluate various parametric effects for the system design and optimized operation. The CFD simulation results and parametric modeling predictions are partially validated through our experimental measurements.

Monday Afternoon, November 7, 2016

4:00pm **VT-MoA8 Vacuum Adventures Encountered Towards a Field-Portable Helium Isotope Detector**, **Gary McMurtry**, SOEST, University of Hawaii; *J.R. DeLuze*, Fusion Energy Solutions of Hawaii; *D.R. Hilton*, Scripps Institution of Oceanography, UCSD; *J.E. Blessing*, MKS Instruments **INVITED** The $^3\text{He}/^4\text{He}$ ratio in volcanic emissions and dissolved gas in groundwater is often co-seismic with, and sometimes precursory to, volcanic unrest and earthquake activity. Because of the extremely low abundance of primordial ^3He to radiogenic ^4He , and difficulties in resolving ^3He in the presence of hydrogen isobars such as HD, the measurement of this ratio has so far been confined to the laboratory. A field-portable He isotope instrument must overcome these analytical hurdles and be small, compact, lightweight and low enough in power consumption to deploy in critical locations.

We use two compact mass spectrometers, an MKS ion trap and a frequency-modified MKS quadrupole MS, with a full-range pressure gauge and waste pumps based upon noble diode ion or turbo-rough pumping. These are coupled to a high-purity quartz glass port that is heated under high vacuum. Gas samples can be separated from waters or directly analyzed by pumped circulation through a sample chamber. We monitor vacuum quality with the ion trap and use the quadrupole MS to obtain sensitive determination of hydrogen and helium isotopes. Two methods of isobaric separation are utilized: a statistical mass-2 vs. mass-3 regression intercept, and an adjusted (threshold) ionization mass spectrometry (AIMS) technique. Comparison of these two independent methods for 44 data pairs in a "blind collection" after heat ramps to a predetermined maximum temperature are completed yields a significant correlation ($r = 0.89$).

Results on laboratory air are within a factor of 2 of the accepted ratio of 1.40×10^{-6} (R_a). We can obtain the exact air ratio ($R/R_a = 1.0$) if we continuously monitor the MS scans during the heat ramps, allowing for differences in the diffusion rates of ^3He and ^4He . With an established power level, keeping to a constant scan time allows air $^3\text{He}/^4\text{He}$ ratios to be obtained to within 0.1 R/R_a . Adventures in vacuum technology encountered along this developmental pathway include the discovery of temperature-dependent differential diffusion of He isotopes in heated glass, quantum tunneling of ^3He , amazing enrichments of ^3He from air, and potential industrial applications of a mass-selective fluid bandpass filter.

4:40pm **VT-MoA10 Use Of A Novel Sensor Using Remote Plasma Emission Spectroscopy For Monitoring And Control Of Vacuum Processes**, **Joseph Brindley**, *T. Williams*, *B. Daniel*, *V. Bellido-Gonzalez*, Gencoa Limited, UK; *F. Papa*, Gencoa USA

Plasma emission monitoring (PEM) has been used for a number of years to either monitor the condition of or actively control vacuum plasma processes. This approach has many advantages such as fast response time, monotonic sensor behaviour and the ability to control uniformity by monitoring different areas of the process. There are however some disadvantages, e.g. there is required a clear line of sight to the plasma that can be obscured by substrate movement, the PEM sensor can become coated by the deposited material and, of course, it can be only be used when the process itself generates a plasma.

A new type of remote plasma generator has been developed, which when combined with advances in miniature spectrometers can be used to perform optical plasma spectroscopy over a wide pressure range of 1 mBar to 1×10^{-6} mBar. Presented are a number of examples of its use as an intelligent pressure gauge (penning pressure measurement in conjunction with plasma spectroscopy), etching process monitoring, vacuum quality monitoring, and reactive deposition control.

A novel, pulsed power, method of enhancing the sputter effect inside the sensor has also been developed. This allows for use of the sputtered cathode emission as a secondary, indirect indicator of the condition of the vacuum and state of the process, enabling monitoring and control of processes otherwise not possible via conventional plasma spectroscopy. Furthermore, this sputter mode of operation has the effect of "cleaning" the sensor's cathode, allowing for extended operation with processes that would otherwise damage the sensor.

5:00pm **VT-MoA11 Calibration of Quadrupole Mass Spectrometers with a Molecular Flow Gas Source**, **Robert Ellefson**, REVac Consulting

In situ calibration of quadrupole mass spectrometers (QMS) after initial calibration is not regularly done. If no calibration gas is available, it requires removal of the QMS from the vacuum system to a calibration test stand where gases and a reference gauge is available. Providing a low-cost calibration gas source dedicated to the QMS enables local calibration checks to qualify the performance of the QMS. This paper describes a molecular flow calibration device that presents known flow rates of gas

species to the ion source. The known flow rate produces partial pressures that can be measured with an ion gauge or calculated knowing the conductance of the QMS molecular flow pumping system. The molecular flow in and molecular flow out preserves the gas composition of even a flowing gas mixture prepared in a volume from attached gas sources. The device prepares a known volume of gas (300 cm^3) at low pressure ($P_{\text{CDG}} < 10 \text{ Torr}$) to assure molecular flow through an orifice with flow proportional to $C_{\text{N}_2}(28/\text{M})^{1/2}$ for each species. With this small volume, the partial pressure depletes for each species in a predictable manner related to the mass of the gas species. By noting the time elapsed since the valve to the molecular leak is opened, the time-dependent partial flow rate, $q_i(t)$ of each species is known and a sensitivity S_i for that species can be calculated as $I_i(t)/[q_i(t)/C_{\text{out}}]$ from the measured ion current, $I_i(t)$. Data showing sensitivity of a QMS as a function of ion source pressures provides information to show stability of sensitivity over a range of pressures. The ability to introduce pure gases and blend or introduce gas mixtures gives conditions to measure QMS accuracy for mixture analysis. The simplicity of the system lends itself to automation of the sensitivity measurement process as the basis for archiving S_i values over extended periods of time as quality assurance performance data.

2D Materials Focus Topic

Room 103B - Session 2D+MI-TuM

Novel 2D Materials

Moderators: Daniel Gunlycke, Naval Research Laboratory, Yuanbo Zhang, Fudan University, China

8:00am **2D+MI-TuM1 Computational Design of 2D Materials and Layered Heterostructures for Opto-electronics, Kristian Thygesen**, Technical University of Denmark **INVITED**

The class of 2D materials is rapidly expanding and now includes semiconductors, insulators, metals, and superconductors. Many of these novel materials exhibit unique properties that are easily tuneable due to their atomically thin nature making them potential candidates for applications in a large range of technological areas. In this talk I will give a general introduction to the electronic structure of 2D materials including the characteristic features of screening and collective excitations. Concrete illustrations will be given from the Computational 2D Materials Repository (1+2) which contains high-accuracy first-principles calculations for a large number of 2D materials. The 2D materials form the basis of a much larger class of materials consisting of vertically stacked 2D layers held together by weak van der Waals forces. I will describe challenges and opportunities for the first-principles modelling of van der Waals heterostructures including our multi-scale Quantum Classical Heterostructure (QEH) model (3) that enables accurate modelling of plasmons, excitons and band structures of general incommensurable heterostructures containing hundreds of layers. Examples of computationally designed heterostructures will be given.

(1) Computational Materials Repository, <https://cmr.fysik.dtu.dk/>

(2) Computational 2D Materials Database: Electronic structure of transition metal dichalcogenides and oxides, F. A. Rasmussen and K. S. Thygesen, *J. Phys. Chem. C* 119, 13169 (2015)

(3) The Dielectric Genome of van der Waals Heterostructures, K. Andersen, S. Latini, and K. S. Thygesen, *Nano Letters* 15, 4616 (2015)

8:40am **2D+MI-TuM3 Mo₂Ga₂C: Structural Determination of a New Nanolaminated Carbide and its 2D Modification by Selective Etching, Chung-Chuan Lai, R. Meshkian, M. Dahlqvist, J. Lu, L.-Å. Näslund**, Linköping University, Sweden; O. Rivin, E.N. Caspi, Nuclear Research Center-Negev, Israel; O. Ozeri, Nuclear Research Center-Soreq, Israel; L. Hultman, P. Eklund, Linköping University, Sweden; M.W. Barsoum, Drexel University; J. Rosen, Linköping University, Sweden

Studies of molybdenum carbides are motivated by, for example, the electric and the catalysis properties, including the recently predicted high Seebeck coefficient of 2D Mo₂C [1]. It has been reported that 2D transition metal carbides (also known as MXenes) can be made by selective etching of corresponding nanolaminated ternary carbides [2], e.g., $M_{n+1}AC_n$ phases where M is typically from group 4 – 6, A is from group 13 – 14, and n is 1 – 4 [3]. However, no suitable precursor has been available to make 2D Mo₂C until most recently, through the discovery of Mo₂Ga₂C [4]. Here, we determined the structure of Mo₂Ga₂C phase from X-ray and neutron diffraction, scanning transmission electron microscopy and X-ray photoelectron spectroscopy, and further validated the structure by ab initio calculations [5]. The structure of Mo₂Ga₂C can be described as Mo₂C layers interleaved by two Ga layers, standing head-to-head along the c -axis of the hexagonal lattice. The Mo₂Ga₂C phase is closely related to another known nanolaminated carbide, Mo₂GaC, in its crystal structures, evident from chemical bonding analysis. However, selective etching of Ga using hydrofluoric acid (HF) is easily attained for the new Mo₂Ga₂C phase, while being more challenging for Mo₂GaC. A reduction in Ga signal with subsequent exfoliation of Mo₂C layers upon etching is here presented for Mo₂Ga₂C, making Mo₂Ga₂C the first precursor for MXene synthesis based on $A = \text{Ga}$, and for MXene synthesis of 2D Mo₂C [6].

References:

[1] M. Khazaei, M. Arai, T. Sasaki, M. Estili, and Y. Sakka, *Phys. Chem. Chem. Phys.* 16 (2014) 7841-7849.

[2] M. Naguib, G. W. Bentzel, J. Shah, J. Halim, E. N. Caspi, J. Lu, L. Hultman, and M. W. Barsoum, *Mater. Res. Lett.* 2 (2014) 233-240.

[3] P. Eklund, M. Beckers, U. Jansson, H. Högborg, and L. Hultman, *Thin Solid Films* 518 (2010) 1851-1878.

[4] C. Hu, C.-C. Lai, Q. Tao, J. Lu, J. Halim, L. Sun, J. Zhang, J. Yang, B. Anasori, J. Wang, Y. Sakka, L. Hultman, P. Eklund, J. Rosen, and M. W. Barsoum, *Chem. Commun.* 51 (2015) 6560.

[5] C.-C. Lai, R. Meshkian, M. Dahlqvist, J. Lu, L.-Å. Näslund, O. Rivin, E. N. Caspi, O. Ozeri, L. Hultman, P. Eklund, M. W. Barsoum, and J. Rosen, *Acta Mater.* 99 (2015) 157-164.

[6] R. Meshkian, L.-Å. Näslund, J. Halim, J. Lu, M. W. Barsoum, and J. Rosen, *Scripta Mater.* 108 (2015) 147-150.

9:00am **2D+MI-TuM4 Synthesis of Borophenes: Anisotropic, Two-Dimensional Boron Polymorphs, Andrew Mannix^{*†}, B. Kiraly**, Northwestern University/Argonne National Lab.; J.D. Wood, M.C. Hersam, Northwestern University; N.P. Guisinger, Argonne National Laboratory

As the lightest metalloid element, bulk boron exhibits great physical and chemical complexity. In contrast, atomic clusters of boron form simple planar and cage-like structures that resemble those of carbon. Theoretical studies suggest that nanostructured boron allotropes (e.g., nanotubes and sheets) should exhibit structures similar to atomic boron clusters. To date, however, boron nanostructures have been scarcely explored experimentally, partly due to difficulties in synthesis and the need for atomically pristine experimental conditions. Recently, we have reported the synthesis of two-dimensional boron sheets (i.e., borophenes) on a silver surface under ultra-high vacuum conditions [*Science* **350**, 1513–1516 (2015)]. Atomic-scale scanning tunneling microscopy shows the growth of two distinct phases, both of which exhibit anisotropic, chain-like structures. We confirm that these sheets are planar, chemically distinct, and atomically thin through extensive ex situ characterization supported by first principles calculations. Furthermore, in situ scanning tunneling spectroscopy of the borophene sheets shows metallic characteristics consistent with theoretical predictions, in contrast to semiconducting bulk boron.

9:20am **2D+MI-TuM5 Atomic and Electronic Structures of Graphitic Carbon Nitride (g-C₃N₄) Monolayers on HOPG, Sangwoo Park, H.M. Kang**, Sungkyunkwan University, Republic of Korea; J.H. Yang, J.H. Choy, Ewha Womans University, Republic of Korea; Y.J. Song, Sungkyunkwan University, Republic of Korea

In this work, we report atomic and electronic studies of graphitic carbon nitride (g-C₃N₄) monolayers on a highly-ordered pyrolytic graphite (HOPG) by using atomic force microscope (AFM), kelvin probe force microscope (KPFM) and low temperature scanning tunneling microscope (LT-STM). The g-C₃N₄ is the most stable allotrope of carbon-nitrides and a very promising candidate for metal-free coordination chemistry and heterogeneous catalyst. Also it is applicable photocatalytic hydrogen production and fuel cell. After successful spin-coating of the g-C₃N₄ monolayers on HOPG, we found the inter-molecular interactions between the flakes or the atomic registries of adsorption on the substrate. This coating mechanism and atomic/electronic properties of g-C₃N₄ on HOPG will be discussed in detail.

9:40am **2D+MI-TuM6 Periodic Array of Graphene Quantum Dots Embedded in a Carbon-Boron-Nitrogen Alloy, Jakob Jørgensen**, Aarhus University, Denmark; L. Camilli, A. Stoot, Technical University of Denmark; A. Cassidy, R. Balog, Aarhus University, Denmark; J. Sadowski, Brookhaven National Laboratory; P. Bøggild, Technical University of Denmark; L. Hornekær, Aarhus University, Denmark

Two-dimensional (2D) materials have received enormous attention in the field of materials science and condensed matter physics in the last decade, with the ultimate goal being developing a new technology based on these materials [1]. A huge variety of promising 2D materials have been identified and the ability to combine these into complex structures is essential. For this reason the synthesis of 2D hetero-structures – i.e., structures resulting from the combination of two or more 2D materials – have been subject to an intense research effort over the last few years [2]. Here we report the first observation of spontaneous formation and self-assembly of graphene quantum dot superlattices embedded in a two-dimensional boron-carbon-nitrogen alloy.

By exposing a hot Ir(111) surface to carbon and boron-nitrogen precursor molecules it is found, using scanning tunnelling microscopy (STM), that the otherwise bulk-immiscible graphene and hexagonal boron nitride (hBN) materials can form a stress induced BCN alloy. Furthermore, pure-phase dislocations are found to co-exist with the alloy resulting in the bright triangular pattern of carbon enriched nanoribbons with a width of approximately 1 nm. Above a critical carbon concentration, an array of quantum dots (QD) of highly regular size and periodicity appears. Based on

^{*} Morton S. Traum Award Finalist

[†] National Student Award Finalist

Tuesday Morning, November 8, 2016

STM in combination with synchrotron x-ray photoemission spectroscopy (XPS) these QDs are determined consist of pure phase carbon, i.e. they are graphene QDs. These findings are consistent with well-established theories on elastic relaxations in ultrathin strained systems [3]. Thus our findings show a pathway to grow a highly periodic array of graphene quantum dots imbedded in a semiconducting BCN alloy.

In addition, using low energy electron microscopy (LEEM), the growth of the alloy structure is followed *in-situ* and diffraction experiments confirm the presence of the ordered quantum dot pattern even on a macroscopic level.

[1] A.C. Ferrari et al. *Nanoscale* 7, (2015) 4598

[2] H. Lim et al., *Chemistry of Materials* 26 (2014) 4891

[3] V. Ozolins et al. *Phys. Rev. Lett.* 88 (2002) 096101

11:00am 2D+MI-TuM10 Electric Field Control of 2D Materials with Electron Correlation, Yoshi Iwasa, University of Tokyo, Japan INVITED

Scaling down materials to an atomic-layer level produces rich physical and chemical properties as exemplified in various two-dimensional (2D) crystals extending from graphene, transition metal dichalcogenides to black phosphorous. These include Dirac physics, quantum Hall physics, and valleytronic functions, which are caused by the dramatic modification of electronic band structures, simply by thinning. In the case of transition metal dichalcogenides (TMDs), the band gap becomes direct in monolayers, and the broken inversion symmetry and the strong spin-orbit interaction causes peculiar valley-dependent spin polarization in zero-magnetic field [1], as well as peculiar opto-valleytronics [2, 3].

In reduced dimensions, on the other hand, the electron correlation effects and their consequence, electronic phase transitions, are also significantly changed from bulk systems, and thus result in new properties and functions. Here we address unique physical properties of correlated 2D electron system 1T-TaS₂, which was achieved simply by thinning. The ordering kinetics of the charge density wave transition was revealed to become extremely slow with reduction of thickness [4], resulting in an emergence of metastable states [5]. Furthermore, we realized the unprecedented memristive switching to multi-step non-volatile states by applying in-plane electric field.

[1] R. Suzuki et al, *Nat. Nano.* 9, 611 (2014).

[2] Y. J. Zhang et al., *Nano Lett.* 12, 1136 (2012), *ibid.* 13, 3023 (2013).

[3] Y. J. Zhang et al., *Science* 344, 725 (2014).

[4] M. Yoshida et al., *Sci. Rep.* 4, 7302 (2014).

[5] M. Yoshida et al., *Sci. Adv.* 1, e1500606 (2015).

11:40am 2D+MI-TuM12 Graphene-based Hybrid Materials by Designer Interfaces for High-Performance Hybrid Supercapacitors, Sanju Gupta, Western Kentucky University

Intense research in renewable energy is stimulated by global demand of electric energy. Electrochemical energy storage and conversion systems namely, supercapacitors and batteries, represent the most efficient and environmentally benign technologies. Moreover, controlled nanoscaled architectures and surface chemistry of electrochemical electrode materials is enabling emergent next-generation devices approaching theoretical limit of energy and power densities and deliver electrical energy rapidly and efficiently. This talk will present our recent activities to advance design, development and deployment of composition, morphology and microstructure controlled graphene-base hybrid multilayer architectures with carbon nanotubes, conducting polymers, transition metal oxides and mesoporous silicon wrapped with graphene sheets as engineered electrochemical electrodes for supercapacitor cathodes and battery anodes. Experimental studies showed significant enhancement towards integrating graphene with other nanomaterials in terms of gravimetric specific capacitance, interfacial capacitance, charging-discharging rate and cyclability. We also present fundamental physical-chemical interfacial processes that govern the underlying mechanisms (surface ion adsorption versus redox reactions) in these electrodes revealed using scanning electrochemical microscopy. The findings are discussed from viewpoint of reinforcing the role played by heterogeneous 'hybrid' electrode surfaces composed of nanoscale graphene sheets (conducting) and other nanomaterials (semiconducting) via higher/lower probe current distribution maps. It allows us to determine ion transfer kinetics and diffusion constant, imaging electrochemical reactions and topography in a microscale at electrode/electrolyte interface.

12:00pm 2D+MI-TuM13 Realization of TaS₂ in the Single-Layer Limit, Charlotte Sanders, M. Dendzik, Aarhus University, Denmark; A.S. Ngankee, Aarhus University; A. Eich, Radboud University, Netherlands; A. Bruix, J.A. Miwa, B. Hammer, Aarhus University, Denmark; A.A. Khajetoorians, Radboud University, Netherlands; P. Hofmann, Aarhus University, Denmark

The electronic properties of bulk TaS₂ have long been a topic of significant interest, due to the fact that the material exhibits unusual charge density wave phases alongside Mott physics and superconductivity. However, little has been known about single-layer (SL) TaS₂. How the electronic properties of this material may change in the SL limit is of great interest, raising questions about the effects of quantum confinement and substrate interactions on exotic electronic states already seen in the bulk. Work on related materials that have been successfully fabricated as SLs points to complex consequences for the CDW and superconducting states. [1] In order to address this topic, one needs to be able to controllably fabricate high-quality, uniform samples with low defect densities for probing *in situ*. We have now succeeded in epitaxially growing high-quality SL TaS₂. We have characterized the SL with angle-resolved photoemission spectroscopy (ARPES), low-temperature scanning tunneling microscopy and spectroscopy (LT-STM/S), and low-energy electron diffraction (LEED). Using the Au(111) substrate as a starting point, we find that the TaS₂ SL on Au(111) assumes a well-defined orientation with respect to the substrate, and a moiré superstructure; simultaneously, and counterintuitively, it adopts a "carpet flow" growth mode over substrate steps, suggesting weak interaction with the substrate. Comparing our measurements to calculations from density functional theory (DFT), we have determined that the SL assumes the trigonal prismatic ("1H") phase. While the bulk parent material is characterized by a CDW transition temperature $T_{CDW} = 75K$ [2], we do not observe either CDWs or superconductivity at temperatures down to 4.7K on Au(111) using STM/STS. We do, however, observe slight doping of the TaS₂ epilayer. While the absence of superconductivity at this temperature is not surprising, considering that the superconducting transition temperature T_c in the bulk is only 600mK [3], the absence of CDWs is of interest. This is particularly so in light of recent research on the closely related system SL-NbSe₂ on bilayer graphene: despite having a lower bulk CDW onset at $T_{CDW} = 33K$, NbSe₂ in the SL exhibits complete transition to the CDW state by $T_{CDW} = 5K$. [1]

[1] M. M. Ugeda et al., *Nat. Phys.* 12, 92 (2016). <http://dx.doi.org/10.1038/nphys3527>

[2] J. A. Wilson and A. Yoffe, *Adv. Phys.* 18, 193 (1969). <http://dx.doi.org/10.1080/00018736900101307>

[3] P. Garoche et al., *J. Low Temp. Phys.* 30, 323 (1978). <http://dx.doi.org/10.1007/BF00114956>

Applied Surface Science

Room 101B - Session AS+AC-TuM

Practical Surface Analysis II: Microanalysis, Nanoanalysis, Atom Probe, and All Things 'Small'

Moderators: Arun Devaraj, Pacific Northwest National Laboratory, Daniel Gaspar, Pacific Northwest National Laboratory

8:00am AS+AC-TuM1 Progress Toward Atomic-Scale Tomography, Thomas Kelly, CAMECA Instruments Inc. INVITED

There have been efforts of late to produce three-dimensional images at the atomic scale where every atom is accounted for and the position information is quite precise. All atoms in a two-dimensional thin film of boron nitride were imaged and identified by Krivanek et al. [1]. Scott et al. were able to produce three-dimensional images using electron tomography that show every atom in a gold nanoparticle containing over 7000 gold atoms [2]. Using atom probe tomography (APT), Moody et al. have shown three-dimensional images of several million atoms in an aluminum alloy where each atom is positioned correctly in a face-centered cubic lattice and 60% of the atoms are detected [3]. These are all impressive and important developments. They suggest what atomic-scale microscopy might ultimately achieve: recording with high precision the position and identity of every atom in a technologically relevant structure. This capability can fairly be termed atomic-scale tomography (AST).

If AST is to be achieved, it appears that APT and electron microscopy should be used synergistically to capture the strengths of one technique to overcome the limitations of the other. This question has been explored in detail [4] and the conclusion is that there are some ways that AST can be achieved. The instrumental developments needed to reach AST with APT

Tuesday Morning, November 8, 2016

and (S)TEM as a basis include: trajectory corrections for precise atom placement and detecting 100% of the atoms without ambiguity in identity. The former may be achieved by imaging the specimen apex to enable precise ion trajectory simulation toward the detector. An electron column integrated into an atom probe can, in principle, record the specimen apex shape throughout an entire atom probe experiment. Detectors for recording all atoms might be based on superconducting materials [5]. If these detectors also record an ion's kinetic energy, then most time of flight-based ambiguities in peak identification can be eliminated [6].

Once these instruments are combined, the full analytical capabilities of each can be used synergistically. This presentation will outline approaches that should be pursued to reach this end and review the current plans to build an atomic-scale tomograph.

[1] O. L. Krivanek, et al., *Nat. Lett.*, vol. 464, p. 571, 2010.

[2] M. C. Scott et al., *Nature*, vol. 483, pp. 444–447, 2012.

[3] M. P. Moody et al., *Micros Microanal.*, vol. 17, pp. 722–723, 2011.

[4] T. F. Kelly et al., *Microsc. Microanal.*, vol. 19, pp. 652–664, 2013.

[5] R. F. McDermott, J. R. Suttle, and T. F. Kelly, “Unpublished research,” 2015.

[6] T. F. Kelly, *Micros Microanal.*, vol. 17, pp. 1–14, 2011.

9:20am AS+AC-TuM5 Atom Probe Tomography and Electron Microscopy Investigation of Composition and Structure of Functionalized Carbon, Chilan Ngo, D.R. Diercks, M.B. Strand, S. Pylypenko, Colorado School of Mines

Carbon is one of the most studied materials due to its broad range of properties, versatility, and low cost. Functionalization or doping of carbon with heteroatoms is an effective way to tailor the properties of carbon and further modify the material for various applications. While significant efforts have been placed on understanding the composition, structure and properties of doped carbon supports, there is a lack of understanding regarding the 3-D distribution of dopant within high surface area materials. In this work, we expand the understanding of nitrogen-functionalized carbon materials by focusing on analysis of nitrogen distribution through atom probe tomography (APT), transmission electron microscopy (TEM), and complementary characterization techniques. Specifically, APT analysis has been applied to provide unique, high-resolution insight into the composition/structure of high-surface area carbon – demonstrating feasibility of the technique towards such materials. Nitrogen-doped carbon nanospheres were prepared by hydrothermal treatment of resorcinol, formaldehyde, and ethylenediamine, followed by pyrolyzation under flowing nitrogen, producing materials with different nitrogen concentration and varied relative distribution of nitrogen functionalities. Sample preparation was performed via focused-ion beam (FIB), in order to isolate C spheres into a workable APT tip. The work presented herein provides a foundation not only for further understanding of N-doped carbon materials and N-containing nonprecious catalysts (NPMCs) employed in a variety of important catalytic reactions, but also to prepare model high-surface area materials, compatible for study via *in situ* liquid and electrochemistry TEM techniques.

9:40am AS+AC-TuM6 Advanced XPS Imaging and Spectromicroscopy: a Review of Current Capabilities, Olivier Renault, CEA-University Grenoble Alps, France

At the practical level, XPS imaging is still poorly used today. This is due to on the one hand to instrumental issues with for instance the difficulty to produce nice secondary electron images to help quick navigation at the surface; on the other hand, lower counting statistics of core-level images necessitate high transmission imaging spectrometer and in some cases post-processing of image data sets using, e.g. PCA. XPS imaging and spectromicroscopy is nevertheless complementary to ToF-SIMS and Auger as it provides quantification and chemical speciation, besides accessing the mesoscopic scale. It should therefore deserve a much broader use to better understand laterally heterogeneous systems. On some instruments, electronic band structure imaging, equivalent to ARUPS microscopy, is becoming possible in routine use, widening significantly the capabilities of photoelectron microscopy with laboratory sources for important applications, e.g., novel 2D materials. In this contribution, we will review through various examples from graphene doping [1] to oxide-based resistive memories and single layer MoS₂, the current capabilities of XPS imaging and spectromicroscopy as implemented with a PEEM-based commercial instrument enabling core-level images with sub- μm scale lateral resolution. The benefits of band structure imaging for 2D

semiconducting materials will be addressed [2]. Finally, perspectives regarding photoelectron microscopy with hard x-rays will be drawn [3].

This work was performed on the Nanocharacterization platform of CEA-MINATEC.

[1] H. Kim, O. Renault et al., *Appl. Phys. Lett.* 105, 011605 (2014).

[2] M. Frégnaux, O. Renault et al., *Surf. Interface Anal.* 2016 (in press).

[3] M. Patt et al., *Rev. Sci. Instrum.* 85 (11) (2014) ; C. Zborowski, O. Renault et al., *Appl. Phys. Lett.* 2016 (accepted).

11:00am AS+AC-TuM10 Challenges and Solutions for Confined Volume Characterization in Semiconductor Systems, Wilfried Vandervorst, IMEC & KULeuven, Belgium

INVITED

Pushing the limits in IC-technology towards the nanometer scale, novel materials and in particular interfacial interactions in 3D-devices play a crucial role leading to a demand for concepts suited to probe very small volumes and enable atomic scale observations.

Atom probe tomography (APT) can provide 3D-composition analysis within very small volumes (a few nm³) with high sensitivity and accuracy. Nevertheless the presence of many materials with different evaporation fields and inhomogeneous laser-tip interactions creates tip distortions and trajectory aberrations inducing severe artefacts in reconstructed profile. Limits in mass resolving power, the presence of multiple charge states, cluster emission and variable detection efficiencies and strong laser power effects do hamper accurate and precise quantification and/or deviation from the correct composition.

Complementary to the resolving power of APT, is the application of scanning probes which enable to grasp the electrical activity of dopants or identify conduction paths within such volumes. As SPM is inherently a 2D-method, concepts for expanding into the depth dimension are explored (cfr Scalpel SPM, ion beam sputtering icw SPM) with applications in logic device engineering, failure analysis and memory cell development.

As APT and SPM suffer from a poor productivity and a lack of statistical averaging over large areas as required in more production oriented metrology. A solution can be found through ensemble measurements whereby spatial resolution is provided by the device under investigation and not by the probing beam. We will illustrate this concept through applications of “self focusing SIMS” which allows to determine the composition from trenches as small as 20 nm without having an ion beam with nm-resolution. Moreover within the area of selective area deposition SF-Sims may provide a unique analysis capability sampling defectivity of self-assembled monolayers and limited selectivity.

Similarly crystallinity in narrow trenches (< 50 nm) can be obtained through channeling RBS whereby again we use a large beam but nevertheless probe the information from an array of very fine features. In all these cases, the averaging over a large array provides excellent statistics and in some cases dramatically improved productivity through the enhanced signal versus the case of a very focused probe beam. The latter is ultimately exemplified in Raman experiments on narrow SiGe-trenches where we demonstrate that very narrow features (20 nm) provide a significantly enhanced (50-100x) compared to its blanket counterpart enabling to probe composition and structural properties from a small volume.

11:40am AS+AC-TuM12 Characterization of Protein G B1 Immobilized Gold Nanoparticles using Time of Flight Secondary Ion Mass Spectrometry and X-ray Photoelectron Spectroscopy, Y.-C. Wang, David Castner, University of Washington

Nanoparticles (NPs) have been widely used in many fields of science due to their unique physical properties. While many applications of NPs such as imaging probes or drug carriers often require the conjugation of proteins or biomolecules, the surface interactions between NPs and biomolecules remains underexplored. For example, the immobilization of immunoglobulin G (IgG) onto nanoparticle surfaces is critical for the development of many immunosensors and drug delivery nanocarriers. Notably, the orientation of the immobilized IgG can have significant impact on the clinical outcomes of these carriers by impacting its biostability and efficacy.

In this work, Protein G B1, a protein that will selectively bind to the Fc tail of IgG, was immobilized onto gold NPs (AuNPs) functionalized with maleimide and oligo-(ethylene glycol)(OEG) self-assembled monolayers (SAMs). Protein G B1 was immobilized onto AuNPs using either carbonyldiimidazole (CDI) chemistry or through a maleimide-cysteine bond. We used the surface sensitive analysis techniques of x-ray photoelectron spectroscopy (XPS) and time of flight-secondary ion mass spectrometry

Tuesday Morning, November 8, 2016

(ToF-SIMS) to characterize the protein G B1 immobilization. Unlike conventional NP characterization techniques such as dynamic light scattering (DLS) and UV/Vis, XPS and ToF-SIMS can provide additional information on the surface elemental composition, protein coverage and orientation.

XPS analysis confirmed the AuNP functionalization with both the maleimide and OEG-SAMs. After incubation with protein, the immobilization of the protein was demonstrated by the increased nitrogen signal on the surface of both SAMs. Loosely bound protein on the AuNPs was effectively removed through conventional centrifugation-resuspension washes and dialysis cleaning.

ToF-SIMS analysis also confirmed the successful functionalization, CDI activation, and protein immobilization by identifying signature secondary ions from each step of the protein immobilization process. Further, by utilizing high surface sensitivity and small sampling depth (2nm) of ToF-SIMS, the orientation of immobilized protein G B1 was determined by comparing the ratio of secondary ion intensity originating from the opposite end of the protein. As expected, the non-site specific CDI chemistry did not lead to a well-defined orientation on the AuNPs. In contrast, we were able to control the orientation of the immobilized protein using maleimide functionalized AuNPs and cysteine mutants of Protein G B1. The systematic characterization of this study provided detailed information about protein-nanoparticle interactions that advances our understanding of the complex protein-NP interface.

12:00pm AS+AC-TuM13 What's New in Wetting? Inorganic Nanotubes at a Water Interface - A Molecular View, Sidney Cohen, O. Goldbart, I. Kaplan-Ashiri, Weizmann Institute of Science, Israel; P. Glazyrina, Ural Federal University, Russia; H.D. Wagner, Weizmann Institute of Science, Israel; A. Enyashin, Ural Ras, Russia; R. Tenne, Weizmann Institute of Science, Israel

Wetting of solid surfaces is a complex and subtle phenomenon which has been studied carefully over the past 200 years. A good understanding of wetting can explain many key physical interactions at interfaces, notable examples being in lubrication, composite materials, and capillarity. Wetting phenomena continue to intrigue the scientific community due to the complexity of this seemingly simple process. In recent years, specific nanoscale aspects of wetting have been revealed, highlighting the importance of a molecular-level understanding of wetting. The study of nanotube wetting encompasses the old/new, as well as nanoscale aspect of these endeavors. Proven importance of nanotubes as fillers in ultra-strength nanocomposites, where the interfacial interactions in the nanocomposite are controlled by wetting, lends a technological push to the field. Inorganic nanotubes (INT) formed from tungsten and molybdenum disulfides disperse very well in a variety of polymers, enabling preparation of nanocomposites with enhanced mechanical properties, thermal stability and improved rheological behavior. Nonetheless, the nature of the interaction between a nanotube and polymer liquid has received little attention and is poorly understood. Here we present a combined experimental and theoretical study on the microscopic interaction of WS₂ nanotubes (INT-WS₂) with water. The unique experimental approach is based on manipulation and pull-out of individual nanotubes from water films while monitoring the forces generated with a cantilever in an atomic force microscope (AFM). This method draws on concepts of the classic Wilhelmy Balance Technique, while exploiting the exquisite force control of the AFM. The AFM experiments were contrasted with parallel experiments in an environmental scanning electron microscope (ESEM). Detailed theoretical calculations based on density functional theory (DFT) predicted well the interaction energy for large, closed cap nanotubes, but vastly underestimated the interaction energy with small, open-ended nanotubes. For those small diameter tubes, force-field molecular dynamics (MD) simulations together with a thermodynamic analysis qualitatively explain the observed behavior, strongly implicating a dominant capillary effect. Visualization of the pullout in the ESEM together with AFM force traces allow precise modelling of the meniscus formation during pullout, reflecting the energetics of the interface at, and inside the nanotube wall. **Acknowledgment:** Supported by the Israel National Nano-Initiative, the Israel Science Foundation, H. Perlman Foundation. and Act 211 Government of the Russian Federation, contract № 02.A03.21.0006.

Electronic Materials and Photonics

Room 102A - Session EM+MN-TuM

New Materials and Devices for TFETs, Spintronics, and Extended CMOS

Moderator: Wilman Tsai, TSMC

8:40am EM+MN-TuM3 Tunneling FET Technology using Ge and III-V Semiconductors, Shinichi Takagi, M. Takenaka, The University of Tokyo, JST-CREST, Japan

INVITED

Since TFETs based on band-to-band tunneling are expected as ultra-low power devices applicable to LSI for IoT, development of the optimum materials, structures and fabrication process have been strongly pursued for realizing both low sub-threshold swing (SS) of sub-60 mV/dec. and high drain Ion/Ioff ratio at the same time. For this purpose, the reduction in the effective band gap is important for enhancing tunneling current. Thus, we are currently focusing planar-type TFETs using Ge/III-V and their hetero-structures.

In this talk, we address two types of planar TFETs utilizing the Ge/strained Si (sSi) hetero-structure and the InGaAs channels. One of the key issues for TFETs is the formation of the steep and high quality source junctions, which provide both high tunneling current and low off current. For InGaAs TFETs, we have introduced solid-phase Zn diffusion through utilizing the inherent diffusion property of Zn in InGaAs creating defect-less extremely-steep profiles. The steepness of the Zn profiles less than 3.5 nm/dec. was obtained, thanks to the diffusion constant of Zn in InGaAs proportional to the square of the Zn concentration, leading to the automatic realization of the steep impurity profile. The small SS of 64 mV/dec and large Ion/Ioff ratio over 1E6 have been realized in the planar-type InGaAs TFETs at room temperature.

For tensile strain Si channel TFETs with Ge sources, in-situ doping p+ Ge/sSi source junctions are employed for realizing steep and defect-less tunneling junction formation. Here, the higher Ev edge of the Ge-source and the lower Ec edge of tensile-strained Si result in reduction in the effective band gap, leading to the increase the tunneling probability with maintaining the relatively large Eg of sSi in the drain regions, which can suppress the ambipolar leakage current. The fabricated Ge/sSi (1.1 %) TFETs show high Ion/Ioff ratio over 1E7 and steep minimum SS of 28 mV/dec.

In conclusion, the enhancement of tunneling probability by utilizing III-V/Ge materials is quite effective in improving the performance of TFETs. Superior source junction formation and MOS interface control technologies are key factors to realize TFETs using III-V/Ge.

This work was partially supported by JST-CREST, and a Grant-in-Aid for Scientific Research (No. 23246058) from MEXT. We would be grateful to Drs. H. Yamada, O. Ichikawa, M. Yokoyama and M. Yamamoto in Sumitomo Chemical Corporation for continuous support on III-V epi substrates, SOITECH for providing strained SOI substrates and, M. Kim, D.-W. Ahn, T. Gotow, T.-E. Bae, M. Noguchi, K. Nishi and S.-H. Yoon in the University of Tokyo.

9:20am EM+MN-TuM5 Thin Film Materials in Novel Spintronic Devices, Gang Xiao, Brown University

INVITED

Tomorrow's spintronic MRAM (Magnetic Random Access Memory) and logic processors could exploit the physics of the giant spin Hall effect (GSHE) for switching bits, but the materials engineering is challenging. Solids with large atomic numbers and resistivities exhibit very large Spin Hall Angle (SHA), a key and characterizing parameter of GSHE. The origin of GSHE is the enhanced spin-orbit coupling (SOC), based on which the search on solids with even larger SHA continues. Some of these solids are difficult to fabricate due to their metastable structures. We have realized robust perpendicular magnetic anisotropy (PMA) in a layered structure combining the elusive, metastable β phase of tungsten and a ferromagnetic thin film. The large spin-orbit coupling in β -W yields, after suitable annealing, a very low critical current density for magnetization switching. Our structures furthermore are easily fabricated, making them even more technologically promising and compatible to modern semiconductor fabrication process.

11:00am EM+MN-TuM10 Tunneling in Low-Dimensional Materials, Joerg Appenzeller, Purdue University

INVITED

Over the last years, two-dimensional (2D) materials are attracting an increasing amount of interest for various electronic applications owing in particular to the ideal electrostatics conditions that can be enabled in a three-terminal field-effect transistor (FET) geometry. Transition metal dichalcogenides (TMDs) as MoS₂, WSe₂, or WS₂, to just name a few, or black phosphorus (BP) offer sizable bandgaps at mobilities that cannot be

Tuesday Morning, November 8, 2016

achieved in three-dimensional, bulk type materials that are scaled down to similar dimensions. The key is the absence of dangling bonds at the 2D semiconductor to substrate or gate dielectric interface that allows for highly conductive channels with sub-nm body thicknesses. In my presentation I will discuss the benefits of an ultra-thin body structure for scaled device applications with a particular emphasis on tunneling field-effect transistors (TFETs). I will also elucidate the critical impact of Schottky barrier (SB) contacts in the context of TMD and BP devices and will present an analytical approach that allows extracting materials and device information as the SB height and bandgap of single- and multi-layer FET structures. Moreover, I will present an analysis on the impact of strain in TMD FETs and discuss the potential relevance of strain for TMD TFETs to achieve ideal performance specs.

11:40am EM+MN-TuM12 Controlled Phase Transition for Ultra Low Power Transistors, Sayeef Salahuddin, University of California, Berkeley **INVITED**
Phase transition materials have long been investigated for fundamental physics and also for potential application in electronics. In this presentation, I shall discuss how a controlled phase transition can lead to fundamentally new switching devices that has significantly less energy dissipation compared to the state of the art. In particular, I shall talk about the state of negative capacitance that can be achieved in certain material systems with stored energy of phase transition. Our recent experiments with ferroelectric materials have shown that such a state of negative capacitance can actually be achieved. I shall also describe our very recent results where such negative capacitance, when combined with conventional transistors, have demonstrated a reduction in supply voltage at a given ON current.

Exhibitor Technology Spotlight Room Hall C - Session EW-TuM

Exhibitor Technology Spotlight Session

Moderator: Chris Moffitt, Kratos Analytical Limited

10:20am EW-TuM8 Toxic, Flammable and Corrosive Waste Gas Treatment. Protect your Employees and Environment, D.K. Prasad, CS CLEAN SYSTEMS, Inc.

Many of the semiconductor processes generate exhaust gases that are highly dangerous to Environment, Health and Safety. Novasafe is a reliable, proven and cost effective solution to allow the handling of toxic, flammable and corrosive waste gas exhaust. Learn more about this product solution in the Spotlight presentation by CS Clean Solutions Air pollution regulations, employee health concerns and growing awareness of toxic agents from semiconductor, industrial and research facilities demand improvements in exhaust gas conditioning. The NOVASAFE dry scrubber reduces the hazards associated with pyrophoric, toxic and corrosive gases and vapors. NOVASAFE effluent gas scrubbers offer an extremely safe and efficient way to treat such process exhausts. The scrubber is a technologically advanced device, containing approximately 10 liters of granulate scrubbing media specific to the process chemistry, and can be used in both production and laboratory and research environments. Operating passively at room temperature, the granulate material reacts on contact with process gases and chemically converts them to non-volatile inorganic solids. NOVASAFE, with its compact form factor, can be integrated with your vacuum pump system to provide a minimal footprint solution. Effluent is abated to sub-TLV levels. The NOVASAFE requires no preventative maintenance, and is replaced and disposed of at its end of life. Granulate is available for many different chemistries, including hydrides, acid gases, metalorganics, etc. making NOVASAFE a cost-effective solution for etch, MOCVD, ALD, ion implant and many other applications.

Manufacturing Science and Technology

Room 103A - Session MS+AS-TuM

Characterization and Processing for IC Manufacturing

Moderator: Alain C. Diebold, SUNY College of Nanoscale Science and Engineering

8:00am MS+AS-TuM1 Thermal Decomposition Properties of Bis(cyclopentadienyl)magnesium for Various Gas Supply System Materials, Hidekazu Ishii, Tohoku University, Japan; *S. Yamashita, M. Nagase, A. Hidaka, K. Ikeda*, Fujikin Incorporated, Japan; *Y. Shiba, Y. Shirai, S. Sugawa*, Tohoku University, Japan

High purity Bis(cyclopentadienyl)magnesium(Cp₂Mg) is used as chemical vapor deposition material of semiconductor devices and dopant for obtaining p-type conduction in GaN based material devices. However, precise control of supply concentration of Cp₂Mg is very difficult because its vapor pressure is very low. Generally, Cp₂Mg is supplied from a precursor container to the film formation chamber by bubbling with the carrier gas. In this method, the tubing for the gas supply must be heated to avoid deposition of Cp₂Mg on the inner surface of tube, which leads to a concern of decomposition of Cp₂Mg. Thus, understanding of thermal decomposition properties of Cp₂Mg for various materials for gas supply tube is important. In this report, we report evaluation results of thermal decomposition properties of Cp₂Mg for various materials such as SUS316L stainless steel and Cr₂O₃, Al₂O₃-passivated stainless steel that are used for gas tubing, as well as Ni-Co alloy and Hastelloy C-22 that are used for a valve diaphragm.

8:40am MS+AS-TuM3 High Volume Materials Characterization in the CMOS Industry, Paul van der Heide, GLOBALFOUNDRIES **INVITED**

In no time in the past has Materials Characterization been as pivotal to CMOS device R&D as it is today. This stems primarily from the fact that since the era of *Denard scaling* (shrinkage alone), new materials/ structures have had to be introduced in order for logic devices to continue to adhere to the dimension shrinkage implied by *Moore's law* (examples lie in the introduction of strain engineering (introduced in 90nm devices rolled out in 2003), HKMG structures (introduced in 45nm devices rolled out in 2007), and 3D structures (introduced in 22nm devices rolled out in 2011)). This timeline also begs the question: *Are we not at the precipice of the next innovation?* What is certain is that the CMOS industry will experience significant and in some cases unforeseen changes over the next 2 decades.

Materials characterization is not only needed to support R&D efforts, but is also required to provide insight into manufacturing issues, along with the qualification of a) new fabrication processes, b) new process equipment, and c) process equipment coming off preventative maintenance cycles. Paramount in these areas is analytical precision, repeatability, data quality and speed (turn around time). This stems from the other aspect of *Moore's law*; that being that the cost associated with the development/implementation of a new device node must remain financially attractive. Topics covered in this presentation include: the support requirements of a high volume CMOS manufacturing site, merits of academia versus industrial labs, financial justifications of onsite lab/s, along with some recent analytical examples/capabilities.

9:20am MS+AS-TuM5 Dynamics in SIMS Characterization for Advanced Nano-Technology: Challenges and Solutions for Novel Materials and 3-D Devices, Marinus Hopstaken, IBM T.J. Watson Research Center **INVITED**

Over the last few decades, SIMS depth profiling techniques and instrumentation has tremendously evolved to keep up with developments in advanced CMOS technology. I will discuss the main technology drivers, their implications for SIMS characterization, and review some of the analytical challenges and solutions:

- Continued dimensional scaling (*i.e.* lower film thicknesses, ultra-shallow junctions USJ) demands for progressive improvement of depth resolution. This has been enabled by continuous instrumental developments to provide high-density, stable, and low-impact energy primary ions beams to enable sub-nm depth resolution (*i.e.* 'Atomic layer' SIMS). I will give various applications of high resolution SIMS analysis of thin-film stacks / USJ, routinely employing sub-500 eV ion beams

- Advanced IC development in a manufacturing context demands at-line SIMS metrology with high throughput and reproducibility, often requiring small area analysis on patterned wafers. Key enablers for advances in SIMS metrology are availability of high-density primary ion beams, high level of automation to allow for unattended operation, and instrumental stability /

Tuesday Morning, November 8, 2016

drift correction. I will discuss implications for high-throughput SIMS full wafer mapping and considerations for patterned device wafer

- Paradigm shift towards 3D device architectures (*i.e.* FinFET) poses one of the greatest challenges, and appears fundamentally incompatible with low-energy (*i.e.* 'broad-beam') SIMS. This can be partially circumvented by averaging over a large regular arrays of FinFET structures, in combination with backfill and planarization to delineate the Fin sidewall ('SIMS through Fin technique'), which we have successfully employed at realistic Fin dimensions and pitch, relevant for 14 nm node and beyond

- Integration of novel and dissimilar material stacks demands novel SIMS calibration methods and/or quantification protocols. Potential solutions to deal with the higher complexity are cross-calibration with absolute external techniques (ion scattering techniques, 3D-APT, advanced TEM-EDX / EELS, etc...) and multi-standard approaches for explicit correction of SIMS yield variations with matrix composition. I will give selected examples for quantification of in-situ doping in SiGe_x for wide variation in Ge% and different doping species in various III-V compounds

11:20am MS+AS-TuM11 Characterization of Electrical Properties of Si and GaN Devices using Scanning Microwave Impedance Microscopy (sMIM) and Nano-scale Capacitance-voltage Curves, Stuart Friedman, F. Stanke, Y. Yang, O. Amster, PrimeNano, Inc

The use of Atomic Force Microscopy (AFM) electrical measurement modes is a critical tool for the study of semiconductor devices and process development. A relatively new electrical mode, scanning microwave impedance microscopy (sMIM), measures a material's change in permittivity and conductivity at the scale of an AFM probe tip [1]. sMIM provides the real and imaginary impedance (Re(Z) and Im(Z)) of the probe sample interface. By measuring the reflected microwave signal as a sample of interest is imaged with an AFM we can in parallel capture the variations in permittivity and conductivity and, for doped semiconductors, variations in the depletion layer geometry. An existing technique for characterizing doped semiconductors, scanning capacitance microscopy, modulates the tip-sample bias and detects the tip-sample capacitance with a lock-in amplifier. A previous study compares sMIM to SCM and highlights the additional capabilities of sMIM [2].

In this talk we focus on the detailed mechanisms and capabilities of the nano-scale C-V curves that can be obtained using sMIM to measure the tip-sample capacitance as a tip-sample bias is swept. Analogous to traditional macro-scale capacitance-voltage experiments, the nano-scale C-V curves probe properties such as doping concentration through their influence on the voltage dependent geometry of the depletion layer. In particular, in this talk we will address the ability to extract semiconductor properties, such as doping concentration, from the C-V curves. This study includes analytical and finite element modeling of tip-bias dependent depletion layer geometry and impedance. These are compared to experimental results on reference samples for both doped Si and GaN doped staircases to validate the systematic response of the sMIM-C channel to the doping concentration.

[1] S. Friedman, O. Amster, Y. Yang, "Recent advances in scanning Microwave Impedance Microscopy (sMIM) for nano-scale measurements and industrial applications." Proceedings of the SPIE, Volume 9173, id. 917308 8 pp. (2014)

[2] B. Drevniok, St.J. Dixon-Warren, O. Amster, S.L. Friedman, and Y. Yang, "Extending Electrical Scanning Probe Microscopy Measurements of Semiconductor Devices Using Microwave Impedance Microscopy", Proceedings of the 41st International Symposium on Testing and Failure Analysis (2015), pp. 77.

11:40am MS+AS-TuM12 Results of the 2016 Triennial Review of the National Nanotechnology Initiative, James Murday, University of Southern California; B.R. Rogers, Vanderbilt University; E.B. Svedberg, The National Academies

INVITED

The National Nanotechnology Initiative is a multi-agency effort to advance nanoscale science, engineering, and technology and to capture the associated economic and societal benefits. The NNI comprises the collective activities and programs among the more than two dozen participating federal agencies with diverse missions and presently a total annual investment of approximately \$1.5 billion. Every three years the National Academies selects a committee of experts to review the NNI in accordance with the provisions of the 21st Century Nanotechnology Research and Development Act. A report on the most recent review has just been released. This report has paid particular attention to examining and commenting on the physical and human infrastructure needs for

successful realization in the United States of the benefits of nanotechnology development and also the mechanisms used by the NNI to advance focused areas of nanotechnology towards advanced development and commercialization. We will report the findings and recommendations of this review.

Nanometer-scale Science and Technology Room 101D - Session NS-TuM

Nanodiamonds, Thin Films and Electronics (8:20–10:00 am)/Health and Environmental Impact of Nanotechnology (11:00 am–12:20 pm)

Moderators: Trevor Wiley, Lawrence Livermore National Laboratory, Leonidas Ocola, Argonne National Laboratory

8:00am NS-TuM1 Formation of Dynamic Topographic Patterns during Electron Beam Induced Etching of Diamond, Aiden Martin, Lawrence Livermore National Laboratory; A. Bahm, FEI Company; J. Bishop, I. Aharonovich, M. Toth, University of Technology, Sydney

Spontaneous formation of complex geometric patterns is an interesting phenomenon that provides fundamental insights into underlying roles of symmetry breaking, anisotropy and non-linear interactions. Here we present dynamic, highly ordered topographic patterns on the surface of diamond that span multiple length scales and have a symmetry controlled by the chemical species of a precursor gas used in electron beam induced etching (EBIE).

We provide an anisotropic etch rate kinetics model that fully explains the observed patterns, and reveals an electron energy transfer pathway that has been over-looked by existing EBIE theory. We therefore propose a fundamental modification, whereby the critical role of energetic electrons is to transfer energy to surface atoms of the solid rather than to surface-adsorbed precursor molecules.

EBIE is a high resolution, direct-write nanofabrication technique in which a precursor gas and an electron beam are used to realize etching. A key advantage of EBIE is the ability to etch materials such as diamond that are resistant to conventional chemical etch processes, without introducing damage to the substrate as observed in ion sputtering techniques. As a result, EBIE has recently been used to fabricate components for photonic and electronic applications. Our findings can be harnessed to engineer specific surface patterns under various electron beam irradiation environments for controlled wetting, optical structuring and other emerging applications that require nano and micro-scale surface texturing.

A portion of this work was funded by FEI Company and the Australian Research Council (Project Number DP140102721). A portion of this work was performed under the auspices of the U.S. DOE by LLNL under Contract DE-AC52-07NA27344. I.A. is the recipient of an Australian Research Council Discovery Early Career Research Award (Project Number DE130100592).

8:20am NS-TuM2 Towards a Gold Standard in Single Digit Detonation Nanodiamond, N.J. Nunn, O.A. Shenderova, M. Torelli, Adamas Nanotechnologies, Inc.; Gary McGuire, International Technology Center

Aggregates of detonation nanodiamond have long been of interest for their numerous potential applications; however, no size of detonation nanodiamond (DND) is perhaps more elusive, yet technologically important, than sub 10 nanometer (or "single-digit") primary particles. Primary particles of DND have a number of potential applications including drug delivery, seeding in microelectronics, polymer nanocomposites, and lubricants. Nevertheless, the challenge associated with obtaining these particles from the initial 200-300nm aggregates of purified detonation soot has made them too expensive for widespread use. Even after overcoming the initial challenge of obtaining the primary particles, they are still often limited in their use due to the assortment of chemical functional groups found on their surface. Therefore, an additional challenge is to tailor the surface chemistry of the particles without sacrificing their size by promoting re-aggregation. A final challenge is to identify useful solvents where stability and size of the functionalized particles are preserved. Here we report our work in obtaining high yields of 5nm particles of DND, progress made toward functionalizing these particles with a number of useful chemical structures including: carboxyl, hydroxyl, amine, hydrophobic chains and the dispersion of these particles in a range of solvents such as DMSO, NMP, DMF, THF, Ethylene Glycol, Synthetic Oils, alcohols, and water.

Tuesday Morning, November 8, 2016

9:20am **NS-TuM5 Field Emission Electron Source Based on UltraNanoCrystalline Diamond Films for Electron Accelerators Applications**, *S. Baryshev, S. Antipov, C. Jing*, Euclid TechLabs LLC; **Anirudha Sumant**, Argonne National Laboratory

Currently, commercially available electron sources for electron accelerators are photocathodes or thermionic cathodes. Both types puts limits onto the resulting duty cycle of an accelerator and adds into increasing its complexity, as they require additional accessories (lasers, pulser compressors etc.). Cold cathode field emission technology based on low work function metals and other materials is an attractive alternative to simplify the electron injector, however, field emission current stability and processing challenges associated with formation of an atomically sharp tip for these field emitters makes it difficult to adopt this technology for accelerator applications

Nitrogen incorporated ultrananocrystalline diamond (N) UNCD films developed at Argonne National Laboratory have demonstrated its remarkable field emission properties. The unique structure of atomically abrupt nitrogen-incorporated grain boundaries provides field emission sites with very high field enhancement and therefore eliminates the need to make sharp nano-tips thus drastically reducing processing steps to fabricate field emission source. More specifically, it delivers significant currents at electric gradients as low as $\sim 10^5$ V/cm, which is far below typical breakdown thresholds in many materials ($> 10^6$ V/cm), and has turn-on voltages as low as 2.5×10^4 V/cm, and have shown excellent emission current stability for extended time periods up to 1000 hrs. Small grain size and a unique grain boundary network ensure more uniform emission properties over large areas and smaller current load per emitting site (i.e., per grain boundary). Taking advantage of these unique properties of (N)UNCD, Euclid TechLabs in collaboration with Argonne conducted a case performance study of a thin film planar (N)UNCD field emitter in an radio frequency(RF) 1.3 GHz electron gun in an electron accelerator. The field emission cathode was a 100 nm thick (N)UNCD film grown on a 20 mm cathode plug. At surface gradients 45-65 MV/m, peak currents of 1-80 mA ($0.3\text{-}25$ mA/cm²) were achieved. Imaging with two YAG screens confirmed emission from the planar (N)UNCD surface with beam emittance of 1.5 mm \times mmrad/mm-rms and longitudinal FWHM energy spread of 0.7% at 2 MeV[1]. The same technology could be adopted for industrial and scientific linear accelerators, both normal-conducting and superconducting, for isotope production for radiopharmacy; X-/gamma-ray production for medicine, non-destructive evaluation, well-logging; and materials processing.

References:

[1] S. V. Baryshev et al., Appl. Phys. Lett. 105, 203505 (2014).

9:40am **NS-TuM6 Time-resolved Small Angle X-ray Scattering during the Formation of Detonation Nanodiamond**, *Michael Bagge-Hansen, M. Nielsen, L. Lauderbach, R. Hodgkin, S. Bastea, L. Fried, D. Hansen, C. May*, Lawrence Livermore National Laboratory; *T. Graber*, Washington State University; *B.J. Jensen, R. Gustavsen, D. Dattelbaum, E. Watkins, M. Firestone*, Los Alamos National Laboratory; *J. Ilavsky*, Argonne National Laboratory; *T. van Buuren, T.M. Willey*, Lawrence Livermore National Laboratory

Most commercial nanodiamond originates from detonation of high explosives, particularly from RDX/TNT mixtures. Models suggest that the phase, crystallinity, and morphology of carbon is strongly dependent on the type of high explosive used and the exact evolution of temperature and pressure conditions during the very early stages of detonation; however, characterization of carbon condensation under the extreme conditions present at 100 ns timescales has been technically challenging. Using time-resolved, synchrotron-based small-angle x-ray scattering, we present a comparative survey of early time carbon condensation from three CHNO high explosives: HNS, Comp B (60% RDX, 40% TNT), and DNTF. We also extend this study to post-mortem TEM analysis of recovered carbon condensates. At later times, the size of particles extracted from SAXS compares favorably with our microscopy results. At early times, models predict that this array of explosives should provide graphitic, nanodiamond, and liquid carbon phases, respectively; our analysis of time resolved SAXS is remarkably consistent with these computational predictions.

This work was performed under the auspices of the US DOE by LLNL under Contract DE-AC52-07NA27344.

11:00am **NS-TuM10 Transformations and Biological Impact of Emerging Energy Storage Nanomaterials**, *Robert Hamers*, University of Wisconsin-Madison **INVITED**

The rapid increase in mobile electronics and electric vehicle technologies is leading to a rapid escalation in the use of complex oxides as cathode materials in the lithium-ion batteries that power these devices. Economic factors are driving a trend toward mixed-oxide materials such as $\text{Li}_x\text{Ni}_y\text{Mn}_z\text{Co}_{1-y-z}\text{O}_2$ ("NMC") that combine high performance with low cost. However, these materials also incorporate substantial amounts of metals such as Ni and Co that may pose environmental risk, and there is not current any national infrastructure for recycling of these materials. We have been investigating the transformation of these emerging nanomaterials and the resulting biological impact as revealed through acute and chronic mortality studies and gene expression studies using *Shewanella oneidensis* and *Daphnia magna* as model organisms. Further molecular-level insights are provided by detailed investigations of NMC interactions with supported lipid bilayers. Our results show that this class of materials induces toxic effects through multiple pathways; with *Shewanella* with effects can be attributed almost exclusively to the redox dissolution of the NMC to form Ni^{2+} and Co^{2+} ions in solution; in contrast, ion-equivalent controls cannot reproduce the effects observed with *Daphnia magna*. These results highlight the need to develop a mechanistic understanding of the transformation of nanomaterials in the environment and the resulting impacts. Some perspectives on potential strategies for redesign to reduce adverse biological impact will be presented.

11:40am **NS-TuM12 Bio-inspired Nanosystems for Healthcare Applications**, *Elena Rozhkova*, Argonne National Laboratory **INVITED**

Nanotechnology offers efficient solutions for virtually all areas of science and technology spanning from energy to healthcare technologies. Owing to rapid development of synthesis, nanofabrication and characterization techniques today we are able to engineer advanced hybrid nanosystems from scratch, at atomic and molecular scale, through controlled assembly of nanoparticles and molecules toward practical devices. Biological phenomena such as self-assembly, electron transfer, photosynthesis and enzyme catalysis, and magnetic field sensing have been a source of inspiration for engineers and scientists. We are using both nature's blueprints and biostructure building blocks for developing smart nano-bio hybrids and devices and then interface them with living systems of various levels of complexity towards advancing modern therapeutic, sensing, imaging and diagnostic methods.

Plasma Processing for Biomedical Applications Focus Topic Room 101A - Session PB+BI+PS-TuM

Plasma Processing of Biological/Biomimetic Surfaces

Moderators: Uroš Cvelbar, Jozef Stefan Institute, Slovenia, Satoshi Hamaguchi, Osaka University, Japan

8:00am **PB+BI+PS-TuM1 Investigation of Discharge Propagation on Cell and Plasmid Suspension in Plasma Gene Transfection**, *Yugo Kido*, Pearl Kogyo Co., Ltd., Japan; *H. Motomura, Y. Ikeda*, Ehime University, Japan; *S. Satoh*, Y's Corp., Japan; *M. Jinno*, Ehime University, Japan

The authors have been developing a plasma gene transfection technique and averaged transfection efficiency up to 20% and cell survivability up to 90% are achieved for more than 20 kinds of cells. A typical procedure of this method is as follows. Target cells are cultured on a 96 well plate and gene suspension is added. The plate is placed between a high voltage electrode made of copper capillary with the diameter of 70 μm and a copper plate grounded electrode. By exposing the suspension to a microplasma generated at the tip of the capillary electrode, the cells are transfected by the genes. In this method, both chemically reactive species (chemical factors) and discharge current (electrical factors) are indispensable to the transfection process and their synergistic effect has been experimentally verified. Moreover, the transfection occurs on the whole area of each well although only the central area is exposed to the microplasma. In this study, to clarify how the discharge current contributes the transfection process with the synergistic effect with the chemical factor, discharge propagation phenomenon on the cell and plasmid suspension is investigated.

As a target, COS-7 cells are cultured on a 35 mm dish and 24 μg of plasmid pCX-EGFP suspended in 120 μL of TE/PBS buffer is added. The applied voltage between the electrodes is 20 kHz sinusoidal waveform and the amplitude is set at 10 kV peak to peak. The gap length between the

capillary electrode and the suspension is set at 1 to 5 mm. The discharge propagation is observed with an ICCD camera equipped with a UV lens.

When only TE/PBS buffer solution exists in the dish, the discharges reach the buffer solution surface and then they propagate radially up to 15-20 mm of diameter. On the other hand, when the cells are cultured on the dish, remarkable radial propagation of the discharge is not observed and the discharge irradiation area is limited within the diameter of about 1 mm, which is narrow compared with the area in which the transfection occurs. Therefore, as a contribution of the electrical factors, not only the direct effect of the discharge current, charge on the plasmids, conduction current in the solution etc. should be analyzed. As a first step of the chemical factor investigation, similar observation is performed by the ICCD camera with an interference filter to observe the emission of OH radicals. The results of the discharge propagation paths study by means of equivalent circuit simulation and comparative analysis between the discharge propagation and the transfection will be shown at the symposium.

8:20am PB+BI+PS-TuM2 Spectroscopic Study of Permeability of Stratum Corneum by Plasma Treatment for Transdermal Drug Delivery, Jaroslav Kristof, N. Tran, M. Blajan, K. Shimizu, Shizuoka University, Japan

Application of drugs by needles presents risk of infections and causes pain. On the other side, oral application of drugs can be toxic for human body because drug has to be transported through alimentary tract and higher amount of active agent is required. Transdermal delivery could be ideal painless and effective way but barrier function of skin has to be reduced for improving permeability of drugs. Research of last years proves that plasma can interact with skin and cause decreasing barrier function of skin [1-3].

We used plasma jet and microplasma discharge for investigation of barrier function of stratum corneum – horny layer of of Yucatan micropig skin. Helium or argon was used as working gas. These rare gases were later enriched by liquids like water or ethanol through the bubbling system to achieve higher amount of active particles like OH.

Physical changes of the pig skin were observed by microscope. As the human body is not non-conductive, we can expect different results when conductivity of layer under skin is changed. We compared effect of plasma on conductive and non-conductive material. Placement of skin on conductive material caused burned spots on skin by plasma jet [3]. While it was isolated, no damage was observed with plasma jet irradiation. In case of treatment of skin by microplasma, physical damage was hardly observed.

Changes in stratum corneum layer were observed by Attenuated Total Reflectance – Fourier Transform InfraRed (ATR-FTIR) spectroscopy. ATR-FTIR spectrum offer information about water, lipid bilayer and proteins in stratum corneum. Permeability of skin for drugs correlates with shift of asymmetric stretch of CH₂ band to higher wavenumbers. This information describes behavior of lipid bilayer. Information about reaction of proteins on plasma treatment content Amide I and Amide II bands. Reaction of stratum corneum layer of pig skin depended on used discharge type and gas. Effectivity of plasma sources and used gases or gas mixtures for transdermal drug delivery was analysed.

References

- [1] Lademann J., A Patzelt A., Richter H., Lademann O., Baier G., Breucker L., Landfester K., *Laser Phys. Lett.* **10**, 083001 (2013).
- [2] Wu A. S. et. al., *Journal of surgical research* **179**(1), E1-E12 (2013).
- [3] Shimizu K., Hayashida K. and Blajan M, *Biointerphases* **10**(2), 029517 (2015).

8:40am PB+BI+PS-TuM3 Cell Attachment to Microwave Plasma-oxidized Titanium and Titanium Alloy Substrates, Denis Dowling, University College Dublin, Ireland; M. Naciri, University Mohamed V of Rabat, Morocco; M. Al-Rubeai, A. Breen, University College Dublin, Ireland

INVITED

Titanium and its alloys have been widely investigated for use in orthopedic and dental implant devices, particularly for osteointegration and biocompatibility. This paper evaluates the influence of titanium surface oxidation using a microwave plasma treatment technique on cell attachment. Commercially pure titanium (CpTi) and titanium alloy (Ti6Al4V) discs were treated in an oxygen atmosphere for 5 min-utes at 850 °C using a microwave (2.45 GHz) plasma system, operating at 2 kPa. After the 5-minute treatment, the thickness of the oxidized layer was 2.3 µm on the CpTi discs and 4.7 µm on the Ti6Al4V discs, with growth rates of 0.5 and 1 µm.min⁻¹ respectively. Reduced plasma oxidation rates were observed on a high surface area beaded surface (Porocoat). In contrast to the plasma treatments, the use of air furnace oxidation only achieved an oxide layer

thickness for the CpTi of 1 µm, when treated at the same temperature. Optical profilometry measurements were performed to determine the surface roughness; XRD, EDX, and SEM examinations were also carried out to determine the properties of the oxide layers and their morphologies. Cell attachment to the treated discs was also assessed after exposure times of 25 and 100 minutes. A 40% increase in MG63 osteoblast cell attachment on the Ti6Al4V discs was observed, when compared with that on the CpTi discs. Alkaline phosphatase (ALP) specific activity of MG63 cells grown on control and plasma oxidised surfaces were compared after 21 days. A statistically significant difference between Ti6Al4V and CpTi oxidised surfaces (P<0.05), when compared to that obtained for the control surface that had not been plasma treated. The acicular morphology of the oxidised Ti6Al4V surface was found to have the most significant influence on enhancing cell attachment, combined with higher oxide layer roughness and thickness.

9:20am PB+BI+PS-TuM5 The Role of Electrical and Chemical Factors in the Molecular/Gene Transfection by Micro-Plasma Irradiation, Masafumi Jinno, Y. Ikeda, H. Motomura, Ehime University, Japan; Y. Kido, Pearl Kogyo Co. Ltd., Japan; S. Satoh, Y's Crop., Japan

INVITED

The plasma gene transfection is expected as a safe and useful method of gene transfection. However, this method had a problem of a difficulty in keeping both high transfection efficiency and less cell damage simultaneously. The authors have evaluated four different plasma sources, such as arc discharge, plasma jet, DBD (dielectric barrier discharge) and microplasma, in terms of the transfection efficiency and the cell viability. High transfection efficiency is achieved by the styles of arc discharge and microplasma in which the electric current flows via the cells. Our experimental results suggests that an electric current may play an important role in plasma gene transfection, and that total volume of the gas flow must be small or zero and the area in which the cells are directly irradiated by plasma must be small in order to achieve higher cell viability. Among the various types of plasmas, which the authors have tried, the microplasma satisfies these conditions and brings both the high transfection efficiency and the high cell viability simultaneously.

We evaluated the contribution weight of three groups of the effects and processes inducing gene transfection, i.e. electrical, chemical and biochemical ones through three experiments. The laser produced plasma (LPP) was employed to estimate the contribution of the chemical factors. The liposomes were fabricated and employed to evaluate the effects of plasma irradiation on membrane under the condition without biochemical reaction. The clathrin-dependent endocytosis, one of the biochemical processes was suppressed. It also turned out the clathrin-dependent endocytosis is the process of the transfection against the 60% in all the transfected cells. The endocytosis and electrical poration are dominant in plasma gene transfection, and neither permeation through ion channels nor chemical poration is dominant processes.

By scavenging the H₂O₂ generated by plasma irradiation using catalase, the transfection efficiency decreased to 40% of that of without catalase. On the other hand, when the H₂O₂ solution is dropped in the cell suspension without plasma irradiation, the transfection is not observed. These results suggest that the synergistic effect of H₂O₂ with electrical factors or with other reactive species generated by plasma irradiation is important. Consequently it becomes clear that chemical factors, radicals such as H₂O₂ and reactive oxygen/nitrogen species, do not work by itself alone, and that the electrical factors (electrical current, charge and field) are essential to plasma gene transfection.

11:00am PB+BI+PS-TuM10 Control of Plant Growth by RONS Produced Using Nonthermal Atmospheric Air Plasma, Kazunori Koga, Kyushu University, Japan; T. Sarinont, Kyushu University; M. Shiratani, Kyushu University, Japan

Nonthermal atmospheric plasmas have been widely used for biomedical applications because of their non-equilibrium feature and synergy effects [1-3]. The non-equilibrium feature allows us to introduce reactive oxygen and nitrogen species (RONS) to biomaterials with a significantly wide dose range compared with the conventional irradiation methods such as X-ray and γ-ray [4]. For an agricultural application, we succeeded in reducing harvest period and enhancing crop yield by plasma irradiation to plant seeds [5]. We found irradiation of RONS with an appropriate dose to seeds brings about growth enhancement in all growth stages of plants. To understand the growth enhancement mechanism, here we have studied dependence of irradiation dose of RONS produced by plasma to seeds on growth of *Arabidopsis thaliana* L. Experiments were carried out using a scalable DBD device [2, 3, 5]. The device consisted of 20 electrodes of a

stainless rod of 1 mm in outer diameter and 60 mm in length covered with a ceramic tube of 2 mm in outer diameter. The discharge voltage and current were 9.2 kV and 0.2 A. 20 seeds of *Arabidopsis thaliana* L. were set 3 mm below the electrodes. The RONS dose was controlled by the irradiation time. After plasma irradiation, they were grown on soil tab in incubators. To evaluate plant growth, the stem length was measured as a function of cultivation days. The stem length was normalized by the stem length of the plants without plasma irradiation. To evaluate statistics of the measured values, we used a two-tailed ANOVA statistically significance different at $\alpha = 0.05$ ($p < 0.05$). The normalized stem length increases to 1.3 for 3 min irradiation, then decreases to zero for 10 min irradiation. The results indicate the plant growth is activated by plasma irradiation less than 3 min and inactivated by plasma irradiation of 5-10 min. Above 10 min irradiation, no seeds were germinated. We have succeeded in growth control of plants from death to activation with irradiation dose of RONS produced by plasma. The mechanism will be discussed in the presentation.

- [1] J. Raiser and M. Zenker, J. Phys. D, 39, 3520 (2006).
- [2] T. Sarinont, et al., JPS Conf. Proc. 1, 015078 (2014).
- [3] S. Kitazaki, et al., Curr. Appl. Phys., 14, S149 (2014).
- [4] A. Pankaj, et al., Scientific Reports, 5, 17781 (2015).
- [5] K. Koga et al., Appl. Phys. Express, 9, 16201 (2016).

11:20am PB+BI+PS-TuM11 Generation of Reactive Species in Medium Irradiated Laser-Induced Plasmas, Yukihiko Kurokawa, N. Kurake, K. Takeda, K. Ishikawa, H. Hashizume, H. Tanaka, H. Kondo, M. Sekine, M. Hori, Nagoya University, Japan

The non-equilibrium atmospheric pressure plasma (NEAPP) was irradiated to the cell culture medium as liquid. The antitumor effect, showing the selective killing effect for cancer cells without killing normal human cells, was reported [1,2]. This effect are considered to be caused by large amounts of reactive nitrogen and oxygen species (RONS) generated by the plasma. However, chemical reactions during transport of plasma in ambient to the liquid surface is complicated; therefore we have applied the laser-induced plasma.

Previously, we reported that the high ratio of $\text{NO}_2^-/\text{H}_2\text{O}_2$, even in low H_2O_2 contained in the plasma activated medium [3]. However, relations of reactive species concentrations with antitumor effects have not been fully elucidated. Here, we focus on the concentrations of reactive species generated in culture media by the laser-induced plasma.

A Nd:YAG laser and harmonic generators (Quanta Ray Pro 230, Spectra Physics) provided the pulsed-laser light with a wavelength of 266 nm, a frequency of 30 Hz, a power at sample surface of 25 mW. The light was focused on the gas-liquid interface of ultrapure water or Dulbecco's Modified eagle Medium (DMEM; cat. no. 5796; Sigma) by using plano-convex lens, made of synthetic quartz. 2 mL of the liquid was typically irradiated for 5 min. This is called as LPAM. Just after irradiation, H_2O_2 and NO_2^- concentrations were measured by using absorption that was measured by ultraviolet-visible near infrared spectrometer (V-650, JASCO). Moreover, HeLa cells were incubated in the LPAM and cell survival was measured after 24 h incubation. For analysis of killing mechanism, activated caspase-3/7 as apoptosis marker (CellEvent Caspase-3/7) was measured after fluorescent staining by a fluorescent microscope.

The LPAM generated effectively H_2O_2 causing by photo-dissociation of water, hydroxyl radicals ($\cdot\text{OH}$) works a precursor of H_2O_2 with the reaction of $\cdot\text{OH} + \cdot\text{OH} \rightarrow \text{H}_2\text{O}_2$. Survival of HeLa cells in the LPAM was dependent on dilution of the LPAM and standard DMEM. We prepared the diluted LPAM for a half of killing of HeLa cells. After the cultivation for 24 h in the diluted LPAM, the caspase-3/7 activity of dead cells as apoptosis death was observed clearly. Notably, the cell-death was almost inhibited by catalase.

We will discuss on the generation mechanism of active species and the mechanism of antitumor effect of the LPAM with comparison of the PAM.

This work was partly supported by MEXT KAKENHI on Innovative Areas Grant no. 24108002.

- [1] H. Tanaka *et al.*, Plasma Medicine, 3, 265 (2013); [2] F. Utsumi *et al.*, PLoS ONE, 4, e81576 (2013); [3] N. Kurake *et al.*, Arch. Biochem. Biophys. (2016) doi:10.1016/j.abb.2016.01.011

11:40am PB+BI+PS-TuM12 Electric Fields in kHz-driven Plasma Jets, ET. Slikboer, Y.N. Nguyen, Eindhoven University of Technology, The Netherlands; O.Y.N. Guaitella, Ecole Polytechnique, Palaiseau, France; G. Sretenović, University of Belgrade; A. Obrusnik, Masaryk University, Brno; Ana Sobota, Eindhoven University of Technology, The Netherlands INVITED
Non-thermal atmospheric pressure plasma jets have been developed for use on thermosensitive targets at atmospheric pressure, for example polymers or for biomedical applications. Diagnostics on these plasma sources is challenging because of their transient nature, often associated jitter and very small volume. Electric fields, fundamental property essential for the understanding of the discharge, are not well known. In this talk two methods of electric field measurements will be shown applied to a He kHz-driven jet, one based on spectroscopy and one on polarimetry and the obtained results will be discussed.

Plasma Science and Technology Room 104B - Session PS-TuM

Plasma Diagnostics, Sensors and Control

Moderator: Michael Gordon, University of California at Santa Barbara

8:00am PS-TuM1 Translational and Vibrational Energy in Cl_2 and O_2 Plasmas Probed by Innovative Optical Diagnostics, Jean-Paul Booth, D. Marinov, M. Foucher, O.Y.N. Guaitella, LPP-CNRS, Ecole Polytechnique, France; C. Drag, Laboratoire Aime Cotton, CNRS-U. Paris-Sud, France; A. Agarwal, S. Rauf, Applied Materials Inc. INVITED

A common assumption for "Low-temperature" plasmas is that neutral molecules and atoms in the system are in thermal equilibrium with the surrounding ambient (room) temperature, and only charged particles, which can acquire energy from applied electric fields, have higher mean energies. In reality, energy can be transferred from electrons or ions to the neutral gas, increasing the gas translational temperature. Furthermore, non-equilibrium vibrational or rotational distributions can occur in molecular gas plasmas. This can have significant effects on the plasma dynamics. Firstly, since most plasma reactors operate in a pressure-controlled regime, high gas temperatures will cause a considerable decrease in gas density (and therefore in electron-neutral collision rates). Secondly, the rates of activated processes may be significantly increased by translational energy. Vibrational excitation can lead to large increases in the rates of electron dissociative attachment and neutral dissociation. We have developed a new, unambiguous technique to measure gas translational temperature of atoms, using Doppler-resolution Two-Photon Absorption Laser Induced Fluorescence (HR-TALIF) employing a specially-built narrow-bandwidth tuneable pulsed UV laser. Initial results have been obtained on oxygen atoms, where a measurement precision of $\pm 10\text{K}$ is readily obtained. In a DC glow discharge in pure O_2 the gas temperature up to 550K are observed. The technique will be extended to the study of lower-pressure inductively-coupled plasmas, where higher temperatures are expected, and to chlorine atoms.

In order to investigate vibrational distributions, we have developed a high-sensitivity ultra-broadband ultraviolet absorption spectrometer. This employs a highly-stable laser-plasma light source and achromatic optics, allowing absorption spectra over a 250nm range to be measured with a baseline stability of the order 10^{-5} . In pure O_2 discharges (both DC glow and in a low-pressure ICP reactor) we were able to observe oxygen molecules in vibrationally-excited levels up to $v=18$ (more than half-way to dissociation), with a "tail" vibrational temperature of 7000K. Vibrational excitation was also detected in Cl_2 molecules in a pure Cl_2 ICP. However, Cl_2 appears to be close to thermal equilibrium with the gas translational temperature, which nevertheless approaches 2000K in this case.

This work was performed within the LABEX Plas@par project, and received financial state aid managed by the Agence Nationale de la Recherche, as part of the programme "Investissements d'avenir" under the reference ANR-11-IDEX-0004-02 and ANR project CleanGRAPH ((ANR-13-BS09-0019). It was also supported by the Applied Materials University Research Partnership Program

Tuesday Morning, November 8, 2016

8:40am **PS-TuM3 Spectroscopic Measurement of Molecular Densities and Temperatures in Processing Plasmas, Yaser Helal^{*}, C.F. Neese, F.C. De Lucia**, The Ohio State University; **A. Agarwal, B. Craver, P.R. Ewing, P.J. Stout, M.D. Armacost**, Applied Materials, Inc.

Processing plasmas are of a similar pressure and temperature to the environment used to study astrophysical species in the submillimeter/terahertz spectral region. Many of the molecular neutrals, radicals, and ions present in processing plasmas have been studied in the laboratory and their absorption spectra have been cataloged or are in the literature for the purpose of astrophysical study. Thus, the methods developed over several decades in the submillimeter spectral region for these laboratory studies are directly applicable for use in the semiconductor manufacturing industry. In this work, a continuous wave submillimeter absorption spectrometer was developed to study its viability as a remote sensor of gas and plasma species. A major advantage of intensity calibrated rotational absorption spectroscopy is that it can be used to determine absolute concentrations and temperatures of plasmas species from first principles without altering the plasma environment. An important part of this work was the design of the optical components which manage the coupling of the 500 – 750 GHz radiation through a commercial inductively coupled plasma (ICP) etch chamber using its existing viewport. A software routine was developed to simultaneously fit for background and absorption signal. The absorption signal determines the concentration, rotational temperature, and translational temperature of polar species. Examples of measurements made in ICPs will be demonstrated.

9:20am **PS-TuM5 Pulsed Capacitively Coupled Plasma Ignition: PROES and RF-IV Diagnostics, John Poullose, M.J. Goeckner, L.J. Overzet**, The University of Texas at Dallas

Pulsed plasma ignition induces rapid changes to the electron energy distribution function. These transitions are of particular interest in the application of etching and deposition of semiconductors. In this article we report temporally and

spatially resolved measurements of the optical emission intensity and RF current and voltage for 1 kHz pulsed plasmas in both electropositive (Ar) and electronegative (CF₄=O₂=Ar) gas mixtures. This allows us to develop a better understanding of the transients during the beginning and end of the powered component of the RF pulse. We are able to show the development of the plasma sheath early in the pulse by combining phase resolved optical emission intensity measurements with measurements of the radio frequency power delivery. In the electronegative discharge we find that the sheath width is minuscule early in the pulse but then expands rapidly. The rapid expansion results in a wave like phenomenon with negative ions bouncing between the growing sheaths.

9:40am **PS-TuM6 Control of Ion Energy Distributions on Insulating Surfaces using Pulsed Plasmas, Tyler List, T. Mu, V.M. Donnelly, D.J. Economou**, University of Houston

As the requirements for plasma etching become more stringent, the need for plasmas that can produce monoenergetic ion energy distributions (IED) keeps increasing. The problem of charging inside of insulating features also becomes magnified at smaller feature sizes, which result in higher aspect ratios. A process in which electrons can reach and neutralize charged features is important to creating nearly monoenergetic IEDs. An argon RF pulsed plasma with synchronous DC boundary voltage was used to generate a nearly monoenergetic IED. To minimize charging of insulating surfaces, short positive voltage pulses were applied to the chuck holding the substrate during the afterglow, capacitively-coupling to the substrate surface and causing electrons to reach the surface and neutralize the surface charge. This allows a self-limited, nearly grounded surface potential to be achieved. Consequently, positive ions can reach the surface without slowing down by positive surface charge. The ion energy therefore is equal to and controlled by the plasma potential relative to ground, set by a synchronous bias voltage in the afterglow of the pulsed plasma. Surface potential measurements confirmed that DC chuck pulses temporarily neutralize the surface charge. Retarding field energy analyzer measurements performed on the floating chuck with the pulsed plasma and no boundary bias or chuck bias pulses showed an IED with a large very low energy peak (~0-2 eV) and a low energy peak (~10 eV, depending on pressure), corresponding to the power off and power on portions of the cycle, respectively. When the boundary bias and chuck pulses are applied in the afterglow, these peaks change slightly and a third peak appears at an

energy near that of the boundary bias voltage. Analysis of the passive charging rate on the surface allowed the prediction of optimal pulsing frequency. Careful tuning of the other chuck pulsing width and amplitude, as well as the pulsed plasma parameters, also improves control of the IED.

11:00am **PS-TuM10 Charged Particle Dynamics in Technological Radio Frequency Plasmas Operated in CF₄, Julian Schulze**, West Virginia University; **B. Berger**, Ruhr-University Bochum, Germany; **S. Brandt**, West Virginia University; **B. Bruneau**, Ecole Polytechnique, Palaiseau, France; **Y. Liu**, Dalian University of Technology; **I. Korolov, A. Derzsi**, Hungarian Academy of Sciences; **E. Schuengel, M. Koepke**, West Virginia University; **T. Mussenbrock**, Ruhr-University Bochum, Germany; **E.V. Johnson, T. Lafleur, J.-P. Booth**, Ecole Polytechnique, Palaiseau, France; **D. O'Connell, T. Gans**, University of York, UK; **YN. Wang**, Dalian University of Technology; **Z. Donko**, Hungarian Academy of Sciences

INVITED

The spatio-temporal dynamics of charged particles and the formation of ion energy distribution functions (IEDF) are investigated in electronegative capacitive RF plasmas operated in CF₄ based on a combination of experiments, PIC simulations, and models. In the experiment, Phase Resolved Optical Emission Spectroscopy is used to access the space and time resolved electron dynamics. The DC self bias and IEDFs are measured at the electrodes. For a single frequency discharge operated at 13.56 MHz and 80 Pa we demonstrate that the presence of an electronegative gas can change the electron power absorption dynamics completely compared to electropositive gases by inducing a heating mode transition. Reducing the driving frequency results in the formation of stable striations of the optical emission and electron impact excitation rate due to the collective response of positive and negative ions to the driving frequency. Based on this fundamental understanding, we show that tailoring the driving voltage waveform using a superposition of multiple consecutive harmonics of a fundamental frequency with individually adjustable harmonics' amplitudes and phases allows for control of the DC self bias, the shape and mean energy of the IEDF, the electron power absorption dynamics, and the spatial division of the discharge into two halves of strongly different electronegativity.

11:40am **PS-TuM12 Correlation of III/V Semiconductor Etch Results with Physical Parameters of High Density Reactive Plasmas Excited by Electron Cyclotron Resonance, Gerhard Franz**, Munich University of Applied Sciences, Germany; **R. Meyer, M.-C. Amann**, Technische Universität München, Germany

Reactive ion etching is the interaction of reactive plasmas with surfaces. For a

detailed understanding, significant properties of reactive composite low pressure

plasmas driven by electron cyclotron resonance were investigated and compared with

the radial uniformity of the etch rate. The determination of electronic properties

of chlorine and hydrogen containing plasmas enabled the understanding of the

pressure dependent resonance behavior and gave a better insight into the electronic parameters of reactive etch gases. With electrical evaluation of I(V) characteristics obtained with a Langmuir probe, differently composed plasmas were investigated and the most important methods of analyzing the I(V)

characteristics were compared. A mathematical model to reduce noise sensitivity

was used and compared to the standard method of Druyvesteyn to derive the electron

energy distribution functions. Special attention was paid to the power of the

energy dependence in the exponent. Especially for plasmas which are generated by

electron cyclotron resonance with EM modes, the existence of Maxwellian distribution functions are not to be taken as a self-evident fact, but it was proven for Ar- and Kr-stabilized plasmas. Aside from the electron temperature,

which could be derived within a certainty of ten percent using the discussed

methods, the global uniform discharge model of Lieberman has been shown to be

useful to calculate the neutral gas temperature. To what extent the invasive

method of using a Langmuir probe could be replaced with the non-invasive optical method of emission spectroscopy, especially actinometry, was investigated and the resulting data showed the same relative behavior as Langmuir data.

12:00pm PS-TuM13 Mapping Plasma Potential of Rotating Ionization Zone in DC Magnetron Sputtering, Matjaz Panjan, Lawrence Berkeley National Laboratory, Slovenia; *A. Anders*, Lawrence Berkeley National Laboratory

In the magnetron discharges formation of dense plasma structures, called ionization zones or spokes, have been extensively studied over the last few years. Ionization zones were first observed in high power impulse magnetron sputtering (HiPIMS) [1] and later in DC magnetron sputtering (DCMS) [2]. In DCMS discharges operated at low-currents and low-pressure a single ionization zone forms with the shape of an elongated arrowhead and rotates in the direction opposite to the electron drift (i.e., in the $-E \times B$ direction). In this work we used emissive and floating probes to measure plasma and floating potentials of rotating ionization zone for a magnetron with a 3" niobium target operated at 2 mTorr (0.27 Pa), -270 V and 100 mA. Both probes showed strong temporal and spatial variations of the signals. From the measurements in the radial and axial directions we reconstructed full three-dimensional distributions of the plasma potential. The potential distribution was compared with the images recorded by an intensified CCD camera. Strongest light intensities in the zone corresponded to maximum plasma potential (i.e., ~0 V for probe positioned over the racetrack and for axial distances above 5 mm), whereas weaker light intensities corresponded to negative potentials (e.g., -70 V for the probe positioned over the racetrack and 5 mm away from the cathode). The plasma potential distribution matches with a previously suggested potential hump model [3]. Sharp drops in the light intensity are associated with large potential gradients, which result in strong in-plane electric fields. The largest in-plane fields are found in the azimuthal direction at the edge of the ionization zone (up to 10 kV/m). Weaker electric fields also form in the radial direction. The presence of the in-plane electric fields changes the paradigm of predominantly axially-directed electric fields. From the plasma potential we calculated the space charge distribution. A double layer is present around the edge of the ionization zone with higher ion density inside the zone and higher electron density just behind the zone's edge. From the difference between the plasma and floating potentials we also reconstructed the three-dimensional distribution of electron temperature. Electrons have largest energies in the area of highest light intensity (i.e., inside the zone and close to the edge) whereas their energy decreases along the drift direction in correlation with the fading light intensity.

[1] A. Anders *et al.*, *J. Appl. Phys.*, **111** (2012) 053304

[2] M. Panjan *et al.*, *Plasma Sources Sci. Technol.*, **24** (2015) 065010

[3] A. Anders *et al.*, *Appl. Phys. Lett.*, **103** (2013) 144103

Novel Trends in Synchrotron and FEL-Based Analysis Focus Topic

Room 103C - Session SA+2D+AC+AS+TF-TuM

Applications of Synchrotron-based Techniques to 2D Materials (8:00-10:00 am)/Complex Functional Materials and Heterostructures (11:00 am-12:20 pm)

Moderators: Nicholas Barrett, CEA Saclay, Giacomo Ceccone, European Commission, Joint Research Centre, IHCP, Italy

8:20am SA+2D+AC+AS+TF-TuM2 A Versatile Method for the Fabrication of 2D-electron Systems at Functional Oxide Surfaces, T.C. Rödel, Université Paris-Sud - SOLEIL, France; *Patrick Le Fèvre*, Synchrotron SOLEIL, France; *F. Fortuna*, *E. Frantzeskakis*, Université Paris-Sud - IN2P3, France; *F. Bertran*, Synchrotron SOLEIL, France; *T. Maroutian*, *P. Lecoeur*, Université Paris-Sud - CNRS, France; *B. Mersey*, Université de Caen, France; *A.F. Santander-Syro*, Université Paris-Sud - IN2P3, France

A critical challenge of modern materials science is to tailor novel states of matter suitable for future applications beyond semiconductor technology. In this prospect, 2D electron systems (2DESs), analogous to those created in semiconductors heterostructures, have been observed at the

LaAlO₃/SrTiO₃ interface [1] and show amazing physical properties like metal-to-insulator transitions, superconductivity or magnetism. It was then demonstrated that 2DES could also be stabilized at the surface of SrTiO₃ [2] or other oxides [3], although it requires the use of intense UV or X-ray synchrotron radiation to desorb oxygen from the surface and dope it with electrons. This opened the way for the use of surface sensitive techniques, like Angle-Resolved PhotoEmission spectroscopy (ARPES) which provided a clear description of the microscopic electronic structure of the quantum well states. However, 2DESs at oxygen-deficient surfaces can be only manipulated and studied in ultra-high vacuum (to preserve the O-vacancies from re-oxidation) and thus, are not suited for experiments or applications at ambient conditions. Here we demonstrate a new, versatile and cost-effective method to generate passivated 2DESs on large areas of UHV-prepared functional oxide surfaces. It consists in a simple evaporation at room temperature of an aluminum film onto the oxide surface. Aluminum acts as a reducing agent and pumps oxygen from the substrate. It oxidizes into an insulating AlO_x layer, protecting an underlying homogeneous 2DES confined in the first atomic planes of the oxide substrate. 2 Å of Al are sufficient to create a saturated 2DES on differently oriented surfaces of SrTiO₃, anatase-TiO₂, or BaTiO₃, which were all studied by ARPES to determine the band structure (effective mass, orbital order and charge carrier densities) [4].

[1] A. Ohtomo, H. Y. Hwang, *Nature* **427**, 423 (2004).

[2] A. F. Santander-Syro, O. Copie, T. Kondo, F. Fortuna, S. Pailhes, R. Weht, X. G. Qiu, F. Bertran, A. Nicolaou, A. Taleb-Ibrahimi, P. Le Fèvre, G. Herranz, M. Bibes, N. Reyren, Y. Apertet, P. Lecoeur, A. Barthélémy, M. J. Rozenberg, *Nature* **469**, 189 (2011).

[3] T. C. Rödel, F. Fortuna, F. Bertran, M. Gabay, M. J. Rozenberg, A. F. Santander-Syro, and P. Le Fèvre, *Phys. Rev. B* **92**, 041106 (2015).

[4] T. C. Rödel, F. Fortuna, S. Sengupta, E. Frantzeskakis, P. Le Fèvre, F. Bertran, B. Mersey, S. Matzen, G. Agnus, T. Maroutian, P. Lecœur, and A. F. Santander-Syro, *Adv. Mater.* **28**, 1976 (2016).

8:40am SA+2D+AC+AS+TF-TuM3 Advanced Spectro-microscopy of Ion Irradiated Graphene-metal Interfaces: From Substitutional Implantation to Nanobubble Formation, Andrea Locatelli, A. Sala, T.-O. Menteş, Elettra - Sincrotrone Trieste, Italy; *G. Zamborlini*, Peter Grünberg Institute (PGI-6) Jülich; *L. Patera*, *C. Africh*, IOM-CNR Laboratorio TASC, Italy; *M. Imam*, *N. Stojić*, *N. Binggeli*, Abdus Salam International Centre for Theoretical Physics, Italy

INVITED

The exploitation of graphene in the next generation electronics depends on our ability of preserving and tailoring its unique electronic and transport properties. Whereas the preservation of the free-standing characteristics of graphene demands to decouple the film from its support, their modification requires functionalization and thus chemical doping. Varied methods have been devised to implant exospecies into and under the C lattice mesh. Among them, irradiation of nitrogen ions has emerged as one of the most powerful approaches, producing enhanced physical and chemical properties rather than detrimental effects. At variance with other methods, ion irradiation enables implementation of lithographic approaches for doping graphene, a feature which is most desirable for creating arrays of devices.

The characterization of complex and laterally-heterogeneous interfaces, such as that of ion-irradiated graphene, demands advanced microscopy tools. Here, we will demonstrate the present capabilities of cathode lens spectro-microscopy. As a first example, we report a proof of principle experiment demonstrating that low energy ion irradiation through an aperture can be used to achieve local control on doping in graphene. Our study tackles the fabrication of a 2-dimensional heterojunction between *n*-doped and almost neutral single-layer graphene on Ir(111). Here, XPEEM is employed to characterize the transition region between areas with metallic and semimetal-like density of states and its thermal stability [1].

Then, we will focus on the irradiation of graphene with low energy Ar and Ne ions, reporting on the formation of nanobubbles upon annealing. The morphology and local stoichiometry of the Ar-ion irradiated interface were characterized by LEEM, XPEEM and STM, specifically addressing the thermal stability of noble gas nanobubbles. These structures display a lateral size up to tens of nanometers and height of several atomic layers. Remarkably, the Ar clusters remain trapped under graphene up to temperatures nearing 1100°C, suffering no material loss through the mesh or its edges. Ab-initio calculations demonstrate that intercalated Ar undergoes extreme pressures, up to few tens GPa. The nanobubble ripening process turns out to be driven by the minimization of the energy

Tuesday Morning, November 8, 2016

cost of film distortion and loss of adhesion [2]. The electronic properties of the ion irradiated interface will be also discussed.

[1] A. Sala, G. Zamborlini, T.O. Menteş, A. Locatelli; Small **11**(44), 5927–5931(2016).

[2] G. Zamborlini, M. Imam, L.L. Patera, T.O. Menteş, N. Stojić, C. Africh, A. Sala, N. Binggeli, G. Comelli and A. Locatelli; Nano Lett. **15**(9), 6162–6169 (2015).

9:20am **SA+2D+AC+AS+TF-TuM5 Gas-source MBE Growth of 2D Materials Examined using X-ray Synchrotron Radiation**, *Hugh Bullen, R.K. Nahm, S. Vishwanath, H.G. Xing, J.R. Engstrom*, Cornell University

Two-dimensional materials, in particular transition metal dichalcogenides, are attracting considerable interest from both fundamental and applied viewpoints. Here we report on the gas-source MBE growth of thin films of WSe_2 using $\text{W}(\text{CO})_6$ and elemental Se, where we monitor the process *in situ* and in real time with X-ray synchrotron radiation. In this work, we have two independent means to introduce the thin film constituents: a (supersonic) gas-source of $\text{W}(\text{CO})_6$ in a carrier gas of He, and an effusion cell containing elemental Se. We can collect both the scattered X-rays, and those emitted due to fluorescence. We have examined growth for a variety of conditions: growth with coincident fluxes of $\text{W}(\text{CO})_6$ and Se, and growth in which one of the two reactant fluxes was gated. These experiments were conducted at several different substrate temperatures, on graphite (HOPG), and on so-called epitaxial graphene (graphene on SiC). First, for continuous exposure to $\text{W}(\text{CO})_6$ and Se we observe, after an short incubation period, continuous growth of both the W and Se intensities. Analysis of this data indicates a stoichiometry consistent with WSe_2 . We also find diffraction features consistent with the crystalline phase of WSe_2 , where the basal plane is in the plane of the substrate. Particularly interesting is what we see when one of the reactants is gated: We have found that growth is halted by gating the incident flux of $\text{W}(\text{CO})_6$, while the film is stable in the presence of a flux of Se. The physical properties of these thin films are essentially the same as those grown using continuous exposure to both reactants. We find a much different result when the flux of Se is gated: the absence of Se, but the presence of $\text{W}(\text{CO})_6$, leads to loss of Se, and an increase in the amount of W. Since the termination of both fluxes does not lead to the loss of either element, it must be that $\text{W}(\text{CO})_6$ is providing the species that leads to the loss of Se. The most likely scenario is that a ligand exchange reaction occurs producing the gas phase species, $\text{SeCO}(\text{g})$. Perhaps our most exciting result involves the growth of WSe_2 on epitaxial graphene. In these experiments, in addition to measuring the X-ray fluorescence, we also measured *in situ* and in real time the intensity at the anti-Bragg condition, which we have shown to be a very effective way to monitor thin film crystal growth. We observe strong and sustained oscillations, indicating layer-by-layer growth of WSe_2 of up to at least 5 monolayers. This is a very exciting result, and it indicates the effective use of synchrotron radiation to examine the growth of TMD thin films.

9:40am **SA+2D+AC+AS+TF-TuM6 Nanostructured Surface of Multilayer Graphene on Cubic-SiC**, *Victor Aristov*, ISSP RAS, Chernogolovka, Russia, Russian Federation; *H.-C. Wu*, BIT, Beijing, China; *O.V. Molodtsova*, S.V. Babenkov, DESY, Hamburg, Germany; *A.N. Chaika*, ISSP RAS, Chernogolovka, Russia, Russian Federation

The results of atomically resolved scanning tunneling microscopy, low energy electron diffraction, low energy electron microscopy, micro-LEED and angle resolved photoelectron spectroscopy studies of graphene synthesized on cubic-SiC will be presented. Uniform few layer graphene was fabricated on SiC/Si wafers using Si-atom sublimation followed by SiC surface layer graphitization during high-temperature annealing in ultrahigh vacuum. Using the new dynamic-XPS end-station, based on the Argus spectrometer installed on the high-brilliance soft X-ray P04 beamline at PETRA III (DESY) one can control layer-by-layer graphene growth in real time following the evolution of the photoemission spectra with an acquisition time of ~ 0.1 sec/spectrum. Recording spectra during graphene growth on the SiC/Si(001) wafer, one can stop the process as soon as the desired number of graphene layers is reached. Angle-resolved photoemission measurements allowed us to extract the information about the electronic structure and the stacking order of the few-layer graphene on SiC(001). The preferential directions of the nanodomain boundaries coincide with the directions of carbon atomic chains on the SiC(001)-c(2x2) reconstruction, fabricated prior to graphene synthesis. Electrical measurements conducted on the vicinal SiC(001) samples demonstrate the opening of a transport gap in the nanostructured trilayer graphene. Our measurements demonstrate that the self-aligned periodic NBs can induce a charge transport gap up to 1.3 eV at low temperatures. The transport gap

opening produces high current on-off ratio of 10^4 . This development may lead to new tuneable electronic nanostructures made from graphene on cubic-SiC, opening up opportunities for a wide range of new applications.

This work was supported by the RAS, RFBR grants No 140200949 and 140201234, by the BMBF-Project No. 05K12GU2, PSP-Element No. U4606BMB1211, by a Marie Curie IIF grant No 12/IA/1264, by SPP 1459 of DFG.

11:00am **SA+2D+AC+AS+TF-TuM10 Full-field Photoelectron Spectromicroscopy of Ferroelectric Surfaces**, *Nicholas Barrett*, CEA Saclay, France **INVITED**

Advanced low energy electron optics combined with synchrotron radiation has transformed photoelectron emission microscopy (PEEM) into a powerful technique for the microscopic study of material surfaces. High lateral, wave-vector and energy resolution makes it possible to probe spatial variations in the chemical and electronic structure of nanoscale materials.

Perovskite based ferroelectrics are one important family of oxide materials requiring such analysis. Their robust polarization, switchable by an external field, makes them extremely interesting candidates for post-CMOS electronics.

First, the principles of fully energy filtered PEEM will be presented. By a combination of both direct and reciprocal space imaging the surface charge, work function, topography, chemistry and band structure of ferroelectric materials can be studied. This will then be illustrated by several examples.

The surface charge and hence the ferroelectric polarization can be estimated from the work function as measured in PEEM. There is a critical film thickness in BiFeO_3 below which the film polarization drops to zero despite constant tetragonality, suggesting the formation of stripe domains in ultra-thin films [1].

The band structure of ferroelectric domains in $\text{BaTiO}_3(001)$ are studied using spatially resolved reciprocal space PEEM and synchrotron radiation. The dispersion relations can be correlated with domain chemistry and in- and out-of-plane ferroelectric polarization [2].

The ferroelectric stability as a function of temperature of piezo force microscopy written domains has been studied using threshold PEEM. A Curie temperature of 490°C is recorded which is also dependent on the poling voltage.

We will conclude with a brief demonstration of an operando PEEM experiment, opening up the perspective of studying the changes in functional oxide properties under electric stimulation.

[1] J. Rault, W. Ren, S. Prosandeev, S. Lisenkov, D. Sando, S. Fusil, M. Bibes, A. Barthélémy, L. Bellaiche and N. Barrett, Physical Review Letters **109**, 267601 (2012)

[2] J. E. Rault, J. Dionot, C. Mathieu, V. Feyer, C. M. Schneider, G. Geneste, and N. Barrett, Physical Review Letters **111**, 127602 (2013)

11:40am **SA+2D+AC+AS+TF-TuM12 Electron Confinement at Magnetic Oxide Interfaces: Insight from Photoemission Spectroscopy**, *Martina Mueller*, Forschungszentrum Juelich GmbH, Germany **INVITED**

Recent advances in the fabrication of oxide heterostructures with atomic-scale precision has enabled interface and size control of complex oxide materials, for which unique phenomena with no bulk analogues have been demonstrated. In designated heterostructures, two-dimensional electron systems can be confined at oxide interfaces -- typically along the growth direction -- which offer possible alternatives to conventional semiconductors in terms of functional (e.g. spin-polarized) electronic transport properties. Using redox-controlled synthesis [1, 2], the electronic properties of oxide heterostructures and interfaces can be engineered -- in terms of quality that were thought to be unique to semiconductors.

The basic idea of electron confinement applies to complex oxides just as to conventional semiconductors, but the physics is much richer. In metal oxides, confined electrons are subject to strong electron-electron interactions leading to a variety of physical phenomena that can be accessed, modified and controlled. For example, using oxides with intrinsic magnetic order allows to explore spin-related phenomena in low dimensions.

We present how to create two-dimensional electronic systems (2DES) in all-oxide heterostructures using EuO , a ferromagnetic insulator [1]. By interfacing Eu metal to SrTiO_3 , a non-magnetic insulator, a redox reaction takes place at the interface which involves the oxidation of Eu metal into

Tuesday Morning, November 8, 2016

ultrathin EuO [2], and the reduction of Ti cations. This redox process strongly suggests that mobile electrons are created at the resulting interface. Using synchrotron-based soft, hard and angle-resolved photoemission spectroscopy [3] we probe the electronic structure and chemical composition at the EuO/STO interface and give a direct indication of a redox-created 2DES. The observed electronic confinement in all-oxide heterostructures provides a route for controlling spin functionality for emerging applications.

[1] G. Prinz, T. Gerber, A. Lorke, M. Müller, submitted (2016)

[2] T. Gerber, M. Müller *et al*, J. Mater. Chem. C, 4, 1813 (2016)

[3] M. Müller *et al*, J. Electron Spectrosc. Relat. Phenom. 208, 24 (2016)

Advanced Surface Engineering

Room 101C - Session SE+NS+TF+TR-TuM

Nanostructured Thin Films and Coatings

Moderators: Jolanta Klemberg-Sapieha, Ecole Polytechnique de Montreal, Canada, Robert Franz, Montanuniversität Leoben, Austria

8:00am **SE+NS+TF+TR-TuM1 Design and Predictive Synthesis of Thin Films and Coatings**, P.A. Salvador, **Gregory Rohrer**, Carnegie Mellon University
INVITED

A fundamental challenge in materials synthesis is to obtain a specific targeted composition in a functional crystal structure. For example, the synthesis of hexagonal BN is relatively easy, but synthesizing thick films of cubic BN is more difficult. In other words, we cannot currently predict exact synthesis conditions of many targeted polymorphs, and so their formation is often left to lengthy "design-of-experiments" (DOE) methodologies or, more commonly, basic trial-and-error practices. It is essential to improve the output of computational and physical experimental practices to move closer to predictive synthesis and design of coatings.

This talk will describe some recent results of a methodology called combinatorial substrate epitaxy (CSE), which we have used to understand the preferred epitaxial orientations (PEOs) of a wide range of heteroepitaxial structures and to fabricate various novel metastable materials. In this approach, the target compound is deposited on polished polycrystalline substrates, rather than commercial single crystals or buffer layers. The primary hypotheses underpinning CSE is that the each grain surface in the polycrystalline substrate can be treated as the equivalent of a single-crystal surface in a traditional DOE experiment, therefore providing every combination of substrate orientation in a single experiment. The local structure is probed in a scanning electron microscope using electron backscatter diffraction and automated orientation assignments. The method not only allows for hundreds of experiments to be carried out in a single growth run, it has the unique advantage of not being restricted to the use of commercially available single crystals.

This talk will focus on three important observations. First, when a film is grown on a polycrystal, the growth occurs by grain-over-grain epitaxy. In other words, films can grow on microcrystalline substrates in the same way they grow on millimeter scale substrates, or every grain is in an independent observation of growth. Second, there are PEOs, regardless of the substrate surface plane, and these can be easily predicted. For many of the cases we have observed, the PEO is the one that aligns the closest packed planes and directions in the eutactic (nearly close packed) arrangement of oxide ions in different structures. Third, we have already fabricated new and novel metastable coatings using this methodology, where novel substrates provide the epitaxial template to control phase formation. Observations relative to functional ceramics, including examples from the BO_2 , B_2O_3 , ABO_3 , A_2BO_4 , and $\text{A}_2\text{B}_2\text{O}_7$ families, will be described.

8:40am **SE+NS+TF+TR-TuM3 Nanoscale Atomic Arrangement in Multicomponent Thin Films Synthesized Far-from-Equilibrium**, V. Elofsson, G.A. Almyras, B. Lü, R.D. Boyd, **Kostas Sarakinos**, Linköping University, Sweden

Synthesis of multicomponent thin films using vapor fluxes with a modulated deposition pattern is a potential route for accessing a wide gamut of atomic arrangements and morphologies for property tuning. In the current study, we present a research concept that allows for understanding the combined effect of flux modulation, kinetics and thermodynamics on the growth of multinary thin films. This concept entails the combined use of thin film synthesis by means of multiatomic vapor

fluxes modulated with sub-monolayer resolution [1], deterministic growth simulations and nanoscale microstructure probes. Using this research

concept we study structure formation within the archetype immiscible Ag-Cu binary system showing that atomic arrangement and morphology at different length scales is governed by diffusion of near-surface Ag atoms to encapsulate 3D Cu islands growing on 2D Ag layers [2]. Moreover, we explore the relevance of the mechanism outlined above for morphology evolution and structure formation within the miscible Ag-Au binary system. The knowledge generated and the methodology presented herein provides the scientific foundation for tailoring atomic arrangement and physical properties in a wide range of miscible and immiscible multinary systems.

[1] "A METHOD OF CONTROLLING IN-PLANE COMPOSITIONAL MODULATION", Patent Pending Application, PCT/EP2014/052831.

[2] V. Elofsson, G.A. Almyras, B. Lü, R.D. Boyd, and K. Sarakinos, "Atomic arrangement in immiscible Ag-Cu alloys synthesized far-from-equilibrium", Acta Mater. 110, 114 (2016).

9:00am **SE+NS+TF+TR-TuM4 Is Intrinsic Nanocrystalline Stability Practically Achievable? Insights from Investigations with Pt-Au Alloys**, **Nicolas Argibay**, T.A. Furnish, D.P. Adams, P. Lu, M. Chandross, M.A. Rodriguez, B.L. Boyce, B.L. Clark, M.T. Dugger, Sandia National Laboratories
The existence of intrinsic thermodynamically stable nanocrystalline binary metal alloys has been proposed recently, supported by some notable demonstrations of stability through annealing of powders. There is a great deal of interest in understanding the impact of stress on this stability. In this presentation we present results of an investigation on the stress and temperature dependent nanocrystalline stability of a noble-metal alloy (Pt-Au) in the form of sputter co-deposited thin films. In situ XRD and TEM annealing revealed an extraordinary degree of thermal stability, confirming literature predictions. Tribological experiments and molecular dynamics simulations were used to further explore the impact of stress as a destabilizing factor.

9:20am **SE+NS+TF+TR-TuM5 Improved Mechanical Properties in Tungsten-Molybdenum Nanostructured Thin Films**, **Gustavo Martinez**, C.V. Ramana, University of Texas at El Paso

Preventing materials failure and improving the performance of materials in nuclear reactors demand novel materials to serve under extreme environment conditions. For nuclear applications, tungsten (W) has been alloyed in the past with La and Re to improve its performance and properties including low fracture and high ductile to brittle transition. In this work, molybdenum (Mo) solute atoms were added to W matrix with the intention of creating interstitial point defects in the crystals that impede dislocation motion, increasing the hardness and young modulus of the material. Nanostructured W-Mo thin films with variable Mo content were deposited by the sputter-deposition. W-Mo films were stabilized in bcc structure of W. Studies showed that as grain size formation increases the residual stress distribution will reach the maximum and stabilize after a deposition temperature of 350 °C. The residual stress still continues to follow a parabolic pattern, indicating that the stresses mainly depend on grain organization rather than atomic packing. From Nano-scratch testing, it is found that depth penetration decreases with increasing sputtering temperature. The effect of Mo on the overall mechanical properties improvement in W-Mo nanostructured thin films will be presented and discussed.

Keywords: Tungsten-Molybdenum Thin Films, Mechanical Properties, Nano-Indentation

9:40am **SE+NS+TF+TR-TuM6 Hierarchical Monolith Scaffolds for Silicon Lithium Ion Battery Electrodes**, **Kevin Laughlin**, Brigham Young University

Research has shown stable high gravimetric capacity lithium ion battery anodes can be made from silicon deposited on carbon nanotubes (CNTs). High stability operation however requires nanostructuring of the silicon to alleviate stresses caused by the large expansion of the silicon upon Li alloying. At high silicon loadings even nanoscale layers of silicon result in stresses large enough to cause mechanical damage to the electrode. Here we present work on a hierarchical approach to structuring carbon nanotube based carbon monoliths that provide for electrode stress management on multiple scales.

11:00am **SE+NS+TF+TR-TuM10 Technological Developments in Coatings for Components and Cutting Tools**, **Roel Tietema**, IHI Hauzer Techno Coating B.V., Netherlands; D. Doerwald, Hauzer, Netherlands; R. Jacobs, G. Negrea, I. Kolev, J. Zhu, J. Landsbergen, Hauzer
INVITED

Nanostructured and amorphous coatings play an important role in today's industrial applications. This is the case both in applications for cutting tools, as well as in applications for components.

Tuesday Morning, November 8, 2016

In cutting tools nanostructured coatings with high hardness, including hot hardness, and ductility have been extremely helpful to increase the productivity of the machining process. On one hand superlattice multilayers have shown here great benefits and on the other hand nanocrystallites in the material have been created to give the coating materials an inherent high hardness and ductility.

In automotive coatings these material properties were leading to technological breakthroughs as well. First coatings on the market were nanostructured WC-C:H sputtered coatings, developed by Prof. Dimiggen of Fraunhofer IST. These developments were soon followed by hybrid a-C:H coatings, combining the WC-C:H developments with a multilayered structure to achieve a gradual adaptation of the Young's modulus of the relatively soft steel as base material to the very hard a-C:H-DLC top layer. In this way it has been possible to produce coatings with a very high ductility, despite the high hardness. Hardness values as applied today on components are ranging from 2000-2500 HV for a-C:H coatings up to 4000-7000 HV for ta-C coatings.

The importance of pretreatment and post treatment steps for cutting tools and components, being as important as the actual coating step, will be addressed in this talk.

The main focus in this talk will be on the equipment aspects. Several technologies for cutting tools and for components will be presented. The equipment design and even the selection of most suitable process technology is however also strongly determined by the productivity. Besides technological properties of the coating there is a focus on the cost reduction of the coating per coated part. Cost reduction is main driver in many fields, especially in the field of components. Reduction of the cost of ownership leads to a tendency to use fast processes in large systems, respectively application of in-line systems.

11:40am SE+NS+TF+TR-TuM12 Influence of Transition Metal Dopants on Target Poisoning and Oxidation Mechanisms of Reactively Sputtered γ - Al_2O_3 Thin Films, Helmut Riedl, B. Kohlhauser, TU Wien, Institute of Materials Science and Technology, Austria; V. Paneta, Uppsala University, Sweden; C.M. Koller, TU Wien, Institute of Materials Science and Technology, Austria; S. Kolozsvári, Plansee Composite Materials GmbH, Germany; D. Primetzhofer, Uppsala University, Sweden; P.H. Mayrhofer, TU Wien, Institute of Materials Science and Technology, Austria

The outstanding oxidation resistance, thermo-mechanical stability and chemical inertness of Al_2O_3 attracts particular attention in various industrial applications. Especially, in the field of protective barrier coatings there are many research activities focusing on the synthesis of the different polymorphs α - and γ - Al_2O_3 (corundum and cubic), respectively. Apart from the fact that the deposition of the thermodynamically stable α - Al_2O_3 is strongly limited by the depositing temperature, the formation of electrically isolating Al_2O_3 at the target surface leads to massive arcing processes and destabilizes the deposition process. These problems could be overcome by varying the powering method to pulsed DC and especially RF sputtering, but at the cost of decreased deposition rates and plasma densities.

Therefore, we study in detail the influence of small amounts of transition metals such as $\text{M} = \text{Cr}, \text{Nb}, \text{Mo}, \text{and W}$ on the process stability and coating properties of reactive DC sputter deposited $(\text{Al}_{1-x}\text{M}_x)_2\text{O}_3$ thin films. To keep the influence of the alloying elements on the outstanding properties of alumina as low as possible only targets with alloying contents of $x = 2$ and 5 at.% are investigated. All micro-alloyed targets allow for significantly improved process stability and massively reduced arcing processes at the target as compared to the non-alloyed Al target. The morphology of all coatings deposited is highly dense, smooth and partly columnar with cubic γ - Al_2O_3 crystalline structure. The mechanical properties of the Cr, Mo, and W containing coatings are slightly enhanced by solid solution hardening in comparison to pure Al_2O_3 obtaining e.g. hardness values of about 25 GPa. In contrast, alloying contents of about 1 at.% Nb are already degrading the mechanical properties of alumina thin films. The significantly enhanced process stability when using Cr, Mo, and W alloyed Al targets, leads to coatings with improved thin film quality. Therefore, the oxidation resistance of these films even outperform the Al_2O_3 DC sputtered film.

Scanning Probe Microscopy Focus Topic

Room 104A - Session SP+AS+MI+NS+SS-TuM

Probing Chemical Reactions at the Nanoscale

Moderator: Tae-Hwan Kim, Pohang University of Science and Technology

8:00am SP+AS+MI+NS+SS-TuM1 In Situ Probing of Oxygen Vacancy Diffusion Across Multilayer Oxide Heterostructures, J. Zhu, University of Massachusetts - Amherst; J.-W. Lee, H. Lee, University of Wisconsin - Madison; R. DeSouza, RWTH Aachen University, Germany; C.-B. Eom, University of Wisconsin - Madison; Stephen Nonnenmann, University of Massachusetts - Amherst

Complex oxide heterostructures display an extraordinary array of exotic collective and correlated physical phenomena that result from exploiting the strong interplay between structural and electronic degrees of freedom. Oxygen vacancies often facilitate or govern the interfacial phenomenon observed at or across well-defined discrete interfaces, ranging from domain wall pinning within ferroic systems to electron donors in conducting systems. Realization of multifunctionality within oxide heterostructures therefore necessitates a direct, proper understanding of the interrelationship exhibited by concomitant, defect-mediated transport mechanisms with adequate spatial resolution. Here we utilize a modified, *in situ* scanning probe technique to measure the surface potential across a multi-layered yttria-stabilized zirconia / strontium titanate (YSZ/STO) heterostructured film at 500 °C. Subsequent application of a classic semiconductor dopant formalism to the work function profile derived from the surface potential enables mapping of the oxygen vacancy distribution within STO with a resolution < 100 nm. The results presented herein demonstrate the promise of *in situ* scanning surface potential microscopy (SSPM) to investigate complex oxide interfacial systems multilayers that exhibit vacancy-dominated properties, under extreme environmental perturbation, on a highly localized scale.

8:20am SP+AS+MI+NS+SS-TuM2 Study of Surface Chemistry on Various Noble Metal Surfaces by Ultrahigh Vacuum Tip-Enhanced Raman Spectroscopy, Naihao Chiang, Northwestern University; D. Chulhai, Pennsylvania State University; G. Goubert, L. Madison, X. Chen, E. Pozzi, M.C. Hersam, T. Seideman, Northwestern University; N. Jiang, University of Illinois at Chicago; L. Jensen, Pennsylvania State University; G. Schatz, R.P. Van Duyne, Northwestern University

During the last few years, there has been an explosion of interest and activity in the field of nanoscale vibrational spectroscopy. Tip-enhanced Raman spectroscopy (TERS) combines the ability of scanning tunneling microscopy (STM) to resolve atomic scale surface features with the single molecule chemical sensitivity of surface-enhanced Raman spectroscopy (SERS). The goal is to understand and manipulate chemistry on the nanometer length scale using the properties of the collective electronic excitations in noble metal nanostructures, known as localized surface plasmon resonance (LSPR).

Two recent advances in ultrahigh vacuum (UHV) TERS which illustrate the power of this nanoscale vibrational spectroscopy will be presented. First, our current understanding of the adsorbate-surface and adsorbate-plasmon interactions involved in the UHV-TERS of the N-N'-bis(2,6-diisopropylphenyl)-perylene-3,4,9,10-bis(dicarboximide) (PDI) on various single crystal surfaces (Ag(111), Ag(100), Cu(111), and Au(111)) which probed by a Ag tip will be discussed. This study demonstrates that TERS is a substrate general technique. Additionally, the LSPR of the Ag tip-Ag sample junction is as broad as a Ag nanoparticle dimer system. Therefore, TERS on Ag tip-Ag sample systems is also excitation general.

Second, new insights into the nature of a conformational dynamics involved at room temperature will be described. We have interrogated the conformational change of meso-tetrakis-(3,5-di-tertiarybutylphenyl)-porphyrin (H_2TBPP) on a Cu(111) surface between two stable conformations. At room temperature, the barrier between the porphyrin ring buckling up/down conformations of the H_2TBPP -Cu(111) system is easily overcome, and our group has achieved unprecedented sub-nm resolution by simultaneous UHV-TERS and STM analysis. This topic illuminates that TERS can unambiguously distinguish the conformational differences between neighboring molecules with single molecule resolution. Furthermore, the sub-nm resolution led to the direct observation of single molecule transitions between states from one scan to the next.

Tuesday Morning, November 8, 2016

8:40am **SP+AS+MI+NS+SS-TuM3 Exploring Surface-assisted Reactions Toward Functional Carbon Nanostructures, Xiaohui Qiu**, National Center for Nanoscience and Technology, China **INVITED**

Understanding the dehydrogenation and dehalogenation reactions of molecular entities on surface is essential for the controlled synthesis of carbon-based nanostructures. Delicately designed precursor molecules exploit the potential of selective activation of functional groups and templating effect of substrates and promise the fabrication of nanoscale building blocks with desired geometries. Here we employed a combination of scanning tunneling microscopy, atomic force microscopy, and theoretical calculation to elucidate self-assembling of halogen-containing molecules on metal surfaces. Metallo-supramolecular assemblies are constructed via coordination bonding between metal atoms and halogen ligands. The spontaneously formed molecular scaffolds are further explored to program the structure and chemical composition of hybrid carbon architecture. We reveal the hierarchic reaction pathway of a few aromatic derivatives in an effort toward realizing carbon-based nanostructures with controllable electronic, optical and magnetic properties.

9:20am **SP+AS+MI+NS+SS-TuM5 Landscapes in Conversion of Quasi-Free-Standing Polymer Chains to Graphene Nanoribbons, Chuanxu Ma**, Oak Ridge National Laboratory; *Z. Xiao*, North Carolina State University; *L. Liang*, Oak Ridge National Laboratory; *W. Lu, J. Bernholc*, North Carolina State University; *K. Hong, B.G. Sumpter, A.-P. Li*, Oak Ridge National Laboratory

Although the cyclodehydrogenation is well known as a key step in the bottom-up preparation of graphene nanoribbons (GNRs), the mechanism is still unclear. To understand and control the cyclodehydrogenation can help to create novel intraribbon heterojunctions of GNR-based structures. Here, we demonstrate the conversion of quasi-free-standing polymer chains to GNRs induced by thermal annealing and manipulations with a scanning tunneling microscope tip. Combined with the density functional theory calculations, a domino-like fashion and the hole-involved cyclodehydrogenation are proposed for the thermal annealing and tip-induced conversion of polymer chains to GNRs, respectively. Our results provide the first direct experimental evidence that the catalytic effect of the Au substrate is critical to the thermal-induced cyclodehydrogenation in forming bottom-up GNRs. Strongly localized density of states in the short GNR segment of the polymer–GNR heterojunction is observed. The significant confinement of the charge carriers is attributed to the big bandgap difference between the two segments of the heterojunction. Our findings might pave new ways to form GNR-based intraribbon heterojunctions by controlling the cyclodehydrogenation during bottom-up preparation, and shed light to the potential applications of the polymer–GNR heterojunctions.

This research was conducted at the Center for Nanophase Materials Sciences, which is a DOE Office of Science User Facility, and partially supported by the Laboratory Directed Research and Development Program of Oak Ridge National Laboratory, managed by UT-Battelle, LLC, for the US DOE.

11:00am **SP+AS+MI+NS+SS-TuM10 Imaging Single Molecule Chemistry, Wilson Ho**, University of California Irvine **INVITED**

Single molecule chemistry can now be probed at unprecedented spatial resolution with a low temperature scanning tunneling microscope (STM) in ultrahigh vacuum. Advances in this field have provided new measurements and insights into the structure and function of molecules through real space imaging and high resolution vibrational spectroscopy. The combination of the STM with optical spectroscopy and femtosecond lasers has added a new dimension of time to space and enabled the probing of single molecule dynamics in light-matter interaction with better than 0.1 nm resolution. The ability to visualize single molecule chemistry has reinvigorated the study of molecules and their transformations on solid surfaces. Much of the scientific advancement and understanding in surface chemistry have derived from the well-defined conditions that have long been championed by surface science in providing unambiguous results that are appealing to the theoretical and experimental communities. Imaging single molecule chemistry has a broader impact on general chemistry due principally to direct visualization of molecules and their inner machinery at the limit of space and time.

11:40am **SP+AS+MI+NS+SS-TuM12 Atomic Force Microscopy: A Tool for Chemical Analysis of Surfaces and Molecules on Atomic Scale, Pavel Jelínek**, Institute of Physics of the AS CR, Czech Republic **INVITED**

Atomic resolution and manipulation is routinely achieved by both scanning tunneling microscopy (STM) and atomic force microscopy (AFM) nowadays.

Tuesday Morning, November 8, 2016

Despite of large activities in development of the scanning probe technique, still some challenges remain, namely the chemical analysis on atomic and molecular level.

First, we will present a novel method extending further the chemical analysis [1,2] by means of AFM. Namely we will discuss a new methodology to measure Pauling's electronegativity of individual atoms on surfaces using AFM. Electronegativity has been an important concept in chemistry, originally defined by Pauling as "*the power of an atom in a molecule to attract electrons to itself*". However, its experimental determination on individual surface atoms was not possible so far.

Second, we will discuss the origin of sub molecular AFM/STM resolution acquired with functionalized tips. We will show that the electrostatic force can substantially affect the sub molecular contrast. We will show, that the electrostatic potential on a single molecule can be mapped out with sub molecular resolution.

[1] Y. Sugimoto et al Nature 446, 64 (2007)

[2] M. Setvin et al ACS Nano 6, 6969 (2012)

[3] P. Hapala et al, Phys. Rev. Lett. 113, 226101 (2014)

[4] J. vad der Lit et al, Phys. Rev. Lett. 096102 (2016)

[5] P. Hapala et al. Nature comm. (accepted 2016)

Surface Science

Room 104D - Session SS1+AS+HC+NS-TuM

Surface Dynamics, Non-Adiabaticity, and Theory and Modeling of Surface and Interfacial Phenomena

Moderator: Greg Kimmel, Pacific Northwest National Laboratory

8:00am **SS1+AS+HC+NS-TuM1 Graphene-Semiconductor Catalytic Nanodiodes for Quantitative Detection of Hot Electrons Induced by a Chemical Reaction, Hyosun Lee***, KAIST & IBS, Republic of Korea; *I. Nedrygailov*, IBS & KAIST, Republic of Korea; *Y.K. Lee, C. Lee*, KAIST & IBS, Republic of Korea; *H. Choi*, Electronics and Telecommunications Research Institute (ETRI), Republic of Korea; *J.Y. Park*, Institute for Basic Science (IBS) & Korea Advanced Institute of Science and Technology (KAIST), Republic of Korea

Direct detection of hot electrons produced by exothermic reactions on catalysts is an effective strategy to quantify the non-adiabatic energy transfer during the elementary steps of the surface reactions, which provides an insight of the catalytic activity.^{1,2} In particular, hot electron dynamics at the surface of metal nanoparticles (NPs) with precisely controlled shape and size is a challenge as well as a key issue in the real-world catalyst system. Herein, we show a novel scheme of graphene catalytic nanodiode composed of a Pt NPs array on graphene/TiO₂ Schottky nanodiode, which allows detection of hot electron flows induced by hydrogen oxidation on Pt NPs. By analyzing the correlation between the turnover rate (catalytic activity) and hot electron current (chemicurrent) measured on the graphene catalytic nanodiodes, we demonstrate that the catalytic nanodiodes utilizing a single graphene layer for electrical connection of Pt NPs are beneficial for the detection of hot electrons due to not only atomically thin nature of graphene but also reducing the height of the potential barrier existing at the Pt NPs/graphene interface. Thereby, the graphene catalytic nanodiodes offer an effective and easy to use approach to study mechanisms of chemical energy conversion in various heterogeneous system, even including composite catalysts with carbon-based supports.

References

1. H. Lee, I. I. Nedrygailov, Y. K. Lee, C. Lee, H. Choi, J. S. Choi, C. Choi, J. Y. Park, Nano Lett. 16 (2016) 1650-1656.

2. H. Lee, I. I. Nedrygailov, C. Lee, G. A. Somorjai, J. Y. Park, Angew. Chem. Int. Ed. 54 (2015) 2340-2344.

8:20am **SS1+AS+HC+NS-TuM2 Adlayer-Structure Dependent Ultrafast Desorption Dynamics: The Coverage Dependence of Substrate-Adsorbate Energy Transfer in Carbon Monoxide on Pd(111), Sung-Young Hong**, Brookhaven National Laboratory; *P. Xu*, Stony Brook University; *N.R. Camillone, M.G. White, N. Camillone*, Brookhaven National Laboratory

We have conducted a detailed investigation of the coverage dependence of the ultrafast photoinduced desorption of CO from the (111) surface of

* National Student Award Finalist

palladium. Because the CO binding site depends on coverage, these measurements present an opportunity to examine the dependence of the substrate-adsorbate energy transfer on adsorption site. Specifically, as the CO coverage is increased, the adsorption site population shifts from all three-fold hollow (up to 0.33 ML), to bridge and near bridge (> 0.5–0.6 ML) and finally to mixed three-fold hollow plus top site (0.6 ML to saturation at 0.75 ML). We show that between 0.24 and 0.75 ML this progression of binding site motifs is accompanied by two remarkable features in the ultrafast photoinduced desorption of the adsorbates: (i) a roughly two-orders of magnitude increase in the desorption probability, and (ii) a nonmonotonic variation in the adsorbate-substrate energy transfer rate observed in two-pulse correlation experiments, with a minimum occurring at intermediate coverages. Simulations using a phenomenological model to describe the adsorbate-substrate energy transfer in terms of frictional coupling indicate that these features are consistent with an adsorption-site dependent electron-mediated energy coupling strength, η_{el} , that decreases with binding site in the order: three-fold hollow > bridge and near bridge > top site. The weakening of η_{el} largely counterbalances the decrease in the desorption activation energy that accompanies this progression of adsorption site motifs and moderates what would otherwise be a rise of several orders of magnitude in the desorption probability. Furthermore, we show that within this framework, the observed energy transfer rate enhancement at saturation coverage is due to interadsorbate energy transfer from the copopulation of molecules bound in three-fold hollows to their top-site neighbors. This conclusion is supported by comparison to desorption of CO from mixed CO+O adlayers where the O adsorbs at three-fold hollow sites and further promotes CO desorption from top sites.

8:40am SS1+AS+HC+NS-TuM3 Evidence for a Spin Accelerated Reaction Mechanism in the Thermal Decomposition of Alkyl Radicals on the Si(100) Surface, A.J. Pohlman, D.S. Kaliakin, S.A. Varganov, **Sean Casey**, University of Nevada

Density functional theory and complete active space self-consistent field calculations were used to probe the thermal decomposition of alkyl radicals on the Si(100) surface. Single dimer and single row double dimer cluster models were used to mimic the Si(100) surface in the calculations, and results indicate an interdimer β -hydrogen elimination reaction is the kinetically favored thermal decomposition pathway for adsorbed alkyl radicals. This pathway occurs via a spin crossing from the initial singlet energy surface to the triplet surface mediated by spin-orbit coupling. On the triplet surface the barrier to the elimination reaction is predicted to be about 40 kJ/mol lower than on the singlet surface. Experimental thermal desorption studies of alkyl chlorides adsorbed onto the Si(100)-(2x1) surface appear to give desorption energies for alkene products that are consistent with the barriers computed for the interdimer β -hydrogen elimination spin accelerated reaction mechanism. Experimental and computational results for the adsorption/desorption energetics of several different alkyl radicals will be discussed, along with results from partial deuteration studies of adsorption of selected haloalkanes.

9:00am SS1+AS+HC+NS-TuM4 Hyperthermal Ion Induced Hot Carrier Excitations in a Metal Probed using Schottky Diodes, Dhruva Kulkarni, D.A. Field, D.B. Cutshall, J.E. Harriss, W.R. Harrell, C.E. Sosolik, Clemson University

We present measurements on hot carrier excitations in a metal irradiated by hyperthermal energy ions.

Specifically, alkali (Na^+/Rb^+) and noble gas (Ar^+) ions were used to irradiate a Schottky diode consisting of

a thin film of Ag (~25nm) grown on an n-type Si (111) wafer. Measurements of the resultant current

through the device were performed as a function of energy, angle of incidence and velocity of the

incident ions. Energy loss of the incident energetic ions inside the metal film leads to the generation of

hot carriers that travel ballistically to the Schottky interface and are detected as a kinetically-induced

current or “kinecurrent” within the device. This kinecurrent is analogous to previous measurements of

“chemicurrent” [H. Nienhaus, *Surface Science*, **45**, 1-78 (2002)], which were linked to the energy

delivered to a surface by exothermic reactions that could non-adiabatically couple to the electronic

structure and generate hot carriers.

9:20am SS1+AS+HC+NS-TuM5 H Atom Scattering, Adsorption, and Absorption in Collisions with Metal Surfaces: the crucial role of electron-hole-pair excitation, M. Alducin, Donostia International Physics Center, Spain; **Daniel Auerbach**, Max Planck Institute for Biophysical Chemistry, Germany; M. Blanco-Rey, Donostia International Physics Center, Spain; O. Bünermann, Y. Dorenkamp, Georg-August University of Göttingen; S.M. Janke, Max Planck Institute for Biophysical Chemistry, Germany; H. Jiang, Georg-August University of Göttingen; A. Kandratsenka, Max Planck Institute for Biophysical Chemistry; G.-J. Kroes, Leiden Institute of Chemistry, The Netherlands; M. Kammler, Max Planck Institute for Biophysical Chemistry; M. Pavenlo, Leiden Institute of Chemistry **INVITED**

When an H atom collides with a solid surface, it can transfer some of its kinetic energy into elementary excitations of the solid like phonons and electron-hole pairs. If the atom loses enough kinetic energy, it can become bound to the solid, either on the surface or in the bulk. For a metal, the availability of a continuum of low lying electronic excitations can lead to the breakdown of the adiabatic Born Oppenheimer approximation and the facile nonadiabatic excitation of electron-hole pairs (ehp). If the H atom loses sufficient energy, it can enter a bound state with the solid, either on the surface or in the bulk.

We have used a combined theoretical and experimental approach to elucidate the relative roles of adiabatic processes (phonon excitation) and nonadiabatic processes (ehp excitation) in collisions of H atoms with metals, insulators, and graphene. The experiments use photolysis to produce nearly mono-energetic beams of H atoms with energies of 1 - 3.3 eV and high resolution energy loss measurements using Rydberg atom tagging time-of-flight analysis. The theory involves calculations of classical trajectories for H atom collisions with two techniques. In the first, we calculate energies and forces on-the-fly during the course of a trajectory using density functional theory (DFT) and ab initio molecular dynamics (AIMD). In the second, we construct a full dimensional potential energy surface (PES) using a flexible functional form fit to DFT energies and bulk properties of the solid.

The measured mean energy loss for H atoms scattering from metals is large, approximately 30% of the initial energy and there is a tail in the energy loss distribution (ELD) extending to the full energy of incidence. The measured ELD is in reasonable agreement with theory only if nonadiabatic effects are included; adiabatic theory drastically underestimates the energy loss. Scattering from insulators (where ehp excitation can be excluded) shows much smaller energy loss and results consistent with adiabatic theory.

For metals, nonadiabatic effects not only dominate the energy loss process, but also change both the magnitude and mechanism for adsorption on metals. With nonadiabatic effects, the most probable pathway to adsorption is for H atoms to penetrate the surface, lose energy in the subsurface region, and then reemerge to adsorb on the surface.

11:00am SS1+AS+HC+NS-TuM10 Progress in Characterizing Submonolayer Island Growth: Capture-Zone Distributions, Growth Exponents, and Transient Mobility, Theodore L. Einstein, University of Maryland, College Park; A. Pimpinelli, Rice University; J.R. Morales-Cifuentes, University of Maryland, College Park; D.L. González, Universidad del Valle, Colombia

Analyzing capture-zone distributions (CZD) using the generalized Wigner distribution (GWD) has proved a powerful way to gain insight into epitaxial growth, in particular to access the critical nucleus size i , as reviewed in [1]. The CZ of an island contains all points closer to that island than to any other and is known as a Voronoi tessellation. This approach complements measurements of the growth exponent α from the scaling (with flux F) of island density $N \sim F^\alpha$ and of the distribution of island sizes. We summarize some extensive Monte Carlo simulations and experiments, especially newer ones, on various systems to which the GWD has been applied. These experiments include atomic or organic adsorbates, sometimes with impurities, and colloidal nano-particles. In some cases, most notably parahexaphenyl (6P) on sputter-modified mica [2], the value i extracted from CZD differs from the [larger] values of i deduced from $N \sim F^\alpha$. Furthermore, while the scaling was good, the values of α differed considerably at small and large F , which was attributed to DLA and ALA dynamics [2]. To reconcile the CZD and scaling measurements, we took into account long-known transient mobility (hot precursors) using a rate-equation approach [3]. We also applied this method to data for pentacene (5A) on the same substrate. In applications of the GWD to social phenomena, notably the areas of secondary administrative units (e.g. counties or French *arrondissements*) [4], lognormal distributions (typically

Tuesday Morning, November 8, 2016

due to multiplicative noise) sometimes arise instead of GWD or gamma distributions; we show this also occurs for some pore-size distributions [5].

*Work at UMD supported by NSF CHE 13-05892

[1] T.L. Einstein, A. Pimpinelli, D.L. González, J. Cryst. Growth **401** (2014) 627; TLE, AP, DLG, J.R. Morales-Cifuentes, J. Physics: Conf. Ser. J. Phys.: Conf. Series **640** (2015) 012024

[2] T. Potocar et al., Phys. Rev. B **83** (2011) 075423 & later work by A. Winkler et al., see [1].

[3] JRM-C, TLE, and AP, Phys. Rev. Lett. **113** (2014) 246101.

[4] R. Sathiyarayanan, Ph.D. thesis, UMD, 2009; R. Sathiyarayanan and TLE, preprint.

[5] A.S. DeLoach, B.R. Conrad, TLE, and D.B. Dougherty, submitted.

11:20am **SS1+AS+HC+NS-TuM11 Hindered Translator and Hindered Rotor Models for Calculating the Entropy of Adsorbed Species, Lynza H. Sprowl***, Oregon State University; C.T. Campbell, University of Washington; L. Arnadottir, Oregon State University

Adsorbed species on surfaces are important for a range of applications including heterogeneous catalysis, corrosion processes, and film growth. The need for a fast and accurate way to predict equilibrium constants and rate constants for surface reactions is important for understanding reaction kinetics and for building microkinetic models of catalytic reactions. Here a method to calculate partition functions and entropy of adsorbed species is presented. Instead of using the vibrational frequencies estimated from density functional theory and the harmonic oscillator approximation to calculate the partition function for all modes of motion, we use hindered translator and hindered rotor models for the three modes of motion parallel to the surface, two translations and one rotation. The energy barriers for translation and rotation were determined using density functional theory and the nudged elastic band method for four different adsorbates on a platinum surface: methanol, propane, ethane, and methane. The hindered translator model was used to calculate the entropy contributions from the two translations parallel to the surface and the hindered rotor model was used to calculate the entropy contribution from the rotation about the axis perpendicular to the surface. When combined with the vibrational entropy contributions and the concentration related entropy contributions, this gives the total entropy of the adsorbate on the surface. The total adsorbate entropies were found to agree well with experimental results, with an average absolute value of the error of only 1.1R or 8% for the four adsorbates. This new model should be useful to future researchers in surface chemistry, since it provides more accurate predictions of standard-state entropies and partition functions, and thus more accurate equilibrium constants and rate constants for surface reactions than provided by the standard harmonic oscillator approximation.

11:40am **SS1+AS+HC+NS-TuM12 Stabilization of X-Au-X Complexes on the Au(111) Surface: A Theoretical Investigation and Comparison of X=Sulfur, Chlorine, Methylthiolate, and Silylthiolate, J. Lee, J.S. Boschen, T.L. Windus, P.A. Thiel, J.W. Evans, Da-Jiang Liu**, Iowa State University

The involvement of Au atoms in the self-assembled methylthiolate (CH₃S) monolayers on Au(111) has been demonstrated experimentally [1], while for S and Cl, chain-like structures with no direct Au involvement were found [2,3]. We find that for S on various coinage metal surfaces, the linear S-M-S complexes (M=Cu, Ag, Au) are prevalent. A systematical theoretical study of the X-Au-X complexes, with X=S, Cl, CH₃S, and SiH₃S, has been performed using DFT and other quantum chemistry methods. Assuming equilibration of the metal substrate, the chemical potential of X are calculated and used to predict the stability of various Au-X complexes. We find good agreement between DFT and available experimental findings. Furthermore, the van der Waals interaction is shown to play a crucial role in the self-assembly of CH₃S observed in experiments [1].

[1] P. Maksymovych, O. Voznyy, D. B. Dougherty, D. C. Sorescu, J. T. Yates Jr., *Prog. Surf. Sci.* **85**, 206 (2010).

[2] V. V. Zheltov et al. *Phys. Rev. B*, **89**, 195425 (2014).

[3] H. Walen, *J. Chem. Phys.* **143**, 014704 (2015).

12:00pm **SS1+AS+HC+NS-TuM13 Contrasting Phonon Confinement and Interface Stability at Fe-Ag and Fe-Cr Multilayers: Insights from Ab Initio Calculations, S. Hong, Talat Rahman**, University of Central Florida

We have performed density functional theory based calculations to compare the characteristics of the interface of Fe-Ag and Fe-Cr multilayers. A perfect interface lattice match between the Fe and Ag layers was obtained by rotating fcc Ag(100) layers by 45° on bcc Fe(100). On the other hand, the Fe-Cr interface could be modeled by epitaxial layers of bcc Fe(100) and Cr(100). In Fe-Ag multilayers, we find the signature peak of Fe bulk phonons (35 meV) to be completely diminished, while the low energy peaks are remarkably enhanced, in agreement with experiment [1]. In contrast, the phonon density of state in the Fe-Cr multilayers do not show any salient feature except a slight decrease in the 35 meV peak for the Fe layer at the interface, as compared to that of the middle Fe layer, again in agreement with experiment [2]. The magnetic moment of the interfacial Fe atoms is larger than that of Fe atoms in other layers, as a result of charge transfer from Fe to Ag at the interface. As compared to the middle layers, more spin-up and less spin-down states are occupied at the interface in such a way that Fe donates a large number of spin-down electrons to Ag but receives only a few spin-up electrons from the latter because of the almost fully occupied Ag d-band. This leads to rather unstable Fe-Ag interface. On the contrary, at the Fe-Cr interface, Cr can easily give and take electrons leading to smooth interfacial coupling and stable environment.

[1] B. Roldan Cuenya et al., to be published

[2] Roldan et al, Phys. Rev. B **77**, 165410 (2008).

Work supported in part by DOE Grant No. DOE-DE-FG02-07ER46354

Surface Science

Room 104E - Session SS2+AS+HC+NS-TuM

Nanostructures: Growth, Reactivity, and Catalysis

Moderator: Bruce Koel, Princeton University

8:00am **SS2+AS+HC+NS-TuM1 Use of Size Correlations to Probe Reaction Mechanisms on Size-selected Model Catalysts, Scott Anderson**, University of Utah **INVITED**

The ability to prepare model catalysts by deposition of mass-selected metal clusters allows the size and density of catalytic sites to be varied independently and precisely, providing a new tool for mechanistic studies. In addition, preparation of truly monodisperse samples alters the kinetics for Ostwald ripening, thus changing the cluster stability under thermal/reactive conditions. This talk will focus on use of size-dependent correlations between catalytic activity and physical properties such as cluster morphology and electronic properties, to probe the factors that control catalysis and electrocatalysis by supported Pt clusters in the <25 atom size range. The stability of the clusters, and how this varies with size under heating, adsorbate exposure, and potential cycling will also be discussed.

8:40am **SS2+AS+HC+NS-TuM3 Role of the Strong Metal Support Interaction on the Catalytic Activity of Platinum Deposited on TiO₂ Supports, R.Paul Hansen, R.S. Phillips**, University at Albany-SUNY; E.T. Eisenbraun, C.A. Ventrice, Jr., SUNY Polytechnic Institute

Several roadblocks prevent the large-scale commercialization of hydrogen fuel cells, including the stability of catalysts and their substrates and the high cost of the Pt involved in the oxygen reduction reaction (ORR). The former of these problems can be solved by replacing the traditional carbon support with a conductive metal oxide such as reduced TiO₂, which will not easily corrode and should result in longer lasting fuel cells. The Pt is necessary in the cathode of the fuel cell to overcome the slow kinetics of the ORR. In this study, Pt was deposited either by atomic layer deposition (ALD) or physical vapor deposition (PVD). The typical size of the Pt islands that were grown using these deposition techniques was 5-8 nm. One factor that can inhibit the catalytic activity of a metal catalyst on a metal oxide is the strong metal support interaction (SMSI). This is where a metal on a reducible metal oxide can be encapsulated by a layer of the metal oxide support material at elevated temperatures. The processing of materials through atomic layer deposition can exceed this temperature. The TiO₂ substrates used in this study were either grown by ALD, which results in a polycrystalline anatase film, or were single-crystal rutile TiO₂(110) samples prepared in ultra-high vacuum (UHV). The Pt/TiO₂ samples were tested electrochemically using cyclic voltammetry (CV) to determine the level of catalytic activity. To determine the effect of the SMSI interaction on the

Tuesday Morning, November 8, 2016

catalytic activity of the PVD grown samples, CV was performed on samples that were annealed in high vacuum after Pt deposition. Additional characterization was performed with scanning electron microscopy (SEM), Auger electron spectroscopy (AES), x-ray photoelectron spectroscopy (XPS), Rutherford backscattering spectrometry (RBS), and four point probe analysis.

9:00am SS2+AS+HC+NS-TuM4 Adsorption and Adhesion Energies of Au, Cu, and Ag Nanoparticles on CeO₂(111), MgO(100) and Other Oxide Surfaces, Charles T. Campbell, S.L. Hemmingson, G.M. Feeley, University of Washington

Heterogeneous catalysts consisting of late transition metal nanoparticles dispersed across oxide supports are ubiquitous in industrial chemistry and energy technology. We have used an ultrahigh vacuum single-crystal adsorption calorimeter to study the adsorption energies of Au, Cu and Ag gas atoms as they adsorb and grow nanoparticles on single-crystal oxide surfaces as models for real catalyst systems. These measurements allow us to determine the chemical potential of metal atoms in supported nanoparticles as a function of particle size and the support upon which they sit. The support effect manifests itself very directly on metal chemical potential via the metal / oxide adhesion energy. Our earlier studies have shown that metal chemical potential can be related to the metal nanoparticle's catalytic activity and deactivation rates through sintering, so there is a great motivation to understand how it varies with particle size and support, and how metal / oxide adhesion energies vary with the nature of the metal and the oxide support material. Through these measurements on a variety of systems, we have discovered systematic trends in these that allow predictions of adhesion energies for system which have not been measured. We have also measured the adsorption energy of isolated Cu atoms on CeO₂(111) terrace sites, which is possible at 100 K. This is the first measurement of the adsorption energy of any late transition metal atom on any oxide surface of the type used as catalyst supports in a situation where the atom sits on the surface as an isolated monomer (as opposed to sitting within a small metal cluster).

9:20am SS2+AS+HC+NS-TuM5 Effects of Nanoparticles on Surface Resistivity: Ni on Au(111), Joshua Cohen, R.G. Tobin, Tufts University

The change in surface resistivity due to the formation of nickel nanoparticles on gold(111) was studied by measuring the resistance of a thin film of Au as a function of Ni coverage, θ . After annealing, Au(111) configures into the herringbone reconstruction and provides a template for the periodic nucleation and growth of Ni nanoparticles. The Ni islands grow radially until $\theta \sim 0.3$ ML, after which, subsequent Ni atoms contribute almost exclusively to a second layer [1].

Surface resistivity arises primarily from the scattering of the substrate's conduction electrons by foreign atoms or defects, and studies of the dependence of surface resistivity on coverage yield insights into growth dynamics, interadsorbate interactions, and interactions between the adsorbed atoms and conduction electrons. For randomly distributed non-interacting scatterers the resistivity change is linear in coverage. Since Ni atoms on Au(111) grow in tight ordered nanoclusters, a nonlinear dependence might be anticipated. Our results, however, show a linear dependence on coverage for Ni atoms in the first layer, as if they were independent point scatterers. At coverages above $\theta \sim 0.3$ ML, there is no further change in resistivity, which we attribute to Ni atoms forming a second layer and making no significant contribution to the surface resistivity.

The samples were 150 nm thick epitaxial Au(111) films on mica prepared by sputtering and annealing in ultrahigh vacuum. The resistance of the film was measured as Ni was thermally evaporated on the surface. Ni coverage was determined using Auger electron spectroscopy (AES), corrected for the inelastic mean free path of the electrons.

The resistance and AES data were analyzed in terms of a growth model that allowed for variation in the coverage at which a second layer begins, the relative probabilities of first- and second-layer growth after that point, and the relative contributions of first- and second-layer Ni atoms to the surface resistivity. The results are consistent with the growth model observed with STM [1], and serve as an indirect probe of the growth kinetics of this interesting system, as well as determining for the first time the contributions of the Ni islands to the surface resistivity of the Au film.

1. Chambliss, D.D., R.J. Wilson, and S. Chiang, *Ordered Nucleation of Ni and Au Islands on Au (111) Studied By Scanning Tunneling Microscopy*. Journal of Vacuum Science & Technology B, 1991. 9(2): p. 933-937.

9:40am SS2+AS+HC+NS-TuM6 Three-Dimensional Control of Nanoparticle Layer Deposition by "Click Chemistry", Mackenzie Williams, A.V. Telyakov, University of Delaware

Our previous studies have focused on the formation of highly-controlled nanoparticle mono- and multilayers of silica and magnetic iron oxide nanoparticles through the copper(I) catalyzed azide-alkyne cycloaddition reaction. By using the specific functionalization scheme in that method, we achieved very high surface coverage and the formation of exactly one nanoparticle layer per deposition cycle, as could be observed with scanning electron microscopy (SEM) and atomic force microscopy (AFM). Formation of the triazole ring from the "click" reaction was confirmed by infrared spectroscopy and X-ray photoelectron spectroscopy (XPS), while density functional theory calculations were used to confirm spectroscopic results and investigate the reasons behind the high coverage. In the current work, a higher level of control over the nanoparticle layers is being sought. Conformal filling of the layer over high aspect-ratio features is being studied and would allow this method to be used as a viable alternative to traditional layer-by-layer techniques. Additionally, control of the spatial resolution of the nanoparticle layers upon the substrate via alternative methods of catalysis initiation is currently being investigated.

11:00am SS2+AS+HC+NS-TuM10 Spherical Metallic Nanostructures Based on Fullerene Scaffolds with Tunable Bandgap, A Scanning Tunneling Microscopy/Spectroscopy (STM/STS) Study, Ehsan Monazami, University of Virginia; J.B. McClimon, University of Pennsylvania; J.M. Rondinelli, Northwestern University; P. Reinke, University of Virginia

The current literature on annealing of fullerene molecules on tungsten surfaces indicates a complete dissociation of the fullerene cage and the formation of a carbide phase. However, our measurements with high resolution STM and STS illustrate a complex intermediate reaction sequence. Upon annealing of C₆₀ adsorbed on a tungsten thin film grown on MgO (001) in UHV, C₆₀ does not dissociate and the spherical C₆₀ shape is retained up to a temperature of at least 973 K. During the annealing, the band gap of the molecular layer decreases gradually from the wide bandgap of fullerene to a fully metallic electronic state. This transition occurs in a narrow temperature range between 600 K and 700 K. After this transition, the near-spherical particles are termed "nanospheres." This progression was observed with a series of high resolution scanning tunneling spectra and detailed spectral mapping. The bandgap variation presents an approach to achieve the formation of densely packed nanoclusters (nanospheres) with variable bandgap, which are stable at elevated temperatures. Experimental results for sub-ML fullerene coverage on tungsten show that the fullerene molecules are mobile at room temperature, but they become stationary after annealing above 500 K. This immobilization of molecules indicates a strong interaction and likely a covalent bond between the molecule and substrate that is triggered by annealing.

The progression to metallic nanospheres is hypothesized to occur either by gradual substitution of W-atoms or by wetting the molecule with W-atoms and thus formation of W-C bonds in a solid state reaction. These models were tested using density functional theory (DFT) calculations. Two simulation strategies were used. In the first, C₆₀ carbon atoms were substituted by W in the molecule and the resulting electronic properties and bandgap were calculated. In the second approach, different adsorption geometries of a C₆₀ molecule on the tungsten (110) surface were considered. The variation of the band gap due to different C₆₀ orientations relative to the tungsten substrate and various types of hetero-fullerenes will be discussed.

11:20am SS2+AS+HC+NS-TuM11 Facile Synthesis of Gold Nanoworms and their Excellent Surface Enhanced Raman Scattering (SERS) and Catalytic Properties, Waqqar Ahmed, COMSATS Institute of Information Technology, Pakistan; J.M. van Ruitenbeek, Leiden University, Netherlands

Gold nanoparticles exhibit interesting optical properties because of the surface plasmon resonance. The shape and size of gold nanoparticles can markedly influence their optical properties. A spherical nanoparticle has a single plasmon peak, while rod-shaped nanoparticles have two plasmon peaks because of their shape anisotropy. Furthermore, slight deviations from the rod morphology can markedly influence the optical properties. For example, worm-shaped gold nanoparticles can have more than two plasmon peaks. Moreover, nanoworms can display very high local field enhancements upon plasmon excitation owing to their special shape and surface roughness.

We have devised a simple, seedless, high-yield protocol for the synthesis of gold nanoworms [1]. Nanoworms were grown simply by reducing HAuCl₄

Tuesday Morning, November 8, 2016

with ascorbic acid in a high pH reaction medium in the presence of growth directional agents. In contrast to the seed-mediated growth of gold nanorods where a seed particle grows into a nanorod, nanoworms grew by oriental attachment of nanoparticles. By varying different reaction parameters we were able to control the length of NWs from a few nanometers to micrometers. Furthermore, the aspect ratio can also be tuned over a wide range.

Owing to their special morphology, gold nanoworms are much superior than the conventional nanorods for numerous applications. For instance, we have seen that they show markedly superior SERS and catalytic properties compared to their nanorod counterparts. This is due to their high-energy rough surface and twisted shape, which not only provides an ideal platform for catalytic activities but also generates local hot-spots upon plasmon excitation. Our study shows that both catalytic and SERS properties of gold nanoworms are strongly dependent on their length.

[1] W. Ahmed, C. Glass, and J.M. van Ruitenbeek, *Nanoscale*, 6, 13222, (2014)

11:40am SS2+AS+HC+NS-TuM12 Surface Hydrogen Enables Sub-Eutectic Vapor-Liquid-Solid Semiconductor Nanowire Growth, *S.V. Sivaram, H. Hui*, Georgia Institute of Technology; *M. de la Mata, J. Arbiol*, Catalan Institute of Nanoscience and Nanotechnology, Spain; *Michael Filler*, Georgia Institute of Technology

Semiconductor nanowires are emerging as indispensable nanoscale building blocks for next generation energy conversion, electronic, and photonic devices. The bottom-up vapor-liquid-solid (VLS) mechanism – whereby a liquid eutectic "catalyst" droplet collects precursor molecules (or atoms) from the vapor and directs crystallization of the solid nanowire – is a nearly ubiquitous method for nanowire synthesis. While VLS growth below the bulk metal-semiconductor eutectic temperature has long been known, the fundamental processes that govern this behavior are poorly understood. Here, we show that hydrogen atoms adsorbed on the Ge nanowire sidewall enable AuGe catalyst supercooling and control Au transport. Our experimental approach combines in situ infrared spectroscopy to directly and quantitatively determine hydrogen atom coverage with a "regrowth" step that allows catalyst phase to be determined with ex situ electron microscopy. Maintenance of a supercooled catalyst with only hydrogen radical delivery confirms the centrality of sidewall chemistry. This work underscores the importance of the nanowire sidewall and its chemistry on catalyst state, identifies new methods to regulate catalyst composition, and provides synthetic strategies for sub-eutectic growth in other nanowire systems. We leverage this newfound understanding of nanowire growth chemistry to fabricate large-area arrays of high quality axial Si/Ge heterostructures for the first time.

12:00pm SS2+AS+HC+NS-TuM13 Ultrafine Sodium Titanate Nanowires with Extraordinary Strontium Ion-Exchange Property, *Koji Nakayama*, Tohoku University, Japan

The removal of radioactive substances released to the environment by a nuclear accident is an emergent issue. The water treatment based on the ion exchange process is the most effective decontamination technology, and inorganic ion exchangers, titanates, have been used for the capture of Sr ions owing to their high radiation stability and extreme ion selectivity. However, the reported adsorption capacity and ion exchange efficiency are not satisfied. We show the formation of sodium titanate nanowires with a few nanometers in diameter, having a mogul-shaped surface, forming hierarchically a three-dimensional network skeletal structure, and exhibiting remarkable Sr ion exchange properties [1]. They are produced by unique and simple non-thermal processes through the simultaneous selective leaching of Al and oxidation of Ti in a rapidly solidified Ti-Al alloy ribbon in NaOH solution. The experimental saturated adsorption capacity is tripled and the uptake rate is at least three hundred times faster than these of the previous reports. The results demonstrate that the newly created nanowires exhibit a potential application in the decontamination and disposal of nuclear waste.

[1] Y. Ishikawa, S. Tsukimoto, K. S. Nakayama, and N. Asao, *Nano Lett.* **15**, 2980-2984 (2015).

Thin Film

Room 102B - Session TF+SA+MI-TuM

Thin Films for Synchrotron and Magnetism Applications

Moderators: Joshua Ballard, Zyvex Labs, Divine Kumah, North Carolina State University

8:00am TF+SA+MI-TuM1 Achieving High-Temperature Ferromagnetic Topological Insulator by Proximity Coupling, *Valeria Lauter*, Oak Ridge National Laboratory

Topological insulators (TIs) are insulating materials that poses conducting surface states protected by time-reversal symmetry, wherein electron spins are locked to their momentum. This exclusive property offers novel prospects for creating next-generation electronic and spintronic devices, including TI-based quantum computation. Introducing ferromagnetic order into a TI system without compromising its distinctive quantum coherent properties could lead to a realization of a number of innovative physical phenomena. In particular, achieving robust long-range magnetic order at the TI surface at specific locations without introducing spin scattering centers could open up new potentials for devices. Here, we demonstrate topologically enhanced interface magnetism by coupling a ferromagnetic insulator (FMI) to a TI (Bi₂Se₃); this interfacial ferromagnetism persists up to room temperature, even though the FMI (EuS) is known to order ferromagnetically only at low temperatures (< 17 K). The induced magnetism at the interface resulting from the large spin-orbit interaction and spin-momentum locking property of the TI surface is found to greatly enhance the magnetic ordering (Curie) temperature of the TI/FMI bilayer system. Due to the short range nature of the ferromagnetic exchange interaction, the time-reversal symmetry is broken only near the surface of a TI, while leaving its bulk states unaffected [1]. The topological magneto-electric response originating in such an engineered TI could allow for an efficient manipulation of the magnetization dynamics by an electric field, providing an energy efficient topological control mechanism for future spin-based technologies. Work supported by U.S. DOE, Office of Science, BES.

[1] F. Katmis, V. Lauter, F. Nogueira, B. Assaf, M. Jamer, P. Wei, B. Satpati, J. Freeland, I. Eremitz, D. Heiman, P. Jarillo-Herrero, J. Moodera, "Achieving high-temperature ferromagnetic topological insulating phase by proximity coupling", *Nature* 2016

8:20am TF+SA+MI-TuM2 Soft X-ray Induced Spin Crossover Transition at Room Temperature, *Paulo Costa, X. Zhang, S. Beniwal*, University of Nebraska-Lincoln; *A.T. N'Diaye*, Lawrence Berkeley National Laboratory; *J.-F. Létard*, Université de Bordeaux; *P.A. Dowben, A. Enders*, University of Nebraska-Lincoln

The spin crossover Fe(II) complex (SCO) of the type [Fe(H₂B(pz)₂)(bipy)] has been previously shown to exhibit spin state transitions between its low spin (LS) and high spin (HS) states as a response to external stimulus such as electric fields, temperature changes, and light. It is well established that this SCO complex exhibits a crossover from its LS state to the HS state if the temperature is increased above approximately 150 K. It is demonstrated here that this spin crossover can be suppressed by mixing the SCO with strongly dipolar *p*-benzoquinonemonoimine zwitterion (PZI) molecules, so that unlike before, the LS state still prevails even at room temperature (RT). With the metastable LS state now locked in at RT, a spin state transition to the HS state can now be triggered optically by soft X-rays over a relatively short time of several minutes. This process is fully reversible, as cooling the mixture to 78 K has been shown to de-excite it back to its original LS state. Experiments were performed using X-ray absorption spectroscopy measurements (XAS) with synchrotron radiation tuned to the Fe L₃ absorption edge as well as accompanying magnetic moment measurements taken by a superconducting quantum interference device (SQUID). The effects of temperature, photon flux, and the stoichiometric ratio between SCO and PZI in the mixture were systematically studied, and the results will be presented here. This study provides a demonstration that the spin crossover transition temperature can be tailored to create a material that exists in a meta-stable LS state at RT wherein spin states can then be switched optically.

8:40am TF+SA+MI-TuM3 Probing Thermochromic Phase Transitions in ALD VO₂ using Synchrotron Radiation, *Alexander Kozen*, U.S. Naval Research Laboratory; *H. Jorress*, Cornell University; *V.D. Wheeler, C.R. Eddy, Jr.*, U.S. Naval Research Laboratory

VO₂ is a thermochromic material, one class of "smart materials" that are receiving considerable interest due to a sharp semiconductor to metal (S-M) phase transition that occurs at a specific, material dependent

Tuesday Morning, November 8, 2016

temperature ($T_c = 68^\circ\text{C}$ for VO_2). The S-M transition occurs as a result of a phase transition between a semiconducting monoclinic phase below T_c and a metallic tetragonal phase above T_c . While VO_2 has been widely utilized as a microbolometer material for IR detectors, current deposition processes used to fabricate thin film VO_2 (PLD, MBE, sputtering) are not adequate to realize complex device architectures. Use of ALD to deposit VO_2 thin films allows for uniform, low temperature coating of large area 3D substrates that could open the door to new applications.

Temperature dependent *in-situ* grazing incidence synchrotron XRD was utilized to probe lattice strain and structural reordering in both as-deposited (amorphous) and annealed (polycrystalline) ALD VO_2 thin films during the S-M transition. GIXRD allows us to selectively sample the bulk or the film-substrate interface of thin ALD films with excellent depth resolution, while the high flux provided by the synchrotron (10^{12} photons/s) enables fast data collection. Initial results show that as-deposited ALD VO_2 films are polycrystalline at the VO_2 -sapphire interface, while the bulk of the as-deposited VO_2 is amorphous. Annealing VO_2 on sapphire in an oxygen-rich environment forms a fiber-textured polycrystalline VO_2 film with a more pronounced S-M transition. We will discuss how substrate selection, ALD growth and processing conditions, and film thickness influence VO_2 morphology and/or structure and relate these materials properties to device data.

The authors wish to acknowledge Cornell University's CHESS synchrotron facilities for GIXRD work and The Office of Naval Research for support. Dr. Kozen acknowledges support by the ASEE-NRL postdoctoral fellows program.

9:00am TF+SA+MI-TuM4 Standing-wave Synchrotron Photoemission Studies of Electronic Structure in SrTiO_3 - LaCrO_3 Superlattices, Ryan Comes, Auburn University; *S.C. Lin*, University of California, Davis; *C.T. Kuo*, Lawrence Berkeley National Laboratory (LBNL); *L. Plucinski*, FZ Juelich; *S. Spurgeon*, Pacific Northwest National Laboratory; *D. Kepaptsoglou*, Q. Ramasse, SuperSTEM; *J.E. Rault*, Synchrotron SOLEIL; *S. Nemsak*, Forschungszentrum Juelich GmbH, Germany; *C. Fadley*, Lawrence Berkeley National Laboratory (LBNL); *P.V. Sushko*, S.A. Chambers, Pacific Northwest National Laboratory

The polar discontinuity at the interface between SrTiO_3 (STO) and LaCrO_3 (LCO) has been shown to produce a varying band alignment between the two materials with a built-in potential gradient.¹ We have recently shown that this built-in potential gradient can be harnessed to induce a polarization in STO-LCO superlattices through interface engineering.² This work demonstrated that by controlling interfacial termination between layers we can induce a built-in polarization in STO, with Ti cations displaced off-center in surrounding oxygen octahedra. To further study this system, we have synthesized a series of STO-LCO superlattices with varying interfacial and surface terminations for synchrotron standing-wave x-ray photoemission measurements.³ These measurements make use of Bragg diffraction from the superlattice to induce an x-ray standing wave that can be scanned across a single period of the superlattice. Through careful material design, we have achieved the strongest standing-wave effects to date, enabling angle-resolved photoemission measurements of electronic dispersion in both the STO and LCO layers of the material. Density functional theory models of the electronic structure of the superlattices are used to corroborate our experimental results with the expected behavior. Monochromated, aberration-corrected scanning transmission electron microscopy electron energy-loss spectroscopy (STEM-EELS) measurements also enable further studies into changes in electronic behavior at interfaces.

¹ S.A. Chambers, L. Qiao, T.C. Droubay, T.C. Kaspar, B.W. Arey, and P.V. Sushko, *Phys. Rev. Lett.* **107**, 206802 (2011).

² R.B. Comes, S.R. Spurgeon, S.M. Heald, D.M. Kepaptsoglou, L. Jones, P.V. Ong, M.E. Bowden, Q.M. Ramasse, P.V. Sushko, and S.A. Chambers, *Adv. Mater. Interfaces*, (2016). DOI: 10.1002/admi.201500779

³ A.X. Gray, C. Papp, B. Balke, S.-H. Yang, M. Huijben, E. Rotenberg, A. Bostwick, S. Ueda, Y. Yamashita, K. Kobayashi, E.M. Gullikson, J.B. Kortright, F.M.F. de Groot, G. Rijnders, D.H.A. Blank, R. Ramesh, and C.S. Fadley, *Phys. Rev. B* **82**, 205116 (2010).

9:20am TF+SA+MI-TuM5 In Situ Synchrotron X-ray Studies of Complex Oxide Thin Film Growth, Dillon Fong, Argonne National Laboratory INVITED Functional materials based on complex oxides in thin film form offer new and exciting strategies for meeting many of our outstanding energy challenges through systematic control of layer sequencing, strain, etc. However, the synthesis of such oxide films can be a major challenge even

when utilizing reactive molecular-beam epitaxy (MBE), a powerful deposition technique that allows the construction of materials atomic plane by atomic plane. To understand the fundamental physics of oxide growth by reactive MBE, we present *in situ* surface x-ray diffraction results on the growth of SrTiO_3 and SrO-SrTiO_3 thin films on (001)-oriented SrTiO_3 substrates. For homoepitaxy, we compare sequential deposition (alternating Sr and Ti monolayer doses) with that of co-deposition of Sr and Ti, both in a background of oxygen pressure, and observe drastically different growth pathways due to the presence of a TiO_2 double layer. For heteroepitaxial growth of Ruddlesden-Popper SrO-SrTiO_3 films, we find that layers rearrange dynamically, resulting in layer sequences distinct from the shutter sequence. In general, the starting surface structure and composition, in combination with local thermodynamic considerations, strongly influence our ability to atomically construct new complex oxides.

Work at Argonne, including the Advanced Photon, is supported by the U.S. Department of Energy.

11:00am TF+SA+MI-TuM10 Probing CVD Growth Mechanisms of SiC with In Operando Synchrotron-based X-ray Diagnostics, Philip DePond, A.A. Martin, J.H. Yoo, M. Bagge-Hansen, J. Lee, S. Elhadj, M. Matthews, T. van Buuren, Lawrence Livermore National Laboratory

Laser chemical vapor deposition (LCVD) of ultra-hard coatings, such as SiC, offers sub-mm spatial control over composition and phase, while addressing multiple growth processes under the same conditions for comparison. Normally, optimization requires extensive and costly "cook and look" experiments. Using an *in situ* approach instead, we develop fundamental insights into the growth mechanisms to unravel the complex roles of deposition parameters. We have conducted a series of *in operando* synchrotron-based X-ray absorption experiments that interrogate the LCVD growth region during growth. SiC was grown in a compact, portable CVD system from tetramethylsilane using a CW 532nm YAG to achieve laser-based pyrolytic precursor decomposition. We will present the results of Si K-edge (1.8keV) X-ray absorption near-edge structure (XANES) measurements conducted concurrently for the film during LCVD growth with an emphasis on the effects of variation of temperature, flow, substrates, and pressure conditions.

11:20am TF+SA+MI-TuM11 Unusual Effects in Organic Thin Film Growth as Revealed by the Use of In Situ Real Time Synchrotron X-ray Techniques, R.K. Nahm, H.J. Bullen, T. Suh, James Engstrom, Cornell University

The effects of molecular scale events on the growth of crystalline thin films has been long been an active area of research as the resulting thin film properties depend sensitively on the microstructure. The growth of high quality, smooth thin films in the vast majority of these systems is favored at low rates of growth and high substrate temperatures. Here we report on the growth of thin films of tetracene, an organic semiconductor that possesses one less aromatic ring as compared to the much more studied pentacene. We examine the growth on SiO_2 using *in situ* real time X-ray synchrotron radiation and *ex situ* atomic force microscopy (AFM). First, using *in situ* X-ray reflectivity, we observe a transition from 3D island growth to 2D layer-by-layer growth as the growth rate of tetracene is increased on SiO_2 at room temperature, $T_s \sim 30^\circ\text{C}$. This unusual phenomenon, 2D growth favored at higher rates, has not been observed in previous work with pentacene, despite the similarities between these two molecules. Results from AFM indicate that tetracene may tend to quickly traverse "upwards" on thin film features such as the edges of islands, making these thin films susceptible to reorganization during and/or after growth. Thus, at sufficiently high rates of growth the rate of ad molecule attachment at the tetracene island/ SiO_2 substrate edges effectively outcompetes the rate of upward step-edge transport, and 2D growth results. We find additional evidence for this mechanism by examining the effect of substrate temperature. In particular we find that the transition to 2D growth occurs at a lower rate of growth at a substrate temperature of $T_s \sim 0^\circ\text{C}$, consistent with suppression in the rate of upward transport at lower values of T_s . Finally, we have also examined the evolution of the thin film crystal structure in real time using *in situ* grazing incidence X-ray diffraction. Many thin film organic semiconductors are known to crystallize in different structures, and tetracene is no exception. At room temperature we find that first a thin film phase grows, then, after a delay, a bulk phase begins to grow, while the growth of the thin film phase saturates. We also find that the film thickness at which X-ray scattering from the bulk phase becomes apparent is found to vary with deposition rate. These phenomena are also dependent on substrate temperature. For example, for the range of thin films thicknesses examined, we found no evidence for growth of the bulk phase at the lower substrate temperature, $T_s \sim 0^\circ\text{C}$. These results

Tuesday Morning, November 8, 2016

highlight the potential complexity of crystalline thin film growth in what appears to be a very simple system, tetracene on SiO₂.

11:40am TF+SA+MI-TuM12 Understanding the Effect of Nitrogen Plasma on Plasma Assisted Atomic Layer Epitaxy of InN Monitored by Real Time GISAXS, Neeraj Nepal, V. Anderson, S.D. Johnson, D.J. Meyer, B.P. Downey, A.C. Kozen, US Naval Research Laboratory; Z.R. Robinson, SUNY College at Brockport; D.R. Boris, S.C. Hernández, S.G. Walton, US Naval Research Laboratory; K.F. Ludwig, Boston University; C.R. Eddy, Jr., US Naval Research Laboratory

III-N semiconductors have found application in a variety of technologies such as high power transistors, emitters, detectors, and solar-cells. The relatively high growth temperature of common III-N synthesis techniques has impeded further development and application of the materials due to challenges with miscibility gaps and strain related to thermal expansion mismatch with non-native substrates. To address these challenges, Plasma assisted atomic layer epitaxy (PA-ALE) offers a new approach to low temperature III-N growth and can be used to epitaxially grow InN by using alternative pulses of trimethylindium and nitrogen plasma [1]. Since growth using this technique is far from thermodynamic equilibrium, understanding how nitrogen plasma affects nucleation and growth kinetics is essential for development.

Real-time grazing incidence small angle x-ray scattering (GISAXS) measurements at the Cornell High Energy Synchrotron Source were used to study the effect of variation in nitrogen plasma pulse conditions on PA-ALE of InN at 250 °C. Current results show the evolution of GISAXS characteristics such as the correlated peak (CP) length scale in the Yoneda Wing (YW) directly relates to the surface roughness, impurities, and electrical properties of the material. During the initial cycles of InN growth, the diffuse specular reflection broadens and CPs start to evolve along the YW with different correlated length scales. For the nitrogen plasma pulse time (t_p) of 15 seconds, the CPs have two different correlated length scales of 33.36 and 8.38 nm. With increasing t_p to ≥ 20 s (the empirically optimal pulse length), a YW with only one CP evolves and the longest correlated length scale of 11.22 nm is for $T_p = 25$ s. The correlated length scale of this single CP decreases to 10.75 nm for $t_p = 30$ s. Additionally at $t_p = 25$ s, the growth rate is largest (0.035nm/cycle – consistent with previously reported self-limited growth [1]) with root mean square surface roughness and carbon impurity at or below AFM and XPS sensitivity limits, respectively. The nature of GISAXS CP correlated length scale directly relates to the material quality. GISAXS also shows that the N₂/Ar flow ratio significantly affect the nucleation and growth of InN. Based on various *ex situ* characterization methods, the quality of the PA-ALE grown films is similar or better than the material grown by conventional growth methods, for example, molecular beam epitaxy at higher temperature (>400 °C).

[1] Nepal et al., Cryst. Growth and Des. **13**, 1485 (2013).

12:00pm TF+SA+MI-TuM13 Spintronics Based on the Chiral Induced Spin Selectivity (CISS) Effect, Yossi Paltiel, The Hebrew University, Israel; R. Naaman, The Weizmann Institute of Science, Israel

The high level of energy dissipation associated with the present semiconductor-based integrated-circuit technology limits the operating frequency of the devices. Therefore there is interest in new concepts that may solve this problem. One such concept that attracts considerable attention nowadays combines spins with electronics (spintronics). In principle, the application of spintronics should result in reducing power consumption of electronic devices and efficiency should be closer to the thermodynamic limit.

Two major issues complicate the use of spintronics; material problems and the inefficiency in producing spin-polarized current. Spintronics devices usually require the use of complicated structures of magnetic material layers and the need for permanent magnetic layers puts constraints on the miniaturization of these devices. In addition, high currents are required to produce highly polarized spin current which results in induced heating.

We present a new concept in which spin current is produced by using the spin selectivity in electron transport through chiral molecules, termed Chiral-Induced Spin Selectivity (CISS). The CISS effect allows realization of simple local and power efficient spintronics devices. Studying the CISS effect, we found that chiral molecules, especially helical ones, can serve as very efficient spin filters at room temperature, with no need for a permanent magnetic layer. Recently, by utilizing this effect we demonstrated a simple magnetless spin based magnetic memory. Moreover, we show that when chiral molecules are adsorbed on the surface of thin ferromagnetic film, they induce magnetization

perpendicular to the surface, without the application of current or external magnetic field.

The CISS-based spintronics technology has the potential to overcome the limitations of other magnetic-based memory technologies and to facilitate the fabrication of inexpensive, high-density memory and other spintronics elements.

Thin Film

Room 105A - Session TF-TuM

Advanced CVD and ALD Processing, ALD Manufacturing and Spatial-ALD

Moderators: Steven M. George, University of Colorado at Boulder, Jesse Jur, North Carolina State University

8:00am TF-TuM1 An Analytic Expression for Reactant Utilization in CVD and ALD Chambers, Edward McInerney, Lam Research Corporation

Recent advances in semiconductor device performance have depended, in part, on the adoption of new materials into the fabrication process. One of the challenges introduced with these materials is cost. In particular exotic reactants for CVD and ALD processes are often quite expensive. To use these materials efficiently, deposition chambers and processes must be designed to maximize reactant utilization while maintaining good deposition uniformity and film properties. In this presentation, an analytic expression for reactant utilization will be developed for CVD and ALD processes in parallel plate stagnation flow reactors. This expression will then be used to highlight the various approaches to achieving good utilization.

8:20am TF-TuM2 Growth of Silicon Films at Room Temperature Using Electron Enhanced Atomic Layer Deposition, Jaclyn Sprenger, A.S. Cavanagh, H. Sun, S.M. George, University of Colorado, Boulder

Electron enhancement can dramatically reduce the temperatures required for ALD. Electrons can desorb surface species, such as hydrogen, and create “dangling bonds”. These “dangling bonds” can facilitate reactant adsorption. Using sequential electron and reactant exposures, low temperature growth should be possible for the ALD of Si, SiN_x, SiC_x, C, and CN_x films that can be grown with hydride precursors. In this work, silicon films were deposited at room temperature using sequential Si₂H₆ (disilane) and electron exposures.

Silicon film growth using an electron flood gun was monitored with an *in situ* spectroscopic ellipsometer in the high vacuum chamber. A silicon growth rate of 0.2 Å/cycle for sequential Si₂H₆ and electron exposures was observed at room temperature with electron energies of 50 eV. *In situ* Auger electron spectroscopy (AES) revealed strong silicon AES signals with ~15 at.% carbon and <4 at.% oxygen impurities. *Ex situ* x-ray photoelectron spectroscopy (XPS) analysis was consistent with the *in situ* AES measurements.

Silicon films were also grown using electrons from a DC glow discharge plasma in a spatial ALD chamber. Deposition was performed at room temperature on 150 mm Si wafers. *Ex situ* spectroscopic ellipsometry measurements obtained a linear growth rate of 0.24 Å/cycle for sequential Si₂H₆ and electron exposures. This growth rate is in excellent agreement with the growth rate measured in the high vacuum chamber. Uniform silicon film thicknesses were obtained with a variation of only 3.0% along the axis of the slit from the DC glow discharge plasma. XPS depth-profiling analysis revealed that the silicon films contained ~10 at.% carbon.

8:40am TF-TuM3 Chemical Vapor Deposition within the ALD window – Quantitative Analysis of Precursor Surface Kinetics in Thin Film Formation, Michael Reinke, Y. Kuzminykh, P. Hoffmann, Empa, Swiss Federal Laboratories for Materials Science and Technology, Switzerland
INVITED

All chemical vapor deposition (CVD) processes rely on the decomposition of precursors on the substrate to deposit the desired material. While in thermal CVD, high substrate temperatures are employed to induce pyrolytic decomposition of the adsorbed precursor molecules, lower temperatures are applied in atomic layer deposition (ALD) to deliberately avoid pyrolysis of the precursor and favor self-saturating surface reactions between two or more reactive partners.

A crucial aspect in ALD processes is the proper separation of reactive partners in order to prevent spontaneous gas phase condensation; this is most commonly achieved in a vacuum process where the reaction volume

Tuesday Morning, November 8, 2016

is sequentially filled with one of the different reactive partners and their exposure is separated by a purge time. Contrary, in spatial ALD the substrate is moved through different reaction volumes that are continuously filled with one reactive partner allowing decreased cycle times and, consequently, increased growth rates.

An alternative way of separating reactive precursor molecules is realized in a high vacuum chemical vapor deposition (HV-CVD) process. If the background pressure during the deposition is sufficiently low, the free mean path of precursor molecules exceeds their trajectory length between effusion source and substrate – in this way gas phase reactions are avoided and the substrate can be simultaneously exposed even to reactive ALD chemistries.

Exemplary, we will review in detail the thin film deposition process of titanium dioxide utilizing titanium tetraisopropoxide (TTIP) and water. We demonstrate the continuous CVD growth of titanium dioxide thin films within the ALD window and show that even selective growth methods applicable in ALD are suitable for HV-CVD processes.

We will discuss a comprehensive surface kinetic model of the TTIP surface reactions, including hydrolysis and pyrolysis. The model was fitted to the large number of experimental results and can describe the experimental observations ranging from thermal CVD depositions to co-depositions with water in the ALD window. The model's good agreement with the experimental data in a wide parameter range suggests its high relevance.

The proposed model and the derived process parameters can be used for quantitative predictions of the precursor behavior in CVD processes, such as prediction of growth rates, deposition efficiencies and pyrolytic decomposition threshold. It reveals furthermore insight in the ALD process itself and allows modelling of the ALD growth rates - including the position of the ALD window.

9:20am TF-TuM5 A Rotation Fluidization Coupled Atomic Layer Deposition Reactor for Nanoparticle Coating, C.L. Duan, State Key Laboratory of Digital Manufacturing Equipment and Technology, School of Mechanical Science and Engineering, Huazhong University of Science and Technology, China; R. Chen, State Key Laboratory of Digital Manufacturing Equipment and Technology, School of Mechanical Science and Engineering, School of Optical and Electronic Information, Huazhong University of Science and Technology, China; Kun Cao, Huazhong University of Science and Technology, Wuhan, China

Atomic layer deposition (ALD) is an attractive approach for atomically controllable and conformal coatings on nanoparticles (NPs) for the fields of catalysts, optical detections, biomedicines, etc. There have been many kinds of ALD reactors for particles. Some of these designs are static reactors which rely on long time precursor diffusion to coat particles. Fluidized bed reactors utilize gas flow to disperse nanoparticles for enhanced gas-solid interactions, though obtaining steady fluidization of nanoparticles and limited precursor residence time are challenges. Rotary reactors disperse particles through rotary agitation and increase precursor usage by a static exposure stage.

In this talk, a rotation fluidization coupled atomic layer deposition reactor will be introduced. Such design allows the fluidization to facilitate the precursor transport in the particle bed and intensify the dynamic breaking up of the particle agglomerates to expose particle surfaces to precursors. In the deposition procedure, the coating process could be expedited due to the enlarged and homogenized void fraction in the particle bed, large gas distribution area and higher particle concentration in the rotating fluidized bed. The rotation not only enhances the gas-solid interactions to stabilize fluidization, but also provides large centrifugal force to break up soft agglomerates together with the fluid drag force derived from gas-solid interactions and the collision between particles. In situ mass spectrometry monitoring of the reaction was performed to optimize the coating process. Under high precursor feed rate, the precursor utilization was improved from below 80% to nearly 100% with thicker rotating bed. The microscale morphology of the coating layers, the macro statistical element mass concentrations and the changes of specific surface area as well as the size distribution after coating confirmed the uniformity and conformity of coatings on individual particles. As an example, magnetic Fe₃O₄ nanoparticles have been uniformly coated with ultrathin Al₂O₃ passivation layers using this reactor. With 5nm coating layer, the nanoparticle could be stable under oxidation resistance with minimum magnetization loss (less than 10%). This is quite attractive in practical magnetic based biomedical applications. Well controllable amorphous Al₂O₃ passivation layers were also deposited on crystalline AlH₃ particles to postpone their decompose

process, which could enhance the safety storage or transportation of these energetic materials.

9:40am TF-TuM6 Atmospheric Pressure ALD in Porous Substrates: The Effect of Pressure on Step Coverage, E. Balder, F. Roozeboom, Paul Poodt, Holst Centre / TNO, Netherlands

ALD is renowned for its ability to deposit thin films into high aspect ratio structures with step coverages realized that are unparalleled by other gas-phase deposition techniques. This is one of the reasons ALD has become a key deposition technique in microelectronics fabrication. In the past years, Spatial ALD concepts have evolved for high throughput, large-area and roll-to-roll ALD applications in e.g. photovoltaics and flexible electronics. A new challenge for Spatial ALD is coating inside porous and 3D substrates, e.g. for applications in energy storage, catalysis and membranes. In many cases, Spatial ALD is performed at atmospheric pressure.

There are several studies where the relation between precursor dose and step coverage has been investigated. The most famous one is the kinetic model derived by Gordon *et al.* [1] that gives an analytical estimation of the precursor dose required to conformally coat a pore as a function of its aspect ratio. The pressure dependence of conformal coating in pores is in the transport of precursor molecules by diffusion along the length of the pore, given by the diffusion coefficient. Unfortunately, the diffusion coefficient is not a variable in the Gordon model.

We have derived an alternative kinetic model that makes use of similar assumptions as used in the Gordon where the pressure dependence of the diffusion coefficient was included. Three regimes can be identified for diffusion inside pores: *pressure dependent* Fickian diffusion for large diameter pores, *pressure independent* Knudsen diffusion for small pore diameters and a transition regime between the two. Combining the pressure dependence of the diffusion coefficient, the kinetic model and experimental data we can calculate the required precursor dose required to conformally coat a pore as a function of pore diameter and reactor pressure. A similar analysis can be performed on the required purge time to empty a pore of reactants.

The main results we will show are that 1) for pores smaller than ~1 μm diameter, there is no difference in atmospheric and low pressure ALD with respect the required precursor dose, 2) for larger pores there is a pressure dependence of the diffusion coefficient and 3) in terms of *deposition rate* it is beneficial to use higher reactor pressures to allow high precursor partial pressures leading to high diffusion- and reaction rates. Based on these experimental and modeling results we will finally give an outlook to the feasibility of large-area or roll-to-roll atmospheric pressure Spatial ALD of conformal coatings in high aspect ratio substrates.

11:00am TF-TuM10 New Spatial ALD platform for Semiconductor Manufacturing, Joseph Yudovsky, Applied Materials, Inc. INVITED

Adoption of Atomic Layer Deposition (ALD) for semiconductor manufacturing has more than doubled over the past 3 years driven by inflections in both logic and memory devices from planar to 3D structures requiring conformal deposition and is set to double again over the next 3 to 5 years as the need for continued device scaling is expected to drive the need for unique and differentiated ALD films. The use of Spatial ALD techniques serves as a disruptive means compared to conventional ALD processes to address the needs of this rapidly growing market. Though Spatial ALD is not new, having been used in volume production for solar cells and Roll-to-Roll systems, adapting spatial ALD technology for the semiconductor market where device performance requirements demand a magnitude higher level of film deposition control faces numerous challenges. In this presentation, we will review the hardware challenges associated with adapting spatial ALD technology to high volume semiconductor manufacturing, and our design approach used in developing a new ALD platform to address those challenges.

11:40am TF-TuM12 Spatial MLD of Polyamide Films on Flexible Substrates using a New Rotating Cylinder Reactor in a Custom Oven, Daniel Higgs, University of Colorado Boulder; S.M. George, University of Colorado at Boulder

Molecular layer deposition (MLD) is usually restricted by the low vapor pressure of the organic reactants. This low vapor pressure could be especially problematic during spatial MLD when rapid substrate speeds limit the reactant exposure times. To address this problem, we have developed a new spatial MLD reactor. The new spatial MLD reactor is based on a rotating cylinder inside an outer fixed cylinder with dosing, pumping and purging modules. In addition, the spatial MLD reactor and the reactants are both located in an isothermal environment using a custom

Tuesday Morning, November 8, 2016

oven. This isothermal environment avoids any possible cold spots in the apparatus.

We have used the new spatial MLD reactor to deposit a polyamide network polymer on a metalized PET polymer substrate. The polyamide network polymer is derived from trimesoylchloride and m-phenylenediamine. This polyamide network polymer has application as a reverse osmosis membrane for desalination. We observed polyamide MLD growth rate of 4.5 Å/cycle at 115°C. The rotating cylinder can be rotated at up to 200 RPM and achieves substrate speeds up to 3 m/s. This reactor can produce growth rates of up to 14 Å/s. The growth of the polyamide MLD film is linear with number of MLD cycles. We could routinely grow polyamide MLD films with thicknesses of 4000 Å in 5 minutes. Polyamide MLD film growth was confirmed using transmission Fourier transform infrared spectroscopy (FTIR) and microRaman spectroscopy.

In addition to the desalination membrane application, these polyamide network polymer films will be useful for flexible gas diffusion barriers. One major difficulty for ALD gas diffusion barriers on polymers is the presence of particles on the initial polymer substrate. These particles mask the polymer surface during ALD and then “fall off” leaving behind pin-hole defects in the ALD film. One solution is to bury all the particles in a thick MLD film and then perform ALD on the surface of the MLD film. We have recently coated a PEN polymer substrate with a MLD polyamide film with a thickness of ~1 µm. After deposition of a 50 nm Al₂O₃ ALD gas diffusion barrier film, the number of pin-hole defects in the Al₂O₃ gas diffusion barrier film reduced by an order of magnitude.

12:00pm **TF-TuM13 Spatial Atomic Layer Deposition for Porous and Fibrous Materials**, *Gregory Parsons, A.H. Brozena, C.J. Oldham*, North Carolina State University

Although there are few thin film deposition methods which can coat complex substrates, such as fibers and membranes, with as high a degree of conformality as atomic layer deposition (ALD), slow growth rates and other scaling limitations have prevented the industrial application of ALD to these materials.

To increase the speed of thin film deposition, researchers have developed spatial ALD as way to scale up traditional ALD systems. By flowing reactants continuously through alternating channels and moving the substrate beneath these reactant flows, thin films can be deposited at rapid speed. However, current spatial ALD systems are designed for solid or solid-backed substrates, such as silicon wafers. The technique has not yet been demonstrated on porous or fibrous substrates, such as woven or non-woven textiles.

To achieve rapid spatial ALD growth on these kinds of porous materials, we modeled and built a flow-through spatial ALD reactor for roll-to-roll deposition of Al₂O₃, using non-woven polypropylene fabric as the test substrate. The tool is operated under open atmospheric conditions and does not use expensive vacuum equipment. The reactor's shower-head design utilizes alternating gas-flows of nitrogen, trimethyl aluminum, and water to produce three complete ALD cycles for a single traversal of the substrate. More ALD cycles can be additively deposited with increasing passes of the substrate. The gases flow through the material and are vented away using a slight negative pressure generated by facility exhaust. With this prototype flow-through spatial ALD reactor, we study how gas flow rates, fabric porosity, and web speed affect self-limiting ALD growth. By monitoring changes to the surface energy of the polypropylene using water contact angle and comparing the spatial ALD coated materials to batch-coated samples, we learn what conditions are necessary to achieve high-throughput, roll-to-roll ALD coatings on porous samples.

Vacuum Technology

Room 104C - Session VT-TuM

Vacuum Pumping and Material Outgassing

Moderators: Martin Wüest, INFICON Ltd., Liechtenstein, Jacob Ricker, NIST

8:00am **VT-TuM1 Applicative Challenges for today's Turbo Molecular Pumps**, *Adrian Wirth, H. Bernhardt*, Pfeiffer Vacuum GmbH, Germany; *N. Cotton*, Pfeiffer Vacuum Inc

INVITED

Since its invention in 1958 by Mr. W. Becker, the turbo molecular pump (TMP) has been a milestone in showing new and effective ways of providing oil-free high vacuum. It soon started to replace available pumping principles and as the need for high vacuum grew, it became the standard for modern high vacuum applications. It has since been

confronted with increasingly diverse customer needs and performance challenges.

In most aspects, the requirements can be subdivided into primary (pump performance related) properties like pumping speed, gas throughput, compression, fore-vacuum compatibility and secondary ones. The latter including attributes of compactness, ease of system integration, corrosion and condensation insensitivity, usability in areas exposed to ionizing radiation, maintenance friendliness, outgassing and particle cleanliness, emission levels of vibrations, sound or electromagnetic radiation, lifetime and costs of ownership—just to name a few.

From the beginning, demanding applications and processes were on the one hand influencing the vacuum performance of the TMP, hence indirectly affecting the effective shape of the rotor and stator parts and its combination with other pumping principles. On the other hand, triggered by specific and extreme applications or operation settings and surroundings, the secondary requirements gained in importance.

Within this scope, some of today's applicative challenges and customer needs for TMPs will be presented. Examples will include the operation of TMPs exposed to magnetic fields in ion implanters or ionizing radiation at particle accelerators, in magnetic stray field and vibration sensitive systems such as electron microscopes, integrated into systems in analytics where low sound levels and the ease of integration are of special interest as well as in corrosive processes. Multi-port characteristic applications with rotor designs being specifically tailored for the individual vacuum performance require sophisticated calculation know-how. Apart from these operation purposes, the utilization in tool coating, nuclear fusion experiments, XUV lithography and mobile employments impose particular specifications. Furthermore an overview and comparison of process/requirement specific TMP designs will be provided.

The TMP had and still has to meet most diverse applications and hence undergoes a change from purely vacuum performance driven specification inputs into a period where also secondary requirements are ever since gaining in importance and hence impose a continuous evolution of the TMP technology.

8:40am **VT-TuM3 Ion Pump Design for Improved Pumping Speed at Low Pressure**, *Alessandro Abatecola, M. Audi*, Agilent Technologies, Italy

Although ion pumps are widely and mostly used in UHV conditions, virtually every existing Ion Pump has its maximum pumping speed around 10 E-6 mbar (10E-4 Pa). The discharge intensity in the Ion Pump Penning cell (the number of ions that bombard the cathode per unit time) is pressure dependent, and it is the main parameter that influences the pumping speed.

A study has been performed to evaluate the influence of magnetic fields and cell dimensions on the Ion Pump Discharge Intensity at different pressure. As a result, a combination of parameters has been defined that allows the design and manufacture of an Ion Pump with maximum pumping speed shifted towards lower pressures.

Experimental results with several different experimental set ups are presented.

A new 200 L/S Ion Pump specifically designed for UHV operation that incorporates these findings to obtain maximum pumping speed in the 10E-8 mbar (10E-6 Pa), and with all components subject to Vacuum Firing prior to assembly to obtain the lowest ultimate pressure is described.

9:00am **VT-TuM4 Multi Scaled Titanium Gettered Surfaces for Enhanced Pumping of H₂**, *Alan Van Drie*, Tri Alpha Energy

The sticking factor for any gas onto a flat surface, whether its physisorbed or chemisorbed can be enhanced by increasing the effective roughness of the flat surface. When done on multiple scale lengths, not unlike a fractal pattern, the sticking factor can approach unity. In the present case, we are interested in pumping H₂ by a fresh coating of titanium, which has a sticking factor of around 3-6% at room temperature on a flat surface. The shape of the fractal pattern and number of scale lengths that can be used is limited by the feasibility of coating titanium on all the exposed surfaces. Using three distinct scale length from ~20 cm, ~2 cm to sub-micron we are able to obtain an estimated 70-80% effective sticking factor. The sub-micron scale is achieved by depositing the titanium onto a cryogenically cooled surface that changes the film's morphology from a dense coating to a porous sub-micron needle like structure. This by itself increases the sticking factor from the normal 3-5% to 20-50%. Some deposition techniques can even create film morphologies with up to 90% sticking factor; eliminating the need for other macroscopic scale lengths. Using these techniques we can create a 2,000 m³/s pump for H₂, with 10 m²

Tuesday Morning, November 8, 2016

entrance area that fits within our 15 m³ vessels. The design principles and preliminary pumping speed and capacity measurements will be presented.

9:40am **VT-TuM6 Outgassing of UHV Stainless Steel Cans**, *Lily Wang, P.D. Honnell*, Los Alamos National Laboratory

UHV stainless steel cans are used to contain material samples in our experiments to study how the materials age under accelerated thermal conditions. In addition to characterizing the material properties after the thermal aging treatment, we also measure the amount of gas released during these thermal aging runs and analyze the off gas collected. In preparing for the experiments, the stainless steel cans were first vacuum-baked at 150°C to remove adsorbed moisture. The vacuum-baked cans were then brought into a dry nitrogen glovebox where the samples were loaded into these cans. The experiments were conducted in static vacuum at various temperatures ranging from 25 to 145°C for a duration ranging from 25 days to several years. The pressure of the gas accumulated in the sample can was measured with a capacitance diaphragm gauge. At each temperature, an empty UHV stainless steel can was also measured. Stainless steel contains dissolved hydrogen that diffuses out and contributes background outgas in vacuum systems. This talk will present the gas evolution results obtained from these empty cans and discuss how this stainless steel outgassing affects our gas evolution measurements.

11:00am **VT-TuM10 Calibration of Reference Samples for Water Vapor Outgassing and Water Vapour Transfer Rate**, *Janez Setina*, Institute of Metals and Technology (IMT), Slovenia; *K. Jousten*, Physikalisch-Technische Bundesanstalt (PTB), Germany

Water vapor is usually main constituent of residual gas in non-baked high vacuum systems. The principal source of water vapor is outgassing from surfaces of vacuum chamber. Significant amount of water vapor is adsorbed on the surfaces every time when the system is vented to moist ambient air. Outgassing rate of water vapor is therefore important parameter of any vacuum material and is needed for proper design of the system to operate in required pressure range.

Traceability of outgassing rate measurements was one of the research activities of the recently finished European project EMRP IND12. For calibration, validation and comparisons of outgassing rate measurement systems different reference outgassing samples were studied. In this presentation we will focus on the reference samples for water vapor outgassing, which were jointly developed and applied for patent by PTB and IMT [1]. For measurement and calibration of outgassing rate from reference samples for different gases, including water vapor, a dedicated vacuum system was developed at IMT. Measurement range of the system for water vapor outgassing rate at room temperature is from 5×10^{-7} mbarL/s to 5×10^{-3} mbarL/s (equivalent to 2×10^{-11} mol/s to 2×10^{-7} mol/s, or 3×10^{-5} g/day to 0.3g/day). Typical relative uncertainty of measured outgassing rate is below 5 %.

Results of calibration of two water vapor reference samples will be presented. One sample had nominal outgassing rate of water vapor 6×10^{-7} mbarL/s (2.5×10^{-11} mol/s, or 4×10^{-5} g/day) and another sample 3×10^{-5} mbarL/s (1.3×10^{-9} mol/s, or 2×10^{-3} g/day). Both samples represent constant outgassing rate over long period of time. Repeated measurements showed time stability of reference samples better than 3%/year.

The newly developed water vapor outgassing reference samples can be also used for calibration of measurement instruments for water vapor transfer rate (WVTR).

[1] Patent DE 102014200907 A1 (2015)

11:20am **VT-TuM11 Simulated and Measured Extreme High Vacuum in the Jefferson Lab Polarized Electron Source**, *Marcy Stutzman*, Thomas Jefferson National Accelerator Facility

The polarized electron source for the Jefferson Lab CEBAF nuclear physics program has stringent vacuum requirements for successful operation. Research projects aimed at improving the static vacuum into the extreme high vacuum range, below 10^{-12} Torr, have investigated outgassing rate reduction through coatings and heat treatments, vacuum characterization optimizing the utilization of commercial extreme high vacuum gauges, and pumping configurations including developments in UHV/XHV cryopumping. Additionally, limitation of dynamic vacuum during operation has been studied using surface analysis and processing toward reducing field emission from the high voltage electrode in the electron source. Both modeling and experimental results of these studies and the impact of incorporating these improvements in the vacuum system for the Jefferson Lab polarized electron source will be presented.

11:40am **VT-TuM12 Outgassing Rate Measurements of 3-D Printed Materials**, *Makfir Sefa, J.A. Fedchak, J. Scherschligt*, National Institute of Standards and Technology (NIST)

3-D printing of parts has many potential advantages over traditional machining. The outgassing rate of these materials is particularly interesting for determining their performance in a vacuum environment and for other practical applications. We measured outgassing rate of 3-D printed stainless steel and titanium samples. The outgassing rate was measured using pressure rate-of-rise method and throughput method. The outgassing rate of each sample was measured at room temperature. The composition of the desorbed gas was also determined. The experimental results and measurement procedure will be discussed in the presentation.

12:00pm **VT-TuM13 Characterization Studies of UHV Polished Surfaces**, *Melisa Buie, C. Fields*, Coherent Inc; *A. Cress*, San Jose State University

Interest continues to remain high in the application of electropolished surfaces. Studies of outgassing and surface treatments dating back to 1969 have remained relevant as science continues to push the lower boundaries of UHV. [1-5] More recently, polished stainless steel surfaces have been tested for use in high voltage applications. [6] The stainless steel flanges must have excellent sealing capability in low compression UHV joints, be able to withstand temperatures above 1200°C, increased corrosion resistance, and provide minimal outgassing.

A characterization study was performed comparing electropolished stainless steel flanges with plated and subsequently hand-polished stainless steel flanges to optimize the flange surface for temperature resistance, corrosion resistance, hermeticity, and outgassing. A randomized designed orthogonal experiment (full factorial) was performed varying the type of polish, the electrolytic exposure time, and post-polish processing temperature. Electropolished surface quality showed a strong interaction between the exposure time to the electrolytic bath and the post-process annealing temperature. Nickel electroplating followed by hand polishing showed resultant plating thickness inconsistencies along with an adverse effect at elevated temperatures.

References:

[1] J. R. Young, J. Vac. Sci. Technol. 6, (1969).

[2] N. Yoshimura, T. Sato, S. Adachi and T. Kanazawa, J. Vac. Sci. Technol. A 8, 924 (1990).

[3] K. Odaka and S. Ueda, J. Vac. Sci. Technol. A 13, 520 (1995).

[4] Y. Sasaki, J. Vac. Sci. Technol. A 25, 1309 (2007).

[5] P. Nunez, E. Garcia-Plaza, A. R. Martin, R. Trujillo and C. Dela Cruz, AIP Conf. Proc. 1181, 130 (2009).

[6] M. BastaniNejad, et. al., J. Vac. Sci. Technol. A 33, 041401 (2015).

Tuesday Lunch, November 8, 2016

Exhibitor Technology Spotlight

Room Hall C - Session EW-TuL

Exhibitor Technology Spotlight Session

Moderator: Chris Moffitt, Kratos Analytical Limited

12:40pm EW-TuL2 Spin-resolved Momentum Microscopy, *Thomas Stempel Pereira*, SPECS Surface Nano Analysis GmbH

We present a newly developed lens design which provides a full 2π solid acceptance angle with highest angular, energy and lateral resolution. In contrast to standard electron analyzers, electronic structure data from and beyond the 1st Brillouin zone is recorded without any sample movement. In addition the lens can work in a lateral imaging mode for microscopy as well. This enables navigation on the sample and reduces the size of the area under investigation down to a few micrometers in diameter. We have combined this lens design with two different kinds of energy dispersive elements: a time-of-flight section or a hemisphere. Both versions combine large acceptance angle, high angular resolution and small acceptance area, making these instruments the ideal tools for electronic structure studies on small samples or sample areas. The functionality of these instruments can be further enhanced by replacing the standard 2D-DLD detector with a spin-resolving imaging detector. The spin-resolved imaging is achieved by electron reflection at a W(100) spin-filter in the [010] azimuth at 45° reflection angle crystal prior to the 2D detector. Varying the scattering energy one can choose positive, negative, or vanishing reflection asymmetry.

1:00pm EW-TuL3 The New Generation of the Hemispherical Energy Analyser in the Novel Surface Science Research, *Lukasz Walczak*, PREVAC Sp z o.o., Rogow, Poland

The complexity and the range of materials and their surfaces studied will be expanded across a wide range of topics, including surface science, catalysis, corrosion, semiconductors research, photoelectrochemical energy conversion, battery technology, or energy-saving technologies [1-5]. An unique and exceedingly flexible analysis cluster with a detection system is needed for these fundamental and applied research. Here it will be described a new energy and angle resolved analyser for photoelectron spectroscopy. The analyser has a hemisphere shape with a mean radius of 150 mm and is based on combining an advanced focusing electron lens system, which can be operated in different modes, transmission, spatial resolution or angular resolution. An angular resolution of better than 0.06° and spatial resolution 100 μ m can be obtained. The spectrometer includes highly stable 6 kV power supply, where each independent voltage module achieves temperature stability below 0.5 ppm of the voltage span per degrees Celsius. The modern 2-D low noise CCD-MCP assembly with a noise level of < 0.01 cps/channel and a 70 fps fast camera are used. Fully automation and environmental software system make it a user-friendly tool for the conducted researches. The combination of the new generation hemispherical energy analyser with a liquid helium/nitrogen manipulators and modular PREVAC surface analysis system as part of multi-technique surface analysis systems will be presented, in order to permit complete characterization of the surface structure via XPS, UPS, ISS and APRES mapping. We will report the first results from this techniques, using analyser and induced by four interaction sources: X-ray, UV, electron or ion impact. Also the results of temperature dependent study on the metallic crystal will be presented. UV excited Xe5p spectra recorded in the gas phase show that the energy resolution is better than 3 meV at 2eV analyser pass energy. The application of the system will be shown on photovoltaic materials, graphene, or self-assembled organic monolayers of organic molecules. This analyser opens up new possibilities for angular/spatial resolved electron spectroscopy, band-mapping and other applications.

References

- [1] S. Bengió, et. al, Surf. Sci. **646**, 126-131 (2016)
- [2] B. Eren et. al, Science **29**, 475-478 (2016)
- [3] Z. Duan et. al, J. of Solid St. Electrochem. **19**, 2265-2273 (2015)
- [4] N. Tomaszewska et. al, Surf. Sci. **632**, 103-110 (2015)
- [5] K. Samson et. al, ACS Catalysis, **4**, 373-374 (2014)
- [6] Yi-Chun Lu et. al, Sci. Rep. **2**, 715 (2012)

1:20pm EW-TuL4 Latest Developments in XPS and Related Methods from Kratos Analytical, *Chris Blomfield, J.D.P. Counsell, S.J. Coultas, S.C. Page*, Kratos Analytical Limited, UK; *C. Moffitt*, Kratos Analytical Limited

The Axis Supra is the latest generation of XPS instrument from Kratos Analytical. In addition to offering enhanced energy resolution and

sensitivity for XPS, it has a 15 μ m small area spectroscopy capability and 1 μ m imaging. The instrument is designed to offer a high level of flexibility and can be fitted with a range of complimentary surface analysis techniques such as UPS, ISS, AES, along with an additional surface science station and a range of sample treatment capabilities. In addition to offering benchmark level performance, the instrument and ESCAPE data system combine to offer a high throughput platform optimized for the multiuser environment of today's surface analysis laboratory. Samples may be pre-aligned and analyses predefined so that, when combined with the automated sample transfer capability, high levels of throughput can be achieved with unattended operation. Applications of high resolution imaging, multispectral imaging, gas cluster ion source and GCIS-UPS studies will be presented on a range of new materials to underline the leading capabilities of the Axis Supra.

1:40pm EW-TuL5 What's New with Physical Electronics, *John Newman*, Physical Electronics USA

Learn about all the new advances with Physical Electronics.

Tuesday Afternoon, November 8, 2016

2D Materials Focus Topic

Room 103B - Session 2D-TuA

Novel Quantum Phenomena in 2D Materials

Moderators: Yoshi Iwasa, University of Tokyo, Japan, Kristian Thygesen, Technical University of Denmark

2:20pm 2D-TuA1 Time-dependent Density-functional Theory Simulation of Local Currents in Pristine and Single-defect Zigzag Graphene Nanoribbons, *S He, A. Russakoff, Y. Li, K. Varga*, Vanderbilt University

The spatial current distribution in H-terminated zigzag graphene nanoribbons (ZGNRs) under electrical bias is investigated using time-dependent density-functional theory solved on a real-space grid. A projected complex absorbing potential is used to minimize the effect of reflection at simulation cell boundary. The calculations show that the current flows mainly along the edge atoms in the hydrogen terminated pristine ZGNRs. When a vacancy is introduced to the ZGNRs, loop currents emerge at the ribbon edge due to electrons hopping between carbon atoms of the same sublattice. The loop currents hinder the flow of the edge current, explaining the poor electric conductance observed in recent

3:00pm 2D-TuA3 Studies of Conductance in Graphene Defects and Junctions using Complex-Injecting Potentials and TDDFT, *Cody Covington, K. Varga*, Vanderbilt University

In order to create nanoscale electronic devices, there is a need for making high quality electrical connections between functional regions or specific defects[1]. However, connecting dissimilar materials such as graphene and metals[2] may pose complications from differing densities of states and work functions, and predicting how the system is effected computationally can be challenging given the system size. To address these challenges, studies of the electrons flow through heterogeneous material junctions, using complex potentials on a real-space grid and Time-Dependent Density Functional Theory have been performed. By confining an electron into the conduction band at a single point and propagating the system in time, the wavefunction for the system in a specific conducting state can be solved. Considerations for junctions and use of injecting and absorbing potentials in regions of diminished electron density will be presented.

[1] J. Lahiri, Y. Lin, P. Bozkurt, I.I. Oleynik, M. Batzill, An extended defect in graphene as a metallic wire, *Nat Nano*, 5 (2010) 326-329.

[2] F. Xia, V. Perebeinos, Y.-m. Lin, Y. Wu, P. Avouris, The origins and limits of metal-graphene junction resistance, *Nat Nano*, 6 (2011) 179-184.

3:20pm 2D-TuA4 Excited Biexcitons in Two-Dimensional Transition Metal Dichalcogenides, *Daniel Kidd, D. Zhang, K. Varga*, Vanderbilt University

Recently, experimental measurements and theoretical modeling have been in a disagreement concerning the binding energy of biexcitons in transition metal dichalcogenides. While theory predicts a smaller binding energy (~20 meV) that is lower than that of the trion, experiments find values much larger (~60 meV), actually exceeding those for the trion. In this work, we show that there exists an excited state of the biexciton which yields binding energies that match well with experimental findings and thus gives a plausible explanation for the apparent discrepancy. Ground and excited states of the five-body exciton-trion are also investigated and shown to be bound.

4:20pm 2D-TuA7 Electron Talbot Effect on Graphene, *Jorge Salas*, Vanderbilt University

The Talbot effect for a graphene sheet as a grating, using electron matter waves, is simulated using density functional theory and solving the Helmholtz equation. The obtained Talbot images show focusing effects suggesting possible applications for reshaping electron wave-packets and interferometry [1].

[1] Salas, J. A., Varga, K., Yan, J.-A. & Bevan, K. H. Electron Talbot effect on graphene. *Phys. Rev. B* 93, 104305 (2016).

4:40pm 2D-TuA8 Femtosecond Hot Electron-Phonon Interactions of Single Layer Graphene and the underlying Substrate, *Zina Jarrahi, J.L. Davidson, N.H. Tolk*, Vanderbilt University

We study the effect of substrate on the femtosecond transient electron and phonon dynamics of single layer graphene transferred on finely polished diamond, sapphire and quartz. Through a comprehensive set of fluence and energy dependent ultrafast optical conductivity measurements, we show that the temporal evolution of the hot carriers in graphene, differ significantly depending on the underlying substrate. We observe much faster (slower) relaxation and less (more) pronounced band filling dynamics for graphene on diamond (quartz). We demonstrate that

the differences in the temporal evolution of the carrier temperature and inter/intraband transition interplay, cannot be accounted for by invoking the different static Fermi-levels of graphene on each substrate. These substrate-dependent dynamics are explained, using a multi-channel cooling picture, involving surface phonons of the substrate, intrinsic optical phonons of graphene, their competing scattering rates, phonon frequencies and the varying Fröhlich coupling strength of the different substrates. In this regard, the sub nm roughness of our studied substrates, enable a strong coupling between the photogenerated carriers in graphene and the surface vibrational modes of the polar substrates. We observe an increase in the carrier relaxation times as photoexcited carrier density is increased. This further confirms the existence of an additional relaxation mechanism through the substrate that competes with the intrinsic phonons of graphene to not only reduce the electron temperature but also carrier and optical phonon lifetimes. These results offer significant potential to selectively activate the desired energy relaxation channels in graphene and tune the carrier and optical phonon lifetimes, by simply varying the substrate and fluence regime. This knowledge will pave the road towards designing graphene-based (opto)electronics with highly tailored functionalities suited for specific device requirements.

5:00pm 2D-TuA9 New Opportunities in Two-Dimensional Material Research, *Yuanbo Zhang*, Fudan University, China **INVITED**

Two-dimensional (2D) atomic crystals, best exemplified by graphene, have emerged as a new class of material that may impact future science and technology. The reduced dimensionality in these 2D crystals often leads to novel material properties that are vastly different from that in the bulk. We refer to such a recurring scheme as "less is different". In this talk I will illustrate this scheme with two 2D materials that we found particularly interesting – black phosphorus and 1T-TaS₂. These two layered materials have vastly different properties. Black phosphorus is a 2D semiconductor, and its superior material quality has recently enabled us to observe the quantum Hall effect. 1T-TaS₂, on the other hand, is a metal with a rich set of charge density wave phases. We explore their electronic properties while the doping and dimensionality of the 2D systems are modulated.

5:40pm 2D-TuA11 Ultrafast Carrier Dynamics in the Quasi-2D Metal Dichalcogenide SnS₂, *Oliver Monti, C. Eads, D. Bandak*, University of Arizona; *D. Nordlund*, SLAC National Accelerator Laboratory; *M. Neupane*, US Army Research Laboratory

We use soft x-ray resonant photoemission and core-hole-clock spectroscopy to investigate the ultrafast carrier dynamics in SnS₂. We show that carriers delocalize on a time-scale of a few hundred attoseconds near the conduction band minimum, but remain localized over an order of magnitude longer in higher lying bands. On the basis of density functional theory calculations we are able to show that this is consistent with the 2D nature of SnS₂. Moreover, we show that these experiments map the wavefunction in the unoccupied bands. Our measurements represent the first of their kind on the carrier dynamics in such materials.

6:00pm 2D-TuA12 MBE Growth of WTe₂ for Novel Electronic and Topologically Protected Devices, *Lee Walsh, R. Yue, A.T. Barton, H. Zhu, L. Cheng, R. Addou, J. Hsu, J. Kim, M. Kim*, University of Texas at Dallas; *L. Colombo*, Texas Instruments; *R.M. Wallace, C.L. Hinkle*, University of Texas at Dallas

Transition metal dichalcogenides (TMDs) are 2D materials which belong to a class known as van der Waals materials where the adjacent layers are held together by weak van der Waals interactions and, in principle, have no surface dangling bonds, which permits a relaxed growth requirement in terms of lattice matching. This relaxed lattice-matching criteria allows us to couple these materials based primarily on their band alignment and electronic properties. WTe₂ is a TMD with an equilibrium structure in the distorted octahedral (1T') phase. This 1T' phase of WTe₂ is a semi-metal and hence may be implemented as a 2D metal in an all-2D heterostructure for new devices. Monolayer 1T' WTe₂ has been separately predicted to be a Weyl semi-metal and to behave as a relatively wide bandgap (>0.1 eV) topological insulator, possessing helical edge states which have a number of interesting properties including time reversal symmetry, spin-momentum locking, and ballistic transport^{1,2}. The trigonal prismatic (2H) phase of WTe₂ is viewed as an integral part of the tunnel field effect transistor (TFET) device due to its bandgap and effective mass and has been theoretically predicted to provide low power operation and sub 60 mV subthreshold swing. WTe₂ is truly a remarkable material with intriguing electronic properties owing to its strong spin-orbit coupling and layered crystal structure.

In this work, we demonstrate the first report of WTe₂ growth by molecular beam epitaxy (MBE) on a variety of substrate materials (Bi₂Te₃, MoS₂, and graphite). We will discuss the optimal MBE growth conditions (substrate temperature, flux rates etc.) along with in-depth structural and chemical characterization of the resultant single crystal thin films. Characterization was conducted via reflection high energy electron diffraction, transmission electron microscopy, scanning tunneling microscopy/spectroscopy, atomic force microscopy, X-ray photoelectron spectroscopy, and Raman spectroscopy. Challenges associated with Te incorporation and simple device and transport measurements will be presented.

This work is supported in part by the Center for Low Energy Systems Technology (LEAST), one of six centers supported by the STARnet phase of the Focus Center Research Program (FCRP), a Semiconductor Research Corporation program sponsored by MARCO and DARPA. It is also supported by the SWAN Center, a SRC center sponsored by the Nanoelectronics Research Initiative and NIST. This work was also supported in part by the Texas Higher Education Coordinating Board's Norman Hackerman Advanced Research Program.

1. A. A. Soluyanov et. al, *Nature***527**, 495 (2015).

2. X. Qian et. al, *Science***346**, 1344 (2014).

Applied Surface Science

Room 101B - Session AS+SS-TuA

Data Analytics in Surface Science and Nanoscience

Moderators: Anders Mikkelsen, Lund University, Sweden, Petra Reinke, University of Virginia

2:20pm **AS+SS-TuA1 Fast Strain Mapping of Nanowire Light-Emitting Diodes Using Nanofocused X-ray Beams**, *T. Stankevici*, Copenhagen University, Denmark; *U. Johansson*, *L. Samuelson*, Lund University, Sweden; *G. Falkenberg*, DESY, Hamburg, Germany; *R. Feidenhans'l*, Copenhagen University, Denmark; **Anders Mikkelsen**, Lund University, Sweden

Nanofocused X-ray beams are nondestructive probes that uniquely allow direct measurements of the nanoscale strain distribution and composition found at the interfaces and surfaces inside the micrometer thick layered structures of many electronic device architectures [1]. While the method has generally been considered time consuming, we demonstrate that by special design of X-ray nanobeam diffraction experiment we can (in a single 2D scan with no sample rotation) measure the individual strain and composition profiles of many structures in an array of upright standing nanowires [2]. We make use of the observation that in the generic nanowire device configuration, which is found in high-speed transistors, solar cells, and light-emitting diodes, each wire exhibits very small degrees of random tilts and twists toward the substrate. Although the tilt and twist are very small, they give a new contrast mechanism between different wires. In the present case, we image complex nanowires for nanoLED fabrication and compare to theoretical simulations, demonstrating that this fast method is suitable for real nanostructured devices.

We then go on to discuss the complications of data analysis as the amount of data available is dramatically increased with the advent of new highly coherent synchrotrons such as MAX IV in Lund Sweden [3] and improved experimental setups [2,4,5]. Using several detectors that give both real space fluorescence and 2D diffraction information combined with scanning both translational, rotational and time coordinates for in operando and in-situ studies in 3D - an enormous multidimensional dataset can be created in a few days. To fully retrieve all the information inside such dataset and pushing resolution and sensitivity limits new computational methods are needed in combination with advanced modelling.

[1] E. Lind et al., IEEE J. El. Dev. Soc. 3, 96 (2015); J. Wallentin et al., Science 339, 1057 (2013).

[2] T. Stankevici et al, ACS Nano 9 (2015) 6978

[3] "Ultimate upgrade for US synchrotron", Nature 501 (2013) 148

[4] U. Johansson, U. Vogt, A. Mikkelsen, Proc. SPIE 8851, X-Ray Nanoimaging: Instruments and Methods, 88510L (September 26, 2013); doi:10.1117/12.2026609

[5] T. Stankevici et al. Appl. Phys. Lett. 107 (2015) 103101

2:40pm **AS+SS-TuA2 Bellerophon Environment for Analysis of Materials (BEAM), A High Performance Computing Workflow Platform for Materials Research**, *E.J. Lingerfelt*, *A. Belianinov*, *E. Endeve*, Oak Ridge National Laboratory; *O.S. Ovchinnikov*, Vanderbilt University; *S. Somnath*, *R.K. Archiblad*, *S.V. Kalinin*, **Stephen Jesse**, Oak Ridge National Laboratory

Improvements in scientific instrumentation allow imaging at mesoscopic to atomic length scales, many spectroscopic modes, and now—with the rise of multimodal acquisition systems and the associated processing capability—the era of multidimensional, informationally dense data sets has arrived. Technical issues in these combinatorial scientific fields are exacerbated by computational challenges best summarized as a necessity for drastic improvement in the capability to transfer, store, and analyze large volumes of data. The Bellerophon Environment for Analysis of Materials (BEAM) platform provides material scientists the capability to directly leverage the integrated computational and analytical power of High Performance Computing (HPC) to perform scalable data analysis and simulation via an intuitive, cross-platform client user interface. This framework delivers authenticated, "push-button" execution of complex user workflows that deploy data analysis algorithms and computational simulations in HPC environments like Titan at the Oak Ridge Leadership Computing Facility (OLCF).

Here, we address the underlying HPC needs for characterization in the material science community, elaborate how BEAM's design and infrastructure tackle those needs, and present a small sub-set of user cases where scientists utilized BEAM across a broad range of analytical techniques and analysis modes. BEAM system will be demonstrated for 4D Ronchigram analysis and property extraction of atomically resolved STEM (Scanning Transmission Electron Microscopy) data, parallel spectroscopic curve fitting in SPM (Scanning Probe Microscopy) data, and image segmentation.

Acknowledgements

This work is partially supported by the Laboratory Directed Research and Development (LDRD) program at ORNL, which is managed by UT-Battelle, LLC, for the U.S. Department of Energy (DOE) under Contract No. DE-AC05-00OR22725 (E.J.L., A.B., E.E., O.O., S.S., C.T.S., S.V.K., M.S., and S.J.). This research was conducted at the Center for Nanophase Materials Sciences and the Spallation Neutron Source, which are DOE Office of Science User Facilities. Research by J.M.B. is supported by the Center for Accelerating Materials Modeling (CMM), which is funded by DOE Basic Energy Sciences under FWP-3ERKCSNL. This research used resources of ORNL's Compute and Data Environment for Science (CADES) and the Oak Ridge Leadership Computing Facility (OLCF), which are supported by the Office of Science of the U.S. Department of Energy under Contract No. DEAC05-00OR22725. The mathematical aspects were sponsored by the applied mathematics program at the DOE by the ACUMEN project.

3:00pm **AS+SS-TuA3 The Center for Advanced Methods for Energy Research Applications (CAMERA): Mathematical Methods for Data Science from Experimental Facilities**, **James Sethian**, University of California at Berkeley

INVITED

The Center for Advanced Methods for Energy Research Applications (CAMERA), jointly funded by the U.S. Department of Energy Offices of Advanced Scientific Research (ASCR) and Basic Energy Sciences (BES), focuses on mathematical models, algorithms, and codes that analyze, interpret, and understand the information contained within experimental data, particularly arising from light sources and nanoscale facilities. Initial focus areas include ptychography, tomography, grazing incidence small-angle scattering, image analysis and reconstruction methods, fluctuation scattering, single particle imaging, fast electronic structure methods, and automatic materials characterization and design. In this talk, we will describe the structure of CAMERA, and summarize some of the major projects. In particular, we will discuss work on: (1) Algorithms for real-time streaming ptychography. Ptychographical phase retrieval is a non-linear optimization problem, made tractable through exploiting redundancy inherent in obtaining diffraction patterns from overlapping regions of the sample. Here, we describe SHARP: our "Scalable Heterogeneous Adaptive Real-time Ptychography" framework that enables high-throughput streaming analysis. (2) New algorithms for fluctuation scattering and single particle imaging: In single particle diffraction (SPD) imaging, a large number of X-ray diffraction images are collected from individual particles, which are delivered to an ultrabright X-ray beam at random and unknown orientations through either a liquid droplet or aerosol delivery system. Recently, a new mathematical and algorithmic procedure has been introduced, known as "Multi-tiered Iterative Phasing" (MTIP), which

Tuesday Afternoon, November 8, 2016

simultaneously determines the orientations, 3D intensity function, complex phases, and the underlying molecular structure together in a single iterative process. (3) Machine learning methods for classification and characterization of scattering patterns. Grazing Incidence Small Angle X-ray Scattering (GISAXS) is an important reciprocal-space imaging modality which provides statistical information about a sample in 3-D. GISAXS is widely used for studying thin films that play a vital role as building blocks for the next generation of renewable energy technology. One challenge in GISAXS imaging is to be able to accurately infer properties of the material such as the crystal lattice corresponding to the sample from a single 2-D diffraction/scatter patterns. We will discuss our work using machine learning algorithms and convolution neural net classifiers to automatically provide structural details about the sample by analyzing the measured GISAXS diffraction patterns.

4:20pm AS+SS-TuA7 New Data Analysis Tools for X-ray Photoelectron Spectroscopy (XPS) and Spectroscopic Ellipsometry (SE), Matthew Linford, B. Singh, J. Bagley, Brigham Young University; J. Terry, Illinois Institute of Technology; A. Herrera-Gomez, CINVESTAV-Unidad, Mexico

Here we discuss a series of new data analysis tools for X-ray photoelectron spectroscopy (XPS) and spectroscopic ellipsometry (SE). For XPS, these include uniqueness plots, and the equivalent and autocorrelation widths. For SE, they include distance, principal component, and cluster analyses. Uniqueness plots are widely used in the SE community for identifying correlation between fit parameters. They are easily interpreted. However, they appear not to have been employed for XPS data analysis. And certainly better tools are needed to identify inappropriate peak fits to XPS narrow scans because (i) XPS is now receiving in excess of 10,000 mentions in the literature each year, and (ii) with the proliferation of the technique, the number of untrained users that are collecting and fitting data has significantly increased. In a number of reported peak fits, too many fit parameters have been introduced into the data modeling, which has reduced or eliminated the statistical meaning of these parameters. Uniqueness plots show the error of a fit as a function of one of the variables in that fit, where the values of a specified variable are systematically fixed to quantities about its optimal value. If the same, low error can be obtained for all the values of the variable in question, a horizontal line is obtained, which signals fit parameter correlation. Here, the same error is obtained because other variables in the fit can compensate for the systematic change to the variable in question. In contrast, if the error in the fit rises as the variable in question is systematically changed about its optimal value, the fit has uniqueness. Uniqueness plots that indicate the absence of fit parameter correlation are often parabolic in shape. We have applied uniqueness plots to the peak fitting of XPS C 1s narrow scans of ozone-treated carbon nanotube (CNT) forests that were obtained as part of a study on CNT-templated thin layer chromatography plates, and Si 2p narrow scans of oxidized silicon. In both cases, uniqueness plots showed that unconstrained fits had poor uniqueness, while more reasonably constrained fits had better uniqueness. These results indicate that uniqueness plots may be a valuable tool for identifying inappropriate peak fits in XPS. In this presentation, I will also briefly mention the use of the equivalent and autocorrelation widths in analyzing XPS narrow scans, and then focus on distance, principal component, and cluster analyses in SE data analysis. Our recent (2016) paper on this topic appears to be only the second example of the application of chemometrics to SE data analysis in the literature.

4:40pm AS+SS-TuA8 A Surface Investigation of Parchments using ToF-SIMS and Principle Component Analysis, Marie-Laure Abel, J.F. Watts, V. Vilde, University of Surrey, UK

Parchments are an historical writing support mostly used during the Middle Ages. Their popularity dates from the second century before Christ (BC) in Pergame, Turkey, from which the name originates. Unlike paper, parchment is made of animal skin with a process similar to that used to produce leather. The products used in the fabrication vary and any animal species can be used, although most historical parchments are made from sheep, goat and calf. Information of species recognition on parchments is currently provided either using proteomics or DNA analysis. However each technique presents difficulties and sometimes it is not possible to obtain an unambiguous result. Many valuable manuscripts are written on parchment such as the Magna Carta or the Codex Sinaiticus, which justifies the effort put towards the study of this material in order to improve the conservation process and to learn more about its history.

In this work, a new technique was used in order to assess if any information may be gleaned and help in the process of recognition or even

providing any further information to conservators to be used for preservation of historical parchment. Time of flight secondary ion mass spectrometry (ToF-SIMS) has been applied to the analysis of parchment specimens. Indeed while ToF-SIMS has been previously applied to a variety of samples of some significance in the cultural heritage field such as paintings or mummies, it has not been applied to parchments. To facilitate the data treatment process, this has been coupled with data analysis using chemometrics, namely principle component analysis (PCA).

A series of specimens of various ages and species were analysed on both sides, "skin" and "flesh". These samples included sheep, goat and calf. In addition, an unknown sample was also introduced to ascertain if its characteristics could be shown to be close to any species. Results indicate that it is fairly straightforward to distinguish between goat and sheep while calf is more difficult to separate from other species which is unexpected as biologically goat and sheep are considered the closest species within the selection. Furthermore the unknown specimen exhibits data which would classify it as a goat specimen. Considering the sides examined separations are seen within one particular species but the direction of the variation is not the same from one species to another. More work is needed to ascertain which side is being analysed for any unknown materials as the behaviour varies amongst the species examined in this work.

5:00pm AS+SS-TuA9 Multivariate Analysis of Very Large Hyperspectral SIMS Datasets: What Can We Do, and What Would We Like to Do?, Henrik Arlinghaus, ION-TOF GmbH, Germany INVITED

Advances in instrumentation capabilities, as well as increases in the complexity of modern materials have resulted in a corresponding increase in the size and complexity of data acquired during sample analysis. The increase in the spatial and spectral resolution of the instrumentation is nominally a boon to the analyst, as the measured data more accurately depicts the sample. However, the resulting hyperspectral images routinely consist of upwards of ten thousand pixel spectra for 2D analyses (e.g. a 128x128 pixel image), or millions of voxel spectra for 3D analyses, each of which may consist of hundreds or thousands of ion peaks. Because of the sheer amount of information contained within such an image, it is often no longer feasible to conduct a full manual analysis of the data. An additional factor exacerbating this issue is the fact that many studies necessitate the analysis of a series of spatially resolved replicate measurements of a single sample, or of multiple similar samples. In these studies the aim is not only to characterize the contents of each individual measurement, but also to determine the similarities and differences between the measurements, while ignoring subtle differences caused by changes in analysis conditions between the individual measurements.

A solution to the problem of information overload is the use of multivariate analysis techniques to help guide the analyst, in order to reduce the time needed for determining the chemical make-up of the analyzed samples. These techniques use different approaches in order to reduce the dimensionality of the measured data, resulting in a small set of factors which recreate a simplified model of the data.

The use of MVA approaches, such as Principal Component Analysis (PCA) and Maximum Autocorrelation Factors (MAF), has become an established method of simplifying the analysis of SIMS data arising from a single measurement. We will discuss alternatives to these commonly used methods, including new variations of Multivariate Curve Resolution (MCR) which use additional optimization criteria, as well as MVA approaches not commonly used in SIMS data analysis. Additionally, we will discuss the unique challenges which may arise when applying MVA techniques to the full hyperspectral data contents of a series of measurements.

5:40pm AS+SS-TuA11 High mass-resolution 3D ToF-SIMS: PCA and visualization in seconds using Graphical Processor Units (GPUs), Peter Cumpson, I.W. Fletcher, N. Sano, A.J. Barlow, Newcastle University, UK

Multivariate analysis offers the exciting prospect of unlocking the information content of 3D SIMS of complex organic and biological samples with sub-micron resolution. However applying principal component analysis (PCA) to large images or 3D imaging depth-profiles has been difficult until now because of the Gb to Tb size of the matrices of data involved. The result has always been an "out of memory" error.

Recently[1] we applied two algorithms, RV1 and RV2, originally developed by Halko *et al*[2] that improve the speed of PCA and allow datasets of unlimited size respectively, even on ordinary personal computers. In this presentation we show results of applying these algorithms to perform PCA on full 3D ToF-SIMS data of several examples of plant and small animal tissue. The datasets we process in this way are typically 128x128 or 256x256 pixel depth-profiles of around 100 layers, each voxel having a

70,000 value mass spectrum associated with it, giving datasets of at least 1Tb in size when uncompressed. These data were acquired using our Ionoptika J105 and IonTOF IV instruments, with Helium Ion Microscope images of particular key features.

Even for such large datasets a rapid PCA calculation is often needed during analysis sessions to inform decisions on the next analytical step. We have therefore implemented the RV1 algorithm on a PC having a Graphical Processor Unit (GPU) card containing 2,880 individual processor cores[3]. This increases the speed of calculation by a factor of around 4 compared to what is possible using the fastest commercially-available desktop PCs, and full PCA is now performed in less than 7 seconds.

We then use the GPU to allow real-time interactive visualization of the principal components in 3D. This leads to some spectacular and information-rich tomographic images that can be an excellent basis for discussion between analysts and the biologists and medics who understand the morphology and anatomy of their tissue samples.

[1] P J Cumpson *et al*, *Surf. and Interface Anal.* **47** (2015) 986-993.

[2] N P Halko *et al*, *SIAM Review, Survey Rev. Sec.* **53** (2011) 217–288.

[3] P J Cumpson *et al*, *Surf. and Interface Anal.*, onlinelibrary.wiley.com/doi/10.1002/sia.6042/full

6:00pm **AS+SS-TuA12 Mass Spectrometry Image Fusion, Bonnie June Tyler**, Universität Münster, Germany; *H.F. Arlinghaus*, University of Muenster, Germany

As mass spectrometry imaging (MSI) has moved from the technique development stage into real world biological studies, the need to combine mass spectrometry images with other biologically relevant imaging techniques has become important. Techniques as diverse as electron microscopy, scanning probe microscopy, XPS imaging, H&E staining, and fluorescent labeling can provide important information that is complementary to the mass spectral images. Combining the information from these complementary measurements is often necessary for accurate understanding of biological samples. Within the field of mass spectrometry imaging alone, combining different imaging modes, such as MALDI/ToF-SIMS, or GCIB ToF-SIMS/LMIG ToF-SIMS, can enhance understanding of the specimens being studied.

In theory, more data should enable more confident conclusions. In practice, however, the challenges of handling and reducing very large imaging data sets, that have disparities in spatial resolution and contrast mechanisms, can result in biased or misleading conclusions. In order to facilitate more consistent, accurate and useful descriptions of real world samples, advanced data exploration tools are needed. Image fusion is an approach to combining data from different sources that is receiving increasing attention within the field of mass spectrometry imaging.

Although many algorithms for image fusion have been developed for applications in remote sensing, medical imaging and photography, the distinctive features of mass spectrometry make many of these techniques inappropriate for use in this field. We have tested algorithms from two major classes of image fusion, those that operate in the spatial domain and those that operate in the frequency domain. Common artefacts caused by the different algorithms have been identified. Two modified algorithms have been developed which can be used to produce satisfactory fused images using mass spectrometry data. The first approach combines multivariate analysis (MVA) and discrete cosine transform (DCT) and is useful for combining MSI images with monochromatic images. The second algorithm, which uses a combination of multivariate methods, is useful for fusing MSI data with a second spectral image. Both of these new image fusion approaches have been tested on simulations, model systems and real tissue samples. We have shown that MVA image fusion can be a valuable technique for reducing noise, improving image contrast and enhancing the sharpness of mass spectrometry images. With appropriate attention to the distinctive features of each imaging method, image fusion can be done without significant artefacts or distortion of the spectral detail.

Biomaterial Interfaces

Room 101A - Session BI+AS+SA-TuA

Biophysics and Characterization of Biological and Biomaterial Surfaces

Moderators: Eva Chi, University of New Mexico, Axel Rosenhahn, Ruhr-University Bochum, Germany

2:20pm **BI+AS+SA-TuA1 Resolving Non-specific and Specific Adhesive Interactions of Catechols at Solid/Liquid Interfaces at the Single Molecular Scale**, *T. Utzig*, Max-Planck Institut für Eisenforschung GmbH, Germany; *P. Stock*, Max Planck Institut für Eisenforschung GmbH, Germany; *Markus Valtiner*, Technische Universität Freiberg, Germany

The adhesive system of mussels evolved into a powerful and adaptive system with affinity to a wide range of surfaces. It is widely known that thereby 3,4-dihydroxyphenylalanine (Dopa) plays a central role. However underlying binding energies remain unknown at the single molecular scale. Here, we use single molecule force spectroscopy to estimate binding energies and binding mechanism of single catechols with a large range of opposing chemical functionalities. Our data demonstrates significant interactions of Dopa with all functionalities, yet most interactions fall within the medium-strong range of 10-20 k_BT. Specifically, Dopa-molecules interact with surfaces exposing different functionalities via different types of interactions ranging from bidentate H-bonding plus metal coordination (titania), monodentate H-bonding (SAMs exposing H-donor or H-acceptor headgroups), the hydrophobic interaction (alkyl SAM) or interactions involving the p-electron system of Dopa's catechol ring (gold). Only bidentate binding to TiO₂ surfaces exhibits a higher binding energy of 29 k_BT. Our data also demonstrates at the single molecule level that oxidized Dopa and amines exhibit interaction energies in the range of covalent bonds, confirming the important role of Dopa for cross-linking in the bulk mussel adhesive. We anticipate that our approach and data will further advance the understanding of biologic and technologic adhesives.

2:40pm **BI+AS+SA-TuA2 Protein-Nanoparticles Interactions: Surface Chemistry, Protein Corona and Secondary Structural Changes**, *I. Ojeda*, R. Capomaccio, L. Calzolari, D. Gilliland, P. Colpo, **Giacomo Cecccone**, EC-JRC-IHCP, Italy; *G. Siligardi*, R. Hussein, Diamond Light Source, Oxfordshire, UK

The characterisation of protein corona formed around nanoparticles is a very important and challenging issue in the investigation of nanomaterials behaviour in biological environment and has been studied by many authors [1, 2, 3,4].

On the other hand, it is recognized that detailed physico-chemical characterization of nanomaterials is becoming increasingly important both from the technological and from health and safety point of view. Moreover, an incomplete characterisation may inhibit or delay the scientific and technological impact of nanoscience and nanotechnology [5]. In this respect, surface chemical analysis methods, such as X-ray Photoelectron Spectroscopy (XPS) and Time of Flight Secondary Ion Mass Spectrometry, can provide an important contribution to more fully characterizing nanomaterials [6].

In this work, we have investigated the interaction of human serum albumin (HSA) with gold nanoparticles (AuNPs) functionalized with thiols. In particular, 15 nm AuNPs functionalized with PEG thiols have been studied before and after interaction with HSA.

The different steps of sample preparation have been characterised by DLS, CPS and TEM, whilst the surface chemistry has been mainly assessed by XPS. Finally, the interaction between nanoparticles and HSA has been studied by Synchrotron Radiation Circular Dichroism (SRCD) to gather information on the protein structure [7]. In particular, XPS and ToF-SIMS data revealed the presence of HSA on pegylated nanoparticles, whilst the use of SRCD in combination with separation techniques allowed the determination of the structure and morphology of HSA-AuNPs complexes [8]. Moreover, SRCD experiments indicate that AuNPs increase the UV and thermal stability of HSA.

[1] Bigdeli A., *et al.*, *ACS Nano*, **2016**, DOI: 10.1021/acsnano.6b00261

[2] Huang R., *et al*, *Nanoscale*, **2013**, *5*, 6928–6935

[3] Winzen S., *et al.*, *Nanoscale*, **2015**, *7*, 2992–3001

[4] Lynch I. and Dawson K.A., *NanoToday*, **2008**, *3*(1-2) 42-47

[5] Baer D, *et al.*, *Anal. Bioanal. Chem.*, **2010**, *396*(3), 983–1002

[6] Grainger D and Castner D, *Adv. Mater.*, **2008**, *20*, 867–877

[7] Laera S., *et al.*, *Nanoletters*, **2011**, *11*, 4480–4484.

Tuesday Afternoon, November 8, 2016

[8] Capomaccio R., et al., *Nanoscale*, **2015**, 7, 17653–17657.

3:00pm **BI+AS+SA-TuA3 Measuring the Impact of the Surface of Protein Stability using Single Molecule Experiments with the AFM, Phil Williams, S. Allen, A. Oyefeso, G. Milson, E. Fornari, University of Nottingham, UK**

INVITED

Seven out of the top eight top-selling medicines of 2014 were biological in origin (so-called biopharmaceuticals or biologics). Successful formulation of such biopharmaceuticals has created new challenges to the pharmaceutical industry since the physical and chemical properties of the biological molecule (protein, peptide, RNA, DNA) differ from those of small 'classical drug' molecules. Whilst single molecule force spectroscopy has given new insight to many ligand/receptor interactions, the requirement to chemically functionalize the surfaces of both the substrate and the tip render the technique of little interest to the pharmaceutical industry since such functionalization, by definition, changes the chemistry of the ligand and receptor. Furthermore, this experimental methodology precludes effective screening of agents binding to a target receptor.

I will highlight our development of a fragment screening methodology using the AFM for single molecule force measurements without chemical modification of the ligands. I will introduce the method validating its approach using the streptavidin/biotin system that is often used as a model. I will then demonstrate the potential of the methodology to find fragments that interact with thrombin, a target for cardiovascular disease therapy.

In developing the above approach, it became apparent that actually neither the tip nor the substrate needs to be functionalized. I will conclude by discussing a promising method to screen for excipients that may stabilize protein structure in formulation and storage, where no chemical functionalization is necessary. The technique permits the measurement of the stability of proteins to be measured through their susceptibility to denaturants, such as urea and guanidinium chloride, and the effect of excipients on the measured stability to be assessed. For some proteins, the stability measured through traditional bulk methods, such as fluorescence, match those measured using the AFM, whereas for others there appears to be a significant difference. I propose, therefore, that this AFM method offers an interesting way to study protein denaturation at an interface.

4:20pm **BI+AS+SA-TuA7 In Vitro Characterization of Interfaces for the Development of Antibacterial and Biocompatible Surfaces, Katharina Maniura, Empa, Swiss Federal Laboratories for Materials Science and Technology, Switzerland**

INVITED

Cell culture and bacterial studies of novel materials and new functional surfaces often show very poor correlation with clinical outcomes. This fact not only poses a major challenge for basic and industrial researchers, it is also associated with high costs.

Generally, the majority of biomaterials are tested using *in vitro* cell monocultures, however, this approach neglects possible synergistic interactions between different cell types and paracrine signalling mediating the tissue-specific response to a material.

Immediately upon implantation, medical implants get exposed to the patient's blood and this initiates the first phase of wound healing and subsequent cell recruitment and response deciding about material integration or non-integration.

We have established that blood pre-incubation of implant surfaces mimics a more physiological situation, providing a more predictive *in vitro* model for the evaluation of novel implant surfaces.

Similarly, many promising antimicrobial materials failed to make the translation from bench to bedside, partially due to insufficient *in vitro* biofilm models used for predicting the long-term *in vivo* antimicrobial and anti-biofilm activity. For the evaluation of novel surfaces the actual forseen implantation location and its biological environment need be considered to design a more predictive bacterial study with conditions mimicking the *in vivo* situation.

5:00pm **BI+AS+SA-TuA9 Vibrational Sum-Frequency Scattering Spectroscopy for Characterization of Biomaterial Interfaces in Biological Environments, Patrik Johansson, C. McDonald, Y.-C. Wang, P. Koelsch, D.G. Castner, University of Washington**

Most biomaterials have a 3-dimensional structure, of which the interfacial properties play an essential role in their interactions with biomolecules in the surrounding environment. The dynamics of protein adsorption onto biomaterials, and the induced conformational changes or selective orientations following such interactions, are phenomena that to a large

extent govern the biocompatibility of such materials. However, direct measurement of these interactions in biological environments are challenging as most techniques often (1) lack interfacial specificity, (2) require model samples with inherent limitations, or (3) lack specificity for the chemistry, orientation, and conformation of the probed species. In this work, we demonstrate how vibrational sum-frequency scattering (SFS) can be used to provide all this information, without the use of labels, from biomolecules specifically at the surface of biomaterials in biological environments.

We first show that SFS can yield chemical information via vibrational spectra selectively from molecules used to functionalize the surface of nanoparticles. Spectral changes upon addition of proteins to the samples do not only confirm adsorption onto the nanoparticles, but also provide information about the secondary conformation for the adsorbed proteins. It is likely that continuous development of SFS will make it an essential tool for evaluating the biocompatibility and other properties of nanoparticles for use in biomedical applications.

We have also applied SFS on protein fibers, for which a detailed understanding of the structure, function, interactions, conformation, and dynamics is critical for refining strategies in tissue engineering, as well as for the development of treatments for progressive diseases involving protein fibers, such as Alzheimer's disease (AD). In our studies, we have found that collagen fibers assembled *in vitro* exhibit a very large SFS cross-section, and that the spectral signatures are dependent on the scattering angle, implying that this parameter can be adjusted to selectively study specific features of the fibers. Data analysis routines, including maximum entropy method calculations, reveal the relative phase of various chemical groups in the fibers, which can be utilized for determining their relative orientations.

Finally, we have demonstrated that amyloid fibers and spherulites, which are structures found in the brain tissue of patients with AD, exhibit strong nonlinear optical properties. We believe that SFS can reveal new details about the development and interactions of these structures, which can provide clues about AD pathology and help finding new biomarkers for the disease.

5:20pm **BI+AS+SA-TuA10 Imaging ToF-SIMS of Human Breast Cancer Tissues: Connecting Chemical Images to Biology, Blake Bluestein, University of Washington; F. Morrish, D. Hockenbery, Fred Hutchinson Cancer Research Center; L.J. Gamble, University of Washington**

Breast cancer, the most common cancer among women, is known to vary in responsiveness to chemotherapy. Therefore, the role of changes in tumor metabolism affecting the response to chemotherapy is under scrutiny. Time-of-flight secondary ion mass spectrometry (ToF-SIMS) provides a powerful approach to attain spatially-resolved molecular data from cancerous tissues. We use imaging ToF-SIMS and principal components analysis (PCA) to study human biopsy tissue samples to clarify links between fatty acid composition within and around tumors and the potential drug resistance of these tumors. An important component of this project is ToF-SIMS analysis of pre and post neoadjuvant frozen patient specimens. Since treatment occurs with the tumor in place, analysis of biopsies taken pre- and post-treatment allows characterization of molecular changes in tumors as a response to treatment. Two sets of pre and post chemotherapeutic treated tissue have been studied. Additionally, 11 triple negative (TN) pre-treatment tissues have been studied using PCA to determine if molecular differences within tumor tissues can be correlated with patient response to treatment.

Data were acquired with an IONTOF TOF.SIMS V using a Bi₃⁺ analysis beam. Multiple 1mm² areas per tissue section were analyzed by stitching together 25 200μm² raster area scans. Data was acquired in both positive and negative polarities. Scores images generated by imaging PCA correlated with cellular and stromal areas were then used as masks to select regions of interest (ROI) that were reconstructed with ToF-SIMS software. Reconstructed spectral data of cellular and stromal areas was subsequently analyzed using PCA to ascertain molecular differences between tumor tissues.

Utilizing ROIs to select specific regions within analysis areas followed by spectral PCA for two different sets of pre and post treatment tumor biopsies showed a near distinctive chemical separation between pre and post. Chemical differences observed between the pre and post treatment tissue biopsies were related to changes in fatty acids, monoacylglycerols, diacylglycerols and cholesterol. Pretreatment samples showed higher loadings for vitamin E and C18:1 while post treatment samples had higher loadings for sphingomyelin and saturated fatty acids (stearic acid and

palmitic acid). Spectral PCA of cellular and stromal region data from the 11 TN tissues separates patients that respond to chemotherapy and those that do not. Patients that respond to chemotherapy show higher loadings of sphingomyelin and saturated fatty acids, while nonresponding patients correlate with loadings of cholesterol, C18:1 and C18:2.

5:40pm BI+AS+SA-TuA11 Some of These Images are Just Like the Others: Finding Similar Images in Imaging Mass Spectrometry Data Sets, Daniel Graham, L.J. Gamble, University of Washington

Mass spectrometry imaging (MSI) has been applied to many areas of research due to the rich chemical information it can provide. However, MSI also brings a set of challenges due to the enormous size of the data sets. Most modern imaging mass spectrometers produce data that consists of a full mass spectrum at every pixel of each image. This data set can be analyzed either as a series of spectra from a given area of the image, or as a series of images from a given set of peak masses. When looking at a series of images, it is of interest to find all masses that have the same spatial distribution since this could provide information about the chemical differences seen throughout a sample, and identify fragments that originate from the same molecules or that co-localize within the analyzed area. In this presentation we demonstrate a simple, useful tool we have developed to process mass spectrometry images and identify which peaks show similar spatial patterns. For this we have created the 'Correlated Image Finder' as part of our NBtoolbox for multivariate analysis of mass spectrometry imaging data. This tool uses one of two methods to find similar images. The first method calculates the correlation coefficient between the pixels of each image and sorts the images according to a user chosen correlation cutoff. The second method uses a simple image subtraction method to find images that match within a user chosen cutoff. For either method, the images are first down binned to reduce image noise and then thresholded and scaled in order to compare all peak images on an equal scale.

The Correlated Image Finder has been tested on a wide variety of images. Examples will be shown from ToF-SIMS and MALDI imaging data. It was seen that the Correlated Image Finder is able to find images showing similar spatial distributions. The Correlated Image Finder can be used on any set of image data and examples will be shown from both 2D and 3D image data sets from tissues, cells and polymers. The results from the Correlated Image Finder can help simplify MSI data interpretation and can also help understand trends seen using other analysis methods such as principal component analysis.

Electronic Materials and Photonics Room 102A - Session EM+MI+MN-TuA

New Materials and Devices for Emerging Memory Technologies

Moderators: Andy Antonelli, Nanometrics, Sean King, Intel Corporation

2:20pm EM+MI+MN-TuA1 Emerging Processing Challenges for Advanced Memory Technologies, Bart Van Schravendijk, Lam Research INVITED

The rapid scaling of semiconductor memory is radically changing the memory industry. Flash memory has switched from lateral scaling to vertical scaling while other new memory technologies are aggressively vying for new opportunities in the memory market. Their targets range from niche applications to replacing any one of the three big memory technologies : SRAM, DRAM or Flash.

For vertical NAND flash largely conventional materials are used in its fabrication at present. However, the unabated drive for higher density is driving aggressive vertical scaling, which poses new problems for stack design and processing. This drives improvements and maybe even changes in the materials.

Newer memory technologies, such as STT-RAM, ReRAM and PCRAM, bring with them different challenges to the processing arena. These new memories come with materials whose full scope of interactions with semiconductor processing are still poorly understood. These materials provide new challenges for the processing tools when scaling these memory technologies to dimensions that are economically attractive.

In this talk we will review some of the more challenging problems for advanced memories and some potential solutions.

4:20pm EM+MI+MN-TuA7 Resistance Change Memory and its Perspective toward 3D Integration, Yoshio Nishi, B. Magyari-Kope, Stanford University INVITED

As we face a situation in the next decade where further scaling of traditional CMOS based devices would not be cost effective from manufacturing issues such as superfine lithography/etching and device physics barriers. Thus non-traditional new materials and devices research have been instigated, which resulted in new principle based non-volatile memories. A short list of such newly emerging memory consists of resistance change memory ReRAM, phase change memory, PCRAM, spin based MRAM/STT RAM, depending upon desirable characteristics to implement.

Though resistance change phenomena in metal oxides have been recognized since early days, it is in the past few years when aggressive research for application as nonvolatile memory has taken off. Basic switching mechanism is formation and annihilation of conductive vacancy chain in the metal oxide sandwiched by two electrodes. Both atomistic and macroscopic models have been investigated. Role of electrode materials and switching oxide interfaces during memory operation have attracted strong attention, as it would imply not only memory characteristics but also device endurance and scalability. Further, development of this type of resistance change memory is toward vertical integration with multi-memory layers which could replace ultra-high density flash memory.

This talk will review progresses made for resistance change memories, covering fundamental physical mechanism, implementation of memory cells including scaling limit studies, and 3 dimensional integration of such devices.

5:00pm EM+MI+MN-TuA9 Atomic Disorder As an Intrinsic Source of Variability in Filamentary Rram Devices – Ab Initio Investigations, Sergiu Clima, IMEC, Belgium; L. Goux, B. Govoreanu, M. Jurczak, G. Pourtois, A. Fantini, IMEC INVITED

Resistive Random Access Memory concept is probably close to production in a new generation of non-volatile memories, but there are still some reliability issues to be fully understood. Resistive RAM devices can be scaled down below 10 nm [1], meaning that the discrete nature of atomic structure of the materials may already be observed in device operation properties. Material-wise, the transition metal oxides attracted the scientific interest due to their CMOS compatibility and their ability to operate on intrinsic defects (oxygen vacancies). For RRAM working with extrinsic defects like metallic inclusions called Conductive Bridge RAM (CBRAM), a larger spectrum of solid electrolytes can be used. Using Density Functional Theory simulations of RRAM materials, we evaluated the kinetics of the defects migration of the conducting species to show that atomic disorder of amorphous state can exhibit large variability in terms of defect stability and kinetic barriers.[2] These have a great impact on filament resistance evolution in time, which can be observed during forming step of the resistive filament, but not only. In the short time immediately after filament formation, the atomic configuration can relax to a metastable state, therefore changing the resistivity of the filament. In a long time retention of the filament resistance we can still measure resistance change. All these observations can be explained with the computed statistical distributions of the defect stability and kinetic barriers in the RRAM materials.

[1] B. Govoreanu et al., Ext.Abstr. SSDM Conf.,Nagoya, Japan, 1005 (2011)

[2] S. Clima et al., Electron Device Lett , 769 (2015)

5:40pm EM+MI+MN-TuA11 Reduction of Radiation Damage to HfOx-Based Resistive Random Access Memory using a Thin ALD HfOx Film, Kaiwen Hsu, T. Chang, University of Wisconsin-Madison; L. Zhao, Z. Wang, Stanford University; R. Agasie, T. Betthausen, J. Nickles, Z. Ma, J. Chang, University of Wisconsin-Madison; Y. Nishi, Stanford University; J.L. Shohet, University of Wisconsin-Madison

Resistive Random Access Memory (RRAM) [1], is considered to be a very promising memory technology for the next generation of computer memory. It has undergone intense research in both industry and academia in the last ten years. As RRAM technology matures and electronic devices using RRAM are likely to be built soon, a RRAM cell which is resistant to radiation will become an important topic in industry to prevent the malfunction of these devices. In this work, neutron and proton-induced effects on two types of RRAM cells are investigated. Type 1 HfOx RRAM cell is different from the Type 2 RRAM cell in two aspects, (1) the thickness of the HfOx film (Type 1 is thicker than Type 2) and (2) the fabrication process

Tuesday Afternoon, November 8, 2016

for depositing the HfOx within the RRAM cell. (Type 1 uses spin-on technology and Type 2 uses ALD technology)

Many Type 1 RRAM cells can be formed under neutron irradiation and end up in the LRS. On the other hand, unformed neutron-irradiated Type 1 RRAM cells only require a lower voltage to form. In addition, the resistance of the HRS increased on the Type 1 RRAM cell. The shift in values of the set voltage can be seen on the I-V characteristic of the neutron-irradiated Type 1 RRAM cell. A similar increase in the resistance of HRS is also observed in proton-irradiated Type 1 RRAM cells. The shift in values of the set voltage can be seen on the I-V characteristic of the proton-irradiated Type 1 RRAM cell.

There are no obvious changes to Type 2 RRAM cells after either neutron or proton irradiation. It is very likely that both the changes in thickness and fabrication are very important since these two modifications can cut down on the number of defects which affect the switching mechanism of the RRAM cell.

This work was supported by the Semiconductor Research Corporation under Contract No. 2012-KJ-2359, by the National Science Foundation under Grant No. CBET-1066231.

[1] H.-S. Philip Wong, H-Y Lee, S. Yu, Y. S. Chen, Y. Wu, P-S Chen, B. Lee, F. T. Chen, and M-J Tsai, "Metal-oxide RRAM," Proceedings of the IEEE 100 1951 (2012).

6:00pm **EM+MI+MN-TuA12 Potential Dependent Resistance of Doped TiO₂ Film Fabricated by Solgel Process: Perspective for Resistive Memory**, R.R. Pandey, *Jyotirmay Sharma*, C. Kant, K. Saini, CSIR-National Physical Laboratory, India

Fastest growth has been registered in the field of electronics. It is the only field which has transformed every corner of the society and every age of the civic society, from youngest child to elderly persons. The growth was outcome of the miniaturization of the basic active device in electronics. The journey started from few millimeter size around 1965 and now reached to few tens of nanometers. At the beginning of this journey, the new smaller size devices not only performed better to its predecessor but were cost effective also. As we reached below ~300nm, the production was no longer economic. At around few tens of nanometer size the device performance also affected and at this junction the need was felt to explore alternate working principles for the device to maintain growth of the field and continue to benefit the society. New devices such as SET, RTD, resistive memory, magnetic memory, spintronic etc. were studied. Working device size of less than ten nanometers is expected from this new class of devices. Here we report fabrication of titanium oxide based resistive memory device by solgel technique. Thin films of high quality doped and undoped titanium oxide were applied on cleaned FTO or Pt-FTO glass substrates by solgel dip process. We doped titanium oxide with aliovalent cations by suitable choice of doped cation salt. Sequence of undoped and doped layers of titanium oxide was altered in different devices. Final structure was completed by thermal evaporation of metal electrode for electrical connection.

A resistance change of 2-3 orders of magnitude was observed up to the maximum applied potential of ± 3.0 volts. The resistance change has complex dependence on nature of the dopant, dopant concentration, electrode material and sequence of the doped and undoped layers. We tried to explore the resistance change behavior and remembrance of resistance on the basis of basic studies viz; XRD, XPS, SEM, etc. cyclic voltametric studies were also carried out to understand the contact between electrode and TiO₂ layer.

Magnetic Interfaces and Nanostructures Room 102B - Session MI-TuA

Magnetic Phenomena in Organic Systems

Moderators: Gary Mankey, University of Alabama, Mikel Holcomb, West Virginia University

2:20pm **MI-TuA1 Promises and Challenges of Organic Spintronics**, *Christoph Boehme*, University of Utah **INVITED**

While the term "Spintronics" was originally introduced as label for technologies that represent information through spin states rather than charge states, it is nowadays oftentimes used solely in the context of spin-polarization, spin-injection, and spin-transport effects, for all of which spin-orbit interaction plays an important role. Many organic semiconductors display only weak spin-orbit coupling and charge transport via hopping

through localized electronic states which are exposed to hydrogen induced strong local and random hyperfine fields. These materials therefore appear at first glance to be entirely unsuitable for spintronics. However, they also exhibit pronounced spin-related effects not seen in materials with strong spin-orbit coupling¹⁻³ which can be used for alternative, different approaches to spintronics based, for instance, on spin-permutation symmetry states of charge carrier pairs which, in contrast to spin-polarization states, are not directly dependent on temperature and magnetic field strength⁴. Weak spin-orbit coupling can also promote long spin-coherence times and thus, allow for electrically readable spin memory of electron⁻⁵ or nuclear-spins⁶. The successful implementation of organic spintronics will require a fundamental understanding of the microscopic electronic processes that are to be utilized for such technologies. In this presentation, some of the progress as well as challenges⁷ for the exploration of these spin-dependent processes will be reviewed. Measurements of spin-coupling types and strengths of charge carriers will be discussed² as well as examples for unusual physical behaviors of these materials, such as an electrically detectable spin-Dicke effect caused by charge carrier spin collectivity⁸ or the presence of an inverse spin-Hall effect⁹.

[1] D. R. McCamey et al., *Nature Materials* **7**, 723 (2008); [2] D. R. McCamey, et al., *Nature Commun.* **6**:6688, 7688 (2015). [4] W. J. Baker et al., *Nature Commun.* **3**, 898 (2012); [5] W. J. Baker et al., *Phys. Rev. Lett.* **108**, 267601 (2012); [6] H. Malissa, et al., *Science* **345** 1487, (2014); [7] C. Boehme and J. M. Lupton, *Nature Nano.* **8**, 612 (2013); [8] D. P. Waters, et al., *Nature Physics* **11**, (11) 910 (2015); D. Sun et al., *Nature Materials* **15**, doi:10.1038/nmat4618 (2016).

3:00pm **MI-TuA3 Spin-Polarized STM Observation of Hybridization at the Interface between Different 8-hydroxyquinolates and the Cr(001) Surface**, *Daniel Dougherty*, J. Wang, A. Deloach, North Carolina State University

The field of organic spintronics has focused dominant attention on organic emitters such as tris-(8-hydroxyquinolate) aluminum (Alq3). This particular molecule has been reported to show large magnetoresistive effects including a 300% effect nanoscale tunnel barriers [1] that is tied to molecular orbital mixing at the magnetic electrode interface. Here we report on a direct study of this orbital mixing using spin polarized scanning tunneling microscopy and local spectroscopy measurements. We focus on the well-known Alq3 molecule adsorbed on a Cr(001) surface and report evidence for spin polarized interface states near the Fermi level. When the adsorbate is replaced with the paramagnetic variant Crq3, the interface remains polarized but the magnetic states are significantly farther from the Fermi level. These results will be discussed in the broad context of molecular orbital control if interfacial polarization in tunneling devices.

[1]Barraud et al., Nat. Phys. 6, 615 (2010).

3:20pm **MI-TuA4 Charge Transport in Thin Films of a Molecular Spin-Crossover Compound**, *Greg Szulczewski*, E. Ellingsworth, The University of Alabama

Spin-crossover in molecular complexes containing divalent Fe ions (six d-electrons) is a phenomena associated with a reversible change in the magnetic state (diamagnetic to paramagnetic and vice versa) as a function of temperature, pressure or optical excitation. In this study we demonstrate the growth of bis(1,10-phenanthroline)dithiocyanato iron (II) or Fe(phen)₂(NCS)₂ thin films, a well-known spin crossover material. A detailed SQUID magnetometry and spectroscopic analysis using Raman, IR, UV-Vis, and XPS, indicates that the as-deposited films are largely a diamagnetic compound that can be best described as Fe(phen)₃(NSC)₂. Upon annealing the films under high vacuum, the diamagnetic compound can be converted into a paramagnetic compound, which is consistent with the formation of Fe(phen)₂(NCS)₂. The annealed films are polycrystalline as revealed by x-ray diffraction and exhibit a spin-crossover transition near 180 K. The DC electrical conductivity of these films was measured from 100-300 K. A small (but repeatable) change in the electrical conductivity was observed. An unequivocal interpretation of this observation is difficult because of competing factors. For example, the unit cell expands across the spin-crossover transition, the geometric structure of the molecule changes, and the frontier molecular orbital energies also change. The relative contribution of these factors will be discussed in detail.

4:20pm **MI-TuA7 Single Organic Radicals on Metal Surfaces: A Model System for Spin-1/2 Kondo Physics**, *Peter Wahl*, University of St Andrews, UK **INVITED**

The Kondo effect is one of the most intensely investigated many-particle problems in solid-state physics. While it was discovered originally in dilute

Tuesday Afternoon, November 8, 2016

magnetic alloys, the same physics emerges in seemingly unrelated contexts, such as the zero-bias anomalies observed in quantum dots or the dynamical behavior close to a Mott transition. The simplicity of the underlying hamiltonian – a single spin coupled by an exchange interaction J to a bath of conduction electrons – contrasts the complex physics emerging from it as well as the challenges met in theoretical calculations. Apart from being a drosophila for electronic correlation effects, the single impurity Kondo effect is an elementary building block for model lattice systems relevant for strongly correlated electron materials such as high temperature superconductors.

Studies of transition metal atoms on metal surfaces by low temperature scanning tunneling microscopy and spectroscopy have renewed interest in the Kondo problem by providing access to local properties; however a quantitative comparison with theoretical predictions remained challenging.

Here I present a study of an organic radical with a single spin $\frac{1}{2}$ on Au(111) [1]. Tunneling spectra reveal a zero bias anomaly as would be expected for a Kondo system, yet comparison of the temperature and magnetic field dependence of the zero bias anomaly with predictions of the Kondo effect in the strong coupling regime are in apparent disagreement. Detailed comparison with theoretical models reveals quantitative agreement with the original Kondo model in the weak coupling regime.

1. Y. Zhang et al., Nat. Commun. 4, 2110 (2013).

5:00pm **MI-TuA9 Tunneling in III-N Heterostructures for Low Power Electronics**, *Patrick Fay*, W. Li, L. Cao, K. Pourang, University of Notre Dame; S. Islam, Cornell University; C. Lund, University of California at Santa Barbara; H. Ilatkhameneh, R. Rahman, T. Amin, Purdue University; D. Jena, Cornell University; S. Keller, University of California at Santa Barbara; G. Klimeck, Purdue University

INVITED

Continuing increases in circuit complexity and capability for logic and computation applications as well as for emerging low-power systems require fundamental advances in device technology and scaling. Due to power constraints, devices capable of achieving switching slopes (SS) steeper than 60 mV/decade are essential if conventional computational architectures are to continue scaling. Similarly, low power systems such as mobile devices and distributed sensing applications also benefit from devices capable of delivering high performance in low-voltage operation. Tunneling field effect transistors (TFETs) are one promising alternative to achieve these objectives. A great deal of work has been devoted to realizing TFETs in Si, Ge, and narrow-gap III-V materials, but the use of III-N heterostructures and the exploitation of polarization engineering in particular offers unique opportunities. From physics-based simulations, GaN/InGaN/GaN heterostructure TFETs offer the potential for achieving switching slopes approaching 20 mV/decade with on-current densities exceeding 100 $\mu\text{A}/\mu\text{m}$ in nanowire configurations. In this talk, the operational principles of III-N-based TFETs will be described, and device design and performance considerations will be discussed. In addition, experimental efforts demonstrating heterostructure backward diodes in III-N heterostructures as well as progress towards nanostructure-based III-N FETs and TFETs will be reviewed.

5:40pm **MI-TuA11 A Spins-Inside Quantum Processor**, *T. Fujita*, Delft University of Technology, The Netherlands; *L.M.K. Vandersypen*, Delft University of Technology, The Netherlands; *T. Hensgens*, Delft University of Technology, The Netherlands

INVITED

A quantum computer holds the promise of solving some problems that are beyond the reach of the most powerful supercomputers. Due to theoretical and experimental breakthroughs in the last few years, we are now at a point where the feeling grows that a large-scale quantum computer can actually be built. Increasingly, this requires bridging the disciplines, from physics to engineering, materials science and computer science. In this talk, I will present the start-of-the-art in quantum computing and outline the challenges ahead, with a focus on electron spin qubits in semiconductors.

Manufacturing Science and Technology

Room 103A - Session MS-TuA

Working with National Labs and User Facilities

Moderator: Bridget Rogers, Vanderbilt University

2:20pm **MS-TuA1 Southeastern Nanotechnology Infrastructure Corridor (SENIC) – A Nano Fabrication and Characterization Resource as part of the National Nanotechnology Coordinated Infrastructure (NNCI)**, *Paul Joseph, D. Gottfried, G. Spinner, O. Brand*, Georgia Institute of Technology

The Southeastern Nanotechnology Infrastructure Corridor (SENIC) is a partnership between two state-of-the-art nanofabrication and characterization facilities located at the Institute for Electronics and Nanotechnology (IEN), an interdisciplinary research institute at the Georgia Institute of Technology, and the Joint School of Nanoscience and Nanoengineering (JSNN), an academic collaboration between North Carolina A&T State University (NCA&T) and the University of North Carolina at Greensboro (UNCG). SENIC is one of 16 members of the National Nanotechnology Coordinated Infrastructure (NNCI), supported by the National Science Foundation, and coordinated by the NNCI Coordinating Office at Georgia Tech. NNCI is an integrated networked partnership of academic nanotechnology user facilities across the US, serving the needs of nanoscale science, engineering, and technology. The NNCI is a research facilitator, providing state-of-the-art equipment, staff expertise, and training to nanotechnology researchers. The shared-user, fee-based laboratories are open to academic, industry, and government clientele, offering a unique and comprehensive nanotechnology laboratory and teaming environment.

At Georgia Tech, the IEN has dedicated expertise and facilities for a broad range of micro and nanofabrication and characterization projects, including a focus on applications to bioengineering and biomedicine. IEN supports cleanroom and characterization facilities used by more than 700 researchers annually, with 20% from external institutions. The external users (off-campus users) can access the desired tool set after training (on-site work) or can send their samples for processing or analysis by IEN staff (remote work). IEN offers unique capabilities in e-beam lithography, photolithography, soft lithography, thin film deposition, etch processing, metallization, packaging, micro scale printing, imaging, metrology, and microanalysis. IEN-supported research themes include nanostructures, nanoelectronics, bio-MEMS, biological/chemical sensors and systems, biomaterials, photonics, materials growth and synthesis.

During this presentation, an overview of NNCI and SENIC will be given. Subsequently, we will discuss shared user lab resources, external user services, and education programs available at IEN.

2:40pm **MS-TuA2 The Cornell NanoScale Science and Technology Facility (CNF)**, *Michael Skvarla*, Cornell NanoScale Science and Technology Facility

The Cornell NanoScale Science and Technology Facility (CNF) is a member of NNCI, a network of open-access facilities partially subsidized by the US National Science Foundation to provide researchers with rapid, affordable, shared access to advanced nanofabrication tools and associated staff expertise. Hundreds of researchers worldwide (from academia, industry, and government) utilize CNF to make structures and systems from the nanometer scale to the centimeter scale. CNF offers unique capabilities in electron-beam lithography, advanced stepper photolithography, dedicated facilities for soft lithography, and direct-write tools for rapid prototype development, along with the flexibility to accommodate diverse projects and to deposit, grow, and etch a wide variety of materials. CNF's technical staff are dedicated full-time to user support, providing one-on-one help with process development, tool training, and troubleshooting. They can offer expertise for a very wide range of fabrication projects, including electronics, nanophotonics, magnetics, MEMS, thermal and energy systems, electrochemical devices, fluidics, and the life sciences and bioengineering (more than 30% of CNF's users now focus on biology). All users are welcome; no experience in nanofabrication is necessary and a central part of CNF's mission is to assist users from "non-traditional" fields seeking assistance to implement nanofabrication techniques for the first time. CNF's user program is designed to provide the most rapid possible access (typically 2 weeks) with the lowest possible barriers to entry (users retain full control of their IP, with no entanglement by CNF or Cornell University). Many of CNF's external academic users come from institutions with their own local cleanroom facilities, but still utilize CNF for advanced capabilities, staff expertise, or tool availability.

This talk will explore the tools and the types of services and advice available to CNF users, and present examples of ongoing work with the

Tuesday Afternoon, November 8, 2016

hope of stimulating ideas and possibilities. We will also provide the latest details on the National Nanotechnology Coordinated Infrastructure (NNCI), a new NSF-sponsored network of shared facilities similar to CNF.

We invite you to explore the CNF and NNCI and discuss ways we can help bring your research visions to fruition. As a first step, CNF's User Program Managers will at no cost provide detailed processing advice and cost estimates for potential new projects. The CNF technical staff also meets every Wednesday afternoon for conference calls where we welcome questions about any topic related to nanofabrication. Visit cnf.cornell.edu to contact us and get started.

3:00pm MS-TuA3 The CNST NanoFab at NIST: Nanofabrication for US Commerce, Vincent Luciani, NIST Center for Nanoscale Science and Technology

The NIST Center for Nanoscale Science and Technology (CNST) supports the U.S. nanotechnology enterprise from discovery to production. As part of the CNST, the shared-use NanoFab provides its users rapid access to a comprehensive suite of tools and processes for nanoscale fabrication and measurement. The CNST NanoFab at NIST is part of the Department of Commerce and therefore puts a high priority on operating a business friendly, easily accessible facility. The same rates are applied to all users, whether from industry, academia or NIST. Applications are accepted at any time and are reviewed and processed every week. Also, NIST does not claim any inherent rights to inventions made in the course of a NanoFab project. Your intellectual property rights are not affected. The NanoFab features a large, dedicated facility, with tools operated within an ISO 5 (class 100), 750 m² (8,000 ft²) cleanroom and in adjacent laboratories that have superior air quality along with temperature, humidity, and vibration control. Over 80 major process tools are available, including but not limited to e-beam lithography, 5x reduction stepper photolithography, nanoimprint lithography, laser writing for mask generation, scanning and transmission electron microscopy, 3 Focused Ion Beam (FIB) systems, metal deposition, plasma etching, chemical vapor deposition, atomic layer deposition, deep silicon etching, ion beam etching and a soft-lithography lab. The NanoFab staff consists of scientists, engineers and technicians that specialize in all areas of nanofabrication and provide training and ongoing technical assistance to users. Our goal is to be a catalyst to our users' success and to help nurture nanotechnology commerce in the United States. Project applications and instructions are easily available on the web at www.nist.gov/cnst/nanofab. Users inside NIST and from all around the country are provided on-line access to tool schedules and the tool reservation system. From physicists, engineers and biologists to medical researchers, users find common ground at the nanoscale in the CNST NanoFab.

3:20pm MS-TuA4 In-Situ Characterization Tools for Materials Growth and Processing at NSLS-II, Klaus Attenkofer, E. Stavitski, K. Evans-Lutterodt, C. Nelson, Brookhaven National Laboratory

Driven by the needs of sub-15nm integrated chip design, power electronics, and energy conversion devices, a wide range of coating and etching processes are in development which allow single layer growth or removal controlled by complex chemical processes on the substrate and/or in the gas phase resulting in self-limiting growth/etching approaches. The invention of new processes for conventional and spatial Atomic Layer Deposition (ALD) is one of the most prominent applications; even if it has a potentially high impact on the technology, used by everybody in future, it faces the challenge of an enormously large parameter space and costly and lengthy experiments developing the various precursor compounds. A theory inspired approach, combining combinatorial methods with computational modeling, may significantly reduce the risks and costs of the development process; however, to connect both approaches, an in-situ characterization tool will be required characterizing structure, and chemistry of the surface compounds, the gas and the film itself. X-ray spectroscopic and scattering/diffraction techniques may be the probes which provides chemical and structural sensitivity under complex reaction conditions.

NSLS-II had developed a set of beamlines which combine high-end state-of-the-art beamline design with optimized endstation design for materials growth. Specifically, the talk will provide an overview on the scattering and spectroscopy capabilities at In-Situ and Resonant scattering (ISR) beamline and the Inner Shell Spectroscopy beamline (ISS); two instruments build to study the growth of amorphous and crystalline films from the early seed formation to the bulk-like film. Next to an introduction into the beamline and its endstation equipment, we will also present experimental data which demonstrate the power of in-situ characterization.

4:20pm MS-TuA7 The Center for Nanophase Materials Sciences, Michael Simpson, Oak Ridge National Laboratory

The Center for Nanophase Materials Sciences (CNMS) at Oak Ridge National Laboratory (ORNL) is a multidisciplinary user facility that provides the research community with access to expertise and equipment to address the most challenging issues in nanoscience. Industrial, government and academic researchers from around the world may access capabilities in functional imaging, atom-precise synthesis, and nanofabrication. The CNMS is a leader in a range of advanced nanofabrication techniques including electron beam assisted deposition on the sub-10 nm level using both gas and liquid precursors as feedstock material, 3D fabrication and atomically precise material sculpting, as well as direct matter manipulation on the atomic level by electron beams to induce material functionality. Spatially resolved quantitative measurements of physical and chemical properties of materials are available to users through unique measurement capabilities of band excitation scanning probe microscopy, scanning transmission electron microscopy, helium ion microscopy, and atom probe tomography. Furthermore, theoretical and computational approaches are available to CNMS users, as frameworks for deep-data analytics methods for imaging, and computational prediction of functional and physical properties in nanostructures, benefiting from the broad ORNL computational capabilities. Located adjacent to the Spallation Neutron Source at ORNL, CNMS acts as a gateway for the nanoscience community to ORNL's world-class neutron science facilities, by providing diverse complementary capabilities such as selective deuteration, sample environments for multimodal measurements, fabrication of templates for neutron reflectivity experiments, and many other materials science capabilities to complement neutron results. As one of the five Department of Energy Nanoscale Science Research Centers (see nsrportal.sandia.gov), CNMS makes all of these capabilities, and the staff expertise to fully benefit from them, available free of charge to users who intend to publish the results, or at-cost for proprietary research, as described at cnms.ornl.gov. [*The CNMS at Oak Ridge National Laboratory is a DOE Office of Science User Facility.*]

4:40pm MS-TuA8 User Opportunities at the Center for Nanoscale Materials, Kathleen Carrado Gregar, Center for Nanoscale Materials at Argonne National Laboratory

The Center for Nanoscale Materials (CNM) at Argonne National Laboratory is a premier user facility providing expertise, instrumentation, and infrastructure for interdisciplinary nanoscience and nanotechnology research. Academic, industrial, and international researchers can access the center through its user program for both nonproprietary (at no cost) and proprietary research.

The CNM is at the forefront of discovery of new materials, visualizing events with high resolution as they occur, understanding the physics and chemistry of energetic processes at the nanoscale, and manipulating nanoscale interactions to create useful, energy-efficient structures with new functionalities. Goals include the hierarchical integration of materials across the nanoscale to the mesoscale, in order to create energy-efficient and affordable functionality that advance the public good.

Unique capabilities at CNM include a premier clean room with advanced lithography and deposition capabilities, expansive synthesis and nanofabrication resources, a hard x-ray nanoprobe at the Advanced Photon Source synchrotron, myriad scanning probes including low temperature, ultrahigh vacuum STMs, TEMs with in situ holders and chromatic aberration-correction, a 30 TFlop supercomputer, and ultrafast optical probes. A key CNM asset includes outstanding staff with expertise in synthesis, nanophotonics, scanning probe and electron microscopy, nanofabrication, and theory, simulation and modeling. Core technological materials range from 2D layered materials to nanocrystalline diamond. All capabilities and expertise are available through peer-reviewed user proposals; access is free of charge for non-proprietary research in the public domain. CNM is one of DOE's premier Nanoscale Science Research Centers serving as the basis for a national program encompassing new science, new tools, and new computing capabilities for research at the nanoscale (<https://nsrportal.sandia.gov>). Recent staff and user research highlights will be presented, painting a picture of present and future nanoscience and nanotechnology at the CNM (www.anl.gov/cnm).

The Center for Nanoscale Materials, an Office of Science user facility, is supported by the U.S. Department of Energy, Office of Science, Office of Basic Energy Sciences, under contract no. DE-AC-02-06CH11357.

Tuesday Afternoon, November 8, 2016

5:00pm MS-TuA9 The Center for Integrated Nanotechnologies--Resources and Capabilities, *Dale Huber*, Sandia National Laboratories

A decade ago, five new Department of Energy user facilities, the Nanoscale Science Research Centers (NSRCs), entered full operations. These facilities offer unique capabilities, at no cost, to qualified researchers in the field. I will describe the Center for Integrated Nanotechnologies (CINT), its capabilities, and where it fits into the broader landscape of the NSRCs and the other major user facilities in the US. While this will necessarily be a broad overview, I will provide details for where and how to obtain further information including important online references, points of contact for general information, and will provide an opportunity to make connections for detailed interests. Sandia National Laboratories is a multi-program laboratory managed and operated by Sandia Corporation, a wholly owned subsidiary of Lockheed Martin Corporation, for the U.S. Department of Energy's National Nuclear Security Administration under contract DE-AC04-94AL85000.

5:20pm MS-TuA10 Using EMSL Capabilities in Combination with those from other User Facilities to Address Fundamental and Applied Problems, *Donald Baer, M.H. Engelhard, T.J. Law*, Pacific Northwest National Laboratory

Increasingly a wide range of advanced research tools and expertise are needed to address important scientific and societal questions. The Environmental Molecular Sciences Laboratory, EMSL, is one of several US Department of Energy user facilities provided to facilitate cutting-edge research. This talk will highlight the focus of EMSL, recent efforts to integrate activities at multiple user facilities and efforts being made to increase industrial use of user facilities. The vision of EMSL is to pioneer discoveries and mobilize the scientific community to provide the molecular science foundations that will address research priorities of the DOE Office of Biological and Environmental Research (BER) and our nation's critical biological, environmental and energy challenges. To accomplish these aims, EMSL science is focused in four areas: biosystem dynamics and design, atmospheric aerosol systems, terrestrial and subsurface ecosystems and molecular transformation. Molecular transformations that occur at surfaces and interfaces are critical in each of these areas, and EMSL provides a wide range of unique and state-of-the-art spectroscopy, microscopy, magnetic resonance and computational capabilities to advance science on these topics (www.emsl.pnnl.gov). Similar to all DOE user facilities, researchers typically use resources at EMSL for little to no cost if results are shared in the open literature, and access is provided by a proposal and peer review process. As a multi-disciplinary facility, we encourage proposals that combine instrumentation across our capability groups to advance scientific understanding. Increasingly, we are focusing on real-time *in situ* measurements in a variety of environments. Efforts over the last few years to enable cross facility access through a single proposal to examine novel ways for scientific user facilities to work together has resulted in the FICUS program—Facilities Integrating Collaborations for User Science. With the opportunity to pursue one research project at two or more institutions under FICUS, scientists can leverage disparate resources, shave years off their project times and amplify the impact of their work. Additional efforts are underway to address access policies and training reciprocity that will further streamline the user's experience and increase industrial use of these facilities as well.

Nanometer-scale Science and Technology

Room 101D - Session NS-TuA

Nanoscale Imaging and Characterization

Moderators: Mehmet Z. Baykara, Bilkent University, Turkey; Sidney Cohen, Weizmann Institute of Science, Israel; Rainer Timm, Lund University, Sweden

2:20pm NS-TuA1 Frontiers of Force Microscopy in Nanoscience and Nanotechnology, *Ricardo Garcia**, CSIC, Spain **INVITED**

This contribution aims to provide an overview of some recent developments as well as some challenges faced by force microscopy in nanoscience and nanotechnology. Specifically, the focus will be oriented to applications to study materials in air and liquid environments. The presentation is divided in three sections. The first section provides an introduction to the physics and key instrumental aspects of advanced force microscopes. The second section describes some applications to generate high resolution (atomic, molecular or nanoscale) maps of soft matter

interfaces (polymer and biomolecules). Those maps combined topography and nanomechanical properties. A method to generate three dimensional and atomically-resolved map of solid-liquid interfaces will be presented. The third section, illustrates how the nanoscale control afforded by scanning probe microscopes has enabled the development of scanning probe-based patterning methods.

References:

- E.T. Herruzo, A.P. Perrino and R. Garcia, *Nature Commun.* **5**, 3126 (2014)
R. Garcia and E. T. Herruzo, *Nature Nanotechnol.* **7**, 217-226 (2012).
R.Garcia, A.W. Knoll, E. Riedo, *Nature Nanotechnology* **9**, 577-587 (2014)

3:00pm NS-TuA3 Elemental and Magnetic Fingerprinting of Materials at the Nanoscale by Synchrotron X-ray Scanning Tunneling Microscopy, *Volker Rose*, Argonne National Laboratory **INVITED**

Recently, substantial progress was made on Argonne's Synchrotron X-ray Scanning Tunneling Microscopy (SX-STM) project. In particular, we demonstrated the power of SX-STM for elemental characterization and topography of individual Ni nano-islands on Cu(111) at 2 nm lateral resolution with single atom height sensitivity [1], tested a new probe tip concept based on carbon nanotubes [2], and demonstrated soft x-ray imaging of nanoscale magnetic domains of an iron thin-film by x-ray magnetic circular dichroism (XMCD) contrast [3]. Further substantial advances are expected using the new low temperature (LT) SX-STM system, which has been developed over the last 3 years and is currently under commissioning.

To fully exploit the special capabilities of the new LT x-ray microscope, XTIP, a dedicated beamline for SX-STM is under construction at the Advanced Photon Source. To meet the scientific objective of the nanoscience and nanomagnetism communities most effectively, we are going to build a soft x-ray beamline with full polarization control operating over the 400-1600 eV energy range.

The dedicated XTIP beamline will provide researchers access to a one-of-a-kind instrument. Among the potential breakthroughs are "designer" materials created from controlled assembly of atoms and molecules, and the emergence of entirely new phenomena in chemistry and physics.

This work was funded by the Office of Science Early Career Research Program through the Division of Scientific User Facilities, Office of Basic Energy Sciences of the U.S. Department of Energy through Grant SC70705. Use of the Advanced Photon Source and the Center for Nanoscale Materials was supported by the U.S. Department of Energy, Office of Science, Office of Basic Energy Sciences, under contract DE-AC02-06CH11357.

- [1] N. Shirato et al., *Nano Letters* **14**, 6499 (2014).
[2] H. Yan et al., *J. Nanomaterials* **2015**, 492657 (2015).
[3] A. DiLullo et al., *J Synchrotron Rad.* **23**, 574 (2016).

4:20pm NS-TuA7 Quantitative Nanomechanics of Soft Materials with AFM: Old and New Methods, *Igor Sokolov*, Tufts University **INVITED**

Quantitative study of mechanical properties of soft materials at the nanoscale, such as the Young's modulus, storage and loss moduli, etc. becomes important in the study of nanocomposites materials, polymers, biological tissues, and cells. Nanoindentation techniques are not capable to attain nanoscale resolution for such materials; whereas atomic force microscopy (AFM) techniques do allow quantitative measurements of soft materials at the nanoscale. Although being attractive and simple, direct extrapolation of macroscopic models to the nanoscale is frequently incorrect. In this talk I will describe the AFM methods suitable for measurements of both static and dynamic moduli of soft materials. I will discuss both well-known modes of operation, such as the force-volume and nonresonant modes (e.g. PeakForce QNM) as well as new modes we recently developed (FT-NanoDMA or imaging nanoindentation and Ringing modes). Comparison of all these modes (including the nanoindentation technique) will be given. Studies of elastic moduli of polymers and cells will be exemplified.

5:00pm NS-TuA9 AFM Based Nanoscale Structure-Property Characterization of Nanoporous Organo-Silicates, *Qichi Hu, K. Kjoller*, Anasys Instruments; *G. Stan*, NIST/Material Measurement Laboratory; *S.W. King*, Intel Corporation

The continued advancement of nanostructured materials and exploitation of nanoscale size effects will ultimately require understanding material structure-property relationships at nanometer length scales. Despite a plethora of metrologies capable of characterizing thermal, mechanical,

* NSTD Recognition Award

Tuesday Afternoon, November 8, 2016

electrical, and optical properties at the nanoscale, combined nanoscale chemical structure-property characterization has only recently become possible with the development of atomic force microscope based IR spectroscopy (ARM-IR). In this regard, we have combined AFM-IR chemical structure and contact resonance AFM (CR-AFM) mechanical property measurements in the investigation of 20 – 500 nm wide fin structures fabricated in a nanoporous organosilicate material. By combining these techniques, we have observed nanoscale modifications in the chemical structure and mechanical properties of the nanoporous fins that correlate with one another, the feature size, and fabrication process. This demonstration should lead the way for nanoscale chemical structure-property characterization of other materials systems where such relationships are deemed essential.

5:40pm NS-TuA11 Scanning Microwave Microscopy Imaging in Liquids through Ultra-Thin Membranes, Alexander Tselev, Oak Ridge National Laboratory; *J. Velmurugan*, National Institute of Standards and Technology (NIST), University of Maryland (UMD); *A. Kolmakov*, NIST/CNST

The growing need in operando imaging of submicron objects immersed in liquids relevant to biomedical or energy applications resulted in a significant effort invested into in situ TEM and SEM. In these techniques, objects of interest are incased inside a chamber equipped with ultra-thin electron-transparent but molecularly-impermeable membrane(s) enabling electron or X-ray probing of the chamber interior. However, local radiation damage and radiolysis induced by high-energy electron or X-ray beams often lead to sample deterioration or adversely affect nanoscale chemical processes. Here, we report a novel concept of in situ near-field scanning microwave microscopy of reactive and biological samples in liquids. Microwaves of a few gigahertz frequencies offer photons of energies ~ 10 μ eV, which ensures non-destructive imaging free from radiolysis and radiation damage associated with use of high-energy electron and X-ray beams. In our approach, the nanoscale objects of interest are separated from ambient by a few-nanometer-thick dielectric membranes transparent for microwave near-fields. The imaging is performed with microwave near-fields formed at a scanning probe of an atomic force microscope in contact with the ultra-thin membrane. In the proposed approach, a liquid and/or a reactive environment of the object of interest are completely isolated from the probe and the rest of the microscope. We performed a comparative, side-by-side study of imaging capabilities of microwave microscopy and SEM in liquids using the same set of biological and inorganic samples. Sensitivity, spatial resolution, probing depth, and probe-induced effects were evaluated and compared. In particular, we demonstrate in situ real-time imaging of growth of metal dendrites at electrode-liquid electrolyte interface during an electrochemical reaction. The demonstrated spatial resolution of the near-field microwave imaging was ca. 250 nm. The resolution can be improved by optimization of probe and membrane geometry, as well as of the membrane material. Under optimal conditions, a resolution of ca. 50 nm can be achieved for metallic objects with commercially available probes. Such resolution is comparable to that demonstrated by in situ SEM in liquids.

The research was supported in part through Scientific User Facilities Division (ORNL), BES, US DOE, US Civilian Research and Development Foundation, and NIST-CNST/UMD-IREAP Cooperative Agreement.

6:00pm NS-TuA12 SnS Nanoplates, Nancy Trejo, A. Hunter, C. Wrasman, S. Ganguly, University of Minnesota; *J. Dwyer*, St. Catherine University; *E.S. Aydi*, University of Minnesota

Two dimensional (2D) layered materials such as graphene, metal dichalcogenides and black phosphorus are of increasing interest because of their unique electronic properties. Tin monosulfide (SnS) has the same crystal structure as black phosphorus. SnS may have potential applications in photovoltaics, photocatalysis, thermoelectrics, and batteries. We have synthesized 3-60 nm thick and up to approximately 10 micron wide SnS nanoplates via decomposition of tin(IV) diethyldithiocarbamate upon hot injection into oleylamine (300-340 °C). The reaction products are characterized using a combination of electron microscopy, energy dispersive X-ray spectroscopy, X-ray diffraction (XRD), atomic force microscopy and Raman spectroscopy. All characterization techniques confirm that the final reaction product is orthorhombic SnS (e.g., after 60 minutes at 340 °C). At low temperatures (300 °C) and short synthesis times (1 minute) we also observe the presence of SnS₂ which suggests that decomposition of tin(IV) diethyldithiocarbamate first produces SnS₂. Tin disulfide is subsequently reduced, likely by oleylamine, to SnS. Orthorhombic SnS grows preferentially as plates, with [010] direction normal to the plate surfaces. In fact, when plates are large (>1 micron) XRD

from films cast from colloidal dispersions in toluene show predominantly the (040) diffraction. The SnS nanoplate sizes could be altered by controlling the temperature, oleylamine concentration, and reaction time. Nanoplate dispersions in toluene exhibit an optical absorption feature in the visible range of the electromagnetic spectrum, which we surmise to be of plasmonic origin. The nanoplate dispersions in toluene also respond to electric fields.

Plasma Science and Technology Room 104B - Session PS+2D-TuA

Plasma Processing for Nanomaterials and 2D Materials

Moderator: Sumit Agarwal, Colorado School of Mines

2:20pm PS+2D-TuA1 Analysis of Microplasma Reduction of Aqueous Silver and Gold Salts to Colloidal Nanoparticles, Caroline De Vos, Université Libre de Bruxelles, Belgium; *M.J. Gordon*, University of California, Santa Barbara; *R.M. Sankaran*, Case Western Reserve University; *F. Reniers*, Université Libre de Bruxelles, Belgium

The remarkable stability of microplasmas at atmospheric pressure and their non-thermal operation facilitate the introduction of liquids such as water for water treatment, medical, and material applications. Recently, there has been interest in the reduction of metal salts in aqueous solutions by microplasmas to produce colloidal nanoparticles (NPs). It is generally accepted that some active species from the plasma react with the solution phase and either directly reduce the metal cation or produce a reducing species. However, it remains unclear how exactly the metal cation is reduced to produce NPs.

In this study, we carried out experiments to understand the formation of silver (Ag) and gold (Au) NPs from their respective metal salt precursors with or without stabilizing capping molecule by reactions at the interface of a microplasma and the aqueous solution phase. The NPs were characterized after synthesis by ultraviolet-visible (UV-vis) absorption spectroscopy and transmission electron microscopy (TEM), and the chemical composition of the solution was characterized before and after microplasma treatment by ionic conductivity, electrochemical potential, and UV-vis absorption spectroscopy.

Our results show that both Ag and Au NP formation are directly proportional to the plasma current and process time. The calculated reduction efficiency based on the number of electrons injected and the number of Ag⁺ reduced is only $\sim 50\%$ while the reduction efficiency for the Au precursor was $\sim 25\%$. Another difference between the two metals is that plasmon band for Au was found to increase even after the plasma treatment was stopped. This was corroborated by a measured decrease in the concentration of the Au complex, confirming that reduction continues to occur without the plasma, presumably because of a long-lived reducing species generated in solution.

Assuming electrons are the important charge carriers, electrons can reduce metal cations, but can also reduce water to form OH radicals which in turn react to form hydrogen peroxide (H₂O₂). H₂O₂ is known to be a weak reducing agent and could also reduce the metal salts but based on our experiments and reduction potentials, we believe that H₂O₂ could only induce the formation of Au NPs.

To gain more insight into the different mechanisms involved, the gas phase above the plasma-liquid system was analysed by optical emission spectroscopy (OES); a variety of species were observed (OH, O, H, NO, N₂) and ultimately linked to the reactions occurring in the liquid phase.

This work was supported by the Belgian Federal Government (IAP research project P7/34 – Physical Chemistry of Plasma Surface Interactions).

2:40pm PS+2D-TuA2 Controllable Optical Properties of Plasmonic TiN Nanoparticles Synthesized by a Scalable Non-Thermal Plasma Method, Alejandro Alvarez Barragan, L. Zhong, L. Mangolini, University of California Riverside

Titanium nitride is a refractory material with optical properties similar to those of gold. It has therefore attracted significant interest, since TiN nanoparticles are expected to show localized surface plasmon resonance in the visible/near-infrared range, all while overcoming the cost and thermal stability limitations of gold. For instance, they are a very attractive substitute of gold nanoparticles in biomedical applications [1]. Most of the methods involving TiN nanopowder synthesis use effective but complicated chemical routes [2,3]. In this contribution, we present a highly scalable method for the production of TiN nanoparticles using a non-thermal

plasma process. A low-pressure non-thermal plasma reactor is used to continuously nucleate and grow crystalline TiN nanoparticles starting from a mixture of ammonia and titanium tetrachloride. Besides achieving a remarkable production rate (~50 mg/h), we were also able to control the particle size and stoichiometry with great precision by tuning process parameters such as gas composition and plasma input power. This finding is of paramount importance because the plasmonic peak position is highly dependent on these two parameters [4]. Absorption measurements of the as-synthesized particles show clear plasmonic resonance in the near-infrared region, ranging between 800 and 1000nm when dealing with the largest and smallest particles, respectively. XRD and high resolution TEM/EDS characterization also provides insight on the nitrogen content of the samples and its close correlation to particle size. The role of process parameters on the surface of the particles, which in turn affects their plasmonic properties, will be discussed extensively.

References

- [1] L.R. Hirsch, R.J. Stafford, J. A. Bankson, S.R. Sershen, B. Rivera, R.E. Price, et al., Nanoshell-mediated near-infrared thermal therapy of tumors under magnetic resonance guidance., *Proc. Natl. Acad. Sci. U. S. A.* 100 (2003) 13549–54. doi:10.1073/pnas.2232479100.
- [2] F. Liu, Y. Li, Y. Yao, H. Zhang, W. Shao, Y. Kang, et al., Preparation of titanium nitride nanoparticles from a novel refluxing derived precursor, *J. Wuhan Univ. Technol. Sci. Ed.* 26 (2011) 429–433.
- [3] S. Kaskel, K. Schlichte, G. Chaplais, M. Khanna, Synthesis and characterisation of titanium nitride based nanoparticles, *J. Mater. Chem.* 13 (2003) 1496.
- [4] U. Guler, S. Suslov, A. V. Kildishev, A. Boltasseva, V.M. Shalae, Colloidal Plasmonic Titanium Nitride Nanoparticles: Properties and Applications, *Nanophotonics*. 4 (2015) 269–276. doi:10.1515/nanoph-2015-0017.

3:00pm **PS+2D-TuA3 Plasma Prize Talk: Nonthermal Plasma Synthesis of Nanocrystal Materials**, *N.J. Kramer, K. Schramke, T. Chen, H. Fu, S. Ehrenberg, K. Reich, B. Shklovskii, Uwe Kortshagen**, University of Minnesota

INVITED

Nonthermal plasma synthesis of nanocrystals is particularly suited for covalently bonded materials that require high temperatures to be produced with good crystallinity. Several years ago, we showed that plasma produced silicon nanocrystals are capable of high-efficiency photoluminescence, different from bulk silicon material. More recently, the capability of nonthermal plasmas to produce substitutionally doped nanocrystal materials has attracted attention, as substitutional doping had presented a significant challenge both for liquid and gas phase synthesis due to effects such as self-purification.

This presentation discusses the physics of plasma synthesis process. High photoluminescence quantum yields are achieved by careful surface functionalization through grafting alkene ligands to the nanocrystal surfaces. We also discuss the substitutional doping of silicon nanocrystals with boron and phosphorous using a nonthermal plasma technique. While the synthesis approach is identical in both cases, the activation behavior of these two dopants is found to be dramatically different. Finally, we present some experimental work on transport in films of highly phosphorous-doped nanocrystals, which indicates the approach to the metal-to-insulator transition.

This work was supported in part by the NSF Materials Research Science and Engineering Center under grant DMR-1420013, the DOE Energy Frontier Research Center for Advanced Solar Photophysics, and the Army Office of Research under MURI grant W911NF-12-1-0407.

4:20pm **PS+2D-TuA7 Initiated Plasma Enhanced Chemical Vapor Deposition of Metalloporphyrins: A Simple Route towards the Deposition of Metal Organic Covalent Networks**, *Nicolas BOSCHER*, Luxembourg Institute of Science and Technology, Luxembourg; *M. WANG, K. GLEASON*, Massachusetts Institute of Technology

Porphyrins and porphyrinoids are robust and versatile functional molecules with varying properties depending on their central metal ion and peripheral and axial substituents. They have proved to be useful in a wide range of applications, including the catalysis and photocatalysis of various chemical reactions, in molecular sensing, light harvesting applications, and for gas storage and gas separation applications. In addition to these functional assets, their rigidity and chemical stability make them ideal as building units for the formation of covalent and coordination metal-organic polymers, including metal-organic frameworks (MOFs). Nevertheless, the

difficult processability of these poorly soluble and non-meltable materials makes difficult their integration into smart devices.

Provided the fact that the monomer to deposit possesses free-radical polymerizable bonds, initiated PECVD (iPECVD) promotes conventional chain-growth polymerisation pathways, ensuring an excellent retention of the monomer structure. Several works have highlighted the radical polymerizability of the exo-pyrrole double bond of the porphyrin rings. The propagation reaction occurs at the beta-position of the porphyrin ring, leading to the formation of a polymer of reduced porphyrins, i.e. chlorin. Based on this wet-chemistry result, we recently investigated the use of zinc (II) meso-tetraphenylporphyrin (ZnTPP) building units in an iPECVD process and formed a new kind of metal-organic covalent network (MOCN) thin films.

5:00pm **PS+2D-TuA9 Plasma-graphene Interaction and its Effects on Nanoscale Patterning**, *A. Harpale*, University of Illinois at Urbana-Champaign; *Huck Beng Chew*, University of Illinois at Urbana-Champaign

INVITED

Graphene is the lightest and strongest known material, and is also an ideal thermal and electrical conductor. Despite its unique properties, graphene has to be patterned to achieve its full engineering and nanotechnological potential. Recent experiments show that a monolayer of graphene deposited on an SiO₂ substrate and subjected to hydrogen plasma treatment either undergoes (a) selective etching from the edges of the graphene sheet while leaving the basal plane intact, or experiences (b) etching of both the edges and basal plane of the graphene sheet which results in the formation of nanoscale holes in graphene. The plasma-etched holes in (b) can be either circular or hexagonal, suggesting that the etching process can be isotropic or anisotropic. Here, we model the hydrogen-plasma etching of monolayer graphene on SiO₂ substrates across the range of plasma energies using scale-bridging molecular dynamics simulations. Our results uncover distinct etching mechanisms, operative within narrow hydrogen-plasma energy windows, which fully explain the differing plasma-graphene reactions observed experimentally. Specifically, our simulations reveal very sharp transitions in the etching mechanisms with increasing hydrogen ion energy: selective edge etching at ion energies of ~1 eV, isotropic basal plane etching at ion energies of between 2 and 5 eV, and anisotropic etching at ion energies > 7 eV. Understanding the complex plasma-graphene chemistry and the relationship to plasma process parameters opens up a means for controlled patterning of graphene nanostructures.

5:40pm **PS+2D-TuA11 A Closer Look at Chemically Modified Graphene**, *Sandra Hernández*, Naval Research Laboratory

INVITED

Graphene has been a research focus due to its numerous unique properties which have motivated vast interdisciplinary research in the search of materials for next-generation technologies. With its unique atomically thin nature, graphene has enabled a closer look at material surface interactions and highlighted the importance of surface interfaces, defects and adsorbates. Purposeful and native defects have demonstrated to have advantageous or adverse influences on the chemical, electrical, optical, mechanical and even magnetic properties of graphene. On the other hand, control of the localization of defects and their arrangement onto ordered and extended structures has enabled new graphene-based materials with novel properties. Surface functionalization has provided the ability to manipulate the material attributes, offering a range of opportunities for the chemically modified materials. It is clear that fundamental understanding of the modification of graphene relies on the understanding of the chemical functionalization dynamics, kinetic barriers, chemical transitions, and diffusion energies experienced by the added adsorbates with the graphene surface as well as the influence of the substrate on each.

Plasmas provide both ease and versatility by enabling a single tool process on a wide range of background gases. In particular, electron-beam generated plasmas can introduce different functional groups over a large coverage range with atomic layer precision, providing the ability to tailor the locality of the surface chemistry on graphene opening up a wide range of reactivity studies and synthesis capabilities. Such unique ability allows for precise nano-engineering of the surface chemistry effecting local electronic properties, electron transfer kinetics, and surface reactivity; opening up a wealth of opportunities in device performance, chemical sensing, bottom-up material growth, plasmonics, and catalysis applications.

This work is supported by the Naval Research Laboratory Base Program.

Novel Trends in Synchrotron and FEL-Based Analysis Focus Topic

Room 103C - Session SA+AS+BI+MI-TuA

Synchrotron and XFEL Advances for Biological Systems (2:20-3:40 pm)/Synchrotron Radiation at the Frontiers of Device Technology (4:20-6:20 pm)

Moderators: David Shuh, Lawrence Berkeley National Laboratory, Olivier Renault, CEA-University Grenoble Alps, France

2:20pm SA+AS+BI+MI-TuA1 Crystal Growth Mechanisms of Biominerals Revealed by Polarization-dependent Imaging Contrast (PIC) Mapping, **Pupa Gilbert**, University of Wisconsin - Madison **INVITED**

X-ray linear dichroism was first shown in natural biominerals by Metzler et al. [1]. Based on this effect, we developed Polarization-dependent Imaging Contrast (PIC)-mapping, which displayed non-quantitative crystal orientation at the nanoscale as gray levels in ratios of images acquired at different linear polarizations [2]. A later development provided grayscale, semi-quantitative PIC-maps by acquiring stacks of 19 images as the linear polarization was rotated in 5° intervals from 0° to 90° [3-7]. The latest development uses the same stacks of images to fully, quantitatively display crystal orientations in colors, including hue and brightness, which represent in-plane and off-plane crystallographic c-axis orientation angles [8-10].

Using PIC-mapping in these 3 subsequent modes, we discovered several biomineral formation mechanisms in nacre [11,7], sea urchin teeth [12-14], ascidian spicules [10], corals, eggshells, modern and fossil sea shell ultrastructure [15].

1. RA Metzler et al., Phys. Rev. Lett. 98, (2007). DOI: <http://dx.doi.org/10.1103/PhysRevLett.98.268102>
2. RA Metzler et al., Phys Rev B 77, 064110-1, (2008). DOI: <http://dx.doi.org/10.1103/PhysRevB.77.064110>
3. PUPA Gilbert et al., Proc Natl Acad Sci USA 108, (2011). DOI: 10.1073/pnas.1107917108
4. PUPA Gilbert, J Electr Spectrosc Rel Phenom, special issue on Photoelectron microscopy, Time-resolved pump-probe PES 185, (2012). DOI: <http://dx.doi.org/10.1016/j.elspec.2012.06.001>
5. IC Olson et al., J Am Chem Soc 134, (2012. JOURNAL COVER). DOI: dx.doi.org/10.1021/ja210808s
6. IC Olson et al., J Struct Biol 183, (2013). DOI: 10.1016/j.jsb.2013.06.006
7. IC Olson et al., J Struct Biol 184, (2013. JOURNAL COVER). DOI: 10.1016/j.jsb.2013.10.002
8. RT DeVol et al., J Phys Chem B 118, (2014). DOI: 10.1021/jp503700g
9. RT DeVol et al., J Am Chem Soc 137, (2015). DOI: 10.1021/jacs.5b07931
10. B Pokroy et al., Chem Mater 27, (2015. JOURNAL COVER.). DOI: 10.1021/acs.chemmater.5b01542
11. PUPA Gilbert et al., J Am Chem Soc 130, 17519, (2008). DOI: 10.1021/ja8065495
12. CE Killian et al., J Am Chem Soc 131, (2009). DOI: 10.1021/ja907063z
13. YR Ma et al., Procs Natl Acad Sci USA 106, (2009). DOI: 10.1073/pnas.0810300106
14. CE Killian et al., Adv Funct Mater 21, (2011). DOI: 10.1002/adfm.201001546
15. PUPA Gilbert et al., in preparation, (2016).

3:00pm SA+AS+BI+MI-TuA3 New Dimensions in Synchrotron IR Spectroscopy, **Michael Martin**, Lawrence Berkeley National Laboratory **INVITED**

Synchrotron infrared beamlines use the diffraction-limited beam properties to enable a variety of cutting edge science - how can we go further?

By combining scattering-scanning near-field optical microscopy (s-SNOM) with mid-infrared synchrotron radiation, synchrotron infrared nano-spectroscopy (SINS) enables molecular and phonon vibrational spectroscopic imaging, with rapid spectral acquisition, spanning the full mid-infrared (500-5000 cm⁻¹) region with nanoscale spatial resolution. This highly powerful combination provides access to a qualitatively new form of nano-chemometric analysis with the investigation of nanoscale, mesoscale, and surface phenomena that were previously impossible to study with IR techniques. We have installed a SINS end-station at Beamline 5.4 at the Advanced Light Source (ALS) at Lawrence Berkeley National Laboratory, making the s-SNOM technique widely available to non-experts, such that it

can be broadly applied to biological, surface chemistry, materials, or environmental science problems. We demonstrate the performance of synchrotron infrared nano-spectroscopy (SINS) on semiconductor, biomineral and protein nanostructures, providing vibrational chemical imaging with sub-septomole sensitivity.

The spatial field localization at the tip apex can also result in a large near-field momentum sufficient to optically excite phonon polaritons (PhPs), which are quasiparticles resulting from the strong coupling of photons with optical phonons. Here, we use SINS to image the PhP spectral response in thin hexagonal boron nitride (hBN) crystals. The large spectral bandwidth of the synchrotron source enables the simultaneous measurement of both the out-of-plane (780 cm⁻¹) and in-plane (1370 cm⁻¹) hBN phonon modes. In contrast to the strong and dispersive in-plane mode, the out-of-plane mode PhP response is weak. Measurements of the PhP wavelength reveal a proportional dependence on sample thickness for thin hBN flakes [2].

This talk will present the novel SINS instrumentation and a variety of scientific examples. Future directions, both technical and scientific, will be discussed.

*With Hans A Bechtel, Markus B. Raschke, Z. Shi, F. Wang, R.W. Johns, D.J. Miliron, E.A. Muller, R.L. Olmon

References

- [1] H.A. Bechtel *et al.*, Proceedings of the National Academy of Sciences of the USA, **111**(20), 7191–7196 (2014)
- [2] Z. Shi, H.A. Bechtel, S. Berweger, Y. Sun, B. Zeng, C. Jin, H. Chang, M.C. Martin, M.B. Raschke, and F. Wang, ACS Photonics **2** (7), 790-796 (2015).

4:20pm SA+AS+BI+MI-TuA7 Sample Delivery Methods for X-ray Free Electron Lasers, **Uwe Weierstall**, Arizona State University **INVITED**

Serial crystallography at XFEL's has shown great promise in recent years for solving crystal structures of proteins, which produce only micron sized crystals. Liquid jets have been very successful for delivery of microcrystals to the X-ray beam. The commonly used liquid injection system will be discussed. High sample consumption has motivated the development of an injector, which uses high viscosity media like Lipidic Cubic Phase (LCP). G-protein coupled receptors are an important group of membrane proteins which are often crystallized in LCP. The injector generates a microscopic stream of LCP with adjustable speed for sample delivery to the X-ray beam¹. Some important GPCR structures could be solved with this device at the LCLS². In addition, new media with similar viscosity to LCP have been developed which enable delivery of soluble or membrane proteins into the X-ray beam with low sample consumption³. The high viscosity injection method has also been shown to facilitate serial diffraction experiments with microcrystals at synchrotron microfocus beamlines. This talk will highlight these developments and discuss the possibilities.

¹ Weierstall, U., James, D., Wang, C., White, T. A., Wang, D., Liu, W., et al. (2014). Lipidic cubic phase injector facilitates membrane protein serial femtosecond crystallography. *Nature Communications*, **5**. <http://doi.org/10.1038/ncomms4309>

² Kang, Y., Zhou, X. E., Gao, X., He, Y., Liu, W., Ishchenko, A., et al. (2015). Crystal structure of rhodopsin bound to arrestin by femtosecond X-ray laser. *Nature*, **523**(7562), 561–567. <http://doi.org/10.1038/nature14656>

³ Conrad, C. E., Basu, S., James, D., Wang, D., Schaffer, A., Zatsepin, N. A., et al. (2015). A novel inert crystal delivery medium for serial femtosecond crystallography. *IUCr*, **2**(4), 421–430.

5:00pm SA+AS+BI+MI-TuA9 Synchrotron-based Spectroscopy Investigation for Electronic Phase Transition at Highly-Charged Electric-Double-Layer Interfaces, **Hongtao Yuan**, SLAC National Accelerator Laboratory **INVITED**

Electric-field control of charge carrier density has attracted much attention since it is remarkably simple for modulating physical properties of condensed matters and for exploring new functionalities with a transistor configuration. Owing to the limitation of dielectric breakdown in most solid dielectrics, the maximum carrier density accumulated in conventional field-effect transistors (FETs) is quite low ($< 10^{13}$ cm⁻²) and thus seriously limits the tunability of electronic states of solids, for example, not sufficient enough to induce insulator-to-superconductor transition. While the electric-double-layer transistor (EDLT) with ionic liquids (ILs, or ionic gel) as gate dielectrics have been proved to be able to effectively attain a high carrier density up to levels of around 10^{15} cm⁻² and to realize a large local electric field up to 50 MV/cm at liquid/solid interfaces. For example, electric-double-layer transistors have been demonstrated for an electric-field control of emergent interfacial quantum phenomena and the

Tuesday Afternoon, November 8, 2016

electronics phase transitions in condensed matters, such as insulator-superconductivity and paramagnetism-ferromagnetism transitions. However, the mechanistic/spectroscopic understanding of the local electronic structures at such highly charged IL/oxide EDL interfaces and also further modification under gate-bias remain elucidated and challenging.

In this talk, we conducted synchrotron radiation based X-ray absorption spectroscopy (XAS) and Auger electron spectroscopy (AES) combined with in situ electrical measurements to directly characterize the evolution of the electronic structure at a representative IL/La_{0.7}Sr_{0.3}MnO₃ (LSMO) thin film interface. We find a significant valence reduction localized to the topmost LSMO layer after interface formation, and that the gate-bias predominantly modulates this surface reduced Mn species effectively converting these top layers into an insulator. We expect the synchrotron radiation based photon science probing techniques will directly shed light on the understanding of interfacial electronic phase control under the electric field.

(This work was done in collaboration with Bongju Kim, Jun-Sik Lee, Yasuyuki Hikita and Harold Y. Hwang. This work was supported by the Department of Energy, Office of Basic Energy Sciences, Division of Materials Sciences and Engineering, under contract DE-AC02-76SF00515.)

5:40pm SA+AS+BI+MI-TuA11 Correlation of the Conductivity/Magnetic Properties and the Electronic, Crystalline and Compositional Structure of Strongly Correlated Complex-oxide Interfaces and Thin Films, Juan Rubio-Zuazo, SpLine CRG Beamline at the ESRF The European Synchrotron, France; *G.R. Castro*, SpLine CRG Beamline at the ESRF The European Synchrotron, France

We study the structural and electronic properties of strongly correlated complex-oxide thin films and interfaces using Hard X-ray Photoelectron Spectroscopy (HAXPES), Electron Energy Loss Spectroscopy (EELS) and Grazing Incidence X-ray diffraction (GIXRD) at the BM25-SpLine beamline (Branch B) at the ESRF. Strongly correlated complex-oxide exhibit a wide variety of interesting physical properties which originate from mutual coupling among spin, charge and lattice degrees of freedom. Usually, the interface drives the magnetic and electric response of the heterostructure. The chemical, mechanical, electric and magnetic properties of such devices are often intimately related to the structure, composition profile and morphology of their surface and internal interfaces. Several mechanisms are present at these interfaces as crystallographic space group modification, presence of oxygen vacancies, dislocations due to lattice strain, deviation from stoichiometry, phase segregation. In general all these phenomena modify the intrinsic properties of the materials used at the heterostructure, offering a unique way to produce artificial correlated materials with tailored properties. The growth of these materials in thin film form opens possibilities for magneto-electronic and spintronic devices applications. The results shown here are focused on the study of the influence of buried interfaces on the electric and magnetic properties of CMR and multiferroics systems. We will show the experimental methodologies at SpLine based on synchrotron radiation techniques to gain quantitative knowledge on the crystallographic and electronic properties at the interface between different complex oxides. There are few techniques able to provide an accurate insight of what is happening at these buried interfaces which in general are buried by several tens of nanometres in the material. The simultaneous combination of hard and soft X-ray photoelectron spectroscopy, electron energy loss spectroscopy with surface/interface X-ray diffraction gives unique capabilities in this respect. Here we will present a series of examples to show how the interface properties can change the magnetic-conductivity properties.

6:00pm SA+AS+BI+MI-TuA12 Interface Passivation of III-V/High-k Materials by High Energy X-ray Photoelectron Spectroscopy: A Quantitative Evaluation, Thierry Conard, V. Spampinato, L. Nyns, S. Sioncke, IMEC, Belgium; *J.M. Ablett*, Synchrotron SOLEIL- Ligne GALAXIES, France; *W. Vandervorst*, IMEC, KU Leuven, Belgium

The use of InGaAs as a high carrier mobility CMOS-channel material requires a proper electrical passivation of its interface with the gate dielectric. One of the passivation schemes investigated involves the use of Sulphur. In this work, high-k stacks on Sulphur passivated InGaAs substrates involving both Al₂O₃ and HfO₂ are investigated. A major question related to the use of Sulphur relates to the chemical states at the interfaces. XPS is traditionally an important technique for interface analysis but faces several challenges in its application to the above mentioned stacks. First, due to the large number of elements involved, numerous peak interferences are present limiting the choice of useful photoemission peaks. Second, relevant stacks have total thicknesses of the order of 4 nm, which lead to very low intensities, certainly for minority elements like

Sulfur. In this work, we discuss the impact of the H₂S passivation temperature as well as the use of TMA pre-pulses in the growth of Al₂O₃. We show that the Sulphur binds to In but that no As-S or Ga-S bonds could be detected. The use of a TMA pre-pulse after surface passivation leads to a reduction of the amount of Sulphur present at the interface and likely increases the amount of In-O bonds. Higher temperature H₂S passivation leads to a reduction of the amount of Sulphur at the surface.

We also observe that the presence/absence of S at the interface, as well as the presence of the Al₂O₃ buffer, which has a major impact on the relative peak position in the spectra between the substrate and the overlayer. This will be compared with the electrical characteristics of the stacks.

Finally, we show that using the Sessa software, full quantification of the stack can be obtained under the condition that all instrumental parameters are correctly taken into account.

Advanced Surface Engineering Room 101C - Session SE+MS+TF-TuA

Innovations in PVD, CVD, Atmospheric Pressure Plasma and Other Surface Technologies

Moderators: Michael Stueber, Karlsruhe Institute of Technology, Germany, Robert Franz, Montanuniversität Leoben, Austria

2:20pm SE+MS+TF-TuA1 Investigation of Critical Processing Parameters on Laser Surface Processing of Mg-Al-Zn Alloys: Impact on Corrosion Kinetics, Michael Melia, D.C. Florian, J.R. Scully, J.M. Fitz-Gerald, University of Virginia

Magnesium (Mg) and its alloys have been the topic of intense research over the past 15 years as the automotive and aeronautic industries strive to increase fuel efficiency by reducing the weight of vehicles. However their wide spread implementation is currently limited by poor intrinsic corrosion resistance. Preferential dissolution of the Mg matrix occurs due to the electrochemically noble secondary phases formed during traditional processing routes of Mg alloys. To mitigate the impact secondary phases (e.g. γ -Al₃Mn₅) have on corrosion, pulsed laser surface processing was employed in the ns time regime. Lasers operating in this time regime are capable of melting and solidification rates on the order of 10⁹ K/s with the ability to extend the solid solubility limit of the alloying elements. The research herein shows the impact laser processing parameters have on the dissolution of the secondary phases and corrosion resistance in the Mg-Al-Zn alloy, AZ31B.

A KrF excimer laser ($\lambda = 248$ nm, pulse duration = 25 ns FWHM) was utilized with a cylindrical focusing lens, a laser spot size of 27 mm x 1.2 mm, and a pulse overlap of 95%. The processing parameters investigated include the laser fluence (0.7, 0.8 and 1.5 J/cm²), irradiation dosage (pulse per area (PPA) = 20 to 400), and processing pressure (1 to 1280 Torr Ar). The dissolution of the γ -Al₃Mn₅ particles was observed by scanning electron microscopy equipped with a backscatter electron detector. Fiducial image recognition was utilized to observe the change in γ -Al₃Mn₅ particle size before and after processing. Analysis of the H₂ evolution reaction rate, related to the quantity and density of electrochemically noble secondary phases, was performed by potentiodynamic polarization measurements in 0.6 M NaCl solution.

Results from the fluence study revealed significant dissolution of the γ -Al₃Mn₅ particles when processing was performed above the ablation threshold suggesting that material transport was afforded by a laser induced plasma pressure acting on the irradiated layer, increasing the extent of dissolution. This was also observed by an order of magnitude reduction in H₂ evolution reaction rate. The lowest pressure of Ar investigated, 1 Torr, consistently exhibited the smallest reduction in H₂ evolution reaction rate from the bulk material. All other processing pressures showed an order of magnitude reduction in H₂ evolution reaction rate when a fluence above the ablation threshold was used. The PPA study revealed a plateau in the reduction of the H₂ evolution reaction rate, observed dissolution of γ -Al₃Mn₅ particles, and time to breakdown of the corroding surface after 100 PPA.

2:40pm SE+MS+TF-TuA2 Engineering a WC/Co Carbide Surface for PVD and CVD coatings, Aharon Inspektor, P.A. Salvador, Carnegie Mellon University; *D. Banerjee, C. McNerny, M. Rowe, P. Mehrotra*, Kennametal Inc.

The emergence of new coating technologies is driving the development of new cutting tools and improved metal cutting techniques. However, to

reach these goals, the coating has to work in concert with the tool substrate material. Hence, building a functional surface that consists of coating and substrate working together, is a key step in the development of new cutting tool. In this paper we will look at the substrate side of the coating - surface interface and discuss how it affects the properties of the subsequent coating. The focus will be on surface engineering of WC/Co carbide surface for Physical Vapor Deposition, PVD, for Chemical Vapor Deposition, CVD, and for CVD diamond coatings. Specifically, Co mobility in the subsurface zone for CVD coatings and surface treatment for PVD coatings. Structure and properties of the resultant surface - coating combination will be presented and discussed.

3:00pm SE+MS+TF-TuA3 Room-Temperature Ductility in Refractory Transition-Metal Carbides: Potential to Create Ultra-Tough, Flexible Thin Films, *Suneel Kodambaka*, University of California at Los Angeles **INVITED**

Transition-metal carbides are high-melting (> 3000 K), extremely hard (10s of GPa), mechanically robust, and chemically resilient compounds capable of operating in extreme environments and are attractive for aerospace and other industries. These hard materials are generally considered to be brittle at low temperatures. Improving their ductility, and hence toughness, is highly desirable but progress thus far has been limited by the lack of a basic understanding of the intrinsic deformation mechanisms in this class of materials. Here, using *in situ* transmission electron microscopy (TEM) coupled with uniaxial compression tests conducted on sub- μm -size pillars, in combination with density functional theory (DFT) calculations, we show that dislocations are mobile at room-temperature and lead to plastic deformation in NaCl-structured group IV and group V transition-metal carbide single crystals, zirconium carbide (ZrC) and tantalum carbide (TaC). We find that the yield strengths of ZrC crystals increase with decreasing size and ZrC(111) is softer than ZrC(100) crystals, an unexpected finding for NaCl-structured compounds. We attribute this anomalous behavior to surprisingly easy dislocation motion and low shear stresses along {001}<1-10> rather than along the commonly assumed {110}<1-10> slip systems. For TaC, in contrast to ZrC, the yield strengths are found to be independent of crystal size and orientation. Our observations suggest that multiple slip systems can be active and operate at room temperature in these hard, refractory ceramics and we expect similar behavior in other transition-metal carbides and nitrides. The insights gained from these studies may help in the development of new material architectures, such as tough and flexible membranes, for new small-scale structural applications.

4:20pm SE+MS+TF-TuA7 Spray-Coated Carbon-Nanotubes for Crack-Tolerant Metal Matrix Composites as Photovoltaic Gridlines, *Omar K. Abudayyeh*, University of New Mexico; *N.D. Gapp*, *G.K. Bradshaw*, *D.M. Wilt*, Air Force Research Laboratories; *S.M. Han*, University of New Mexico

Microcracks developing in photovoltaic cells, due to growth defects or due to external mechanical factors, can lead to substantial power loss in solar cells. Microcracks can be critical as they propagate from the semiconductor bulk to the metal gridlines isolating portions of the cell and leading to decreased cell performance. In this work, multiwalled carbon nanotubes are being investigated for reinforcement of metal contacts on photovoltaic solar cells that serve as a secondary conductive network in the presence of cracks. In this effort we have focused on a silver-carbon-nanotube layer-by-layer microstructure. We present the use of a simple, cost-effective, and manufacturable method of depositing carbon nanotubes onto electroplated metal films to create metal matrix composite gridlines for photovoltaic cells. Carbon nanotubes are deposited using a spray coating method to create layer-by-layer microstructure composites. To increase adhesion strength to metal and achieve efficient metal-nanotube stress transfer, carbon nanotubes are chemically functionalized with carboxylic group prior to deposition. Initial strain failure tests show the ability of composite lines to remain electrically connected with fractures up to 28- μm -wide on average, where carbon nanotubes electrically bridge the gap. The metal-carbon-nanotube composites are electrically characterized through current-voltage (*I-V*) sweeps. Our composite lines can carry current densities ranging from 500 to 2500 A/cm² in the presence of cracks (5, 10, and 15- μm -wide). MMC gridlines are successfully integrated on commercial triple-junction solar cells with measured fill factor and efficiency 86% and 26.8% respectively, closely comparing to current triple-junction cells with standard metallization. Dark *I-V* measurements indicate further improvement in the series and shunt resistances of the cells with the optimization of MMC integration process.

4:40pm SE+MS+TF-TuA8 Atmospheric Pressure Plasma Enhanced CVD of High Quality Silica-Like Bilayer Encapsulation Films, *Fiona Elam*, FUJIFILM Manufacturing Europe B.V., Netherlands; *A.S. Meshkova*, DIFFER, Netherlands; *S.A. Starostin*, *J.B. Bouwstra*, FUJIFILM Manufacturing Europe B.V.; *M.C.M. van de Sanden*, Dutch Institute for Fundamental Energy Research (DIFFER), Netherlands; *H.W. de Vries*, DIFFER, Netherlands

Atmospheric pressure-plasma enhanced chemical vapour deposition (AP-PECVD) is an innovative technology that can be integrated into many existing manufacturing systems to facilitate the mass production of functional films; specifically encapsulation foils. These barrier films are essential to the flexible electronics industry, envisioned to protect devices such as flexible solar cells and organic light emitting diodes against degradation from oxygen and water.

Roll-to-roll AP-PECVD was recently used to produce smooth, 90 nm silica bilayer thin films comprising a 'dense layer' and 'porous layer' that demonstrated exceptionally good encapsulation performance with effective water vapour transmission rates in the region of $6.9 \times 10^{-4} \text{ g m}^{-2} \text{ day}^{-1}$ (at 40°C, 90% relative humidity). By using the same material in the multilayer film architecture, and by having AP-PECVD as the deposition method, rendered this investigation highly industrially and commercially relevant to the eventual large scale production of flexible encapsulation foils. It was discovered that increasing the input energy per precursor gas molecule during the deposition of the dense layer, resulted in an improved encapsulation performance. However, the individual role performed by each layer in the overall success of the bilayer films is not yet fully understood, nor is the potential for energy conservation by varying process throughput.

A glow-like AP dielectric barrier discharge in a roll-to-roll set-up was used to deposit silica bilayer thin films onto a polyethylene 2,6 naphthalate substrate by means of PECVD. Tetraethyl orthosilicate (TEOS) was used as the precursor gas, together with a mixture of nitrogen, oxygen and argon. In each case, the deposition conditions for the synthesis of the dense layers were varied in order to study the effect of input energy per TEOS molecule and process throughput on the chemical composition and porosity of the layer. Deposition conditions for the porous layers were kept constant, with process throughput the only exception. Each film was characterised in terms of its water vapour transmission rate, its chemical composition and its morphology as a function of the input energy per TEOS molecule during the dense layer deposition and overall process throughput.

For the first time in AP-PECVD, it was found that the porous layer plays a critical role regarding encapsulation performance and surface smoothing of silica bilayer films. Due to increased throughput, the bilayer architecture also enables a 50% reduction in deposition energy consumption per barrier area, with respect to single layer silica films of equivalent encapsulation performance and thickness.

5:00pm SE+MS+TF-TuA9 Plasma Polymerization of Organic Coatings at Atmospheric Pressure: Relationship between the Precursor Chemistry, the Plasma Chemistry and the Final Coating Chemistry, *B. Nisol*, *N. Vandecasteele*, *J. Hubert*, *C. De Vos*, *J. Ghesquière*, *D. Merche*, *François Reniers*, Université Libre de Bruxelles, Belgium

The synthesis of organic coatings using plasma technologies has been developed since many decades. This paper investigates a full series of organic coatings, synthesized in the same dielectric barrier discharge system, in the same operational conditions. The >10 precursors vary from fully saturated molecules, with or without heteroatoms (hexamethylnonane, CxCl_y, CxF_y), to anhydrides, acrylates, with or without double or triple bonds. It is shown that the presence of double bonds not only significantly increase the polymerization rate, but also protect the ester function in acrylates. A combined effect of the plasma power and the presence of double bonds on the C/O ratio is observed for all the relevant precursors used. Correlation between the plasma chemistry and the fragment pattern in the gas phase, as recorded by atmospheric mass spectrometry, with the final chemical composition of the coatings, determined by XPS and FTIR is established. Coatings properties can be easily tuned either by combining precursors, by varying the plasma power or by changing the main plasma gas. By an appropriate combination of the plasma parameters and the precursor, very high deposition rates can be achieved, highly hydrophobic or hydrophilic coatings can be synthesized. These macroscopic results are interpreted in terms of plasma properties, and chemical reactivity.

This work was supported by the Belgian Federal Government (IAP research project P7/34 – Physical Chemistry of Plasma Surface Interactions).

Tuesday Afternoon, November 8, 2016

5:20pm **SE+MS+TF-TuA10 Innovations in Atmospheric Pressure Plasma Technologies for Surface Engineering**, *David Ruzic, Y.L. Wu, L. Na, S. Hammouti, I.A. Shchelkanov*, University of Illinois at Urbana-Champaign

INVITED

The growing need for high efficiency-low cost coating tools for large area surfaces drives research efforts for development of innovative techniques. One of the options is an Evaporative Coating at Atmospheric Pressure process (ECAP). The principal of this deposition method is an evaporation of a material, with-in a plasma environment. The appealing advantage of this deposition technique is its atomic nature, and its environmentally safe process as no harmful chemicals compounds are used. With ECAP the evaporated material atoms end up deposited molecule-by-molecule or atom-by-atom as in a Physical Vapor Deposition but without the need for a vacuum chamber. This effect is achieved by using a thermal energy from the microwave plasma, when solid 99.99%+ purity metallic and ceramic target such as Al, Sn, Cr, Au, Ag and AlCl_3 could be evaporated and then produce a PVD-like coating on a work piece. The tool is designed to have the evaporated material being submerged into the center of the atmosphere microwave discharge. As the result evaporation occur in a controlled environment where a pure metals can be deposited or their compounds. For example in the aluminum case, a pure alpha phase of Al_2O_3 can be deposited using oxygen from the environment, or if a metallic coating of such a reactive metal as Al, is desired, the deposition can be performed in a pure Ar argon environment with the help of a special gas curtain. The tool provides deposition rate for metals as high as 1-5 $\mu\text{m}/\text{min}$ with high adhesion. The measured adhesion for copper on steel was at least 250 g/mm^2 . The ECAP technology opens broad possibilities for surface processing at atmosphere without environmental impact.

6:00pm **SE+MS+TF-TuA12 Solid-state Dewetting: Control and Applications**, *Lukasz Borowik, Y. Almadori, N. Chevalier, J.-C. Barbé*, CEA, LETI, MINATEC Campus, France

The dewetting of ultrathin silicon layers, induced by the thermal budget, is an issue to develop Silicon On Insulator (SOI) and Silicon Germanium On Insulator (SGOI) based technologies. However, dewetting can be controlled to obtain well-arranged agglomerates with similar size or even inhibited. This experimental study aims at demonstrating: the effect of the strain, surface contamination, ion sputtering on the dewetting mechanism, and further applications of dewetting thanks to interfacial reaction between agglomerates and the silicon dioxide. For that purpose, we present the results obtained on: (1) (001) oriented ultrathin (8-22 nm) silicon layers on silicon dioxide, (2) (001) oriented 12 nm silicon-germanium layers on silicon dioxide. In order to understand the dewetting mechanism, samples were heated up to $\sim 800^\circ\text{C}$ under ultra-high vacuum (1×10^{-9} mBar) during tens of minutes. The dewetted samples were characterized by Atomic Force Microscopy (AFM) to put in evidence the influence of the different factors on dewetting mechanism.

In first part of our presentation we will present various methods to control dewetting process by using different parameters such as: strained silicon, [1] surface contamination [2] or argon pre-sputtering. [3] These parameters allow tuning agglomerates size, shape and density. In second part of the talk we will show possible applications of dewetting to form porous silicon dioxide via agglomerates interfacial reaction, and finally how to master stoichiometry of silicon germanium agglomerates. [4] All these methods are promising since permit an easy and fast implementation, it is thus of real interest, since it opens up Si and SiGe agglomerates with tuned Ge concentration to application in innovative technologies.

This work was performed in the frame of the ANR LOTUS project. The measurements were realized on the CEA Minattec Nanocharacterization Platform (PFNC).

References:

- [1] Ł. Borowik et al. Journal of applied physics 114, 063502 (2013)
- [2] Ł. Borowik et al. Thin solid films 527, 133–136 (2013)
- [3] F. Leroy et al. Surface Science Reports accepted
- [4] Y. Almadori et al., 120, 7412–7420 (2016)

Scanning Probe Microscopy Focus Topic
Room 104A - Session SP+AS+MI+NS+SS-TuA

Probing Spin-Dependent Phenomena

Moderators: Phillip First, Georgia Institute of Technology, Shivani Rajput, Oak Ridge National Laboratory

2:20pm **SP+AS+MI+NS+SS-TuA1 Spin Sensing and Magnetic Design at the Single Atom Level**, *Alexander Khajetoorians*, Radboud University, The Netherlands

INVITED

Unraveling many of the current dilemmas in nanoscience hinges on the advancement of techniques which can probe the spin degrees of freedom with high spatial, energy, and ultimately high temporal resolution. With the development of sub-Kelvin high-magnetic field STM, two complementary methods, namely spin-polarized scanning tunneling spectroscopy (SP-STs) [1] and inelastic STs (ISTS) [2-3], can address single spins at the atomic scale with unprecedented precession. While SP-STs reads out the projection of the impurity magnetization, ISTs detects the excitations of this magnetization as a function of an external magnetic field. They are thus the analogs of magnetometry and spin resonance measurements pushed to the single atom limit. We have recently demonstrated that it is possible to reliably combine single atom magnetometry with an atom-by-atom bottom-up fabrication to realize complex atomic-scale magnets with tailored properties [4-6] on metallic surfaces [1,7]. I will discuss the current state of the art of this growing field as it pertains to single spin information storage, and how the functionality of coupled magnetic adatoms can be tailored on surfaces by substrate mediated interactions. I will discuss our recent efforts toward realizing tailored chiral magnets [8] and present an outlook on future perspectives toward probing quantum matter at ultra-low temperatures.

[1] A.A.K., et al., PRL, 106, 037205 (2011); [2] A. J. Heinrich, et al., Science, 306, 466 (2004); [3] A.A.K, et al., Nature, 467, 1084 (2010); [4] A.A.K., et al., Nature Physics, 8, 497 (2012) [5] A.A.K., et al., Science, 332, 1062 (2011), [6] A.A.K., et al., Science, 339, 55 (2013), [7] A.A.K., et al., PRL, 111, 126804 (2013). [8] A.A.K., et al. Nature Comm, 7, 10620 (2016).

3:00pm **SP+AS+MI+NS+SS-TuA3 Electron Spin Resonance of Single Atom and Engineered Spin Structures**, *Taeyoung Choi, W. Paul, C.P. Lutz, A.J. Heinrich*, IBM Almaden Research Center

INVITED

The scanning tunneling microscope (STM) has been one of the most versatile tools for atomic-scale imaging, manipulation, and tunneling spectroscopy. Inelastic spin excitation and spin-polarized tunneling have been employed to study spin physics of individual atoms and engineered structures, demonstrating nanoscale memory bits [1] and logic gates [2]. However, the energy resolution of the STM is mainly limited by a temperature of a system surrounding the atomic spins ($>100 \mu\text{eV}$).

Here, we successfully combine electron spin resonance (ESR) and STM, coherently driving spin resonance of individual iron (Fe) atoms on surfaces ($\text{MgO}/\text{Ag}(100)$) [3]. A radio-frequency electric field ($\sim 20 \text{ GHz}$), applied at the tunneling junction, modulates the spin state of the Fe atoms. The spin resonance signal is detected by a spin-polarized tunneling current. The ESR signals from individual Fe atoms differ by a few GHz ($\sim 10 \mu\text{eV}$) while the ESR linewidth is in the range of only a few MHz ($\sim 10 \text{ neV}$). Such a high energy resolution enables us to distinguish spin distributions down to single-atom level and to investigate weak magnetic interactions.

When we placed two Fe atoms close together with controlled atom manipulation, we found that the ESR signal from each Fe atom splits into doublet, of which separation depends on the distance between two atoms. Our measurements show $r^{-3.024 \pm 0.026}$ distance-dependent splitting, in excellent agreement of magnetic dipole-dipole interaction. We utilized this precisely measured dipolar interaction to determine the location and magnetic moment of unknown spin centers with sub-angstrom and one hundredth of Bohr magneton precision [4].

Coherent quantum control of individual atoms on surfaces combined with atom manipulation may promise the STM as a new and unique platform for a quantum sensor, investigating spin-labeled molecular structures and a quantum information processor, modeling quantum magnetism.

We gratefully acknowledge financial support from the IBM and Office of Naval Research.

[1] S. Loth, S. Baumann, C.P. Lutz, D.M. Eigler, A.J. Heinrich, Science **335**, 196 (2012).

[2] A.A. Khajetoorians, J. Wiebe, B. Chilian, and R. Wiesendanger, Science **332**, 1062 (2011).

Tuesday Afternoon, November 8, 2016

[3] S. Baumann*, W. Paul*, T. Choi, C.P. Lutz, A. Ardavan, A.J. Heinrich, Science **350**, 417 (2015).

[4] T. Choi et al., *manuscript in preparation*.

4:40pm **SP+AS+MI+NS+SS-TuA8 Controlling Kondo Effect of Magnetic Molecules on Au(111) by Small Molecule Binding, MinHui Chang, S.J. Kahng**, Korea University, Republic of Korea; Y.H. Chang, Korea Advanced Institute of Science and Technology (KAIST), Republic of Korea; H.W. Kim, S.H. Lee, Korea University, Republic of Korea; Y.-H. Kim, KAIST, Republic of Korea

Controlling and sensing spin states of magnetic molecules at the single molecule level is essential for spintronic molecular device applications. Here, we demonstrate that spin interactions of Co-porphyrin on Au(111) can be controlled by adsorption and desorption of small molecules, and be sensed using scanning tunneling microscopy and spectroscopy (STM and STS). Bare Co-porphyrin showed a clear zero-bias peak, a signature of Kondo effect in STS, whereas Co-porphyrin adsorbed small molecules showed modified zero-bias peaks, with reduced full width half maximum or Kondo temperature. Our density functional theory calculation results explain it with spatial redistribution of unpaired spins in d_{z^2} Orbitals. Our study opens up ways to tune molecular spin interactions by means of chemical binding.

5:00pm **SP+AS+MI+NS+SS-TuA9 Spin-polarized Scanning Tunneling Microscopy on Surfaces Prepared by Molecular Beam Epitaxy, Arthur Smith**, Ohio University Nanoscale and Quantum Phenomena Institute
INVITED

Spin-polarized scanning tunneling microscopy (SP-STM) has proven to be a powerful *in-situ* technique for obtaining detailed information about spin structures at surfaces down to atomic scale.¹ It has been applied extensively to investigate pristine ferromagnetic and antiferromagnetic (aFM) transition metal surfaces, with many great results in the case of model systems such as nano-sized magnetic islands and single magnetic monolayers.² This has led to fascinating discoveries of nanoscale magnetic domains, domain walls, spin spirals, spin skyrmions, and much more.^{3,4} Although not simple in practice, SP-STM can in principle also yield unprecedented spin characterization on a broad spectrum of material surfaces, including practical, real world systems. For example, it could be applied to investigate surfaces of intermetallic compounds, superconductors, complex magnetic oxides, and magnetic semiconductors.

We are applying SP-STM to study various magnetic systems grown *in-situ* by molecular beam epitaxy, including transition metal nitrides,⁵ magnetic-doped nitride semiconductors, and several bi-metallic magnetic systems. I will present our recent work using STM and SP-STM, beginning with a discussion of manganese nitrides, including our work on aFM θ -phase MnN and ferrimagnetic ϵ -phase Mn₃N. The θ -phase films are very complex due to the expectation of canted spins within each atomic layer with four unique canting angles, while the ϵ -phase films contain two types of spins (Mn^I and Mn^{II}) with equally complex spin arrangements.

A second material we are working on is the chromium nitride system in which we investigate its electronic and spin properties in a low-temperature SP-STM system. Spectroscopy results to date suggest a d -wave resonance on the surface and a Kondo signature for nanoscale iron islands grown on atomically-smooth CrN surfaces.

I will also present results for Mn δ -doped semiconducting gallium nitride surfaces in which we find atomic layer ferromagnetism within a unique and stable $\sqrt{3} \times \sqrt{3} - R30^\circ$ MnGa₂N surface reconstruction. Spectroscopy clearly reveals spin-polarized and spin-split Mn states, as predicted by first principles theory calculations. SP-STM measurements map out ferromagnetic domains at *room temperature*, and the additional presence of magnetic rim states seen at the edges of ferromagnetic islands, as well as magnetic hysteresis, give further interest to this intriguing system.

¹ R. Wiesendanger, Rev. Mod. Phys. **81**, 1495 (2009).

² M. Bode et al., Phys. Rev. Lett. **92**, 67201 (2004).

³ P. Ferriani et al., Phys. Rev. Lett. **101**, 027201 (2008).

⁴ S. Loth et al. Science **335**, 196 (2012).

⁵ K.K. Wang and A.R. Smith, Nano Lett. **12**, 5443 (2012).

5:40pm **SP+AS+MI+NS+SS-TuA11 The Use of Scanning Probe Techniques to Study the Behaviour of Second Phase Particles in Beryllium and Their Role in Localised Corrosion, Christopher Mallinson, J.F. Watts**, University of Surrey, UK

Scanning Kelvin probe force microscopy (SKPFM) has been employed to examine the galvanic activity of a wide range of second phase particles in S-65 beryllium that are believed to have a role in the localised corrosion of the metal. SKPFM and AFM analysis has been combined with additional surface and bulk analysis techniques of scanning electron microscopy, energy dispersive x-ray spectroscopy and Auger electron spectroscopy to provide a detailed overview of the link between the bulk and surface composition of particles and their Volta potential or surface contact potential.

Initial results appear to show that all second phase particles are more noble than the beryllium matrix with the greatest potential difference observed for AlFeBe₄ and alumina or carbide like particles. The more negative Volta potential indicates that the particles should act as local cathodes when the metal is exposed to an aqueous environment.

The initial investigation, which is being performed in-air, will be expanded to determine the effect of increasingly higher humidity environments on the behaviour of the particles. It is hoped that this will provide a greater understanding about the onset of pitting corrosion in beryllium.

6:00pm **SP+AS+MI+NS+SS-TuA12 Many-body Interaction induced Spin-split States of Single Vacancy in Graphite, Wonhee Ko**, Samsung Advanced Institute of Technology, Republic of Korea; H.W. Kim, Y. Cho, Samsung Advanced Institute of Technology; Y. Kuk, Seoul National University, Korea, Republic of Korea; S.W. Hwang, Samsung Advanced Institute of Technology Although carbon atoms have no magnetic states, it has been known that defects in graphene or graphite can have magnetic states induced by many-body interaction. By utilizing ultra-low-temperature scanning tunneling microscopy, we observed the spin-split states of single vacancy in graphite, which is a hallmark of magnetic states. Evolution of the spin splitting in the magnetic field did not follow the Zeeman effect of single electron states, and can be explained only when we consider electron-electron interaction. Quantitative analysis showed that the strength of the electron-electron interaction is in the range of 1~3 meV. Our observation implies that the simplest defect in graphite like single vacancy can behave as magnetic, which would be an important ingredient for development of carbon-based spintronic devices.

Surface Science

Room 104E - Session SS+AS-TuA

Structure and Characterization of Oxides

Moderator: Robert Bartynski, Rutgers, the State University of New Jersey

2:20pm **SS+AS-TuA1 Phase Formation and Stability of Reactive Sputtered Zirconium Dioxide Thin Films, Mohsin Raza, D. Cornil, J. Cornil**, University of Mons, Belgium; S. Lucas, University of Namur, Belgium; A.L. Thomann, A. Caillard, M. El Mokh, GREMI CNRS/Université d'Orléans, France; J.F. Pierson, P. Boulet, Université de Lorraine, France; R. Snyders, S. Konstantinidis, University of Mons, Belgium

As materials properties are greatly influenced by their phase constitution, therefore it's of high importance to understand and address the mechanisms driving their phase formation and stability. In this respect, zirconium oxide (ZrO₂) has been the focus of a special attention for the last couple of decades regarding the stabilization of its cubic (c) phase at room temperature.

In the present study, the role of the film chemistry i.e. of oxygen vacancies and of energy deposited during the film growth is investigated. To this purpose, 100 nm thick films of zirconium oxide are grown in the poisoned mode as well as in the transition zone with the help of voltage feedback control unit (Speedflo mini from Gencoa UK). During the film growth, to have a fast response from the feedback unit and thus a tight control over the film chemistry (i.e. O/Zr ratio), oxygen is injected just at the target surface. By systematically varying the working parameters, it is observed that for films grown at 200 mA, 10 mTorr in the poisoned mode, the XRD diffractograms only exhibits reflections from the low-temperature stable monoclinic (m) phase. To the contrary, while working inside the transition zone i.e. by growing sub-stoichiometric zirconium oxide thin films as demonstrated by careful elemental characterization, the film phase is dramatically modified and only the c reflections are observed. Theoretical calculations at the Density Functional Theory level are in remarkable

agreement with the experimental data, hence highlighting that the incorporation of oxygen vacancies is the sole responsible mechanism for the stabilization of the c-phase. It is also observed that any deviation from the optimized working conditions i.e. change in discharge current or pressure leads to the change in film phase constitution. Thermal annealing analysis performed in air and N₂ shows the oxygen vacancy stabilized zirconia films are stable up-to 750 °C. Above 750 °C, the mechanical stress, generated in the film due to the mismatch of the thermal expansion coefficients of both the zirconia film and the substrate, apparently surpasses a critical value and leads to the appearance of m-phase.

In conclusion, c-phase of zirconia can be stabilized at room temperature (up to 750 °C) by solely incorporating oxygen vacancies in the zirconia lattice. However, increasing the energy flux during film growth or the mechanical stress may induce the transformation of the oxygen vacancy stabilized cubic phase of zirconia into the m-phase.

2:40pm SS+AS-TuA2 W-oxide on Ag(100): a Flexible Decoupled 2-D Oxide Layer, T. Obermüller, S. Surnev, Falko P. Netzer, Karl-Franzens University, Austria

Two-dimensional (2-D) transition metal oxide layers have attracted significant interest during the past decade due to their novel emergent properties and high potential for nanotechnology applications [1,2]. For practical reasons 2-D oxide layers are usually supported on metal surfaces. This leads to a coupling of the oxide overlayer to the metal substrate, thus creating a hybrid system with properties largely determined by the oxide-metal interface. Here, we report the formation of a 2-D W-oxide layer on a Ag(100) surface, where the oxide appears to be essentially *decoupled* from the substrate. The W-oxide has been prepared by vapor phase deposition of (WO₃)₃ clusters at 500°C substrate temperature. The WO_x grows as a well-ordered incommensurate 2-D wetting layer in large domains with variable orientation with respect to the substrate. This gives rise to a variety of oxide domains with different azimuthal orientation, which can easily be recognized in the STM by their different Moiré patterns. The overlayer lattice can be imaged with atomic resolution in the STM and analyzed using the Moiré formula, from which the square overlayer lattice constant can be accurately evaluated to $a = 3.72 \text{ \AA}$; this is close to the respective WO₃ bulk lattice constant. AES and XPS spectra indicate an overlayer stoichiometry close to WO₃, but the W 4f binding energy suggests a lower oxidation state than W⁶⁺. A structure model in terms of a 2-D WO_x sheet is discussed. It is conjectured that this WO_x sheet on Ag(100) behaves essentially like an isolated 2-D oxide layer.

[1] G. Pacchioni, *Two-dimensional oxides: multifunctional materials for advanced technologies*. Chem. Eur. J. 18(2012) 10144

[2] *Oxide materials at the two-dimensional limit*. F.P. Netzer, A. Fortunelli, Eds. (Springer Series in Materials Science, April 2016)

3:00pm SS+AS-TuA3 Growth and Termination of a Rutile IrO₂(100) Layer on Ir(111), Rahul Rai, T. Li, Z. Liang, University of Florida, Gainesville; M. Kim, A. Asthagiri, Ohio State University; J.F. Weaver, University of Florida, Gainesville

Iridium oxide is an effective catalyst for promoting electrochemical water splitting and is a promising material for effecting other chemical transformations as well. In this talk, I will discuss our recent investigations of the growth and termination of a crystalline IrO₂(100) film that develops during the oxidation of Ir(111) by gaseous O-atoms. We characterized the oxidation of Ir(111) using temperature programmed desorption (TPD), low energy electron diffraction (LEED), low energy ion scattering spectroscopy (LEISS) and density functional theory (DFT) calculations. We find that a well-ordered surface oxide with ($\sqrt{3} \times \sqrt{3}$)R30° periodicity relative to Ir(111) develops as the oxygen coverage increases to 1.4 ML (monolayer). Continued oxidation produces a rutile IrO₂(100) layer that reaches a kinetic saturation, under the conditions employed, after the growth of about four atomic layers and decomposes during TPD to yield a sharp O₂ desorption peak at ~770 K. We assert that favorable lattice matching at the IrO₂(100)/Ir(111) interface is responsible for the preferential growth of the IrO₂(100) facet during the initial oxidation of Ir(111), as LEED reveals the formation of a well-defined (6 × 1) coincidence structure. TPD experiments show that CO and H₂O probe molecules bind weakly on the IrO₂(100) surface, and LEISS measurements reveal that the oxide surface is strongly enriched in O-atoms. These characteristics provide evidence that the rutile IrO₂(100) layer is oxygen-terminated, and therefore lacks reactive Ir atoms that can strongly bind molecular adsorbates. Finally, I will discuss our DFT predictions of the stability of so-called on-top and bridging oxygen atoms on rutile IrO₂ and RuO₂ surfaces. The DFT results support the conclusion that IrO₂(100) is oxygen-terminated at the growth temperatures that we

employed (< 650 K), and further reveal that on-top oxygen atoms significantly destabilize bridging oxygen atoms on the rutile (100) surfaces; such destabilization is less pronounced on the (110) surfaces. This destabilization may explain our observation that the desorption of on-top oxygen atoms and complete decomposition of the IrO₂(100) film occur over a similar range of temperatures during TPD. Our findings have implications for understanding the generation of rutile IrO₂ layers for model surface chemistry studies.

3:20pm SS+AS-TuA4 Vibrational Spectroscopy of Iron Oxide Nanostructures and Thin Films Supported on Graphite, Joel Langford, F. Rosner, J.Y. Kwon, J.C. Hemminger, University of California Irvine

Iron oxide nanostructures supported on highly oriented pyrolytic graphite have been investigated with high resolution electron energy loss spectroscopy (HREELS) and Auger electron spectroscopy (AES). The average O:Fe ratio, as measured by AES, can be increased or decreased by annealing in an oxygen background of 1×10^{-7} Torr or *in vacuo*, respectively. Depending on annealing temperature, and oxygen exposure, the O:Fe ratio can range from near metallic to hematite (Fe₂O₃) stoichiometry. Regardless of stoichiometry, no iron oxide vibrational modes were observed in the specular HREELS spectra. Only the collective free charge carrier excitation of the graphite substrate was observed. The absence of iron oxide modes in specular HREELS is due to an electrostatic screening from the surface dipole generated by the collective graphite excitation. This screening effect is supported by calculations of the electron energy loss function for a thin iron oxide film supported on graphite. Off specular HREELS shows that the graphite phonon dispersion is unperturbed by the presence of iron oxide nanostructures. Thus, there is minimal interaction between the graphite substrate and the supported iron oxide nanostructures. HREELS spectra of water and carbon monoxide adsorbed on iron oxide nanostructures show hindered vibrational modes. The intensity of the hindered mode is high when compared to the intramolecular modes and the elastic peak. The intensity enhancement is due to a resonance effect between the hindered mode and a longitudinal phonon mode of the nanoparticle i.e. a substrate Fermi resonance. A more descriptive interpretation of this resonant enhancement and finite relaxation lifetime based off perturbation theory will be discussed.

4:20pm SS+AS-TuA7 Electron Transfer Processes on Single Crystalline Alkaline Earth Metal Oxide Films, Thomas Risse, Freie Universität Berlin, Germany

INVITED

Charge transfer processes are central ingredients to understand the chemical and physical properties of matter in general and on surfaces in particular. These processes may be classified into transient charge transfer states as created e.g. after photo excitation and processes, which create metastable charge transfer products such as molecular radicals. The Presentation will be restrict to the discussion of spontaneous charge transfer processes and will among other techniques discuss results obtained by electron paramagnetic resonance (EPR) spectroscopy to characterize paramagnetic species.

We will focus on results obtained on single crystalline, epitaxial MgO(001) film and show how film thickness, defects as well as dopants in the film are involved in charge transfer processes both between intrinsic species within the MgO as well as adsorbates such as molecular oxygen or metal atoms.

5:00pm SS+AS-TuA9 Tungsten Trioxide Monolayer on Pd(100), N. Doudin, M. Blatnik, Karl-Franzens University, Austria; D. Kuhness, Karl-Franzens University, Germany; A. Fortunelli, CNR-ICCOM & IPCF Pisa, Italy; F.P. Netzer, Svetlozar Surnev, Karl-Franzens University, Austria

Tungsten trioxide (WO₃) is a key material in several applications including smart windows technology, photo-electrochemical water splitting, gas sensors and heterogeneous catalysis. In particular, tungsten oxides are important acid-base and redox catalysts, and they show excellent activity for many catalytic reactions, such as alcohol dehydrogenation, alkane hydrogenation and metathesis [1]. WO₃ has been produced in single crystal form or as supported thin films with the bulk crystal structure. Recently, the formation of an ordered two-dimensional (2D) tungsten oxide layer on Pt(111) has been reported, where W atoms show a mixture of 5+ and 6+ oxidation states [2].

Here we report on the preparation of a well-ordered 2D WO₃ layer on a Pd(100) surface and the characterization of its geometric, electronic and vibrational structure by a combination of STM, LEED, XPS, HREELS measurements, supported by DFT calculations. The WO₃ monolayer on Pd(100) surface and features a surface network consisting of small (~ 4 nm) square-shaped domains, separated by narrow (~ 0.3 nm) trenches (Fig. 1a).

The latter are identified as anti-phase domain boundaries, as evidenced by atomically-resolved STM images (see inset of Fig. 1a) and the characteristic spot splitting in the LEED pattern (Fig. 1b). The STM image shows that each domain exhibits a square surface structure with a lattice constant of 0.39 nm, which corresponds to a $c(2 \times 2)$ superstructure. Another important feature is the presence of few dark depressions inside the domains, which we attribute to missing terminal O atoms (see model in Fig. 1d), in corroboration with HREELS results and high-resolution W 4f core-level spectra (Fig. 1c). The latter consist of three $4f_{7/2} - 4f_{5/2}$ doublet components, due to W atoms at different surface locations: within the defect-free areas (major component at 34.4 eV), with missing terminal oxygens (minor component at 33.3 eV), and at the domain boundaries (35.2 eV). The DFT derived structure model of the WO_3 monolayer is shown in Fig. 1d and consists of a layer of O atoms adsorbed in on-top Pd positions, followed by a $c(2 \times 2)$ layer of W atoms, which are connected at the top to terminal O atoms via strong W=O bonds, as suggested by the HREELS results. It can be viewed in a way as a 2D analogue of a cubic $WO_3(001)$ crystal, featuring a similar lattice constant (0.39 nm vs. 0.38 nm) and polyhedral linkage, but with a modified W-O coordination sphere due to the contact with the Pd(100) surface.

[1] D. Gazzoli et al, J. Phys. Chem. B 101 (1997) 11129

[2] Z. Li, et al, J. Phys. Chem. C 115 (2011) 5773

This work has been supported by the FWF Project P26633-N20 and by the EU COST Action CM1104.

5:20pm SS+AS-TuA10 Electron Energy Loss Study of Excess Electrons in Reducible TiO_2 : Dual Behaviour or Coexistence of Trapped and Free States? Bulk or Surface Defects?, Remi Lazzari, J. Li, J. Jupille, Institut des NanoSciences de Paris, France

Stoichiometry defects play a tremendous role in the surface chemistry of titanium oxide [1,2]. Reduced rutile is indubitably a n-type semiconductor in terms of electrical transport but electron-based spectroscopies and scanning tunnelling microscopy show the existence of a defect-related gap state lying 0.8-1eV below the Fermi level [1,2]. Its nature *i.e.* surface oxygen vacancies [2,3] versus sub-surface interstitial titaniums [4] is still highly debated in the literature as well the actual (de)localisation of the associated excess electrons [4,5,6].

In our work, electron energy loss spectroscopy in low and high resolution modes was used to probe band gap state and phonon excitations in $TiO_2(110)$ as a function of oxygen exposure at 100 and 300K. By comparing surfaces, from reduced to fully oxidized obtained by various means including electron bombardment, and by using EELS depth sensitivity in out-of-specular detection, a contribution from sub-surface defects is clearly evidenced. A method to prepare defect-free surfaces (as observed by EELS) is even proposed. Using dielectric modelling of spectra including phonons, carriers, gap state and interband transitions and multiple excitations, it was shown that "free-like" carriers characterized by their plasmon excitation coexists with band gap states. While the latter give rise to an obvious peak in the band gap, the former induce a temperature dependent broadening of the quasi-elastic peak and a sizeable screening and upward frequency shift of phonons compared to stoichiometric samples. Through data fitting, both surface and bulk carrier densities and dampings could be quantified as well their profile. A very different dynamics of the healing of the associated signals upon O_2 exposure was also observed. The implication of such findings in terms polaronic nature of excess electron will be discussed.

[1] U. Diebold, Surf. Sci. Rep. 48 (2003) 43; C. Pang et al., Chem. Rev. 113 (2013) 3887

[2] C. Yim et al., Phys. Rev. Lett. 104 (2010) 036806

[3] P. Kruger et al., Phys. Rev. Lett 100 (2008) 055501

[4] S Wendt et al., Science 320 (2008) 1755

[5] M. Setvin et al., Phys. Rev. Lett. 113 (2014) 086402

[6] A. Janotti et al., Phys. Stat. Solidi RRL 7 (2013) 199

6:00pm SS+AS-TuA12 Vanadium on Anatase TiO_2 , Stig Koust, L. Arnarson, iNANO, Aarhus University, Denmark; P.G. Moses, Haldor Topsøe Research Lab, Denmark; I. Beinik, J.V. Lauritsen, S. Wendt, iNANO, Aarhus University, Denmark

Tighter regulations concerning nitrogen oxides (NOx) and an increased public concern, highlighted recently by a study from ICCT [1], demonstrating that new diesel cars emit more than seven times the allowed NOx, has clearly shown the urgent need for the development of more effective catalysts for the removal of NOx. The Selective Catalytic Reduction (SCR) is widely used to reduce NOx into N_2 and H_2O in flue and

exhaust gasses. This reaction is best catalyzed using a TiO_2 -anatase supported sub-monolayer VOx-based catalyst.

Unfortunately, the detailed reaction mechanism(s) are still debated, and the nature of the active site is uncertain [2]. To tackle these issues, the preparation and characterization of good model catalyst model systems may provide new fundamental insights.

Here we present atomically resolved STM images of sub-monolayer vanadium (V) supported on anatase TiO_2 (101). Upon V deposition at liquid nitrogen temperature (LT), the surface is covered with small isolated V clusters, distributed homogeneously on the terraces. Further characterization with XPS revealed the oxidation state of V being 2+, indicating a preferred binding between V clusters and surface oxygen atoms. This conclusion is further supported by the observed reduction of the titanium surface atoms.

Surprisingly, our STM studies revealed an embedding of vanadium into the near-surface region already at room temperature (RT). A significant decrease in the density of V clusters is observed after annealing at RT and new features in the STM images appeared, which we assign to monomeric V atoms at regular titanium lattice sites, substituting the surface titanium. This change in the surface is accompanied by a shift of the V2p XPS feature to higher binding energy, revealing the oxidation of the vanadium to be 3+/4+ as compared to only 2+ upon LT deposition. The V2p area is unaltered after annealing at RT, suggesting no loss of V due to re-evaporation or migration into the bulk. Our DFT calculations confirm the substitution of vanadium with surface titanium atoms.

Additionally we present STM and XPS studies of vanadia (V_2O_5) deposited on a- TiO_2 (101) in comparison to metallic vanadium on the same surface. Vanadia displays weaker interaction with the surface compared to vanadium and we observe diffusion in to the sub-surface for vanadia after annealing at ~700K, however subsequent oxidation pulls vanadia back out to the surface.

1. Vicente, B., et al. *REAL-WORLD EXHAUST EMISSIONS FROM MODERN DIESEL CARS*. 2014.

2. Busca, G., et al., *Applied Catalysis B: Environmental*, 1998. (1–2): p. 1-36.

Surface Science

Room 104D - Session SS+HC-TuA

Photocatalysis and Photochemistry at Surfaces

Moderator: Arthur Utz, Tufts University

2:20pm SS+HC-TuA1 Investigations of Surface Chemistry for Pyridine-catalyzed CO_2 Reduction on GaP, C.X. Kronawitter, Bruce Koel, Princeton University

The surface chemistry of N-containing heteroaromatics, molecular co-catalysts that enable the selective electrochemical reduction of CO_2 to fuels, is discussed. The presented experimental results focus on elucidating the role of the electrode surface in CO_2 reduction reactions that are co-catalyzed by pyridine. For this catalysis, exceptionally high selectivity for reduced fuels has been reported when the reaction occurs at the surface a GaP photocathode. For this reason, experimental emphasis is placed on assessing preferential adsorption sites and bonding interactions of adsorbates on surfaces of GaP. A surface science approach is used, whereby ultra-high vacuum conditions facilitate the fabrication of highly characterizable electrode-adsorbate systems. The use of single crystal surfaces permits analysis of surface chemistry independent of complicating factors such as grain boundaries and morphology. Surface-sensitive core-level and vibrational spectroscopy techniques, including high-resolution X-ray photoelectron spectroscopy, synchrotron-based photoemission, and high-resolution electron energy loss spectroscopy, are used to probe adsorbate-substrate and adsorbate-adsorbate interactions for pyridine, water, hydrogen, and carbon dioxide on GaP. Scanning tunneling microscopy was used to obtain molecular orbital-resolved images of adsorbed molecules. Conclusions from experimental results on these model systems are supported by calculations using density functional theory. This work assists in generating a molecular-level understanding of the heterogeneous processes important to the reaction mechanisms involved in the efficient photoelectrocatalytic generation of carbon-containing fuels with high energy densities.

Tuesday Afternoon, November 8, 2016

2:40pm SS+HC-TuA2 Photoreactivity of Benzoate Monolayers on TiO₂: Comparison of Anatase (001) and Rutile (110), Erik Skibinski, W.J.I. DeBenedetti, A. Song, A. Ortoll-Bloch, M.A. Hines, Cornell University

The photoreactivity of organic self-assembled monolayers (SAMs) on TiO₂ surfaces is of considerable importance to applications such as dye-sensitized solar cells and photocatalytic environmental remediation. Despite extensive research, there remains little information about the reactivity of well characterized TiO₂ surfaces under ambient conditions. Here, we study the surface structure and photoreactivity of near-ideal benzoate monolayers prepared from dilute aqueous solutions and reacted at atmospheric pressure on anatase (001) and rutile (110) surfaces using scanning tunneling microscopy, infrared and x-ray photoelectron spectroscopies, and density functional theory.

We show that self-assembled monolayers of benzoate, an analogue of the organic linkage used in dye-sensitized solar cells, undergo rapid photodecomposition on both rutile (110) and anatase (001) under ultraviolet illumination in ambient and oxygen-rich conditions. Interestingly, while the two surfaces have similar, although not identical, reactivities, they differ in their reaction products, with the anatase polymorph producing a surface-bound ketene.

3:00pm SS+HC-TuA3 Light-driven H₂ Generation using Multicomponent Semiconductor-metal Colloidal Nanorod Heterostructures, Tianquan Lian, Emory University

INVITED

Quantum confined semiconductor nanocrystals have been widely investigated as light harvesting and charge separation components in photovoltaic and photocatalytic devices. The efficiency of these semiconductor nanocrystal-based devices depends on many processes, including light harvesting, carrier relaxation, charge separation and charge recombination. The competition between these processes determines the overall solar energy conversion (solar to electricity or fuel) efficiency. Compared with single component quantum dots (QDs), semiconductor nanoheterostructures, combining two or more materials, offer additional opportunities to control their charge separation properties by tailoring their compositions and dimensions through relative alignment of conduction and valence bands. Further integration of catalysts (heterogeneous or homogeneous) to these materials form multifunctional nanoheterostructures. Using CdSe/CdS/Pt, dot-in-rod nanorods (NRs) with Pt tips, as a model system, we are examining the mechanism of long-lived charge separation and H₂ generation in the presence of sacrificial electron donor. The rates of electron transfer, hole transfer and charge recombination are directly monitored by transient absorption and time-resolved fluorescence spectroscopy. In this talk, we will discuss the mechanism of exciton dissociation, the dependence of the rates of elementary charge transfer processes on the dimension (size and length) and band alignment in these materials, and how these rates affect the overall H₂ generation efficiency.

4:20pm SS+HC-TuA7 Quenching of Electron Transfer Reactions through Coadsorption: A Study of Oxygen Photodesorption from TiO₂(110), Greg Kimmel, N.G. Petrik, M. Shen, M.A. Henderson, Pacific Northwest National Laboratory

Using temperature programmed desorption (TPD) and photon stimulated desorption (PSD), we show that coadsorbates of varying binding energies on the rutile TiO₂(110) surface exert a commensurate inhibiting influence on the hole-mediated photodesorption of adsorbed O₂. A variety of coadsorbates (Ar, Kr, Xe, N₂, CO, CO₂, CH₄, N₂O, acetone, methanol or water) were shown to quench O₂ photoactivity, with the extent correlating with the coadsorbate's gas phase basicity, which in turn determines the strength of the coadsorbate-Ti⁴⁺ bond. Coadsorbed rare gases inhibited the photodesorption of O₂ by ~10-25%, whereas strongly bound species (water, methanol and acetone) nearly completely inhibited O₂ PSD. We suggest that coadsorption of these molecules inhibit the arrival probability of holes to the surface. Band bending effects, which vary with the extent of charge transfer between the coadsorbate and the TiO₂(110) surface, are not expected to be significant in the cases of the rare gases and physisorbed species. These results indicate that neutral coadsorbates can exert a significant influence on charge transfer events by altering the interfacial dipole in the vicinity of the target molecule.

4:40pm SS+HC-TuA8 Different Effects of Oxygen Adsorption on the Band Bending of TiO₂ Nanoparticles Studied by Photoluminescence Spectroscopy, Shiliang Ma, M. Reish, Z. Zhang, I. Harrison, J.T. Yates, Jr., University of Virginia

By employing photoluminescence (PL) spectroscopy, it was found that oxygen adsorption on powdered TiO₂ changes the band bending of anatase

in different ways. On the one hand, oxygen exposure leads to molecular chemisorption of oxygen molecules, which take up negative charge, but can be reversibly removed by ultraviolet photodesorption from the TiO₂ surface. Molecular chemisorption of oxygen molecules increases the upward band bending of TiO₂ and decreases the PL emission. On the one hand, oxygen can adsorb through irreversible reaction with defects, which occurs through an intermediate state of molecularly chemisorption, reducing the intrinsic upward band bending at the TiO₂ surface resulting in PL emission increase. Since band bending plays an important role in charge carrier migration to the surface, this finding that oxygen adsorption can have two different effects on the band bending of TiO₂ provides a new perspective on how oxygen and oxygen vacancies may modulate photocatalytic reaction efficiencies.

5:00pm SS+HC-TuA9 Imaging Photodecomposition of Trimethyl Acetic Acid on Cross-linked (1 × 2) Rutile TiO₂(110), Y. Xia, K. Zhu, Zhenrong Zhang, K.T. Park, Baylor University

Photoreactivity of reduced TiO₂ is important in photocatalytic applications. Cross-linked (1 × 2) rutile TiO₂(110) has been extensively studied, yet the exact atomistic model remains a point of contention. Employing a carboxylic acid as a probing molecule, we studied the structure of cross-linked (1 × 2) TiO₂(110) through the interaction of trimethyl acetic acid (TMAA) with various sites on the surfaces using *in situ* scanning tunneling microscopy (STM). We compared three specific atomistic models for (1 × 2) reconstructed TiO₂(110), Ti₂O₃, Ti₂O, and Ti₃O₆. The adsorption of TMAA on strands at room temperature strongly supports the Ti₂O model for cross-linked (1 × 2) reconstructed TiO₂(110). Photodecomposition of TMAA shows the dependence on the initial TMA coverage and O₂ pressure.

5:20pm SS+HC-TuA10 Non-Fullerene Acceptors for Organic Photovoltaics: PTCDA versus C₆₀, Steven Robey, National Institute of Standards and Technology

Extensive development of new polymer and small molecule donors has helped produce a steady increase in the efficiency of organic photovoltaic (OPV) devices. However, OPV technology would benefit from the introduction of non-fullerene acceptors. Unfortunately, efforts to replace fullerenes have typically led to significantly reduced efficiencies. A number of possible explanations for reduced efficiencies with non-fullerene acceptors compared to fullerene acceptors have been suggested, including the formation of unfavorable morphologies in non-fullerene systems and/or favorable excitation/carrier delocalization in fullerenes. In addition, enhanced exciton dissociation associated with fundamental characteristics of the fullerene molecular electronic states has also been suggested. We employed time-resolved two-photon photoemission (TR-2PPE) to directly compare exciton dissociation at interfaces between zinc phthalocyanine (ZnPc) interfaces and the non-fullerene acceptor, perylene tetracarboxylic dianhydride (PTCDA) versus dissociation measured at the analogous interface with C₆₀, and thus help discriminate between these potential explanations. Exciton dissociation rates are comparable for phthalocyanine interfaces with both acceptors, allowing us to suggest a hierarchy for effects influencing higher efficiencies with fullerene acceptors.

5:40pm SS+HC-TuA11 Use of Photoluminescence to Monitor Surface Chemistry of Metal Oxide Nanoparticles, S. Kim, D. Somaratne, James Whitten, University of Massachusetts Lowell

Many metal oxides nanoparticles are photoluminescent upon irradiation with ultraviolet light, with visible emission arising from surface states and surface defects. Because of the sensitivity of the surface to adsorption and electron transfer to and from even weakly adsorbed molecules, photoluminescence (PL) is proving to be a convenient method of monitoring chemisorption and physisorption. Experimental and theoretical results are presented related to adsorption of various gases and organic vapors on zinc oxide, zirconium oxide, and titanium dioxide nanoparticles toward the goal of correlating adsorption to PL changes. X-ray and ultraviolet photoelectron spectroscopy (XPS and UPS) and Raman spectroscopy measurements have been performed on metal oxide nanoparticles and single crystals to investigate whether chemisorption occurs at room temperature and the details of adsorbate bonding. These results are combined with density functional theory (DFT) calculations to understand how adsorption influences the PL changes. In addition to atmospheric gases, examples of adsorbates that have been examined include ammonia, methanethiol, methanol, benzene, and pyridine. This research provides a convenient method of monitoring adsorption and lays the foundation for optochemical sensing, in which metal oxides may serve as a new type of gas sensor.

Tuesday Afternoon, November 8, 2016

6:00pm **SS+HC-TuA12 Exploring Pd Adsorption, Diffusion, Permeation, and Nucleation on Bilayer SiO₂/Ru as a Function of Hydroxylation and Precursor Environment: From UHV to Catalyst Preparation, William Kaden**, University of Central Florida

The hydroxylation-dependent permeability of bilayer SiO₂ supported on Ru(0001) was investigated by XPS and TDS studies in a temperature range of 100 K to 600 K. For this, the thermal behavior of Pd evaporated at 100 K, which results in surface and sub-surface (Ru-supported) binding arrangements, was examined relative to the extent of pre-hydroxylation. Samples containing only defect-mediated hydroxyls showed no effect on Pd diffusion through the film at low temperature. If, instead, the concentration of strongly bound hydroxyl groups and associated weakly bound water molecules was enriched by an electron-assisted hydroxylation procedure, the probability for Pd diffusion through the film is decreased via a pore-blocking mechanism. Above room temperature, all samples showed similar behavior, reflective of particle nucleation above the film and eventual agglomeration with any metal atoms initially binding beneath the film. When depositing Pd onto the same SiO₂/Ru model support via adsorption of [Pd(NH₃)₄]Cl₂ from alkaline (pH 12) precursor solution, we observe notably different adsorption and nucleation mechanisms. The resultant Pd adsorption complexes follow established decomposition pathways to produce model catalyst systems compatible with those created exclusively within UHV despite lacking the ability to penetrate the film due to the increased size of the initial Pd precursor groups.

Thin Film

Room 105A - Session TF-TuA

Thin Film Photovoltaics

Moderators: Eray Aydil, University of Minnesota, Colin Wolden, Colorado School of Mines

2:20pm **TF-TuA1 Perovskite Solar Cells: Material Synthesis, Device Operation and Charge Carrier Dynamics, Kai Zhu**, National Renewable Energy Laboratory **INVITED**

Organic-inorganic hybrid halide perovskites have rapidly become a focal point of the photovoltaic (PV) community as a promising next-generation PV technology. Various perovskite absorbers (e.g., CH₃NH₃PbI₃ and HC(NH₂)₂PbI₃) and device architectures (e.g., mesoporous, planar, and mesoporous-planar hybrid cell configurations) have been examined with promising results by using either solution processing or thermal evaporation. The certified efficiency of a single-junction perovskite solar cell (PSC) has reached 22% after only a few years of active research. In addition to solar cell application, the fascinating optical and electronic properties of these perovskite systems have enabled their usage for various electronic devices including light emitting diodes, photodetectors, and transistors. Despite this remarkable progress associated with perovskites, there are still many fundamental questions to be addressed at both material and device levels. Further improvements are required to advance our understanding on the material effects on the fundamental physical and chemical processes that are important to device operations. In this presentation, I will present our recent studies toward a better understanding and control of perovskite nucleation, grain growth, and microstructure evolution using solution processing. The precursor chemistry and growth conditions are found to affect significantly the structural and electro-optical properties of perovskite thin films. Devices based on different grain sizes and film thicknesses were investigated to correlate the grain sizes with device performance. The impact of grain size on charge carrier dynamics was also studied. Tuning tolerance factor through solid state alloying is shown as an effective way for stabilizing perovskite structures. In addition, I will discuss briefly the role of grain boundary on charge carrier dynamics and device characteristics. These results and others will be discussed.

3:00pm **TF-TuA3 Perovskite Film Growth And Degradation Mechanisms In Graphene-Based Perovskite Solar Cells By In Situ Spectroscopy, Muge Acik**, Argonne National Laboratory; *S.B.D. Darling*, Argonne National Laboratory, University of Chicago

High power conversion efficiency of perovskite-based solar cells offers promise for low-cost and scalable production of renewable energy. Hybrid organic-inorganic methylammonium lead halides, MAPbX₃ (X=I, Br, Cl)/mixed-halides (I_{1-x}Cl_x, I_{1-x}Br_x) have been reported as light harvesting layers with tunable bandgaps, long electron-hole diffusion lengths and high electron/hole mobility. Nevertheless, halide-based perovskites require *in situ* investigation for film growth mechanisms to overcome detrimental

effects of incomplete lead precursor conversion, inconsistent crystallite formation/film uniformity, and weak cation-anion-solvent coordination (1). Graphene-derived hybrids has recently emerged as an ETL/HTL replacement in these devices. Graphene/perovskite structure-property relationships are, however, not well understood due to unclear chemistry at the ETL/perovskite/HTL interfaces. Moreover, effect of film thickness, lead content, stoichiometry control, overlayer/underlayer morphology/composition, and cation-anion electrostatic interactions ought to be examined for better charge transport at the graphene/perovskite interfaces. Stability factors also need to be studied for charge mechanisms to unravel device performance challenges. Indeed, underlayer ETLs (TiO₂/Al₂O₃) and overlayer HTLs (spiro-OMeTAD) were rarely studied with graphene. To address scalability and stability issues, we investigated degradation, nucleation and growth mechanisms in reduced graphene/graphite oxide (RGO) upon halide-based (I, Cl, Br) perovskite deposition. Chemical interactions were interpreted at perovskite/RGO interfaces for the grain size, orientation, boundaries, and surface/bulk effects using variable-temperature (≤600°C, Ar(g)) *in situ* spectroscopy (infrared absorption, micro-Raman, UV-vis-NIR, luminescence). Controlled perovskite formation was achieved at room temperature for bromide/chloride-based perovskites resulting in improved chemical stability with heat (vs. iodide derivative). Perovskite decomposition was observed at ~150°C. Oxygen-induced chemical reactions occurred at ≤150°C, eliminated hydroxyls/ carboxyls in RGO, and maintained ethers/epoxides upon perovskite decomposition (2). Poor perovskite formation was observed on RGO due to varying electron affinity and reactivity of precursor halides, resulting in film degradation in air (O₂, H₂O). Film morphology was explored by SEM, XRD, XPS, TEM, and AFM.

(1) M Acik, SB Darling. J. Mater. Chem. A (2016) Advance Article. Doi: 10.1039/C5TA09911K (2) M Acik, G Lee, C Mattevi, M Chhowalla, K Cho, YJ Chabal. Nature Mater. (2010) 9 (10), 840-845

Acknowledgment: Use of the Center for Nanoscale Materials was supported by the U.S. Department of Energy, Office of Science, Office of Basic Energy Sciences, under Contract No. DE-AC02-06CH11357. The abstract has been created by UChicago Argonne, LLC, Operator of Argonne National Laboratory ("Argonne"). Argonne, a U.S. Department of Energy Office of Science laboratory, is operated under Contract No. DE-AC02-06CH11357. The U.S. Government retains for itself, and others acting on its behalf, a paid-up nonexclusive, irrevocable worldwide license in said article to reproduce, prepare derivative works, distribute copies to the public, and perform publicly and display publicly, by or on behalf of the Government. Office of Science User Facility under Contract No. DE-AC02-06CH11357. M.A. also acknowledges support from the Joseph Katz Named Fellowship at Argonne National Laboratory.

3:20pm **TF-TuA4 ALD Processing for Organo-Metal Halide Perovskite Solar Cells: Opportunities and Challenges, V. Zardetto**, Eindhoven University of Technology, Netherlands; *F. di Giacomo, R. Andriessen*, Solliance/TNO, Netherlands; *T.M. Brown, A. di Carlo*, University of Rome "Tor Vergata", Italy; *W.M.M. Kessels, Mariadriana Creatore*, Eindhoven University of Technology, Netherlands

Within the class of emerging photovoltaic technologies, organo-metal halide perovskite solar cells have exhibited a sky-rocketing conversion efficiency above 20% in just a few years. In this contribution we will address the opportunities which ALD offers to perovskite solar cells by highlighting its merits of low temperature processing and compatibility with 3D-structures.

Specifically, we will present two studies aimed at the suppression of charge carrier recombination processes at the complex interface ITO/mesoscopic TiO₂ scaffold/ mixed halide perovskite absorber.

In the first study we investigate the role of thin plasma-assisted ALD TiO₂ blocking layers on PET/ITO substrates, developed at a substrate temperature of 150°C [1,2]. The ALD TiO₂ layer is found to exhibit an excellent blocking behaviour towards charge carrier recombination at the above-mentioned interface, leading to open circuit voltage (V_{oc}) values as high as 900 mV (with respect to the pristine PV device exhibiting no rectifying behaviour with a V_{oc} of 50 mV) and superior device performance (9.2%) with respect to a sol-gel TiO₂ blocking layer (4%).

In the second example we carry out few ALD cycles of Al₂O₃ in a 250 nm-thick mesoscopic TiO₂ scaffold. Next to the conformality of the process, we demonstrate by means of electrochemical impedance spectroscopy that just one ALD cycle is sufficient to suppress the charge recombination processes. Specifically, the V_{oc} is found to increase from 860 to 960 mV upon 1 ALD cycle of Al₂O₃.

This contribution will end by discussing the challenges yet to be met by ALD processing directly on perovskite. In all these cases, a careful interface engineering needs to include several aspects potentially affecting the optochemical and morphological stability of the active components of the device. For example, methylammonium lead iodide perovskite solar cells already degrade under prolonged (i.e. few hours) annealing at 80°C, as witnessed by the appearance of a PbI₂-related peak in the XRD spectrum. However, when the Al₂O₃ plasma-assisted ALD process at 30°C is compared with the thermal process at 80°C, the plasma step is found to be responsible for abstraction of the methylammonium cation and the formation of iodate species. Instead, the thermal ALD process does not affect the chemistry of the perovskite. These selected examples point out that processing temperature and choice of reactant (moisture or plasma radicals) need to be carefully considered when dealing with processing of hybrid materials, such as perovskite solar cells.

[1] F. Di Giacomo *et al.*, Adv. Energy Mat. 5, 1401808 (2015)

[2] V. Zardetto *et al.*, ECS Transactions 69 (7), 15 (2015)

4:20pm TF-TuA7 Identification of Critical Defects in Thin Film CdTe Solar Cells Deposited by Magnetron Sputtering. P.M. Kaminski, A. Abbas, S. Yilmaz, John Walls, Loughborough University, UK

The exceptional uniformity of deposition provides magnetron sputtering with important advantages as a deposition technique for some applications of thin film cadmium telluride (CdTe) solar cells. Efforts to develop a viable sputtering process for CdTe have been conducted in many laboratories around the world. These efforts have been moderately successful but the conversion efficiency achieved has not matched that obtained using lower energy deposition techniques such as Close Space Sublimation or Vapour Transport Deposition. In particular, sputtered CdTe is less tolerant to the cadmium chloride activation process. Delamination of the films at the cadmium sulphide junction is often observed. Catastrophic void formation within the CdTe layer has also been reported. This behaviour has often been attributed to film stress even though this can be mitigated in the as-deposited films. Using state-of-the-art High Resolution Transmission Electron Microscopy, we will report on the identification of the nanoscale defects that are responsible for the poor response of sputtered CdTe films to the cadmium chloride treatment. Identification of the atomic scale mechanisms at work provides a way to significant process improvement.

4:40pm TF-TuA8 Solar Energy Conversion Properties and Defect Physics of ZnSiP₂. Aaron Martinez, Colorado School of Mines; E.L. Warren, P. Gorai, National Renewable Energy Laboratory; K.A. Borup, Aarhus University, Denmark; D. Kuciauskas, P.C. Dippo, National Renewable Energy Laboratory; B.R. Ortiz, Colorado School of Mines; R.T. Macaluso, University of Texas at Arlington; S.D. Nguyen, University of Northern Colorado; A.L. Greenaway, S.W. Boettcher, University of Oregon, Eugene; A.G. Norman, National Renewable Energy Laboratory; V. Stevanovic, E.S. Toberer, Colorado School of Mines; A.C. Tamboli, National Renewable Energy Laboratory

Implementation of an optically active material on silicon has been a persistent technological challenge. For tandem photovoltaics using a Si bottom cell, as well as for other optoelectronic applications, there has been a longstanding need for optically active, wide band gap materials that can be integrated with Si. ZnSiP₂ is a stable, wide band gap (2.1 eV) material that is lattice matched with silicon and comprised of inexpensive elements. From bulk single crystal growth, we have demonstrated the first ZnSiP₂ photovoltaic device, and shown that ZnSiP₂ has excellent photoresponse and high open circuit voltage of 1.3 V, as measured in a photoelectrochemical configuration. The high voltage and low band gap-voltage offset are on par with much more mature wide band gap III-V materials. Photoluminescence data combined with theoretical defect calculations illuminate the defect physics underlying this high voltage, showing that the intrinsic defects in ZnSiP₂ are shallow and the minority carrier lifetime is 7 ns. The favorable results obtained from characterization of bulk material encourage the development of ZnSiP₂ as a photovoltaic absorber material. To pursue this development, we have constructed a thin film growth reactor. This reactor employs a combination of ultra high vacuum chemical vapor deposition, using silane and phosphine as precursor gases, and physical vapor deposition, using an effusion cell to evaporate elemental Zn. The preliminary results of the first stages of thin film growth will be presented in addition to an overview of our characterization of bulk ZnSiP₂.

5:00pm TF-TuA9 Controlling the Composition of Zn(O,S) Alloys Grown by Atomic Layer Deposition. Diane K. Lancaster, H. Sun, University of Colorado, Boulder; S.M. George, University of Colorado at Boulder

Zn(O,S) alloys are promising conduction band buffers for solar cells. The tunable conduction band of Zn(O,S) alloys improves electron transfer between electron absorber and electron transport materials. Zn(O,S) alloys are produced with atomic layer deposition (ALD) by alternating between ZnO ALD and ZnS ALD using diethylzinc (DEZ) and H₂O or H₂S as the reactants. However, controlling the composition of Zn(O,S) alloys is complicated by an efficient exchange reaction between H₂S and ZnO to produce H₂O and ZnS. This H₂S + ZnO → H₂O + ZnS exchange reaction dramatically increases the sulfur content of the Zn(O,S) alloys. Because of this exchange reaction, the growth temperature and the H₂S exposure have an effect on the Zn(O,S) alloy composition that is nearly equivalent to the ratio between the alternating numbers of ZnO ALD and ZnS cycles. For example, the exchange reaction is much more efficient at higher temperatures. Increasing the growth temperature from 100°C to 225°C changed the composition for films grown with an alternating sequence of 3 ZnO ALD cycles and one ZnS ALD cycle from 65% ZnS to 90% ZnS, respectively. To overcome the complexity of the exchange reaction, we have developed a new method of growing Zn(O,S) alloy films that avoids alternating between numbers of ZnO ALD and ZnS ALD cycles. This new growth method exposes the H₂O and H₂S simultaneously in sequence with the DEZ exposures. The simultaneous H₂O and H₂S exposures allow competition between the forward exchange reaction (H₂S + ZnO → H₂O + ZnS) to produce ZnS and the reverse exchange reaction (H₂O + ZnS → H₂S + ZnO) to recreate ZnO. Film composition using this method was determined by the mole fraction of the H₂S in the dosing mixture. The bandgaps of the Zn(O,S) alloys were measured versus film composition. Composition determined the bandgaps of the Zn(O,S) alloys regardless of growth conditions. Controlling the Zn(O,S) band gap was also much more reproducible using the simultaneous H₂O/H₂S exposures. Bandgaps varied linearly from 3.06 eV to 3.39 eV for H₂S mole fractions in the H₂O/H₂S dosing mixture from 0.03 to 0.39, respectively. We are now able to prepare tunable conduction band buffers for solar cell applications.

5:20pm TF-TuA10 ALD Ta-doped ZnO Transparent Conducting Oxide. Zhengning Gao, Y. Myung, R. Mishra, Washington University in St. Louis; R. Kanjolia, SAFC, Sigma; J. Park, Korea University, Republic of Korea; P. Banerjee, Washington University in St. Louis

ZnO based transparent conducting oxides (TCOs) offer earth abundant alternatives to conventional indium tin oxide (ITO) films. At the same time, ALD enables discretized doping of substitutional cations at a monolayer level, providing fine and exquisite control over dopant concentration and resultant properties. In this work, we present the ALD of tantalum (Ta) doped ZnO (TZO) films. Compared to dopants such as Ga³⁺ and Al³⁺, a Ta cation exists in +5 oxidation state and thus, can ideally transfer 3 electrons by substitutionally doping a Zn²⁺ site. We show that 30 nm TZO films with 2 at% Ta provides a minimum resistivity of 4 mW.cm and optical transmissivity of > 86% in the visible range.

The precursors used for Zn, O and Ta are diethyl Zn (DEZ), H₂O and pentakis-dimethylamido Ta (PDMAT). The targeted % Ta is varied from 2 to 20% by introduction of PDMAT pulse between DEZ and H₂O pulses. Downstream quadrupole mass spectrometry (QMS) tracks the interaction chemistry of the PDMAT with Zn-ethylated surface and the DEZ with a Ta-dimethyl amido saturated surface. Electron concentration and mobility are measured using Hall measurements. A minimum resistivity of 4 mW.cm with carrier density of 9.0x10¹⁹ cm⁻³ and a mobility of 17.7 cm²/V-sec is observed at 2 at% Ta. UV-Vis spectroscopy indicates a monotonic increase in bandgap of ZTO from 3.2 to 3.4 eV upon addition of Ta. Photoluminescence (PL) shows a quenching of the green band emission of ZnO associated with oxygen defects upon the addition of 2 at% Ta. Upon further Ta addition, a red shifted defect peak appears which is attributed to formation of new Zn vacancies. This data is supported by X-ray photoelectron spectroscopy (XPS), showing removal of O vacancies and a clear Ta-O-Zn bond formation for higher Ta doping. The results provide a clear understanding on the mechanism of Ta doping in ZnO and its direct impact on vacancies and resulting electronic and optical properties.

Finally, ALD TZO is deposited on flexible glass substrates and inside nanoporous anodic alumina templates to demonstrate formation of transparent conducting electrodes, conformally on a variety of platforms of relevance to photovoltaic research.

Tuesday Afternoon, November 8, 2016

5:40pm **TF-TuA11 Leveraging Small Molecules to Control Interfacial Stability of Transparent Conductive Oxides**, *Ina Martin, R. Matthews, E.B. Pentzer, T.J. Peshek*, Case Western Reserve University

Transparent conductive oxide (TCO) degradation is a known failure mode in thin-film photovoltaic (PV) devices through mechanisms such as resistivity increase and delamination. Degradation studies encompassing accelerated aging of the individual TCO, material combinations (e.g. the TCO interacting with an encapsulant) and full devices are necessary to elucidate the complicated mechanistic pathways of degradation that occur in thin-film PV devices. We have previously demonstrated quenching of the damp-heat-induced degradation of Al:ZnO (AZO), used as a front contact in CIGS modules, by depositing a mere 1 nm of a silane modifier, 3-aminopropyltriethoxysilane (APTES). Here we present results on the effect of the application of thin interfacial modifiers on AZO degradation, for thin films and within full CIGS (Cu(In,Ga)Se₂) thin film PV devices. Accelerated aging was performed under damp-heat (DH) and thermal-cycling protocols (from the IEC 61646 testing protocol for PV modules), ASTM G155 and outdoor testing. Modifiers include a monofunctional amine terminated silane (APDMES, 3-aminopropyltrimethoxysilane), and a trifunctional amine terminated silane (APTES, 3-aminopropyltriethoxysilane).

6:00pm **TF-TuA12 Thickness Dependence of Electro-optical Properties of Pb_{0.95}La_{0.05}Zr_{0.54}Ti_{0.46}O₃ Thin Films for Photovoltaic Applications**, *Vaishali Batra, S. Kotru*, The University of Alabama

Exploring the viability of alternate materials to increase efficiency of the solar cells, and to decrease the fabrication cost, has gained momentum in the past decade. Ferroelectric materials are one of those materials which have become a subject of intense research for future energy applications. These materials are well established in memory and MEMS industry and nowadays are being investigated to design photovoltaic (PV) devices. These materials show PV effect without a need of p-n junction as required in semiconductor devices. Additionally they exhibit bulk PV effect due to internal electric field originating from electric polarization. Of all the materials, lanthanum doped lead zirconate titanate (Pb_{0.95}La_{0.05}Zr_{0.54}Ti_{0.46}O₃/PLZT) of perovskite type crystalline structure is considered to be promising ferroelectric material for solar cell applications. The practical realization of these devices requires high PV response which is still a challenge. In this work, an innovative method based on orientation control of PLZT thin films is used to improve the PV response.

Promoting (001) orientation and suppressing (110) orientation in the PLZT films is observed to improve the electrical and optical properties of these films. This work focusses on effect of varying thickness of PLZT films on their electrical and optical properties. The reflectance and band gap energies strongly depend on film thicknesses and are found to be in the range of 3.30-3.57 eV. AFM demonstrates the change in morphology and improvement in roughness with respect to orientation. The roughness in the films is observed to increase with the increase in film thickness in the range of 2.92 nm to 4.06 nm. Raman spectroscopy reveals the shift in longitudinal and transverse optical modes with the change in film thickness suggesting the change in ferroelectric phases and crystallinity in the films. The electrical properties were studied using the model for metal-ferroelectric-metal (MFM) heterostructures with Schottky contacts using Pt electrodes. High polarization, free carrier concentration and higher photovoltaic properties are obtained from thicker PLZT films. The photovoltaic efficiency is observed to increase by ~4-10 times by controlling the orientation of the films.

Vacuum Technology

Room 104C - Session VT-TuA

Accelerator and Large Vacuum Systems

Moderators: Marcy Stutzman, Thomas Jefferson National Accelerator Facility, Marcelo Ferreira, European Spallation Source-ESS, Sweden

2:20pm **VT-TuA1 Vacuum Design of the European Spallation Source Target Monolith System**, *Peter Ladd*, European Spallation Source, Sweden

INVITED

The European Spallation Source (ESS) is a multi-disciplinary research center based on the world's most powerful neutron source being built in Lund, Sweden. The facility design and construction includes the most powerful linear proton accelerator ever built, helium-cooled tungsten target wheel, state-of-the-art neutron instruments, a suite of laboratories, and a supercomputing data management and software development center. The LINAC will deliver 5 MW of power to the target at 2000 MeV. Ground

breaking took place in September 2014 and construction is rapidly progressing towards first neutron on target scheduled for mid 2019.

ESS is a long pulse superconducting linac that accelerates protons in 2.86 ms long pulse stream with a repetition rate of 14 Hz at a 4 % duty cycle providing an average beam power of 5 MW. The stream of protons is intercepted by a helium cooled tungsten target wheel where about 10% are converted to mass, through the nuclear reactions in the spallation process and the remaining 90% is deposited as heat within a distance of about 1m from the target wheel. The moderators and reflectors maximize the yield directing the flow of neutrons to a suite of neutron instruments through neutron guides.

The "Target 'Monolith Vessel'" (CPMV) is a vacuum vessel nominally 6m in diameter x 9m high fabricated of 304 stainless steel. The major equipment located within this vessel are the helium cooled target wheel, 42 actively cooled neutron beam port inserts that connect to the external neutron guides, actively cooled moderators and reflector plugs and water cooled radiation shielding blocks. The CPMV is designed to operate either under a helium atmosphere, normally at 1 bar pressure, or under high vacuum and is directly connected to the accelerator beam-line that operates under ultra high vacuum conditions. A proton beam window (PBW) physically separates the two environments when the monolith is under a helium atmosphere and in the vacuum mode the PBW is removed and the two vacuum environments are directly connected.

The paper presented reviews the various aspects of the Vacuum Design of the Target Monolith System including material selection, surface finishes and construction issues, equipment sizing and selection and the development of a Strategic Installation and Test Strategy in order to minimize project risk.

3:00pm **VT-TuA3 Achievements and Problems in the First Commissioning of SuperKEKB Vacuum System**, *Yusuke Suetsugu, K. Shibata, T. Ishibashi, M. Shirai, S. Terui, K. Kanazawa, H. Hisamatsu*, KEK, Japan

The SuperKEKB is an electron-positron collider with asymmetric energies, that is, 7 GeV electrons and 4 GeV positrons, aiming the goal luminosity of 8x10³⁵ cm⁻²s⁻¹. Most of the vacuum components of the main rings (MR), especially in the positron ring, were newly fabricated to manage the high power of synchrotron radiation and the electron cloud effect (ECE), and to reduce the beam impedance, which are essential to keep the low-emittance beams stable in the operation with high beam currents. The construction of the new vacuum system had finished by the end of December 2015, and the beam commissioning started in February 2016. The maximum stored beam currents steadily increased from the beginning, and reached to 650 mA and 590 mA for the positron and electron rings, respectively, by the end of April. The average pressures at these beam currents were on the order of 10⁻⁶ Pa and 10⁻⁷ Pa for the positron and the electron ring, respectively. The vacuum scrubbing of the new beam pipes by the synchrotron radiation processed steadily. The pressure rises per unit beam current were on the order of 10⁻⁶ Pa A⁻¹ and 10⁻⁷ Pa A⁻¹ for the positron and electron ring, respectively. The high gas desorption in the positron ring was due to the electron stimulated gas desorption at aluminum parts in the ring. On the other hand, the reused beam pipes of the electron ring well memorized the surface condition of that in KEKB, which lead to the low gas desorption. The residual gas during the beam operation was continuously monitored using a quadrupole mass analyzer. The main components were hydrogen, methane, carbon monoxide and carbon dioxide. The electron numbers around the positron beam were also monitored at an arc section in relation to the electron cloud issues. The effect of antechambers and TiN coating on the suppression of electron cloud was confirmed. Newly developed vacuum components, such as the bellows chambers and gate valves with a comb-type RF-shield, and the MO-type flanges with little step inside, worked well as expected. One annoying problem was frequent pressure bursts accompanying beam aborts observed in the positron ring. Discharges at gaps or collision of the beam with dusts were suspected, but the investigation is still in progress. Here the major achievements and problems obtained in the first beam commissioning of the SuperKEKB MR vacuum system are presented.

4:20pm **VT-TuA7 Saving Megawatts in a Micron: Tailoring the Surfaces of Superconducting RF Cavities**, *Sam Posen**, Fermi National Accelerator Laboratory

INVITED

In particle accelerators, superconducting radiofrequency (SRF) cavities are specially-shaped chambers in which intense electromagnetic fields are built up through resonant excitation, in order to transfer energy to beams of

* VTD Early Career Award

Tuesday Afternoon, November 8, 2016

charged particles as they pass through. Large AC currents are generated in the region in which magnetic fields penetrate into the superconductor—just hundreds of nanometers below the surface—dissipating power that must be absorbed in the liquid helium bath that cools the cavities. Because of the significant cost of removing heat at cryogenic temperatures, accelerator scientists take great care in tailoring the surfaces of these superconducting materials to minimize dissipation, as well as to maximize the accelerating electric field. This contribution will present an overview of modern techniques used in SRF surface preparation, including doping with nitrogen, high temperature deposition of tin, and plasma processing. These processes, which generate micron-scale modifications of the surface, will be outlined, and their substantial impact on the accelerator will be presented.

5:00pm VT-TuA9 NEG Coating of Narrow-Gap Insertion Devices and Beam Pipes: Recent Achievements and Future Perspectives, Paolo Manini, M. Puro, S. Raimondi, T. Porcelli, F. Siviero, E. MacCallini, G. Bongiorno, SAES Getters S.p.A., Italy

Non-evaporable getter (NEG) coatings are nowadays successfully employed in several accelerator facilities, where stringent ultra-high vacuum (UHV) conditions should be met.

NEG coatings are able to provide high distributed pumping speeds for every getterable gas; in addition, the thermal outgassing and secondary electron yield of a NEG-coated beam pipe are considerably reduced, thus allowing the achievement of better results in terms of base pressure and, consequently, beam lifetime and luminosity.

The use of NEG coatings is especially suitable for narrow-gap beam pipes and insertion devices, which could not otherwise be pumped with the same effectiveness by a series of traditional UHV lump pumps. This aspect is particularly significant in view of next-generation machines, for which long and small-aperture tubes (*i.e.*, down to 4 mm) are envisaged in order to reach even higher luminosities and lower emittances.

Such stringent requirements should be carefully addressed, as a number of technical issues arise—both in terms of coating deposition and characterisation—when dealing with narrow-gap beam pipes of this kind.

SAES' recent achievements in this field are here presented, together with an overview of the ongoing R&D activities, whose aim is to demonstrate the feasibility and pumping effectiveness of narrow pipes under 10 mm of diameter. These include SEM morphological inspections, chemical composition analyses and thickness profiling made by EDX and, finally, measurements of the getter film's sorption capacity for CO. Future perspectives and issues—including the possibility to coat very long and narrow chambers and to perform transmission factor measurements on them—are also reviewed.

5:20pm VT-TuA10 Realisation of a Vacuum System of an EUV Exposure System, Freek Molkenboer, N.B. Koster, A.F. Deutz, B.A.H. Nijland, P.J. Kerkhof, P.M. Muilwijk, B.W. Oostdijk, J. Westerhout, C.L. Hollemans, E. te Sligte, W.F.W. Mulckhuysen, M. van Putten, A.M. Hoogstrate, P. van der Walle, J.R.H. Diesveld, A. Abutan, TNO Technical Sciences, Netherlands
TNO is designing and building an Extreme Ultra-Violet (EUV) exposure facility, as presented last year. This system, called EUV Beam Line 2 (EBL2) will be capable of exposing a wide range of samples, including 6" EUV reticles.

The EBL2 system combines 6 major sub systems;

An atmospheric and vacuum handler connected through a load lock, enabling both molecular and particle clean handling of the sample. Samples will be loaded on the atmospheric handler using SEMI standardised EUV dual pods.

The vacuum handler transports the samples to and from all the attached sub systems. The particle cleanliness of the EBL2 system shall ensure that the EUV reticles can re-enter into EUV lithography tools to assess the imaging impact of the exposure after handling and exposure.

The EUV radiation is generated with a Sn fuelled EUV source and focussed with two collectors, providing EUV irradiation on the sample. The two collectors are mounted in a differentially pumped vacuum system which ensures good vacuum quality in the exposure chamber while maintaining the increased pressure in the EUV source.

The exposure chamber is an ultra-clean vacuum chamber which enables exposure of the sample in an ultra-clean environment. The vacuum design also enables a controlled introduction of various contaminants and process gasses to facilitate the customer's request. The sample or EUV reticle is mounted on a clamp that can be moved in XYZ and rotated around X and Z.

This movement is achieved with a large hexapod which is located in atmosphere. The vacuum barrier between the hexapod and the exposure chamber is a 1 meter long, CF250 mm edge welded bellow.

The last sub system is an X-ray Photoelectron Spectroscop (XPS) which is capable of analysing the full surface area of an EUV reticle, as well as performing angle resolved analysis on smaller samples in a specially designed sample holder that can be loaded in the exposure chamber for exposure to EUV.

This presentation will focus on the realisation of the vacuum system of the EBL2 system and will highlight the design choices made to meet the stringent vacuum and particle contamination requirements. Preliminary results of vacuum qualification of chambers will be shown together with progress in building the system.

EBL2 will be publicly accessible as a test facility for EUV lithography related research after qualification, which is expected to be finished end of Q1 2017.

5:40pm VT-TuA11 Cleaning and Verification Strategies for UCV and UHV Components, Michael Flämmich, VACOM, Vakuum Komponenten & Messtechnik GmbH, Germany; C. Worsch, S. Gottschall, R. Bauer, U. Bergner, VACOM Vakuum Komponenten & Messtechnik GmbH, Germany
INVITED

The requirement of high quality vacuum components for ultra clean vacuum (UCV) and ultra high vacuum (UHV) has become stronger over the last years, especially driven by industrial applications, research institutions and accelerator facilities. Besides the prerequisite of ultra clean surfaces, the outgassing properties from the bulk material are critical for in-situ baked UHV systems. For these applications stainless steel has been and still is the most commonly used raw material. The challenge of suppressing hydrogen outgassing from the bulk material has extensively been discussed in the past. Some approaches seem to be promising, but at the same time they are quite expensive and economically hardly viable. As an alternative to stainless steel, aluminum is regarded as a promising raw material due to some fundamental advantages, even though metal sealed CF components and chambers made from aluminum are hardly available and rarely used.

The present talk focusses on vacuum components and chambers for UCV and UHV applications made from both raw materials, stainless steel and aluminum. In this context, a viable cleaning strategy applying some state-of-the-art cleaning methods will be presented. In order to carefully characterize the extremely low outgassing of components for these vacuum sectors (UCV: non baked; UHV: in-situ baked), appropriate setups for outgassing rate measurements (throughput, accumulation, and pressure rise) will be discussed and respective experimental data will be shown. Measuring, verifying, controlling, and, at the end, knowing the outgassing rate of the produced components enables to explicitly specify, classify and guarantee the cleanliness and outgassing properties of UCV & UHV vacuum components.

As a further focus of the talk, metal-sealed CF vacuum components made from aluminium are introduced. In this context, adequate knife edge stability, complicated weldability and reliable outgassing properties have always been discussed as major challenges. It will be shown that these challenges have been solved lately and that Alu-CF components and chambers (AluVaC®) are today a serious alternative to the established components made from stainless steel.

Tuesday Evening Poster Sessions, November 8, 2016

Actinides and Rare Earths Focus Topic

Room Hall D - Session AC-TuP

Chemistry and Physics of the Actinides and Rare Earths Poster Session

AC-TuP1 Spatially Resolved Uranium Speciation in Nuclear Materials by Scanning Transmission X-ray Microscopy, Joseph Pacold, Lawrence Berkeley National Laboratory; *M.J. Kristo, K.B. Knight, K.S. Holliday,* Lawrence Livermore National Laboratory; *W.W. Lukens, C.H. Booth, S.G. Minasian, T. Tyliszczak, D.K. Shuh,* Lawrence Berkeley National Laboratory

The production and manipulation of nuclear material can leave distinct physical and chemical signatures, which can later be characterized to provide evidence of the origin and process history of an unidentified specimen, a field known as 'nuclear forensics'. A broad variety of analytical chemistry techniques can provide information about interdicted and post-detonation materials. Here, we present the results of several research studies of uranium-bearing forensic specimens by soft X-ray scanning transmission X-ray microscopy (STXM). STXM yields X-ray absorption spectroscopy data with 25-nm or better spatial resolution, making it possible to quantitatively evaluate variations in oxidation state and other chemical properties across a heterogeneous specimen. Operating in the soft X-ray regime provides access to the $M_{IV,V}$ edges of the actinides and the oxygen K edge, which is highly sensitive to variations in U-O bonding, and consequently carries unique fingerprints of uranium oxides and their hydrates. Thus, this approach makes it possible to evaluate the oxidation state and the heterogeneity of nuclear forensic samples, yielding information on formation or process history, and/or past storage conditions. In studies of U-bearing glassy materials, the L edges of some transition metals (particularly iron, which influences the redox behavior of uranium) can provide additional insights. Technical developments in STXM operations relevant to forensics are also summarized. In particular, we report on improvements in sample preparation and rapid data analysis methods implemented in STXM experiments at Beamline 11.0.2 of the Advanced Light Source.

AC-TuP2 XPS Investigation on the Reduction of Aged UO_2 Powders during Exposure to Vacuum, Scott Donald, M. Davisson, Z. Dai, A.J. Nelson, Lawrence Livermore National Laboratory

The evolution in vacuum of UO_2 powder samples, previously aged under a controlled environment composed of 20% O_2 and relative humidity varying from 34% to 98%, was studied using core level x-ray photoelectron spectroscopy. Upon exposure to ultra-high vacuum, the U 4f peak position was found to shift to a lower binding energy with time, consistent with a decrease in the overall oxidation state of the uranium. No samples were found to reduce fully to stoichiometric UO_2 under vacuum; those exhibiting the greatest decay with time asymptotically approached a mean uranium valence of +4.5, analogous to U_4O_9 , within 14 days. The reaction rate was found to be variable with the initial mean uranium valence, with more oxidized samples reducing more quickly. Scanning electron microscopy images of the aged powders showed corresponding structural variation and enhanced surface cracking, both of which may serve to facilitate the reduction process.

The work was performed under the auspices of the U.S. Department of Energy by Lawrence Livermore National Laboratory under Contract DE-AC52-07NA27344.

Applied Surface Science

Room Hall D - Session AS-TuP

Applied Surface Science Division Poster Session

AS-TuP2 Observing the Effects of Jetting from Sputtering with Both Monatomic Argon and Argon Gas Clusters of Multi-layered Samples Using XPS with Rapid Mapping, Timothy Nunney, Thermo Fisher Scientific, UK; *R. Simpson,* University of Surrey, UK; *C. Deeks, P. Mack, J.P.W. Treacy,* Thermo Fisher Scientific, UK

Nano-scale multi-layered materials are becoming more common, especially in the microelectronics industry. Components used in applications such as flexible electrical circuitry are often made of stacked layers of material. These can include both organic and inorganic materials in a single component. Complications arise in depth profiling these kinds of components when transitioning across the interface between the two material types.

Depth profiling from an inorganic layer to an organic layer can produce an effect known as "jetting". This is where material from the lower organic layer is rapidly ejected and redeposited around the etch crater, as a result of the high energy penetration of the inorganic material layer. As soon as the organic layer is exposed to the ion beam, the relative high energy ion beam needed to etch the inorganic layer, will cause material from the organic layer to burst out in this jetting effect.

This presentation will demonstrate the effects of jetting on a range of samples, illustrating how the ejection on deposition occurs depending on the type of sample and the ion beam mode type used. It will show differences between monatomic sputtering and cluster sputtering and showcase the benefits of both of these methods of depth profiling. A new form of rapid XPS mapping will be demonstrated allowing the jetting effect to be quickly observed.

AS-TuP3 Multitechnique Surface Analysis for Advanced Microelectronics Materials, James Lallo, Thermo Fisher Scientific; *C. Deeks, P. Mack, T.S. Nunney, J.P.W. Treacy,* Thermo Fisher Scientific, UK

Multitechnique analysis is becoming increasingly common for characterisation of materials. Performing X-ray Photoelectron Spectroscopy (XPS) is now routine in many laboratories to give surface information (0-10 nm). Energy Dispersive X-ray Spectroscopy (EDS or EDX) is also widely used in laboratories to help detect elemental information from smaller areas within the bulk (1-2 μm) of the material. A combination of both EDS and XPS can help to give a wider picture of samples being analysed, giving both elemental and chemical information from both the 'surface' and the 'bulk' of samples over a wide ranging spatial area.

EDS is often used in microelectronics laboratories to observe if any contaminants are present on the surface. A big contaminant is copper as it has poor adhesion to most insulators, so the ability to observe this is key. We will demonstrate on advanced microelectronic samples that EDS alone is not enough for detecting contaminants such as this, and we will show that XPS is also needed to give the full elemental and chemical details of these types of samples.

This presentation will look at a range of microelectronics samples, and demonstrate by using both XPS and EDS combined on a single system, that no one technique is enough to obtain the full picture of what is in the sample, and show that by having the ability to have both these techniques on a single system, it can provide a wealth of complementary information from the surface and near-surface regions of a material.

AS-TuP4 Surface Analysis of Human Hair – a Multi-technique Approach, Sarah Coultas, J.D.P. Counsell, C.J. Blomfield, Kratos Analytical Limited, UK; *M. Openshaw,* Shimadzu - MALDI Technologies Group; *C. Moffitt,* Kratos Analytical Inc.

In 2016, the global hair care market is estimated to be worth about USD 83.1 billion [1] and the size of the market is growing year on year. There are thousands of products available used for both cosmetic and medical purposes and the industry is constantly developing new formulations to improve performance and safety.

There are numerous treatments and modifications made to hair which involve complex surface chemistry. Products contain many ingredients designed to clean, condition, add volume, shine or treat medical conditions such as dandruff to name but a few. Techniques such as XPS, ToF-SIMS and MALDI-ToF have all been used to characterise the surfaces of natural fibres and investigate the efficacy of such treatments. Recent developments in organic depth profiling using argon cluster sources have also been applied to hair samples opening up an interesting extra dimension [2].

Each of the techniques has its own strengths: XPS provides quantitative elemental identification whereas ToF-SIMS and MALDI are rich in molecular information. Here we use the combination of all three to fully characterise the surface treatment of human hair, in particular the application of conditioner. A range of treatment conditions have been studied, including various concentrations of active ingredients and application methods. As well as investigating the distribution with depth using ARXPS and cluster depth profiling we explore the spatial distribution of species via imaging.

[1] <http://www.statista.com/statistics/254608/global-hair-care-market-size/>

[2] Ishikawa, Kazutaka and Okamoto, Masayuki and Aoyagi, Satoka, *Biointerphases*, 11, 02A315 (2016)

Tuesday Evening Poster Sessions, November 8, 2016

AS-TuP5 Exploring the Surface and Sub-Surface Nature of Nuclear Graphite, J.D.P. Counsell, S.J. Coultas, C.J. Blomfield, Kratos Analytical Limited, UK; **Chris Moffitt**, Kratos Analytical Limited; A. Theodosiou, University of Manchester

Graphite is a key material used in the current generation of UK nuclear reactors. Graphite has been recognised as an excellent neutron moderator and reflector in reactors, allowing sustainable, controlled fission. Contaminants in moderator rods are a major problem as they can act as neutron absorbers. This causes decreased fission and production of unwanted isotopes – a common cause of radioactive waste. The goal of this study is to understand the surface chemistry of graphites used in the UK nuclear industry today.

The surface compositions of Pile grade A (PGA) and Gilsco coke graphites are determined using X-ray photoelectron spectroscopy (XPS). The results are compared to commercially available highly-ordered pyrolytic graphite (HOPG). The degree of sp²/sp³ character is determined for each graphite using Auger parameter analysis. Significant variation in sp² character was observed between graphites. Depth profiling of the surface was performed utilising both monatomic Ar⁺ ions and cluster Ar_n⁺ ions. The mechanics of cluster/monatomic ion bombardment are discussed with respect to surface damage and a suitable method for graphite bulk analysis is proposed.

AS-TuP6 Comparison of Angle Resolved XPS and Ultra-shallow Ar Gas Cluster Depth Profiling of Organometallic Multilayer Materials, **Simon Hutton**, Kratos Analytical Limited, UK; T. Bendikov, Weizmann Institute of Science, Israel; K. Macak, W. Boxford, S.C. Page, S.J. Coultas, C.J. Blomfield, J.D.P. Counsell, Kratos Analytical Limited, UK

Angle resolved X-ray photoelectron spectroscopy (ARXPS) is a widely used technique for investigating the depth distribution of species over the first few nanometres of the sample surface. An important property of the technique is that it is non-destructive; the sample is not damaged during the measurement process. This is in contrast to sputter depth profiling where an ion beam removes the surface layer to reveal the underlying material. A major shortcoming of the ARXPS technique is that it provides information only from the surface region of the material. It is limited to the maximum escape depth of the photoelectrons generated during measurement. This limitation is not shared by sputter depth profiling, which can delve deep into the material by employing multiple sputter / analysis cycles.

Chemical damage of the analysed material is an ever present consideration during sputter profiling. One method of reducing this chemical damage is to vary the nature of the sputtering ion. This has proved very successful for organic materials and thin films where massive gas cluster ions have found widespread use. We have previously demonstrated the successful use of massive Ar clusters to sputter depth profile through multi-layer organometallic thin films [1]. In this study we compare the results of non-destructive ARXPS measurements with ultra-shallow sputter depth profiling using massive Ar cluster ions on similar multi-layer organometallic thin films.

The films consist of two well defined and iso-structural osmium and ruthenium polypyridyl complexes. These complexes are deposited from solution in a sequence-dependent assembly regime leading to self-propagating molecular assemblies with distinct internal interfaces and composition. [2] The films were assembled on indium tin oxide (ITO) coated glass slides. ARXPS data was collected by tilting the sample with respect to the analyser / X-ray source. The results were processed using a maximum entropy method software package developed specifically for this type of application [3].

Shallow sputter profiles through the thin films were achieved using massive Ar cluster ions with approximately 2000 Ar atoms per cluster. Ion acceleration voltages were kept low to ensure a very low energy per Ar atom and hence limit the sputtered region to the sample surface.

[1] S. Hutton, T. Bendikov, W. Boxford, S. Page, J. Counsell, A. Roberts, C. Blomfield, S. Coultas, *AS-THP3 AVS 62nd International Symposium & Exhibition*.

[2] G. de Ruiter, M. Lahav, G. Evmenenko, P. Dutta, D. A. Cristaldi, A. Gulino and M. E. van der Boom, *J. Am. Chem. Soc.* 2013, 135, 16533-16544.

[3] K. Macak, *Surf. Interface. Anal.* 2011.

AS-TuP7 Pd deposited on Al₂O₃ analyzed by Low Energy Ion Scattering (LEIS), P. Bruener, T. Grehl, ION-TOF GmbH, Germany; **Nathan Havercroft**, ION-TOF USA; J.Z. Mundy, G.N. Parsons, North Carolina State University
Low Energy Ion Scattering (LEIS) is uniquely able to provide quantitative elemental characterization of the outermost atomic layer of a sample. In Tuesday Evening Poster Sessions, November 8, 2016

addition, the LEIS spectra contain information about the composition of the first few nm of the samples. These properties make it an ideal tool for the characterization of thin films, from the initial nucleation stage to complete films. The analysis gives insight into growth modes (island vs. layer-by-layer), growth rates and impurities, as well as accurate information about layer closure.

For the LEIS analysis, noble gas ions with kinetic energy of a few keV are scattered by individual atoms in the sample surface. The energy loss of the ions in this scattering process is dependent on the mass of the surface atom it was scattered from. The peaks in the energy spectrum of the backscattered ions are used to identify and quantify the elemental composition of the outer surface.

Ions that are scattered in deeper atomic layers are first of all efficiently neutralized and lose energy by nuclear and electronic stopping on their way through the sample. This causes a shift in energy proportional to the distance traveled in the solid, and a lower intensity of those ions. Due to this, the scattering from the first atomic layer can be distinguished from sub-surface scattering, leading to the extreme surface sensitivity of just one atomic layer [1].

However, even ions scattered below the surface can be detected if the surface promotes the reionization of neutralized primary ions after their travel through sub-surface layers. This can be used to determine layer thickness and elemental distribution in the first few nm of the sample in a fast and non-destructive measurement. The required stopping power values are calculated using SRIM [2].

In this study we applied LEIS to a range of samples of ALD deposited Pd on Al₂O₃ substrates. The currently used process for the Pd deposition requires high temperatures to facilitate the desorption of residuals from the Pd precursor, which poison the substrate surface and inhibit the further nucleation of Pd. This leads to island growth of Pd clusters. We demonstrate how LEIS can be used to analyze the surface coverage of the deposited Pd, the Pd cluster dimensions, and the amount of precursor residual. This information is crucial to develop a lower temperature process for the deposition on temperature sensitive substrates, such as polymers.

[1] Surface composition analysis by low-energy ion scattering, Brongersma, H. H.; Draxler et al., *Surf Sci Reports*, 62, 2007, 63-109

[2] The Stopping and Range of Ions in Solids (Pergamon, New York, 1985)

AS-TuP8 Real-time Monitoring of Surface Reactions by Means of Cluster-induced Desorption/Ionization Mass Spectrometry, A. Portz, Justus Liebig University Giessen, Germany; **Christoph R. Gebhardt**, Bruker Daltonics Bremen, Germany; M. Durr, Justus Liebig University Giessen, Germany

The reactions of biomolecules on surfaces are of great interest both from a fundamental point of view as well as with respect to applications such as surface functionalization. However, the chemical information obtained by standard surface analysis tools is limited. Recently, we have shown that desorption/ionization induced by neutral clusters (DINeC) is a soft and matrix-free ion source for mass spectrometry of biomolecules. DINeC employs molecular clusters of 10³ to 10⁴ SO₂ molecules; the clusters do not only provide the energy necessary for desorption but, due to the high dipole moment of SO₂, also serve as a transient matrix in which the desorbing molecule is dissolved during cluster-surface impact. Thus desorption takes place at comparably low cluster energies (< 1 eV/molecule); shattering of the clusters during and after surface impact furthermore leads to a rapid redistribution of the system's energy. As a consequence, desorption takes place without fragmentation of the desorbing molecules.

In this contribution, we demonstrate that DINeC can be used for real-time monitoring of surface reactions of larger molecules such as porphyrins and oligo-peptides. The quantitative nature of the method was demonstrated using angiotensin II molecules individually adsorbed on gold substrates by means of electrospray ion-beam deposition. These adsorbates were desorbed and detected as intact molecules down to a coverage of 10⁻¹³ mol/cm² (0.001 ML); a linear relationship between surface coverage and signal intensity was observed over three orders of magnitude. Real-time monitoring of surface reactions is demonstrated for isotope-exchange experiments with angiotensin II and different types of porphyrins. Dosing D₂O led to a broadening of the isotopic pattern and a continuous shift towards higher m/z values. When the D₂O pressure was chosen high enough, the H/D exchange rate was determined by the exchange process itself. The results were modeled by means of Monte Carlo simulations taking into account reaction and back-reaction of H/D exchange. Several

Tuesday Evening Poster Sessions, November 8, 2016

different rate constants could be extracted and are assigned to the different types of functional groups in the respective molecules.

AS-TuP9 Improved X-ray Photoelectron Spectroscopy Analysis using the PHI VersaProbe III, Jennifer Mann, J.S. Hammond, J.F. Moulder, B. Schmidt, Physical Electronics USA

Based on its proven scanning X-ray Photoelectron Spectroscopy (XPS) microprobe core technology, Physical Electronics has introduced the newest version of its VersaProbe product line; the VersaProbe III. Multiple improvements over the VersaProbe II model have been incorporated into this new design including:

1. Higher sensitivity for all analysis areas
2. Increased number of detector channels for faster imaging
3. Collection angle defining aperture for angle dependent studies
4. Improved hot/cold stage temperature range
5. Dedicated high temperature mount for increased temperature experiments
6. Dedicated 4-contact sample mount for in-situ controlled potential experiments

This poster will discuss these improvements in more detail and show examples where they are beneficial in XPS experiments.

AS-TuP10 Multiple Technique Investigation of UV-grafted Polymers, Lopamudra Das, M.J. Kelley, College of William and Mary

The major increased-value opportunities for polyesters depend on affordable, environmentally-friendly surface modification. We report the use of 172 nm UV light to induce surface radicals that offer graft sites for desirable functionalities on PET, PTT, PBT and PEN. Obtaining insight into the mechanisms and results requires multiple techniques, notably XPS, ToF-SIMS, AFM and FTIR.

AS-TuP11 Analysis of Thin Phase-Shifter Films using Surface Analysis Techniques, Vincent Smentkowski, General Electric Global Research Center; L. Le Tarte, GGeneral Electric Global Research Center; H. Piao, General Electric Global Research Center; M. Marko, Wadsworth Center

Many types of phase-shifters have been developed for use in place of the TEM objective aperture. The phase shifters act to increase phase contrast by providing high transfer of information over a very wide spatial-frequency range. Unfortunately, many of these devices fail shortly after being installed into the instrument due to charging in the electron beam, so we have been experimenting with surface deposition of novel thin-film metals. In some cases, it is essential that the electron-scattering cross-section of the metal film be as small as possible, so the films must often be quite thin (less than 10 nm thick). Accurate analysis of such thin films is required to understand the composition of the layers, unexpected impurities both in the films and at the interfaces, the oxidation state of the layers, and the lateral uniformity of the layers.

In this poster we use a suite of surface analysis techniques to monitor the distribution of species through one multilayer phase plate stack comprised of 2nm Rh, 6nm C, and 2nm Al using depth profiling protocol. The pros and cons of each of the surface analysis techniques are illustrated via the sample analyzed. Each of the three techniques used here were able to successfully identify and resolve each of the 3 layers with a sufficient number of data points defining the thin layers. Each of the techniques also revealed oxygen in the aluminum layer with a stoichiometry of about Al₂O₃.

An advantage of ToF-SIMS for depth profiling is the ability to rapidly collect an image at every depth, allowing for 3D rendering of the data sets. The 3D ToF-SIMS renderings do not reveal discontinuous regions at a length scale of a few hundred nm (the conditions used here); ruling out holes at a length scale of less than a few hundred nanometers in the Rh layer would require ToF-SIMS analysis using a pulsing mode with a smaller analytical spot size. Another advantage of ToF-SIMS is that a full mass spectrum is saved at every voxel and hence all elements and high mass molecular fragments are analyzed. Often unexpected species are revealed sub surface. A disadvantage of ToF-SIMS is the ion yield varies depending on the composition of the matrix and this makes quantitative analysis more difficult. In contrast sensitivity factors have been developed for both AES and XPS and these reported sensitivity factors are typically valid to within 10% and hence quantitative analysis is easier.

Mike Marco acknowledges funding through NIH grant GM103555.

AS-TuP12 Improving the Performance of the Cylindrical Mirror Analyzer by Electrode Segmentation, David Edwards, Jr, IJL Research Center

Electrode segmentation of the cylindrical mirror analyzer has been shown to significantly improve the resolution of the standard instrument. The high precision solution which had been found for the 42.3 device is shown in this report to exist in fact for an extended set of input angles or equivalently for a range of sample positions. This has allowed a significant limitation of the CMA, namely the critical dependence of instrument performance on sample position, to be largely overcome. In addition by placing the sample at the minimum in the curve of resolution vs sample position, a resolution of ~0.00045 has been obtained for a +6 degree bundle an improvement of a factor of ~40 over the standard spectrometer. Thus electrode segmentation has been found not only to significantly improve the device performance, but in fact to enable its high precision to be realized.

AS-TuP15 Impact of Surface Contaminants on ToF-SIMS analysis of Wood Polymer Composites (WPCs), Laura D. Brunelle, Z.A. Gernold, C.S. Swagler, E.R. Welton, R.E. Goacher, Niagara University

Wood Polymer Composites (WPCs) are a promising material for outdoor applications, such as decking and marine structures, because they have improved properties over wood or plastic alone. WPCs also allow for the recycling of plastics and use of reclaimed wood. However, the use of WPCs poses questions regarding the breakdown and weathering of WPCs. The importance of the interface between wood and polymer components of the composite may make analysis with a chemical imaging technique such as Time-of-Flight Secondary Ion Mass Spectrometry (ToF-SIMS) advantageous. Due to the high surface sensitivity of ToF-SIMS, an understanding of the surface contaminants on WPCs is required. Contaminants on WPCs may arise from handling, storage, or from lubricants and other components used in the manufacturing process. As such, even new material surfaces can be considered contaminated. Therefore, the interiors of the WPCs were used as references, as the interior is an unhandled surface. The removal of contaminants by solvents (including purified water, isopropyl alcohol, and mixtures thereof) was evaluated to identify appropriate cleaning methods. Furthermore, it may be desirable to remove contaminants prior to or after controlled weathering experiments. Therefore, the chosen cleaning method was applied to previously weathered samples. Comparisons of ToF-SIMS spectra of the WPCs were performed using Principal Component Analysis (PCA) and Multivariate Curve Resolution (MCR). This work provides insight into how the surface and interior of the WPCs differ, how treatment with common solvents alter the obtained spectra, and how weathered surfaces appear with and without cleaning.

AS-TuP16 Examining the General Applicability of ToF-SIMS for Wood Polymer Composite (WPC) Analysis, Christopher S. Swagler, L.D. Brunelle, M.R. Michienzi, E.R. Welton, R.E. Goacher, Niagara University

The interface between hydrophobic plastic and hydrophilic wood in Wood Polymer Composites (WPCs) is important for the strength and durability of the materials. WPCs are used in decking and marine structures because they have improved properties over wood or plastic alone. WPCs are relatively new materials and prior research into their weathering and durability has focused on the issue of interface adhesion. Such studies have used Scanning Electron Microscopy (SEM) for morphological analysis, and many have included chemical analysis using X-ray Photoelectron Spectroscopy (XPS). However, XPS has poor imaging resolution and only provides elemental and functional group analysis. For a more detailed analysis of the wood-plastic interface, Time-of-Flight Secondary Ion Mass Spectrometry (ToF-SIMS) offers higher imaging resolution than XPS, and can provide more detailed molecular information.

To date, ToF-SIMS analysis of WPCs has been limited to preliminary studies involving the weathering and cleaning of a single commercially available product. These analyses have shown ToF-SIMS to have promise for the analysis of weathering, using spectral, imaging, and depth profiling approaches. The present study expands this analysis to include a wider variety of sample types, such as those made from polypropylene, nylon or styrene maleic anhydride plastics, with and without added dyes. The composition of these samples is better known than the composition of the previously analyzed commercial material, which aids in identification of peaks from the polymer, wood, and any additives. The analysis of a wider set of unweathered WPCs provides baseline information about the observable chemical distributions for comparison to weathered samples. ToF-SIMS results are also compared to visual light microscopy, SEM, and XPS to illustrate complementarity with these techniques. This work

Tuesday Evening Poster Sessions, November 8, 2016

provides insight into how the ToF-SIMS spectra and images vary for WPCs of different composition, including new and reclaimed materials.

AS-TuP17 Swift Heavy Ion Irradiation for Designing Planar Field Emitters and Exchange Bias Layers, *Debalaya Sarker*, S. Bhattacharya*, Indian Institute of Technology Delhi, India; *S. Ghosh, P. Srivastava*, Indian Institute of Technology Delhi

In this talk, I shall give a brief overview of engineering ferromagnetic metal-insulator (FM_M/SiO_2 $\text{FM}_M=\text{FeCo}$, Ni) nano-composites having application in device physics. Increasing demand of flat displays necessitates to design planar emitters which not only miniaturize the device but also have several other advantages like mechanical durability, temporal stability etc. FM_M nanoparticles (NPs) inside SiO_2 matrix, when subjected to Swift Heavy Ion (SHI) irradiations get elongated. Using this, we demonstrate here a planar field emitter with maximum current density of $550 \mu\text{A}/\text{cm}^2$ at an applied field of $15 \text{ V}/\mu\text{m}$. The film, irradiated with 5×10^{13} ions/ cm^2 fluence (5e13) of 120 MeV Au^{3+} ions, shows very high electron emitting quantum efficiency in comparison to its unirradiated counterpart. We find experimental evidence of enhanced valence band (VB) density of states (DOS) for 5e13 film from XPS, which is further verified in the electronic structure of a model FM_M cluster from combined density functional theory (DFT) and *ab initio* molecular dynamics (MD) simulations. The MD temperature is taken from the lattice temperature profile from thermal spike model. Increasing the SHI fluence beyond 5e13, results in reduced VB DOS and melting of surface protrusions, thus causing reduction of FE current density. We finally conclude from DFT that change in fluence alters the co-ordination chemistry followed by the charge distribution and spin alignment, which influence the VB DOS and concurrent FE as evident from our experiment^{1,2}. More recently, we have explored the effect of shape and structural anisotropies on magnetic properties of SHI irradiated FM_M/SiO_2 films. Magnetic anisotropy (MA) and exchange bias effect (EBE) were tuned by monitoring SHI irradiation fluence. The in-plane and out-of-plane M-H loops show that the perpendicular MA reaches a maximum value at 5e13 and then decreases. At highest fluence an EBE is observed. Underlying electronic structure was not only probed with XANES and XPS VB, but also is validated from our non-collinear theoretical calculations. We conclude this EBE is an outcome of formation of anti-ferromagnetic domains due to spin-flipping at high temperature. In summary, elongated FM_M NPs inside SiO_2 matrix are designed using controlled SHI irradiation. Due to its high current density and mechanical/chemical durability, the irradiated films open new possibilities for the development of electronic displays. They also show sufficient promise in magnetic storage media for their interesting MA and EBE properties.

Reference:

¹D. Sarker *et al.*, ACS Appl. Mater. Interfaces, 8, 4994 (2016).

²D. Sarker *et al.*, J. Appl. Phys, 115, 174304 (2014).

AS-TuP18 Improving Relative Quantitation in Imaging Lipidomics using ToF-SIMS, *Marwa Munem, J.S. Fletcher*, University of Gothenburg, Sweden

Introduction
ToF-SIMS is of increasing value to clinicians and has been used on a number of tissue samples to successfully identify and localise different chemical components to various areas of the tissue and answer disease related questions [1]. Compared to traditional histology or fluorescence staining, the main advantage of ToF-SIMS is the label free detection of a large number of different molecules simultaneously on the same tissue section. New gas cluster ion beams (GCIBs) provides benefits for imaging larger molecular species [2]. These improvements still leave issues such as greatly varying ionisation efficiencies for different molecules and matrix effects. In some biological samples changes in Na or K concentration through the sample can lead to different pseudo-molecular ions being preferentially generated from different parts of the sample.

Methods

A J105 ToF-SIMS instrument (Ionoptika Ltd, UK) was used to analyse salt adduct effects on lipids ionization by exposing different standard lipids and tissue samples to different concentrations of sodium and potassium salts mixtures. Tissue sections from mouse heart, rat brain and cancer biopsy samples were imaged on the same instrument adduct formation assessed.

Results

In positive ion mode the relative intensity of $[\text{M}+\text{H}]^+$, $[\text{M}+\text{Na}]^+$ and $[\text{M}+\text{K}]^+$ ions from phosphatidylcholine phospholipids changes dramatically with just

a small change in the Na:K ratio in the sample. The situation is further complicated by changes in relative intensities of fragment ions. The ratio of the $[\text{M}+\text{Na}-59]^+$ to the $[\text{M}+\text{Na}]^+$ peak is significantly smaller than the equivalent ratio from potassium adduct ions. Using these different peaks corrected images of different lipids can be generated from images of tissue sections obtained by ToF-SIMS.

Conclusions

Matrix effects, in this case variation in salt content in biological samples, can lead to difficulties in (relative) quantitation of different biological species. The changes in ionisation and fragmentation observed in ToF-SIMS measurements show similar trends to those observed with other mass spectrometry methods where adduct formation is used as a tool for influencing fragmentation in tandem MS experiments[3].

[1] David Toubel, Sandrine Roy, Dominique P. Germain *et al.*, *Int. J. Mass Spectrom.* 2007, 260(2-3), 158-165, Sjövall Peter, Björn Johansson *et al.*, *App. Surf. Sci.* 2008, 255 (4), 1177-1180, Michael A. Robinson, Daniel J. Graham, Fionnuala Morrish *et al.*, *Biotinterphases*, 2016, 11, 02A303

[2] T. B. Angerer, P. Blenkinsopp, J. S. Fletcher, *Int. J. Mass Spectrom.* 2015, 377, 591-598

[3] Rian L. Griffiths and Josephine Bunch, *Rapid Commun. Mass Spectrom.* 2012, 26, 1557-1566

AS-TuP19 XPS Investigation of UHP Mg and Mg Alloys Exposed to Water: Peak Fitting the Mg 2p Core Level Spectra to Distinguish Oxide from Hydroxide, *Harry Meyer, D. Leonard, M.P. Brady*, Oak Ridge National Laboratory

Magnesium alloys are increasingly used in structural materials applications requiring high strength and light weight. Alloys containing Mg are also of interest in biomedical applications (implants) and energy materials applications (fuel cells, batteries, and hydrogen storage). The Department of Energy has aggressive materials research projects aimed at increasing the use of magnesium and magnesium-based alloys for vehicle applications. The primary interest in vehicles is to reduce the overall vehicle weight by substituting lighter weight Mg-alloys. One of the primary obstacles for increased use of Mg-alloys is the corrosion behavior of these materials. Oak Ridge National Laboratory has been studying aqueous corrosion behavior for several years to try to develop an understanding of the corrosion film formation mechanism. The material presented in this poster is a portion of that larger program and is focused on using x-ray photoelectron spectroscopy (XPS) to study Mg-alloy corrosion. In this study we have exposed four Mg materials (UHP Mg; Mg-0.27Zr; Mg-0.14Nd; and Mg-2Al) to water for 4 hours to elucidate early film formation. Ar-ion depth profiling was used to compare the thickness of the corrosion films and to try to understand the partitioning between oxide and hydroxide growth. This poster demonstrates the Mg 2p peak fitting strategy that was employed. This abstract has been authored by UT-Battelle, LLC under Contract No. DE-AC05-00OR22725 with the U.S. Department of Energy.

AS-TuP20 Root-Cause Analysis of an Interfacial Adhesive Failure Based on Time-of-Flight Secondary Ion Mass Spectrometry (ToF-SIMS), *James Ohlhausen, P. Vianco*, Sandia National Laboratories

Low Temperature Co-fired Ceramic (LTCC) substrates are used for high frequency electronics assemblies. The LTCC material is comprised of alumina particles in a silica-based, glassy phase; the latter also includes Na, Mg and Ca oxides. The surface conductor traces and pads are a Au/Pt/Cu/Ti metallization where Ti is the adhesion layer. Delamination was experienced at the interface between the Ti layer and LTCC. Determining a root-cause to the delamination was made difficult by the complexity of the LTCC material and air exposure of the test samples before being introduced into the vacuum chamber for surface analysis. This air exposure of already de-adhered interfaces potentially compromises the cleanliness of the mutual, interface surfaces due to oxidation and adventitious contamination that caused significant challenge for the Time-of-Flight Secondary Ion Mass Spectrometry (ToF-SIMS) assessment.

ToF-SIMS was used to analyze the de-adhered interfaces as well as to evaluate the unexposed interface by means of the depth profile mode. The ToF-SIMS tool was able to identify key Pb, Na, K, and Ca markers that confirmed the widespread coverage of the surface by the glassy phase. The role of organic contamination was similarly documented at the de-adhesion sites. The data obtained from these ToF-SIMS assessments confirmed that delamination was caused primarily by the propensity of the glassy phase to cover the LTCC surface. Small variations to the glass phase composition accounted for the intermittent presence of delamination. This poster will outline the specific ToF-SIMS test steps as well as the data

Tuesday Evening Poster Sessions, November 8, 2016

analysis and methodologies that allowed for a conclusion to be developed for the delamination event.

****Sandia National Laboratories** is a multi-program laboratory managed and operated by Sandia Corporation, a wholly owned subsidiary of Lockheed Martin Corporation, for the U.S. Department of Energy's National Nuclear Security Administration under contract DE-AC04-94AL85000.

AS-TuP21 Surface and Bulk Property Studies of Newly Developed High Performance Transparent Conductor Material, Lei Zhang, W. Wu, N.G. Tassi, D. Walls, DuPont Science and Engineering

Nowadays, transparent conductor (TC) materials have been widely applied into various areas including displays such as LCD & OLED, touchscreens, and photovoltaics. While indium tin oxide (ITO) has been used as a dominant TC material, due to the rareness of indium metal, scientists have been working to develop new/alternative TC materials to meet special needs in different application areas.

In the area for large touch screen panel application, copper mesh material can be a good TC candidate because of Cu's high electrical conductivity and low material cost. However, Cu is unstable in air and easily forms Cu(I)/Cu(II) oxides, plus Cu atoms are easily diffused to other layers in the devices to cause device malfunctioning. To stabilize the Cu surfaces, graphene is selectively deposited on the surfaces of the micro-grids by atmospheric pressure chemical vapor deposition (CVD) method. Integrated analytical techniques including X-ray photoelectron spectroscopy (XPS), Raman, and others were applied to characterize the surface, bulk, and electrical properties of the graphene coated Cu/Ni micro-grid systems. Results indicated the realization of long-term stability of the new TC structure. This presentation will cover the development and study of this high performance and stable graphene coated copper/nickel micro-grids transparent conducting structure.

AS-TuP22 Optimizing the Surface of Perovskite Oxide/Carbon Composites as Catalysts for the Oxygen Reduction Reaction in Alkaline Media, Michael Dzara, C. Ngo, Colorado School of Mines; **J. Christ,** National Renewable Energy Laboratory; **P. Joghee, C. Cadigan, T. Batson, R. Richards, R. O'Hayre, S. Pylypenko,** Colorado School of Mines

Developing non-precious metal catalyst (NPMC) materials for the oxygen reduction reaction (ORR) is a critical research area in order to drive the widespread commercial adoption of low temperature fuel cells. Current technology uses Pt or other precious metal-based catalysts; by replacing these expensive precious metals with inexpensive, earth-abundant NPMCs, the economic feasibility of low temperature fuel cells can be significantly improved. However, improvements in the performance of NPMCs are needed in order to compete with precious metal-based catalysts. Perovskite oxide structures (ABO₃) are one of the candidates among themany materials being evaluated as NPMCs for the ORR in alkaline media. Many elements can form perovskite oxide structures that are stable in alkaline media, and the properties of these structures can be tuned by doping the A and B sites, providing an extremely vast range of possible structures to explore.¹ Performance of perovskite oxides has been shown to improve by creating a perovskite oxide/carbon composite, as carbon improves the conductivity of the composite and has an active role in catalyzing the ORR.² However, like other NPMC chemistries perovskite oxides are heterogeneous by nature, and it is therefore difficult to correlate material properties with catalytic performance.

Here, our work focuses on understanding the interplay of surface chemistry and surface morphology of Ca_{0.9}La_{0.1}Al_{0.1}Mn_{0.9}O_{3-δ} perovskite oxides and their composites with carbon. An aerogel synthesis method was used to produce Ca_{0.9}La_{0.1}Al_{0.1}Mn_{0.9}O_{3-δ} perovskite oxides with surface areas from approximately 5-80 m²/g. By varying synthesis parameters, materials with different surface chemistry and morphology were produced. Detailed characterization of surface composition and morphology are performed using physisorption, x-ray photoelectron spectroscopy, and transmission electron microscopy equipped with energy dispersive X-ray spectroscopy. This information is correlated to rotating ring-disk electrode electrochemical measurements in alkaline media. These techniques help provide understanding of the surface properties of Ca_{0.9}La_{0.1}Al_{0.1}Mn_{0.9}O_{3-δ} perovskite oxides and their impact on performance, providing a path towards optimization of the surface chemistry and morphology for improved catalytic performance.

References

1. Hardin, W. G., et al. (2014). Tuning the electrocatalytic...interactions. *Chem. Mater.*, 26(11), 3368–3376.

2. Poux, T., et al. (2012). Dual role...reaction. *Catalysis Today*, 189(1), 83–92.

AS-TuP23 Tuning of N-Doping in Carbon Nanospheres for Investigation of Catalyst-Support Interactions, Matthew Strand, C. Ngo, A. White, J. Hagen, S. Pylypenko, Colorado School of Mines

Continued increase of worldwide energy consumption necessitates the development of renewable energy resources. Fuel cells can utilize a wide variety of renewable fuels, but poor long term stability of the catalyst impacts their economic viability. High surface area carbon is utilized as a state-of-the-art catalyst support, and research has shown that the presence of dopants such as nitrogen can improve the stability of catalyst nanoparticles.^{1,2} The interplay between nitrogen concentration, graphiticity, and specific nitrogen functionalities and their effect on catalyst-support interactions is still not well understood. Such investigations require the use of model high-surface area materials and multi-technique characterization approach.

In this work, a series of nitrogen-doped carbons was created to serve as model high-surface area substrates with the goal to: investigate in more detail the effect of nitrogen and specific nitrogen functionalities on the stability of metal nanoparticles; enable in situ microscopy analysis of catalyst-support interactions; and serve as a platform for atomistic analysis of dopants in high-surface area carbon materials. N-doped carbon nanospheres were synthesized using a previously published sol-gel method,³ varying both the amount of nitrogen precursor and pyrolysis temperature in order to vary nitrogen concentration and speciation. Samples were first characterized by scanning electron microscopy (SEM) and transmission electron microscopy (TEM) to determine nanosphere sizes, then by nitrogen physisorption for surface area and porosity analysis. Detailed analysis with Raman and X-ray photoelectron spectroscopies was completed to correlate changes to the parameter space of the synthesis with ratio of amorphous to graphitic carbon, relative concentrations of nitrogen, and different nitrogen functionalities.

¹ K. N. Wood, R. O'Hayre, S. Pylypenko. *Energy Environ. Sci.* **2014**, 7, 1212-1249.

² S. Pylypenko, A. Queen, T. S. Olson, A. Dameron, K. O'Neill, K. C. Neyerlin, B. Pivovar, H. N. Dinh, D. S. Ginley, T. Gennett, R. O'Hayre. *J. Phys. Chem. C* **2011**, 115, 13667-13675.

³ N. P. Wickramaratne, J. Xu, M. Wang, L. Zhu, L. Dai, M. Jaroniec. *Chem. Mater.* **2014**, 26, 2820-2828.

AS-TuP24 Electron Microscopy Study of Fission Product Migration in Irradiated TRISO Nuclear Fuel, Rachel Seibert, Illinois Institute of Technology; **C. Parish, P. Edmondson, K. Terrani,** Oak Ridge National Laboratory; **J. Terry,** Illinois Institute of Technology

High temperature gas cooled reactors (HTGRs) may use tristructural-isotropic (TRISO) coated nuclear fuel particles. Fuel performance is limited by the interaction of fission products with the barrier SiC layer. In particular, Ag is released from intact TRISO fuel, and Pd may locally corrode the SiC. Additionally, uranium and plutonium migration are of interest. An understanding of the reaction mechanisms and kinetics of these interactions under normal operation as well as accident conditions is critical for the development of advanced nuclear reactors. We have studied TRISO particles produced at ORNL under the Advanced Gas Reactor fuel program. The fuel was irradiated at the Advanced Test Reactor at Idaho National Laboratory. The local chemical structure of three TRISO SiC shells was examined through X-ray absorption fine structure spectroscopy (XAFS) at the Materials Research Collaborative Access beamline at the Advanced Photon Source. To complement these results, electron microscopy studies have been conducted on various samples prepared from these SiC fragments at the Low Activation Materials Development and Analysis (LAMDA) facility at ORNL. Specifically, samples were prepared from the inner, outer, and middle interfaces of the SiC fragment to obtain a full cross-sectional image of the fission product migration. These results have provided key information on the fission product transport behavior through irradiated SiC at varying temperatures. Knowledge of these reaction pathways will allow for better simulation of the long-term behavior of TRISO fuels. They may also suggest ways to modify the SiC layer to improve fuel performance and mitigate fission product release, which is critical for safety strategies required to commercialize HTGRs.

Tuesday Evening Poster Sessions, November 8, 2016

AS-TuP26 X-ray Photoelectron Spectroscopy Analysis of Titanium Nitride-Nickel Nanocomposite Catalyst, Samuel Gage, Colorado School of Mines; V. Molinari, D. Esposito, Max Planck Institute of Colloids and Interfaces, Germany; S. Pylypenko, Colorado School of Mines

Titanium nitride-nickel (TiN-Ni) nanocomposites have been recently found to be an efficient catalyst for the hydrogenolysis of aryl ethers as models for lignin biomass refining. As compared to Ni catalysts supported on carbon, TiN-Ni nanocomposites showed superior catalytic activity. One possible explanation for the improved performance is a change in the electronic structure of nickel due to the TiN support. In order to test this hypothesis, a series of TiN-Ni nanocomposites with varying amounts of Ni loadings (1, 10, 20 and 50 wt.%) were synthesized and investigated using X-ray Photoelectron spectroscopy (XPS) and microscopy techniques. A series of TiO₂-Ni reference materials with identical Ni loadings served as a reference.

The binding energy of Ni in the TiN-Ni samples is higher than those measured for Ni supported on TiO₂, indicating that Ni in TiN-Ni nanocomposites is more electron poor. At Ni loadings greater than 1 wt.%, higher concentrations of Ni were measured on the surface of the TiN support as compared to the TiO₂ support. The increase in the Ni loading appears to preferentially block TiN surface sites. In contrast at 1 wt.% loadings, the amount of Ni detected on the surface of TiN support is lower than that observed on the surface of TiO₂ support, suggesting incorporation of Ni into the TiN structure.

AS-TuP27 Redox Active Cerium Oxide Immobilized on Highly Ordered Polymer Nanopillars as Dopamine Sensor, Swetha Barkam, M. Peppler, S. Das, S. Saraf, C. Li, J. Thomas, S. Seal, University of Central Florida

Dopamine, is one of the main neurotransmitters which plays a significant role in the function of human metabolism, hormonal, cardiovascular and central nervous systems. Several diseases and neurological disorders such as Parkinson's disease, schizophrenia and Huntington's disease can be caused due to deficiency of dopamine. Therefore lower concentration detection of dopamine in biological samples such as sweat and/or urine containing dopamine metabolites is very crucial. In this study, we propose cerium oxide coated polymer nanopillars based sensor to achieve lower limit detection of dopamine with high sensitivity and selectivity for diagnostic applications. Cerium oxide nanoconstructs (nanoceria) that have the potential to act as antioxidant attributed to its switching of oxidation state from +3 to +4 mediated at the oxygen vacancies. The unique inter action between dopamine and the redox active nanoceria is studied using *in-situ* UV-visible spectro-electrochemistry and surface characterization methods. It has been previously observed that there is a strong attachment of dopamine to nanoceria surface through oxidation followed by formation of a charge transfer complex, there by motivating to develop a sensor to detect dopamine. In this study, cerium oxide is immobilized on high aspect ratio nano-pillars made of polyacrylonitrile polymer. The nanopillars fabricated using soft lithography increased the surface area of exposed cerium oxide, thereby increasing the interaction of the nanoparticles with dopamine. The changes in the redox potential and surface chemistry of cerium oxide coating upon reaction with dopamine were recorded using electrochemical and optical techniques. Cerium oxide coatings were obtained using different techniques such as sputter coating, atomic layer deposition, electrodeposition and spin coating to obtain different surface chemistry (ratio of Ce³⁺:Ce⁴⁺ on the surface) to improve the detection limit of the dopamine.

AS-TuP28 X-ray Photoelectron Spectroscopy of Raw Material for Metal Additive Manufacturing, David Wieliczka, A.S. Choi, J.A. Crow, C.J. Cook, L.F. Elder, R.D. Koch, T.A. Pond, B.C. Sartin, D.R. Shinault, S.E. Van Slyke, Honeywell Federal Manufacturing and Technology

Understanding the effects of powder reuse on metallurgical properties of components fabricated via laser powder bed fusion is critical to ensure the production of functional components. The inability to reuse metal AM powder will have a significant negative economic impact on this manufacturing method. In mid-2015, the KC NSC initiated a 316L powder study on a consistent run of components. This paper will present surface analysis results from both virgin metal powder and powder sampled from the overflow bin after a build. In addition to XPS, the powders have been examined with SEM/EDS to provide morphology and composition, direct probe mass spectroscopy to examine the outgassing of the material, and ICP-MS to examine the impurities at ppm levels. The XPS data was obtained from the surface of the powder as well as a function of depth utilizing

argon ion sputtering and provides unique information on the elemental composition of the surface. Specifically, we were tracking the elemental surface enrichment due to vapor created during the build process. We are also examining the oxide chemistry of both the surface and near surface region.

AS-TuP29 Characterization of Bonding between Super-hard Ceramics and Polymer Substrate, Ranganathan Parthasarathy, Tennessee State University; J.B. Beam, Vanderbilt University; F.E.H. Hoff, Tennessee State University; A. Misra, University of Kansas; L.Z. Ouyang, Tennessee State University; C.M.L. Lukehart, Vanderbilt University

Superhard coatings improve the durability of biomedical polymer implants due to their excellent wear resistance. We study the bond strength between Rhenium Diboride (ReB₂), a superhard ceramic, and Teflon, which is widely used as an implant material in load-bearing biomedical applications. As part of a proof-of-concept study, ReB₂ is coated onto Teflon using confined-plume chemical deposition at room temperature and pressure. For the coating to function effectively in load-bearing conditions, the bond strength between the polymer and the coating must well exceed in-situ stresses. Accurate local measurement of bond strength using nano-indentation is difficult owing to platelet microstructure of the ReB₂; hence an experimental workflow was designed to determine the average macro-scale bond strength between Teflon substrate and ReB₂ coating. The inert nature of Teflon makes conventional pull-out challenging. Therefore, we performed a) Tensile pull-out of the deposited ceramic coating based on a modified version of ASTM D4541, b) Imaging of failure surfaces using light microscopy and Scanning Electron Microscopy (SEM) c) Image segmentation to determine area of failure, and d) Calculation of average stress at pull-out. The tests reveal average bond strength of 2.5 MPa between Teflon and ReB₂ for coatings deposited on an untreated Teflon surface and 4.5 MPa for those on a sanded and etched Teflon surface. The pull-out occurs in a brittle manner, with no observable yield or plastic flow. The SEM images reveal strands of Teflon on the pull-out side, indicating that the true bond strength is likely higher than the measured average. Imaging of the Teflon surface under the coating reveals that the confined-plume chemical deposition creates a laminate surface of ReB₂ on the substrate, as opposed to anchored platelets. The results confirm the development of a robust and repeatable workflow for the measurement of average bond strengths of super-hard ceramic coatings on comparatively soft polymer substrates.

Biomaterial Interfaces

Room Hall D - Session BI+PB-TuP

Biomaterial Interfaces Poster Session (preceded by Oral Flash Presentations)

BI+PB-TuP2 Quantitative Sensing of Pancreatic Enzymes using Gelatin, George Banis, University of Maryland, College Park; L. Beardslee, Walter Reed National Military Medical Center; R. Ghodssi, University of Maryland, College Park

We present an investigation of gelatin film response to an array of pancreas-specific enzymes using a Quartz Crystal Microbalance (QCM) system. In fluids secreted from the pancreas into the upper small intestine, highly concentrated enzymes (α -amylase, trypsin, and lipase) are mixed to complete digestion of partially broken-down materials entering from the stomach. Sensors, such as that illustrated in Fig 1, are utilizing biomaterials such as gelatin, as it can be used to enter the body due to its biocompatibility and tailorability both chemically and structurally. Gelatin is known to be highly sensitive to degradation by trypsin, one of the aforementioned enzymatic pancreas biomarkers, thereby offering potential to indirectly monitor trypsin levels [1]. The composition of pancreatic fluid is a biomarker in testing exocrine function of the pancreas, a process often involving invasive procedures toward quantifying losses in enzyme levels [2]. However, its interactions with other interfering enzymes such as lipase or α -amylase have not been studied. While these enzymes are believed to cleave specific to bonds not found in gelatin, it is critical to be able to determine how these non-specific enzymes impact the signals produced when gelatin interacts with specific enzymes, i.e. trypsin, when they are each in the media.

In this work, we utilize a QCM system in sensing the mass change of gelatin films deposited onto standard crystals with gold electrodes. Films are subjected to a constant flow rate of buffer before introducing pancreatic enzymes in the setup illustrated in Fig 2. After system stabilization under

Tuesday Evening Poster Sessions, November 8, 2016

buffer flow, material loss is quantified from the surface of the crystal. For trypsin, as expected, we observe degradation in a concentration-dependent manner, shown in Fig. 3. With either lipase or α -amylase, however, we observe no change, as illustrated in the top of Fig 4. After rinsing with buffer, we reintroduce trypsin in combination with each enzyme to determine if the presence of nonspecific enzymes affected the sensitivity of the gelatin to proteolytic activity, shown in the bottom of Fig 4. Digestion rates are found to decrease by -----83% and 77% with exposure to lipase or α -amylase, respectively, indicating a decrease in gelatin sensitivity to trypsin in the presence of these enzymes. The next phase in this work will be to combine all three enzymes to further model pancreatic juices. This work emphasizes the necessity in characterizing gelatin's response to other enzymes in understanding its sensitivity and specificity in the digestive environment, leading the avenue for devices designed to monitor gastrointestinal health.

BI+PB-TuP3 Evaluation of Printed Cell Viability, Proliferation, and Insulin Production on Various Alginate-Gelatin Hydrogels, Luis Solis, J. Rincon, A. Varela-Ramirez, R. Aguilera, T. Boland, University of Texas at El Paso

Over the past couple of decades, encapsulation of islets or beta cells has emerged as the new modality for the treatment of Type 1 Diabetes Mellitus (T1DM). A major setback in bioengineering encapsulated cells however, is the formation of fibrosis from immunologic defenses rendering the cells ineffective. This study proposes the use of an inkjet bioprinter to allow arrangement of β TC-6 mouse pancreatic beta cells and improve vascular ingrowth among alginate hydrogels. In addition, different concentrations of gelatin were tested in order to determine printable alginate-gelatin ratios for optimal vascular ingrowth, proliferation, viability, and insulin production of cells. Cell proliferation cultures were monitored daily for a total duration of 14 days. Cell viability and glucose stimulated insulin production were assessed at day 14. In-vitro alginate-gelatin hydrogels promoted proliferation of spherical insulinoma clusters and increased insulin secretion as compared to the monolayer of cells without hydrogels. These findings demonstrate that the alginate-gelatin hydrogels support the proliferation, viability, and insulin production of β TC-6 cells. These results will also allow to formulate improved bioinks for automated cell encapsulation applications.

BI+PB-TuP4 Synchrotron Radiation Studies of the Bonding and X-Ray Induced Reactions of Bacteriorhodopsin Adsorbed on Gold, Richard Rosenberg, Argonne National Laboratory; D. Mishra, R. Naaman, Weizmann Institute of Science, Israel

Bacteriorhodopsin (bR) is the integral protein of the purple membrane of *Halobacterium salinarum* and is the most studied proton pump. It is a chiral system composed of seven parallel, upright-oriented α -helices. Recent photoemission and electrochemical studies have shown that it can act as a natural electron spin filter as a result of the chiral-induced spin selectivity effect.[1] Previous structural studies using hard x-ray synchrotron radiation (SR) have shown that such radiation can significantly impact the structural integrity of bR,[2] while earlier work has demonstrated that X-ray-induced, low energy secondary electrons can play a major role in surface chemical reactions of adsorbed biological molecules.[3] In the present study we use SR x-ray absorption and photoelectron spectroscopy (XPS) to characterize the initial state of the adsorbed bR. Time-dependent changes in the core-level XPS spectra are utilized to follow the dynamics of the X-ray/secondary electron induced reaction. The results will be discussed in terms of previous studies of x-ray induced reactions in bR and other biological molecules.

The work performed at the Advanced Photon Source was supported by the U.S. Department of Energy, Office of Science, Office of Basic Energy Sciences under Contract No. DE-AC02-06CH11357.

REFERENCES

- 1 D. Mishra, T. Z. Markus, R. Naaman et al., Proc. Nat. Acad. Sci. **110**, 14872 (2013).
- 2 V. I. Borshchevskiy, E. S. Round, A. N. Popov et al., J. Mol. Biol. **409**, 813 (2011).
- 3 B. Boudaiffa, P. Cloutier, D. Hunting et al., Science **287**, 1658 (2000); R. A. Rosenberg, D. Mishra, and R. Naaman, Angew. Chem. Int. Ed. **54**, 7295 (2015); R. A. Rosenberg, J. M. Symonds, K. Vijayalakshmi et al., Phys. Chem. Chem. Phys. **16**, 15319 (2014).

BI+PB-TuP5 Investigations on Peptide Incorporation and Peptide Yields in ME-SIMS, Martin Körsen, A. Pelster, M. Heeger, B.J. Tyler, K. Dreisewerd, H.F. Arlinghaus, Universität Münster, Germany

Time-of-flight secondary ion mass spectrometry (ToF-SIMS) is a powerful technique for the nanoanalysis of biological samples, but improvements in Tuesday Evening Poster Sessions, November 8, 2016

sensitivity are needed in order to detect large biomolecules, such as peptides, on the individual cell level at physiological concentrations. An increase in the detection efficiency for larger molecules and reduced fragmentation rates could be obtained by a) the use of cluster ion beams such as Au_n^+ , Bi_n^+ , C_{60}^+ , or even large Ar_n^+ clusters in order to maximize the energy deposited close to the surface or b) by modifying the surface by organic matrices in the so-called matrix-enhanced SIMS (ME-SIMS). This approach is based on embedding analyte molecules in low weight organic matrices, like common MALDI matrices, prior to ion bombardment

We used dual beam ToF-SIMS to image the incorporation of three peptides with different hydrophobicities, bradykinin, substance P, and vasopressin, into two classical MALDI matrices, 2,5-dihydroxybenzoic acid (DHB) and α -cyano-4-hydroxycinnamic acid (HCCA) prepared with dried droplet sample preparation method. For depth profiling, an Ar cluster ion beam was used to gradually sputter through the matrix crystals without causing significant degradation of matrix or biomolecules. A pulsed Bi_3^+ ion cluster beam was used to image the lateral analyte distribution in the center of the sputter crater. Using this dual beam technique, the 3D distribution of the analytes and spatial segregation effects within the matrix crystals were imaged with sub- μm resolution.

Combining cluster ion beams and ME-SIMS we were able to investigate the molecular yield of two peptides (bradykinin and melittin) under various primary ions and preparation methods. Large argon clusters in the mass range between 1000 and 2500 atoms per cluster and several bismuth primary ions were used to determine molecular yields. Preparation utilized spin coating of pure peptide solutions and spray coating of matrix-peptide mixtures on silicon wafers. With the data obtained we were able to describe the molecular yield of the analyzed peptides. For bismuth primary ions the yield obtained by the use of cluster primary ions is nearly constant in the case of ME-SIMS, whereas for the neat sample an increase of the molecular yield is observable. In contrast to the molecular yield decrease with larger argon clusters for neat samples, an increase of the molecular yield is observable for larger argon clusters in the case of ME-SIMS.

BI+PB-TuP6 Developments of Non-Stick Surfaces for Medical Devices: Beneficial Effects of Thin Film Metallic Glass Coating, G.H. Jiang, C.C. Yu, C.L. Li, Y. Tanatsugu, Jinn P. Chu, National Taiwan University of Science and Technology, Taiwan, Republic of China; M.J. Chen, S.H. Chang, Mackay Memorial Hospital Tamsui Campus, Taiwan, Republic of China

This presentation reports on the use of Zr-based ($\text{Zr}_{53}\text{Cu}_{33}\text{Al}_9\text{Ta}_5$) thin film metallic glass (TFMG) for the coating of various medical devices and compares the results with those obtained using conventional titanium nitride and pure titanium coatings. TFMG was selected as the coating material for its unique properties such as good biocompatibility and antibacterial property due to its amorphous atomic structure, revealing a great potential for biomedical applications. The TFMG coating was shown to reduce insertion forces and retraction forces by up to over seventy percent when tested using polyurethane rubber block. The benefits of TFMG-coated needles were also seen when tested using pig muscle tissues. Based on the nano-scratch test, the TFMG coatings achieved a low coefficient of friction (COF), about one order of magnitude lower than those of bare surface and other coatings. Furthermore, the adhesions of cancer cells and platelets to coatings are also examined. TFMG coating is shown to appreciably minimize the attachment of cancer cells and platelets by more than eighty percent in relative to those of Ti coating and bare surface. The low COF and non-stick coated surfaces by TFMG can be attributed to the absence of grain boundaries in the TFMG coating, smooth surface and low surface free energy.

BI+PB-TuP7 Polyurethane Degradation by Wild Type and Hydrolase Deficient *Pseudomonas protegens* Pf-5 Unsaturated Biofilms, Daniel Barlow, US Naval Research Laboratory; L.I. Nadeau, C.S. Hung, Air Force Research Laboratory; J.C. Biffinger, US Naval Research Laboratory; A.L. Crouch, Air Force Research Laboratory; J.N. Russell, US Naval Research Laboratory; W.J. Crookes-Goodson, Air Force Research Laboratory

Two hydrolases secreted by *Pseudomonas protegens* Pf-5 bacteria, PueA and PueB, have been demonstrated to be active towards polyester - polyurethane (PU) hydrolysis. In this work, the impact of these enzymes towards PU degradation was directly compared at biofilm / PU interfaces through deletion of PueA and PueB genes. Unsaturated biofilm assays were used where biofilm growth took place on solid, hydrated PU discs in air. PU degradation was analyzed using confocal Raman microscopy of intact samples. Additionally, cross-sectional analysis of microtomed sections was done using FTIR microscopy and combined atomic force microscopy - infrared spectroscopy (AFM-IR). Results showed varying degrees of biofilm

Tuesday Evening Poster Sessions, November 8, 2016

related permeation and polymer degradation within the ~300 um thick discs. Degradation took place through a pitting process involving preferential loss of the ester component. Wild type and PueB knockout mutants showed the highest levels of hydrolysis, measured by loss of carbonyl intensity in vibrational spectra, while the PueA and double knockout mutants showed lower hydrolysis levels. The apparent higher level of PueA activity is consistent with higher enzymatic activity for the hydrophobic lipase substrate, p-nitrophenyl palmitate. Relationships between biofilm morphology and PU degradation were also observed for the wild type and mutant biofilms.

BI+PB-TuP8 Laser Irradiation of Mg Alloys: Reduced Kinetics and Enhanced Biocompatibility, M.A. Melia, David Florian, W. Steuer, J.R. Scully, J.M. Fitz-Gerald, University of Virginia

Until recently, biodegradable implants have exclusively been used in non-load bearing applications such as stents and sutures. Mg-Al-Zn alloys like AZ31B are currently being considered as biodegradable materials because of their similar mechanical properties to that of bone. In addition, the corrosion product resulting from Mg alloys in body fluid contains Mg and Ca-phosphates (hydroxyapatite) and has been shown to stimulate bone regeneration. The degradation of Mg alloys is also considered non-toxic when corroding in the human body. However, the structural integrity is poor due to rapid corrosion caused by microstructural heterogeneities in the form of electrochemically noble secondary phases leading to micro-galvanic couples and preferential dissolution of the α -Mg matrix in physiological media. Laser surface processing of the Mg-Al-Zn alloy, AZ31B, reduced the corrosion rate in simulated body fluid (SBF) experiments by minimizing the impact of secondary phases.

Experiments utilized a pulsed excimer laser ($\lambda = 248$ nm and FWHM = 25 ns) in combination with a novel surface modification chamber. Samples of AZ31B in the as-received and laser processed condition were submerged in a 27 mM HCO_3^- Tris ($(\text{HOCH}_2)_3\text{CNH}_2$) variant of SBF. The corrosion resistance was investigated through optical microscopy, scanning electron microscopy (SEM), energy dispersive spectroscopy (EDS), gravimetric mass loss, and polarization measurements.

No major corrosion product variations were observed for the as-received / laser processed specimens by SEM and EDS, both showing a similar amount of Ca and P. The laser processed alloy exhibited a reduction in anodic kinetics compared to the as-received material, suggesting the corrosion product is more compact and passivating. Furthermore, the laser processed surface exhibited a 50% reduction in mass loss after 24 hours immersion in SBF in comparison to the as-received samples. Optical micrographs of samples immersed in SBF reveal a reduction in the H_2 evolution rate of the laser processed versus as-received material. In addition, the laser treated specimens exhibited a significant increase in wettability with a 10° contact angle compared to the 45° angle of the as-received materials. The increased wettability of the laser processed samples may decrease the time required for osseointegration through allowing cells to more readily bind to the surface of an implant.

BI+PB-TuP9 Plasma-assisted Fabrication of Silver/Bacterial Cellulose/Chitosan Functional Nano-composites and Their Properties, Shuquan Chang, A.R. Shetty, S.L. Arias Suarez, J.P. Allain, University of Illinois at Urbana-Champaign

Bacterial cellulose and chitosan are renewable natural polymers and have many favorable properties such as biocompatibility, biodegradability and low toxicity. So, they have been extensively used in drug delivery systems, gene therapy, tissue engineering, and biosensor applications. Silver nanoparticles have attracted much attention for their unusual chemical and physical properties and have been widely applied in sensors, antibacterial and photocatalytic areas. The synthesis of nanomaterials with different chemical composition, size distribution, and controlled monodispersity has become an important research area in nanotechnology. Many kinds of methods such as vapor deposition, solvent-thermal, sol-gel, electrochemistry and microwave have been developed to fabricate nanomaterials. So far, plasma technology has become an important approach to prepare and reinforce materials and surfaces. This work seeks to fabricate nanoparticles/natural polymer functional composites via an atmospheric pressure plasma method. Comparing many traditional methods, atmospheric pressure plasma jet can induce chemical reactions in mild conditions, which can guarantee the purity of system and will not destroy the structure of natural polymers.

In this work, silver/bacterial cellulose/chitosan functional composites are fabricated via an atmospheric pressure plasma method. Plasma can produce many active radicals including reduction species and oxygen

species, which can trigger chemical reaction. Ag^+ in the reaction system can attach to the surface of bacterial cellulose and chitosan via bonding. By controlling the reaction condition, Ag^+ can be reduced to $\text{Ag}(0)$ and form Ag nanoparticles under plasma treatment. The existence of bacterial cellulose and chitosan can limit the growth and prevent the aggregation of particles, which is very critical to form nanostructure. SEM, XRD, XPS, FT-IR are employed to examine the morphology and structures of as prepared nano-composites. The biocompatibility and antibacterial properties are also studied. All results reveal that Ag nanoparticles are successfully formed and well dispersed in bacterial cellulose/chitosan. The as prepared silver/bacterial cellulose/chitosan nano-composites have excellent biocompatibility and antibacterial abilities, which can be used in biomedical areas. This convenient synthesis strategy based on atmospheric pressure plasma could be extended to fabricate other nanoparticles/bacterial cellulose/chitosan composites.

BI+PB-TuP11 A Non-toxic, Super-Hydrophilic Anti-Fog Coating for Lenses used in Closed Body Cavity Surgery: VitreOx™– In Vivo Animal Clinical Trials, Nicole Herbots, SiO2 NanoTech LLC; C.F. Watson, SiO2 NanoTech LLC/Arizona State University Physics Dept; E.J. Culbertson, University of California at Los Angeles; P.R. Thilmany, IPO. Martins, SiO2 NanoTech LLC

Laparoscopes, arthroscopes, and laryngoscopes lenses are hydrophobic and fog during closed body surgery, due to bodily fluids and differences between body and operating room temperatures [1,2]. Surgeons must repeatedly remove, clean, and reinsert scopes obscured by fog. Hencesurgery duration, infection risks, and scarring from air exposure increase. Methods to address fogging introduce other complications [3]. Alcohol-based coatings scar tissue and quickly evaporate, heated lenses require reheating every 5 to 20 minutes. A non-toxic, super-hydrophilic, anti-fog coating that is pH neutral (7.2-7.4), long-lasting has been developed VitreOx™. [4] VitreOx™ can be used wet or dry, without alcohol, heat, or fluid evacuation. When applied in liquid form, it easily espouses a lens's surface and edges, and dries within seconds to form a permanently super-hydrophilic surface on silica and most polymer surfaces. VitreOx™ avoids current shortfalls by foregoing frequent reapplications.

VitreOx™'s anti-fog properties can be explained by nucleation and growth theory, and the three mechanisms for condensation: 1) 3-D droplets, resulting in fogging; 2) 2-D sheets resulting in a flat transparent film; or 3) mixed, resulting in optical distortion. On hydrophobic surfaces (e.g. optical lenses), condensation occurs with fogging via spherical 3-D droplets (Volmer-Weber model). 3-D droplets scatter light in all directions through refraction yielding opaque or translucent films, or fog. VitreOx™ applied to hydrophobic lenses renders them super-hydrophilic. Similar to the 2-D Frank Van-der-Merwe growth mode, **condensation with uniform wetting** yields transparent 2-D films that don't distort light.

In-vitro and *in-vivo* animal studies of VitreOx™ were conducted to measure performance and duration of anti-fog effectiveness and bio-compatibility. *In-vitro* testing spanned from 3 to 72 hours over a 3-year range. Side-by-side *in-vivo* gastro-endoscopies were conducted using a lens coated with VitreOx™ and a Covidien Clearify™ warmer with anti-fog, on Yucatan™ swine for 90 minutes. The VitreOx™ coating lasted without fogging nor reapplication, while Covidien Clearify™ only lasted for 38 minutes without fogging, and required retreatment and reapplication. No adverse reaction was observed on swine in surgery, and in the 18 months that follows.

[1] Knuth A et al "Anaesthesist. 2012 Dec;61(12):1036-44.

[2] Lawrentschuk N, et al "Laparoscopic Lens Fogging" (2010). *Journal of Endourology*. 24(6):905-913

[3] US Pat. 5,518,502 (1994) and its 129 cites.

[4] Herbots N, Watson CF, patents pending

Magnetic Interfaces and Nanostructures Room Hall D - Session MI-TuP

MIND Poster Session

MI-TuP1 Static and Dynamic Magnetic Properties of FeGa/NiFe Multilayer Heterostructures for Multiferroic Applications, C.R. Rementer, Q. Xu, P. Nordeen, G.P. Carman, Y. Wang, Jane P. Chang, University of California Los Angeles

Iron-gallium (FeGa) is one of the most promising magnetic materials for use in composite multiferroics due to its high piezomagnetic coefficient (3 ppm/Oe) and high stiffness (70 GPa). It has been integrated into several

Tuesday Evening Poster Sessions, November 8, 2016

multiferroic systems, but generally in MHz range or below.¹ In order to make it suitable for high frequency (GHz) applications, metalloid dopants have been used to soften magnetic materials and enhance their frequency dependent properties, but at the cost of the saturation magnetization as well as magnetoelastic properties.² A viable approach to circumvent this trade-off problem is to integrate a magnetic material with complementary properties into magnetic heterostructures. In this work, multilayer laminates were fabricated with FeGa and NiFe, a material with excellent properties in high frequency regimes.

FeGa (hard) and NiFe (soft) were sputtered via alloy targets with compositions Fe₈₅Ga₁₅ and Ni₈₁Fe₁₉ (at%) into multilayers with layer thicknesses ranging from 3-50 nm, with FeGa being used as the first and last layer in the stack. XPS confirmed the composition and showed there was no intermixing of the layers. Static magnetic properties were evaluated via SQUID magnetometry, and it was found that the incorporation of NiFe layers reduced the coercivity by up to 85%, from 30 Oe to 4 Oe. FMR studies showed a reduction of the linewidth of up to 50%, from 70 Oe to 38 Oe. It is believed that this effect is largely due to the decrease of magnetic anisotropy dispersion in the multilayers.³ The multilayer films maintained a high magnetostriction of up to 190 ppm, on the same order of magnitude as giant magnetostrictive materials such as thin film Terfenol-D.⁴ FeGa/NiFe heterostructures have been shown to be an excellent candidate for strain-coupled microwave multiferroics.

References:

1. M Hamashima, C Saito, M Nakamura and H Muro, ECJ (5), 1-7 (2012).
2. J Lou, RE Insignares, Z Cai, KS Ziemer, M Liu and NX Sun, APL (18) (2007).
3. R. Nakatani, T Kobayashi, S Ootomo and N Kumasaka, JJAP **27** (6) (1988).
4. KP Mohanchandra, SV Prihodko, KP Wetzlar, WY Sun, P Nordeen and G. P. Carman. AIP Advances **5** 097119 (2015).

MI-TuP2 The Microstructure and Isotope Effects on Spin Response in Organic Spintronic Devices, Nuradhika Herath, J. Keum, H. Zhang, K. Hong, J. Jakowski, J. Huang, J. Browning, S. Bennett, C. Rouleau, I. Ivanov, V. Lauter, Oak Ridge National Laboratory

There is currently a strong drive to realize magnetoelectronic heterostructures with controls of magnetic ordering and electron-spin transport for use in the next generation spintronic devices. One proposed method to gain such controls is the use organic spintronics (OS). The general configuration of OS device consists of two ferromagnetic (FM) electrodes separated by an organic layer to form a sandwich structure. While basic concepts of OS device have been demonstrated, there is very little understanding about the detailed effects of the organic layer and the interface interactions within the multilayers on the physical properties of the system. Amongst the difficulties limiting high performances OS are the subtle structural variations, including i.e., interdiffusion of FM electrode into the soft organic layer during the fabrication. Using the depth sensitive method of polarized neutron reflectometry we have been able to probe the fine details of the structural and magnetic properties of prototype spintronic devices (STO\LSMO\polymer\Co\Ag). We fabricated heterostructures using two electron conducting polymers (P3HT and PFO) and their deuterated substitutions to study the isotope effect of polymer layer in the spintronic devices. While our main goal is on understanding the effect of deuterium substitution on the spin-dependent electron transport, in this presentation, we will focus the details of the structural and magnetization profiles on both LSMO\Polymer and polymer\Co interfaces and their impact on the coupling between magnetic layers.

Acknowledgements: This work was sponsored by Oak Ridge National Laboratory Directed Research and Development (LDRD 7938) and conducted at the Center for Nanophase Materials Sciences (CNMS) and Spallation Neutron Source (SNS), which are sponsored at Oak Ridge National Laboratory by the Scientific User Facilities Division, Office of Basic Energy Sciences, U.S. Department of Energy.

Manufacturing Science and Technology

Room Hall D - Session MS-TuP

Aspects of Manufacturing Science and Technology Poster Session

MS-TuP2 Study of Mechanical Properties of Nanographene/Al Composite Materials for Purpose of Industrial Applications, Yusuke Oguro, A. Matsumuro, Aichi Institute of Technology, Japan

Basic science of graphene with various superior characteristics has been made clear rapidly on the frontier technology. Especially, development of superior nano-scale electronic devices and bio systems has been studied energetically. Nevertheless, various surprising mechanical properties of graphene have been not attracted great attention, such as extreme low density, tensile strength with 100 times stronger than steel by weight, Young's modulus with 1 TPa and more flexible than rubber. Since our original successful isolation techniques of creating single layer nanographene sheets from nanographene with a several sheet and uniforming dispersion of nanographene within based materials, we have been challenging in fabrication innovative nanographene reinforced Al composite sintered materials and established the fabrication method. It has already been demonstrated that Vickers hardness of nanographene/Al composite pellet-formed sintered materials showed the maximum value of 323 Hv, which means about 5 times up in comparison with that of Al bulk material, and the density decreased down to 2.45 g/cm³. So, the specific strength increased up to 414 kN·m/kg. The value increased up to 1.4 times for sintered Al material, and the value surprisingly exceeded that of commercial used magnesium alloys. These results would suggest bringing a change in the concept of industrial use materials.

In this study, we investigated possibility that industrial applications of our nanographene /Al composite materials would take advantage of their bulk properties. Standard flat-plate type specimens consisted of our nanographene/Al composite materials were fabricated under the same sintered condition in order to compare various mechanical properties of the standard data. Bending, tensile and fatigue mode tests were performed in precisely. Elastic and fracture properties were analyzed using four-point bending test apparatus without few artificial errors. The results revealed that Young's modulus increased from 40 GPa of sintered Al up to 45 GPa of nanographene/Al composite materials. Fracture characteristics showed that the breaking stress of the composite material showed drastic improvement up to 75 %, and the breaking strain of the composite material also increased up to 70 %. These great improvements of mechanical properties can be attributed to reinforcement effect of nanographene. Other mechanical properties tests should show the same tendency. Therefore, nanographene/Al composite materials give us excellent possibility of the innovative industrial use materials with a promising future.

MS-TuP3 Development of High-Strength Resin Composite Materials Reinforced with Nanocarbon for 3D Printing Manufacturing, Hiroaki Sakaguchi, A. Matsumuro, Aichi Institute of Technology, Japan

Now technologies related to 3D printing are strongly leading the industrial revolution in all fields. However, unavoidable basic technical problems of 3D printing have prevented from an ideal technology of manufacturing products with conventional characteristics. This serious problem must be caused by the layer structure of products used by additive process, and the insufficient mechanical strength of the molding materials specific to each type of 3D printer.

In this study, we strongly focused on develop innovative high strength resin-based composite materials reinforced with nanocarbon, i.e. C₆₀, CNT and graphene. These nanocarbon show extraordinary mechanical, physical and chemical properties with each superior characteristics. It is worth noticing that the mechanical properties, such as a strength, elastic modulus, hardness and so on, can be investigated incommensurably high values compared with those of commercial materials. Furthermore, these kinds of nanocarbon have superior geometric and nanometer-scale dimension characteristics as reinforcement materials considering various 3D printing processes. We researched the possibility of the application of nanocarbon composite materials with ABS base resin used widely in industry for the purpose of innovative strength increment of 3D printed products. To clarify each characteristic of C₆₀, CNT and graphene to ABS resin composites, these three-type nanocarbon composite specimens were fabricated. The fabrication method with a uniform composite material reinforced with distributed each nanocarbon have established on our own.

Tuesday Evening Poster Sessions, November 8, 2016

The uniform and dispersion of nanocarbon around ABS base powder particles should be the key point for fabrication of specimen by melt and solidification method. We applied our original technique using ultrasonic vibration with isopropyl alcohol as a solvent for 4 hours. And we investigated the optimal composition rates of each composite material. Each pellet-type solidified specimens was prepared at about 500 K for 30 minutes by atmospheric furnace cooling.

As the result of one of representative mechanical property, Vickers hardness for each specimen excellently increased up to about 10 % for 7.0 wt.% C₆₀ and 7 % for 1.0 wt.% graphene in comparison with the value of pure ABS resin bulk sample. The evaluation of important other mechanical properties such as pulling strength, break strength, fatigue strength, elastic modulus and so on have been examined in detail. These results should give us great conclusive evidence for achievement of this study.

MS-TuP4 Development of Innovative 3D Printer with Superior Multifunctional Surface Modification, Kentaro Horiuchi, Y. Hasegawa, A. Matsumuro, Aichi Institute of Technology, Japan

Direct manufacturing process using 3D printing technologies is spreading rapidly in all fields. Many difficult problems should be overcome in order to establish 3D printing technologies as the general industrial products manufacture method. One of the representative problems is the durability or strength of the products. But now this problem is overcoming rapidly by passionate R&D for specific products, and the material steady studies with various characteristics to satisfy the requirement of each product have conducted wide fields. Furthermore, studies of 3D printing systems with superior functions of various post processes at molding simultaneously are indispensable. The particular expected functions are removal of support materials from printed products, full-color painting, and surface modification for improvement of the mechanical, electrical, chemical and biological properties. The development of removal of support materials and full-color molding have been already solved using automatic machine cutting machine and ink-jet-type paint system equivalent to the same mechanism of a printer used in the office as typical examples, respectively. On the other hand, the surface modification technologies have been applied in wide industrial field in order to control great various characteristics of hardness, wear resistance, electrical conductivity, thermal conductivity and so on at arbitrary places of metal products using vacuum apparatus. So the surface modification technologies should be necessary applied to 3D printing products using resin materials.

In this study, our unique 3D printing system with multifunctional surface modification has been developed using the conventional air brush painting technique for resin and metal products. The air brush apparatus consist of only three parts: paint flow nozzle, paint container and air compressor. So high extensibility of the function and the mechanism of the spray system, the synchronization with the printer and numerical flexibility of the air brush can be possible easily. For confirmation of our trial apparatus, the full-color painting on the surface of 3D printing products has been succeeded by mix-spraying from three air brushes with suitable spray ratio using paint of cyan, magenta and yellow. The commercial paints using a air brush or a spray gun are widely used due to improve many kinds of charming surface characteristic such as lubricity, electric property, glossiness, fireproof property, corrosion resistance, luminous color property, et cetera. Therefore we could find great attractive possibility of realization of development of the innovative 3D printer with multifunctional surface modification.

MS-TuP5 Controlling the Diameter, Uniformity, and Spatial Distribution of Electrospun PVDF Nanofibers through Experiment and Simulation, Omar Ali, T. Grier, A. Ueda, C. Marvinnay, S. Avanesyan, C.S. Carson, W.E. Collins, Fisk University; J. DeCoste, US Army Research, Development, and Engineering Command; R. Mu, Fisk University

Polyvinylidene fluoride (PVDF) is a polymer which has important applications in insulation, sensors, and battery production. The thermal, electrical, elastic, and morphological behaviors and properties of PVDF, on which the applications depend, are intimately related to the structure of the polymer on various physical length scales. Retained PVDF solid structures on different scales are also related. For example, stretching and poling a PVDF membrane causes the PVDF monomer chain to change phase from the non-polar alpha phase to the polar beta phase, which imparts significant piezoelectric and pyroelectric properties. Controlling the properties of PVDF by tuning the solid structures is, therefore, of key importance for various applications. Efforts have been made by our team into electrospinning technology, which is a relatively simple and scalable

method of nanofiber production, for energy storage and biomedical applications.

We have investigated the effect of varying the electrospinning conditions and polymer solution properties on the diameter size and uniformity, and the spatial distribution of the produced PVDF nanofibers. Experimentally, we varied both the concentration of PVDF in the initial solution, and the voltage applied during electrospinning. Using optical imaging and scanning electron microscopy (SEM), we obtained a set of images for several voltage-concentration parameter pairs. Based on the experimental data, we were able to examine the diameter and uniformity as functions of the concentration and applied voltage. Additionally, we simulated different electric field distributions in an effort to design a method for controlling fiber deposition area.

The results indicate that increased concentration can lead to a significant increase in average fiber diameter. Fibers produced at lower concentrations are not only thinner, but also had significantly less uniform diameters and a greater number of beads in the fibers. The effect of voltage on diameter size and uniformity was somewhat less clear. There does not appear to be any correlation between voltage and average diameter size. However, voltages around the middle of the range we studied seem to lead to slightly more uniform fibers. Further, COMSOL simulation has been conducted and showed that using conduction rings to manipulate the electric field lines can make the field diverge sufficiently at first to allow for the electrospinning process to take place and then converge to direct the fibers to a smaller area of the grounded substrate. Such control over where the fibers are distributed can be very useful when producing fibrous mats and other macro-structures from nanofibers.

Nanometer-scale Science and Technology Room Hall D - Session NS-TuP

Nanometer-scale Science & Technology Poster Session

NS-TuP1 tPA Loaded Fe₃O₄ Nanorods to Enhance and Target Stroke Treatment, Weijie Huang, University of Georgia; J.N. Hu, S.W. Huang, K.L. Jin, University of North Texas; Y.P. Zhao, University of Georgia

Stroke remains the 4th leading cause of death in United States and the No. 1 cause of adult disability among the world. Current stroke treatment with tissue plasminogen activator (tPA) therapy faces a lot of challenges due to its side effect. For example, the administration time window of tPA to lyse clots is within the first 3 hours after the initial onset of stroke since the risk of tPA-related hemorrhage is significantly increased after that. Besides this, the traditional tPA therapy also fails to lyse the clot and recanalize the middle cerebral artery in about half cases.

We propose an active drug loaded Fe₃O₄ nanorod strategy to improve the stroke treatment therapy. Fe₃O₄ nanorods were fabricated by oblique angle deposition technique and loaded with tPA using glutaraldehyde as the cross-linker. *In-vitro* study showed that the tPA loaded nanorods could achieve a mass loading ratio (drug mass over rod mass) of 6% and a release time of 30 min. Once the nanorods were immersed in liquid and stimulated by an external rotating magnetic field, about 11% of loaded tPA was released and the thrombolysis efficiency was increased by about 40%. Such an enhancement is due to the increased tPA local concentration and the enhanced mass transport in the fluid, which could help more tPA be delivered into the clot. Such a strategy has been demonstrated using *in vitro* blood clot experiments. We believe that this strategy could improve thrombolysis and recanalization rates, reduce the risk of tPA-mediated hemorrhage, and maybe applied for other disease treatment.

NS-TuP2 Gelatin Nanoparticle Encapsulation of Anti-Parasitic Compound and Characterization for Treatment of Leishmaniasis Disease, Carlos Serna, A. Ornelas, E. Iniguez, K. Michael, R. Maldonado, T. Boland, The University of Texas at El Paso

Leishmania major is azoonotic flagellate protozoan transmitted to humans and other mammals through phlebotomine female sand flies. *L. major* is mainly responsible for causing cutaneous leishmaniasis (CL) in endemic areas of the Old World, with about 1 million new infections each year [1]. The Mannich base compound 1-acetyl-3,5-dibenzylidene-4-piperidone(2) has been found to have effective anti-parasitic properties, but lacks solubility making it difficult to deliver using standard methods. In this study, we synthesized gelatin nanoparticles (GNP) as carriers for the treatment molecule and demonstrate an effective method of delivering anti-parasitic treatment enhancing drug delivery and reducing toxicity in treatment.

Tuesday Evening Poster Sessions, November 8, 2016

Materials and Methods: 1-acetyl-3,5-dibenzylidene-4-piperidone(2) was synthesized by dissolving 3,5-dibenzylidene-4-piperidone(1) in a mixture of 10% acetic anhydride and 5% diisopropylethylamine in dichloromethane while stirring at room temperature. The Ofokansi et al. [2] two-step desolvation method was applied to produce GNP. To maximize the encapsulation yield of the compound, the preparation method was further modified by limiting the drop-wise cross-linking agent (glutaraldehyde) rate to 30 min and replacing DI water with phosphate buffer saline (PBS) for higher pH stability. Unloaded GNP sizes were determined using a particle size analyzer (Nanosight) in order to test for GNP swelling in varying pH levels. UV visible spectroscopy was used to identify the release rate and total concentration of the compound encapsulated. A viability and cytotoxicity assay was conducted in the testing of loaded and unloaded GNP.

Results and Discussion: The mode values of size distributions using PBS pH 5, 7, and 9 in the production of GNP were found to be 73 nm, 91 nm, and 121 nm respectively. Using UV visible spectroscopy, the concentration of compound encapsulated by the GNP was found to be 4.01 µg/mL released over a time frame of 96 h in 2.4 g of GNP. A viability assay showed an EC50 value of 2.26 µM for 1-acetyl-3,5-dibenzylidene-4-piperidone(2) in *L. major*; cytotoxicity for the murine intraperitoneal macrophages showed an IC50 value of 6.35 µM.

Conclusions: GNP characterization showed an increase in size with respect to increasing pH in PBS used in the production process; the swelling initiated by exposing GNP produced at pH 5 to a PBS solution of pH 8 showed a release rate of 1 µg/mL per day for 4 days. Viability assays showed the GNP to be effective against *L. major* when encapsulated and non lethal when lacking a molecule payload.

References:

1. Alrajhi A.A. N Engl J Med. 2002, 346:891-895.
2. Ofokansi K. Eur. J. Pharm. Biopharm. 2010,76,1-9.

NS-TuP4 Templated Annealing of Gold Nanowires formed by Directed Assembly on DNA Origami, Tyler Westover, M. Stoddard, B. Uptrey, R.F. Davis, J. Harb, A. Woolley, Brigham Young University

The formation of gold nanowires using bottom up nanofabrication has resulted in wires of small dimension or high conductivity, but not both. We form nanowires on DNA origami through directed assembly of nanoparticles, electrochemical plating, or a combination of the two. These metal deposition processes result in non-ideal microstructure and correspondingly low conductivities. To remedy this we have sought to reduce the grain boundary density and surface roughness through annealing. However annealing causes the wires to coalesce into beads. We will present results on using polymer layers to maintain overall wire morphology during low temp (200° C) annealing.

NS-TuP5 Zinc Oxide Nanoprobe Spectroscopy for Sensing Trace Levels of Molecular Species in Solution, Andrew Cook, Vanderbilt University; C.S. Carson, Fisk University; J. DeCoste, Edgewood Chemical Biological Center; T.D. Giorgio, Vanderbilt University; R. Mu, Fisk University

Surface-enhanced Raman spectroscopy (SERS) has great potential to revolutionize clinical diagnostics, yet is limited by an extreme intensity drop-off with distance from the sensing surface. For this reason, much research into SERS-based biosensing relies on chemical or physical adsorption of analytes to the active surface, which limits the types of analytes that can be detected, as well as detection sensitivity. Using the 3-dimensional closely packed architecture of zinc oxide nanowires decorated with silver nanoparticles, the enhancement drop-off can be effectively mitigated, allowing for adsorption-free biosensing. This greatly improves the viability of Raman spectroscopy as a biosensing technique. We demonstrate a significant SERS enhancement from silver nanoparticle-decorated zinc oxide nanoprobes to the Raman spectrum of crystal violet molecules in water, as a model system. More importantly, we demonstrate the detected SERS signal is from molecules un-adsorbed to the sensing surfaces via time-dependent Raman analysis. We also demonstrate growth of high quality zinc oxide nanowires and deposition of silver nanoparticles on the nanowire sides as a surface-enhanced sensing platform.

NS-TuP7 Effect of Deposition Temperature on the Formation of the SiO₂/ZnO/SiO₂ Heterostructure Deposited by Reactive RF Sputtering*, R. Escobedo-Alcaraz, C. Atzin-Mondragon, Cinvestav-IPN, Mexico; A. Hernandez-Hernandez, Escuela Superior de Apan, Mexico; A. Garcia-Sotelo, MiguelAngel Melendez-Lira, Cinvestav-IPN, Mexico

The roughness associated with the sputtering deposition process has been employed to explore the possibility to produce ZnO nanoparticles Tuesday Evening Poster Sessions, November 8, 2016

embedded within a silicon oxide matrix on soda-lime glass and p-silicon substrates. Silicon dioxide and metallic Zn films were deposited employing silicon and zinc targets. An oxygen rich working plasma was employed. Oxygen content of the working plasma was modulated through argon partial pressure. A sequential deposition of SiO₂/Zn/SiO₂ films was employed ; SiO₂ layer was produced at 400 °C while deposition temperature of Zn layer was changed between 100 and 500 °C. Results of the chemical, structural and electronic properties are presented. The Results indicated the successful production of ZnO with properties depending on deposition temperature. X-ray diffraction characterization do not shown the presence of metallic zinc. Secondary ion mass spectroscopy shown an interdiffusion of zinc toward the SiO₂ matrix. TEM micrographs indicated the presence of ZnO nanoparticles. XPS corroborates the ZnO formation under specific growth parameters. Photoluminescence emission at room temperature for samples grown on silicon substrates was not observed. Electrical transport properties are discussed on terms of deposition parameters.

*: Partially funded by CONACyT-Mexico

NS-TuP8 Design of High Performance Compact Plasmonic Optical Devices Based on Low Loss Silicon Hybrid Dielectric Loaded Plasmonic Waveguides, Cheng-Hung Hsieh, C.M. Kuo, National Tsing Hua University; M.J. Huang, Naitoal Tsing Hua University; R.J. Sun, National Tsing Hua University; K.C. Leou, National Tsing Hua University, Taiwan, Republic of China

Here we present the design of several plasmonic optical devices which have gained a great deal of attention recently for potential application in nano photonic circuits. A unique ultra low loss surface plasmon polariton (SPP) waveguide, top metal silicon (Si) hybrid dielectric-loaded plasmonic waveguide (TM-SiHDLW), was first designed. The waveguide adopted a top metal stripe structure for easier process integration with conventional micro fabrications and a thick (200 nm) metal stripe was found to yield optimal performance due to reduced Ohmic loss in conductor around the stripe edge/corner. Moreover, a relatively thick (150 nm) dielectric spacer between the Si ridge and the metal stripe was employed to achieve both long propagation length and good field confinement. Results from numerical simulation show that a long propagation length of 350 µm and a small mode area of 0.03 m² are obtained. The TM-SiHDLW structure was also adopted for design of several compact high performance plasmonic optical devices, including a directional coupler, a disk resonator and an switch. The directional coupler adopted a coupled waveguide structure. A coupling length as low as 2.95 µm, only ~ 0.85% of the propagation length, was obtained. The second device is a disk resonator operating at the low loss TE mode. Simulation results demonstrate that a quality factor as high as 2000 can be achieved at a size much smaller than that of a conventional ring resonator. Another plasmonic optical device we have explored was an electro-optical (E-O) switch where an organic E-O material was chosen for low switching voltage along with having a better compatibility with conventional microfabrication processes. The switch we proposed employed a coupled waveguide structure configured in a way that the optical wave can be switched between to two waveguides, depending on the voltage applied on the switch electrodes. All these SPP waveguides and devices were designed to operate at the standard 1550 nm wavelength.

* Work supported by the Ministry of Science and Technology of ROC. The authors also thank the "National Center for High-Performance Computing" of ROC for providing simulation code.

References

- 1) C. H. Hsieh, et al., *IEEE Photon. Technol. Lett.*, (2015) 27(10), 1096-1099.
- 2) C. H. Hsieh, et al., *IEEE Photon. Technol. Lett.*, (2015), 27(23), 2473-2476.

NS-TuP9 Carbon Nanotube Based Digital X-ray Tube for a Very Short X-ray Pulse with High Dose Rates, Jun-Tae Kang, J.W. Jeong, J.W. Kim, Y.C. Choi, S.H. Kim, H. Jeon, S. Park, M.S. Shin, J.H. Yeon, E. Go, J.W. Lee, Y.H. Song, Electronics and Telecommunications Research Institute (ETRI), Republic of Korea

Carbon nanotube (CNT) field emitters are being considered as a promising electron source of x-ray tube, which is expected to overcome the limitations of conventional thermionic tubes. The thermionic x-ray tube has been fabricated using a hot cathode, causing analog behaviors like slow response time. On the other hand, the field-emission x-ray tube with CNT emitters can be digitally addressed, which makes it possible to give a very short exposure time. The high x-ray dose rate in a very short exposure time is very important for achieving clear x-ray images.

Tuesday Evening Poster Sessions, November 8, 2016

We have successfully fabricated a digital x-ray tube with CNT field emitters for medical applications. The x-ray tube sealed in a vacuum level of below 5×10^{-6} Torr consists of a CNT field emission gun and a rotating anode made of W/Re target on a Mo block. The field emission current over 100 mA is attained by the gate bias of several kV and is fast modulated through an active-current control at the cathode node, showing a very short x-ray pulse under submicron seconds at a high dose rate. The developed x-ray tube is expected to be used in the advanced diagnostic imaging system with a very short exposure time and high x-ray dose.

Novel Trends in Synchrotron and FEL-Based Analysis Focus Topic

Room Hall D - Session SA-TuP

Novel Trends in Synchrotron and FEL-Based Analysis Poster Session

SA-TuP1 Transmission X-Ray Microscopy Characterization of PtNi Extended Surface Catalysts within MEAs for PEMFCs, Sarah Shulda, Colorado School of Mines; **J. Nelson Weker,** SLAC National Accelerator Laboratory; **C. Ngo,** Colorado School of Mines; **S. Mauger, K.C. Neyerlin, S. Alia, B. Pivovar,** National Renewable Energy Laboratory; **S. Pylypenko,** Colorado School of Mines

Proton exchange membrane fuel cells (PEMFCs) have a high power-to-weight ratio making them well suited for transportation applications. Platinum (Pt) nanoparticles on high surface area carbon is the current state of the art catalyst for the oxygen reduction reaction at the cathode. However, the high cost and inherent durability issues of this catalyst significantly limit the commercialization potential of PEMFCs in automobiles. Pt nanowires are a promising alternative to the carbon-supported Pt nanoparticles. High surface area platinum nickel (PtNi) nanowires have been synthesized and demonstrated exceptionally high activity and durability in electrochemical studies using rotating disk electrodes (RDEs). The incorporation of nanowire catalysts into full membrane electrode assemblies (MEAs) is not straightforward due to significant differences in the morphology of these materials as compared to traditional catalysts based on carbon-supported nanoparticles, and requires optimization of electrode composition and structure. Factors effecting the performance of the electrodes include catalyst content, amount of ionomer, amount and type of carbon additive, the three dimensional morphology of the nanowires, and nanowire contact with each other and with the other constituents of the MEA. In the specific case of NiPt nanowires, preventing Ni leaching is also imperative as Ni will poison the fuel cell and inevitably cause a significant drop in performance. Optimization of these parameters requires detailed understanding of the electrode structure, preferably using non-destructive techniques.

Transmission x-ray microscopy (TXM) allows for non-destructive three-dimensional analysis of full MEAs providing detailed information on electrode composition and structure. Ni and Pt are imaged separately through selective tuning of the incident x-ray energy, making their relative distribution throughout the MEA readily discernible. A series of MEAs with varying ink compositions was analyzed with TXM to study the effects of ionomer content, amount and type of carbon, and addition of poly(acrylic acid) (PAA) on electrode structure. MEAs pre-leached with acid to remove Ni were also imaged. Results demonstrated that ink formulations and acid leaching significantly impacted the nanowire morphology within the MEA. The addition of graphitized carbon nanofibers (GCNFs) resulted in more homogeneous and less densely packed nanowire distribution. Scanning electron microscopy (SEM), transmission electron microscopy (TEM), and scanning transmission electron microscopy (STEM) with energy dispersive elemental mapping complemented the TXM studies.

SA-TuP2 In Operando X-ray Imaging and Scattering from Detonating High Explosives, M. Bagge-Hansen, M. Nielsen, L. Lauderbach, R. Hodgins, S. Bastea, L. Fried, D. Hansen, C. May, T. van Buuren, Trevor Willey, Lawrence Livermore National Laboratory

The detonation of CHNO high explosives can generate an array of carbon nanomaterials including nano-onions, nano-diamond, and graphene products. The formation of these solid carbon phases occurs rapidly over the first several hundred nanoseconds, and a means to experimentally interrogate carbon nanomaterial formation during detonation will improve computational modeling and predictions of detonation phenomena. Experimental probes of carbon condensation under the extreme pressure and temperature conditions present during detonation at 100 ns

timescales have been technically challenging to-date. Here, we present a new time-resolved small-angle x-ray scattering (SAXS) end-station, developed at LLNL and deployed at the Advanced Photon Source. This end-station at the Dynamic Compression Sector is capable of synchronously initiating detonation, and acquiring either small-angle x-ray scattering, or x-ray transmission radiographic images from discrete 80 ps x-ray pulses, which arrive every 153.4 ns during 24-bunch mode. The endstation can be trivially switched between SAXS and imaging modes. Images reveal densification within the explosive reaction zone, as well as detonation front curvature, and detonation velocity. The SAXS patterns demonstrate dramatic variation in the morphology and size of particles produced by different explosives. This work was performed under the auspices of the US DOE by LLNL under Contract DE-AC52-07NA27344

Advanced Surface Engineering

Room Hall D - Session SE-TuP

Advanced Surface Engineering Poster Session

SE-TuP1 Room Temperature Bonding of Polymer and Silicon Wafer using Vacuum Ultraviolet Surface Activation, Yoshihiro Fujiwara, T. Utsunomiya, T. Ichii, H. Sugimura, Kyoto University, Japan

Vacuum ultraviolet (VUV; $\lambda < 200$ nm) light and active oxygen species generated by VUV light chemically introduce polar functional groups to the surface of organic materials, which are related to adhesive property and wettability. In our previous research [1][2], we investigated the VUV decomposition and chemical conversion of the chemisorbed self-assembled monolayers (SAMs) and polymers surfaces. Using the VUV treatment under the atmospheric pressure, we have succeeded in bonding of Cyclo-olefin polymer (COP) films, which is a nonpolar hydrocarbon polymer, and in bonding between the polymer film and metals such as copper and aluminum at temperature lower than the glass transition temperature of each polymer. However, because of the surface roughness, thermal stress and the presence of intermediate oxide layer, the bonding mechanism is still unclear. In this research, we carried out the surface activated bonding of COP and silicon(111) single crystal wafer as a model surface with atomic-scale flatness. The atomically flat surface enables us to bond different materials at room temperature. Bonding condition without roughness and thermal effects is desirable to reveal the effectiveness of VUV treatment of the surface. A bond strength test was conducted to elucidate the effect of surface modification and bonding conditions such as VUV-irradiation distance, VUV-irradiation time, terminal functional groups of SAMs.

References:

- [1] Y. Kim, Y. Taniguchi, K. Murase, Y. Taguchi, H. Sugimura, Appl. Surf. Sci. **255**, 3648-3654 (2009).
- [2] A. Soliman, T. Ichii, T. Utsunomiya, H. Sugimura, Soft Matter, **11**, 5678-5687 (2015).

SE-TuP2 Improvement in Organic Solvent Resistance of Cyclo-Olefin Polymer by Coating with Silica-like Thin Film, Taiki Kanzawa, T. Utsunomiya, T. Ichi, H. Sugimura, Kyoto University, Japan

Cyclo-olefin polymer (COP) is an amorphous polymer and has the great optical properties like silica glass.¹ Therefore, COP is suitable for microfluidic devices with the optical detection. However, COP is not durable to many organic solvents such as toluene and ether. For utilizing COP to wider range of application fields, this problem must be solved.

Several methods for fabricating the silica-like thin film on polymer substrates have been reported.^{2,3} We optimized the coating methods to improve organic solvents resistance of COP. Vacuum ultra-violet (VUV) light of 172 nm wavelength was used in order to photochemically activate the hydrophobic surface of COP plate. Then, tetramethylcyclotetrasiloxane (TMCTS), which has similar component to silica, was chemisorbed onto VUV light-irradiated COP surface by vapor phase deposition. Finally, the sample coated with TMCTS thin film was irradiated by using VUV light again.

The X-ray photoelectron spectroscopy (XPS) and the attenuated total reflection Fourier transform infrared spectroscopy (ATR-FT-IR) measurements clearly indicated that TMCTS thin film was converted to silica-like thin film after VUV light-irradiation. Then, we dropped some organic solvents onto the sample coated with silica-like thin film. After evaporation, there were no traces of osmosis, showing the no permeation

Tuesday Evening Poster Sessions, November 8, 2016

of organic solvents to bulk polymer. These results showed that coating with silica-like thin film greatly improved the resistance to organic solvents.

- [1] M. Yamazaki, *J. Mol. Catal. A: Chem.*, **213**, 81 (2004)
- [2] M. Ouyang, C. Yuan, R. J. Muisener, A. Boulares, J. T. Koberstein, *Chem. Mater.*, **12**, 1591 (2000)
- [3] V. -M. Graubner, R. Jordan, O. Nuyken, B. Schnyder, T. Lippert, R. Koetz, A. Wokaun, *Macromolecules*, **37**, 5936 (2004)

SE-TuP3 Microstructure and Properties of (ZrHf)N Thin Films Deposited by Sputtering at Room Temperature, *N.N. Chu, Yu-Wei Lin, C.-N. Hsiao*, ITRC, National Applied Research Laboratories, Tainan, Republic of China

This study investigated the microstructure and properties of nanocrystalline (ZrHf)N films on Si substrate at room temperature. (ZrHf)N films were prepared by reactive magnetron sputtering based on our previous optimum coating conditions (substrate temperature, system pressure, nitrogen flow etc.) for HfN and ZrN thin films. Based on the early studies, metal nitride coatings have attracted attention for good mechanical properties, hardness up to 30 GPa. In the study, we should have a generalized definition for substitutional solid solution. The addition of Hf into ZrN (or addition of Zr into HfN) forms the substitutional solid solution ZrHfN (or HfZrN). Different ratios of Hf/Zr will form various structure for (Zr,Hf_{1-x})N with interesting properties, and many characteristics, such as nanostructure and hardness remain to be studied further. Characterizing the structure and properties of single ZrHfN layer coating with the different ratio of Hf-Zr to find out the optimum processing parameters, and further to tailor a variety of surface coating applications is the objective of this project.

SE-TuP4 Nanopatterned ZnO on Si-based Materials via Decoupled Ion Beam Modification and Metal Co-deposition, *Zachariah Koyn, B. Holybee, J.P. Allain*, University of Illinois at Urbana-Champaign

Ion beams have been shown to create nano-scale surface patterning on polycrystalline thin metal films, including ripples and dots [1,2]. Additionally, oxygen ion beams have been shown to induce fluence-dependent surface oxidation on metal surfaces [3]. This work seeks to unravel the directed irradiation synthesis of metal oxide thin-films and nanostructures, specifically ZnO, with irradiation-driven mechanisms on dissimilar, polymer-based substrates via in-situ, in-operando high-pressure XPS. This examines the dual effects of oxygen irradiation as a means to both oxidize and pattern metal thin-films at ambient temperatures. This represents a scalable process in growing and functionalizing metal-oxide thin-films on polymers, which are sensitive to the high temperatures required in thermal oxidation processes. Recent work utilized a single ion beam to simultaneously irradiate and sputter deposit metal impurities on Si, creating nanostructures [4]. The work here decouples these processes by using two ion beams to independently control the metal deposition and surface modification fluxes and energy distributions. The ratio of these fluxes is the primary tool used to explore the creation and control over size and shape of nanostructures. Beam energies of 500-1500 eV are used at ambient temperatures to protect the substrate, with an inert beam used for metal sputter deposition and both inert and reactive (O₂⁺) normal incidence beams used for surface modification. Both Si and PDMS substrates are explored with fluences of 1E16–1E18 ions/cm². Surface chemistry is monitored in-operando in the new Ion-Gas-Neutral Interactions with Surfaces (IGNIS) facility. XPS is performed at pressures up to 5 mTorr, allowing for the real-time monitoring of Zn deposition and oxidation. The ability to functionalize flexible, transparent substrates with metal-oxide nanostructures offers exciting applications in areas such as flexible and wearable electronics, gas sensors, biosensors, and photonics [5].

- [1] D. Ghose, *J. Phys. Condens. Matter* **21**, 224001 (2009).
- [2] P. Gailly, C. Petermann, P. Tihon, and K. Fleury-Frenette, *Appl. Surf. Sci.* **258**, 7717 (2012).
- [3] N. V. Alov, *Nucl. Instruments Methods Phys. Res. Sect. B Beam Interact. with Mater. Atoms* **256**, 337 (2007).
- [4] K. Zhang, M. Brötzmann, and H. Hofsäuss, *AIP Adv.* **2**, 0 (2012).
- [5] I.-S. Hwang, Y.-S. Kim, S.-J. Kim, B.-K. Ju, and J.-H. Lee, *Sensors Actuators B Chem.* **136**, 224 (2009).

SE-TuP5 Propagating Exothermic Reactions in Al/Pt Multilayers of Varied Stoichiometry, *D.P. Adams*, Sandia National Laboratories; *R.V. Reeves*, Lawrence Livermore National Laboratory; *M. Abere*, *Cathy Sobczak*, Sandia National Laboratories

Reactive bimetallic multilayers are a form of energetic material that can be ignited at a point and undergo rapid, exothermic, self-propagating reactions. Providing a burst of heat, these materials continue to find use for different joining, battery and fusing applications. Much has been learned about the properties of these materials, yet little is known about the compositional limits of reactivity. In this presentation, we describe the propensity of sputter-deposited Al/Pt multilayers to undergo rapid, self-propagating formation reactions. Reactivity has been evaluated across a broad range of stoichiometry (nAl:mPt) and layer periodicity. Experiments demonstrate self-propagating reactions in ~1.6 micron-thick Al/Pt multilayers when the molar ratio of reactants is in the range 4Al:1Pt to 1Al:4Pt. This rather large compositional range is characterized by different reaction rates and behaviors. High-speed photography shows that equimolar Al/Pt multilayers undergo the most rapid reactions with wavefront speeds as large as 80 m/s. Al- and Pt-rich multilayers react at reduced rates with speeds as low as 1 m/s. A previously developed, analytical method by Mann et al. (*J. Appl. Phys.* 1997) is utilized to reveal additional details of reactions in the various multilayers. Models that account for the reactant layer thicknesses, composition, the adiabatic temperatures, the flame temperatures, and the measured heats of reaction are used to predict wavefront speeds that closely match measured values. These results are further analyzed to extract information regarding the mass transport characteristics of reactant species.

This work was supported by a Sandia Laboratory Directed Research and Development (LDRD) program. Sandia National Laboratories is a multi-program laboratory managed and operated by Sandia Corporation, a wholly owned subsidiary of Lockheed Martin Company, for the United States Department of Energy's National Nuclear Security Administration under Contract DE-AC04-94AL85000.

SE-TuP7 Time-resolved Ion Energies in the Pulsed Cathodic Arc Plasma from Composite Niobium-aluminum Cathodes, *Siegfried Zoehrer*, Montanuniversität Leoben, Austria; *A. Anders*, Lawrence Berkeley National Laboratory; *R. Franz*, Montanuniversität Leoben, Austria

Cathodic arc plasmas are utilized in industry to synthesize a wide variety of functional thin films and coatings. However, the plasma properties present during the deposition processes are not yet fully understood, in particular when composite cathodes are used.

For pulsed cathodic arc plasmas, it is known that the plasma properties like ion energies and ion charge states are time dependent, but the influence of the cathode composition is not much studied. We therefore recorded time-resolved ion energy distribution functions in vacuum arc plasmas from composite NbAl cathodes with the Nb/Al atomic ratios 75/25, 67/33 and 25/75, as well as from single-element Nb and Al cathodes. The mass and charge-state-resolved detection of ions was realized using a commercial mass-energy analyzer modified to allow us having a time resolution of 100 ns (Tanaka et al., 2015). Three dimensional data sets were obtained, where the intensity, that is proportional to the ion count rate, is displayed as a function of time and energy for Nb and Al ions with charge states up to 5+ and 4+, respectively.

Regardless of the cathode composition, the highest mean charge states and ion energies were observed in the beginning of the pulses. There is also a clear influence of the cathode composition. Namely, the fraction of higher ion charge states being significantly lower in the plasma from the composite compared to the single-element cathodes. The current results regarding the time dependence of the ion charge state and energy distributions represent a first step towards a comprehensive understanding of how the cathode composition is affecting the plasma properties.

Tanaka, K.; Han, L.; Zhou, X. & Anders, A. (2015), 'Adding high time resolution to charge-state-specific ion energy measurements for pulsed copper vacuum arc plasmas', *Plasma Sources Science and Technology* **24**(4), 045010.

Tuesday Evening Poster Sessions, November 8, 2016

Scanning Probe Microscopy Focus Topic

Room Hall D - Session SP-TuP

Scanning Probe Microscopy Poster Session

SP-TuP1 New Directions in Ultrahigh Vacuum Tip-Enhanced Raman Spectroscopy with Molecular-Resolution Scanning Tunneling Microscopy, Z. Porach, P. Whiteman, University of Illinois at Chicago; N. Chiang, Northwestern University; **Nan Jiang**, University of Illinois at Chicago

During the last few years, the study of ultrahigh vacuum tip-enhanced Raman spectroscopy (UHV-TERS) has been raised to an unprecedented level. While scanning probe microscopy (SPM) is commonly used to study individual molecules, its information content can be severely compromised by surface diffusion, irregular packing, or three-dimensional adsorbate geometry. Here we demonstrate the simultaneous chemical and structural analysis of single molecules on the solid surface by UHV-TERS. In situ lenses can increase the collection efficiency with large numerical aperture. The strongly enhanced Raman signal makes the detection of single molecules possible. The adsorption configurations are able to be determined at unprecedented spatial resolution ($<1\text{nm}$).

SP-TuP3 Temperature-dependent Nanoscale Conductance on Water-Intercalated Graphene, JinHeui Hwang, H. Lee, J.Y. Park, Institute for Basic Science (IBS) & Korea Advanced Institute of Science and Technology (KAIST), Republic of Korea

We investigated the nanoscale conductance of water-intercalated graphene using current-sensing atomic force microscopy (C-AFM). The intercalation of water between graphene and mica was enabled by transfer of chemical vapor deposition (CVD) graphene on mica substrate. Water molecules were captured in the liquid water bath during the graphene transfer process. We show that the surface conductance are significantly influenced by the presence of water layer between graphene and mica. We found that the edge of water island exhibits the lower conductance, compared to that of bare graphene. We further showed conductance of graphene on the first water layer were fluctuated depending on the temperature. The anomalous behavior of conductance is originated by structural defects of water layer and bonding nature between edge of the water islands and mica substrate, which lead to the suppression of the local current.

SP-TuP4 Phase Coexistence in Vanadium Dioxide Crystal Probed via Scanning Probe Microscopy, Christina McGahan, Vanderbilt University; S. Gamage, Georgia State University; J. Liang, Tianjin University, China; B.G. Cross, Georgia State University; R.E. Marvel, R.F. Haglund, Vanderbilt University; Y. Abate, Georgia State University

For the past decade, scattering-scanning near-field optical microscopy (s-SNOM) has been employed to image the coexisting metallic and insulating domains in single-crystal nanorods and platelets of vanadium dioxide (VO_2) during the insulator-to-metal phase transition. In virtually all studies, the coexisting domains appear as alternating stripes perpendicular to the c_R (growth axis) of the nanocrystals and extending from one side of the beam to the other.

We employed s-SNOM with a laser wavelength of $\lambda=10.7\text{ }\mu\text{m}$ and polarized far-field optical microscopy to examine a single VO_2 microcrystal decorated with gold (Au) plasmonic dipole antennas. Metallic and insulating domains can be easily distinguished during the thermal phase transition in VO_2 using s-SNOM due to the large dielectric contrast between metallic and insulating VO_2 at that wavelength. Plasmonic dipole antennas are positioned on the crystal, designed to be resonant at the s-SNOM probe wavelength to allow simultaneous probing of the pattern of coexisting phases of VO_2 and the nanorod plasmon.

We observe a novel herringbone pattern of phase coexistence, seen in cracked epitaxial thin films but never in single crystals, in a VO_2 single crystal which is large enough that the phase coexistence is not constrained by high aspect-ratio geometry. The herringbone pattern is altered by the presence of ferroelastic strain domains that form to relieve stress and can nucleate metallic domains. These ferroelastic domains are imaged with polarized far-field optical microscopy. Though the local dielectric environment of the crystal changes during the phase transition, as indicated via s-SNOM, the plasmon resonance frequency of Au nanoantennas atop the crystal does not change in response to the growth of metallic domains. This indicates that the metallic domains nucleate in the bulk of the single crystal, beyond the range of the plasmon field, which only penetrates tens of nanometers below the crystal surface but in range of the s-SNOM due to the penetration depth of $10.7\text{ }\mu\text{m}$ laser light. The domain pattern is insensitive to the locations and orientations of the

resonant Au antennas because the field, as determined through simulations, is not high enough to induce the VO_2 phase transition. Simulations indicate that a bowtie antenna has sufficient field to locally switch VO_2 from insulating to metallic, enabling localized induction of the phase transition near the surface of the VO_2 .

SP-TuP5 Single Virus Particle Spectroscopic Nano-Imaging, Brendan Cross, S. Gamage, M. Howard, J.R. Terrell, M. Luo, Y. Abate, Georgia State University

We present the spectroscopic nano-imaging of single influenza virus particles in the mid infrared spectral region. The X-31 strain of Influenza A is an enveloped virus, which has a lipid and protein layer that contains the nucleocapsid. Virions are drop cast on silicon substrates for near-field imaging. High-resolution near-field microscopy is used to map the amide and phosphate bands of the envelope proteins on a single virion. We have also investigated the evolution of the virus as a function of time, acid treatment and laser radiation.

SP-TuP6 Spectroscopic Nano-Imaging Patterned InGaN Nanolayers, Alireza Fali, S. Gamage, D. Seidlitz, I. Kankanamge, N. Dietz, Georgia State University; Y. Abate, Georgia state university

Ternary InGaN compound semiconductors are of interest for many device applications such as light-emitting diodes, laser diodes, solar cells, etc., because they cover a broad spectral range from deep ultraviolet to near infrared as a function of the composition. This study focuses on nanoscopy of patterned structures of InGaN compound. To achieve this goal, InGaN film has been grown on top of the InN substrate. Scattering-type scanning near-field optical microscopy was used for nano-spectroscopic studies in the mid infrared spectral region of various thickness and composition of $\text{In}_{1-x}\text{Ga}_x\text{N}$ nanolayers grown on InN substrates.

SP-TuP7 Nanoscopy of Black Phosphorus Degradation, Sampath Gamage, Georgia State University; L. Zhen, University of Southern California; V.E. Babicheva, M. Javani, V.S. Yakovlev, Georgia State University; H. Wang, S. Cronin, University of Southern California; Y. Abate, Georgia State University
Black phosphorus (BP) is a promising layered material for optoelectronics applications due to its outstanding physical properties. Importantly, the thickness-dependent tunable direct bandgap of BP excited material scientists over graphene that lacks a natural bandgap. Similar to graphene, BP can be prepared commonly and simply by mechanical exfoliation. However, the major impediment of the BP based research is its surface degradation when exposed to atmospheric water and oxygen. In order to develop BP as a material for aforementioned applications, it is essential to understand degradation process at nanoscale chemical resolved resolution. In this poster contribution, we present our findings of the nanoscale spectroscopy degradation study of BP using scattering type scanning near-field optical microscopic (s-SNOM) technique at several mid infrared wavelengths. We have experimentally investigated the thickness dependence and substrate influence of a set of uncoated and Al_2O_3 coated samples and theoretically modeled the degradation evolution.

SP-TuP8 Periodically-pulsed Laser-Assisted Tunneling May Generate Terahertz Radiation, Mark Hagmann, University of Utah

Background: Periodic excitation of the tunneling junction in a scanning tunneling microscope by a mode-locked ultrafast laser superimposes a frequency comb at harmonics of the pulse repetition frequency on the DC tunneling current.¹ The power measured at the first 200 harmonics (74.254 MHz to 14.85 GHz) varies inversely with the square of the frequency—decaying only due to shunting by the stray capacitance.

Hypothesis: The tunneling junction is much smaller than the laser wavelength so effectively the laser superimposes a time-dependent voltage on the DC bias. Quasi-static conditions cause the time-dependent tunneling current to be related to the time-dependent voltage by a cubic polynomial as in the DC case. Thus, the waveform of the current in the tunneling junction is similar to the envelope of the laser radiation.

Analysis: The time-dependent voltage is modeled as a random process including pulse-jitter and finite coherence length of the laser. The current in the tunneling junction is shown to be a wide-sense stationary random process. For a laser with a pulse-width of 15 fs and pulse repetition frequency of 74.254 MHz the power spectral density in the tunneling junction has an intrinsic decay of 3 dB at the 2.4×10^5 th harmonic of 18 THz. The power measured at the first harmonic corresponds to a peak current of 5.7 nA. But the frequency of this harmonic is low enough that the decay caused by stray capacitance is negligible so this value, adjusted for the intrinsic decay, is the peak current at each harmonic in the tunneling junction.

Tuesday Evening Poster Sessions, November 8, 2016

Results and conclusions: Under the conditions for our measurements of the frequency comb we predict that in the tunneling junction the peak current for each pulse is approximately 690 mA. This value would be higher with a laser having greater coherence length or lower timing-jitter. It appears that the finest spatial resolution so far achieved in terahertz imaging is 40 nm by the near-field confinement of plane-wave illumination at a conical metal tip.² Our simulations suggest it may be possible to achieve atomic resolution by using the terahertz radiation at the tunneling junction in periodically-pulsed laser-assisted scanning tunneling microscopy. Much higher power is expected in periodically-pulsed laser-assisted field emission because of the greater current and much lower stray capacitance.

References

¹M. J. Hagmann, A. J. Taylor, and D. A. Yarotski, Appl. Phys. Lett. **101**, 241102 (2012).

²A. J. Huber, F. Keilmann, J. Wittborn, J. Alzpurua, and R. Hillenbrand, Nano Lett. **8**, 3766-3770 (2008).

Surface Science

Room Hall D - Session SS-TuP

Surface Science Poster Session

SS-TuP1 Adsorption and Decomposition Properties of Dimethyl Trisulfide Over Au(111), Isao Nakamura, National Institute of Advanced Industrial Science and Technology (AIST), Japan; *M. Tokunaga*, Kyushu University, Japan; *T. Fujitani*, National Institute of Advanced Industrial Science and Technology (AIST), Japan

It is known that dimethyl trisulfide (DMTS) is mainly responsible for an off-flavor that develops during the storage of Japanese sake. Recently, we found that the supported gold catalysts are effective for the adsorption and removal of DMTS. In this study, in order to clarify the reaction properties of DMTS over gold, we investigated the adsorption and decomposition of DMTS using the Au(111) single-crystal surface.

First, we examined the influence of the exposure temperature on the adsorption properties of DMTS. X-ray photoelectron spectroscopy (XPS) results indicated that DMTS is dissociatively adsorbed as CH₃S and CH₃SS species at 100–300 K. Furthermore, both the dissociative adsorption rate and the saturation coverage were the same regardless of the exposure temperature.

In contrast, the thermal decomposition properties of CH₃S and CH₃SS strongly depended on their formation temperatures. On the Au(111) surface formed at 100 K, the CH₃S was shown to be associatively desorbed as dimethyl disulfide (DMDS), and the production of ethane and atomic sulfur by the cleavage of C–S bond in CH₃SS were confirmed from temperature-programmed desorption and XPS measurements. Thus, CH₃S and CH₃SS reacted individually. On the other hand, the reaction of CH₃S with CH₃SS to produce DMDS and atomic sulfur was also confirmed for the surface at 150 K. At 200 K or 300 K, only the reaction of CH₃S with CH₃SS was observed. We consider that the difference in the decomposition reaction is due to that the adsorption structure of CH₃S and CH₃SS species on Au(111) changes by their formation temperatures. That is, the CH₃S and CH₃SS species are present in separate islands each other at 100 K, whereas the adsorption structure of CH₃S and CH₃SS becomes random with rising their formation temperatures.

SS-TuP2 Spectroscopically Monitoring the Surface and Crystallinity of Titania Nanopowders Treated with Hydrogen Peroxide: an Endeavor in Simplifying the Atomic Picture of Complex Substrates, Maria Kipreos, M. Foster, University of Massachusetts, Boston

Metal oxide substrates are often riddled with defect sites, imperfections in metal-oxide atomic arrangements. One such defect is an oxygen vacancy at the surface. Commonly, the substrate is exposed to O₂ to reestablish the proper metal-oxygen coordination. Much like O₂, hydrogen peroxide may be used to oxidize the surface of metal oxide nanopowders, such as titania (TiO₂), as well as drive off impurities remaining and/or derived from the synthesis of these materials, to establish a more pristine surface. Various commercially available nanosized rutile and anatase structured titania nanopowders are treated with hydrogen peroxide and any changes in crystallinity are monitored using a confocal Raman microscope as well as powder X-ray Diffraction. In situ DRIFTS coupled with a high temperature reaction chamber is used to assess any changes in the substrate upon treatment, including evolving water and hydroxyl features on the surface

and the disappearance of impurities, both as the pretreatment conditions change and as a function of substrate temperature.

SS-TuP3 Efficacy of Ar⁺ CIRD Removal of Adsorbed O from Rh(111), Marie Turano, R.G. Farber, D.R. Killelea, Loyola University Chicago

Subsurface oxygen (O_{sub}) on Rh(111) is formed via gas-phase deposition of atomic oxygen (AO). Total O coverages of over 3 ML equivalence are possible, and results in an oxygen saturated surface and O_{sub}. In order to study the geometric and electronic effects of O_{sub} on a surface alone requires a technique to remove the adsorbed oxygen (O_{ad}) while retaining O_{sub} and minimizing damage to the metal surface. Here, we present results from our development of collision-induced recombinative desorption (CIRD) of O_{ad} from Rh(111) using Ar⁺ ions from a commercial sputter gun. We show that with proper selection of the Ar⁺ energy and electronic bias of the metal surface, O_{ad} can be removed leaving behind a cleared Rh(111) surface still charged with O_{sub}. We characterized the surface with a combination of structural probes (LEED, STM) and temperature programmed desorption to quantify total oxygen and Auger electron spectroscopy for the surface coverage.

SS-TuP4 Adsorption and Oxidation of n-Butane on the Stoichiometric RuO₂(110) Surface, Tao Li, R. Rai, Z. Liang, University of Florida, Gainesville; *M. Kim*, *A. Asthagiri*, Ohio State University; *J.F. Weaver*, University of Florida, Gainesville

The surface chemistry of late transition-metal (TM) oxides has drawn significant attention due to the observation and prediction of facile C-H bond cleavage of molecularly adsorbed n-alkanes at low temperatures. Previous studies have shown that PdO(101) readily promotes the dissociation of alkanes by a mechanism in which adsorbed σ -complexes serve as precursors to initial C-H bond cleavage. Density functional theory (DFT) calculations further predict that the formation and facile C-H bond activation of alkane σ -complexes should also occur on RuO₂ and IrO₂ surfaces, suggesting that the σ -complex mechanism is a common pathway for alkane activation on late TM oxides.

In this study, we investigated the adsorption and oxidation of n-butane on the stoichiometric RuO₂(110) surface using temperature-programmed reaction spectroscopy (TPRS) and DFT calculations. At low coverage, molecularly adsorbed n-butane achieves a binding energy of ~100 kJ/mol on RuO₂(110), consistent with a strongly bound σ -complex that forms through dative bonding interactions between the n-butane molecule and coordinatively unsaturated (cus) Ru atoms. We find that a fraction of the n-butane reacts with the RuO₂ surface during TPRS to produce CO, CO₂, and H₂O that desorb above ~400 K and present evidence that adsorbed σ -complexes serve as precursors to the initial C-H bond cleavage and ultimately the oxidation of n-butane on RuO₂(110). From measurements of the product yields as a function of surface temperature we estimate that the initial reaction probability of n-butane on RuO₂(110) decreases from 9% to ~4% with increasing surface temperature from 280 to 300 K and show that this temperature dependence is accurately described by a precursor-mediated mechanism. From kinetic analysis of the data we estimate a negative, apparent activation energy of -35.1 kJ/mol for n-butane dissociation on RuO₂(110) and an apparent reaction prefactor of 6×10^{-8} . The low value of the apparent reaction prefactor suggests that motions of the adsorbed n-butane precursor are highly restricted on the RuO₂(110) surface. DFT calculations confirm that n-butane forms strongly bound σ -complexes on RuO₂(110) and predict that C-H bond cleavage is strongly favored energetically. The n-butane binding energies and energy barrier for C-H bond cleavage predicted by DFT agree quantitatively with our experimental estimates. Our results support the idea that the σ -complex mechanism is a common pathway for alkane activation on late TM oxide surfaces that expose pairs of cus metal and oxygen atoms.

SS-TuP5 Step-type Dependence of Water Desorption from Single-Crystalline Ag Surfaces, Sabine Auras, Leiden University, Netherlands; *J. Janlamarol*, Chulalongkorn University, Bangkok

Many heterogeneously catalyzed reactions have been shown to be strongly structure dependent.^[1] Catalytically active materials can feature a wide spectrum of defect densities on the same sample and may include various step types.^[2] Thus, curved crystals with continuously changing average step densities provide a good alternative to flat single crystals for the investigation of surface structure dependencies.^[3] In this study we use two curved Ag single crystals to exemplify the strength of this approach to studying structure dependencies. The crystals have two different apex orientations. One Ag crystal with a [111] apex contains two different step sites on either side of the center, generally referred to as the (100) and (111) or A and B step types. The step density gradually increases until at

Tuesday Evening Poster Sessions, November 8, 2016

the edges of the crystal we reach 5-atom wide (111) terraces. The crystal with the [100] apex has only one step type, that resembles the B step type from the first crystal, but has adjacent (100) terraces. We study the surface structure of the clean crystals with LEED and STM and show that the surface behaves as may be expected with single-atom high steps.

Subsequently, water adsorption to the steps and their effect on the water-metal interface are investigated using spatially resolved Temperature Programmed Desorption. As Ag binds water only weakly, effects resulting from the available steps are expected to be rather small. We show how the different step types affect the desorption of water and how it would be nearly impossible to measure the effects using multiple flat Ag samples.

1. Somorjai, G.A. The structure sensitivity and insensitivity of catalytic reactions in light of the adsorbate induced dynamic restructuring of surfaces. *Catal. Lett.* **1990**, 7, 169–182.

2. Walter, A.L.; Schiller, F.; Corso, M., et al. X-ray photoemission analysis of clean and carbon monoxide-chemisorbed platinum(111) stepped surfaces using a curved crystal. *Nat. Commun.* **2015**, 6, 8903.

3. (a) Besocke, K.; Krah-Urban, B.; Wagner, H. Dipole moments associated with edge atoms; A comparative study on stepped Pt, Au and W surfaces, *Surf. Sci.* **1977**, 68, 39–46.

(b) Hopster, H.; Ibach, H.; Comsa, G. Catalytic oxidation of carbon monoxide on stepped platinum(111) surfaces, *J. Catal.* **1977**, 46, 37–48.

(c) Pluis, B.; van der Gon, A.W.D.; Frenken, J.W.M.; van der Veen, J.F. Crystal-Face Dependence of Surface Melting, *Phys. Rev. Lett.* **1987**, 59, 2678–2681.

SS-TuP6 Topographical Changes of Liquid-Metal Alloys as a Function of Temperature, *Nelson Bello*, University of Massachusetts, Boston; *I. Tevis*, SAFI-Tech; *M. Thuo*, Iowa State University; *M. Foster*, University of Massachusetts, Boston

Gallium-indium metal alloys are remarkable materials that, at the eutectic composition, are liquid at room temperature and form a very thin (0.7 nm) passivating oxide film on the surface. This makes them valuable in the field of molecular electronics as soft conformal electrical contacts and as, potentially, self-repairing wires. For this project, EGaln is put through a fluidic shearing process that produces 3-layered core-shell nano/micro-spherical particles composed of a chemisorbed organic outer layer on an oxide film around the liquid metal core that prevents their coalescence. We used Atomic Force Microscopy (AFM) and Scanning Electron Microscopy (SEM) to monitor topographical changes in these particles as a function of temperature. The liquid metal has a different rate of expansion from the oxide shell, and AFM coupled with SEM are especially well-suited to monitor these changes both as a function of the rate of change of the temperature and the thickness of the oxide film. The nature of the external coating can also be tuned through exposure of the particles to strong oxidants or shearing the metal in the presence of different surfactants. The effect of the different film coatings and the expansion of the particles upon application of heat will be discussed.

SS-TuP7 Interaction of Ethylene with Partially Chlorinated RuO₂(110) Surfaces, *Zhu Liang*, *T. Li*, *R. Rai*, *J.F. Weaver*, University of Florida

Partial replacement of surface oxygen atoms with chlorine atoms may provide a means for modifying the activity and selectivity of oxide surfaces toward hydrocarbon oxidation. In this study, we investigated the adsorption and oxidation of ethylene on partially chlorinated RuO₂(110) surfaces using temperature programmed reaction spectroscopy (TPRS) and X-ray photoelectron spectroscopy (XPS). Chlorination of the RuO₂(110) surface occurs when exposing the stoichiometric surface to gaseous HCl at 700 K, where the bridging oxygen atoms are selectively replaced by chlorine atoms. The degree of chlorination is controlled by the amount of HCl gas introduced, and characterized by XPS. Compared with stoichiometric RuO₂(110), we find that bridging Cl atoms weaken the binding and suppress the oxidation of ethylene, without shifting the selectivity toward partially oxidized products. We also find that on-top oxygen atoms significantly enhance the activity of both s-RuO₂(110) and chlorinated RuO₂(110) surfaces toward the complete oxidation of ethylene. The enhanced reactivity arises from an increase in the ethylene coverage achieved on the O-rich surfaces as well as more facile C–H bond cleavage of ethylene via H-transfer to on-top vs. bridging oxygen atoms. Our results provide evidence that ethylene molecules achieve high coverages on the O-rich surfaces by preferentially binding to stranded Ru sites located between on-top oxygen atoms, and that such configurations are responsible for the high activity of the O-rich RuO₂ and RuO_xCl_y surfaces. These findings demonstrate that the relative reactivity of on-top vs. bridging oxygen

atoms plays a decisive role in determining the chemical activity of partially-chlorinated RuO₂ surfaces, and that high reactivity can be achieved on O-rich RuO_xCl_y surfaces.

SS-TuP8 Supramolecular Assemblies of Halogenated Molecules on the Si(111) v3xv3-Ag and Cu(100) Surfaces, *Renjie Liu*, Lakehead University, Canada; *C. Fu*, *A.G. Moiseev*, *D.F. Perepichka*, McGill University, Canada; *M.C. Gallagher*, Lakehead University, Canada

The surface-confined assembly of two-dimensional (2-d) covalent organic frameworks (COF) has gained much attention [1]. One approach to COF formation is the adsorption of halogenated aromatic precursors onto a noble metal surface, followed by dehalogenation of the precursors, and subsequent covalent coupling. We have studied the adsorption of a halogenated organic molecule, 2,4,6-tris(4-iodophenyl)-1,3,5-triazine (TIPT), on both the Cu(100) and Si(111)-v3xv3-Ag surfaces by scanning tunneling microscopy (STM). Recently, we found that the Si v3–Ag surface can provide an inert, high-mobility template for the adsorption of halogenated organic molecules [2].

STM images reveal that TIPT monomers are quite mobile on the Cu(100) surface at room temperature. At low coverage, molecules readily migrate and accumulate at step edges. We observe very few supramolecular features at the surface, and these structures often decompose after repeated STM scanning. In contrast to the as deposited samples, after annealing to 420°K more robust open pore structures are observed. The structure and size of these molecular frameworks are consistent with covalent linking. We have also studied TIPT adsorption on the v3-Ag surface. The structure of these films as a function of coverage and annealing temperature will be discussed.

1. D.F. Perepichka, and F. Rosei, *Science* **323**, 216–217 (2009).

2. R. Liu et al., *Surf. Sci.* **647**, 51–54 (2016).

SS-TuP9 Synthesis and Reduction of Graphene Oxide, *Heike Geisler*, *J.M. Bacher*, *N.A. LaScala*, SUNY College at Oneonta

Graphite oxide was successfully synthesized from graphite powder using the modified Hummers method*. The graphite oxide was then exfoliated to yield graphene oxide which was subsequently reduced to give reduced graphene oxide. This employed two different chemical reduction methods, and one effective combination of the two. The two methods being a weaker sodium borohydride/calcium chloride catalyst and a hydrogenation through hydrogen produced from the reaction of hydrochloric acid and aluminum. This can be seen through the removal of various functional groups from our graphene oxide sample after each reduction method, as shown in FTIR spectra of each sample. While the reduction methods employed did remove a number of oxygenated functional groups on the graphene oxide sheet, we still observe the presence of hydroxyl and some carboxylic acids that persist through. We also notice the appearance of a well-defined peak at ~1600 cm⁻¹ representing the conjugated system in the combined reduction method.

* *W. S. Hummers and R. E. Offeman, J. Am. Chem. Soc., 1958, 80, 1339*

SS-TuP10 Nanomechanical Properties of Eutectic Gallium-Indium Particles by Atomic Force Microscopy, *Syeda Akhter*, University of Massachusetts, Boston; *I. Tevis*, SAFI-Tech; *M. Thuo*, Iowa State University; *M. Foster*, University of Massachusetts, Boston

Eutectic Gallium-Indium (EGaln) alloy is a liquid metal at room temperature that, under air, forms a passivating native thin (~0.7 nm) oxide layer. This oxide layer plays an important role in the overall mechanical properties of the alloy. The metallic and physical properties of EGaln make it effective at conducting, and dissipating, heat away from temperature sensitive components. Being a deformable liquid metal, EGaln is consistently electrically conductive even when a supporting polymeric channel is excessively stretched. EGaln particles, with a liquid core and a thin oxide shell, are created with diameters that range from 6.4 nm to >10 µm using fluidic shearing. The mechanical properties, such as the flexibility of the oxide shell, especially on nano- and micro-particles, are unknown. Atomic Force Microscopy, however, is a versatile instrument for imaging surface topography as well as for characterizing material properties, such as elasticity and film thickness at the micro- and nanoscale via force-distance curves (F-D curves). F-D curves are the result of interactions, upon contact, between an AFM tip and the surface of the sample due to the elastic force of the cantilever and values can be measured with resolutions up to piconewtons. This poster describes our studies on mechanical properties of EGaln thin film and particles of various sizes via AFM F-D curves.

Tuesday Evening Poster Sessions, November 8, 2016

SS-TuP11 Reactivity of CO₂ at Single-site Vanadium in Metal-Organic Coordination Networks at Surfaces, *C. Tempas, B. Cook*, Indiana University; *David Wisman*, Indiana University; *NAVSEA Crane; T. Morris, A. Polezhaev, D. Skomski, K. Smith, K. Caulton, S.L. Tait*, Indiana University

Driven by growing concern of the effect of greenhouse gases on the environment, CO₂ chemistry has become an increasingly active area of research. The interaction of CO₂ with metal-organic complexes offers opportunities for CO₂ recycling, but those chemistries have not been developed in surface catalysts, which could offer much higher efficiency. We have developed a prototypical metal-organic network that shows chemical activity toward CO₂ by co-depositing bis-pyridinyltetrazine (DPTZ) and metallic vanadium on a Au(100) surface. These organize at room temperature into highly-ordered one-dimensional metal-organic chains. We characterized the assembly by high-resolution scanning tunneling microscopy. The chains align in specific orientations relative to the underlying gold surface due to their interaction with the gold. The assembly occurs by a redox-active self-assembly process, in which the vanadium oxidizes to the +2 state and there is corresponding reduction of the ligand, as observed by X-ray photoelectron spectroscopy. Exposure to CO₂ gas leads to a shift in the vanadium oxidation state to +4; the shift is gradual with increasing CO₂ exposure. The 1D chains generally remain intact during the CO₂ exposure, but become somewhat less ordered with increasing exposure time. Following gas exposure, the surface was annealed at various temperatures. At annealing temperatures of 250 °C and greater we observe desorption of the ligand and the shift of vanadium back to the +2 state, indicating a residual vanadium-oxo species on the surface. Developing single-site metal center surfaces systems with chemical activity toward CO₂ may lead to the development of new methods for CO₂ capture and recycling, as well as providing more general insight into the development of next-generation catalysts.

SS-TuP12 CO₂ Optical Phonons for Constraining Mixing in Interstellar Ices, *Ilsa Cooke*, University of Virginia; *K.I. Öberg*, Harvard University

CO₂ is an important ice species in interstellar environments, often the second most abundant ice after H₂O. Astronomical infrared spectra of interstellar objects have revealed abundant CO₂ in a variety of protostellar environments as well as in cold dark clouds. The CO₂ ν₂ band has been used as a tracer of thermal processing due to its dependence on the ice temperature and local environment; however, there are still uncertainties involved in fitting the laboratory ν₂ band to astronomical spectra. We report laboratory spectra of the CO₂ longitudinal optical (LO) phonon mode for a series of CO₂ ices at low temperature and for ice mixtures with polar (H₂O) and non-polar (CO, O₂) components. We show that the LO phonon mode is particularly sensitive to the mixing ratio of various ice components of astronomical interest. These spectra may be useful in constraining the bulk environment of CO₂ in astronomical ices as well as for tracing ice mixing in laboratory experiments.

SS-TuP17 Probe the Degradation Mechanism of Hybrid Perovskite by In Situ DRIFTS, *Q. Peng, X. Yu, Amanda Volk*, University of Alabama

Methylammonium Lead Iodide Perovskite (MAPbI₃) is a promising photoelectronic material for photovoltaics and LEDs. However, the stability of MAPbI₃ under the external application environments is a big concern. The underlying mechanism of decomposition of MAPbI₃ is not well understood yet. In this poster, we will use *in-situ* Diffuse reflectance infrared fourier transform spectroscopy for the first time to understand the surface reaction mechanism in the decomposition of MAPbI₃ in various related applications environments. With the unique setup and high-surface-area configuration, our results showed that the degradation rate is strongly affected by the temperature and chemical composition of the application environments. The degradation mechanism of MAPbI₃ changes with the application environments. Our results provide a fresh view of the degradation pathways of MAPbI₃ and will help optimize the synthesis of MAPbI₃ and provide potential solutions for stabilizing MAPbI₃.

SS-TuP19 Interaction of Atomic Oxygen with Ag(111) and Ag(110) Surfaces: Oxygen Adsorption at Surface versus Subsurface, *Sara Isbill, S. Roy*, University of Tennessee, Knoxville

While transition metals are commonly used to catalyze the oxidation of small organic compounds, the mechanisms of these reactions are not yet completely understood. Silver surfaces are important industrial catalysts for the partial oxidation of ethylene to ethylene oxide and methane to methanol. While significant strides have been taken towards revealing the complex chemical pathways of oxidation reactions by silver surfaces, several aspects of the catalysis, particularly the different ways in which oxygen interacts with the silver surface have yet to be elucidated. This

understanding is critical to determine the catalytically active oxygen-silver species that interacts with the reactants. It is also important to know how these active species change with reaction conditions, such as surface structure, surface temperature, and oxygen coverage, such that the conditions can be tuned to design the most effective catalysts. In the present study, density functional theory (DFT) was used to probe atomic-oxygen adsorption at the surface and subsurface of Ag(111) and Ag(110) surfaces. The main goal was to investigate the competition between surface and subsurface oxygen at different oxygen coverages, and study their participation in oxidation catalysis by silver surfaces. On the Ag(111) surface, it was found that adsorption energies for all surface and subsurface sites decreased with coverage; however, surface adsorption was compromised much more than subsurface adsorption. This difference causes a flip in preference from surface adsorption at low coverages to subsurface adsorption at high coverages. Calculated potential energy curves of oxygen moving from surface to subsurface on Ag(111) and Ag(110) show a complex interplay between adsorption energies and energy barriers that is sensitive to monolayer coverage. Results provide valuable insight into the competition between surface adsorption and subsurface adsorption of oxygen on the silver surface, the role of subsurface oxygen in catalysis by the silver surface, and the importance of charge transfer in the adsorption and dynamics of oxygen on the silver surface.

SS-TuP20 Isotope Fractionation Effect in Secondary Ions Mass Spectroscopy Analysis for Boron Quantification, *Yibin Zhang*, GLOBALFOUNDRIES U.S. Inc.

Secondary Ion Mass spectroscopy (SIMS) analysis is heavily used in semiconductor, lighting/LED, solar/PV industries for routine manufacturing and research/development due to its versatility, fast turnaround time and excellent accuracy/precision. There are some factors that affect the accuracy of SIMS quantification. Fractionation is one of them. It is very important for isotope abundance measurement and for applying RSFs from one isotope to another. If fractionation is ignored during SIMS quantification by applying RSFs from one isotope to another, over 10% error could be introduced. Boron is a useful dopant for such semiconductors as silicon, germanium, and silicon carbide. Having one fewer valence electron than the host atom, it donates a hole resulting in p-type conductivity. Then to accurately monitor Boron concentration in semiconductor manufacturing process is very important. In this study, the Boron isotope fractionation was investigated on Cameca IMS WF, Cameca 7f, Quad SIMS. A methodology to quantify Boron was demonstrated by applying RSF from ¹⁰B implanted standard to unknown sample by monitoring ¹¹B.

Vacuum Technology

Room Hall D - Session VT-TuP

VT Poster Session (and Student Poster Competition)

VT-TuP1 Smart Measurement and Diagnostics Module for Dry Vacuum Pumps, *Wan-Sup Cheung, K. Baik, J.Y. Lim*, KRISS, Republic of Korea

This paper addresses recent industrial demands for more reliable predictive maintenance and diagnostics for the failure protection of dry vacuum pumps operated in the semiconductor and flat display chemical processes. Korean leading companies are very expecting to improve the predictive maintenance and self-diagnostics capability sufficient to meet such higher demands for dry vacuum pumps. This project has started to satisfy Korean industrial demands. On the onset of this work, the first technical issue was to examine what kinds of state variables are measured from dry vacuum pumps. Most of them were found to be the static properties such as body and exhaust temperatures, N₂-flow rate, motor supply currents of booster and dry pumps, exhaust pressure, etc. Most vacuum pump manufacturers have reported that most of vacuum pump failures come from their rotating machinery parts such as rotors, bearings and/or gears. It became apparent that reliable self-diagnostics of vacuum pumps cannot be realized without vibration measurement of those rotating parts. A vacuum pump vibration measurement (VPVM) module has been developed to enable the measurement of three vibration harmonics of rotors, bearings and gears. Tested results of the VPVM module are shown to provide harmonic vibration measurements of rotors, bearings and gears. In addition to the

Tuesday Evening Poster Sessions, November 8, 2016

vibration measurement capability of the VPVM module, another technical challenge was to collect the measurements of the state variables available from each vacuum pump via the digital communication interface. This work has attempted to integrate both the traditional state variables and the three harmonic vibration levels into an extended set of state variables required to realize more reliable predictive maintenance and diagnostics of dry vacuum pumps. To obtain the extended state variables, the VPVM module was developed to support three kinds of serial communication ports (RS232C/RS485, CAN and/or SPI) to an individual vacuum pump controller. Furthermore, the VPVM module was designed to provide a 128 MB backup flash ROM to record a time series of the extended state variables in real-time. These records of the extended state variables are used to implement the self-diagnostics and predictive maintenance algorithms of dry vacuum pumps developed and patented by KRISS.

VT-TuP2 Vacuum System of Positron Damping Ring for SuperKEKB, Kyo Shibata, Y. Suetsugu, T. Ishibashi, M. Shirai, S. Terui, K. Kanazawa, H. Hisamatsu, KEK, Japan

SuperKEKB, which is an upgrade of the KEKB B-factory (KEKB), is a next-generation high-luminosity electron-positron collider. Its design luminosity is $8.0 \times 10^{35} \text{ cm}^{-2} \text{ s}^{-1}$, which is about 40 times than the KEKB's record. To satisfy tight requirements on beam quality for positron injection, a new damping ring (DR) with a circumference of 135.5 m is constructed in the positron injection system. For beam quality improvement, the positron beam extracted from an injection linac with an energy of 1.1 GeV stays in the DR for 40 ms. Maximum stored current is 70.8 mA, and the number of bunches is 4.

The DR has two arc sections (~110 m) and two straight sections (~20 m). In the arc sections, walls on both sides of the beam pipes are irradiated with synchrotron radiation (SR, critical energy: ~1 keV). To deal with SR and photoelectrons, the beam pipes in the arc sections have antechambers on both sides of a beam channel. The antechamber is also effective in reduction of the beam impedance. The height of the beam channel in the arc sections is 24 mm and the width including the antechambers is 90 mm. To remove the heat by SR irradiation, a water cooling system is also required in the arc sections. In the straight section, on the other hand, an antechamber structure and a water cooling system are not necessary. The cross-section of the beam pipe is octagon with an inscribed circle diameter of 46 mm.

Required beam lifetime due to residual gas scattering is longer than 1000 sec and averaged pressure should be lower than $1 \times 10^{-5} \text{ Pa}$. In the arc sections, pumping speed should be much larger than that in the straight sections because a major dynamic gas load during the beam operation is photon stimulated desorption by SR. Non-evaporable getter (NEG) pumps are mainly used with auxiliary ion pumps, and the average effective pumping speed in the arc sections is about $0.05 \text{ m}^3 \text{ s}^{-1} \text{ m}^{-1} \text{ (CO)}$ just after NEG activation. If the photon stimulated desorption coefficient drops to below $1 \times 10^{-4} \text{ molecules photon}^{-1}$ by the sufficient SR irradiation (i.e. scrubbing), the target pressure can be achieved even after the average pumping speed reduces by nearly half.

The material of the beam pipes is aluminum alloy. The number of the beam pipes is about 100, and almost all beam pipes are coated with titanium nitride films as a countermeasure against the electron cloud issue. Moreover, the beam pipes in the arc sections have the grooved surfaces on upper and lower sides of the beam channel to reduce the secondary electron yield structurally.

Installation work of the beam pipes will start on May of 2016, and the construction of the vacuum system will finish by the summer of 2017.

VT-TuP3 Testing Pump Speed & Thermal Loading of Titanium Arc-Gettered High Speed (~2,000 m³/s for H₂) Cryoboxes, Ernesto Barraza-Valdez, Tri Alpha Energy

We have a need for very high pump speed for H₂ and D₂ with a finite capacity that can be periodically refreshed. Special pumps are being developed to achieve $S_{\text{H}_2} \sim 2,000 \text{ m}^3/\text{s}$ and $S_{\text{D}_2} \sim 1,500 \text{ m}^3/\text{s}$ with an inlet area of 10 m² that fits within our 15 m³ vessel. The pumps are an array of LN₂ (Liquid Nitrogen) cooled cryoboxes with multifaceted surfaces that are coated with titanium using cathodic-arc gettering. Since these are rather large cryoboxes, ~1m² inlet area each, the standard AVS test dome pump speed method is not practical in our case. This poster will present our own test methods, which are guided by and checked against simulated pump speeds using Molflow+. Additionally, experimental cooling and thermal stress tests will be presented on the cryoboxes and VCR fittings used to make the LN₂ connections between pumps. This will be compared to our simulated cooling and thermal stress analysis.

Tuesday Evening Poster Sessions, November 8, 2016

VT-TuP4 Formation and Characterization of Hydrogenated Amorphous Silicon (a-Si:H) Thin Films Deposited by ECR-CVD with Different RF Powers, Hugo Alvarez, A.R. Santos, J.G. Fo, F.H. Coidin, J.A. Diniz, Universidade Estadual de Campinas, Brazil

Hydrogenated amorphous silicon (a-Si:H) films have been deposited on Si substrates using electron cyclotron resonance (ECR) plasmas. ECR systems are downstream plasma reactors, which allow a separate control of ion energy and ion flux, and can operate at low pressures (1-50mTorr) and can allow reducing sharply ion surface sputtering. A 2.45GHz microwave ECR source generates the plasma at high power (up to 1000W). A 13.56MHz RF power source biases separately the sample chuck. The 2.45GHz ECR source and RF chuck power control the ion flux and ion energy, respectively, allowing low temperature (20°C), low pressure (4mTorr) and low damage chemical vapor deposition (CVD). Due to high discharge power conditions in ECR plasmas, high dissociation degree of silane (SiH₄), gas molecules can be obtained. SiH₄ diluted in 98% of Ar allows low silane concentration in the ECR plasma that, with high degree of dissociation, can reduce the Si-H bond incorporation in the films deposited. Moreover, to optimize the composition and the microstructure of the deposited a-Si:H films, the H incorporation should be kept at less than 20%, depending on RF power source bias. In this work, to study the effects of RF chuck power in the H incorporation into films, different RF powers of 1, 3 and 5W were deposited on silicon substrates, with fixed parameters: ECR power of 500W, pressure of 4mTorr, substrate temperature of 20°C, gas flows of SiH₄ and Ar, 200 and 20 sccm and 20 minutes. The hydrogen incorporation in the films was determined by FTIR (Fourier Transformed Infrared). These films were annealed at 1000°C, during 60s (Rapid Thermal Annealing (RTA) process). Thus, before and after the RTA annealing, for films deposited with RF powers between 1 and 5W: i) The crystalline level of each film, obtained by Raman spectroscopy, changed from totally amorphous film to amorphous and polycrystalline (19.4% - 32.4%) structures; ii) The images from optical microscopy were used to identify the presence of pin holes on the film surfaces. Using scan profiler system, it was extracted the depth (100µm - 2.2µm) and diameter (1800Å - 90 Å) of them. For that, it can be concluded that if the RF power values increases, the crystalline level increases and pin holes dimensions and densities decreases. Considering that the pin holes are generated due to H incorporation into the films, if RF chuck power is higher, the intensities due to Si-H bonds are reduced (extracted from FTIR analyses), indicating the low H concentration into the films. Thus, the a-Si:H films deposited by ECR-CVD that are part of the hybrid solar cells with a-Si:H-p+/c-Si-n++ structures are going to be presented at the conference.

VT-TuP7 Low-carbon Steel Chamber and Double Viton O-ring Sealing for Electron Microscope, In-Yong Park, N.-K. Chung, B. Cho, KRISS, Republic of Korea

Generally, EM(Electron Microscope) consists of an electron beam generation part, beam control part and a specimen chamber. Among them, in order to get a high imaging resolution, condition and function of electron gun are the most important. Firstly, vacuum level of electron gun chamber is maintained properly depends on the method of electron beam generation. Secondly, gun chamber should be shielded from stray magnetic field which influences the electron beam. Lastly, gun chamber had better have adjustable parts for precise alignment of gun position. In this work, we center around on a simple and cheap electron gun structure for EM. For the purpose of it, we adopt the low-carbon steel for gun chamber material and double Viton O-ring for gun chamber sealing, thereby succeeding in making adjustable gun system maintaining UHV(Ultra High Vacuum) condition.

Recently, B. Cho shows that Low-carbon steel (C≤0.2 wt. %) has a sufficiently low outgassing rate for constructing UHV chamber [1]. Low-carbon steel is a soft magnetic material that is relatively inexpensive and has a high magnetic permeability, so it block out the stray magnetic field. O-ring is usually used for motion vacuum part and also possible to align electron gun in high vacuum. Schottky emitter and cold field emitter are used for high resolution EM, however those require the UHV condition for preventing contamination of tip surface. For EM based on Schottky emitter, we designed the electron gun with low-carbon steel and double O-rings which support UHV condition by pumping out the permeated gases between double O-rings. We compared the performance of double Viton O-rings and double Kalrez O-rings experimentally after 150 °C baking process. The Viton material is better than Kalrez in our system and the vacuum pressure of electron gun arrived at ~10⁻⁸ Pa at room temperature. The vacuum pressure is maintained as UHV when the electron gun chamber surface is moved at the double O-ring surface. We applied the

Tuesday Evening Poster Sessions, November 8, 2016

Viton double O-ring electron gun system to commercial EM replacing original electron gun to get EM images. We observed the evaporated gold nano-particles and got the magnification up to 200K. Also, we measured the electron beam current stabilities of extractor and probe beam. We demonstrated that Low-carbon steel and double Viton O-ring can be used for EM with Schottky emitter and show highly magnified images of gold nano-particles. We anticipated that these methods could replace the existing electron gun system of EM, thereby providing a simple structure and reducing the cost of production of EM.

[1] C. Park, T. Ha and B. Cho, J. Vac. Sci. Technol. A 34(2), (2016).

2D Materials Focus Topic

Room 103B - Session 2D+TF-WeM

2D Materials: Growth and Fabrication

Moderator: Masoud Mahjouri-Samani, Oak Ridge National Laboratory

8:00am **2D+TF-WeM1 Synthesis and Characterization of Two-dimensional WSe₂ Grown using Chemical Vapor Deposition**, *Avra S. Bandopadhyay, G.A. Lara Saenz, C. Biswas, A.B. Kaul*, University of Texas at El Paso

Semiconducting Transition Metal Dichalcogenides (TMDCs) have attracted a lot of attention recently, because of their interesting electronic, optical, and mechanical properties [1]. Among large numbers of TMDCs, monolayers of tungsten diselenides (WSe₂) are of particular interest since WSe₂ possesses a direct band gap (~1.6eV) and tunable charge transport behavior, which makes it suitable for a variety of electronic and optoelectronic applications. Direct synthesis of large domains of monolayer WSe₂ and their growth mechanism studies are important steps toward applications of WSe₂. In this work, we have synthesized Tungsten Diselenide via Chemical Vapor Deposition Method using WO₃ powder and Se pellets as the precursors. Selenium was placed at the upstream side of the furnace at a temperature zone of 260-270°C. The temperatures and distances of these two sources were carefully controlled and adjusted. We used silicon with 300 nm thermally grown SiO₂ as the substrate and it was placed at some distance from the WO₃ source. The substrates for growing WSe₂ are put at the downstream side, where the Se and WO₃ vapors were brought to the targeting substrates by an Ar/H₂ (4:1) flowing gas with a flow rate of 120sccm. The pressure was maintained at 5Torr throughout the experiment. The temperatures at the Se source, WO₃ source and Substrates are maintained 260°C, 950°C and 750-850°C respectively. After the growth, the temperature of the furnace was naturally cooled down to room temperature and the samples were taken out for characterization. The size and shape of the as-grown flakes were observed under an Optical Microscope. Raman spectroscopy was used to determine the number of layers by noting the location of the Raman peaks and the relative Raman shift. In this paper we will discuss our work on the synthesis and characterization of 2D WSe₂, where we have also succeeded in forming monolayer structures for electronic device applications.

References:

- [1] A. B. Kaul, *Journal of Materials Research*, vol. 29, pp. 348-361, 2014.
- [2] H.Sahin et al, *Physics Review B*, vol. 87, pp. 1654091-1654096, 2013.

8:20am **2D+TF-WeM2 Reduction of Graphene Oxide by a Selective Surface Modification Process via Chemical Route for Achieving Higher Proportion of Graphene**, *K. Dave*, CSIR Centre for Cellular and Molecular Biology (CCMB), India; *KyungHee Park*, Chonnam National University, Republic of Korea; *M. Dhayal*, CCMB, India

The primary objective of the study was to target the removable of remaining oxygen available as carboxylic acid functionalities from the surface of first level of reduced graphene oxide. Hence, first we describes preparation of highly exfoliated graphene oxide (GO) from graphite which was further reduced by hydrazine and sodium borohydride. Further we used soda lime for removing carboxylic functional group from the surface of reduced GO by decarboxylation. X-ray photoelectron spectroscopic analysis confirm the synthesis of exfoliated graphene oxide by chemically introduced oxygen as -COOH), -OH and C-O-C. A very high % proportion of carbon atoms as carboxylic functionality observed in the synthesized GO whereas the reduction of it with NaBH₄ and Hydrazine significantly reduced it. The use of soda lime had further reduced the carboxylic group in both the NaBH₄ and N₂H₄ reduced GO. Raman spectroscopic analysis showed two distinct peaks of graphene oxide and reduced graphene in Raman spectra which were correlated with breathing mode of sp² atom and graphitic carbonic sp² of carbon atoms. A strong red shift in the G-band position was observed after oxidation of graphite into GO due to increase in the number of layers of graphene whereas the reduced GO by both reducing agent NaBH₄ and N₂H₄ had showed a decrease in the red shift of the D-band. Above finding confirms better conversion of GO into graphene due to increased SP₂ carbon proportion after selective reduction of the GO. In the future we planned to use these materials for biomedical applications.

8:40am **2D+TF-WeM3 Scalable Production of Molybdenum Disulfide-based Biosensors**, *A.T. Charlie Johnson*, University of Pennsylvania **INVITED** We demonstrate biosensor arrays based on CVD-grown molybdenum disulfide (MoS₂) field effect transistors (FETs) coupled to a computationally-redesigned soluble variant of the μ -opioid receptor

(MOR). By transferring dense films of monolayer MoS₂ crystals onto prefabricated electrode arrays, we obtain clean, high-quality FETs that allow reproducible protein attachment. The yield of MoS₂ FETs and biosensors exceeds 95%, with average mobility of 2.0 cm²V⁻¹s⁻¹ (36 cm²V⁻¹s⁻¹) under ambient (in vacuum). An atomic length linker chemistry enables target binding very close to the MoS₂ surface to maximize sensitivity. The biosensor calibration curve for a synthetic opioid peptide target indicates binding affinity that matches values determined using traditional techniques and a limit of detection ~ 3 nM. The combination of scalable array fabrication and rapid readout enabled by MoS₂ transistors offer the prospect of a solid-state drug testing platform for rapid readout of the interactions between novel drugs and their intended protein targets.

9:20am **2D+TF-WeM5 Growth of Graphene on Cubic Silicon Carbide on Silicon Substrates**, *Mehdi Rezaee, G.L. Harris, J. Griffin, C. Taylor*, Howard University; *E. Hu, D. Bell*, Harvard University

Graphene is a two-dimensional sheet of sp² carbon atoms with extraordinary high mobility and quantum properties that makes it a promising candidate for future electronics. Large-scale production of graphene is paramount for the development of graphene-based electronics. This thesis focused on the synthesis and characterization of graphene layers. Two methods were used to grow graphene films. First, graphene films were epitaxially grown on silicon carbide substrates by thermal decomposition of SiC at high temperatures and low pressures. An in-house built reactor consisting of an induction furnace was used to form epitaxial films for electronic applications. Second, chemical vapor deposition was used for direct graphene synthesis on 3C-SiC using copper as a catalyst. In the thermal CVD processes, hydrogen and methane gases were used as precursors. Methane acts as a carbon source, while annealing and cooling were done in a hydrogen environment. Different polytypes of silicon carbide (6H-SiC and 3C-SiC) and their crystal orientations were exploited as substrates to form epitaxial graphene. A hetero-epitaxial 3C-SiC epilayer was first deposited on Si substrate using the chemical vapor deposition technique in the cold wall, low-pressure horizontal CVD reactor. The reactor temperature, argon pressure, flow rate and concentration of different gases (propane, silane, hydrogen and argon) was investigated to control the growth of 3C-SiC and graphene sublimation rate. The resulting graphene films were confirmed using Raman spectroscopy. Further, graphene films have been characterized with the tools of atomic force microscopy (AFM) and scanning electron microscopy (SEM). Mobility, electrical resistivity and carrier density measurements were taken using Hall effect measurements.

This work was supported by the STC Center for Integrated Quantum Materials, NSF Grant No. DMR-1231319 and the PREM NSF Program.DMR-1205608 grant.

9:40am **2D+TF-WeM6 Growth of Graphene on Cu Single Crystal Substrates**, *Tyler Mowll*, University at Albany-SUNY; *Z.R. Robinson*, College at Brockport-SUNY; *C.A. Ventrice, Jr.*, SUNY Polytechnic Institute

Copper foils are frequently used to grow single-layer graphene by chemical vapor deposition (CVD). The primary reasons for this are the low costs of the Cu foils, the low solubility of carbon in Cu, and the relatively low cost of the equipment needed to grow the films. However, the polycrystalline nature of Cu foils can lead to numerous crystalline defects in the graphene, resulting in a reduction in the transport properties. To provide a systematic study of the CVD graphene growth process, a study of the growth of graphene on single crystal Cu substrates, with terminations along the (100), (110), and (111) planes, was performed. Synthesis was performed in an ultra-high vacuum (UHV) chamber using a modified setup to allow growth at pressures as high as 1 Torr. Ethylene was used as the precursor gas. To control Cu sublimation at the elevated growth temperatures, an Ar overpressure was used. This arrangement allowed for the preparation of clean Cu surfaces by sputtering and annealing the Cu crystals in UHV, followed by graphene growth at low pressure, and analysis with low energy electron diffraction in UHV without breaking vacuum. This avoided exposure of the crystal to atmospheric contaminants. It was found that surface termination plays a strong role in the rotational alignment of the nucleating graphene grains and the decomposition rate of the ethylene. It was observed that single-domain epitaxy is possible on Cu(111) when the ethylene pressure is 5 mTorr or less. However, growth on both Cu(100) and Cu(110) result in a minimum of two domains. In addition, ex-situ EELS is currently being performed on well-ordered epitaxial graphene films grown on Cu(111) and Cu(100) to determine the effect of the graphene-Cu interaction on the electronic properties of the graphene.

Wednesday Morning, November 9, 2016

11:00am 2D+TF-WeM10 Atomic Layered Large Area Growth of 2D Monolayers Over Different Substrates, Joseph Waters, S. Garg, S. Balci, S. Kim, P. Kung, University of Alabama

Atomically-thin transition metal dichalcogenides (TMDCs) such as molybdenum disulfide (MoS_2) and tungsten disulfide (WS_2) are of great interest because of their unique semiconducting and optical properties. For example, unlike graphene, MoS_2 is a semiconductor whose band gap changes from indirect (~ 1.2 eV) to direct (~ 1.85 eV) as the material thickness reduces from bulk to a monolayer state. This makes MoS_2 promising for numerous optoelectronic and biosensing applications. TMDC monolayers have originally been realized through exfoliation. However, the ability to synthesize monolayers over larger areas than those achievable with exfoliation requires scalable techniques such as chemical vapor deposition.

Here, we report the large area growth of monolayer thin films of TMDCs, such as MoS_2 and WS_2 , by low-pressure chemical vapor deposition in an oxygen-free inert argon atmosphere. The growth of these materials has been compared on various substrates, such as basal plane sapphire, (001) SiO_2/Si , and GaN/sapphire substrates. The effects of growth conditions, including growth temperature, on the characteristics of the resulting material have been studied. The physical properties of the monolayers have been characterized using electron microscopy and atomic force microscopy to study their topology over the various substrates, in conjunction with confocal micro-Raman and micro-photoluminescence spectroscopy to correlatively assess their optical characteristics. The terahertz time domain spectroscopy of MoS_2 and WS_2 monolayer thin films will also be presented. We will further discuss the impact of these monolayer materials for robust optoelectronic device applications.

11:20am 2D+TF-WeM11 Growth of Doped Graphene from Fullerene Precursors, X. Fei, J. Neilson, V. Lopez, California State University Northridge; H.J. Gao, Chinese Academy of Sciences, People's Republic of China; L. Gan, Peking University, People's Republic of China; Li Gao, California State University Northridge

Heteroatom-doped graphene materials have potential applications in electronic devices, energy storage and conversion systems, and gas storage. Chemical doping with various heteroatoms is an effective strategy for tuning the properties of graphene in order to expand its applications. Toward the practical applications as well as fundamental studies of doped graphene materials, it is an urgent task to explore effective approaches to synthesize these materials with a high level of control over their doping properties. In this talk, we will discuss the synthesis of heteroatom-doped graphene materials from fullerene precursors. Initial success has been achieved on the iridium and ruthenium surfaces. The growth process and the properties of grown doped graphene materials are characterized by using scanning tunneling microscopy on the atomic scale. We will discuss how the growth process and the properties of grown doped graphene depend on precursor/metal systems and experimental conditions. This new synthesis approach is an important complement to the existing strategies for the preparation of heteroatom-doped graphene.

11:40am 2D+TF-WeM12 Evaluation of Precursor Chemistry for Controllable Growth of Molybdenum Disulfide by Pulsed Chemical Vapor Deposition, Berc Kalanyan, J.E. Maslar, W.A. Kimes, B.A. Sperling, E. Garratt, B. Nikoobakht, R. Beams, S.J. Stranick, A.V. Davydov, National Institute of Standards and Technology (NIST)

Layered two dimensional (2D) transition-metal dichalcogenides (TMDs), e.g., MoS_2 , are of increasing interest for next-generation nanoelectronic and optoelectronic devices due to their thickness dependent optical and electrical properties. For many applications, high volume manufacturing of devices based on TMDs will require deposition techniques that are capable of reproducibly growing wafer-scale films with monolayer control. To date, TMD deposition processes largely rely on powder vaporization and transport, with minimal control over precursor fluxes and chemistry. A detailed understanding of metal and chalcogen precursor chemistry in relation to film properties remains an important step toward the design of highly-controllable deposition processes suitable for large-scale 2D synthesis.

We aim to identify promising chemistries for chemical vapor deposition (CVD) processes for TMDs. We focus on MoS_2 CVD using organometallic and organosulfur compounds in a research grade single-wafer deposition system equipped with *in situ* optical diagnostics. The precursor flux is measured using optical mass flow meters installed on the delivery lines while deposition chemistry is characterized in the reactor volume above the deposition surface using *in situ* Fourier transform infrared (FTIR)

spectroscopy. As-deposited and annealed films are characterized with *ex situ* techniques, including Raman and photoluminescence spectroscopy, scanning and transmission electron microscopy, and X-ray photoelectron spectroscopy.

Large-area thin films of MoS_2 were prepared from (η^5 -ethylcyclopentadienyl)-dicarbonylnitrosyl molybdenum, cycloheptatriene tricarbonyl molybdenum, bis(ethylbenzene) molybdenum, 1-propane thiol, and diethyl disulfide sources. Film composition and growth rates on SiO_2 and c-plane Al_2O_3 were characterized for each compound as a function of precursor exposure time. Gas phase reaction chemistry and thermal stability of precursors were evaluated using FTIR spectroscopy. The full-width at half-maximum values for in-plane (E_{2g}^1) and out-of-plane (A_{1g}) Raman modes for MoS_2 were used as indicators of film quality. By relating film properties to gas-phase chemistry for various metal precursors, we will highlight precursor design and process conditions that lead to high quality CVD films.

12:00pm 2D+TF-WeM13 In-situ Scanning Tunneling Microscopy Studies of Chemical Vapor Deposition of hexagonal Boron Nitride Monolayers on Pd(111), Pedro Arias, A. Ebnonnasir, F. Fankhauser, University of California at Los Angeles; C. Ciobanu, Colorado School of Mines; S. Kodambaka, University of California Los Angeles

Using *in-situ* ultra-high vacuum variable-temperature scanning tunneling microscopy (STM), we investigate the chemical vapor deposition kinetics of hexagonal boron nitride (hBN) monolayer growth on Pd(111) substrates as a function of substrate temperature, borazine flux, and deposition time. All of the experiments were carried out on sputter-deposited Pd(111)/ Al_2O_3 (0001) thin films. In each experiment, STM images were acquired while resistively heating the Pd(111) samples on the STM stage at temperatures between 300 K and 773 K and in the presence of borazine ($10^{-7} \sim 10^{-6}$ Torr) for times between 60 s and 2500 s. We observe the nucleation and growth of chemisorbed (and presumably partially dissociated) borazine islands on the Pd surfaces. From the STM images, we measured the island density and size as a function of time, temperature, and borazine flux. We find that both the island density and size increase with increasing borazine flux and deposition time. We also find that borazine islands form on Pd(111) 'up-steps.' After achieving monolayer coverage of borazine, the samples are annealed in ultra-high vacuum at 1020 K for 60 seconds to form hBN monolayers. We then determined of the number density of rotational domains in the hBN layers, based upon which we identify the deposition parameters critical to the growth of single-domain hBN layers on Pd(111).

Actinides and Rare Earths Focus Topic Room 103C - Session AC+MI-WeM

Magnetism, Complexity, and Superconductivity in the Actinides and Rare Earths (8:00-11:00 am)/Actinide and Rare Earth Theory (11:00 am-12:20 pm)

Moderators: Tomasz Durakiewicz, Los Alamos National Laboratory, Ladislav Havela, Charles University, Prague, Czech Republic, Alexander Lichtenstein, University of Hamburg

8:00am AC+MI-WeM1 Local Magnetic Properties of Uranium Compounds Probed with XMCD, Fabrice Wilhelm, A. Rogalev, ESRF, France INVITED

In these last years actinides and actinide compounds, mainly Uranium based compounds, have been the subject of increasing interest due to their very different magnetic behaviors, such as Pauli paramagnetism, localized and itinerant magnetism, and heavy fermions. The element specific X-ray Magnetic Circular Dichroism (XMCD) spectroscopy technique has been proven over two decades to be the best suitable technique to probe the orbital and spin magnetism and to isolate those different contributions separately using the magneto-optical sum-rule under given assumption regarding the magnetic dipole contribution. XMCD experiments have been reported for a great number of uranium compounds and have permitted to understand which is the ground state. It has also revealed differences between localized and itinerant systems that are not yet fully understood. This talk reviews recent advances in use of polarized x-rays to study local magnetic properties and electronic structure of uranium based compounds.

Wednesday Morning, November 9, 2016

8:40am **AC+MI-WeM3 Neutron and X-ray Scattering as a Probe of Complex Order in Actinides, Helen Walker**, STFC, UK **INVITED**

Neutron and X-ray scattering are powerful probes of complex ordering in the actinides, giving access to the spatial and temporal fluctuations of structural and electronic degrees of freedom. To demonstrate the vast array of different types of information obtainable using different scattering techniques, I will focus on the question of the elusive hidden order parameter in URu_2Si_2 .

Innumerable different theories have been proposed for the nature of the hidden order [1], with a preponderance directed towards multipolar order. With this in mind I will discuss how X-ray Resonant Elastic Scattering has shown that no quadrupolar ordering is present [2], and future opportunities for probing higher order multipoles. I will also discuss the valence state, which is of vital significance for any multipolar model, and how this might be investigated by probing the f-states at the M-edges using Resonant X-ray Emission Spectroscopy.

More recently, there is a growing consensus pointing towards some electronic nematic state, resulting in an orthorhombic distortion [3,4,5]. Inelastic neutron and X-ray scattering experiments, which have searched for a change in the band structure associated with such a distortion, will be discussed.

[1] J.A. Mydosh and P.M. Oppeneer, *Rev. Mod. Phys.* **83**, 1301 (2011)

[2] H.C. Walker, *et al.*, *Phys. Rev.* **B83**, 193102 (2011)

[3] R. Okazaki, *et al.*, *Science* **331**, 439 (2011).

[4] S. Kambe, *et al.*, *Phys. Rev. Lett.* **110**, 246406 (2013).

[5] S. Tonegawa *et al.*, *Nat. Comms.* **5**, 4188 (2014)

9:20am **AC+MI-WeM5 Hydrogen Contributing to 5f-localization in UTX Compounds, Silvie Maskova**, Charles University in Prague, Czech Republic; K. Miliyanchuk, Ivan Franko National University of Lviv, Ukraine; S. Danis, B. Vondrackova, Charles University in Prague, Czech Republic; O. Stelmakhovych, Ivan Franko National University of Lviv, Ukraine; L. Havela, Charles University in Prague, Czech Republic

U-based ternary compounds, which were studied in large isostructural series, allow large variations of the 5f localization due to variable 5f-5f overlap and the 5f hybridization with the d- and p-states. An additional tuning parameter is the H absorption, working primarily as a negative pressure. At 5f-band systems it leads to enhancement of magnetic properties in most of cases [1]. However, this tool is restricted to cases in which substantial H absorption can be achieved. In the system of UTX compounds (T = later transition metal, X = p-metal) with the ZrNiAl structure type, a high absorption was registered only for UNiAl , leading to $\text{UNiAlH}_{2.3}$, in which the Neel temperature is enhanced from 19 K to 95 K. Recently we discovered a new UTX compound, UNiZn [2], which is itself non-magnetic, as the 5f-p hybridization is stronger in the case of smaller Zn than for larger Al. This material forms an equivalent hydride, $\text{UNiZnH}_{2.3}$, which is antiferromagnetic (below 50 K). This opened a possibility to study systematically the onset of antiferromagnetism in the system UNiZn-UNiAl and variations of properties of related hydrides. We found that the magnetic order in the precursors sets in between 10 and 30 at.% Al. The Sommerfeld coefficient of electronic specific heat γ increases from 94 mJ/mol.K^2 in UNiZn and reaches 360 mJ/mol.K^2 in the critical area and then it decreases for a higher Al concentration to 164 mJ/mol.K^2 in UNiAl , which is known as a mid-weight heavy fermion. [3]. The hydrides exhibit lower γ -values. $\gamma = 100 \text{ mJ/mol.K}^2$ in the UNiZn hydride decreases monotonously to 67 mJ/mol.K^2 in the hydride of UNiAl . The situation implies that reducing the 5f-p hybridization even more, we may proceed with strengthening of magnetism in the sense of further increasing T_N and decreasing γ . The natural counterpart of UNiAl is UNiGa with the same structure type but larger X-ligand. However, no attempt to synthesize a hydride of UNiGa was successful in the past. In the present work we undertook a study of the hydrides of quasi-ternary system UNiAl-UNiGa [4], and found that the H absorption can be reached even for high Ga concentrations. Physical properties of Ga-substituted hydrides are currently explored.

[1] S. Maskova, L. Havela, E. Santava, and K. Miliyanchuk, *J. of Physics: Conf. Ser.* **200** (2010) 032040.

[2] S. Maskova, S. Danis, K. Miliyanchuk, O. Stelmakhovych, B. Vondrackova, A.V. Kolomiets, L. Havela, *J. Alloys Comp.* **646** (2015) 885-892.

[3] L. Havela, K. Miliyanchuk, A. Kolomiets: *Int.J.Mat.Res.* **100** (2009) 1182-1186.

[4] H. Maletta, V. Sechovsky, P.A. Veenhuizen, F.R. de Boer, L. Havela, and G. Hilscher, *Z.Phys. B – Cond. Matter* **72** (1988) 455-460.

9:40am **AC+MI-WeM6 Radiation damage: Experimental Investigation of Aluminum Containing Helium Bubbles at Static High Pressure in a Diamond Anvil Cell, Itzhak Halevy**, Physics Department; B. Glam, NRC Soreq, Israel; S. Maskova, Charles University, Prague, Czech Republic; D. Moreno, NRC Soreq, Israel; S. Eliezer, NRC Soreq Shalom Eliezer2, Israel

High pressure investigation of the crystallographic structure and bulk modulus of aluminum containing helium bubbles is presented. The targets were obtained by melting pure aluminum with 0.15% wt. ^{10}B powder. The solid targets were neutron irradiated in the Soreq nuclear reactor to get homogeneous helium atoms inside the aluminum boron 10 matrix according to the reaction $^{10}\text{B} + n \rightarrow ^7\text{Li} + ^4\text{He}$. The irradiated aluminum was heat treated for accumulation of helium atoms into nanometric bubbles by diffusion. The helium bubbles formation in $\text{Al-}^{10}\text{B}$ metal was observed by TEM.

The crystallographic structure and the bulk modulus of aluminum loaded up to pressure of 39 GPa in a diamond anvil cell (DAC) were studied in different samples: (1) $\text{Al-}^{10}\text{B}$, (2) Irradiated $\text{Al-}^{10}\text{B}$ with helium bubbles (3) The irradiated $\text{Al-}^{10}\text{B}$ foil with helium bubbles that was used for TEM observation.

The data was analyzed by the X'Pert Plus (Philips) Rietveld analysis software packages. The high-pressure energy dispersive X-ray diffraction studies were taken at the X17-C beam-line of the National Synchrotron Light Source (NSLS) at BNL [1]. The energy dispersive data was collected with a high purity germanium detector at a fixed Bragg angle ($2\theta \approx 12^\circ$). The high-pressure X-ray powder diffraction measurements were taken at discrete pressure steps in the range of 0–35 GPa. The data was collected by the EDS technique, using the white beam of the superconducting wiggler magnet at the X17-C beam-line. Typical data collection time was about 10 min. In the lower range of the high-pressure range, angle dispersive measurements were carried out in transmission configuration using the image plate technique. The data was analyzed using a commercial Rietveld analysis software packages [2].

The Pressure as function of V/V_0 was fitted by Vinet equation to yield the B_0 and B_0' of the EOS. B_0 and B_0' are the bulk modulus and its pressure derivative at the equilibrium volume V_0 at zero pressure. For our pure Al $B_0=68.6 \text{ GPa}$ while B_0' was kept at 3.6.

Our early work with SEM and TEM showed He bubbles as the sample was irradiated.

Quantum Design SQUID equipment was used for magnetic studies of bulk Al-15wt.\% B and pure Al. Magnetic measurements were performed in the temperature range 2-300 K and fields up to 7 T.

Results of the susceptibility measurements, $c(T)$, are summarized. The susceptibility is field independent in the whole temperature range studied. All “samples” have similar weak temperature dependence, with c-values somewhat below $1 \cdot 10^{-10} \text{ m}^3/\text{mol}$.

References

[1] Hu, J.: High pressure X-ray beam line X17C. www.bnl.gov/x17c. Updated 07/01/2007

[2] Rietveld, H.M.: *J. Appl. Crystallogr.* **2**, 65 (1969)

11:00am **AC+MI-WeM10 AVS Gaede Langmuir Award Talk: Multiplets and More for Core-Level Spectra, Paul Bagus***, University of North Texas **INVITED**

Multiplets are an essential aspect of electronic spectroscopies and they must be taken into account to correctly describe these spectra. In particular this is true for the core-level spectra of open-shell systems including both X-Ray Photoelectron Spectroscopy, XPS, and Near-edge X-Ray Adsorption Fine Structure, NEXAFS. Unfortunately, the significance of multiplets for the interpretation and analysis of XPS and NEXAFS is often neglected, quite possibly because of the complex mathematical formalism that is required to obtain formal expressions for the multiplets and their energies. In this talk, the focus will be on using the familiar rules for the quantum mechanical addition of angular momentum and for multiplet energies, as given, for example, by Hund's rules, to provide a qualitative guide to the importance of these splittings. The combination of these qualitative guides with rigorous electronic structure calculations of energies and intensities allows us to understand the origins of the XPS and NEXAFS features in terms of the chemical and physical interactions in a

* Gaede Langmuir Award Winner

Wednesday Morning, November 9, 2016

system. This combination also allows us also to understand how ligand field mixings modify atomic descriptions of these core-level spectra. For XPS, we show that the value of multiplet splittings to identify oxidation states depends on the choice of core-level ionized. [1] For NEXAFS, we show that decomposing a spin-orbit split level, or multiplet, into its composition in terms of Russell-Saunders, RS, multiplets gives insight into the origin of the often complex features of the spectra.[2] This is because the selection rules are stricter for the RS multiplets. The role of “shake” excitations from occupied bonding orbitals into un-occupied anti-bonding orbitals will also be considered. Several examples for the spectra of heavy metal oxide systems will be presented to illustrate the value of the methods described.

We acknowledge support for this work by the Geosciences Research Program, Office of Basic Energy Sciences, U.S. DOE.

1. P. S. Bagus, *et al.*, Surf. Sci. **643**, 142 (2016).

2. P. S. Bagus, M. J. Sassi, and K. M. Rosso, J. Electron Spectrosc. Relat. Phenom. **200**, 174 (2015).

11:40am AC+MI-WeM12 Complex Magnetism of Gd Intermetallics: Ab-initio Theory and Experiment., Leon Petit, Daresbury Laboratory, UK; *D. Paudyal, Y. Mudryk, K.A. Gschneidner, V.K. Pecharsky*, Ames Laboratory, Iowa State University; *M. Lueders, Z. Szotek*, Daresbury Laboratory, UK; *J.B. Staunton*, Warwick University, United Kingdom of Great Britain and Northern Ireland

Using an ab-initio electronic structure theory which includes disordered local moments and strong f-electron correlations, we have investigated the magnetic ordering and critical temperatures of Gd-intermetallics.¹ The theory correctly finds GdZn and GdCd to be simple ferromagnets and predicts a remarkably large increase of Curie temperature with pressure (+1.5 K kbar⁻¹) for GdCd, confirmed by our experimental measurements. In our calculations for GdMg, a transition from ferromagnetic to AF1 is observed with increasing pressure, whilst a canted magnetic state is seen to emerge from either the ferromagnetic or anti-ferromagnetic state with lowering the temperature. Replacing 35% of the Mg atoms with Zn removes this transition, in excellent agreement with long-standing experimental data. We conclude that despite being filled and situated at low binding energies, the non-lanthanide metal d-states strongly influence the electronic structure at the Fermi level as well as the magnetic ordering.

¹ L. Petit, D. Paudyal, Y. Mudryk, K. A. Gschneidner, Jr., V. K. Pecharsky, M. Lueders, Z. Szotek, R. Banerjee, and J. B. Staunton, Phys. Rev. Lett **115**, 207201 (2015)

12:00pm AC+MI-WeM13 Thermodynamics of the Doped Sm(Co_{1-x}Fe_x)₅ Alloys: Ab Initio Study, Alexander I. Landa, A. Söderlind, E.A. Turchi, Lawrence Livermore National Laboratory

SmCo₅ (in the hexagonal CaCu₅-type structure) magnets exhibit enormous uniaxial magnetocrystalline anisotropy ($K_1 \sim 17.2$ MJ/m³) substantially higher than for the Nd₂Fe₁₄B (Neomax) magnets ($K_1 \sim 4.9$ MJ/m³), and SmCo₅ magnets have almost twice higher Curie temperature ($T_C \sim 1020$ K) than Nd₂Fe₁₄B magnets ($T_C \sim 588$ K). However the world market of permanent magnets is currently dominated by Neomax magnets (~ 62 %), which possess the highest energy performance with a record energy product of 470 kJ/m³ that is twice as high as the energy product of SmCo₅ magnets, of 231 kJ/m³. Although SmCo₅ magnets are more suitable for high temperature applications than Neomax, due to their relatively low energy performance SmCo₅ magnets occupy only ~ 3% of the world market. From a cost point of view, it would be beneficial to substitute Co atoms with Fe because Fe in the Earth's crust is ~ 2000 times more abundant than Co and consequently much cheaper. In addition, Fe is a ferromagnetic metal with the largest magnetization at room temperature. However SmFe₅ is unstable, and does not appear in the equilibrium Sm-Fe phase diagram. Our presentation show results of *ab initio* Density Functional Theory based on the Exact Muffin-tin Orbital (EMTO) method for the heat of formation of Sm(Co_{1-x}Fe_x)₅ alloys doped with different metals (Me). The Coherent Potential Approximation (CPA) implemented in the *ab initio* EMTO method allows us to gradually substitute the Co atoms by Fe atoms on the Cu-types sites of the CaCu₅-type structure. Previous neutron diffraction studies of Th(Co_{1-x}Fe_x)₅ alloys show that the larger Fe atoms prefer to occupy the 3g-type sites whereas the smaller Co atoms prefer to occupy the 2c-type sites. EMTO-CPA calculations reveal very small region ($x \leq 0.05$) of stability of Sm(Co_{1-x}Fe_x)₅ alloys. The Full-Potential Linear Muffin-tin Orbital (FPLMTO) calculations for SmCo₅ and SmFe₅ end points of SmCo₅-SmFe₅ phase diagram give similar results to those given by the EMTO method. We calculate the heat of formation of the pseudo-binary SmFe₃(Me_{1-x}Co_x)₂ alloys where Fe atoms occupy all the 3g-type sites and the occupation of the 2c-type sites gradually changes from pure Me (SmFe₃Me₂ compound)

Wednesday Morning, November 9, 2016

to pure Co (SmFe₃Co₂ compound) within the CPA. Our calculations show that SmFe₃(Me_{1-x}Co_x)₂ alloys could remain stable until approximately half of Me atoms are substituted by Co atoms. This work performed under the auspices of the US DOE by LLNL under Contract DE-AC52-07NA27344. This research is supported by the Critical Materials Institute, an Energy Innovation Hub funded by the US Department of Energy, Office of Energy Efficiency and Renewable Energy, Advanced Manufacturing Office.

Applied Surface Science

Room 101B - Session AS+SS-WeM

Applications where Surface Analysis is Your Only Hope

Moderators: Jeffrey Fenton, Medtronic, Svitlana Pylypenko, Colorado School of Mines

8:00am AS+SS-WeM1 Accurate Ion Beam Analysis of Electrolytes via Rutherford Backscattering (RBS) and Positive Ion X-ray Emission (PIXE) of Uniform Thin Solid film of Blood congealed via HemaDrop™, Yash Pershad, N.X. Herbots, SiO₂ NanoTech LLC; *C.F. Watson*, SiO₂ NanoTech LLC/Arizona State University Physics Dept; *E.J. Culbertson*, University of California at Los Angeles

Medical diagnostics needs new methods of blood analysis using mL of blood rather than the standard 7 mL to improve care. Theranos has been recently challenged about their “finger-stick method,” where blood drops are used for complete blood diagnostics, not just glucose. They only approved by the FDA for qualitative detection, rather than accurate blood composition. Motivated by these accuracy issues, along with the great need for diagnostics from microliters of blood, we use MeV Rutherford Backscattering Spectrometry (RBS) to measure elemental composition (H, C, N, O, K, Mg, Ca, Na, Fe) in microliters of blood congealed into smooth, planar, Homogeneous Thin Solid Films (HTSF). These planar HTSF of blood are prepared with a new technology that congeal blood drops, called HemaDrop™ [1, 2] Measurements on HTSF prepared via HemaDrop™ are compared and found much more reproducible and accurate than those taken for comparison on dried blood drops, such as the so called “Dried Blood Spot (DBS)” that can only be used in microvolume sampling for drug metabolism, not blood composition. HTSF prepared with HemaDrop™ yields reproducible elemental composition regardless of substrate used or area of analysis with < 6% sampling error. Ion damage from RBS is accounted for via the 0-dose intercept damage curve method, which graphs RBS yield of elements detected, as a function of analysis dose, using several sequential cumulative spectra. Positive Ion X-ray Emission (PIXE) is used to verify the reproducibility and accuracy of RBS. RBS and PIXE analysis on HTSF prepared with HemaDrop™ using 6 microliter of blood are found in excellent agreement within the 6% sampling error. Thus, HemaDrop™ successfully creates homogeneous thin solids film from blood that can be analyzed in vacuum and can also be used for Infrared (IR) spectroscopy and Tapping Mode Atomic Force Microscopy for molecular identification and counting. HTSF enable for the first time blood analysis via vacuum-based methods. IR and TMFAM are also being investigated to add molecular identification and counting.

[1] US Patent Pending, Assignee: SiO₂ NanoTech, Inventors: Herbots, N, Watson CF, Krishnan A, Pershad Y, et al (2016)

[2] Electrolytes Detection by Ion Beam Analysis, in Continuous Glucose Sensors and in Microliters of Blood using a Homogeneous Thin Solid Film of Blood, HemaDrop™. Yash Pershad, Ashley A. Mascareno, Makoyi R. Watson, Alex L. Brimhall, Nicole Herbots, Clarizza F. Watson, Abijith Krishnan, Nithin Kannan, Mark W. Mangus, Robert J. Culbertson, B. J. Wilkens, E. J. Culbertson, T. Cappello-Lee, R.A. Neglia Submitted to MRS Advances, April 2016

8:20am AS+SS-WeM2 Surface Analysis As a Valuable Tool to Study Chemistry of Metals in Environmental Problems, Kateryna Artyushkova, University of New Mexico; *J. Blake*, New Mexico Water Science Center; *L. Rodriguez-Freire, S. Avasarala, A. Ali, A. Brearley, E. Peterson, J.M. Cerrato*, University of New Mexico

This talk will present application of X-ray Photoelectron Spectroscopy to understand the role of chemistry of metals in several environmental problems. In the first study, the chemical interactions of U and co-occurring metals in abandoned mine wastes in a Native American community in northeastern Arizona were investigated using spectroscopy, microscopy and aqueous chemistry. Elevated concentrations of metals are of concern due to human exposure pathways and exposure of livestock currently ingesting water in the area. This study contributes to understanding the

Wednesday Morning, November 9, 2016

occurrence and mobility of metals in communities located close to abandoned mine waste sites. Elevated U (6,614 mg/kg), V (15,814 mg/kg), and As (40 mg/kg) concentrations were detected in mine waste solids. The power of XPS in specific identification of the chemical states of these elements as U (VI), As (-I and III) and Fe (II, III) will be presented.

In the second study, the goal is to investigate the effect of metals associated with wildfire ash from wood collected from the Valles Caldera National Preserve, Jemez Mountains, New Mexico on water chemistry. Metals and other constituents associated with wildfire ash can be transported by storm event runoff and negatively affect water quality in streams and rivers. Microscopy and spectroscopy analyses were conducted to determine the chemical composition of ash. Metal-bearing carbonate and oxide phases were detected through X-ray spectroscopy analyses.

Finally, we integrated spectroscopy, microscopy, diffraction, and water chemistry to investigate the presence of metals in water and sediment samples collected 13 days after the Gold King Mine spill (occurred on August 5, 2015). Spectroscopy, microscopy, and XRD analyses suggest that Pb, Cu, and Zn are associated with metal-bearing jarosite ($\text{KFe}_3(\text{OH})_6(\text{SO}_4)_2$) and other minerals (e.g. clays, Fe-oxides and oxyhydroxides) identified in sediments from Cement Creek, CO. The presence of sulfates and phosphates, Fe as 75% Fe^{2+} and 25% Fe^{3+} , and 100% Pb^{2+} in the near surface region of these sediments was detected by XPS analyses.

Additionally, phosphates and nitrogen species were found with XPS in the sediments from Farmington, NM, downstream the Animas River. The interaction of these metal-bearing minerals with biogeochemical processes occurring downstream could cause metal mobilization into the water.

8:40am AS+SS-WeM3 Surface Analysis Techniques – Hope Springs Eternal, John Newman, S.R. Bryan, D.M. Carr, G.L. Fisher, J.S. Hammond, J.E. Mann, Physical Electronics USA; T. Miyayama, ULVAC-PHI, Japan; J.F. Moulder, D. Paul, Physical Electronics USA; R. Inoue, ULVAC-PHI, Japan; B. Schmidt, Physical Electronics USA

INVITED

In today's technologically advanced laboratories there are many dozens of different, and very specialized, analytical techniques being used to attempt to solve problems and characterize materials. When choosing the proper technique for a particular application, the needs of the study are matched to the attributes of a particular method – its depth of analysis, detection sensitivity, analytical spot size, type of information provided, and whether or not the technique is appropriate for the sample in question. For applications where the region of interest is measured in atomic layers, surface sensitive methods such as Auger Electron Spectroscopy, X-ray Photoelectron Spectroscopy, and Time-of-Flight Secondary Ion Mass Spectrometry have always been the methods of choice and, in most cases, really the only hope for a successful analysis.

However, when we look at the relatively recent technological advances in these three methods, we find that their increased capabilities expand their usefulness to much more than the traditional types of surface experiments. For example, gas cluster beams now allow for intact organic information to be obtained from depth profiles or cross-sectioned samples; higher energy x-ray beams allow for deeper analysis depths compared to traditional XPS x-ray beams; and tandem mass spectrometry technology can provide unambiguous peak identification in TOF-SIMS. This presentation will look at applications where some of these advancements are used; exemplifying how newer technologies are making these techniques our only hope for a much wider array of studies.

9:20am AS+SS-WeM5 What Came First? The Black Ink or the Black Ink? That Is the Question, Robyn E. Goacher, L.G. DiFonzo, K.C. Lesko, Niagara University

Determining the order of deposition of ink markings in questioned documents (forgeries) is an important forensic task. Time-of-Flight Secondary Ion Mass Spectrometry (ToF-SIMS) has received attention as a possible technique for this purpose because it is a surface sensitive technique that can provide chemical images, potentially resolving the top ink from the bottom ink. Furthermore, static SIMS imaging is non-destructive, which is important for the preservation of unique evidence. Prior work demonstrated that ToF-SIMS can correctly determine deposition order of intersections between inks of dissimilar colors¹, and that the order of deposition between fingerprints and ink can be elucidated if the fingerprint is on top of the ink². In order to further test the abilities and robustness of the method, intersections between similar inks need to be examined. In this study, three different black ink samples were tested (BicTM, PapermateTM, and StaplesTM brand pens). Preliminary work produced inconsistent results, and indicated that a more thorough analysis of the

Wednesday Morning, November 9, 2016

primary ions striking the sample and of the polarity of the secondary ions collected needed to be done. Therefore, chemical images of the ink intersections were collected using Ar^{1000+} , Bi_3^+ , and Bi_3^{2+} primary ions, with both positive and negative secondary ion spectra. Data were analyzed using Principal Component Analysis (PCA) and Multivariate Curve Resolution (MCR). Data analysis included consideration of regions of interest as well as full image analysis, with and without restrictions to the secondary ion mass range. The results point to issues regarding incorrect apparent order of deposition, potentially based on the interactions of inks of different types. This brings the forensic use of ToF-SIMS for determining the order of deposition in ink forgeries into question, and points to the need for further research on factors that can result in incorrect apparent deposition orders.

1. A. He, D. Karpuzov and S. Xu, "Ink identification by time-of-flight secondary ion mass spectrometry", *Surface and Interface Analysis*, **2006**, 38 (4), 854-858.

2. N.J. Bright, R.P. Webb, S. Bleay, S. Hinder, N. Ward, J.F. Watts, K.J. Kirby and M.J. Bailey. "Determination of the Deposition Order of Overlapping Latent Fingerprints and Inks Using Secondary Ion Mass Spectrometry", *Analytical Chemistry*, **2012**, 84, 4083-4087.

9:40am AS+SS-WeM6 ToF-SIMS Analysis of Aerospace Topcoat Degradation, Taraneh Bozorgzad Moghim, M.L. Abel, J.F. Watts, University of Surrey, UK

Aircraft coatings are subjected to a multitude of environments during their service life time, including high humidity, extreme temperatures and solar radiation. The major source of degradation derives from ultra-violet (UV) radiation. With commercial aircrafts flying at altitudes between 9 and 13 km, their exposure to UV radiation and ozone significantly increases. Therefore photooxidation of an aircraft topcoat must be understood in order to monitor topcoat degradation. The main laboratory technique used to establish the degradation phenomena from UV radiation is through QUV chambers, however the effect of ozone is not considered in this method. The novelty of the approach used here, is in the use of a desktop cleaner, intended for SEM sample preparation, as the exposure method. This combines the effects of UV and ozone. The topcoat was subject to UV/ozone exposure for varying durations and analysed using time of flight-secondary ion mass spectrometry (ToF-SIMS).

The detail provided by ToF-SIMS is vital in understanding the degradation phenomena and enables a degradation mechanism to be established. ToF-SIMS produces a significant amount of data and therefore when combined with principal component analysis (PCA) a more detailed analysis of the data can be obtained. The main changes observed are the rise of inorganic components with exposure time, as the polymer resin decomposes and the inorganic pigments of the coating are exposed. However this does not describe the degradation of the organic components. Therefore by filtering out the inorganic contributions in the PCA, the changes to the organic components could be isolated and observed. This allows the positive identification of cluster ions of the reactants from the resin and those from the reaction products. In this manner it was possible to deduce the degradation mechanism.

11:00am AS+SS-WeM10 Surface And Bulk: Are They Always The Same? X-Ray Photoelectron Spectroscopy Study, Tatyana Bendikov, D. Barats-Damatov, B. Butschke, J. Bauer, J. Pellegrino Morono, T. Zell, R. Neumann, D. Milstein, Weizmann Institute of Science, Israel

X-ray Photoelectron Spectroscopy (XPS) is a surface sensitive technique (top 10-15 nm) with sensitivity down to single atomic layer. XPS provides unique information about elemental composition and on the chemical and electronic state of the element in the material. The importance of XPS analysis is essential when the top surface and bulk of the material are different in chemical composition and, consequently, in their properties.

We present here two systems where XPS analysis shows significant differences in elemental composition of the top surface, compared to bulk material characterized by various analytical techniques, such as X-ray crystallography, NMR, EPR, Raman and infrared (IR) spectroscopies, etc.

In the first system, influence of temperature on the crystal packing and secondary structure of phosphovanadomolybdic acid, $\text{H}_5\text{PV}_2\text{Mo}_{10}\text{O}_{40}$ was studied.¹ After high temperatures treatment (400-600°C) XPS analysis reveals enrichment of the top surface of the $\text{H}_5\text{PV}_2\text{Mo}_{10}\text{O}_{40}$ by amorphous vanadate/phosphate layer.

In the second system, series of iron-PNN complexes were synthesized and characterized in terms of their stability, elemental composition and metal center oxidation state.²⁻³ Using example of two complexes,

Wednesday Morning, November 9, 2016

$[(t\text{BuPNN})\text{Fe}(\text{NO})_2]^+[\text{BF}_4]^-$ and $[(t\text{BuPNN})\text{Fe}(\text{NO})_2]^{2+}2[\text{BF}_4]^-$; PNN = 2-[(Di-tert-butylphosphinomethyl)-6-diethylaminomethyl]pyridine, it is shown by XPS study that NO ligands are not stable and easily escape from the complex. This reveals changes in structure and in paramagnetic/diamagnetic behavior of these complexes.

1. Barats-Damatov D., Shimon L.J., Feldman I., Bendikov T., Neumann R. *Inorg. Chem.* **2015**, *54*, 628-634.

2. Zell T., Milko P., Fillman K.L., Diskin-Posner Y., Bendikov T., Iron M.A., Leitun G., Ben-David Y., Neidig M.L., Milstein D. *Chem. Eur. J.* **2014**, *20*, 4403-4413.

3. Butschke B., Fillman K.L., Bendikov T., Shimon L.J., Diskin-Posner Y., Leitun G., Gorelsky S.I., Neidig M.L., Milstein D. *Inorg. Chem.* **2015**, *54*, 4909-4926.

11:20am AS+SS-WeM11 *In Situ* Chemical Imaging of Biointerfaces Using Microfluidics and Molecular Imaging, Xiao-Ying Yu, Pacific Northwest National Laboratory

The surfaces of aqueous phases and films have unique kinetics and thermodynamics, distinct from the bulk. However, major surface analytical techniques are mostly vacuum-based and direct applications for volatile liquid studies are difficult. We developed a vacuum compatible microfluidic interface, System for Analysis at the Liquid Vacuum Interface (SALVI), to enable direct observations of liquid surfaces and liquid-solid interactions using time-of-flight secondary ion mass spectrometry (ToF-SIMS). SALVI was recently applied to investigate biomolecules and biological interfaces in living biofilms and single mammalian cells. Specifically, a variety of hydrated protein thin films were studied, providing the first *in situ* observation of interfacial water or biological water. In the single cell study, ion transport through the ion channel in the cell membrane was mapped in wet cells. In our most recent biofilm research, characteristic fragments of the extracellular polymeric substance (EPS) were obtained for the first time, including proteins, polysaccharides, lipids, polymers, and distinct biomarkers. These species are useful to track the metabolic and electron transfer processes in the microbial communities. For example, biomarkers characteristic of quorum sensing as a result of biofilm response to environmental stressors such as $\text{Cr}_2\text{O}_7^{2-}$ exposure and subsequent dispersion of the biofilm can be observed using this novel approach. Correlative imaging was employed to achieve a more holistic view of complexed biological systems across different space scales. In addition, electron transfer mechanisms of living biofilms as the electrode material are being studied using the electrochemical version of our microfluidic reactor. Our results demonstrate that interfacial chemistry involving important biomolecules and biological systems can be studied from the bottom up all based on microfluidics. Our transferrable microfluidic reactor sets the analytical foundation toward chemical imaging of complex phenomena occurring in multiple time and length scales, or the mesoscale, underpinning chemical changes at the molecular level in the condensed phase.

11:40am AS+SS-WeM12 Capturing the Transient Species at the Electrode-Electrolyte Interface by SALVI and Liquid ToF-SIMS, Jiachao Yu, Y. Zhou, X. Hua, Pacific Northwest National Laboratory; S. Liu, Southeast University, China; Z. Zhu, X.-Y. Yu, Pacific Northwest National Laboratory

In situ time-resolved identification of interfacial transient reaction species were captured using imaging mass spectrometry, leading to the discovery of unexpected and more complex elementary electrode reactions and providing unprecedented understanding of the reaction mechanism on the electrode surface and solid-electrolyte interface using dynamic molecular imaging. This unique approach was enabled by a vacuum compatible electrochemical microfluidic reactor, namely System for Analysis at the Liquid Vacuum Interface (SALVI). The chemical mechanism of iodine oxidation at the electrode surface was revisited using simultaneous cyclic voltammetry (CV) and dynamic ToF-SIMS. Our dynamic ionic and molecular imaging results suggested that more complex surface reactions exist concerning the gold adlayer formation on the electrode surface, providing the discovery of more short-lived transient species and new insights of elementary electrode reactions unknown in the textbook. Such findings further illustrated the importance of truly observing electron transfer reactions in real-time with high spatial chemical mapping. This innovated approach is suitable for fundamental kinetic studies in electrochemistry at the solid-liquid (s-l) interface or the solid-electrolyte interface with many potential applications such as energy storage, material conversion, and electrocatalysis. The ability to capture and elucidate complex reaction mechanisms at the dynamic s-l interface opens a new door to control, mitigate, design, and engineer reactive pathways toward predictive

material synthesis, efficient energy storage, and favorable catalytic conversion.

12:00pm AS+SS-WeM13 Energy Storage Materials – Investigating the Surface, Jonathan Counsell, S.J. Coultas, C.J. Blomfield, Kratos Analytical Limited, UK; C. Moffitt, Kratos Analytical Limited

Lithium ion batteries are commonly found in home electronic equipment. In recent times there have been significant efforts to improve the durability, cycle time and lifetime decay of the batteries and in particular the electrode/electrolyte material. Novel materials have been developed to also increase the energy storage density. Lithium phosphorus oxynitride (LiPON) has become the most commonly used solid electrolyte thin-film in energy storage devices. Obviously due to the widespread use of this material there is significant interest in understanding the characteristics and properties with a view towards optimisation.

Here we apply XPS and UPS to explore both the surface and bulk properties of several $\text{Li}_x\text{PO}_y\text{N}_z$ surfaces prepared via atomic layer deposition ALD [1]. The distribution of elements below the surface is explored via ion and angular-resolved depth profiling methods. This technique has been used extensively across a broad range of applications however the damage caused by impinging ions on the structure of the analysis material has always been a concern for the analyst. More recently Argon gas cluster ion sources have been employed to reduce the chemical damage of organic materials and broaden the range of materials amenable to this type of analysis. Here we extend the application of cluster ions beyond organics to inorganic oxides. Herein we discuss how, with the use of $\text{Ar}250\text{-}3000^+$ ions, where the energy per atom can be 2.5-40 eV, it is possible to obtain more accurate information regarding the true nature of the LiPON thin-film. A comparison is made with conventional monatomic depth profiles in particular the differences in stoichiometry obtained with the two ion sources. Ion implantation is also discussed as are the unfortunate chemical effects of carbon deposition from organic cluster ions. We will demonstrate how the analyst can now confidently depth profile through inorganic metal oxide thin-films without the worry of reduction or preferential sputtering.

[1] Alexander C. Kozen, Alexander J. Pearse, Chuan-Fu Lin, Malachi Noked, Gary W. Rubloff, DOI: 10.1021/acs.chemmater.5b01654

Biomaterial Interfaces

Room 101A - Session BI+MI-WeM

Biosensors and Diagnostics

Moderators: Daniel Graham, University of Washington, Tobias Weidner, Max Planck Institute for Polymer Research, Germany

8:00am BI+MI-WeM1 Bacteriophage-Derived Surfaces for the Targeting of Pathogenic Bacteria, Stephane Evoy, University of Alberta, Canada

Bacterial pathogens cause a high level of morbidity and mortality, specifically for infants, young children, elderly and immunocompromised individuals. Antibodies have been exploited as molecular probes in order to impart specificity to bacterial biosensing platforms. Antibodies however suffer from degradation and reliability issues. The high specificity of phages offers a potent alternative for the targeting of pathogens. More specifically, recombinant phage receptor binding proteins (RBPs) responsible for phage-host specificity can be used as biological probes and present numerous advantages over the use of whole phage.

We successfully coupled phage RBP Gp047 from phage NCTC12673 onto magnetic beads. These beads were then employed for the extraction of *Campylobacter* cells from food matrices. Recovery rates were greater than 80% in samples spiked with as low as 10^2 cfu mL^{-1} of cells. Phage lysins have also been employed as capturing probes. We coupled recombinant lysin Gp10 from the mycobacteriophage L5 onto magnetic Dynabeads 280 for the capture of *Mycobacterium avium* subsp. *paratuberculosis* (MAP) cells from complex media. The study employed skim cow milk spiked with MAP cells, skim milk spiked with both MAP and *Escherichia coli* cells and Middlebrook 7H9 medium spiked with MAP cells as test matrices. The functionalized beads were incubated with the spiked sample, separated, cleaned, and subjected to DNA extraction. The resulting solution was analyzed by real time PCR. The entire test was completed within 24 hours. The capture process significantly increased the PCR sensitivity and demonstrated high specificity towards MAP cells.

Further, we demonstrated the use of cysteine-tagged P22 phage RBPs on gold surface for the specific SPR detection of *Salmonella enterica serovar Typhimurium*. These results demonstrate that N-terminus Cys tagged

Wednesday Morning, November 9, 2016

proteins capture bacteria efficiently compared to the C-terminus Cys tagged protein due to preferential orientations. Finally, micromechanical devices have also been proposed for the detection and enumeration of bacteria. We designed and developed a microresonator array optimized for such detection. This large array-based design offers a large total area for the capture of cells, while maintaining the ability to detect the attachment of a single cell anywhere on the array. The devices were functionalized with phage GST-Gp48 tail-spike proteins to impart specificity of detection. We successfully employed these arrays for the specific detection of *Campylobacter jejuni* from clean buffer. The devices did not show any sensitivity to *Escherichia coli* bacteria confirming the specificity of detection.

8:20am BI+MI-WeM2 Biomolecule Sensing at Attogram Levels via Nanophotonic-Optomechanical Resonators, Anandram Venkatasubramanian, University of Alberta, Canada; V.T.K. Sauer, S.K. Roy, National Institute of Nanotechnology, Canada; D. Wishart, W.K. Hiebert, University of Alberta, Canada

The Gas chromatography (GC) – Mass spectrometry (MS) system is the industry benchmark in chemical analysis. However the need for complex instrument such as the ionizer makes the Mass spectrometry unsuitable for portable detection applications. Recent demonstrations with nano-optomechanical (NOMS) resonators at atmospheric pressure show they are promising for portable GCs, matching the mass detection limits of NEMS sensors in only the first generation. Owing to their superior displacement sensitivity compared to NEMS, NOMS may have competitive advantages going forward. In this regard, a free space interferometry system was used for NOMS sensing of biomolecules. The primary motivation to develop sensors for portable applications is to develop point of care diagnostic devices for health monitoring. As the state of our health is a product of our interactions with our environment, metabolomics is useful in health monitoring. Among the different human biofluids, urine is “favoured” due to their precise portrayal of metabolic breakdown products, sterility and easy to obtain large volumes. Hence we have demonstrated multiple component (5+) biomolecule detection from derivatized human urine metabolomes (HUM) as they elute from the GC. Derivatized HUMs such as ethyl malonic acid (EMA) were tested as a single component sample to obtain the limit of detection. From the results it was observed that the minimum detectable mass was about 20 attograms with a concentration threshold of 25 μM with EMA, which is in the normal physiological range in human adults. To the best knowledge of the authors, this is the first time a NOMS based gas sensor has been used in conjunction with a gas chromatographic system and has demonstrated physiological range of detection of biomolecules.

8:40am BI+MI-WeM3 Hole-mask Colloidal Lithography Method to Fabricate Chiral Metal-Nanoparticles for Plasmon Enhanced CD Measurements, Gunnar Kläs, Aarhus University, Denmark; D.S. Sutherland, Aarhus, Denmark

Hole-mask colloidal lithography is a well studied method [1] for a reliable high throughput fabrication of metal nanoparticles (NP). The plasmonic resonances and their electromagnetic near field dependencies of such NPs are widely used as bio-sensors, e. g. for high sensitivity refractive index sensing [2]. Rather recently it was also shown that the near field interactions of planar plasmonic chiral NPs can be used for sensitive chiroptical measurements of very dilute amounts of chiral material [3], allowing structural characterization of even small amounts of many biomolecules. So far the fabrication of such chiral NPs is based on time-consuming techniques such as e-beam lithography [4].

Here, I present a novel method for the fabrication of chiral Au nanocrescents based on a modified version of hole-mask colloidal lithography. This reliable and efficient method utilizes the shrinking of the hole due to the material evaporated through it, adding an additional parameter to the control over the shape of the resulting NP.

The method allows the fabrication of nanocrescents with an outer diameter of 100nm-200nm that show plasmonic responses similar to previous Au structures [2]. Furthermore, when analyzed with circular polarized light, they show a considerable circular dichroism response.

Hence, this fabrication method is a promising technique for the time- and cost-efficient production of sensitive biosensors for the structural analysis of chiral materials.

[1] Bochenkov, V. E. and Sutherland, D. S. " *NanoLett*, Vol. 13, 1216-1220, 2013.

[2] Guerreiro, J. R. L. et al. *ACS nano*, Vol. 8, No. 8, 7958–7967, 2014.

[3] Hendry, E. et al. *NNANO*, Vol. 5, 783-786, 2010.

[4] Hentschel, M. et al. *NanoLett*, Vol. 12, 2542-2547, 2012.

9:00am BI+MI-WeM4 Neuraminidase Assay using Glycan-Functionalized Graphene Field-Effect Transistors, Kaho Kamada, T. Ono, Y. Kanai, Osaka University, Japan; Y. Ohno, Tokushima University, Japan; K. Maehashi, Tokyo University of Agriculture and Technology, Japan; K. Inoue, Osaka University, Japan; Y. Watanabe, Kyoto Prefectural University of Medicine, Japan; T. Kawahara, Y. Suzuki, Chubu University, Japan; S. Nakakita, Kagawa University, Japan; K. Matsumoto, Osaka University, Japan

A lot of the anti-influenza virus drugs such as Tamiflu® and Relenza® prevent the viruses from infecting to the next cell. Influenza viruses enter the host cells of the throat and trachea by binding to the host cell's surface receptor molecules which contains sialic acid. After the proliferation into the cell, the viruses cleave the sialo oligosaccharides by the action of the enzyme neuraminidase (NA), and propagated viruses are detached from the cells on the infection to the next cell. Therefore, it is possible to suppress the chain of propagation of virus by inhibiting the NA. Currently, the evaluation of antiviral drugs has been conducted mainly using cultured cells, there are problems in accuracy and quantitative property. In addition, it is difficult to evaluate the mechanism of reaction. Therefore we aim to build a useful new biological model platform for drug evaluation and drug discovery research. We modified sialoglycoprotein chain on the graphene surface, and fabricated the glycan-functionalized Graphene Field-Effect Transistors (G-FET), which reproduce cell surface environment on the graphene. The reaction behavior of the virus is highly detected as the current by the G-FET. So we can quantitatively evaluate drug reaction by the physical indicators. As a first step here, we electrically measured NA reaction by the glycan-functionalized G-FET.

G-FET was produced by evaporating the electrodes on graphene obtained by the exfoliation method. 1-Pirenbutan acid succinimidyl ester as a linker, was modified human sialoglycoprotein chain having a modified amino group on the graphene channel. After dropping the NA on it, we measured time course of the neuraminidase reaction monitored by the graphene-FET.

When dropping the NA, the current value is decreased exponentially. This is because the sialic acid negatively charged was disconnected from the sugar chain, and the hole carriers induced on graphene were decreased. The rate of decrease in current value with neuraminidase dropping is in good agreement with the activity value obtained by the absorption method (A NA molecule cuts the 1.7 of molecules per second). This shows that the rate constant obtained from electrically measurement by G-FET reflects the enzyme reaction rate.

This study has received the support of JST-CREST.

9:20am BI+MI-WeM5 Surface-sensitive Imaging of Supported Membranes and Single Lipid Vesicles for Medical Applications, Fredrik Höök, Chalmers University of Technology, Sweden

INVITED

Measurements of ligand-binding events to membrane-protein receptors in a near-natural environment display an opportunity in mechanistic studies of membrane receptors. Furthermore, the residence time of drug-target interactions is being increasingly recognized as a key parameter in evaluating drug efficacy, but is hampered by the technical challenge to perform such studies for membrane proteins. However, with membrane proteins embedded in nanoscale lipid vesicles and detection methods with single molecule sensitivity, such information can be gained in a broad dynamic range, as requested in both drug-screening and diagnostic applications. A diverse set of tools with single-nanoparticle sensitivity is now available, to which we recently contributed a concept that enables simultaneous fluorescent and scattering-based label-free imaging of thousands of surface-bound nanoscale entities [Agnarsson B et al., *ACS Nano*, 2015]. The principle is based on the use of lipid vesicles as enhancer elements in optical waveguide based fluorescence and label-free evanescent-wave scattering microscopy, making the concept compatible with analysis of both water-soluble and cell-membrane bound receptors. The concept is currently evaluated as a diagnostic assay for biomarker detection and in drug-screening applications, previously explored by us using conventional total internal reflection fluorescence (TIRF) microscopy [Gunnarsson et al., *Anal Chem* (2015)]. The use of scattering microscopy in the context of single-enzyme detection in complex biological fluids will be presented, with focus on single-molecule biomarker detection in cerebrospinal fluid from individuals suffering from Alzheimer's disease [Angew Chemie, 2015]. A new means to utilize the two-dimensional fluidity of supported cell-membrane derived lipid bilayers in microfluidic designs

Wednesday Morning, November 9, 2016

for nanoparticle size determination and sorting applications will also be presented [Simonsen et al., JACS, 2011 and Pace et al., Anal Chem, 2015].

11:20am BI+MI-WeM11 Non-invasive Thermal Sensing using Thermographic Phosphors, Firouzeh Sabri, University of Memphis; S. Allison, EMCO; P. Parajuli, University of Memphis
F. Sabri¹, S. W. Allison², and P. Parajuli¹

1. University of Memphis, Department of Physics and Materials Science
2. Emerging Measurements Co.

Thermal measurements involving thermographic phosphors, whether in the form of powder, crystal, or glass, continues to be of interest for a wide range of applications and temperature ranges. The investigation of phosphor-doped polymer films is a promising avenue for thermometry applications. Phosphor thermometry has been investigated recently for non invasive thermal assessment of biological and biomedical surfaces. For thermographic phosphors to be useful for biomedical applications they must first be encapsulated in a biocompatible, biostable, and transparent "host" that would allow optical access to the embedded phosphors. The work here demonstrates the feasibility of thin film thermographic phosphor-based thermometry where $\text{La}_2\text{O}_2\text{S:Eu}$ particles have been embedded in a clear silicone encapsulant at different concentrations. The composite materials were prepared by means of spin-coating technology and the effect of spin speed and spin time on the thickness and distribution of the powder was investigated. . In order to improve the thermal conductivity of the composite material, a layer of carbon has been incorporated into the multilayer structure. The results presented will compare the excitation-emission behavior of the composite materials mentioned above with the properties of pure powder, at various temperatures. The effect of the tensile properties of the composite material on the excitation/ emission behavior of the materials will also be discussed. Measurements were conducted at low temperatures and at elevated temperatures and the decay characteristics were investigated as a function of temperature.

11:40am BI+MI-WeM12 Imaging Time-of-Flight Secondary Ion Mass Spectrometry to Characterize Tumor Progression and Regression, Lara Gamble, B.M. Bluestein, D.J. Graham, University of Washington; F. Morrish, D. Hockenbery, Fred Hutchinson Cancer Research Center

The tumor microenvironment has been associated with regulating tumor cell growth, metastatic potential, and chemotherapeutic drug resistance. However, very few techniques are capable of directly probing the tumor microenvironment on the micron scale. A new perspective is required to interpret and characterize this complex environment. Using imaging time-of-flight secondary ion mass spectrometry (ToF-SIMS) and a mouse model with Myc-dependent inducible and regressible pancreatic β -cell neoplasia, it is possible to relate changes in the composition and distribution of metabolic related molecules with tumor development. Myc, one of the most frequently deregulated oncogenes in human cancers, contributes to tumorigenesis through various mechanisms, including the deregulation of cell proliferation and growth, protein and mitochondrial biogenesis, and metabolic alterations. Pancreatic tissues were harvested and frozen in optimal cutting temperature (OCT) at 6 days post Myc induction. 4 μm cryosections were serially cut, with one used for H&E staining, one for ToF-SIMS analysis, and another for immunohistochemistry. ToF-SIMS data was acquired on an IONTOF TOF V with pulsed 25 keV Bi_3^+ ion beam. Principal component analysis (PCA) of ToF-SIMS image data separated regions of tumor cells from stroma within the first principal component and revealed subtle differences in chemistry between the tumor and surrounding tissue. ToF-SIMS data suggests a preferential uptake of fatty acids 18:3, and 18:2 within the tumor. The tumor also shows an increased localization of sphingomyelin fragments and vitamin E compared to the surrounding tissue. PCA was also applied to selected tumor regions to spatially and chemically analyze within the tumor and compare chemistries between different tumor sizes. Distinct chemical differences were identified between control and 6 day Myc activated β -cell islet tissues using multivariate analysis techniques. The results from C14:0 and phosphatidylcholine fragments present within the tumor are suggestive of *de novo* fatty acid synthesis. This work further demonstrates the high resolution capability of ToF-SIMS as the data clearly reveals intra-tumor chemical heterogeneity as localized high intensity regions, but histologic correlations are needed to discern the purpose and function of these structures.

12:00pm BI+MI-WeM13 $\text{SrI}_2(\text{Eu}^{2+})$ Gamma Camera for SPECT Imaging in Medical Applications, LaNell Williams, M. Groza, E. Rowe, J. Butler, Fisk University; T. Peterson, Vanderbilt University; A. Burger, Fisk University

The detection of gamma rays for nuclear imaging has become increasingly important in designing non-invasive imaging tools for biological research and modeling. Although imaging techniques such as computed tomography (CT) and Positron Emission Tomography (PET) have been previously used, and improved spatial resolution and sensitivity continue to be an issue. Thus, improvements in these detection devices are needed to create better images for more accurate modeling in research [Cressey, 2011]. Scintillators such as Cesium Iodide (CsI), and Sodium Iodide (NaI) have been used for many imaging techniques for their ease of growth, energy resolution, and overall effectiveness as a gamma ray detectors. In more recent studies, Strontium Iodide doped with Europium ($\text{SrI}_2(\text{Eu}^{2+})$) has shown to be a promising scintillator compared to NaI and CsI. Because of $\text{SrI}_2(\text{Eu}^{2+})$ improved energy resolution ($\sim 2.7\%$), fast decay time ($\sim 1.2 \mu\text{s}$) and light yield (110,000 photons/MeV), it is an ideal replacement for technologies that have used previously been made with NaI and CsI. [Cherepy, 2008]. In addition, $\text{SrI}_2(\text{Eu}^{2+})$ also has an emission centered around 420 nm making it an ideal scintillator to be used with silicon photomultipliers that provide lower energy consumption than the standard photomultiplier tube. The improved energy resolution of $\text{SrI}_2(\text{Eu}^{2+})$ in a gamma camera will result in an promising detector for nuclear imaging.

Electronic Materials and Photonics Room 102A - Session EM+NS-WeM

Nanoparticles for Electronics and Photonics

Moderators: Joseph Tischler, U.S. Naval Research Laboratory, Jessica Hilton, Mantis Deposition

8:00am EM+NS-WeM1 Nanostructures on Surfaces: From Cluster Deposition to Low Energy Ion Bombardment, Luke Hanley, K. Steeves Lloyd, M.W. Majeski, I.L. Bolotin, University of Illinois at Chicago; M. Schmeling, Loyola University Chicago; I.V. Veryovkin, University of Illinois at Chicago

INVITED

Two strategies are described for the preparation of unique nanostructures on surfaces or within thin films: cluster beam deposition and low energy ion beam irradiation. In cluster beam deposition, copper sulfide nanoparticles were prepared by magnetron sputtering under a flow of argon and hydrogen sulfide, then codeposited with evaporated pentacene to form a composite thin film (M.W. Majeski, *et al.*, ACS Appl. Mater. Interf., 2014, <http://dx.doi.org/10.1021/am5028428>). This all-gaseous method can prepare a variety of semiconductor nanoparticles without the surface ligand capping and oxidation effects often observed for colloiddally prepared nanoparticles that can inhibit charge transfer or cause self-doping. X-ray photoelectron spectroscopy, transmission electron microscopy, and high-angle annular dark-field scanning transmission electron microscopy were used to determine that $2.3 \pm 0.4 \text{ nm}$ Cu_{2-x}S nanoparticles with copper in the +1 oxidation state were deposited into pentacene films. In low energy ion beam irradiation, nanocone and nanoripple arrays were prepared on Si surfaces by grazing incidence irradiation with 1 keV Ar^+ ion beams that simultaneously sputtered away surface atoms and sputter-deposited metal impurity atoms from adjacent targets (K. Steeves Lloyd, *et al.* Surf. Sci., 2016, <http://dx.doi.org/10.1016/j.susc.2016.03.016>). Scanning electron microscopy and atomic force microscopy observed that when Si, Cu, or stainless steel was employed as a co-sputtering target, only stainless steel was found to assist the growth of dense arrays of nanocones. The structural characterization of samples further correlated the role of incident ion fluences on the formation of nanoripples vs. nanocones. Characterization of sample chemical composition by total reflection X-ray fluorescence and X-ray photoelectron spectroscopy revealed that the concentration of metal impurities originating from stainless steel (Fe, Cr and Ni) was relatively high in the regions with high density of nanocones and much lower in the region of nanoripples. Overall, these two strategies open up multiple possibilities for the preparation of complex nanostructures on surfaces and in thin films that are compatible with more common lithographic strategies.

8:40am EM+NS-WeM3 Designer Nanocrystal Electronic and Optoelectronic Materials through Controlled Coupling and Doping, Cherie Kagan, University of Pennsylvania

INVITED

Semiconductor nanocrystals (NCs) are prized for their size- and shape-dependent electronic and optical properties and as building blocks in the

Wednesday Morning, November 9, 2016

assembly of NC solids. However, the long, insulating ligands commonly employed in the synthesis of colloidal NCs inhibit strong interparticle coupling and charge transport once NCs are assembled into the solids state as NC arrays. In this talk, I will describe methods to introduce atoms, ions, and more compact molecules at the NC surface that allows us to increase interparticle coupling and dope NC solids. NC coupling and doping provide control over the density of states, the carrier statistics and the Fermi energy. I will also describe the importance of engineering device interfaces to study the fundamental physics of NC solid transport and to design device architectures for applications. Examples of strong coupling and doping in II-VI and IV-VI semiconductor NC solids will be given that yield high-mobility, high-conductivity NC solids. Temperature-dependent transport measurements of these materials are consistent with a transition from localized to extended-state charge transport. These high mobility n- and p-type materials are used as the semiconductors to construct large-area, flexible, field-effect transistors and integrated circuits and for solar photovoltaics.

9:20am EM+NS-WeM5 Au Nanoparticle Modified Indium Tin Oxide Ultramicroelectrode for Single Particle Spectro-electrochemistry Study and Ultrasensitive Electrochemistry Sensing, Yanxiao Ma, The University of Alabama; S. Pan, The University of Alabama

Plasmonic active metal NPs are broadly used in electrochemical and optical sensing of molecular recognition events. However, it is extremely challenging to resolve chemical and physical transformation at single NP level using conventional optical and electrochemical methods for resolving their local structure-function relationship. We are developing an optical and electrochemical technique to resolve electrocatalytic property of single NPs. Combined methods of photolithography and electrodeposition are used for fabricating Au NP modified indium tin oxide ultramicroelectrode (ITO UME). Dark field scattering (DFS) microscopy and scanning electron microscopy (SEM) were used to characterize NPs on the surface of ITO UME. The electrochemistry voltammetric study shows that Au and Pt NPs are ideal catalytic materials for hydrazine oxidation reaction. Dark field spectroelectrochemical study of hydrazine oxidation at planar ITO and ITO UME confirmed the formation of nanobubbles on NPs surface. Relationship between DFS light intensity and hydrazine oxidation current profile was obtained.

9:40am EM+NS-WeM6 Band Gap-Control of Spray Pyrolysis Synthesized CZTS Nanoparticles, Stephen Exarhos, E. Palmes, A. Alvarez-Barragan, L. Mangolini, University of California, Riverside

An innovative and scalable synthesis approach to the formation of phase-pure $\text{Cu}_2\text{ZnSnS}_4$ (CZTS) nanoparticles has been developed using aerosol spray pyrolysis. CZTS material is an inherent direct-band gap *p*-type semiconductor with a band gap of ~ 1.5 eV and absorption coefficient of $>10^4 \text{ cm}^{-1}$, making it suitable for solar absorption applications. As an earth-abundant absorber material, it has been well-studied for application in thin film photovoltaics [1]. Little experimental work has been done to test the viability of the material as a photocatalyst, though the material shows low activity in driving water splitting or pollutant degradation unless synthesized in a noble metal heterostructure [2]. By its nature, CZTS is a very adaptable material system. It is relatively straightforward to alloy into the material primarily as a method of band gap control. By optimizing the band gap and band alignment of alloyed CZTS-like nanoparticles, we intend to improve the catalytic quality of CZTS-based heterostructures. We have previously shown that aerosol spray pyrolysis is an effective inexpensive and scalable technique for the synthesis of CZTS [3]. By processing a solution with copper-, tin-, and zinc-diethyldithiocarbamate precursors dissolved in a toluene solvent, we can form phase-pure, surface-ligand-free, kesterite CZTS nanoparticles with a size distribution average of ~ 20 nm. Using the same process, by adding hydrogen-terminated silicon nanoparticles — synthesized in-house by a non-thermal plasma process — to the precursor solution, we can alloy silicon into the material (making CZTSiS), and in turn increase the band gap of the material from the 1.5 eV for pure CZTS. We also have the ability to decrease the band gap by alloying different transition metals in place of zinc in the crystal lattice. We present preliminary studies characterizing CZTS and CZTSiS nanoparticles for potential use as a photocatalytic heterostructure material.

[1] Liu, Xiaolei, Yu Feng, Hongtao Cui, Fangyang Liu, Xiaojing Hao, Gavin Conibeer, David B. Mitzi, and Martin Green. Progress in Photovoltaics: Research and Applications, January 1, 2016.

[2] Yu, Xuelian, Alexey Shavel, Xiaoqiang An, Zhishan Luo, Maria Ibáñez, and Andreu Cabot. Journal of the American Chemical Society 136, no. 26 (July 2, 2014): 9236–39.

[3] Exarhos, Stephen. eScholarship, January 1, 2015. <http://escholarship.org/uc/item/1pw1t81k>.

11:00am EM+NS-WeM10 Designer Nanomaterials by Magnetron Sputtering and Ion Soft Landing, Grant Johnson, V. Prabhakaran, Pacific Northwest National Laboratory; T. Moser, Michigan Technological University; M.H. Engelhard, N. Browning, J. Laskin, Pacific Northwest National Laboratory

Clusters and nanoparticles comprised of controlled amounts of different atoms are of interest for applications in optics, magnetics, catalysis, sensors, and biotherapeutics. Alloy nanoparticles, in particular, may possess enhanced properties compared to single-metal species due to the additional interplay between their different elemental components. By reducing the quantity of precious metals in alloys by substitution with cheaper base metals, it is possible to achieve equivalent or superior performance to noble metal nanoparticles at reduced material cost. In addition, alloying of elements that are immiscible in the bulk is possible at the nanoscale because the enthalpy of mixing decreases and becomes negative at small particle sizes. As a result, a broad array of alloy species may be generated in the form of clusters and nanoparticles. Magnetron sputtering of multiple targets in the same region of gas aggregation is demonstrated to produce ionic alloy clusters and nanoparticles with defined composition and morphology that are not obtainable through solution synthesis. Introduction of reactive gases into the sputtering and aggregation region is shown to result in the formation of complex morphologies. A suite of characterization techniques including atomic force microscopy, scanning and transmission electron microscopy, and x-ray photoelectron spectroscopy is utilized to determine how the size, shape, and elemental composition of soft landed particles may be tuned through variations in source parameters. The electrochemical activity of the soft landed nanomaterials toward the oxygen reduction reaction, a critical process occurring in proton exchange membrane fuel cells, is evaluated ex-situ using cyclic voltammetry in solution and in-situ using an ionic liquid membrane in vacuum.

11:20am EM+NS-WeM11 A Facile Electrodeposition Method for Vertically Standing Plasmonic Nanorods for Surface Enhanced Photoelectrochemical Catalysis, Jue Wang, S. Pan, The University of Alabama

A facile template-free electrodeposition technique is developed for large-scale fabrication of vertically standing plasmonically active silver nanorods (NRs). The diameter, length, and surface coverage of Ag NRs are dependent on the electrodeposition time. The growth mechanism of the vertically standing Ag NRs is investigated by tracking their morphology evolution as a function of deposition time. Because of their large specific surface area, oriented alignment, broad range light scattering, and light absorption tunability, these NRs are ideal substrates for thin layer photocatalysts for enhancing light absorption and charge collection. The Preliminary tests on plasmon-induced photocurrent of bare Ag NRs, Ag NR converted to Ag_2S NRs, and coated with CdS nanoparticles (NPs) are presented to demonstrate surface enhancement characteristics. This simple NR fabrication method can be extended to other conductive substrates and other materials for obtaining vertically standing NR structures.

11:40am EM+NS-WeM12 Influence of Surface Reaction on the Infrared Localized Surface Plasmon Resonance of Indium Tin Oxide Nanocrystals, Weize Hu, M.A. Filler, Georgia Institute of Technology

Heavily doped oxide nanocrystals exhibit a tunable plasmonic response in the infrared, a capability that is promising for future photonic, spectroscopic, and energy harvesting/transport technologies. Nanocrystal carrier density, and thus spectral response, is adjustable via chemical reaction; however, the fundamental processes governing this behavior are poorly understood. Here, we study the oxidation and reduction of indium tin oxide (ITO) nanocrystals with O_2 and H_2 , respectively, with in situ diffuse reflectance infrared Fourier transform spectroscopy (DRIFTS). We show that the main absorption feature redshifts upon oxidation more than 1000 cm^{-1} and blueshifts to its original position upon reduction. The same magnitude spectral shift is observed over many cycles of oxidation and reduction. A kinetic model, which includes surface reaction and bulk diffusion, allows us to quantitatively rationalize the process, revealing that surface reaction is rate limiting under the conditions studied. Our experiments provide a deeper understanding of the connection between surface reaction and carrier density in oxide nanocrystals, and open the door to a priori control of plasmonic response.

Wednesday Morning, November 9, 2016

12:00pm **EM+NS-WeM13 Electrochemical Synthesis of Nanostructured Cu and Cu_xO Electrodes for the Reduction of CO₂ to Usable Fuels**, *Nelly Kaneza, S. Pan*, The University of Alabama

In effort to controlling carbon dioxide (CO₂) levels in the atmosphere, the conversion of CO₂ into useful products, although very challenging, has emerged as a very attractive area of research. In this work, a series of Cu based nanostructures are synthesized and characterized to demonstrate a low cost approach to reduce CO₂ electrochemically to specific fuel products at low overpotential. The synthesized Cu and Cu_xO nanostructures are characterized with X-ray diffraction (XRD), transmission electron microscopy (TEM), and scanning electron microscopy (SEM) and their performance evaluated in terms of their activity, selectivity and stability using cyclic voltammetry (CV), gas chromatography (GC) equipped with a mass spectrometry (MS).

Exhibitor Technology Spotlight

Room Hall C - Session EW-WeM

Exhibitor Technology Spotlight Session

Moderator: Chris Moffitt, Kratos Analytical Limited

10:20am **EW-WeM8 From Surface Spectrometry to 3D Analysis - Latest Trends and Instrumentation for TOF-SIMS**, *Nathan Havercroft*, ION-TOF USA; *R. Moellers, A. Pirkel*, ION-TOF GmbH, Germany

During the last 25 years IONTOF has continuously made significant development efforts to further improve the instrumentation for Time-of-Flight Secondary Ion Mass Spectrometry (TOF-SIMS) and related techniques. Some of the most recent achievements include in-situ sample preparation and tomography by FIB, enhancement of maximum count rates and dynamic range in conventional depth profiling of inorganic materials, the design of a TOF-SIMS / SPM combination instrument, as well as the integration of an Orbitrap™ mass spectrometer with unrivalled mass resolution and mass accuracy into the TOF.SIMS 5 instrument.

IONTOF's, new TOF.SIMS NCS instrument platform combines all the well-known options of our high-end TOF.SIMS 5 system with the possibility to perform in-situ SPM measurements. The sophisticated, large area SPM unit has a scan range of up to 80 x 80 μm² and is ideally suited to provide topographic information for SIMS measurements. Beside AFM, MFM, KPFM and multi-frequency modes it also supports a unique surface profiler mode which allows for fast measurements of large SIMS craters. The new piezo sample stage with submicron position accuracy ensures fast and precise movement between the TOF-SIMS and the SPM measurement position.

Depth profiling of organic materials, e.g. layer systems for optical and electronic devices, can be ideally performed using gas cluster ion beams (GCIB) in combination with TOF-SIMS. For optimum performance, a dual-beam approach is usually utilized, employing a lower energetic quasi DC sputter beam for material removal and a short-pulse small-spot analysis beam for optimal mass spectral and imaging performance.

However, molecular identification of unknown substances, e.g. contaminants, is usually hampered by constraints in mass resolution and mass accuracy of the TOF analyzer. Furthermore, ions generated in the sputter phase of the dual-beam experiment are lost for analysis. In order to overcome these limitations, a TOF / Orbitrap™ SIMS hybrid instrument has been developed in order to combine all advantages of a state-of-the-art TOF-SIMS with the mass spectrometry performance of a Q Exactive™ HF mass analyzer. The Q Exactive™ HF provides a mass resolution of more than 240,000 @ m = 200 u, <1 ppm mass accuracy, and full MS/MS capabilities for structural analysis of complex molecules. By utilizing these unique features, the SIMS analyst can make peak identifications with much greater confidence.

Fundamental Discoveries in Heterogeneous Catalysis Focus Topic

Room 103A - Session HC+SS-WeM

Bridging Gaps in Heterogeneously-catalyzed Reactions

Moderator: Ashleigh Baber, James Madison University

8:00am **HC+SS-WeM1 Vinyl Acetate Formation Pathways and Selectivity on Model Metal Catalyst Surfaces**, *Theodore Thuening*, University of Wisconsin-Milwaukee

Surface reaction pathways are explored on model single crystal catalyst surfaces using a combination of surface science experiments in ultrahigh vacuum, in-situ monitoring of the surface intermediates during reaction, and by using density functional theory (DFT) calculations. This approach enables detailed reaction pathways to be obtained and is illustrated using palladium catalyzed synthesis of vinyl acetate monomer (VAM). It is shown that vinyl acetate is formed on a Pd(111) and Pd(100) model catalysts via the so-called Samanos pathway, where reaction is initiated by coupling between ethylene and surface acetate species to form an acetoxyethyl intermediate that decomposes by β-hydride elimination to form VAM. The way in which adsorbate coverage affects both reactivity and selectivity is discussed.

8:20am **HC+SS-WeM2 In situ Monitoring of Acetylene Hydrogenation over a Pd/Cu(111) Single Atom Alloy Surface with Polarization Dependent Infrared Spectroscopy**, *Christopher M. Kruppe, J.D. Krooswyk, M. Trenary*, University of Illinois at Chicago

Low coverages of catalytically active metals deposited onto less active metal surfaces can form single atom alloys (SAAs), which often display unique catalytic properties. Such alloys are particularly attractive for selective hydrogenation reactions. It is therefore of interest to probe the surface structure and chemistry of such alloys in the presence of gas phase reactants. We have used polarization dependent reflection absorption infrared spectroscopy (PD-RAIRS) to monitor the in situ hydrogenation of acetylene to ethylene over a Pd/Cu(111) SAA surface. The coverage and morphology of the deposited Pd is elucidated with Auger spectroscopy (AES), temperature programmed desorption (TPD) of H₂, and PD-RAIRS of CO. After exposing clean Cu(111) and Cu(111) with various Pd coverages to 10 L CO at 100 K, the RAIR spectra show that the surface is largely unchanged by the presence of less than 0.5 ML of Pd. In the presence of 1×10⁻² Torr of CO at 300 K, significant CO coverages are only achieved when Pd is present on the surface. The Pd coverage determined from the areas of the CO peaks in the PD-RAIR spectra is approximately equal to the Pd coverage calculated from peak-to-peak ratios in the Auger spectra. Surface species and gas phase products of C₂H₂ hydrogenation are monitored between 180 K and 500 K on clean Cu(111) and Pd/Cu(111). With a total pressure of 1 Torr and a C₂H₂:H₂ ratio of 1:100, annealing a SAA-Pd/Cu(111) surface to 360 K results in complete conversion of all gas phase C₂H₂ to gas phase ethylene (C₂H₄), without producing any gas phase ethane (C₂H₆). The results demonstrate the utility of PD-RAIRS for monitoring the selective hydrogenation of acetylene to ethylene.

8:40am **HC+SS-WeM3 Novel in Situ Techniques for Studies of Model Catalysts**, *Edvin Lundgren*, Lund University, Sweden **INVITED**

Motivated mainly by catalysis, gas-surface interaction between single crystal surfaces and molecules has been studied for decades. Most of these studies have been performed in well-controlled environments, and has been instrumental for the present day understanding of catalysis. We have in recent years explored the possibilities to perform experiments at conditions closer to those of a technical catalyst, in particular at increased pressures. In this contribution, results from catalytic CO oxidation over Pd single crystal surfaces using High Pressure X-ray Photo emission Spectroscopy (HPXPS), Planar Laser Induced Fluorescence (PLIF), and High Energy Surface X-Ray Diffraction (HESXRD) will be presented.

Armed with structural knowledge from ultra-high vacuum experiments, the presence of adsorbed molecules and gas-phase induced structures can be identified, and related to changes in the reactivity and/or to reaction induced gas-flow limitations. The strength and weaknesses of the experimental techniques will be discussed.

9:20am **HC+SS-WeM5 Metastable Cluster Formation and Polymorphism of Hydrogen-bonding Molecules on Gold are a Consequence of the Pulse-deposition of a Solution into Vacuum**, *Ryan Brown, S.A. Kandel*, University of Notre Dame

A primary motivation in studying the assembly of molecules at an interface is to determine the underlying principles which drive the spontaneous

Wednesday Morning, November 9, 2016

formation of supramolecular structures under specific environmental conditions, with the ultimate goal being an understanding which allows control over such processes. Recently we have postulated the importance of solution-phase cluster formation during the pulse-deposition, in vacuum, of small organic and organometallic molecules which contain strong hydrogen bonding components, namely carboxylic acid functional groups, in addition to weak hydrogen bonding donors. Specifically, we have studied the cluster formation of 1,1'-ferrocenedicarboxylic acid, $\text{Fc}(\text{COOH})_2$, which has been pulse deposited on Au(111)-on-mica substrates. We employed low temperature scanning tunneling microscopy (LT-STM) to observe which molecular clusters persist at the interface following pulse-deposition from solution. We subsequently performed annealing experiments to determine which of these species represent stable conformations, and which are metastable species formed in the solution droplet during deposition. LT-STM images of $\text{Fc}(\text{COOH})_2$ show a coexistence between dimer, chiral hexamer, and square tetramer clusters. Since the bulk crystal structures for $\text{Fc}(\text{COOH})_2$ are all comprised entirely of molecular dimers, the most stable 2D supramolecular structure likely is some array of dimers, whereas the other species present are metastable. We attribute the initial strong presence of metastable species to the formation of clusters in solution, followed by their precipitation as predicted by Ostwald's rule, then their adsorption on to the substrate in a kinetically-trapped conformation. Electrospray ionization mass spectrometry (ESI-MS) of $\text{Fc}(\text{COOH})_2$ solutions supports the presence of hexamer clusters in solvent droplets, which confirms the possibility that the chiral hexamers observed after deposition precipitate from the solution droplet. Sequential mild annealing steps of this surface results in the formation of linear rows of square tetramers, chiral dimer domains, and eventually tilted dimer arrays. The prevalence of each of these species is related to the surface's thermal history, and this is characteristic of a system evolving under kinetic control. We propose that injection of solution into a vacuum environment can be exploited to produce supramolecular 2D-structures not observed in the bulk crystal, and that the frequency of nature of the metastable species present should be dependent on variables such as the solution concentration, solvent, and droplet size.

9:40am **HC+SS-WeM6 Understanding the Activity of Pt-Re Bimetallic Clusters on Titania and Pt-Re Alloy Surfaces in the Water Gas Shift Reaction**, *Donna Chen, A.S. Duke, K. Xie, A.J. Brandt, T.D. Maddumapatabandi*, University of South Carolina

The chemical activities of bimetallic Pt-Re clusters supported on $\text{TiO}_2(110)$ and single-crystal Pt-Re alloy surfaces are investigated as model systems for understanding Pt-Re catalysts in the water gas shift (WGS) reaction. The activities of these Pt-Re bimetallic surfaces are studied in a microreactor coupled to an ultrahigh vacuum chamber so that the surfaces can be characterized by X-ray photoelectron spectroscopy (XPS) before and after reaction. Bimetallic clusters consisting of a Re core covered by a Pt shell have turnover frequencies that are almost twice as high as that of the pure Pt clusters at 160 °C. Furthermore, the Re in the active bimetallic clusters remains in its metallic state because Re is not readily oxidized when it remains subsurface; there is no evidence that ReO_x is active in promoting the WGS reaction. Pure Re clusters are not active for the WGS reaction, and bimetallic clusters with significant Re at the surface are less active than pure Pt clusters. Surface Re is oxidized under reaction conditions and sublimates as Re_2O_7 . Post-reaction infrared spectroscopy studies show that CO and hydroxyls are detected on the surface.

11:00am **HC+SS-WeM10 Fundamental Studies of the Water-gas Shift and CO_2 Hydrogenation on Metal/oxide Catalysts: From Model Systems to Powders**, *Jose Rodriguez*, Brookhaven National Laboratory **INVITED**

In this talk, it will be shown how a series of *in-situ* techniques {X-ray diffraction (XRD), pair-distribution-function analysis (PDF), X-ray absorption spectroscopy (XAS), environmental scanning tunneling microscopy (ESTM), infrared spectroscopy (IR), ambient-pressure X-ray photoelectron spectroscopy (AP-XPS)} can be combined to perform detailed studies of the structural, electronic and chemical properties of metal/oxide catalysts used for the production of hydrogen through the water-gas shift reaction (WGS , $\text{CO} + \text{H}_2\text{O} \rightarrow \text{H}_2 + \text{CO}_2$) and the hydrogenation of CO_2 to methanol (MS , $\text{CO}_2 + 3\text{H}_2 \rightarrow \text{CH}_3\text{OH} + \text{H}_2\text{O}$). Under reaction conditions most WGS and MS catalysts undergo chemical transformations that drastically modify their composition with respect to that obtained during the synthesis process. The active phase of catalysts which combine Cu, Au or Pt with oxides such as ZnO , CeO_2 , TiO_2 , $\text{CeO}_2/\text{TiO}_2$ and Fe_2O_3 essentially involves nanoparticles of the reduced noble metals. The oxide support undergoes partial reduction and is not a simple spectator, facilitating the dissociation of water, or the adsorption of CO_2 , and in some cases modifying the chemical

properties of the supported metal. Therefore, to optimize the performance of these catalysts one must take into consideration the properties of the metal-oxide interface. IR and AP-XPS have been used to study the reaction mechanism for the WGS and MS on the metal/oxide catalysts. Data of IR spectroscopy indicate that formate species are not necessarily involved in the main reaction path for these reactions on Cu-, Au- and Pt-based catalysts. Thus, a pure redox mechanism or associative mechanisms that involve either carbonate-like (CO_3 , HCO_3) or carboxyl (HOCO) species should be considered. In the last two decades, there have been tremendous advances in our ability to study catalytic materials under reaction conditions and we are moving towards the major goal of fully understanding how the active sites for the production of hydrogen through the WGS or the hydrogenation of CO_2 to methanol actually work.

11:40am **HC+SS-WeM12 The Use of EC-STM to Study the Chemical Reactivity and Nanoscale Structure of Metal Surfaces**, *A. Phillips, L. Jackson, H. Morgan, G. Jones, Erin Iski*, University of Tulsa

In the development of surfaces as efficient catalysts, it is critical to understand and control the surface reactivity in a defined manner. Electrochemical Scanning Tunneling Microscopy (EC-STM) is an advantageous technique in that in addition to providing a local probe of the atomic surface structure, EC-STM also functions as a 3-electrode cell in which redox chemistry can be performed to harness the chemical reactivity of the surface. This technique offers a unique window to study catalysis at conditions outside of a UHV environment, specifically at ambient temperatures and in liquids. Also, cyclic voltammograms (CVs) can be generated to provide specific information regarding the nature of the redox events occurring at the surface. Within this framework, it is possible to study how certain surfaces can become activated and/or deactivated as a result of electrochemical manipulation. One specific example of a thermally deactivated surface is a single Ag layer on a Au(111) crystal. The Ag layer is deposited on the Au(111) surface using Underpotential Deposition (UPD), which is an extremely controllable electrochemical technique for the application of a monolayer (or less) of a metal onto a more noble metal. Surprisingly, this atomically-thin Ag layer when formed in the presence of halides remains on the Au surface after heat treatments as high as 1,000 K. Importantly, thermal stabilization can be contrasted and compared with catalytic activity in which chlorine has shown to be a promoter of ethylene epoxidation over Ag(111), demonstrating why this system is intriguing from multiple vantage points. From a general standpoint, EC-STM offers an environmentally unique handle on how the chemical reactivity of a metal surface can be altered and how that surface can then be studied on a fundamental level.

12:00pm **HC+SS-WeM13 Formation and Stability of Surface Oxides on Ag(111)**, *Daniel Killelea, J. Derouin, R.G. Farber, M.E. Turano*, Loyola University Chicago; *E.V. Iski*, The University of Tulsa

A long-standing challenge in the study of heterogeneously catalyzed reactions on silver surfaces has been the determination of what surface phases are of greatest chemical importance. This is due to the coexistence of several different surface phases on oxidized silver surfaces. A further complication is subsurface oxygen (O_{sub}). O_{sub} are O atoms dissolved into the near surface of a metal, and are expected to alter the surface in terms of chemistry and structure, but these effects have yet to be well characterized. We studied oxidized Ag(111) surfaces after exposure to gas-phase O atoms with a combination of surface science techniques to determine the resultant surface structure; we observed that once 0.1 ML of O_{sub} has formed, the surface dramatically, and uniformly, reconstructs to a striped phase at the expense of all other surface phases. Furthermore, O_{sub} formation is hindered at temperatures above 500 K. We also observed a coexistence of several surface oxides at intermediate deposition temperatures, and the predominance of the $p(4 \times 5\sqrt{3})$ surface reconstruction at elevated temperatures.

MEMS and NEMS

Room 102B - Session MN-WeM

Multiscale Phenomena & Emerging Technologies in Micro- and Nano-Systems

Moderators: Max Zenghui Wang, Case Western Reserve University, Robert Davis, Brigham Young University

8:00am **MN-WeM1 Designing Microrobots to Interact with the Real World**, *Sarah Bergbreiter*, R. St. Pierre, D. Vogtmann, University of Maryland, College Park; A. Gerratt, Ecole Polytechnique Fédérale de Lausanne (EPFL)

INVITED

Research on mobile microrobots has been ongoing for the last 20 years, but the few robots that have walked have done so at slow speeds on smooth silicon wafers. However, ants can move at speeds over 40 body lengths/second on surfaces from picnic tables to front lawns. At larger scales, bio-inspired robots have taken advantage of a wide array of materials to provide passive mechanical properties used by insects to locomote effectively. We have developed a micro-molding process to incorporate materials with widely varying moduli and functionality along with traditional silicon MEMS for similar complexity in smaller packages. Mechanisms useful for locomotion like legs and energy storage elements are demonstrated, including a 4mm jumping mechanism that can be launched approximately 35 cm in height. In addition, magnetic materials can be incorporated in this process and we have used press-fit, commercially available NdFeB magnets down to 250 μm in size to provide untethered, off-board actuation of these robotic mechanisms. Both magnetic and molded materials have been characterized to better model robot mechanisms using this process. In addition, magnetic actuation is used to characterize legged locomotion in a 25 mg 6-legged microrobot over flat and rough terrain with speeds demonstrated up to 5.9 body lengths/second.

8:40am **MN-WeM3 Ferroelectric and Piezoelectric Properties of [100]-textured PZT (52/48) Films Deposited on Pb_xTiO₃ Nano-seed Layered Platinized Silicon**, *Sushma Kotru*, J. Zhong, V. Batra, The University of Alabama

Lead zirconate titanate (PZT) films are used in micro electro mechanical systems (MEMS) due to the self-generating sensing, large actuation amplitude with low voltage, and compatibility to integrated circuit process. PZT films exhibit higher values of effective transverse piezoelectric coefficient ($d_{31,e}$) and effective longitudinal piezoelectric coefficient ($d_{33,e}$), compared to any other available piezoelectric materials, both of which are important properties for such applications. Further improvement in the piezoelectric coefficients of PZT films is still being investigated.

In our previous work, the effect of Pb content and solution concentration of lead titanate (Pb_xTiO₃) seed layer on the texture and electric properties of Pb_{1-x}(Zr_{0.52}Ti_{0.48})O₃ thin films (190 nm) was investigated. The results indicated that 0.02 M Pb_xTiO₃ favors (100)/(001) orientation and suppresses (111) orientation in PZT films, thereby improving the electrical properties. The optimized conditions of the seed layer were further used to prepare thicker PZT films. Seed layer of 0.02 M Pb_xTiO₃ with varying Pb content ($x = 1.0, 1.05, 1.1, 1.2$) was used to prepare 1.3 μm PZT films by chemical solution deposition method. From the results, it was observed that PZT films deposited on seed layer with 1.0 Pb content exhibit maximum {100}-texture, highest remnant polarization (50.25 $\mu\text{C}/\text{cm}^2$), coercive field (38.20 kV/cm), and permittivity (2086). However, maximum transverse piezoelectric coefficient of -13.3 C/m² was obtained for films with 1.05 Pb content in the seed layer. Thus use of a seed layer is a promising route to promote {100}-textured PZT films, thereby improving the electrical properties and effective transverse piezoelectric coefficient of PZT films required for actuators and/or sensors.

9:00am **MN-WeM4 Methodology for Electromechanical Characterization of Resonant Micro Structures Actuated by Acoustic and Fringing Electrostatic Fields**, *S. Lulinsky*, T. Shmilovich, Tel Aviv University, Israel; B.R. Ilıc, National Institute of Standards and Technology; *Slava Krylov*, Tel Aviv University, Israel

In resonant micro and nanoelectromechanical sensors (MEMS/NEMS), the excitation of vibratory motion is usually achieved through implementation of electrostatic, piezoelectric, magnetic, thermal or optical transduction. Most of these methods require additional conductive layers, which broaden the vibrational characteristics of the device and induce residual stresses. In addition, often nonlinear actuation forces may alter the spectral characteristics of the structure. Inertial excitation by an external

shaker is widely used for mechanical dynamic characterization. However, simultaneous electrical excitation and detection requires wire bonding and packaging, which is not always suitable at the initial stages of characterization or for wafer level testing. In this work we report on a methodology for efficient electromechanical characterization of resonant micro structures using a combination of acoustic and fringing electrostatic fields. We show that omnidirectional acoustic excitation of unpackaged, electrically connected using micromanipulators, devices is a convenient alternative to inertial excitations.

Using deep reactive ion etching (DRIE), 500 μm long and 16 μm wide cantilevers were fabricated from silicon on insulator (SOI) wafers with 5 μm and 2 μm thick device and buried thermal silicon dioxide layers, respectively. A cavity was etched within the handle of the wafer to allow for high unobscured out-of-plane vibrational amplitudes. An actuating electrode was fabricated from the device layer and was located symmetrically at the two sides of the beam. First, in order to investigate the mechanical response, flexural out-of-plane vibrations of microcantilevers were excited by a miniature acoustic speaker. The transducer frequency band was chosen near the fundamental mode of the cantilevers. Resonant frequencies and quality factors of the devices were measured optically with a laser Doppler vibrometer (LDV). An acoustic field was simultaneously monitored by a microphone located in a proximity of the cantilever. The microphone output, after re-normalization, was subtracted from the LDV output in order to eliminate the influence of the spectral characteristics of the transducer itself. Next the devices were operated simultaneously by the acoustic and electrostatic fields. The distributed electrostatic force acts in the direction opposite to the deflection and serves as an effective elastic foundation. As a result, the stiffness of the cantilever increases with increasing voltage. By applying a steady DC voltage of 100 V we demonstrate that the fundamental frequency of the beam harmonically excited by an acoustic field can be tuned upward by 2.5%.

9:20am **MN-WeM5 Nonlinear Interactions of Micromechanical Cantilevers through Fringing Electrostatic Fields**, *Christopher Wallin*, Center for Nanoscale Science and Technology (CNST), National Institute of Standards and Technology (NIST), and University of Maryland (UMD); D.A. Westly, National Institute of Standards and Technology, Center for Nanoscale Science and Technology, Gaithersburg, MD; S.J. Grutvik, A.T. Zenhnder, R.H. Rand, Cornell University; V. Aksyuk, National Institute of Standards and Technology, Center for Nanoscale Science and Technology, Gaithersburg, MD; S. Krylov, Tel Aviv University, Israel; B.R. Ilıc, National Institute of Standards and Technology, Center for Nanoscale Science and Technology, Gaithersburg, MD

Micro- and nano-electromechanical systems (M/NEMS) have enormous potential in and provide new opportunities for applications such as detection of mass, force and energy, microwave amplification, optomechanics, and energy harvesting. Micro and nanoscale mechanical resonators offer significant advantages over their macroscopic counterparts, including their low mass, high mechanical quality factor, Q, and compatibility with integrated electronics. Architectures consisting of interacting M/NEMS arrays exhibit rich dynamical phenomena. For instance, excitations in periodic, strongly-interacting nonlinear systems give rise to wave propagation and intrinsically localized modes. The dynamics of these systems are highly sensitive to local changes in their environment which makes them an attractive platform for realizing ultra-sensitive chemical, biological, and force sensors. In our work, we report experimental observations of parametric electrostatic excitation, synchronization and abrupt transitions between standing wave patterns in the interacting cantilever array systems.

Interdigitated, electrostatically-actuated cantilever devices were fabricated using a silicon-on-insulator (SOI) wafer with a highly-doped single-crystal silicon device layer. First, Au electrodes with a Cr adhesion layer were defined using lift-off with a bilayer resist process. The devices, consisting of two sets of 100 interdigitated cantilevers, were lithographically defined and etched using deep reactive ion etching (DRIE). The two structures were electrically isolated by the underlying ≈ 3 micrometer thick buried silicon dioxide layer (BOX). Using an aligned backside exposure, the silicon handle wafer was bulk etched within the active array area. This allowed the excitation of nonlinear vibrations with large amplitudes by eliminating the possibility of impacts between the cantilevers and the substrate. Interactions between cantilevers take place *via* both fringing electrostatic fields within the overlap region and mechanical coupling through the overhang. The out of plane, translational motion was directly visualized using a high resolution CMOS camera at a frame rate of $\approx 30 \text{ s}^{-1}$. Device

Wednesday Morning, November 9, 2016

dynamics were first measured in vacuum at a pressure of $\approx 2 \times 10^{-3}$ Pa and then under ambient air conditions. In vacuum, where mechanical quality factors are high, the drive voltage was significantly lower than in air where considerable damping occurs. Our results show distinct propagation bands, abrupt transitions between standing wave patterns, and the influence of missing-beam defects on system dynamics.

9:40am **MN-WeM6 Reduction in Frequency Noise through Mode Coupling in a MEMS Oscillator**, *David Czaplewski, C. Chen, D. Lopez*, Argonne National Laboratory; *P.M. Polunin, O. Shoshani, S.W. Shaw, M.I. Dykman*, Michigan State University

MEMS and NEMS oscillators have been proposed as frequency generators to replace quartz as timing components in applications that require low power and a small footprint. The accuracy of a time measurement using a frequency generator is related to the fluctuations in both the generator amplitude and frequency. In many oscillators, the relative magnitude of frequency fluctuations is suppressed by increasing the vibration amplitude and choosing an operating point before the onset of non-linear response. Operating in a nonlinear region is generally avoided, primarily due to an additional contribution to the frequency fluctuations arising from the conversion of amplitude fluctuations into frequency fluctuations. However, we demonstrate a non-linear frequency generator that suppresses frequency fluctuations through means of an internal resonance. An internal resonance is accompanied by a pronounced transfer of energy between two coupled modes of a resonant structure [1,2]. For our frequency generator, the primary mode of operation is an in-plane flexural mode, which is actively controlled, and the second mode is a torsional mode with an eigenfrequency about three times larger than the flexural mode, which is passively coupled to the flexural mode. We present a theoretical model of the modal coupling and show, from our model and experimental observations, that the frequency fluctuations are reduced by several orders of magnitude due to a broad range of near-zero dispersion, i.e., near independence of the vibration frequency on the amplitude imposed by the presence of internal resonance. Within this near-zero dispersion region, a subset of operating conditions is found where frequency fluctuations are reduced even further due to a zero-dispersion point created by relationships of the parameters of the coupled equations. We present data on the stability of the frequency as a function of time (Allan deviation) and the spectrum of the frequency fluctuations (phase noise versus offset frequency) at different operating points of the generator. We also discuss the prospect of further increasing the frequency stability of MEMS/NEMS oscillators by reducing the noise floor of the system and approaching the thermomechanical noise limit of such systems.

[1] A. H. Nayfeh and D. T. Mook, *Nonlinear oscillations* (John Wiley & Sons, 2008).

[2] D. Antonio, D. H. Zanette, and D. Lopez, *Nature communications* 3 806 (2012).

11:00am **MN-WeM10 Characterization of MEMS-based, Thin Film Silicon Carbide Diaphragms Using Multimode, Resonance Frequency Analysis**, *A.C. Barnes, Christian Zorman*, Case Western Reserve University

This paper presents an investigation into the resonant frequency behavior of large area diaphragms made from silicon carbide thin films and the development of a plate-under-tension model to determine the Young's modulus and residual stress from resonant frequency data. Test specimens consisted of single crystalline (100) 3C-SiC, polycrystalline (111) 3C-SiC and amorphous SiC thin films that were fabricated into nominally 1×1 mm² diaphragms by silicon bulk micromachining. Single crystalline diaphragms ranged in thickness from ~ 1.5 μ m to 125 nm while the polycrystalline and amorphous diaphragms were held in the 1.5 μ m thickness range. A thin (~ 50 nm) Si₃N₄ diaphragm was also included in the study. Test specimens were excited into resonance using a PZT crystal and interferometry was used to detect the vibrational modes. Testing was performed in vacuum to eliminate damping.

Initial testing involved measurement of resonant frequencies between 50 kHz and 2 MHz at various drive amplitudes. Each diaphragm exhibited at least 50 resonant peaks in this range, with at least one diaphragm having 250 peaks. Every diaphragm exhibited at least 5 peaks with quality factors (Q) > 10,000. The highest quality factor, as well as the largest number of high Q peaks, was observed in the diaphragm with the highest residual stress.

A method to determine the Young's modulus and residual stress of a diaphragm from the resonant frequency data using a plate-under-tension model was proposed and developed. This method, which relies on the identification of numerous high order modes, was shown to be effective for

the thicker films in the study (> 1 μ m); however, the technique was only able to determine the residual stress for the submicron-thick films. Based on these observations, an equation that relates the Young's modulus and residual stress to diaphragm thickness, side lengths and mode number was derived to identify diaphragm parameters that are well suited for this method.

11:20am **MN-WeM11 High-resolution, MEMS-based Calorimeter for Quantitative Studies of Superconducting Phase Transitions in Thin Film Samples**, *Zhu Diao, D. Campanini, A. Rydh*, Stockholm University, Sweden

Quantitative calorimetric studies of minute amount of material is a notoriously sophisticated task. It requires a high-resolution calorimeter design that contributes a negligible background signal (addenda). The issue is further complicated when the electronic specific heat of a sample is concerned, e.g. in the case of characterising the superconducting phase transition of a superconductor in thin film form. Over a wide temperature range, the electronic specific heat in most materials is one or two orders of magnitude lower than its lattice counterpart, raising even more stringent requirements on the resolution and accuracy of calorimetric measurements.

In this work, we describe a state-of-the-art, microelectromechanical system (MEMS)-based differential calorimeter operating in the ac steady-state mode that addresses this challenge. The calorimeter cell, consisted of two 150-nm-thick SiN_x windows placed side by side, is fabricated with a batch processing routine utilising silicon bulk micromachining techniques. Active components of the calorimeter include a gold-germanium resistive thermometer, an AC heater for delivering a well-defined alternating power to the sample, and a DC heater for locally heating the sample above the base temperature. They are defined using UV lithography and deposited onto the centre of the membrane window in the form of a stack of thin film layers [1]. The addenda of the calorimeter cell are as low as a few tens of nJ/K at room temperature, and further decrease down to 10 pJ/K at 1 K. Calorimetric measurements are carried out in a sample-in-vacuum ³He cryostat, under an automatic frequency adjusting, true differential-mode using custom-designed FPGA-based advanced electronics [2]. This provides both absolute accuracy and high resolution, where the addenda from the calorimeter cell are largely eliminated.

Thin films of superconducting niobium and tantalum in the range of hundreds of nanometers are used in demonstrating the capability of our calorimeter. They are deposited onto prefabricated silicon nitride windows, sculptured with a focused ion beam, and then transferred onto one of the calorimeter windows with a micromanipulator under an optical microscope. Specific heat jumps at the respective superconducting phase transition are still found to display an excellent signal-to-noise ratio while in-field measurements allow quantitative studies of the suppression of superconducting order parameters by applied magnetic fields.

[1] S. Tagliati, V. M. Krasnov, and A. Rydh, *Rev. Sci. Instrum.* **83** (2012) 055107.

[2] <http://www.synktek.com>

11:40am **MN-WeM12 Microelectrode Array of Carbon Nanotube Posts with High Aspect Ratio and Millimeter-length, and Its Electrochemical Response**, *Guohai Chen, R.R. Vanfleet, R.F. Davis*, Brigham Young University

Carbon nanotubes (CNTs) have been demonstrated to be capable of making excellent electrodes/microelectrodes due to the combination of high aspect ratio, nanometer-sized dimensions, good electrical conductivity, and high chemical and thermal stability. Microelectrode array of CNT posts with high aspect ratio and millimeter-length was fabricated using carbon-nanotube-templated microfabrication with a sacrificial hedge. The electrochemical response (cyclic voltammetry) to both methyl viologen and dopamine in phosphate buffered saline solution was measured on an individual CNT post microelectrode with a diameter of 25 μ m and a length of 1 mm. In addition of the detection of the characteristic peaks, the CNT post microelectrodes show a fast electrochemical response, which may be enabling for in-vivo and/or in-vitro measurements.

Wednesday Morning, November 9, 2016

Plasma Science and Technology

Room 104C - Session PS+TF-WeM

Atomic Layer Etching

Moderator: Eric A. Hudson, Lam Research Corporation

8:00am **PS+TF-WeM1 Selective Cyclic Plasma Etching of Thin Films in Two Heating Way, Ion Bombardment and Infrared Irradiation.**, *M. Izawa*, Hitachi High-Technologies Corp., Japan; *Kazunori Shinoda*, *N. Miyoshi*, *H. Kobayashi*, Hitachi, Japan; *N. Yasui*, *M. Tanaka*, *Y. Sonoda*, *K. Kuwahara*, Hitachi High-Technologies Corp., Japan; *K. Ishikawa*, *M. Hori*, Nagoya University, Japan

INVITED

With shrinking device size and introduction of 3D FinFET transistor structure, cyclic Atomic Layer Etching (ALEt) becomes one of the key technologies in thin film etch. To achieve extreme high selectivity against mask and etch-stop layers, atomic level etching as a method to meet these etching requirements and eliminate physical damage has been investigated. Further, isotropic ALEt will be required for use in nanoscale patterning for formation of more complex 3D structures. In cyclic ALE technology, a modification layer is formed on a thin film layer by supplying etching species. After that, the modification layer is removed by heating. We investigated two types of ALEt tools; one is an anisotropic ALE tool based on Microwave ECR plasma and the other is a isotropic ALE based on ICP type down-flow plasma.

Recently, we have reported results of isotropic ALEt of Silicon Nitride (SiN) film [1]. High-throughput and high-selectivity ALEt of SiN using IR irradiation and down-flow plasma was also demonstrated [2]. Modification layer, ammonium hexafluorosilicate ((NH₄)₂SiF₆), was synthesized by fluorocarbon gas plasma and nitrogen supplied from SiN film. Because the modification layer is formed only on SiN film, SiN film can be removed with high selectivity at IR radiation heating step. This technology can be also applicable to ALEt of TiN.

Anisotropic ALEt was also investigated by using Microwave-ECR plasma [3]. In this study, Ar ion irradiation was utilized instead of heating. To achieve high selectivity, the ion energy lower than sputtering threshold is required. Because microwave-ECR plasma has low plasma potential and is not fluctuated by wafer RF power, lower ion energy is available. In addition, it is known that excessive dissociation of gases and by-products causes reverse reaction and degradation of selectivity. We therefore used high gas flow rate and pulsed plasma to reduce dissociation. This ALEt technology has been applied to high selective etching of Si, HfO₂, and SiN film.

[1] K. Shinoda *et al.*, AVS Atomic Layer Etching workshop 2015.

[2] N. Miyoshi *et al.*, 62 nd AVS, , PS+SS+TF-WeM5, 2015.

[3] M.Tanaka *et al.* , SPIE Advanced Litho., 9428-23, 2015.

8:40am **PS+TF-WeM3 Concurrent Engineering of Atomic Layer Etch Patterning Processes Involving Oxide and Nitride Materials**, *Mingmei Wang*, *P. Chan*, TEL Technology Center, America, LLC; *P. Ventzek*, Tokyo Electron America; *A. Ranjan*, TEL Technology Center, America, LLC

Atomic layer etching (ALE) of Si has been the focus of extensive research and development for over two decades. [1] However, the precision etch of dielectric materials (SiO₂, Si₃N₄) in patterning schemes employing self-aligned contacts (SACs) and self-aligned multiple patterning (SAMP) at the 10nm technology node and beyond are where ALE has significant potential. In both SAC and SAMP schemes, an oxide layer must be etched selective to a thin nitride layer with a corner with a thickness and radius of curvature of less than 10 nm. Fortunately precision etch using cyclic deposition/etch schemes have been proven effective at preserving the thin nitride corner. Unlike atomic layer etching of silicon using chlorine, fluorocarbon chemistry etching of nitride and oxide is not self-limiting process. The thin fluorocarbon polymer layers that protect the nitride layer corner deep in a feature are difficult to measure with common in-line metrology. Both these facts make trial-and-error development of processes for cyclic etch of oxide materials selective to nitride underlayers challenging. We have used concurrent engineering approaches including both modeling and experiment to bypass these difficulties. The core of the approach is a new integrated chamber (HPem)-feature scale MCFPM (Monte Carlo Feature Profile Model) model [2] for oxide nitride etch experiments conducted on a dual frequency plasma source using a benchmark Ar/C₄F₈/O₂ chemistry. The concurrent engineering approach comprises stages of development and prediction tests using both blanket wafer and patterned coupon data and finally process parameter optimization. By using this approach, we have minimized nitride corner loss and optimized nitride/oxide etch selectivity with a minimum of engineering resources. The presentation will

survey both experimental and computational results representing a case study in SAC process development. Furthermore, insights into the relationship between chamber function and critical surface processes will be discussed.

[1] A.Ranjan, M.Wang, S.Sherpa, V. Rastogi, A. Koshiishi, and P.Ventzek, J. Vac. Sci. Technol. A34, 2016.

[2] M.Wang and M.Kushner, J. Appl. Phys 107, 2010.

9:00am **PS+TF-WeM4 System Trade-offs of Atomic Layer Etching (ALE) of High Aspect Ratio 3D Features**, *Chad Huard*, University of Michigan; *Y. Zhang*, *S. Sriraman*, *A. Paterson*, Lam Research Corp.; *M.J. Kushner*, University of Michigan

Atomic layer etching (ALE) is a method for decoupling process parameters that, with continuous etching, are usually difficult to separately control. ALE does so at the trade-off of decreased etch rate. Of particular interest is the ability of ALE to separate the consequences of plasma parameters, such as ion to neutral flux ratios and ion energies, from issues of transport into and out of the feature. By using separate and self-limited reactions for surface passivation and material removal, ALE offers a way to deliver the optimum neutral/ion ratio at any aspect ratio at the trade-off of increasing etch time.

Using a 3-dimensional voxel based Monte-Carlo feature profile model, the trade-off between etch time and etch fidelity encountered in the ALE regime has been investigated. The poly-silicon gate etch process of a high-k metal replacement finFET is the base case for this study. The time-multiplexed scheme to achieve ALE is an Ar/Cl₂ plasma passivation step followed by an Ar plasma step having higher ion energies to remove Si. We found that the change in neutral conductance of the feature as the aspect ratio increases requires adjusting process step times to optimize etch rates. We also found that ALE is able to clear corners in 3D features more effectively than continuous etching, requiring less over-etch. A measure of clearing efficiency is the amount of over-etch required to clear the corners compared to the total etch time. The clearing efficiency was investigated for an entirely ALE process and a hybrid approach using a continuous main etch followed by an ALE clearing etch, over a range of geometries including varying fin spacing and side-wall slope.

Work was supported by Lam Research Corp., Department of Energy Office of Fusion Energy Science and the National Science Foundation.

9:20am **PS+TF-WeM5 Molecular Dynamics Simulations of Atomic Layer Etching**, *Jun-Chieh Wang*, *S. Rauf*, *J.A. Kenney*, *L. Dorf*, *K.S. Collins*, Applied Materials, Inc.

INVITED

Sub-nm precision is increasingly being required of many critical plasma etching processes in the semiconductor industry. As such, atomic layer etching (ALE) has become a potential candidate for accurate control of a variety of critical etching processes. In ALE, the target substrate is first exposed to a reactive gas that passivates the surface followed by ion bombardment with energy below the sputtering threshold. It is essential to precisely control the ion/radical energy and flux during the etching process to remove the topmost passivated surface without damaging the underlying substrate. Once the passivation layer is removed, the etch process stops. The passivation and etching steps repeat until one has etched to the desired thickness. In contrast to conventional radio-frequency (RF) plasma etching processes, microfabrication using ALE promises high selectivity and low damage to the substrate. In this talk, we discuss the properties of ALE on a patterned surface using results from molecular dynamics (MD) simulations. A chlorinated Si/SiO₂ surface was bombarded by Ar⁺ or Cl⁺ ions to remove the modified surface layers. With Ar⁺ energy below the sputtering threshold, etch process stops after the Si surface becomes deficient in Cl atoms; while at high bombarding energy, Si removal continuous with lower rate partly due to physical sputtering. For Cl⁺ ion bombardments, the Si surface is continuously etched at a constant rate, and the etch rate increases with Cl⁺ ion energy. Results for different aspect ratios will also be discussed. These fundamental studies are used to interpret our layer-by-layer ALE experiments.

11:00am **PS+TF-WeM10 Isotropic Atomic Layer Etching of Titanium Nitride Using Formation and Desorption of Ammonium Salt**, *Kazunori Shinoda*, *N. Miyoshi*, *H. Kobayashi*, *M. Kurihara*, Hitachi, Japan; *S. Sakai*, *M. Izawa*, Hitachi High-Technologies, Japan; *K. Ishikawa*, *M. Hori*, Nagoya University, Japan

There is growing interest in atomic layer etching (ALEt) as 3D devices become widely used and feature sizes continue to scale down. The development of isotropic ALEt for various materials will be important for existing and future 3D devices such as a 3D NAND, Fin FET, and GAA FET.

Wednesday Morning, November 9, 2016

Recently, the authors developed an isotropic ALEt for SiN using formation and desorption of an ammonium hexafluorosilicate-based modified layer [1]. High-throughput high-selectivity ALEt of SiN using IR irradiation was also demonstrated by the authors [2]. In this work, isotropic ALEt of TiN using formation and desorption of an ammonium salt-based modified layer is developed.

The experimental apparatus used in this study is composed of a reaction chamber and an x-ray photoelectron spectroscopy (XPS). TiN deposited by atomic layer deposition was used as the sample material. Several samples were exposed to radicals that were generated in fluorocarbon-based gas mixtures. The samples were then annealed by using circulating fluid. The surface of the samples was analyzed by XPS. Photoemission spectra obtained after radical exposure and after thermal annealing of the TiN samples are compared. The etching depth was evaluated by ellipsometry.

A nitrogen 1s peak (402 eV), which has been assigned as ammonium salt, was observed after radical exposure. Titanium 2p peaks (462 and 467 eV), which originate from a Ti-F bond, were observed simultaneously. These results imply that the surface of the radical exposed TiN consists mainly of ammonium salt such as ammonium fluorotitanate. After the samples were annealed on the wafer stage heated at 210°C, the nitrogen 1s peak at 402 eV, which is assigned as ammonium salt, disappeared. A nitrogen 1s peak at 396 eV, which is attributed to TiN, appeared after the ammonium salt-related peak disappeared. This phenomenon implies that the film of ammonium salt decomposed and desorbed from the TiN surfaces at elevated temperatures.

The preliminary tests of cyclic etching are carried out by repeating radical exposure and thermal annealing. For one cycle of etching, the etching depth increases with increasing radical exposure time and saturates at 0.7 nm. For multiple cycle etching, the etching depth increases with an increasing number of repetitions of the cycle. Tuning of the etched amount per cycle (EPC) in the range from 0.3 to 0.7 nm was demonstrated by changing the composition of gas mixtures. From these results, it is concluded that the ALEt of TiN was successfully demonstrated.

[1] K. Shinoda et al., Atomic Layer Etching Workshop 2015, July 1–2, p. 572 (2015).

[2] N. Miyoshi et al., AVS 62nd International Symposium & Exhibition, PS+SS+TF-WeM5 (2015).

11:20am PS+TF-WeM11 Organic Etchants Toward Atomic Layer Etching of Magnetic Metals, Nicholas Altieri, L. Minardi, E.L. Chen, J.P. Chang, University of California Los Angeles

The continued advancement in logic and memory devices relies heavily on the introduction of new materials. Of specific interest in the field of memory application is the utilization of magnetic metals and alloys such as Co, Fe, and CoFe as well as additional doped alloys such as CoFeB. Contemporary techniques for patterning these materials rely on noble ion beam milling which, although effective, leaves much to be desired in achieving selectivity and retaining pattern transfer fidelity for high aspect ratio features. One solution is the pursuit of atomic layer etching through reversal of the atomic layer deposition scheme and generation of volatile metal-organic species reminiscent of ALD precursors. Due to the etch-resistant nature of the materials studied, removal at an atomic level is enabled by chemical modification of the surface through plasma exposure and subsequent introduction of organic ligands.

Selected single element Co and Fe films as well as the magnetic metal alloy CoFeB (30nm) were studied using this scheme. Organic chemistries, such as acetylacetone (acac) and hexafluoroacetylacetone (hfac) were first investigated to determine the feasibility of metal-organic formation through direct exposure. The efficacy of acetylacetone and hexafluoroacetylacetone etching chemistries were confirmed through previous solution-based studies on Co and Fe, respectively, via formation of $\text{Co}(\text{acac})_2$ (257 amu) and $\text{Fe}(\text{hfac})_3$ (680 amu) as confirmed through mass spectrometry. Use of these organics was extended to the boron-doped alloy in the form mixtures with volumetric ratios of 1:3, 1:1, and 3:1 (acac:hfac). $\text{Co}_{30}\text{Fe}_{45}\text{B}_{25}$ was shown to etch at rates up to 15 nm/min in the 1:1 solution and ~1 nm/min at an organic mixture partial pressure of 60 Torr. The composition of the film as well as its metallic nature were preserved as seen by x-ray photoelectron spectroscopy (XPS) through the detection of Co and Fe metallic peaks present at 778.2 and 706.7 eV, respectively.

Chemical modification of the surface was then investigated as a means of controlling the amount of material removed and determining effects on material properties under various process conditions. XPS analysis of Co

and Fe films processed under O_2 plasma show increasing thickness of CoO and Fe_2O_3 up to 3.7nm and 4.6nm, respectively after 5 min exposure. Magnetic properties of both single element and alloyed films were characterized using superconducting quantum interference device magnetometry (SQUID) and displayed degraded magnetic properties through increasing coercivity with increasing oxidation time.

11:40am PS+TF-WeM12 Conformality of Thermal Al_2O_3 Atomic Layer Etching in High Aspect Ratio Structures, Amy Marquardt, H. Sun, University of Colorado Boulder; S.M. George, University of Colorado at Boulder

Thermal atomic layer etching (ALE) is the reverse of atomic layer deposition (ALD). Conformal deposition in high aspect ratio structures is one of the key features of ALD. The conformality of etching in high aspect ratio structures will also be important for thermal ALE. In this study, the conformality of thermal Al_2O_3 ALE was investigated in channels with high aspect ratios ranging from 60 to 200. Al_2O_3 ALD was used to deposit the initial Al_2O_3 films in the channels. The Al_2O_3 ALE was performed at 300°C using HF and $\text{Al}(\text{CH}_3)_3$ as the reactants. HF is known to fluorinate Al_2O_3 and form an AlF_3 layer on the Al_2O_3 surface. The $\text{Al}(\text{CH}_3)_3$ then undergoes a ligand-exchange transmetalation reaction with the AlF_3 layer. $\text{Al}(\text{CH}_3)_3$ accepts fluorine and donates methyl ligands to the surface. This ligand-exchange allows the Al in the AlF_3 layer to leave as a volatile reaction product such as $\text{AlF}(\text{CH}_3)_2$ or $\text{Al}(\text{CH}_3)_3$. The conformality of Al_2O_3 etching was examined in high aspect ratio channels defined by stainless steel foil spacers between silicon substrates. Spectroscopic ellipsometry was used to measure the Al_2O_3 film thickness in the channels. Increasing the aspect ratio increased the reactant exposure and purge times necessary to maintain conformal etching. Longer times were required to allow the reactants and products to diffuse in and out of the high aspect ratio channels. Increasing the reactant pressures also lowered the required reactant exposure times. However, increasing the reactant pressures from 0.1 to 9 Torr also increased the Al_2O_3 etching rate. The higher etching rates were attributed to a thicker AlF_3 layer formed at higher reactant partial pressures. Using longer reactant exposure or purge times or higher reactant pressures, conformal Al_2O_3 etching was obtained in the high aspect ratio channels.

12:00pm PS+TF-WeM13 Thermal Atomic Layer Etching of Crystalline Aluminum Nitride Using Sequential, Self-Limiting HF and $\text{Sn}(\text{acac})_2$ Reactions and Enhancement by H_2 and Ar Plasmas, Nicholas Johnon, H. Sun, K. Sharma, S.M. George, University of Colorado at Boulder

Thermal atomic layer etching (ALE) has been recently demonstrated for a variety of oxides such as Al_2O_3 , HfO_2 and ZrO_2 using sequential, self-limiting fluorination and ligand-exchange reactions. In this work, the thermal ALE of aluminum nitride, a III-V metal nitride, was performed for the first time. Crystalline aluminum nitride (AlN) films were etched using hydrogen fluoride (HF) and tin(II) acetylacetonate ($\text{Sn}(\text{acac})_2$) as the reactants. The AlN films were in the crystalline wurtzite phase with the (0001) plane parallel to the surface. Film thicknesses were monitored versus number of ALE reaction cycles at 275°C using in situ spectroscopic ellipsometry (SE). A low etch rate of 0.07 Å/cycle was measured during etching of the first 40 Å of the film. These small etch rates corresponded with the AlO_xN_y layer on the AlN film. The etch rate then increased to 0.36 Å/cycle for the AlN films. In situ SE experiments established the HF and $\text{Sn}(\text{acac})_2$ exposures that were necessary for self-limiting surface reactions. In the proposed reaction mechanism for thermal AlN ALE, HF fluorinates the AlN and produces an AlF_3 layer on the surface. The metal precursor, $\text{Sn}(\text{acac})_2$, then accepts fluorine from the AlF_3 layer and transfers an acac ligand to the AlF_3 layer in a ligand-exchange reaction. The volatile etch products are $\text{SnF}(\text{acac})$ and either $\text{Al}(\text{acac})_3$ or $\text{AlF}(\text{acac})_2$. Adding a H_2 or Ar plasma exposure to the reaction sequence enhanced the etching rates. A H_2 or Ar plasma exposure after the $\text{Sn}(\text{acac})_2$ exposure increased the AlN etch rate from 0.36 Å/cycle to 1.96 Å/cycle or 0.9 Å/cycle, respectively, at 275°C. The enhanced etch rates are believed to result from either H radicals or photons from the H_2 plasma or ions or photons from the Ar plasma. The H radicals may be able to remove acac surface species that may limit the etch rate. The photons or ions may also lead to the desorption of surface species or substrate excitation that enhances the etch rate.

Wednesday Morning, November 9, 2016

Plasma Science and Technology

Room 104B - Session PS-WeM

Plasma Sources and Novel Mechanisms for Generating Plasmas

Moderator: Sumit Agarwal, Colorado School of Mines

8:00am **PS-WeM1 Multifrequency Impedance Matching Solutions for Plasma Excitation by Tailored Voltage Waveforms**, *Erik V. Johnson*, Ecole Polytechnique, Palaiseau, France; *S. Dine*, SOLAYL SAS, France; *J.-P. Booth*, Ecole Polytechnique, Palaiseau, France

Tailored Voltage Waveforms (TVWs) and the Electrical Asymmetry Effect they induce in plasmas are useful tools to both optimize plasma processes and gain insight into the role of specific plasma parameters (ion bombardment energy, species flux) in processing outcomes. However, the multi-frequency nature of these waveforms, which are composed of a fundamental frequency in the MHz range and a number of its harmonics (e.g. 13.56MHz + 27.12MHz + 40.68MHz....), leads to a practical technical challenge, namely multi-harmonic impedance matching. Although impedance matching the 50 ohm output of an amplifier to a plasma processing chamber with a large reactive component is easily achieved for a single frequency using a passive component matchbox, doing the same at multiple harmonics is much more challenging due to the frequency response of every circuit element (including the chamber).

One strategy that has been employed and deployed as a commercial product is the use of multiple amplifiers, matchboxes, and filter sets, one for each frequency used. Although technically effective, using individual amplifiers for each frequency may not be the most cost-effective solution. Alternatively, we have previously proposed a technique to simultaneously match at multiple frequencies using a passive multi-frequency matchbox (MFMB), but this minimal-component solution is difficult to control due to variations in components affecting the response at pairs of frequencies.

In this work, we present results from a new design of MFMB using only passive components. Critically, this new design allows (1) independent control of the frequency response at each harmonic, and (2) the use of a single high-power amplifier. Circuit simulation results as well as experimental results are shown for a small area, laboratory plasma processing chamber during an argon plasma for three-frequency operation, and for fundamental frequencies between 9 and 15 MHz. It is demonstrated that although adjusting the matching condition for the fundamental frequency (1f) changes the matching for the other two (2f, 3f), the converse is not true; adjusting the matching on the higher harmonics does not impact that of the fundamental. Furthermore, we show that this improved matching is indeed due to better power transfer and not parasitic losses in the matching network.

8:20am **PS-WeM2 Effect of Tailored Voltage Waveforms on Surface Nanotexturing of Silicon in Capacitively Coupled SF₆/O₂ Discharges**, *Guillaume Fischer*, Institut Photovoltaïque d'Ile-de-France (IPVF), France; *E. Drahi*, *G. Poulain*, Total MS-Energies Nouvelles, France; *B. Bruneau*, *E.V. Johnson*, LPICM, Ecole Polytechnique, France

The nanotexturing of the surface of a crystalline silicon (c-Si) wafer for improved photovoltaic performance can be achieved through the use of an SF₆/O₂ reactive ion etching (RIE) capacitively coupled plasma (CCP). The resulting surfaces typically consist of nano-sized structures resembling cones (sizes ranging from 30 to 500nm) with little preferential crystallographic orientation. The process occurs through competing mechanisms involving Si etching by fluorine radicals, formation of in-situ micro-masking species, and physical etching by ions, all these mechanisms being strongly influenced by plasma conditions.

As has been done for previous processes and chemistries, we attempt to decouple the influence of various plasma properties through the use of Tailored Voltage Waveforms (TVWs), and thus obtain insights into the mechanisms involved in the dry nanotexturing of silicon. TVW excitation consists of adding harmonic frequencies with controlled amplitudes and phase-shifts to the RF (13.56 MHz) driving voltage, and allows one to quasi-independently control parameters such as species flux and ion bombardment energy (IBE). Furthermore, in an electronegative chemistry such as the SF₆/O₂ mixture, waveforms resembling "sawtooths" induce high ionization asymmetries due to plasma sheath dynamics, and may impact the type of reactive species arriving at the surface.

In this study, the phase-shift of the harmonic frequencies of the TVW excitation is varied at constant discharge power in an SF₆/O₂ mixture, therefore modifying (by an up to fourfold increase in absolute value) the

self-bias voltage (V_{DC}) at the powered substrate holder and therefore the maximum IBE. The impact of varying the TVW shape is observed through both the plasma properties (V_{DC} , optical emission) and the morphological and optical properties of the obtained nanotexture. The effectiveness of the texture is quantified by the surface effective reflectance (R_{eff}) which is the average reflectance weighted by the solar spectrum irradiance.

It is here shown that the use of TVW excitation allows, at constant discharge power, to switch from a regime with no etching (almost no change of R_{eff} , no nanostructures observed) to a texturing regime where the decrease of R_{eff} scales with the IBE (R_{eff} decreasing up to 30% and nanocones observed). Moreover, new types of nanostructures have been observed for some particular etching regimes, showing partial dependence on the crystallographic orientation of the substrate.

8:40am **PS-WeM3 Plasma Enhanced CVD processes: Dual Frequency PECVD with pulsing of liquid precursors and PEALD for Selective Deposition**, *Christophe Vallee*, LTM, Univ. Grenoble Alpes, CEA-LETI, France; *R. Gassilloud*, CEA, LETI, MINATEC Campus; *R. vallat*, LTM, Univ. Grenoble Alpes, CEA-LETI; *F. Piallat*, Altatech, France; *M. Aoukar*, LTM, Univ. Grenoble Alpes, CEA-LETI; *P. Kowalczyk*, LTM - CEA/LETI, France; *P.D. Szkutnik*, LTM, Univ. Grenoble Alpes, CEA-LETI; *P. Noé*, CEA, LETI, MINATEC Campus; *A. Bsiesy*, *P. Gonon*, LTM, Univ. Grenoble Alpes, CEA-LETI **INVITED** With this presentation we will address two topics concerning the development of specific Plasma Enhanced CVD processes for microelectronics applications: Dual Frequency (DF) with pulsed liquid injection of precursors and selective deposition.

First, we will talk about Dual Frequency processes for PECVD applications. Since the excitation frequency has extensive effects on the spatial distribution of species and their concentrations, the dissociation of the precursor can also be increased by crossing the discharge excitation frequency to the basic ion plasma frequency. This route is considered here with comparison and discussion over the improvements brought by Dual Frequency LF/RF plasmas in the case of thin metal gate (TiN) and Phase Change Material (GeSbTe) deposition. For this study we used 200 mm and 300 mm commercial PECVD tools from Altatech with a pulsed liquid injection of precursors. We will show that during TiN deposition the plasma enters a g-mode due to secondary electron heating. Then adding LF to RF modifies the sheath thickness of the plasma, increases the electron temperature of the gas and thus leads to strong modification of the carbon content, density and growth rate. For PCM applications, very different cycles (amorphous to crystalline) are obtained for GeTe materials elaborated in RF mode or DF mode. Moreover, we observe a very strong improvement of the gap filling capability of the process by using the DF mode.

The second part of this talk will be dedicated to the development of a selective deposition process by PEALD. One of the main challenges brought by the reduction of the transistor size below 10 nm is the development of selective deposition processes (for a self-forming Cu diffusion barrier for example). ALD is a suitable technique for selective deposition since it is a self-limited surface reaction process. The resulting selective process, called SeALD (Selective ALD) or AS-ALD (Area Selective ALD) is usually based on a specific surface treatment before deposition. Indeed, in ALD process, thin film nucleation depends strongly on the surface chemistry, so that by using a specific treatment one can transform a chemically reactive site into a nonreactive one. In this part, we propose a new selective ALD process, without surface treatment before deposition but using a Plasma assistance ALD process and by playing on the plasma chemistry. We will show for example that we are able to deposit selectively Ta₂O₅ oxide on top of metal (TiN) while no deposition is obtained on Si or SiO₂ surfaces. The process and its potential application will be described in more details during the talk.

9:20am **PS-WeM5 Customizing Ion Energy Distributions in Pulsed Plasmas with Chirped Bias Power**, *Steven Lanham*, *M.J. Kushner*, University of Michigan

Control of the ion energy distribution (IED) in plasma material processing reactors is necessary to maintain the critical dimensions (CD) needed to produce modern microelectronic devices. An effective way to customize IEDs is using pulsed power. For example, electronegative (e.g. halogen) plasmas used in etching processes form ion-ion plasmas during the power off period, where low energy ions can be preferentially extracted. This also allows for extraction of negative ions during the afterglow, which can help negate charge induced damage. Pulsed power parameters such as duty cycle and pulse repetition frequency need to be optimized for different electronegative plasmas chemistries due to varying attachment rates and

Wednesday Morning, November 9, 2016

heavy particle reaction mechanisms. The choice of frequency for the bias is a first-order decision in forming the IED, even in pulsed systems, which has in turn resulted in multi-frequency biases to aid in further customization. The use of multi-frequency biases brings additional complexity to pulsed systems.

In this work, based on a computational investigation, we discuss methods to produce customized IEDs in pulsed, electronegative inductively coupled plasmas. A 2-dimensional model, the Hybrid Plasma Equipment Model (HPEM), was used for this study. For pulsed biases in inductively coupled plasmas, IEDs will be discussed for various halogen plasma chemistries. Chirped biases in which the frequency is ramped during a pulsed period are discussed as a means to replicate IEDs that can otherwise only be formed in dual or triple frequency systems.

Work was supported by the Department of Energy Office of Fusion Energy Science and the National Science Foundation.

9:40am **PS-WeM6 Nonlinear Frequency Pull in Pulsed Capacitively Coupled Plasmas**, *J. Poulou, Lawrence Overzet, M.J. Goeckner*, The University of Texas at Dallas; *S. Shannon*, North Carolina State University; *D. Coumou*, MKS Instruments

Plasma ignition induces abrupt impedance changes due to the plasma sheath and bulk formation. These transitions can induce nonlinear changes in the instantaneous RF voltage and current frequencies despite the fact that the RF frequency is typically assumed to be fixed. These transitions are of particular interest in the application of frequency tuning of matching networks to maximize power transfer in pulsed plasma. In this presentation, we report on time resolved studies of the RF frequency and plasma impedance during pulsed plasma ignition using both electropositive (Ar) and electronegative (CF₄/O₂/Ar) gas mixtures. The center frequency is found to vary in time corresponding to fast changes in the complex plasma impedance when the plasma sheath is re-forming.

11:00am **PS-WeM10 Plasma Source Development for Fusion Relevant Material Testing**, *John Caughman, R.H. Goulding, T.M. Biewer, T.S. Bigelow, I.H. Campbell, S.J. Diem, A. Fadnek, D.T. Fehling, D.L. Green, C.H. Lau, E.H. Martin, P.V. Pesavento, J. Rapp*, Oak Ridge National Laboratory; *H.B. Ray, G.C. Shaw, M.A. Showers*, University of Tennessee; *P. Piotrowicz, D.N. Ruzic*, University of Illinois at Urbana-Champaign; *G.-N. Luo*, Chinese Academy of Sciences

INVITED

Plasma facing materials in a magnetic fusion reactor have to tolerate plasma heat fluxes of 10 MW/m². The Prototype Materials Plasma Experiment (Proto-MPEX) is a linear high-intensity radio frequency (RF) plasma source that combines a high-density helicon plasma generator with electron and ion heating sections. It is being used to study the physics of heating over-dense plasmas in a linear configuration with the goal of producing up to 10 MW/m² of plasma heat flux on a target. The helicon plasma is operated at 13.56 MHz with RF power levels up to 100 kW. Microwaves at 28 GHz (~150 kW) are coupled to the electrons in the over-dense helicon plasma via Electron Bernstein Waves (EBW), and ion cyclotron heating (~30 kW) is via a magnetic beach approach. Plasma diagnostics include Thomson Scattering and a retarding field energy analyzer near the target, while a microwave interferometer and double-Langmuir probes are used to determine plasma parameters elsewhere in the system. Filterscopes are being used to measure D-alpha emission and He line ratios at multiple locations within the device, and IR cameras image the target plates to determine heat deposition both upstream and downstream of the helicon source region. High plasma densities have been produced in helium (>3x10¹⁹/m³) and deuterium (>2x10¹⁹/m³), with electron temperatures that can range from 2 to >10 eV. Operation with on-axis magnetic field strengths between 0.6 and 1.4 T is typical. The plasma heat flux delivered to a target can be > 10 MW/m², depending on the operating conditions. Plasma parameters vary depending on the operating pressure/gas flow, and skimmer plates are used to try to control the neutral pressure in the device. The ion energy distribution varies radially/axially and is related to changes in the electron temperature and antenna coupling conditions. The helicon antenna coupling is being modeled with the COMSOL and VORPAL programs to help explain and guide operations. Details of the experimental results and operating parameters related to ion energies and delivered plasma heat flux will be presented.

11:40am **PS-WeM12 Linear Magnetron Magnet Pack for High Power Pulsed Magnetron Sputtering**, *Jake McLain, P. Raman, I.A. Shchelkanov*, University of Illinois at Urbana Champaign; *J. Hrebik*, Kurt J. Lesker Company; *B. Jurczyk, R. Stubbers*, Starfire Industries; *D.N. Ruzic*, University of Illinois at Urbana-Champaign

High Power Pulsed Magnetron Sputtering (HPPMS) is an ionized physical vapor deposition technique that utilizes high power pulses applied to the sputtering target. The high power densities allow for an increased percentage of sputtered particles to be ions, and the ions allow for more control over the deposition process. The enhanced control allows for improved film quality and surface adhesion when compared with DC magnetron sputtering (DCMS). The primary reason for the lack of industrial implementation is the intrinsically low deposition rate that HPPMS provides. The Center for Plasma-Material Interactions has designed a high deposition rate HPPMS magnet pack that produced comparable deposition rates in HPPMS when compared with a conventional magnet pack using DCMS for a 4-inch circular magnetron with a titanium target at 500W. This magnet pack also increased the HPPMS deposition rate twofold when compared with the conventional magnet pack using HPPMS [1]. To allow for industrial implementation of HPPMS, a similar high deposition rate magnet pack is designed and built for a linear magnetron, capable of being scaled to any desired length. This work focuses on the similarities and differences in the process and physics of the standard and new magnet packs. The properties explored in this work include deposition rate, deposition uniformity, plasma parameters, and film quality.

[1] P. Raman, et al., Surf. Coat. Technol. (2015), <http://dx.doi.org/10.1016/j.surfcoat.2015.12.071>

Advanced Surface Engineering Room 101C - Session SE+TR-WeM

Protective Coatings for Tribological Applications in Surface Engineering

Moderators: Andrey Voevodin, University of North Texas, Michael Stueber, Karlsruhe Institute of Technology, Germany

8:00am **SE+TR-WeM1 Correlative Theoretical and Experimental Investigation of the Formation of AlYB₁₄ and Competing Phases**, *Oliver Hunold, Y.T. Chen, D. Music*, RWTH Aachen University, Germany; *P.O.A. Persson*, Linköping University, Sweden; *D. Primetzhofer*, Uppsala University, Sweden; *M. to Baben*, GTT-Technologies; *J. Achenbach, P. Keuter, J.M. Schneider*, RWTH Aachen University, Germany

The phase formation in the boron rich section of the Al-Y-B system has been explored by a correlative theoretical and experimental research approach. The structure of coatings deposited via high power pulsed magnetron sputtering from a compound target was studied using elastic recoil detection analysis, electron energy loss spectroscopy spectrum imaging, as well as X-ray and electron diffraction data. The formation of AlYB₁₄ together with the (Y,Al)B₅ impurity phase, containing 1.8 at. % less B than AlYB₁₄, was observed at a growth temperature of 800 °C and hence 600 °C below the bulk synthesis temperature. Based on quantum mechanical calculations we infer that minute compositional variations within the film may be responsible for the formation of both icosahedrally bonded AlYB₁₄ and cubic (Y,Al)B₅ phases. These findings are relevant for synthesis attempts of all boron rich icosahedrally bonded compounds with the space group: *Imma* that form ternary phases at similar compositions.

8:20am **SE+TR-WeM2 Investigation of Friction and Wear for the Oxide-Oxide Contact in the Piston Ring-liner System**, *P. Ernst, P. Luethy, Ch. Bohnheio*, Oerlikon Metco AG, Wohlen, Switzerland; *F. Seibert, B. Widrig, Jürgen Ramm*, Oerlikon Balzers, Oerlikon Surface Solutions AG, Liechtenstein

The reduction of friction and wear are important issues in the development and optimization of internal combustion engines increasing their efficiency and reducing the service interval times. One possibility to increase the efficiency of an engine is an operation at higher temperature. Surface coating could help to keep the standard materials and extend their operation range to higher temperatures. In this work, the friction and wear of oxide coatings are investigated and compared with coatings which are standard for an engine like Nikasil and Fe- based liner coatings and CrN for piston rings. The oxide coating material was first tested in a SRV test and the coefficient of friction against steel and alumina was measured for dry and lubricated conditions. In addition, the wear of the coatings and the steel or alumina counter-part was inspected. The most promising coating

Wednesday Morning, November 9, 2016

combinations were tested in a motor-bike engine configuration and compared with standard material.

8:40am SE+TR-WeM3 Local Characterization Tools as the Key for Optimized Performance of Hard Coatings, Christian Mitterer, Montanuniversität Leoben, Austria INVITED

Advanced tribological hard coatings providing multi-functional properties like wear and oxidation resistance combined with high toughness require sophisticated selection and design of materials and architectures. For a knowledge-based development of such coatings, advanced characterization techniques on the nano-scale are needed to establish the necessary link of their microstructure to their properties. Within this contribution, recent progress in coating characterization techniques is highlighted. The application of focused ion beam techniques, electron backscatter diffraction and synchrotron X-ray nanodiffraction enables previously unrevealed insights in microstructure evolution. For the determination of mechanical and tribological properties at elevated temperatures, high-temperature nanoindentation and high-temperature ball-on-disk tests in combination with in-situ measurement techniques and site-specific sample preparation for damage analysis are discussed. Utilization of micromechanical tests for coatings provides information about their fracture toughness and rupture strength. The available portfolio of characterization techniques enables the determination of a complementary microstructural and mechanical fingerprint of tribological hard coatings, which allows to understand the complex structure-property relations in these materials and subsequently to further improve their performance.

9:20am SE+TR-WeM5 High Temperature Oxidation in Pure Steam Environment of HIPIMS Deposited CrN/NbN Nanostructured Coatings, Papken Hovsepian, A.P. Eghasarian, Y. Purandare, Sheffield Hallam University, UK; F.J. Perez, M.I. Lasanta, M.T. de Miguel, A. Illana, Universidad Complutense de Madrid, Spain; J. Juez-Lorenzo, Fraunhofer Institute für Chemische Technologie ICT, Germany; A. Aguero, Instituto Nacional de Técnica Aeroespacial (INTA), Spain

The demand for new materials to be used in supercritical steam power plants for efficient and clean coal utilization is ever growing. A significant reduction of CO₂ emissions is expected by increasing the efficiencies of the steam turbines to $\eta > 50\%$ which can be achieved by moving from subcritical low pressure/ low temperatures, (180 bar/540 °C) to high pressure/high temperature, (300 bar/600-620 °C) ultra-supercritical regime of operation. The main challenges faced by different steel components of the power plant with this approach however, consist of material failure due to high temperature oxidation, and phenomenon such as creep, erosion and descaling after a stipulated period of time. Over the years considerable research has been done in finding solution to the above problems in terms of protective surface layers with limited success.

In the current work, 4 μm thick CrN/NbN coating utilising nanoscale multilayer structure with bi-layer thickness of $\Delta = 3.4$ nm has been used to protect low Cr content P92 steel widely used in steam power plants. The uniquely layered coatings have a combination of nitrides of chromium and niobium which are not only resistant to aqueous corrosion, corrosion erosion and excellent tribological properties, but also have oxidation resistant in dry air up to a temperature of 850 °C. The novel High Power Impulse Magnetron Sputtering (HIPIMS) deposition technology has been used to deposit CrN/NbN with enhanced adhesion (critical scratch adhesion value of $L_c = 80\text{N}$) and very dense microstructure as demonstrated by XTEM imaging. These superior coating properties are achieved due to the unique high metal ion content (up to 90%) in the HIPIMS plasma, which allows particle acceleration and trajectory control by external electrical and magnetic fields thus delivering highly energetic material flux on the condensing surface.

P92 bare and coated samples were oxidised at 650°C in 100% steam atmosphere up to 2000 h, in order to simulate the future operation conditions of steam turbines employed in power plants. The oxidation kinetics was evaluated by mass gain measurements in a five decimal balance. In these conditions CrN/NbN provided a reliable protection of the P92 steel and outperformed other coatings such as ceramic Al₂O₃ and intermetallic Fe₄₄Cr₅₆Al used for the same application. The paper also discusses the effect of the growth defects and high temperature crack formation analysed by SEM and FIB- SEM techniques on the high temperature corrosion resistance in pure steam atmosphere thus revealing the coatings failure mechanisms.

9:40am SE+TR-WeM6 Improved Thermo-Mechanical Properties and Oxidation Resistance of Ti-Al-N Coatings by Alloying Ta and Modifying the Coating Architecture, Christian Martin Koller, A. Kirnbauer, Technische Universität Wien, Austria; H. Bolvardi, Oerlikon Balzers, Liechtenstein; P. Polcik, Plansee Composite Materials GmbH, Germany; P.H. Mayrhofer, Technische Universität Wien, Austria

In recent years, different approaches towards the enhancement of physical vapor deposited TiAlN hard coatings were made. Among these, the alloying of additional elements to form quaternary compounds proved to be extremely efficient. In addition to as-deposited film properties also the coatings' thermo-mechanical behaviour and the performance in oxidizing environments, both constitute fundamental requirements for cutting applications, can be significantly increased.

One example is the substitution of Ti or Al by Ta, which chemically strengthens the face-centred cubic cell, leading to higher hardness values and increased Young's moduli. Furthermore, Ta prevents the formation of anatase TiO₂ by directly promoting rutile-structured TiO₂. Consequently, a thermal-induced phase transformation of anatase into rutile TiO₂ and its therewith associated generation of crack networks is avoided.

In the present study two subsets of multilayers based on TiAlN/TaAlN and TiAlTaN/TaAlN were investigated. The coatings were synthesised using powder-metallurgically manufactured Ti_{0.5}Al_{0.5}, Ta_{0.5}Al_{0.1}, Ta_{0.75}Al_{0.25}, Ta_{0.5}Al_{0.5}, Ti_{0.475}Al_{0.475}Ta_{0.05}, and Ti_{0.45}Al_{0.45}Ta_{0.10} targets. The TiAlN and TiAlTaN-base layers were arc evaporated (arc), whereas the TaAlN layers were either arc evaporated or reactively sputtered (rsd) [1][2]. The multilayer architecture was realised by the use of a shutter system or through the continuous two-fold rotation of the substrate holder, resulting in sharp and slightly blurred layer interfaces. The overall Ta-content and TaAlN-layer thickness was varied by different power settings of the Ta_{0.75}Al_{0.25} cathode and shutter-open times, respectively.

We can show that a coating architecture of TiAlN^{arc} and TaAlN^{arc} allows for thermo-mechanical properties comparable to TiAlTaN, whereas superior oxidation resistance only can be achieved by a TiAlN^{arc}/TaAlN^{rsd} arrangement. For both rsd-multilayer arrangements the critical factor in terms of thermo-mechanical performance and oxidation resistance is the TaAlN layer thickness as well as the overall interface volume. Results are discussed based on X-ray diffraction and electron microscopy studies.

[1] C.M. Koller, R. Hollerweger, C. Sabitzer, R. Rachbauer, S. Kolozsvári, J. Paulitsch, P.H. Mayrhofer, *Surf. Coat. Technol.* **259** (2014) 599–607.

[2] C.M. Koller, R. Hollerweger, R. Rachbauer, S. Kolozsvári, J. Paulitsch, P.H. Mayrhofer, *Surf. Coat. Technol.* **283** (2015) 89–95.

11:00am SE+TR-WeM10 Tribochemistry between Graphene and Fe, Fe₂O₃, and Fe₃C Surfaces, J. David Schall, Oakland University INVITED

Tribosystems containing both iron and hydrocarbon-based lubricants are ubiquitous and an understanding of the chemistry that takes place in such systems is essential to the development of new lubricant additives designed to reduce friction and wear. Graphene nanoparticle additives have been proposed by numerous researchers due to the excellent friction and wear properties of graphene. Recent experiments have shown that even single layers of graphene in the absence of lubricants on steel components can greatly reduce wear (Berman, Carbon, 54, 2013, 454). Berman *et al* have hypothesized that graphene forms a conformal protective layer on the steel surface with or without additional lubrication. Simulations show vanishingly small friction when continuous sheets of graphene are sandwiched between Fe surfaces; however, real graphene has various functional groups including -carboxyls, -alkyls, -hydroxyls among others along the edges. Graphene can also be oxidized. In this talk simulations that illustrate the triboinitiated mechanochemistry between graphene with various functional edge groups and Fe, Fe₂O₃ and Fe₃C surfaces will be presented. These molecular dynamics simulations were conducted with a REAX-FF interatomic potential function for Fe, O, C and H (Zou, JOM, 64, 2012, 1426) that includes terms for chemical reactivity with charge transfer enabling investigation of tribochemistry in the sliding interface.

11:40am SE+TR-WeM12 Tribological Testing of Leather Treated with Ag/TiO₂ Nanoparticles for Footwear Industry, M. Rebelo de Figueiredo, Montanuniversität Leoben, Austria; I. Carvalho, S. Carvalho, Universidade do Minho, Portugal; C. Gaidau, Leather and Footwear Research Institute, Romania; Robert Franz, Montanuniversität Leoben, Austria

Ecologic and health effects of applying materials with advanced functions for leather surface finishing contribute to increasing the added value and durability of leather and fur articles. The innovative properties of Ag/TiO₂

Wednesday Morning, November 9, 2016

nanoparticles on leather surface are due to their antimicrobial, self-cleaning and flame retardant characteristics. Furthermore, it leads to a reduction of chemicals with high pollutant potential, e.g. volatile organic biocides, organic solvents and halogenated flame retardants typically used during leather manufacturing.

The efficient anchoring of Ag/TiO₂ nanoparticles on leather surface ensures minimum risk of human skin penetration. To this aim, two different technologies for the functionalisation of the leather surfaces were explored: (1) physical mixing of Ag/TiO₂ nanoparticles with film forming polymers and leather surface covering by conventional technologies and (2) leather surface activation by cold plasma pre-treatment and magnetron sputter deposition of transparent Ag/TiO₂ nanoparticle layers.

In order to test the adhesion of the deposited Ag/TiO₂ nanoparticles to the leather substrates, a series of tribological tests in ball-on-disc configuration has been performed using different counterpart materials ranging from rubber (e.g. nitrile rubber) to polymers (e.g. PTFE, PUR or POM). The analysis of the coating wear by light optical and scanning electron microscopy as well as Raman spectroscopy revealed details regarding the adhesion of the Ag/TiO₂ nanoparticles depending on the deposition method and parameters applied. In a similar way, the sticking behaviour of the Ag/TiO₂ nanoparticles to the different counterpart materials was used to emulate the uptake of the released nanoparticles by the human skin. The conducted experiments represent a first step towards a systematic study of the mechanical performance of leathers treated with nanoparticles in order to evaluate their suitability for future applications in the footwear industry.

12:00pm SE+TR-WeM13 Phase Formation of Cathodic Arc Evaporated Al_xCr_{1-x} and Al_xCr_{1-x}O₈ Thin Films, Valentin Dalbauer, CDL AOS TU Wien, Austria; *J. Ramm*, Oerlikon Balzers, Oerlikon Surface Solution AG, Liechtenstein; *S. Kolozsvári*, Plansee Composite Materials GmbH, Germany; *C.M. Koller*, CDL AOS TU Wien, Austria; *P.H. Mayrhofer*, Vienna University of Technology, Austria

Aluminium-based oxides and oxide scales are highly valued for various demanding applications due to their outstanding thermo-mechanical properties as well as their superior resistance in oxidising and chemically hazardous environments. However, the polymorphic character of Al₂O₃ (and consequentially also (Al_xCr_{1-x})₂O₃) synthesised at deposition temperatures lower than 800 °C is impeding its large-scale utilisation. Especially high Al-containing films, being dominated by transient oxides, are susceptible for thermally-induced phase transformations, which are associated with the formation of crack networks. Therefore, the growth of the thermodynamically stable α-Al₂O₃ at deposition temperatures ~ 400-600 °C has been in the focus of research for many years. Although considerable advances were made, none of them proved to be applicable to industrial utilisation. A comprehensive and in-depth understanding of mechanisms, leading to the growth of transient oxides within the quasi-binary system Al₂O₃-Cr₂O₃ synthesised by cathodic arc evaporation is therefore still of major interest, as this knowledge is crucial for being able to grow coatings with dedicated crystallography and microstructure.

In the present work, we approach this issue by investigating the structural evolution of intermetallic Al_xCr_{1-x} and Al_xCr_{1-x}O₈ films synthesised by arc evaporation. Depositions were carried out in non-reactive as well as reactive atmosphere, using low to intermediate O₂ flow rates to examine its impact on film morphology and phase composition. In order to correlate the chemical aspect and process conditions (i.e., Cr-content and O₂ partial pressure) with the accessible microstructure and crystallographic evolution, powder-metallurgically manufactured Al_xCr_{1-x} targets with different compositions were selected. By this, the significant phase regimes within the binary Al-Cr phase diagram are accessible.

In detail, arc evaporation of Al_{0.9}Cr_{0.1}, Al_{0.7}Cr_{0.3}, Al_{0.5}Cr_{0.5}, and Al_{0.25}Cr_{0.75} targets leads to the formation of intermetallic films dominated by Al₁₃Cr₂, Al₈Cr₅ or AlCr₂ phases, which well-agrees with the equilibrium Al-Cr phase diagram. Chemical analyses demonstrate that differences in the Al/Cr-ratio between targets and films increase towards the Cr-rich side, which decrease by introducing O₂ to the deposition process. Furthermore, the simultaneous broadening and intensity reduction of dominant intermetallic XRD peaks is accompanied by the emergence of weak broad signals indicative for the development of X-ray amorphous areas. Between 70 and 90 at.% Al we find a compositional window, which is characterised by a maximum target evaporation and minimum film growth rate.

Scanning Probe Microscopy Focus Topic

Room 104A - Session SP+SS+TF-WeM

Probing Electronic Properties

Moderator: Carl Ventrice, Jr., SUNY Polytechnic Institute

8:00am SP+SS+TF-WeM1 Local Probe Investigation of 1D Structures and Interfaces in 2D Materials, Chenggang Tao, Virginia Tech INVITED

Emerging two-dimensional (2D) materials, such as graphene and atomically thin transition metal dichalcogenides, have been the subject of intense research efforts for their fascinating properties and potential applications in future electronic and optical devices. The interfaces in these 2D materials, including domain boundaries and edges, strongly govern the electronic and magnetic behavior and can potentially host new quantum states. On the other hand, these interfaces are more susceptible to thermal fluctuation and external stimuli that drive mass displacement and generate disorder. In this talk we will present our scanning tunneling microscopy (STM) and spectroscopy (STS) explorations of edges of few layered molybdenum disulfide (MoS₂) nanostructures with unique structural and electronic properties and show how step edges on titanium diselenide (TiSe₂) surfaces change dynamically due to electrical fields. We will also discuss temperature evolution of quasi-1D C₆₀ nanostructures on graphene. Through careful control of the subtle balance between the C₆₀ surface mobility and the linear periodic potential of rippled graphene, C₆₀ molecules can be arranged into a novel 1D C₆₀ chain structure, and this chain structure can further transition to a compact hexagonal close packed stripe structure by tuning the annealing temperature.

8:40am SP+SS+TF-WeM3 Investigation of Electronic Structures from Monolayers to Multilayers in Charge Transfer Complex, TTF-TCNQ using Low-temperature Scanning Tunneling Microscopy/Spectroscopy, Seokmin Jeon, P. Maksymovych, Oak Ridge National Laboratory

The properties of few-layer molecular films are in general distinct from both bulk and monolayer phases, particularly in the case of metallic substrates, whose high-density electronic structure dominate the monolayer electronic structure and hamper characterization of the intrinsic properties of the molecular layer. This is especially true for charge transfer molecular solids, whose interesting electronic properties derive from a subtle alignment of each individual component's states, balance of dielectric screening, long-range electrostatic interactions, and relative molecular geometry. In contrast to vast effort on bulk phase study of the historic organic charge-transfer complex, TTF-TCNQ, study of its low-dimensional phases has been limited to monolayer phases. We investigated the evolution of the electronic structure of TCNQ and TTF-TCNQ multilayers using STM/STS at 4.3 K.

Thanks to submolecular resolution STM data and DFT calculations we were able to accurately determine the stacking relationship between the overlying layer and the underlying layer at an atomic scale. In such a well-defined layered model structure, we scrutinize the electronic structures of multilayered TCNQ and TTF-TCNQ using STS. Double-periodic charge ordering and Coulomb gap features are observed in the bilayer TTF-TCNQ. The effect of substrate variation (Ag, Au, and HOPG) on multilayer growth and electronic properties are discussed. The STS data from the multiple combinations of adsorbates and substrates allow us to assign states reliably and understand of transition of the surface, molecular, and charge transfer states clearly in the multilayer systems.

This research was conducted at the Center for Nanophase Materials Sciences, which is a DOE Office of Science User Facility.

9:00am SP+SS+TF-WeM4 Investigation of Initial Stages of Oxidation of Ni-Cr and Ni-Cr-Mo Alloys by Scanning Tunneling Microscopy/Spectroscopy (STM/STS), Gopalakrishnan Ramalingam, P. Reinke, University of Virginia

Ni-Cr based superalloys are excellent candidates for use in highly corrosive environments due to their exceptional oxidation and corrosion resistance. Our work focuses on unraveling the initial reaction steps of alloy oxidation as a function of composition, moving from the clean Ni-surface to a Ni-base alloy with 33wt% Cr. In the study presented here, we used STM/STS to investigate the initial stages of oxidation reaction in Ni-Cr (0-35wt.% Cr) alloys and the impact of Mo (2-10 wt.%) on the reaction. We developed spectroscopy maps which yield highly coveted information on the spatial distribution of oxide nuclei and the transition from chemisorbed oxygen to oxide. The STS maps capture the evolution of oxide during various stages of oxidation and provides valuable insight into the reaction as a function of composition of alloy.

Wednesday Morning, November 9, 2016

Cr is the main alloying addition in Ni-based superalloys and the minimum amount of Cr necessary to form a continuous, passive oxide layer is 6-13 wt.% based on empirical observations. The passivating quality of an oxide layer strongly depends on the initial nucleation of the oxide, the oxide growth during continued oxidation, and eventual coalescence to form a complete oxide layer. However, the effect of Cr content on the initial nucleation and growth behavior of the oxide is not well understood. Similarly, the underlying mechanisms at the atomic scale and the role of electronic structure changes due to Mo addition are not well understood.

In this study, alloy thin films grown on MgO(100) substrates in an ultrahigh vacuum chamber are oxidized in situ at 300 °C with O₂ exposure up to 130 L. In the initial stages of oxidation (0.5-7 L of O₂), oxide nuclei are initially formed at the step-edges with some nucleation also present on the flat terraces. Subsequent oxygen exposure (>30 L) results in growth of existing oxide islands with additional nucleation of oxide. The amount of oxygen required for complete oxide coverage depends strongly on the Cr content of the alloy: >85% of the surface is covered with oxide in a Ni-14wt.%Cr alloy after 80 L oxidation while the same coverage is achieved in Ni-33wt.%Cr alloy after only 11.5 L. In contrast, we do not observe a complete oxide layer on Ni surface even after 180 L oxidation. Scanning tunneling spectroscopy maps provide spatially resolved electronic structure information and the variation of bandgap of the oxide as a function of oxide thickness and Cr content will be discussed. Preliminary data on the changes in the atomic and electronic structure of the thin film and oxidation behavior due to the addition of Mo will be presented.

9:20am **SP+SS+TF-WeM5 Au(111) Characterization, Single Atom Manipulation and Si(100):H Surface Imaging by LT-UHV-4 STM, Corentin Durand, D. Sordes, C. Joachim, CNRS, France** **INVITED**

Advance in nanotechnology requires the development of new instruments capable of imaging, communicating, manipulating and measuring at the atomic scale. The performances of the new ScientaOmicron LT-UHV 4-STM microscope have been certified by a series of state-of-art STM experiments on an Au(111) surface at 4.2 K [1]. During the STM operation of the 4 STM scanners (independently or in parallel), a $\frac{1}{2}$ Z stability of about 2 pm per STM was demonstrated. With this LT-UHV 4-STM stability, single Au atom manipulation experiments were performed on Au(111) by recording the pulling, sliding and pushing manipulation signals. Jump to contact experiments lead to perfectly linear low voltage I-V characteristics on a contacted single Au ad-atom with no need of averaging successive I-V's. Our results show that the 4 scanners of this new instrument working in parallel have performances equivalent to single tip state-of-art LT-UHV-STM. Two tips surface conductance measurements were performed on Au(111) using a lock-in technique in a floating sample mode of operation to capture the Au(111) surface states via two STM tips dI/dV characteristics. The capabilities of this microscope being demonstrated, we now move on to our next project, the realization of atomic devices. The hydrogen passivated Si(100) surface is a good candidate to achieve this goal. Here, I will show our preliminary results regarding the investigation of this surface and its topography. The surface has been prepared by a "wafer-bonding" method [2]. Large scale STM images show that this technique provides large and clean terraces essential to the fabrication of atomic circuits. Atomic resolution imaging enables us to confirm the position of the dimers, these latter ones having a different aspect depending on the polarity of the tunneling junction [3]. Finally, I will introduce the route of our project, the different steps we must achieve in order to build up a device made of few atoms on this surface [2].

[1] J. Yang et al. Eur. Phys. J. Appl. Phys, 73, 10702, 2016

[2] M. Kolmer et al. Appl. Surf. Sci., vol. 288, p. 83, 2014

[3] T. L. Yap et al. Surf. Sci., vol. 632, p. L13, 2015

11:00am **SP+SS+TF-WeM10 Heterochiral to Homochiral Transition in Pentahelicene 2D Crystallization induced by 2nd-layer Nucleation, Anaïs Mairena, Universität Zürich, Switzerland**

Chirality is ubiquitous in our world (human body, pharmaceuticals, liquid crystals...). Nevertheless, the principles of intermolecular recognition are still poorly understood. Therefore, it is not possible to predict the outcome of crystallization, which is still the most important method to separate chiral molecules into their enantiomers, or to explain why a minority of chiral compounds crystallize into conglomerate. A promising approach towards a better understanding of chiral interactions is the study of self-assembly of chiral molecules on single crystal surfaces with STM (sub-molecular resolution).

We studied the 2D self-assembly of racemic-pentahelicene ([5]H, C₂₂H₁₄) on Cu(111) with STM. Adsorption of [5]H leads, already at very low coverages to formation of homochiral pairs, i.e. both molecules have the same handedness.

At coverages close to the saturated monolayer, two distinct long-range ordered structures have been observed. Both structures have the homochiral pairs as building blocks. However, while one structure consists of a conglomerate of homochiral domains, the second structure is racemic, i.e. composed of homochiral pairs with opposite handedness. At monolayer coverage, only the racemic structure prevails. Above monolayer coverage, the dense racemate phase in the monolayer disappears on the expense of a homochiral conglomerate phase with lower density due to 2nd-layer-nucleation. Our results indicate that a long-range chiral communication between 2nd layer islands and other areas on the surface are at work.

These findings are also compared with those obtained for heptahelicene (C₃₀H₁₈) on Cu(111). A surface-mediated selection mechanism, taking different intermolecular interactions into account, will be presented.

11:20am **SP+SS+TF-WeM11 Two-stage Chiral Selectivity in the Molecular Self-Assembly of Tryptophan, Nathan Guisinger, Argonne National Laboratory; B. Kiraly, Northwestern University; R. Rankin, Villanova University**

Both chirality and molecular assembly are essential and key components to life. In this study we explore the molecular assembly of the amino acid tryptophan (both L- and D- chiralities) on Cu(111). Our investigation utilizes low temperature scanning tunneling microscopy to observe resulting assemblies at the molecular scale. We find that depositing a racemic mixture of both L- and D- tryptophan results in the assembly of basic 6 molecule "Lego" structures that are enantiopure. These enantiopure "Legos" further assemble into 1-dimensional chains one block at a time. These resulting chains are also enantiopure with chiral selectivity occurring at two stages of assembly. Utilizing scanning tunneling spectroscopy we are able to probe the electronic structure of the chiral Legos that give insight into the root of the observed selectivity.

11:40am **SP+SS+TF-WeM12 Mask Free Approach to Selective Growth of Transition Metal Dichalcogenides Heterostructures enabled with Scanning Probe based Nanolithography, R. Dong, L. Moore, N. Aripova, C. Williamson, R. Schurz, Saint Louis University; L.E. Ocola, Argonne National Laboratory; Irma Kuljanishvili, Saint Louis University**

Advances in graphene research ignited interest in other type of two-dimensional (2D) atomic crystals, such as hexagonal boron nitride and layered transition metal dichalcogenides (TMDCs). Among these new types of 2D materials, the applications of TMDCs in logic electronics and optoelectronics are promising because of their sizable bandgaps and natural stability. The techniques which enable heterostructure formation with different TMDCs systems have provided further solution to the design of high performance electronic devices such as those for photovoltaics and optoelectronics. The existing heterostructures fabrication methods, based on mechanical exfoliation and/or wet chemical transferring rely on traditional fabrication methods such as photo- and e-beam lithography.

To realize the selective growth and layered assembly of heterostructures at predefined location, here, we report on application of mask free, scanning probe based direct writing method. With the use of AFM cantilevers and developed water based "inks", we demonstrate arrays of MoS₂ and WS₂ dots and ribbon arrays at predefined locations on variety of substrates. Employing this SPM based patterning method we have also fabricated MoS₂/WS₂ heterostructures of sub-micrometer scales in a controlled fashion. The quality of MoS₂/WS₂ heterostructures was confirmed by Raman spectroscopy, AFM characterization and electrical transport measurements. Our mask free nanolithography approach offers an alternative route for patterning and growth of TMDCs with added benefit of potential reduced contamination of the TMDCs surfaces and interfaces between materials and substrates. It demonstrates a promising unconventional technology for fabrication of high quality TMDCs heterostructures in convenient manner capable of nanoscale precision.

Acknowledgements

Use of the Center for Nanoscale Materials was supported by the U. S. Department of Energy, Office of Science, Office of Basic Energy Sciences, under Contract No. DE-AC02 06CH11357. I.K. acknowledges support of NSF MRI program (Award No. 1338021), and the Saint Louis University seed funds.

Wednesday Morning, November 9, 2016

12:00pm **SP+SS+TF-WeM13 Non-Destructive Electrical Depth Profiling across Nanometric SiO₂ Layers, Hagai Cohen**, Weizmann Institute of Science, Israel; A. Givon, Tel Aviv University, Israel

The access to sub-nm scale depth information in thin dielectric layers, considering both the compositional and the electrical sub-surface characteristics, is challenging. A remarkable answer may be provided by CREM (chemically resolved electrical measurements), a technique based on x-ray photoelectron spectroscopy (XPS). CREM exploits the chemical contrast within a given structure to gain rich electrical information, or alternatively, apply electrical tests to gain improved structural/compositional analyses. Yet, for compositionally uniform domains, CREM becomes rather insensitive to the fine profiling details. Here, we show that this principal limitation can be overcome and the CREM resolution be improved significantly. Applied to nanometric silica layers, we reveal hidden impurity concentration profiles and further correlate them with the depth-dependent dielectric quality. Based on this leap improvement in resolution and sensitivity, our advanced CREM analysis promises diverse applications in device contact-free electrical studies.

Surface Science

Room 104D - Session SS+2D-WeM

Synthesis, Characterization, and Surface Science of Novel Materials and Interfaces

Moderator: Talat Rahman, University of Central Florida

8:00am **SS+2D-WeM1 Early Stages of the Thermal-Induced Mobility of Ag in SiC, Daniel Velázquez, R. Seibert, J. Terry**, Illinois Institute of Technology
Tri-structural isotropic (TRISO) particles are the fuel of choice for very-high temperature reactor technology. At the core, these spherical particles consist of an inner fuel kernel of UO₂, UC₂ or a combination of both, which is coated radially outward by successive layers of low density pyrolytic graphite, an inner high density pyrolytic graphite layer, silicon carbide (SiC) and an outer high density pyrolytic graphite layer. SiC is the main diffusion barrier against the release of fission products due to its hardness and high melting point. Nonetheless, irradiation testing of TRISO particles indicates that trace amounts of metallic fission products, such as Ag (which as a ~41 day half-life), diffuse through SiC. Competing theoretical and experimental observations that indicate that Ag diffuses through the bulk and through grain boundaries. Diffusion through grain boundaries is usually amplified due to the formation of large grains upon crystallization by heating. This leads to the formation of triangular micro pits in thin films, suggesting that a 3D version of this form of crystallization could facilitate even more the release of Ag. Previously XAFS and XPS have shown that Ag remains metallic in a SiC matrix, indicating that bulk diffusion is perhaps interstitial rather than substitutional. In this work we discuss the mobility of Ag films enclosed on layers of 3C-SiC by analyzing SEM images taken before and after annealing. Image analysis supported by surface spectroscopic and crystallographic techniques are used in order to estimate the release of Ag through SiC for Ag interlayers at various thicknesses and annealing temperatures. Preliminary analysis by SEM/EDS show that upon annealing Ag escapes through the SiC surface by three different mechanisms, which roughly in chronological are: 1) escape through triangular pits and grain boundaries in SiC; 2) agglomeration and formation of sub-surface blisters which eventually rupture; 3) diffusion through the bulk of SiC when the trapped amounts of Ag are insufficient to form large blisters. During the third mechanism, we still observed sub-surface mobility in the form of dendritic paths. When the starting amount of Ag is reduced sub-surface diffusion is limited and the release of Ag is dominated by the escape through the triangular pits of SiC and bulk diffusion.

8:20am **SS+2D-WeM2 Quantitative Chemical State base on XPS Energy Scan Image Applied to Ni Fe corroded Samples, Vincent Fernandez, J. Keraudy**, Université de Nantes, France; N. Fairley, Casa Software Ltd, UK; P.Y. Joan, Université de Nantes, France

1. Introduction

Corrosion is a natural phenomenon where metals have a tendency to revert back to their natural, lower energy state. During many years, the most effective corrosion protection systems were based on the use of chromate-rich surface treatments. However, recently, the legislation imposed by the European Commission, REACH (Registration, Evaluation, Authorization and Restrictions of Chemicals) prohibited the use of hexavalent chromium. Many alternatives have been explored so far, including the protection with monolayer and/or multilayers of thin films

(Cr, CrN, Ti, TiN, NbN) deposited by magnetron sputtering process. Corrosion is a physical-chemical interaction between the metal and its environment. Most hard coatings (TiN, CrN, NbN) possess an higher corrosion resistance than less noble materials like steel, Al or Mg alloys. When the coatings are deposited on such less noble substrates and exposed to a corrosive atmosphere (ex : NaCl), the coated parts suffer from serious corrosive attack (pitting corrosion) due to inherent coating defects or inhomogeneities. This kind of corrosion is localized to the defect area and is characterized by the anodic dissolution of the substrate material with a high anodic current density at the defect site. It is generally called galvanic corrosion. In this study, Nickel thin film (2 micrometers) was deposited on steel substrate (XC38) using Direct Current Magnetron Sputtering from a Ni target. In order to simulate the corrosive attack, the coated part was exposed to a corrosive medium, i.e salt spray test. The test was conducted under continuous spray (24 hours) conditions (5wt.% NaCl) at a temperature of 35 °C according to the ASTM B117 standard procedure.

The morphology and the chemical environment of the corrosion products were analyzed respectively by optical microscopy and XPS investigations.

2. Results

The samples have conducting and isolating regions to avoid spatial differential potential the samples were measured in a floating condition. The Parallel XPS images of 128 pixels by 128 pixels were done with FOV of 900 x 900 microns at an energy resolution of about 1eV and an energy step of 0.2 eV for O 1s, Na KLL, Ca 2p, C 1s, Ni 3p and Fe 3p with charge compensation. Ni and Fe were measured in one region. To treat the 735 images corresponding of more than 1.2 10⁷ intensity points, images were smoothed and projected on PCA images. All images were projected on 6 abstract factors. Then images were converting in 81920 spectra. After spectra quantification, energies regions were converting back in quantitative images. Then Fe map was classified in 5 false colors part by intensity.

8:40am **SS+2D-WeM3 Novel Approaches to Form Organic-Inorganic Interfaces: Parallels between Coupling and Surface Modification Schemes in Vacuum and in Wet Chemistry, Andrew Teplyakov**, University of Delaware

Recent interest towards controlled formation of organic-inorganic interfaces affected greatly the approaches used for surface modification of semiconductors. Despite substantial progress in designing chemical pathways for surface modification of these materials and synthetic capabilities to build a variety of precursor molecules, two major issues remain: 1) Can the same level of precision achieved for surface characterization in vacuum be achieved for surfaces modified by wet chemistry methods; and 2) Can the elemental and compound semiconductor surfaces be modified with chemical groups that are both oxygen- and carbon-free. These two questions will be addressed by drawing parallels between cyclocondensation processes on modified semiconductor surfaces and cycloaddition in vacuum. Mixed surface modification schemes will be discussed for silicon and ZnO materials to produce high-coverage chemical “hooks” and the use of these functionalities will be demonstrated for initial stages of film deposition or depositing large constructs (nanoparticles and buckyballs) by chemical addition to produce strong covalent bonds. The addition across double bonds of carbonaceous constructs and the production of chemical bonds by straightforward chemical reactions will be discussed. The reactions for producing amino-functionalities and the platforms for “click” reactions will be presented. The experimental evidence of the reactions will be based on infrared spectroscopy, X-ray photoelectron spectroscopy (XPS), time-of-flight secondary ion mass spectrometry (ToF-SIMS) and a combination of microscopic techniques. The selected results of the experimental work will be compared with the experimental observables predicted by density functional theory (DFT).

9:00am **SS+2D-WeM4 Adsorption of Hetero-bifunctional Urea on Ge(100)-2x1 Surface, Tania Sandoval, S.F. Bent, A.M. Crow**, Stanford University

Organic functionalization of Group IV semiconductor surfaces is of interest due to the need for new pathways in surface chemistry modification. This is important in applications such as molecular layer deposition, molecular electronics, and biosensors where the ability to control and tune surface properties requires a deep understanding of the interactions between molecules and solid surfaces. In this study, adsorption of the heterobifunctional urea molecule on the Ge(100)-2x1 surface was investigated. Both the amine and carbonyl group of the urea molecule are known to react with the Ge surface. The aim of this study is to determine if

Wednesday Morning, November 9, 2016

any preferential reaction pathways exist and to understand the driving forces toward the final products.

Density functional theory (DFT) calculations suggest that NH_2 dissociation is the most thermodynamically favorable pathway for the single reaction. The reaction can occur through two possible precursor states: a nitrogen dative bond with the surface or an oxygen dative bond that can further undergo an enolization reaction. Interestingly, the oxygen dative bond is 7 kcal/mol more stable than the nitrogen bond, suggesting a preference for the latter reaction pathway. Furthermore, calculations show that the dual reactions provide less stabilization gain and a higher kinetic cost than single reactions, as the dual NH_2 dissociation has an activation barrier greater than 30 kcal/mol and only provides 5 kcal/mol of additional exothermicity, indicating that the urea molecule will likely react only through a single functional group. X-ray photoelectron spectroscopy (XPS) and multiple internal reflection Fourier transform infrared (MIR-FTIR) spectroscopy were used to determine the final reaction products. Results suggest that urea adsorbs on Ge(100) forming a mix of surface products. One of the products can be identified by the downshift in binding energy of the N(1s) XP peak and the Ge-H stretching mode in IR as NH_2 -dissociated urea on Ge. This assignment is also consistent with the presence of a carbonyl group in the IR and XPS spectra, which is expected to remain unchanged in this surface configuration. Another reaction product exists that is evident by second O(1s) and C(1s) XPS peaks downshifted from that of the parent urea molecule, suggesting a loss of the carbonyl group by a reaction with a more electropositive atom. Moreover, coverage results support our DFT findings by suggesting that each urea molecule will occupy a Ge dimer by reacting through a single functional group per molecule.

9:20am **SS+2D-WeM5 Electronic Structure of Ferroelectric Nanodomains**, *Erie Morales, C. Perez, M. Brukman, D. Bonnell*, The University of Pennsylvania

The local measurement of structure and properties enabled by scanning tunneling microscopy and atomic force microscopy in conjunction with systematic control of in situ environments has yielded insight into the fundamental behavior of ferroelectric compounds. Many atomic structures on BaTiO_3 surfaces have been determined, the thermodynamic stability of structures on (001) surfaces has been described, and the polarization dependence of several classes of surface reactions has been demonstrated. In addition the polarization behavior at the nanoscale has received much attention.

Here we report unusual impact of local poling on the electronic structure of ferroelectric surfaces. Scanning Tunneling Microscopy in situ poling was performed on BaTiO_3 (001) in ultra high vacuum (UHV). The voltage pulse produces apparent anti-parallel ferroelectric domains. Domain size can be controlled by changing conductivity of the crystal and/or by changing the bias set point; the smallest domain we pole is 24 nm. We use a 4-D analysis of geometric and electronic structure data to characterize the variations in electronic structure. Patterns of variations in the surface band gap are consistent with existing theoretical calculations of anti parallel domain orientations.

9:40am **SS+2D-WeM6 Using Data Analytics and Informatics in Understanding Enhanced Conductivity, Mobility, and Transparency in ITO Bearing ZrO_2 and reduced SnO_2** , *Timothy Peshek*, Case Western Reserve University; *J.M. Burst, T. Coutts, T.A. Gessert*, National Renewable Energy Laboratory

We deposited high quality tin-oxide-doped indium oxide (ITO) by RF magnetron sputtering with varying oxygen partial pressure in the sputter ambient and using targets with a nominal concentration of 5 wt% SnO_2 , instead of a typical 10 wt%, and between 0-3 wt% ZrO_2 . We demonstrate mobilities of $>45 \text{ cm}^2/\text{Vs}$ for sputtered ITO films at zero added oxygen. We demonstrate resistivities in the range of $10^{-5} \Omega\text{-cm}$ at zero added oxygen with 1 wt% ZrO_2 added, mobilities at $>55 \text{ cm}^2/\text{Vs}$ and the films showed a modest increase in optical transmission with increasing Zr-content. [orptio](http://orptio.com)

Hypothetically the increase in mobility that apparently accompanies the addition of ZrO_2 yields enhanced optical clarity in the IR due to reduced free carrier absorption from reduced doping concentration for any given resistivity.

Anomalous behavior was discovered for films with no Zr-added, where a bimodality of high and low mobilities were discovered for nominally similar growth conditions. We examined this anomalous behavior using modern data science and visualization techniques of big data and materials informatics. We used these techniques to gain insights into the mechanistic behavior of the relationship between stoichiometry, process variables, *Wednesday Morning, November 9, 2016*

material morphology and electrical properties. We will summarize these findings and describe the methods used in the analysis and a path forward for continuing utilizing data analytics in material characterization and learning.

11:00am **SS+2D-WeM10 Surface Composition and Atomic Structure of Topological Insulator Materials**, *Jory Yarmoff, W. Zhou, H. Zhu*, University of California - Riverside

INVITED

A topological insulator (TI) is a two-dimensional material that behaves as an insulator in the bulk, but conducts along the surface via topologically protected surface states. TI's have attracted intense interest because of their fundamental importance combined with great potential for applications in areas such as spintronics and quantum computation. Because the critical electronic states in TI's are localized in the near-surface region, it is critical to understand their surface composition, surface atomic structure and surface chemistry, and there are several outstanding issues that have not been fully resolved. For example, the materials are often naturally doped leading to the Fermi energy residing in the conduction band. Some materials have also been observed to change over time, the so-called "aging effect". In addition, the surface termination of the prototypical TI, Bismuth Selenide (Bi_2Se_3), has been an area of recent debate. Although some studies have demonstrated that the cleaved surface is terminated with Se, as expected from the bulk crystal structure, there are other reports that show either a Bi-rich or mixed-termination.

We are using low energy ion scattering (LEIS), in conjunction with other surface analysis tools, to investigate the surface composition and atomic structure of TI materials prepared in numerous ways. LEIS is uniquely suited to measure surface termination and atomic structure, as it provides the elemental identification of the near-surface region and can be deployed to probe only the outermost atomic layer. We compared surfaces prepared by *ex situ* cleaving, *in situ* cleaving and Ar^+ ion bombardment and annealing (IBA) in ultra-high vacuum. LEIS measurements do not indicate any substantial differences between the Se-terminated surfaces prepared by IBA or *in-situ* cleaving. Samples inserted into the vacuum chamber following *ex-situ* cleaving are less well-ordered, show adsorbed oxygen and can be either Se-terminated or Bi-rich, which suggests a critical dependence on the level of contamination. We have also used molecular beam epitaxy to investigate the structure and stability of Bi overlayers grown on Bi_2Se_3 . Additional experiments involve exposure of clean surfaces to gaseous species such as O_2 , H_2 and Br_2 .

11:40am **SS+2D-WeM12 Impact Collision Ion Scattering Spectroscopy of Bi_2Se_3 and Bi/ Bi_2Se_3** , *Weimin Zhou, H. Zhu, J.A. Yarmoff*, University of California - Riverside

Bismuth selenide (Bi_2Se_3) and isolated bilayers of bismuth both behave as topological insulators, which are two-dimensional materials that conduct along the surface through topological surface states (TSS). These materials show great promise for use in spintronics and quantum computation. Because the TSS are located at the surface, it is important to understand the relationships between the surface atomic and electronic structures. Low energy ion scattering (LEIS) is a simple, but powerful surface sensitive technique that is ideal for structural analysis. LEIS, using Na^+ projectiles, is employed here in two distinct modes. First, time-of-flight (TOF) spectra are collected using low index incidence directions. This allows for a direct measure of the surface termination with minimal beam damage. Second, impact collision ion scattering spectroscopy (ICISS), which involves the collection of angular distributions using a large scattering angle, is employed to study the structure of the outermost few atomic layers. This work investigates the surfaces of clean Se-terminated Bi_2Se_3 and after a Bi bilayer has been grown on top by molecular beam epitaxy (MBE). Molecular dynamics (MD) simulations of ICISS are compared to the experimental data in order to ascertain the surface structures.

12:00pm **SS+2D-WeM13 Feature Scale Simulation for Materials Processing**, *Paul Moroz*, TEL Technology Center, America, LLC; *D.J. Moroz*, University of Pennsylvania

Modern materials processing often includes complex chemistries and surface interactions, and variety of species incoming to the wafer from gas and/or plasma in the chamber. It also often involves many time-steps, each one utilizing different chemistry and different gas/plasma parameters resulting in time-varying composition of fluxes coming to the wafer, and different energy and angular distributions of incoming species. Chemically or physically active species interact with material surfaces, generally resulting in etching, deposition, and implantation, and such processes might even happen together at the same time. The FPS3D feature scale simulator [1-3] is capable of handling very different and complex cases due

Wednesday Morning, November 9, 2016

to its special structure and numerical techniques, from atomic layer etching and atomic layer deposition to large-scale Bosch processing. Numerical models of surface and molecular interactions are flexible enough to describe most general cases. For this presentation, we selected three types of simulation cases. The first type considers simulation of mostly etching and implantation, such as during Si etching by chlorine-argon plasma. The 2nd type considers ALE (atomic layer etch) when etching is done by a cyclic process of surface passivation/activation with the following process of etching/removal of a single atomic layer per cycle or per a few cycles, allowing ultimate processing accuracy. The 3rd type of simulations considers deposition cases, such as Cu seed layer deposition. Some results will be presented for 2D simulations and some others – for 3D simulations.

References:

- [1] P. Moroz, IEEE Trans. on Plasma Science, **39** (2011) 2804.
- [2] P. Moroz, D. J. Moroz, ECS Transactions, **50** (2013) 61.
- [3] P. Moroz, D. J. Moroz, J. Physics: CS **550** (2014) 012030.

Surface Science

Room 104E - Session SS+AS-WeM

Environmental Interfaces, Ambient Surfaces, and In-Operando Studies

Moderator: R. Scott Smith, Pacific Northwest National Laboratory

8:00am SS+AS-WeM1 In-situ Electron Microscopy of Synthesis, Chemistry and Self-assembly of Colloidal Nanostructures, Eli Sutter, University of Nebraska - Lincoln

INVITED

In-situ microscopy, particularly real-time imaging of dynamic processes has developed into an active field of research and is expected to be one of the key enabling techniques for understanding the formation of nanostructures, catalytic reactions, phase transformations, self-assembly, and other central issues in nanoscience and technology. *In-situ* transmission electron microscopy can be used to follow the behavior and measure the properties of nanostructures over a wide range of environmental conditions with resolution down to the atomic scale. While processes at variable temperatures and gas-solid interactions have been accessible for some time, observations in liquids have emerged only in recent years with the development of special membrane cells. Liquid-cell electron microscopy has developed into a powerful technique that allows the imaging of various processes in wet environments, such as liquids, solutions, or colloidal suspensions, and the investigation not only of a wide range of inorganic nanoscale objects but of biological systems as well.

I will illustrate the power of liquid-cell electron microscopy applied to imaging colloidal synthesis (nanoparticles, core-shell structure), electrochemistry (galvanic replacement reactions) and the self-assembly of nanocrystal superstructures in solution. Our results demonstrate that real-time electron microscopy can substantially advance our understanding of a wide range of processes involving nanoscale objects in bulk liquids.

8:40am SS+AS-WeM3 Low Energy Electron Microscopy at Near Ambient Pressures, Andreas Thissen, SPECS Surface Nano Analysis GmbH, Germany
Low-energy electron microscopy (LEEM) is a spectromicroscopy technique, which allows the study of dynamic processes at surfaces and interfaces, such as thin-film growth, surface reactions, and phase transitions. With the FE-LEEM P90 from SPECS, which is based on the instrument design by Rudolf Tromp from IBM [1,2], lateral and energy resolution of below 5 nm and 250 meV, respectively, can be achieved. Depending on the excitation source and the settings on the instrument a variety of different imaging modes are possible: mirror electron microscopy, low energy electron diffraction (LEED), phase contrast imaging, reflectivity contrast, dark field imaging and bright field imaging, as well as photoelectron emission microscopy and spectroscopy.

We have enhanced the technical capabilities of the FE-LEEM P90 towards studies under near ambient conditions by developing a special sample geometry. This enables the analysis of materials and devices under near ambient conditions and even in situ during operation.

9:00am SS+AS-WeM4 Probing Liquid-Vapor Interfaces of Ionic Solutions with Lab-based APXPS, John Newberg, C. Arble, Y. Khalifa, A. Broderick, S. Rani, University of Delaware

Ionic interfaces are ubiquitous in physical, chemical, biological, environmental and technological processes. Herein we will present recent efforts examining ionic liquid and deliquescent salt interfaces using lab-

based ambient pressure X-ray photoelectron spectroscopy (APXPS) in the presence of water vapor. The onset to water uptake into the top few nm of a hydrophilic ionic liquid is surprisingly similar to hydrophilic solid surfaces. A hydrophilic salt zinc bromide was also probed as it transitions from a solid to a liquid. It will be shown for ionic solutions that the uptake of water leads to variable shifts in the binding energy of anion and cation moieties driven by their interaction with water.

9:20am SS+AS-WeM5 Effect of Surface Passivation on Stability of Methylammonium Lead Iodide Perovskite, Q. Peng, Xiaozhou(Joe) Yu, University of Alabama

Methylammonium Lead Iodide Perovskite (MAPbI₃) is a promising photoelectronic material for various applications. However, the stability of MAPbI₃ is a big concern for its applications in outdoor application environments. Its stability is affected the interfaces between MAPbI₃ and other layers of materials, temperature, moisture, and O₂. Currently the detail decomposition mechanism is not clear yet. In this presentation, we will employ a suite of in-situ characterization methods including in-situ Fourier Transform Infrared spectrometer, quartz crystal microbalance, and quadrupole mass spectrometer to understand the decomposition mechanism when expose MAPbI₃ to different simulated application environments (such as Fig. 1). The effect of various surface passivation methods on the stability of MAPbI₃ will be presented to help illustrate the mechanism that govern the stability of MAPbI₃.

9:40am SS+AS-WeM6 STM Reveals the Formation of Near-Ideal Self Assembled Monolayers on TiO₂ in Air and Solution, William DeBenedetti, M.A. Hines, E.S. Skibinski, A. Song, A. Ortol-Bloch, Cornell University

The surface chemistry of TiO₂ in air and solution is an important, but understudied, topic for next-generation photovoltaics, environmental remediation, and CO₂ photoreduction. Using scanning tunneling microscopy (STM), polarized infrared spectroscopy and other techniques, we will show that surprisingly stable, near-ideal organic monolayers spontaneously form on rutile (110) in a variety of environments.

First, we will show that under ambient conditions, the rutile (110) surface is terminated by a monolayer of bicarbonate, HCO₃⁻, and H formed from the reactive adsorption of CO₂ and H₂O — a reaction that has never been observed in ultrahigh vacuum. Contrary to conventional wisdom, this bicarbonate monolayer displaces H₂O bound to the surface, remaining intact even in vacuum up to ~700 K. The spontaneous formation of a HCO₃⁻ monolayer has important implications for the mechanism of CO₂ photoreduction on TiO₂.

Second, we will show that near-ideal organic monolayers form when rutile (110) is immersed in a variety of aqueous solutions. As an example, highly ordered benzoate monolayers with a characteristic “paired” geometry can be formed from aqueous solutions. Using polarized infrared spectroscopy, we show that this pairing is not due to dimerization, as suggested by previous researchers. Instead, DFT simulations confirm that π - π interactions lead to long-range ordering and a tetrameric bonding geometry. The structure of these monolayers is further confirmed by disrupting the π - π interactions using a variety of fluoro-substituted precursors.

11:00am SS+AS-WeM10 Study of the Electrical Double Layer of Calcium Carbonate Minerals, Yijue Diao, R.M. Espinosa-Marzal, University of Illinois at Urbana-Champaign

Understanding the interactions taking place at the calcite-solution interface is crucial to elucidate many natural geochemical processes on or near the Earth's surface, such as biomineralization and CO₂ sequestration capture of inorganic contaminants by minerals, and enhanced oil recovery. Being the most stable crystalline phase of calcium carbonate, and one of the most abundant minerals, calcite has been studied intensively at the microscale. However, when it comes to the nanoscale, little is known about the molecular details of the calcite-solution interface. Not until recently have experimental and computational works, including our previous force spectroscopy studies, shown that unlike the conventional model of Stern layer, the calcite interface in aqueous phase is well defined by two layers of water molecules on top of which loosely bound hydrated calcium ions are located. Our previous work by colloidal probe atomic force microscopy (AFM) reveals the influence of confinement on the calcite surface under equilibrium conditions.

In this study, AFM with both a microsphere and a sharp tip is employed to perturb the electrical double layer (EDL) of calcite. By performing force measurements with a short interval that does not allow the EDL reaching equilibrium between consecutive force measurements, we perturb the EDL

Wednesday Morning, November 9, 2016

and afterwards scrutinize the kinetics of EDL re-formation. It has been shown that the calcite interface can be tuned by varying calcium concentration and hence, the influence of calcium concentration on the kinetics of EDL formation is also studied. On the other hand, we directly probe into the behavior of the Stern layer by resolving the film thickness transitions (FTTs) that result from squeezing-out layers of molecules confined between the tip and calcite. The significant difference in the confined area, which therefore induces confinements of different extent between the colloidal probe and the sharp tip, allow understanding the influence of the confinement on the EDL.

Calcium carbonate is stored in nanopores of marine organisms and of rocks. Knowing the nanoconfined interfacial structure of calcite from our previous study, we take one step further in this work to investigate the kinetics of the EDL formation under the perturbation induced by consecutive confinement, which allows us not only to spatially elucidate the calcite-solution interface, but also with time resolution.

11:20am SS+AS-WeM11 Observation of Water Adsorption Structures on Ultrathin ZnO/Au(111), Junseok Lee, D.C. Sorescu, X. Deng, National Energy Technology Laboratory

Adsorption of water at the nanostructured metal oxide surfaces has implications in catalysis and serves as a prototypical system in studying water-oxide interfaces. In this work, the adsorption of water on ultrathin ZnO nanostructures grown on Au(111) substrate is investigated using scanning tunneling microscopy (STM) and density functional theory (DFT) calculations. Water overlayers are grown on well-defined monolayer and bilayer of ZnO nanostructures. STM images of water overlayer structures on the monolayer and the bilayer of ZnO nanostructures at low temperature are analyzed in detail at different water coverages with the help of DFT calculation results. Moire pattern is found to influence the adsorption structure of water on the ZnO nanostructure surfaces and the brightness of the Moire pattern of the ZnO structure is observed to be significantly modulated by the adsorption of water molecule. Various hydrogen bonded water network structures are observed on ZnO bilayer after desorbing excess water molecules. The edge of the ZnO monolayer is found to be decorated by water molecules up to room temperature but there was no evidence of adsorption of water at the edge of ZnO bilayer.

11:40am SS+AS-WeM12 Surface and Bulk Crystallization Kinetics of Amorphous Solid Water Nanoscale Films, Chunqing Yuan, R.S. Smith, B.D. Kay, Pacific Northwest National Laboratory

We investigate the crystallization kinetics of nanoscale amorphous solid water (ASW) films using temperature-programmed desorption (TPD) and reflection absorption infrared spectroscopy (RAIRS). ASW is a metastable form of water created by vapor deposition on a cold substrate (T<130 K). We directly measure the surface (using TPD) and bulk (using RAIRS) ASW crystallization kinetics as a function of film thickness and temperature. The results show that nucleation and crystallization begins at the ASW/vacuum interface and then the crystallization growth front propagates linearly into the bulk. The linear propagation is further confirmed by adding a thin layer of isotopic D₂O ice indicator at different positions in the ice. These results show that the closer the isotopic layer is to the vacuum interface, the sooner the isotopic layer crystallizes, which confirms the top-down propagation of the crystallization front. Further evidence for ASW/vacuum interface nucleation mechanism comes from experiments where a decane layer is deposited on top of the ASW film. The presence of the decane layer impedes surface nucleation and dramatically decreases the crystallization rate. By separating surface nucleation and bulk propagation processes, we are able to extract the nucleation and growth rates of ASW crystallization between 140-160 K.

This work was supported by the US Department of Energy (DOE), Office of Science, Office of Basic Energy Sciences, Division of Chemical Sciences, Geosciences & Biosciences. The research was performed using EMSL, a national scientific user facility sponsored by DOE's Office of Biological and Environmental Research and located at Pacific Northwest National Laboratory, which is operated by Battelle operated for the DOE.

12:00pm SS+AS-WeM13 Capture of Hyperthermal Atoms and Molecules by Amorphous Water Ice via Ballistic Embedding, Grant Langlois*, S.J. Sibener, University of Chicago

We present comprehensive work detailing the capture and aggregation of hyperthermal atoms and molecules (CO₂, CF₄, Xe, Kr) by amorphous solid

water (ASW) under ultra-high vacuum conditions at 125 K, near the amorphous/crystalline transition. Using time-resolved *in situ* reflection-absorption infrared spectroscopy (RAIRS), the gases prepared in supersonic molecular beams with translational energies above ~3.0 eV are observed to directly embed underneath the vacuum-ice interface to become absorbed within amorphous ice films despite an inability to adsorb at 125 K. Embedding into crystalline films, when observed, is less effective. Upon embedding, resultant mobility within the ice and the strength of intermolecular interactions can yield segregation of these gases into clusters, as seen in the case of CO₂. Tracing the kinetics of these embedding events under different energetic conditions allows for elucidation of the underlying dynamics, and we draw comparison between all studied gases to promote generalized conclusions in regards to empirical prediction of embedding probability. Through application of a classical model of the entrance barrier for atoms and molecules colliding with amorphous ice, we provide direct evidence for a unified connection between embedding probability and momentum of the incoming atoms and molecules; an account of all embedding data measured by our group traces a singular barrier. This work highlights the interplay between translational energy and momentum accommodation during collisions with ice; atoms and molecules can become trapped in an icy surface despite an inability to simply stick to the interface. These results are of considerable importance to studies of both the astrochemistry and evolution of interstellar bodies and dust, and detailing the capture and release of gases by permafrost relating to global climate forcing.

Thin Film

Room 105A - Session TF+MI+NS-WeM

ALD and Nanostructures

Moderators: Sean King, Intel Corporation, Mariadriana Creatore, Eindhoven University of Technology, Netherlands

8:00am TF+MI+NS-WeM1 Scalable Manufacturing of Nanostructured Materials by Gas-Phase Deposition Techniques, Ruud van Ommen, Delft University of Technology, Netherlands

INVITED

Core-shell nanoparticles and other nanostructured particles have high potential in applications such as catalysis, energy storage and pharma. However, a hurdle in their utilisation is that typically large amounts of such materials are required. Current liquid-phase and gas-phase synthesis methods often lack the high precision required or do not lend themselves to large-scale production. Gas-phase coating can be used to provide the surface of a particle with either a thin continuous coating or a decoration of nanoclusters. Coating techniques that can be used are chemical vapour deposition (CVD) [1], atomic layer deposition (ALD) [2], and molecular layer deposition (MLD) [3].

When carried out in a so-called fluidized bed, gas-phase coating is an attractive way of producing nanostructured particles with excellent scale-up potential. In such a system, the particles are suspended in an upward gas flow. We can do this both for nanoparticles and micron-sized particles. Nanoparticles – contrary to what is typically observed for larger particles – are fluidized as very dilute agglomerates with distinctive fluidization characteristics. I will discuss the challenges related to coating of nanoparticles using CVD, ALD, and MLD with such a system. Moreover, I will give a number of examples of the applications of nanostructured particles produced in this way.

[1] Valdesueiro, D., Meesters, G., Kreutzer, M., and van Ommen, J.R., 'Gas-phase deposition of ultrathin aluminium oxide films on nanoparticles at ambient conditions', *Materials* 8: 1249-1263 (2015).

[2] Goulas, A. and van Ommen, J.R., 'Atomic layer deposition of platinum clusters on titania nanoparticles at atmospheric pressure', *Journal of Materials Chemistry A* 1(15): p. 4647-4650 (2013).

[3] Vasudevan, S.A., Xu, Y., Karwal, S., van Ostaay, H.G.M.E., Meesters, G.M.H., Talebi, M., Sudhölter, E.J.R., and van Ommen, J.R., 'Controlled release from protein particles encapsulated by molecular layer deposition', *Chemical Communications* 51: 12540-12543 (2015).

8:40am TF+MI+NS-WeM3 Surface Passivation of InP Nanowires by Atomic Layer Deposition, Lachlan Black, Y. Cui, A. Cavalli, M.A. Verheijen, E.P.A.M. Bakkers, W.M.M. Kessels, Eindhoven University of Technology, Netherlands
III/V semiconductor nanowires offer a variety of novel properties that make them of interest for electronic and optoelectronic device applications, including enhanced light trapping/concentration, reduced material use,

* Morton S. Traum Award Finalist

† National Student Award Finalist

Wednesday Morning, November 9, 2016

and relaxation of lattice-matching constraints, which enables novel heterostructures and growth on inexpensive substrates. However, the greatly increased surface-to-volume ratio of nanowires compared to planar devices significantly increases the importance of surface recombination and hence of effective passivation of the nanowire surface.

In this work, we focus on nanowires of InP, a material of particular interest for optoelectronic devices. In contrast to the situation for GaAs, the bare or natively oxidized surface of InP presents relatively few electronically active defect states to facilitate surface recombination. However, in order to form InP device structures it is necessary to deposit an insulating dielectric layer on part of the InP surface, and this tends to result in significant depassivation of the surface, to the extent that the performance of InP devices is commonly limited by surface recombination.

Atomic layer deposition (ALD), as a relatively "soft" deposition technique capable of forming well-controlled, high-quality dielectric layers, would seem to offer the best chance of successfully passivating InP nanowire surfaces. ALD can be performed at low substrate temperatures, which is important to avoid phosphorus out-diffusion and resulting damage of the InP surface, while its excellent conformality allows for uniform deposition on nanowire surfaces. Nevertheless, previous attempts to passivate InP surfaces by ALD have encountered similar difficulties to other techniques in achieving low surface recombination for deposited dielectric layers of appreciable thickness.

In this work, we demonstrate successful dielectric passivation of InP planar and nanowire surfaces in the presence of a relatively thick (>10 nm) ALD Al_2O_3 layer deposited from trimethylaluminum (TMA), through the use of a thin phosphate interlayer deposited at low temperature in the same system from trimethyl phosphate (TMP), in both cases using an O_2 plasma oxidant. Time-resolved photoluminescence measurements show that carrier lifetimes are increased relative to the native surface for both planar and nanowire InP samples (e.g. from 1.6 to 2.4 ns for one nanowire sample), in contrast to a strong depassivation observed following ALD of Al_2O_3 and other dielectrics on the bare InP surfaces. X-ray photoelectron spectroscopy (XPS) and transmission electron microscopy (TEM) are used to elucidate the composition and structure of the deposited phosphate layers.

9:00am TF+MI+NS-WeM4 Selectivity and Nucleation Effects in Atomic Layer Deposition of Copper for Plasmonic Nanostructures, Jie Qi, B.G. Willis, University of Connecticut

Plasmonic nanostructures made of conducting metals such as copper, silver, and gold have been intensively investigated due to their capability for enabling optics beyond the diffraction limit and making it possible to manipulate visible and near-IR radiation at the nanometer scale. The interaction between metallic nanostructures and incident light induces large enhancements of the local electromagnetic fields via the excitation of localized surface plasmon resonances (LSPRs). These confined and enhanced fields have many exciting applications in optical detection, cancer therapeutics, biological and chemical sensors, spectroscopy, catalysis, and photovoltaics. A key feature of nanoscale plasmonic materials is a strong dependence of the plasmon resonance on size, shape, composition, and surroundings of the nanostructures. Selective area atomic layer deposition (SA-ALD) offers a promising nanofabrication technique to further tune the properties of plasmonic nanostructures with composition and thickness control at an atomic level. Successful application of SA-ALD requires good control of nucleation and surface morphology evolution, as well as good selectivity. Unfortunately, there are very few studies that report selectivity and/or nucleation characteristics, and their dependence on growth conditions.

In this work, we investigate the growth characteristics of Cu SA-ALD for tuning plasmonic nanostructures. Pd nanostructures are fabricated by electron-beam lithography and used as template layers. Samples are analyzed by AFM, high-resolution SEM, and image processing to investigate nuclei size and density, and morphology evolution. It has been found that nucleation is greatly affected by deposition temperature and co-reactant H_2 partial pressure. Poor nucleation leads to a rough surface with randomly distributed nanoparticles, while good nucleation leads to smooth, conformal growth over the entire feature. Sample surface pretreatments are found to be more critical for initiating growth on nanostructures compared to planar films, which might be related to residual impurities from photoresist layers or other contaminants from nanofabrication processing. Several preparation cleaning methods have been investigated for their effects on Cu film nucleation and growth selectivity including: UV-

Ozone, O_2 plasma, annealing in H_2 , annealing in He, boiling in water, and dipping in dilute HF.

9:20am TF+MI+NS-WeM5 Metal Oxide Aerogel Patterning by CO_2 Laser Etching of ALD-coated Carbon Nanotube Macro-Structures, C. Aksu, P.D. Bradford, Jesse Jur, North Carolina State University

Patterning techniques of metal oxide foam architectures embedded within an ALD-coated carbon nanotube interconnected matrix are defined. Three dimensionally interconnected networks of carbon nanotube are produced from spinnable vertically aligned CNT arrays in which CNTs make. Atomic layer deposition is used to functionalize the surface of the CNTs in the array. Prior work has demonstrated that the CNT networks can be sacrificially removed to form aerogel architectures of the ALD material. In this study, we present a simple and scalable method to fabricate macro-sized structures of ALD alumina foams embedded in the carbon nanotube foam architecture via a CO_2 continuous wave laser etching. Specifically, we have demonstrated the ability to ALD modify the CNT in large macro-structures (>1 cm 2) and subsequently remove the CNT from specified areas, leading to the complex hybrid alumina-CNT periodic structures. The effects of ALD coating thickness are inspected by in-situ heating transmission electron microscopy methods and by high resolution scanning electron microscopy. Factors relating to manufacturability (i.e. etching speed and power) and dimension stability (i.e. laser etch size) are defined to identify scale-up opportunities.

9:40am TF+MI+NS-WeM6 Tungsten ALD in Porous Carbon Nanotube Forests, K. Hinton, N. Hollingworth, D.D. Allred, Richard Vanfleet, Brigham Young University

We have deposited tungsten on carbon nanotube (CNT) forests by CVD (WF_6 & H_2) and ALD -the silane reduction of WF_6 . Resulting structures are studied by scanning electron and transmission electron microscopy. We observed that the CNT forest provides a scaffolding for the nucleation and growth of the tungsten. Such structures may be a useful avenue for metal MEMS that does not require extensive etching. The present study may provide insight into the mechanisms of ALD in highly porous structures. In conventional ALD on surfaces which are largely planar, the amount of reactants needed to completely cover the surface does not change much from step-to-step. In contrast the surfaces of carbon nanotube forests consist of cylindrical tubes largely oriented perpendicular to the sample surface. Thus, the surface area increases with deposition. This is in addition to the changes in surface area associated with incubating early stage nucleation sites. When beginning with adequate tungsten or silane one might expect to move to starvation mode as the number of cycles increases if the amount of each reactant is kept constant. We see evidence for tungsten starvation in our research results. For low number of cycles the CNT fibers have a spatially uniform nucleation of tungsten. For low amounts of WF_6 or low "soak" times, as cycles increase, growth on the top surface and sidewalls of the carbon nanotube forest outpaces growth within the structure. Post deposition cross-sections show distinct bands witnessing the starvation of tungsten growth in the interior as more of the tungsten is deposited on regions that have direct access to the WF_6 gas. EDX analysis across such a cross-section shows distinct plateaus in the amount of tungsten present corresponding to the bands.

11:00am TF+MI+NS-WeM10 Rational Design of Hyperbranched ZnO Nanowire Systems for Superomniphobic Surfaces Enabled by ALD, Ashley Bielinski, M. Boban, University of Michigan, Ann Arbor; Y. He, Pacific Northwest National Laboratory; E. Kazyak, University of Michigan, Ann Arbor; C. Wang, Pacific Northwest National Laboratory; A. Tuteja, N.P. Dasgupta, University of Michigan, Ann Arbor

Semiconductor nanowires (NWs) are powerful 1D building blocks for a range of technologies including electronics and optics, sensors, mechanical resonators, and energy conversion [1]. NW arrays are synthesized with careful control of morphology and composition using both top-down and bottom-up approaches. However, the hierarchical assembly of these NWs into heterogeneous systems remains challenging, largely due to lack of deterministic control of feature size, shape and position in 3D assemblies. Here we demonstrate that Atomic Layer Deposition (ALD) is a powerful tool for modifying interfaces to control the fabrication of ordered hyperbranched NW systems. Hierarchical branched NWs bridge the nano and micro length scales, while providing an exponential increase in surface area. Examples have been synthesized for a variety of applications, but the ability to tune the morphology along a spectrum in order to optimize the structure requires development.

Nanoscale patterning techniques for NW placement, while slow and costly on planar substrates, often become impossible on high aspect ratio

Wednesday Morning, November 9, 2016

structures. Solution-based techniques offer scalability and lower cost, but the results are often disordered and difficult to tune. Our approach uses ALD to catalyze the nucleation of NWs on the substrate during hydrothermal growth. ALD is essential for this approach because it deposits conformal films on ultra-high aspect ratio substrates, with atomic-scale control of film composition and structure. We've demonstrated that by varying the thickness of ALD ZnO films, their crystallographic orientation, roughness, and surface stress can be controlled [2]. These catalyst seed layers allow us to tune the NW array morphology, including density and orientation, over a range of substrate materials and geometries.

We further show that ALD can overcome challenges that arise when transitioning from simple NW arrays to complex branched structures [3]. First, amorphous ALD TiO₂ over-layers are used to reduce nanowire density creating space for subsequent levels of hierarchy. Next, ALD interlayers are used to block the crystallinity of the previous level of ZnO NWs to allow for non-epitaxial deposition of the subsequent ALD seed layer, forming core-shell NWs. These new techniques were used to grow hierarchical branched NW arrays, which were shown to be superomniphobic (repellent to high and low surface tension liquids) with tunable contact angles for different liquids using ALD to control the array properties.

[1] Dasgupta, N. P.; et al. *Adv. Mater.* **2014**, 26 (14), 2137–2184.

[2] Bielinski, A. R.; et al. *Chem. Mater.* **2015**, 27 (13), 4799–4807.

[3] Bielinski, A. R.; et al. *Submitted* **2016**

11:20am TF+MI+NS-WeM11 Bio-Templated Morpho Butterfly Wings by ALD for Photocatalysis, Robin E. Rodriguez, D. Das, S.P. Agarwal, University of Michigan, Ann Arbor; W. Shang, T. Deng, Shanghai Jiao Tong University, China; N.P. Dasgupta, University of Michigan, Ann Arbor

Hierarchical nanostructures found in biology have unique properties that inspire bio-mimetic engineering. These natural nanostructures present design principles of bottom-up nanomanufacturing for materials with tunable properties. For example, structural coloration is a phenomenon observed in a wide range of natural materials that take advantage of nanoscale hierarchical structures to tune their reflection and absorption properties through periodic diffraction and photonic resonances. Here we demonstrate *bio-templating* via Atomic Layer Deposition (ALD) as an approach to manufacture atomically-precise synthetic materials that manipulate the natural structural coloration found in *Morpho* butterfly wings for enhanced photocatalytic activity.

Until recently, conventional approaches to bio-templated nanomaterial synthesis have been limited in their ability to create highly conformal 3-D interfaces between temperature- and chemically-sensitive bio materials and functional thin films. ALD is uniquely suited for scalable and conformal bio-templating, which allows us to use the nanoscale structural complexity that nature provides to tune the interfacial properties of natural systems by coating them with functional materials. By varying the geometric and optical properties of the surface, ALD is able to tune structural coloration to manipulate the light absorbing and photocatalytic properties of natural materials with nanostructured surfaces.

Morpho butterflies are particularly interesting examples of structural coloration, which occurs due to hierarchical nanostructures on their wing surfaces. The combination of strong photonic resonances and high surface area in these wings represent an ideal template for photocatalysis. To demonstrate this, proof-of-concept tests were performed on *Morpho* wings coated by ALD of TiO₂ and ZnO. Electron microscopy images showed conformal coating of the wing geometries at the nanoscale. The structural coloration of the butterfly wings could be tuned using this approach, which was modeled using finite-difference time-domain simulations of the modified wing geometry. The viability of this approach was further demonstrated in the photocatalytic degradation of methylene blue dyes in water, which led to an increase in photocatalytic activity relative to planar thin film samples. The ALD deposited materials show superior photocatalytic activity which was attributed to enhanced light absorption and increased surface area from the butterfly's hierarchical structures.

Vacuum Technology

Room 101D - Session VT-WeM

Vacuum Technology – History and Innovation (8:20-10:00 am)/Transfer and Manipulation (11:00 am-12:20 pm)

Moderator: Jay Hendricks, National Institute of Standards and Technology

8:20am VT-WeM2 A New Approach to Vacuum Technology Education at a Distance, Del Smith, N. Louwagie, Normandale Community College

Education and training for technicians who work in the vacuum and vacuum coating industries is becoming more critical as the complexity of the equipment and processes increases. In addition, many of those currently working as technicians are approaching retirement age, with no obvious source for the large number of replacement personnel that will be needed. Many technicians will benefit from a formal educational program giving them grounding in the basic sciences and developing their soft skill set. Several local companies utilizing vacuum and coating technologies partnered with Normandale Community College in 1998 to develop a formal educational program to train technicians in the basic concepts of vacuum and thin film technology. Recently, the need for the expansion of this program to geographic areas that are currently underserved and cannot support a college program in these specialties became apparent. Normandale Community College in Bloomington, MN, is in its second year of a three year project, funded by the National Science Foundation, Division of Undergraduate Education, Advanced Technological Education. The focus of this project is to develop the vacuum technology curriculum, processes and equipment needed to train technicians at locations remote from the primary instructor. This paper presents the current status of this project, with details about curriculum development, remote classroom technology and the development and use of advanced vacuum training hardware systems for use at the remote learning site that include features not previously available.

8:40am VT-WeM3 It's All Because of the Vacuum..., H. Frederick Dylla, American Institute of Physics

INVITED

A number of key scientific demonstrations from the 18th century to the present were enabled by the essential task of obtaining a low enough level of vacuum. This talk explores a number of well-known events in the history of science and technology that depended on achieving a remarkable level of high vacuum for the era contemporary to the demonstration. We start with Franklin's lyceum experiments where he applied static voltages across glass cylinders where pressures were lowered below ambient conditions with crude air pumps. This work presaged subsequent work on gas discharges and modern accelerator cavities. A century later, J. J. Thomson was the first to make an electron beam by lowering vacuum levels sufficiently to prevent ionized residual gas ions from shielding the negative particle beam. Fast-forward to the early 1960's where G.K. O'Neill invented the now standard configuration for contemporary particle physics experiments- the high intensity storage ring. This configuration demanded and achieved true ultrahigh vacuum levels on an industrial scale. The story concludes with this year's remarkable detection of gravity waves using LIGO - the kilometer-scale laser interferometers that required extreme high vacuum levels for all residual gas components.

9:20am VT-WeM5 The Next Generation Quantum-based Metrology for Miniaturized Sensors and Standards, Gregory F. Strouse, National Institute of Standards and Technology

INVITED

Development of innovative sensors and standards that—through improvements in cost, size, speed, and durability—will enable new manufacturing processes, tools and products of tomorrow. The NIST vision is that these innovations will improve the dissemination of standards to the point where routine exchange of artifacts for measurement quality assurance is no longer needed. Quantum and photonic based rugged small-scale vacuum sensors open new horizons in measurement science and represent a paradigm shift in how metrology is done. Networks of small and precise sensors embedded within structures and composite materials could improve their performance and reliability. These sensors draw upon a range of technologies not previously exploited for these applications, such as nanofabrication, photonics, and atomic physics. Photonic and quantum-based vacuum sensors will allow both the absolute sensing of vacuum and the realization of the SI at the user site and will allow the user to calibrate other sensors or directly measure process vacuum levels for critical applications. Several related research programs at NIST are geared towards realizing the vision of small or chip sized absolute sensors for practical applications. NIST is building a sensor program, with the goal to establish a set of chip-scale tools that enable real-world use. An example is

Wednesday Morning, November 9, 2016

the chip-scale cold-atom technology requires maintaining UHV conditions throughout the operating lifetime of the device, posing practical technical challenges to the vacuum engineering. Our program to replace primary mercury manometers with photonic-based primary standard relies on lasers and Fabry-Pérot optical cavities that are stable from several atmospheres of pressure down to high-vacuum. These cavities will be field-deployable absolute sensors requiring no calibration. Other quantum and photonic based sensors include dynamic pressure measurements and thermometry. These programs will be discussed in terms of the larger programmatic view of how quantum-based, chip scale technologies will disrupt vacuum technology, primary standards, and pressure, vacuum and temperature measurement.

11:00am VT-WeM10 Vacuum Transport for Realization and Dissemination of the Redefined Kilogram at NIST, *Eric Benck, E. Mulhern*, NIST INVITED

In 2018 the unit of the kilogram will be redefined. Instead of being based on the physical artifact known as the International Prototype Kilogram (IPK), the kilogram will be defined by fixing the value of a fundamental physical constant, Planck's constant. It will now be realized using watt balance or x-ray crystal density (Avogadro) experiments. This will enable any research group throughout the world to realize the unit of mass if they have sufficient technical expertise and equipment. Both of these experimental methods are optimally designed to operate in vacuum. As a result, mass metrology must now deal with the issues of maintaining, manipulating and moving masses under vacuum.

At the National Institute of Standards (NIST), at least five different experimental systems operating in vacuum will be used for the realization and dissemination of the kilogram. First, the kilogram will be realized using the NIST-4 watt balance. Second, NIST is developing a unique apparatus called the magnetic suspension mass comparator (MSMC) to transfer the unit of mass in vacuum to a mass in air. Third, a commercial vacuum comparator will be used to directly compare different masses in vacuum and for sorption studies. Fourth, a new plasma cleaning station is being developed to use a downstream hydrogen plasma source to clean a mass. And finally, there will be a vacuum mass storage facility where multiple calibrated masses can be kept for later mass comparisons.

In order to transport a mass under vacuum between the different apparatus, a custom built mass transport vehicle (MTV) has been constructed. It is essentially a mobile vacuum chamber made out of a 4 way cross and gate valve. It has a wide range pressure gauge and a battery powered getter pump. The vacuum chamber is supported by an aluminum frame mounted on casters. The MTV can maintain a vacuum below 1.3×10^{-3} Pa for 30 minutes without pumping which is sufficient time to transport a mass between the different rooms housing the experimental apparatuses. The MTV can be attached to a load lock on each apparatus which can extract the mass and transfer it inside while maintaining the mass in vacuum. The complete transfer process of a mass from one machine to another with the MTV takes on the order of an hour. Most of this time is due to the evacuation time of the load lock after the MTV has been attached.

11:40am VT-WeM12 Handling, Transfer, Storage, and Shipping of Commercial Thin Film Hydride Disk Target Samples, *James Provo*, J. L. Provo, Consulting

Handling, Transfer, Storage, and Shipping of Commercial Thin Film Hydride Disk Target Samples

James L. Provo*

Consultant, J. L. Provo Consulting, Trinity, FL 34655-7179

Thin film hydride targets are important for many applications including, accelerator research, various neutron devices, contraband detection, etc.

They are very sensitive to air-oxidation and easily contaminated by improper

handling. Air-exposure, which oxidizes Group IIIB, IVB, and rare earth film materials, affects their operating properties. This paper will discuss the development of handling techniques, and special transfer and shipping containers for hydride target samples from post processing to transfer and shipment to a customer. Studies were performed to determine the best physical

handling devices, procedures for reducing particulate contamination, and for

reducing air-exposure and moisture from samples before actual use. Initially, as

an example, samples in an air-exposure hydriding system, were backfilled with

an inert gas just before opening into an environmentally controlled clean room,

quickly moved to an inert gas glove box, and then placed in special vacuum transfer or shipping containers, as quickly as possible, and then pumped down

to a vacuum of $\sim 1 \times 10^{-7}$ Torr (1.33×10^{-5} Pa) or less. For optimum handling

conditions, a system was developed with the major components being a hydride

loading system in a double-sided stainless steel glove box contained in an environmentally controlled room. This glove box contained a loader vacuum

chamber, a video microscope, a HEPA filter/fan module and a hydriding gas

manifold. The glove box had an inert Ar or N₂ atmosphere, achieved by circulating

the gas through a commercially made purifier which stripped oxygen and water

vapor. The glove box atmosphere was monitored by an oxygen monitor, and a

water vapor analyzer. When loaded samples are removed from the chamber

of such a system, samples are automatically in a pristine environment, with very

low particulate contamination, and a minimum amount of water vapor.

On the other side of the glove box, samples are placed into transfer and/or shipping containers, which are then pumped down to high vacuum conditions for

shipment. Examples of sample handling clips, and sample containers are given.

Results have shown, that by using such methods and techniques, hydride target

disk samples can be successfully processed, handled, transferred and shipped in a

condition very close to that as processed out of a loader.

* Formerly, Principle Member of the Technical Staff at Sandia National Laboratories,

Albuquerque, New Mexico 87185 (Retired); electronic mail: jprovo@verizon.net

Wednesday Lunch, November 9, 2016

Exhibitor Technology Spotlight

Room Hall C - Session EW-WeL

Exhibitor Technology Spotlight Session

Moderator: Chris Moffitt, Kratos Analytical Limited

1:00pm EW-WeL3 Why Test Inks Cannot Tell the Full Truth About Surface Free Energy, *Thomas Willers, M. Jin, KRUSS*

There are a range of methods for activating the surface when treating materials before coating, bonding or printing. These include thermal or electrical methods, such as plasma, flame or corona treatment, and chemical treatment with oxidizing gases. Equally important are cleaning steps which remove hydrophobic substances from the surface. All these methods increase the surface free energy (SFE) and therefore improve wettability and adhesion. Norms such as DIN 55660 for coating materials and DIN EN 828 for adhesive processes specify contact angle measurement as the method for determining the SFE of surfaces and for checking an activating or cleaning pre-treatment process. In addition, these inks, which are intended to reflect the SFE based on liquids with set surface tension (SFT) are also frequently used. According to the ink test method, complete wetting always occurs when the values of the SFE of the solid and the SFT of the liquid are equal. Many scientific authors have refuted this wetting theory and have shown that only an analysis of the polar and dispersive interaction fractions of the SFE and the SFT provide a complete picture of the wetting process. Contact angle measurements, which take these interactions into account, and ink tests should accordingly lead to different evaluations of surfaces and therefore also to different assessments of the quality of a pre-treatment process. In the present study, we have compared SFE results from contact angle measurements with those from ink tests for 13 very different materials. We also carried out comparative measurements on three plasma-treated plastics. Both the small number of consistent results and the large number of deviations can be conclusively explained when we take the effect of polar and dispersive interactions into account. It appears that the SFE result of an ink test must be called into question for many samples. In this discussion, we also point out some advantages of the contact angle method in measurement practice.

1:20pm EW-WeL4 A Vacuum Species Sensor using Remote Plasma Emission Spectroscopy for Direct Monitoring of Vacuum Processes, *Joseph Brindley, D. Benoit, V. Bellido-Gonzalez, Genco Limited, UK*

Some form of monitoring of the vacuum environment is essential for the efficient operation of any vacuum processes. This can be achieved through a variety of sensors; from simple total pressure sensors, to highly sensitive quadrupole mass spectrometers. In particular, residual gas analysis (RGA) can be performed with quadrupole mass spectrometers. Residual Gas Analysis allows for detection and identification of individual species within the vacuum. This can result in higher process yields through faster troubleshooting, scrappage reduction through contamination detection, more efficient use of pumping time, or a more controlled vacuum environment. The limiting factor for Quadrupole RGAs is the pressure range over which they can operate. Above 1×10^{-4} mbar damage will occur to the sensor's filament – restricting its use above this pressure. To overcome this obstacle a differential pump can be used to bring the local pressure at the sensor down to the required range. However, this is a costly addition and spurious readings can be generated from the differential pump itself. An alternative residual gas monitoring sensor that operates directly at pressures above 1×10^{-4} has been built around plasma emission monitoring. A small “remote” plasma can be generated inside a sensor that is part of the main vacuum. Consequently, species that are present within the vacuum will become excited in the sensor's plasma, emitting light at certain wavelengths, which can then be used to identify the emitting species. Advances in miniature spectrometers in combination with advanced spectrum identification software has resulted in a robust, lower-cost, multi-purpose vacuum sensor. Presented are a number of examples of its use in monitoring a variety of vacuum conditions such as contaminant detection, water vapour outgassing, etching process monitoring, pump down analysis and reactive deposition control.

1:40pm EW-WeL5 Raman Imaging of Samples with Complex surface Topographies Using Renishaw's inVia Qontor, *Tim Prusnick, RENISHAW, INC.*

Recent advancements in hardware and software have been made to enable micro-Raman focus to be maintained over large areas during data collection. These developments allow analysis of samples that in the past were impractical or even impossible because of variations in surface topography. With the addition of Renishaw's latest innovation, Live Track™

focus tracking technology, the inVia Qontor enables users to analyze samples with uneven, curved or rough surfaces.

2:00pm EW-WeL6 Ampoules and Bubblers 101, *William Kimmerle, K.S. Kimmerle, NSI*

NSI Bubblers and Ampoules are commonly used in Atomic Layer Deposition, Chemical Vapor Deposition, Epitaxial growth on crystalline substrates and numerous other applications. The drive for smaller structures continues to demand new materials and molecules as well as methods for depositing these new materials. Bubblers and ampoules provide a means of safely transporting and precisely delivering these new molecules to wafer substrates. Additionally, as higher vapor pressure materials are utilized, temperature control and ampoule content monitoring become salient. A discussion of safety (Code of Federal Regulations - DOT 4B), various types of ampoules and bubblers for use with liquids and or solids at increasingly higher temperatures will be discussed. NSI – is the largest premium quality manufacturer of Ampoules and Bubblers for use in ALD, CVD, Compound Semi and Epi in the world.

Wednesday Afternoon, November 9, 2016

2D Materials Focus Topic

Room 103B - Session 2D+NS-WeA

Nanostructures including Heterostructures made of 2D Materials

Moderators: Charlie Johnson, University of Pennsylvania, Arkady Krashenninikov, Helmholtz Zentrum Dresden-Rossendorf, Germany

2:20pm 2D+NS-WeA1 Single- and Few-Layer WTe₂ Nanosheets: New Raman Fingerprints, Nanomechanical Resonances, and Environmental Instability Studies, Fan Ye, J. Lee, Case Western Reserve University; J. Hu, Z.-Q. Mao, J. Wei, Tulane University; P.X.-L. Feng, Case Western Reserve University

Among recently emerging two-dimensional (2D) materials, 1T'-phase semi-metallic tungsten ditelluride (WTe₂) [4] possesses unique properties – large, non-saturating magnetoresistance [1] that originates from perfect balance between electrons and holes populations [2], a metallic to insulating transition under low temperature with varying number of layers [3] and superconductivity under high pressure [5]. These properties are not easily accessible in other 2D materials, thus making WTe₂ highly attractive for further investigations on their basic properties, especially in the single layer (1L) to few-layer regime.

In this work, we have systematically investigated new Raman signatures, nanomechanical properties [6], and environmental instability of single- and few-layer WTe₂. In Raman study, we have observed up to 12 peaks in few-layer WTe₂. We find clear softening, stiffening and invariant behaviors in the measured 12 Raman modes as thickness decreases from 8L to 1L. These Raman fingerprints could be an effective 'thickness indicator' for identifying layer number in atomically thin WTe₂. We have also investigated mechanical properties of few-layer suspended WTe₂ by measuring their resonances, and further determined its Young's modulus to be $E \sim 80$ GPa. In addition, by employing surface sensitive material characterization tools such as Raman spectroscopy, XPS, and AES, we carefully study the degradation behavior of single- and few-layer WTe₂ in ambient conditions [7]. We find that oxidation is the main driving force of WTe₂ degradation and it is a self-limiting process. In particular, 1L WTe₂ quickly oxidize in ~ 13 mins, while 2L and 3L WTe₂ exhibit relatively slower, saturating and self-limiting degradation process over two weeks.

This work paves the way for future investigations and utilization of the multiple new Raman fingerprints of few-layer WTe₂, and for exploring mechanical control of WTe₂ atomic layers.

[1] X. L. Fan, *et al J. Mater. Chem. A*, **2**, 20545–20551 (2014).

[2] M. N. Ali, *et al., Nature* **514**, 205-208 (2014).

[3] P. L. Cai, *et al., Phys. Rev. Lett.* **115**, 057202 (2015).

[4] L. Wang, *et al., Nat. Comm.* **6**, 8892 (2015).

[5] X.C. Pan, *et al., Nat. Comm.* **6**, 7805 (2015).

[6] J. Lee *et al., Nanoscale*, **8**, 7854–7860 (2016).

[7] F. Ye *et al., In Submission* (2016).

3:00pm 2D+NS-WeA3 Laser-based Synthesis and Processing of Two-dimensional Monolayers and Heterostructures, Masoud Mahjouri-Samani, C. M. Rouleau, A.A. Puzos, D.B. Geohegan, Oak Ridge National Laboratory

INVITED

Two-dimensional (2D) materials, such as metal chalcogenides, graphene, and oxides, have emerged as an exciting class of materials with extraordinary physical, chemical, electrical, and optical properties. These classes of 2D materials have the potential to enable numerous new technological applications ranging from electronics to photonics. However, realization of this potential requires (i) novel synthesis approaches for growth of high-quality 2D materials, (ii) controllable chemical and structural modification of the crystals, and (iii) a fundamental understanding of their structural properties and device characteristics.

In this talk, I will demonstrate the use of non-equilibrium laser-based approaches to form and deliver atoms, clusters, or stoichiometric nanoparticles with tunable kinetic energies for the synthesis and processing of 2D layered semiconductors. Utilizing stoichiometric nanoparticles as feedstock, we have shown the growth of either small domain nanosheet networks (~ 20 nm) or large crystalline domains (~ 100 μ m) of GaSe, MoSe₂, and WSe₂ with controlled orientation, number of layers, crystallite size, and growth location. We have also shown that atomic precursors with tunable kinetic energies can be used for doping, alloying, and conversion of 2D monolayers. I will show the structural,

optical, and electrical properties of monolayer crystals modified by defect formation, healing, doping, and conversion processes. I will then highlight our newly developed method that enables the formation of patterned arrays of lateral heterojunctions between two different 2D semiconductors necessary for ultrathin electronics. These non-equilibrium approaches provide unique synthesis and processing opportunities that are not easily accessible through conventional methods.

4:20pm 2D+NS-WeA7 Pulsed Laser Deposition of Single Layer, Hexagonal Boron Nitride on Fiber-oriented Ag(111)/SrTiO₃(001), Jeff Terry, D. Velazquez, R. Seibert, L. Spentzouris, Illinois Institute of Technology

We have grown thin films of hexagonal boron nitride (h-BN) of thickness 1-10 ML on fiber-oriented Ag buffer films on SrTiO₃(001) by pulsed laser deposition. We used Ag buffer films of 40nm thickness to substitute for expensive single crystal metallic substrates. Reflection high-energy electron diffraction (RHEED) was used to monitor the surface structure of the Ag films and to observe the formation of the characteristic h-BN diffraction pattern. Attenuated total reflectance spectroscopy showed the characteristic h-BN peaks at 780 cm⁻¹ and 1367.4 cm⁻¹. Ex-situ photoelectron spectroscopy showed that the surface of the h-BN films was stoichiometric. Scanning electron microscopy showed that the h-BN films grew as large, sub-millimeter sheets with nano- and micro-sheets scattered on the surface. The h-BN sheets were easily exfoliated by the micromechanical adhesive tape method. The use of thin film Ag allowed us to adjust the surface morphology of the thin film prior to h-BN growth.

4:40pm 2D+NS-WeA8 Fracture Toughness Measurements of Graphene Oxide, Tobin Filleter, C. Cao, University of Toronto, Canada; J.Y. Howe, Hitachi High Technologies Canada Inc., Canada; D. Perovic, University of Toronto, Canada; Y. Sun, University of Toronto, Canada

Graphene Oxide (GO) is a functionalized form of graphene that we have recently shown to possess high tensile strength [1-2]. These studies on the strength of GO have revealed a size dependent mechanical behavior in which the strength is found to increase with decreasing thickness, a behavior which is controlled by a transition in the fracture mechanism [2]. In real engineering applications in which materials exhibit pre-existing flaws, the fracture toughness of a material is also a critical property in predicting the failure of the material. Here we present studies of GO with preexisting defects that enable the first measurements of the fracture toughness of GO nanosheets. Application of traditional experimental techniques used to measure the fracture toughness (and monitor the fracture behavior) of bulk materials is not feasible for the measurement of ultra-thin films such as GO. In this work, we apply a micro-electro-mechanical system (MEMS) based *in situ* transmission electron microscope (TEM) method to measure the fracture toughness of GO and directly characterize its fracture behavior through high resolution TEM imaging. GO nanosheets suspended on monolithic MEMS devices *in situ* TEM were first controllably etched by high-energy electrons to create well defined holes in the GO nanosheets used for fracture toughness measurements. After a defect was created, *in situ* TEM tensile tests allowed both measurement of the stress at the onset of fracture, as well as direct monitoring of the fracture response via TEM imaging.

[1] C. Cao, M. Daly, C. V. Singh, Y. Sun, and T. Filleter, "High strength measurement of monolayer graphene oxide", Carbon, vol. 81 (2015) p.g. 497-504

[2] C. Cao, M. Daly, B. Chen, J. Howe, C. V. Singh, T. Filleter, and Y. Sun, "Strengthening in graphene oxide nanosheets: bridging the gap between interplanar and intraplanar fracture", Nano Letters, vol. 15 (2016) p.g. 6528-6534

5:00pm 2D+NS-WeA9 Strain, Solitons, and Bimorphs with 2D Materials, Paul McEuen, Cornell University

INVITED

Two-dimensional sheets combine many remarkable properties in a single, atomically thin package. For example, a graphene sheet can be made into a high-performance transistor, but it is also the ultimate realization of a thin mechanical sheet. In this talk, I will discuss some of the fascinating properties of heterostructures of these materials, touching on everything from creating the world's thinnest bimorph to the electronic and mechanical properties of interlayer strain solitons.

Wednesday Afternoon, November 9, 2016

5:40pm **2D+NS-WeA11 Strain-Engineered Graphene Grown on Boron Nitride and Hexagonal Boron Nitride Grown on Graphite using High-Temperature Molecular Beam Epitaxy**, *Alex Summerfield*, A. Davies, T.S. Cheng, V.V. Korolkov, Y. Cho, C.J. Mellor, E.F. Smith, C.T. Foxon, A.N. Khlobystov, University of Nottingham, UK; K. Watanabe, T. Taniguchi, National Institute for Materials Science (NIMS), Japan; L. Eaves, S.V. Novikov, P. Beton, University of Nottingham, UK

To scale up the production of graphene-hexagonal boron nitride (hBN) heterostructure devices, direct epitaxial growth of these materials will be necessary. As an alternative to commonly used techniques such as the exfoliation of graphene/hBN flakes or growth using chemical vapour deposition we have investigated high-temperature molecular beam epitaxy (HT-MBE) in order to produce high-quality graphene and hBN monolayers.

We show that graphene grown using HT-MBE on hBN surfaces form continuous domains with dimensions of order 20 μm , and exhibits moiré patterns with large periodicities, up to ~ 30 nm, indicating that the layers are highly strained. Topological defects in the moiré patterns are observed using atomic force microscopy (AFM) and attributed to the relaxation of graphene islands which nucleate at different sites and subsequently coalesce. In addition, cracks are formed leading to strain relaxation, highly anisotropic strain fields, and abrupt boundaries between regions with different moiré periods. These cracks can also be formed by modification of the layers with a local probe resulting in the contraction and physical displacement of graphene layers. The Raman spectra of regions with a large moiré period reveal split and shifted G and 2D peaks confirming the presence of strain.

We also demonstrate the epitaxial growth of high-quality hBN atomic layers on graphite using plasma-assisted HT-MBE. AFM reveals mono- and few-layer island growth, while conductive AFM measurements show that the grown hBN has a resistivity which increases exponentially with layer thickness comparable with exfoliated hBN samples. Furthermore, X-Ray photoelectron spectroscopy, Raman and spectroscopic ellipsometry confirm the formation of sp^2 -bonded hBN with a band gap of 5.87 eV. Hexagonal moiré patterns of 15-17 nm are also observed on the hBN surface, suggesting that the grown layers may be strained due to the lattice mismatch with the graphite surface.

Our work demonstrates a new approach to the growth of epitaxial graphene/hBN and provides a route to the production of vertical superlattice structures for use in future devices.

6:00pm **2D+NS-WeA12 Metallic Edges in Atomically Thin WSe_2** , *Rafik Addou*, C.M. Smyth, The University of Texas at Dallas; Y.-C. Lin, The Pennsylvania State University; J. Noh, The University of Texas at Dallas; S.M. Eichfeld, The Pennsylvania State University; K.J. Cho, The University of Texas at Dallas; J.A. Robinson, The Pennsylvania State University; R.M. Wallace, The University of Texas at Dallas

Transition metal dichalcogenides (TMDs) is a unique class of layered two-dimensional (2D) crystals with extensive promising applications. Tuning their electronic properties is vital for engineering new functionalities. Surface oxidation is of particular interest because it is a relatively simple and low-cost method compared with other processes involving complicated steps. By means of scanning tunneling microscopy and spectroscopy (STM and STS), and X-ray photoelectron spectroscopy (XPS), we show here the observation of metallic step edges in atomically thin WSe_2 monolayers grown by chemical vapor deposition (CVD) on epitaxial graphene (Gr). STM images show the shape and the structure of WSe_2 step edges and STS reveals their metallic nature. Photoemission demonstrates that the formation of metallic sub-stoichiometric tungsten oxide (WO_x , $x < 3$) is responsible of high conductivity measured along the WSe_2 step edges. DFT Calculations [1,2] revealed that the $\text{W}_{18}\text{O}_{49}$ have a metallic behavior which is in excellent agreement with our photoemission estimated WO_x with $2.61 \leq x \leq 2.72$. Our findings are in contrary with reported results of air-exposed WSe_2 edges with large band gap measured at ~ 3.1 eV. [3] We explain this discrepancy by considering the differences in WO_x stoichiometry. [1]

This work was supported in part by the Center for Low Energy Systems Technology (LEAST), one of the six SRC STARnet Centers, sponsored by MARCO and DARPA, and by the SWAN Center, a SRC center sponsored by the Nanoelectronics Research Initiative and NIST, and the US/Ireland R&D Partnership (UNITE) under the NSF award ECCS-1407765.

[1] D. B. Migas *et al.* *J. Appl. Phys.* **108**, 093714 (2010)

[2] M. Remskar *et al.* *Adv. Funct. Mater.* **17**, 1974-1978 (2007)

[3] J. H. Park *et al.* *ACS Nano* **10**, 4258-4267 (2016)

Actinides and Rare Earths Focus Topic Room 103C - Session AC+MI-WeA

Actinide and Rare Earth Theory (2:20-3:40 pm)/Nuclear Power, Waste Remediation and Applications (4:20-6:20 pm)

Moderators: Paul Bagus, University of North Texas, Leon Petit, Daresbury Laboratory, UK, Alexander I. Landa, Lawrence Livermore National Laboratory, Melissa Denecke, University of Manchester, UK, David Geeson, AWE, UK, Stefan Minasian, Lawrence Berkeley National Laboratory (LBNL)

3:00pm **AC+MI-WeA3 First-Principle Calculations of Magnetic Properties of Actinide Complexes**, *Hélène Bolvin*, IRSAMC, Université de Toulouse III **INVITED**

The calculation of properties of open-shell 5f molecules is a challenge for the methods of quantum chemistry : these complexes have many low lying configurations, spin-orbit effects are important and correlation effects must be taken into account. The SO-CASPT2 method gives results that compare well to experimental data : it is a two-step wave function based method. The multiconfigurational nature of the wave functions is described by starting with a CASSCF calculation, correlation effects are calculated by 2nd order theory and spin-orbit effects are introduced in the very last step by a state interaction procedure.

We will show by several examples how calculations have become a complementary tool to the experimental data in order to get information about the nature and the magnetization of the ground and excited states.

1. calculation of EPR parameters : the ground state and excited states of actinyl complexes depend strongly on the nature of the equatorial ligands. All calculations are rationalized using a model based on crystal field theory. [1,2,3]

2. calculation of the susceptibility of aquo An(III) , An(IV) , An(V) and An(VI) cations and comparison to the LS coupling scheme. [4]

3. calculation of the pNMR shifts in the An(Et-DPC)_3^{3+} series and comparison with the lanthanide series. The variation in temperature of this shift will be discussed.

[1] D. Paez Hernandez, H. Bolvin *J. Electron. Spectrosc. Relat. Phenom.* **194**, 74 (2014).

[2] F. Gendron, D. Paez Hernandez, F. P. Notter, B. Pritchard, H. Bolvin, *J. Autschbach Chem. Eur. J.* **20**, 7994 (2014).

[3] F. Gendron, B. Pritchard, H. Bolvin, *J. Autschbach Inorg. Chem.* **53**, 8577 (2014).

[4] M. Autillo, L. Guerin, H. Bolvin, P. Moisy, C. Berthon *Phys. Chem. Chem. Phys.* **18**, 6515 (2016).

4:20pm **AC+MI-WeA7 Observations of Actinide-mineral Precipitation in Solution by In Situ Electron Microscopy**, *E.C. Buck, Michele Conroy, J.A. Soltis*, Pacific Northwest National Laboratory **INVITED**

In this presentation, the history of Pu contamination at the Hanford site will be reviewed, including the various disposal locations, the quantities of Pu and co-contaminants disposed, and recent research efforts designed to unravel the chemical form of Pu in the environmental samples. Microanalytical information will also be presented for the sediments at the Z-9 site. The information will include the chemical characterization of the sediments at two bore holes drilled at the Z-9 sites. Although the majority of the plutonium is present as oxide, using both electron microscopy (EM) and x-ray absorption spectroscopy evidence was found for the formation of nano-sized mixed Pu and iron phosphate hydroxides that are structurally related to rhabdophane-group minerals. The Pu-phosphate formation may depend on the local microenvironment in the sediments, availability of phosphate, and hence the distribution of these minerals may control long-term migration of Pu in the soil. The presentation will also focus the role of

Wednesday Afternoon, November 9, 2016

in-situ EM can play in understanding nanoparticle formation and its subsequent interaction with substrates.

Iron (II) minerals, when in isolation, will control the fate of Pu; however, in a sediment with clay, calcite, and other soil minerals present as we observed in the Z9 sediments, other phases and elements may have a significant impact on the Pu chemistry. Nevertheless, the complexity found in the natural environments may lead to the formation of phases that may not be predicted in laboratory set-ups. Understanding the chemistry of Pu in complex media requires tools that can probe micro-environments. We have been exploring the use of *in-situ* EM to investigate the precipitation of Pu. All designs of cells for *in-situ* electron microscopy incorporate a membrane that prevents evaporation of the liquid sample in the microscope vacuum. We will describe other observations of Pu behaviour, morphology, and compositional changes studied with these new EM methods.

5:40pm **AC+MI-WeA11 PES Study of Surface Passivation in U-Zr Alloys, Ladislav Havela, M. Paukov**, Charles University, Prague, Czech Republic; *F. Huber, T. Gouder*, European Commission, Joint Research Centre (JRC), Institute for Transuranium Elements

High temperature *bcc* structure of Uranium (γ -U) can be retained to low temperatures by alloying with different *d*-metals. Such alloys are used, due to enhanced resistance to radiation damage and better mechanical properties comparing to α -U, as nuclear fuels. Alloying leads also to reduced surface reactivity. Such "stainless" uranium is much more resistant to oxidation, and reaction with hydrogen gas needs high H_2 pressures. This raises questions about phenomena at the surface of such alloys. We performed a photoelectron spectroscopy study of the alloy $U_{0.80}Zr_{0.20}$, prepared by rapid solidification (splat cooling). The concentration of 20% Zr was chosen as the lowest concentration which still gives a safe margin for single-phase *bcc* phase. In particular, we studied the properties of the surface exposed to oxidation and/or annealing.

The surface in the initial state is Zr-rich (approx. 85% Zr), and the Zr excess is only slowly removed by Ar-ion sputtering. In the cleaned state the U-4f spectra indicate that the degree of the 5f localization is not changed between the α -U and γ -U phases, which can be understood considering that the U-U spacing even in the γ -U phase remains far below the Hill limit. Also the valence-band spectra in UPS exhibit only small differences with respect to pure U, which adopts the α -U phase.

Exposing the clean surface of $U_{0.80}Zr_{0.20}$ to O_2 , one observes relatively rapid oxidation. The dose of 5 Langmuir of O_2 converts 35-40% of metal into a dioxide, while Uranium oxidizes slightly more than Zirconium.

Isochronal annealing for 900 s leaves the clean surface unchanged for temperatures below 500 K. However, above this temperature the concentration of Zr in the surface layer fast increases. Repeated cleaning and annealing cycles lead to the same picture of surface enriched by Zr. The oxide formation of such surface is much more sluggish. This is true particularly for U, which has difficulty to form UO_2 . The oxidation can be stimulated by elevated temperatures, pointing to the fact that such oxidation is modulated by diffusion of O through the Zr overlayer. Still for 100 L of O_2 at 473 K the large part of U remains in metallic state and the amount of oxide is lower than for room-temperature oxidation of stoichiometric surface after 5 L O_2 . The finding demonstrates that the U-Zr alloys are coated by Zr or Zr-rich film when exposed to 500-600 K and such film leads to a passivation of the surface.

This work was supported by the Czech Science Foundation under the Grant 15-01100S. The work at ITU was supported by the European FP7 TALISMAN project, under contract with the European Commission.

6:00pm **AC+MI-WeA12 XPS and SIMS Study of the Surface and Interface of Aged C'Implanted Uranium, Art Nelson, S. Donald, J. Siekhaus**, Lawrence Livermore National Laboratory

Core-level photoelectron spectroscopy in combination with X-ray excited Auger peak energies were blended with secondary ion mass spectrometry depth profiling to investigate the surface and interfacial chemistry of oxidized C^+ ion implanted polycrystalline uranium exposed to air for over 10 years at ambient temperature. Implantation of 33 keV C^+ ions into U^{238} with a dose of $4.3 \times 10^{17} \text{ cm}^{-2}$ produced a physically and chemically modified surface layer that was characterized and shown to initially prevent air oxidation and corrosion of the uranium. The evolution of the previously characterized surface and interfacial layers were now examined by using a combination of the C KLL and U NOV Auger peak energies with the associated chemical shift of the C 1s and U 4f photoelectron lines that defines the Auger parameter resulting in a reliable method for conclusively

determining oxidation states independent of binding energy calibration. Results showed definitive Auger line-shapes and were used to produce a chemical state (Wagner) plot for select surface oxide and interfacial carbide. In addition, valence band spectra were used to explore the electronic structure of the aged carbide surface and interface layer. Furthermore, the time-of-flight secondary ion mass spectrometry depth profiling results for the aged sample confirmed an oxidized UC layer over the carbide layer/U metal interface.

The work was performed under the auspices of the U.S. Department of Energy by Lawrence Livermore National Laboratory under Contract DE-AC52-07NA27344.

Applied Surface Science Room 101B - Session AS-WeA

Multiple Technique Approaches for Real-World Industrial Problem Solving

Moderators: Kateryna Artyushkova, University of New Mexico, Xia Dong, Eli Lilly and Company

2:20pm **AS-WeA1 Integrated XPS/ Raman Spectroscopy for Comprehensive Structural, Molecular and Chemical Surface Analysis, Christopher Deeks, P. Mack, T.S. Nunney, J.P.W. Treacy, M. Meyer, N. Hibbard**, Thermo Fisher Scientific, UK

Advanced materials present ever increasing challenges to the analytical scientist. Composite materials built from nanostructures or ultra-thin films, often with complex chemistries present, are now required in a broad range of applications, and achieving full characterization is rarely managed using only one analysis method. To maintain confidence in the results from the utilization of several different methods, it is advantageous to be able to perform experiments on the same platform. Ideally, this should be without having to move the sample, removing the need for additional registration or processing to ensure that the data is being collected from the same position.

Often in surface analysis many related techniques are integrated onto the same system. These can include such practices as Ultraviolet Photoelectron Spectroscopy (UPS) for valence band and work function measurements. Ion Scattering Spectroscopy (ISS) is often used to give much more elemental surface information compared to XPS alone. Reflected Electron Energy Loss Spectroscopy (REELS) can also give information on hydrogen in samples which cannot be detected by any of the previously named techniques, allowing full elemental analysis of samples with these combined.

An integrated system that has a Raman spectrometer with a micro-focused, monochromated XPS system can be used for even further analysis. The focal points are aligned such that data can be acquired from the same point simultaneously, and that the sizes of the analysis areas are comparable in size. This combined approach is particularly powerful when analyzing carbon nanomaterials. Chemical modifications of the material can be easily determined and quantified with XPS, and Raman offers a fast way of determining the quality and conformity of the material. Vibrational structure can also give more precise chemical information in some cases. The greater depth of field of the Raman spectrometer also offers bulk information to complement the surface sensitive XPS data.

In this presentation we will discuss the strengths of this combined, in-situ approach to surface analysis, illustrated with examples from a range of applications including carbon nanomaterials, microelectronics and geology.

2:40pm **AS-WeA2 Extended Molecular Identification with TOF-SIMS Imaging MS/MS, John Hammond, G.L. Fisher, S.R. Bryan**, Physical Electronics; *S. Iida, T. Miyayama*, ULVAC-PHI, Japan

TOF-SIMS has become widely accepted as the most powerful spectroscopy and imaging surface analysis tool for organic and polymer samples based on the capabilities of 2 nm surface sensitivity and 100 nm spatial resolution. For most polymer additives as well as lipids, disease markers and fatty acids on biological tissue samples, the molecular ions have masses up to m/z 1000. At this higher mass range, traditional TOF-SIMS lacks the mass resolution and mass accuracy to uniquely identify the detected ions. A new TOF-SIMS instrument combining, in parallel, imaging MS and imaging MS/MS provides the capability to provide a multi-technique approach to real world problem solving with extended molecular identification of higher mass ions [1].

A series of saturated and unsaturated fatty acid standards as well anti-oxidant polymer additives were analyzed with a PHI *nanoTOF II* TOF-SIMS

Wednesday Afternoon, November 9, 2016

Parallel Imaging MS/MS. The MS/MS spectra were generated with a 1 daulton precursor selection window followed by 1.5 keV collision-induced dissociation (CID). The MS¹ and MS² parallel imaging of polymer surfaces with a mixture of polymer additives were obtained with a raster scanned Bi₃⁺ ion source with a sub-micron spatial resolution

The structural elucidation of the fatty acid CID MS/MS spectra can be interpreted by charge-remote fragmentation [2]. The location of unsaturated bonds in the fatty acids can be defined from these spectra. The complex structures of the anti-oxidants can be easily identified with the high energy CID MS/MS. Using the high signal/background of the MS² images, bunched or unbunched imaging with the Bi₃⁺ ion source can produce sub-micron spatial resolution with unique molecular identification of additives on the polymer films. These results also point to a broader utility of this technique for biological tissue imaging.

4. References

[1] P.E. Larson, J.S. Hammond, R.M.A. Heeren, G.L. Fisher, *Method and Apparatus to Provide Parallel Acquisition of MS/MS Data*, U.S. Patent 20150090874, 2015.

[2] M. L. Gross,, Int. J. Mass Spectrom., 200 (2000) 611

3:00pm **AS-WeA3 Practical Aspects of Multiple Technique Problem-Solving: Making it Work, Kathryn Lloyd**, DuPont Corporate Center for Analytical Sciences **INVITED**

Although there do exist types of problems or research support for which one analytical technique is sufficient to provide useful guidance or an answer, it is more the norm that multiple analytical techniques are required to address technical problems involving coatings, layered structures, and other industrial materials. In fact, basing action (e.g., a change in manufacturing process) on data from a single analytical technique -- especially a surface-specific technique -- would not be advisable in most cases.

Some technique combinations seem intuitive -- for example, combining the high-lateral-resolution detail from electron microscopy with the higher level of chemical information available from either secondary ion mapping (ToF-SIMS) or Raman microprobe analysis. However, there are still challenges with sample preparation, data acquisition from the same area, and data integration that need to be addressed.

Other technique combinations arise from the business need -- for example, finding a combination of techniques that both describe the chemistry and correlate with end-use performance. This usually involves combining a vacuum-based technique with an ambient or "macroscopic" technique such as contact angle, porosity, or friction measurements.

As most practitioners know, the surface specificity of XPS and ToF-SIMS can be both an advantage and a disadvantage. In this regard, the introduction of GCIB (Gas Cluster Ion Beam) sources has opened up new opportunities for multiple-technique problem-solving.

This talk will present some experiences and examples that provide a flavor of multiple-technique problem-solving in an industrial environment.

4:20pm **AS-WeA7 Adhesion Aspects of Polymeric Methylene Diphenyl Diisocyanate on Different Steel Surfaces by XPS and ToF-SIMS, Jorge Bañuls Ciscar**, M.L. Abel, J.F. Watts, University of Surrey, UK

Polymeric methyl diphenyl diisocyanate (p-MDI) is a versatile isocyanate commonly used in coatings and adhesives applications because of its excellent mechanical properties. In this work, we are aiming to understand the chemistry involved at the interface between p-MDI and a specific stainless steel as a result of different processing parameters. This steel has distinct surface properties. On one side the surface has been ground and the composition is mostly iron oxide (Fe₂O₃) whereas on the other side the steel has a mill-finished surface and the composition is predominantly chromium oxide (Cr₂O₃). Therefore, in our system of interest, the stainless steel has different physical and chemical properties on each side. As such, understanding the adhesion aspects of p-MDI on each side could lead to an improvement of its use in many steel applications.

Preliminary work using XPS and ToF-SIMS has shown an interaction between nitrogen and chromium oxide at the interface. A low binding energy peak (~397 eV) was identified in the N1s high resolution XPS spectrum. This peak represents nitrogen atoms which have a higher electronic density as a result of the electron withdrawing effect of the MDI on the metal substrate. Additionally, peaks of characteristic fragments of N-Cr interaction were found in the ToF-SIMS spectra. This will form the basis of further work to determine the exact chemistry involved in such interfacial regions.

4:40pm **AS-WeA8 Migration of Erucamide in Polyethylene Films, Michaeleen Pacholski, R. Sharma, J. Ngunjiri, K. Laughlin, M. Kapur, V. Kalihari**, The Dow Chemical Company

Polyolefins are often formulated with additives to provide stability and processability depending on their end use. Reduction of coefficient of friction (COF) for polyolefin films is a critical property. A common additive for COF reduction is erucamide. Films made using this fatty amide are known to have diminished COF performance when exposed to elevated temperatures that might be found in hot trucks or warehouses. Characterization of these materials during and after thermal aging can provide useful understanding in deterioration of film performance. Here we use a multitechnique approach to characterize the surface chemistry and morphology of this relatively simple, yet common, system of polyethylene and erucamide.

5:00pm **AS-WeA9 Probing the Impact of Process and Materials Variability of Medical Device Components with Surface Characterization, Jeffrey Fenton**, L. Nygren, B. Tischendorf, R. Jahnke, J. Heffelfinger, Medtronic plc

Since the first pacemaker implant in 1958, engineering and medical advances have greatly improved device capabilities and patient outcomes. Advances in materials chemistry have increased the need for deep understanding of process-material interactions and their role in device or component longevity. This presentation will focus on the utilization of X-ray photoelectron spectroscopy (XPS) and scanning electron microscopy (SEM) on processes related to two device components, feedthroughs and printed wire boards, as a means to improve processing conditions, expand processing boundaries, and understand failure modes.

In pacemakers or like devices, feedthroughs are evaluated using various electrical tests to determine the insulation resistance which is typically in the Megaohm or Gigaohm range. XPS and SEM analysis will be shown to aid in the determination of yield loss root cause by identifying sources of foreign materials. For example, fibers from clothing may deposit onto the insulator and graphitize during high temperature processes. The graphitized materials may then provide a pathway for conductivity during electrical testing. Compositional and morphological identification with SEM allows for root cause identification and elimination of those yield losses.

Laser soldering, which is relatively new to the industry, is utilized in new Medtronic products. During the laser soldering process localized heat results in a different wetting dynamic from the conventional furnace reflow. The laser soldering process may be used after preceding thermal exposure in the upstream processes resulting in changes to the surface condition of the soldering pads. The surface chemistry may change during thermal exposure which may cause reduced wettability and create one of the biggest challenges during the process development to overcome. XPS, SEM and XRF (x-ray fluorescence) methods provide key insight on the inter-diffusion between the metallization layers on the PBW and migration to the surface species that can limit pad solderability. The main outcome of the analysis was establishing design rules for the PWB plating, including metallization materials and layer thickness in multilayer metallization.

5:20pm **AS-WeA10 Multi-technique Characterization of PtNi Extended Surface Catalysts for Improvement of Electrocatalytic Activity and Durability, S. Shulda, C. Ngo**, Colorado School of Mines; **S. Alia**, National Renewable Energy Laboratory; **J. Nelson Weker**, SLAC National Accelerator Laboratory; **B. Pivovar**, National Renewable Energy Laboratory; **Svitlana Pylypenko**, Colorado School of Mines

Transition metal nanowires are emerging as an effective structure for various heterogeneous catalysis applications. Metal and metal oxide nanowires have demonstrated high activity for the oxidative coupling of methane into higher value products, hydrogenation of aromatic compounds, and water splitting, among others. Of particular interest is the application of platinum-nickel and platinum-cobalt nanowires as oxygen reduction catalysts in polymer electrolyte membrane fuel cells (PEMFCs) as they have shown activities that significantly surpass the current state of the art Pt nanoparticles supported on high surface area carbon and are considered a promising alternative. The activity and durability of Pt nanowires is dependent on both the surface and bulk properties, which continuously evolve during different steps of the synthesis, electrode preparation, and fuel cells operation, making a multi-technique analysis approach necessary.

High surface area platinum nickel (PtNi) nanowires have been synthesized via spontaneous galvanic displacement. Various post-processing treatments were applied altering the chemistry and structure of the nanowires to improve their activity and durability. This work focuses on the analysis of the surface and bulk composition and structure and their

Wednesday Afternoon, November 9, 2016

evolution with various treatments. X-ray photon spectroscopy (XPS), energy dispersive x-ray spectroscopy (EDS) via transmission electron spectroscopy (TEM), x-ray absorption near edge structure (XANES) and extended x-ray absorption fine structure (EXAFS) spectroscopies, and transmission x-ray microscopy (TXM) were utilized. All of the processing treatments altered the surface chemistry and in some instances the morphology of the nanowires, with some treatments resulting in increased activity and durability while others being detrimental to the performance. The extensive characterization of the nanowires pre- and post-processing provided a robust understanding of each treatments effect on the nanowires and guided the optimization of the post-processing treatments. Moreover, this study highlights the challenges associated with the characterization of nanowires structures, where evolution of both surface and bulk composition and structure are extremely important.

5:40pm **AS-WeA11 Compositional Analysis for Additive Manufacturing**, *Michael Brumbach, N. Argibay, D. Susan, J. Rodelas, J. Reich, B.L. Boyce, A. Roach*, Sandia National Laboratories

The implementation of characterization in additive manufacturing (AM) demands new perspectives for a setting traditionally adapted to support basic science research. As the development of AM continues, the need for diagnostics and control of AM processes is critical and begins with an understanding of materials composition. This exploration of characterization techniques for analyzing bulk composition will give particular consideration for low detection limits, high-throughput analyses, and the ability to quantify light elements. Comparisons between optical emission spectroscopy (OES) from various excitation sources including glow-discharge (GDS), arc-spark, and inductively coupled plasma (ICP) will be discussed. The results are compared to X-ray fluorescence (XRF) and wavelength dispersive spectroscopy (WDS/microprobe). Combustion analysis will be discussed for carbon, sulfur, oxygen, nitrogen, and hydrogen from traditional wrought metals and AM analogs. The role of surface analysis and comparison to bulk techniques will also be demonstrated.

Sandia National Laboratories is a multi-program laboratory managed and operated by Sandia Corporation, a wholly owned subsidiary of Lockheed Martin Corporation, for the U.S. Department of Energy's National Nuclear Security Administration under contract DE-AC04-94AL85000.

6:00pm **AS-WeA12 Ambient Mass Spectrometry for the Analysis of Organic Monolayers**, *Han Zuilhof*, Wageningen University, Netherlands

The characterization of organic monolayers is critically dependent on highly surface-sensitive methods. While a wide variety of methods has been developed over the last decades, *structural information* of organic species, including information relating to their three-dimensional structure, was often very difficult to obtain.

The current presentation sets out to detail the potential of ambient ionization mass spectrometry for this purpose, by giving examples of where it can extend the analysis, where e.g. XPS, scanning probe microscopies and IR fall short.

Lit: Langmuir 2016, 32, 3412; Anal. Chem. 2014, 86, 2403.

Electronic Materials and Photonics

Room 102A - Session EM+NS+SP+SS-WeA

Nanoscale Imaging of Metals and Compound Semiconductor based Nanostructures, Surfaces and Interfaces

Moderators: Yohannes Abate, Georgia State University, Andy Antonelli, Nanometrics

2:20pm **EM+NS+SP+SS-WeA1 The Importance of Contact Engineering for 2D Devices**, *Saptarshi Das*, Pennsylvania State University **INVITED**

Contact resistance is one of the most important factors which could potentially limit the performance of novel electronic and optoelectronic devices based on two-dimensional (2D) materials like graphene, black phosphorus, various transition metal dichalcogenides (TMDs) like MoS₂, WSe₂ and beyond [1-3]. It is now widely accepted that metal-2D contacts are mostly Schottky barriers type [1-3]. Hence, various contact engineering strategies have been adopted to minimize the Schottky barrier height at the metal-2D interface and thereby reduce the contact resistance. In this talk I will provide a comprehensive overview of different contact engineering schemes metal work function engineering, interface engineering and phase engineering [4-6]. Additionally, I will also talk about

Wednesday Afternoon, November 9, 2016

the scalability of the contact resistance since an aggressively scaled 2D device will also have aggressively scaled contacts.

1. Das S, Chen H-Y, Penumatcha AV, Appenzeller J: **High performance multilayer MoS₂ transistors with scandium contacts**. *Nano letters* 2012, **13**(1):100-105

2. Das S, Appenzeller J: **WSe₂ field effect transistors with enhanced ambipolar characteristics**. *Applied Physics Letters* 2013, **103**(10):103501

3. Das S, Demarteau M, Roelofs A: **Ambipolar phosphorene field effect transistor**. *ACS nano* 2014, **8**(11):11730-11738.

4. Das S, Appenzeller J: **Where does the current flow in two-dimensional layered systems?** *Nano letters* 2013, **13**(7):3396-3402

5. Das S, Gulotty R, Sumant AV, Roelofs A: **All two-dimensional, flexible, transparent, and thinnest thin film transistor**. *Nano letters* 2014, **14**(5):2861-2866.

6. Kappera R, Voiry D, Yalcin SE, Branch B, Gupta G, Mohite AD, Chhowalla M: **Phase-engineered low-resistance contacts for ultrathin MoS₂ transistors**. *Nature materials* 2014, **13**(12):1128-1134.

3:00pm **EM+NS+SP+SS-WeA3 Imaging Stress-Directed Compositional Patterning in Silicon Germanium with μ -Raman Spectroscopy**, *Brian Rummel, S.M. Han*, University of New Mexico

We have previously demonstrated that a patterned elastic stress field can be used to change the near-surface atomic composition in an epitaxial compound semiconductor film.¹ This compositional patterning laterally manipulates quantum barriers within the film in a press-and-print manner. In this example, an array of silicon pillars is pressed against a relaxed Si_{0.8}Ge_{0.2} substrate in a mechanical press, and the entire assembly is heated to high temperatures. This serves to promote a diffusive separation of the germanium into highly localized regions. Here, the difficulty in analyzing these structures is due to the lack of surface detail on the stress-annealed substrate as there is only elastic deformation observed during the fabrication process. To visualize the regions compressively stressed by the pillars and therefore compositionally altered regions, we report the use of μ -Raman spectroscopy to produce a 2D compositional map of a substrate. The substrate is patterned with feature sizes on the order of 1 to 3 microns to remain within the spatial resolution of μ -Raman spectroscopy for the purpose of demonstration. The first-order Raman spectrum for pure silicon and germanium produces peaks at 520.2 and 300.7 cm⁻¹, respectively. The deviations from these relaxed silicon and germanium peaks have been attributed to residual tensile stress in the Ge-depleted regions. Lateral line scans are performed to map the compositions of the stressed and annealed substrate, which provides a clear image of the resulting diffusion process. This imaging also allows the quantum structures to be addressable.

¹ S. Ghosh, D. Kaiser, J. Bonilla, T. Sinno, and S. M. Han, "Stress-Directed Compositional Patterning of SiGe Substrates for Lateral Quantum Barrier Manipulation," *Applied Physic Letters* **107**, 072106-1:5 (2015).

3:20pm **EM+NS+SP+SS-WeA4 Atomic-scale Characterization of III-V Nanowire Heterostructures and Devices**, *J. Knutsson, S. McKibbin, M. Hjort, J. Colvin, S. Yngman, A. Troian, O. Persson, A. Mikkelsen, Rainer Timm*, Lund University, Sweden

III-V semiconductor nanowires (NWs) have a large technological potential within electronics, optoelectronics, and energy harvesting [1]. With their flexibility in creating heterostructures, by radial and axial stacking during epitaxial growth, comes an increasing complexity of device structure. Furthermore, due to their small diameter and their very large surface-to-volume-ratio, the performance of NW devices is strongly determined by surface properties. It is therefore essential to study the structural and electronic properties of NW surfaces down to the atomic level and across interfaces regarding doping, material composition, or crystal phase.

We recently obtained atomically resolved scanning tunneling microscopy (STM) images of various GaAs, InAs, and InP NW surfaces [2,3]. By combining STM imaging with scanning tunneling spectroscopy (STS) measurements, we correlate the surface structure and local electronic properties [3]. Here, we will present examples from InAs NWs with interfaces between different crystal phase. Our low-temperature STM/S results show that even the smallest possible insertion of zincblende phase within a wurtzite segment, a single bilayer stacking fault, shows a clear zincblende signature. We observe transitions in the local density of states with sub-nm lateral resolution. Furthermore, we map the interface band alignment and measure quantum confinement energies of single and double bilayer stacking faults.

Wednesday Afternoon, November 9, 2016

Beyond traditional steady-state surface characterization, it is desirable to even investigate nanostructure devices *in-situ*, meaning while they are operating under an external bias. We are now using simultaneous STM, AFM, and electrical transport measurements for studying individually contacted NWs during device operation [4], complemented by Kelvin probe force microscopy and scanning photoemission microscopy. We will present initial results of such combined *in-situ* studies on axial *pn*-junctions in InP and GaInP NWs, where we also investigate the influence of NW surface modification (e.g. removal of native oxide by atomic hydrogen) on photovoltaic properties.

[1] E. Lind *et al.*, IEEE J. El. Dev. Soc. **3**, 96 (2015); J. Wallentin *et al.*, Science **339**, 1057 (2013).

[2] M. Hjort *et al.*, ACS Nano **6**, 9679 (2012); J. Knutsson *et al.*, ACS Appl. Mat. & Interf. **7**, 5748 (2015).

[3] M. Hjort *et al.*, Nano Lett. **13**, 4492 (2013); M. Hjort *et al.*, ACS Nano **8**, 12346 (2014).

[4] O. Persson *et al.*, Nano Lett. **15**, 3684 (2015); J. L. Webb *et al.*, Nano Res. **7**, 877 (2014).

4:20pm EM+NS+SP+SS-WeA7 Revealing Optical Properties of Reduced-Dimensionality Materials at Relevant Length Scales using Nanospectroscopic Imaging, P. James Schuck, The Molecular Foundry, Berkeley Lab **INVITED**

Reduced-dimensionality materials for photonic and optoelectronic applications including energy conversion, solid-state lighting, sensing, and information technology are undergoing rapid development. The search for novel materials based on reduced-dimensionality is driven by new physics. Understanding and optimizing material properties requires characterization at the relevant length scale, which is often below the diffraction limit. The nano-optical imaging community has now crossed the boundary from insufficient to sufficient resolution, mapping critical optoelectronic properties in these exciting materials at their native length scales. Here, I will describe the recent near-field imaging advances that lay groundwork for generally-applicable nano-optical studies of these low-D materials, and will show recent results on 0, 1, and 2D systems. I will spend time discussing the importance of near-field polarization in probing these materials, and will also highlight recent applications in 2-D semiconductor transition metal dichalcogenides (TMDCs), where we and others have uncovered new optoelectronic regions and spatially-varying features that were hidden in prior optical studies. These findings have broad implications for the development of atomically thin transistors, quantum optical components, photodetectors and light-emitting devices.

5:00pm EM+NS+SP+SS-WeA9 Polarizability Mapping of Nanolayers Based on Near-Field Edge Fringes, Viktorii Babicheva, V.S. Yakovlev, S. Gamage, M.I. Stockman, Y. Abate, Georgia State University

Scattering-type scanning near-field optical (s-SNOM) microscopy enable spectroscopic imaging with nanoscale resolution and provide chemical and structural information of surfaces [1]. In this work, we investigate identification of material type using an approach based on analyzing near fields at the sample edge [2]. We develop theoretical approach that includes full-wave numerical simulations and calculations of s-SNOM signal in different demodulation orders. This model allow characterization of structures of any shape and material, as well as different tips, and does not include any fitting parameters. In this way, we defined that metallic edge has bright and dark fringes in near-field characterization, whereas a bright edge of dielectric material has no outside fringe. Similar behavior is observed for anisotropic material with hyperbolic dispersion (boron nitride in mid-IR range): depending on the wavelength, it shows either metallic or dielectric properties.

1. Y. Abate, R.E. Marvel, J.I. Ziegler, S. Gamage, M.H. Javani, M.I. Stockman, and R.F. Haglund "Control of plasmonic nanoantennas by reversible metal-insulator transition" Sci. Rep. **5**, 13997 (2015).

2. Y. Abate, S. Gamage, L. Zhen, S.B. Cronin, H. Wang, V. Babicheva, M.H. Javani, M.I. Stockman, "Nanoscopy reveals metallic black phosphorus," Light: Science & Applications, accepted (2016). <http://arxiv.org/abs/1506.05431>

5:20pm EM+NS+SP+SS-WeA10 Wedding Cake Growth Mechanism in One-Dimensional and Two-Dimensional Nanostructure Evolution, Xin Yin*, University of Wisconsin-Madison; J. Shi, Rensselaer Polytechnic Institute; X. Niu, Northeastern University; D. Geng, University of Wisconsin-Madison; H. Huang, Northeastern University; X.D. Wang, University of Wisconsin-Madison

Morphology is one essential element that gives rise to extraordinary physical, chemical, and mechanical properties in nanomaterials. Precise morphology control of nanomaterials is a notorious task, which heavily relies on fundamental understanding of the governing atomistic mechanisms and kinetics at the nanoscale. Despite numerous studies on the growth and application of nanostructures, current understanding of kinetics that governs the nanocrystal evolution is yet limited.

By programming deposition conditions at time domain, we observed the wedding cake growth mechanism in the formation of 2D ZnO nanostructures. Within a narrow growth window, the surfaces of 2D structures were covered with a unique concentric terrace feature. This mechanism was further validated by comparing the characteristic growth rates to the screw dislocation-driven model. An interesting 1D to 2D morphology transition was also found during the wedding cake growth, when the adatoms overcome the Ehrlich-Schwoebel (ES) barrier along the edge of the top crystal facet triggered by lowering the supersaturation. The evolution of 2D plate structure from 1D pillars represents a dynamic crystal growth behavior transition when the local deposition conditions were tuned *in-situ*. It lively recorded the wedding cake growth model in nanostructure formation from vapor phase, which was rare to be observed when the deposition conditions were remained constant. The terrace feature on these nanostructures provided a valuable platform for understanding the wedding cake growth kinetics that could be an important mechanism to design and predict the nanocrystal morphology formation from the bottom-up. Analyzing the supersaturation and temperature-related growth behavior provides a new insight into nanostructure growth mechanisms and morphology control.

Wedding cake growth is a layer-by-layer growth model commonly observed in epitaxial growth of metal films, featured by repeated nucleation of new atomic layers on the topmost surface owing to the confinement of the Ehrlich-Schwoebel (ES) barrier. This study expands the application of the wedding cake growth mechanism to the nanostructure growth. It enriches our understanding on the fundamental kinetics of nanostructured crystal growth and provides a transformative strategy to achieve rational design and control of nanoscale geometry.

5:40pm EM+NS+SP+SS-WeA11 Detecting the Invisible - The Atomic Structure of Radiation Sensitive Nano-Materials, Christian Kisielowski, Molecular Foundry, Lawrence Berkeley National Laboratory; P. Specht, University of California Berkeley **INVITED**

As heterogeneous materials scale below 10 nm, a suitable combination of single digit nanocrystals with their rich variety of tunable surfaces and interfaces allows tailoring unprecedented materials with novel structure-function relationships. The design of new catalysts [1], investigations of polymers at atomic resolution [2] or analyses of deviations from a random doping distributions at atomic resolution [3] may serve as examples. This contribution describes research that aims at exploiting the emerging ability to analyze and understand such materials by directly determining their atom arrangement in three-dimensions using aberration-corrected transmission electron microscopy [4]. Attempts to unravel the atomic structure of such nanoscale composites in this manner must explicitly address their pronounced sensitivity to the probing radiation that can unintentionally alter their pristine structure, often beyond recognition. We address this challenge by applying low dose-rate in-line holography [5], which allows operating electron microscopes with dose rates as low as 5-10 e/Å²s that help maintaining structural integrity at atomic resolution to an unexplored end. The approach mimics best practices in biological research but achieves atomic resolution with single atom sensitivity by the acquisition of large image series. We observe a variety of previously unknown atom configurations in surface proximity of CoO_x nanocrystals and coatings that are hidden behind unusually broadened diffraction patterns but become visible in real space images because the phase problem is solved. The observed structures are drastically altered by an exposure of the material to water vapor or other gases, which is investigated at atomic resolution in environmental electron microscopy. It is shown for Rh/W catalysts that electron beam-induced atom dynamics can be entirely suppressed even for atom clusters made from less than 10

* NSTD Student Award Finalist

atoms. Resultantly, chemical compositions can be determined by contrast measurements alone and functional processes can be triggered and tracked in real time at atomic resolution.[6]

[1] J. A. Haber et al., **Advanced Energy Materials** 5 (2015) 1402307

[2] D. Lolla et al., **Nanoscale** 8 (2016) 120 - 128

[3] P. Specht, C. Kisielowski, On the chemical homogeneity of InxGa1-xN alloys - Electron microscopy at the edge of technical limits, submitted (2016)

[4] F.R. Chen et al., **Nature Commun.** 7:10603 doi: 10.1038/ncomms10603 (2016)

[5] C. Kisielowski, **Advanced Materials** 27 (2015) 5838-5844

[6] The Molecular Foundry, which is supported by the Office of Science, the Office of Basic Energy Sciences, the U.S. Department of Energy under Contract No. DE-AC02-05CH11231

Fundamental Discoveries in Heterogeneous Catalysis Focus Topic

Room 103A - Session HC+NS+SS-WeA

Nanoscale Surface Structures in Heterogeneously Catalyzed Reactions

Moderator: Arthur Utz, Tufts University

2:20pm **HC+NS+SS-WeA1 Ceria Nanoclusters on Graphene/Ru(0001): A New Model Catalyst System**, Z. Novotny, Pacific Northwest National Laboratory; F.P. Netzer, Karl-Franzens University, Austria; **Zdenek Dohnalek**, Pacific Northwest National Laboratory

Cerium oxide is an important catalytic material known for its ability to store and release oxygen, and as such, it has been used in a range of applications, both as an active catalyst and as a catalyst support. Using scanning tunneling microscopy and Auger electron spectroscopy, we investigated the growth of ceria nanoclusters and their oxygen storage/release properties on single-layer graphene (Gr) on Ru(0001) with a view towards fabricating a stable system for model catalysis studies. The ceria nanoclusters are of the CeO₂(111)-type and are anchored at the intrinsic defects of the Gr surface and display a remarkable stability against reduction in ultrahigh vacuum up to 900 K, but some sintering of clusters is observed for temperatures > 450 K. The evolution of the cluster size distribution suggests that the sintering proceeds via a Smoluchowski ripening mechanism, i.e. diffusion and aggregation of entire clusters. To follow the cluster redox properties we examined their oxygen storage and release in an oxygen atmosphere (<10⁻⁶ Torr) at elevated temperature (550 – 700 K). Under oxidizing conditions, oxygen intercalation under the Gr layer is observed. Time dependent studies demonstrate that the intercalation starts in the vicinity of the CeO_x clusters and extends until a completely intercalated layer is observed. Atomically resolved images further show that oxygen forms a p(2x1) structure underneath the Gr monolayer. Temperature dependent studies yield an apparent kinetic barrier for the intercalation of 1.2 eV. At higher temperatures, the intercalation is followed by a slower etching of the intercalated Gr (apparent barrier of 1.6 eV). Vacuum annealing of the intercalated Gr leads to the formation of carbon monoxide and causing etching of the Gr film thus revealing that the spillover of oxygen is not reversible. These studies demonstrate that the easily reducible CeO_x clusters act as intercalation gateways capable of efficiently delivering oxygen underneath the Gr layer.

3:00pm **HC+NS+SS-WeA3 Lowering the Barrier to C-H Activation using Pt/Cu Single Atom Alloys**, **Matthew Marcinkowski**, M. El Soda, F.R. Lucci, E.C.H. Sykes, Tufts University

Due to the increased in shale gas production in recent years the availability of light alkanes such as ethane and propane has increased significantly. Although these chemicals are typically considered inert, the ability to cleave C-H bonds in alkanes would allow for production of alkenes, which are important precursors to polymers. In this work, we use a surface science approach to model C-H activation on a Cu(111) surface using methyl iodide. Methyl iodide is known to decompose to produce methyl groups and iodine atoms on Cu(111) below 200 K. The methyl groups are then stable on the surface up until 450 K, at which temperature they decompose to form a number of products including methane, ethylene, ethane, and propylene. The rate limiting step to forming these products is the activation of one of the C-H bonds in the methyl group to produce surface bound hydrogen and methylene. Pt(111) is also able to activate the

C-I bond in methyl iodide, but methyl groups on this surface only produce methane, hydrogen, and surface bound methylene groups at 290 K. While the barrier to C-H activation is lowered on Pt compared to Cu, the Pt surface is unable to perform carbon coupling reactions. Inspired by these previous results, we fabricated surfaces consisting of 1% Pt in the Cu(111) surface. At this concentration, Pt exists as single, isolated atoms substituted into the Cu(111) lattice. These *single atom alloys* exhibit synergistic chemistry and yield the desirable properties of each of the two pure metal surfaces. They are able to produce carbon coupling products like pure Cu, but are able to activate the C-H bond necessary to begin these reactions at 340; 110 K cooler than on Cu(111). Increasing the concentration of Pt further decreases the temperature necessary to activate C-H bonds, but also decreases the amount of carbon coupling products formed as the surface becomes more similar to Pt(111). Single atom alloys therefore provide an ideal model catalyst for the decomposition of methyl iodide, allowing for more facile activation of the C-H bond than pure Cu while also producing the desired coupling products, which Pt(111) is unable to do.

3:20pm **HC+NS+SS-WeA4 Formation, Migration and Reactivity of Au-CO Complexes on Gold-Surfaces**, **Jun Wang**, Oak Ridge National Laboratory; M. McEntee, W. Tang, M. Neurock, University of Virginia; A.P. Baddorf, P. Maksymovych, Oak Ridge National Laboratory; J.T. Yates, Jr., University of Virginia

We report experimental as well as theoretical evidence that suggests formation of Au-CO complexes upon the exposure of CO to active sites (step edges and threading dislocations) on a Au(111) surface. Room-temperature scanning tunneling microscopy (STM), X-ray photoelectron spectroscopy, transmission infrared spectroscopy, and density functional theory calculations point were combined to investigate morphological changes of the Au(111) surface with an intentionally created array of etch-pits. Room-temperature STM of the Au(111) surface at CO pressures in the range from 10⁻⁸ to 10⁻⁴ Torr (dosage up to 10⁶ langmuir) indicates Au atom extraction from dislocation sites of the herringbone reconstruction, mobile Au-CO complex formation and diffusion, and Au adatom cluster formation on both elbows and step edges on the Au surface. The formation and mobility of the Au-CO complex result from the reduced Au-Au bonding at elbows and step edges leading to stronger Au-CO bonding and to the formation of a more positively charged CO (CO^{δ+}) on Au. Our studies indicate that the mobile Au-CO complex is involved in the Au nanoparticle formation and reactivity, and that the positive charge on CO increases due to the stronger adsorption of CO at Au sites with lower coordination numbers.

ACKNOWLEDGEMENTS: Part of this research was conducted at the Center for Nanophase Materials Sciences (CNMS), which is a DOE Office of Science User Facility .

Reference: J. Wang, M. McEntee, W. Tang, M. Neurock, A. P. Baddorf, P. Maksymovych, and J. T. Yates, Jr., *J. Am. Chem. Soc.* 138, 1518 (2016)

4:20pm **HC+NS+SS-WeA7 Sulfur-Metal Complexes on Surfaces of Copper, Silver, and Gold**, **Patricia A. Thiel**, Iowa State University; H. Walen, RIKEN Surface and Interface Science Laboratory, Wako, Saitama, Japan; D.-J. Liu, Ames Laboratory, Ames, IA; J. Oh, RIKEN Surface and Interface Science Laboratory, Wako, Saitama, Japan; H.J. Yang, University College London, UK; Y. Kim, RIKEN Surface and Interface Science Laboratory, Wako, Saitama, Japan

INVITED

The nature of sulfur interaction with surfaces of coinage metals (M=Cu, Ag, Au) is relevant to aspects of heterogeneous catalysis, corrosion, and self-assembled monolayers. We have discovered a number of unexpected complexes—independent, molecule-like MxSy species—that form on low-index M surfaces. In a sense, these complexes are iidway between the well-known phenomena of chemisorption and adsorbate-induced reconstruction. Our primary experimental tool is scanning tunneling microscopy (STM) used in ultrahigh vacuum. We tailor our experimental conditions to isolate the complexes, by working at ultra-low sulfur coverage to avoid competition from surface reconstructions. Furthermore, we prepare the surface at 300 K, but image at 5 K, in order to immobilize these small species. Density functional theory (DFT) is used to interpret the experimental results. For instance, application of DFT is essential to identify the complexes that form on Cu(111), Ag(111), and Au(100), and this identification is made both on the basis of their physical characteristics in real vs. stimulated STM images (size, orientation, shape) as well as their calculated stability. On other surfaces, including Au(111), Cu(100), and Au(110), MxSy complexes do not form under comparable conditions. This

Wednesday Afternoon, November 9, 2016

broad database and extensive analysis provides insights into factors that favor complexation in this class of systems.

5:00pm **HC+NS+SS-WeA9 Titania/Gold Inverse Model Catalysts for Acetaldehyde Formation from Ethanol, Ashleigh Baber, D.T. Boyle, W. Andahazy, V. Lam, D. Schlosser, N. Tosti, J. Wilke**, James Madison University
The fundamental investigation of the catalytic chemistry of ethanol at interfaces is important for many fields including the automotive industry due to the use of ethanol as a fuel. The redox chemistry of small alcohols, including methanol and propanol, has been studied on Au(111) supported TiO₂ nanoparticles, yet the active site for the chemistry has not yet been elucidated. Here, the systematic study of ethanol has been investigated on Au(111) and TiO₂/Au(111) via temperature programmed desorption in an effort to gain insight on the interfacial role of the reactivity for ethanol, as a function of titania coverage. Ex situ atomic force microscopy was used to image the gold-supported titania particles, and X-ray photoelectron spectroscopy was used to confirm the presence of titania on the surface. The presence of TiO₂ nanoparticles on Au(111), ~25 nm in diameter, led to the catalytic conversion of ethanol to acetaldehyde at temperatures greater than 400 K. The interaction of ethanol with Au(111)-supported TiO₂ nanoparticles is markedly different than its interaction with the individual counterparts: bulk titania and gold, which both lead to the desorption of molecular ethanol at temperatures lower than 400 K.

5:20pm **HC+NS+SS-WeA10 Shape and Support Interaction of Size Selected Pt Nanoparticles in Presence of H₂, Mahdi Ahmadi, F. Behafarid**, University of Central Florida; **B. Roldan Cuenya**, Ruhr-University Bochum, Germany
Pt nanoparticles (NPs) supported on TiO₂ have been widely used as catalysts in industrial applications.

Strong metal-support interaction (SMSI) is expected to occur for this system under reducing environments

such as vacuum and H₂. Since the morphology of NPs depends on their surface energy and their interaction

with the support, investigating the shape of NPs could be an excellent pathway to understand the metal

support interactions. In this study we have investigated the in situ shape evolution of TiO₂ supported Pt NP

using grazing incidence small angle X-ray scattering (GISAXS) during annealing in H₂ environment. The

size selected Pt NPs with an initial spherical shape were synthesized via inverse micelle encapsulation

method. The sample was step annealed up to 700°C in H₂ environment and the onset for NPs faceting was

found to be 600°C. Annealing at a higher temperature (700°C) did not cause any further change in NPs

structure. The presence of a sharp scattering ray at 45° with respect to the surface normal indicates the (110)

facet to be the dominant side facet for Pt NPs and the top and interfacial facets to be Pt(100). These features

point out that the shape of Pt NPs supported on TiO₂ under hydrogen environments is pyramidal. The

specific shape of Pt NPs are discussed based on the SMSI phenomenon.

5:40pm **HC+NS+SS-WeA11 Single Atom Alloys as a Strategy for Selective Heterogeneous Hydrogenation and Dehydrogenation Reactions, Charles Sykes**, Tufts University **INVITED**

Catalytic hydrogenations are critical steps in many industries including agricultural chemicals, foods and pharmaceuticals. In the petroleum refining, for instance, catalytic hydrogenations are performed to produce light and hydrogen rich products like gasoline. Typical heterogeneous hydrogenation catalysts involve nanoparticles composed of expensive noble metals or alloys based on platinum, palladium, rhodium, and ruthenium. We demonstrated how single palladium and palladium atoms can convert the otherwise catalytically inert surface of an inexpensive metal into an ultrasensitive catalyst.⁽¹⁻³⁾ High-resolution imaging allowed us to characterize the active sites in single atom alloy surfaces, and temperature programmed reaction spectroscopy to probe the chemistry. The mechanism involves facile dissociation of hydrogen at individual palladium atoms followed by spillover onto the copper surface, where ultrasensitive catalysis occurs by virtue of weak binding. The reaction selectivity is in fact much higher than that measured on palladium alone, illustrating the system's unique synergy.

Our *single atom alloy* approach may in fact prove to be a general strategy for designing novel bi-functional heterogeneous catalysts in which a catalytically active element is atomically dispersed in a more inert matrix. Very recently we demonstrated that this strategy works in the design of real catalysts. Platinum/copper nanoparticles can perform the industrially important butadiene hydrogenation at lower temperature using just 1% platinum.⁽³⁾ Moreover, some of the best industrial alloy catalysts to date may already be operating via this mechanism, but there is currently no method to directly probe the atomic geometry of a working catalyst. Our scientific approach allows one to parse out the minimal reactive ensembles in an alloy catalyst and provide design rules for selective catalytic nanoparticle. *From another practical application standpoint, the small amounts of precious metal required to produce single atom alloys generates a very attractive alternative to traditional bimetallic catalysts.*

References:

- 1) G. Kyriakou, M. B. Boucher, A. D. Jewell, E. A. Lewis, T. J. Lawton, A. E. Baber, H. L. Tierney, M. Flytzani-Stephanopoulos and E. C. H. Sykes – **Science** 2012, 335, 1209
- 2) M. D. Marcinkowski, A. D. Jewell, M. Stamatakis, M. B. Boucher, E. A. Lewis, C. J. Murphy, G. Kyriakou and E. C. H. Sykes - **Nature Materials** 2013, 12, 523
- 3) F. R. Lucci, J. Liu, M. D. Marcinkowski, M. Yang, L. F. Allard, M. Flytzani-Stephanopoulos, and E. C. H. Sykes - **Nature Communications** 2015, 6, 8550

Advanced Ion Microscopy Focus Topic Room 104A - Session HI-WeA

10 Years of GFIS Microscopy

Moderators: Gregor Hlawacek, Helmholtz-Zentrum Dresden Rossendorf, Germany, Richard Livengood, Intel Corporation

2:20pm **HI-WeA1 A Spectacular Collision of Entrepreneurial Spirit and a Doomed Technology... Transforming the Impossible into the Helium Ion Microscope, Bill Ward**, Entrepreneur, Scientist, Inventor, and Consultant **INVITED**

More than 50 years of research by many of the top physicists in our field culminated in a final effort to resolve the formidable problem of stabilizing the Gas Field Ion Source. It was the collective opinion that several of the physical problems were unsolvable before our efforts began at Micron nearly 20 years ago.

Our inventive process, the scientific breakthroughs and the many failures are presented in story-like fashion to explain how we successfully created the brightest ion source known to mankind. The human side of our first ten years of research which led to the successful creation of the Single Atom Ion Source and the Helium Ion Microscope is discussed. How the Entrepreneurial Spirit played a significant role in solving the final technical issues will be presented.

This perspective is offered with the hope of inspiring others to dream beyond their perceived limits.

3:00pm **HI-WeA3 Recent Developments of the Gas Field Ion Source, John A. Notte**, Carl Zeiss Microscopy, LLC

Since the commercial introduction of the Gas Field Ion Source in 2006, there has been a steady progression in both the GFIS technology and the GFIS applications. The majority of the technological developments were motivated by the goal of making the helium beam more stable and more versatile. This includes improvements to the high voltage stability, cryogenic system, the gun vacuum, and gas purity. Other changes were adopted to simplify the installation process and make the facilities requirements less demanding. Other efforts made the instrument more compatible and consistent with the larger family of Zeiss instruments.

Simultaneously, there have been changes to the GFIS *applications*, largely driven by insightful customers wanting to exploit this unique beam. This gradual change is reflected in the marketing literature which promoted the original instrument as a microscope (e.g. the "ORION Helium Ion Microscope"), whereas we now emphasize the descendant product as an instrument for nanofabrication (e.g. the "ORION NanoFab"). The new applications include lithography, nanoscale milling, structural modification, beam induced chemistry, transmission imaging, and various analytical methods. The latest NanoFab includes automated scripting, to allow for mass production and parametric investigations.

Wednesday Afternoon, November 9, 2016

In support of these new applications, there is a desire to operate the GFIS with gas species other than helium to produce, for example a focused neon beam. The operation of the GFIS with neon introduces challenges not present with helium. And many of the newest developments of the GFIS are aimed towards making the neon operation more reliable. The changes include improvements to the base vacuum, column, the gas manifold, and gas purity. Other changes are operational, helping to define the circumstances where neon can operate most successfully.

This talk will review the evolution of the ORION product family over the last 10 years. Special attention will be given to the most recent efforts undertaken to produce a stable neon ion beam.

3:20pm HI-WeA4 Monte-Carlo Simulations of Ion Beam Milling in Compound Targets, Kyle Mahady, P.D. Rack, University of Tennessee; S. Tan, R.H. Livengood, Y. Greenzweig, A. Raveh, Intel Corporation

In this talk, we will present an experimental and simulation based study of the evolution of nanostructures resulting from ion beam sputtering. We have updated our Monte-Carlo based code EnvizION, which simulates the sputtering and milling process for a variety of target compositions and structures. The computational efficiency of the updated code permits the simulation of more detailed physics in larger scale problems, with doses involving millions of ions and targets with hundreds of millions of atoms. In particular, we can now simulate milling in compound targets, as well as replacement of target atoms with impinging ions of single atom targets. We study the development of nanostructures in compound and single atom targets, and the evolution of the composition in the near surface region. Simulations of targets composed of SiO₂ demonstrate preferential sputtering of oxygen, and associated enrichment of Si in the near surface region. For ion beams in targets composed of crystalline Si, we study the replacement of target Si atoms, and relate the amorphization of the Si with the energy implanted due to the beam. Simulation results are compared with experiments.

4:20pm HI-WeA7 Characterization of Structural Changes During HIM and SEM Imaging of Organic Films, Shinichi Ogawa, National Institute of Advanced Industrial Science and Technology (AIST), Japan; T. Ohashi, S. Oyama, Nissan Chemical Industries, Ltd.

Acrylic organic films of 100 nm thick were spin coated on Si substrates, and then a helium ion or electron beam was irradiated at a dose of 2×10^{15} at 30 kV and $1 \times 10^{17}/\text{cm}^2$ at 0.7 kV of an adequate observation condition, respectively. Morphological and structural changes after the beam irradiations were characterized by AFM, IR, Raman, and TOF-SIMS. Although the helium beam energy is higher, the combination of the lower helium ion current and the longer range of the ions means that the power density to the organic materials is nearly a factor of 10^3 lower with the 30 keV helium ion beam than it is with the 0.7 keV electron beam [1]. One might therefore expect the materials to shrink less and be less damaged during HIM imaging than during SEM imaging.

AFM showed less decrease in the film thickness in a case of the ion than the electron. It indicated that the electrons might damage the film heavier than the helium ions. IR showed larger signal intensity decrease with less peak broadening and OH system remained in a case of the electrons, while it was completely destroyed in the helium ions case. Raman showed more amorphous carbon in the helium ions irradiated film, which was probably formed by destruction of CH system. Those results mean that helium ions irradiations brought about less surface morphological transformation while it resulted in larger chemical change in a deeper region of the film than the electron irradiations. This phenomenon is probably because heavier helium ions with higher energy came into deeper than electrons to the organic film cutting chains of the organic material with amorphous. TOF-SIMS showed the similar results for larger decrease of signal intensities of CH and CHO systems by the electron irradiation. Those results mean there were a lot of trade-off between irradiations of helium ions and electrons. Based on the above results with optimization, cross sections of filling of the organic materials into trenches were imaged by the HIM and SEM. As described, helium ions damaged the organic materials heavier in depth direction than electrons, while it kept original surface morphology with less transformation or shrink, so imaging of the filled organic materials into trenches by the HIM presumably shows more realistic than the SEM imaging.

T. Iijima and S. Migita are acknowledged for the usage of helium ion microscope at AIST SCR station.

References

[1] S. Ogawa, et al., "Helium ion secondary electron mode microscopy for interconnect material imaging", Jpn. J. Appl. Phys. 49 04DB12 (2010)

4:40pm HI-WeA8 Laser-Assisted Focused Helium and Neon Beam Induced Processing, M.G. Stanford, The University of Tennessee Knoxville; S. Tan, R.H. Livengood, Intel Corporation; B.B. Lewis, University of Tennessee Knoxville; J.D. Fowlkes, Center for Nanophase Materials Sciences, Oak Ridge National Lab; Philip D. Rack, The University of Tennessee Knoxville

He⁺ and Ne⁺ ion beam induced nanoscale processing has been extensively studied as an alternative ion source to the standard liquid Ga⁺ source. While superior imaging and nanomachining resolution has been achieved, perhaps the Achilles heel of higher exposure dose nanomachining operations is the cumulative damage that occurs beneath the region of interest. To this end, we have developed a laser-assisted focused He⁺ and Ne⁺ beam induced process in which a pulsed laser photothermally facilitates the helium diffusion, and for instance silicon interstitial/vacancy recombination, and thus inhibits the amorphization and the nanobubble formation. Furthermore, we have recently studied gas-assisted and laser-gas(XeF₂)-assisted He⁺ etching and have realized both reduced swelling as well as enhanced etch rates for titanium thin films. We will overview the processing parameters and the ion/photon/reactive gas fluxes that lead to both damage mitigation as well as laser- and gas-assisted etching.

5:00pm HI-WeA9 Imaging and Lithography of Two-Dimensional Nanostructures with Helium Ions, André Beyer, Bielefeld University, Germany

INVITED

In my talk, I will give an overview about imaging and local milling of two-dimensional nanostructures with helium ion microscopy (HIM). In particular, carbon nanomembranes (CNMs), graphene and biological cell membranes will be discussed. CNMs are made by a combination of molecular self-assembly, radiation-induced cross-linking and the detachment of the cross-linked monolayer from its substrate. Although free-standing CNMs cannot be imaged by light microscopy, charged particle techniques can visualize them. However, CNMs are electrically insulating, which makes them sensitive to charging. The same is true for biological cell membranes. I will demonstrate that HIM is particularly well suited for imaging such insulating membranes due to its efficient charge compensation tool. In particular, I will discuss the effects of sample charging, imaging of multilayers and imaging artefacts for CNMs as a model system. Furthermore, I will show that the focused helium ion beam of the HIM can be utilized to create nanopores with diameters down to 1.3 nm in insulating as well as conducting membranes. An analysis of the nanopore growth behaviour allows determination of the profile of the helium ion beam.

5:40pm HI-WeA11 High Resolution Elemental Imaging on the Helium Ion Microscope, David Dowsett, J.-N. Audinot, F. Vollnhals, T. Wirtz, Luxembourg Institute of Science and Technology (LIST), Luxembourg

The Helium Ion Microscope (HIM) has become an ideal tool for imaging and nano-patterning [1]. Imaging with helium ions leads to resolutions of 0.5 nm for secondary electron (SE) based imaging, while structures with sub 20 nm feature sizes may be rapidly patterned using Ne. Despite these advantages, the analysis capability of the instrument is currently limited. At beam energies of 35 keV helium or neon ions do not lead to the emission of characteristic X-rays from a sample. While some compositional information can be obtained from back scattered helium [2], identifying elemental information is more difficult. Secondary Ion Mass Spectrometry (SIMS) is a powerful ion beam based technique for analysing surfaces capable of high sensitivity and high mass resolution. SIMS is based on the generation and identification of characteristic secondary ions by irradiation with a primary ion beam (in this case helium or neon). The typical interaction volume for SIMS is around 10 nm in the lateral direction. As the probe size in the HIM is substantially smaller (both for He and Ne) the lateral resolution is limited only by fundamental considerations [3-4] and not, as is currently the case on commercial SIMS instruments, the probe size.

We have developed a prototype SIMS spectrometer specifically adapted to the Zeiss ORION NanoFab. Notably the instrument is capable of producing elemental SIMS maps with lateral resolution limited only by the fundamental interaction between the primary beam and the sample. All elements/isotopes and small clusters with masses up to 500 amu are detectable with a mass resolution $M/\Delta M$ greater than 400 and parallel detection of 4 mass channels (Figure 1).

The prospect of adding SIMS to the HIM yields not just a powerful analytical capability, but opens the way for in-situ correlative imaging

Wednesday Afternoon, November 9, 2016

combining high resolution SE images with elemental and isotopic ratio maps from SIMS [5]. This approach allows SE images of exactly the same zone analysed with SIMS to be acquired easily and rapidly. Figure 2 shows a combined SE-SIMS image of a lithium titanate and boron nitride nanoparticle mixture. The SE image has a resolution of a few nanometres, clearly showing the structure of individual nanoparticles, while the SIMS image has a resolution of a few tens of nanometres and allows unambiguous identification of individual nanoparticles.

We will present the performance characteristics of the spectrometer along with the latest results in the field of materials science.

In-Situ and Operando Spectroscopy and Microscopy for Catalysts, Surfaces, & Materials Focus Topic Room 101C - Session IS+HC-WeA

Ambient Pressure XPS Studies of Surface and Chemistry of Catalysts

Moderators: Franklin (Feng) Tao, University of Kansas, Anatoly Frenkel, Yeshiva University

2:20pm **IS+HC-WeA1 The Electronic Structure of Electrochemically Active Interfaces**, V. Pfeifer, Fritz-Haber-Institut der Max-Planck-Gesellschaft and Helmholtz-Zentrum Berlin, Germany; J.J. Velasco-Velez, Max-Planck-Institut für Chemische Energiekonversion, Germany; R. Arrigo, Diamond Light Source Ltd., UK; T.E. Jones, Fritz-Haber-Institut der Max-Planck-Gesellschaft, Germany; M. Hävecker, Max-Planck-Institut für Chemische Energiekonversion, Germany; E. Stotz, Fritz-Haber-Institut der Max-Planck-Gesellschaft, Germany; R. Schlögl, Fritz-Haber-Institut der Max-Planck-Gesellschaft and Max-Planck-Institut für chemische Energiekonversion, Germany; **Axel Knop-Gericke**, Fritz-Haber-Institut der Max-Planck-Gesellschaft, Germany

INVITED

In this presentation I will describe the application of near ambient pressure photoelectron spectroscopy (NAPXPS) to the investigation of electrochemically active gas-solid and liquid-solid interfaces during electrochemical processes. Understanding the oxygen evolution reaction (OER) on a molecular level has become increasingly important over the last few years, because energy storage of renewables is becoming more relevant now that CO₂ emission has been identified as a source of climate change.

Nafion membrane based NAPXPS experiments performed on Pt electrodes during the OER demonstrate that Pt oxides are detrimental for the OER. An oxygen induced species characterized by an Pt4f binding energy 0.6 eV above the metallic Pt4f peak was observed. However, these experiments were done in water vapor and the relevance of the results for the OER in liquid water is questionable [1]. Therefore a new approach to study the liquid-solid interface during an electrochemical process in liquid water was developed.

In this new process the electrode material is deposited on a bilayer of graphene that is stabilized by a silicon nitride window with a pinhole structure. The electrode is exposed to the aqueous electrolyte and is irradiated at the same time by synchrotron light through the bilayer graphene membrane. The emitted photoelectrons have to pass the graphene membrane before being detected in the photoelectron analyzer [2]. Recent progress in the study of the electronic structure of noble metal electrodes used in OER reaction will be discussed [3,4].

References:

1. R. Arrigo et al., In Situ Study of the Gas-Phase Electrolysis of Water on Platinum by NAP-XPS, *Angew. Chem. Int. Ed.* **52**, 11660-11664 (2013)
2. J. J. Velasco-Velez et al., Photoelectron spectroscopy at the graphene-liquid interface reveals the electronic structure of an electrodeposited cobalt/graphene electrocatalyst, *Angew. Chem. Int. Ed.* **54**, 14554-14558 (2015)
3. V. Pfeifer et al., The electronic structure of iridium oxide electrodes active in water splitting, *PCCP*, **18**, 2292-2296 (2016)
4. V. Pfeifer et al., The electronic structure of iridium and its oxides, *Surf. Interface Anal.*, **48**, 261-273 (2016)

3:00pm **IS+HC-WeA3 In situ AP-XPS and NEXAFS Studies on CO Oxidation and CO₂ Dissociation on Copper Surfaces**, B. Eren, Christian Heine, G.A. Somorjai, M.B. Salmeron, Lawrence Berkeley National Laboratory (LBNL)

This presentation contains three parts: 1- Surface science approach to CO oxidation reaction on the low-index Cu surfaces which shows at oxygen

lean conditions where the Cu surface is not oxidized to Cu₂O, (111) face of Cu is more active than more open (100) and (110) faces. This is due to high binding energy of atomic oxygen on Cu, i.e., poisoning of the lower coordinates sites of Cu. 2- Chemical state of the surface and subsurface, and adsorbate coverage on Cu(111) in steady state conditions. Here, we provide phase diagram of the surface under reaction conditions. Interestingly, no CuO phase occurs between 273K-413K when the CO:O₂ ratio is chosen as 2:1 or above. Cu₂O phase appears to be to more active phase, however it still unclear whether the reaction on Cu₂O is a MvK or LH type. 3- Finally, we present the chemical state and the surface morphology of Cu during CO₂ dissociation at ambient pressures, which appears to be different than in the presence of CO or O₂ alone.

3:20pm **IS+HC-WeA4 Alcohol Adsorption and Reaction on La_{0.7}Sr_{0.3}MnO₃(100) by APXPS**, David Mullins, T.Z. Ward, S.H. Overbury, Oak Ridge National Laboratory

Perovskite materials that are characterized by the composition ABO₃ can be formed by a wide variety of A and B cations. This enables the catalytic properties to be altered by selectively choosing the constituents while maintaining nominally the same structure. The adsorption and oxidation of simple alcohols such as methanol and ethanol have been identified as probe reactions to characterize and compare the catalytic properties of different oxide surfaces.

Methanol and ethanol oxidation on doped La_{0.7}Sr_{0.3}MnO₃(001) have been studied using ambient pressure x-ray photoelectron spectroscopy (APXPS). La_{0.7}Sr_{0.3}MnO₃(001) was grown on single crystal Nb-doped SrTiO₃(001) by pulse laser deposition. The growth of this film has been extensively characterized as a function of temperature, oxygen pressure and laser fluence in order to produce near ideal crystallinity and morphology in the film. The APXPS experiments were performed on the end station at the recently commissioned Beamline CSX-2 at NSLS II. In order to investigate the so-called "pressure gap" that may occur between reactions studied under vacuum conditions and at pressure approaching atmospheric pressure, experiments were conducted at nominally 10⁻⁵ torr and at 0.1 torr between 250° C and 350° C.

Methanol forms methoxy when adsorbed on the perovskite surface at 250° C. The surface coverage was four times greater at 0.1 torr compared to 10⁻⁵ torr. Methoxy was the only C-containing surface species observed at 10⁻⁵ torr with or without O₂. Methoxy was also the dominant surface species at 0.1 torr in the absence of O₂. However, small amounts of formate and atomic C were also evident. At the higher pressure the Mn 2p spectra indicated that the alcohol partially reduced Mn³⁺ to Mn²⁺. There was also an indication in the O 1s spectra that O was removed from the surface.

When O was present at 0.1 torr formate became the dominant surface species with only trace amounts of methoxy and C also evident. Gas phase CO₂ and H₂O products were also detected in the C 1s and O 1s spectra.

Results using ethanol rather than methanol as the reactant were generally the same, i.e. only ethoxy on the surface at lower pressures, a mixture of ethoxy and acetate at higher pressure in the absence of O₂, and exclusively acetate on the surface when O₂ was present. The only significant difference between methanol and ethanol was a greater tendency for ethanol to form the carboxylate in the absence of O₂.

Operando experiments are planned to monitor the products with a mass spectrometer to determine whether the different pressures, and resulting surface species, lead to different products.

5:00pm **IS+HC-WeA9 In situ Spectroscopy for Catalyst Design**, Rosa Arrigo, Diamond Light Source, Oxfordshire, UK

INVITED

Observing structural dynamics of heterogeneous catalysts in action yields important mechanistic insights to guide the synthesis towards improved materials. Synchrotron-based ambient pressure X-ray photoemission spectroscopy (AP-XPS) has become very popular worldwide to serve this purpose.¹⁻³ One expanding field of application of this technique is electrocatalysis²⁻³ due to its central role in a renewable energy scenario. In this contribution, I will present two examples of the application of this technique to study the gas/solid interface of electro-catalysts for a polymeric electrolyte membrane-based electrode assembly.⁴ The first example is the oxygen evolution reaction (OER), which occurs at the anode side of an electrochemical cell for water electrolysis. Herein, the highly debated descriptions of the electronic structure of the oxygen evolving Pt⁴ and Ir⁵ surfaces are clarified. The second example is the CO₂ reduction reaction (CO₂RR) to fuel over Fe on N-functionalised carbon-based electrocatalysts. These catalysts proved to be active for the CO₂ reduction but the competing hydrogen evolution reaction (HER) from water reduction is

Wednesday Afternoon, November 9, 2016

avored. Results of this research will be presented which enable us to shine light onto the nature of the H evolving sites and CO₂ reducing sites on this type of catalyst.

[1] H. Bluhm, M. Hävecker, A. Knop-Gericke, M. Kiskinova, R. Schlögl, M. Salmeron, *MRS Bulletin* 32, 2007, 1022.

[2] J. J. Velasco-Velez, V. Pfeifer, M. Hävecker, R. S. Weatherup, R. Arrigo, C.-H. Chuang, E. Stotz, G. Weinberg, M. Salmeron, R. Schlögl, A. Knop-Gericke, *Angewandte Chemie International Edition* 54, 2015, DOI: 10.1002/anie.201506044.

[3] Z. Liu, H. Bluhm, *Hard X-ray Photoelectron Spectroscopy (HAXPES)*, 447-466. DOI: 10.1007/978-3-319-24043-5_17.

[4] R. Arrigo, M. Hävecker, M. E. Schuster, C. Ranjan, E. Stotz, A. Knop-Gericke, R. Schlögl, *Angewandte Chemie International Edition*, 52, 2013, 11660-11664.

[5] V. Pfeifer, T. Jones, J.-J. Velasco-Velez, M. Greiner, C. Massué, R. Arrigo, D. Teschner, F. Girgsdies, M. Scherzer, J. Allan, M. Hashagen, G. Weinberg, S. Piccinin, M. Hävecker, A. Knop-Gericke, R. Schlögl, *Physical Chemistry Chemical Physics* 18, 2015, DOI: 10.1039/C5CP06997A.

5:40pm IS+HC-WeA11 *In Situ* and *Operando* Characterization of Model Metal Nanoparticle Catalysts: Size, Shape, and Chemical State Effects, Beatriz Roldan Cuenya, Ruhr-University Bochum, Germany INVITED

In order to comprehend the properties affecting the catalytic performance of metal nanoparticles (NPs), their dynamic nature and response to the environment must be taken into consideration. The working state of a NP catalyst might not be the state in which the catalyst was prepared, but a structural and/or chemical isomer that adapted to the particular reaction conditions. This talk provides examples of recent advances in the preparation and characterization of NP catalysts with well-defined sizes and shapes. It discusses how to resolve the shape of nm-sized Pt, Au, Pd, and Cu catalysts via a combination of *in situ* microscopy (AFM, STM, TEM), and *in situ* and *operando* spectroscopy (XAFS, GISAXS) and modeling, and how to follow its evolution under different gaseous or liquid chemical environments and in the course of a reaction. It will be highlighted that for structure-sensitive reactions, catalytic properties such as the reaction rates, onset reaction temperature, activity, selectivity and stability against sintering may be tuned through controlled synthesis.

Examples of catalytic processes which will be discussed include the gas-phase oxidation of alcohols (methanol, propanol, butanol), the oxidation and reduction of NO, the electrochemical oxidation of propanol and electrochemical reduction of CO₂. Emphasis will be given to elucidating the role of the NP size, shape and chemical state in the activity and selectivity of the former reactions.

MEMS and NEMS

Room 102B - Session MN+NS-WeA

Optomechanics, Photonics, and Quantum Nanosystems

Moderators: Leonidas Ocola, Argonne National Laboratory, Robert Illic, National Institute of Standards and Technology, Center for Nanoscale Science and Technology

2:20pm MN+NS-WeA1 Transducing between Microwaves and Light using Mechanics, Andrew Cleland, University of Chicago INVITED

In this talk, I will describe my group's progress in developing technology that would serve as a fundamental component of a quantum repeater, a hypothetical device that will be a central component for practical long-range quantum communication. The devices we have developed to date rely on the parametric conversion of signals between microwave and optical frequencies, via a strong optomechanical interaction in a suspended one dimensional photonic/phononic crystal. The device is coupled to a fiber optic line for transmission of classical (ultimately quantum) optical information, and its microwave frequency (few GHz) mechanical mode is strongly coupled to a piezoelectric transducer. This device would ultimately be coupled to a microwave frequency quantum bit, either based on superconducting or semiconducting quantum technology, which would serve to purify and/or entangle quantum information. I will include a brief description of our approach and a description of the current status of development. Worked is supported by grants from AFOSR and NSF.

3:00pm MN+NS-WeA3 Single Laser Modulated Drive and Detection of a Nano-Optomechanical Cantilever, Vincent Sauer, J.N. Bachman, Z. Diao, M.R. Freeman, W.K. Hiebert, University of Alberta and The National Institute for Nanotechnology, Canada

Nano-optomechanical systems (NOMS) offer many advantages in transducing nanomechanical motion including very high displacement sensitivities and large frequency detection bandwidths due to their optical nature. It follows from this that NOMS are a promising avenue for on-chip nanomechanical mass sensing. To take full advantage of the operational frequency properties that NOMS devices possess it is important to drive the devices optically as well. Here, a single laser modulated drive and detection (SLMDD) system is modeled and demonstrated. The setup operates similarly to a traditional NOMS pump/probe system, but instead of using a separate probe laser with a constant output power, the probe laser is power modulated to coherently drive the nanomechanical resonator using an optical gradient force. Using the SLMDD system the second laser source and its optical filter can be removed from a standard NOMS measurement system reducing the cost and complexity. This results in signal mixing between the modulated optical pump power and the Lorentzian response of the nanomechanical cantilever. The response at 1f gives a fano-like shape, but we are still able to track this characteristic mechanical frequency within a phase-lock loop. This demonstrates that the device could still be used for inertial mass loading experiments which rely on mechanical frequency tracking. Interestingly, the SLMDD system also enables homodyne detection through the DC response. As such, this can circumvent some difficulties of measuring high frequency devices with lower frequency equipment.

3:20pm MN+NS-WeA4 Optomechanical Limit Cycle Oscillations in Metallic Nanowires, Roberto De Alba, T.S. Abhilash, R.H. Rand, J.M. Parpia, Cornell University

Guitar strings are possibly the most common example of mechanical systems in which the frequency is temperature dependent. MEMS devices are similarly subject to thermal forces, and can be parametrically controlled by them under the correct conditions. Silicon domes and suspended graphene membranes are two systems that have been shown to self-oscillate when illuminated with intense laser light -- both resulting from optical absorption and associated temperature fluctuations. Here we study these optomechanical effects in metallized silicon-nitride nanowires with 50 nanometer square cross-sections and 40 micrometer length. We observe stable limit-cycle behavior with an amplitude of roughly one-eighth of the impinging laser wavelength, and characterize entrainment of this motion with inertial forcing. Lastly, we attempt to overcome viscous air damping in these nanowires using these optical interactions. In future MEMS designs, self-driven motion using on-chip optical sources could be a viable alternative to external drive electronics or active feedback circuits.

4:20pm MN+NS-WeA7 Transducer Array with Optomechanical Read-out and Integrated Actuation for Simultaneous High Sensitivity force Detection, Thomas Michels*, Ilmenau University of Technology, Germany; B.R. Illic, V. Aksyuk, National Institute of Standards and Technology; I.W. Rangelow, Ilmenau University of Technology, Germany

Research and development of transducers based on cavity optomechanics is a topic of high interest particularly because these transducers enable measurement of mechanical motion down to the fundamental limit of precision imposed by quantum mechanics. We have developed an on-chip cavity optomechanical transducer array that combines high bandwidth and high sensitivity with compactness, robustness, small size, and potential for low cost batch fabrication inherent in MEMS. The parallelization of multiple probes within one transducer array allows the simultaneous measurement of serial forces or mass detection.

Our fully-integrated, fiber-pigtailed transducer array combine high sensitivity ($\approx 0.5 \text{ fm Hz}^{-1/2}$ to $\approx 10 \text{ fm Hz}^{-1/2}$), high bandwidth optomechanical readout and built-in thermal actuation. We use a wafer-scale microfabrication process combining one e-beam patterning, six stepper, and three contact mask aligner lithography steps. These define the silicon nitride (SiN) cantilever, the single-crystal silicon-on-insulator (SOI) microdisk optical cavity with high optical Q (up to 2×10^6), SOI optical waveguides, and the patterned gold layer for bimorph actuation. Back and front side anisotropic potassium hydroxide (KOH) silicon etch allows to overhang the cantilever over the edge of the silicon chip and to define v-grooves for single mode optical fiber attachment. Two sacrificial silicon

* NSTD Student Award Finalist

dioxide layers are removed by an isotropic hydrofluoric acid (HF) etch to free the mechanically movable structures.

The SiN cantilever can be excited by an electrical signal supplied to an integrated thermal actuator. The cantilever is evanescently coupled to a high-Q optical whispering gallery mode of the optical microdisk cavity and the motion is detected by measuring the resonance frequency shift of the optical cavity mode. The actuator can be used to individually address the cantilever and dynamically move them as well as to tune the distance between the cantilever and the optical cavity, to change the sensitivity and range of measurement of the cantilever. One side of the cantilever overhangs the edge of the chip, where it can be easily coupled to a variety of off-chip samples and physical systems of interest. A 10 μm long probe is currently designed to have a stiffness of 0.1 N/m to 5 N/m and a resonance frequency of 50 kHz to 2 MHz, while the design can be easily and broadly tailored for specific sensing applications.

4:40pm MN+NS-WeA8 Magnetic Resonance Spectroscopy with Torsional Optomechanics, Mark Freeman, University of Alberta and The National Institute for Nanotechnology, Canada **INVITED**

A broadband magnetic resonance spectrometer based on optomechanical detection will be described. Demonstrations of inductive detection of spin precession in the early 1940s launched magnetic resonance spectroscopy as a general-purpose tool. As an easily miniaturizable complement to this, a resonant AC torque on a mechanical torsion sensor is choreographed from the precessing transverse RF moment via frequency mixing and then recorded through optical interferometry.

Comprehensive electron spin resonance spectra of a single-crystal, mesoscopic yttrium iron garnet disk at room temperature will be presented to illustrate the approach. A key feature of the method is that it is broadband to DC, enabling measurements of the intricate magnetostatics of individual mesoscopic magnetic objects to be performed simultaneously with the spin resonance studies. Progress in enhancing the detection sensitivity with nanocavity optomechanics also will be reported.

Work performed in collaboration with J Losby, F Fani Sani, D Grandmont, Z Diao, M Belov, J Burgess, S Compton, W Hiebert, D Vick, T Firdous (University of Alberta and National Institute for Nanotechnology, Edmonton), M Wu, N Wu, P Barclay (University of Calgary and NINT), and K Mohammad, E Salimi, G Bridges, D Thomson (University of Manitoba, Winnipeg). We are grateful for support from NSERC, NINT, AITF, and CRC.

Plasma Science and Technology Room 104B - Session PS+TF-WeA

Plasma Deposition and Plasma Assisted ALD

Moderators: Noemi Leick, Colorado School of Mines, Adrie Mackus, Eindhoven University, Netherlands

2:20pm PS+TF-WeA1 High Quality Film and Interface Formation using Appropriate Reaction Species, Akinobu Teramoto, Tohoku University, Japan **INVITED**

The strong reactive species are required for the high quality film deposition by CVD or ALD. For oxides or nitrides formation, oxygen radicals or nitrogen radicals generated by the microwave exited plasma are very effective(1-3) because of high density and low plasma damages. The integrity of SiO₂ film formed by the microwave exited PECVD is the same as that formed by the thermal oxidation on Si(100) surface, and is superior than that formed by the thermal oxidation on any other surface of Si(100)(1, 2). The SiO₂ deposition rate of the microwave PECVD is sufficiently large for the practical use. For the SiNx film formation, the microwave PECVD is also effective. The quality of SiNx film formed by the PECVD at 400 °C is the same as that formed by thermal CVD(4, 5). However, the relatively long deposition time is required for high quality film deposition, and relatively low pressure is also required, as a result, the gap fill characteristics is weaker than the thermal CVD. The high quality SiNx film deposition at low temperature and relatively high pressure are required. The nitrogen radical generated by the atmospheric pressure discharge is attractive for these applications(6, 7).

We have to choose the reactive species more carefully when the depositing material is different from the substrate, such as Al₂O₃ on Si or GaN, SiO₂ on GaN. If the reactive species is excessively active, the species react not only the precursor but also the substrate, and the materials of the substrate and the film are mixed at the film/substrate interface, as a result, those mixed materials make defects and interface traps. Al₂O₃ can works as the gate

insulator for the GaN-based MOSFET(8, 9) because of the large band gap and the high resistivity to Ga diffusion. The H₂O which has relatively lower oxidation ability than oxygen radical was used as the oxidant at the initial stage of Al₂O₃ ALD for suppressing the oxidation of GaN surface. Following radical oxygen treatment by microwave exited plasma is very effective for improving the film quality of Al₂O₃(9). It is noticed that the oxidation of GaN at the Al₂O₃/GaN interface must not occur during the oxygen treatment.

References

1. T. Ohmi, et al., *J. Phys. D: Appl. Phys.*, **39**, R1 (2006).
2. H. Ueda, et al., *Jpn. J. Appl. Phys.*, **48**, 126001 (2009).
3. A. Teramoto, et al., *ECS Trans.*, **66**, 151 (2015).
4. Y. Nakao, et al., *ECS Trans.*, **45**, 421 (2012).
5. Y. Nakao, et al., *SSDM*, p. 905, Nagoya (2011).
6. O. Gaku, et al., *J. Phys. D: Appl. Phys.*, **41**, 155204 (2008).
7. Y. Shiba, et al., *ECS Trans.*, **69**, 1 (2015).
8. P. D. Ye, et al. *Appl. Phys. Lett.*, **86**, 063501 (2005).
9. H. Kambayashi, et al., *Jpn. J. Appl. Phys.*, **52**, 04CF09 (2013).

3:00pm PS+TF-WeA3 The Synergy of Diamond-like Carbon Film PECVD Systems: Plasma Diagnostics and Film Properties, Tara Van Surksun, E.R. Fisher, Colorado State University

Diamond-like carbon (DLC) films have numerous potential applications because of their appealing mechanical and electronic properties (e.g., hardness, thermal conductivity, and high electrical resistance). Plasma enhanced chemical vapor deposition (PECVD) is a widely used technique in the production of DLC films, but to date, little is known about the underlying molecular-level chemistry involved in DLC plasma processing. In particular, energy partitioning within plasmas used to either produce or modify DLC films is not well understood. The present work focuses on investigating the fundamental chemistry of hydrocarbon plasmas used in DLC film processing as a means of understanding and ultimately controlling film fabrication. Here, we present a more holistic assessment of PECVD system used to create DLC films, including analysis of the gas-phase as well as the resulting materials. This comprehensive evaluation utilizing optical spectroscopy techniques and surface analysis tools (e.g., profilometry, contact angle goniometry, and Fourier transform infrared spectroscopy) is part of a larger effort to elucidate fundamental physical and chemical information on plasma processes that control deposition. For example, developing an understanding of energy partitioning within these plasma systems is a central component of this work as we have employed optical emission spectroscopy and broadband absorption spectroscopy to determine rotational and vibrational temperatures (T_r and T_v , respectively) of the CH radical in a variety of hydrocarbon precursor plasma systems. In CH₄ plasmas, $T_r(\text{CH})$ ranges from ~3000 to ~5000 K under most plasma conditions, whereas T_v generally reaches values ranging from 1000-2000 K. Both values appear to be correlated with system pressure and applied rf power. These results will also be presented in relationship to the properties of the deposited films. More importantly, data such as these provide valuable insight regarding possible mechanistic details in hydrocarbon plasmas linked to DLC film fabrication and help to unravel these complex systems with and without the presence of a substrate.

3:20pm PS+TF-WeA4 ULK Film Dielectric Constant Restoration through Enhanced Organic Plasma Treatment, Zhiguo Sun, J. Shu, P. Mennell, Q. Yuan, A. Madan, S. Molis, J. Mody, Y. Zhang, J. Shepard Jr, GLOBALFOUNDRIES

Ultra low k (ULK) films has been successfully integrated into Back End of Line(BEOL) interconnect to maintain a lower RC delay to take advantage of transistor continuous scaling, and to keep power consumption at a low level. However, due to its intrinsic composition and porosity, ULK films are susceptible to damage during the following process, especially patterning process and wet process such as wet clean and CMP. It is desirable to restore the dielectric constant to its original number to get full benefit if low k value. In this study, We will report a novel plasma treatment method being able to enhance the film resistance to plasma damage and repair the plasma damage. Through the detailed comparison between the pristine films,, damaged films and repaired films through analytical methods including Ellipsometry Porosimetry(EP) ,Fourier transform infrared spectroscopy (FTIR), X-ray photoelectron spectroscopy (XPS) and Hg-probe, we find the organic plasma treatment capable of restoring the surface porosity, restore the lost methyl groups and restore the dielectric constant to its original value.

4:20pm **PS+TF-WeA7 Understanding of Low Temperature ALD of Silicon Nitride**, *H.C.M. Knoops*, Oxford Instruments Plasma Technology, UK; *R.H.E.C. Bosch, T. Faraz, M. van Drunen, L.E. Cornelissen, M. Creatore, Erwin Kessels*, Eindhoven University of Technology, Netherlands

This contribution highlights insights into atomic layer deposition (ALD) of silicon nitride (SiN_x) and shows how considering these results in high material quality at low deposition temperatures. Thermal ALD processes generally require high temperatures for sufficient SiN_x quality and therefore plasma ALD has been studied extensively in the last few years. The model system discussed here consists of ALD processes using aminosilane precursors, such as $\text{SiH}_2(\text{NH}^t\text{Bu})_2$ (BTBAS) and $\text{SiH}_3\text{N}^t(\text{Bu})_2$ (DSBAS), and N_2 plasma as reactant.

Most plasma ALD processes for nitrides utilize NH_3 or H_2/N_2 plasmas, but for SiN_x it was found that the presence of H-containing species in the plasma strongly inhibits precursor adsorption.¹ DFT calculations demonstrated that groups with H on the surface have low reactivity with aminosilane precursors. Under-coordinated surfaces however, such as those obtained after N_2 plasma, have a much higher reactivity. To determine the nature of the surface, surface FT-IR studies were carried out. These indicated that the surface chemistry is rather complex as C and H species typically remain on the surface after the plasma step. Mass spectrometry showed that this can be related to reaction products that are created by the plasma step but which dissociate in the plasma and subsequently redeposit.² Shorter gas residence times reduce this redeposition effect and provide improved film properties (e.g., wet-etch rate, impurity content, and refractive index). The surface chemistry during the precursor step is relatively straightforward as gas-phase IR measurements and mass spectrometry measurements reveal that amino-groups from the precursor are released from the surface (e.g., in the form of $\text{H}_2\text{N}^t\text{Bu}$). Note that not all the groups are released during the precursor step, as evidenced by the aforementioned redeposition effect.

Taking these aspects into account, high quality SiN_x layers were prepared by ALD at low temperatures. One particular example is that films prepared at 120 °C using BTBAS precursor and Ar/N_2 plasma were found to have excellent barrier properties against moisture.³ Intrinsic water-vapor transmission rates in the range of 10^{-6} g/m²/day were obtained for films as thin as 10 nm.³ When DSBAS is used as precursor the redeposition effect appears to be reduced further, likely due to the fact this is a mono-aminosilane precursor. Precursor saturation, material quality and conformality vary with precursor and plasma employed and these aspects will be discussed in the contribution.

¹ Ande et al., *J. Phys. Chem. Lett.* **6**, 3610 (2015)

² Knoops et al., *Appl. Phys. Lett.* **107**, 014102 (2015)

³ Andringa et al., *ACS Appl. Mat. Inter.* **7**, 22525 (2015)

4:40pm **PS+TF-WeA8 Plasma Assisted Atomic Layer Deposition of SiC_xN_y Films with Methylamine as the Carbon Source**, *Rafael Ovanessian, N. Leick, R.J. Gasvoda*, Colorado School of Mines; *K.M. Kelchner, D.M. Hausmann*, Lam Research Corporation; *S. Agarwal*, Colorado School of Mines

The introduction of 3-D device architectures in integrated circuits has created a need for atomic layer deposition (ALD) of highly conformal ultra-thin films. In particular, ALD of low-dielectric-constant, carbon-containing silicon nitride (SiC_xN_y) films at temperatures ≤ 400 °C is required. However, controlled incorporation of C atoms into SiN_x during ALD remains challenging.

In this work, we report the C incorporation mechanism during two plasma-enhanced SiC_xN_y ALD processes. The first ALD process consisted of three steps, Si_2Cl_6 /thermal $\text{CH}_3\text{NH}_2/\text{N}_2$ plasma, while the second process consists of two steps, $\text{Si}_2\text{Cl}_6/\text{CH}_3\text{NH}_2$ plasma. In both ALD processes, we have determined the film composition, reactive sites, and adsorbed surface species using in situ attenuated total reflection Fourier transform infrared (ATR-FTIR) spectroscopy. In addition, the growth per cycle (GPC) and refractive index were determined using in situ four-wavelength ellipsometry.

Our IR spectra show that in the first ALD process, the CH_3NH_2 thermally reacts with $-\text{SiCl}_x$ surface species created after the Si_2Cl_6 half-cycle to form $-\text{CH}_x$ terminated surface amides. During the subsequent N_2 plasma half-cycle, in addition to nitridation of Si, a fraction of the surface CH_x groups were incorporated into the SiC_xN_y film as $-\text{N}=\text{C}=\text{N}-$ species, which appear as a strong vibrational mode at ~ 2170 cm⁻¹. The composition of the SiN_x films in the two-step ALD process was very similar, with C incorporated primarily as $-\text{N}=\text{C}=\text{N}-$ groups created during the CH_3NH_2 plasma half-cycle. We find

that during the exposure of the film to Si_2Cl_6 following an CH_3NH_2 plasma half-cycle, surface carbodiimides ($-\text{N}=\text{C}=\text{NH}$) rearrange to nitriles ($-\text{NH}-\text{C}\equiv\text{N}$), while most of the surface is terminated with $-\text{SiCl}_x$ species. The subsequent CH_3NH_2 plasma half-cycle, shows that the $-\text{NH}-\text{C}\equiv\text{N}$ species formed during the Si_2Cl_6 half-cycle are removed, and the $\text{N}=\text{C}=\text{NH}$ surface species are restored along with $-\text{NH}_x$ groups. For the $\text{Si}_2\text{Cl}_6/\text{CH}_3\text{NH}_2$ plasma ALD process, SiN_x films grown at 400 °C show a carbon content of ~ 4 at.% as measured through Rutherford backscattering spectroscopy combined with hydrogen forward scattering. Transmission electron microscopy shows a conformality of $>95\%$ for the SiC_xN_y films. The GPC for both processes was ~ 0.9 Å, with a refractive index of 1.95 and 1.86 for the N_2 plasma and CH_3NH_2 plasma ALD processes, respectively.

5:00pm **PS+TF-WeA9 Plasma Enhanced Atomic Layer Deposition in the Semiconductor Industry**, *Adrien LaVoie*, Lam Research Corporation
INVITED

Atomic layer deposition (ALD) has emerged as a key and enabling technology for $<2\text{X}$ node fabrication methods in the modern semiconductor manufacturing toolbox. Today's applications range from front-end-of-line (FEOL) spacers and liners, isolation gapfill, FinFet conformal doping, multi-patterning layers, and through-Si-via (TSV) 3D liners. When considering ALD for HVM applications, the appropriate selection of platform and tool architecture is imperative with the goal of optimizing performance, reliability, cost, and throughput. In the first section, platform architecture features and requirements will be correlated to ALD market applications. In the second section, we focus on increasing throughput. Throughput demands have led to several hardware and process innovations including driving ALD towards operation in sub-saturation regimes. The greatest advantage of ALD is the self-limiting nature of the two half reactions which provides precise thickness control, extremely high film uniformity and conformality. However, the first half reaction of precursor adsorption requires saturation at longer times with diminishing growth per unit time when considering the dose saturation curve. The self-limiting nature is achieved at the expense of lower throughput and higher chemical consumption. An alternative is to perform "sub-saturated" processing in the sub-saturated regime. This presents a paradigm shift for ALD that permits conformal film deposition without satisfying saturated half reactions. Herein we demonstrate the modulation of dosing uniformity and conversion uniformity using various process parameters to achieve excellent wafer-to-wafer thickness control, within wafer non-uniformity and compositional uniformity. The utilization of the sub-saturation processing regime provides advantages in terms of throughput and chemical usage and has driven novel hardware designs.

5:40pm **PS+TF-WeA11 Substrate Biasing during Remote Plasma-ALD On Planar and 3D Substrates**, *Tahsin Faraz*, Eindhoven University of Technology, The Netherlands; *H.C.M. Knoops*, Oxford Instruments Plasma Technology, UK; *D.M. Hausmann, J. Henri*, Lam Research Corporation; *W.M.M. Kessels*, Eindhoven University of Technology, The Netherlands

Ion-surface interactions during plasma-enhanced atomic layer deposition (PEALD) can influence the physical and chemical properties of the growing material. The limit to which ion-surface interactions can influence the deposition process depends on the energy and flux of the ions which are governed, in principle, by various process parameters. In a low pressure, remote inductively-coupled-plasma (ICP) reactor (e.g., Oxford Instruments FlexAL) capable of producing a wide range of ion fluxes, the ion energy can be controlled independently of the ion flux if equipped with substrate biasing. Previously, our group demonstrated that the material properties of thin films deposited on planar substrates using remote plasma-ALD can be tailored by controlling the energy of the impinging ions through substrate biasing.¹

In this contribution, we will investigate the role of the ion energy via substrate biasing during remote plasma-ALD on both planar and 3D topologies. An upgrade to enable substrate biasing (up to 100 W, 13.56 MHz RF power, -500 V resulting DC bias) has been implemented in the FlexAL system in our laboratory. PEALD processes for SiN_x , a material used as gate spacers and hard masks during CMOS fabrication, were developed using aminosilane precursors and N_2 plasma.² The processes were modified by incorporating a tunable RF bias signal on the substrate table during the N_2 plasma exposure step which enabled control over the energy of the nitrogen ions impinging on the growing film. SiN_x films were simultaneously deposited on planar Si wafers and 3D trench nanostructures (AR $\sim 4.5 : 1$) using bias powers up to 10 W (~ -65 V resulting DC bias). The planar films deposited with biasing typically exhibited lower refractive indices and densities (~ 1.71 and 2.75 g/cm³ respectively for -65V) compared to those

deposited without biasing ($\sim 1.93, 3.13 \text{ g/cm}^3$). A 30s dilute HF etch treatment was performed on the films deposited on 3D trench nanostructures. Horizontal SiN_x film regions located at the top and bottom surfaces of the trench exhibited very high wet etch rates (WER) and were completely removed after the etch. However, vertical SiN_x film regions exhibited very low WERs ($\sim 3 \text{ nm/min}$) and remained selectively at the trench sidewalls post-etch. It will be discussed that the results observed could hold potential applications in multiple patterning and area-selective processing techniques, relevant for the fabrication of state-of-the-art FinFETs and next-generation “gate-all-around” FETs.

¹ Profijt, Van de Sanden, Kessels., *J. Vac. Sci. Technol. A* **31**, 01A106 (2013)

² Knoops, Braeken, de Peuter, Potts, Haukka, Pore, Kessels, *ACS App. Mat. Interfaces* **7**, 19857 (2015)

6:00pm PS+TF-WeA12 A Novel ABC-type ALD Process for Cobalt using CoCp_2 and N_2 and H_2 Plasmas, Martijn Vos, N.F.W. Thissen, A.J. Mackus, W.M.M. Kessels, Eindhoven University of Technology, Netherlands

Cobalt is a transition metal which is receiving much interest, among others due to its ferromagnetic properties. One of the promising applications is in multilayers and alloys of Co/Pt, which are used in nonvolatile memory devices such as magnetic random-access memory (MRAM). For many of the applications of Co the key strengths of atomic layer deposition (ALD), i.e. conformality and ultimate thickness control, can be very beneficial. In previous work, the ALD processes using cobaltocene (CoCp_2) and NH_3 or N_2/H_2 plasma showed a decent growth-per-cycle (GPC) and good material properties, including a low resistivity.^{1,2} It was found that the best material properties were obtained for a N_2/H_2 mixing ratio of ~ 0.33 , corresponding to the highest production of NH_3 in the plasma. This result suggests that NH_3 is necessary for obtaining high purity Co films.

In this contribution we address ALD of Co films using CoCp_2 and subsequent N_2 and HHfddfd H_2 plasmas. By comparing this ABC process to the AB process with a combined N_2/H_2 plasma the role of NH_3 can be further investigated. Moreover the ABC process offers additional flexibility over the AB process, such as different powers and pressures during the subsequent plasma steps. Films were deposited on different substrates, including Si, SiO_2 and Pt, at temperatures from 100 to 300°C yielding a GPC between 0.2 and 0.4 \AA . It will be shown that despite the absence of NH_3 in the plasma, the ABC process can be used to deposit high-purity films of Co on ALD Pt films, with contamination levels as low as 1 at.%, as measured by X-ray photoelectron spectroscopy (XPS). On the other hand, considerable amounts of C, O and N contamination (2-10 at.%) in Co films deposited on Si and SiO_2 suggest that NH_3 is a prerequisite for high purity films on these substrates. This difference between deposition on Pt and Si/SiO_2 is likely due to the catalytic activity of the Pt, causing the reduction or ‘cleaning’ of the deposited Co. In addition the fabrication of Co/Pt multilayers using ALD will be discussed.

1. Lee, H.-B.-R. *et al.*, *Electrochem. Solid-State Lett.* **9**, G323 (2006).

2. Yoon, J. *et al.*, *J. Electrochem. Soc.* **158**, H1179 (2011).

Plasma Science and Technology

Room 104C - Session PS-WeA

Atomic Layer Etching and Low Damage Processing

Moderator: Eric Joseph, IBM Research Division, T.J. Watson Research Center

2:20pm PS-WeA1 Plasma-Based Removal of Native Oxide Layers on Si and SiGe Substrates While Minimizing Surface Residues, D. Metzler, Chen Li, University of Maryland, College Park; C.S. Lai, E.A. Hudson, Lam Research Corporation; G.S. Oehrlein, University of Maryland, College Park

The evaluation of a plasma-based native oxide surface cleaning process for Si and SiGe substrates is described. Objectives include removal of the native oxide while minimizing substrate damage and surface residues. This work is based on recent advances in atomic layer etching (ALE) of SiO_2 [1]. To achieve controlled etching of SiO_2 at the Ångström level a cyclic approach consisting of a deposition step and etch step was initially employed. The deposition step deposits fluorocarbon (FC) films up to 10 \AA thick on the surface. Subsequent low energy Ar^+ ion bombardment during the etch step induces mixing of the FC film with the substrate and removal of the FC film together with the mixed, reacted substrate material. Oxide layer thicknesses were measured using *in situ* ellipsometry and surface chemistry was analyzed by X-ray photoelectron spectroscopy. The cyclic ALE approach did not remove native oxide from a Si substrate at the level

required. A modified process was evaluated which used continuously biased Ar plasma with periodic CF_4 injection. By eliminating a dedicated FC film deposition step, optimizing process times and ion energies, significant O removal from the Si surface was achieved, while leaving residual C. An additional H_2/Ar plasma exposure performed at higher pressure and minimizing ion bombardment successfully removed residual C and F originating from the surface cleaning process. The combined treatment reduced O and C levels to about half compared to as received Si surfaces but removed $\sim 37 \text{ \AA}$ of Si. Similar to Si substrates, SiGe substrate oxide removal was seen upon applying this cleaning process, while the H_2/Ar post treatment subsequently removed F and C-related species. O and C levels are reduced to $\sim 70\%$ after the combined treatment while $\sim 55 \text{ \AA}$ of SiGe are removed. In addition, the surface is Ge richer after the cleaning process compared to SiGe surfaces as received. This feasibility study of Ar/FC based native oxide cleaning approaches for Si and SiGe substrates shows the potential to reduce O levels but at the cost of substantial substrate material loss and introducing low levels of C and F.

The authors gratefully acknowledge the financial support of this work by the National Science Foundation (CBET-1134273) and Lam Research Foundation.

References:

[1] D. Metzler and *et al.*, *J Vac Sci Technol A* **32**, 020603 (2014)

2:40pm PS-WeA2 Electrical Characterization of SiN Modified by Hydrogen and Helium Plasma for New Atomic Layer Etching Processes, Florentin Chambettaz, L. Vallier, O. Joubert, Univ. Grenoble Alpes, France

As downscaling pace the microelectronic industry, current plasma etching processes show their limits. Actually for critical dimension smaller than 10 nm, atomic precision has to be reached. In this study, we are characterizing an Atomic Layer Etching (ALE) process by focusing on the induced damages related to the chemical and physical interaction(s) with hydrogen and helium plasmas. Hydrogen plasmas have been used for years in the microelectronic industry and studied in the fields of deposition (PECVD, Plasma Enhanced Chemical Vapor Deposition), surface processing (surface passivation, hydrogenation) [1] and plasma etching. However the mechanisms related to these processes are not fully understood yet mainly because hydrogen is an element with peculiar characteristics such as its low mass and electronegativity. Helium plasmas have been also used for many years in the microelectronics industry, mainly as an additives gas thanks to its low chemical reactivity and low mass. In order to modify the surface of ultrathin layers without damaging the materials, a very low ion bombardment is required (conditions similar to those obtained in a pulsed ICP reactor [2]). At the same time, dense plasmas are required to obtain satisfying etch rates when several nanometers have to be etched away. In this study we focus on plasma etching of silicon nitride by hydrogen and Helium plasma exposure in a commercially available 300 mm reactor, in order to develop an ALE process for spacer etching of future transistors [3]. Several process conditions are achieved with different ion energies and ion densities, on thin silicon nitride blanket samples. The quantity and the position in the silicon nitride of generated traps are studied with an electrical characterization. The effect of those plasma process condition on the silicon nitride etch rate will be discussed.

1. E.Despiau-Pujo, A.Davydova, G.Cunge, L.Delfour, L.Magaud, and D. B.Graves, *Journal of Applied Physics*, **113** (2013)

2. C. Petit-Etienne, M. Darnon, P. Bodart, M. Fouchier, G. Cunge, E. Pargon, L. Vallier, O. Joubert, and S.Banna, *Journal of Vacuum Science & Technology B*, **31** (2013)

3. N. Posseme, O. Pollet, and S. Barnola, *Applied Physics Letters*, 105 (2014)

3:00pm PS-WeA3 Electron Beam Generated Plasmas Produced in Fluorine-Containing Gases, David Boris, G.M. Petrov, Tz.B. Petrova, S.C. Hernandez, S.G. Walton, Naval Research Laboratory

Electron beam generated plasmas are characterized by high plasma density ($>10^{10} \text{ cm}^{-3}$), and very low electron temperatures ($<1 \text{ eV}$) making them well-suited for next generation processing techniques where high fluxes of low energy ions are desirable. In addition, both modeling and optical emission spectroscopy indicate relatively low concentrations of radicals compared to discharges. In this work, we focus on the characteristics these plasmas in fluorine-containing chemistries (SF_6 , C_2F_6 , etc.), due to their relevance to industrial etching applications. We discuss the electron density and temperature, electronegativity, excited F^* atom emission, as well as ion flux and energy at adjacent surfaces for plasmas produced in Ar/SF_6 Ar/F_2 and Ar/CF_4 mixtures, with particular attention paid to the influence of reactive gas concentration. These parameters are measured using

Wednesday Afternoon, November 9, 2016

Langmuir probes, optical emission spectroscopy, and energy-resolved mass spectrometry. The results are then compared with a one-dimensional, steady-state hydrodynamic model developed for electron beam generated plasmas produced in low pressure Ar-SF₆ mixtures.

3:20pm PS-WeA4 Plasma-Enhanced Germanium Atomic Layer Etching (ALE), Wenbing Yang, S. Tan, K. Kanarik, R. Arghavani, T.B. Lill, Y. Pan, Lam Research Corp.

Atomic layer etching (ALE) has been studied in the laboratory for more than 25 years and is being driven today by the semiconductor industry [1]. The case study ALE system is silicon ALE etched with alternating chlorine dosing and argon ion bombardment. Besides silicon, over 20 other materials have been reported with ALE including oxides, III-V compounds, and metals. Germanium, due to its superior hole mobility, is a prime candidate to replace silicon channel for use in future semiconductor devices. Two previous studies reported on germanium ALE in 1997. In the first study, Ikeda et al reported isotropic ALE of Ge by removing the chlorinated layer thermally [2]. In the second study, Sugiyama et al reported directional ALE of Ge by removing the chlorinated layer using argon ions [3]. In both reports, the chlorine was delivered thermally as a gas, without the use of plasma. Here we report on plasma-enhanced, directional Ge ALE. We will show results on both Ge blanket and patterned wafers and compare the behavior to the silicon case study.

References

1. Kanarik et al, J. Vac. Sci. Technol. A 33(2), Mar/Apr 2015
2. Ikeda, Imai, and Matsumura, Applied Surface Science 112, 1997
3. Sugiyama, Matsuura, Murota, Applied Surface Science 112, 1997

4:20pm PS-WeA7 Damage Monitoring of GaN Film for Material Processing, Daisuke Ogawa, Y. Banno, Y. Nakano, K. Nakamura, Chubu University, Japan

INVITED

Gallium nitride (GaN) is one of the candidate materials to realize miniaturized high power devices due to the wide band gap. The miniaturization of individual power devices, such as small inverters, are necessary to increase the electrical capacity, in particular, in upcoming electric vehicle era. In the last several decades, low-temperature plasma plays a role to speed computers up by fabrication. And now, the plasma is about to be applied to miniaturize high power devices. The advantage of the plasma processing is that a lot of semiconductor industries already have their own manufacture lines with the plenty of their processing experiences. However, it is also well known that plasma can create undesired change on the processing devices. This is called plasma induced damage (PID), which is created by ions, radicals, radiations, dusts etc. GaN cannot be the exception of the damage creation so that better understanding of damage developments is important to increase manufacture productivity.

We have been analyzing the evolution of GaN condition during plasma processing to clarify the damage creation mechanism. In-situ monitoring is a key diagnostic to understand the mechanism so that we have mainly utilized photoluminescence (PL) from the GaN that is exposed in processing plasma. The PL gives us the information of the volume-averaged damages from the surface to approximately 45 nm depth. The depth range is important because the change in the range affects the device performance when fabricated. The PL also gives us the indication of the optically-emissive intermediate states that are mostly caused by impurities and crystal defects in GaN. In particular, it is possible to know what kind of damage a specific plasma creates by observing a specific wavelength range of the PL, such as near-band-edge (NBE), blue (BL) and yellow luminescence (BL) range.

In this presentation, we will summarize our damage analysis on GaN that is exposed in processing (etching) plasma. Understanding of damage creation mechanism from the plasma is not trivial because plasma creates the surface damage in addition to the temperature increase due to the ion bombardments. The temperature can assist physical deformation of GaN and chemical reactions on the surface. This means that the isolation between the damage creation and the temperature rise by the plasma might be a good idea to understand the mechanism. Interestingly, our former PL measurements showed that cooling GaN kept PL better than non-cooling GaN even when exposing argon plasma.

5:00pm PS-WeA9 Neutral Beam Etching of Germanium Microstructure for Ge Fin-FET Devices, E.T. Lee, Shuichi Noda, Tohoku University, Japan; W. Mizubayashi, AIST; K. Endo, AIST; S. Samukawa, Tohoku University, Japan

Germanium Fin-FET has becoming a promising candidates for highly scaled CMOS FETs to solve the limitation of device scaling of Si CMOS FET due to large carrier mobility of Ge itself. However, it seems that the etching mechanisms of Ge and optimization of etching method have not investigated deeply in spite of its importance forming basic channel structures in FET devices. Since we have already succeeded to apply a neutral beam etching (NBE) method to damage-free Si Fin-FET fabrication process and shown excellent device performances¹⁾, much more advantages in the low-damage NBE can be expected for Ge fin etching because thermal annealing is difficult due to a heat resisting property of Ge.

The NBE characteristics of Ge Fin were evaluated using pure Cl₂ gas chemistry which is the same for the Si Fin etching and compared results each other. The NBE system consists of an inductive coupled plasma (ICP) source and a carbon aperture plate where energetic negative ions are effectively converted to the neutral beam utilizing a pulse time modulated plasma. Ge Fin structure were etched with TEOS-CVD SiO₂ hard masks which were patterned by an EB lithography and a conventional ICP RIE. The sample substrate was set on the cooled stage at -15°C. The Ge profile was optimized by adjusting the beam energy which was controlled by changing the RF bias power to the carbon aperture.

The Ge Fin was etched at the etch rate of more than three times larger than Si. However, the large bottom tails were observed with different profile from the Si Fin structure. The etch rate difference can be explained due to the different etch yield and chlorination density on the surfaces²⁾. The large bottom tails of Ge Fin structure are considered to be caused by lower evaporation pressure of GeCl₄ than that of SiCl₄. The profile optimization was made by controlling RF bias power on the aperture plate. The bottom tail was reduced with increasing the bias power. The side-etching under the SiO₂ hard mask hardly increased during long over etch period. Conversely, the etch rate of Ge was almost constant regardless of the RF bias power. This results indicate that the etching reaction is limited by Cl supply, which chlorinates adsorption site on the Ge surface. The lateral etching is limited because the Cl radical density is low and the samples are cooled down to -15°C. The bottom tails seemed to be reduced in according to beam divergence narrowing. High magnification TEM images showed extremely smooth side wall surface in the substantially atomic level.

- 1) K. Endo *et al.*, IEDM Tech. Dig. (2005) pp. 840-843. 2) J-Y Choe, *et al.*, J. Vac. Sci. Technol. A, **16**, 3266 (1998).

5:20pm PS-WeA10 Selective Trimming of Surface Oxygenated Groups through Vacuum Ultraviolet Light Irradiation in an Evacuated Environment, Ahmed Soliman, T. Utsunomiya, T. Ichii, Kyoto University, Japan; H. Sugimura, Kyoto University, Japan

Vacuum ultraviolet (VUV) light of 172 nm is widely used for modifying the surfaces of polymers and self-assembled monolayers (SAMs) to be applicable in microfluidics, lithography and microelectromechanical systems (MEMS) devices. The influences of VUV light on the surface modifications are dependent on the irradiation environment. In an atmospheric environment, the VUV light generates active oxygen species (O), which can functionalize and etch the organics at the irradiated surface.¹ While in high vacuum condition (HV), the rate of oxidation process at the VUV-irradiated surface decreased,² and other photochemical reactions, such as photo-cleavage can proceed apparently.

In this work, we examined the influence of HV-VUV treatment on the surface oxygenated groups of SAMs. We used VUV/(O)-modified hexadecyl (HD-) SAMs in this study, because of their highly-dense and well-defined structure. Furthermore, these modified-SAMs were homogeneously terminated with different oxygenated groups.¹ These modified-SAMs were HV-VUV irradiated for different periods. The changes of the chemical constituents after HV-VUV treatment were characterized by X-ray photoelectron spectroscopy (XPS) and chemical derivatization using different fluorinated reagents.

After VUV/(O) treatment, the XPS results showed that the oxygenated groups at the surface of SAM contained both derivatizable (such as OH, CHO and COOH) and nonderivatizable (C-O-C, C-CO-C and C-COO-C) groups.¹ The HV-VUV affected the surface components; the decrease of COO and C-O moieties, while the slight increase of C=O moieties. The C-C components were slightly influenced by the HV-VUV irradiation. Considering the changes of the chemical constituents, wettability and

morphology, the routes and mechanisms of the chemical conversions at the HV-VUV irradiated surface were discussed.

We concluded that the HV-VUV treatment to the surface oxygenated groups could only dissociate the components containing C-O bonds without significant influence on the C-C skeleton. The HV-VUV can be considered as a selective-trimming modification technique with less degradation, as the components containing C-O bonds were only dissociated.

References

1. A. I. A. Soliman et al., *Soft Matter*, 2015, **11**, 5678–5687.
2. S. Ichikawa, *J. Appl. Phys.*, 2006, **100**, 033510 (1–5).

5:40pm **PS-WeA11 Transistor Performance Improvement Through Low-Damage Plasma-Enhanced ALD Metal Gates**, *Christopher Brennan, C. Neumann, S. Vitale*, MIT Lincoln Laboratory

Metal gate materials have now replaced polysilicon gates for advanced silicon CMOS fabrication of both planar silicon MOSFETs and FinFETs. However, plasma processes employed for metal gate deposition can cause significantly more damage to the gate dielectric material than with traditional chemical vapor deposition polysilicon gates, resulting in reduced device performance and reliability. Titanium nitride (TiN) is one such metal gate material, possessing both thermal stability and compatibility with gate dielectric materials. Additionally, the workfunction of TiN can be tuned to make mid-gap metal gates for undoped-body fully depleted silicon-on-insulator (FDSOI) transistors for subthreshold, ultra-low power operation. Gate dielectric quality remains critical for advanced device fabrication, especially for these low power, low leakage devices.

This work compares plasma-induced gate oxide damage by two different metal gate deposition processes: magnetron sputtering and plasma-enhanced atomic-layer-deposition (PE-ALD). FDSOI transistors fabricated with either gate deposition process showed similar electrostatic performance, with good short channel performance including subthreshold swing, DIBL, and V_t roll-off. However, gate dielectric quality metrics were significantly better when PE-ALD TiN was used compared to plasma sputtered TiN. CV measurements exhibited stretching of the curves and increased hysteresis with sputtered TiN compared to PE-ALD TiN, indicative of a higher density of interface states in the former case. In addition, gate leakage was 1200x higher for the plasma sputtered TiN devices, which is consistent with a high density of defects in the gate oxide leading to trap-assisted tunneling. Finally, transistors fabricated with both methods show that those fabricated with PE-ALD TiN demonstrate a significantly lower gate oxide failure probability.

Taken together, the electrical results suggest that plasma sputtering damages the gate dielectric through energetic ion and vacuum ultra-violet (VUV) photon bombardment which breaks Si-O bonds and leaves defect states. In addition to higher leakage, these defect states can lead to device reliability issues and high early failure rates. Alternatively, inductively coupled plasma PE-ALD produces a much lower energetic ion and VUV flux at the wafer surface, resulting in markedly less damage. Instead of damaging the gate oxide, PE-ALD initially deposits a sub-nm TiOCN film which may serve as a passivating layer. This layer does not seem to induce any undesirable device characteristics except for a slight increase in EOT.

6:00pm **PS-WeA12 In situ Optical Diagnostics during Atomic Layer Etching of SiO₂ using Alternating Cycles of C₄F₈ and Ar Plasma**, *N. Leick, Ryan Gasvoda*, Colorado School of Mines; *A. van de Steeg*, Eindhoven University of Technology, Netherlands; *R.A. Ovanesyan*, Colorado School of Mines; *R. Bhowmick*, E.A. Hudson, Lam Research Corporation; *S. Agarwal*, Colorado School of Mines

Due to the continuous shrinking of semiconductor devices combined with the 3D architecture, the demands on dry etching processes have become increasingly stringent. Therefore, the development of more precise etching methods is necessary, and atomic layer etching (ALEt) is a promising technique to enable atomic-level thickness control, directional etching and material selectivity. Recently, ALEt of SiO₂ has been extensively studied, using a cyclic process that involves plasma deposition of a fluorocarbon (CF_x) layer, followed by an Ar plasma exposure to activate the fluorine for etching.

In this work, SiO₂ was etched using an ALEt process based on an octafluorocyclobutane (C₄F₈) plasma to deposit the CF_x layer and an Ar plasma for the removal of the material. In each ALEt half-cycle, *in situ* attenuated total reflection Fourier transform infrared (ATR-FTIR) spectroscopy and *in situ* four-wavelength ellipsometry were simultaneously used to study the film composition and the change in film thickness, respectively. From these measurements, it was possible to conclude that

under the C₄F₈ plasma conditions used, the CF_x layer can be deposited at a growth rate of ~1.65 Å/s, while minimizing the SiO₂ removal to negligible amounts. At the end of the CF_x deposition step, the predominant IR feature was centered at 1220 cm⁻¹, and can be attributed to CF_x (x=1,2,3), while some surface Si-C, Si-F and C-O can also be observed, suggesting the formation of an intermixed SiO₂/CF_x layer. In line with this result, the IR from the first 10 s of Ar plasma clearly shows the instantaneous removal of SiO₂. This removal continues for the 60 s of Ar plasma exposure, and ellipsometry enables us to distinguish between two etch regimes. The first regime has a high etch rate, ~0.5 Å/s, indicating a high F concentration in the intermixed SiO₂/CF_x layer. As the film etching proceeds, the intermixed layer becomes F-deficient which slows down etching, until finally the SiO₂ removal is dominated by inefficient Ar⁺ sputtering. From these results, SiO₂/CF_x intermixing seems to be the dominant etching mechanism in this ALEt process.

In addition to the instantaneous removal of SiO₂, an increase in the CF_x signal was initially detected in the IR during the first 10 s of the Ar plasma exposure. Because at the end of the 60 s Ar plasma step no net incorporation of CF_x can be observed, we propose that CF_x is initially redeposited from the reactor surfaces and participates in the etching process. This redeposition increases the etch rate during the Ar plasma cycle by providing additional amounts of F from the gas phase, but also undesirably increases the etch rate with increasing ALEt cycles.

Advanced Surface Engineering

Room 101D - Session SE+2D+EM-WeA

Multifunctional Thin Films and Coatings

Moderators: Jolanta Klemberg-Sapieha, Ecole Polytechnique de Montreal, Canada, Michael Stueber, Karlsruhe Institute of Technology, Germany

2:20pm **SE+2D+EM-WeA1 Investigation of H₂S Poisoning Process on Composite Material Made of Metal Oxides and Carbon Nanotubes**, *Yichen Duan, A.V. Teplyakov*, University of Delaware

The composite material based on a combination of SnO₂, CuO and acid-treated carbon nanotubes is considered to be promising for H₂S sensing applications. By applying large dosage of H₂S (1% in volume) to the composite and evaluating the chemical changes spectroscopically via XPS, SEM and EDS, the poisoning mechanism of this type of sensing material is revealed. Specifically, metal sulfides (CuS and SnS₂), metal sulfate (Sn(SO₄)₂) and thiols are formed as the products following the introduction of H₂S. In fact, all the three components of the material are affected by H₂S. Moreover, when oxygen is present, metal sulfides can be reoxidized back into metal oxides while metal sulfate and thiols remain unchanged. The measurements of the model sensor response also support the assessment of the poisoning process.

2:40pm **SE+2D+EM-WeA2 Graphene-family Nanomaterials Co-assembled with Nanostructured Cobalt Oxide Polymorphs as Hybrid Supercapacitive Electrodes and Enzymeless Glucose Detection Platforms**, *Sara Carrizosa, B. McDonald, S. Gupta*, Western Kentucky University

Graphene-family Nanomaterials Assembled with Cobalt oxides and Cobalt Nanoparticles As Hybrid Supercapacitive Electrodes and Enzymeless Glucose Detection Platforms We developed graphene/cobalt oxides and graphene/cobalt nanoparticles hybrid assembly highlighting the impacts of nanoscale surface morphology and microstructure producing tailored interfaces for improved electrochemical and electroanalytical properties. Molecular electrodeposition and facile hydrothermal synthesis techniques followed by thermal treatment are demonstrated to be effective approaches for nanoengineered electrochemical electrodes. Hybrid electrodes consisting of supercapacitive graphene nanosheets and pseudocapacitive nanostructured cobalt oxide polymorphs (CoO and Co₃O₄) as well as cobalt nanoparticles (CoNP) synthesized on two- and three-dimensional graphene nanosheets facilitate chemically bridged (covalently and electrostatically anchored) yet tunable graphene-cobalt interfaces. The intrinsic microstructure and surface of these hybrids were characterized by electron microscopy combined with elemental mapping, X-ray diffraction and Raman spectroscopy. The graphene/cobalt hybrid composites were investigated as asymmetric supercapacitor cathodes and as electroanalytical platforms for enzymeless detection of glucose. We demonstrate that Co₃O₄/ErGO and Co₃O₄/multilayer graphene hybrids are capable of delivering high specific capacitance of > 600 F g⁻¹ at a current density of 10 A g⁻¹ is achieved when the mass ratio of Co₃O₄ to ErGO is equal to 80:20 as compared with other hybrids with excellent cycling

Wednesday Afternoon, November 9, 2016

stability in voltage range 0–1.2 V. It can also detect glucose with ultrahigh sensitivity of 4.57 mA mM⁻¹ cm⁻² and a remarkable lower detection limit of < 50 nM in the following order Co₃O₄/rGO_{HT} < CoO/ErGO < CoNP/MLGNiFoam < Co₃O₄/MLGNiFoam. We attribute all of these remarkable findings due to interplay of (a) open pore system beneficial to ion diffusion and transport kinetics owing to larger accessible geometric surface area, (b) three-dimensional topologically multiplexed and highly conductive pathways provided by MLG, ErGO and rGO_{HT} nanoscaffold architectures to ensure rapid charge transfer and electron/ion conduction (< 10 ms), and (c) synergistic integration of functional nanomaterials devoid of graphene sheets agglomeration with optimal transition metal (oxides) nanoparticles loading.

3:00pm SE+2D+EM-WeA3 Cross-Bonding between Silicon, Silica and III-V Surfaces at the Nano-Scale Using Energy Analysis via Three Liquid Contact Angle Analysis (3LCAA) to achieve Hermetic Wet NanoBonding™, Ashley Mascareno, SiO₂ NanoTech LLC/Arizona State University Physics Dpt; *N.X. Herbots*, SiO₂ NanoTech LLC; *C.F. Watson*, SiO₂ NanoTech LLC/Arizona State University Physics Dpt

Mobile ions such as Na, percolate from saline environments into marine and atmospheric sensors and limit their reliability to less than a week. Implantable glucose monitors for diabetics require replacement about every 3-7 days, with finger blood samples re-calibration daily. Hermetic bonding can yield economic, medical, and human benefits by extending lifetime of such integrated sensors from days to years. Si-based surfaces such as thermally-grown amorphous a-SiO₂ on Si(100), and on III-V surfaces can be hermetically bonded with Wet NanoBonding™ to yield dense, hermetic cross-bonding. In Wet Nonbonding™, planarization is first accomplished at the nano-scale, then a-SiO₂ is etched with HF, while a 2 nm precursor β-cSi₂O₄H₄ phase is grown on Si(100) to initiate cross-bonding. Next, both surfaces are put into mechanical contact in a class 10 clean-room and nano-bonded under low temperature (T<180° C) steam pressurization.

Modifying the surface energy components of 2 surfaces can help optimize hermeticity by increasing the density of cross-bonding. Surface energy γ^T can be measured via 3 Liquid Contact Angle Analysis (3LCAA) using the the Van-Oss theory, which models γ^T for semiconductor and insulators in 3 interactions: (1) Lifschitz-Van der Waals molecular dipole interactions γ^{LW}, (2) electron donor interactions γ⁺, and (3) electron acceptor interactions γ⁻. Successful NanoBonding™ can occur between one surface with high γ⁺ and one with high γ⁻. 3LCAA extracts these from contact angles between several liquids with known surface energies and the surface. Sessile drop analysis with water, glycerin, and α-bromonaphthalene is conducted in a Class 100 hood using 4-8 drops per liquid for statistical accuracy. RCA cleaned Si(100) and Si(100) terminated with 2-nm β-cSi₂O₄H₄ via the Herbots-Atluri (H-A) process are used, in combination with Rapid Thermal Anneal and Oxidation (RTA and RTO), to grow a-SiO₂ [3]. The γ^T of hydrophilic RCA-cleaned Si(100) is 47.3±0.5 mJ/m², 25% higher than the γ^T of ordered, hydrophobic β-cSi₂O₄H₄ Si(100), 37.3±1.5mJ/m², and 30% higher than RTO oxides 34.5±0.5 mJ/m². Interactions from γ^{LW} account for 90-98±2% of γ^T in ordered oxides, but only 76.5±2.0% of those in hydrophilic surfaces. Thus, 3LCAA detects changes in surface reactivity from defects, impurities, and dangling bonds. While γ⁺ accounts for little to none of γ^T for all but one surface, 180° C annealing during Wet NanoBonding significantly increases γ⁺ in β-cSiO₂. Conversely, HF etching significantly increases γ⁻ for a-SiO₂. When matching acceptor with donor interactions between surfaces via 3LCAA, cross-bonding density appears to increase, and NanoBonding™

3:20pm SE+2D+EM-WeA4 Porous Materials for Solid Phase Microextraction by Sputtering and Chemical Vapor Deposition, Tuhin Roychowdhury, A. Diwan, B. Singh, M. Kaykhali, M.R. Linford, Brigham Young University

Solid phase microextraction (SPME) is an important sampling tool. It consists of placing a coated fiber above a sample (headspace mode) or immersing it in a liquid such that molecules (analytes) of interest can be selectively extracted and concentrated. The captured species are then released by heating into a chromatograph for separation and identification. It is a 'green' method because no additional solvent is used in this process. We have developed a new class of SPME fibers that offer extraordinary capacity and speed. They are prepared by sputtering a material under conditions that lead to a nanoporous coating on the fiber. When silicon is sputtered under these conditions, its outermost surface can be additionally oxidized, leading to a high density of silanol groups than can be subsequently silanized. For example, the fibers can be derivatized with

octadecyldimethylmethoxysilane by chemical vapor deposition (CVD), which creates a hydrophobic extraction medium. The performance of our 2 micron sputtered coatings has been compared to that of thicker (7 micron) commercial coatings. Our fiber consistently outperforms the commercial fiber, showing significantly higher capacity for alcohols, amines, aldehydes, and esters. Real world samples, e.g., hops and PAH from water, have also been analyzed. Different coating thicknesses have been prepared and evaluated. Sputtered coatings have been characterized by X-ray photoelectron spectroscopy (XPS), scanning electron microscopy (SEM), and wetting.

4:20pm SE+2D+EM-WeA7 Ferroelectric Thin Films for Memory Applications, Joyprakash Chakrabarty, Institut national de la recherche scientifique (INRS), Canada

Ferroelectric (FE) oxides draw attention in science community because of its spontaneous switchable polarization often used in electronic devices. FEs are earth abundant, easy to synthesis and low degradation of electronic properties while exposed to room atmosphere. One of its promising applications is in computer memory devices. FEs function as memory by storing data in its two polarization states normally defined as up and down state. However the challenges lie in enhancing data bit density at room temperature. Here we show four step ferroelectric polarization switching in BiFeO₃(BFO)/SrRuO₃(SRO)/BiMnO₃(BMO) heterostructure thin films which act as FE memory devices. All crystalline films are grown on (100) oriented Niobium doped SrTiO₃ (NSTO) single crystal substrates by pulsed laser deposition. Our experimental results show a promising device concept, unique in FE memories that can enhance the data storage capacity in heterostructure capacitor devices at room temperature.

4:40pm SE+2D+EM-WeA8 Thermoelectric and Optical Properties of Advanced Thermoelectric Devices from Ni/Bi₂Te₃/Ni and Ni/Sb₂Te₃/Ni Thin Films, Satilmis Budak, Z. Xiao, J. Cole, A. Kassu, D. Price, T. Davis, T. Strong, J. Gray, Alabama A&M University

Thermoelectric devices were prepared from Ni/Bi₂Te₃/Ni and Ni/Sb₂Te₃/Ni thin films using DC/RF magnetron sputtering and E-beam deposition systems. Thermoelectric devices were annealed at different temperatures to form nanostructures in the multilayer thin films to increase both the Seebeck coefficients and electrical conductivity and decrease thermal conductivity. The thin film devices were characterized using Seebeck coefficient measurement systems; four probe van der Pauw measurement system to measure resistivity, sheet resistance, density, mobility and type of the charge carrier concentration. In addition to the Seebeck coefficient and van der Pauw measurements, the laser thermal conductivity system was used for the thermal conductivity measurements. The surface morphology of the fabricated thermoelectric films is characterized using Scanning Electron Microscope (SEM). Raman Spectroscopic technique is used for identification of inherent molecular specificity and analysis of chemical compositions of the films. The resonant features of the scattering spectra measured under the 532 nm and 785 nm wavelength excitation lasers are analyzed.

Acknowledgement

Research was sponsored by NSF with grant numbers NSF-HBCU-RISE-1546965, NSF-EPSCOR-R-II-3-EPS-1158862, DOD with grant numbers W911 NF-08-1-0425, and W911NF-12-1-0063, U.S. Department of Energy National Nuclear Security Administration (DOE-NNSA) with grant numbers DE-NA0001896 and DE-NA0002687, Department of Homeland Security-Scientific Leadership Award, Grant No. DHS-SLA 2014-ST-062-000060.

5:00pm SE+2D+EM-WeA9 Effects of Composition and Strain on Band Gaps of Pseudomorphic Ge_{1-x-y}Si_xSn_y on Ge, Nalin Fernando, New Mexico State University; R. Hickey, J. Hart, R. Hazbun, D. Zhang, J. Kolodzey, University of Delaware; S. Zollner, New Mexico State University

Ge-Si-Sn alloys are interesting for CMOS applications for a variety of reasons. For example, adding Sn to Si-Ge lowers the band gap, which reduces parasitic contact resistance. Also, the lattice constant of Ge-Sn alloys increases when adding Sn. Therefore, such alloys could be used to impart strain on PMOS devices with Ge channels. We used deformation potential theory to determine the compositional dependence of the direct, indirect, E₁, and E₁+Δ₁ band gaps of pseudomorphic Ge_{1-x-y}Si_xSn_y on Ge and theoretical predictions are validated through spectroscopic ellipsometry measurements of the band gaps of pseudomorphic Ge_{1-y}Sn_y on Ge grown by MBE.

The band structure of Ge is a strong function of strain and alloy composition, and a transition from an indirect to a direct band gap has been observed for y~6-10% for relaxed Ge_{1-y}Sn_y indicating the possibility of

Wednesday Afternoon, November 9, 2016

widespread applications of Ge-based photonic devices. The pseudomorphic nature of the Ge-based alloy layer on a substrate is important to keep dislocation densities low at the interface to improve the performance of the device. Band gap engineering of Ge by controlling strain and alloying with Si and Sn has attracted great interest since a $\text{Ge}_{1-x}\text{Si}_x\text{Sn}_y$ ternary alloy with two compositional degrees of freedom allows decoupling of the lattice constant and electronic structures.

The pseudomorphically grown $\text{Ge}_{1-x}\text{Si}_x\text{Sn}_y$ layer on Ge experiences a biaxial stress due to the lattice mismatch between the alloy layer and the Ge. The strain resulting from the stress affects the band structure of the alloy. Deformation potential theory is used to determine the compositional dependence of the band gaps of pseudomorphic $\text{Ge}_{1-x}\text{Si}_x\text{Sn}_y$ on Ge as a function of Si (x) and Sn (y) compositions. The predictions of the deformation potential theory are validated for pseudomorphic $\text{Ge}_{1-y}\text{Sn}_y$ (for Si=0) on Ge through measurements of the optical properties. The complex pseudodielectric functions of pseudomorphic $\text{Ge}_{1-y}\text{Sn}_y$ alloys grown on Ge by MBE were measured using ellipsometry in the 0.1-6.6 eV energy range for Sn contents up to 11%, to investigate the compositional dependence of the band gaps. Critical point energies (CP) and related parameters were obtained by analyzing the second derivative spectrum of the dielectric function. Our experimental results for E_g^{dir} , E_1 and $E_1 + \Delta_1$ gaps are in good agreement with the theoretically predicted CP energies. We will discuss the strain and compositional dependence of the band gaps and the effects of the growth temperature of the Ge buffer layer on Si to the band gaps.

This work was supported by AFOSR (FA9550-13-1-00222). FTIR measurements were performed at CINT.

5:20pm SE+2D+EM-WeA10 MBE Growth of Hexagonal Boron Nitride for use in Novel Electronic Devices, Adam Barton, R. Yue, C.M. Smyth, R. Addou, L. Cheng, R.M. Wallace, J. Kim, M. Kim, J. Hsu, K.J. Cho, The University of Texas at Dallas; L. Colombo, Texas Instruments; C.L. Hinkle, The University of Texas at Dallas

2D materials offer unique opportunities in device fabrication due to the weak van der Waals interaction between crystalline layers that allows for the growth of high-quality heterostructures with significantly less impact from lattice mismatch with the substrate. Hexagonal boron nitride (hBN) has a honeycomb structure similar to graphene except with alternating boron and nitrogen atoms. The hexagonal rings are composed of six sp^2 -hybridized atoms (three boron atoms and three nitrogen atoms). The electronic structure results in a bandgap of 5-7eV, a low- κ dielectric constant of 2-4 ϵ_0 , and an electron affinity of roughly 2 eV. These electronic properties make hBN an exciting material for a wide range of applications in electronic devices. In particular, we are interested in coupling hBN with transition metal dichalcogenides (TMDs) for low-power tunnel FET applications. Previous publications have primarily utilized chemical vapor deposition (CVD) to grow hBN on catalyzing transition metal substrates (Co, Ni, Cu, etc.) at growth temperatures ranging from 800-1200°C. However, these substrates and growth temperatures are not practical for the majority of device applications. Chalcogen loss in TMDs, for example occurs well below those temperatures.

In this work we report on our recent findings on the growth and characterization of hBN thin films grown by molecular beam epitaxy (MBE). This will include a detailed discussion of the growth mechanism on a variety of substrates (MoS_2 , HOPG, WSe_2 , Bi_2Se_3 , and sapphire) using substrate growth temperatures ranging from 300-800°C. The impact of the source fluxes, substrate temperatures, and in particular, the presence of atomic hydrogen during growth will be presented. The hexagonal phase of BN is achieved as determined by diffraction, Raman, and XPS. AFM, TEM, and RHEED are also used to assess film quality and the experimentally determined bandgap and band alignment will be presented. We will also present our recent work on coupling hBN with ALD-deposited Al_2O_3 to enable higher-k gate dielectrics on top of 2D materials heterostructures.

This work is supported in part by the SWAN Center, a SRC center sponsored by the Nanoelectronics Research Initiative and NIST. This work was also supported in part by the Texas Higher Education Coordinating Board's Norman Hackerman Advanced Research Program.

5:40pm SE+2D+EM-WeA11 Passivation of Interfaces Between High-k Dielectrics and SiGe: Ex Situ Wet Sulfur Clean vs. In Situ Plasma Nitridation, Kasra Sardashti*, M.S. Clemons, UC San Diego; M. Yakimov, SUNY College of Nanoscale Science and Engineering; K. Tang, Stanford University; S. Oktyabrsky, SUNY College of Nanoscale Science and Engineering; P.C. McIntyre, Stanford University; L. Dong, N. Yoshida, Applied Materials, Inc.; A.C. Kummel, UC San Diego

Silicon-Germanium is a promising channel material to be used in novel CMOS device architectures such as FinFET and Nanowire FET, due to its high hole mobility. Moreover, it enables control of carrier mobility by mechanical stress and band gap by variation in Si/Ge content in multilayer design. One of the important issues to address in the integration of SiGe in the MOS devices is formation of low-defect interfaces with very thin high-k gate dielectrics such as Al_2O_3 , HfO_2 and ZrO_2 . Due to adverse effect of Ge sub-oxide (GeO_x) formation and subsequent Ge out-diffusion on the performance of the devices, robust strategies to control the Ge reactions during and after oxide deposition are essential to further the development of SiGe FETs. This study determines the effects of two passivation methods on the quality of the interfaces between SiGe and high-k dielectrics: 1) Ex-situ wet sulfur passivation using $(\text{NH}_4)_2\text{S}$ solution; 2) In-situ NH_3 plasma nitridation. Al_2O_3 and HfO_2 were deposited on SiGe surfaces by atomic layer deposition (ALD). Electrical and chemical properties of the interfaces were evaluated by capacitance-voltage (C-V) spectroscopy, angle-resolved photoelectron spectroscopy (AR-XPS) and time-of-flight secondary ion mass spectroscopy (ToF-SIMS). Both sulfur passivation and plasma nitridation resulted in smaller density of interface traps with a large majority of the trap energy levels adjacent to the valence band edge. Ex-situ sulfur passivation was found to improve the interface quality by reducing the extent of GeO_x formation at the high-k/SiGe interface, therefore constraining the extent of Ge out-diffusion within the oxide. The mechanism is distinct; sulfur forms much stronger bonds to Ge than to Si due to the d-orbitals on the Ge; this promotes selective oxidation of the Si and prevents formation of GeO_x . Using plasma nitridation, a thin layer of SiON forms selectively at the high-k/SiGe interfaces, preventing the presence of thermally-unstable species such as GeO_x and GeON . In addition, SiON can act as a physical diffusion barrier to Ge out-diffusion. The nitridation is selective due to the higher enthalpy of formation for Si vs Ge oxynitrides. Both ex-situ sulfur passivation and in-situ NH_3 plasma nitridation were found to be effective approaches in preparing low-defect $\text{Al}_2\text{O}_3/\text{SiGe}$ and HfO_2/SiGe interfaces; the different chemical mechanisms show there are multiple paths to selective bond formation to SiGe which can be utilized to engineer low-defect stable interfaces.

6:00pm SE+2D+EM-WeA12 Enhanced Voltage Control of Perpendicular Magnetic Anisotropy in Magnetic Tunnel Junctions Using Ultrathin PZT Composite Oxide Tunneling Barriers, Kevin Fitzell, X. Li, K. Wong, G. Yu, S. Robbenolt, S.H. Tolbert, P.K. Amiri, K.L. Wang, J.P. Chang, University of California at Los Angeles

In contrast to manipulating magnetization with applied current, using an applied electric field can significantly reduce the required energy and result in less heat generation, leading to increased energy density. This can be accomplished using the voltage-controlled magnetic anisotropy (VCMA) effect, which forms the basis of next-generation magnetoelectric MRAM devices. Specifically, applying an electric field across a CoFeB/MgO interface can decrease the perpendicular magnetic anisotropy field as a result of the altered electron density at the interface, thus destabilizing the magnetization state and allowing for its efficient and deterministic reorientation with a small applied magnetic field. This operation principle stands in contrast to that of STT-RAM, which uses upwards of 100 fJ to write a single bit (300,000 times more energy than the actual energy barrier to switching).

Previous research on $\text{CoFeB}/\text{oxide}$ interfaces has shown that increasing the dielectric constant of the oxide layer also increases the sensitivity of the interfacial magnetic anisotropy energy to an applied electric field. Lead zirconate titanate (PZT), having excellent ferroelectric properties including a large dielectric constant, is therefore a prime candidate for integration into such oxide layers in an attempt to maximize the VCMA effect. Using atomic layer deposition (ALD), PZT was thus incorporated into magnetic tunnel junctions having $\text{MgO}/\text{PZT}/\text{MgO}$ multilayer composite tunneling barriers. Our group has shown that MRAM devices fabricated using these $\text{MgO}/\text{PZT}/\text{MgO}$ tunneling barriers resulted in a 40% increase in the VCMA coefficient (and thus substantial energy savings) over magnetic tunnel junctions simply employing MgO tunneling barriers, despite the PZT layer

being amorphous. Our most recent work has focused on the crystallization of these ultrathin PZT layers, which would cause an even larger dielectric response (even greater energy savings) and open an avenue toward four-state memory devices relying on the ferroelectric polarization of the PZT.

Surface Science

Room 104D - Session SS+AS+EM-WeA

Semiconductor Surfaces and Interfaces

Moderator: Andrew Gellman, Carnegie Mellon University

2:20pm SS+AS+EM-WeA1 Adsorption of Triethylenediamine on Si(100)-2x1 Surface via N-Si Dative Bonding and C-N Dissociation, Jing Zhao, M. Madachik, University of Delaware; K. O'Donnell, Curtin University, Australia; O. Warschkow, University of Sydney, Australia; L. Thomsen, Australian Synchrotron, Australia; G. Moore, S. Schofield, University College London; A.V. Teplyakov, University of Delaware

The functionalization of silicon surfaces with thin layers of organic materials is an important area of studies with current and potential applications in microelectronics, catalysis, and bio-sensing. Triethylenediamine (also known as 1,4-diazabicyclo[2.2.2]octane, or DABCO) presents an interesting case study for silicon functionalization because of its symmetric structure with two x nitrogen atoms in tertiary amine configuration. Each of these atoms could potentially form a dative bond with a clean Si(100)-2x1 surface while the other may remain accessible for further modification. We applied infrared spectroscopy (MIR-FTIR), X-ray photoelectron spectroscopy (XPS), and temperature programmed desorption (TPD) supported by density functional theory calculations (DFT) to investigate the reaction mechanism of triethylenediamine with a clean Si(100)-2x1 surface, focusing specifically on dative bond formation and C-N dissociation.

2:40pm SS+AS+EM-WeA2 Chemoselective Adsorption of Functionalized Cyclooctynes on Silicon, M. Reutzel, N. Munster, M.A. Lipponer, Philipps-Universität Marburg, Germany; C. Langer, Justus Liebig University Giessen, Germany; U. Hofer, U. Koert, Philipps-Universität Marburg, Germany; Michael Durr, Justus Liebig University Giessen, Germany

The adsorption of organic molecules on silicon surfaces has been subject of intense research due to the potential applications of organic functionalization of silicon surfaces in semiconductor technology. The high reactivity of the silicon dangling bonds, however, presents a major hindrance for the first basic reaction step of such a functionalization, i.e., chemoselective attachment of bifunctional organic molecules on the pristine silicon surface. Due to the high reactivity of the dangling bonds, each functional group of a bifunctional molecule adsorbs with an initial sticking coefficient close to unity and thus the final adsorption product will typically consist of a mixture of molecules adsorbed via different functional groups.

We overcome this problem employing cyclooctyne as the major building block of our strategy. Using scanning tunneling microscopy and X-ray photoelectron spectroscopy, cyclooctyne derivatives with different functional side groups are shown to react on Si(001) selectively via the strained cyclooctyne triple bond while leaving the side groups intact. The origin of this chemoselectivity is traced back to the different adsorption dynamics of the functional groups involved. We show that cyclooctyne's strained triple bond is associated with a direct adsorption channel on the Si(001) surface, in contrast to most other organic molecules which adsorb via weakly bound intermediates. In these intermediate states, the molecules have a finite lifetime and are often mobile and free to rotate on the surface. This allows the bifunctional molecule to sample the surface with the strained triple bond during its finite lifetime in the trapped state and in consequence, bifunctional molecules with a strained triple bond as one functional group will end up with this group attached to Si(001) even if the initial interaction proceeds via the second functional group.

Chemoselectivity can thus be achieved even on the highly reactive Si(001) surface when exploiting the adsorption dynamics of the respective reaction channels.

3:00pm SS+AS+EM-WeA3 Compositions, Structures, and Electronic Properties of Grain Boundaries of Cu(InGa)Se₂, Xudong Xiao, Chinese University of Hong Kong

INVITED

Polycrystalline semiconductors are important energy materials and the grain boundaries play crucial role in their electrical transport property. While in general grain boundary is detrimental, for Cu(InGa)Se₂ (CIGS), it

was found that the grain boundary is benign to the electrical transport and a record solar cell energy conversion efficiency of 22.3%, the best among all thin film solar cells, has been achieved with a polycrystalline film. This peculiar benign behavior has attracted great attention in the materials science community, unfortunately, even with tremendous effort, the mechanism of the benignity of CIGS grain boundary remains as an outstanding problem, mostly due to the lack of convincing experimental evidences.

We performed our study by design and prepare well controlled CIGS samples with two different Cu content. By careful treatment of the samples to remove artifacts, we used a combination of techniques, namely AFM, STM, and TEM, to probe at nanoscales the composition, structure, and electrical properties of the individual grain boundary in direct comparison to those of the individual grain interior. We discovered that the grain boundary in fact consists of a boundary layer of finite thickness in addition to the grain boundary surface/interface for the non $\Sigma 3$ grain boundaries. This boundary layer has a definitive composition, structure, and electronic band, independent of the overall Cu content in the CIGS films. The observation of similar grain interior and similar grain boundary except the boundary layer thickness for the two samples with very different overall Cu content is indeed a surprising finding that has never been reported before. The band alignment between grain boundary and grain interior was discovered to be of type II with downward offset for both conduction and valence bands at grain boundary, well correlating to the local copper deficiency and structure. Our findings expressively support the type inversion and large hole barrier in this grain boundary layer, and establish a comprehensive mechanism for the suppression of carrier recombination therein.

4:20pm SS+AS+EM-WeA7 Thermal Self-limiting CVD Silicon and ALD Silicon Nitride Containing Control Layers on In_{0.53}Ga_{0.47}As(001)-(2x4), Si_{0.5}Ge_{0.5}(110), and Si_{0.7}Ge_{0.3}(001), Steven Wolf, M. Edmonds, T. Kent, K. Sardashti, University of California at San Diego; M. Chang, J. Kachian, Applied Materials; R. Droopad, Texas State University; E. Chagarov, A.C. Kummel, University of California at San Diego

Compound semiconductors with high mobilities such as InGaAs and SiGe are being employed in metal oxide semiconductor field effect transistors (MOSFETs) to increase transistor performance. However, these surfaces contain dangling bonds that can affect the surface Fermi level; thus, depositing a control layer via ALD or self-limiting CVD on multiple materials and crystallographic faces is required. Silicon uniquely bonds strongly to all crystallographic faces of InGa_{1-x}As, In_xGa_{1-x}Sb, In_xGa_{1-x}N, SiGe, and Ge enabling transfer of substrate dangling bonds to silicon, which can then be passivated by atomic hydrogen. Subsequently, the surface may be functionalized with an oxidant such as HOOH in order to create a terminating Si-OH layer, or a nitriding agent such as N₂H₄ in order to create an Si-N_x diffusion barrier and surface protection layer. This study focuses on depositing saturated Si-H_x and Si-OH seed layers via a self-limiting CVD process on InGaAs(001)-(2x4), and depositing a Si-N_x seed layer on Si_{0.5}Ge_{0.5}(110) and Si_{0.7}Ge_{0.3}(001) via an ALD process. XPS in combination with STS/STM were employed to characterize the electrical and surface properties of these control layers on the various surfaces. A thin Si-H_x capping layer (2.5 monolayers) was deposited in a self-limiting CVD fashion on InGaAs(001)-(2x4) by exposing to Si₂Cl₆ at 350°C. This layer allows for multilayer silicon or Si-O_x growth by ALD through cyclically dosing Si₂Cl₆ with either atomic H or anhydrous HOOH. STM and STS measurements show the Si₂Cl₆ exposed InGaAs(001)-(2x4) surface is atomically locally ordered and has an unpinned surface Fermi level. Exposure to anhydrous HOOH at 350°C terminates the surface with Si-O bonds and does not lead to oxidation of substrate peaks. The HOOH treated surface then nucleates TMA at 250°C and ultimately further high-k gate oxide growth. MOSCAP device fabrication was performed on n-type InGaAs(001) substrates with and without a Si-H_x passivation control layer deposited by self-limiting CVD in order to determine the effects on C_{max}, frequency dispersion, and midgap trap states. Deposition of a SiO_xN_y diffusion barrier and surface protection layer was achieved on the Si_{0.5}Ge_{0.5}(110) and Si_{0.7}Ge_{0.3}(001) surfaces via an ALD process at 275°C through cyclically dosing Si₂Cl₆ and anhydrous N₂H₄. MOSCAP device fabrication was performed on Si_{0.7}Ge_{0.3}(001) with and without a SiO_xN_y passivation control layer to compare device performance. Ultimately, the Si-H_x passivation layer gave less frequency dispersion at flat band and a lower D_{it}, and the SiO_xN_y passivation layer yielded lower gate leakage and D_{it} when compared to the respective wet clean only devices.

4:40pm **SS+AS+EM-WeA8 Formation of Atomically Ordered and Chemically Selective Si-O-Ti Monolayer on $\text{Si}_{0.5}\text{Ge}_{0.5}$ (110) for a MIS Structure via $\text{H}_2\text{O}_2(\text{g})$ Functionalization, SangWook Park, J.Y. Choi, University of California, San Diego; E. Chagarov, University of California, San Diego; B. Sahu, S. Siddiqui, GLOBALFOUNDRIES; N. Yoshida, J. Kachian, Applied Materials; A.C. Kummel, University of California, San Diego**

To overcome challenges when scaling down silicon-based complementary metal-oxide semiconductor (CMOS) devices, SiGe has received much attention due to its high carrier mobility and applications in strain engineering. Extremely thin oxides with appropriate band offsets can be utilized to form unpinned contacts on SiGe for a metal-insulator-semiconductor (MIS) structure. The TiO_2 interfacial layer on Ge is known to form a MIS structure which reduces the tunneling resistance due to the nearly zero conduction band offset (CBO) between TiO_2 and Ge. In this study, formation of TiO_x monolayer on SiGe(110) via $\text{H}_2\text{O}_2(\text{g})$ functionalization was investigated using *in-situ* scanning tunneling microscopy (STM), scanning tunneling spectroscopy (STS), and x-ray photoelectron spectroscopy (XPS). $\text{H}_2\text{O}_2(\text{g})$ was employed instead of the conventional $\text{H}_2\text{O}(\text{g})$ oxidant since $\text{H}_2\text{O}_2(\text{g})$ can form a uniform monolayer of -OH ligands on the surface without subsurface oxidation which should be ideal for forming the most stable possible interface which is a layer of Si-O-Ti bonds. STM verified that clean $\text{Si}_{0.5}\text{Ge}_{0.5}$ (110) surfaces were terminated with both Si and Ge adatoms. STS measurements indicated that the Fermi level of clean $\text{Si}_{0.5}\text{Ge}_{0.5}$ (110) surfaces was pinned near midgap between the valence and conduction band edges due to the half-filled dangling bonds of the adatoms. In order to passivate the dangling bonds, atomic H was dosed onto clean $\text{Si}_{0.5}\text{Ge}_{0.5}$ (110) at 300°C which unpinned the Fermi level as demonstrated by STS. XPS analysis showed a saturation dose of $\text{H}_2\text{O}_2(\text{g})$ at 25°C left the $\text{Si}_{0.5}\text{Ge}_{0.5}$ (110) surfaces terminated with a monolayer of both Ge-OH and Si-OH sites. STS indicated that the Fermi level on $\text{H}_2\text{O}_2(\text{g})$ dosed $\text{Si}_{0.5}\text{Ge}_{0.5}$ (110) was shifted to near the valence band edge due to the formation of surface dipoles induced by hydroxyl bonds. Tetrakis(dimethylamido)titanium (TDMAT) or titanium tetrachloride (TiCl_4) was subsequently dosed onto hydroxyl-terminated $\text{Si}_{0.5}\text{Ge}_{0.5}$ (110) at 25°C forming Ti bonds on surface. Both TDMAT and TiCl_4 dosed $\text{Si}_{0.5}\text{Ge}_{0.5}$ (110) surfaces were annealed at 300°C and XPS verified that the Ti-O bonds were totally transferred from Ge atoms to Si atoms forming exclusively Ti-O-Si bonds on $\text{Si}_{0.5}\text{Ge}_{0.5}$ (110) surfaces consistent with the strong bonding between Si and oxygen pulling Si atoms toward the surface to bond with oxygen while pushing Ge atoms into the subsurface during the annealing. STM demonstrated an ordered TiO_x monolayer was formed with a row spacing which doubles the spacing of adatoms on clean $\text{Si}_{0.5}\text{Ge}_{0.5}$ (110). In addition, STS indicated a TiO_x monolayer on SiGe(110) was unpinned and therefore can serve as an ultra-thin insulating layer for a MIS structure.

5:00pm **SS+AS+EM-WeA9 The Effect of Ultrasonic Treatment (UST) on the Defect Structure of the Si-SiO₂ System, Daniel Kropman, T. Laas, Tallinn University, Estonia**

The effect of ultrasonic treatment (UST) on the defect structure of the Si-SiO₂ system by means of electron spin resonance (ESR), selective etching, MOS capacitance technique and secondary ions mass-spectroscopy is presented. The non-monotonous dependence of the defect densities on the US wave intensity has been observed. The influence of the UST frequency on the ESR signal intensity of the defect centres depended on the defects type and may be caused by vibration energy dissipation, which are a function of defect centres type. In the ESR spectra of Si samples a signal with $g=1.9996$ (Pa centres) connected with vacancy complexes is observed. After UST appears another signal with $g=2.0055$ (broken bonds of Si atoms). The influence of the US frequency and sample orientation on the ESR signal intensity varies for different centres. The frequency and orientation dependence of the ESR signal with $g=1.9996$ and the lack of this dependence for the centres with $g=2.0055$ show that vibration energy dissipation depends on the type of defect centers. Defect density at the interface grows with an increase of US wave intensity or changes nonmonotonously depending on the oxide thickness and crystallographic orientation. In the samples with thick oxide/0,6 mkm there is a maximum in the dependence of the charge carriers lifetime on the US wave amplitude and in the samples with thin oxides /0,3 mkm/ there is a minimum. This shows that the structural defects form electrically active centres and their density can be varied by US. The density of point defects and absorbed impurities at the Si-SiO₂ interface can be reduced and its electrical parameters improved by an appropriate choice of the UST and oxidation condition. US is widely used not only for materials treatment but in medicine as well (cancer treatment).

References:

[1] D. Kropman, V. Poll, L. Tambek, T. Karner, U. Abbru. Ultrasonics 36(1998)10211025

[2] D. Kropman, S. Dolgov. Physica stat. Sol. (c) v.9, issue 10-11, pp.2173-2176, 2012.

5:20pm **SS+AS+EM-WeA10 Adsorption of C₆₀ Buckminster Fullerenes on a Carbon-free Hydrazine-modified Silicon Surface, Fei Gao*, A.V. Teplyakov, University of Delaware**

Buckminster fullerene C₆₀ was used as a model to understand the attachment chemistry of large molecules on amine-terminated semiconductor surfaces. The resulting interface may serve as a foundation for devices in such fields as solar energy conversion, biosensing, catalysis, and molecular electronics. In this work, a monolayer of buckminster fullerenes C₆₀ was covalently attached to silicon surfaces using an efficient wet chemistry method. The starting chlorine-terminated Si(111) surface was initially modified with hydrazine to produce NH-NH functionality. Then the C₆₀ fullerenes were reacted directly with this surface. The chemical state and surface topography of the C₆₀-modified surface were characterized by surface analytical spectroscopic and microscopic methods, including X-ray photoelectron spectroscopy (XPS), time-of-flight secondary ion mass spectrometry (TOF-SIMS), and atomic-force microscopy (AFM). The experimental results were also supported by computational investigation, density functional theory (DFT) calculations, that were performed to predict core-level energies of surface species formed and to propose the possible mechanism of surface reactions.

5:40pm **SS+AS+EM-WeA11 Passivation of SiGe Surfaces with Aqueous Ammonium Sulfide, Stacy Heslop, A.J. Muscat, University of Arizona**

Ge and SiGe are promising materials for future p-type metal-oxide semiconductor field effect transistors (MOSFETs) due to their higher hole mobilities and narrower bandgap compared to Si. In contrast to silicon, Ge and SiGe readily oxidize in ambient air forming nonstoichiometric Ge oxides that are detrimental to the electrical performance of the device. One approach is to remove these oxides and passivate the surface. SiGe with molar ratios of 25 and 75% Ge were treated with aqueous ammonium sulfide, (NH₄)₂S, to deposit sulfur. The composition of the surface was measured using x-ray photoelectron spectroscopy (XPS) as a function of concentration and pH. The (NH₄)₂S concentration was varied from 3 mM to 3 M, and the pH was varied from 10 to 8 using HCl and HF. Film thicknesses were measured with spectroscopic ellipsometry.

A fresh SiGe starting surface was produced by immersing in SC-1 (1:1:500 v/v) to form oxides and stripping the oxides using HF:HCl:H₂O (1:3:300 v/v). In the case of SiGe 25%, sulfides were not detected based on the S 2p XPS state for surfaces treated with (NH₄)₂S (Figure 1a). The oxygen coverage increased with increasing (NH₄)₂S concentration, forming primarily SiO₂ and a small coverage of GeO. The surface was enriched in Si and oxidized, and there was not enough Ge atoms exposed for S to bond to. HCl and HF were added to remove the Si and Ge oxides that formed. The addition of HCl and HF resulted in the deposition of sulfides on SiGe 25% (Figure 1b). The Si/Ge peak area ratio after oxide removal was 1.7. After immersion in 30 mM (NH₄)₂S at a pH of 10 the surface composition was unchanged (Si/Ge=1.7). For the same (NH₄)₂S concentration at a pH of 8 the surface was only slightly enriched with Si (Si/Ge=2.4). Overall, (NH₄)₂S is not an effective passivation reagent for Si-rich SiGe surfaces due to the lack of S deposited and the undesirable oxides which form during processing. By dropping the pH to 8, less than a monolayer of S is deposited but oxides still remain. In contrast, SiGe 75% did not oxidize as a function of the (NH₄)₂S concentration. Sulfur was detected based on the S 2p XPS state and the S coverage was independent of (NH₄)₂S concentration. The sulfur thickness increased from about 2.3 Å for (NH₄)₂S (30 mM or 1:100 v/v) at a pH of 10 to 3.4 Å for the same (NH₄)₂S dilution at a pH of 8 (Figure 1c and d). These film thicknesses were approximated from XPS peak areas based on a single layer model for S on Ge. The deposition of the S layer did not affect the surface stoichiometry between oxide removal steps (Si/Ge=0.19) and 30 mM passivation (Si/Ge=0.20).

6:00pm **SS+AS+EM-WeA12 Novel Electrical Circuit Model for the Design of InGaAs/GaAs (001) Strained-Layer-Super-Lattice, Tedi Kujofsa, J.E. Ayers, University of Connecticut**

Understanding lattice relaxation and dislocation dynamics has important implications in the design of highly functional and reliable semiconductor device heterostructures. Strain-layer-superlattices (SLs) have been commonly used as dislocation filters whereby threading dislocations (TDs)

can be removed by the insertion of a series of mismatched interfaces. The reduction of the threading dislocation in SLSs can be explained by the bending over of TDs associated with misfit segments of one sense by misfit dislocations having the opposite sense. Furthermore, the use of multilayered metamorphic buffer layers (MBLs) with intentionally mismatched interfaces may be used to take advantage of the strain compensation mechanism.

Previously, we developed a generalized energy minimization model, which determines the equilibrium configuration of an arbitrary compositionally-graded or multilayered heterostructure. The present work focuses on the development of a *novel electrical circuit* model for understanding equilibrium lattice relaxation in InGaAs/GaAs (001) strained-layer-superlattice heterostructures. This work focuses on the design of the SLS buffer layer of $\text{In}_x\text{Ga}_{1-x}\text{As}$ deposited on a GaAs (001) substrate. The SL contains a set of 10 uniform layers with alternating mismatch. In other words, the SSL contains alternating uniform layers of $\text{In}_x\text{Ga}_{1-x}\text{As}$ with indium compositions x and $x + \Delta x$ respectively. For each structure, we present minimum energy calculations and show that for a given SLS total layer thickness h_{SLS} , it is possible to find the combination x and Δx such that it provides tight control of the in-plane strain of the strained-layer-superlattice. In addition, for each structure type we present minimum energy calculations by studying the (i) depth profile of strain and (ii) the misfit dislocation density profile. Most importantly, the use of the electrical circuit model allows the analysis of semiconductor heterostructures using a standard SPICE circuit simulator and provides an intuitive understanding of the relaxation process in these multilayered heterostructures.

Thin Film

Room 105A - Session TF+EM+MI-WeA

Thin Films for Microelectronics

Moderators: Paul Poodt, Holst Centre / TNO, Netherlands, Christophe Vallee, LTM, Univ. Grenoble Alpes, CEA-LETI, France

2:20pm TF+EM+MI-WeA1 Impact of ALD VO_2 Film Thickness on the Electrical and Optical Properties of the Metal-Insulator Phase Transition, Virginia Wheeler, B.P. Downey, J. Roussos, M. Currie, A. Giles, C. Ellis, J. Tischler, J. Caldwell, D.J. Meyer, C.R. Eddy, Jr., U.S. Naval Research Laboratory

VO_2 films are known to undergo a metal-insulator phase transition (MIT) at a critical temperature ($T_c = 68^\circ\text{C}$) near room temperature which results in significant changes in thermal emittance, optical transmittance and reflectance, and intrinsic electrical properties; thus attracting interest in a variety of new electronic, optoelectronic, and photonic applications. Atomic layer deposition (ALD) provides a way to obtain large area film uniformity, abrupt interfaces and angstrom-scale control of thickness conformally across planar, as well as three-dimensional, high surface area nanostructures, which could be used to integrate VO_2 films into complex electronic and optical devices for additional functionality. In this work, VO_2 electrical devices and VO_2 coated SiC-based nanoresonators are used to investigate the impact of film thickness on electrical and optical properties.

The influence of VO_2 thickness on electrical performance was investigated using a simple two-terminal device structure. Sheet resistance measurements as a function of temperature revealed that the $R_{\text{off}}/R_{\text{on}}$ ratio increased with increasing VO_2 thickness, up to $R_{\text{off}}/R_{\text{on}}$ of ~ 7000 for a 92 nm film. Similarly, the T_c increased slightly with increasing thickness ($T_c = 66^\circ\text{C}$ for 35nm, 73°C for 92nm), while all films show relatively low hysteresis ($\Delta T < 8^\circ\text{C}$). Initial small-signal rf measurements using the 92 nm ALD VO_2 film demonstrated a cut-off frequency of greater than 1 THz, indicating the potential for rf-switch applications into millimeter wavelength frequencies using these ultra-thin ALD films, and the potential of these films to be conformally integrated into complex circuits with an ALD process.

For applications in the infrared, surface phonon-polariton-based SiC nanoresonators exhibiting strong, narrowband absorption features within the 10-12.5 μm range were coated with different thickness ALD VO_2 films. Since these films are transparent to infrared light below the T_c and reflective above the T_c , conformally coating these SiC nanostructures provides a way to add functionality to these structures by modulating the amplitude of the resonances with temperature. Initial results show that the magnitude of the resonance suppression increases with increasing VO_2 thickness and a VO_2 film thickness greater than 16nm is required to fully inhibit the signal. It was also determined that the SiC resonances become increasingly shifted and broadened with increasing thickness of the VO_2

coating. These results suggest that VO_2 can add active tunability and integrated switching to optical structures.

2:40pm TF+EM+MI-WeA2 Study of Ru Silicidation with and without Sub-nm ALD TiN and TaN Barrier/nucleation Layers for Ru Interconnect Applications, Sonal Dey, SUNY College of Nanoscale Science and Engineering; K.-H. Yu, S. Consiglio, K. Tapily, C.S. Wajda, G.J. Leusink, TEL Technology Center, America, LLC; J. Jordan-Sweet, C. Lavoie, IBM T.J. Watson Research Center; A.C. Diebold, SUNY College of Nanoscale Science and Engineering

With continual shrinkage of the feature size in devices, contribution of the Cu interconnects, liners, and barrier layers to the RC time-delay is becoming a significant obstacle at the 10 nm technology node and below. Ru is a potential candidate to replace Cu as an interconnect material for ultra-scaled line widths where scaling effects on Cu line resistance become increasingly problematic. Ru has already been demonstrated to be useful as the seed layer for Cu electroplating but has been shown to be an inadequate barrier to prevent Cu diffusion into surrounding BEOL dielectrics and requires the use of an additional barrier layer such as a Ta-based nitride. In addition, TaN deposited by PVD is reaching a limit in its ability to conformally coat aggressively scaled structures in the sub 10 nm node. Accordingly, in this study we evaluated the thermal stability of thin Ru films (3 nm) with and without ultra-thin (~ 0.5 nm) highly conformal ALD TiN and TaN films as nucleation and/or barrier layers for Ru interconnect applications in advanced technology nodes. Si (100) substrates were chemically cleaned to remove the native oxides followed by deposition of ultra-thin ALD TiN and TaN barrier films. TiCl_4 and $\text{Ta}(\text{NMe}_2)(\text{NetMe})_3$ precursors, along with NH_3 , were used for deposition of the TiN and TaN layers, respectively. Using $\text{Ru}_3(\text{CO})_{12}$, 3 nm of Ru was deposited by CVD on top of these refractory metal nitride films and also directly on Si. We also used PVD Cu (25nm)/Si as a control stack for our experiments. The diffusion kinetics of metal-silicide formation was evaluated using in-situ rapid thermal anneal (RTA) synchrotron x-ray diffraction (XRD) measurements and a Kissinger-like analysis to determine the transition temperatures of the metal-silicidation in these stacks and the effective activation energy (E_a) using three different ramp rates (0.3, 3, and 10°C/s). The Ru/Si stack showed higher $E_a = 2.48$ eV as compared to the Cu/Si stack ($E_a = 1.88$ eV). A 0.5 nm thick TaN ($E_a = 2.88$ eV) was found to act as a more effective barrier as compared to 0.5 nm thick TiN ($E_a = 2.64$ eV). Scanning electron microscopy (SEM) data shows that both TaN and TiN act as nucleation layers for the growth of Ru microstructure on top. A fewer number of pin holes was observed for Ru films deposited on TaN although there was not significant change on the wettability properties of the Ru film with either TiN and TaN nucleation layers underneath. Additional physical and chemical characterization with XPS and TOF SIMS were also performed to gain understanding of the film stack properties before and after silicide formation.

3:00pm TF+EM+MI-WeA3 2D - Material and Process Challenges of the Ultimate Thin Films in Nanoelectronics, Stefan de Gendt, KU Leuven, IMEC, Belgium; S. Brems, D. Chiappe, IMEC, Belgium; M. Heyne, K. Verguts, KU Leuven, IMEC, Belgium; R. Philipson, KU Leuven, Belgium; C. Lockhart de la Rosa, A. Delabie, KU Leuven, IMEC, Belgium; S. De Feyter, KU Leuven, Belgium; C. Huyghebaert, IMEC, Belgium

INVENTED
Graphene has emerged as one of the promising candidates for post-Si electronics, both for channel (Logic, RF, sensors) and interconnect applications. Further, other two-dimensional (2D) materials such as transition metal dichalcogenides (MX_2 , with M a transition metal of group 4-7 and X a chalcogen) have versatile properties that complement or even supersede those of graphene. Both categories however share similar problems, related to the absence of good quality synthesis processes, subsequent layer transfer processes and doping and contacting challenges. To tackle the **first challenge** – growth – chemical vapor deposition (CVD) is widely considered to be the most economically viable method to produce both graphene and MX_2 materials for high-end applications. However, in most cases, this deposition technique typically yields undesired grain boundaries in the 2D crystals, which drastically increases the sheet resistance of the layer. Strategies w.r.t. template and process development will be presented. Further, given growth temperature and template, direct growth on devices is often unfeasible, thus a **second challenge** relates to the requirement for a transfer process. For graphene, several transfer process possibilities have been evaluated, but up to now, the graphene transfer suffers from contamination often coming from the temporary support layer and/or etching products, wrinkle formation during bonding, crack formation during graphene handling, ... Moreover, with improvement in 2D quality the release from the growth template is hindered due to

increased adhesion forces. At least for MX₂ materials, the transfer challenge can be avoided through area selective growth. A process based on a reductive two step CVD process will be presented, whereby in a first step the metal precursor (WF₆) is reduced to a lower oxidation state through sacrificial reaction with Si. Subsequently, the metallic film is allowed to react with a sulphur precursor (H₂S). Challenges are again related to the (poly)crystallinity of the films and the control of lateral 2D versus crystal 3D growth. Last but not least, a **third challenge** related to 2D materials resides in the contacting and doping of these materials. Different strategies have been proposed to achieve doping, but in this presentation we will demonstrate the self-assembly of organic molecules physisorbed on top bulk and thin 2D layers as a means to achieve controlled doping.

4:40pm TF+EM+MI-WeA8 Atomic Layer Deposition of Stoichiometric TaSi₂ on Si(001), JongYoun Choi, S.W. Park, University of California San Diego; R. Hung, Applied Materials Inc.

Transition metal disilicides are of great interest in Metal-Oxide-Semiconductor Field Effect Transistors (MOSFETs) due to their ability to tune the work function at the metal contact in the source/drain regions. Various kinds of transition metal silicides such as TiSi₂, NiSi₂ and WSi₂ have been studied in previous decades, however, nanoscale studies of TaSi₂ are relatively scarce. Previously, Lemonds *et al.* successfully demonstrated atomic layer deposition (ALD) of tantalum silicide (TaSi_x) on SiO₂ using TaF₅ and Si₂H₆. In this work, it is demonstrated that using similar reaction conditions TaSi₂ can be grown by ALD process on oxide-free clean Si(001). The growth rate of TaSi₂ on Si(001) was monitored *in-situ* using a Quartz Crystal Microbalance (QCM) during the deposition. This enabled optimization of the TaF₅ and Si₂H₆ dosing to avoid chemical vapor deposition (CVD) components. Scanning tunneling microscopy (STM), X-ray photoelectron spectroscopy (XPS), scanning tunneling spectroscopy (STS) and atomic force microscopy (AFM) have been used to investigate the atomic and electronic structure of Si(001) surface after TaSi₂ thin film deposition. HF cleaned Si(001) was used for the substrate. The chemical composition was determined by XPS after ALD to be that of a stoichiometric TaSi₂ film formed on the Si substrate. The key variables in forming stoichiometric TaSi₂ are the ratio of the precursors and the surface temperatures. In the ALD process, a 100x fold excess of Si₂H₆ is required to prevent formation of TaOx; in addition, the surface temperature must be above 240C. These requirements for excess Si₂H₆ and a high surface temperature are likely due to high activation barrier to break the residual Ta-F bonds on the surface after the TaF₅ half pulse since the Ta-F bonds are stronger than the Si-H bonds.

5:00pm TF+EM+MI-WeA9 Different Approaches for Enhancing the Thermal Stability of Ge₂Sb₂Te₅ Thin Films by Carbon Addition, David Adams, K. Childs, T. Gurrieri, W. Rice, Sandia National Laboratories

Different forms of carbon-doped Ge₂Sb₂Te₅ chalcogenide thin films have been evaluated for potential use in phase change memory and thermal sensor applications. This includes films sputter deposited from single, carbon-doped targets and refined multilayers made by sequential deposition of chalcogenide and C layers. In both forms, the crystallization temperature (T_{crys}) and the resistance change through crystallization vary with carbon content. Doped chalcogenide films sputter deposited from single targets exhibit increased T_{crys} as the concentration of C is made larger. For example, films having ~7 at.% C exhibit a T_{crys} that is approximately one hundred and fifteen degrees above that of undoped Ge₂Sb₂Te₅. Films with reduced C content, in the range 1-6 at.%, show intermediate crystallization temperatures. Multilayers fabricated by the sequential deposition of thin chalcogenide and C layers behave much like films grown from single targets, provided that multilayer periodicity is made small, < 3 nm. The crystallization temperature of multilayers also increases with C concentration and a prompt transition to a crystalline phase is observed when the carbon content is low. Interestingly, multilayers made with ≥ 9 at.% C do not transition abruptly to a crystalline state. Instead, a transformation occurs over a broad range of elevated temperature. Each form of chalcogenide thin film exhibits a decreased resistivity upon crystallization. In most cases, resistivity is reduced by 5 decades upon transforming to a face centered cubic structure or a subsequent hexagonal close packed lattice at higher temperature. The changes to microstructure and thickness associated with phase change will also be described. These film properties are investigated by cross-section and plan view electron microscopy.

This work was supported by Sandia National Laboratories. Sandia National Laboratories is a multi-program laboratory managed and operated by Sandia Corporation, a wholly owned subsidiary of Lockheed Martin

Company, for the United States Department of Energy's National Nuclear Security Administration under Contract DE-AC04-94AL85000.

5:20pm TF+EM+MI-WeA10 Comparison of Electromigration and Resistivity in On-chip Co and Cu Damascene Nanowires, C.-K. Hu, J. Kelly, J.H.-C. Chen, H. Huang, Y. Ostrovski, R. Patlolla, B. Peethala, P. Adusumilli, T. Spooner, IBM Research Division, Albany; L. Gignac, S. Cohen, IBM Research Division, T.J. Watson Research Center; R. Long, G. Hornicek, T. Kane, G. Lian, M. Ali, IBM Systems; V.M. Kaminen, F. Mont, S. Siddiqui, GLOBALFOUNDRIES

Cu metallization has been used for back end of the line (BEOL) on-chip interconnections since 1997. However, scaling Cu BEOL dimensions has increased Cu resistivity and degraded electromigration (EM) reliability. The Cu effective resistance has increased rapidly as the interconnect size has reduced and the ratio of liner area to total interconnect cross sectional area has increased. This size effect was caused primarily by increasing the probability of electron scattering with interfaces and grain boundaries. The EM lifetime degradation was caused by an increase in the volume fractions of diffusing atoms at interfaces and grain boundaries and a decrease in the void volume required to cause EM failure. It is estimated that ~ 70% of interconnect metal area could be occupied by the liner in the 5 nm technology node for reliable Cu metallization. To this end, an alternate metal, Co, was investigated. Multi-level Co BEOL was fabricated using typical 10 nm node technology wafer processing steps. A Co dual damascene process was used to fill the interconnect trenches and holes. The present Co resistivity study showed a similar size effect in Co as in Cu. This can be explained by the fact that the slope of resistivity vs. interconnect size is proportional to the product of the electron mean free path and resistivity, with the two slopes being about the same for Cu and Co. The effective resistivity difference between Co and Cu becomes small when no liner is used in Co lines. EM in 22 nm to 88 nm wide Co lines was tested using sample temperatures from 376°C to 425°C. Two-level EM structures consisted of either Co M1 to Co V1 to Co M2 or W CA to Co V0 to Co M1. The EM stress conditions for Co were far more severe than those for Cu. For comparison, EM in 24 nm wide Cu lines with a Co cap was also included. These data showed that both Co and Cu BEOL were highly reliable EM.

This work was performed by the Research Alliance Teams at various IBM Research and Development Facilities

5:40pm TF+EM+MI-WeA11 UV/VUV Curing Process for Low-k Organosilicate Dielectrics, Huifeng Zheng, X. Guo, D. Pei, W. Li, J. Blatz, K. Hsu, D. Benjamin, University of Wisconsin-Madison; Y. Lin, H. Fung, C. Chen, National Synchrotron Radiation Research Center, Taiwan, Republic of China; Y. Nishi, Stanford University; J.L. Shohet, University of Wisconsin-Madison

Porous SiCOH films are of great interest in semiconductor fabrication due to their low-k properties. Post-deposition treatments of SiCOH thin films are required to decompose labile pore generators (porogens) and to ensure optimum network formation to improve the electrical and mechanical properties of low-k dielectrics. The goal of this work is to optimize the vacuum-ultraviolet spectrum to identify those wavelengths that will have the most beneficial effect on improving dielectric properties and minimizing damage without the need for thermal heating of the dielectric. Vacuum ultraviolet (VUV) irradiation between 8.3-8.9 eV was found to increase the hardness and elastic modulus of low-k dielectrics at room temperature. Combined with UV exposure of 6.2 eV, it was found that this UV/VUV curing process compares favorably with current UV curing. The results also show that UV/VUV curing can overcome many of the drawbacks of UV curing and improve properties of dielectrics more efficiently without the need for high-temperature heating of the dielectric.

This work was supported by the Semiconductor Research Corporation under Contract 2012-KJ-2359

6:00pm TF+EM+MI-WeA12 Effects of Cesium Ion Implantation on the Mechanical and Electrical Properties of Organosilicate Low-k Films, Weiye Li, D. Pei, X. Guo, M.-K. Cheng, S. Lee, University of Wisconsin-Madison; Q. Lin, IBM Research Division, T.J. Watson Research Center; S.W. King, Intel Corporation; J.L. Shohet, University of Wisconsin-Madison

The effects of cesium (Cs) ion-implantation on uncured plasma-enhanced chemical-vapor-deposited (PECVD) organosilicate low dielectric constant (low-k) (SiCOH) films have been investigated and compared with the effects of ultraviolet (UV) curing. The mechanical properties, including the elastic

Wednesday Afternoon, November 9, 2016

modulus and hardness, of the films were improved by up to 30% with Cs implantation, and further up to 52% after annealing at 400°C in a N₂ ambient for one hour. These improvements in mechanical properties are either comparable with or better than the effects of UV-curing. These improvements are attributed to an enhancement of the Si-O-Si network structure. The k-value of the SiCOH films increased slightly after Cs implantation, and increased further after annealing. These increases are attributed to two carbon-loss mechanisms, i.e. the carbon loss due to Si-CH₃ bond breakage from implanted Cs ions, and the carbon loss due to oxidation during the annealing. The time-zero dielectric breakdown strength was improved after the Cs implantation and the subsequent annealing, and were shown to be better compared with the UV-cured SiCOH films. Within the investigated range of implantation dose, an optimal dose can be found to achieve the best effects. These results indicate that Cs ion implantation has the potential to be a supplement to or a substitution for the incumbent UV curing method for processing SiCOH low-k films.

This work was supported by the Semiconductor Research Corporation under Contract 2012-KJ-2359.

[1] Y. Kayaba, K. Kohmura, H. Tanaka, Y. Seino, T. Odaira, F. Nishiyama, et al., "Electrical reliabilities of highly cross-linked porous silica film with cesium doping," *Journal of the Electrochemical Society*, **155**, G258 (2008)

Thin Film

Room 104E - Session TF+MI-WeA

Thin Films for Magnetic and Optical Applications

Moderator: Subhadra Gupta, University of Alabama

2:20pm **TF+MI-WeA1 Tuning Static and Dynamic Magnetic Properties of FeGa/NiFe Multilayer Heterostructures via Magnetic anisotropy Dispersion**, **Colin Rementer**, Q. Xu, P. Nordeen, G.P. Carman, Y. Wang, J.P. Chang, University of California Los Angeles

Iron-gallium (FeGa) is one of the most promising magnetic materials for use in composite multiferroics due to its high piezomagnetic coefficient (3 ppm/Oe) and high stiffness (70 GPa). It has been integrated into several multiferroic systems, but generally in MHz range or below.¹ In order to make it suitable for high frequency (GHz) applications, metalloid dopants have been used to soften magnetic materials and enhance their frequency dependent properties, but at the cost of the saturation magnetization as well as magnetoelastic properties.² A viable approach to circumvent this trade-off problem is to integrate a magnetic material with complementary properties into magnetic heterostructures. In this work, multilayer laminates were fabricated with FeGa and NiFe, a material with excellent properties in high frequency regimes.

FeGa (hard) and NiFe (soft) were sputtered via alloy targets with compositions Fe₉₅Ga₅ and Ni₈₁Fe₁₉ (at%) into multilayers with layer thicknesses ranging from 3-50 nm, with FeGa being used as the first and last layer in the stack. XPS confirmed the composition and showed there was no intermixing of the layers. Static magnetic properties were evaluated via SQUID magnetometry, and it was found that the incorporation of NiFe layers reduced the coercivity by up to 85%, from 30 Oe to 4 Oe. FMR studies showed a reduction of the linewidth of up to 50%, from 70 Oe to 38 Oe. It is believed that this effect is largely due to the decrease of magnetic anisotropy dispersion in the multilayers.³ The multilayer films maintained a high magnetostriction of up to 190 ppm, on the same order of magnitude as giant magnetostrictive materials such as thin film Terfenol-D.⁴ FeGa/NiFe heterostructures have been shown to be an excellent candidate for strain-coupled microwave multiferroics.

References:

1. M Hamashima, C Saito, M Nakamura and H Muro, *ECJ* (5), 1-7 (2012).
2. J Lou, RE Insignares, Z Cai, KS Ziemer, M Liu and NX Sun, *APL* (18) (2007).
3. R. Nakatani, T Kobayashi, S Ootomo and N Kumasaka, *JJAP* **27** (6) (1988).
4. KP Mohanchandra, SV Prikhodko, KP Wetzlar, WY Sun, P Nordeen and G. P. Carman. *AIP Advances* **5** 097119 (2015).

2:40pm **TF+MI-WeA2 Magnetic Anisotropy of CoFe₂O₄ Nanotubes Synthesized by Radical-Enhanced ALD**, **Puilaam(Cyrus) Cheung**, J. Chang, University of California Los Angeles

Multiferroic materials, exhibiting ferroelectricity and ferromagnetism simultaneously, have attracted interests for energy efficient multifunctional applications at nanoscale such as memories, antennas and

actuators. While room temperature single-phase multiferroic materials such as bismuth ferrite provide insufficient magnetoelectric effect, composite systems have enhanced magnetoelectric properties by combining piezoelectric materials and magnetostrictive materials through strain. However, such strain-mediated approach in thin film composites is limited by interfacial area and substrate clamping. Ferromagnetic nanowires, on the other hand, provides a new degree of freedom in manipulating magnetic properties through shape anisotropy.

In this work, cobalt ferrite (CoFe₂O₄) nanotubes were grown on anodic aluminum oxide membranes using radical enhanced atomic layer deposition (RE-ALD) to study magnetic shape anisotropy. The deposition was achieved using metal tmhd precursors (tmhd = 2,2,6,6-tetramethyl-3,5-heptanedionato) and oxygen radicals at 200°C. The ALD growth rate of cobalt ferrite was 0.18nm/cycle. Nanotubes array were formed inside the cylindrical pores of the membrane with diameter of 18nm, 35nm and 80nm. The morphology and magnetic properties of the nanotubes were studied using scanning electron microscopy, SQUID and energy dispersive X-ray spectroscopy. It was observed that as the wall thickness of the nanotube increases from 16nm to 32nm, the magnetic easy axis was switched from perpendicular to parallel to the nanowires axis, with a doubled saturation magnetization of 5.12x10⁵ emu. The out-of-plane anisotropy field was observed to be 18.7% higher than that from in-plane axis, indicating the out-of-plane axis was magnetically more favorable. As cobalt ferrite nanowires were formed, the preferential easy axis was reversed, which could potentially be implemented in manipulating of magnetization orientation if coupled to a piezoelectric material for device applications.

3:00pm **TF+MI-WeA3 Magnetic Anisotropy and Relaxation in Spintronic Materials**, **Claudia Mewes**, T. Mewes, J. Beik Mohammadi, A. Farrar, K. Cole, The University of Alabama

INVITED

Functional materials with optimized properties, such as the magnetic anisotropy and magnetic relaxation rate, are crucial for the next generation of spintronic devices. Therefore technological progress in this area depends heavily on the successful search for new materials as well as on a deeper understanding of the fundamental mechanisms of the magnetic relaxation and the magnetic anisotropy. This talk will focus on different aspects which can influence the magnetic relaxation as well as the magnetic anisotropy within a confined device setting.

For many spintronic applications the use of thin films with perpendicular anisotropy is often essential for the functionality of the device. For example the use of thin films with perpendicular anisotropy in spin transfer torque magnetic random access memories (STT MRAMs) leads to a reduction of the current density needed to switch the device state. In addition to the perpendicular anisotropy it is often crucial to have materials with a low magnetization relaxation rate. Therefore many spintronic applications rely on ultra-thin magnetic films with a low magnetization relaxation in which the perpendicular anisotropy is created through surface anisotropy. This approach is very sensitive to the interface morphology and chemical environment. In this talk I will discuss the effect of spatial fluctuations of the first order perpendicular anisotropy in thin films and its influence on the effective anisotropy for these materials.

Similar to the magnetic anisotropy the magnetic relaxation in thin ferromagnetic films can be affected by neighboring layers. Spin pumping is a well-known contribution that has to be taken into account for practical applications using multilayer structures. More recently a strong unidirectional contribution to the relaxation in exchange bias systems has been observed experimentally. To describe this phenomenon theoretically we use the formalism of an anisotropic Gilbert damping tensor that takes the place of the (scalar) Gilbert damping parameter in the Landau-Lifshitz-Gilbert equation of motion. In this talk I will discuss this approach to study the modified magnetization dynamics under the influence of unidirectional damping.

ACKNOWLEDGMENTS

C.K.A. Mewes acknowledges support by the NSF-CAREER Award No. 1452670, T. Mewes acknowledges support by the NSF-CAREER Award No. 0952929.

4:20pm **TF+MI-WeA7 Vacuum Furnace Annealing Block Copolymers for Bit Patterned Advanced Media**, **Allen Owen**, S. Gupta, University of Alabama

Hard disk drive storage media is trending towards both smaller physical size and greater storage capacity, there by increasing the areal density of the magnetic storage media. Bit patterning shows potential as a method

for increasing this areal density. A block copolymer template can be used to provide an etch mask for bit patterning a magnetic thin film. A statistical design of experiments was carried out to optimize the effect of nanopatterning via ion milling Co/Pd multilayers for PS-PFS block copolymers. The design of experiments varied the etch angle and etch time during ion milling. Samples that were sputter-deposited with Co/Pd multilayered thin films were spin-coated with PFS block copolymer and vacuum furnace annealed at 140 °C for 48 hours at a pressure of $\sim 5 \times 10^{-5}$ Torr. After vacuum furnace annealing, the films were ashed in oxygen plasma to remove the PS, leaving the PFS spheres as masks for the subsequent ion milling. The stack used was Pd5/[Co0.3Pd1.0]₁₄/Pd 5 nm sputter deposited onto a Si substrate. The as deposited coercivity was ~ 1.3 kOe. After ion milling for 2 min at an angle of 45°, the coercivity was found to be ~ 0.6 kOe. Ion milling at 45° for 4 min resulted in a coercivity of ~ 0.07 kOe. This is in comparison with previous experiments using thermal annealing in atmosphere and solvothermal annealing with heptane, where the coercivity increased at ~ 4 min at the same 45° ion milling angle. The difference can be explained by the fact that for the previous experiments, the stack used was Ta5/[Co0.3Pd1.0]₁₄/Ta5 nm. The Ta capping layer must be more resistant to ion milling than Pd, which means the ion milling times must be adjusted to transfer the bit pattern to the media.

4:40pm TF+MI-WeA8 Atomic Layer Deposition Enabled Synthesis of Multiferroic Composite Nanostructures, Jeffrey Chang, A. Buditama, University of California at Los Angeles; A. Rosenberg, Stanford University; L. Kornblum, Yale University; S.H. Tolbert, University of California at Los Angeles; K.A. Moler, Stanford University; C.H. Ahn, Yale University; J.P. Chang, University of California at Los Angeles

Multiferroic materials, which exhibit controllable ferromagnetic (ferroelectric) properties via electric (magnetic) field, are of great interest due to their potential in enabling new device applications. Due to the scarcity of single-phase multiferroics in nature and their weak responses at room temperature, composite multiferroics are proposed to realize robust multiferroic behaviors by coupling the functional properties from the constituent phases. A strain-mediated coupling strategy is achieved by interfacing magnetostrictive ferromagnets with piezoelectric materials, where the interfacial area per volume, as well as the material crystallinity, play important roles in the attainable functional properties. With the aim of enhancing the composite magnetoelectric behavior by nanostructuring, atomic layer deposition (ALD), with its high quality and conformal film growth, shows considerable potential in achieving high quality multiferroic composites with industrial scalability.

In this work, lead-free ferroelectric/antiferromagnetic BiFeO₃ (BFO) and ferrimagnetic CoFe₂O₄ (CFO) thin films were grown on SrTiO₃ (001) substrates by ALD using tmdh-based metalorganic precursors (tmdh = 2,2,6,6-tetramethylheptane-3,5 dione). The use of oxygen radicals as the oxidant provides a low temperature process capability at $\sim 200^\circ\text{C}$. The growth rates for BFO and CFO are $\sim 3.3\text{\AA}/\text{cycle}$ and $\sim 2.4\text{\AA}/\text{cycle}$, respectively. The BFO films showed epitaxial single crystalline growth in (001) pseudocubic orientation after being annealed under 650°C , while the CFO films are oriented polycrystalline due to the lattice mismatch between the film and substrate. The BFO piezoelectric properties were confirmed using piezo force microscopy, while tunable CFO magnetic properties were demonstrated by thickness-related strain relaxation measurements.

Multiferroic composite nanostructures were synthesized by implementing ALD processes with different substrates. Room-temperature magnetoelectric behaviors ($\alpha \sim 64 \times 10^{-3}$ Oe cm/V) and tunable magnetic anisotropies were observed in the BFO/CFO system with 2-2 and 1-3 orientations, respectively. The microscopic magnetic domain structures were characterized by the scanning SQUID systems. 0-3 CFO/PZT composites were enabled by using mesoporous PZT structures. The change in lattice parameters after poling was observed by high-resolution XRD measurements, showing that the strain interactions lead to the magnetoelectric behavior in the composite. Besides, the integration of the BFO/CFO system onto Si platforms demonstrated the versatility of the ALD processes, illustrating a path for integrating novel multiferroic materials into current industrial processes by ALD.

5:00pm TF+MI-WeA9 Thin Film Challenges for High Performance Ir Plasmon Enhanced Photodiodes: from Simulation to Focal Plane Array Integration and Characterization, François Boulard, Univ. Grenoble Alpes, France; O. Gravrand, Univ. Grenoble Alpes, France; D. Fowler, Univ. Grenoble Alpes, France; G. Badano, Univ. Grenoble Alpes, France; P. Ballet, Univ. Grenoble Alpes, France; M. Duperron, Univ. Grenoble Alpes, France; L. Adelmini, R. Espiau de Lamaestre, Univ. Grenoble Alpes, France **INVITED**

For several decades now, Surface Plasmons (SP) have been increasingly studied for applications in many fields from chemistry, biology, to materials science. In the IR sensor community, the use of SPs to concentrate and channel light offers new possibilities to increase sensitivity or modify spectral response. However, the incorporation of metallic nanostructures in technologically mature components is challenging. This paper deals with the design and integration of a sub-wavelength photonic structure to add spectral functionalities to mid wave and longwave IR HgCdTe photodiodes. Based on simulation and experimental results, tradeoffs to reach the full potential of SP enhancement are discussed. The relationship between the metallic grating geometry and the excited optical mode is illustrated using numerical simulations. The agreement between the simulated and measured spectral response and dispersion relation on a test photodiode array is shown. The influence of the absorber, passivation, and adhesion layer properties and thicknesses on the resonance intensity and photodiode noise is experimentally illustrated. Finally, results of multicolor midwave IR focal plane arrays with shot noise limited operation and less than 0.3% defective pixels are presented.

6:00pm TF+MI-WeA12 Watching Thin-film Aluminum Oxidize, David Allred, M. Miles, S. Thomas, S. Willett, M.J. Greenburg, A. Vance, R.S. Turley, Brigham Young University

In three years NASA will be in the midst of its decadal review, establishing priorities for the 2020s. Very likely one of the chief astrophysical missions will contain a LUVOIR (large, UV-optical-IR) telescope. This space-based observatory will likely contain the largest mirrors ever flown and will probe the cosmos seeking to address key questions of the origin, current status and evolution of our universe. These investigations will profit from a truly broad-band mirrors. Thus, the reflective coating will almost certainly be aluminum. To be viable, the top surface of such a space mirror needs to be bare without the tarnish layers that naturally form in air. This could open up the 11-15eV band for space-based astrophysics without sacrificing IR, visible and UV reflectance. We report on two techniques aimed at clarifying the oxidation mechanism for Al. First, we have used VUV (>10 eV) reflectometry of bare, freshly deposited aluminum mirrors as they age in controlled atmospheres, and second, variable-angle, spectroscopic ellipsometry is shown to be capable of measuring changes at the angstrom level in multilayers consisting of aluminum, protected by various vacuum-applied barrier layers. These ultrathin barrier layers included polymers such as parylene and inorganic films, such as MgF₂ and AlF₃. For example, we saw that the growth in oxidation thickness of aluminum protected by a 7nm MgF₂ film is logarithmic over a period of time of more than 1000 hrs.

Tribology Focus Topic

Room 101A - Session TR+AS+NS+SS-WeA

Nanoscale Wear: Applications to Nanometrology and Manufacturing

Moderators: Tevis Jacobs, University of Pittsburgh, Filippo Mangolini, University of Leeds, UK

2:20pm TR+AS+NS+SS-WeA1 A Multi-Bond Model of Single-Asperity Wear at the Nano-Scale, Y. Shao, Johns Hopkins University; T.D.B. Jacobs, University of Pittsburgh; Michael L. Falk, Johns Hopkins University **INVITED**

Single-asperity wear experiments and simulations have identified different regimes of wear including Eyring- and Archard- like behaviors. A multi-bond dynamics model based on Filippov *et al.* [Phys. Rev. Lett. **92**, 135503 (2004)] captures both qualitatively distinct regimes of single-asperity wear under a unifying theoretical framework. In this model, the interfacial bond formation, wear-less rupture and transfer of atoms are governed by three competing thermally activated processes. The Eyring regime holds under the conditions of low load and low adhesive forces; few bonds form between the asperity and the surface and wear is a rare and rate-dependent event. As the normal stress increases the Eyring-like behavior of wear rate tends to break down. A nearly rate-independent regime holds under high load or high adhesive forces; bonds form readily and the resulting wear is limited by the sliding distance. In a restricted regime of

Wednesday Afternoon, November 9, 2016

normal load and sliding velocity, the dependence of wear rate on normal load is nearly linear and independent of sliding velocity, as described by the Archard equation. Detailed comparisons to experimental and molecular dynamics simulation investigations have illustrated both Eyring and Archard regimes and an intermediate cross-over between the two.

3:00pm **TR+AS+NS+SS-WeA3 Surface Chemical and Tribological Studies of Solid Lubricants for Space**, *Jeffrey Lince*, The Aerospace Corporation **INVITED**

Successful operation of satellites and launch vehicles requires using multiple moving mechanical assemblies (MMAs). The correct choice of lubricants and tribocoatings is critical for the operation of spacecraft MMAs. However, the space environment is challenging. Examples include vibration during launch, thermal cycling on orbit, and the need to work effectively for missions up to twenty years in duration without lubricant replenishment. Especially challenging is the need for tribomaterials to withstand the vacuum of space during lengthy missions. As such, they must exhibit low vapor pressures, since evaporation of lubricants can result in loss from and premature failure of devices, as well as contamination of sensitive spacecraft components. Although unique synthetic liquid lubricants are used heavily in spacecraft for a variety of applications, solid lubricants are used with many devices because of their low vapor pressure, lack of migration, relative insensitivity to temperature changes, and low contamination potential. Soft solid lubricants such as molybdenum disulfide (MoS_2) and polytetrafluoroethylene (PTFE) have been used traditionally. More recently, hard low friction coatings such as hydrogenated diamond-like carbon have shown promise for operation in vacuum with existing spacecraft lubricants, or even unlubricated operation in vacuum. In addition, increasing interest in low friction nanoparticles has highlighted their potential utility. Tribomaterials show performance in vacuum that differs from that in air. This issue is important for spacecraft hardware, because it is often prohibitive to test them in a space-like environment, including vacuum, before launch. In addition, degradation during long-term storage can occur, and real-time storage studies correlating surface chemical changes with tribological performance are lacking. In this talk, results will be presented from studies done at The Aerospace Corporation that elucidate the effects of vacuum and temperature extremes on the tribological performance of important spacecraft tribomaterials. Emphasis will be on correlating surface chemical and tribological properties.

4:20pm **TR+AS+NS+SS-WeA7 Molecular Control of Friction**, *Roland Bennewitz*, INM - Leibniz Institute for New Materials, Germany; *J. Blass*, *BL. Bozna*, INM - Leibniz Institute for New Materials; *M. Albrecht*, *G. Wenz*, Saarland University **INVITED**

Molecular films on surfaces can be used to control friction if it is dominated by adhesive shear rather than surface deformation. The underlying molecular mechanisms can be explored by high-resolution friction force microscopy.

We have developed a molecular toolkit for the control of friction and adhesion by supramolecular interactions in aqueous environments. The contacting surfaces are functionalized by cyclodextrin molecules. The interaction is mediated by ditopic connector molecules with hydrophobic end groups which form inclusion complexes with the cyclodextrin molecules on opposing surfaces. Significant friction and adhesion has been measured in atomic force microscopy experiments for connector molecules with adamantane, ferrocene, and azobenzene end groups.

For adamantane connector molecules, adhesion is found to be strongly dependent on the pulling rate due to a transition from subsequent peeling of individual bonds for slow pulling to multivalency effects at fast pulling. In contrast, friction does not depend on the sliding velocity [1].

The use of azobenzene connector molecules allows for switching of adhesion and friction by light stimuli [2]. Switching of friction by electrochemical stimuli for ferrocene connector molecules is less effective due to molecular interactions which are specific to the connector molecules but do not change with the potential [3]. We will discuss differences in rupture and rebinding dynamics for the three connector molecules and their influence on the rate dependence of adhesion and friction.

Cyclodextrin molecules have also been included in stiff polymers whose end groups are attached to tips or surfaces. The polymer-functionalized surfaces exhibit interesting variations of shearing and peeling mechanisms.

1. Blass, J., et al., Dynamic effects in friction and adhesion through cooperative rupture and formation of supramolecular bonds. *Nanoscale*, 2015. 7(17): p. 7674-7681.

2. Blass, J., et al., Switching adhesion and friction by light using photosensitive guest-host interactions. *Chemical Communications*, 2015. 51(10): p. 1830-1833.

3. Bozna, B.L., et al., Friction Mediated by Redox-Active Supramolecular Connector Molecules. *Langmuir*, 2015. 31(39): p. 10708-10716.

5:00pm **TR+AS+NS+SS-WeA9 Plasticity Controlled Friction and Wear in Single-Asperity Contacts**, *Izabela Szlufarska*, *L. Zhao*, *A. Li*, *C. Tangpatjaroen*, *D. Grierson*, University of Wisconsin - Madison **INVITED**

One of the critical challenges in designing materials with superior tribological properties is the current lack of understanding of the microstructural evolution that takes place in sliding contacts. Phenomena that contribute to such evolution are grain growth and refinement, evolution of dislocation networks, and interaction of dislocations with interfaces. In this talk I will discuss examples of how we use multi-scale simulations and atomic force microscopy (AFM) experiments to determine the role of microstructural evolution and plastic deformation in friction and wear. Specifically I will discuss: (i) Our developments of a continuum model that couples grain growth, plastic deformation, and mechanics. This model combines for the first time the phase field method, crystal plasticity, and finite element analysis of mechanical contacts, and parameters for this model are determined from atomistic simulations and experiments. The new model is capable of simulating deformation at strain rates comparable to those encountered in AFM experiments. (ii) Results from our molecular-level simulations on the effects of dopants on strength and wear resistance of nanostructured metal alloys. (iii) Discovery from our complementary AFM and nanoindentation experiments that, although a harder material (silicon carbide) is typically more wear resistant than a softer material (silicon), this trend can be reversed with smaller contact sizes. The contact pressure is the same in both sets of experiments, and both are carried out in the regime where a plastic zone is well-developed. We demonstrate that this surprising finding is due to a transition from abrasive to adhesive wear, which for the first time is observed in single-asperity contacts. Our results show that surface chemistry can have a significant effect on sub-surface plastic deformation.

5:40pm **TR+AS+NS+SS-WeA11 Applying Analytical Roughness Models to Real Surfaces: Reconstructing the Power Spectral Density from Surface Topography Measurements**, *Tevis Jacobs*, *A. Gujrati*, *S.R. Khanal*, University of Pittsburgh; *T. Junge*, *L. Pastewka*, Karlsruhe Institute of Technology (KIT), Germany

Surface topography is a critical factor for optical, mechanical, and tribological properties of materials. Many studies report single scalar roughness parameters that contain information over just a limited range of wavelengths. Analytical models of roughness have shown in recent years that properties such as stiffness, adhesion, and friction depend on the nature of roughness across many length scales. The power spectral density (PSD) is the mathematical instrument that provides a description of surface roughness as a function of scale. A truly quantitative analysis of surface roughness in terms of the PSD is necessary to validate and apply these analytical roughness models. However, this is currently limited by: (A) inconsistencies in the way that the quantitative PSD is computed; (B) bandwidth-limits of conventional surface metrology; and (C) instrumental artifacts at the smallest scales. Here, we demonstrate these limitations – first, by comparing the various forms of the PSD, then by computing the PSDs both for simulated and experimental surfaces.

We show that experimentally-determined PSDs suffer three types of systematic error, each of which will hinder quantitative comparison to models. We demonstrate strategies for detection and mitigation of these artifacts, to ensure accurate and reliable PSDs. A novel web-based application has been created and made available for general use which computes accurate PSDs and assesses the limits of their reliability. This enables the application of analytical roughness models to calculate upper and lower bounds of surface properties.

Finally, we report on the roughness characterization of an ultrananocrystalline diamond (UNCD) surface over the range from Angstroms to centimeters. This range of characterization enables quantitative comparison with rough-surface adhesion models. By elucidating experimental barriers to accurate surface characterization, and by demonstrating solutions to these barriers, this work facilitates the application of analytical roughness models to real-world surfaces – both to predict and tailor surface properties.

Wednesday Afternoon, November 9, 2016

6:00pm **TR+AS+NS+SS-WeA12 Universal Ageing Mechanism for Static and Sliding Friction of Metallic Nanoparticles**, *M. Feldmann, Dirk Dietzel, A. Schirmeisen*, Institute of Applied Physics, Justus-Liebig-University Giessen, Germany

On the macroscale, the distinct difference between static and sliding friction can well be explained by the phenomenon of contact ageing, which is typically related to an increase of contact area with time within a multi asperity interface model. On the nanoscale, however, the role of contact ageing is less clear, especially when considering nanoscale asperities of constant size.

Recently, the role of contact ageing for nanoscale friction dynamics was analyzed for antimony nanoparticles sliding on HOPG. The antimony nanoparticles have been prepared by thermal evaporation on HOPG and comprise an ideal model system with atomically flat interfaces of constant size where friction can be described by the concept of structural superlubricity [1]. Friction of the particles was assessed by nanomanipulation techniques and it was found, that sliding friction can be described as a complex process of thermally activated contact ageing and bond breaking [2]. Further measurements have now revealed, that the particle movement follows an irregular stick slip pattern, where the slip events can be considered as recurring contact renewal, while the stick times can be interpreted as the age of the contact. By correlating the stick times with the lateral force values measured for contact breaking, we found that our system can well be described by logarithmic ageing [3], as it might be expected by assuming atom by atom relaxation processes at the interface.

To check whether ageing during sliding motion is fundamentally different from ageing under stationary conditions, we have performed additional “slide hold slide” measurements [4] and found that in both cases ageing can be described by exactly the same logarithmic function. This indicates, that the strength of the contact is determined by the ageing time but independent of the kinetic conditions. This means that static and sliding friction can be described by a universal ageing law where the age of the contact is the crucial parameter.

[1] D. Dietzel, M. Feldmann, H. Fuchs, U.D. Schwarz, A. Schirmeisen, *Phys. Rev. Lett.* 111, 235502 (2013)

[2] M. Feldmann, D. Dietzel, H. Fuchs, A. Schirmeisen, *Phys. Rev. Lett.* 112, 155503 (2014)

[3] M. Feldmann, D. Dietzel, A. Tekiel, J. Topple, P. Gruetter, A. Schirmeisen, *Phys. Rev. Lett.* 117, 025502 (2016)

[4] Q. Li, T.E. Tullis, D. Goldsby, R. W. Carpick, *Nature* 480, 233-236 (2011)

2D Materials Focus Topic

Room 103B - Session 2D+MI-ThM

Properties of 2D Materials including Electronic, Magnetic, Optical, Mechanical, Thermal Properties

Moderators: Paul Sheehan, US Naval Research Laboratory, Zhaohui Zhong, University of Michigan, Ann Arbor

8:00am 2D+MI-ThM1 Mechanics and Fracture of 2D Materials with Defects and Grain Boundaries, Zhao Qin, G.S. Jung, Massachusetts Institute of Technology; S. Wang, University of Oxford, UK; F.J. Martin-Martinez, Massachusetts Institute of Technology; J.H. Warner, University of Oxford, UK; M.J. Buehler, Massachusetts Institute of Technology

Two dimensional materials including graphene, silicene, MoS₂ and so forth represent ideal materials composed of a single layer of atoms organized in a lattice form. Their unique geometry and intriguing mechanical and thermal properties make them perfect candidates for nano scale engineering applications. The robustness of the materials, especially those with defects is important to prevent their catastrophic failure and contribute to their durability in usage. Here we combine both large-scale molecular dynamics simulations based on reactive force fields and experiments via transmission electron microscopy to investigate their fracture behavior under extreme mechanical loading conditions. We focus on how defects and grain boundaries in 2D materials affect the critical conditions and the dynamics process of their fracture. Our results reveal that certain forms of atomic defects and grain boundaries are beneficial to enhance the mechanical strength of 2D materials that are subjected to cracks. For example, we find that poly-crystalline graphene under fracture releases up to 50% more energy than the pristine graphene. We find that grain boundaries increase the critical energy release rate to fracture by reducing stress concentration and making branches near the crack tip. We find atomic defects can cause crack deflections during crack propagation, effectively extending the crack length during propagation and thus increase the energy dissipation. Together, these molecular irregularities taking place at the atomic scale level can significantly affect the lattice characteristics of the 2D materials at larger scale levels and thereafter enhance their fracture toughness, making its crack propagation different from pristine ones, and such a mechanism explains the reduced crack propagation speed by adding vacancies as what is seen in experiments.

8:20am 2D+MI-ThM2 Effects of Non-local Screening and Effective Mass Anisotropy on Excitons in 2D Materials, I.I. Oleynik, Joseph Gonzales, University of South Florida

The optical excitations in semiconductors are substantially influenced by electron-hole interactions resulting in formation of excitons. Although the exciton binding energies in the bulk are much smaller than the fundamental band gaps, the excitonic effects in 2D materials are significantly amplified due to combined effect of quantum confinement and non-local screening of electron-hole interactions in two dimensions. An effective mass theory of 2D excitons, which takes into account the combined effect of the anisotropy and non-local 2D screening, is used to systematically investigate the variation of monolayer exciton binding energies E_x across a representative set of layered chalcogenides, both isotropic, such as MoTe₂, MoSe₂, WSe₂, and WS₂, and anisotropic including phosphorene, TiS₂, ReS₂, and SnSe₂. The markedly different values of E_x are correlated with corresponding variations in atomic polarizabilities of constituent atoms.

8:40am 2D+MI-ThM3 2D Materials: A New Platform for Strong Light-Matter Interactions, Ajit Srivastava, Emory University **INVITED**

A recent addition to low-dimensional materials are monolayer transition metal dichalcogenides (TMDs), such as WSe₂, with an atomically thin, honeycomb lattice and optical band gaps. In addition to spin, charge carriers in TMDs exhibit a "valley" degree of freedom which can be optically addressed using circularly polarized light, opening up exciting possibilities for "valleytronics". Another curious aspect of TMDs lies in the non-trivial geometry of their band structure which gives rise to equal but opposite Berry curvature, an effective magnetic field in the momentum space. Owing to unusually strong Coulomb interactions in truly 2D limit, optical spectra of monolayer TMDs is dominated by tightly bound excitons which are expected to strongly couple to light and form stable polaritons - half light, half matter excitations.

In this talk, I will begin by presenting our recent results on valley Zeeman effect, where in analogy to spins, valleys shift in energy with magnetic field. Next, I will discuss our theoretical results on how the non-trivial geometry of Bloch bands modifies the excitonic fine structure of TMDs resulting in an

orbital Zeeman effect in reciprocal space and a Lamb-like shift of levels. Finally, I will present our recent results on the observation of microcavity polaritons confirming the strong light-matter interactions in these materials. The presence of valley degree of freedom, non-trivial geometry of bands, and the possibility of introducing non-linearities in form of quantum emitters makes polaritons in TMDs particularly appealing for studying correlated many-body physics and topological states of matter.

9:20am 2D+MI-ThM5 Electronic Transport and Localization in Nitrogen-Doped Graphene Devices Using Hyperthermal Ion Implantation, Adam Friedman, C.D. Cress, Naval Research Laboratory; S.W. Schmucker, National Research Council postdoc working at Naval Research Laboratory; J.T. Robinson, O.M.J. van 't Erve, Naval Research Laboratory

Chemical alteration of graphene facilitates doping and may add a usable transport gap. For most published studies, atomic species (e.g., fluorine or hydrogen) are chemically bonded to the surface out-of-plane, breaking the sp² symmetry and replacing it with an sp³ bond. These methods produce functionalized graphene, rather than substitutionally-doped graphene, where the former is typically only chemically stable for days (e.g., fluorine) or weeks (e.g., hydrogen) or less, depending on environmental conditions. Hyperthermal ion implantation offers a controllable method of producing high-quality substitutionally doped graphene with nitrogen, an n-type dopant that has great potential for graphene electronics and spintronics applications where high carrier concentration, uniform doping, and minimal vacancy defect concentration is desired [1]. Here we examine the transport properties of monolayer graphene sheets as a function of implantation beam energy and dose. We observe a transition from weak (metal) to strong (insulator) localization that varies as a function of carrier concentration, and we find that the transition is suppressed near the Dirac point for higher amounts of nitrogen [2]. For nominally equivalent doses, increased N ion energy results magnetoresistance magnitude increases, reaching a value as approximately -5.5% at 5,000 Oe, which we discuss in the context of dopant concentration and defect formation. We use a model for the temperature dependence of the conductivity that takes into account both temperature activation, due to the formation of a transport gap, and Mott variable-range hopping, due to the formation of defects, to further study the electronic properties of the doped films as a function of dose and N ion energy. We find that the temperature activation component dominates the behavior, further indicating that the implanted nitrogen, rather than defects, is responsible for the observed result.

[1] C.D. Cress, et al. ACS Nano 10, 3714 (2016).

[2] A.L. Friedman, et al. Phys. Rev. B, 93 161409(R) (2016).

9:40am 2D+MI-ThM6 Metal Contacts to Transition Metal Dichalcogenide Films: Understanding and Avoiding the Formation of a Schottky-like Barrier, M. Gomez, J. Martinez, M. Valentin, E. Preciado, V. Klee, C. Merida, Ludwig Bartels, University of California - Riverside

We utilize a combination of X-ray photoelectron spectroscopy, transport measurements and optical as well as acoustic excitation to study the impact of the formation of metal contacts to transition metal dichalcogenide films on the electronic structure of the films. Photoelectron spectroscopy permits us to follow the formation of a Schottky-like barriers with increasing metal film thickness on the Angstrom scale. We utilize core level spectroscopy to indicate the evolution of the MoS₂ valence band during metal deposition. Our findings indicate that single layer MoS₂ films adopt the character of the metal (Fermi-level pinning) resulting in a Fermi-level position in the MoS₂ semiconducting gap that is – depending on the metal work function – indicative of a p-type semiconductor, even though the native carriers in an MoS₂ film are electrons. As a consequence, metal-TMD-metal junctions may best be understood as p-n-p junctions. Numerous ancillary measurements support this hypothesis.

11:00am 2D+MI-ThM10 Multilayer Graphene Suspension Over Millimeter Size Openings and Mechanical Testing, Joseph Rowley, R.F. Davis, R.R. Vanfleet, Brigham Young University; J. Abbott, Moxtek, Inc.

Because of its high ultimate tensile strength, a single atomic layer of graphene has been able to suspend micron size holes reliably. However, to extend into regimes where devices have dimensions measured in millimeters, a single layer of graphene is insufficient. Films made from a few layers of graphene, although not as strong as pristine single layer graphene, have been shown to still retain a high level of strength. Using chemical vapor deposition on a nickel catalyst, we have fabricated many layer graphene films and suspended these membranes over millimeter size holes. Mechanical properties were measured on suspended films using a custom bulge test instrument.

Thursday Morning, November 10, 2016

11:20am **2D+MI-ThM11 Modeling Excitons in Transition-Metal Dichalcogenides**, *F. Tseng*, NRC Research Associate; *E. Simsek*, George Washington University; **Daniel Gunlycke**, Naval Research Laboratory

Using a triangular lattice exciton (3ALE) model, we explore exciton states in semiconducting monolayer transition-metal dichalcogenides. We show that the hydrogen model for excitons breaks down due to lattice effects and that the excitons are neither Wannier nor Frenkel excitons and instead span an intermediate size regime. The model is formulated on sparse form in direct space, leading to a computationally efficient $N \log(N)$ scaling and the ability to calculate over lattice grids with tens of thousands of sites, more than sufficient to converge exciton states in this intermediate exciton regime. In this presentation, we will also discuss the Coulomb potential generated from a dielectric substrate and how the exciton binding energies could be tuned by the thickness and permittivity of an oxide layer.

11:40am **2D+MI-ThM12 Characterization of Collective Ground States in Single-layer NbSe₂**, **Miguel M. Ugeda**, CIC nanoGUNE, Spain; *A.J. Bradley*, University of California at Berkeley; *Y. Zhang*, Advanced Light Source, Lawrence Berkeley National Laboratory; *S. Onishi*, *W. Ruan*, *Y. Chen*, *C. Ojeda-Aristizabal*, University of California at Berkeley; *H. Ryu*, Advanced Light Source, Lawrence Berkeley National Laboratory; *M.T. Edmonds*, *H.Z. Tsai*, *A. Riss*, University of California at Berkeley; *S.K. Mo*, Advanced Light Source, Lawrence Berkeley National Laboratory; *D. Lee*, *A. Zettl*, University of California at Berkeley; *Z. Hussain*, Advanced Light Source, Lawrence Berkeley National Laboratory; *Z.X. Shen*, Stanford Institute for Materials and Energy Sciences, SLAC National Accelerator Laboratory; *M.F. Crommie*, University of California at Berkeley

INVITED

Layered transition metal dichalcogenides (TMDs) are ideal systems for exploring the effects of dimensionality on correlated electronic phases such as charge density wave (CDW) order and superconductivity. In bulk NbSe₂ a CDW sets in at $T_{CDW} = 33$ K and superconductivity sets in at $T_c = 7.2$ K. Below T_c these electronic states coexist but their microscopic formation mechanisms remain controversial. In this talk I will present the electronic characterization study of a single 2D layer of NbSe₂ by means of low temperature scanning tunneling microscopy/spectroscopy (STM/STS), angle-resolved photoemission spectroscopy (ARPES), and electrical transport measurements (1). I will show that 3x3 CDW order in NbSe₂ remains intact in 2D. Superconductivity also still remains in the 2D limit, but its onset temperature is depressed to 1.9 K. Our STS measurements at 5 K reveal a CDW gap of $\Delta = 4$ meV at the Fermi energy, which is accessible via STS due to the removal of bands crossing the Fermi level for a single layer. Our observations are consistent with the simplified (compared to bulk) electronic structure of single-layer NbSe₂, thus providing insight into CDW formation and superconductivity in this model strongly-correlated system. Furthermore I will show that CDW order is also present in 2D semiconducting TMDs around 1D mirror twin boundaries (2).

(1) M. M. Ugeda, et al., Nature Physics 12, 92 (2016).

(2) S. Barja, et al., Nature Physics, in press (2016).

Actinides and Rare Earths Focus Topic Room 103C - Session AC+AS+SA-ThM

Chemistry and Physics of the Actinides and Rare Earths

Moderators: David Shuh, Lawrence Berkeley National Laboratory, Art Nelson, Lawrence Livermore National Laboratory

8:00am **AC+AS+SA-ThM1 Covalency in Oxidized Uranium**, **James G. Tobin**, University of Wisconsin-Oshkosh

INVITED

Actinides, the 5f elements and their compounds, alloys, and mixtures, are a crucially important part of modern technological societies. Moreover, uranium dioxide is the most widely used nuclear fuel for the generation of electricity. Yet, because of the complexity of the 5f/6d electronic structure in the actinides, a fundamental understanding of their physical behavior, in actinides in general and uranium dioxide in particular, has not been achieved.

Theoretically, it has been proposed that covalency is an important part of the electronic structure of actinide dioxide, although some disagree. Experimentally, spectroscopic studies have been reported which support the hypothesis of 5f covalency. However, a crucially important and absolutely essential component has been missing: a systematic study where the nature of the oxidant is changed, so the specifics of the 5f and 6d covalencies could be varied and monitored. The turning-on and turning-off of an effect is the essence of a true benchmarking. The work reported here clearly and irrevocably establishes experimentally the strong presence

of U 5f–O 2p covalency in the unoccupied density of states of UO₂, the most important of our nuclear fuels.

This comparative study will feature the isoelectronic systems uranium dioxide (UO₂) and uranium tetrafluoride (UF₄). While isoelectronic, both being U⁴⁺ 5f² in the formal limit, they exhibit substantially different structures. UO₂ is a fluorite (cubic) material, while UF₄ is monoclinic. However, both exhibit very similar U L₃ extended x-ray absorption fine structure (EXAFS) behavior, indicative of quantitatively similar interatomic distances. The result of this comparative study is that UF₄ exhibits continued 6d covalency but the almost complete loss of 5f covalency, while UO₂ clearly displays both strong 5f and 6d covalencies. Here we have direct experimental demonstration that 5f covalency is important in actinide oxides but can be lost with a more powerful oxidizing agent such as fluorine.

To summarize: Using x-ray emission spectroscopy and absorption spectroscopy, it has been possible to directly access the states in the unoccupied conduction bands that are involved with 5f and 6d covalency in oxidized uranium. By varying the oxidizing agent, the degree of 5f covalency can be manipulated and monitored, clearly and irrevocably establishing the importance of 5f covalency in the electronic structure of the key nuclear fuel, uranium dioxide.

Collaborators on this work include: S.-W. Yu, R. Qiao, W. L. Yang, C. H. Booth, D. K. Shuh, A. M. Duffin, D. Sokaras, D. Nordlund, and T.-C. Weng. [*See PHYSICAL REVIEW B **92**, 045130 (2015)]

8:40am **AC+AS+SA-ThM3 An In Situ X-ray Diffraction Study of Plutonium Oxidation**, **Paul Roussel**, *W. Lake*, AWE, UK

X-ray diffraction was used to follow the oxidation of α -phase plutonium in oxygen at a pressure of 500 mbar. The composition of the growing oxide scale consisted of the trivalent cubic sesquioxide α -Pu₂O₃ and tetravalent fluorite dioxide PuO₂. The hexagonal β -sesquioxide phase was not detected. The quantity and lattice parameters of the oxide phases were determined from Rietveld analysis of the diffraction patterns. The lattice parameters of both oxides were found to decrease with increasing oxide quantity. Decreasing lattice parameters occur from increasing oxygen anion concentration in each oxide phase. The rate of oxidation for the total oxide composition at various temperatures below 100 °C was found to be linear, indicative of possible moisture enhanced oxidation. A detailed analysis of the contributions of the individual oxide compositions will be presented. Post oxidation optical microscopy of the coherent oxide scale showed areas of thicker scale typical of island growth. When the oxidation reaction was allowed to proceed to form olive green spalled oxide, X-ray diffraction analysis of the powder showed it to consist of a mixture of both cubic oxide phases.

Our initial XRD work presented at this meeting in 2012 suggested the initial oxide film grown on δ -plutonium might be amorphous. This work has been repeated using the XRD in-situ environmental reaction cell and the results will be presented.

© British owned Crown Copyright 2016/AWE

9:00am **AC+AS+SA-ThM4 Advanced Applications of Synchrotron Sources to Describe Water Soluble Plutonium Colloids**, **Thomas Dumas**, CEA, France; *E. Dalodière*, *M. Viot*, ICSM Marcoule; *V. Morosini*, CEA Marcoule; *T. Chave*, ICSM Marcoule; *C. Hennig*, Helmholtz Zentrum Dresden-Rossendorf; *T. Wiss*, European Commission, Joint Research Centre (JRC), Institute for Transuranium Elements; *D.K. Shuh*, *T. Tyliszcaak*, Lawrence Berkeley National Laboratory; *P. Moisy*, CEA Marcoule; *I. Nikitenko*, ICSM Marcoule

Colloidal species of Pu(IV) were shown to play a central role in the speciation of plutonium in various aqueous wastes and in biosphere [1-3]. However, a comprehensive understanding of the behavior and structure of Pu colloids remains elusive and hinders progress on the development of reliable processes of their management. Preparation of plutonium colloidal species with controlled composition and properties is still a challenge. Herein, we report the preparation of stable Pu(IV) colloids by the action of ultrasonic waves on PuO₂ in salt-free water conditions. Sonochemical colloid was compared with hydrolytic colloid using HRTEM, Pu LIII-edge EXFAS and STXM/NEXAFS techniques.

HRTEM revealed nanostructured morphology for both colloids composed of particles of PuO₂ (fcc, space group) measuring about 7 nm and 3 nm, respectively. The EXAFS spectra of colloidal PuO₂ nanoparticles were fitted on the basis of PuO₂ crystal structure. Combined HRTEM and EXAFS results revealed the correlation between the coordination numbers (i.e. Pu-O and Pu-Pu) and atomic surface-to-volume ratio of studied PuO₂ nanoparticles.

The STXM/NEXAFS technics implemented at ALS BL 11-0-2 was used for the first time to study plutonium colloids. It offers a new topographic angle to describe colloids combined to spectroscopic measurements at oxygen K edge. It first revealed that the oxygen state of hydrolytic Pu colloid is influenced by hydrolyzed Pu(IV) species in much more extend than the sonochemical colloids. Moreover the topographic analysis highlight discrepancies in plutonium and oxygen distribution for hydrolytic Pu colloid on the contrary to sonolitic one.

Complementarily to previous studies, this work confirmed that plutonium colloids (hydrolytic and sonochemical) can be described as core-shell nanoparticles composed of quasi stoichiometric PuO₂ core and hydrolyzed Pu(IV) moieties at the surface shell. Nevertheless, the application of soft X-ray technics highlight the strong influence of the synthetic route on colloid chemical composition and hence its expectable reactivity.

1. A. B. KERSTING, Plutonium Transport in the Environment, *Inorg. Chem.*, **52**, 3533 (2013).
2. A. I. ABDEL-FATTAH, D. ZHOU, H. BOUKHALFA, S. TERIMALA, S. D. WARE, A. A. KELLER, Dispersion Stability and Electrokinetic Properties of Intrinsic Plutonium Colloids: Implications for Subsurface Transport, *Env. Sci. Technol.*, **47**, 5626 (2013).
3. C. WALTER, M. A. DENECKE, Actinide Colloids and Particles of Environmental Concern, *Chem. Rev.*, **113**, 995 (2013).

9:20am AC+AS+SA-ThM5 In *Pristinum* Observation of Plutonium Hydride, Martin Brierley, J.P. Knowles, AWE

The reaction of plutonium with hydrogen creates plutonium hydride in an energetic process which often liberates the reaction product as a powder. Plutonium hydride is pyrophoric; therefore study of the reaction product usually requires that it is passivated by careful exposure to oxygen prior to removal from the reaction chamber. The passivation process is highly energetic with the potential to significantly affect the microstructure of the reaction product and surrounding metal. In this study we used a scanning electron microscope with an adjoining reaction chamber to maintain vacuum between reaction and analysis to grow plutonium hydride and subsequently analyse the reaction products as formed.

Initial work on electro refined Pu gave a slow reaction to hydrogen, requiring an *in situ* heat treatment to form hydride. Analysis of the reaction product was made *in vacuo* following reaction, preventing oxygen from accessing the sample. Subsequent cross sectional analysis of the reaction product morphology was performed, showing a coating of a hydride product layer with an open structure under the original surface oxide [1].

A sample of mixed α/δ phases was successively exposed to hydrogen for increasing durations of 60, 7200 and 70320 s. No evidence of reaction was evident following the 60 s and 7200 s exposures, unlike that observed in experiments on gadolinium [2] and uranium [3]. Following the 70320 s exposure, 96 % of the available hydrogen was consumed and several large anisotropic reaction sites had formed. The hydride sites on this mixed phase sample exhibited anisotropic growth similar to δ -stabilised plutonium samples investigated previously [4]. Deformation of the δ -phases surrounding hydride sites occurred via slip processes. Cracks formed in the overlying oxide layer above the deformed material allowing facile access for hydrogen to reach fresh Pu at the metal/oxide interface. Subsequent cross sectional analysis revealed anisotropic growth of hydride reaction sites, strongly supporting our previously proposed mechanism for anisotropic growth [4]. The α -phase domains resisted deformation and instead transferred the stresses from the hydride reaction front further into the surrounding metal. Post experimental cross sections through reaction sites suggest that hydride regions associated with α -domains had not undergone complete reaction.

References

1. M. Brierley et al., Journal of Nuclear Materials 469 (2016) 39-42
2. G.M. Benamar, et al., Journal of Alloys and Compounds 520 (2012) 98-104.
3. R.M. Harker, A.H. Chohollo, MRS Online Proceedings Library Archive, 1444 (2012) 189
4. M. Brierley, et al., Journal of Nuclear Materials 469 (2016) 145-152

9:40am AC+AS+SA-ThM6 Evidence for f- and d-orbital Mixing in Lanthanide and Actinide Dialuminides, MAI₂ (M = Ce, Sm, Eu, Yb, Lu, U, Pu), Stefan Minasian, Lawrence Berkeley National Laboratory (LBNL); A.B. Altman, J. Arnold, University of California at Berkeley; E.D. Bauer, Los Alamos National Laboratory; C.H. Booth, J.I. Pacold, C.D. Pemmaraju, D.G. Prendergast, D.K. Shuh, T. Tylliszczak, Lawrence Berkeley National Laboratory (LBNL)

For most scientific and technical applications, aluminum is well-regarded as a trivalent, electropositive and Lewis-acidic metal. However, this textbook model fails to adequately explain the unusual chemical and physical properties of many f-element molecules, materials, and alloys incorporating aluminum and other group 13 elements. In order to develop a more nuanced model of aluminum electronic structure, we have turned to metal K-edge X-ray Absorption Spectroscopy (XAS), which is an established technique for evaluating electronic structure in bioinorganic and inorganic compounds. Pre-edge peaks in K-edge XAS correspond to bound state transitions between core and unoccupied orbitals. Therefore, by comparing pre-edge features to established references, information can be gathered on the electronic structure of a system and the orbitals involved in bonding. However, there is very little precedent for the measurement and interpretation of aluminum K-edge XAS for molecules and materials.

This presentation will describe our recent efforts to develop Al K-edge XAS as a probe of chemical bonding and electronic structure in Al molecules and materials with lanthanide and actinide metals. Work began by examining a series of molecular aluminum compounds and by systematically varying supporting ligands and oxidation states. Features in the Al K-edge spectra were fully assigned through a comprehensive polarization study and comparison with the results of XCH and DFT calculations. Results were interpreted within a molecular orbital framework, providing unique insight that could not be obtained from analysis of NMR or metrics from single-crystal X-ray diffraction. These results have laid a foundation for ongoing efforts with lanthanide and actinide aluminum alloys, MAI₂ (M = Ce, Sm, Eu, Yb, Lu, U, and Pu). Comparisons between the Al K-edge spectra and earlier resonant X-ray emission spectra for the MAI₂ compounds provide unique insight into how electronic structure influences the desirable physical properties of these materials. For EuAl₂ and YbAl₂, the increasing occupancy of the 4f orbitals enhances screening of the 5d orbitals, resulting in enhanced Al 3p and Ln 5d orbital mixing for Eu and Yb that is not observed for Ce, Sm, or Lu. For UAl₂ and PuAl₂, the Al K-edge XAS and theory results also provides convincing evidence of Al 3p and 6d orbital mixing. Because of the enhance radial extension of the 6d orbitals, 6d orbital involvement in bonding for PuAl₂ is more likely to have an impact on the stability of the Pu-Al bonds. Current efforts are focused on evaluating f-element interactions with aluminum in other stoichiometric and non-stoichiometric alloys.

11:00am AC+AS+SA-ThM10 Comparative Analysis of Uranium Oxide Films, Miguel Santiago Cordoba, Los Alamos National Laboratory

Depleted Uranium (DU) Oxide thin films are considered to be employed as surrogates and reference compounds for systematic studies on the elucidation of fundamental properties of actinide materials. The goal of this work is to compare surface morphologies of DU oxide thin films fabricated by two techniques, polymer assisted deposition (PAD) and electron beam evaporation (EBE). In this contribution, we utilized a MultiMode atomic force microscope (AFM) operating in tapping mode in order to compare and establish a contrast among the three dimensional surface structures of polycrystalline U₃O₈ and UO₂ films fabricated by PAD, and UO₂ thin films deposited by EBE. Differences in surface morphology are analyzed, and the information provided by AFM is compared against other complementary techniques such as transmission electron microscopy (TEM) and scanning electron microscopy (SEM). Reported results revealed that films fabricated by both techniques had granular structure, with morphologies strongly depending on the fabrication methods and conditions.

*Approved for public release LA-UR-16-22993

11:20am AC+AS+SA-ThM11 Soft X-ray Spectroscopy of Actinide Materials, David Shuh, S.G. Minasian, C. Pemmaraju, A. Canning, D.G. Prendergast, Lawrence Berkeley National Laboratory; T. Tylliszczak, Lawrence Berkeley Lab, University of California, Berkeley; A. Modin, S. Butorin, J. Nordgren, L. Werme, P. Oppeneer, Uppsala University, Sweden

Soft X-ray synchrotron radiation methodologies are being developed and employed at the Advanced Light Source (ALS) of Lawrence Berkeley National Laboratory to elucidate the electronic structure of actinide materials. Results from these investigations have begun to provide

improved fundamental knowledge that can be used as a scientific basis for the enhanced design of special-purpose actinide materials and the overall understanding of actinide materials. The experimental developments at the ALS have centered on the use of the Molecular Environmental Science (MES) scanning transmission X-ray microscope (STXM) at Beamline 11.0.2 for near-edge X-ray absorption fine structure spectroscopy (NEXAFS), and on X-ray emission spectroscopy (XES) at several beamlines, focusing primarily on light atom constituents (C, N, O, F) for ligand K-edge XAS, and on metal-ion centers plus light-atom signals for XES. The spectromicroscopy capabilities of the STXM provide the means to investigate and determine the speciation in actinide materials and environmentally-relevant systems with spatial resolution that reaches to the true nanoscale. An absolutely critical and key enabling component for all of the soft X-ray investigations is the contribution of theory, that when combined with experiment, has firmly provided more detailed knowledge of electronic structure in actinide materials in terms of orbital composition and mixing, and oxidation state.

Applied Surface Science

Room 101B - Session AS+SS-ThM

Depth Profiling, Buried Interfaces, and 3D Analyses

Moderators: Gregory Fisher, Physical Electronics USA, Karen Gaskell, University of Maryland, College Park

8:00am AS+SS-ThM1 Pushing the Limits of Bonded Multi-Wafer Stack Heights while Maintaining High Precision Alignment, Alireza Narimannezhad, J. Jennings, M.H. Weber, K.G. Lynn, Washington State University

The last decade in advanced microelectronics has shown great interest in three-dimensional architectures, which was paved by multi-wafer alignment technologies. However, many limitations remain in the fabrication of ultrathin stacks as the alignment becomes more challenging and very costly. In this paper, a new cost-effective alignment technique was employed using a set of sapphire rods in through-wafer holes. Cross-sectional analysis, edge profilometry, and electron transmission tests showed ~2 µm alignment tolerances over 1 cm and ~4 µm over 10 cm tall stacks. An off-angle gold sputtering method was developed to fully coat vias of 5:1 aspect before bonding. Also, a new *Stamping* technique is introduced to coat the vias to a desired height where necessary. In this study, parallel microtubes with aspect ratios of 1,000:1 were formed by aligning ~200 wafers, each including 20,000 gold-coated vias for storing charged particles.

8:20am AS+SS-ThM2 Porous Si Stack Analysis by Model Based Infrared Reflectometry (MBIR), Sukti Chatterjee, L. Scudder, P. Narwankar, Applied Materials Inc.

In 1956, Porous silicon (PS) was accidentally discovered by Uhlir at Bell Laboratories [1], and the material was very much ignored. Later (70's and 80's) porous Si was found to be useful because its high surface area [2-5] for various applications, like microcavity, broadband AR coating, mid infrared LEDs, chemical Sensors, smart Dust, pressure Sensor, photonic crystal. Recent interest of porous Si is in the biomedical field [6] with wide range of applications, ex. drug delivery, cancer therapy, and tissue engineering. For diverse applications, single or multilayers porous Si stacks are required. In this abstract we present our metrology invention for single or multilayers porous Si stacks analysis.

We introduce a novel approach to characterize the different Si film stacks by using Model Based Infrared Reflectometry (MBIR). We believe, we are first group to apply the technique for analyzing various multilayer Si stacks. The film stack thickness has varied between 1 µm to more than 100 µm. Thick layers of silicon are opaque in the UV-VIS wavelength range, and IR wavelengths are ideal for measurements of such films. The ability to specify a film stack in the MBIR analysis model makes the technique more versatile, compared to traditional FTIR. We will present in the conference how the IR optical properties of PS can be described by Bruggeman Effective Medium Approximation (EMA), employing a standard multilayer reflectance model. To validate the MBIR results x-SEM and Gravimetric analysis have been used. The results have shown MBIR to be a suitable technique for characterization and production monitoring of the process steps associated with the new porous silicon applications field.

References

1. Uhlir, A., Electrolytic shaping of germanium and silicon. Bell System Tech. J., 1956. 35: p. 333-347.

2. Gupta, P., V.L. Colvin, and S.M. George, Hydrogen desorption kinetics from monohydride and dihydride species on Si surfaces. Phys. Rev. B, 1988. 37(14): p. 8234-8243.

3. Gupta, P., et al., FTIR Studies of H₂O and D₂O Decomposition on Porous Silicon. Surf. Sci., 1991. 245: p. 360-372.

4. Dillon, A.C., et al., FTIR studies of water and ammonia decomposition on silicon surfaces. J. Electron Spectrosc. Relat. Phenom., 1990. 54/55: p. 1085-1095.

5. Dillon, A.C., et al., Diethylsilane Decomposition on Silicon Surfaces Studied using Transmission FTIR Spectroscopy. J. Electrochem. Soc., 1992. 139(2): p. 537-543.

6. Porous Silicon for Biomedical Applications, Edited by: H.A. Santos ISBN: 978-0-85709-711-8

8:40am AS+SS-ThM3 Applications of Atom Probe Tomography on 3D Semiconductor Devices, AjayKumar Kambham, D. Flatoff, P.A.W. van der Heide, GLOBALFOUNDRIES U.S. Inc.

One of the aims in CMOS device development is to reduce power consumption while increasing performance. Pivotal to this, is the critical need to engineer dopant profiles, and to define the formation of the appropriate junctions. Tied to this is the increased severity of short channel effects (SCEs) as dimensions are decreased, hence the reason to move to 3D structures in the form of FinFETs. One type of SCE that is known to cause performance degradation is Drain Induced Barrier Lowering (DIBL). To reduce DIBL, dopant junction profiles are made more abrupt. This can be done through the introduction of Sigma/cavity, fully depleted silicon-on-insulator (FDSOI) structures and the modulation of stress through optimal engineered epitaxial buffer layers. To assess the quality of interfaces in these different structures over nanometer scale regions requires the use of analysis techniques such as Atom Probe Tomography (APT) and Transmission Electron Microscopy (TEM). This presentation will discuss the ability of APT to extract the critical information of interest to device engineering.

9:20am AS+SS-ThM5 Analysis of ALD/CVD Thin Film Conformality using Lateral High Aspect Ratio (LHAR) Structures: Experimental Characteristics and Proposed Classifications, Riikka Puurunen, VTT Technical Research Centre of Finland; J. Dendooven, V. Cremers, C. Detavernier, Ghent University, Belgium

High conformality—the ability of a thin film to cover a complex three-dimensional substrate uniformly—is a key advantage of atomic layer deposition (ALD) compared to chemical vapor deposition (CVD) and physical vapor deposition (PVD) processes. More than 700 ALD processes (with unique reactant pairs/activation) have been reported, as calculated from Ref. [1]. Conformality has been experimentally studied for a small minority of these, most likely because of the lack of easily available test structures and accessible methods of analysis.

When conformality is investigated, most typically, vertical trenches (or holes) etched into silicon, typically with aspect ratio (AR) up to around 50:1, are used and the results are analysed point by point by cross-sectional electron microscopy. Comparison of results obtained in different studies is difficult because of the lack of standard test structures and standard means of analysis, and the large variety of process conditions that are used. The theoretical framework for interpreting the conformality results is also underdeveloped.

To develop the conformality analysis, we have reported on macroscopic [2, 3] and microscopic [4] lateral high aspect ratio (LHAR) test structures. In contrast to vertical HAR, LHAR structures allow one to investigate thin film thickness and properties in very demanding aspect ratios (>10 000:1) and obtain accurate information of film thickness and properties along the feature by standard means of measurement such as ellipsometry and reflectometry. The purpose of the present work is to compare results obtained for different thin film processes in different test structures (our own + literature) using the highly studied [1, 5] Me₃Al/H₂O ALD process as baseline. We propose a classification scheme for how the thickness line profiles are expected to vary inside LHAR structures in different cases of characteristic governing growth chemistries.

Acknowledgements: This work has been funded by the Finnish Centre of Excellence in Atomic Layer Deposition, BOF-UGent, FWO-Vlaanderen and SIM-Flanders (TRAP-FUNC project). Feng Gao and Meeri Partanen are thanked for fabricating the microscopic LHAR structures.

References:

- [1] V. Mikkilainen et al., J. Appl. Phys. 113 (2013) 021301.

- [2] J. Dendooven et al., J. Electrochem. Soc. 156 (2009) P63.
[3] J. Dendooven et al., J. Electrochem. Soc. 157 (2010), G111.
[4] F. Gao et al., J. Vac. Sci. Technol. A, 33 (2015), 010601.
[5] R. L. Puurunen, J. Appl. Phys. 97 (2005) 121301.

9:40am AS+SS-ThM6 *In Situ* Liquid SIMS Investigation of Chemical Components of the Solid-Electrolyte Interface in Li Ion Batteries, Zihua Zhu, C. Wang, Y. Zhou, D.R. Baer, W. Xu, R. Cao, X. Yu, P. Yan, R. Zhao, Pacific Northwest National Laboratory

Since the birth of Li-ion battery, Solid-Electrolyte Interface (SEI) has been a hot research topic, and numerous efforts have led to some information about its chemical composition, formation mechanism and degradation process. However, critical questions that can enable the design of advance battery systems remain unanswered because it has been very difficult to molecularly examine the SEI layer during battery operation. For example, in situ TEM has been used to study the formation process of the SEI layer in Li ion batteries; however, mostly morphological information, but very limited chemical information is obtained. In situ liquid SIMS was developed in Pacific Northwest National Laboratory (PNNL) in the last several years, and it has proven a very promising new technique to provide both elemental and molecular information at solid-liquid interfaces. In this work, a model Li-ion battery was designed for in situ liquid SIMS analysis of SEI layer. A ~70 nm thick Cu film was deposited onto a SiN membrane, which served as anode. Cathode was traditional LiCoO₂. 1.0M LiPF₆ in EC (ethylene carbonate)/DMC (dimethyl carbonate) was used as electrolyte. Li₂O and LiOH are found in the SEI layer, while very little LiF is observed, indicating LiF is not an important component in the SEI layer. More interestingly, solvent molecules are found in the SEI layer, and the major component is DMC but not EC. In addition, very little PF₆⁻ is found in SEI layer. This is the first time that molecular information of the SEI layer is obtained, and the new information will greatly advance understanding formation mechanism and degradation process of SEI layer.

11:00am AS+SS-ThM10 Electronic and Physical Changes to Soft Materials Caused by Gas Cluster Sputtering, Christopher Goodwin, Z.E. Voras, T.P. Beebe, Jr., University of Delaware

The development and application of gas cluster ion sputtering (GCIS) of soft materials opens the ability to perform 3D analysis without removing the sample from a vacuum environment. GCIS has been used to remove material from the surface of some samples without leaving behind a significant amount of damaged material. This allows for depth profiling and sample cleaning in vacuum, without loss of chemical information. The soft sputtering standard Irganox 1010 has been used to study topological effects of GCIS with atomic force microscopy (AFM) while chemical changes were monitored with X-ray Photoelectron Spectroscopy (XPS). In addition to Irganox 1010, polyaniline has been studied due to its importance as an organic conductive material, allowing for many applications such as a solar cells, antistatic and corrosion-resistant coatings, and superconductors. GCIS was used to depth profile into thin films of polyaniline, resulting in some topological (AFM) and chemical changes (XPS). Our interest is in exploring how these changes caused by GCIS sputtering affect the electronic band structure of conductive polymers.

11:20am AS+SS-ThM11 FIB-TOF Characterization of Organic and Organic/Inorganic Structures, David Carr, G.L. Fisher, S.R. Bryan, Physical Electronics; S. Iida, T. Miyayama, ULVAC-PHI, Japan

1. Introduction

Probing the sample chemistry beyond the surface region with ion beam sputtering is subject to practical limitations which include preferential sputtering, accumulated sputter beam damage, inclusions, and voids. These effects can result in a distortion or complete loss of the true chemical distribution as a function of depth.

In situ FIB milling and sectioning with TOF-SIMS chemical imaging (3D FIB-TOF tomography [1]) is an alternative approach to achieve 3D chemical imaging of complex matrix chemistries. The FIB milling can minimize or eliminate artifacts caused by sputter depth profiling from the surface.

For matrices with organics components, however, FIB beam-induced chemical or molecular damage may limit the detection of characteristic molecular signals. The characteristic molecular signals can often be recovered with cluster ion polishing to remove the organic FIB damage.

2. Method

The 3D chemical characterization of organic and organic/inorganic mixed composition structures was achieved utilizing FIB-TOF on a PHI TRIFT nanoTOF II (Physical Electronics, USA) imaging mass spectrometer Thursday Morning, November 10, 2016

equipped with the new parallel imaging MS/MS [2,3]. The spectrometer's large angular acceptance and depth-of-field maintain high mass resolution and high mass scale linearity in this challenging geometry.

3. Results

Results will be presented for structures with mixed organic phases and mixed organic/inorganic phases. The FIB-TOF results will be compared with corresponding sputter depth profiling results to highlight the relative advantages of the two techniques along with potential complicating factors to the analyses. The high sensitivity of the TOF-SIMS technique is not limited to strong organic matrix peaks. Data will be presented showing the ability to probe the 3D distribution of polymer additives in a sample. The identity of the additives is confirmed using the newly developed parallel imaging MS/MS option for the nanoTOF II. The ability to study buried organic structures with FIB-TOF and then conclusively identify the detected species using MS/MS is a powerful new development for the field of TOF-SIMS.

4. References

- [1] A. Wucher, G.L. Fisher and C.M. Mahoney, Three-Dimensional Imaging with Cluster Ion Beams (p. 207-246) in *Cluster Secondary Ion Mass Spectrometry: Principles and Applications*, C.M. Mahoney (Ed.), Wiley & Sons, N.J. (2013).
[2] P.E. Larson, J.S. Hammond, R.M.A. Heeren, G.L. Fisher, *Method and Apparatus to Provide Parallel Acquisition of MS/MS Data*, U.S. Patent 20150090874, 2015.
[3] G.L. Fisher, J.S. Hammond, P.E. Larson, S.R. Bryan, R.M.A. Heeren, *SIMS XX Proceedings*, D. Castner (Ed.), Wiley, N.J. (2016) DOI: 10.1116/1.4943568.

11:40am AS+SS-ThM12 Molecular Depth Profiling with a New Hybrid 3D SIMS instrument for Improved Molecular Identification, Alexander Pirkel, R. Moellers, H.F. Arlinghaus, ION-TOF GmbH, Germany; N.J. Havercroft, ION-TOF USA; E. Niehuis, ION-TOF GmbH, Germany; A.A. Makarov, S. Horning, Thermo Fisher Scientific; R. Havelund, M.K. Passarelli, A.G. Shard, I.S. Gilmore, National Physical Laboratory, UK

Introduction

Depth profiling of organic layers for optical and electronic devices can be ideally performed using gas cluster ion beams (GCIB) in combination with time-of-flight secondary ion mass spectrometry (TOF-SIMS). For optimum performance a dual beam approach is utilized, employing a lower energetic quasi DC sputter beam for material removal and a short pulsed small spot analysis beam for optimal mass spectral and imaging performance.

However molecular identification of unknown substances, e.g. contaminants, is usually hampered by constraints in mass resolution and mass accuracy of the TOF analyser. Furthermore ions generated in the sputter phase of the dual beam experiment are lost for the MS analysis. In order to overcome these limitations a TOF/Orbitrap™-SIMS hybrid mass analyser instrument was developed.

Methods

A prototype SIMS instrument with a hybrid TOF/Orbitrap mass analyser was utilized for acquisition of organic depth profiles. During sputtering with 5-20 keV argon clusters secondary ions can be detected using the Q Exactive™ HF mass analyser. Selective ion gating was implemented to avoid artefacts from the crater walls. *In situ* tandem MS analyses of the most abundant peaks were used to confirm the mass assignments. Imaging TOF analysis with high lateral resolution was performed on the same instrument using short pulses from a 30-60 keV Bi-liquid metal ion gun (LMIG) and a dedicated TOF-SIMS V analyser for comparative measurements.

Preliminary Data

Molecular depth profiles were acquired using GCIB induced desorption in a single beam approach from organic test structures and organic LED materials. The high mass resolution of 240 000 of the Q Exactive HF mass spectrometer proved to be essential for separation of otherwise overlapping ion signals. Molecular assignments based on the high mass accuracy below 3 ppm were validated using tandem MS analysis. Up to 5 decades of dynamic range and a depth resolution below 8 nm were found to be possible with this approach leading to unprecedented depth profiling results.

Depth profiles and according spectra are compared to the classical dual beam approach. While depth resolution is similar, differences in the relative signal intensities were observed in spectra from the two different

ion beams. Implications for the analysis of biological samples will be discussed.

12:00pm AS+SS-ThM13 3-D Analysis of Binding-Medium Degradation as Related to Renaissance-Era Artwork, Zachary Varas, C.M. Goodwin, University of Delaware; J.L. Mass, Rijksmuseum; K.R. DeGhetaldi, Winterthur Museum; T.P. Beebe, Jr., University of Delaware

In historical art objects, binding-medium degradation involves complex chemistries that can occur at the surface or interface of a paint layer. These can propagate inward toward the bulk material, caused by inherent impurities within the paint that migrate throughout the paint layer. These effects can cause mechanical failure due to binding-medium degradation, primarily observed as paint-layer flaking, spalling, and fracture. Our prior research performed on Renaissance-era artwork has indicated two major correlations to the severity of binding-medium degradation: i) depletion of long-chain fatty acid components within the binding medium of a paint layer, and ii) alteration of the amino-acid composition of proteinaceous materials comprising the binding medium. In this study, the effects of controlled aging factors (i.e., heat, humidity, and UV exposure) on thin films of egg tempera were observed through the use of x-ray photoelectron spectroscopy (XPS) and time-of-flight secondary ion mass spectrometry (ToF-SIMS). The newly available technology of gas cluster ionization sources (GCIS) allows for the ability to depth profile through some soft organic and biological materials with no little or no ion-induced damage. By using an argon-cluster ion beam to depth profile through a degraded thin film, a 3-dimensional analysis of short- and long-range degradation effects, followed by XPS and ToF-SIMS, respectively, was performed. Since ultramicrotomy is an established sample-preparation technique in the art conservation field, results of GCIS will be compared to ultramicrotomy as sample preparation method for organic and biological thin films.

Biomaterial Interfaces

Room 101A - Session BI+AS+SA-ThM

Synthesis and Processing of Biomaterials/Biologically Inspired Materials

Moderators: Daniel Barlow, US Naval Research Laboratory, Lara Gamble, University of Washington

8:00am BI+AS+SA-ThM1 Response of PC 12 Cells to Mesoporous Substrates with and without DC Bias, F. Sabri, University of Memphis; Kyle Lynch, University of Memphis; O. Skalli, University of Memphis

The interaction of nerve cells with nanostructured surfaces and substrates is of great importance to the field of tissue engineering and artificial substrates developed for biomedical applications. It has been established that cells respond to different polymer surface characteristics such as roughness, surface free energy, topography, chemistry, charge, and other properties including electrical conductivity. It has also been recognized that the nanotopography can affect and influence cell morphology, cell alignment, cell signaling and extension of neurites. Here, we discuss the influence of the mesoporous structure of crosslinked silica aerogels on the adhesion, proliferation, and neurite extension of PC 12 cells, in the presence and absence of applied DC bias. The behavior of cultured PC 12 cells on the aerogel substrates is compared to the behavior of cells cultured on cell culture plastic (control) and the affect of applied DC bias of different magnitudes is carefully investigated. The neurite extensions clearly show a preferred growth direction and the rate of growth of extensions is also influenced by the varying conditions.

8:20am BI+AS+SA-ThM2 Collagen Functionalized with ALD-TiO₂: A Novel Biomaterial for Bone Grafting, Arghya Kamal Bishal, C. Sukotjo, C.G. Takoudis, University of Illinois at Chicago

In medicine, the use of implants is growing rapidly. Some patients may not have enough bone to support such implants.¹⁻² Therefore, those patients are required to have augmentation, a procedure to increase the height or width of inserted bone-like supporting materials, prior to implantation.¹ Collagen resorbable membrane is used as a bone grafting material which acts as supporting material and facilitates new bone formation.³ Sometimes, titanium reinforced collagen membrane is used for improved stability.²

Collagen is an important biomaterial which is used in several biomedical applications. It has a triple helix structure made of polypeptide chains.^{3,4} Hydrogen bonds play an important role in keeping together these peptide chains. Glycine, proline are the most abundant amino acids found in its

structure. Collagen has also the ability to be reorganized and crosslinked and thus turn into flexible fibrils with higher tensile strength.³ There are four main types of collagen: type I, II, III and V. Among them mostly type I and little amount of type V construct the bone structure by forming a composite with hydroxyapatite (HA) crystals.⁴

Titanium (TiO₂) itself is biocompatible.⁵ Additionally, it has the ability to attract Calcium and Phosphate in a liquid environment.⁶ Therefore TiO₂ coated collagen may be used as an excellent bone grafting material to nucleate Ca and P and thus reconstructing a stable bone structure. In this work, we present ALD of TiO₂ on collagen membrane in a custom-made ALD reactor. The deposition was performed at room temperature. Tetrakis(dimethylamido)titanium (TDMAT) and ozone were used as metal precursor and oxidizer, respectively. Samples were characterized for their surface morphology, composition and mechanical properties. Energy dispersive spectroscopy confirmed the presence of Ti on coated collagen and electron microscopy showed an increase in fiber diameter after deposition by more than a factor of 2:

References:

1. Chiapasco M, Casentini P, Zaniboni M. International Journal of Oral & Maxillofacial Implants. 2009 Oct 2;24.
2. Cucchi A, Ghensi P. The open dentistry journal. 2014 Nov 14;8(1).
3. Khan R, Khan MH. Journal of Indian Society of Periodontology. 2013 Jul 1;17(4):539.
4. Cen L, Liu W, Cui L, Zhang W, Cao Y. Pediatric research. 2008 May 1;63(5):492-6.
5. Healy KE, Ducheyne PA. ASAIO transactions/American Society for Artificial Internal Organs. 1990 Dec;37(3):M150-1.
6. Järn M, Areva S, Pore V, Peltonen J, Linden M. Langmuir. 2006 Sep 12;22(19):8209-13.

8:40am BI+AS+SA-ThM3 Nanostructure Formation on Biomaterials by Directed Irradiation Synthesis (DIS) for Tissue Regeneration and Maximize Corrosion Resistance, Jean Paul Allain, A.R. Shetty, University of Illinois at Urbana-Champaign; S. Arias, A. Barnwell, University of Illinois at Urbana Champaign; F. Echeverria, L.F. Berrio, University of Antioquia, Colombia

An important aspect of tissue engineering is to create a favorable extracellular microenvironment, mainly the extracellular matrix (ECM) which can guide cell differentiation and tissue regeneration. The ECM consists of a number of cues that can be guided by surface topography and matrix stiffness [1]. Recent studies [2,3] have demonstrated that depending on the type of surface structuring and patterning, cell adhesion can be controlled with potential applications in smart cell culture systems and biosensors. Many of the desired biomaterial properties that require a combination of metal alloy and soft material interfaces cannot be processed with conventional bottom-up techniques. Directed irradiation synthesis (DIS) address this limitation by introducing a synthesis process that is scalable to high-volume manufacturing by virtue of its intrinsic large-area simultaneous exposure of materials surfaces and interfaces.

In this study, we have employed directed irradiation synthesis to induce nanostructure formation on two commonly used biomaterials: 1) Ti6Al4V and 2) magnesium (Mg). The goal is to examine the role of surface nanostructuring on the stimulation of cells and tissues in order to provide important cues for tissue regeneration as well as guarantee a good corrosion resistance and to minimize bacteria adhesion. Detailed characterization, establishing processing conditions and correlating them to surface and biomaterial properties have been successfully performed on nanostructured medical grade Ti6Al4V and Mg. These irradiated surfaces were biologically evaluated by using human aortic smooth muscle cells (HASMCs) for cytotoxicity and cell/surface adhesion and interactions. This analysis allowed us to determine connections with processing, structure, surface energy, and biointerface properties. Biological response of these new surfaces has also lead us, for the first time, to establish correlations between nanostructuring by DIS and cell stimulation, as well as to show the real potential of these new surfaces to favorably stimulate cells and tissues different than bone. The corrosion behavior of these biomaterials in a phosphate buffered simulated body fluid (SBF) has also been investigated for bone implant application.

References:

- 1) Evelyn, K.F., Darling, E.M., Kulangara, K., Guilak, F., and Leong K.W., *Biomaterials* **2010**, 31, 1299–1306.

2) Guasch, J. Diemer, J., Riahinezhad, H., Neubauer, S., Kessler, H., and Spatz, J.P., *Chem. Mater.* **2016**, 28, 1806–1815

3) Slater, J.H, Boyce, P.J, Jancaitis, M.P., Gaubert, H.E, Chang, A.L., Markey, M.K., and Frey

W., *ACS Appl. Mater. Interfaces* **2015**, 7, 4390–4400.

9:00am BI+AS+SA-ThM4 Controlled Peptide Surfaces of Various Ratios that Guide Neural Stem Cell Differentiation, *HalaShakib Dhowre, M. Zelzer, H. Sahaf, C. Towilson, N.A. Russell*, University of Nottingham, UK
Cell instructive biointerfaces represent an essential aspect for the advancement of regenerative medicine. Currently, a major issue in biointerface design is the limited ability to mimic the complex interactions of the natural processes in the extracellular matrix (ECM) with artificially designed surfaces and interfaces¹. While biomaterial surfaces have been shown to be able to elicit specific cell responses (e.g. adhesion, proliferation, differentiation), precise control akin to that of natural cellular environments is still lacking².

AIM:

The present work aims to address this challenge by designing new synthetic peptide surfaces with well controlled composition and functionality able to impact control over the differentiation of neuronal stem cells with the ultimate goal to understand and control how neuronal networks function.

METHODS:

Compositionally well defined surface concentrations of two short laminin peptide sequences, Arg-Gly-Asp (RGD) and Ile-Lys-Val-Ala-Val (IKVAV) were prepared of various ratios via the “grafting from” stepwise approach and the surface modification was confirmed with surface analysis techniques to indicate successful peptide functionalisation. The neural stem and progenitor cells (NSPC) were set up from embryonic rat hippocampi (E18). Immunocytochemistry (ICC) observed cell viability and differentiation to specific NSPC lineages for Nestin, β III-Tubulin and GFAP.

RESULTS:

Surface characterising techniques (WCA, AFM and ToF-SIMS) verified the successful amino acid build-up to peptides on the surfaces, allowing modification of the surfaces with RGD and IKVAV. Enhanced NSPC adhesion, proliferation and differentiation were observed on the peptide surfaces. ICC demonstrated Nestin expression decrease after the removal of the growth factors (EGF and FGF) and an increase in the expression of β III-Tubulin and GFAP; thus illustrating cells differentiating from stem cells to neurons or astrocytes due to peptide surface influence.

CONCLUSION:

Well defined peptide surfaces were designed successfully, the various ratios of RGD and IKVAV surfaces demonstrated cell adhesion, proliferation and desirable effects in controlling different populations of stem cell fate. These surfaces may advance new insight in understanding how surface properties affect the regulation of physiological relevance in directing neural cell differentiation, which will be essential to understand how neural networks function.

References

1. Zelzer, M. & Ulijn, R.V., *Chem.Soc.Rev.*, **39**,3351-3357 (2010)
2. Ricault, S.G. et al., *Biomaterials.*, **35**, 727-736 (2014)
3. Cooke, M.J. et al., *J.Biomed.Mater.Res-Part A.*, **93**,824-832 (2010)

9:20am BI+AS+SA-ThM5 Biofunctional Hydrogels for Tissue Repair, *Andres Garcia*, Georgia Institute of Technology

INVITED

Hydrogels, highly hydrated cross-linked polymer networks, have emerged as powerful synthetic analogs of extracellular matrices for basic cell studies as well as promising biomaterials for regenerative medicine applications. A critical advantage of these synthetic matrices over natural networks is that bioactive functionalities, such as cell adhesive sequences and growth factors, can be incorporated in precise densities while the substrate mechanical properties are independently controlled. We have engineered poly(ethylene glycol) [PEG]-maleimide hydrogels to study epithelial morphogenesis and identified independent contributions of biophysical and biochemical properties of these materials to this developmental process. In another application, we have developed synthetic hydrogels that support improved pancreatic islet engraftment, vascularization and function in diabetic models. These studies establish these biofunctional hydrogels as promising platforms for basic science studies and biomaterial carriers for cell delivery, engraftment and enhanced tissue repair.

11:00am BI+AS+SA-ThM10 Nanoscale Domain Formation Induced by Partial Polymerization Creates Planar Supported Lipid Bilayers that are Fluid and Stable, *N.Malithi Fonseka, B. Liang, K.S. Orosz, C.A. Aspinwall, S.S. Saavedra*, University of Arizona

Planar supported lipid bilayers (PSLBs) are widely explored bilayer platforms for receptor-based biosensors. PSLBs composed of fluid lipids lack the stability necessary for many technological applications due to the relatively weak non-covalent interactions between lipid molecules. Lipid polymerization enhances bilayer stability, but may greatly reduce lipid mobility and membrane fluidity. In an effort to enhance bilayer stability while maintaining fluidity, we have prepared and characterized PSLBs composed of mixtures of the polymerizable lipid bis-Sorbyl phosphatidylcholine (bis-SorbPC), and the fluid lipid diphytanoyl phosphatidylcholine (DPhPC) to form mixed PSLBs. We measured lateral diffusion coefficients (D) as a function of the bis-SorbPC/DPhPC molar ratio using fluorescence recovery after photobleaching (FRAP). In pure DPhPC PSLBs, $D = 0.66 \mu\text{m}^2/\text{sec}$. In equimolar poly(bis-SorbPC)/DPhPC, $D = 0.36 \mu\text{m}^2/\text{sec}$, whereas when the ratio is greater than 0.7, D decreased to $0.13 \mu\text{m}^2/\text{sec}$. These data show that considerable fluidity is retained even when the poly(bis-SorbPC) fraction is substantial, which suggests that these bilayers are phase segregated, composed of polymerized and fluid domains. However domains were not observed with fluorescence microscopy techniques. The sub- μm morphology of these PSLBs was therefore investigated using atomic force microscopy (AFM). Nano-scale phase segregation of the two lipids was observed. DPhPC forms a continuous lipid matrix that is 0.2-0.4 nm thicker than the island-like poly(bis-SorbPC) domains. This height difference agrees with bilayer thicknesses measured for pure DPhPC and poly(bis-SorbPC) PSLBs. Furthermore, it was observed that the size of the poly(bis-SorbPC) domains increased with the percentage of poly(bis-SorbPC) in the PSLB. In summary, mixed lipid bilayers composed of poly(bis-SorbPC) and DPhPC form nano-structured membranes with retained lipid diffusivity, and thus they have considerable potential for creating membrane-based biosensors in which receptor activity depends on bilayer fluidity.

11:20am BI+AS+SA-ThM11 Stabilization of Lipid Films by Hyaluronic Acid and Polymeric Substitutes in a Joint Model System, *Felicitas Schwoerer*, Universität Heidelberg, Germany; *M. Trapp, R. Steitz*, Helmholtz-Zentrum Berlin für Materialien und Energie GmbH; *R. Dahint*, Universität Heidelberg

In the United States there are 27 million people suffering from osteoarthritis. The disease is primarily caused by the degeneration of cartilage, which covers the bone ends of the joints and is in turn decorated with a phospholipid (PL) layer. The bone ends are separated by the synovial fluid containing the polysaccharide hyaluronic acid (HA) as a main component. It is generally assumed that both HA and PLs reduce friction and protect the cartilage. Based on the observation that HA concentration is reduced in diseased joints, a new cure called viscosupplementation has been developed, where HA or mixtures of HA and PLs are injected into the joints. However, until now the positive effect of such therapy is under debate.

To elucidate the importance of HA and PLs for joint lubrication and protection on a molecular level we investigate their interaction using a simplified model system for natural joints. A silicon wafer (representing the bone end) is covered with PL oligobilayers and incubated in an aqueous solution containing HA or polymeric substitutes (representing the synovial fluid). To mimic the forces in joint movement, we expose the model surfaces to a home-built shear apparatus facilitating *in situ* measurements at a rotational speed between 0 rpm and 6000 rpm. Measurements were performed at *BioRef* (Helmholtz-Zentrum Berlin), a time-of-flight neutron reflectometer with integrated infrared spectroscopy.

Upon contact with both HA and poly(allylamine hydrochloride) (PAH) solutions a tremendous swelling of the lipid film occurs. Film thickness increases by a factor of about four compared to pure D_2O exposure due to a drastic increase in the thickness of the interstitial water layers located between adjacent lipid bilayers. This effect is most likely due to the adsorption of charged polymers at the lipid headgroups leading to electrostatic repulsion. Despite their high film thickness and water content, the polymer-exposed lipid films exhibit approximately ten times higher shear stability than the respective systems incubated in pure water. With increasing rotational speed the lipid films contain substantially enhanced water fractions, which we attribute to increasing lateral fragmentation. Present investigations aim at the question whether HA and PAH are incorporated into the lipid tail region and bridge adjacent bilayers as this might explain the observed higher stability.

Thursday Morning, November 10, 2016

11:40am **BI+AS+SA-ThM12 New Substrates and Patterning Methods for Supported Lipid Bilayers**, *Sally McArthur, L. Askew*, Swinburne University of Technology, Australia **INVITED**

The cell membrane encases and protects cellular components and plays an important role in transport, signalling and disease. Studying membrane behaviour is a challenging task due to the complexity and scale on which these processes occur. Supported lipid bilayers (SLBs) have provided researchers with stable and reproducible platforms to recreate cell membrane environments. The planar structure of the model means a variety of patterning techniques can be employed to recreate membrane architecture on both a micro and nanoscale. In particular, pre-patterned substrates are of great interest as they eliminate complications associated with preserving membrane integrity during patterning. Plasma polymers provide a versatile method of creating thin films with a variety of different surface chemistries. In this work we explore the behaviour of plasma coatings in aqueous conditions and the use of plasma films for creating patterned SLBs using vesicle collapse. The results demonstrate that variations in plasma polymer chemistry can be used to control lipid bilayer formation and the locations of different lipid species. Characterisation of film behaviour and bilayer formation was conducted using a variety of techniques including ellipsometry, quartz crystal microbalance with dissipation (QCM-D), confocal microscopy, atomic force microscopy (AFM) and Time-of-Flight Secondary Ion Mass Spectrometry (ToF-SIMS).

Electronic Materials and Photonics

Room 102A - Session EM+AC+SS+TF-ThM

Radiation Detection Materials and Devices

Moderators: Sean King, Intel Corporation, Michelle Paquette, University of Missouri-Kansas City

8:00am **EM+AC+SS+TF-ThM1 Novel High Energy Resolution Scintillator Detectors**, *Arnold Burger, E. Rowe, L. Matei, P. Bhattacharya, M. Groza*, Fisk University; *K. Stassun*, Vanderbilt University; *A. Stowe*, Consolidated Nuclear Security Y-12; *N. Cherepy, S. Payne*, Lawrence Livermore National Laboratory **INVITED**

This presentation will review the status of bright scintillators for gamma and thermal neutrons applications. The scintillators are based on single crystals of halides or selenides that are activated by rare earth ions or are self activated. The main features that make them attractive for biological, medical, space and national security applications are: (i) high stopping power of radiation, (ii) high energy resolution, (iii) fast decay time, (iv) crystal growability at low cost, (v) good gamma/neutron discrimination via pulse shape analysis, and (vi) good spectral matching with silicon photodetectors for compact and low power devices and instrumentation.

8:40am **EM+AC+SS+TF-ThM3 Improved p-n Heterojunction Device Performance Induced by Irradiation in Amorphous Boron Carbide Films**, *George Peterson, Q. Su*, University of Nebraska - Lincoln; *Y. Wang*, Los Alamos National Laboratory; *P.A. Dowben, M. Nastasi*, University of Nebraska - Lincoln

Amorphous hydrogenated boron carbide films ($a\text{-B}_{10}\text{C}_{2+x}\text{H}_y$) on Si p-n heterojunctions were fabricated utilizing plasma enhanced chemical vapor deposition (PECVD). These devices were found to be robust when irradiated with 200 keV He^+ ions. For low doses of irradiation, contrary to most other electrical devices, the electrical performance improved. On the heterojunction I(V) curve, reverse bias leakage current decreased by 3 orders of magnitude, series resistance across the device decreased by 64%, and saturation current due to generation of electron-hole pairs in the depletion region also decreased by an order of magnitude. It is believed that the improvements in the electrical properties of the devices are due to an initial passivation of defects in the $a\text{-B}_{10}\text{C}_{2+x}\text{H}_y$ film resulting from electronic energy deposition, breaking bonds and allowing them to reform in a lower energy state, or resolving distorted icosahedron anion states.

9:00am **EM+AC+SS+TF-ThM4 Amorphous Hydrogenated Boron Carbide for Direct-Conversion Solid-State Neutron Detection**, *Gyanendra Bhattacharai, T.D. Nguyen, S. Dhungana, A.N. Caruso, M.M. Paquette*, University of Missouri-Kansas City

The trade-off between conversion layer thickness and penetration depth of primary reaction products inherently limits the efficiency of conversion-layer solid-state neutron detectors, motivating the need for direct-conversion solutions. Direct-conversion devices, in principle, offer nearly unity detection efficiency, a minimum of fabrication steps, large-area scalability, and high efficiency density, all of which are essential for small-

sized neutron spectrometers as well as for large-area detectors. However, to date, there is a lack of well-developed semiconductor materials with high thermal neutron absorption that also lead to energetic reaction products amenable to detection. Amorphous hydrogenated boron carbide ($a\text{-B}_{10}\text{C}_{2+x}\text{H}_y$), a complex disordered semi-insulating material, is a promising candidate because of its high neutron absorption and high resistivity. Additionally, excellent mechanical, chemical, and thermal stability make it suitable for harsh detection environments. The main challenges, however, in the study of $a\text{-B}_{10}\text{C}_{2+x}\text{H}_y$ are its low charge carrier mobility, the difficulties associated with making proper electrical contacts for accurate charge transport measurements, and the inefficacy of traditional experimental techniques and interpretations to address the complex nature of the material (i.e., it is a high-resistivity, disordered, molecular solid). This contribution will present an overview of how $a\text{-B}_{10}\text{C}_{2+x}\text{H}_y$ may lead to high-efficiency neutron detectors based on theoretical simulations, the study of its charge transport metrics focusing mainly on charge carrier mobility and lifetime, and the development of proper electrical contacts on PECVD grown thin films of this material.

9:20am **EM+AC+SS+TF-ThM5 Radiation Damage of Low- κ Interlayer Dielectrics Studied with Electrically Detected Magnetic Resonance**, *Michael Mutch, P.M. Lenahan*, Pennsylvania State University; *S.W. King*, Intel Corporation

Radiation effects of MOS devices have been extensively studied due to the demand for electronic devices in space applications.[1] The scaling of these MOS devices will lead to an eventual need for low-dielectric constant (i.e., low- κ) dielectrics to reduce parasitic capacitances associated with scaling of back-end-of-line interlayer dielectrics (ILDs). However, little is known about radiation effects of low- κ ILDs. We utilize electrically detected magnetic resonance (EDMR) via spin-dependent trap-assisted tunneling (SDTAT) to study point defects in porous low- κ a-SiOC:H systems before and after exposing samples to radiation damage. SDTAT/EDMR has the sensitivity and analytical power to specifically identify only those defects which are involved in electronic transport. Due to the inherent complexity of the a-SiOC:H systems, multiple frequency EDMR is utilized to better understand defect structure when featureless spectra are present.

The a-SiOC:H films are grown via PECVD, and exhibit carbon dangling bonds prior to porogen removal via UV-annealing.[2] After porogen removal via UV treatment, it has been shown, via multiple frequency EDMR, that silicon dangling bonds are the dominating defect center responsible for SDTAT in these films.[2] The porous a-SiOC:H systems were subjected to a 15 Mrad total dose via a cobalt-60 dry cell gamma-ray source while simultaneously applying either positive, negative, or no bias. We find that the post-radiation IV curves are a strong function of the biasing conditions which were applied during radiation. This likely indicates that electron and hole traps will both play a role in radiation damage effects in these systems. We find that the EDMR response amplitude is greatly increased (by a factor of 4 or greater) after irradiation for all biasing conditions. This result indicates a substantial increase in the density of defects involved in electronic transport. Multiple frequency EDMR measurements suggest that the generated defects are primarily silicon dangling bonds.

[1] J. R. Schwank et al., IEEE Trans. Nuc. Sci. **55**, 1833 (2008).

[2] M. J. Mutch et al., J. Appl. Phys. **119**, 094102 (2016).

9:40am **EM+AC+SS+TF-ThM6 Modeling Unit Displacement Damage in Amorphous Silicon Oxycarbides**, *Hepeng Ding, M. Demkowicz*, MIT

Amorphous silicon oxycarbide (SiOC) is of great technological interest. To study its potential application as a radiation-resistant material, we present *ab initio* modeling investigations of unit displacement damage processes in it using density functional theory. We model 0.1 keV primary knock-on atoms (PKA) in SiO_2 , SiOC, and hydrogenated SiOC (SiOCH) with different hydrogen levels. We find that PKAs affect the carbon-clustering tendency in both SiOC and SiOCH. Our results also suggest that SiOCH is irradiation indifferent, i.e., upon PKA, the potential energy does not increase and there is no major structural change.

This work was funded by the DOE Office of Nuclear Energy, Nuclear Energy Enabling Technologies, Reactor Materials program, under contract No. DE-NE0000533. Computational support was provided by DOE-NERSC and DOE-OLCF.

Thursday Morning, November 10, 2016

11:00am **EM+AC+SS+TF-ThM10 Position-Sensitive 3D CZT Gamma-Ray Detectors with Thickness Up to 50 mm**, **Ralph James**, A.E. Bolotnikov, G.S. Camarda, Y. Cui, G. De Geronimo, J. Fried, A. Hossain, G. Mahler, U. Roy, E. Vernon, G. Yang, Brookhaven National Laboratory

INVITED

High-granularity position-sensitive detectors allow for accurate charge-signal corrections to overcome non-uniformities in the devices' responses caused by crystal defects. The operational principle of position-sensitive detectors is analogous to the well-known drift ionization chambers used for tracking charged particles and detecting the interaction events generated by gamma rays. Advantages of the position-sensitive designs were realized in a number CZT detectors, including CAPture™, hemispherical, Frisch-ring, capacitive Frisch-grid and even pixel detectors in which pixel contacts act like shielding electrodes. In our virtual Frisch-grid (VFG) devices, the sensing strips are separated from the crystal surfaces by a thin insulating layer, as it was originally done in other Frisch-grid designs. The amplitudes of the signals readout from the strips are used to measure the coordinates of the interaction points and correct the response non-uniformities. The drift time and the cathode-to-anode ratio were used to independently evaluate the location of the interaction points in Z directions, correct for electron loss, and identify and reject the events for which the charge losses caused by defects are so great that they cannot be corrected accurately. Combining these two techniques allows us to significantly enhance the spectral responses of position-sensitive VFG detectors, and to significantly improve their performance. Such high-granularity position-sensitive detectors open up the opportunity for using thicker, less expensive crystals. We demonstrated that today's CZT material is suitable for detectors with up to 40-50-mm drift distances, provided that the detectors have the ability to correct their response non-uniformities on a scale comparable to the sizes of electron clouds, which is ~100 m. We employed an ASIC and data-acquisition system developed by BNL's Instrumentation Division for arrays of VFG detectors. For each detector we used 6 ASIC channels to read the negative signals from the cathode and from four position-sensing pads, and the positive signals from the anode. For each interaction event, the anode signal correlates with the X and Y values converted from the 4 strip signals and Z coordinate evaluated from the cathode signal. This relationship allows us to correct each anode signal in accordance with the location of the interaction point. We selected the voxel sizes to achieve the best performance, typically ~30x30 pixels in XY-space and ~100 segments in the Z-direction. The performance of thick position-sensitive VFG detectors fabricated from CZT crystals will be reported for a variety of radioactive sources and testing conditions.

11:40am **EM+AC+SS+TF-ThM12 Understanding the Electrical Properties of U₃O₈ for Direct Conversion Neutron Detectors**, **Brandon Shaver**, S. Lawson, B. Musicó, The University of Tennessee Knoxville; S. Dhungana, G. Bhattarai, M.M. Paquette, A.N. Caruso, University of Missouri-Kansas City; T. Meek, The University of Tennessee Knoxville

With a high neutron fission cross section for ²³⁸U, U₃O₈ is one of a series of uranium oxide semiconductors that may be suitable for direct-conversion neutron detectors. However, the electrical transport properties of U₃O₈ are not well-characterized: the literature that does exist reports largely inconsistent resistivity values, and similarly contradictory values for work function. One of the reasons for these wide ranges is that slight changes in stoichiometry in uranium-based systems, UO₂ for example, can have a tremendous influence on electrical properties; however, the details of these effects are not well-understood. We seek to rigorously characterize the electrical transport properties in U₃O₈ to understand the range of values that can be achieved and—importantly—their relationship to fabrication method as well as composition/microstructure. Samples of U₃O₈ pellets have been made by uniaxial pressing of U₃O₈ powder and subsequent sintering under various conditions. These samples have then been characterized to determine their microstructure, exact stoichiometric composition, and electrical properties. By carefully studying the relationship between sample preparation and electrical properties, we aim to establish the ability to control and optimize the electrical transport metrics of U₃O₈ critical for detection applications.

12:00pm **EM+AC+SS+TF-ThM13 Radiation Damage in 4H SiC nMOSFETs Detected by Electrically Detected Magnetic Resonance**, **Ryan Waskiewicz**, M.A. Anders, P.M. Lenahan, Pennsylvania State University; A.J. Lelis, U.S. Army Research Laboratory

Metal oxide semiconductor field effect transistors (MOSFETs) based upon 4H-SiC have great promise in high power and high temperature applications. An area of substantial interest is in outer space, where the devices will be subjected to ionizing radiation. The effects of ionizing radiation have been well studied in Si-based MOS devices, where E' and Pb

centers play dominating roles as oxide and interface traps respectively. Very little is known about the types of defects created in radiation damage in SiC MOSFETs. In order to develop a fundamental understanding of ionizing radiation effects, we have performed a study utilizing electrically detected magnetic resonance (EDMR) via the bipolar amplification effect (BAE) [1]. We observe several changes between the pre- and post-irradiation EDMR results, which strongly indicate change in the structure of the SiC/SiO₂ interface region but relatively little change in the number of observed interface defects.

The devices used in this study had 50 nm thick thermally grown gate oxides in N₂O. After oxidation, the devices were subjected to the standard post-oxidation NO anneal at 1175°C. The n-channel 4H-SiC MOSFETs have been subjected to 6MRads of gamma radiation from a 60Co gamma source while a 10V bias applied to the gates. Standard transistor characteristic measurements made on the devices before and after irradiation indicate a threshold voltage shift of approximately -4V. We observed several significant changes in the EDMR response, the most obvious EDMR differences are in the amplitude of the BAE EDMR measurements as a function of applied gate voltage. The maximum EDMR amplitude increased by a factor of 7 as a result of the irradiation, and the gate bias at which the peak occurred shifted by approximately -4V, consistent with the approximate -4V shift in threshold voltage. BAE measurements measure spin dependent recombination due to deep level defects at and very close to the SiC/SiO₂ interface. We find significant change in the EDMR line shapes, observing significant post-irradiation broadening of the spectra. Surprisingly, we are unable to observe either silicon or carbon dangling bond defects in these preliminary measurements. It is clear from the measurements that both the pre-irradiation and post-irradiation measurements are dominated by silicon vacancies on the SiC side of the interface. EDMR measurements as a function of microwave power show quite significant changes in the saturation behavior of the magnetic resonance. These results suggest significant structural changes in the interface region.

[1] Thomas Aichinger and Patrick M. Lenahan, Appl. Phys. Lett. **101**, (2012)

Fundamental Discoveries in Heterogeneous Catalysis Focus Topic

Room 103A - Session HC+SS-ThM

Dynamics of Gas-surface Interactions in Heterogeneous Catalysis

Moderator: Daniel Killelea, Loyola University Chicago

8:00am **HC+SS-ThM1 Adsorption and Hydrogenation of Acrolein on Ru(001)**, **Dominic Esan**, Y.D. Ren, University of Illinois at Chicago; I.B. Waluyo, Brookhaven National Laboratory; M. Trenary, University of Illinois at Chicago

The partial hydrogenation of α , β -unsaturated aldehydes is an important step in several synthetic industrial processes especially in the fine chemicals and pharmaceutical industries. Generally, it has been established that the thermodynamics of the catalytic hydrogenation of these unsaturated aldehydes favor the formation of saturated aldehydes via the hydrogenation of the C=C bond while the manipulation of the kinetics of the process may yield the desired unsaturated alcohol product via the hydrogenation of the C=O bond. Most of the studies done on single metal surfaces using acrolein (CH₂=CH=CHO), the smallest of these aldehydes, show that the thermodynamically-preferred product (propanal) is always the favored product. However, bimetallic systems have been shown to possess unique properties, compared to their single metal counterparts, including novel reaction pathways. Thus, our aim is to study acrolein hydrogenation on a bimetallic Pt/Ru(001) system to determine if the presence of the Pt atoms can enhance the selectivity and activity towards the formation of the unsaturated alcohol (2-propenol).

In this initial study, temperature programmed desorption (TPD) and reflection absorption infrared spectroscopy (RAIRS) were used to determine if the bare Ru(001) surface is active towards (partial and complete) hydrogenation of acrolein and if it's selective for the desired product (2-propenol). At low coverages, acrolein was found to adsorb on the surface, at 90 K, via the C=O bond and completely decomposes to CO(g) around 460 K. As the coverage increases, adsorption via the C=C bond predominates and most of the acrolein desorbs molecularly or decomposes to CO(g). However, some of the acrolein also self-hydrogenates to yield all the possible hydrogenation products – propanal, 2-propenol, and 1-

propanol with TPD peak temperatures at 180, 210, and 280 K respectively – with propanol having the highest yield. Co-adsorption with $\text{H}_2(\text{g})$ enhances the adsorption via the C=C bond and the yield of all the products. These results will serve as a guide for the study on the Pt/Ru(001) system.

8:20am HC+SS-ThM2 Dynamics of Formate Synthesis from CO_2 and Formate Decomposition on Cu Surfaces, *J. Quan, T. Kozarashi, T. Ogawa, T. Kondo, Junji Nakamura*, University of Tsukuba, Japan

Much attention has been paid to methanol synthesis by hydrogenation of CO_2 as a promising chemical conversion of CO_2 . It has been well-known that Cu-based catalysts show high activity for the methanol synthesis, in which the initial elementary step of CO_2 is formation of formate species by the reaction of CO_2 with surface hydrogen atoms on Cu. Previous kinetic measurements of the formate synthesis by hydrogenation of CO_2 have suggested an Eley-Rideal (E-R) typed mechanism that CO_2 directly attacks a hydrogen atom on Cu surfaces. We have thus tried to prove the E-R typed mechanism by molecular beam experiments assuming that the reaction between incoming CO_2 molecules and Cu surfaces is thermally non-equilibrated. We first prepared hydrogen atoms on cold Cu(111), Cu(110), and Cu(100) kept around 200 K and then hot CO_2 molecular beams were illuminated onto the surfaces with controlling its vibrational and translational energy. It is found that the formate synthesis proceeds significantly without heating Cu samples if vibrational and translational energies are supplied to gaseous CO_2 . The results clearly indicate the thermal non-equilibrium dynamics. Possibility of a tunneling mechanism between CO_2 and a hydrogen atom on Cu was discarded because no significant H/D effect was observed on the reaction rate of formate synthesis. On the other hand, we have studied the dynamics of the formate decomposition as a reverse reaction of the formate synthesis. We measured the angular distribution and the translational energy of desorbed CO_2 formed by the decomposition of formate on Cu(110) under a steady state reaction of HCOOH and O_2 . The angular distribution showed a sharp collimation, $\cos^2\theta$, perpendicular to the surface. The translational energy of CO_2 was independent of the surface temperature of Cu(110). It is thus found that the formate decomposition is also thermal non-equilibrium dynamics. However, the translational energy was as low as 100 meV, which is much lower than that required for formate synthesis, about 600 meV. The discrepancy will be discussed in the presentation.

8:40am HC+SS-ThM3 Step-Type Selective Oxidation on Pt Surfaces, *Rachael Farber*, Loyola University Chicago; *C. Badan*, Leiden Institute of Chemistry, The Netherlands; *H. Heyrich*, Leiden Institute of Chemistry; *L.B.F. Juurlink*, Leiden Institute of Chemistry, The Netherlands; *D.R. Killelea*, Loyola University Chicago

The development of predictive models of heterogeneously catalyzed systems relies on a sound understanding of the atomic-level details of the interactions of gas-phase species with the metal surface. A key factor in this tapestry is how the surface geometry influences reactivity. Single metal crystals with low Miller indices have often been used to probe the interactions between the reactive adsorbates and catalytic metal substrate. These low index surfaces are more accessible both computationally and experimentally, and have been essential to our current understanding of metal surface-catalyzed chemistry. However, the decreased complexity, because of the absence of active surface defects, can result in incomplete models of actual catalytic systems. Actual catalytic surfaces are believed to possess many defect sites that contribute to the overall reactivity of the catalyst. It has been recently shown that differences in the (110) and (100) step edge greatly influences water structures on the Pt surface. By using highly stepped Pt crystals with (110) and (100) steps, we see that the slight geometric differences between the (110) and (100) step also has profound effects on oxygen adsorption on stepped Pt crystals.

By utilizing highly stepped Pt crystals to study oxygen adsorption, along with ultra-high vacuum (UHV) surface science techniques such as temperature programmed desorption (TPD) and low temperature UHV scanning tunneling microscopy (STM), we are able to further understand O-Pt interactions on a surface that better mimics actual catalytic environments. Pt(553), with (110) step edges, was studied via STM to support the different behavior seen in oxygen adsorption between the (110) and (100) step edges in TPD experiments. The combination of TPD, STM, and variation in crystal step edge geometry allows for a more complete understanding of O_2 adsorption and dissociation on the Pt(553) surface and, more generally, (110) and (100) type step edges on Pt crystals.

9:00am HC+SS-ThM4 Vibrational Symmetry Effects in the Dissociative Chemisorption of CH_2D_2 on Ni(111), *Arthur Utz, N. Chen, E.H. High*, Tufts University

Vibrational state resolved reactivity measurements have established that mode-selective chemistry, in which the reaction probability, S_0 , depends on the identity of the reactant's vibrational state, and bond selective chemistry, in which the product identity depends on the reagent's vibrational state, is widespread in the dissociation of methane and its isotopologues on Ni and Pt surfaces. Two factors lead to the observed mode- and bond-selectivity. First, methane's distorted transition state geometry introduces a bias that favors those vibrational motions that best access the transition state geometry. The sudden vector projection (SVP) model of Guo and coworkers predicts selectivity based on this factor. As the methane molecule approaches the surface, the molecule-surface interaction potential can also perturb the molecule's vibrations and lead to vibrational energy redistribution in the entrance channel for the reaction. Reaction path Hamiltonian calculations by Jackson and coworkers, quantum dynamics calculations by Kroes et al., and the vibrational adiabatic predictions of Halonen et al. focus on how this second factor impacts reactivity. In all of these calculations, the incident molecule's vibrational state symmetry can influence the vibrational coupling channels and energy flow pathways for the molecule as it approaches the surface.

This talk will focus on state-resolved experimental measurements of CH_2D_2 dissociation on a 90K Ni(111) surface. Unlike CH_4 , the C_{2v} symmetry of the CH_2D_2 molecule results in both the ν_1 symmetric- and ν_6 antisymmetric C-H stretching vibrations being infrared active. Therefore, we can use state-resolved infrared laser excitation of CH_2D_2 in a supersonic molecular beam to measure the reaction probability for these two C-H stretching states as a function of incident translational energy (E_{trans}). By performing the measurements at 90K, we observe a sharp energy threshold for reaction that permits an unusually precise measure of the efficacy of each vibration in promoting reaction. Our choice of excitation transitions further reduces experimental error in comparing the two states' reactivity. Contrary to the predictions of a vibrationally adiabatic model, the two states have nearly identical reaction probability. We will compare these results with recent reaction path Hamiltonian calculations from the Jackson group to explore how the symmetry of these two vibrational states impacts their reactivity.

9:20am HC+SS-ThM5 Elementary Steps in Surface Reactions: Mechanisms, Kinetics and Thermodynamics, *Swetlana Schauer mann*, Christian-Albrechts-Universität Kiel, Germany **INVITED**

Atomistic-level understanding of surface processes is a key prerequisite for rational design of new catalytic and functional materials. In our studies, we investigate mechanisms, kinetics and thermodynamics of heterogeneously catalyzed reactions and adsorption processes on nanostructured model supported catalysts by combination of multi-molecular beam techniques, infrared reflection-absorption spectroscopy and single crystal adsorption calorimetry. By employing these methods under well-defined ultra high vacuum conditions, we study mechanistic details of complex multi-pathway surface reactions, such as hydrocarbon transformation in presence of hydrogen or selective hydrogenation of multi-unsaturated hydrocarbons. The ultimate goal of our research is obtaining detailed correlations between reactivity, selectivity and the particular structure of the catalytic surface.

Specifically, it will be shown that selective hydrogenation of the C=O bond in acrolein to form an unsaturated alcohol is possible over Pd(111) with nearly 100 % selectivity. However, this process requires a very distinct modification of the Pd(111) surface with an overlayer of oxopropyl spectator species that are formed from acrolein during the initial stages of reaction and turn the metal surface selective towards propenol formation.

In the second part, a mechanistic picture of interaction of water with model $\text{Fe}_3\text{O}_4(111)/\text{Pt}(111)$ surface will be discussed. A combination of single crystal adsorption calorimetry and infrared spectroscopy was employed to determine the adsorption and dissociation heats of water and identify the surface species. We show that water dissociates readily on iron oxide surfaces forming a dimer-like hydroxyl-water complex and proved that the generally accepted model of water dissociation to two individual OH groups is incorrect.

11:00am **HC+SS-ThM10 CO₂ Hydrogenation on Rhodium: Comparative Study using Field Emission Techniques and 1-D Atom Probe, *Sten Lambeets*, Université Libre de Bruxelles, Belgium; *C. Barroo*, Harvard University; *S. Owczarek*, *N. Gilis*, Université Libre de Bruxelles, Belgium; *N. Kruse*, Washington State University; *T. Visart de Bocarmé*, Université Libre de Bruxelles, Belgium**

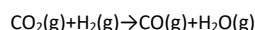
Valorization of CO₂ into useful products is one way to fulfill current environmental and economic imperatives. This can be done via the selective reduction of CO₂ using heterogeneous catalysts. To get a better understanding of the fundamental processes, we studied the CO₂ adsorption as well as its interaction with H₂ on single nanosized Rh crystals. For this, Field Emission Microscopy (FEM), Field Ion Microscopy (FIM) and 1-D Atom Probe (1DAP) were used. These methods use samples prepared as sharp needles, the extremity of which is imaged with nanoscale (FEM) and even with atomic lateral resolution (FIM).

The structure of the Rh nanocrystals is characterized by FIM, and CO₂ adsorption, dissociation and hydrogenation is studied in FEM mode. The brightness intensity of the FEM pattern depends on the presence and the nature of adsorbates. Probing and analyzing the brightness signal over time allows to qualitatively monitor the variations of surface composition, and thus the presence of surface reactions, during the ongoing processes.

Finally, 1DAP, which corresponds to the combination of a FIM device with mass spectrometry, is used to identify the nature of the different surface species.

The FEM pattern of a clean sample essentially highlights {012} facets. During CO₂ exposure, the brightness of these facets drastically decreases and remains dark, reflecting the CO₂ dissociative adsorption over these facets - leading to the formation of O(ad) species. The presence of O(ad) at the surface induces a new FEM pattern where {113} facets become the most visible. This pattern reflects the formation of subsurface oxygen O(sub) beneath the {113} facets, which is confirmed by comparison with N₂O, O₂ and CO on Rh systems. To study the hydrogenation of CO₂, pure H₂ gas is introduced while the pressure of CO₂ is kept constant. Reaction phenomena, proved by variations in the brightness pattern, were observed from 650 to 734 K.

The adsorption of hydrogen at the surface leads to the formation of H(ad) species reacting with O(ad) to form H₂O(ad). Similar reaction phenomena were also observed with N₂O+H₂/Rh and O₂+H₂/Rh systems in the same temperature range, but not with the CO+H₂/Rh system, proving the role of O(ad) in the mechanism. Our observations allow to identify the reaction as the Reverse Water Gas Shift:



These assumptions are in line with direct local chemical first analyses performed by 1DAP. Rhodium oxides species - RhO²⁺ and RhO₂²⁺ - and CO₂ with its dissociation products, i.e. CO₂⁺, CO⁺ and O⁺, are detected in the first layers of a (115) facet of the Rh nanoparticle during an exposure to pure CO₂ at 325 K.

11:20am **HC+SS-ThM11 State-resolved Reactivity of Methane on Ir(110)-(1x2), *Eric Peterson*, *E. Nicotera*, *E.K. Dombrowski*, *A.L. Utz*, Tufts University**
The rate-limiting step in the steam reforming reaction, in which methane and water react to form hydrogen gas and carbon monoxide (syngas), is the initial cleavage of a C-H bond in the methane molecule. Methane's dissociative chemisorption is highly activated on catalytically active transition metal surfaces. To date, experimental measurements have focused on CH₄ molecules whose internal (vibrational) energy is less, and frequently much less than the threshold energy for reaction. Under those conditions, significant incident translational energy (TE) or energy transfer from the surface is required to activate dissociation, and reactions most often proceed via a direct dissociative chemisorption mechanism. Using a molecular beam in conjunction with an OPO-OPA continuous-wave IR laser, we are able to prepare methane molecules with a sharply defined kinetic energy and 36 kJ/mol of internal vibrational energy, which approaches or even exceeds the threshold energy for dissociative chemisorption. These molecules possess sufficient energy to react via direct or precursor-mediated mechanisms. The direct channel is characterized by an increase in reactivity with increasing TE, and is dominant for molecules with >10 kJ/mol of TE. Molecules with <10 kJ/mol of energy react through precursor-mediated channel, in which reactivity decreases with increasing TE. This low-TE precursor channel is especially interesting in a catalytic context, as most molecules under typical industrial reactor conditions have TEs where trapping, and therefore physisorption probabilities are high.

In studies of CH₄ dissociation on Ir single crystal surfaces, we observe both the precursor and direct channels for reaction. On Ir(111) we observe that 36 kJ/mol of E_{vib} in the n₃ C-H stretch enhances reactivity in both channels at a surface temperature of 1000K. On the corrugated Ir(110)-(1x2) surface, we still observe vibrational-energy enhancement in both channels, but the TE dependence of S₀ differs for the vibrationally hot and ground state CH₄ molecules at T_{surf} = 1000K. Upon lowering T_{surf} to 500K, vibrational ground state molecules no longer have a pronounced precursor-mediated reaction channel, but the vibrationally excited molecules do. We will discuss the origin of these similarities and differences. The observed reactivity of vibrationally hot methane molecules with thermal TE points to the potentially important role that vibrationally hot precursor molecules may play in industrially catalyzed reactors.

11:40am **HC+SS-ThM12 Curved Single Crystals As Tools to Study Structure Dependences in Surface Science and Gas-Surface Reactions Dynamics, *Ludo Juurlink*, Leiden University, Netherlands** **INVITED**

The surface science approach has benefited for many decades from the availability of flat single crystal samples of high purity and high surface quality. The traditional flat, polished samples provide the user with a single surface structure that dominates over macroscopic length scales. However, a single sample that provides the user with multiple surface structures may provide additional benefits. For example, in attempts to relate chemical reactivity or selectivity to surface structure, having a continuous range of vicinal surfaces in a single sample can speed up scientific research and circumvent experimental difficulties. Also for studies focusing on either short or long-range effects in adsorbates and electronic states that are perturbed by steps, a single sample with a range of surface structures is an excellent tool. Therefore, we have revived the implementation of curved single crystal surfaces in traditional surface science studies and elaborated the implementation toward gas-surface reaction dynamics. Depending on the bulk crystal structure and the directions of the apex and curvature, many different surface structures are available in a single sample. We show how we now use LEED, AES, STM, TPD, RAIRS and supersonic molecular beam techniques to directly relate surface structure to molecular and dissociative adsorption, desorption, and chemical reactions. We exemplify the possibilities by showing recent results from studies that used a cylindrical Ni single crystal, two curved Ag samples, a Co curved sample and two Pt curved single crystal surfaces with various apex directions.

Advanced Ion Microscopy Focus Topic Room 104A - Session HI+NS-ThM

Fundamentals of Ion Beam Microscopy

Moderators: Armin Götzhäuser, Bielefeld University, Germany, Philip D. Rack, The University of Tennessee Knoxville

8:00am **HI+NS-ThM1 Generation of Hydrogen Beams using Single Atom and Trimer Nanotips, *Radovan Urban*, University of Alberta and The National Institute for Nanotechnology, Canada; *K. Nova*, University of Alberta, Canada; *M. Salomons*, National Institute for Nanotechnology, Canada; *R.A. Wolkow*, University of Alberta and The National Institute for Nanotechnology, Canada; *J.L. Pitters*, National Institute for Nanotechnology, Canada**

Hydrogen ion beams have been discussed as useful for scanning ion microscopy (SIM) due to their low mass and low sputtering rates. However, hydrogen ion beams are known to occur as mixtures of H⁺, H₂⁺ and H₃⁺ depending on the electric field strength. There is some evidence that various tip orientations contribute differently to the ratios of the ions and also that site-specific regions also affect the gas species but it has not been clearly determined. Understanding the relationship between the field strength dependence, tip shape, and apex termination with specific hydrogen ion creation is therefore critical to prepare pure hydrogen ion beams of a single species. We employed W and Ir to prepare atomically sharp nanotips with various atomic arrangements at the very apex to compare the ratios of H⁺, H₂⁺ and H₃⁺.

The experimental setup included a custom field ion microscope (FIM) operating in ultrahigh vacuum (base pressure <5x10⁻¹¹ Torr). The tip was mounted on a heating loop wire for degassing and could be cooled with a liquid helium flow cryostat. Nanotips were prepared from tungsten single crystal W(111) wire and polycrystalline Ir wire using the field assisted chemical etching method. A magnetic field of ~1T was generated using two permanent magnets mounted between the extractor and the micro-channel plate.

Thursday Morning, November 10, 2016

The hydrogen beam composition from a single atom W(111) and Ir nanotips at different applied tip voltages was recorded and analyzed. At low voltages the H_2^+ beam dominates. As the voltage is increased, H_3^+ is also observed until it dominates at larger voltages. In this manner, a particular species can be selected depending on the operating voltage. Furthermore, comparing the hydrogen beam composition between W(111) single atom tip and trimer structure reveal important differences. For trimer nanotip, H_2^+ becomes a significant species and equals the H_3^+ current. However, in the case SAT, H_3^+ becomes the only contribution to ion current at higher voltages resulting in pure H_3^+ beam suitable for imaging.

Relative ratios of H^+ , H_2^+ and H_3^+ were studied as a function of tip material (tungsten and iridium), applied voltage, and tip apex structure (single atom and trimer nanotips). We have determined that the tip structure and apex termination for both tungsten and iridium nanotips play important roles in the production of hydrogen ion beams. It has been found that single atom tip at high tip voltages produces nearly pure H_3^+ beam.

8:20am HI+NS-ThM2 High-brightness Xenon Gas Field Ion Source from a Single-Atom Tip, Ing-Shouh Hwang, Institute of Physics, Academia Sinica, Taipei, Taiwan, Taiwan, Republic of China; *W.T. Chang, W.C. Lai, P.-C. Li*, Institute of Physics, Academia Sinica, Taipei, Taiwan; *T.Y. Fu*, Department of Physics, National Taiwan Normal University, Taipei, Taiwan; *T.T. Tsong*, Institute of Physics, Academia Sinica, Taipei, Taiwan

Current focused ion beam systems are mainly equipped with liquid metal ion sources (LMISs). Even though LMISs are very reliable in operation, their relatively large source size and high energy spread limit the current density. In contrast, gas field ion sources (GFISs) can reach higher beam currents at smaller beam diameters because of their atomic-scale source size and a small energy spread (<1 eV). Since 2006, Zeiss Orion helium ion microscope (HIM) has demonstrated superior performance with a spatial resolution better than 0.5 nm [1]. To expand the application of GFISs, it is essential to develop GFISs of various ion species, particularly, ions of high mass.

Here we present Xe-GFIS emitted from a noble metal covered W(111) single-atom tip (SAT) [2,3]. This type of SATs are thermally and chemically stable, and high-brightness helium, neon, argon, hydrogen, oxygen, and nitrogen GFISs have been generated [4,5]. The Xe-GFIS also exhibits a very narrow beam with a half opening angle of $\sim 0.5^\circ$. The ion current stability is good (instability $\sim 2\%$). The reduced brightness of Xe-GFIS is measured to be 1.3×10^8 Am $^{-2}$ sr $^{-1}$ V $^{-1}$ at the gas pressure of 10^{-4} torr, 3 orders of magnitude higher than that of Ga-LMIS and several orders of magnitude higher than that of Xe magnetically enhanced inductively coupled plasma ion source (5.4×10^3 Am $^{-2}$ sr $^{-1}$ V $^{-1}$) [6]. In principle, the brightness of the Xe-GFIS can be further enhanced at a higher gas pressure or by using an emitter of a larger radius. The operation temperature can be ~ 200 K, which is much higher than the cryogenic temperature required for HIM. Thus Xe-GFIS-FIB would be easier to implement than HIM and may become a powerful tool for nanoscale milling and secondary ion mass spectroscopy.

[1] Ward, B.W., J.A. Nottle, and N.P. Economou, *J. Vac. Sci. & Technol. B* 24, 2871 (2006).

[2] T. Y. Fu, L. C. Cheng, C. H. Nien & T. T. Tsong, *Phys. Rev. B* 64 113401(2001).

[3] H.-S. Kuo, I.-S. Hwang, T.-Y. Fu, J. Y. Wu, C. C. Chang & T. T. Tsong, *Nano Lett.* 4 2379 (2004)

[4] H.-S. Kuo, I.-S. Hwang, T.-Y. Fu, Y. C. Lin, C. C. Chang & T. T. Tsong, *Jap. J. Appl. Phys.* 45 8972 (2006).

[5] H.-S. Kuo, I.-S. Hwang, T.-Y. Fu, Y.-H. Lu, C.-Y. Lin, and T. T. Tsong, *Appl. Phys. Lett.* 92 063106 (2008).

[6] N. S. Smith et al., *J. Vac. Technol. B* 24, 2902 (2006).

8:40am HI+NS-ThM3 New Ion Source for Nanofabrication and Microscopy, Adam Steele, B. Knuffman, A. Schwarzkopf, zeroK NanoTech Corporation; *J.J. McClelland*, National Institute of Standards and Technology (NIST)

INVITED

Performance measurements from a recently constructed focused ion beam (FIB) prototype that employs a new ion source technology will be presented. The performance of any FIB system, and hence the tasks to which it is best suited, are typically determined by its ion source. The high brightness and low energy spread of the Low Temperature Ion Source (LoTIS) employed here has the potential to enable significantly smaller focal spot sizes across a range of beam currents and beam energies in an optimized FIB.

The LoTIS consists of a laser-cooled atomic beam of cesium which is compressed and then photoionized within a volume of a few cubic micrometers. A uniform electric field is applied to form an ion beam. The micro-kelvin temperature of the neutral atoms results in a Cs^+ beam with a low intrinsic transverse velocity spread, yielding low emittance. The small energy spread is determined in this source by the finite spatial extent over which ions are created in a uniform electric field of approximately 10^5 V/m. Previous measurements have shown that LoTIS can achieve a brightness in excess of 1×10^7 A m $^{-2}$ sr $^{-1}$ eV $^{-1}$ and an energy spread less than 0.34 eV [1].

This brightness and energy spread imply that, when coupled to an optimized ion acceleration and focusing column, a d_{50} spot size of 1 nm should be achievable at 1 pA. The source has also achieved total currents over 5 nA, albeit at a reduced brightness. Among other benefits, these source characteristics are expected to enable a FIB with better nanomachining performance and reduced subsurface damage.

The presentation will also briefly discuss FIB equipped with a similar Li^+ ion source technology that offers a unique capability to site specifically deposit lithium into target substrates.

[1] B Knuffman, AV Steele, and JJ McClelland. *J. Appl. Phys.* **114**, 4 (2013).

9:20am HI+NS-ThM5 Recent Liquid Metal Ion Source developments for Improving Focused Ion Beam Machines, Jacques Gierak, LPN-CNRS, Route de Nozay France; *L. Bischoff*, Helmholtz-Zentrum Dresden-Rossendorf, Institute of Ion Beam Physics and Materials Research, Germany; *P. Mazarov, L. Bruchhaus*, Raith GmbH, Germany; *P. Lozano, C. Perez Martinez*, Massachusetts Institute of Technology

INVITED

Nowadays Focused Ion Beams (FIBs) machines have become very important tools capable of fulfilling many challenges ranging from micro- to nanofabrication. These tools are widely used both for industrial¹ and emerging nanosciences applications².

Traditionally FIB technology has been mainly based on gallium Liquid Metal Ions Source. The very high brightness, long lifespan, small source size of the gallium LMIS, and its easy handling, remain its chief and most decisive advantages, but some weaknesses are also well known that inhibit improvements in the resolution of LMIS-based FIB. Therefore progress on ion sources operational characteristics remains very desirable.

In this presentation we will first summarize our recent efforts aiming at optimizing gallium LMIS “needle type” within a dedicated environment for stable operation at lowest possible emission currents. This effort and the important performance gains³, we will detail, are a firm evidence that progresses can still be expected from this technology.

We will then review and detail the advantages of Liquid Metal Alloy Ion Sources (LMAIS) that represent a promising alternative to expand the already remarkable application field of FIB machines. Incoming ion species are found to influence significantly the properties of FIB-patterned nanostructures, in particular their electrical, optical, magnetic, and mechanical properties. A selection of the best suited elements transported in a focused ion beam will open new nanofabrication routes. In this presentation we will explain how nearly half of the elements of the periodic table can be made available to the FIB technology as a result of continuous research in this area during the last forty years⁴ and how, in our opinion, nanotechnology can now take benefit of these.

Finally we will introduce Ionic Liquid Ion Sources (ILIS) that are capable to produce ion beams through field-evaporation from room temperature molten-salts⁵. The possibility of extracting both positive and negative ions having a composition that can be tuned by the selection of the polarity, the liquid chemical composition, the ion emission current and the ion landing energies represents a formidable perspective for FIB technology.

In conclusion we will summarize our vision on the future of FIB technology with improved performances, versatility and on the science frontiers it might help to push.

11:00am HI+NS-ThM10 Elucidating the Directed Nanoscale Transformations when Building with Ions in Liquid, A. Ievlev, V. Iberi, J. Jakowski, M.J. Burch, H. Hysmith, A. Belianinov, R.R. Unocic, Olga Ovchinnikova, Oak Ridge National Laboratory

In-situ direct writing by ion beams from solutions opens a pathway for resistless fabrication of nanostructures with higher purity than standard gas phase deposition approaches like IBID. In particular the use of the helium ions with the opposite charge and shorter mean free path offers the potential for the localization of the reaction zone on the single digit nanometer scale. However, to fully control the interaction of the ion beam

Thursday Morning, November 10, 2016

with the liquid to allow for single digit fabrication a comprehensive understanding of the radiolytic process as well as role of secondary ISE generated in solution has to be developed. Here we will present our results on the visualizing nanoparticle nucleation and growth parameters through data analytics on acquired in-situ growth movies and correlate these results to a fully encompassing time-dependent quantum dynamical simulation that takes into account both quantum and classical interactions. Additionally, with optimized instrument parameters and solution chemistry we are able to demonstrate writing of platinum structures from liquid (beam induced electroplating) in a platinum chloride solution using helium ions with sub-10 nm resolution. Furthermore, we will discuss opportunities for using in situ flow cell technology for understating of diffusion processes as they relate to direct writing with ions in solution.

Acknowledgements

This work was conducted at the Center for Nanophase Materials Sciences, which is a Department of Energy (DOE) Office of Science User Facility

11:20am HI+NS-ThM11 Determination of an Upper Limit of Ionization Probability during SIMS Experiments using Laser Post-ionization, Nicholas Popczun, L. Breuer, Pennsylvania State University; A. Wucher, University of Duisburg-Essen, Germany; N. Winograd, Pennsylvania State University

The prospect of secondary ion mass spectrometry (SIMS) as a method of molecular imaging and molecular depth profiling of organic materials has grown with the implementation of polyatomic primary ion sources. These sources increase the total sputter yield and reduce chemical damage, creating a phenomena where the rate of damage removed by the primary ion beam exceeds the rate of damage created. Improving the sensitivity for molecular imaging and molecular depth profiling further relies on increasing the secondary ion yield of the molecular species. The most obvious suggestion to accomplish this is to increase the ionization probability, which has been estimated to be as low as 10^{-7} for atomic primary ion sources. Our lab has developed a method of directly measuring the total ionized and neutral sputtered molecular species located in the same volume sensitive to extraction. This measurement is accomplished by rastering a mid-IR femtosecond pulse for laser post ionization (LPI) of secondary neutral molecules in a two-dimensional plane perpendicular to the direction of laser propagation.

Here, we apply this technique for the first time to organic molecules coronene and guanine. Two-dimensional representations of the spatial distribution of neutral molecular species sputtered by C_{60}^{+} bombardment are presented. Correction for undersampling of the laser volume and subsequent photofragmentation yields an upper limit for the ionization probability for each molecule. In general, this work provides a visual representation of the spatial distribution of sputtered, organic neutral molecules, delivering additional information for the improvement post-ionization techniques.

11:40am HI+NS-ThM12 Studying Gas Cluster Ion Beam Sputter Yields and Surface Topography in the Helium Ion Microscope, Anders Barlow, N. Sano, J.F. Portoles, P.J. Cumpson, Newcastle University, UK

The applications of ion beams in surface analysis are large and clear in the recent literature. In our multi-user facility most projects benefit from the use of an ion beam processing step, whether for cleaning or oxide removal prior to chemical analysis, or for sputter depth profiling through an interface or layer. In our facility we have access to a number of different ion beams: argon monoatomic and gas cluster ion beams (GCIB), C_{60} ion beams, and on our ORION NanoFab, helium/neon ion beams and a gallium focussed ion beam (FIB). These beams serve numerous purposes, from cleaning of surfaces prior to chemical analysis in X-ray photoelectron spectroscopy (XPS) and time-of-flight secondary ion mass spectrometry (ToF-SIMS), to depth profiling in these techniques, to imaging and FIB milling. In all cases however, the ion beam is interacting with the surface under analysis, and this interaction needs to be studied and well-understood. In chemical analysis such as XPS and ToF-SIMS, this requires knowledge of damage mechanisms that impact the reported chemistry from the technique [1]. Understanding how the ion beam can generate nanoscale topography that directly affects the measurements is paramount [2,3].

We are applying helium ion microscopy (HIM) to studying how the ion beams on our instruments change the surfaces we are analysing. The ultra-high resolution of the HIM allows us to see nanoscale topography on surfaces with new-found sharpness at very high magnification, elucidating the mechanisms behind topography formation during treatment. We have investigated the GCIB etching of indium phosphide (InP) using 8keV Ar_{300} clusters (i.e. 300 Ar atoms per cluster). InP is known to generate significant

topography following ion beam irradiation. We observe with a spectacular level of clarity the mechanisms behind topography formation, surpassing other commonly used imaging techniques such as scanning probe and scanning electron microscopy. We can also relate the stages of nanotopography growth with total ion beam dose, from a single GCIB etch crater. With this new technique we can more confidently relate the results we obtain from XPS and ToF-SIMS with the topography we observe in the HIM.

[1] Barlow A.J et al., *J. Appl. Phys.* **116**, 054908 (2014)

[2] Radny, T. and Gnaser, H., *Nanoscale Research Letters* **9**, 403 (2014)

[3] Seah, M.P. et al., *Applied surface science* **144**, 151-155 (1999)

[4] Cumpson, P.J. and Seah, M.P., *Measurement Science and Technology* **1**, 544 (1990)

[5] Cumpson, P.J. et al., *J. Appl. Phys.* **114**, 124313 (2013)

In-Situ and Operando Spectroscopy and Microscopy for Catalysts, Surfaces, & Materials Focus Topic Room 101C - Session IS-ThM

In-situ and Operando Spectroscopy and Microscopy with Infrared Absorption Spectroscopy

Moderators: Franklin (Feng) Tao, University of Kansas, Judith Yang, University of Pittsburgh

8:00am IS-ThM1 In-situ and Operando Characterization of Catalytic Reactions with Infrared Absorption Spectroscopy, Francisco Zaera, University of California, Riverside
INVITED

Infrared absorption spectroscopy has been used in our laboratory to study a number of catalytic systems, from model flat surfaces to catalysts with novel nanostructures, under in situ and operando conditions, and in both gas and liquid-solid interfaces. Examples of these applications will be discussed in this presentation, including adsorption on flat metal surfaces probed by reflection-absorption infrared spectroscopy (RAIRS) under ultrahigh vacuum, in operando conditions at atmospheric pressures, and in situ at liquid/solid interfaces. The liquid-solid interface has been characterized in total attenuated reflection (ATR) mode as well. In transmission mode, IR has been used to probe diffusion through different nanostructures, including dendrimers and silica and titania shells. Finally, diffuse-reflectance (DRIFT) IR absorption spectroscopy has been employed to follow reactions on yolk-shell nanocatalysts.

8:40am IS-ThM3 Studying Birth, Life and Death of Catalytic Solids with In-situ and Operando Spectroscopy, Bert Weckhuysen, Utrecht University, Netherlands
INVITED

The search for new or more effective catalysts would benefit from a multiscale science approach bridging the molecular world with the macroscopic world. Recent breakthroughs in chemical imaging techniques, based on optical, electron and X-ray methods, demonstrate that such approach is within reach.

This lecture discusses the advances in spectro-microscopy of catalytic solids at different length scales, starting from single molecules and single atoms up to the level of individual catalyst particles. Special emphasis will be devoted to the exploration of mesoscale effects in heterogeneous catalysis.

9:20am IS-ThM5 Direct Observation of CVD Graphene Growth and the Dynamics of Active Catalysts by In situ Scanning and Transmission Electron Microscopy, Z.-J. Wang, J. Cao, R. Farra, R. Schlögl, Marc Georg Willinger, Fritz Haber Institute of the Max Planck Society, Germany
INVITED

During the last three years, we have modified the set-up of a conventional scanning electron microscope in order to enable the observation of catalyst surface dynamics under controlled atmosphere and temperature. Using this instrument, we investigate chemical vapor deposition (CVD) growth of graphene on different metal catalysts. Since the experiments are performed in the chamber of a microscope, it is possible to observe a complete CVD process from substrate annealing through graphene nucleation and growth and, finally, substrate cooling in real time at nanometer-scale resolution without the need of sample transfer. The nucleation and growth of single layer graphene can be investigated at temperatures of up to 1000°C, while at the same time, surface dynamics of the active metal catalyst can be imaged and directly related to the catalytic activity [1]. Due to the high sensitivity of the secondary electron signal to changes in the work function and charge transfer at the surface, we are able to visualize different degrees of graphene-substrate coupling [2] as

Thursday Morning, November 10, 2016

well as the stacking sequence of few layer graphene. In addition, the *in situ* SEM images of edge misalignment between mutual layers and individual sheets provide real-time information on the evolution of the rotation angle between growing layers and formation of the stacking order. The growth behavior of graphene on nickel, copper and platinum substrates shows characteristic differences that are related to the catalytic activity and carbon solubility of the respective catalysts. In the case of Cu and Pt substrates, we observe grain orientation dependent growth dynamics. Real-time imaging during growth thus allows us to directly visualize and study the catalytic activity of differently oriented surfaces. ESEM observations during graphene growth highlight the dynamic nature of catalysts and reveal the sensitive response of the surface to changes in the chemical potential of the gas phase. *In situ* scanning electron microscopy furthermore covers the spatial resolution of complementary *in situ* techniques that provide spectroscopic information, such as ambient pressure X-ray and Raman spectroscopy. It completes the spectroscopic data with visual information and spatially resolved chemical dynamics. Finally, in combination with *in situ* TEM, it allows to correlate locally observed phenomena with collective dynamics of active catalysts.

References:

- [1] Zhu-Jun Wang et al., ACS Nano, **2015**, 9 (2), 1506-1519
- [2] Piran R. Kidambi et al., Nano Lett., **2013**, 13 (10), 4769-4778

11:00am IS-ThM10 Characterizing Working Catalysts with Correlated Electron and Photon Probes, Eric Stach, Brookhaven National Laboratory; Y. Li, Yeshiva University; S. Zhao, University of Illinois at Urbana Champaign; A. Gamalski, Brookhaven National Laboratory; D. Liu, R. Nuzzo, University of Illinois at Urbana Champaign; J.G. Chen, Columbia University/Brookhaven National Laboratory; A.I. Frenkel, Yeshiva University

INVITED

Heterogeneous catalysts often undergo dramatic changes in their structure as the mediate a chemical reaction. Multiple experimental approaches have been developed to understand these changes, but each has its particular limitations. Electron microscopy can provide analytical characterization with exquisite spatial resolution, but generally requires that the sample be imaged both *ex situ* and *ex post facto*. Photon probes have superior depth penetration and thus can be used to characterize samples in *operando* (i.e. when they are actively working). But they generally lack spatial resolution and thus give only ensemble average information.

We have taken advantage of the recent developments in closed-cell microscopy methods to develop an approach that allows us to successfully combine electron, x-ray and optical probes to characterize supported nanoparticle catalysts in *operando*. By measuring the reaction products at each stage of the reaction, we can directly correlate the information that can be obtained from each approach, and thus gain a deep insight into the structural dynamics of the system.

In this work, we will show how a combination of x-ray absorption near edge (XANES) and scanning transmission electron microscopy (STEM) can be used to characterize the changes that occur in a model NiPt bimetallic catalyst during oxidation and reduction. Bimetallics are of broad interest in heterogeneous catalysis as they provide the opportunity to selectively tune reactivity and selectivity. However, the characterization of their structure by averaged probes such as x-ray absorption spectroscopy is comprised by the heterogeneity that such systems may proscribe.

The presentation will focus on the development and application of experimental methods used to describe the morphological changes that occur in this model bimetallic system. These will include high temperature atmospheric pressure electron microscopy, the direct measurement of reaction products using gas chromatography-mass spectrometry and the ability of a newly developed electron microscope for *operando* microscopy (based on the FEI Talos platform) to characterize bimetallic nanoparticles through energy dispersive x-ray spectroscopy.

11:40am IS-ThM12 Tracking Atoms and Charges in Metal Catalysts under Reaction Conditions, Anatoly Frenkel, Yeshiva University

In the last decade, complexity of catalytic nanoparticles attracted much attention as a major factor in catalytic processes. Atomic and electronic structure and dynamics of particles, as well as their interactions with support and adsorbates, are important descriptors of their catalytic activity. The main challenge is how to investigate these factors in a working catalyst, at high temperature and pressure, and how to do so without breaking the correlations between components of this complex system. I will give a brief overview of new methods developed recently to enable

such combined studies under realistic reaction conditions. Our approach is to single out electronic charge of metal atoms in a cluster as an “observable” quantity and develop methods to “observe” it experimentally under realistic reaction conditions, and model theoretically. In this framework, complex interactions between metal and adsorbates, metal and support, and support and adsorbates can be all accounted for in terms of their effects on the cluster charge. I will review recent results utilizing this approach for a prototypical catalyst, 1nm Pt nanoparticles supported on silica. Using high energy resolution methods of X-ray absorption and emission spectroscopies (HERFD and RIXS), as well as *in situ* IR spectroscopy (DRIFTS) and electron microscopy, aided with first-principles (DFT) modeling, we deduced that the structure of atoms and charges in the catalyst is strongly heterogeneous and that it changes dynamically with the change in temperature and pressure of adsorbates (H₂ or CO).

12:00pm IS-ThM13 STEM Imaging of Catalysts to the Single-Atom Level, via Closed-Cell In Situ Gas Reaction Technology, Lawrence Allard, Oak Ridge National Laboratory; S. Duan, J. Liu, Arizona State University

In recent years, catalysis by single-atom species dispersed on supports has been shown to be an exciting and viable possibility, for catalytic reactions in many systems [e.g. ref. 1]. The stability of single metal atoms on a support during elevated temperatures typically seen in “real” reaction processes is a critical issue, and is necessary to characterize appropriately in order to develop robust single-atom catalysts (SACs). Imaging single heavy atoms on lower Z supports via aberration-corrected high-angle annular dark-field (HAADF) imaging techniques in modern electron microscopy has become routine over the past decade, and extending this imaging capability into the realm of *in situ* gas-reaction technology is a natural goal for the catalytic scientist to better understand dynamical movement and the anchoring of noble metal atoms on specific support sites. This understanding will allow the ability to synthesize SACs with significant loadings of catalytic species while maintaining the full dispersion at the single-atom level.

Novel *in situ* gas-reaction technologies that utilize MEMS-based heater devices retained in a “closed-cell” reactor specimen holder for use in aberration-corrected (S)TEM instruments have shown the remarkable ability for imaging atomic columns in a crystal structure even at elevated temperatures and at pressures up to a full atmosphere [e.g. ref 2]. The possibility to extend this imaging capability to SACs has been a goal of our work, and will be demonstrated in this talk. The effects of the electron beam on the sample, and the effects of electron scattering processes within the gas and window materials that comprise the gas-cell are problematical questions that are being addressed. An “ideal” SAC catalyst comprising Pt atoms on NiO nanocrystals has been used as the model sample for HAADF images to demonstrate cases from material on a standard TEM grid to material in the full geometry of the closed gas-cell reactor.

References:

- 1. B. Qiao, A. Wang, X. Yang, L.F. Allard, Z. Jiang, Y. Cui, J. Liu, J. Li and T. Zhang, “Single-atom catalysis of CO oxidation using Pt1/FeOx,” *Nature Chemistry* **3** August 2011, pp. 634-641.
- 2. L.F. Allard, S.H. Overbury, W.C. Bigelow, M.B. Katz, D.P. Nackashi and John Damiano; “Novel MEMS-Based Gas-Cell/Heating Specimen Holder Provides Advanced Imaging Capabilities for *In Situ* Reaction Studies,” *Microsc. Microanal.* **18**, 2012, pp. 656-666.

MEMS and NEMS

Room 102B - Session MN+BI-ThM

‘Fantastic Voyage’ – the New Micro/Nano/Bio Systems Frontiers

Moderators: Reza Ghodssi, University of Maryland, College Park, Christian Zorman, Case Western Reserve University

8:00am MN+BI-ThM1 Living Micromachines, M. Taher Saif, B. Williams, University of Illinois at Urbana Champaign

INVITED

Industrial revolution of the 19th century marked the onset of the era of machines that transformed societies. Late 20th century marked the beginning of miniaturization resulting in micro-nano electronics and MEMS/NEMS. This revolution connected every individual with all the others in the planet. However, all of these machines are non-living, and they do not have inherent intelligence. On the other hand, since the discovery of genes, there is a considerable body of knowledge on

engineering living cells. It is thus appropriate to envision biohybrid micro machines that are made from microfabricated scaffolds and living cells. These machines have the potential of unprecedented capabilities, as they would carry the footprints of millions of years of evolution. These machines may emerge from an interaction between the living cells and the micro-nano scaffolds. Thus, they might be the unique products of both the bottom-up and top-down methods. In this talk we will present such an elementary micro machine consisting of a soft slender string and rat cardiomyocytes. The string is made from PDMS by filling a microfabricated channel using capillary draw. Cells are cultured on one region of the string. These cells interact with the string as well as with each other, and beat in synchrony as a single actuator. This living actuator bends the string, and a bending wave propagates from the actuator site towards the end, as a bending of a sperm. This artificial machine thus swims in fluids as the engineered living swimmer. These swimmers might be used in vivo for autonomous intelligent drug delivery.

8:40am MN+BI-ThM3 Inertial Imaging with Nanoelectromechanical Systems, Selim Hanay, Bilkent University, Turkey

Nanoelectromechanical Systems (NEMS) resonators can be used as exquisite sensors of physical quantities, such as mass, force and spin. As the size of a mechanical sensor shrinks, its responsivity increases: combining this advantage with low-noise readout schemes has enabled extreme sensitivity levels to be achieved such as the detection of electronic spins, single-cells in liquid and volatile chemicals at low concentration. It has become possible to use NEMS sensors for single-molecule analysis: for instance, the mass of single molecules can be measured by NEMS, paving the road for sensitive biochemical analysis. Another sensing modality, for single-biomolecule analysis, has been recently discovered. It was shown that spatial properties of analyte particles, such as its size and degree of asymmetry, can be extracted by tracking multiple mechanical modes of a sensor. Such multimodal measurement provides both size and shape information, as well as, the mass of the analyte. Furthermore, by combining spatial information, an image of the analyte can be constructed. The new technique, Inertial Imaging, transforms the capabilities of nanomechanical sensors to a new level: the combined data of molecular mass, size and shape of the analyte can enable previously unattainable information in biomolecular analytics. In this talk details for the implementation of this technique as well as experimental progress for single molecule detection will be presented.

9:00am MN+BI-ThM4 Dynamic Patterning of Breast Cancer Cells Using Silicon Nitride Multimode Membrane Resonators, Hao Jia*, H. Tang, P.X.-L. Feng, Case Western Reserve University

Manipulating and patterning biological cells on surfaces has gained great interest due to its fundamental importance for cell-level biophysical studies, and implications for potential biomedical applications.¹ In this work, we report the first experimental demonstration of non-invasive, fast, dynamic patterning of clusters of cancer cells with micrometer-scale spatial precision, by using multimode silicon nitride (Si_3N_4) membrane resonators that feature very large aspect ratios (~600nm-thick, and hundreds of microns in lateral dimensions), in rectangular and square shapes. The fabricated Si_3N_4 membranes exhibit robust multiple flexural resonances (within 50–500 kHz) in liquid solutions. We observe that the breast cancer cells (MDA-MB-231) can be dynamically manipulated into diverse Chladni patterns² within a few seconds, via the multimode resonances of the membrane. Multiple spatially signatory cell patterns are observed for rectangles (~300×120 μm^2) and squares (~350×350 μm^2), respectively. We further demonstrate that cell patterns can be dynamically switched. We model and explain the cell patterns by oscillating boundary induced acoustic streaming flows of the fluid.

As an important cell line for breast cancer metastasis studies, MDA-MB-231 cells are selected in this work and genetically-engineered to express green fluorescent protein (GFP), a biomarker for gene expression and cell identification. Dilution in EDTA solution allows suspended individual cells with reduced surface viscosity. Cancer cells are locally delivered to the device area using micropipettes, and the cell distributions are imaged in real time by a high-speed fluorescent microscope. We observe that cancer cells are allocated into '1D' array of clusters on the rectangular membrane under excitation frequencies corresponding to its 1st, 2nd and 3rd modes (in Fig. 1), while they cluster into multiple '2D' patterns when the multiple modes of square membrane are excited individually (in Fig. 2).

Furthermore, the cell patterns can be readily changed when switching between resonance frequencies.

The demonstrated Si_3N_4 membrane platform provides new capabilities for manipulating breast cancer cells, which could further lead to studies involving cancer cell signaling and interaction with neighboring cells, probing and controlling cancer cell metastatic behaviors using multimode mechanical resonators.

[1] B. Guillotin, *et al.*, *Trends in Biotechnology*4, 2011.

[2] E.F.F. Chladni, *Entdeckungen über die Theorie des Klanges*, 1787.

9:20am MN+BI-ThM5 Smart Drug Delivery through Gut, W. Yu, R. Rahimi, M. Ochoa, Babak Ziaie, Purdue University

INVITED

This paper reports on a magnetic-proximity-fuse method for site-specific drug release in the gut. As an embodiment, a capsule is comprised of two compartments; one houses a charged capacitor and a reed switch (magnetic switch) while the other accommodates the drug reservoir, whose lid is latched by a taut nylon thread intertwined with a NiCr wire. Meanwhile, the wire is connected to the capacitor via the switch. Once within the proximity of a magnet, the switch closes and the capacitor discharges on the wire, melting the fusible thread and opening the reservoir.

Pharmaceutical companies have been interested in releasing medications at specific sites in the gut. Many drug absorption studies (DASS) use Enterion [1] capsule which incorporates a loaded spring that is RF-actuated, pushes a piston and forces the drug out through a hole. The capsule location is monitored via γ -ray scintillating-imaging. Other similar devices include IntelliSite [2] (tracked by x-ray) and IntelliCap (tracked by pH). Though suitable for DASS in clinical settings, these approaches are not practical for use in larger populations. This is mainly due to the problems related to the need for real-time localizing the capsule. Thus, we present an alternative approach using a Smart Capsule incorporating a magnetic-proximity fuse.

Fig. 1 depicts a capsule traveling through the gut in proximity to a magnet. The capsule consists of two chambers. The right one contains a capacitor (1F, 2.7V) and a reed switch. The capacitor is charged before use. A NiCr wire is connected to the capacitor and the switch, with two ends in the right chamber and the rest intertwined with a nylon fuse in the drug reservoir. Along the axis is a rubber band linking the fuse to a cap, covering the reservoir with an elastic layer for reliable sealing. Additionally, an elastic rod is used as a loaded spring pushing the cap out once the fuse breaks. As in Fig. 2, the band holds the cap initially. When the capsule meets a magnetic field to close the switch, the NiCr wire is heated, melting the fuse (60~85°C) and opening the cap. Fig. 3 shows a photo of a Smart Capsule (9mm×26mm).

Fig. 4 shows snapshots of the capsule traveling in a tubing at various points with respect to the magnetic marker. The capsule starts to open in frame "a" (1sec) at a separation distance of 1mm from the magnet, with the opening completed (cap totally separated from the capsule) in frame "e" (17sec). Considerable diffusion and mixing of the powdered dye in water is observed within a minute, frame "f". Fig. 5 shows the relationship between the capacitance and the charging voltage necessary for melting the fuse through a NiCr wire (~0.23ohms).

11:00am MN+BI-ThM10 Biopsy with Untethered Microgrippers, David Gracias, Johns Hopkins University

INVITED

An important requirement to enable the vision of the Fantastic Voyage is to develop tiny mechanized devices that can be used to perform functional surgical tasks. As an example, I will describe a decade long effort in our laboratory to develop sub-millimeter sized biopsy forceps in the shape of hands or microgrippers. I will discuss challenges in fabrication, materials choice, deployment, guidance, safety, power harvesting and practical surgical operation of these devices. In addition to in vitro and ex vivo studies, I will discuss in vivo operation of such devices in live pigs to enable statistical sampling of tissues, targeted biopsy and drug delivery. I will also discuss the creation of microgrippers out of bioresorbable and biodegradable silicon based and polymer materials as well as devices as small as single red blood cells. Our studies highlight feasibility and proof-of-concept for the implementation of small untethered devices in medicine and surgery.

11:40am **MN+BI-ThM12 Bacterial Biofilms on 3D-printed Implant Materials**, *Ryan Huiszoon**, *S. Subramanian*, *T.E. Winkler†*, University of Maryland, College Park; *H.O. Sintim*, Purdue University; *W.E. Bentley*, *R. Ghodssi*, University of Maryland, College Park

New technologies, like capsule microsystems (Fig.1), have the potential to revolutionize medical care by autonomously locating and treating *in vivo* infections. Such implantable systems require 3D structures that cannot be fabricated using traditional photolithography. Additive manufacturing is the ideal tool that allows for rapid and detailed fabrication of such complex structures. However, 3D-printed implants, like their metal and ceramic counterparts, are vulnerable to biofilm infections [1]. Thus, it is essential to characterize treatments for these films on emerging 3D printable materials. In this work, we evaluate bacterial biofilm treatment on 3D-printed implant materials such as MED610.

Bacterial biofilms are the leading cause of implant infections. They form when planktonic bacteria adhere on a surface, secrete protective extracellular matrix and grow. They are highly resistant to antibiotics, allowing the infection to persist [2,3]. Microfluidics is a common and effective tool to evaluate biofilms in a controlled environment as it offers more clinically relevant data about biofilm growth and treatment [4].

In this work, we 3D printed open microfluidic channels (750µm wide x 400µm deep) on a Stratsys Connex3 polyjet printer. The open channels were sealed using sealing wrap, PDMS and glass, and clamped together using binder clips (Fig.2). *Escherichia coli* W3110 biofilms were grown in the micro-channels under Lysogeny Broth (LB) media flow at 120µl/hr for 24 hours. Subsequently, treatment with LB media (control), 10µg/mL gentamicin, 100µM autoinducer-2 (AI-2) analog (quorum sensing disruptor), or a combination of the latter two treatments was introduced into the various channels at the same flow rate for an additional 24 hours. The biofilms were then imaged through the open channels using an Olympus BX60 microscope (Fig.3). Treatment efficacy was evaluated as a percent change in channel surface coverage quantified using ImageJ. Bacterial biofilm coverage was reduced by 21%, 31% and 50% for gentamicin, analog and combination treatments respectively as compared to the untreated control, consistent with previous results (Fig.4) [2]. The combination treatment proved most effective, reducing biofilm coverage by 37% compared to the standard antibiotic-only therapy [2].

3D printed microfluidic test platforms offer an affordable way to experiment on new materials and can hasten the development of novel treatments. Additionally, the characterization of these materials brings us a step closer to making this technology a viable option for fabricating complex structures for implantable multi-purpose microsystems.

Plasma Science and Technology

Room 104C - Session PS1-ThM

Modeling of Plasmas and Plasma-Surface Interactions

Moderator: Sumit Agarwal, Colorado School of Mines

8:00am **PS1-ThM1 The role of the Singlet Metastables and Energy-dependent Secondary Electron Emission Yields in Capacitively Coupled Oxygen Discharges**, *Jon Gudmundsson*, *H. Hannesdottir*, University of Iceland

We explore the effects of including the singlet metastable molecules $O_2(a^1\Delta_g)$ and $O_2(b^1\Delta_g)$ in the discharge model of a capacitively coupled rf driven oxygen discharge. We furthermore examine the addition of energy-dependent secondary electron emission yields from the electrodes to the discharge model. The one-dimensional object-oriented particle-in-cell Monte Carlo collision code oopd1 is used for this purpose [1], with the oxygen discharge model considering the species $O_2(X^3\Sigma_g^-)$, $O_2(a^1\Delta_g)$, $O_2(b^1\Delta_g)$, $O(^3P)$, $O(^1D)$, $O(^1S)$, O^+ , O^+ , O^- , and electrons. The effects on particle density profiles, the electron heating rate profile, the electron energy probability function and the sheath width are explored including and excluding the metastable oxygen molecules and secondary electron emission. We have demonstrated that adding the metastable $O_2(a^1\Delta_g)$ to the discharge model changes the electron heating from having contributions from both bulk and sheath heating to being dominated by sheath heating for pressures above 50 mTorr [2,3]. However, at a low pressure (10 mTorr), Ohmic heating in the bulk plasma (the electronegative core) dominates, and detachment by $O_2(a^1\Delta_g)$, has only a small influence on

the heating process. Thus at low pressure, the electron energy probability function (EEPF) is convex and as the pressure is increased the number of low energy electrons increases and the number of higher energy electrons (>10 eV) decreases, and the EEPF develops a concave shape or becomes bi-Maxwellian [3]. We find that including the metastable $O_2(b^1\Delta_g)$ further decreases the Ohmic heating and the effective electron temperature in the bulk region. The effective electron temperature in the electronegative core is found to be less than 1 eV in the pressure range 50 - 200 mTorr which agrees with recent experimental findings. Furthermore, we find that including an energy-dependent secondary electron emission yield for O_2^+ ions has a significant influence on the discharge properties, including decreased sheath width.

[1] J. T. Gudmundsson, E. Kawamura and M. A. Lieberman, Plasma Sources Sci. Technol., 22(3) (2013) 035011

[2] J. T. Gudmundsson and M. A. Lieberman, Plasma Sources Sci. Technol., 24(3) (2015) 035016

[3] J. T. Gudmundsson and B. Ventéjou, J. Appl. Phys., 118(15) (2015) 153302

8:20am **PS1-ThM2 A Computational Model for Magnetron Sputtering Devices using VSim**, *James McGugan*, *C.D. Zhou*, Tech-X Corp.; *J.D. Smith*, Tech-X UK Ltd.; *C.M. Roark*, *A.Y. Pankin*, *P.H. Stoltz*, Tech-X Corp.

A 2D, axisymmetric model for a cylindrical magnetron is presented. The model is PIC based and performed in the software tool, VSim for Plasma Discharges. The effects of an external feedback circuit are investigated and an IV curve for the device is presented. The sputtering rate and erosion profile are obtained, and the erosion profile is input as an iterative geometry modification. The effects of this non-planar surface are calculated using a second-order cut-cell algorithm within the PIC algorithm. The modifications of the non-planar surface on the sputtering rate and yield are presented. Finally, the results are used to quantitatively predict device performance, longevity, and the atomic layer distribution of sputtered atoms on the target.

8:40am **PS1-ThM3 Three Dimensional Monte Carlo Simulation of Surface Charging on a Contact Hole during Pulsed Plasma Etching**, *Yugo Osano*, *Y. Higuchi*, *Y. Nishizawa*, Samsung R&D Institute Japan; *M.H. Cha*, Samsung Electronics, Republic of Korea; *H. Kubotera*, Samsung R&D Institute Japan; *K.H. Lee*, Samsung Electronics, Republic of Korea

Three-dimensional (3D) simulation model has been developed to analyze the surface charging on a contact hole during plasma etching process, with emphasis placed on surface charging mitigated by employing pulse-time-modulated (TM) plasma. Surface charging and its influence on the trajectories of ions and electron are investigated with Monte Carlo (MC) procedure in level-set represented 3D-polygon geometries under uniform square lattice. The distribution of steady state surface charging is achieved by recursive calculation of charge accumulation from the ion/electron transport under the self-consistent electric field, and electric field is calculated by solving Poisson's equation for the accumulated charge. For the plasma description, time averaged ion/electron flux is used for continuous wave (CW) plasma, and the TM plasma is modeled by alternating two different sets of fluxes and incident energies of ions and electrons which corresponds to pulse-on and pulse-off states. The incident energy of electrons is set to be significantly lower in pulse-off state than in pulse-on state, to simulate decreased electron temperature during pulse-off. Calculations are performed for a silicon oxide contact hole with mask, where the surface geometry is shaped in an inversed truncated circular cone of aspect ratio ~10. Numerical results reproduced accumulation of surface charging showing distinct difference between CW and TM plasma. In a CW condition, surface charging is simply accumulated until the fluxes of electrons and ions become locally equivalent owing to their deflection by local electric field. Meanwhile, the distribution of surface charging varies at all time in a TM condition and exhibits significant contrast to CW (including sign of charging) upon TM plasma conditions such as duty ratio, frequency, etc. In accordance with charging distribution, the potential distribution is also significantly different between CW and TM plasma. The potential increases deeper in the contact hole with its maximum shown near at the bottom of the hole in a CW condition, whereas it shows fluctuating distribution in a TM condition.

9:00am **PS1-ThM4 Characteristics of Capacitively Coupled Plasmas Excited by Tailored Voltage Waveforms**, *Ankur Agarwal*, *S. Rauf*, *K.S. Collins*, Applied Materials Inc.

Critical scaling limitations in microelectronics fabrication are increasingly driving the transition to 3D solutions such as multi-gate MOSFETs and 3D

* MEMS/NEMS Best Paper Award Finalist

† National Student Award Finalist

Thursday Morning, November 10, 2016

NAND structures. These structures create significant challenges for dielectric and conductor etching, especially given the high aspect ratio (HAR) of the features. Etching of HAR features require careful balance of the reactive species (ions and radicals) flux and ion energies else the via-like features may physically twist/turn due to the stochastic nature of fluxes entering the feature as the size of the opening shrinks or the critical dimension varies significantly along the depth of the HAR feature.[1] Capacitively coupled plasma (CCP) sources, commonly used for dielectric etching, enable separate control over the fluxes of ion and radicals and ion energies by utilizing multiple frequencies. The high frequency source allows for generation of large plasma density while biasing the wafer at low frequency controls the energy of the ions. However, interference effects between the driving frequencies have been shown where in even the low frequency contributes to plasma density and thereby affects ionization dynamics.

Recently, techniques such as electrical asymmetry effect and non-sinusoidal voltage waveforms have been developed which purport to overcome the interference effect and thereby provide active separation of ionization level and ion energy distributions.[2,3] Much of this work has focused on either a geometrically symmetric system or for high pressure deposition processes. In this work, we investigate the plasma characteristics of CCPs driven by non-sinusoidal voltage waveforms in a geometrically asymmetric chamber as is typically utilized for plasma etching. Results will be discussed from a 2-dimensional plasma equipment model will be discussed for varying voltage waveforms which are generated using up to 5 harmonics similar to Bruneau et al.[3] Characterization of active species identity, fluxes and energies will be discussed for varying gas pressure in argon and fluorocarbon gas mixtures.

[1] M. Wang and M.J. Kushner, J. Appl. Phys. **107**, 023309 (2010).

[2] B.G. Heil, et al., J. Phys. D **41**, 165202 (2008).

[3] B. Bruneau et al., Plasma Sources Sci. Technol. **23**, 065010 (2014).

9:20am **PS1-ThM5 Multi-zone Equilibrium of ICP Discharge for Plasma Processing. Mechanism of Plasma Heating, Vladimir Nagorny**, Mattson Technology

ICP discharges and plasma sources are quite common in semiconductor plasma processing. Many

observations, plasma measurements and even simulations, including multiple species were published

through the years. However theoretical considerations were limited to a case when plasma

equilibrium can be characterized as global. In a real processing plasma this kind of equilibrium is

unstable. Here we analyze more real case when equilibrium consists of at least two areas - one is a

band-like area with self-sustaining plasma, where most of plasma generation occurs is linked on one

side to the induction coil and absorbs all the energy directly from the coil. On the other side

this band is linked to the second - plasma transfer area, which is fed by the energy and particles

escaping from the first area. The second area is also linked to surrounding walls. In a way, this

structure of ICP discharge reminds a glow discharge structure. The first - plasma generating area

functions similar to a cathode fall, and the plasma transfer area - similar to a positive column.

The number of plasma generating zones depends on the number of coils and construction of the coil,

and is usually more than one plasma generating zones are linked to a common plasma transfer zone.

Keywords - Plasma Processing, Inductively coupled plasma, ICP discharge, Plasma Sources

9:40am **PS1-ThM6 Characterization of Transients in Pulsed Capacitively Coupled Plasmas, Wei Tian**, A. Agarwal, S. Rauf, K.S. Collins, Applied Materials Inc.

Plasma etching processes for microelectronics fabrication at future technological nodes are extremely challenging. The requirements regarding the uniformity (both etch rate and critical dimensions) and selectivity are also more stringent than ever. To meet these strict requirements, it is Thursday Morning, November 10, 2016

important to control the flux of ions and radicals to the substrate and energy of the ions incident on the substrate. In capacitively coupled plasmas, this control is typically achieved by varying the gas mixture, frequency, or pressure. Pulsing the plasma also enables one to modulate the electron energy distributions and the electron impact source functions of reactive species, which may be not otherwise possible using traditional methods.[1,2] Although pulsed capacitively coupled plasmas (CCPs) has been experimentally and computationally investigated before, there is little understanding of the transients during a given pulse. Of particular interest is the characterization during transition from after-glow to active-glow and vice-versa when the plasma impedance varies rapidly.

In this work, we will discuss the transients in pulsed CCPs using results from a 2-dimensional plasma equipment model. The model is validated against experimental measurements for Ar/O₂/CF₄ mixtures.[3] Asymmetric ignition of the plasma is observed in some cases which can have significant consequences on time-averaged plasma uniformity. Depending on the operating conditions, oscillations in bulk plasma are also observed which last many rf cycles. These oscillations can be attributed to the negative ions bouncing between the rapidly expanding sheaths during early active-glow. The consequences of gas mixture, pulse duty cycle and pulse frequency on the plasma characteristics during the initial active-glow phase and after-glow phase will be assessed.

[1] S.-H. Song and M.J. Kushner, Plasma Sources Sci. Technol. **21**, 055028 (2012).

[2] A. Agarwal, S. Rauf, and K. Collins, J. Appl. Phys. **112**, 033303 (2012).

[3] J. Poulou, et al., 62nd AVS Symposium 2015.

11:00am **PS1-ThM10 Modeling and Simulation of Nonequilibrium Atmospheric Pressure Plasma Flows, Juan Trelles**, University of Massachusetts Lowell

INVITED

Atmospheric pressure plasmas are at the core of diverse technological applications, from materials processing and chemical synthesis, to waste treatment and environmental remediation. These plasmas display high collision frequencies among electrons and heavy-species (molecules, atoms, and ions). The interaction of atmospheric pressure plasmas with the processing media, such as a gas stream, produces significant deviations from the Local Thermodynamic Equilibrium (LTE) state, manifested by dissimilar velocity distributions between electrons and heavy-species, leading the plasma to a state of thermodynamic nonequilibrium (non-LTE or NLTE). Moreover, such interactions are characterized by large variations in flow properties and complex coupling among fluid flow, heat transfer, chemical kinetics, and electromagnetic phenomena. These characteristics impose severe challenges to numerical modeling and simulation approaches, which include resolution of multiscale features, multiphysics coupling, and robustness in the presence of large solution field gradients. An overview of the modeling and simulation of nonequilibrium plasma flows using the Variational Multiscale (VMS) Finite Element Method (FEM), one of the most robust, versatile, and widely used techniques for the numerical solution of multiphysics problems, is presented. The plasma is modeled as a compressible reactive electromagnetic fluid in chemical equilibrium and thermodynamic nonequilibrium. Material properties vary in a markedly nonlinear manner and by several orders of magnitude, which severely stresses the robustness required from the numerical methods. The VMS methodology treats the plasma flow model as a coupled system of transient-advective-diffusive-reactive transport equations, which naturally allows the extension of the approach to other plasma models. Simulation results of canonical and industrially-relevant atmospheric pressure nonequilibrium plasmas, namely the plasma flow in transferred and non-transferred arc plasma torches and the free-burning arc, demonstrate the effectiveness of the method. Particularly, the simulation approach is capable to capture the complex arc dynamics inside plasma torches, including the arc re-attachment process, as well as the spontaneous formation of self-organized anode patterns in the free-burning arc. The results indicate the suitability of the VMS-FEM for its application to other types of plasma flow models and the simulation of other plasma-related processes.

11:40am **PS1-ThM12 Multiscale Approach for Deep Silicon Etching Simulation under Bosch Process using SF₆ and C₄F₈ Plasma Chemistry, Guillaume Le Dain**, A. Rhallabi, Institut des Matériaux Jean Rouxel – Université de Nantes, France; M. Boufnichel, F. Roqueta, ST Microelectronics, France

Deep silicon etching is now used in many semi-conductor devices such as high power devices, Micro-Electro-Mechanical-Systems (MEMS) and Systems In Package (SIP). The aim of deep silicon etching is to perform high

8:00 AM

aspect ratio profiles with a minimum of geometrical defects such as roughness and undercut. Bosch process is one of dry etching processes used for silicon deep etching. It is based on cyclic process consisting of alternating etching and deposition pulses. The optimization of this kind of etching processes for different applications requires a good understanding of the plasma surface interactions. Etching simulator can be considered as a complementary tool to improve the quality and the reliability of the silicon etch profile. In this context, we have developed a multi-scale approach to simulate the silicon etch profile evolution as a function of the operating conditions of Bosch process, performed in ICP reactor. Etching pulse is ensured by SF_6/Ar plasma mixture while the deposition pulse is ensured by C_4F_8 plasma.

Our silicon etching simulator is thus composed of three models:

- 0D plasma kinetic models of SF_6 and C_4F_8
- Sheath models of SF_6 and C_4F_8
- 2D Surface model

0D kinetic model is based on the solving of the mass balance equations of all neutral and ion species considered in the reaction scheme coupled to charge neutrality equation and power balance equation. The solving of the non linear equation system, until it reaches to steady state. This solving allows to calculate the fluxes of neutral and ion species as well as the electron density and temperature. Those information are introduced as input data in the sheath and etching models. The sheath model provides angular and energetic ion distribution functions which are required in the quantification of the ion sputtering on the local etched surface.

The surface model is the third model which is based on the cellular Monte-Carlo method to describe the plasma surface interactions in a probabilistic way for silicon etching through the mask. Atomic fluorine and positive ions produced during SF_6 plasma discharge are considered as the reactive species in the etching process steps while the C_xF_y radicals and positive ions are considered as the reactive species in the surface passivation steps.

The simulation results show the pressure variation which affects the etch profile especially the scalloping and the undercut effects. On the other hand the comparisons between the simulation and the experiment in terms of trenches aspect show a satisfactory agreement.

12:00pm PS1-ThM13 Molecular Dynamics Simulation of Ni Etching by CO Plasmas, Akito Kumamoto, N. Mauchamp, M. Isobe, K. Mizotani, H. Li, T. Ito, K. Karahashi, S. Hamaguchi, Osaka University, Japan

Magnetic random access memory (MRAM) is a nonvolatile storage device of high speed operation with low operating voltage. It has the potential to replace static random access memory (SRAM), dynamic access memory (DRAM), and flash memory if the MRAM integration becomes comparable to that of DRAMs. One of the key challenges for high integration of memory cells in an MRAM device is to establish low-damage highly anisotropic etching technologies for magnetic thin films. Although Ar ion milling processes have been widely used to etch magnetic thin films for MRAM chip manufacturing, plasma etching based on chemically reactive gases such as CO/NH_3 and CH_3OH have been also studied as possible reactive ion etching (RIE) processes. In this study, we have used molecular dynamics (MD) simulations and ion beam experiments to understand etching mechanisms of magnetic thin films by chemically reactive plasmas. More specifically the current goal of this research is to develop classical interatomic reactive potential functions for MD simulation to emulate etching processes of magnetic thin films (Ni, Co, Fe, and CoFeB alloys) with high accuracy. In this study, we have used Ni as a sample film and developed Ni-C-O interatomic potential functions to examine self-sputtering and physical sputtering by energetic inert gas ions as well as oxidation and carbonization of Ni surfaces by incident O^+ , C^+ , and CO^+ ions. The metal-metal interactions are modeled with embedded atom method (EAM). However, the existing EAM potentials for most metals do not reproduce their self-sputtering yields well and therefore require modification of the functions in the short range. The metal-oxygen or metal-carbon interaction model used in our MD simulation is based on bond-order potential functions or Stillinger-Weber type angle dependent three-body functions. The potential function model also includes coordination bonds to allow the possible formation of metal carbonyls such as $\text{Ni}(\text{CO})_4$. The parameters of these potential models have been optimized based on experimental data of sputtering yields as well as potential energy data obtained from first-principle quantum mechanical (QM) simulations. The MD simulation results for Ni etching based on the newly developed reactive potential functions are also compared with data obtained from ion beam experiments.

Plasma Science and Technology

Room 104B - Session PS2-ThM

Plasma Processing of Challenging Materials

Moderator: David Ruzic, University of Illinois at Urbana-Champaign

8:00am PS2-ThM1 Epitaxy of Doped Diamond for Electronics and Energy Applications Using Microwave Plasma CVD, Robert Nemanich, F.A. Koeck, Arizona State University

INVITED

Diamond has been considered as the ultimate power semiconductor because of its wide bandgap, high electron and hole mobilities, low dielectric constant and highest thermal conductivity. Recent availability of CVD diamond plates with defect densities less than $1\text{E}5\text{ cm}^{-2}$ has presented the opportunity to fabricate and characterize diamond devices. While p-type doping with boron has been known for a number of years, n-type doping during CVD growth has recently been achieved using phosphorus as the dopant. The early studies established that phosphorus can be incorporated for growth on (111) surfaces, but the incorporation is much less efficient for growth on (100) surfaces. This report describes microwave plasma CVD approaches for P-doping on both 100 and 111 surfaces while maintaining high quality epitaxy. For the (100) surfaces a pulsed growth approach is presented which results in a P-incorporation density greater than $1\text{E}18\text{ cm}^{-3}$. For growth on (111) surfaces incorporations rates approaching $1\text{E}20\text{ cm}^{-3}$ have been obtained. Using these growth approaches pin diodes have been prepared on both (111) and (100) substrates. Diodes on (100) surfaces with breakdown voltages greater than 600V have been prepared and characterized. These diodes show high forward current densities of greater than 100 A/cm^2 at 5V. The diodes prepared on (111) substrates show a turn-on between 4 and 5 V indicating bipolar characteristics. An approach for fabricating pnp bipolar junction transistors is described. Simulation results indicate operation at high voltage and high power with a gain that could approach 100. The use of P-doped layers for thermionic emitters and thermionic energy conversion is also described. The P-doped diamond layers show a workfunction less than 0.8 eV which could enable a leap in thermionic energy conversion efficiency.

This research supported by ARPA-E through the SWITCHES program and by the Office of Naval Research.

8:40am PS2-ThM3 Magnetic Degradation of Perpendicular CoFeB Film caused by Hydrogen Plasma, Masaki Yamada, Hitachi High-Technologies Corporation, Japan; M. Satake, Hitachi High-Technologies Corporation

The RIE etching of p-MTJ (Perpendicular Magnetic Tunnel Junction) device is one of big issues to realize the high density STT-MRAM (Spin Transfer Torque Magnetoresistive Random Access Memory). In the view point of high etching selectivity or corrosion-less, $\text{Ar}/\text{CH}_3\text{OH}$ or CO/NH_3 is generally used in MTJ etching. On the other hand, according to recently report, the hydrogen plasma in etching gas may cause the electrical degradation [1]. In this study, we investigate the influence of hydrogen plasma on magnetic properties by using thin CoFeB blanket film.

The stacked film structure is $\text{Ta}(t_{\text{Ta}}) / \text{MgO}(2.0\text{nm}) / \text{CoFeB}(t_{\text{CoFeB}}) / \text{Ta}(5\text{nm})$ / substrate, which were deposited on Si substrate by UHV RF-sputtering apparatus. In this study, CoFeB film thickness t_{CoFeB} were varied from 1.0 nm to 2.0 nm. Then they were annealed at 300 degC for 1 hour with $\mu_0 H = 0.6\text{ mT}$. After that, the hydrogen plasma was irradiated to the film for 5 min through Ta capping layer by using Inductively Coupled Plasma etcher. The magnetization of blanket CoFeB films were evaluated by using Vibration Sampling Magnetometer.

At first we evaluate the CoFeB film thickness dependence of magnetic anisotropy. Without plasma irradiation, the magnetization of CoFeB film shows a perfect perpendicular anisotropy at $t_{\text{CoFeB}} = 1.2\text{ nm}$ and its coercivity $\mu_0 H_c$ is obtained as $\mu_0 H_c = 0.8\text{ mT}$. On the other hand, when the hydrogen plasma is irradiated to stacked film, the coercivity decreases down to $\mu_0 H_c = 0.2\text{ mT}$. And also its effective perpendicular anisotropy field $\mu_0 H_k$ also decreases from $\mu_0 H_k = 330\text{ mT}$ to $\mu_0 H_k = 220\text{ mT}$ with hydrogen plasma irradiation. In the case of $t_{\text{CoFeB}} = 1.4\text{ nm}$, the magnetization shows weak perpendicular anisotropy before plasma irradiation. In this situation, the magnetization drastically changes from the weak perpendicular to in-plane anisotropy by hydrogen plasma irradiation. These results imply that the interfacial perpendicular anisotropy energy decreases by hydrogen plasma irradiation. Next we evaluate capping layer thickness t_{Ta} dependence of magnetic anisotropy. In the case of $t_{\text{Ta}} < 20\text{ nm}$, the coercivity of CoFeB film increases with increasing Ta capping film thickness with hydrogen plasma irradiation. And it shows approximately constant value at $t_{\text{Ta}} > 50\text{ nm}$ even with hydrogen plasma irradiation. This behavior is

well described by the hydrogen plasma diffusion model in Ta capping layer, which is calculated by Monte Carlo simulation. From present study, we found that hydrogen plasma may attack to MgO layer chemically and it may deteriorate the perpendicular magnetization of CoFeB.

[1] J. H. Joeng, *et al.*, J. Appl. Phys., vol.115, 17C727 (2014)

9:00am **PS2-ThM4 Roughness and Selectivity Trade Off during Patterning using Next Generation Resist**, *Vinayak Rastogi, A. Ranjan*, TEL Technology Center, America, LLC

Optical lithography has reached its physical limit and eventual capacity to extend validity of Moore's law. Augmentation of 193i with multiple patterning, Extreme Ultraviolet Lithography and Directed Self Assembly are viable contenders to enable scaling for future technology nodes. However each patterning technique comes with common challenges of 'high initial pattern roughness' and 'etch resistance', the correction/compensation of which becomes more critical as we work on smaller dimension features. Plasma Etch processes have the potential to improvise upon the incoming pattern roughness and improve LER/LWR downstream with enhanced selectivity to thinner resist for expediting sub 10nm technology development.

In this work we demonstrate the specific role of passivation control in the dual-frequency Capacitively Coupled Plasma (CCP) with thin (EUV) resist patterning as an example process to improve LER/LWR, resist selectivity and CD tunability for line/space patterns. We will draw the implicit trends between different passivation chemistry and their effectiveness for roughness improvement. The effect of relative C:F and C:H ratio in feed gas on CF_x and CH_x plasma species and in turn the evolution of pattern roughness is drawn. Data that evinces the role of plasma etch parameters impacting the key patterning metrics of CD, resist selectivity and LER/LWR will be presented.

9:20am **PS2-ThM5 Fabrication of Large Superhydrophobic Surfaces with Hierarchical Structures on Polymer Films – Influence of the Roughening and the Fluorination**, *Jérôme Durret, N. Frolet, C. Gourgon*, CNRS - LTM, France

Superhydrophobic (SH) surfaces exhibit many useful characteristics for various industrial applications [1]. Many strategies have been put forward [2] on small surfaces including efficient plasma treatment [3]. It is of great interest to create large and flexible SH surfaces, making polymer films a promising solution. In this work, a two-step method for producing SH large and flexible surfaces from hydrophobic or hydrophilic polymer film materials is described.

Hierarchically structured SH surfaces were fabricated using NIL for submicro scale structuration and plasma treatment for nanoscale structuration. Hydrophobic (FEP) and hydrophilic (PMMA) polymer film materials were used. The roughening of nanoimprinted films by plasma treatment with Ar/CF₄ gas flow is reported in a capacitive coupled parallel reactor. Water contact angles (WCA) greater than 160° and contact angle hysteresis (CAH) less than 1° have been measured for a plasma treatment of only 10s. The effect of the input power (600 to 1800 W) has been investigated in terms of roughening and fluorine percentage (%F), see Fig. 1, and Fig. 2 for XPS spectra. This representation enables us to discriminate the influence of the roughness and %F. Indeed, from 800 W plasma treatment, and despite variations of the %F, the wettability remains unchanged due to a sufficient roughness. Fig. 3 shows corresponding SEM images. Additionally, Fig. 4 shows that during plasma treatment, PMMA becomes first hydrophobic as the fluorination increases (from 0 to 39%) and finally superhydrophobic with the increasing roughness.

A modification of the dot dimensions during the plasma treatment is observed as can be seen in Fig. 5. Moreover, fracture defects still remain when fabricating high aspect ratio patterns by NIL [4]. We propose to overpass this limitation by using NIL patterning only as a preliminary step to define the dot diameter. Then the desired height can be achieved by a plasma transfer. Promising results were obtained on rough dots, see Fig. 6.

In the prospect of an industrial application, all process were developed on large areas (50 in² or 320 cm²). Thus, large, flexible and transparent SH films were obtained. Finally, thanks to the combination of NIL and plasma transfer, these films may be used to fabricate high aspect ratio patterns.

This work has been partially supported by the Direction Générale de l'Armement (DGA) and the Renatech network.

[1] Nosonovsky *et al.* (2009). Current Opinion in Colloid & Interface Sci, 14(4), 270-280

[2] Xue *et al.* (2016). Sci and Tech of Adv Materials

[3] Durret *et al.* (2016). Microelectronic Engineering

[4] Schiff (2008). Journal of Vacuum Sci & Tech B, 26(2), 458-480

9:40am **PS2-ThM6 Chlorine-based Etching of InP Laser : Effect of Plasma Chemistry on Sidewall Roughness and Damages**, *Guillaume Gay, E. Pargon, C. Petit-Etienne*, LTM - CEA/LETI, France; *M. Brihoum, S. Barnola*, CEA, LETI, MINATEC Campus, France; *S. Labau, S. Arnaud*, LTM - CEA/LETI, France

Development of photonic devices on silicon could open the path to the design of new components, mixing optoelectronics and microelectronics. However, indirect band of silicon makes an all-silicon photonic device impossible. An alternative is the hybrid integration which consists in building active laser emitters with III-V materials, and other components (waveguides, filters, photodetectors) with silicon-based materials. In this study, we will focus on the dry etching of Indium-Phosphide (InP) for laser emitter fabrication reported on 200mm silicon-on-insulator wafer by molecular bonding. The major challenges related to this integration are (i) high InP etch rates necessary for micrometric high lasers, (ii) high selectivity toward silicon oxide to preserve the underneath passive components, (iii) anisotropy and (iv) smooth and undamaged surfaces. Plasma etching experiments are carried out in an inductively coupled plasma reactor from applied materials equipped with a hot cathode. In order to achieve these objectives, two plasma chemistries were developed: Cl₂/CH₄/Ar and Cl₂/N₂. They will be compared in terms of profile, roughness, surface chemical composition, and a particular attention will be paid on the chemical and physical damages induced on the pattern sidewalls. The pattern profiles are characterized by electron microscopies. The sidewalls roughness is measured by AFM using a homemade setup where the sample is tilted to allow the tip to scan the sidewalls. The sidewalls chemical composition and stoichiometry after etching is analyzed by EDX. In Cl₂/CH₄/Ar, the process performance is mainly driven by the CH₄ flow. The anisotropy is ensured by the redeposition of SiO_xC_y byproducts, coming from the SiO₂ wafer, on the InP sidewalls. A compromise has been found to ensure anisotropy and sufficient selectivity of InP over the SOI substrate. Sidewall roughness on InP patterns is very close to the one measured on the mask sidewalls before etching, thus proving that this etching process does not produce supplementary roughness. Concerning Cl₂/N₂ plasma, etching selectivity is high and leads to highly anisotropic profile. In that case, the sidewall passivation layer is formed by the preferential etching of indium by chlorine, leading to a phosphorus-rich layer. The counterpart is that this P-rich layer also forms on the open-area and is responsible for roughness formation. Afterwards, we will also consider different strategies to remove these passivation layers so as to obtain clean InP ribbons sidewalls suitable for laser emitter fabrication.

11:00am **PS2-ThM10 Using a Dielectric Barrier Discharge (DBD) Device to Produce Proton Exchange Membranes at Atmospheric Pressure for PEMFC Technology**, *Joffrey Baneton, D. Merche*, Université Libre de Bruxelles, Belgium; *G. Caldarella, N. Job*, Université de Liège, Belgium; *F. Reniers*, Université Libre de Bruxelles, Belgium

The polymer electrolyte membrane is one of the most important components of proton exchange membrane fuel cells (PEMFC) because it transports the ions from one side of the cell to the other one while it prevents the passage of the electrons and then the offsetting of the accumulated charges at each electrode. It is also important for device structure and gas permeability considerations [1]. Over the years, several methods have been developed to replace conventional techniques that involve many steps and the use of solvents and expensive reagents. Some studies exhibit an interest for low-pressure plasma devices to produce sulfonated polystyrene membranes [2]. In this work, we propose an innovative approach using an atmospheric-pressure dielectric barrier discharge (DBD) with styrene as carbon matrix reagent and acid precursors (such as trifluoromethanesulfonic acid) to integrate proton exchange groups. Using this atmospheric plasma device allows to produce membranes in a 'one-step' process, avoiding solvents and vacuum constraints [3]. X-ray photoelectron spectroscopy (XPS) and infra-red reflection absorption spectroscopy (IRRAS) are used to determine the chemical composition of the membranes. Stylus profilometry and scanning electron microscopy (SEM) are applied to analyze their morphology. Electrochemical measurements are also performed to determine the membrane proton conductivity.

In the case of pure polystyrene films, it is shown that the plasma leads to the polymerization of the monomer without altering their chemical structure. Moreover, the optimization of the reactor geometry and the experimental variables such as the flow rate, the injected discharge power,

the precursor temperature or the duty cycle (in the case of pulsed plasma) can lead to the formation of homogeneous and uncontaminated films. In the case of copolymerized membranes using an acid precursor, a high content of fragmented and distributed proton exchange groups can be observed on the XPS and IRRAS spectra.

This work was financially supported by the Walloon Region (HYLIFE project n°1410135, Energinsere program) and by the Belgian Federal Government (Interuniversity Attraction Belgian Science Policy IAP research project P7/34 – Physical Chemistry of plasma surface interactions).

[1] J. Larminie and A. Dicks. *Fuel Cell Systems Explained* (Second Edition), John Wiley & Sons Ltd, UK, **2003**, 67–72.

[2] S. Roualdes et al. *Journal of Power Sources*, **158** (2006), 1270–1281.

[3] D. Merche et al. *Plasma Processes and Polymers*, **7** (2010), 836–845.

11:20am PS2-ThM11 Laser-Enhanced Plasma Etching of Semiconductors and Metals, Jason Peck, G.A. Panici, I.A. Shchelkanov, S. Hammouti, D.N. Ruzic, University of Illinois at Urbana-Champaign

Dry etch assisted by laser (DEAL) of silicon and copper via Ar/C4F8/O2, Ar/SF6, and Ar/CCl4 capacitively-coupled plasma was studied, with goals including form control for sub-22 nm features and uniformity for 450 mm wafer processes. The first phase of the study consisted of wavelength (1064, 532, 266 nm) investigation, variation of gas chemistry, and laser intensity ramping. Multiple lasers were employed to vary repetition rate, from CW, 100 Hz, or 100 kHz, as well as varied pulse width, 350 fs to 7 ns, to understand instantaneous laser power against gas dynamics timescales.

The second phase of the study explored multiple material candidates, focusing particularly on metal etch. The etch rate enhancements were determined in the case of Si and Cu etch. Etch activation in zero-etch recipes was achieved upon introduction of 532/266 nm wavelength in the case of silicon and 1064 nm in the case of copper. In particular, Cu etch was demonstrated at substrate temperatures (40-70°C) far below the required temperature to produce a volatile etch product. Scalability and the ease of incorporating this technique into industry processes will be discussed.

11:40am PS2-ThM12 Highly Selective Isotropic Etching of Silicon in Preference to Germanium, Christopher Ahles, A.C. Kummel, University of California, San Diego

As CMOS technology is scaled down to <10nm, new MOSFET architectures are required in order to maintain control over the device. The optimal design for such a device is the gate-all-around (GAA) architecture. Whereas in previous CMOS generations the MOSFETs were planar structures, GAA structures require highly selective isotropic etching for device fabrication. Previous isotropic gas phase selective etching of silicon employed sulfur passivation of Ge which can dope silicon, corrode process equipment, and cause ion mobility in dielectrics. In this report a sulfur-free isotropic selective etch is reported which has essentially infinite Si/Ge etch rate ratio (ERR) using in a downstream plasma. The etch rates of Si and Ge were simultaneously measured in-situ using a reactor chamber equipped with dual quartz crystal microbalances (QCMs). The gold-coated quartz crystals were sputter-coated with Si and Ge. After in-situ removal of the surface oxides with a downstream NF3/H2 plasma, the Si and Ge films were dosed with gas from a downstream plasma of H2, CF4 and Ar. It was found that a high Si/Ge ERR can be obtained over a wide range of H2/CF4 gas flow ratios, QCM temperatures, chamber pressure and plasma power. For the optimal process window, there is an etch rate >1nm/min for Si and deposition of carbon onto Ge. The nature of the passivation layer is being investigated via XPS as well as isotopic labeling in conjunction with secondary ion mass spectrometry (SIMS) studies. It is hypothesized that the high selectivity occurs due to the occupied Ge d-orbitals backbonding with an unsaturated carbon ligand, such as a CF2 carbene. This backbonding promotes the polymerization of a carbonaceous film on the Ge surface and thereby passivates the Ge against etching. Since Si does not possess occupied d-orbitals it is unable to promote the polymerization of a passivation layer as efficiently as Ge.

12:00pm PS2-ThM13 Thermodynamic Prediction and Experimental Verification of Etch Selectivity for EUV Mask Materials, Luke Minardi, N.D. Altieri, E.L. Chen, J.P. Chang, University of California Los Angeles

Extreme ultraviolet (EUV) lithography is a promising candidate to replace optical lithography and extend Moore's Law. EUV lithography requires reflective optics due to the strong absorption of EUV light by most materials. The exposed wafer area is defined by the absorbing and reflecting regions of the EUV mask. The absorber stack in the EUV mask consists of 2-10 nm TaON antireflective coating (ARC) and 50-60 nm TaN bulk absorber. The final EUV mask must have a ±1 nm absorber thickness

uniformity and a mean-to-target critical dimension of 2.0 nm^{1,2}. The etch process to pattern the EUV mask must be highly selective and anisotropic to meet the stringent requirements on mask dimension.

In this work, a generalized thermodynamic approach was used to screen viable etchants and predict selectivity. Gibbs energy minimization (GEM) was used to screen a library of halide containing etchants for efficacy on Ta-based compounds. Using GEM, Cl-based etchants indicated a high selectivity of Ta to Ta2O5. For example, at 350 K and 10⁻⁵ atm, 1 kmol of Ta(s) in the presence of 33 kmol of Cl2 forms 1 kmol of TaCl5(g) while 0.5 kmol Ta2O5(s) remains unreacted in 33 kmol of Cl2. Volatility diagrams were constructed for the Cl2-Ta and Cl2-Ta2O5 systems to compare etch product volatility at specified Cl2 pressure. For the Cl2-Ta system at a chlorine pressure of log(PCl2)=-5 atm, it is predicted that TaCl5(s) is in equilibrium with TaCl5(g) at a partial pressure of log(PTaCl5)=-6 atm. For the Cl2-Ta2O5 system at a chlorine pressure of log(PCl2)=-5 atm, it is predicted that Ta2O5(s) is in equilibrium with TaCl5(g) at a partial pressure of log(PTaCl5)=-40 atm. Using GEM and volatility diagrams it was predicted the etch rate of Ta(s) >> Ta2O5(s) in a Cl2 environment. Selectivity predictions have been tested and verified experimentally through etch rate experiments using an inductively coupled plasma etcher. Experiments conducted at 250 W power, 10 mTorr, and 20 sccm Cl2 determined selectivity to be 360 and 68 at bias powers of 0W and 10W, respectively. Although plasma processing is inherently non-equilibrium, thermodynamic prediction of product volatility is a powerful tool indicating trends in etch rate.

References:

1. B. Wu and A. Kumar, *J. Vac. Sci. Technol. B* **25** (6), 1743-1761 (2007)
2. J. Mathuni, J. Rau, F.-M. Kamm, G. Ruhl, Ch. Holfeld, F. Letzkus, C. Kopernik, and J. Butschke, *Proc. SPIE Vol. 5504*, 105-110 (2004)

Surface Science

Room 104D - Session SS-ThM

Chirality and Enantioselectivity on Surfaces; Ionic Liquid Interfaces

Moderator: Eddy Tysoe, University of Wisconsin-Milwaukee

8:00am SS-ThM1 Self-assembly and Dynamics for Chiral Conformational Switches on Surfaces Studied by UHV-STM, Trolle Linderroth, Aarhus University, Denmark

INVITED

Chiral self-assembled structures formed from organic molecules adsorbed on surfaces can be studied at high resolution by Scanning Tunneling Microscopy under Ultra-High Vacuum conditions. Through collaboration between UHV-STM experiments and organic synthesis, we have investigated how molecular conformational flexibility can lead to new chiral effects in the form of chiral switching, chiral accommodation and chiral induction, allowing transfer of chirality from the molecular to the supra-molecular level [1-5]. To generalize these principles, we have recently developed a new system of 3-bit binary conformational switches (Oligo-Naphthalene Ethynyls) [6, 7] and in particular quantified their dynamic conformational switching and collective effects in ordering using time-resolved STM movies.

[1] Weigelt, S.; Busse, C.; Petersen, L.; Rauls, E.; Hammer, B.; Gothelf, K.V.; Besenbacher, F.; Linderroth, T.R. *Nature Materials*, **2006**, **5** 11.

[2] Bombis, C.; Weigelt, S.; Knudsen, M. M.; Nørgaard, M.; Busse, C.; Lægsgaard, E.; Besenbacher, F.; Gothelf, K. V.; Linderroth, T. R. *ACS NANO* **2010**, **4**, 297.

[3] Knudsen, M.; Kalashnyk, N.; Masini, F.; Cramer, J.; Lægsgaard, E.; Besenbacher, F.; Linderroth, T. R.; Gothelf, K. V. *J. Am. Chem. Soc.* **2011**, **133**, 4896.

[4] Masini, F.; Kalashnyk, N.; Knudsen, M. M.; Cramer, J. R.; Lægsgaard, E.; Besenbacher, F.; Gothelf, K. V.; Linderroth, T. R. *J. Am. Chem. Soc.* **2011**, **133**, 13910.

[5] Nuermaimaiti, A.; Bombis, C.; Knudsen, M. M.; Cramer, J.; Lægsgaard, E.; Besenbacher, F.; Gothelf, K. V.; Linderroth, T. R. *ACS Nano* **2014**, **8**, 8074.

[6] Cramer, J. R.; Ning, Y.; Shen, C.; Nuermaimaiti, A.; Besenbacher, F.; Linderroth, T. R.; Gothelf, K.V. *Eur. J. Org. Chem.* **2013**, 2813.

[7] Ning, Y.; Cramer, J. R.; Nuermaimaiti, A.; Svane, K.; Yu, M.; Lægsgaard, E.; Besenbacher, F.; Xue, Q.-K.; Ma, X.; Hammer, B.; Gothelf, K. V.; Linderroth, T. R. *J. Chem. Phys.* **2015**, **142**, 101922.

Thursday Morning, November 10, 2016

8:40am **SS-ThM3 Chiral Recognition among Non-planar Aromatic Hydrocarbons on Metal Surfaces**, A. Mairena, Empa, Swiss Federal Laboratories for Materials Science and Technology; M. Parschau, Karl-Heinz Ernst, Empa, Swiss Federal Laboratories for Materials Science and Technology, Switzerland

Molecular recognition among chiral molecules on surfaces is of paramount importance in biomineralization, enantioselective heterogeneous catalysis, and for the separation of chiral molecules into their enantiomers via crystallization or chromatography. Understanding the principles of molecular recognition in general, however, is a difficult task and calls for investigation of appropriate model systems. One popular approach is thereby studying intermolecular interactions on well-defined solid surfaces, which allows in particular the use of scanning tunneling microscopy (STM). We present an elucidation of chiral recognition of helical and bowl-shaped hydrocarbons in monolayers and in multilayers. For pentalicene, a unique coexistence of 2D conglomerate and racemate is observed on a copper surface. Chiral bias in form of small enantiomeric excess leads to single enantiomorphism in multilayered samples of racemic heptahelicene.¹ Only the majority enantiomer is allowed to exist in the bottom layer, whereas the top layer consists exclusively of the minority enantiomer, i.e., enantioselective de-wetting occurs.

Pentagonal substituted chiral buckybowls form 2D racemate crystals, but chiral hemifullerene restructures a copper surface such that special chiral kinks become stabilized by the enantiomers.²

1 M. Parschau, K.-H. Ernst, *Angew. Chem. Int. Ed.* **2015**, *54*, 14422.

2 W. Xiao, K.-H. Ernst et al., *Nature Chemistry* **2016**, in press.

9:00am **SS-ThM4 Competing Forces in Chiral Surface Chemistry: Enantiospecificity versus Enantiomer Disproportionation**, Andrew Gellman, Y. Yun, Carnegie Mellon University

{The enantiospecific adsorption of chiral molecules on chiral surfaces is dictated by two competing forces the enantiospecificity of adsorption energetics and the propensity of enantiomers to disproportionate into homochiral (conglomerate) or heterochiral (racemate) clusters. These phenomena have been studied by measuring the surface enantiomeric excess, ee_s , of mixtures of chiral amino acids adsorbed on Cu surfaces and in equilibrium with gas phase mixtures of varying enantiomeric excess, ee_g . Alanine adsorption on Cu{3,1,17}^{R&S} surfaces is non-enantiospecific, $ee_s = ee_g$, because alanine enantiomers do not interact with either the surface or one another enantiospecifically. Aspartic acid adsorbs enantiospecifically on the Cu{3,1,17}^{R&S} surfaces; $ee_s \neq ee_g$, even during exposure to a racemic mixture in the gas phase, $ee_g = 0$. Exposure of the achiral Cu{111} surface to non-racemic aspartic acid, $ee_g \neq 0$, results in local amplification of enantiomeric excess, $|ee_s| > |ee_g|$, as a result of homochiral disproportionation. Finally, in spite of the fact that the Cu{653}^{R&S} surfaces are chiral, the adsorption of aspartic acid mixture is dominated by homochiral disproportionation of adsorbed enantiomers rather than enantiospecific adsorbate-surface interactions, $|ee_s| > |ee_g|$. All of these types of behavior are captured by a Langmuir-like adsorption isotherm that also describes competition between enantiospecific adsorption and both homochiral (conglomerate) and heterochiral (racemate) clustering of adsorbed molecules.}

9:20am **SS-ThM5 Probing Individual Binding Sites around Individual Chiral Molecules on a Metal Surface: Chemisorption and Non-Covalent Bonding in Heterogeneous Asymmetric Hydrogenation**, Peter McBreen, Laval University, Canada; B. Hammer, Aarhus University, Denmark; M. Goves, Aarhus University; J.-C. Lemay, Y. Dong, Laval University, Canada

There is rapid progress in the design and application of chirally-modified metal particles for heterogeneous catalytic enantioselective reactions. Modification is achieved by adsorbing chiral molecules to create asymmetric active sites. Great advances are being made in *operando* studies, surface science studies and theoretical studies of such systems. We will describe combined experimental and theoretical work related to the enantioselective hydrogenation of activated ketones on chirally-modified Pt(111). We will present results from combined variable temperature STM and optB88-vdW DFT studies of individual bimolecular docking complexes formed between enantiopure 1-(1-naphthyl)ethylamine, and related molecules, and representative prochiral substrates. The experiments reveal sub-molecularly resolved site-specific and stereospecific data. Single chemisorbed enantiomers simultaneously present several chiral pockets, each displaying a specific prochiral ratio for a given substrate molecule. A hierarchy of chemisorption and intermolecular interactions is found to control prochiral selection at each pocket. Fine-tuning the structure of the modifier reveals how sensitive the stereochemical outcome is to even

minor molecular changes. Time-lapsed STM measurements of individual substrate molecules sampling a set of chiral pockets provide new insight on stereocontrol, and on reaction paths and barriers at individual binding sites.

9:40am **SS-ThM6 Enhanced Hydrogenation Activity and Diastereomeric Interactions of Methyl Pyruvate Co-adsorbed with R-1-(1-Naphthylethylamine) on Pd(111)**, Mausumi Mahapatra, W.T. Tysoe, University of Wisconsin-Milwaukee

The diastereomeric interactions and reactivity of co-adsorbed methyl pyruvate (MP) and R-1-(1-naphthyl)ethylamine (NEA) are studied on a Pd(111) model single crystal catalyst using temperature-programmed desorption (TPD) and scanning tunneling microscopy (STM) with the aim of identifying the nature of the interactions and understanding the observed enhancement in hydrogenation activity of MP to methyl lactate on NEA-modified surfaces. The enhancement in hydrogenation activity of chirally modified sites is critical in designing heterogeneous enantioselective catalysts by mitigating the effect of unmodified racemic sites. TPD experiments of coadsorbed MP and hydrogen or deuterium on Pd(111) reveal that NEA accelerates the rates of both MP hydrogenation and H/D exchange. The measured STM images of docking complexes on Pd(111) are classified according to the angles between the long axes of MP and the naphthyl ring of NEA, which fall into well-defined ranges of $10 \pm 5^\circ$, $45 \pm 5^\circ$ and $70 \pm 5^\circ$. Docking structures are modeled using first-principles density functional theory (DFT) calculations that include van der Waals interactions, and STM image simulations. Excellent agreement is found both between the shapes of the calculated and simulated images and their theoretical and experimental dihedral angle distributions, thereby confirming the validity of the calculations. Diastereomeric interactions between NEA and MP occur predominantly by binding of the carbon-carbon double bond of the *enol* tautomer of MP to the surface, while simultaneously optimizing C=O...H₂N hydrogen-bonding interactions. The combination of chiral-NEA driven diastereomeric docking with a tautomeric preference enhances the hydrogenation activity since C=C bonds hydrogenate more easily than C=O bonds. This model provides a rationale for the catalytic observations.

11:00am **SS-ThM10 Structural Transitions of Ionic Liquids at Nanoconfined Interfaces**, Rosa M. Espinosa-Marzal, University of Illinois at Urbana-Champaign

INVITED

Ionic liquids (ILs) have remarkable properties including vanishingly low vapor-pressures, are non-flammable, and have wide thermal and electrochemical stability windows that make them ideal for several applications, including electrolytes in supercapacitors and lubricants. Our interest is to understand the interfacial behavior of ILs under nanoconfinement. Several studies have demonstrated the layered structure of ILs in nanoconfinement. The confined ions resist being “squeezed out” when surfaces are compressed, with the result that an IL film remains between the surfaces up to high pressures, thus preventing direct contact between the surfaces, also under shear, which can aid in reducing friction.

Laboratory studies have mainly focused on atomically flat and chemically homogeneous substrates, i.e. on ideal surfaces, to understand fundamental mechanisms. In our current work we are exploring the influence of nanoscale heterogeneities on ionic-liquid interfacial properties. Such heterogeneities can be composed of contamination, roughness or chemical surface groups. The strong molecular interactions still facilitate self-assembly of ILs on the surfaces, but they reveal new aspects of the IL behavior. We address diverse fundamental questions about the interfacial IL structure and the response to shear in the presence of heterogeneities. Further, these studies are of relevance to extend studies performed on ideal systems to real applications.

11:40am **SS-ThM12 Ionic Liquid Ordering at a Model Electrode Interface: 1-butyl-3-methylimidazolium Tetrafluoroborate, [C4C1Im][BF4], Interaction with the Anatase TiO₂ (101) Surface**, Michael Wagstaffe, University of Manchester, UK

Ionic liquids are room temperature molten salts comprised entirely of cations and anions. They have an array of unique physico-chemical properties that have led to their use in a wide variety of electrochemical systems.^[1] These include actuators, corrosion inhibitors, energy storage for batteries, supercapacitors, displays and as the electrolyte in photovoltaic devices. Both the function and performance of devices employing ionic liquids are dependent on how the ionic liquid behaves at phase boundaries, interfaces and near interfacial areas. Previous studies have shown that ionic liquids have a tendency to self organize at the IL/solid interface.^[2]

Thursday Morning, November 10, 2016

Such ordering has been shown to reduce the barrier to charge injection when ionic liquids are used in oxide solar cells.^[3] As such, the ordering and chemistry of ionic liquids at the anatase TiO₂(101) surface is of some interest since this is the dominant surface in mesoporous TiO₂ films used in dye sensitized solar cells.

Although there is a growing body of work on the surface chemistry of bulk ionic liquids studied by photoelectron spectroscopy, studies of their interaction with solid surfaces are still relatively rare. On this basis, in an attempt to address the gap in the work, we adopted a surface science approach in which we utilized a combination of X-ray photoelectron spectroscopy and near-edge X-ray absorption fine structure (NEXAFS) spectroscopy. From this we were able to successfully determine the orientation of the cation on the surface of anatase(101), at both high and low coverage, and also the manner in which it adsorbs. Additionally, a surface induced degradation reaction of the anion was observed at room temperature.

[1] K. R. J. Lovelock *et al.* *Chem. Rev.*, 2010, **110**, 5158–90.

[2] E. Binetti *et al.* *J. Phys. Chem. C*, 2013, **117**, 12923–12929.

[3] B. R. Lee *et al.* *J. Mater. Chem.*, 2011, **21**, 2051.

12:00pm SS-ThM13 In-Situ Photocurrent Measurements in Liquid-Phase Molecular Layer Deposition (LP-MLD), Shi Bai, Tokyo University of Technology, Japan

[Introduction] A solution of the loss of heat by using black dye in a dye-sensitization solar cell is expending the width of the light absorbing wavelength by growing multi-dye with narrow wavelength to reduce the loss of heat. So, we supply and make the molecules grow according to the reaction between the molecules, and apply the multi-dye layer film by using Liquid-Phase Molecular Layer Deposition. By way of LP-MLD, the multi-dye layer forms on the surface of ZnO, and we test the expansion effect of the photocurrent spectrum width.

[Growth of multi-dye layer film] First, adsorb the p-type dye(Rose Bengal)molecules p1 on the surface. Because there is no reaction between the same molecules, and they don't combine each other. So the first layer is completed on the surface of the substrate which the surface is filled with p1. Second, remove the p1 by IPA(isopropyl alcohol), then supply the n1,molecules of n-type dye(Brilliant Green).p1 and n1 react and they combined. The same as step 1,the p1 layer is filled with n1,then the second layer is completed. Step 3 is using p-type dye(Eosin Y) molecules again. Repeat these steps, adsorb the molecules in the array as designed, and complete the multi-dye molecule layer film.

[Measurement of the photocurrent in LP-MLD] LP-MLD is a technology using the combination power between molecules of p-type dye and molecule of n-type dye to make a layer. Use IPA as the solvent to make a solution with the concentration of 1.6×10^{-2} mol/L. Set the substrate in a cell, inject the cell with IPA until the cell is full of it. Then inject the solution of p1 to make the dye molecules adsorbed by the substrate. After 20 minutes, in order to remove p1 solution in the cell, inject the cell with IPA again. After putting the laser on the substrate and measuring the photocurrent, repeat the process with other dye solution. Base on the measurement, the expansion effect of the photocurrent spectrum width was deduced.

Thin Film

Room 104E - Session TF1-ThM

Control and Modeling of Thin Film Growth and Film Characterization

Moderators: Berc Kalanyan, National Institute of Standards and Technology (NIST), Richard Vanfleet, Brigham Young University

8:00am TF1-ThM1 Adventures in Group IV Ordering: Super-periodicities at the Atomic/Nano/Meso/scale, Jerrold Floro, J. Amata, C. Duska, C.W. Petz, University of Virginia; **D. Yang, J. Levy**, University of Pittsburgh

INVITED

This talk will examine the perils, pitfalls, and possibilities for creating order across different lengthscales and dimensionalities in heteroepitaxial Group IV thin films and nanostructures. I will review our results in three projects: (i) Direct writing of ordered arrays of 3C-SiC quantum dots on Si (001); (ii) Directed self-assembly of 2D and 3D ordered arrays of Ge quantum dots on Si (001); and (iii) chemical ordering in Si_{1-x}Ge_x alloys on Si (001). Herein, all the materials are grown by molecular beam epitaxy. Even though Group IV materials are amongst the most heavily studied epitaxial growth systems,

Thursday Morning, November 10, 2016

in all three cases discussed here there were significant surprises, some “good” and some “bad”. First I will briefly review our goal of using carbonaceous bumps, written on Si (001) by fine-spot electron-beam cracking of hydrocarbons, to direct the self-assembly of Ge quantum dots. We did not observe the latter to occur, but the formation of epitaxial 3C-SiC was itself interesting, and the carbide dots were successfully encapsulated in a Si matrix under optimized overgrowth conditions. We then used Ga focused ion beams (FIB) to create surface morphology that directs the self-assembly of Ge quantum dots. Atomic force microscopy (AFM) showed beautiful long-range order, both in single layers of dots, and in multiple layers of dots. However, cross-section transmission electron microscopy told a rather different story to the AFM, and this ultimately led us to abandon FIB as our patterning method of choice, in favor of electron beam lithography (ongoing). Finally, we recently revisited *chemical* ordering in Si_{1-x}Ge_x alloys, which was intensively studied in the 1990's. Our work was driven by predictions that chemical ordering, with large order parameters, could produce observable effects on thermal transport, and likely on electrical transport as well. This could improve the thermoelectric figure of merit. However, despite an extensive survey of growth-parameter space, we never observed order parameters to exceed 0.24. We found it necessary to be very careful in our quantification of the order parameter. More interestingly, our results seem to suggest three mutually inconsistent results with regard to how ordering is affected by step density. Hence there is much more to be understood about the interactions of strain, steps, faceting, and dislocations on chemical ordering. We gratefully acknowledge the support of the Department of Energy Office of Basic Energy Sciences, the II-VI Foundation, and the National Science Foundation Division of Materials Research. Research was performed in part at the NIST Center for Nanoscale Science and Technology.

8:40am TF1-ThM3 Combinatorial Fabrication of Cu-Fe₂O₃ Composite Nanostructures by Oblique Angle Co-Deposition, S. Larson, W.J. Huang, Yiping Zhao, University of Georgia

Traditionally, new materials have been explored and discovered via the one by one trial-and-error method. This can require decades of research to identify and optimize a material system for technological application and commercialization. From an experimental point of view, to speed up materials discovery, a large amount of materials need to be synthesized/fabricated and characterized simultaneously. Such a parallel production and characterization process has been traditionally targeted by a so-called high throughput or combinatorial materials science. The adaptation of the combinatorial techniques to nanofabrication has been slow due to the complexity and variety of fabrication techniques. To-date, only few groups have realized combinatory nano-synthesis via multi-well hydrothermal and solvothermal methods. However, based on combinatory thin film deposition technique and shadowing growth mechanism, a new and versatile combinatory nanofabrication technique called the oblique angle co-deposition can be easily facilitated. It can be used to generate a library of nanomaterials with different morphology and structure. In this talk we demonstrate the feasibility of such a nanofabrication technique. Using the Cu-Fe₂O₃ system as an example, by carefully characterizing the vapor plumes of the source materials, a composition map can be generated, which is used to design the locations of all the substrate holders. The resulting nanostructures at different locations show different thickness, morphology, crystallinity, composition, as well as inhomogeneity in microstructures. In addition, material maps of all these structural parameters are established, which can be used to correlate their properties. By further oxidizing or reducing the composite nanostructures, the properties of the nanostructures such as band gap, photocatalytic performance, and magnetic properties can be easily linked to their composition and other structural parameters. Optimal materials for photocatalytic and magnetic applications are efficiently identified. It is expected that the oblique angle co-deposition and its variations could become the most powerful combinatory nanofabrication technique for nanomaterial survey.

9:00am TF1-ThM4 Structural and Electronic Properties of Titanium Doped Ga₂O₃ Thin Films, Sandeep Manandhar, E. Rubio, C.V. Ramana, The University of Texas at El Paso

Gallium oxide (Ga₂O₃) has garnered significant interest due numerous applications of this material in gas sensing, optoelectronic devices, transparent electronic devices, and spintronics. From optical applications point of view, Ga₂O₃ finds attractive applications in luminescent phosphors, antireflection coatings, and solar cells. Ga₂O₃ has been recognized as a deep ultraviolet transparent conducting oxide (UV-TCO), which makes the material a potential candidate for transparent electrode applications in UV

8:00 AM

optoelectronics. However, while the large band gap makes it useful for far UV applications, it is possible to tune the properties and make it suitable for visible or low-UV applications if the band gap and electrical conductivity of Ga₂O₃ thin films are tuned. In this context, we propose and investigate to modify the properties of Ga₂O₃ by selectively doping with titanium (Ti). β -Ga₂O₃ thin films with variable Ti content were deposited by co-sputtering of the Ga-oxide ceramic and Ti metal by varying the sputtering power applied to these targets. The effect of Ti on the crystal structure and optical properties of β -Ga₂O₃ thin films is significant. For low Ti-content, films crystallize in β -phase of Ga₂O₃. However, increased Ti content induces amorphization of the Ga₂O₃ thin films. Band gap values showed a corresponding shift from ~5 eV to lower side indicating that the Ti incorporation induce changes in the electronic structure. A correlation between Ti-chemistry, structure and optical properties of Ga-Ti-O films will be discussed.

9:20am TF1-ThM5 Characterizing Patterns and Order in Self-Assembled Langmuir Films of Quantum Dots, Zachary Whitfield, J.J. Weimer, University of Alabama in Huntsville

The goal of this analytical study is to establish methods to quantify the uniformity of self-assembled Langmuir monolayers of quantum dots (QDs) in an efficient and reliable manner. Gradient-core quantum dots (QDs) were selected for creating the thin films because of their growing popularity for use in industries. The QDs were cast as Langmuir films on a water subphase, and the Langmuir films were deposited onto substrates using the Langmuir-Schaefer (LS) technique. Images were taken using an iSight digital camera of both the Langmuir and LS films with a black light source. Agglomerations, voids, islands, and ridges were some of the artifacts found when surveying the Langmuir films. These artifacts were seen to template directly to the LS films. Emission spectra of the LS films were mapped using fluorescence spectroscopy. Scanning probe microscopy was also performed to study surface morphology of samples. Image processing software was used to quantify the intensities of the variations at different spatial locations across the films. A direct correlation was made between the spatial variations in image brightness and the intensities of fluorescence spectra at the same given point on the LS films.

9:40am TF1-ThM6 Radical-Based MBE Growth, Structure, Defects and Transport in High-Mobility Epitaxial La-doped BaSnO₃ Films, A. Prakash, P. Xu, J. Dewey, Bharat Jalan, University of Minnesota

We will present on the growth of phase-pure, epitaxial BaSnO₃ films using a novel radical-based molecular beam epitaxy (MBE) approach with scalable growth rates [1]. In this approach, we use a metal-organic precursor (hexamethylditin) as a tin source, a solid effusion cell for barium, and an rf plasma source for oxygen. BaSnO₃ films were grown on SrTiO₃ (001), LaAlO₃ (001) and LSAT (001) substrates. The substrate temperature and oxygen pressure were kept fixed at 900° C, and 5x10⁻⁶ Torr respectively whereas Ba/Sn beam equivalent pressure (BEP) ratio was varied to optimize cation stoichiometry. The unstrained lattice parameter determined using high-resolution X-ray diffraction, and the Rutherford backscattering spectroscopy (RBS) were used to optimize cation stoichiometry. Lanthanum was used as n-type dopants.

Stoichiometric composition yielded an unstrained lattice parameter value of 4.116±0.001Å, which is identical to that of bulk BaSnO₃. This value was found to increase for Ba-rich films whereas Sn-rich films resulted into secondary phase formation. A range of Ba/Sn flux ratio was identified where films cation stoichiometry was self-regulating indicating the presence of a "MBE growth window". Time-dependent reflection high-energy electron diffraction (RHEED) intensity oscillations were observed during film growth indicating films grew in a layer-by-layer fashion. Atomic force microscopy confirmed smooth surface morphology for stoichiometric films. Non-stoichiometry films showed surface nanocrystallites, which correlated with the film stoichiometry. Most remarkably, phase-pure BaSnO₃ could also be grown with the molecular oxygen (i.e. without any rf plasma) suggesting an important role of reactive radical chemistry during film growth. We will discuss these results in the context of highly reactive Sn radicals growth mechanism that assist with the reaction and compound formation.

Finally, we will present a comprehensive electrical characterization of La-doped BaSnO₃ and will discuss how electrical transport is influenced by the presence of structural defects such as dislocations, non-stoichiometry, and dopant concentration. We will also present different scattering mechanisms in La-doped BaSnO₃ that limits the room temperature electron mobility. We will present pathways to suppress these scattering rates - a

step closer towards defect-managed high mobility oxide thin films and heterostructure.

Work supported by the NSF, and the AFOSR YIP Program.

[1] A. Prakash, J. Dewey, H. Yun, J.S. Jeong, K.A. Mkhoyan, and B. Jalan, "Hybrid molecular beam epitaxy for growth of stoichiometric BaSnO₃", J. Vac. Sci. Technol. A, **33**, 060608 (2015).

11:00am TF1-ThM10 Reduction of Extended Defects in SiC Epilayers Grown on 2° Offcut Substrates, Rachael Myers-Ward, N. Mahadik, R. Stahlbush, P. Klein, K.M. Daniels, A. Boyd, K. Gaskill, Naval Research Laboratory

Silicon carbide is a material of interest for high-voltage and high-power switching device applications. Basal plane dislocations (BPDs) are a major concern for SiC bipolar devices as they source Shockley-type stacking faults in the presence of an electron-hole plasma and reduce minority carrier lifetimes. Many researchers have investigated methods to reduce the BPD density by experimenting with pre-growth treatments, substrate orientation, growth parameters and growth interrupts. This work investigates extended defects, morphology and lifetime in 4H-SiC epilayers grown on substrates offcut 2° toward the [11-20].

Epilayers were grown on 2° offcut substrates in a horizontal hot-wall reactor using the standard chemistry of silane (2% in H₂) and propane. Epilayers were grown at various growth rates, C/Si ratios, and growth temperatures. The pressure was maintained at 100 mbar for all growths. Some samples were grown with a 5 μ m highly doped n⁺ buffer layer using ultra high purity nitrogen prior to the low doped epilayers. Ultraviolet photoluminescence (UVPL) imaging was used to identify BPDs in the low doped epilayers. Time resolved photoluminescence measurements were performed to determine the minority carrier lifetime of the layers and Raman spectroscopy was used to analyze polytype inclusions. Electron trap concentrations were determined using deep level transient spectroscopy (DLTS). Surface roughness was measured by atomic force microscopy and the morphology was also characterized using Nomarski microscopy.

When a 15 μ m epilayer was grown without a buffer layer, step bunching was observed and the surface roughness was 6.0 nm RMS. For comparison, a standard 4° offcut sample typically has 3.0 nm RMS for a 20 μ m epilayer. Using UVPL, it was found that after 4 μ m of epi, 90% of the BPDs had converted in the low doped layer as compared to 70% in a 4° offcut sample, indicating the conversion is faster in the lower offcut material. 3C-SiC inclusions were present in the epilayers as verified using Raman spectroscopy for both unintentionally doped (UID) and N⁺ epilayers. These inclusions were reduced by increasing the growth temperature and lowering the C/Si ratio for N⁺ epilayers, but increasing C/Si ratios for UID films. Changing these growth parameters resulted in specular film morphology and resulted in minority carrier lifetimes on the order of 1 μ s.

11:20am TF1-ThM11 Modeling the Structure and Medium Range order of ALD Amorphous Oxide Thin Films, Angel Yanguas-Gil, J.W. Elam, Argonne National Laboratory

The evolution of microstructure during the early stages of growth is crucial for the chemical and electronic properties of oxide materials at the core of a wide range of applications, from gate dielectrics for conventional and power electronics to energy storage and catalysis. Through a combination of synchrotron studies and atomistic models we have studied the evolution of the structure for a variety of oxide materials including ZnO, In₂O₃, TiO₂, and HfO₂.

We have leveraged ALD's unique ability to grow conformally on high surface area materials to characterize the evolution of the coordination environment and medium range order using EXAFS, XANES, and PDF. We have compared these results with atomistic simulations, which have allowed us to calculate the pair correlation function and the EXAFS of the simulated material as a function of thickness and temperature.

We have combined these molecular dynamic calculations with simple Monte Carlo simulations to understand the evolution of microstructure during the early stages of growth. Our results are consistent with local structural relaxation mechanisms having a key role in allowing the transition from isolated cluster to bulk-like coordination and medium range. In particular, using the REAXFF potential we were able to look at the impact that hydroxyl groups have on delaying the formation of crystalline phases for low temperature ALD ZnO.

Thursday Morning, November 10, 2016

11:40am **TF1-ThM12 From Nano-porosity to Macro-scale Defects: Ellipsometric Porosimetry and Electrochemical Impedance Spectroscopy Characterization of Thin Inorganic Films, Alberto Perrotta^{*}, W.M.M. Kessels, M. Creatore**, Eindhoven University of Technology, Netherlands

Nano-porosity is an intrinsic property of thin films, and it is identified in inorganic layers by the size of rings (e.g., -SiOSi-) and ring termination units (e.g., Si-OH). Porosity control is the key to several technological applications and selected examples are separation membranes, low- k dielectrics, and permeation barrier layers.

In moisture permeation barriers, H₂O permeation is known to occur through nano-porosity and the so-called macro-scale defects (from few nm to hundreds of μ m). Therefore, the development of methodologies able to follow both permeation paths and predict the quality of a barrier layer are needed.

In this study, an in-depth analysis of nano-porosity in thin films and its impact on their moisture barrier performance are presented.¹ Several inorganic layers (SiO₂, Al₂O₃, SiN_x) deposited by plasma enhanced-chemical vapor deposition (PE-CVD) and (plasma assisted-) atomic layer deposition (ALD) have been considered. Ellipsometric porosimetry (EP) and electrochemical impedance spectroscopy (EIS) have been adopted as complementary techniques for the analysis of nano-porosity ranging from H₂O kinetic diameter (0.27 nm) up to 1 nm. The role of the specific nano-pore range in controlling the *intrinsic* barrier properties has been disclosed. In detail, absence of porosity with diameter above 0.27 nm led the transition from mediocre (10^{-4} gm⁻¹day⁻¹) to excellent (10^{-6} gm⁻²day⁻¹) H₂O barrier properties. Moreover, PA-ALD Al₂O₃ and SiN_x (10-40 nm) layers showed no porosity in the 0.27-1 nm range, and therefore excellent *intrinsic* barrier properties.

Also, next to nano-porosity, macro-scale defect detection is shown possible by both EIS and EP. Specifically, EIS was shown able to directly detect such defects for barriers deposited on c-Si. With EP, the permeation of probe molecules through barriers deposited on polymers can be followed in time. It is thereby possible to discern diverse events, i.e., filling of nano-porosity in the barrier layer and swelling of the polymer.² The rate of permeation through the polymer and its swelling has been found to decrease of one order of magnitude upon deposition of porous barriers. The application of a denser layer, impermeable to the probe molecule, showed a further decrease in permeation rate and limited uptake in the polymer. This allowed the isolation of the permeation through macro-scale defects and, thus, their detection.

This research forms part of the research program of the Dutch Polymer Institute (DPI), project #752.

¹ Perrotta *et al.*, *Microp. Mesop. Mat.* 188 (2014) 163; *Appl. Mater. Interfaces*, 7 (2015) 15968; *Plasma Processes Polym.* 12 (2015) 968.

² Perrotta *et al.*, to be submitted.

12:00pm **TF1-ThM13 Thermal Conductivity and Mechanical Properties of AlN-based Thin Films, Vincent Moraes, H. Riedl**, Technische Universität Wien, Austria; *H. Bolvardi*, Oerlikon Balzers, Liechtenstein; *S. Kolozsvári*, Plansee Composite Materials GmbH, Germany; *M. Ikeda, L. Prochaska, S. Paschen, P.H. Mayrhofer*, Technische Universität Wien, Austria

While many research activities concentrate on mechanical properties and thermal stabilities of protective thin films, only little is known about their thermal properties being essential for the thermal management in various industrial applications. Based on the 3 ω -method, we show the influence of Al and Cr on the temperature dependent thermal conductivity of single-phase cubic structured TiN and single-phase wurtzite structured AlN thin films, respectively, and compare them with the results obtained for CrN thin films.

The dc sputtered AlN thin films revealed a highly c-axis oriented growth for deposition temperatures of 250 to 700 °C. Their thermal conductivity was found to increase strongly with the film thickness, indicating progressing crystallization of the interface near amorphous regions during the sputtering process. For the 940 nm AlN film, we found a lower boundary for the thermal conductivity of 55.3 W·m⁻¹·K⁻¹. By the substitution of only 10 at.% Al with Cr, κ significantly reduces to \sim 5.0 W·m⁻¹·K⁻¹, although the single-phase wurtzite structure is maintained. The single-phase face centered cubic TiN and Ti_{0.36}Al_{0.64}N thin films exhibit at room temperatures κ values of 3.1 W·m⁻¹·K⁻¹ and 2.5 W·m⁻¹·K⁻¹, respectively. Hence, also here, the substitutional alloying reduces the thermal conductivity, although at a

significantly lower level. Single-phase face centered cubic CrN thin films show κ values of 3.6 W·m⁻¹·K⁻¹.

For all nitride based thin films investigated, the thermal conductivity slightly increases with increasing temperature between 200 and 330 K. This rather unusual behavior is based on the high defect density (especially point defects) within the films prepared by physical vapor deposition.

PACS numbers: 68.60.Dv; 68.55.Jj;

Keywords: Thermal conductivity; Nitride based thin films; Alloying effects; 3 ω -method;

Thin Film

Room 105A - Session TF2-ThM

Area-selective Deposition and Sequential Infiltration Synthesis

Moderator: Giovanna Scarel, James Madison University

8:00am **TF2-ThM1 Area Selective Deposition from an Aqueous Fog, N. Murari, R.H. Mansergh, Y. Huang, D.A. Keszler, John F. Conley, Jr.**, Oregon State University

As ULSI technology continues to scale towards the sub-10 nm regime, lithographic patterning and registration to existing features have become increasingly difficult, expensive, and time consuming. Direct patterning or area selective deposition of materials only on desired areas of a substrate has been proposed as a way to overcome these lithographic challenges. Recently, several groups have demonstrated area selective atomic layer deposition (ALD) through approaches such as area deactivation - the use of polymers and self-assembled monolayers (SAMs) to inhibit ALD nucleation. While this work shows promise, alternatives to elevated temperature, vacuum based deposition techniques are desired by the microelectronics, photovoltaics, and display industries. Solution based deposition techniques offer a lower cost, more sustainable approach. Traditional spin-coating, however, is primarily limited to planar substrates and lacks the ability to form uniform films over large surface areas. A number of mist based deposition techniques have attempted to address the limitations of spin coating, but typically suffer from one or more disadvantages such as the requirement of high volatility precursors, uneven mist distribution, complex vapor transport, and/or poor control of film uniformity. A new aerosol based technique overcomes these problems by employing a novel atomizer consisting of two opposing jets located within the deposition chamber. Head-on collision of the opposing jets shears the precursor droplets into a fine mist / fog, allowing the use of low volatility precursors. The uniform generation of mist is scalable for deposition on arbitrarily large substrate areas. In this work we use this method to demonstrate area selective deposition from an aqueous fog at room temperature and pressure.

Aerosol deposition was conducted on a BENEQ ACS 200-101at room temperature and pressure using precursor fog of aqueous based aluminum phosphate inorganic clusters. An octyltrichlorosilane (OTS-8) based SAM with a hydrophobic tail group is used as a growth inhibitor. OTS-8 is patterned on a hydrophilic Si wafer surface. Selective deposition of oxide thin films from an aqueous precursor aerosol fog is achieved with growth occurring only in the hydrophilic regions and not on the areas covered by OTS-8. Smooth films with sharp boundaries are deposited with average surface roughness of less than 1 nm RMS. Deposition selectivity is investigated as a function of pattern size, shape, and half pitch. Overall, room temperature area selective aerosol deposition is shown to be a potentially promising sustainable alternative to AS-ALD for large area electronics.

8:20am **TF2-ThM2 "Patterned-by-Printing" ZnO Vertical TFTs, Carolyn Ellinger, S.F. Nelson**, Eastman Kodak Company

"Patterned-by-printing" uses selective area deposition (SAD) as an alternative approach to printed electronics: an inhibiting polymer ink is printed and the active materials are deposited via spatial atomic layer deposition (SALD). We have previously illustrated the use of this methodology to make planar ZnO thin-film transistors (TFTs) with equivalent device performance to TFTs fabricated from the same materials but patterned by conventional photolithographic means. We have further shown how patterned-by-printing enables freedom in circuit design due to the orthogonal nature of the patterning process, demonstrating facile fabrication of circuits with architectures that can be difficult to obtain using subtractive processing methods.

Thursday Morning, November 10, 2016

This talk will address fully patterned-by-printing vertical thin-film transistors (VTFTs), fabricated without any vacuum metallization steps. Using our standard toolset of SALD, inkjet printing and cleaning, we have explored the unique advantages offered by a patterned-by-printing approach for vertical TFT and circuit architectures. In addition to controlling the inhibitor pattern on the substrate by the print pattern, surface structures can be used to control the spatial location of the inhibitor ink via capillary forces. These vertical transistors have liberal design rules and low print resolution requirements as a result of self-aligned source and drain contacts. Starting with a gate structure having a re-entrant profile on the edge, conformal Al_2O_3 gate dielectric and ZnO semiconductor are patterned at low resolution using a printed inhibitor ink and SALD. The same inhibitor ink is printed at the same low resolution so that it is drawn into the reentrant profile, defining the semiconductor channel between SALD-deposited AZO source/drain contacts. The VTFTs have considerably shorter channel lengths than directly obtainable by the printed resolution, and correspondingly higher device performance from a simple additive patterning process. Furthermore, since each step is the same as used for our planar TFTs, circuits having mixed transistor architectures can be used to optimize performance. Individual device characteristics as well as circuit performance will be discussed.

8:40am TF2-ThM3 Area-selective Atomic Layer Deposition of Metal and Magnetic Films, John Ekerdt, H. Nallan, Z. Zhang, S. Chopra, University of Texas at Austin **INVITED**

In this work, we demonstrate the selective atomic layer deposition of Co onto MgO/Si and HfO_2/Si substrates. Magnetic materials such as Ni and Co are used in a wide variety of devices ranging from microelectronics to RF technology to energy. Recently, Co films have been explored as the magnetic material for a magnetic tunnel junction structure of an STT-RAM heterostack. Previous efforts to deposit Co metals using ALD precursors bis(N-tert butyl, N'ethylpropionamidato) cobalt (II) and H_2 have suffered from carbon and nitrogen incorporation into the film. Furthermore, etching ferromagnetic films typically relies on plasma processes that can generate side products and are detrimental to device performance.

Here we offer an alternative to this deposition and patterning approach through a sequence of area-selective atomic layer deposition (A-SALD) followed by an oxide reduction. A-SALD is a process by which the energy of a surface can be manipulated such that there is preferential wetting and nucleation of ALD precursors only in desired regions. It is shown that CoO ALD is successfully blocked on MgO or HfO_2 surfaces that have been treated with a self-assembled monolayer such as n-octadecyltrichlorosilane or a diblock polymer such as poly(trimethyl)silylstyrene/polystyrene. Once patterned, these organic blocking layers are used to prevent CoO deposition in particular areas of the substrate. The CoO deposition is performed at a temperature of $\sim 180^\circ$ using cobalt bis(diisopropylacetamidate) and water as co-reactants. Following deposition, it is shown that the CoO can be reduced to form Co metal using a reducing gas such as H_2 or CO at elevated temperature and/or by capping the CoO film with an oxygen-scavenging layer of Al that reacts to Al_2O_3 . With this approach, we are able to deposit Co metal in only desired regions of the substrate. X-ray photoelectron spectroscopy is used to determine the oxidation state of cobalt and film stoichiometry. Film crystallinity and structure of the films are analyzed with X-ray diffraction and reflection high-energy electron diffraction. Using a scanning superconducting quantum interference device, we explore how the magnetic properties of the Co films can be manipulated using different CoO thickness and capping metals.

9:20am TF2-ThM5 Selective Area Epitaxy of Magnesium Oxide Thin Films on Gallium Nitride Surfaces, Mark Losego, Georgia Institute of Technology; J-P. Maria, North Carolina State University; E.A. Paisley, Sandia National Laboratories

Selective area growth of thin films reduces the number of steps in microfabrication processing and enables novel device structures. Here we report for the first time selective area epitaxy of an oxide material on a GaN surface. Chlorination of the GaN surface via wet chemical processing is found effective to disrupt Mg adsorption and selectively prevent molecular beam epitaxy (MBE) growth of MgO. MgO films grown on neighboring, non-chlorinated surfaces are epitaxial with a (111) MgO || (0001) GaN crystallographic relationship. In-situ XPS studies reveal that a surface monolayer of adsorbed chlorine acts to prevent MgO deposition. Better than 3 micron lateral resolution for the selective area growth of MgO on GaN is demonstrated. This talk will present our current understanding of

this selective growth process and detail our studies of the surface chemistry mechanisms.

9:40am TF2-ThM6 Sequential Infiltration Synthesis (SIS) and its Applications in Nanofabrication, Qing Peng, University of Alabama

Chemical assembly of materials with atomic/molecular precision is the key to enable new generation technologies. Such sophisticated controllability relies on the understanding of fundamental mechanisms during atomic/molecular assembly processes. In this presentation, I will present the applications of sequential infiltration synthesis (SIS) in nano materials fabrication. The SIS method is based on the coupled diffusion and substrate site-limited reaction process. It shows great promise in the modification of the properties of polymers, and in the scalable and controllable manufacture of nanomaterials. The underlying mechanisms involved in the SIS process will be discussed along with its applications in the advanced lithography, nanostructure engineering and catalyst fabrication.

11:00am TF2-ThM10 Understanding Growth of Infiltrated ZnO an Atomic Step at a Time, Leonidas Ocola, D.J. Gosztola, A. Yanguas-Gil, Argonne National Laboratory; A. Connolly, Vassar College

We have investigated a variation of atomic layer deposition (ALD), called sequential infiltration synthesis (SiS), as an alternate method to incorporate ZnO and other oxides inside polymethylmethacrylate (PMMA) and other polymers. The precursors used to synthesize ZnO in PMMA are water (H_2O) and Diethylzinc (DEZ). SiS of ZnO in PMMA was accomplished by infiltrating ($\text{H}_2\text{O}:\text{DEZ}$) cycles at 95°C for periods of up to 4 min per cycle. Energy dispersive spectroscopy (EDS) results show that we synthesize ZnO up to 300 nm inside a PMMA film.

A key feature of an ALD process is the ability to add an atomic layer at a time. This characteristic allows for a detailed study of the formation of ZnO in the polymer matrix after each atomic step is formed. We followed each growth step of ZnO in PMMA using ex-situ photoluminescence (PL), Raman spectroscopy and x-ray photoemission spectroscopy (XPS). These studies show clear differences between mono, dimer and trimer Zn atom configurations. Mono Zn atoms (O-Zn and O-Zn-O) are formed with a single DEZ precursor pulse and one or two H_2O pulses and exhibit pure UV emission with no evidence of oxygen vacancy states (V_O). Dimer Zn atoms (O-Zn-O-Zn and O-Zn-O-Zn-O) are formed with two pulses of DEZ and two or three pulses of H_2O . They do not form yet a continuous film as shown with Raman spectroscopy. Dimers do show strong PL emission from V_O states. In addition, XPS data show no evidence of ZnO wurtzite bonding. After 3 precursor cycles we observe first evidence of film formation inside the polymer matrix with Raman spectroscopy and wurtzite formation with XPS. The evolution of ZnO properties studied with PL, Raman and XPS from these initial stages up to 12 cycles of SiS ZnO will be presented. Such detailed study allows insight to growth mechanisms of ZnO in a non-traditional environment, which may lead to novel applications of ZnO as sensors or detectors.

This work was supported by the Department of Energy under Contract No. DE-AC02-06CH11357. Use of the Center for Nanoscale Materials was supported by the U. S. Department of Energy, Office of Basic Energy Sciences, under Contract No. DE-AC02-06CH11357.

11:20am TF2-ThM11 Investigation of Vapor Phase Infiltration Kinetics: Infusing Metalorganic Vapors in Polymer Thin Films, Collen Leng*, M.D. Losego, Georgia Institute of Technology

Polymers can be chemically modified via infiltration and reaction with gaseous metalorganic precursors to create new hybrid organic-inorganic materials with novel electrical, chemical, and/or physical properties. These new materials can have applications as chemical barriers, filtration media, or photolithographic hard masks. Here, the focus is to have a better knowledge of the diffusion and reaction kinetics during this vapor phase infiltration process with the goal of understanding how both polymer structure and processing conditions can maximize the depth of inorganic infiltration. In this study, we use the model system of poly(methyl methacrylate) (PMMA) films exposed to trimethylaluminum (TMA) gaseous precursors. Spectroscopic ellipsometry is used to track infiltration by film swelling and changes in refractive index. At a process temperature of 60°C , films are found to initially swell in thickness with the square root of time, suggesting that kinetics are dominated by Fickian-like diffusion behavior. A maximum film swelling of 60% is measured at any exposure time exceeding 1000 minutes. Using these swelling curves as a proxy for infiltration amount, we calculate effective diffusion coefficients for TMA in PMMA at

60° C to be on the order of 10^{-15} cm²/s, with faster diffusion in PMMA films of lower molecular weight. At higher temperatures (160° C), swelling is less significant, but refractive indices of infiltrated films increase by 2% to 3%. We interpret the decrease in swelling as a result of faster chain relaxation when processing above the glass transition temperature of the polymer. To determine whether polymer films infiltrated and swollen below T_g can also undergo similar polymer relaxation behaviors, a systematic study of post-annealing was carried out at 150° C. In these instances, the amount of swelling decreases by approximately half and refractive index increases but to a lesser degree than those from the initial high process temperatures. The results of this study will be put in context with other ongoing research in the field to help build a phenomenological model that can be used to better design vapor phase processing schemes to form organic-inorganic hybrid materials.

11:40am **TF2-ThM12 Pyrolysis of Organic-Inorganic Hybrid Materials Formed by Sequential Organometallic Vapor Infiltration**, *Halil Akyildiz*, Uludag University, Turkey; *P.D. Bradford*, *J.S. Jur*, North Carolina State University

Organic inorganic hybrid materials are of interest for wide variety of applications including flexible electronics and catalysis. This work explores the use of a sequential vapor infiltration (SVI) process by which organometallic ALD precursors are infiltrated into the bulk polymer materials and react with the available functional sites to form a network of organic-inorganic hybrid materials. In this study, thermal degradation characteristics of the SVI hybrid materials are studied with thermogravimetric analysis (TGA) under inert atmosphere. Higher thermal stability of the fibers of SVI hybrid materials is observed compared to the pristine PET fibers and different degradation steps in TGA are defined. Furthermore, increased thermal stability of hybrid materials is demonstrated by pyrolysis of SVI treated nylon-6 and polyester fiber mats at 900°C with high heating rates (up to 200°C/min). It is shown by SEM imaging that fabrics with SVI treatment retain their fibrous structure and high surface area, whereas pristine fabric samples are either completely degraded. Raman spectroscopy analysis of these carbon fibers confirms the graphitic and disordered carbon structures formation.

12:00pm **TF2-ThM13 Carbon Nanofibers Derived from a Cellulosic Polymer Enabled by Vapor Infiltration of Diethyl Zinc for Carbon Based Supercapacitors**, *Wenyi Xie*, *O.J. Rojas*, *S. Khan*, *G.N. Parsons*, North Carolina State University

Common thermoplastic polymers, such as polyvinyl alcohol and cellulose derivatives are viable precursors to prepare carbon materials for supercapacitor electrodes. These polymers can be readily processed to prepare high external surface area nanofibers. However, thermoplastic polymers undergo melting transition upon heating, therefore result in loss of initial morphology and low carbon yield. In this study, vapor infiltration of diethyl zinc is applied to modify cellulose based nanofibers as the carbon precursor. Our goal is to investigate the effect of inorganic modification on the morphology, surface area and pore volume, as well as the supercapacitor performance of the carbon product from the modified cellulose based nanofibers.

Vapor infiltration of diethyl zinc (DEZ), was performed using a home-built viscous-flow hot-wall tube reactor. One cycle of the vapor infiltration chemistry consisted of a short dose of DEZ (1 s), followed by a DEZ-hold step (60 s) to enable the reactant to diffuse into the nanofibers, and then followed by a N₂ purge step (40 s) to remove excess reactant and byproducts. *Scanning electron microscopy* (SEM) revealed that the fiber structure of cellulose-based nanofibers could be preserved with at least ~ 8.0 wt % of Zn. Nitrogen sorption measurements at 77 K showed that the surface area and pore volume could be tuned by the DEZ infiltration process. Two-electrode symmetric capacitors were fabricated using the carbon materials from the DEZ modified cellulose based nanofibers. Cyclic voltammetry measurements were performed using 1 M KOH as the electrolyte to determine the specific capacitance. The carbon materials obtained from the DEZ modified cellulose based nanofibers showed a specific capacitance in range of ~25 to 50 F/g.

In this work, vapor infiltration of DEZ has enabled the preparation of carbon nanofibers from cellulose based nanofibers. By varying the loading of Zn, the surface area and pore volume of the resulting carbon nanofibers can be tuned to enhance the supercapacitor performance. Therefore, we believe that inorganic modification by vapor infiltration of DEZ is promising for modifying thermoplastic polymers to produce high performance nanostructured carbon materials for supercapacitors

Thursday Afternoon, November 10, 2016

2D Materials Focus Topic

Room 103B - Session 2D-ThA

Surface Chemistry, Functionalization, Bio and Sensor Applications of 2D Materials

Moderator: Li Tao, The University of Texas at Austin

2:20pm 2D-ThA1 Nanoelectronic Heterodyne Sensor: A New Electronic Sensing Paradigm, *Zhaohui Zhong*, University of Michigan, Ann Arbor

INVITED

Nearly all existing nanoelectronic sensors are based on charge detection, where molecular binding changes the charge density of the sensor and leads to sensing signal. However, there are several fundamental limitations to the charge-detection based electronic sensors. The examples include the ionic screening effect in high ionic strength solution, and the sensitivity-speed tradeoff for vapor phase sensing. In this talk, I will discuss our group's recent works on a new paradigm of electronic sensing by exploring the heterodyne mixing response between the molecular dipole and a nanoscale transistor. First, we successfully demonstrated that the fundamental ionic screening effect can be mitigated by operating single-walled carbon nanotube field effect transistor as a high-frequency heterodyne biosensor. Electrical detection of streptavidin binding to biotin in 100 mM buffer solution is achieved at a frequency beyond 1 MHz. The results should promise a new biosensing platform for point-of-care detection, where biosensors functioning directly in physiologically relevant condition are desired. Second, we demonstrated the concept of nanoelectronic heterodyne sensor for vapor detection in a graphene device. The dipole detection mechanism is confirmed by a plethora of experiments with vapor molecules of various dipole moments, particularly, with *cis*- and *trans*-isomers that have different polarities. Rapid (down to 0.1 s) and sensitive (down to 1 ppb) detection of a wide range of vapor analytes is achieved, representing orders of magnitude improvement over state-of-the-art nanoelectronics sensors. Finally, we demonstrated electrical probing and tuning of the non-covalent physisorption of polar molecules on graphene surface by using graphene nanoelectronic heterodyne sensors. Our results provide insight into small molecule-nanomaterial interaction dynamics and signify the ability to electrically tailor interactions, which can lead to rational designs of complex chemical processes for catalysis and drug discovery.

3:20pm 2D-ThA4 Study of the Photoresponse and Transport Properties of Photoexcited Carriers in MoS₂ Nanoflakes for Sensing Applications, *Sourav Garg, J. Waters, A. Shahab, M. Singla, S. Kim, P. Kung*, University of Alabama

Although graphene has been widely studied for its 2D properties, its zero band gap nature limits its potential role in semiconducting applications. Molybdenum disulphide (MoS₂) is a semiconductor whose bandgap changes from indirect to direct due to the disappearance of the inversion symmetry when the material is in a monolayer form and in addition this breaking of the symmetry between the K and K' valleys intensifies its use in valleytronic applications. Understanding the correlation between electrical and optical characteristics of MoS₂ is important in order to realize optoelectronic devices based on these materials, including for sensing and biological applications.

In the present work, we investigate and compare the electrical transport characteristics of MoS₂ in monolayer and bilayer forms under the influence of an optical excitation and temperature, through the realization and measurement of MoS₂ interdigitated patterned devices. MoS₂ monolayer and bilayer sheets were synthesized by chemical vapor deposition in an oxygen-free environment on basal plane sapphire substrates. Interdigitated metal contacts were realized using conventional optical lithography with channel lengths ranging from 5 to 10 micrometer. The response of the resulting device was characterized as a function of incident light intensity, wavelength, applied bias, and temperature. We further investigate the impact of these properties on the realization of chemical sensor devices using MoS₂.

4:00pm 2D-ThA6 Surface Engineering with Chemically Modified Graphene and other 2D Materials, *Paul Sheehan, SC. Hangarter, W.K. Lee, S.P. Mulvaney, J.T. Robinson, S.D. Tsoi, K.E. Whitener*, US Naval Research Laboratory

INVITED

Atomically-thin 2D materials such as graphene, boron nitride, or transition metal dichalcogenides can radically alter the chemistry and physics of surfaces they are placed on. Indeed, the appropriate choice of 2D material and subsequent chemical functionalization can dictate all the principal

surface forces including van der Waals, acid-base interactions, electric double layers, and even magnetism. For instance, while graphene completely screens the van der Waals forces of the underlying substrate, boron nitride is completely transparent to these forces. A second example is hydrogenation which enables rapid patterning of ferromagnetic domains in graphene. Such control over surface forces should enable us to master technologically critical processes ranging from ice formation to bacterial adhesion to oriented crystal growth. The methods we have developed for chemically functionalizing and patterning graphene will be presented as well as experimental and theoretical work describing how these changes control the various surface forces. Finally, we will discuss a new technique to transfer surface functionalities *in toto* from one substrate to another.

4:40pm 2D-ThA8 Passivation of Transition Metal Chalcogenide Surface via Sulfur Layer to Enhanced Metal Contact, *JunHong Park*, University of California, San Diego; *A. Rai*, University of Texas at Austin; *I.J. Kwak*, University of California, San Diego; *S. Bhattacharjee, K. Ganapathi, N. Bhat*, Indian Institute of Science, Bangalore; *S.K. Banerjee*, University of Texas at Austin; *A.C. Kummel*, University of California, San Diego

The performance of FETs based on transition metal chalcogenide (TMD) is limited by the contact resistance between metal and TMD channels, resulting from the interface degradation during metal deposition on TMDs, metal reaction at defect sites or work function differences between TMDs and metals. In this presentation, the amorphous sulfur layers are formed on MoS₂ to protect the surface of MoS₂ during metal deposition and form an interfacial layer between MoS₂ and metal. The MoS₂ (bulk) flake is emerged into ammonium sulfide 40 % (NH₄)₂S in H₂O at 523 K (technique of Karr et al). Afterwards, the sulfur treated MoS₂ (bulk) is transferred into a UHV chamber to observe the atomic and electronic transformations of the surface *via* scanning tunneling microscopy (STM) and spectroscopy (STS). In the STM and STS, the sulfur-treated surface band gap is measured 1.85 ± 0.03 eV, while the bare MoS₂ bulk has 1.27 ± 0.02 eV band gap, consistent with existence of sulfur layer on MoS₂. Annealing the sample at 623 K for 60 mins results an increase in the band gap to 2.30 ± 0.03 eV. Additional annealing at 793 K of sulfur treated MoS₂ results in observation of crystalline sulfur clusters on MoS₂. However, this sulfur layer can be desorbed from MoS₂ by just direct heating to 793 K for 1 hr without intermediate step. Afterward, no missing sulfur atoms are observed nor any surface residues; however, there are sulfur clusters inside of the large native defects. The amorphous sulfur layer can be used as interface control for contact deposition. The MoS₂ devices were fabricated to elucidate the impact of sulfur treatments on MoS₂ FETs. After sulfur treatment of multilayer MoS₂, the metal contacts are defined by electron beam lithography and deposition, afterwards the samples were annealed at 673 K for 15 mins. In the electronic measurements, the contact resistance of multilayer MoS₂ and metal decrease to half of non-treated MoS₂ FET. The present sulfur treatment can expand to other TMD materials to improve the contact of TMDs and metal by providing both defect passivation and an interfacial control monolayer to prevent TMDA reaction and an ultrathin metal-sulfide interfacial control layer.

5:20pm 2D-ThA10 Substrate Effects in CVD Synthesized Monolayer WS₂, *Kathleen McCreary, A.T. Hanbicki*, Naval Research Laboratory; *G. Kioseoglou*, University of Crete; *M. Currie, B.T. Jonker*, Naval Research Laboratory

The unique electronic band structure in single layer WS₂ provides the ability to selectively populate a desired valley by exciting with circularly polarized light. The valley population is reflected through the circular polarization of photoluminescence (PL). We investigate the circularly polarized PL in WS₂ monolayers synthesized on SiO₂/Si substrates using chemical vapor deposition (CVD).^[1] The resulting polarization is strongly dependent on the sample preparation. As-grown CVD WS₂ (still on the growth substrate) exhibits PL emission from the neutral exciton and polarized emission that is unaffected by laser power. Removing WS₂ from the growth substrate and repositioning on the same substrate significantly impacts the optical properties. In transferred films, the excitonic state is optically controlled via high-powered laser exposure such that subsequent PL is from either the charged exciton state or the neutral exciton state, similar to the recently observed behavior in mechanically exfoliated WS₂ flakes.^[2] Additionally, the neutral excitonic emission in transferred CVD films exhibits low polarization whereas the trion polarization can exceed 25% at room temperature, demonstrating the ability to optically control the degree of circularly polarized emission. The removal process may modify the strain, sample-to-substrate distance, and chemical doping in the WS₂ monolayer, and work is underway to determine how these factors influence the valley populations. This work was supported by core

Thursday Afternoon, November 10, 2016

programs at NRL and the NRL Nanoscience Institute, and by the Air Force Office of Scientific Research #AOARD 14IOA018-134141.

[1] K. M. McCreary, A. T. Hanbicki, G. G. Jernigan, J. C. Culbertson, B. T. Jonker, *Sci. Rep.* **2016**, 6, 19159.

[2] M. Currie, A. T. Hanbicki, G. Kioseoglou, B. T. Jonker, *Appl. Phys. Lett.* **2015**, 106, 201907.

5:40pm **2D-ThA11 Driving Mechanochemical Wear on Graphene Using Local Stress and Heat**, S. Raghuraman, Jonathan Felts, Texas A&M University

Here we investigate the chemical dynamics of local graphene oxide reduction through the application of local temperature and stress using a heated atomic force microscope (AFM) tip. Specifically, a silicon AFM cantilever with an embedded Joule heater applies both local stress and heat to chemically functionalized graphene surfaces during tip sliding. The friction of the graphene sheet depends linearly on chemical group concentration, so monitoring friction force provides an *in situ* measure of chemical functionality on the surface over time. We demonstrate bond cleavage of oxygen via both local temperature and force during tip sliding on graphene oxide. Monitoring friction change over time for constant tip temperatures between 310 – 355 C and a load of 40 nN provides the kinetics of the reduction process, with an activation energy for bond scission of 0.7 ± 0.3 eV. Measurement noise contributed significantly to error and precluded determination of reaction order. In an effort to reduce measurement time and error, we introduce a new technique, called Scanning Thermal Desorption Microscopy (SThDM). The working principle of SThDM is similar to bulk thermal analysis techniques such as thermogravimetry or differential scanning calorimetry, where thermal kinetics are calculated from mass loss over time during a linear temperature ramp. We demonstrate the technique on graphene oxide during a linear temperature ramp between 50 - 450 C at low mechanical loads, providing an activation energy 0.62 ± 0.07 and a reaction order $n \sim 1$. Raising the applied load during the temperature ramp shifted the mass loss curve to lower temperatures, due to a lowering of the thermal energy barrier. The results show that the force lowers the energy barrier non-linearly—at odds with current models of mechanochemical atomic attrition found in the literature—where higher loads begin to impede the reaction rate. The results are compared to bulk measurements from the literature and current theoretical models of mechanochemical reactions. Based on the observed energy barriers and reaction order, a diffusion mechanism is proposed.

6:00pm **2D-ThA12 Functionalized Metallic Island Films as Enhancement Substrates for Raman and IR Microscopic Biosensing**, C. Kratz, Leibniz-Institut für Analytische Wissenschaften - ISAS - e.V., Germany; D. Gkogkou, F. Rösicke, Humboldt-Universität zu Berlin, School of Analytical Sciences Adlershof (SALSA), Germany; T. Shaykhutdinov, T. Oates, A. Furchner, Leibniz-Institut für Analytische Wissenschaften - ISAS - e.V., Germany; J. Rappich, Helmholtz-Zentrum Berlin für Materialien und Energie GmbH, Germany; Karsten Hinrichs, Leibniz-Institut für Analytische Wissenschaften - ISAS - e.V., Germany

Metallic island covered substrates for Surface Enhanced Infrared Absorption (SEIRA) [1] and Surface Enhanced Raman Scattering (SERS) [2] are excellent candidates for enhancement templates in biosensing applications. The specific enhancement behavior of the surfaces is due to their effective optical properties as well as localized and coupled surface plasmon effects. For a detailed understanding of this behavior Au and Ag silver island films on SiO₂/Si with a lateral gradient in size distribution were characterized by IR laser ellipsometry [3] and VIS ellipsometry [4] in combination with numerical and analytical calculations. Along the gradient of the metallic island film, measurements of the IR enhancement of vibrational bands of a Self-Assembling Monolayer adsorbed on the surface as well as a band of the SiO₂ below the island film were performed. The metallic island substrates increase the detection limit and enable new applications, anisotropic substrates allow to separate signals from solvated molecules from adsorbed ones. [2] On the way towards applications as biosensors, the effective and reliable functionalization of these surfaces is an important step. For this we studied a direct electrochemical functionalization of the metal particles from diazonium compounds [5-6] and an indirect route by transferring pre-functionalized graphene sheets to our substrates. [7] For quantitative evaluation the surfaces were characterized in a multi-method approach using UV-VIS ellipsometry, IR ellipsometry, IR microscopy, Raman spectroscopy and IR-AFM.

References

[1] C. Kratz, T. W. H. Oates, K. Hinrichs, Thin Solid Films (2016) in press.

Thursday Afternoon, November 10, 2016

[2] D. Gkogkou, B. Schreiber, T. Shaykhutdinov, H.K. Ly, U. Kuhlmann, U. Gernert, S. Facsko, P. Hildebrandt, N. Esser, K. Hinrichs, I.M. Weidinger, T.W.H. Oates, ACS Sensors, 1 (2016) 318-323.

[3] A. Furchner et al, submitted to Appl. Surface Science.

[4] D. Gkogkou et al, submitted to Appl. Surface Science

[5] P. Kanyong, G. Sun, F. Rösicke, V. Syritski, U. Panne, K. Hinrichs, and J. Rappich; Electrochem. Commun. **51**, 103 (2015).

[6] X. Zhang, A. Tretjakov, M. Hovestaedt, G. Sun, V. Syritski, J. Reut, R. Volkmer, K. Hinrichs, and J. Rappich; Acta Biomaterialia **9**, 5838 (2013).

[7] F. Rösicke et al, to be submitted.

Applied Surface Science

Room 101B - Session AS-ThA

Advances for Complicated Sample Preparation Strategies and Complex Systems

Moderators: Christopher R. Anderton, Pacific Northwest National Laboratory, Michaeleen Pacholski, The Dow Chemical Company

2:20pm **AS-ThA1 Measuring Nanoparticle Properties: Are We High and Dry or All at Sea?**, Caterina Minelli, National Physical Laboratory (NPL), UK
INVITED

Reliable and reproducible measurement methods for nanoparticles will significantly impact the uptake of these materials in commercial applications and allow industry to comply with regulation. However, there are significant challenges in the analysis of nanomaterials due to, among other factors, the interdisciplinary nature of the field, the lack of adequate reference materials to calibrate analytical tools and the difficulties associated both with sample preparation for analysis and the interpretation of data. Furthermore, the inconclusive outcomes of nanoparticle toxicity risk assessments can largely be traced to a failure to address these measurement challenges.

The preparation of nanoparticle samples for analysis can significantly alter both the nanoparticles themselves and the results of the analysis. Measuring colloidal nanoparticles using vacuum-based techniques is particularly prone to artefacts and irreproducibility introduced by sample preparation. In order to produce relevant and meaningful data from nanoparticle analysis it is therefore important to establish sound sample preparation protocols. It is good practice to use a combination of techniques which can be employed directly to the colloidal suspension and on the dried particles to ensure a meaningful interpretation. Examples which will be discussed include the measurement of the density of polymeric nanoparticles by small angle X-ray scattering (SAXS) and analytical centrifugation, and the analysis of the protein coatings on gold nanoparticles in liquid media (*in-situ*) and *ex-situ* with high vacuum techniques such as X-ray photoelectron spectroscopy (XPS) and low energy ion scattering (LEIS). The challenges in sample preparation for these methods and the difficulties of data interpretation will be described in detail. The *in-situ* measurement of nanomaterials in complex matrices is highly sought after by industry and regulatory bodies, but remains an unmet challenge. The potential application of new methods, such as non-linear optical techniques, will be considered.

Inter-laboratory studies enable the refinement of sample preparation protocols, which in turn have a positive impact on the broader adoption of the analytical method for nanoparticle characterisation. We will discuss the main outcomes of a VAMAS inter-laboratory study whose aims included to assess the inter-laboratory variability in the measurement of nanoparticle coatings using XPS and LEIS and identify sources of variability in sample preparation procedures. This work will directly input into ongoing efforts in ISO TC201 to standardize the surface chemical analysis of nanoparticles.

3:00pm **AS-ThA3 The Secret Life of Nanoparticles: Often Ignored Characteristics of Nano-Objects That Limit Reproducibility and an Approach to Improving Data Collection and Reporting to Address the Challenges**, Donald Baer, Pacific Northwest National Laboratory

The literature is filled with images of nanoparticles and nanostructured materials along with descriptions of how they were synthesized and some aspects of their new and exciting properties. However, nano-objects present fundamental synthesis, characterization, and handling challenges that are often ignored or unrecognized by parts of the scientific and technical community. The frequent tendency of such particles to interact with surrounding media and to respond to environmental changes

Thursday Afternoon, November 10, 2016

complicates understanding their properties as a function of time in different environments but also presents interesting opportunities for the design of particles with desired time dependent properties. Particle variation due to time and environmentally dependent changes raise a number of issues associated with particle preparation for analysis, especially surface analysis. Issues include knowing the nature of changes and the rate at which they change after synthesis, during storage and processing, and in different media. This presentation will highlight some of the behaviors of nanoparticles we have observed drawing on research on Fe oxide-shell metal-core, ceria, and Ag nanoparticles. Examples will include the impact of particle structure on the dissolution and toxicity of Ag nanoparticles, the environmentally induced changes in the chemical state of ceria nanoparticles and the impact of synthesis details on the ability of iron metal-core oxide-shell particles to reduce contaminants in ground water. Some of the inconsistencies in the literature are aggravated by the under-recording and under-reporting details of particle synthesis and handling. An ISO standard being developed to help address the problem will be described. This draft document includes both a standard on reporting of the preparation of particles for surface analysis and information about a range of sample preparation methods optimized for the types of information desired. One focus of the document is in on the extraction of nanoparticles from solution for analysis of surface coatings.

3:20pm AS-ThA4 Combined XPS/ISS/UPS Study of Ultra-thin HfO₂ films on SiO₂/Si Substrates, *Paul Mack*, Thermo Fisher Scientific, UK

Hafnium oxide (HfO₂) films are often found in microelectronic devices, where they are used as gate dielectrics, for example. As device dimensions become smaller and smaller, it becomes necessary to make thinner HfO₂ films, which may only be a few nanometers thick. X-ray Photoelectron Spectroscopy (XPS) is an analysis technique which non-destructively provides chemical bonding information from the top few nanometres of a surface. It is the ideal technique to analyse the hafnium or silicon chemical bonding environment or to measure the thickness of these ultra-thin films. XPS cannot easily measure the coverage of ultra-thin films, however, but the complementary technique of Ion Scattering Spectroscopy (ISS) can be used for this purpose.

There is also a requirement for understanding the electronic structure of ultra-thin HfO₂ films. Ultraviolet Photoelectron Spectroscopy (UPS), using a helium discharge lamp for generate He(I) or He(II) photons (with energies of 21.2eV and 40.8eV, respectively), can be used to measure the work function of conductive films and to investigate valence electronic structure.

This talk will present data from XPS/ISS/UPS studies of a series of ultra-thin HfO₂ film films on SiO₂/Si substrates. The samples were created with varying numbers of ALD cycles, to generate HfO₂ films of different thickness and coverage. The results will demonstrate that using a complementary analytical approach, with all three techniques available on a single tool, provides a much more comprehensive analysis of the HfO₂ films than would be possible with only one analytical technique.

4:00pm AS-ThA6 A Novel Method for Matrix Application in Matrix Enhanced SIMS Imaging, *Matthias Lorenz, A.G. Shard, J.-L. Vornig, I.S. Gilmore*, National Physical Laboratory, UK

We report on a novel method for controlled and versatile application of matrix compound for the purpose of matrix enhanced secondary ion mass spectrometry (ME SIMS). General applicability of this approach for ion signal enhancement of drug molecules and endogenous compounds in drug dosed tissue homogenate is demonstrated.

A major problem for SIMS imaging in life-sciences is the signal-limited spatial resolution and matrix effects that suppress ion yields. In severe cases, the ion signal may be lost all together. This leads to the adage that not seeing a molecule in SIMS does not mean it is not there. One route forward is to use a molecule to enhance the signal as done in matrix assisted laser desorption/ionization (MALDI). However, it is well-known that this causes redistribution of analytes (such as drugs) over tens of microns. This circumvents the resolution benefit of SIMS over MALDI. Furthermore, methods used for MALDI are not suitable for 3D imaging, where the matrix layer would be sputtered away. We report on a novel technique for the controlled application of matrix compounds specifically for ME SIMS that overcomes these two major barriers.

The new approach provides high flexibility and precise control of the timing and amount of material applied. It is applicable for a wide range of matrix compounds. The general approach and critical instrumental parameters of the technique will be discussed, and its applicability for the enhancement of SIMS ion signals will be shown on examples of drug compounds and drug molecules embedded in tissue homogenate. We show that ion signals of

clozapine could be enhanced by a factor of 3 for the protonated molecule [M+H]⁺ by adding 2,5-dihydroxybenzoic acid (2,5-DHB), a common matrix compound used in MALDI. The [M+H]⁺ ions of the drug molecules chloroquine and tamoxifen show an enhancement with 2,5-DHB matrix application. A factor of 7 enhancement of clozapine could be achieved with 3-nitrobenzonitrile (3-NBN), a species utilized for primary ion formation in the matrix assisted ionization vacuum (MAIV) technique. The abundance and intensity of lipid related signals (e.g., the phosphocholine fragment at *m/z* 184) in the spectra are significantly enhanced for the analysis of the tissue homogenate. The addition of formic acid shows another example for signal enhancement using the new approach, with an increase of the [M+H]⁺ signal of the drug molecule by a factor greater than 3 and of the phosphocholine signal (*m/z* 184) by a factor of 6.

4:20pm AS-ThA7 ToF-SIMS Imaging of Bee Brain Tissue – Comparing Lipid Distributions and Varying Sample Preparation Methodologies, *Jordan Lerach, E. Amsalem, C.M. Grozinger*, The Pennsylvania State University

Time-of-flight secondary ion mass spectrometry (ToF-SIMS) with cluster-based primary ion sources enables researchers to elucidate molecular information from complex samples with sub-micron imaging resolution. This technique is becoming more commonly applied to complex biological systems due to its excellent molecular imaging capabilities. The following research details, with chemical specificity, the location of molecules of interest in brain tissue of the common eastern bumble bee (*Bombus impatiens*). Microtomy was used to create thin tissue sections of both frozen-hydrated and freeze-dried tissues and the differences in the data sets are reported. A ToF-SIMS instrument with a Bi₃⁹⁺ primary ion source selected for Bi₃⁺⁺ ions is used for analysis. This ion source is shown to produce large molecular ions in excess of 1,000 amu on the tissue samples which yields information from larger biomolecules such as lipids. In this analysis specific attention is paid to the lipid distribution since site-specific chemical imaging of lipids in the brain tissue remains relatively unexplored.

4:40pm AS-ThA8 Understanding Matrix Effects in Mass Spectrometry, *Amy Walker, L.D. Gelb*, University of Texas at Dallas

Chemical imaging methods, including imaging mass spectrometry (MS), are becoming widely used for the analysis of a variety of samples from biological tissues to electronic devices. A significant barrier to wider adoption of imaging mass spectrometry is the presence of matrix effects which complicate quantitative analysis. Interactions between an analyte molecule and its surroundings (the “matrix”) can substantially alter both the yield and type of ions observed. These matrix effects result in both significant nonlinearity of signal intensity with concentration and changes in the characteristic spectrum of a given species with environment. We present progress towards the quantitative extraction of chemical concentration profiles, component spectra, sample topography, and other information from imaging mass spectrometry data in the presence of matrix effects. Our approach is based on maximum *a posteriori* (MAP) reconstruction against physically motivated models rather than statistical dimensionality-reduction techniques such as Principal Components Analysis. We demonstrate our methodology using several different samples as well as synthetic data sets. These include systems that demonstrate “weak” matrix effects, such as mixed self-assembled monolayers, and “strong” matrix effects such as those observed in ionic liquid matrix enhanced secondary ion mass spectrometry.

5:00pm AS-ThA9 Reducing Matrix Effects in Organic Secondary Ion Mass Spectrometry, *Lars Breuer, H. Tian, N.J. Popczun*, The Pennsylvania State University; *A. Wucher*, University of Duisburg-Essen, Germany; *N. Winograd*, The Pennsylvania State University

Secondary ion mass spectrometry (SIMS) is a powerful tool for surface analysis. With the development of cluster ion beams, this technique now has the capability to analyze organic materials while maintaining molecular information of the analyte. A challenging aspect in SIMS applications in multi-components systems are so called *matrix effects* in the ionization probability of sputtered material. Unfortunately, there is no theory to date which is capable of predicting these matrix effects. Results are presented here to show one physical and one chemical approach to address and reduce matrix effects in an organic model systems of Irganox 1010 and 1098.

The first, and perhaps most straightforward approach in overcoming matrix effects is to decouple the ionization from the sputtering process. For this purpose, the plume of sputtered material above the sample, mainly consisting of neutral species, is intersected with an intense ultrafast laser pulse in the near infrared region with power densities up to several 10¹⁵

Thursday Afternoon, November 10, 2016

W/cm². This pulse ionizes neutral particles within the plume and makes their detection feasible

The second approach presented is based upon the idea of enhancing protonation at the bombardment sites. HCl doped Ar_n⁺ gas cluster ions, in which the HCl molecules are incorporated into the gas clusters, are used as the primary ion beam. During analysis, H₂O is precisely leaked into the analysis chamber while the sample is cooled with liquid nitrogen. In this way, a thin ice overlayer is formed at the sample surface to facilitate the dissociation of the HCl molecules incorporated in the Ar_n gas clusters. The free hydronium ions become available at the impact site, which aid the protonation of intact molecules. During the entire analysis, a dynamic equilibrium between deposition and sputtering of ice is well maintained to yield a quantitative depth profile.

5:20pm AS-ThA10 Image Fusion for Improving the Visualization of Elemental and Isotopic Distributions in SIMS, Jay Tarolli, B. Naes, B. Garcia, A. Fischer, D. Willingham, Pacific Northwest National Laboratory

While secondary ion mass spectrometry (SIMS) is a technique that offers a substantial amount of chemical information of an analysis area, it comes with inherent limitations that often reduce the signal-to-noise ratio of desired species as well as the achievable spatial resolution. A growing approach to overcoming these limitations is to acquire complementary information from other analytical imaging techniques, such as optical and electron microscopy. Image fusion is a post-acquisition data analysis technique that has been recently applied to new and more diverse SIMS experiments in order to improve the perceived spatial resolution, intensity, and contrast of chemical images. The basis of image fusion is to combine information from two or more input images in order to create an output visualization that better represents the analysis area than any of the input images could alone. Thus, multimodal imaging analyses that incorporate SIMS and a second higher resolution analytical technique, followed by post-acquisition image fusion, are able to provide a representation of chemical information with greater detail at a smaller scale.

In this work, a new source of higher resolution data, X-ray energy-dispersive spectroscopy (EDS), is explored to improve the visual quality of SIMS images, combining elemental information with chemical information. First, a workflow was developed to register and fuse EDS images of an Al-Si-Cu alloy at various microscope magnifications with dynamic SIMS images to better visualize the localization of Cu and Si domains. A new implementation of image fusion was then developed to improve the screening process of U-bearing particles. In this case, elemental information provided by EDS is used to improve the spatial resolution of uranium isotopic distributions in order to differentiate particles which may potentially be enriched. These particles can then be screened individually to verify the isotopic distributions. In this case, image fusion has been applied not simply in a proof-of-concept scenario, rather an implementation that improves an existing process in order to obtain SIMS results with higher accuracy and precision.

5:40pm AS-ThA11 Evaluating the Utility of Uranium-Molybdenum Foils as Nuclear Fuels via Elemental and Isotopic Imaging, David Willingham, J. Tarolli, B. Naes, M. Rhodes, M. Dahl, A. Guzman, D. Burkes, Pacific Northwest National Laboratory

We aim to characterize the elemental and isotopic composition of uranium (U) metal and U metal alloys by electron microscopy (EM) and secondary ion mass spectrometry (SIMS). This type of characterization is important in understanding the behavior and performance of nuclear fuels and targets, and could potentially be utilized to interrogate processing history of the material. One example of such nuclear alloys is the uranium-molybdenum (U-Mo) system, development of which is being actively pursued throughout the world for use in research and test reactors (NA-23 Reactor Conversion Program), light water power reactors (DOE-NE Accident Tolerant Fuel), and pulse reactors (DoD – Army).

Previous EM characterization of approx. 19.75% enriched ²³⁵U-10wt% Mo fuel foils produced for the NA-23 Reactor Conversion Program revealed a complex grain structure of coarse, highly elongated regions interspersed with finer, more equiaxed grains. The distribution of grains was also organized within regions containing significant Mo variation produced during casting of this particular alloy. During post-irradiation examination, these regions and structures have been observed to behave differently depending upon the irradiation conditions that the fuel was subjected to. Elemental and isotopic heterogeneities in the fuel, particularly at boundaries between grains, have been hypothesized to lead to non-uniform swelling regions (i.e., volume growth) within the fuel. Understanding the elemental and isotopic distribution of alloying metals

and other impurities is important to reasonably predict behavior of the fuel in a particular reactor system, ultimately enabling successful qualification for its use.

SIMS image analysis revealed several key characteristics of the U-Mo foil system. First, Mo rich grains could be observed by SIMS imaging. These grains are highly elongated along the length of the foil. Secondly, carbon inclusions, likely a result of U carbides, were found in the SIMS images. These inclusions can be seen to track with the previously observed Mo rich elongated grains. Finally, the U within the foil is much more homogenized than the Mo and appears to be much less mobile. The ²³⁵U/²³⁸U is consistent with the known value at approx. 20% enrichment of ²³⁵U and the U isotopic distribution is homogenous in all regions of the U-Mo foil. It is, therefore, likely that non-uniform swelling of these foils under irradiation is due primarily to U-Mo elemental heterogeneities rather than U isotopic variations.

6:00pm AS-ThA12 Investigation of the Interaction Between a High Poly Vinylpyrrolidone Content Silicone Hydrogel Contact Lens and a Natural Humectant using Surface Imaging Techniques, Katarzyna Wygladacz, D.J. Hook, Bausch + Lomb

Background: Optimum surface wettability and high water content are both important factors that can influence successful contact lens wear. In the case of the silicone hydrogel contact lens, samfilcon A, polyvinylpyrrolidone (PVP) was engineered into the material to increase the water content and provide a wettable lens surface. As a complement to high level of PVP in the lens chemistry another way to improve lens wettability is to take advantage of interactions between the lens material and the lens care solution. This study assessed the interaction of hyaluronate (HA), a natural humectant, present in Biotrue multi-purpose solution (MPS) with the high PVP-content samfilcon A lens, using multiple analytical techniques.

Method: X-ray Photoelectron Spectroscopy (XPS) characterization was used to confirm the presence of HA on the lens surface. The distribution of HA over the samfilcon A surface was assessed by quantitating lens surface roughness (RMS), before and after incubation with 0.1% (w/v) HA by atomic force microscopy (AFM) imaging. Confocal laser scanning (CLSM) and differential interference contrast (DIC) microscopies were used to characterize the association of HA to the surface of samfilcon A lenses after exposure to 0.1% (w/v) HA and HA present in Biotrue MPS.

Results: Differences in the XPS C1s spectra recorded for samfilcon A before and after exposure to 0.1% (w/v) HA were detected. Samfilcon A surface roughness (RMS) was 2.5 ± 0.4 nm before exposure to HA and was significantly decreased after incubation with 0.1% (w/v) HA, (RMS=0.6 ± 0.1nm; p<0.05). CLSM and DIC imaging illustrated a comparable confluent, stained HA network that extended across the entire surface with 0.1% (w/v) HA and commercial HA-containing MPS.

Conclusion: XPS analysis show evidence for samfilcon A surface modification with hyaluronate. CLSM and DIC imaging offered a comprehensive view of the lens surface and demonstrated an extensive coverage of HA on samfilcon A. AFM measurements confirmed that HA adsorption reduced roughness of the lens surface. Together, the combination of imaging techniques provided a unique picture of the interaction of HA and PVP containing silicone-hydrogel lenses.

Spectroscopic Ellipsometry Focus Topic Room 104C - Session EL+AS+BI+EM+TF-ThA

Optical Characterization of Nanostructures and Metamaterials (2:20-3:40 pm)/Application of Spectroscopic Ellipsometry for the Characterization of Thin Films (4:00-6:00 pm) and Biological Materials Interfaces

Moderators: Tino Hofmann, University of North Carolina at Charlotte, Stefan Zollner, New Mexico State University, Heidemarie Schmidt, Technische Universität Chemnitz, Germany

2:20pm EL+AS+BI+EM+TF-ThA1 Optical Properties of (Self-assembled) Nanostructured Surfaces Studied by Spectroscopic Mueller Matrix Ellipsometry and Local Direct Imaging Techniques, Morten Kildemo, Norwegian University of Science and Technology, Norway INVITED

This paper covers several applications of ex-situ and in-situ Spectroscopic Mueller Matrix Ellipsometry (SMME) for the study of self-assembled nanostructured surfaces, with applications ranging from antireflection coatings, PV-absorbers, nanoimprinting masks, plasmonic polarizers, plasmonic meta-materials and in particular hyperbolic metamaterials and

Thursday Afternoon, November 10, 2016

meta-surfaces. The optical analysis is systematically supported by AFM, SEM and TEM. As nanostructured surfaces are often inherently anisotropic, SMME with variable angle of incidence and full azimuthal rotation of the sample is shown to be a powerful optical technique to fully characterize such anisotropic and sometimes bi-anisotropic materials. The first part of the presentation briefly reviews an uniaxial effective medium approach to model the kinetics of the optical response of self-assembled straight and tilted GaSb nanopillars [Le Roy et al., Phys. Rev. B 2010, Nerbo et al. Appl. Phys. Lett. 2009], and SiO₂-nanopillars containing plasmonic Cu [Ghadyani et al., Opt. Exp. 2013]. The second part of the presentation discusses the experimentally extracted uniaxial and biaxial optical properties of self-assembled plasmonic hyperbolic meta-materials [X. Wang et al., *Block-copolymer based self-assembled hyperbolic metamaterials in the visible range*. (manuscript in preparation), 2016] and metasurfaces [Aas et al., Opt. Expr. 2013]. Hyperbolic metamaterials use the concept of controlling the propagative modes through the engineering of the dispersion relation, and are considered highly promising to reach different meta-properties. The presentation is closed by the discussion of the fascinating Mueller matrix response of a highly organized array of hemispherical Au nanoparticles produced by Focused-Ion-Beam milling, and the response is discussed in the context of highly organized meta-surfaces and plasmonic photonic crystals [Brakstad et al. Opt. Express 2015]

3:00pm EL+AS+BI+EM+TF-ThA3 Optical Properties of Nanocrystalline Si₃N₄:TiN Thin Films, Neil Murphy, Air Force Research Laboratory; L. Sun, General Dynamics Information Technology; J.G. Jones, Air Force Research Laboratory; J.T. Grant, Azimuth Corporation

Nanocomposite films comprised of mixed nitrides, especially Si-Me-N (Me=Ti, Zr, Hf), have generated significant attention due to their robust thermal and mechanical properties. In addition to their desirable structural characteristics, the mixing of dielectric Si₃N₄ with various metallic nitrides has the potential for the deposition of hybrid thin films with controllable optical absorption based on the fraction of metallic nitrides present within the Si₃N₄ matrix. In this work, nanocrystalline Si₃N₄ thin films, doped with varying amounts of TiN (1-20 at.%), are deposited using reactive magnetron co-deposition. Note that the Berg model for reactive sputtering is utilized to select the initial conditions for the deposition of the films, which are sputtered from elemental targets within a mixed nitrogen-argon environment and characterized *in-situ* using spectroscopic ellipsometry. The TiN content is varied through systematic adjustment of the current applied to the Ti cathode concurrent with pulsed DC deposition of Si₃N₄ at a constant current of 0.4 A. The use of *in-situ* ellipsometry, interrogating wavelengths from 381-1700 nm, allows for the real-time measurement of the refractive index, extinction coefficient, and thickness of the growing films. Additionally, *in-situ* ellipsometry data is used to observe the behavior of the films at the onset of growth, indicating the onset of Volmer-weber type nucleation. All ellipsometric data are fit using a Bruggeman effective medium approximation, varying the amount of TiN present within the films. Optical characterization of the Si₃N₄:TiN thin films indicates that the refractive index at 550 nm decreases gradually from 2.05 to 1.99 as the TiN content is increased from 0-20 at%, while the extinction coefficient rises from 0 to 0.35. These films demonstrate strong absorption features starting from 550 nm out to 1500 nm, allowing for efficient absorption of visible and near-infrared wavelengths. Variation of the TiN content within Si₃N₄:TiN films allows for the user to select the magnitude of extinction coefficient and refractive index, leading to potential applications as mechanically robust layers in interference filters, or as alternatives to lossy metallic configurations in plasmonic devices.

3:20pm EL+AS+BI+EM+TF-ThA4 The Effect of Aluminum Content on Properties of Al-doped Zinc Oxide Thin Films Grown at Room Temperature, Lirong Sun, General Dynamics Information Technology; N.R. Murphy, Air Force Research Laboratory; J.T. Grant, Azimuth Corporation; J.G. Jones, Air Force Research Laboratory

Transparent conductive Al-doped zinc oxide (AZO) thin films have shown excellent structural, optical and electrical properties for applications in photovoltaic and optoelectronic devices, transparent conducting electrodes, solar cells, liquid crystal displays, touchscreens, energy efficient window coatings and heat reflective coatings. In this work, the AZO thin films were deposited at room temperature by multi-target reactive magnetron sputtering using metallic Zn and Al targets simultaneously. The Al doping content of the AZO films by x-ray photoelectron spectroscopy (XPS) had great impacts on optical properties in the near infrared (NIR) and in the UV regions and were strongly correlated to their electrical properties. The spectroscopic ellipsometry data in three incident angles and transmission intensity data were measured and fitted simultaneously

with a Tauc-Lorentz oscillator and a Drude model in the wavelength of 270 -2500 nm. The transmittance and reflectance spectra, the derived refractive index and extinction coefficient, were tailored in the NIR region by Al content and correlated to the electrical resistivity. The blue shift of the absorption edge in the UV region and the widening of the optical band gap were associated with the increase of the Al content. Structural, optical and electrical properties were characterized using x-ray diffraction, scanning electronic microscopy, UV-Vis-NIR spectra and four-point probe methods.

4:00pm EL+AS+BI+EM+TF-ThA6 Optical Monitoring of Growth (and Death) of Thin Film Materials for Solar Cells, Nikolas Podraza, K. Ghimire, M.M. Junda, A.A. Ibdah, P. Koirala, University of Toledo; S. Marsillac, Old Dominion University; R.W. Collins, Y. Yan, University of Toledo

INVITED
Performance of thin film solar cells depends on (i) electronic quality of the components (doped and undoped semiconductors, metallic and transparent conducting contact layers), (ii) component optical response, and (iii) full opto-electronic response of the photovoltaic (PV) device structure dictated by layer properties and thickness. Spectroscopic ellipsometry probes (ii) and (iii) through measurement of both thickness and optical response ($N = n + ik$, $\epsilon = \epsilon_1 + i\epsilon_2$, $\alpha = 4\pi k/\lambda$) of multiple layers in thin film device structures. Assessing (i) electronic quality of materials or devices optically relies on understanding other property information deduced from the optical response, such as connecting variations in film structure (crystallinity, degree of disorder) or growth evolution to device performance. In situ, real time spectroscopic ellipsometry (RTSE) monitors growth evolution and post-deposition processes to better understand property changes with thickness, phase transitions and separation, and process kinetics. RTSE of hydrogenated silicon (Si:H), cadmium telluride (CdTe), and copper indium gallium diselenide (CIGS) absorbers have been used to understand growth and its relationship to the respective device performance. All of these are relatively mature PV technologies, where knowledge gained from RTSE during growth can potentially improve metrology and manufacturing. The potential impact of RTSE is equally strong when applied to developing technologies. Organometal lead halide perovskite semiconductors (CH₃NH₃PbI₃) are used in >20% initial efficiency solar cells but suffer from degradation with temperature, bias, moisture, and ultraviolet light exposure. The time scale of device performance degradation is much shorter than that of other polycrystalline PV (CdTe, CIGS). RTSE has been applied during co-evaporation of CH₃NH₃I and PbI₂ to produce the perovskite, but also during decomposition of the perovskite. Significant fractions of CH₃NH₃I and PbI₂ at the substrate / perovskite and perovskite / ambient interfaces after deposition even under simple atmospheric exposure begin to appear in a matter of minutes. The ability to track the degradation – or death of this material – in addition to growth may be equally important to assessing the ultimate stability and manufacturability of these next generation PV materials.

4:40pm EL+AS+BI+EM+TF-ThA8 Monitoring Nanometer-Thin Film Formation using Ellipsometry, Bert Müller, F.M. Weiss, T. Töpfer, B. Osmani, University of Basel, Switzerland

Elastomers can transform electrical energy into mechanical one. They have a wide variety of applications including powering wipers, sound generation, and operating camera lenses. Sandwiched between electrodes the deformable but incompressible elastomer laterally expands when applying a voltage. To provide the necessary strain of at least 10 %, micrometer-thick silicone membranes need an operation voltage of several hundred volts, which is inappropriate for the human body. Nanometer-thin membranes, however, require only a few volts. To generate forces as necessary for artificial sphincters, i.e. muscles to treat incontinence, several ten thousand membranes have to be sandwiched. Currently, the manufacturing methods such as organic molecular deposition only reach deposition rates of about one micrometer per hour, which does not allow fabricating the sandwiched nanostructures in an efficient way. We have developed an alternative deposition method to prepare extremely flat silicone membranes that are below one micrometer thick. The root-mean-square-roughness is smaller than one nanometer. For this purpose, silicone polymers in solution are sprayed by electrospray deposition [1,2]. Usually electrospraying is based on direct current mode. Here, we have employed, however, an alternating current to avoid charge accumulation on the substrate. Spectroscopic ellipsometry has been used to monitor the formation of confluent organic films and electrodes as well as the changes of the organic thin films during ultra-violet radiation treatments. This in situ technique enabled us to derive the refractive index, the porosity, the surface roughness, and the film thickness. The derived quantities on surface roughness and film thickness were validated using

Thursday Afternoon, November 10, 2016

atomic force microscopy. The combination of electrospraying, ultra-violet light curing, and in situ ellipsometry has a huge potential to efficiently create and monitor nanometer-thin, ultra-flat elastomeric membranes, which may become part of artificial muscles for medical applications and beyond.

[1] F.M. Weiss, T. Töpfer, B. Osmani, S. Peters, G. Kovacs, and B. Müller Electrospraying Nanometer-Thin Elastomer Films for Low-Voltage Dielectric Actuators *Advanced Electronic Materials* (2016) 1500476; DOI: 10.1002/aem.201500476

[2] F.M. Weiss, T. Töpfer, B. Osmani, H. Deyhle, G. Kovacs, and B. Müller Thin Film Formation and Morphology of Electro-sprayed Polydimethylsiloxane *Langmuir* 32 (2016) 3276-3283

5:00pm **EL+AS+BI+EM+TF-ThA9 Optical Determination of Electrical Response for Thin Film Transparent Conductors: Spectral Range Dependence**, *Prakash Uprety, M.M. Junda, K. Lambright, R. Khanal, A. Phillips, M. Heben, D. Giolando, N.J. Podraza*, University of Toledo

Thin films with simultaneous high transparency and electrical conductivity have applications in photovoltaics, displays, and other opto-electronic devices. Accurate characterization of electrical transport properties along with optical properties in these transparent conductors, particularly when in the device structure, is of critical importance to their use. Spectroscopic ellipsometry (SE) provides a widely applicable method for determining such properties without many of the complications and limitations that accompany other methods that make use of physical contact to the film. As is described by the Drude model, free carrier optical absorption has increasing effect on the complex dielectric function ($\epsilon = \epsilon_1 + i\epsilon_2$) with decreasing photon energies. Thus, extracting ϵ from SE measurements spanning the visible to terahertz (THz) frequency ranges provides sensitivity to film thickness and morphology at higher energies and free carrier absorption dominating the optical response at low energies. In this work fluorine doped tin oxide (SnO₂:F), aluminum doped zinc oxide (ZnO:Al), and sprayed single walled carbon nanotube (CNT) thin films are measured with ex situ SE over a spectral range of 0.035 to 5.9 eV using a single rotating compensator multichannel ellipsometer (0.75 - 5.9 eV) and a single rotating compensator Fourier transform infrared ellipsometer (0.035 - 0.75 eV). Additionally, the ZnO:Al and CNT films are measured using a single rotating compensator THz ellipsometer (0.4 - 5.8 meV) to further extend the measured spectral range to lower energies. Due to the wide spectral range measured, a single model describing ϵ and layer thicknesses has sufficient sensitivity to simultaneously determine electronic transitions, vibrational phonon modes, and free carrier absorption. The electrical properties in the Drude model are described by the bulk material resistivity ρ and scattering time τ . Optically extracted ρ has increasing correspondence to ρ deduced from four point probe electrical measurements as increasing low photon energies are included in the fitting (< 5% variation in ρ for ZnO:Al analyzing the full measured range); a behavior that demonstrates the benefit of extending the measurement spectrum to very low energies. The analyzed spectral range dependence of optically determined transport properties in these examples is considered to illustrate how narrower spectral range measurements impact deduced ρ and τ .

5:20pm **EL+AS+BI+EM+TF-ThA10 Spectroscopic Ellipsometry Studies of CdS-CdSe-CdTe Alloys: Applications in Thin Film Solar Cells**, *Maxwell Junda, C.R. Grice, Y. Yan, N.J. Podraza*, University of Toledo

Recent studies have demonstrated that photovoltaic (PV) device performance of thin film cadmium telluride (CdTe) solar cells is improved when a thin cadmium selenide (CdSe) layer is added at the cadmium sulfide (CdS) / CdTe interface and when oxygen is added to the CdS window layer (CdS:O). Specifically, devices fabricated with this configuration show increased short circuit current density without a corresponding degradation in open circuit voltage. The high temperature close spaced sublimation (CSS) deposition of the CdTe layers in these devices effectively anneals the existing CdS:O / CdSe window layer creating alloyed regions between these three materials as opposed to distinct, separate layers at the front side of the device. To better understand the sources of performance gain, we begin by using ex situ spectroscopic ellipsometry (SE) from the near infrared to the ultraviolet (0.74 - 5.9 eV) to study the optical and structural properties of these alloys. Films of CdS:O, Cd_{0.9}Se_{0.1}, and CdSe_{0.9}Te_{0.1} are fabricated on soda lime glass substrates by radio frequency sputtering a stack of layered combinations of CdS, CdSe, and/or CdTe followed either by annealing at the CdTe CSS deposition temperature or actual CSS of CdTe. A parameterized model describing the critical point transitions in the optical response ($\epsilon = \epsilon_1 + i\epsilon_2$) is developed, allowing for tracking of the changes in ϵ as a result of film composition and processing

for each alloy. Additionally, structural and compositional variations introduced by the alloying of materials is considered and supported by complementary x-ray diffraction and energy dispersive x-ray spectroscopy measurements. The database of ϵ developed for these materials can be used to assess how the oxygen introduced in the CdS:O layer and diffusion of CdSe into both CdTe and CdS:O modify that interface and impact PV device performance.

5:40pm **EL+AS+BI+EM+TF-ThA11 Development of Growth Evolution Diagrams for RF Sputtered Nanocrystalline Hydrogenated Silicon Thin Films via Real Time Spectroscopic Ellipsometry**, *Dipendra Adhikari, M. M. Junda, N. J. Podraza*, University of Toledo

As a result of its increased visible light absorption and increased stability in comparison to hydrogenated amorphous silicon (a-Si:H), hydrogenated nanocrystalline silicon (nc-Si:H) thin films are of considerable interest for a variety of opto-electronic applications, including photovoltaic (PV) devices. Radio frequency (RF) sputtering in an Ar + H₂ ambient provides a cost effective deposition technique for Si:H films and has advantages over conventional plasma enhanced chemical vapor deposition as a result of the potential to improve deposition rates and the elimination of hazardous precursor gasses. In this work we investigate how pressure, RF power, and Ar/H₂ ambient gas composition ratio influence film structure (thicknesses; amorphous, nanocrystalline, mixed phase composition) and optical response of Si:H films deposited by RF sputtering onto native oxide covered crystalline silicon wafer substrates using in situ real time spectroscopic ellipsometry (RTSE) over the near infrared to ultraviolet spectral range. Through analysis of RTSE measurements and application of virtual interface analysis where appropriate, the time evolution of bulk layer thickness, surface roughness, and complex dielectric function ($\epsilon = \epsilon_1 + i\epsilon_2$) spectra are extracted. Variations in nucleation and evolution of crystallites forming from the amorphous phase as a function of pressure, power, or Ar/H₂ ratio can be deduced from the growth evolution and used to create growth evolution diagrams. Overall film quality, crystallinity, and hydrogen incorporation (assessed using infrared extended measurements), are also determined from ϵ . X-ray diffraction measurements provide complementary information about how deposition conditions influence the density, size, and preferred orientation of crystallites. In addition to controlling film phase and structure, improvement of the deposition rate is also of practical interest and is explored here.

Electronic Materials and Photonics Room 102A - Session EM+SS+TF-ThA

Materials and Interfaces for Energy Storage

Moderators: Michelle Paquette, University of Missouri-Kansas City, Lee Walsh, University of Texas at Dallas

2:20pm **EM+SS+TF-ThA1 Strain Engineering of Ultrathin Metal Oxide Coatings Deposited using Atomic Layer Deposition for Controlled Electrochemical Energy Storage**, *Nitin Muralidharan, R.E. Carter, A.P. Cohn, L. Oakes, C.L. Pint*, Vanderbilt University

Strain engineering has transformed applications in the semiconductor electronics industry, but has not been widely explored as a tool for electrochemical applications. Here we study the role of strain on the electrochemistry of metal oxide coatings deposited using atomic layer deposition onto super-elastic NiTi alloy surfaces. Specifically, we focus on vanadium pentoxide (V₂O₅) due to its well-known capability to function as a cathode for the intercalation of lithium ions. Exploiting the capability of NiTi to "lock-in" strain in the elastic regime, which extends up to ~ 15% strain, we study the correlation between strain transferred to the V₂O₅ active material and the electrochemical performance during lithium intercalation. Overall, our results indicate that pre-straining the material changes both the kinetics and energetics for intercalation properties. Furthermore, the diffusion coefficient of lithium ions in the V₂O₅ lattice can be effectively doubled through the application of elastic strains as low as ~0.25%. These results provide a route to controllably engineer bulk materials using principles of mechanics to improve battery or other electrochemical application performance.

Thursday Afternoon, November 10, 2016

2:40pm **EM+SS+TF-ThA2 Probing Li-Ion Transport in All-Solid-State Batteries through Electron Transparent Electrodes**, *Alexander Yulaev*, Center for Nanoscale Science and Technology, NIST, Gaithersburg, MD, USA; *A.A. Talin*, Sandia National Laboratories; *M.S. Leite*, University of Maryland; *A. Kolmakov*, NIST/CNST

All-solid-state batteries demonstrate a high power-to-weight ratio and high energy density, offering prospective opportunities for miniaturized micro-electronics and medical devices. Moreover, solid state batteries reduce the safety risk of thermal runaway that may occur in electrochemical cells with liquid electrolytes. In spite of growing interests, the details of lithium transport in solid electrolytes and their interfaces are not yet well understood due to a scarcity of experimental methods to probe electrochemical processes at the nanoscale. For instance, the factors controlling the rate and reversibility of Li ion intercalation are still an active area of research. Here we apply a combination of optical and scanning electron microscopies to resolve spatially Li-ion transport across a thin LiPON electrolyte. Using lithographically patterned electrodes, we monitor Li-ion transport through optically and electron transparent ultrathin anodes made either of high capacity silicon or carbon. The variation of the probing depth is achieved by altering the energy of the primary electron beam from 1 keV to 15 keV. Analogous to SEM tomography, the sequence of depth dependent 2D images can be employed to reconstruct the 3D diffusion pathways of Li ions in the electrolyte. In addition, we investigate Li plating/intercalation reactions, which occur at the anode-electrolyte interface during charge/discharge cycles. We foresee that this approach will help elucidate the effects of chemical and ion transport inhomogeneity inside the electrolyte and electrodes on the overall performance of the battery.

3:00pm **EM+SS+TF-ThA3 Thin Film Battery Materials for Fundamental Studies and Applications**, *Nancy Dudney*, *K. Kercher*, *M. Veith*, Oak Ridge National Laboratory

INVITED

Although most commercial rechargeable batteries are prepared by bulk and powder processing methods, vapor deposition of materials has led to important advances for fundamental research, modification of battery materials and interfaces, and also for commercialization of thin film batteries. Each of these areas will be illustrated with our studies of thin film materials for electrolyte, anode, and cathode components of rechargeable lithium and lithium-ion batteries with both planar and 3-dimensional architectures.

Acknowledgement: This work was supported by the U. S. Department of Energy, Office of Science, Basic Energy Sciences, Materials Science and Engineering Division.

4:00pm **EM+SS+TF-ThA6 Silicon Compatible Pseudocapacitors Based on Nickel Hydroxide Functionalization of Carbonized Porous Silicon**, *Joshua Fain*, *J.W. Mares*, *S.M. Weiss*, Vanderbilt University

We report on silicon (Si) compatible energy-storage supercapacitors (SCs) that incorporate pseudocapacitive nickel hydroxide [Ni(OH)₂] coupled with an electric double layer capacitance (EDLC) contributed by constituent Ni(OH)₂ and carbon layers. SCs can charge and discharge their energy much more rapidly than conventional batteries (within a few seconds to minutes), while possessing a higher energy storage capability than traditional capacitors (specific capacitances can reach thousands of F/g). Although SCs have made a commercial impact in regenerative braking, there remains untapped potential for this technology in on-chip energy storage that could lead to reduced size and weight of microelectronic devices. However, advancements in Si-based on-chip energy storage has been hindered due to the rapid corrosion of Si by most electrolytes necessary for energy storage. Recently, it has been shown that conformal carbonization of high surface area porous silicon (PSi) electrodes protects the Si matrix from corrosion while also contributing to energy-storage EDLC behavior. Here, we show that functionalization of carbonized PSi with pseudocapacitive Ni(OH)₂ leads to significantly improved energy-storage capabilities of the SC electrode from a few to over 100F/g (with respect to the mass of the entire electrode), and up to 1400 F/g (with respect to the mass of only the Ni(OH)₂ - corrected for EDL contribution of the carbon). The electrodes were fabricated by electrochemical etching of PSi, followed by carbonization using chemical vapor deposition, and finally inclusion of Ni(OH)₂ into the matrix via a sol-gel process or electrochemical deposition. Cyclic voltammetry (CV) and charge/discharge experiments were carried out to investigate the energy storage capabilities of composite pseudocapacitive electrodes prepared with varying sol-gel concentrations and different electrochemical deposition parameters. Scan rates of 1-50 mV/s were used. Clear oxidation and reduction peaks were evident in the

CV curves along with the EDLC contribution. We observed a tradeoff between specific surface area and Ni(OH)₂ quantity: the higher the Ni(OH)₂ coverage in the PSi matrix, the lower the accessible surface area. The highest specific capacitance of 1400 F/g was measured on an electrode with a modest concentration of Ni(OH)₂ (5 mg/mL nickel acetate tetrahydrate:2-methoxyethanol) at 50 mV/s. The results of these studies suggest that PSi is an excellent high surface area host template for Ni(OH)₂ that enables high specific capacitance to be achieved on a Si-compatible platform that could be directly integrated into microelectronic devices.

4:20pm **EM+SS+TF-ThA7 In-situ Raman of Sodium Ion Cointercalation into Highly Crystalline Few-Layered Graphene**, *Adam Cohn*, *C.L. Pint*, Vanderbilt University

A maximum sodium capacity of ~ 35 mAh/g has restricted the use of crystalline carbon for sodium ion battery anodes. We demonstrate that a diglyme solvent shell encapsulating a sodium ion acts as a “non-stick” coating to facilitate rapid ion insertion into crystalline few-layer graphene and bypass slow desolvation kinetics. This yields storage capacities above 150 mAh/g, cycling performance with negligible capacity fade over 8000 cycles, and ~ 100 mAh/g capacities maintained at currents of 30 A/g (~ 12 second charge). Raman spectroscopy elucidates the ordered, but non-destructive cointercalation mechanism that differs from desolvated ion intercalation processes. In-situ Raman measurements identify the Na⁺ staging sequence and isolates Fermi energies for the first and second stage ternary intercalation compounds at ~ 0.8 eV and ~ 1.2 eV.

4:40pm **EM+SS+TF-ThA8 Using X-ray Reflectivity to Measure the Vacuum Ultraviolet Absorption Spectrum in Low-k Dielectrics**, *Faraz Choudhury*, *H.M. Nguyen*, *W. Li*, University of Wisconsin-Madison; *Y. Nishi*, Stanford University; *J.L. Shohet*, University of Wisconsin-Madison

During plasma processing, low-k dielectrics are exposed to high levels of vacuum ultraviolet (VUV) radiation that can cause severe damage to the dielectric material. The degree and nature of VUV-induced damage depends on the VUV photon energies.[1] In this work, we determine the VUV absorption spectrum of low-k organosilicate glass (OSG) using specular X-ray reflectivity (XRR). Low-k SiCOH films were exposed to synchrotron VUV radiation with energies ranging from 7 to 25 eV and the electron density depth profile of the VUV irradiated films were extracted from the fitting of the XRR experimental data using the Parratt method. The results show that the depth of the VUV induced damage layer is sensitive to the photon energy. Between 7 to 11 eV, the depth of the damaged layer decreases sharply from 110 nm to 60 nm and then gradually increases to 85 nm at 21 eV. The maximum VUV absorption in low-k films occurs between 11 and 15 eV. This method is also utilized to investigate the penetration depth of 5 to 25 eV photons in porous SiCOH films with porosities ranging from 15 to 50%. It is seen that the penetration depth of photons increases with porosity. This work shows that XRR electron density depth profiling can be a very effective, non-destructive tool to determine the penetration depth and absorption coefficients of photons and other reactive species from a plasma in various kinds of dielectric films.

This work was supported by the Semiconductor Research Corporation under Contract 2012-KJ-2359

[1] T. V. Rakhimova et al, J. Phys. D: Appl. Phys. 47 (2014) 025102

5:00pm **EM+SS+TF-ThA9 On-chip [¹⁸F]fluoride Concentration for Microfluidic PET Tracer Synthesis**, *Xin Zhang*, *J. Buck*, *M. Nickels*, *C. Manning*, *L. Bellan*, Vanderbilt University

Positron emission tomography (PET) is a valuable medical imaging method that relies on radioactive tracers that target specific sites in the body. Development of these tracers is currently hindered by the enormous infrastructure requirements to perform the necessary radioisotope production and subsequent reactions. To overcome this hurdle and facilitate PET tracer development, we are designing simple, modular microfluidic systems that support on-chip radiosynthesis reactions with small volumes of reagents. In this work, [¹⁸F]fluoride (a positron emitter widely used in PET imaging due to its convenient half-life of 110 minutes) is concentrated with a miniaturized anion exchange column located in a microfluidic device fabricated in polydimethylsiloxane (PDMS). By employing a microfluidic device, we aim to achieve more controlled diffusion and reactive kinetics. Instead of relying on complicated flow control elements (e.g. valves), in this microfluidic system, a channel containing pillars with a spacing less than the average diameter of the anion exchange beads is used to trap relatively monodispersed, rigid polystyrene/divinyl benzene beads. We characterized the ability of this

Thursday Afternoon, November 10, 2016

miniaturized on-chip exchange column to capture and release quantities of [^{18}F]fluoride appropriate for human imaging (a typical dose is 10 mCi).

Our device is composed of a main chamber with larger microchannels (9 mm long) connected to an inlet and outlet. A laser writer (Heidelberg μPG 101) was used to create patterns on a silicon wafer using a 60 μm thick layer of mr-DWL resist; this template was subsequently used to pattern a microfluidic structure in PDMS. The desired quantity (2.9 mL) of anion exchange beads was trapped by a double row of square pillars near the outlet of the chamber, and the beads subsequently activated with 1.0 M of KHCO_3 . Diluted [^{18}F]fluoride (100 mCi/mL) sourced from a nearby cyclotron was introduced into the system using a syringe pump, flowing at 0.05 mL/min for 10 minutes.

By quantifying the radioactivity of the [^{18}F]fluoride introduced, the radioactivity of the chip, and the radioactivity of the outflow, we could determine trapping and release efficiency. We observed near complete capture of [^{18}F]fluoride (50 mCi) on our chips in a relatively short time. Moreover, elution with a small volume (less than 200 mL) of Kryptofix (K_{222})/ K_2CO_3 was able to release nearly all the [^{18}F]fluoride (49 mCi). Thus, this device is capable of simply and efficiently trapping [^{18}F]fluoride and controllably releasing the concentrated radiolabel in small volumes for downstream reaction with desired molecules.

5:40pm EM+SS+TF-ThA11 The Role of Electron-Beam Deposition Rate in Controlling Properties of the Titanium/Semiconductor Interface, Keren Freedy, A. Giri, B.M. Foley, University of Virginia; J. Bogan, R. O'Connor, Dublin City University, Ireland; P.E. Hopkins, S. McDonnell, University of Virginia

Electron beam evaporation under high vacuum is very widely used for contact deposition in electronic device fabrication. Ti has a low work function and is commonly deposited as a contact or adhesion layer for other metals in silicon-based devices and more recently in 2D semiconductors. Previous work on Ti/ MoS_2 contacts suggests that electron beam evaporation of Ti under high vacuum results in the formation of TiO_2 at the interface while UHV deposition results in unintentional reactions between metallic Ti and the MoS_2 substrate (McDonnell et al., 10.1021/acsami.6b00275). Since the majority of reports using Ti as a contact metal utilize HV rather than UHV e-beam processes, understanding the role of process conditions on the properties of this contact/semiconductor interface is of the utmost importance. To avoid the large variability observed in metal/ MoS_2 contacts, we focus on Si as a case study to investigate the thermal and electronic properties of the Ti/semiconductor interface. The present study examines the effect of deposition rate on the properties of the Ti/Si interface. Electron beam evaporation of Ti onto both hydrogen-terminated and native oxide (001) Si surfaces is performed at varied deposition rates ranging from 0.1 to 5 Å/s at pressures of $\sim 10^{-6}$ Torr. Prior to ex-situ characterization, the samples are capped with Au in the evaporator to prevent further oxidation in air. Photoelectron spectroscopy measurements reveal that oxide composition is inversely proportional to the deposition rate. X-ray diffraction data shows no evidence of metallic Ti at slower deposition rates. Due to an appreciable partial pressure of O_2 at high vacuum, the composition of the deposited material is sensitive to the impingement rate of Ti on the surface. It follows that higher deposition rates should result in a smaller fraction of oxide phases. Electron and phonon transport across the interface will be studied as a function of deposition rate.

6:00pm EM+SS+TF-ThA12 Single Crystal Study of Layered $\text{U}_n\text{RhIn}_{3n+2}$ Materials: Case of the Novel U_2RhIn_8 Compound, Attila Bartha, M. Kratochvílová, Charles University, Czech Republic; M. Dušek, Institute of Physics ASCR, Czech Republic; M. Diviš, J. Custers, V. Sechovský, Charles University, Czech Republic

Materials of reduced dimensionality appear in many contemporary fields of research and technology, because they encompass a wide variety of interesting electronic phenomena. For instance carbon can be prepared in 3D (diamond), quasi-2D (graphite), 2D (graphene) or 1D (carbon nanotubes). All of these structures have distinct electronics. Diamond is an insulator. Graphene is semimetal. However, when the dimensionality is increased by putting several graphene layers together (eventually making graphite), the resulting band structure moves to that of a more trivial metal. Another example is high temperature superconductors being quasi-2D materials as well.

The role of dimensionality in f -electron systems has been mainly discussed in the context of quantum phase transitions and related phenomena. The series $\text{Ce}_n\text{TmIn}_{3n+2m}$ ($n = 1, 2$; $m = 0, 1, 2$; T = transition metal) of layered compounds has been extensively investigated. CeIn_3 is cubic (3D) and

orders antiferromagnetically (AFM) at $T_N = 10.2$ K. Under hydrostatic pressure superconductivity appears with highest $T_c = 0.3$ K at $p = 2.5$ GPa. In CeRhIn_5 , the anisotropic crystal structure leads to a quasi-2D electronic and magnetic structure. The AFM order is reduced ($T_N = 3.8$ K) while superconductivity is supported, T_c increases to 1.9 K at $p = 1.77$ GPa.

We report on the properties of the novel U_2RhIn_8 compound studied the single crystal form in the context of parent URhIn_5 and UIn_3 systems [1]. The compounds were prepared by In self-flux method. U_2RhIn_8 adopts the Ho_2CoGa_8 -type structure with lattice parameters $a = 4.6056(6)$ Å and $c = 11.9911(15)$ Å. The behavior of U_2RhIn_8 strongly resembles features of related URhIn_5 and UIn_3 with respect to magnetization, specific heat, and resistivity, except for magnetocrystalline anisotropy developing with lowering dimensionality in the series UIn_3 vs. U_2RhIn_8 and URhIn_5 . U_2RhIn_8 orders AFM below $T_N = 117$ K and exhibits slightly enhanced Sommerfeld coefficient $\gamma = 47$ mJ.mol $^{-1}$.K $^{-2}$. Magnetic field leaves the value of Néel temperature for both URhIn_5 and U_2RhIn_8 unaffected up to 9 T. On the other hand, T_N increases with applying hydrostatic pressure up to 3.2 GPa. Results of thermal expansion measurement will be discussed in the framework of Ehrenfest relations. The character of uranium $5f$ electron states of U_2RhIn_8 was studied by first principles calculations based on the density functional theory combined with the Hubbard model. The overall phase diagram of U_2RhIn_8 is discussed in the context of magnetism in related UTX_5 and UX_3 (T = transition metal, $X = \text{In, Ga}$) compounds.

[1] A. Bartha et al., J. Magn. Magn. Mater. 381 (2015) 310-315

Fundamental Discoveries in Heterogeneous Catalysis Focus Topic

Room 103A - Session HC+SS-ThA

Advances in Theoretical Models and Simulations of Heterogeneously-catalyzed Reactions

Moderator: Donna Chen, University of South Carolina

2:20pm HC+SS-ThA1 Theoretical Pathways to Predict (meta-)stability of Gas Phase Metal Oxide Clusters: Beyond the Static Mono-Structure Description, Saswata Bhattacharya, Indian Institute of Technology Delhi, India; L.M. Ghiringhelli, Fritz-Haber-Institut der Max-Planck-Gesellschaft; N. Marom, Tulane University

This talk is driven by the vision of computational design of cluster-based nanocatalysts. The discovery of the extraordinary activity in catalysis exhibited by small metal-oxide clusters has stimulated considerable research interest. However, in heterogeneous catalysis, materials property changes under operational environment (e.g. temperature (T) and pressure (p) in an atmosphere of reactive molecules). Therefore, a solid theoretical understanding at a realistic (T , p) is essential in order to address the underlying phenomena. In this talk, I shall first introduce a robust methodological approach that integrates various levels of theories combined into one multi-scale simulation to address this problem[1]. I shall show one application of this methodology in addressing (T , p) dependence of the composition, structure, and stability of metal oxide clusters in a reactive atmosphere at thermodynamic equilibrium using a model system that is relevant for many practical applications: free metal (Mg) clusters in an oxygen atmosphere[2].

More recently, I have extended this development in designing clusters with desired properties. The novelty of this implementation is that it goes beyond the interpretation of experimental observations and addresses the challenging “inverse problem” of computationally designing clusters with target properties. The methodology is applied and thoroughly benchmarked on $(\text{TiO}_2)_n$ clusters [$n=2, 3, \dots, 10, 15, 20$][3]. All the results are duly validated using the highest level of theories currently achievable within Density Functional Theory (DFT).

References:

[1] S. Bhattacharya, S. Levchenko, L. Ghiringhelli, M. Scheffler, New J. Phys. 16, 123016 (2014).

[2] S. Bhattacharya, S. Levchenko, L. Ghiringhelli, M. Scheffler, Phys. Rev. Lett. 111, 135501 (2013).

[3] S. Bhattacharya, B. Sonin, C. Jomonte, L. Ghiringhelli, N. Marom, Phys. Rev. B 91, 241115 (R), (2015).

Thursday Afternoon, November 10, 2016

2:40pm HC+SS-ThA2 Role of Oxygen at the Surface and Subsurface during Catalytic Oxidation by Silver, *Sharani Roy*, University of Tennessee

Catalytic oxidation by the silver surface is used in several important industrial processes, such as epoxidation of ethylene to form polyethylene or partial oxidation of methane to form methanol. To understand the mechanisms of catalytic oxidation at the molecular level, it is essential to understand the interactions of atomic oxygen with the silver surface. We present a detailed theoretical study of oxygen adsorbed on the surface and subsurface of silver based on density functional theory and molecular dynamics simulations. Our ultimate goal is to develop a conceptual model of reactivity of surface oxygen and subsurface oxygen in catalytic oxidation by the silver surface. While the detailed quantum chemical calculations serve to accurately model the ground-state potential energy landscape of the oxygen-silver system, molecular dynamics simulates the motion of oxygen on the surface and subsurface at realistic laboratory or catalytic temperatures. We focus on several important phenomena, including surface-site preference, coverage dependence, and temperature dependence of oxygen adsorption at the surface and subsurface. We also investigate the changes in the surface structure of silver induced by the presence of oxygen. Due to the differences in structure, interatomic spacing, and binding sites of the (111) and (110) faces of the silver crystal, the adsorption properties of atomic oxygen vary for the two surfaces. Our study determines some fundamental differences in silver-oxygen interactions on the two surfaces, and provides qualitative insight on how the choice of surface can affect the participation of surface and subsurface oxygen in catalytic oxidation by silver. Future work will explore the interactions of surface oxygen and subsurface oxygen with reactant molecules such as methane or ethylene.

3:00pm HC+SS-ThA3 Using Theory and Computation to Understand Plasma Enhanced Dry Reforming on Nickel Catalysts, *George Schatz*, Northwestern University **INVITED**

Dry reforming is a process wherein CH_4 and CO_2 react to give synthesis gas and/or liquid fuels. Dry reforming is normally done under high temperature and pressure conditions, with a Ni catalyst, however it has recently been discovered that if a plasma is also present near the catalyst, then it is possible to get this reaction to go under modest conditions close to room temperature and atmospheric pressure. The role of the plasma in this process is poorly understood. In this talk I will describe several electronic structure studies that my group is doing which are designed to describe the processes involved in plasma enhanced dry reforming, including both the role of the plasma, and the gas-surface chemistry that occurs in the presence of plasma species. The plasma is known to fragment the reacting gases, especially CH_4 , so we will study the interaction of methane fragments with various Ni surfaces, to show how this enhances chemisorption, surface dissociation, and subsequent reaction with species already on the surface. A highlight of this work involves the reaction of subsurface hydrogen with adsorbed CO_2 to give CO , water and other products. We have also studied the influence of ions and electrons on surface chemistry.

4:00pm HC+SS-ThA6 The Impact of Structure on the Catalytic Behavior of Cu_2O Supported Pt Atoms, *Andrew Therrien**, Tufts University Department of Chemistry; *E.C.H. Sykes*, Tufts University

Single site catalysts composed of individual atoms on various oxide supports have been a major research focus in recent years. Such catalysts exhibit novel reactivity with the benefit of 100% atom efficiency and a dramatic reduction in the precious metal loading. However, despite several experimental examples of efficient single atom catalysts, there is much debate regarding the structure and catalytic mechanisms of such catalysts and debate over whether single atoms or nanoparticles are the active species. Given the complexity of heterogeneous catalysts and the size scale of the active sites, there is a need for a surface science and microscopy approach to understand the structure and reactivity of atomically dispersed atoms on oxides.

We have studied the structure and reactivity of individual Pt atoms supported on oxidized Cu using scanning tunneling microscopy (STM) and temperature programmed reaction (TPR). We first elucidated the structure of the support, a previously observed but unsolved Cu_2O overlayer on Cu, by density functional theory (DFT) and comparison of simulated STM images with experimental STM. We discovered that the oxide surface is inert towards CO oxidation, while the single Pt atom decorated surface is efficient for low-temperature CO oxidation. This system is also capable of

water activation. Our combination of TPR and STM studies suggest that single Pt atoms supported on the oxide are indeed catalytically active and may be a good catalyst for the water-gas shift reaction.

4:20pm HC+SS-ThA7 Energetics of Water Dissociative Adsorption on $\text{NiO}(111)\text{-}2\times 2$, *Wei Zhao*, University of Washington; *M. Bajdich*, Stanford University; *S. Carey*, University of Washington; *M. Hoffmann*, *A. Vojvodic*, *J. Nørskov*, Stanford University; *C.T. Campbell*, University of Washington

The energetics of the reactions of water with metal oxide surfaces are of tremendous interest for catalysis and electrocatalysis, yet the energy for the dissociative adsorption of water was only previously known on one well-defined oxide surface, $\text{Fe}_3\text{O}_4(111)$.^[1] Here we report the first calorimetric measurement of the heat of reaction for the dissociative adsorption of water on $\text{NiO}(111)\text{-}2\times 2$ as a function of coverage, showing that the heat of dissociative adsorption decreases with coverage from 177 kJ/mol to 119 kJ/mol in the first 0.25 ML of coverage. These measurements provide an important benchmark for validating computational estimates of adsorption energies of molecular fragments on correlated metal-oxide such as NiO and for oxide surface chemistry in general, which is more challenging in this respect than for metal or wide-gap semiconductor surfaces. We also present DFT calculations of the energetics of this reaction, and compare it to the calorimetric results.

[1] P. Dementyev, K.-H. Dostert, F. Ivars-Barceló, C.P. O'Brien, F. Mirabella, S. Schauermaier, X. Li, J. Paier, J. Sauer, H.-J. Freund, Water Interaction with Iron Oxides, *Angewandte Chemie International Edition*, 54 (2015) 13942-13946.

4:40pm HC+SS-ThA8 Challenges in the First-Principles Description of Reactions in Electrocatalysis, *Axel Groß*, Ulm University, Germany **INVITED**

In spite of its technological relevance in the energy conversion and storage, our knowledge about the microscopic structure of electrochemical electrode-electrolyte interfaces and electrical double layers is still rather limited. The theoretical description of these interfaces from first principles is hampered by three facts. i) In electrochemistry, structures and properties of the electrode-electrolyte interfaces are governed by the electrode potential which adds considerable complexity to the theoretical treatment since charged surfaces have to be considered. ii) The theoretical treatment of processes at solid-liquid interfaces includes a proper description of the liquid which requires to determine free energies instead of just total energies. This means that computationally expensive statistical averages have to be performed. iii) Electronic structure methods based on density functional theory (DFT) combine numerical efficiency with a satisfactory accuracy. However, there are severe shortcomings of the DFT description of liquids, in particular water, using current functionals.

Despite these obstacles, there has already significant progress been made in the first-principles modeling of electrochemical electrode-electrolyte interfaces. In this contribution, I will in particular focus on how the electrochemical environment can be appropriately taken into account using numerically efficient schemes. In the presence of an aqueous electrolyte, metal electrodes are in general covered by either cations or anions. Based on the concept of the computational hydrogen electrode, the equilibrium coverage of $\text{Pt}(111)$ with hydrogen (1,2) and halides (3) as a function of the electrode potential has been derived showing that halide and hydrogen adsorption is competitive, in agreement with experimental findings. The presence of the aqueous electrolyte has been taken into account modeling water layers either implicitly through a polarizable medium (2) or explicitly in ab initio molecular dynamics runs (3). To obtain a proper description of the water-water and the water-metal interaction, it turns out that the consideration of dispersion corrections is essential (4). The importance of the electrochemical environment in electrocatalytic processes will be demonstrated using the methanol electrooxidation on $\text{Pt}(111)$ (5) as an example.

References

- (1) S. Sakong, M. Naderian, K. Mathew, R. G. Hennig, and A. Gross, *J. Chem. Phys.* **142**, 234107 (2015).
- (2) T. Roman and A. Gross, *Catal. Today*. **202**, 183 (2013).
- (3) F. Gossenberger, T. Roman, and A. Gross, *Surf. Sci.* **631**, 17 (2015).
- (4) K. Konigold and A. Gross, *J. Comput. Chem.* **33**, 695(2012).
- (5) S. Sakong and A. Gross, submitted.

* Morton S. Trauma Award Finalist

Thursday Afternoon, November 10, 2016

5:20pm **HC+SS-ThA10 Beyond the 2D Lattice Gas and 2D Ideal Gas Models for Adsorbates: The Hindered Translator / Hindered Rotor Model**, *Liney Arnadottir, L.H. Sprowl*, Oregon State University; *C.T. Campbell*, University of Washington

With the recent explosion in computational catalysis and related microkinetic modeling, the need for a fast yet accurate way to predict equilibrium and rate constants for surface reactions has become more important. In such calculations, adsorbates are usually treated within either the 2D lattice gas or 2D ideal gas approximation to estimate their partition functions and entropies. Here we present a fast new method to estimate the partition functions and entropies of adsorbates that is much more accurate than those approximations, and recognizes the true oscillating nature of the adsorbate's potential energy for motions parallel to the surface. As with previous approaches, it uses the harmonic oscillator (HO) approximation for most of the modes of motion of the adsorbate. However, it uses hindered translator and hindered rotor models for the three adsorbate modes associated with motions parallel to the surface, and evaluates these using an approach based on a method that has proven accurate in modeling the internal hindered rotations of gas molecules. The translational and rotational contributions to the entropy of a hindered translator / hindered rotor calculated with this new method are, in general, very closely approximated (to within $<0.25R$ error per mode) by the corresponding harmonic oscillator (i.e., 2D lattice gas) entropy when kT is less than the barrier. When kT exceeds the barrier, the hindered translator / hindered rotor model is closely approximated (to within $0.1 R$) by the entropy of an ideal 2D gas. The harmonic oscillator / lattice gas model severely overestimates the entropy when kT greatly exceeds the barrier. The cutoff between the temperature ranges of applicability of these simple two approximations is very sharp but with our combined hindered rotor/hindered translator approach the whole temperature range is covered with the same approach.

5:40pm **HC+SS-ThA11 Methanol Partial Oxidation Catalyzed by Singly-dispersed Pd on ZnO(101 $\bar{0}$)**, *Takat B. Rawal¹, S.R. Acharya, S. Hong, T.S. Rahman*, University of Central Florida

Heterogeneous catalysis by singly-dispersed metal atoms on non-metallic surfaces offers great potential for maximizing the efficiency of metal atoms, and optimizing their activity and selectivity. Herein, we present results from our *ab-initio* density functional theory (DFT) calculations for methanol partial oxidation (MPO), an industrially important reaction for the production of H_2 , on $Pd_1/ZnO(101\bar{0})$. To begin with we find that the Pd atom prefers to adsorb at the oxygen vacancy site i.e. the anion vacancy is responsible for stabilizing singly-dispersed Pd atom on $ZnO(101\bar{0})$. We discuss the adsorption characteristics of a set of gas molecules (CH_3OH , O_2 , CO , CO_2 , H_2O , H_2), and the potential energy profile including activation barriers for the reaction processes associated with MPO on $Pd_1/ZnO(101\bar{0})$, and compare them with those on $Pd_{16}Zn_{16}$ nanoparticle and pristine $ZnO(101\bar{0})$. We find that the singly dispersed Pd sites offer a high activity towards the formation of CO_2 and H_2 over that of CO and H_2O . We trace this reactivity to the electronic structure of the single Pd site as modified by its local environment which in turn facilitates a strong binding of CO to the Pd site, thereby increasing the CO desorption barrier and stabilizing O_2 on $ZnO(101\bar{0})$, which is essential for further oxidation steps. With activation energy barriers and pre-exponential factors calculated from DFT, for a large set of reaction intermediates, we perform kinetic Monte Carlo simulations to determine the turn over frequencies and rate limiting steps in the formation of CO_2 and H_2 on $Pd_1/ZnO(101\bar{0})$, under ambient conditions.

Work supported in part by DOE grant DE-FG02-07ER15842.

6:00pm **HC+SS-ThA12 Simulations of Surface Induced Dissociation, Soft Landing, and Reactive Landing in Collisions of Protonated Peptide Ions with Organic Surfaces**, *William Hase, S. Pratihari*, Texas Tech University

Chemical dynamics simulations have been performed to explore the atomistic dynamics of collisions of protonated peptide ions, peptide- H^+ , with organic surfaces. Overall, the results of the simulations are in quite good agreement with experiment. The simulations have investigated the energy transfer and fragmentation dynamics for peptide- H^+ surface-induced dissociation (SID), peptide- H^+ physisorption on the surface, soft landing (SL), and peptide- H^+ reaction with the surface, reactive landing (RL). The primary structure of biological ions is determined by SID, as well as information regarding the ions' fragmentation pathways and energetics. SID occurs by two mechanisms. One is a traditional mechanism in which

peptide- H^+ is vibrationally excited by its collision with the surface and then dissociates in accord with the statistical, RRKM unimolecular rate theory after it rebounds off the surface. For the other mechanism, the ion *shatters* via a non-statistical mechanism as it collides with the surface. The simulations have also provided important dynamical insight regarding SL and RL of biological ions on surfaces. SL and RL have a broad range of important applications including preparation of protein and peptide microarrays. The simulations indicate that SL occurs via multiple mechanisms consisting of peptide- H^+ physisorption on and penetration in the surface. An important RL mechanism is intact deposition of peptide- H^+ on the surface.

Advanced Ion Microscopy Focus Topic

Room 104A - Session HI+MI+NS-ThA

Ion Beam Based Imaging and Nanofabrication

Moderators: Jacques Gierak, LPN-CNRS, Shinichi Ogawa, AIST, Japan

2:20pm **HI+MI+NS-ThA1 Mask Repair Technology using Gas Field Ion Source**, *Anto Yasaka, F. Aramaki, T. Kozakai, O. Matsuda*, Hitachi High-Tech Science Corporation, Japan

INVITED

We developed a new ion beam based mask repair system using a gas field ion source (GFIS). For conventional photomasks, nitrogen ions were used to repair defects, while hydrogen ions were used for EUVL masks. We evaluated the performance of the mask repair system on $MoSi$ based phase shift masks and EUV masks. The results demonstrate that GFIS technology is a reliable solution of repairing defects on high end photomasks for 1Xnm generation and beyond.

3:00pm **HI+MI+NS-ThA3 Application of an Advanced Bi Cluster LMIS for TOF-SIMS Analysis at the Nano-scale**, *F. Kollmer, W. Paul, D. Rading, R. Moellers*, ION-TOF GmbH, Germany; *N.J. Havercroft*, ION-TOF USA; *E. Niehuis, Julia Zakel*, ION-TOF GmbH, Germany

In recent years, the application of cluster primary ions has become standard for all kinds of TOF-SIMS applications. Organic surfaces, in particular, benefit from the cluster bombardment due to a more efficient emission of molecular species compared to mono-atomic bombardment. However, the ultimate spot size so far has been obtained by Ga based liquid metal ion sources. In our contribution we will show that a Bi based cluster LMIS has the potential to outperform the established Ga LMIS even in terms of TOF-SIMS imaging at the highest lateral resolution.

We will discuss fundamental emission properties such as energy spread and virtual source size for the main species of a Bi cluster LMIS. Via a consistent optimisation of emission parameters and an adaption of the ion-optical column, a lateral resolution in the 20 nm range can be achieved. At this scale it seems that we are approaching the physical limits since not only the primary ion beam spot size, but also the size of the sputter cascade as well as the signal intensity limit the obtainable useful lateral resolution. Further progress requires the combination of the SIMS data with complementary imaging techniques of higher lateral resolution or sophisticated sample preparation methods such as bevelling of the surface region with an FIB column.

In this respect we will show that a combined TOF-SIMS Scanning Probe Microscopy (SPM) provides the required information on the nanometer level. Moreover, information on surface topography and other physical properties of the scanned surface area can be obtained in-situ. The investigated samples include inorganic reference samples, alloys, biological samples, hybrid sample systems and thin films.

3:20pm **HI+MI+NS-ThA4 Nanoscale Imaging and Characterization of Interface Driven Assembly of Soft Materials via He-Ion Beam Microscopy**, *Matthew Burch, A. Belianinov, D. Chang, Y. Luo, K. Hong, O.S. Ovchinnikova*, Oak Ridge National Laboratory

The ability to directly image and characterize nanoscale structures and features of soft materials is key to understanding the role growth, interfaces and extrinsic stimuli have on the functionality of these materials. In particular, the arrangement and architecture of bottlebrush block copolymer systems is of interest, as material properties depend greatly on the organization and interfaces of these polymers during growth. However, due to the insulating nature of these materials, directly imaging surface features at the nanoscale using traditional electron microscopy based techniques is challenging. Alternatively, He-ion beam microscopy (HIM) has been developed to the level where it can now characterize and directly image the nanoscale surface features of these soft materials directly.

* National Student Award Finalist

Thursday Afternoon, November 10, 2016

In this work, He-ion microscopy is utilized to investigate the nanoscale structures of copolymer systems. In particular, the ordered periodic structures of bottle brush copolymer thin film systems are investigated to understand how different substrates and growth conditions impact the final periodic lamella and domain structures. Of particular interest is how the interface driven separation leads to different short range molecular and long range surface ordering. Furthermore, we will discuss how surface ordering of the copolymers effects the functionality of the material by correlating HIM imaging results with local probing of electromechanical and electrochemical using scanning probe microscopy.

Acknowledgements

This work was conducted at the Center for Nanophase Materials Sciences, which is a Department of Energy (DOE) Office of Science User Facility.

4:00pm HI+MI+NS-ThA6 Advances in *Ex Situ* Lift Out and Manipulation Techniques for FIB Applications, Lucille Giannuzzi, ExpressLO LLC

The focused ion beam (FIB) *ex situ* lift out (EXLO) technique was the first lift out technique developed for transmission electron microscopy (TEM), surface science, and other site specific analysis of materials [1,2]. EXLO is well known for its ease, speed, and reproducibility, and is perfectly suited for manipulation of thick or electron transparent thin specimens for site specific microscopy or analytical characterization. EXLO is also perfectly suited for manipulation of electron transparent specimens to MEMS carrier devices used for *in situ* TEM holders. Micromanipulation techniques also aid in specimen preparation for particulates and fibers that require subsequent FIB milling. A review of EXLO and advances of the technique using a new slotted grid specimen carrier will be presented. This new grid negates the need for a carbon film specimen support and allows for additional specimen FIB milling or other post processing after manipulation [3].

[1] L.A. Giannuzzi et al., *Mat. Res. Soc. Symp. Proc.* 480 (1997) 19-27.

[2] F.A. Stevie et al., *Surf. Interface Anal.* 31 (2001) 345–351.

[3] L.A. Giannuzzi et al., *Microsc. Microanal.* 21 (2015) 1034-1048.

4:20pm HI+MI+NS-ThA7 Helium Ion Microscopy Imaging of Carbon Nanofoams from Hydrothermal Carbonization of Sucrose, Natalie Frese, Bielefeld University, Germany; S.T. Mitchell, A. Bowers, K. Sattler, University of Hawaii; A. Götzhäuser, Bielefeld University, Germany

Carbon nanofoam is considered as potential hydrogen storage material as well as cathode material for metal-air batteries. It is known that carbon nanofoam contains both sp^2 - and sp^3 -bonded carbon atoms. However, there is still a lack of knowledge about the atomic structure of this material. In this work, different types of carbon nanofoams were produced by low-temperature hydrothermal processing of carbon precursor materials. It was found that the produced foams have a low density and are uniform in their appearance. Helium-ion microscopy, X-ray photoelectron spectroscopy and Raman spectroscopy were used to characterize the foam samples. The results show good consistency between the micro- and nanostructure as well as the elemental composition. We conclude that hydrothermal processing of carbon precursor materials is an effective method to produce high-quality carbon nanofoams of graphitic nature.

4:40pm HI+MI+NS-ThA8 Nanofabrication Limits in Layered Ferroelectric Semiconductors via He-ion Beam, Alexei Belianinov, A. Ievlev, V. Iberi, H. Hysmith, M.A. Susner, M. McGuire, S. Jesse, S.V. Kalinin, O.S. Ovchinnikova, Oak Ridge National Laboratory

Manipulating matter at progressively finer and ultimately atomic scales enables new functionality and effectively drives nanoscience. Currently, well understood, robust resist-based lithography, carries the brunt of nanofabrication, however local electron, ion and physical probe methods are improving as well, driven largely in part of their ability to fabricate without multi-step preparation processes that contaminate the sample with processing resists and solvents. Furthermore probe based methods extend beyond nanofabrication to nanomanipulation and imaging, vital ingredients to rapid transition to testing and manufacturing of layered 2D heterostructured devices.

In this work we demonstrate chemical and physical changes induced by a helium ion beam in a Helium Ion Microscope (HIM) with the surface of bulk copper indium thiophosphate (CITP) $CuM_{III}P_2X_6$ ($M = Cr, In$; $X = S, Se$) library of compounds of varying copper concentration; from 4–100%. Physical changes in micro- and nano-fabrication are explored via Atomic Force Microscopy, (AFM), and chemical changes are probed by Secondary Ion Mass Spectrometry, (SIMS). Our work illustrates controlled loss of ferroelectric domains, and nanostructure growth with material volumes

scaling to the dosage of the helium ion beam. The nanostructures are oxygen rich, sulfur poor, with the copper concentration virtually unchanged. Effects of varying copper concentration on the quality of the fabricated nanostructures, as well as the differences in their chemical make-up will be discussed.

Acknowledgements

Research was supported (A. B., V. I., A. I., H. H., S. J. S. V. K. O. S. O) and partially conducted (AFM, HIM, SIMS) at the Center for Nanophase Materials Sciences, which is sponsored at Oak Ridge National Laboratory by the Scientific User Facilities Division, Office of Basic Energy Sciences, US Department of Energy. This work was also supported (M. S., M. M.) and partially conducted (material growth) by the U.S. Department of Energy, Basic Energy Sciences, Materials Sciences and Engineering Division.

5:00pm HI+MI+NS-ThA9 Focused Ion Beam Technology Challenges for Circuit Edit, Yuval Greenzweig, Y. Drezner, A. Raveh, Intel Corporation

The challenges of Circuit Edit (CE) using focused ion beam (FIB) are driven by the perpetual down-scaling of minimum features per VLSI process technology generation. The recent emergence of FIBs with much reduced probe sizes relative to Ga LMIS based tools, may provide a long-needed revitalization of FIB nanomachining capabilities such as FIB image resolution and machining acuity, necessary for nanomachining tasks such as CE. However, other requirements must go along, driving preferences of ion species, ion energies, and requirements for system performance in several areas.

Among the challenging requirements of CE is the task of milling in a controlled and planar fashion through layers of parallel metal lines with intervening dielectric, and end-pointing on a metal layer of choice. The end-pointing is based on the real-time secondary electron (SE) image during ion milling, and the requirement is leaving most of the target metal intact. If linear dimensions of features, such as minimum metal widths, reduce by a factor α from one VLSI generation to the next, then maintaining quality realtime milling images, i.e., sufficient resolution and signal to noise, requires milling vertically through a layer proportional to α^2 relative to the previous generation - same number of ions, but in a smaller pixel. On the other hand, the vertical thickness of the metals has also decreased by α , causing the etching to scale as α^3 relative to the thinner new metal thicknesses. Previous VLSI process generation scaling factors have been approximately $\alpha = 0.7$, so that the severity of this challenge has been getting worse by $\sim 3X$ for several generations and is now at the feasibility limit. To improve on this, SE emission and collection efficiency must improve, and in particular SE collection efficiency of normally emitted SEs, which are the bearers of the information from the bottom of these milling boxes. The figure of merit representing this challenge is the SE yield times the SE detector collection efficiency, divided by the sputter yield (or etch rate), this provides opportunity for GFIS sources.

Other challenges of the CE application which providing preferences of ion species and ion energy will be discussed.

5:20pm HI+MI+NS-ThA10 Ion-milling of Graphene Nanostructures While Supported and Unsupported: Considerations of Graphene Contamination, Substrate Scattering and Beam Tailing, J. Swett, Lockheed Martin Space Systems Company; V. Iberi, D. Cullen, Adam Rondinone, Oak Ridge National Laboratory

Graphene and other 2D materials offer novel characteristics and opportunities compared to traditional thin films. Common nanofabrication techniques including e-beam and nanoimprint lithography can be used to pattern atomically thin 2D systems but the multi-step processes they utilize result in exposure of the film to solvents and resists, and hence degradation of the material's novel electronic properties. Herein we demonstrate that helium and neon-ion milling are effective tools for the creation of very fine features with arbitrary geometries in supported and unsupported graphene, to include conductive structures, arrays of pores, and engineered defects. Properties of graphene, including contamination levels, play an important role in determining millability, as do instrumental parameters such as beam tailing and substrate scattering.

Acknowledgement

This research was conducted at the Center for Nanophase Materials Sciences, which is a Department of Energy (DOE) Office of Science User Facility.

Thursday Afternoon, November 10, 2016

5:40pm **HI+MI+NS-ThA11 Interaction of Gas Field Ionized Nitrogen with Silicon, Marek Schmidt, Y. Oshima, L.T. Anh, X. Zhang, T. Kanzaki, M. Akabori**, Japan Advanced Institute of Science and Technology, Japan; A. Yasaka, Hitachi High-Tech Science Corporation, Japan; M. Muruganathan, T. Shimoda, H. Mizuta, Japan Advanced Institute of Science and Technology, Japan

A larger number of gas molecules (among them helium, nitrogen and neon) can be ionized by the gas field ion source (GFIS) and used as projectiles in focused ion beam (FIB) systems. Among them, the nitrogen stands out as it forms a very strong covalent bond. It is not yet fully understood how this N₂ molecule behaves during field ionization and sample interaction, i.e. if and when the bond is broken. Previously, it has been shown that cross section studies are very useful in analyzing beam/sample interaction [1]. Here, we report scanning transmission electron microscopy (STEM) analysis of cross sections extracted from silicon bombarded with ionized N₂ molecules. The extracted implantation depths for ion energies of 25 and 16 keV are compared with theoretical values and suggest that the bond is broken during sample interaction. We use first principle molecular dynamics simulation to support this finding, in particular that the covalent bond is broken within the first few atomic layers of the impinged silicon target.

All nitrogen ion implantation was carried out in the GFIS-FIB nanofabrication system [2] located at the Japan Advanced Institute of Science and Technology. Line implantation was carried out on cleaned silicon. Following the cross section preparation STEM observation was conducted. For the 25 keV beam, an implantation depth of ~75 nm is observed, while this decreases to ~35 nm for the case of 16 keV. These values match the theoretically predicted values for the case that two nitrogen atoms are ionized with a single charge (N₂⁺), and split upon impact. The splitting is also predicted by the molecular dynamics simulation we conducted.

These results help to give a clearer picture of the nitrogen ionization in a GFIS and the resulting beam. After ionization of the N₂ molecule through electron tunnelling into the atomically sharp emission tip, the ion is accelerated to the energy $E = E_0$ and focused onto the sample. Upon interaction with the sample surface, the covalent bond is momentarily split. Consequently, each of the nitrogen atoms has only half of the energy $E = E_0/2$. The ion charge is dissipated in the substrate by transfer of an electron.

The help of M. Uno with the usage of the GFIS-FIB is acknowledged. The authors thank M. Ito for the help with TEM cross section preparation. This work is supported by the Center Of Innovation (COI) program of the Japan Science Technology Agency.

[1] R. H. Livengood et. al, *Nucl. Instrum. Methods Phys. Res. Sect. Accel. Spectrometers Detect. Assoc. Equip.*, vol. 645, no. 1, pp. 136–140, Jul. 2011.

[2] F. Aramaki et. al, in *Proc. SPIE 8441*, Yokohama, Japan, 2012, vol. 8441, p. 84410D–84410D–6.

6:00pm **HI+MI+NS-ThA12 Spatially Controlled Ripple Formation in the HIM using Low Voltages and High Temperatures, Gregor Hlawacek, L. Sottili, M. Engler, S. Facsko**, Helmholtz-Zentrum Dresden Rossendorf, Germany

Ripple formation is a well known phenomenon that is observed for many materials under low energy ion bombardment. Often broad beam noble gas ion irradiation using energies of a few keV is employed to create these self-organized patterns on various metal, semiconductor and insulator surfaces. In addition to the fundamental interest in the formation and evolution of these structures they can be utilized in a number of new applications. Creating nano scale periodic roughness can be of interest for various microfluidic applications or to control friction in new MEMS and NEMS devices. However, these applications are not realized at their full potential today as the required sub micron patterning which can not easily be realized using broad beams.

Here, we present for the first time ripple patterns that have been created on the GaAs(001) surface using 5 keV Ne ions and elevated temperatures of up to 600 K in a Helium Ion Microscope (HIM). We will present the home built sample heater that can be loaded through the load lock of the Carl Zeiss Orion NanoFab and describe the influence on the device performance, as well as HIM operation at 5 keV.

The evolution of the ripple wavelength changes from 30 nm at low 1e17 Ne/cm² to 80 nm at 1e18 Ne/cm². The orientation of the ripples with respect to the shape can be changed by rotating the pattern on the surface and the influence of the geometrical constraints of the irradiated area on the ripple pattern is studied.

In-Situ and Operando Spectroscopy and Microscopy for Catalysts, Surfaces, & Materials Focus Topic
Room 101C - Session IS-ThA

Ambient Pressure Photoelectron Spectroscopy and Scanning Probe Techniques

Moderator: Xiao-Ying Yu, Pacific Northwest National Laboratory

2:20pm **IS-ThA1 The Influence of Oxygen on the Catalytic Interaction between CO₂ and Copper studied by High Pressure X-ray Photoelectron Spectroscopy, A. Regoutz, G. Kerherve, I. Villar-Garcia, C.K. Williams, David Payne**, Imperial College London, UK

CO₂ is a source for the production of carbon based fuels, such as methanol, and presents an attractive alternative to fossil fuels. Copper is an ideal catalyst for the reduction of CO₂, as it is able to direct reactions through stable intermediates, e.g. CO. An important question concerns the influence of oxygen on the catalytic activity and whether oxides are formed on the surface. As this system is an excellent material for the reduction of CO₂ a detailed understanding of the basis of its catalytic activity is essential and absolutely necessary for any further development.

X-ray photoelectron spectroscopy (XPS) is used widely in the solid-state sciences but due to its nature as an ultra high vacuum technique (pressure 10⁻⁹ mbar) it is not possible to study gas-solid interfaces. High-pressure XPS (HPXPS) is an advanced method which allows the measurement of solid samples at elevated pressures of between 1 and 30 mbar. This work presents results on the interaction of CO₂ and CO₂/O₂ with the surface of polycrystalline Cu followed by HPXPS. Cu 2p core levels, as well as the Cu L₃M_{4,5}M_{4,5} Auger line are used to investigate the state of the Cu surface. The C 1s and O 1s core levels are used to track the interaction between CO₂/O₂ and Cu and are compared to CO₂/O₂ gas phase measurements.

Ultimately, the presented results provide a starting point for the detailed understanding of these catalysts and lead to the identification of possible ways to further improve and develop their properties.

2:40pm **IS-ThA2 Graphene Membranes for Atmospheric Pressure Photoelectron Spectroscopy, Robert Weatherup, B. Eren, Y. Hao, H. Bluhm, M.B. Salmeron**, Lawrence Berkeley National Laboratory (LBNL)

Determining the chemical state of a catalyst under realistic reaction conditions is of crucial importance in designing catalytic systems with improved activity and selectivity towards sought after products, and a key step in developing or improving existing industrial processes. Ambient pressure X-ray photoelectron spectroscopy APXPS has proved a powerful technique for providing quantitative and surface sensitive (within a few nm) information on the chemical composition of surfaces/interfaces, with commercial analyzers available that allow measurements at pressure in the tens of mbar regime.[1] However numerous reactions of interest occur at atmospheric pressures and above, and thus the behavior observed in existing APXPS systems may not be truly representative of such reactions.

Here we demonstrate atmospheric pressure XPS using single-layer graphene membranes as photoelectron-transparent barriers that sustain pressure differences in excess of 6 orders of magnitude.[2] The graphene-based membranes are produced by transferring graphene grown by chemical vapor deposition,[3] onto metal (Au or Al) coated silicon nitride grids using a polymer-free transfer technique. The graphene serves as a support for catalyst nanoparticles under atmospheric pressure reaction conditions (up to 1.5 bar), where XPS allows the oxidation state of Cu nanoparticles and gas phase species to be simultaneously probed. We thereby observe that the Cu²⁺ oxidation state is stable in O₂ (1 bar) but is spontaneously reduced under vacuum. We further demonstrate the detection of various gas-phase species (Ar, CO, CO₂, N₂, O₂) in the pressure range 10–1500 mbar including species with low photoionization cross sections (He, H₂). Pressure-dependent changes in the apparent binding energies of gas-phase species are observed, attributable to changes in work function of the metal-coated grids supporting the graphene. We expect atmospheric pressure XPS based on this graphene membrane approach to be a valuable tool for studying nanoparticle catalysis.

[1] Starr, D. E.; Liu, Z.; Hävecker, M.; Knop-Gericke, A.; Bluhm, H. Investigation of Solid/vapor Interfaces Using Ambient Pressure X-Ray Photoelectron Spectroscopy. *Chem. Soc. Rev.* **2013**, 42, 5833–5857.

[2] Weatherup, R. S.; Eren, B.; Hao, Y.; Bluhm, H.; Salmeron, M. B. Graphene Membranes for Atmospheric Pressure Photoelectron Spectroscopy. *J. Phys. Chem. Lett.* **2016**, 7, 1622–1627.

Thursday Afternoon, November 10, 2016

[3] Hofmann, S.; Braeuninger-Weimer, P.; Weatherup, R. S. CVD-Enabled Graphene Manufacture and Technology. *J. Phys. Chem. Lett.* **2015**, 6, 2714–2721.

3:00pm IS-ThA3 Development of Graphene Environmental Cells for Atmospheric Pressure Photoelectron Spectroscopy and Microscopy, Andrei Kolmakov, Center for Nanoscale Science and Technology, NIST
INVITED

Atmospheric pressure electron spectroscopy and microscopy are fast growing branches of the chemical and morphological analysis of the practically important interfaces relevant to catalysis, energy storage, harvesting and conversion as well as biomedical research. A great progress in this area achieved so far is largely due to meticulously engineered differentially pumped electron energy analyzers installed now at many laboratories and at synchrotron radiation facilities. Very recently a new approach for truly atmospheric pressure XPS, SEM, and TEM was demonstrated, which radically reduces the requirements to analytic instrumentation and, in principle, makes it possible high-pressure research using the standard laboratory electron spectrometers and microscopes. The core of this method are electron transparent membranes made of novel 2D materials, which separate high-pressure liquid (or gas) sample compartment from the UHV conditions of the spectrometer or microscope. In this report, we survey different designs and application practices of the graphene liquid cells and demonstrate their potential using X-ray Photoelectron Spectroscopy, X-ray Absorption Spectroscopy, Auger Electron Spectroscopy, Photoemission and Scanning Electron Microscopies of liquid interfaces.

4:00pm IS-ThA6 Probing Surface Structural and Chemical Evolutions at Atomic Scale in Bi-metallic Catalysts using In Situ STEM, Miaofang Chi, Oak Ridge National Laboratory; C. Wang, Johns Hopkins University; K. More, Oak Ridge National Laboratory; Y. Xia, Georgia Institute of Technology
INVITED

The catalytic performance of nanocatalysts in terms of activity, selectivity, and durability, is primarily determined by the precise nature of the surface and near-surface atomic configurations. The surface atomic arrangements of nanoparticles (NPs), both in structure and chemistry, however, are highly dynamic during synthesis treatments and reaction conditions. Precisely understanding the complete evolution of NPs as a function of synthesis and reaction environments is imperative towards the rational design of nanocatalysts with optimized performance. With the ability of chemical-sensitive imaging at atomic resolution and the simultaneous acquisitions of electron energy loss spectroscopy (EELS) and energy dispersive X-ray (EDX) analysis, *in situ* scanning transmission electron microscopy (STEM) plays an important role in such studies. In this presentation, we will demonstrate how atomic-scale surface arrangements respond dynamically to *in situ* thermal annealing and gas reaction conditions in bi-metallic nanocatalysts. In particular, by tracking the *same individual* NPs during *in situ* annealing, the influence of post-synthesis treatments on Pt₃Co NPs will be discussed. Five distinct stages of surface elemental rearrangements are discerned at the atomic scale: initial random (alloy) elemental distribution; surface Pt-skin-layer formation; nucleation of structurally ordered domains; ordered framework development; and finally, initiation of amorphization. Furthermore, the responses of surface atomic configurations in alloyed Pd-Au NPs to different reactive environments, including both reducing and oxidizing gases, will be discussed. In both cases, comprehensive interplays among phase evolution, surface faceting, and elemental inter-diffusion are revealed.

Acknowledgements: This work was supported by the Center for Nanophase Materials Sciences, which is U. S. Department of Energy Office of Science User Facility.

4:40pm IS-ThA8 Calculations of Electron Inelastic Mean Free Paths for Liquid Water at Energies from 50 eV to 30 keV, H. Shinotsuka, B. Da, S. Tanuma, H. Yoshikawa, National Institute for Materials Science (NIMS), Japan; Cedric Powell, DR. Penn, National Institute of Standards and Technology

We calculated electron inelastic mean free paths (IMFPs) for liquid water from its optical energy-loss function (ELF) for electron energies from 50 eV to 30 keV. These calculations were made with the relativistic full Penn algorithm (FPA) that has been used for previous IMFP and electron stopping-power calculations for many elemental solids [1]. We also calculated IMFPs of water with three additional algorithms: the relativistic single-pole approximation (SPA), the relativistic simplified SPA, and the relativistic extended Mermin method. These calculations were made using the same optical ELF in order to assess any differences of the IMFPs arising

from choice of the algorithm. We found good agreement among the IMFPs from the four algorithms for energies over 300 eV. For energies less than 100 eV, however, large differences became apparent. IMFPs from the relativistic TPP-2M equation for predicting IMFPs were in good agreement with IMFPs from the four algorithms for energies between 300 eV and 30 keV but there was poorer agreement for lower energies. We made comparisons of our IMFPs with earlier calculations from authors who had used different algorithms and different ELF data sets. IMFP differences could then be analyzed in terms of the algorithms and the data sets. Finally, we compared our IMFPs with measurements of IMFPs and of a related quantity, the effective attenuation length (EAL). There were large variations in the measured IMFPs and EALs (as well as their dependence on electron energy). Further measurements are therefore required to establish consistent data sets and for more detailed comparisons with calculated IMFPs.

[1] H. Shinotsuka, S. Tanuma, C. J. Powell, and D. R. Penn, *Surf. Interface Anal.* **47**, 871 (2015).

5:00pm IS-ThA9 Structural Response of Compact Copper Surfaces to CO Adsorption and its Effects of Reactivity, Baran Eren, G.A. Somorjai, M.B. Salmeron, Lawrence Berkeley National Laboratory (LBNL)

The most compact and stable surfaces of copper, namely the (111), (100), and (110) faces undergo massive reconstructions in the presence of carbon monoxide at room temperature at pressures in the Torr range. They decompose into two-dimensional nanoclusters. This is a double effect of low cohesive energy of copper compared to other active metals and the high gain in adsorption energy at under-coordinated sites. With atomically resolved STM images and DFT calculations we provide a rationale for this behavior. Finally, we show that the surfaces which are broken up into clusters are more active for water dissociation, a key step in the water gas shift reaction.

5:20pm IS-ThA10 Using a Novel In-situ/Operando Chemical Cell to Investigate Surface Reactions such as the Reduction of Oxygen and Surface Oxides, Philipp Kerger, D. Vogel, M. Rohwerder, Max-Planck-Institut fuer Eisenforschung, Germany

A novel in-situ/operando electrochemical cell for doing Ambient Pressure X-ray Photoelectron Spectroscopy (APXPS) studies was developed. The cell allows treating the electrode surface with various preparation techniques such as sputtering and deposition as well as analyse it by XPS and other complementary characterisation methods. The electrode is covered under full electrochemical control by a nanoscopic electrolyte layer. This allows in-situ/operando investigations of electrochemical reactions such as oxygen reduction or oxide reduction by ambient pressure XPS. Examples will be presented and discussed in detail.

5:40pm IS-ThA11 Monitoring of Electrochemical Reactions on Metal Surfaces with Sub-monolayer Sensitivity by Means of Polarization Optical Spectroscopy and EC-STM, Christoph Cobet, M.-H. Chien, R. Sharif, V. Solokha, Gh. Barati, K. Hingerl, Johannes Kepler University, Austria

We combine spectroscopic ellipsometry (SE), reflection anisotropy spectroscopy (RAS), and a homemade electrochemical scanning tunneling microscope (EC-STM) to study the surface of electrodes on the atomic level in liquids i.e. electrochemical environments. This combination of in-situ methods provides complementary information in comparison to conventional cyclic voltammetry (CV). While in CV the integrated charge and ion-exchange is measured, EC-STM provides direct snapshots of the surface morphology and electron corrugation. Polarization optical spectroscopy, on the other hand, is known for high surface/interface sensitivity regarding chemical modifications, sub-monolayer film formation and morphology transformations. The optical information can be additional recorded with almost the same time resolution like in conventional CV and allows the study of reaction kinetics. Thus it is finally possible to relate measured Faraday-currents to different surface processes.

Here, we report on the results on Cu single crystal surfaces of different orientation in halide solutions. The observed processes include halide adsorption, Cu(I) and Cu(II) dissolution, hydrogen evolution, as well as the initial formation of CuO. These studies are motivated by questions concerning e.g. the corrosion behavior and the catalytic functionality of Cu surfaces. The adsorption of Cl on Cu(110) at anodic potentials for example minimizes the surface energy by a formation of monoatomic steps parallel to the [001]-direction which finally ends up in a faceting of the surface. It turns out that some of the characteristic redox peaks in CV correlate with the surface transformation while others relate to a Cu(I) dissolution. The observed morphology transformations compares in parts with the

Thursday Afternoon, November 10, 2016

oxide/chloride induced surface structures as measured UHV. This behavior is only observed at the more "open" and instable (110) surface. The (111) surface, in contrast, retains a smooth surface upon halide adsorption but with a distinct surface reconstruction. At more cathodic potentials we could monitor the hydrogen absorption and the hydrogen gas evolution at Cu surface by RAS and SE, respectively.

6:00pm IS-ThA12 A Liquid-Jet AP-XPS Study of TiO₂ Nanoparticles in an Aqueous Electrolyte Solution, Randima Galhenage, M.J. Makowski, J.M. Langford, J.C. Hemminger, University of California, Irvine

To our knowledge, this is the first attempt to understand a true colloidal titania nanoparticle/water interface using Ambient Pressure X-ray Photoelectron Spectroscopy (AP-XPS). Titania has attracted a significant amount of research interest due to its broad catalytic applications, many of which involve titania nanoparticles in aqueous solution. Therefore, understanding the titania nanoparticle/water interface is critical for the rational development of such systems. Here, we have employed liquid-jet Ambient Pressure X-ray Photoelectron Spectroscopy (AP-XPS) to investigate the solid/liquid interface of 20 nm diameter TiO₂ nanoparticles in 0.1M aqueous nitric acid solution. Liquid-jet AP-XPS experiments were conducted at beamline 11.0.2 of the Advanced Light Source at the Lawrence Berkeley National Laboratory. The temperature controlled liquid jet system generates a 25 μ m diameter liquid beam at a constant flow rate. The jet is irradiated by x-rays of variable photon energies which, therefore, enables us to probe different depths of the solution. Ejected electrons travel through a small aperture and are analyzed by a differentially pumped electrostatic analyzer. A combination of the Ti2p line shape and the absolute binding energies of Ti2p and O1s reflect a stoichiometric titania lattice and no indication of oxygen vacancies (Ti³⁺). Further, by increasing the x-ray excitation energy, the difference in O1s binding energies between that of liquid water (O1s_{liq}) and the titania lattice (O1s_{lat}) oxygen was measured over an increasing experimental probe depth into the particle. The titania lattice, O1s_{lat}, binding energy decreases by 250 meV when probing from the surface into the bulk of the particle. This binding energy difference cannot be accounted for by any other interfacial species as they should have a larger binding energy shifts with respect to the lattice oxygen. Moreover, due to the lack of characteristic Ti³⁺ signal, it is clear that further dissociation of water does not occur on the colloidal particles during the course of our XPS study. The observed change in binding energy is interpreted as downward band bending at the surface, resulting from accumulated charge on the surface of the titania nanoparticle.

MEMS and NEMS

Room 102B - Session MN+2D+NS-ThA

Focused Session on Atomic Layer Nanomechanics and 2D MEMS

Moderators: Wayne Hiebert, National Institute of Nanotechnology & University of Alberta, Canada, Max Zenghui Wang, Case Western Reserve University

2:20pm MN+2D+NS-ThA1 Exploring New Degrees of Freedom by Reducing Dimensions, Lincoln Lauhon, Northwestern University

INVITED
Nanomechanical resonators fabricated additively from 1-D and 2-D nanomaterials present a wealth of scientific opportunities beyond those of conventional resonators fabricated in a subtractive manner from dielectric thin films. This talk will describe the interesting mechanical behaviors of 1-D VO₂ nanowires and 2-D MoS₂ membranes measured by scanning fiber optic interferometry and modeled using finite element methods. In the first case, nanowire resonators provide a compelling platform to investigate and exploit phase transitions coupled to mechanical degrees of freedom because resonator frequencies and quality factors are exquisitely sensitive to changes in state, particularly for discontinuous changes accompanying a first-order phase transition. To that end, correlated scanning fiber-optic interferometry and dual-beam Raman spectroscopy were used to investigate mechanical fluctuations VO₂ nanowires across the first order insulator to metal transition (*Nano Lett.* **14**, 1898 (2014)). Unusually large and controllable changes in resonator frequency were observed due to the influences of domain wall motion and anomalous phonon softening on the effective modulus. In addition, extraordinary static and dynamic displacements were generated by local strain gradients, suggesting new classes of sensors and nanoelectromechanical devices with programmable discrete outputs as a function of continuous inputs. The same interferometric measurement method has been extended to study

thermally driven displacements in square few-layer MoS₂ membranes (*Nano Lett.* **15**, 6727 (2015)). Mechanical mode frequencies can be tuned by more than 12% by optical heating with the above gap illumination, and modes exhibit avoided crossings indicative of strong inter-mode coupling. When the membrane is optically excited at the frequency difference between vibrational modes, normal mode splitting is observed, and the inter-mode energy exchange rate exceeds the mode decay rate by a factor of 15. Finite element and analytical modeling quantifies the extent of mode softening necessary to control inter-mode energy exchange in the strong coupling regime. The observation of strong coupling suggests the feasibility of coherent control of mechanical modes in TMDs resonators, which would provide novel basis for developing phononic devices or exploring mechanical motions that mimic quantum phenomena.

3:00pm MN+2D+NS-ThA3 Manipulating Nonlinearities in 2D NEMS, Akshay Naik, Indian Institute of Science, India

INVITED
Nanoelectromechanical systems (NEMS) are exquisitely sensitive to various stimuli and make fantastic sensors. NEMS devices fabricated using top down fabrication techniques have already demonstrated the ability to measure mass of individual protein macromolecules and their potential use in mass spectrometry applications. NEMS devices fabricated using atomically thin membranes have the potential to bring the resolution of these devices down to single Dalton. However, nonlinearities in these 2D NEMS are quite prominent and can dramatically reduce the dynamic range of these sensors. It is thus imperative to employ strategies to minimize the effect of nonlinearities as well as to exploit them to improve the performance of these devices.

In this talk, I'll present two distinct ways in which we manipulate the nonlinearities in these atomically thin NEMS devices and improve their performance for sensing and oscillator applications. In the first method we manipulate bias voltages and strain in these devices to partially cancel out the nonlinearities present in the system. In the second method, we exploit the strong coupling between various vibrational modes to initiate internal resonance. The frequency stability, and thus the mass resolution, can be improved by orders of magnitude by operating these devices at internal resonances.

4:00pm MN+2D+NS-ThA6 Wide Bandgap β -Ga₂O₃ Nanomechanical Resonators, Xu-Qian Zheng, S. Rafique, J. Lee, L. Han, C.A. Zorman, H. Zhao, P.X.-L. Feng, Case Western Reserve University

Among wide bandgap oxide semiconductors, β -Ga₂O₃ has recently been emerging as a promising candidate for future high-power electronics. Thanks to its direct wide bandgap, $E_g \approx 4.9$ eV [1,2], power devices made of β -Ga₂O₃ may provide higher breakdown voltage even than that in high-power devices based on mainstream 4H-SiC and GaN materials. In addition to its excellent chemical and thermal stability [1, 2], β -Ga₂O₃ also possesses excellent mechanical properties (Young's modulus, $E_Y \approx 300$ GPa) [3], providing opportunities for creating next generation nano- and micro-electromechanical systems (NEMS and MEMS) which can be suited for operations in harsh and extreme environments.

In this work, we describe the construction of β -Ga₂O₃ nanosheets and their suspended structures, toward the first demonstration of vibrating β -Ga₂O₃ drumhead nanomechanical resonators. The nanomaterials were synthesized on 3C-SiC film covered Si substrate using a growth temperature of 950°C for 1.5hrs. No metal catalyst was used for the synthesis of the nanomaterials. The nanosheets have a width of ~ 7 μ m and thickness of ~ 20 -140 nm. The crystal structure and the morphology of the nanosheets were investigated by field emission scanning electron microscopy (FESEM) and transmission electron microscopy (TEM). From high resolution FESEM image, it was confirmed that the nanosheets originated from the sidewall of the nanorods. The selected area electron diffraction pattern (SAED) taken along the [10-1] zone axis reveals that the synthesized nanosheets are single crystalline β -Ga₂O₃. We investigate the elastic properties and resonant characteristics of such devices, by measuring flexural-mode resonances using ultrasensitive laser interferometry. We fabricate circular drumhead β -Ga₂O₃ resonators with a diameter of ~ 3 μ m using a dry transfer technique. Then, by measuring undriven thermomechanical noise spectra of β -Ga₂O₃ resonators, we observe the resonance characteristics of such resonators at 37 MHz to 66 MHz in high frequency (HF) range with quality (Q) factors ranging 100 to 420. In addition, we observe static mechanical behaviors of β -Ga₂O₃. We perform nano-indentation on these drumhead structures using AFM tips to further study the elastic modulus of β -Ga₂O₃. By combining measured elastic properties from resonances and nano-indentation, this study provides quantitative understanding of mechanical

Thursday Afternoon, November 10, 2016

properties of β -Ga₂O₃, and paves the way for future nanomechanical devices engineering based on this new crystal.

- [1] S. Rafique, *et al.*, *Phys. Status Solidi (a)* **213**, 1002-1009 (2016).
- [2] S. Rafique, *et al.*, *Cryst. Growth Des.* **16**, 511-517 (2016).
- [3] M.-F. Yu, *et al.*, *IEEE Sensors J.* **5**, 20-25 (2005).
- [4] R. Yang, *et al.*, *J. Vac. Sci. & Tech. B* **32**, 061203 (2014).

4:20pm MN+2D+NS-ThA7 Nonlinear Mode Coupling and Internal Resonances in MoS₂ Nanoelectromechanical System, Chandan Samanta, P. Gangavarapu, A.K. Naik, Indian Institute of Science, India

Molybdenum-disulphide (MoS₂), a layered material has attracted attention for nanoelectro-mechanical system (NEMS) applications due to its ultralow mass density and extraordinary mechanical properties. Along with this, its direct band gap of 1.8eV (for monolayer MoS₂) offers the possibility of a new kind of transducer where its mechanical properties can be strongly coupled to its optical properties in visible range. MoS₂-NEMS has been realized recently using optical detection technique. This approach has its own difficulties to drive the resonator into nonlinear regime. On the other hand, mechanical nonlinearities play a crucial role in the performance of NEMS as its dimension shrinks down to atomically thin membrane. A clear understanding of nonlinear effects and the ability to control them are important from both fundamental and application points of view. In this report, we demonstrate fabrication of few layer MoS₂-NEMS and its characterization by three distinct all electrical actuation and detection schemes. We are able to detect multiple vibrational modes in our devices using all the three schemes. We are also able to drive the devices deep into nonlinear regime. Our devices show strong nonlinear coupling between multiple modes. The nonlinear modal coupling is so strong that it leads to multiple internal resonances. Although, there is a report on internal resonance in micromechanical system (MEMS), there is no reported evidence of internal resonance in NEMS made from atomically thin membrane. The observed internal resonances in our devices open the possibility for realizing high stability oscillator in very high frequency range.

4:40pm MN+2D+NS-ThA8 Very-High-Frequency (VHF) Molybdenum Disulfide (MoS₂) Nanomechanical Resonators Operating in Liquid, H. Jia, Rui Yang, P.X.-L. Feng, Case Western Reserve University

Micro/nanoelectromechanical systems (NEMS/NEMS) have demonstrated versatile device technologies for sensing applications by exploiting their miniaturized dimensions and increasing sensitivities upon scaling.^{1,2} However, quite limited flexural-mode resonators (mostly cantilevers and doubly-clamped beams) have been reported, with only fundamental-modes are often utilized that suffer from very low quality factors ($Q < 5$) in viscous media.³⁻⁶

In this work, we experimentally demonstrate the operation of molybdenum disulfide (MoS₂) nanoscale drumhead resonators (1–5 μ m in diameter, 50–60nm in thickness) in fluidic environment (water), which exhibit robust multimode resonances in the high- and very-high-frequency (HF/VHF) bands. We observe ~ 10 flexural modes up to ~ 150 MHz in water. The Q factors can easily exceed 10 for fundamental modes, and achieve as high as ~ 30 for higher modes.

Atomic-layer MoS₂, an emerging two-dimensional semiconductor, has attracted tremendous attention due to its ultralight weight and high surface-to-volume ratio. These attributes suggest that MoS₂ nanoresonators hold potential for ultrasensitive sensing capabilities even in fluids. Meanwhile, drumhead structure exhibits sealed air cavity and multimode resonance characteristics, which help maintain device performance in liquid.

The MoS₂ resonators are directly immersed in water, and optothermally driven by an amplitude-modulated 405nm diode laser. The multimode resonances are interferometrically read out using a 603nm He-Ne laser. We observe ~ 10 flexural modes up to ~ 150 MHz with Q factors exceeding 10 for fundamental modes, and reach as high as ~ 30 for higher modes in water. We attribute the improved resonance performance (higher f and Q , as compared to cantilever beams) to the drumhead structure consisting of an air cavity on one side. We also demonstrate the degradation of resonance characteristics (f , Q dramatically drop) if water gradually leaks into the imperfectly-sealed nanodrum cavities.

- [1] J.L. Arlett, *et al.*, *Nature Nanotech.* **6**, 2011.
- [2] B.N. Johnson, *et al.*, *Biosens. Bioelectron.* **32**, 2012.
- [3] J. Tamayo, *et al.*, *Ultramicroscopy* **86**, 2001.
- [4] A. Vidic, *et al.*, *Ultramicroscopy* **97**, 2003.

[5] S.S. Verbridge, *et al.*, *Nano. Lett.* **6**, 2006.

[6] A.P. Davila, *et al.*, *Biosens. Bioelectron.* **22**, 2007.

Nanometer-scale Science and Technology Room 101D - Session NS+BI-ThA

Applied Nanoscale Microscopy Techniques/Biomaterial Interfaces – New Advances

Moderators: Stephanie Allen, The University of Nottingham, UK, Leonidas Ocola, Argonne National Laboratory

2:40pm NS+BI-ThA2 Advancing the Development of Nanocrystal Emitters via Advanced Electron Microscopy Techniques, James McBride, K.R. Reid, S.J. Rosenthal, Vanderbilt University

The key tool for the characterization of nanoparticles has long been transmission electron microscopy. This technique can provide the size, shape, crystal structure and chemical composition of a nanocrystal. Aberration-corrected Z-STEM has enabled the visualization of the true core/shell structure of colloidal quantum dots, accelerating their commercial development.¹ Through dynamic STEM movies we have visualized the beam-induced motion of the surface atoms of nanocrystals and learned about the instability of the atomic structure of ultrasmall nanocrystals and the surface/sub-surface of large nanocrystals.² However, Z-contrast can be difficult to directly interpret due to the choice in shell material or uncertainty of the 3D morphology of large, thick-shelled quantum dots. Advancements in the detector design for performing STEM energy dispersive spectroscopy mapping (STEM-EDS) have greatly facilitated the chemical imaging of nanocrystals, enabling rapid identification of their chemical structure before significant beam damage occurs. With this technological advance, we have obtained the chemical composition of an individual nanocrystal and directly correlated to its individual photophysics using our recently developed correlation technique.³ The unique combination of optical, structural and chemical information allowed us to determine the origin of the low quantum yield plaguing non-blinking CdSe/CdS quantum dots.⁴ Further, STEM-EDS imaging will be presented showing development of InP/CdS and Zn₃N₂ nanocrystals. Included in the presentation will be specifics on sample preparation and the choice of beam current/spatial resolution and sample damage.

1. McBride, J.; Treadway, J.; Feldman, L.C.; Pennycook, S.J.; Rosenthal, S.J. Structural Basis for Near Unity Quantum Yield Core/Shell Nanocrystals *Nano Lett.* **2006**, *6* (7), 1496-1501.

2. McBride, J.R.; Pennycook, T.J.; Pennycook, S.J.; Rosenthal, S.J. The Possibility and Implications of Dynamic Nanoparticle Surfaces *ACS Nano* **2013**, *7* (10), 8358-8365.

3. Orfield, N.J.; McBride, J.R.; Keene, J.D.; Davis, L.M.; Rosenthal, S.J. Correlation of Atomic Structure and Photoluminescence of the Same Quantum Dot: Pinpointing Surface and Internal Defects That Inhibit Photoluminescence *ACS Nano* **2015**, *9* (1), 831-839.

4. Orfield, N.J.; McBride, J.R.; Wang, F.; Buck, M.R.; Keene, J.D.; Reid, K.R.; Htoon, H.; Hollingsworth, J.A.; Rosenthal, S.J. Quantum Yield Heterogeneity among Single Nonblinking Quantum Dots Revealed by Atomic Structure-Quantum Optics Correlation *ACS Nano* **2016**, *10* (2), 1960-1968.

3:00pm NS+BI-ThA3 Demonstration of Electron Mirror for Quantum Electron Microscopy, Navid Abedzadeh, C.S. Kim, R.G. Hobbs, K.K. Berggren, MIT

Electron mirrors have been used in electron microscopy techniques such as low-energy electron microscopy, mirror-corrected scanning electron microscopy and photoemission electron microscopy due to their ability to introduce chromatic and spherical aberrations of arbitrary sign. More recently, a design for a quantum electron microscope (QEM), an imaging approach based on interaction-free measurement, was proposed that could take advantage of an electron mirror whose surface was patterned with a topographic grating. This grating would produce a periodically varying potential close to its surface when a voltage was applied. As a result, the grating would diffract an incident electron plane wave, presenting an opportunity to develop a low-loss electron beam splitter. The diffracted beams produced by such a beam splitter could be used to probe a sample within an electron cavity to achieve an interaction-free measurement. An electron cavity could be formed when another electron mirror is placed slightly behind the back focal plane of the grating mirror. If a sample were placed inside this cavity, repeated weak interactions with

Thursday Afternoon, November 10, 2016

the reflected/diffracted electron beam can be used to image the sample while keeping beam-induced sample damage arbitrarily low.

The approach outlined here will be used to characterize diffraction from the patterned mirror surface. Demonstration of electron diffraction from a patterned surface in a FESEM will represent a significant advancement toward the demonstration of a QEM system.

3:20pm **NS+BI-ThA4 Nanoscale Chemical Imaging by Photo-induced Force Microscopy**, *Ryan Murdick*, Molecular Vista

Nanoscale Chemical Imaging with Photo-induced Force Microscopy

Sung Park

Molecular Vista, Inc.

Infrared Photo-induced Force Microscopy (IR PiFM) is based on an atomic force microscopy (AFM) platform that is coupled to a widely tunable mid-IR laser. PiFM measures the dipole induced at or near the surface of a sample by an excitation light source by detecting the dipole-dipole force that exists between the induced dipole in the sample and the mirror image dipole in the metallic AFM tip. This interaction is strongly affected by the optical absorption spectrum of the sample, thereby providing a significant spectral contrast mechanism which can be used to differentiate between chemical species. Due to its AFM heritage, PiFM acquires both the topography and spectral images concurrently and naturally provides information on the relationship between local chemistry and topology. Due to the steep dipole-dipole force dependence on the tip-sample gap distance, PiFM spectral images have spatial resolution approaching the topographic resolution of AFM, demonstrating sub 10 nm spatial resolution on a variety of samples. PiFM spectral images surpass spectral images that are generated via other techniques such as scanning transmission X-ray microscopy (based on synchrotron source), micro confocal Raman microscopy, and electron microscopes, both in spatial resolution and chemical specificity. The breadth of the capabilities of PiFM will be highlighted by presenting data on various organic, inorganic, and low dimensional materials. By enabling imaging at the nm-scale with chemical specificity, PiFM provides a powerful new analytical method for deepening our understanding of nanomaterials and facilitating technological applications of such materials.

Bio: Sung Park is the CEO of Molecular Vista, which he co-founded with Prof. Kumar Wickramasinghe (UC Irvine, formerly of IBM) in 2011 to provide research and industrial tools for rapid and nanoscale imaging with chemical identification. Sung has 25 years of experience of industrial R&D, engineering, marketing and sales, and operations. Sung co-founded Park Scientific Instruments (PSI), which was one of the first commercial companies to develop and sell scanning tunneling microscopes (STM) and atomic force microscopes (AFM); PSI was acquired by Thermo Instruments in 1997, by which point PSI had sold upwards of 1,000 instruments to customers worldwide. Prior to founding Park Scientific Instruments, Sung worked as a post-doc at IBM Watson Research Center. Sung earned a Ph.D. in Applied Physics from Stanford University and BA in Physics from Pomona College.

4:00pm **NS+BI-ThA6 Strong Coupling of Localized Surface Plasmon Resonances to Light-Harvesting Complexes from Plants and Bacteria**, *A. Tsargorodskaya, M. Cartron, C. Vasilev*, University of Sheffield, UK; *G. Kodali*, University of Pennsylvania; *J. Baumberg*, University of Cambridge, UK; *PL Dutton*, University of Pennsylvania; *CN. Hunter*, University of Sheffield, UK; *P. Torma*, University of Aalto; *Graham Leggett*, University of Sheffield, UK

Plants and bacteria harvest solar energy with extraordinary efficiency. In chloroplasts, the quantum efficiency, defined as the fraction of captured photons that goes on to cause charge separation, is estimated to be ca. 90%. The mechanisms by which such extraordinary efficiencies are realised have been the subject of intense interest. We have explored the potential offered by plasmonic techniques for the investigation of biological light harvesting complexes. Macroscopically extended arrays of gold nanostructures are fabricated by interferometric exposure of an alkythiolate SAM on gold, enabling the fabrication of macroscopically extended arrays of gold nanostructures in a rapid, simple process. After annealing, these structures yield strong localized surface plasmon resonances (LSPRs). In contrast to the behaviour observed for most proteins, the LSPRs are split when light-harvesting membrane proteins from purple bacteria and plants are attached to the gold nanostructures, yielding pronounced changes in their extinction spectra. The splitting is large, and is different for mutant proteins containing different pigment molecules, indicating that it is sensitive to the electronic structures of the membrane proteins. The splitting is attributed to strong coupling between

the LSPRs and excitons in the light-harvesting complexes. The splitting is suggestive of an asymmetric Fano-type resonance, and the plasmon-exciton coupling has been modelled with coupled harmonic oscillators. The model yields good fits to the experimental spectra. It indicates that in light harvesting complexes 1 and 2 (LH1/2) from purple bacteria, coupling to the carotenoid S2 state dominates, with a strength of ~ 0.2 eV. However, in a carotenoid-free mutant of LH1 the LSPR couples with a strength of ~ 0.1 eV to the bacteriochlorophyll Q_x transition, which has a smaller transition dipole moment than do the carotenoids. The coupling varies with the square root of the surface coverage of the protein, consistent with strong coupling theory. Strong coupling was also observed for self-assembling polypeptide maquettes that contain only chlorins. However, it was not observed for monolayers of bacteriochlorophyll, indicating that strong plasmon-exciton coupling is sensitive to the specific presentation of the pigment molecules.

4:20pm **NS+BI-ThA7 Microfluidic Device For Aptamer-Based Cancer Cell Capture And Genetic Mutation Detection**, *Sarah Reinhold, H.G. Craighead*, Cornell University

Genetic mutations in cancer cells are not only fundamental to the disease, but can also have tremendous impact on the efficacy of treatment. Identification of specific key mutations in a timely and cost-effective way would allow clinicians to better prescribe the most effective treatment options. Here, we present a novel microfluidic device as a platform for specifically capturing cancer cells and isolating their genomic DNA (gDNA) for specific amplification and sequence analysis. To filter out rare cancer cells from a complex mixture containing a diversity of cells, nucleic acid aptamers that specifically bind to cancer cells are immobilized within a microchannel containing micropillars to increase capture efficiency. The captured cells are then lysed and the gDNA is isolated via physical entanglement within a secondary micropillar array. This type of isolation allows the gDNA to be retained within the channel, and enables multiple consecutive rounds of isothermal amplification in which different individual genes are amplified separately. The amplified gene samples undergo sequencing, and the resulting sequence information is compared against the known wildtype gene to identify any mutations. Cervical and ovarian cancer cells have been initially tested for mutations in the *TP53* gene using this technology. This approach offers a way to monitor multiple genetic mutations in the same small population of cells, which is beneficial given the wide diversity in cancer cells, and requires very few cells to be extracted from the patient sample. With this capability for genetic monitoring, precision medicine should be more accessible for the treatment of cancer.

4:40pm **NS+BI-ThA8 Molecular Processes in an Electrochemical Clozapine Sensor**, *Thomas Winkler*, University of Maryland, College Park; *S.L. Brady*, East Carolina University; *E. Kim*, University of Maryland, College Park; *H. Ben-Yoav*, Ben-Gurion University of the Negev, Israel; *D.L. Kelly*, University of Maryland, Baltimore; *G.F. Payne*, *R. Ghodssi*, University of Maryland, College Park

Selectivity presents a crucial challenge in electrochemical sensing. One example is schizophrenia treatment monitoring of the redox-active antipsychotic clozapine (CLZ). To accurately assess efficacy, differentiation from its metabolite *N*-desmethylclozapine (NDMC) – similar in structure and redox potential – is critical. Here, we leverage biomaterials integration to study, and effect changes in, diffusion and electron transfer kinetics of these compounds. A key finding in our present work is differing dynamics between CLZ and NDMC once we interface the electrodes with chitosan-based biomaterial films. These additional dimensions of redox information can thus enable selective sensing of largely analogous small molecules.

Our study utilizes gold working electrodes either bare, coated with chitosan, or with our previously demonstrated redox cycling system (RCS). In the RCS, electrodeposited chitosan serves as a matrix to immobilize electroactive catechol near the electrode *via* electrografting. Small redox species diffuse through the film for oxidation at the electrode; the nearby catechol enables subsequent reduction of the analyte, establishing a signal-amplifying redox cycle. We execute cyclic voltammetry at 1m–10V/s sweep rates with CLZ, NDMC, or the model redox couple 1,1'-ferrocenedimethanol (FC).

With bare gold, both CLZ and NDMC exhibit similar ($R^2=0.99$) drastic increases in peak separation even at 0.5V/s, indicating slow electron transfer kinetics, in contrast to FC (Nernstian up to 3V/s). With both chitosan and the RCS we find that similarity broken. For diffusion, the coefficients *D* reveal two regimes in chitosan: dominance of bulk solution below 10mV/s (values match those from bare gold and theory), and

Thursday Afternoon, November 10, 2016

diffusion inside the film becoming limiting at higher scan rates. This is reflected in D decreasing by $1.9\times$ for FC, $17\times$ for CLZ, and $31\times$ for NDMC. The sharp difference between FC and the other larger two suggests a size-restriction phenomenon. The consistently $2\times$ lower D for NDMC over the similarly sized CLZ points to possible electrostatic effects. With the RCS, signal amplification translates into apparent D increases – $9\times$ over bare for FC, $5\times$ for CLZ, and $3\times$ for NDMC. Only at high scan rates does D decrease toward the chitosan-only value as true diffusion asserts dominance.

In conclusion, our results demonstrate the intricate interplay between biomaterials, biomolecules, and electrochemistry. They reveal intriguing distinguishing characteristics of CLZ from both the largely analogous NDMC as well as the model FC. This opens up avenues of utilizing diffusion and kinetics information to enhance selectivity in electrochemical sensing.

5:00pm NS+BI-ThA9 Quantitative Quartz Crystal Microbalance Measurements across Transients Produced by Switching Fluid Properties, V. Mugnaini, Dmitri Petrovykh, International Iberian Nanotechnology Laboratory, Portugal

We systematically investigated Quartz Crystal Microbalance with Dissipation (QCM-D) measurements in aqueous solutions of model strong electrolytes that are commonly used in experiments with biological surfaces. In particular, we examined the quantitative behavior of both frequency and dissipation responses in transitions between two different aqueous solutions.

The abrupt changes in the QCM-D responses upon such transitions are sometimes referred to as “jumps” associated with switching the bulk properties of the fluid flowing through the QCM-D cell. Switching between fluids of different compositions may be important in a variety of QCM-D measurements for biointerfaces, e.g., when switching between a baseline/rinsing solution and a measurement solution, or switching between optimal buffers used for probe immobilization and for biorecognition steps [1-3]. In specialized quantitative biointerface measurements, such as measuring stabilities of DNA hybrids [2-3], switching among different solutions multiple times actually provides the basis for the measurement.

In typical QCM-D measurements, the baseline is reset after a “bulk jump”, so the data are typically only quantified between any transients, but not across them, i.e., quantification is carried out for a constant fluid composition, but not between different fluids. By considering the underlying viscoelastic formalism [4-5], we demonstrate in a series of systematic measurements for solutions of strong electrolytes that the QCM-D responses upon switching between different solutions can be quantitatively predicted and exhibit interesting scaling behavior. Classical theory of the viscosity of electrolyte solutions provides additional insight into correlations between the results measured for different salts.

[1] D. Y. Petrovykh, H. Kimura-Suda, L. J. Whitman, M. J. Tarlov, J. Am. Chem. Soc. 125, 5219 (2003)

[2] S. M. Schreiner, D. F. Shudy, A. L. Hatch, A. Opdahl, L. J. Whitman, D. Y. Petrovykh, Anal. Chem. 82, 2803 (2010)

[3] S. M. Schreiner, A. L. Hatch, D. F. Shudy, D. R. Howard, C. Howell, J. Zhao, P. Koelsch, M. Zharnikov, D. Y. Petrovykh, A. Opdahl, Anal. Chem. 83, 4288 (2011)

[4] K. K. Kanazawa, J. G. Gordon II, Anal. Chim. Acta, 175, 99 (1985)

[5] M. Rodahl, F. Höök, A. Krozer, P. Brzezinski, B. Kasemo, Rev. Sci. Instrum. 66, 3924 (1995)

5:20pm NS+BI-ThA10 ToF-SIMS/XPS Characterization of Frozen-Hydrated Hydrogels, Michael Taylor, M.R. Alexander, The University of Nottingham, UK; **M. Zelzer,** National Physical Laboratory, UK

Over the last decade the beneficial properties of hydrogels as artificial cell culture supports have been extensively investigated¹. Certain synthetic hydrogels have been proposed to be similar in composition and structure to the native extracellular matrix of the stem cell niche, their *in vivo* cell habitat, which is a powerful component in controlling stem cell fate². The stem cell differentiation pathway taken is influenced by a number of factors. When culturing cells within or upon hydrogels this choice can be strongly dependent on the underlying 3D hydrogel chemistry which strongly influences hydrogel-cell interactions³. The interrelationship between hydrogel chemistry and that of biomolecules in controlling cellular response ideally requires analysis methods to characterise the chemistry without labels and often in 3D. Time-of-flight secondary ion mass spectrometry (ToF SIMS) has the potential to be utilised for through thickness characterisation of hydrogels. The frozen-hydrated sample

format is well suited to minimise changes associated with dehydration or the chemical complexity of ‘fixation’, a challenging aspect in vacuum analysis conditions⁴. Frost formation can occur in the ambient atmosphere preventing ready depth profiling of the frozen hydrogels⁵. We develop a simple method to remove this frost by blowing with gas prior to entry into the instrument which is shown to produce remarkably good profiles on a poly(2-hydroxyethyl methacrylate) (pHEMA) hydrogel film where a model protein, lysozyme, is incorporated to demonstrate how biomolecule distribution within hydrogels can be determined. A comparison of lysozyme incorporation is made between the situation where the protein is present in the polymer dip coating solution and lysozyme is a component of the incubation medium. It is shown that protonated water clusters $H(H_2O)_n^+$ where $n=5-11$ that are indicative of ice are detected through the entire thickness of the pHEMA and the lysozyme distribution through the pHEMA hydrogel films can be determined using the intensity of characteristic fragment secondary ions. We also expand the developed methodology to X-Ray Photoelectron Spectroscopy (XPS) for through thickness analysis of the similar pHEMA / lysozyme hydrogels, and show that lysozyme distribution can be quantitatively mapped in hydrogels.

5:40pm NS+BI-ThA11 GCIB-SIMS for Studying Bacterial Surfaces, John Stephen Fletcher, P. Wehrli, University of Gothenburg, Sweden; **A. Farewell,** University of Gothenburg, Sweden; **T.B. Angerer, J. Gottfries,** University of Gothenburg, Sweden

For many years ToF-SIMS has shown the promise of delivering new information of direct relevance to biological research. However, inadequacies in the ability to generate intact molecular ion species and then detect them with precise mass resolution and accuracy have held the technique back. Recent advances in ToF-SIMS, through the implementation of gas cluster ion beams (GCIBs) coupled to non-conventional MS systems, now permit the analysis of higher mass species from native, underivatized, biological specimen i.e. intact bacterial cells. Being able to characterise and understand changes in bacterial biochemistry as a result of environmental, biological or pharmacological stress is critical to address the global challenge of antibiotic resistance. For example, *E. coli* is able to rapidly adjust the biophysical properties of its membrane phospholipids to adapt to environmental challenges including starvation stress. Here, these membrane lipid modifications were investigated in glucose starved *E. coli* cultures and compared to a *DrelADspoT* (ppGpp⁰) mutant strain of *E. coli*, deficient in the stringent response, by means of time-of-flight secondary ion mass spectrometry (ToF-SIMS). Cultures in stationary phase were found to exhibit a radically different lipid composition as compared to cultures in exponential growth phase. Wild-type *E. coli* reacted upon carbon starvation by lipid modifications including elongation, cyclopropanation and increased cardiolipin formation. Observations are consistent with variants of cardiolipins (CL), phosphatidylglycerols (PG), phosphatidylethanolamines (PE), phosphatidic acids (PA), and fatty acids. Notably, despite having a proteomic profile and a gene expression profile somewhat similar to the wild-type during growth, the ppGpp⁰ mutant *E. coli* strain was found to exhibit modified phospholipids corresponding to unsaturated analogues of those found in the wild-type. We concluded that the ppGpp⁰ mutant reacts upon starvation stress by elongation and desaturation of fatty acyl chains, implying that only the last step of the lipid modification, the cyclopropanation, is under stringent control. These observations suggest alternative stress response mechanisms and illustrate the role of the RelA and SpoT enzymes in the biosynthetic pathway underlying these lipid modifications.

**Plasma Science and Technology
Room 104B - Session PS-ThA**

Plasma Chemistry and Plasma Surface Interactions

Moderator: Steven Vitale, MIT Lincoln Laboratory

2:20pm PS-ThA1 Nonthermal Plasma Driven Power to Gas, Tomohiro Nozaki, Tokyo Institute of Technology, Japan

INVITED

Renewable energy is recognized as indispensable CO₂-free energy source in our future society and tremendous increase in renewable energy has been demanded worldwide. However, it is also well-known that energy generation and timing strongly fluctuate depending on the climate and geological conditions. Energy storage by secondary batteries and smart grid concept have been investigated extensively by now. More recently, power to gas (PtG) concept is highlighted. The key component of PtG is the electrochemical conversion of H₂O into H₂ and O₂ with renewable electricity, enabling direct conversion of electrical energy to chemical

energy. Basic concept of PtG can be extended to the synthetic CH₄ production from CO₂ and renewable hydrogen for increased energy storability and transportability. The key strategy is that electrochemical H₂O conversion and conventional C1 chemistry, which utilizes thermal energy at various temperature range, is combined appropriately in order to maximize overall electrical to chemical conversion processes.

In this study, nonthermal plasma enhanced catalytic conversion of CH₄ and CO₂ into syngas (CO and H₂) is presented. Electrical energy is converted into chemical energy of syngas via nonthermal plasma (electrical energy) driven endothermic reaction. Syngas is then converted into not only CH₄, but also carbon containing liquid fuels with the existing C1 chemistry. Liquid hydrocarbon would be more preferable than synthetic CH₄ because transport and storage capability of liquid hydrocarbons is improved with great flexibilities. CH₄ and CO₂ reforming is known as dry methane reforming (DMR): CO₂ can be oxidizer as well as carbon source for C1 chemistry. There are two major problems in DMR: one is coke formation which readily deteriorates catalyst activity. The other is high temperature thermal energy is needed (above 800 °C). Therefore, combustion of initial feed is unavoidable. Nonthermal plasma enables low temperature conversion of CH₄ and CO₂ at relatively low temperature (below 600 °C), yet fast reforming is guaranteed because plasma-generated reactive species promote catalytic surface reaction. We have developed pulsed dry methane reforming as comprehensive diagnostic method of plasma catalytic methane reforming [1]. This diagnostic method is further enhanced by the combination of optical emission spectroscopy, isotope labeling, and admixture of reaction promoters. In the symposium, mechanistic study of plasma catalysis and prospects for practical application (PtG) will be presented.

[1] S. Kameshima, K. Tamura, Y. Ishibashi, T. Nozaki, *Catalysis Today*, **256** (2015) 67-75.

3:00pm PS-ThA3 Plasma-based CO₂ Conversion: Experiments and Modeling, A. Bogaerts, *Ramses Snoeckx*, University of Antwerp, Belgium INVITED

Plasma-based CO₂ conversion is gaining increasing interest. We try to obtain better insight in the underlying mechanisms by experiments and computer modeling. Our experiments are carried out in a (packed bed) DBD and in a vortex-flow gliding arc (GA) reactor, focusing mainly on the conversion and energy efficiency at different conditions and reactor setups. Our model calculations focus especially on the detailed plasma chemistry in a DBD, GA and microwave (MW) plasma, for pure CO₂ as well as mixtures of CO₂ with N₂, CH₄ and H₂O. For this purpose, we make use of a zero-dimensional chemical kinetics model.

When studying the plasma chemistry in pure CO₂, we focus especially on the the role of vibrationally excited CO₂ levels, which are the key species for enhanced energy efficiency of the CO₂ conversion [1].

We have also studied the plasma chemistry in CO₂/CH₄ [2,3] and in CO₂/H₂O [4] mixtures in a DBD reactor, for producing value-added chemicals. The main products formed are a mixture of H₂ and CO, or syngas, with a tuneable H₂/CO ratio depending on the gas mixing ratio. The production of oxygenated compounds is very limited. A detailed chemical kinetics analysis allows to elucidate the different pathways leading to the observed results, and to propose solutions on how to improve the formation of value-added products.

Finally, we also studied the plasma chemistry in a CO₂/N₂ mixture, both in a DBD [5] and in a MW [6] plasma, to investigate the effect of this important impurity in effluent gases on the CO₂ conversion, energy efficiency and product formation. Our model and experiments reveal that N₂O and NO_x compounds are produced in the range of several 100 ppm. The reaction pathways for the formation of these compounds are again explained based on a kinetic analysis, which allows proposing solutions on how to prevent the formation of these harmful compounds.

References

1. T. Kozák, A. Bogaerts, *Plasma Sources Sci. Technol.* **23** (2014) 045004.
2. R. Snoeckx, R. Aerts, X. Tu, A. Bogaerts, *J. Phys. Chem. C* **117** (2013) 4957-4970.
3. R. Snoeckx, Y.X. Zeng, X. Tu, A. Bogaerts, *RSC Advances* **5** (2015) 29799-29808.
4. R. Snoeckx, A. Ozkan, F. Reniers and A. Bogaerts, paper in preparation.
5. S. Heijckers, R. Snoeckx, T. Kozák, T. Silva, T. Godfroid, N. Britun, R. Snyders and A. Bogaerts, *J. Phys. Chem. C* **119** (2015) 12815-12828.

6. R. Snoeckx, S. Heijckers, K. Van Wesenbeeck, S. Lenaerts and A. Bogaerts, *Energy & Environm. Sci.* **9** (2016) 999-1011

4:00pm PS-ThA6 Revisiting HgCdTe Etching Mechanism in High Density CH₄-H₂ Plasmas in Terms of Langmuir Adsorption Kinetics and Taking into Account Etching Inhibition, *Christophe Cardinaud*, A. Pageau, CNRS - IMN, France; L. Le Brizoual, IETR - Univ. Rennes, France; F. Boulard, J. Baylet, CEA, LETI, MINATEC Campus, France

In the past 20 years, intrinsic properties of Hg_(1-x)Cd_xTe have placed this semiconductor compound as the standard material for the fabrication of high performance infrared detection devices [1]. CH₄-H₂ based plasmas have proven to be efficient to etch HgCdTe [2]. In terms of mechanism, it is usually admitted that methyl radicals, coming from the dissociation of methane CH₄, form volatile metal organic species, mainly Cd(CH₃)₂ and Te(CH₃)₂, while atomic hydrogen, coming from CH₄ and H₂ dissociation, forms volatile TeH₂, and that Hg, due to its high vapor pressure, desorbs spontaneously from the surface. Strong Cd accumulation is always observed on the processed surface, underlining that Cd removal is the limiting step of HgCdTe plasma etching. In a previous study we have identified that the surface stoichiometry change appears as soon as the etching starts and that the etch rate is closely related to the incoming flux of methyl species [3]. Consequently, the Hg_(1-x)Cd_xTe alloy removal takes place through a Cd-rich surface layer rather than through the bulk material itself. Low-pressure high-density plasma sources and independent control of sample bias enable operation of the process with more chemical than physical etching mechanisms. Such conditions should meet the main fabrication requirements: high anisotropy, smooth sidewalls, reasonable etch rate, and low level of surface damage. However they typically fall in the HgCdTe etching / hydrocarbon deposition borderline.

Plasma-surface interaction mechanisms are investigated when varying source power, sample bias, CH₄ flow rate and total pressure. Mass spectrometry and electrostatic probes are respectively used to evaluate methyl and positive ion flux onto the surface. X-ray photoelectron spectroscopy provides surface composition. Results and etch rate measurements are discussed in the view of an ion-neutral species synergy model based on Langmuir adsorption kinetics [4] and taking into account the competition between hydrocarbon film formation and HgCdTe etching.

- 1 A. Rogalski, *Infrared Phys. and Technol.* (2011) **54**, 136
- 2 R.C. Keller, M. Seelmann-Eggbert, and H.J. Richter, *J. Electron. Mater.* (1995) **24**, 1155
- 3 F. Boulard, J. Baylet, and C. Cardinaud, *J. Vac. Sci. Technol. A* (2009) **27**, 855
- 4 T.M. Mayer and R.A. Barker, *J. Vac. Sci. Technol.* (1982) **21**, 757

4:20pm PS-ThA7 Temporal Evolution of Surface Chemistry in Ion and Radical Dominated Etch of Hydrocarbon Polymers, *Barton Lane*, P. Ventzek, N. Eibagi, Tokyo Electron America, Inc.; A. Ranjan, V. Rastogi, TEL Technology Center, America, LLC

Precise and selective etching requires the control of the chemical and physical nature of thin surface layers. We discuss here the specific example of hydrocarbon polymer etching in an argon/oxygen chemistry. An important issue is the temporal evolution of the layer started from an initial condition established by a preceding step. It is important to ascertain whether the surfaces evolve continuously or not. We find for this chemistry and film set, that there are transients which give way at longer times to steady state conditions. Through the use of a novel *in situ* OES based technique which mimics traditional SIMS surface analysis we demonstrate the time dependent effect of argon ions on a hydrocarbon polymer surface which has been previously oxidized and separately the re-oxidation of a previously graphitized surface. Both these processes show sharp transients followed by much less active steady states. We characterize how these transients depend on the starting surface condition. We apply these same analytic techniques to the more complicated situation of the time evolution of photoresist lines which have been defined by 193i lithography. We show that the time dependence of the morphology of the surfaces of these lines which can be related to the lamellar structure of the photoresist.

Thursday Afternoon, November 10, 2016

4:40pm PS-ThA8 Etching Mechanisms of Transparent Conducting Oxides by Hydrocarbon Plasmas, *Hu Li*, Osaka University, Japan; *P. Friederich*, K. Fink, Karlsruhe Institut für Technologie (KIT); *K. Karahashi*, Osaka University; *M. Fukasawa*, *K. Nagahata*, *T. Tatsumi*, Sony Corporation, Japan; *W. Wenzel*, Karlsruhe Institut für Technologie (KIT); *S. Hamaguchi*, Osaka University, Japan

Zinc oxide (ZnO) and tin-doped indium oxide (ITO) are some of the most promising transparent conducting oxides (TCOs) for optoelectronic devices such as solar panels and head-mounted liquid crystal displays. With the demand of high-resolution optoelectronic devices increasing in the market, more efficient fabrication technologies for sub-micron- or nano-scale patterning of TCOs are required. Reactive ion etching (RIE) is a key technology for such fine patterning of materials, which has been widely used in the fabrication of semiconductor devices. RIE processes for TCOs have been developed with non-corrosive gases such as CH₄. However, etching reactions and mechanisms of such processes are not fully understood yet. The goal of this study is therefore to clarify plasma-surface interactions of CH₄ based plasmas with TCOs.

It has been found in our earlier beam experiments that the etch rate of ZnO by energetic CH_x⁺ ions strongly depends on the amount of hydrogen (i.e., value of x) of each incident CH_x⁺ ion. The results have also shown that ZnO stores hydrogen after the surface was exposed to energetic hydrogen ions. The modified surface layer of ZnO, which we call a "hydrogen-embedded ZnO" layer, has a higher sputtering yield for incident (inert) ions. In this study, we have examined how hydrogen can be stored in a hydrogen-embedded ZnO layer, using *ab initio* calculations. It has been found that, when a hydrogen atom is introduced to the surface or bulk of ZnO, it forms a hydroxyl group and weakens the Zn-O bond, converting ZnO to ZnOH. The result indicates that, in terms of energy levels, ZnOH has a higher sputtering yield than ZnO. A similar discussion of hydrogen effects on ITO will be also given in this presentation.

5:00pm PS-ThA9 The Role of the Dense Amorphous Carbon (DAC) Overlayer in Photoresist Etching, *Adam Pranda*, *Z. Tomova*, *S. Gutierrez Razo*, *J.T. Fourkas*, *G.S. Oehrlein*, University of Maryland, College Park

Multicolor photolithography is an alternative to extreme ultraviolet (EUV) lithography in attaining device feature sizes below 10nm. The use of this technique requires modification of existing acrylate-based photoresists in order to enable selective photochemistry with multiple wavelengths of light. In the following work, we establish the viability of multicolor photoresists by comparing their plasma etching behavior to industry-standard 193nm and 248nm photoresists.

The 193nm and 248nm photoresist polymers commonly used in industry are abundant in C-H bonds that scission when exposed to high energy ions that are characteristic of plasma etching. The rapid removal of volatile hydrogen- and oxygen-based carbon products results in the formation of a dense amorphous carbon (DAC) overlayer in the nm range. Steady-state etching of the bulk photoresist entails the constant removal and reformation of this overlayer, and the DAC layer acts as an etch-inhibiting layer on top of the bulk resist. The overall density of the overlayer will determine the etching behavior of the underlying photoresist.

In this work, we define a baseline for comparing multicolor photoresists by investigating the relationships between chamber conditions, formation of the DAC overlayer, and the resultant etch yields for a poly(methyl methacrylate)-based 193nm photoresist polymer (PR193) and a polystyrene-based 248nm photoresist polymer (PR248) using an inductively-coupled plasma (ICP) reactor as well as an electron cyclotron wave resonance (ECWR) reactor. The thickness and refractive index of both the DAC overlayer and bulk photoresist layer were monitored in real-time using *in-situ* ellipsometry.

We observe a correlation between the ambient chamber oxygen concentration, magnitude of the DAC overlayer refractive index (reflective of material density), and photoresist steady state etch rate. In the absence of ambient oxygen, the primary steady-state etching mechanism is physical sputtering. In the presence of ambient oxygen, the etching mechanism has contributions from physical and chemical sputtering, the latter mainly through adsorbed oxygen on the sample surface. Removal of carbon from the overlayer is enhanced by chemical sputtering, resulting in a less dense DAC overlayer which yields a higher steady state etch rate compared to the oxygen-deficient condition. These observations are useful as a baseline for evaluating the behavior of multicolor photoresists and provide a benchmark to guide which photoresists to synthesize to achieve the desired etching behavior.

The authors gratefully acknowledge the financial support of this work by the National Science Foundation (NSF CMMI-1449309).

5:20pm PS-ThA10 Transport Mechanism on Reactive Species in Downflow Reactors for F-based Etch, *Kenji Ishikawa*, *T. Tsutsumi*, *Y. Zhang*, *M. Sekine*, *T. Hayashi*, *M. Hori*, Nagoya University, Japan; *Y. Horiike*, Tsukuba University, Japan

In chemical dry etching (CDE) of F-based etch chemistry such as CF₄, SF₆, etc. [1], it has been believed that F atoms transport as long as 1 meters downflow of plasma source and etch Si with etch rates around 500 nm/min [2]. The etch results for SiO₂ and Si₃N₄ films were shown stable even low rates but relevant values regardless of the distance [3,4]. Otherwise, whilst the cases of NO + F₂ gas mixture generates F atoms, the etch rates significantly decreases with the distance from the location generated F atoms [5]. These apparently paradoxical results remain an open question, which needs to revisit. In particular of O₂ addition, the etch rate-dependence versus distance is evident, thus the effects of peroxy radicals, OOF, and peroxides, F₂O₂, are hypothesized. Here, we report the transport mechanism on reactive species in downflow for F-based etch.

The chemical dry etching apparatus was constructed by a long-length quartz tube. A mixture of CF₄ and O₂ gases was flown into the tube and a microwave cavity (2.45 GHz, 50W) was used for plasma generation. At the downflow, F atom or FOO signals were measured by electron spin resonance (ESR) instrument [6,7]. Quantum-chemical calculations were done with B3LYP/6-311+G(d) by Gaussian 09.

Ground-state of O₂ (³Σ_g) is reacted with F atom and stabilized 0.36 eV to generate OOF. Subsequently, OOF reacts with F atom to form F₂O₂. The OOF and Si reaction takes place Si + OOF → SiF + O₂(³Σ_g), rather than Si-oxidation pathways.

Experimentally, concentrations of F atoms at downflow depended on mixture ratio of O₂ and distances from the plasma source. The O₂ addition enhanced to transport F atom toward further positions. In general, although F atom recombination to F₂ is known to be relatively low reaction rate, however the recombination cannot be negligible during transport. Thus, we revisited the radical complex mechanism, i.e., F + O₂ → OOF and OOF → F + O₂, *vice versa*. In summary, we suggest that the transport of reactive species needs to revisit effects of the radical complex of F atom with O₂, in particular of the O₂ added F-based chemistry.

[1] Y. Horiike *et al.* Jpn. J. Appl. Phys. suppl. 15 (1976) 13; [2] N. Hayasaka *et al.*, 11th Proc. DPS (1989), p.57; [3] B. E. E. Kastenmeier *et al.*, J. Vac. Sci. Technol. A 14 (1996) 2802; [4] G. S. Oehrlein *et al.*, Plasma Sources Sci. Technol. 5 (1996) 193; [5] S. Tajima *et al.*, J. Phys. Chem. C 117 (2013) 5118; [6] H. E. Radford *et al.*, Phys. Rev. 123 (1971) 153; [7] A. D. Kirshenbaum *et al.*, J. Am. Chem. Soc. 88 (1966) 2434.

5:40pm PS-ThA11 Surface Reactions of Magnetic Materials by CO Cluster Beams, *Kazuhiro Karahashi*, Osaka University, Japan; *T. Seki*, *J. Matsuo*, Kyoto University, Japan; *K. Mizotani*, *K. Kinoshita*, *S. Hamaguchi*, Osaka University, Japan

Dry etching of magnetic thin films is a critical issue in the fabrication of magnetic random access memories (MRAMs). Currently argon (Ar) ion milling seems the only etching technique available in the manufacturing processes. However Ar ion milling is incapable of achieving anisotropic and selective etching of magnetic films and therefore extensive research is underway to establish highly selective anisotropic reactive ion etching (RIE) processes for magnetic thin films [1]. The formation of volatile metal carbonyl compounds produced by reactions of a metal surface with incident CO molecules may be used as a chemical etching process but such reaction probabilities are known to be very small. In this study we propose gas cluster beam processes as a means to etch magnetic metal surfaces. Gas clusters can provide a large number of reactant molecules to the metal surface at low incident energies and are expected to cause multiple collision processes at impact [2]. Especially we have examined surface reactions of Ni thin films by CO neutral clusters as well as energetic CO ion clusters. First we studied Ni etching reaction by incident CO cluster ion irradiation with typical single cluster ion energy being E_{cluster} = 20 keV (and a single CO molecule ion incident energy being E_{CO} = 11 eV). It was found that amorphous carbon deposition occurred on Ni surfaces and the beam did not etch the Ni films. These results suggest that each CO cluster is broken apart to CO molecules at impact by the excessive kinetic energy. Such excess kinetic energy prevents the formation of carbonyl compounds. Second, we examined interactions between low-energy incident CO neutral clusters (E_{cluster} = 300 eV, E_{CO} = 60 meV) with Ni surfaces. NiCO (Mass 86), which are fragments of nickel carbonyl compound [Ni(CO)₄], were detected with a quadrupole mass spectrometer equipped in the chamber of the

Thursday Afternoon, November 10, 2016

beam system. These results suggest that carbonyl formation reaction occurred by CO neutral cluster irradiation. Currently the probability of such carbonyl-formation reaction seems low and we shall discuss how the carbonyl-formation reaction rate on a metal surface can be increased. This work was supported by the Semiconductor Technology Academic Research Center (STARC)

References

- [1] K. Kinoshita et al., Jpn. J. Appl. Phys. 49(2010) 208JB02.
- [2] I. Yamada, J. Matsuo, et al., Mater. Sci. Eng. A, 253(2005) 249.

6:00pm **PS-ThA12 A Method to Accelerate Creation of Plasma Etch Recipes Using Physics and Bayesian Statistics**, *Meghali Chopra, R.T. Bonnecaze*, The University of Texas at Austin

Creating and optimizing plasma etch recipes for microelectronic and other nanostructured devices is costly and time consuming. Fully optimized plasma etch recipes can take several months to two years to create, which slows time to market. Here we introduce a method combining physics-based global plasma models, Bayesian statistics and experimental data to rapidly develop and optimize recipes for plasma etching. The method predicts optimal process windows with two- to three-fold fewer experiments than using factorial design of experiments. We first demonstrate this method for prediction of etch rates in CCP and ICP-RIE plasma reactors. These predictions are then successfully compared to synthetic and experimental data. We next use the method to determine the anisotropic etch rates through a single material including level set modeling. Lastly, we apply the method to the etch recipe development of a high aspect ratio trench through a multi-layer stack. Our results show that we can reduce three-fold the cost and time required to develop an etch recipe.

Surface Science

Room 103C - Session SS+AS-ThA

Celebrating a Life in Surface Science: A Symposium in Honor of JOHN T. YATES, JR.

Moderators: John Russell, Jr., Naval Research Laboratory, Vincent Smentkowski, General Electric Global Research Center

2:20pm **SS+AS-ThA1 Introductory Remarks About Prof. John T Yates Jr. and his Scientific Legacy**, *V. Smentkowski*, General Electric Global Research Center; *John Russell*, US Naval Research Laboratory
Introductory remarks about Prof. John T Yates Jr. and his scientific legacy

2:40pm **SS+AS-ThA2 JOHN T. YATES, JR. - The Energizer Bunny (Invited Talk)**, *J. William Gadzuk*, NIST

My friend and colleague John Yates was a joy to share life with. His perpetual enthusiasm, imagination, and sincere interest in whatever happened to be the topic of the moment whether a complex issue in surface science, the fate of an astronomically distant galaxy, the program for Lorin Maazel's next Pittsburgh Symphony concert, the well-being of his scientific "children" and real family, or speculation on what's likely to be tonight's specialties on the menu of our favorite Il Pizzico Restaurant near NIST, was infectious. John's retirement in 2006 from his chair at the University of Pittsburgh [which he went to from NBS/NIST in 1982] brought him to an emeritus-like guest faculty desk at the University of Virginia. Soon upon settling in at the university, his "desk" became an office became a full-fledged surface science lab with an active group of students and post docs supported by research grants that totaled among the highest within UVA chemistry, all of which was built up from scratch after John "retired". He was the only person I know who confessed that he really liked writing research proposals. He lived and executed his retirement with more excitement, energy, and enthusiasm than a young, tenure-seeking assistant professor; the energizer bunny personified.

I will present a number of anecdotal/amusing illustrative vignettes drawn from my experiences with "the energizer bunny" and discuss why his seminal JCP papers on thermal broadening in ESD [51,1264(1969)] and on resonance ESD [90,5793(1989)] were so influential in my own conceptualization and realizations in surface dynamics.

Finally, John and I had the privilege of being co-participants in two NIST Oral History interviews in 2014 and 15, once as a "target" and then as an interviewer [of each other]. This was a great way for us to summarize our

nearly half a century of being a part of each other's life, a privilege that I feel very fortunate and honored to have had. [transcripts available upon request: gadzuk@nist.gov [mailto:gadzuk@nist.gov]]

3:00pm **SS+AS-ThA3 Polymer Precursors Studied by Mass Spectrometry, Ion Mobility and Computational Strategies (Invited Talk)**, *David M. Hercules*, Vanderbilt University

There has been considerable interest recently in using mass spectrometry and related methods to address structures of complex systems, including block copolymers. Polyurethanes (PURs) are polymers that contain multiple "hard" and "soft" blocks that have different sequences of the same units along the chain. The ultimate goal in studying such materials would be the ability to determine the exact sequence along the chain and to correlate specific sequences with polymer performance. We have established a protocol on smaller molecules that can address this type of issue using the combination mass spectrometry, collision-induced dissociation, ion mobility spectrometry (IMS), and molecular dynamics simulations. A key component of the of the project is the synthesis of model PUR oligomers having authentic component sequences. The individual components are methylene diphenyl diisocyanate (MDI), bis-diol terminated polybutylene adipate (PBA), and 1,4-butane diol (BD), each containing 3 MDIs, 4 PBAs and 4 BDs (MW = 1910). The main collision-induced dissociation fragmentation reactions occur between the PUR and PBA carbonyl groups and BD hydrogen atoms. Additionally, a 1,3 H-shift reaction occurs between the PUR N-H group and BD oxygen. Different fragment ions are observed depending on the unit size and the sequences of the units in the chain. An important aspect of the research is to use IMS to separate compounds that have identical masses but different molecular-ion scattering cross sections. Computational strategies are important for calculation of IMS collisional scattering cross sections and to aid in the interpretation of fragmentation mechanisms. They help to identify synthetic targets that will show the largest effects of the experimental measurements.

3:20pm **SS+AS-ThA4 From Symmetry to Applications: One of Many Journeys Touched by John Yates (Invited Talk)**, *Ellen Williams*, Advanced Research Projects Agency - Energy

In the 1970's John Yates spent a sabbatical year at Caltech, where he touched the lives of many students and postdocs working in the group of Prof. Henry Weinberg. My story starts as a young student, fascinated with symmetry and statistical mechanics, who was privileged to work in the laboratory with John, in those early days of surface science when it seemed that every observation opened new horizons.

I will provide highlights of some of the exciting research that followed from those early days of surface science, discussing the impact of scanning tunneling microscopy, the linkages of surface science and nano-electronics, and the practical impacts of many years of fundamental studies from the perspectives of industry and ARPA-E.

4:00pm **SS+AS-ThA6 A Tribute to John T. Yates Jr. and His Pioneering Work with Graphitic Surfaces (Invited Talk)**, *Patricia A. Thiel*, Ames Laboratory

John T. Yates, Jr. directed pioneering work on graphitic surfaces. In one case, he and his group prepared graphene on SiC surfaces long before graphene was popularized. In another case, they developed a method to induce surface intercalation of Cs at a graphite surface. In this talk, I will review his contributions and describe the ways in which his work has inspired some of my own. For instance, we have studied adsorption, nucleation, growth, and reaction of dysprosium (Dy) on the basal plane of graphite, and the way that these phenomena are influenced by surface defects. Dysprosium islands nucleate homogeneously on terraces at room temperature. With increasing temperature the shape changes, with islands becoming taller and more faceted. At still higher temperature, Dy reactions with graphite to form carbide. Using the technique developed by John and his group, we can also induce surface intercalation at elevated temperature. We show that this surface intercalation differs significantly from bulk intercalation.

4:20pm **SS+AS-ThA7 Surface Science influenced by Dopants (Invited Talk)**, *Hajo Freund*, Fritz Haber Institute of the Max Planck Society, Germany
Model systems are useful to establish structure/morphology reactivity relations in heterogeneous catalysis. Here we use a Metal-Insulator-Metal (MIM) structure to advice CO₂.

We had shown before that ultra-thin oxide films could be used as effective barriers to charge Au islands with electrons from the metal below the support. The idea is to use the electrons stored in the islands to activate

Thursday Afternoon, November 10, 2016

molecules by electron transfer. Such a molecule is the energy economy relevant carbon-dioxide for example. We demonstrate adsorption of CO₂ at gold islands and the reversible formation of CO₂ anions and oxalates based on information from microscopy and spectroscopy.

We show how to transfer those ideas developed for thin film systems to bulk materials, where we use appropriate dopants within the support material to provide the electron source. The electron transfer to Au islands as well as the activation of oxygen will be demonstrated.

4:40pm SS+AS-ThA8 Desorption: Out of the Vacuum, into the Liquid (Invited Talk), Michael Grunze, KIT, Germany; **H.J. Kreuzer**, Dalhousie University, Canada

The first paper on thermal desorption John Yates published with Ted Madey was entitled: *Nitrogen Desorbs with Complex Kinetics*. Thermal Desorption Spectroscopy, in more and more sophisticated experimental set-ups including flow reactors, became then a prominent techniques in John's Laboratory to study simple and complex surface chemical reactions. In this short report, we look further into "complex kinetics" and find that the theoretical framework of a thermally activated process can not be applied to the detachment of particles in a micro-fluidic shear-flow experiment.

The theoretical description of the desorption process treats bond breaking as a thermally activated process, which can be described by the Arrhenius equation. The activation energy and the pre-exponential factor can be determined from a series of TPD experiments with either varying coverage or at constant coverage, using different heating rates. Here we experimentally and theoretically analyze the detachment of microscopic polystyrene beads from different self-assembled monolayer (SAM) surfaces in a shear flow to develop a mechanistic model for the removal of cells from surfaces. The detachment of the beads from the surface is treated, as in thermal desorption experiments, as a thermally activated process to determine activation barrier and attempt frequency of the rate determining step in bead removal. The statistical analysis of the experimental shear detachment data, obtained in phosphate-buffered saline solution, results in an activation energy of detachment around 20 kJ/mol. This value is orders of magnitude lower than the adhesion energy measured by atomic force microscopy (AFM). The same order of magnitude for the adhesion energy measured by AFM is derived from ab initio calculations of the van der Waals interaction energy between the polystyrene beads and the SAM-covered gold surface. We hence conclude, that the rate determining step for detachment of the beads is the initiation of rolling on the surface (overcoming static friction), and not physical detachment as would be the case in a gas desorption experiment.

5:00pm SS+AS-ThA9 Infrared Spectroscopy in Surface Science: The Legacy of John T. Yates, Jr. (Invited Talk), Michael Trenary, University of Illinois at Chicago

A constant theme throughout the long scientific career of John T. Yates, Jr. was the use of infrared spectroscopy to probe the properties of surfaces and of adsorbed molecules. In his very first publication in 1961, based on his PhD thesis from MIT, he used transmission infrared spectroscopy to study the interaction of carbon monoxide with alumina-supported nickel surfaces. He continued to use innovative methods of transmission infrared spectroscopy in his laboratories at the National Bureau of Standards, the University of Pittsburgh, and the University of Virginia. The final publication of his career, which appeared in 2016, featured transmission IR spectra of CO interacting with the surfaces of titania-supported gold. In addition to transmission IR spectroscopy of high-area powdered samples, he was also a leader in the use of reflection absorption infrared spectroscopy (RAIRS), also known as infrared reflection absorption spectroscopy (IRAS), a method that allows IR spectra to be obtained on small-area metal single crystals. RAIRS is one of the few surface science techniques that can be used both under UHV conditions as well as in the presence of an ambient pressure of gas. John Yates was a pioneer in bridging the so-called pressure gap by using RAIRS to probe gas-surface interactions in the presence of elevated gas pressures. Recent examples from other research groups will be presented to highlight the continuing impact John Yates has had in the use of infrared spectroscopy in surface science.

5:20pm SS+AS-ThA10 From Surface Science to New Catalysts (Invited Talk), Ib Chorkendorff, Technical University of Denmark

In this presentation I will give a brief overview of how my post-doc with John T. Yates Jr. influenced my way of working and how that philosophy could be used too go from fundamental investigations of reactions on surfaces to actually understand and make new heterogeneous catalysts.

First we shall discuss how mass-selected nanoparticles of CuZn alloys to elucidate the dynamics of the methanol synthesis catalysts. The produced nanoparticles will be compared to the conventional CuZnAl at 1 bar for synthesizing methanol from CO₂ and H₂ [1, 2, 3]. The methanol synthesis on CuZn will also be discussed with respect to our very recent findings of using alloys of NiGa for methanol synthesis [4]. The use of mass-selected nanoparticles will be further demonstrated for electrochemical Oxygen Reduction Reaction, which is really the limiting reaction in Proton Exchange Membrane Fuel Cells. Here we have found entirely new classes of electrocatalysts by alloying Pt with early transition metals [5] or the lanthanides [6]. We have also shown that it is possible to make mass-selected nanoparticles of these alloys with very good activities [7] and PtGd alloys [8].

References

1. S. Kuld, C. Conradsen, P.G. Moses, I. Chorkendorff and J. Sehested, *Angew. Chemie* 53 (2014) 1.
2. C. Holse, C. F. Elkjær A. Nierhoff, J. Sehested, I. Chorkendorff, S. Helveg, J. H. Nielsen, *J. Chem. Phys.* 119 (2015) 2804-2812.
3. S. Kuld, M. Thorhauge, H. Falsig, C. Elkjær, S. Helveg, I. Chorkendorff, J. Sehested, *Accepted SCIENCE* (2016).
4. F. Studt, F. Abild-Pedersen, I. Sharafutdinov, C. F. Elkær, J. S. Hummelshøj, S. Dahl, I. Chorkendorff, and J. K. Nørskov, *Nature Chemistry* 6 (2014) 320.
5. J. Greeley, I.E.L. Stephens, A.S. Bondarenko, T. P. Johansson, H. A. Hansen, T. F. Jaramillo, J. Rossmeisl, I. Chorkendorff, J. K. Nørskov, *Nature Chem.* 1 (2009) 522.
6. M. Escudero-Escribano, P. Malacrida, M- Hansen, U. G. Vej-Hansen, A. Velázquez-Palenzuela V. Tripkovic, J. Schøtitz, J. Rossmeisl, I. E.L. Stephens, I. Chorkendorff, *SCIENCE* 352 (2016) 73-76.
7. P. Hernandez-Fernandez, F. Masini, D. N. McCarthy, C. E. Streb, D. Friebe, D. Deiana, P. Malacrida, A. Nierhoff, A. Bodin, A. M. Wise, J. H. Nielsen, T. W. Hansen, A. Nilsson, I. E.L. Stephens, I. Chorkendorff, *Nature Chemistry* 6 (2014) 732-8.
8. A. Velázquez-Palenzuela, F. Masini, A. F. Pedersen, M. Escudero-Escribano, D. Deiana, P. Malacrida, T. W. Hansen, D. Friebe, A. Nilsson, I. E.L. Stephens, I. Chorkendorff, *J. Catal.* 328 (2015) 297-307.

5:40pm SS+AS-ThA11 Activation of Carbon Dioxide on Metal and Carbide Surfaces (Invited Talk), Jingguang Chen, Columbia University

Converting CO₂ into valuable chemicals and fuels is one of the most practical routes for reducing CO₂ emissions while fossil fuels continue to dominate the energy sector. The catalytic reduction of CO₂ by H₂ can lead to the formation of three types of products: CO through the reverse water-gas shift (RWGS) reaction [1], methanol via selective hydrogenation [2], and hydrocarbons through combination of CO₂ reduction with Fischer-Tropsch (FT) reactions. In the current talk we will discuss some of our recent results in CO₂ conversion [3]. Our research approaches involve the combination of DFT calculations and surface science studies over single crystal surfaces, catalytic evaluations over supported catalysts, and in-situ characterization under reaction conditions. We will also discuss challenges and opportunities in this important research field [4].

References:

- [1] M.D. Porosoff, X. Yang, J.A. Boscoboinik, and J.G. Chen, "Molybdenum carbide as alternative catalysts to precious metals for highly selective reduction of CO₂ to CO", *Angewandte Chemie International Edition*, 53 (2014) 6705-6709.
- [2] X. Yang, S. Kattel, S.D. Senanayake, J.A. Boscoboinik, X. Nie, J. Graciani, J.A. Rodriguez, P. Liu, D.J. Stacchiola and J.G. Chen, "Low pressure CO₂ hydrogenation to methanol over gold nanoparticles activated on a CeOx/TiO₂ interface", *Journal of the American Chemical Society*, 137 (2015) 10104-10107.
- [3] M.D. Porosoff, M. Myint, S. Kattel, Z. Xie, E. Gomez, P. Liu and J.G. Chen, "Identifying different types of catalysts for CO₂ reduction by ethane through dry reforming and oxidative dehydrogenation", *Angewandte Chemie International Edition*, 54 (2015) 15501-15505.
- [4] M.D. Porosoff, B. Yan and J.G. Chen, "Catalytic reduction of CO₂ by H₂ for synthesis of CO, methanol and hydrocarbons: Challenges and opportunities", *Energy & Environmental Science*, 9 (2016) 62-73.

Thursday Afternoon, November 10, 2016

6:00pm **SS+AS-ThA12 Thermodynamic Control of TTF-TCNQ Molecular Layers on Metallic Surfaces (Invited Talk), Petro Maksymovych**, Oak Ridge National Laboratory

Bulk molecular ionic solids exhibit a fascinating diversity of electronic ground states, including unconventional superconductivity. The electronic properties of these systems have historically avoided surface analytical studies due to the intrinsic difficulty with surface preparation. We are therefore pursuing epitaxial growth of charge-transfer compounds, toward understanding their fundamental properties and creating new kinds of metal-organic or organic-organic interfaces [1,2]. A primary challenge is to assure compatibility of supported epilayers with the redox processes so as to enable, enhance but not eliminate significant charge transfer and electron correlations with supported structures.

In this talk, I will discuss 2D molecular structures of TTF and TCNQ molecules supported on metal and graphitic surfaces. We established that these molecules self-organize into a "zoo" well-ordered structure with a wide-range of TTF:TCNQ ratios [3] - a marked deviation from a single stable 1:1 ratio in the bulk. We propose that the formation these structures is governed by a surface phase diagram that exhibits at least four distinct stable compositions. The diagrammatic picture explains many of the properties of such systems that often seem incidental: the morphology of epilayers, governed by nucleation and growth; coexistence and abundance of various phases, and the distinct molecular structure of phase boundaries. Using coupled image and computational analysis, we conclude that the observed shapes are dictated by the preferential formation of a well-defined "quad"-motif involving TTF(TCNQ) molecules coordinated by at least four of its matching neighbors. Thus enabled deterministic control is beneficial to both electronic properties of surface phases (which can develop local magnetic moments) and the formation of quasi-2D TTF-TCNQ solids, which develop decidedly non-bulk Mott-insulating state despite having 1:1 bulk ratio. We anticipate that these properties are quite general for multicomponent molecular compounds, providing new opportunities for self-organized and electronically interesting molecular systems.

This research was conducted at the Center for Nanophase Materials Sciences, which is a DOE Office of Science User Facility.

[1] G. A. Rojas et. al, and P. Maksymovych, "Ionic Disproportionation of Charge Transfer Salt Driven by Surface Epitaxy", J. Phys. Chem. C, 117 (2013) 19402.

[2] C. Park et. al, and P. Maksymovych, "Weak competing interactions control assembly of strongly bonded TCNQ ionic acceptor molecules on silver surfaces", Phys. Rev. B 90 (2014) 125432.

[3] S. Jeon et. al and P. Maksymovych, ACS Nano in review (2016).

Thin Film

Room 104E - Session TF+BI-ThA

Thin Films for Bio-related Applications

Moderator: Angel Yanguas-Gil, Argonne National Lab

2:20pm **TF+BI-ThA1 Self-healing Antifouling Fluorinated Monolayers and Polymer Brushes: One Fluorine Goes a Long Way!**, *Zhanhua Wang, H. Zuilhof*, Wageningen University, Netherlands

Organic monolayers or polymer brushes, often in combination with surface structuring, are widely used to prevent nonspecific adsorption of polymeric or biological material on sensor and microfluidic surfaces. Here we show how robust, covalently attached alkyne- derived monolayers or ATRP-produced polymer brushes, with a varying numbers of fluorine atoms, on atomically flat Si(111), effectively repel a wide range of apolar polymers without the need for micro- or nanostructuring of the surface. We have studied the antifouling property of fluoro-hydro monolayers and of fluorine-containing polymer brushes towards a range of commonly used polymers/plastics with comparable molecular weight in non- aqueous solvent, and have investigated the effect of polymer molecular weight on the fouling behavior. In addition, we show how for fluorinated polymer brushes this property can be self-repaired upon damage. These studies relied on a range of characterization methods: wettability studies, ellipsometry, X- ray photoelectron spectroscopy (XPS) and atomic force microscopy (AFM). We developed a novel surface morphology survey by AFM characterization that can accurately quantify the degree of fouling.

These findings and analysis offer significant potential for antifouling applications of ultrathin and covalently bound fluorine- containing coatings for a range of micro- and nanotechnological applications.

Lit:

J. Mater. Chem. A, 2016, 4, 2408-2412

Adv. Mater. Interfaces 2016, 3, 1500514

2:40pm **TF+BI-ThA2 Sensitivity Enhancement in Grating Coupled Bloch Surface Wave Resonance by Azimuthal Control**, *Vijay Koju, W.M. Robertson*, Middle Tennessee State University

Bloch surface waves (BSWs) are electromagnetic excitation modes that exist at the interface of truncated dielectric multilayer structures and a homogeneous medium. Although BSWs are intrinsically present at such interfaces, they cannot be directly excited by light incident from the homogeneous medium due to their non-radiative and evanescent nature. The use of a grating coupler or a prism mitigates this inability by providing an additional momentum to the free-space wave vector required to satisfy the phase matching condition with the BSW wave vector. Since Grating-coupled Bloch surface wave resonance (GCBWR) bio-sensors do not require a bulky prism to couple light into BSWs, they are strong candidates for nanoscale bio-sensors. But GCBWR bio-sensors, based on either wavelength or angular interrogation, are observed to be less sensitive compared to prism-coupled Bloch surface wave resonance (PCBWR) bio-sensors. However, due to their inhomogeneous surface architecture, GCBWR bio-sensors can be interrogated by rotating the grating platform azimuthally. Exploiting this ability, here we present a new method for improving sensing capability of GCBWR bio-sensors. We demonstrate computationally, using a three-dimensional scattering matrix based rigorous coupled wave analysis method, that the proposed azimuthal angle interrogation technique highly enhances the sensitivity of GCBWR bio-sensors. For our study we use a sixteen layered TiO₂-SiO₂ multilayer with SiO₂ gratings on the top sensing platform. We fix the wavelength and incident angle of the incoming light, and sweep over the azimuthal angle to simulate the sensitivity as a function of changing refractive index of the sensing layer. Furthermore, we show that contrary to conventional GCBWR bio-sensors that only work for transverse electric mode, azimuthal angle based GCBWR bio-sensors work for both transverse electric and transverse magnetic modes.

4:00pm **TF+BI-ThA6 Thin Film Technologies for Biomedical Devices-Current State of Art and Future Opportunities**, *Mallika Kamarajugadda*, Medtronic plc **INVITED**

Thin film coatings are becoming ubiquitous in the medical device industry. Capabilities of medical devices and implants are greatly enhanced by thin films, which impart different properties such as adhesion, wear resistance, corrosion resistance, lubricity, radiopacity, electrical insulation, and bio response. Thin film deposition processes for medical devices are often challenging due to the complex substrate geometry of the components and the requirement for biocompatibility. In biomedical thin film coatings, the shape of a surface controls its interaction with biological components. Optimizing the interactions that occur at the surface of implanted biomaterials will be the key to further advances in this field. Furthermore, as treatment options shift towards non-invasive methods, and device size is reduced, researchers will need to work towards overcoming technological challenges to leverage thin film technology in medical devices. This talk will provide current examples of thin film coating applications in the medical device industry along with the future opportunities.

4:40pm **TF+BI-ThA8 Preparation and Characterization of Amino Coatings for Peptide Arrays**, *Gaurav Saini, L. Howell, M. Greving, P. Walsh, D. Smith*, HealthTell Inc. **INVITED**

Amine-functionalized substrates are among the most commonly used materials in solid-phase peptide synthesis. Chemical stability and amine loading of the amino coating are two important properties that determine silane selection as a building layer in peptide synthesis. We synthesized three different amino coatings *i.e.*, APTES (3-aminopropyltriethoxysilane), APDEMS (3-aminopropyl-diethoxymethylsilane) and APDIPES (3-aminopropyl-diisopropylethoxysilane), and determined their strengths and limitations as a building layer in peptide array synthesis. Here, amino coatings were synthesized via gas-phase deposition of the corresponding silanes on thermal oxide-terminated silicon substrates in a commercial chemical vapor deposition system. A 16-mer peptide coating was then synthesized on the amino surfaces and the chemical stability of the surface to highly acidic side chain deprotection (SCD) treatments was determined. After SCD, the coating thicknesses decrease to different degrees on the surfaces: it is greatest for the APDIPES surface, lowest for the APTES surface and intermediate for the APDEMS surface, which indicates that peptide-functionalized APTES and APDIPES surfaces are chemically most

Thursday Afternoon, November 10, 2016

and least stable to SCD treatment, respectively. The effect of amine loading on peptide density and purity was also determined for the three amino surfaces. Four different trimers were synthesized on the amino surfaces, and the density and purity of these trimers for the three surfaces was determined. A positive correlation between the amine loadings and peptide densities was observed; peptide density was highest for the APTES surface and lowest for the APDIPES surface. However, high amine loading is found to have a negative impact on peptide purity; peptide purity is highest for the APDIPES surface and lowest for APTES surface. Coated surfaces were characterized by spectroscopic ellipsometry, contact angle goniometry, X-ray photoelectron spectroscopy (XPS), atomic force microscopy (AFM), spectrophotometry, and MALDI-MS.

5:20pm TF+BI-ThA10 Electronic Characterization of SWCNT/Block Copolymer-based Nanofiber for Biosensor Application, Amrit Sharma, Clark Atlanta University

The aim of this research is to fabricate an electrically conducting, smooth, continuous and sensitive nanofiber using polystyrene (PS), triblock copolymer (PS-*b*-PDMS-*b*-PS) and single-walled carbon nanotubes (SWCNTs) by electrospinning. The electronic nanofibers may be utilized for effective bio-sensing applications. The SWCNTs have been of great interest to researchers because of their exceptional electrical, mechanical, and thermal properties. The nanoscale diameter, high aspect ratio, and low density make them an ideal reinforcing candidate for novel nano composite material.

Electrically conducting nanofibers have been prepared by electrospinning a solution of PS, PS-*b*-PDMS-*b*-PS and functionalized SWCNTs in the ratio 5:1:0.05 using solvent DMF. The nanofibers formed had an average diameter of 5 μm and height 4 μm . These nanofibers were characterized by scanning electron microscopy (SEM), atomic force microscopy (AFM), optical microscopy and electrical characterization.

The electrical characterization of a single fiber shows an almost linear graph of current vs voltage using four-point probe (also known as Kelvin sensing) method. This linear graph exemplifies the conducting nature of the nanofiber. From the graph, a resistance, resistivity and conductivity of the single were measured. The study suggests that the SWCNT/block copolymer nanofibers have superior performance in the development of ultra-high sensitive sensor for the detection of single molecule relative to conventional materials due to significantly larger surface-to-volume ratio. Future work includes preparing nanofibers decorated with functional groups and binding with specific type of enzyme or protein to study their I-V behavior. This approach or method can be utilized for bio-sensing activities, especially for the detection of various antibodies and protein molecules.

References:

- [1] Ramakrishna, S.; Fujihara, K.; Teo, W.-E.; Lim, T.-C.; Ma, Z. *An Introduction to Electrospinning and Nanofibers*; World Scientific: Singapore, 2005.
- [2] Charlier, J.-C.; Issi, J.-P. Electrical Conductivity of Novel Forms of Carbon. *Journal of Physics and Chemistry of Solids*. **1996**, 57, 957–965.
- [3] Zhao, B.; Hu, H.; Haddon, R. C. Synthesis and Properties of a Water-Soluble Single-Walled Carbon Nanotube–Poly (m-Amino benzene Sulfonic Acid) Graft Copolymer. *Advanced Functional Materials*. **2004**, 14, 71–76.

Funder Acknowledgement(s): This research was funded and supported by the National Science Foundation, CREST, DMR-0934142 and the Center for Functional Nanoscale Material Research program at Clark Atlanta University.

Faculty Advisor/ Mentor: Dr. Michael D. Williams, mdwms@cau.edu

Thin Film

Room 105A - Session TF-ThA

Self-assembled Monolayers and Organic/Inorganic Interface Engineering

Moderators: Matthew Linford, Brigham Young University, Adrienne Stiff-Roberts, Duke University

2:20pm TF-ThA1 Surface Affinity Control by Polymer Brushes for Direct Self-Assembly, R. Tiron, A. Gharbi, M. Argoud, F. Delachat, P. Pimenta Barros, CEA-LETI, MINATEC, France; X. Chevalier, ARKEMA FRANCE; S. Bouanani, STMicroelectronics, France; G. Claveau, C. Lapeyre, CEA-LETI, MINATEC; G. Chamiot-Maitrala, CEA-LETI, France; C. Monget, V. Farys, STMicroelectronics, France; C. Nicolet, C. Navarro, ARKEMA FRANCE
INVITED

The ongoing progress in nanoscience and nanotechnology leads to a continual device miniaturization. Until now, lithography has been the main driving force of this process. Block copolymers have become of great interest for high-resolution patterning due to their low fabrication cost, ease of use and high throughput potential. Self-assembling materials used in conjunction with the most advanced exposure tools may extend the current manufacturing practices to dimensions of 10nm and beyond. Density multiplication of patterned templates by DSA of block copolymers stands out as a promising alternative to overcome the limitation of conventional lithography.

In this paper, we investigate the potential of DSA to address both contact via level patterning as well as line and space application. Using the 300mm pilot line available in LETI and Arkema materials, our approach is based on the graphoepitaxy of PS-*b*-PMMA block copolymers. Our integration scheme is based on BCP self-assembly inside organic hard mask guiding patterns obtained using 193i nm lithography. The process is monitored at different steps: the generation of guiding patterns, the directed self-assembly of block copolymers and PMMA removal, and finally the transfer of PS patterns into the metallic under layer by plasma etching.

Furthermore, several process flows are investigated, either by tuning different material related parameters such as the block copolymer intrinsic period or the interaction with the guiding pattern surface (sidewall and bottom-side affinity). The final lithographic performances are finely optimized as a function of the self-assembly process parameters such as the film thickness and bake (temperature and time).

Finally, DSA performances as a function of guiding patterns density are investigated. Thus, for the best integration approach, defect-free isolated and dense patterns for both contact shrink and multiplication (doubling and more) have been achieved on the same processed wafer.

These results show that contact hole shrink and multiplication approach using DSA is well compatible with the conventional integration used for CMOS technology.

3:00pm TF-ThA3 Measuring the Rate of Organic Reactions on Surfaces, Rickdeb Sen, J. Escorihuela, M.M.J. Smulders, H. Zuilhof, Wageningen University, Netherlands

Ultrathin coatings like self-assembled monolayers and polymer brushes have been used for a wide variety of studies and applications. Reactions within such monolayers or brushes are often difficult to follow, and their rates are typically not measurable: apart from a handful of cases in which electrochemical methods have been used, no rigorously measured kinetics on reactions within e.g. self-assembled monolayers are available.

The current presentation will outline a generic approach, combining ambient mass spectrometry and XPS, to fill this gap, and provide a novel method to measure the rate of intramonolayer or intrapolymer organic reactions. Examples will include a variety of so-called click reactions, as these display a very high potential in materials science.

Reference: *Langmuir* 2016, 32, 3412–3419

4:00pm TF-ThA6 Operando Investigation of Chemical Bonding at Hybrid Interfaces: the Effect of Humidity on Polymer/metal Oxide Bonds, Sven Pletincx, Vrije Universiteit Brussel, Belgium; L. Trotochaud, A.R. Head, O. Karslioglu, Lawrence Berkeley Lab, University of California, Berkeley; L.I. Fockaert, J.M.C. Mol, TU Delft, Netherlands; H. Bluhm, Lawrence Berkeley Lab, University of California, Berkeley; H. Terryn, T. Hauffman, Vrije Universiteit Brussel, Belgium

Stability in aqueous and corrosive environments of formed bonds between carboxylic acid functional groups of a polymer and a hydroxylated surface of aluminium oxide has a great relevance to a broad range of applications.

Thursday Afternoon, November 10, 2016

One of the most important industrial problems of adhesion phenomena includes the loss of desired chemical interactions at the interface as a result of humidity and ionic compounds present in the atmosphere. Conventional vacuum techniques do not permit analysis under atmospheric conditions or can nullify the influence of ex-situ atmospheric modifications upon exposure of the sample to an ultra-high vacuum environment. Also, because of the relatively thick polymer layer present in conventional hybrid systems, a buried interface exists, which is difficult to characterize with surface-sensitive analytical techniques. Recent developments in the field of ambient-pressure x-ray photoelectron spectroscopy (APXPS) enable a novel approach to probe these interfaces. A broad range of relative humidities can be reached in the analysis chamber, making it possible to unravel interfacial chemistry changes *operando*.

The amount of bonds formed at the hybrid interface and their binding mechanism (monodentate, bidentate, Brønsted interactions, Lewis interactions) are largely determined by oxide properties such as surface hydroxyl content, acid/base character, and dielectric properties. In this work, aluminium oxide is synthesized by electropolishing and anodizing pretreatment steps to carefully control oxide properties on the nanoscale and fully characterized by different analysis techniques. Polyacrylic acid coatings are made sufficiently thin to access the interface with surface analysis techniques with probing depths between 5-10 nm.

Complementary to APXPS, a vibrational spectroscopy technique using the so-called Kretschmann configuration is used to characterize the formed bonds at the metal oxide/polymer interface. An Al layer is sputtered on an IR transparent crystal, with the Al thickness selected such that the FTIR signal from the oxide/polymer interface is amplified as a result of the Kretschmann effect, and thus an interface-specific spectrum of the oxide/polymer surface is attained. This way, we have direct access to the interface, and the influence of an above-the-polymer electrolyte (i.e. H₂O) can be probed. Preliminary results show an increase in the amount of bonds at the oxide/polymer interface, together with an increase in water content directly at this interface. It seems that water, at least during the first 24 hours of interaction, triggers an increased wet adhesion.

4:20pm TF-ThA7 Integration of Redox-Active Diruthenium-based Molecular Layer onto Electrodes for Memory Device Applications, Sujitra Pookpanratana, National Institute of Standards and Technology (NIST); H. Zhu, George Mason University; J.W.F. Robertson, NIST; S.N. Natoli, Purdue University; E.G. Bittle, C.A. Richter, NIST; T. Ren, Purdue University; Q. Li, George Mason University; C.A. Hacker, NIST

Attaching and integrating electrochemically-active molecules to a variety of different surfaces is of importance for applications in catalysis, memory devices, and molecular electronics. With the increasing demand for personal electronics, growth in Flash-based memory has increased dramatically. However, the dimensional scaling of memory components faces many critical material limitations. A critical component to the memory device is the floating gate or charge trapping layer. To scale the charge trapping layer to nanometer dimensions, one approach is to use a discrete charge storage layer that is based on organic molecules.^{1,2,3} Reduction-oxidation (redox) active organic molecules hold potential for memory devices due to their nanoscale dimensions, potential for high charge density, and synthetic flexibility that could be tailor-made for specific electronic functionality.

Here, we investigated the potential of diruthenium-bearing organometallic molecules as the charge trapping layer for memory devices. Diruthenium-bearing organometallic molecules display multiple redox states,⁴ which makes them ideal to incorporate within non-volatile memory devices. Monolayer assembly is performed in a stepwise fashion by first forming azide-terminated monolayer on SiO₂ by using azidoundecyl trimethoxysilane followed by a Cu-catalyzed azide-alkyne cycloaddition click reaction to attach diruthenium (Ru₂) compounds (note: SiO₂ serves as the tunneling layer).⁵ Infrared spectroscopy and X-ray photoelectron spectroscopy confirmed the Ru₂ attachment. Ultraviolet photoelectron spectroscopy identified the occupied electronic levels of the hybrid organic-inorganic surfaces before and after click reaction. Voltammetric measurements on Ru₂-terminated SiO₂/Si and Au electrodes confirm that the Ru₂ is still electrochemically-active with accessible electronic states integrated on both surfaces.

To complete the memory capacitor device, an Al₂O₃ layer (serving as a charge blocking layer) was deposited by atomic layer deposition over the molecular layer followed by a metal Pd gate. The impact of different Ru₂ compounds on the electronic structure and electrochemical properties of the electrodes and properties of the memory devices will be compared.

Our results will provide future design considerations and limitations for molecular-integrated memory devices.

1. T. Shaw et al., IEEE T. Electron. Dev. **58** (3), 826-834 (2011).
2. D. Beckmeier and H. Baumgärtner, J. Appl. Phys. **113** (4), 044520 (2013).
3. H. Zhu, et al., Appl. Phys. Lett. **103** (5), - (2013).
4. W.-Z. Chen and T. Ren, Inorg. Chem. **45** (20), 8156-8164 (2006).
5. S. Pookpanratana, et al., Langmuir **30** (34), 10280-10289 (2014).

4:40pm TF-ThA8 Fabrication Methods of Organic-Inorganic Hybrids Based on Atomic Layer Deposition, Myung Mo Sung, Hanyang University, Korea
INVITED

Organic-inorganic hybrid materials are particularly attractive because they can provide means for not only combining the distinct properties of organic and inorganic components, but outperforming their constituents. The incorporation of inorganic layers into organic layers, therefore, provides the opportunity for developing new hybrid materials with synergic behavior, leading to improved performance. In this presentation, we report three fabrication methods of organic-inorganic hybrid materials using atomic layer deposition (ALD). (1) Molecular layer deposition (MLD) is a gas phase process analogous to ALD and also relies on sequential saturated surface reactions which result in the formation of a self-assembled organic monolayer in each sequence. The MLD method can be combined with ALD to take advantages of the possibility of obtaining organic-inorganic hybrid thin films. The advantages of the MLD technique combined with ALD include accurate control of film thickness, large-scale uniformity, excellent conformality, good reproducibility, multilayer processing capability, sharp interfaces, and excellent film qualities at relatively low temperatures. (2) Large-area graphene films produced by means of chemical vapor deposition (CVD) are polycrystalline and thus contain numerous grain boundaries that can greatly degrade their performance and produce inhomogeneous properties. A better grain boundary engineering in CVD graphene is essential to realize the full potential of graphene in large-scale applications. Here, we report a defect-selective atomic layer deposition (ALD) for stitching grain boundaries of CVD graphene with ZnO so as to increase the connectivity between grains. In the present ALD process, ZnO with hexagonal wurtzite structure was selectively grown mainly on the defect-rich grain boundaries to produce ZnO-stitched CVD graphene with well-connected grains. (3) ALD under high pressure showed that precursors often diffuse sub-surface into polymers. This subsurface diffusion and reaction cold result in the change of the chemical composition and the physical properties of the bulk polymers. Atomic layer infiltration provides a new approach for preparation of organic-inorganic hybrid materials from polymers.

Tribology Focus Topic

Room 101A - Session TR+BI+SE+TF-ThA

Materials Tribology

Moderator: Michael Chandross, Sandia National Laboratories

2:20pm TR+BI+SE+TF-ThA1 Reaction Pathways and Tribofilm Formation Kinetics at a Solid-Solid Interface, H.L. Adams, University of Wisconsin-Milwaukee; A. Martini, University of California Merced; **Wilfred Tysoe**, University of Wisconsin-Milwaukee
INVITED

Perhaps the most difficult surface-science challenge is to monitor reaction pathways and kinetics at sliding solid-solid interfaces, in particular for opaque contacting materials [1]. Optical techniques can be used to interrogate the interface when one of the contacting surfaces is transparent, but they are often not sensitive to the first monolayer. Strategies for measuring reaction pathways and their kinetics for well-defined surfaces in ultrahigh vacuum (UHV) are described using the example of sliding-induced decomposition of adsorbed methyl thiolate species, formed by exposure to dimethyl disulfide, on copper. Surface science experiments show that methyl thiolates are stable up to ~425 K on copper, but decompose during rubbing; the effect of the external force is to lower the reaction activation barrier so that it proceeds at room temperature. The surface reaction products can be monitored immediately after sliding in UHV using surface spectroscopies (for example, Auger spectroscopy). However, the reaction kinetics can also be monitored in situ first, by measuring the gas-phase species evolved as a function of the number of times the surface is rubbed, where methane and ethane are detected and second, by measuring the change in friction force due to the evolution of the nature of the species present on the surface. This allows

Thursday Afternoon, November 10, 2016

the elementary steps in the tribofilm formation pathway to be identified and their rates measured.

[1] Heather L. Adams, Michael T. Garvey, Uma Shantini Ramasamy, Zhijiang Ye, Ashlie Martini, and Wilfred T. Tysoe, *Journal of Physical Chemistry C*, **119**, 7115–7123 (2015)

3:00pm TR+BI+SE+TF-ThA3 Nanotribology of Graphene Revisited: The Influence of Contact Size and Substrate Topography, A. Balkanci, Bilkent University, Turkey; Z. Ye, A. Martini, University of California Merced; **Mehmet Z. Baykara**, Bilkent University, Turkey

Two-dimensional (2D) materials have been the focus of intense research in recent years thanks to their outstanding electronic and mechanical attributes. In particular, graphene exhibits exceptional potential as a solid lubricant appropriate for use in nano-/micro-scale mechanical systems. As such, a comprehensive evaluation of its frictional properties on such small length scales is of crucial concern. While pioneering studies toward this purpose have revealed strongly layer-dependent frictional behavior [1], the precise roles that contact size and substrate topography (important design parameters for mobile components in nano-/micro-scale devices) play in the lubricative nature of graphene have not been explored yet in detail.

In this contribution, we present a combined experimental and numerical study aimed at evaluating the influence of contact size and substrate topography on the nanotribological characteristics of graphene. In particular, atomic force microscopy (AFM) is employed under ambient conditions to measure friction forces on mechanically-exfoliated graphene as a function of applied load, number of graphene layers, and contact size. To study the influence of contact size on measured frictional properties, AFM probes with different tip apex sizes are obtained by thermal evaporation of gold and platinum onto the probes. In conjunction with the experiments, molecular dynamics (MD) simulations are performed that involve the calculation of friction forces experienced by model tip apexes of varying size on single- and few-layer graphene. Moreover, substrates with various RMS roughness and correlation length values are employed in the MD simulations to investigate the effect of substrate topography on frictional behavior. Results reveal that a subtle interplay between contact size and substrate topography determines the layer-dependent frictional behavior of graphene, providing a new perspective to the nanotribology of this remarkable material.

[1]: C. Lee *et al.*, *Science* **328**, 76 (2010)

3:20pm TR+BI+SE+TF-ThA4 Iron-Doped Diamond-Like Carbon Coatings (Fe-DLCs): Synthesis, Characterization, and Tribology--Seminal Results, **Parag Gupta**, Northwestern University/Argonne National Lab.; **M.E. Graham**, Northwestern University

Iron-doped diamond-like carbon coatings (Fe-DLCs) of ≈ 0.1 to 35 at.% Fe content have been synthesized, characterized, and tribologically tested. Coatings were deposited on Si(111), 52100 steel ball, and H-13 steel flat substrates using a closed-field unbalanced magnetron sputter deposition process with unmodified and modified graphite target states, the latter with press-fit cast gray iron slugs. Process parameters of target modification, target power, acetylene flowrate, and substrate bias were varied and used in establishing a process-conditioning window to create predictable coatings.

Mechanical characterization was done to determine deposition rate, thickness, internal stress, and hardness. Cross-sectional characterization was done to determine coating uniformity, to understand coating adhesion and morphology, and to confirm interlayer presence and morphology (if deposited). Surface characterization was done to determine surface roughness and mechanical anisotropy. Chemical characterization was done to determine elemental concentration and chemical anisotropy. Finally, structural characterization was done to determine carbon bond order.

Using a ball-on-flat reciprocating tribometer, highly-doped Fe-DLCs were studied at either room temperature or ≈ 100 °C and with either coating / coating or steel / coating contact. Electrical contact resistance between interfaces was measured *in situ*. A contact pressure of ≈ 1 GPa was employed alongside an average sliding speed of 1.0 cm / s, except when non-monotonic sequential speed stepping was prescribed. The boundary-lubricated sliding tests were conducted in the presence of poly-alpha-olefin SAE grade 30 synthetic base stock oil (PAO10) with and without molybdenum dithiocarbamate (MoDTC) and zinc dialkylidithiophosphate (ZDDP) additives, both at 0.5 wt.%. Coatings were also tested in unlubricated conditions.

Friction responses were determined, and wear assessments were conducted. Tribofilm and debris analyses were done. The results were

compared to those from DLC, CrN + DLC, Si-DLC, and W-DLC coatings obtained from Oerlikon Balzers. Results indicate that Fe-DLC samples containing between 12 and 35 at.% Fe exhibit negligible wear in the presence of PAO10 with MoDTC and ZDDP, affirming the influence of iron in catalyzing protective tribofilms. Additionally, wear on such samples in both lubricated and unlubricated conditions is far lower than that observed for other coatings, indicating that these Fe-DLCs are robust in any conditions.

4:00pm TR+BI+SE+TF-ThA6 Tribo-Rheometry of Soft Matter, **J. Kim, Alison Dunn**, University of Illinois at Urbana-Champaign **INVITED**

Hydrogel surfaces are biomimics for sensing and mobility systems in the body such as the eyes and large joints due to their compliance, controllable chemistry, permeability, and integrated aqueous component. Recent studies have shown that polymer concentration gradients in the top microns of crosslinked hydrogel surfaces result in a less dense surface region. In addition, the lubrication of hydrogel interfaces is driven by the effective mesh size, a parameter which follows from the local density. Given the similarity of a dilute crosslinked hydrogel surface with a dilute polymer solution, we probe the surface of a polyacrylamide hydrogel using stepped-velocity tribo-rheometry over 5 decades of sliding speed, with an annular aluminum countersurface. Three distinct lubricating regimes emerge based on a) hysteretic torque response depending upon increasing or decreasing sliding speeds, and b) characteristic torque overshoot following velocity step changes. This evidence supports the analogy of a rheology-like lubrication response. We postulate that the mechanisms of hydrogel-against-hard material lubrication are due to distinct complex fluid behavior characterized by weakly or strongly time-dependent response. Tribo-rheometry is particularly suited to uncover the lubrication mechanisms of complex interfaces such as are formed with hydrated hydrogel surfaces and biological surfaces.

4:40pm TR+BI+SE+TF-ThA8 Friction Coefficient Lowering in High-hardness Boron Nitride Films Under Ultra-high Vacuum, **Masao Noma**, Shinko Seiki Co., Ltd, Japan; **K. Eriguchi**, Kyoto University, Japan; **M. Yamashita**, Hyogo Prefectural Institute of Technology, Japan; **S. Hasegawa**, Osaka University, Japan

Solid lubricant material with low friction coefficient is of technological interest for its usage under harsh environments such as ultra-high vacuum. At present, MoSi-containing films [1] are the most widely employed for space applications because of their low friction coefficients (0.02–0.05) in vacuum [2]. However, the mechanical hardness and the oxidation resistance temperature are 10–20 GPa [3] and 360 °C [4], respectively, inapplicable to a long term operation in space. Boron nitride (BN) films have been considered an alternative material because of their superior high hardness and oxidation resistance temperature, 45 GPa and 1200 °C, respectively [5]. We have proposed a novel reactive plasma-assisted coating technique (RePAC) for forming 1- μ m-thick high-hardness BN films (~ 50 GPa) [6][7]. In this study, we present "friction coefficient lowering" phenomena in the high-hardness BN films under ultra-high vacuum ($\sim 10^{-6}$ Pa), which is in sharp contrast to "friction coefficient increase" usually observed for other hard coating materials. The time-dependent high-vacuum friction measurement revealed that the friction coefficient decrease from 0.1 to 0.03 was found for the substrate bias voltage from -90 to -180 V in the RePAC. In this (incident ion energy) region, the cubic BN phase was formed in the turbostratic BN background, leading to the high-hardness of ~ 50 GPa at atmosphere [7]. Moreover, the obtained low friction coefficient was confirmed to be stable (<0.05) for long time exposures to the vacuum (~ 96 hrs). The friction coefficients of the present BN films are comparable to widely reported values of MoS₂ films. The BN film prepared by the RePAC is one of promising hard coating materials for harsh environment (e.g., space) applications.

[1] M. Chhowalla, and G. A. J. Amarutunga, *Nature* **407** (2000) 164.

[2] G. Colas *et al.*, *Wear* **305** (2013) 192.

[3] N. M. Renevier *et al.*, *Surf. Coat. Technol.* **142-144** (2001) 67.

[4] K. C. Wong *et al.*, X. Lu, *Wear* **264** (2008) 526.

[5] C. B. Samantaray and R. N. Singh, *Int. Mater. Rev.* **50** (2005) 313.

[6] M. Noma *et al.*, *Jpn. J. Appl. Phys.* **53** (2014) 03DB02.

[7] K. Eriguchi *et al.*, AVS 61st Int. Symp. & Exhibition, SE+NS+TR-TuM3 (2014).

Thursday Afternoon, November 10, 2016

5:00pm **TR+BI+SE+TF-ThA9 Nanoscale Friction Properties of Water Intercalated Graphene on Mica and its Isotope Effects**, *Hyunsoo Lee*, Institute for Basic Science (IBS) & Korea Advanced Institute of Science and Technology (KAIST); *J.-H. Ko*, KAIST, Republic of Korea; *J.S. Choi*, Electronics and Telecommunications Research Institute, Republic of Korea; *J.H. Hwang*, IBS & KAIST, Republic of Korea; *Y.-H. Kim*, KAIST, Republic of Korea; *M.B. Salmeron*, Lawrence Berkeley National Laboratory (LBNL); *J.Y. Park*, IBS & KAIST, Republic of Korea

We demonstrate that the frictional behavior of hydrophobic graphene on hydrophilic mica is affected by water intercalation after exposure to humid air using atomic force microscopy. The single- and multi-layer graphene were formed by mechanical exfoliation on freshly cleaved muscovite mica. The adsorption of the ice-like water layer between graphene and mica led to friction enhancement, as compared with a pristine graphene/mica sample, which is presumably due to additional frictional energy dissipation at the solid-liquid interface. Moreover, friction on the graphene increased as the number of stacking water layers increased. The magnitude of friction increase was, on the other hand, reduced as following increase of the number of covering graphene layer above intercalated water layer, and then the friction is eventually not distinguished from the multi-layer graphene stack excluded water adsorption. Using the first-principle density functional theory calculations we explain this unexpected behavior by the increased spectral range of vibration modes of graphene caused by water, particularly the low frequency flexural modes, and by the better overlap of the graphene vibration modes with the mica phonons, which favors a more efficient dissipation of the frictional energy. Additionally, we found that the intercalation of deuterium oxide (D_2O) leads to the lower friction, compared to H_2O intercalated graphene on mica. We attribute this isotope effect with to the low vibrational frequency of D_2O adsorbate, which results in the low rate of frictional energy dissipation at the interface.

5:20pm **TR+BI+SE+TF-ThA10 The Remarkable Friction Behavior of Copper at Cryogenic Temperatures**, *Andrew Kustas*, Sandia National Laboratories; *J. Curry*, Lehigh University; *T. Babuska*, *M. Chandross*, *P. Lu*, *T.A. Furnish*, *N. Argibay*, Sandia National Laboratories

It is commonly accepted that unlubricated, self-mated pure metal contacts over the course of sliding invariably cold-weld and gall, leading to undesirably high friction and wear. Recent work with nanostructured pure metals has shown that in fact it is possible to obtain low friction ($\mu < 0.5$) with pure bare metals such as pure Cu and Au at room temperature. Here we discuss those findings, and more recent work that shows the impact of temperature, stress and microstructure evolution on friction of self-mated pure metals. Variable temperature friction experiments were used to show the existence of a temperature-dependent transition for Cu from high ($\mu > 1$) to low ($\mu = 0.25$) friction, achieved by sufficiently reducing temperature and promoting the development of nanocrystalline surface films that are unachievable at room temperature at the relatively high applied stresses imposed. In-situ electrical contact resistance (ECR) measurements were used to indirectly measure the evolution of the microstructure (grain size) at the interface throughout the experiment. Microscopy was then used to verify claims of nanocrystalline surface film formation at low temperatures. Lastly, an analytical model based exclusively on materials properties is presented that incorporates stress and temperature over time to predict grain size, connecting grain size to friction behavior, for pure FCC metals. While more work is needed to develop the proposed framework, a model that intrinsically connects grain size to friction behavior of metals based exclusively on materials properties is transformational to alloy design, and raises a number of compelling and highly fundamental questions for further research.

5:40pm **TR+BI+SE+TF-ThA11 Understanding Friction in MoS₂, Part 1: Stress, Time and Temperature**, *Tomas Babuska*, Sandia National Laboratories; *J. Curry*, Lehigh University; *M. Chandross*, *M.T. Dugger*, Sandia National Laboratories; *B. Krick*, Lehigh University; *N. Argibay*, Sandia National Laboratories

In the 90 years since the first patent was issued for molybdenum disulfide (MoS_2) as a friction and wear reducing additive, great strides have been made in understanding its remarkable lubricity. However, much remains to be understood about the mechanisms of friction at the molecular scale. Firstly, we present results of investigations into the origins of the well-known non-Amontonian behavior of MoS_2 . We show that the apparent return to Amontonian behavior previously reported with steel is in fact associated with an elasto-plastic transition of the contact, and that the stress-dependent friction predictable varies as a function of substrate composition and microstructure (hardness). Time-dependent friction evolution (i.e. run-in behavior) was also found to be strongly a function of

substrate material composition and stress; these results imply a potentially useful connection between stress and microstructure evolution in both film and substrate that is discussed. We also report on investigations into the temperature-dependent friction and wear behavior of pure MoS_2 . In the range -150 to 250°C, we report dramatic deviations from previous literature, as well as the existence of transitions between thermal and athermal behavior as a function of temperature. Evidence of deviations from classical Arrhenius behavior is presented, and the implications of these findings discussed in the context of thermally-activated friction models at the molecular scale. Finally, we end with a discussion of how these findings collectively advance our ability to develop a practical predictive friction model for MoS_2 that includes temperature, stress, substrate effects, defect density and commensurability as their foundation.

6:00pm **TR+BI+SE+TF-ThA12 Understanding Friction in MoS₂, Part 2: Water, Oxidation and Run-in**, *John Curry*, Lehigh University; *M. Chandross*, *T. Babuska*, Sandia National Laboratories; *N.C. Strandwitz*, *H. Luftman*, Lehigh University; *M.T. Dugger*, *N. Argibay*, Sandia National Laboratories; *B. Krick*, Lehigh University

Effects of water vapor and oxidation resistance for amorphous (sputtered) and highly ordered (N_2 sprayed) MoS_2 were investigated with a high-sensitivity, low energy ion scattering (HS-LEIS) spectrometer, molecular dynamics simulations and accompanying tribological testing in each environment of interest. Recent studies have shown that N_2 sprayed MoS_2 coatings possess a preferential surface parallel basal plane texture as deposited due to the kinetic energy imparted during spraying, effectively shearing MoS_2 particles onto the surface. As such, the highly ordered structure of the sprayed coatings both at the surface and throughout the bulk of the film are hypothesized to act as a diffusion barrier to environmental contaminants. Coatings were exposed to molecular oxygen at 250°C and atomic oxygen at 20°C for 30 minutes each and subsequently depth profiled in the HS-LEIS. Results show that N_2 sprayed coatings were successful in limiting the depth of oxidation for both types of exposure. The main contributor, however, to increased initial friction post exposure was the type of coating (amorphous vs highly oriented). Tribological experiments in dry and humid nitrogen showed the initial friction response to be unaffected for sprayed samples while greatly affected for sputtered. Spiral orbit tribological testing was utilized in dry and humid nitrogen environments to further assess the effect of prolonged sliding on purely amorphous MoS_2 with and without formation of a transfer film. It is hypothesized that water does not poison friction behavior of established films of highly oriented MoS_2 , but it does poison the ability to form long range order and sintering of crystallites.

Thursday Afternoon Poster Sessions, November 10, 2016

2D Materials Focus Topic

Room Hall D - Session 2D-ThP

2D Materials Poster Session

2D-ThP1 Vacuum Properties and Operation Stability of the RFQ Accelerator in J-PARC Linac, *Takatashi Morishita*, Japan Atomic Energy Agency, Japan

The J-PARC accelerator comprises an injector linac, a 3-GeV Rapid-Cycling Synchrotron and a 50-GeV Main Ring. The beam energy of the linac has been upgraded from 181 MeV to 400 MeV in 2013. For the beam current upgrade, the new frontend (RF ion source, RFQ, chopping system) has been installed for 1 MW operation at RCS. The new RFQ, which is designed for 50 mA beam acceleration from 0.05 MeV to 3 MeV, has been high-power tested and beam acceleration tested at the test station before the installation. The existing RFQ, which is 30 mA design, was replaced to 50 mA RFQ in the accelerator tunnel in summer 2014. After two weeks vacuum pumping, the high-power RF conditioning has been started in the middle of September, then, the user operation started in the beginning of November, 2014. Since then, the RFQ operates without serious problems for more than one year, however, the operation stability with beam acceleration was not enough due to the sparking in the RFQ cavity. We consider that the impurities in the vacuum chamber are related to this sparking phenomena. In this paper, the relation between the sparking rates, the residual gas species in the cavity, beam operation parameters are described.

2D-ThP2 Inkjet Printing Of Liquid-Exfoliated, Highly Conducting Graphene Nanosheets, *J. Desai, M. Michel, C. Biswas, R. Hossain, Jorge Catalan, A.B. Kaul*, University of Texas at El Paso

Graphene consisting of just one sheet of carbon atoms arranged in a honeycomb lattice is a thinnest two-dimensional (2-D) material known since its discovery in 2004. It finds applications in printed electronics, flexible displays, fuel cells, solar cells and range of other applications due to its high strength and good thermal and electrical properties. Two-dimensional materials are formed from layered materials which can be defined as materials having strong in-plane covalent bonding but weak out-of-plane van der Waals bonding. Exfoliation, i.e., shearing of individual monolayers of layered materials to get two-dimensional materials, can lead to breakage of van der Waals bonding and production of thin atomic two-dimensional nanosheets. Liquid-phase exfoliation refers to exfoliation in suitable solvents. It is a versatile, scalable and sustainable route for production of 2-D nanosheets. Inkjet printing is a material-conserving deposition technique used for printing patterns and devices using liquid-phase materials. The present challenges in printed electronics include finding an appropriate common solvent for exfoliation and printing, printing highly conductive and uniform graphene patterns, preventing nozzle clogging and non-uniform spread of ink on substrate, promoting adsorption and preventing absorption of inks. In our work, we demonstrate highly conductive graphene patterns produced by liquid-phase exfoliation of layered graphite in N-Methyl-2-pyrrolidone (NMP) followed by inkjet printing. We have found an avenue to tailor the viscosity of NMP through the addition of PEDOT: PSS or Poly (3,4 ethylenedioxythiophene)-poly(styrenesulfonate), making it suitable for inkjet printing. Our ink jet printed dispersions show a uniform microstructure, good optical absorbance values and higher concentration of graphene in our final exfoliated solvent using the novel techniques we have developed.

2D-ThP3 Electronic Transport Properties of Hybrid Graphene-C60 Structures, *S. Chugh, C. Biswas, Avra S. Bandopadhyay, G. Lara, L. Echegoyen, A.B. Kaul*, University of Texas at El Paso

Since graphene was first mechanically exfoliated in 2004 using scotch tape [1], it has attracted intense interest due to its unique electrical, mechanical and thermal properties. Since then, rapid advances have been made in the large-area deposition of graphene films and its ensuing applications. At the same time, C₆₀ fullerenes and their derivative structures also display remarkable chemical reactivity [2]. Various hybrid materials created by organic functionalization of fullerenes have generated intense attention, driven by the possibility of combining some of the outstanding properties of these zero-dimensional materials with those of higher order dimensionality [3]. In this work, we report on the electrophoretic deposition of C₆₀ on the graphene. The synthesized graphene films were characterized using Raman spectroscopy and Scanning Electron Microscopy (SEM), and electrical contacts were made to the graphene flakes of varying sizes using a lift-off process. Then, C₆₀ was synthesized and deposited via an electrophoretic deposition technique. Electronic characterization of the

structures was conducted before and after the attachment of C₆₀ over a wide range of temperatures. A comparative study was made to analyze the resistivity and conductivity as a result of the interaction with the Si/SiO₂ substrate. Also, we discuss the potential application of graphene based C₆₀ structures as flexible transparent electrodes in photovoltaic devices.

Keywords: Graphene, CVD, Raman Spectroscopy, SEM, electrophoretic deposition, C₆₀

[1]Novoselov, KS, et al.; Science 306, 666-669 (2004).

[2]Dirk M, Acc. Chem. Res., 33 (10), 695-703 (2000).

[3] Dingshan Yu, J. Phys. Chem. Lett., 2 (10), 1113-1118 (2011).

2D-ThP4 Comparative Study of the Optical and Electrical Properties of Fluorine-doped Tin Oxide Films Obtained by Spray Pyrolysis Techniques, *Karim Monfil-Leyva, R.C. Ambrosio-Lázaro, J.A. Luna-López*, Benemerita Universidad Autónoma de Puebla, Mexico; *A.L. Muñoz-Zurita*, Universidad Politécnica Metropolitana de Puebla, Mexico

Research and development of Transparent Conducting Oxides (TCOs) has increased due to their many industrial applications. In particular, Fluorine doped Tin Oxide (FTO) is actually needed to develop semiconductor devices because this material has repeatable optical and electrical properties. This work shows a comparative study of the optical and electrical properties of FTO thin films obtained by electronic spray pyrolysis and ultrasonic spray pyrolysis techniques. A chemical solution for spraying purposes was prepared with stannic chloride (SnCl₄) dissolved in ethanol (C₂H₆O₂) mixed with ammonium fluoride (NH₄F). FTO thin films were deposited on glass substrates varying the distance from the nozzle to the hot plate. Spray pyrolysis system was controlled by an electronic trigger. Ultrasonic pyrolysis system was controlled by a resonant frequency. The transmittance and reflection properties were measured using an UV-Vis Spectrophotometer and the band gap energy was determined. The average transmittance in the visible range of FTO films was even above 85%. All FTO films were characterized using X-Ray Diffraction (XRD) and Scanning Electron Microscopy (SEM). The X-ray diffraction patterns showed that main growth orientations were [110], [101] and [211]. SEM images showed homogeneous surface on FTO films but they also indicated a change on nano-cluster sizes and density according to the distance from the nozzle to the hot plate and according to the used spray pyrolysis technique. XRD results were used to calculate the grain size and lattice parameters. The chemical composition of the FTO films was also analyzed using Electron Diffraction Scanning (EDS) and the obtained atomic concentration was compared. Sheet resistance was measured using a four points arrangement and the minimum sheet resistance was 14 Ω/square. Optical and electrical results of the FTO thin films showed suitable properties for photovoltaic and optoelectronic applications using fast, cheap and large area deposition techniques.

2D-ThP5 Selective Molecular attachment for 3D Printing of 2D Circuits, *A.T. Juhl, N.R. Glavin, G.M. Leuty, R.J. Berry, R.R. Naik, M.F. Durstock, E.M. Heckman, R.S. Aga, E.B. Kreitz*, Air Force Research Laboratory; *Wenbi Lai, C. Muratore*, University of Dayton

Recently, we utilized phage display techniques to identify peptides that selectively bind to 2D targets such as electrically conductive graphene and semiconducting MoS₂ in the forms of micro-scale fine powder, bulk crystals, and ultra-thin films (<1.5-5 nm). To examine the nature of peptide binding to these materials, we produced different 'inks' comprised of peptide molecules known to selectively bind to each material in solvents for printing on diverse surfaces including SiO₂, gold, and PDMS. Each ink only binds to one type of particle (graphene or MoS₂). We then exposed the substrates printed with peptides to suspensions of 2D particles. The particles demonstrate strong binding to the printed peptide surfaces, demonstrating a new scalable technique for large area device fabrication from 2D materials on diverse surfaces. To further understand peptide-MoS₂ surface binding mechanisms, molecular dynamics simulations employing a newly developed atomic force field predicting the surface energy of MoS₂ films were conducted. Integration of binding peptides into the model in conjunction with experimental results promote fundamental understanding of molecular interactions with MoS₂ and other TMD materials for development of novel sensors and devices.

2D-ThP6 Image Potential State of Graphene on Iridium Modulated by Oxygen Dosing, *Yi Lin, Y.Z. Li, J. Dadap, R. Osgood*, Columbia University

Image potential state are an important class of surface states, which can be used to probe the chemical and structural properties of metallic or dielectric crystals. Recently the existence of image states has been reported for graphene and graphene on metal such as the Fauster and

Thursday Afternoon Poster Sessions, November 10, 2016

Osgood, Hoefler, and Petek Groups. However, understanding of the effects of adsorbates on Gr surfaces has not been extensively studied either theoretically or experimentally. An important issue is the change of the electronic structure of the image potential states at graphene-metal interface due to oxygen absorption. Thus we have recently carried out the study on the image potential system for graphene on iridium (111) as altered by oxygen dosing.

The epitaxial graphene on iridium is prepared by repeated cycles of temperature programmed growth (room-temperature ethene exposure 2×10^{-5} torr for 45 s and then flashing to 1450 K. This procedure is known to lead to self-limited growth such that exactly one graphene monolayer are formed on the single crystal Iridium substrate (*in situ* cleaned by many annealing and sputtering cycles). The oxygen adsorption is done simply by pure oxygen gas injection by 10^{-5} Torr. The cleanness of the iridium substrate, the growth of monolayer graphene on iridium and the absorption of oxygen are monitored by *in situ* low energy electron diffraction (LEED) patterns. Our 2PPE experiments are conducted using either monochromatic or bichromatic femtosecond pulses with the pump photon energy generally in the 4.2 eV range. An optical parametric amplifier, driven by 250 kHz Ti-sapphire laser, generates tunable laser pulses from 1.5-6.1 eV, pulse duration 90 fs and pulse energy 1 nJ. Photoemission electrons are detected along the M-G-M direction of the Brillouin zone using a spherical-sector energy analyzer with 50 meV energy resolution. Care is taken to prevent distortion of the photo-emitted electron energy distribution by space charge effects.

With this instrument, the state energy, its dispersion and the decay time of the first image potential states of the oxygen-absorbed graphene on iridium are measured. We compare our results of oxygen-dosed graphene on iridium with previous reported results of pure graphene on iridium. The shift of the states, the broadening of the dispersion and the change of the dynamic process are modeled and discussed, which provides new insight on using image states for surface probing, as well as the effects of dosing on image state physics.

This work was supported by the Department of Energy, Office of Basic Energy Sciences, Division of Materials Sciences and Engineering under Award Contract No. DE-FG 02-04-ER-46157.

2D-ThP7 Raman Spectroscopy and Optical Characterization of Thermoelectric Devices From Ni/Bi₂Te₃/Sb₂Te₃/Ni Thin Films, Aschalew Kassu, S. Budak, Z. Xiao, R. Hammond, X. Crutcher, A. Sharma, Alabama A&M University

Thermoelectric devices from Ni/Bi₂Te₃/Sb₂Te₃/Ni thin films were prepared. The thin films are deposited by using DC/RF magnetron sputtering and E-beam deposition systems. The surface morphology of the fabricated thermoelectric films is characterized using Scanning Electron Microscope (SEM). Raman spectroscopic technique is used for identification of inherent molecular specificity and analysis of chemical compositions of the films. The resonant features of the scattering spectra measured under the 532 nm and 785 nm wavelength excitation lasers are analyzed.

Acknowledgement

This research was supported by NSF with grant numbers NSF-HBCU-RISE-1546965, NSF-EPSCOR-R-II-3-EPS-1158862, DOD with grant numbers W911 NF-08-1-0425, and Department of Homeland Security-Scientific Leadership Award, Grant No. DHS-SLA 2014-ST-062-000060

2D-ThP8 Thermoelectric Generators from SiO₂/SiO₂+Au Thin Films For Energy Harvesting, S. Budak, Z. Xiao, M. Curley, Justin Cole, C. Birchfield, M. Howard, B. Rodgers, T. Strong, Alabama A&M University

Thermoelectric generators were prepared from multilayered SiO₂/SiO₂+Au thin films using DC/RF magnetron sputtering system. Thermoelectric devices were annealed at different temperatures to form nanostructures in the multilayer thin films to increase the Seebeck coefficients and electrical conductivity and decrease thermal conductivity. The prepared devices were characterized using Seebeck coefficient measurement; four probe van der Pauw measurement resistivity and the laser thermal conductivity systems. The surface morphology of the fabricated thermoelectric films is characterized using Scanning Electron Microscope (SEM+EDS). TE devices will also be characterized as if they are wave-guides. Mode index, propagation loss, refractive index profile with respect to the dose, depth of the thin films will be analyzed as a function of annealing temperatures.

Acknowledgement

Research was sponsored by NSF with grant numbers NSF-HBCU-RISE-1546965, NSF-EPSCOR-R-II-3-EPS-1158862, DOD with grant numbers W911

NF-08-1-0425, and W911NF-12-1-0063, U.S. Department of Energy National Nuclear Security Administration (DOE-NNSA) with grant numbers DE-NA0001896 and DE-NA0002687.

2D-ThP9 Advanced Thermoelectric Devices from Ni/Bi₂Te₃/Sb₂Te₃/Ni Thin Films for Energy Harvesting, S. Budak, Z. Xiao, M. Curley, Cody Birchfield, J. Cole, M. Howard, B. Rodgers, T. Strong, Alabama A&M University

Thermoelectric devices were prepared from Ni/Bi₂Te₃/Sb₂Te₃/Ni thin films using E-beam deposition and DC/RF magnetron sputtering systems. Fabricated devices were annealed at different temperatures to form nanostructures in the multilayer thin films to increase both the Seebeck coefficients and electrical conductivity and decrease thermal conductivity. The thermoelectric devices were characterized using Seebeck coefficient measurement system; four probe van der Pauw measurement resistivity system and the laser thermal conductivity system. The surface morphology of the fabricated thermoelectric films is characterized using Scanning Electron Microscope (SEM). TE devices will also be characterized as if they are wave-guides. Mode index, propagation loss, refractive index profile with respect to the dose, depth of the thin films will be analyzed as a function of annealing temperatures.

Acknowledgement

Research was sponsored by NSF with grant numbers NSF-HBCU-RISE-1546965, NSF-EPSCOR-R-II-3-EPS-1158862, DOD with grant numbers W911 NF-08-1-0425, and W911NF-12-1-0063, U.S. Department of Energy National Nuclear Security Administration (DOE-NNSA) with grant numbers DE-NA0001896 and DE-NA0002687.

2D-ThP10 VUV-photoassisted Chemical Doping on Graphene Oxide, Masahiro Soga, Y. Tu, T. Utsunomiya, T. Ichii, H. Sugimura, Kyoto University, Japan

Chemical doping on graphene and its derivatives is a powerful technique for modulating their electronic properties¹. Especially, nitrogen doping can help the electron transfer and enhance the electrocatalytic activity. Nitrogen doped graphene have been synthesized by thermal annealing approach and hydrothermal reduction of graphene oxide (GO) in the presence of N₂H₄ and NH₃ in general^{1,2}. However, these methods are high cost, complicated and suffer from toxic chemicals. In this research, nitrogen doped and reduced graphene oxide (N-rGO) was synthesized by vacuum ultraviolet (VUV) irradiation.

Colloidal dispersion of GO sheets was prepared by the modified Hummers' method. NH₃ aqueous solution (14.8 M) was added to the GO dispersion and was magnetically stirred for 24 hours. After that, the dispersion was centrifuged at 13.5 krpm for 10 min and washed ten times with ultra pure water, and then aqueous dispersion of nitrogen modified GO (N-GO) was obtained. The N-GO dispersion was spincoated on Si substrate and VUV light ($\lambda = 172$ nm, 10 mW cm⁻²) was irradiated on this sample under high vacuum condition ($< 10^{-3}$ Pa) for 64 min. The sample was characterized by Fourier transform infrared spectroscopy (FT-IR) and X-ray photoelectron spectroscopy (XPS).

XPS and FT-IR analysis of the samples revealed that chemically reactive oxygen functional groups in a GO sheet reacted with ammonia and the formation of C-N bond proceeded after stirring in NH₃ aqueous solution. After VUV irradiation, XPS and FT-IR analysis showed that N-GO was reduced and bonding configuration of nitrogen was changed.

1. X. Li, H. Wang, J. T. Robinson, H. Sanchez, G. Diankov, H. Dai, J. Am. Chem. Soc. 131, 15939 (2009)

2. D. Long, W. Li, J. Miyawaki, I. Mochida, S. Yoon, Langmuir 26, 16096 (2010)

2D-ThP11 Tungsten Diselenide Nanoribbons Formed by Focused Helium Ion Beam Induced Etching, Michael G. Stanford, P.R. Pudasaini, A.T. Wong, A. Hoffman, D.G. Mandrus, P.D. Rack, The University of Tennessee Knoxville

The helium ion microscope (HIM) has garnered much attention in recent years due to its high resolution and precision as a nanoprocessing tool. In this work, we introduce a focused helium ion beam induced etching (FIBIE) process which enables direct-write patterning of WSe₂. The etching process utilizes the XeF₂ precursor molecule to provide a chemical etch assist for rapid material removal. The FIBIE process enables the high fidelity patterning of WSe₂ with He⁺ doses an order of magnitude lower than standard He⁺ milling procedures. Of particular interest, transition metal dichalcogenide (TMD) nanoribbons exhibit unique magnetic properties depending upon edge termination. However, few experimental studies have been conducted on TMD nanoribbons due to difficulty of fabrication.

Thursday Afternoon Poster Sessions, November 10, 2016

The FIBIE process enables the straightforward direct-write fabrication of aligned arrays of WSe₂ nanoribbons with dimensions as low as 8 nm. The WSe₂ nanoribbons demonstrate high optical anisotropy and electrical measurements are reported for the first time. We also study the magnetic properties and report magnetoresistance of devices fabricated from WSe₂ nanoribbon arrays.

2D-ThP12 Tuning the Electronic Structure of Metallic Single Crystal Surfaces through Ultra Thin Hetero-Junctions for Photocathode Applications, ZhengRong Lee, R. Seibert, D. Velázquez, L. Spentzouris, J. Terry, Illinois Institute of Technology

The development of photocathodes for the next generation of state-of-the-art laser-driven photoinjectors requires the use of photoemissive materials with specific characteristics depending upon their application (FELs, ERLs, Wakefield acceleration, etc.). The ability to tune the emissive properties of photocathodes to match the requirements of the specific accelerator device could have a important impact in research and development. In this work we show that such photoemissive tunability can be achieved through the engineering of single crystal metallic surfaces by coating them with metal-insulator heterojunctions of various thicknesses. Ultrathin multilayered MgO/Ag(001)/MgO films were grown by pulsed laser deposition, tuning the thickness n of the flanking MgO layers to 0, 2, 3, and 4 monolayers. We observed an increase in quantum efficiency and simultaneous decrease in work function with layer thickness. The scale and trend direction of measurements are in good but not excellent agreement with theory. Angle resolved photoemission data for the multilayered sample $n = 3$ showed that the emission profile has a metallic-like momentum dispersion. Deviations from theoretical predictions [K. Németh et al., PRL 104, 046801 (2010)] are attributed to imperfections of real surfaces in contrast with the ideal surfaces of the calculation.

2D-ThP13 Electronic Structure of Bulk WSe₂ and Multilayer WS₂, Iori Tanabe, University of Nebraska-Lincoln; **T. Komesu,** University of Nebraska - Lincoln; **E.F. Schwier,** Hiroshima Synchrotron Radiation Center; **M. Gomez, L. Bartels,** University of California - Riverside; **M. Zheng, Y. Kojima,** Hiroshima University; **E.M. Echeverria,** University of Nebraska-Lincoln; **A.V. Barinov, S.K. Balijepalli, V. Kandyba, Elettra - Sincrotrone Trieste; K. Shimada,** Hiroshima Synchrotron Radiation Center; **P.A. Dowben,** University of Nebraska - Lincoln

WSe₂ and WS₂ and the related transition metal dichalcogenides (TMDs) MX₂ (with M = V, Mo, W, Ta and X = S, Se, Te) are layered structures, where each plane consists of a hexagonal honeycomb lattice reminiscent of graphene or graphite. The distinguishing features of TMDs compared to graphene are that TMDs are semiconductors and TMDs monolayers have C_{3v} symmetry, not C_{6v} symmetry, since the metal and chalcogen planes are offset from each other. We investigated the valence band structure of bulk WSe₂ and multilayer WS₂ using angle resolved photoemission spectroscopy (ARPES). These ARPES studies of the electronic band structure of bulk WSe₂ and multilayer WS₂ provide a means to compare the effective hole mass and the splitting of the top of the valence band at K, due to spin-orbit coupling for various transition metal dichalcogenides. The splitting of the top of the valence band at K was measured to be 0.49±0.01 eV and 0.42±0.03 eV, for bulk WSe₂ and multilayer WS₂ respectively. In both cases, the splitting due to spin orbit coupling are far larger than that for MoS₂, but smaller than that for monolayer WSe₂. We found that the effective mass at the top of the valence band at K of WSe₂ and WS₂ were very small, which indicates very high intrinsic mobility and is consistent with expectations from density functional theory. The electron effective masses, as derived from angle-resolved inverse photoemission, are found to be much greater than anticipated.

Spectroscopic Ellipsometry Focus Topic Room Hall D - Session EL+AS+EM+TF-ThP

Spectroscopic Ellipsometry Poster Session

EL+AS+EM+TF-ThP1 FTIR Ellipsometry Studies of Thermally Grown GeO₂ on Ge, Jaime Moya, T.N. Nunley, N.S. Fernando, N. Samarasingha, S. Zollner, New Mexico State University

To study the vibrational modes of GeO₂, we produced a set of thermal GeO₂ oxides ranging from 45 to 136 nm in thickness. Receiving a set of Ge Bulk wafers, we cleaved and roughened the back sides via an aluminum abrasive to avoid backside reflections. To remove carbon-containing surface contaminants and leave a stable oxide on the wafer, we performed a hybrid dry/wet clean. The dry clean was done by subjecting the wafer to an

ozone clean in an ultrapure oxygen environment while heating the sample to 150°C for 1 hour, followed by a 30 minute incubation period. The samples were then cleaned ultrasonically for 20 minutes in deionized water followed by 20 minutes in isopropanol. No harsh chemicals were used. The samples were then dried with nitrogen and annealed at 270 kPa and 550°C in ultrapure oxygen for a few hours to achieve different oxide thicknesses.

Using Fourier-transform infrared ellipsometry, the ellipsometric angles ψ and Δ were measured from 250 to 6000 cm⁻¹ at several angles of incidence (60° to 75°). The infrared lattice absorption peak of the amorphous GeO₂ was fit with a Lorentz oscillator.

When comparing our results to Lippincott's *et al.* [1] transmission measurements of vitreous GeO₂ formed by quenching hexagonal GeO₂, we see a negative shift in vibrational frequency. The difference can be attributed to the different Ge-O bond length comparing the vitreous GeO₂ and our amorphous thermal oxide. Our amorphous thermal oxide GeO₂ samples have a longer bond length, corresponding to a weaker bond and a lower vibrational frequency. This shift also shows a lower density of our samples compared to Lippincott *et al* [1].

References

[1] E.R. Lippincott, A. Van Valkenburg, C.E. Weir, and E.N. Bunting, J. Res. Natl. Bur. Stand. **61**, 61 (1958).

EL+AS+EM+TF-ThP2 Anisotropic Bruggeman Effective Medium Approach for Modeling Spectroscopic Ellipsometry Data of Porous Samples, Stefan Schöeche, J. VanDerslice, J.A. Woollam, J.A. Woollam Co., Inc.

Porous materials are widely used with applications including filtration devices, low-k dielectrics, catalysts, optical coatings, and more. The porous medium is described by its total porosity, pore diameter and specific surface area. The overall properties of the porous material are a result of the combined constituents and can often be approximated using effective medium theories. Due to complicated microstructure, these effective properties may vary along different directions or within the material resulting in anisotropic optical properties or gradients in pore size and total porosity.

Spectroscopic ellipsometry (SE) based porosimetry monitors the optical and structural changes of a porous sample during an adsorption and desorption cycle, i.e., insitu monitoring while the sample is exposed to an atmosphere with solvent partial pressure P varied between zero and the saturation vapor pressure of the solvent over flat surface P_0 . Ellipsometric porosimetry based on the Lorentz-Lorenz equation is widely used to characterize thin porous films since it is simple (only requires refractive index at one wavelength) and the skeletal material refractive index is not needed for the calculation. However, the theory is based on invalid assumptions on the microscopic nature of the film, the choice of refractive index is random, it is applicable only to isotropic and homogeneous samples, makes assumptions on the filling of pores at relative pressures $P/P_0=0$ and $P/P_0=1$, ignores potential inaccessible pores, and does not provide access to the skeletal refractive index.

We present an alternative approach to analyze porous samples based on the anisotropic Bruggeman effective medium approximation (ABEMA). The model uses well established theory to best match the SE data over a wide spectral range, is easily extendable to more constituents, accounts for optical anisotropy due to the shape of the pores or the pore network, allows determination of the skeletal refractive index in unknown materials, is sensitive to inaccessible pores, and allows grading of relevant sample properties such as the total porosity. A comparison of the two model approaches for data obtained on a porous SiO₂ film on Si substrate will be shown.

EL+AS+EM+TF-ThP3 Optical Constants of M2-phase VO₂ Measured by Spectroscopic Ellipsometry, Samuel T. White, R.F. Haglund, K. Hallman, Vanderbilt University

Vanadium dioxide (VO₂) is a highly interesting material due to changes in its electronic and optical properties associated with the reversible phase transition from a monoclinic (M1) to a rutile (R) crystal structure. This transition makes VO₂ a promising candidate for many applications, including ultrafast electrical switching and optical modulation. There exists another, distinct monoclinic phase (M2) which also can undergo the transition to R, and which is structurally similar to a possible transient phase appearing in the M1-R phase transition. Thus, M2 is important to understanding the M1-R transition, besides being potentially useful for application in its own right; however, M2 and its phase transition are not as well-characterized as M1. Establishing the optical constants for M2-phase

Thursday Afternoon Poster Sessions, November 10, 2016

vanadium dioxide is an important step in characterizing this phase and will help provide understanding of its relationship to the other phases.

Here, variable-temperature spectroscopic ellipsometry is used to measure the optical constants of thin-film M2-phase VO₂ below and above the phase-transition temperature, for wavelengths ranging from 370 to 1690 nm. Samples were prepared by electron-beam deposition onto a silicon substrate, with Cr doping to prepare the M2-phase. Experiments were performed both at room temperature and at 95°C with a JA Woolam M-2000 Spectroscopic Ellipsometer equipped with a heated sample stage. VO₂ layer thickness was established by profilometry measurements, and the optical constants were extracted by fitting data to a sum of three Lorentz oscillators. The results are compared to those obtained for thin-film M1-phase VO₂.

The optical constants for M2 and M1 are found to have similar wavelength-dependence, and to agree generally with results obtained for M1 by other researchers. The extinction coefficient, k , is very close for both samples over all wavelengths measured. The index of refraction, n , on the other hand, is larger for M2 than for M1 by ~5-10% for almost all wavelengths measured, with the greatest difference occurring at wavelengths near the peak value, ~430 nm. At elevated temperatures, both samples show optical constants typical of R-phase VO₂, though the index of refraction again appears to be higher for the M2 sample than for the M1 sample. Repeating this experiment with samples prepared by another method may help to distinguish effects due to phase difference due to those due to other sample differences.

Electronic Materials and Photonics

Room Hall D - Session EM-ThP

EMPD Poster Session

EM-ThP1 The Effects of VUV Radiation on Low-k Organosilicate Glass (SiCOH) as Measured with Electron-Spin Resonance, *Panpan Xue, W. Li,* University of Wisconsin-Madison; *J. de Marneffe, M. Baklanov,* IMEC, KU Leuven Belgium; *V. Afanas'ev,* Catholic University of Leuven, Belgium; *Y. Nishi,* Stanford University; *J.L. Shohet,* University of Wisconsin-Madison

The effects of VUV radiation on defect concentrations in SiCOH are investigated. Electron-spin resonance (ESR) spectroscopy is a very effective tool to detect defects in dielectrics. ESR has been used on various high-k dielectrics, such as HfO₂. Here, in order to obtain a clear spectroscopic signal, 60-nm thick SiCOH ($k=2.4$) was deposited on high-resistivity (3000 Ω -cm) wafers. There are at least two kinds of detectable defects in SiCOH: Si dangling bonds ($g=2.0054$) and Oxygen vacancies ($g=2.0020$). In this work, we concentrate on the silicon dangling-bond defects. In order to eliminate dangling bonds from the silicon substrate as well as its edges, CP4 and HF treatments were used. To investigate the influence of VUV radiation, the samples were exposed to synchrotron radiation with a range of photon energies from 7.3 to 21 eV. The ESR measurements showed that the defect concentration of the silicon dangling bonds increased after VUV exposure with photon energies higher than 8 eV. In addition, when the photon energy was less than 15 eV, the defect concentration increased with higher photon energy, but did not increase further for VUV exposures with higher photon energies. This is likely caused by electron depletion by photoemission from defects during VUV irradiation. That is, before VUV irradiation, the silicon dangling bonds are filled with electrons. The electrons are then depleted by photoemission during irradiation. Since the band gap for SiCOH is approximately 8 eV, this is also consistent with the fact that the energy threshold for Si-H bond photolysis at the surface of H-passivated Si is ~7.9 eV. Moreover, VUV exposure can cause a loss of methylated species. It is possible that the loss of -CH₃ groups results in additional Si dangling bonds near the surface of the SiCOH films. The ESR signals have a Lorentzian shape and the Bloch model fits these well. We conclude that silicon dangling bond defects in SiCOH and its interface with silicon can be detected using ESR and that VUV exposure increases the defect concentration.

Work supported by the Semiconductor Research Corporation under Contract No. 2012-KJ-2359 and the National Science Foundation under Grant No. CBET-1066231.

H. Zheng, S. W. King, V. Ryan, Y. Nishi and J.L. Shohet, Appl. Phys. Lett. 104, 062904 (2014).

2 A. Puse, U. Wetterauer, and P. Hess, Phys. Rev. 81, 645 (1998).

3 T.V. Rakhimova, A.T. Rakhimov, Yu. A. Mankelevich, D.V. Lopaev, A.S. Kovalev, A.N. Vasil'eva, S.M. Zyryanov, J. Phys. D: Appl. Phys. 47, 025102 (2014).

4 J. Lee and D.B. Graves, J. Phys. D: Appl. Phys. 44, 325203 (2011)

EM-ThP2 Effect of Initial Substrate Conditioning on Structural and Optoelectronic Properties of In_xGa_{1-x}N Grown by MEPA-MOCVD, *Indika Senevirathna, D. Seidlitz, A. Fali, Y. Abate, N. Dietz,* Georgia State University
Fabrication of high quality Indium rich- In_{1-x}Ga_xN layers is still a challenge due to the immiscibility between the binaries InN and GaN. The lack of lattice-matched substrate is an additional challenge for the growth of In_{1-x}Ga_xN layers. The lattice mismatch between the substrate template and the In_{1-x}Ga_xN layer generate residual strains and threading dislocations at the interface that propagate into the In_{1-x}Ga_xN layers, and consequently, degrade the quality of the In_{1-x}Ga_xN epilayer. To mitigate these effects, different approaches such as the use of buffer layers (e.g. GaN, InN, AlN) between the In_{1-x}Ga_xN layers are explored.

In this contribution, we present our findings on the effects of substrate treatments on the structural and optoelectronic properties of In_{1-x}Ga_xN layers grown by Migration-Enhanced, Plasma-Assisted MOCVD (MEPA-MOCVD). Furthermore, the analysis consist the data for In_{1-x}Ga_xN layers grown on different nitrided sapphire substrates as well as layers grown on sapphire substrates templates, containing InN, GaN or AlN interlayers.

The optoelectronic properties – e.g. free carrier concentration, the mobility of the carriers, high-frequency dielectric constant ϵ_{∞} , and layer thickness in the In_{1-x}Ga_xN layers have been analyzed by simulating the reflectance spectra, obtained via Fourier Transform Infra-red (FTIR) spectroscopy, using a multilayer stack model and a dielectric function based on Lorentz-Drude model. AFM topography has been used to study the surface morphology of the layers. Raman spectroscopy has been utilized to analyze the local crystallinity ($E_2(\text{high})$ mode) of the In_{1-x}Ga_xN layers as well as the composition via the shift of the $A_1(\text{LO})$ mode and its broadening with In_{1-x}Ga_xN target composition.

EM-ThP3 An In-Depth Study of Cu₂ZnSnS₄ Films Synthesized by Sulfurization of Stacked Metallic Layers, *A. Alvarez Barragan, S.A. Exarhos, Lorenzo Mangolini,* University of California Riverside

The quaternary chalcogenide Cu₂ZnSnS₄ (CZTS) is composed of earth-abundant elements and has interesting optoelectronic properties that project it as an important candidate for thin-film photovoltaics. Among several synthesis methods, sulfurization of metallic stacked layers has been heavily used because it does not rely on toxic compounds and provides good control over the final stoichiometry of the sample [1-3]. We present an in-depth structural and compositional analysis of CZTS synthesized by this technique. A first study exhibits preferential segregation of hexagonal SnS₂ when increasing the sulfurization pressure in a closed annealing chamber. Variations in film morphology suggest that different reaction pathways take place as the pressure is raised. Formation of gaseous SnS is favored at lower pressure, while nucleation of solid SnS₂ preferentially occurs at higher pressure. In addition to this investigation, an individual grain study sheds light on the complexity of this material system. Elemental analysis shows significant grain-to-grain variations in composition despite dealing with an overall close-to-ideal stoichiometry. High resolution Raman spectroscopy indicates that this is accompanied by grain-to-grain structural variations as well. The intensity from the 337 cm⁻¹ Raman peak, generally assigned to the kesterite phase of CZTS, remains constant over a large area of the sample. On the other hand, signals from secondary phases at 376 cm⁻¹ (copper-tin-sulfide) and 351 cm⁻¹ (zinc-sulfide) show significant variation over the same area. These results demonstrate how a seemingly homogeneous CZTS thin film can actually have considerable structural and compositional variations that are often overlooked.

References

[1] Dhakal, T. P.; Peng, C.; Tobias, R. R.; Dasharathy, R.; Westgate, C. R. Characterization of a CZTS thin film solar cell grown by sputtering method. *Sol. Energy* **2014**, 100, 23–30.

[2] Hong, S.; Kim, C. Characteristics of Cu₂ZnSnS₄ Thin Films Fabricated by Sulfurization of Two Stacked Metallic Layers. *Mol. Cryst. Liq. Cryst.* **2014**, 602, 134–143.

[3] Cheng, A.-J.; Manno, M.; Khare, A.; Leighton, C.; Campbell, S. A.; Aydil, E. S. Imaging and phase identification of Cu₂ZnSnS₄ thin films using confocal Raman spectroscopy. *J. Vac. Sci. & Technol. A: Vacuum, Surfaces, Films* **2011**, 29.

Thursday Afternoon Poster Sessions, November 10, 2016

EM-ThP4 Optical and Magneto-Optical Properties of ZnO/Zn_{1-x}Co_xO Thin Films Grown by Pulsed Laser Deposition, Da-Ren Liu, C.J. Weng, Instrument Technology Research Center, National Applied Research Laboratories

Diluted magnetic semiconductors (DMS) have recently attracted considerable attention due to their potential applications for spintronic devices, such as spin-valve transistors, nonvolatile memory, and magneto-optical switches. ZnCoO is one of the most promising DMS materials due to its predicted above room temperature ferromagnetism. In this study, ZnO layer was conformally deposited on the Si substrates by atomic layer deposition (ALD). Then the Zn_{1-x}Co_xO (0.01 < x < 0.10) coatings were grown on ZnO layer by Nd:YAG pulsed laser deposition (PLD). The thickness and roughness of the films were characterized by grazing-incidence x-ray reflectivity (GIXR). According to the results of high-resolution x-ray diffraction, the ZnO/ Zn_{1-x}Co_xO thin films are polycrystalline with a preferential growth direction of (002). Photoluminescence spectra demonstrate ultraviolet emission peaks which have shift with the increase of Co ion concentration. The temperature-dependent magnetization (M-T) curves of the ZnO/ Zn_{1-x}Co_xO thin films were measured by a superconducting quantum interference device (SQUID) magnetometer and the magneto-optical properties were measured by micro-MOKE spectroscopy. The results show the room temperature ferromagnetism of the ZnO/ Zn_{1-x}Co_xO thin films suggested that the possibility for the application to diluted magnetic semiconductors.

EM-ThP5 A bi-functional Bolometer with Sensitivity to IR Radiation and Hot Air Induced Temperature Variation, Evgenia Vaganova, The Hebrew University of Jerusalem, Israel

ABSTRACT We have shown previously that doping a poly(4-vinyl pyridine)/pyridine gel with an ester group-containing polymer (e.g. poly(butyl methacrylate)) (polymer acids as additives) expands the wavelength range of the gel photoelectrical sensitivity from the uv into the infra-red. Here we characterize the temporal response of the gel resistivity and demonstrate its ability to operate as a bi-functional bolometer. At constant room temperature, the bolometer can function as a rapidly responding IR detector. It can also respond to temperature variation produced by hot air, but with a much longer time constant. Measurements are shown in the figure below.

b)

Figure. a) Time dependence of the resistance changes of the polymer gel due to IR irradiation at 1 μm . The down pointing arrows indicate switch-on of the radiation source while the up pointing arrows indicate switch-off. b) Time dependence of the resistance changes of the polymer gel in response to temperature variation produced by hot air. The maximum temperature change was 4C (26C - 30C).

The fractional change in resistance caused by IR irradiation at 1mm is $\Delta R/R_0 = 0.13$; the fractional change caused by hot air induced temperature variation - $\Delta R/R_0 = 0.06/1^\circ\text{C}$. The relaxation rate of the IR response following switch-off is 260%/s. The temperature-induced relaxation curve could be fit to an exponential function with two time constants - $\tau_1=0.148\text{s}$ and $\tau_2=17.11\text{s}$. Analysis of the relaxation of the photo-response was limited by the time resolution of the resistance measurements, i.e. 0.02s.

Polymer/liquid pyridine interactions² are considered to be responsible for this interesting functionality of the polymer blend and they will be discussed.

References:

E. Vaganova, E. Wachtel, A. Goldberg, S.Yitzchaik, *J. Phys. Chem. C*, **2012**, 116, 2508.

B. Sedlacek, J. Spevachek et al. *Macromolecules*, **1984**, 17, 825.

EM-ThP6 Proton-Induced Effects on HfO_x-Based Resistive Random Access Memory, K. Hsu, T. Chang, University of Wisconsin-Madison; L. Zhao, Z. Wang, Stanford University; R. Agasie, T. Betthausen, J. Nickles, J. Chang, University of Wisconsin-Madison; Y. Nishi, Stanford University; Z. Ma, J. Leon Shahet, University of Wisconsin-Madison

Resistive Random Access Memory (RRAM) [1], is considered to be a very promising memory technology. As RRAM technology matures and electronic devices using RRAM are likely to be built soon, malfunctions of

RRAM caused by radiation will become an important problem in industry since the size of these devices will continue to decrease. The goal of this work is the measurement of proton-induced effects on HfO_x RRAM cells. Proton irradiation in the MeV range of energies were initially chosen since most cosmic-ray protons are in this range. However, protons lose energy when they pass through matter and thus, lower-energy protons were also investigated. According to TRIM code calculations, there is more interaction between protons and HfO_x films when the proton energy decreased to several keV.

Two proton fluences were chosen ($\sim 2 \times 10^{15}\text{cm}^{-2}$ and $\sim 2 \times 10^{14}\text{cm}^{-2}$). The proton-induced effects on HfO_x RRAM cell include forming rate, modification to forming voltage, resistance of high resistance state (HRS) and shifts in set/reset voltage. After proton irradiation, no RRAM cells were formed and ended up in the low resistance state (LRS) and no changes were observed in the forming voltage of irradiated RRAM cells even when exposed to very high fluence ($\sim 2 \times 10^{15}\text{cm}^{-2}$).

An increase in the resistance of HRS was observed in proton-irradiated RRAM cells. RRAM cells irradiated with 60 keV protons have a higher increase in their HRS state than RRAM cells irradiated with 5 MeV protons. The shift in values of the set voltage can be seen on the I-V characteristic of the proton-irradiated RRAM cell. It is very likely that there is an annealing process occurs and it might be a result of defect reordering after proton irradiation.

The shift in set voltage after 5 MeV proton irradiation (fluence $\sim 2 \times 10^{15}\text{cm}^{-2}$) is from 3.5 V to 7 V. The shift in set voltage after 60 keV proton irradiation (fluence $\sim 2 \times 10^{15}\text{cm}^{-2}$) is from 3.5 to 11 V. Such shifts of set voltages may create problems in real device applications. These shifts are likely to be attributed to atomic-structure changes in HfO_x caused by proton irradiation.

This work was supported by the Semiconductor Research Corporation under Contract No. 2012-KJ-2359, by the National Science Foundation under Grant No. CBET-1066231.

Reference:

[1] H.-S. Philip Wong, H.-Y. Lee, S. Yu, Y. S. Chen, Y. Wu, P.-S. Chen, B. Lee, F. T. Chen, and M.-J. Tsai, "Metal-oxide RRAM," *Proceedings of the IEEE* **100** 1951 (2012).

EM-ThP7 SiGe_x (100) (x=0.25, 0.5, 0.75) and Ge (100) MOSCaps with Aqueous Ammonium Sulfide Passivation, Lauren Peckler, S.L. Heslop, A.J. Muscat, University of Arizona

SiGe_x is a potential semiconductor for next generation transistors because it could be incorporated into current, silicon-based semiconductor manufacturing processes and it would improve transistor performance due to the high carrier mobility of Ge. Despite these advantages, one major challenge is to reduce the number of Ge defects at the SiGe/dielectric interface because they degrade electrical performance of the transistor. While a relatively stable SiO₂ layer can be grown on Si with relatively few defects, the same is not true for Ge. One approach to forming a high quality interface is to remove Ge oxides by passivating the Ge atoms on the surface. SiGe and Ge metal oxide semiconductor capacitors (MOSCaps) were fabricated (10 nm Al₂O₃) and tested to evaluate the effect of sulfur-based chemical passivation on electrical performance. The (100) faces of three SiGe_x substrates - x = 0.25, 0.5, 0.75 - and one Ge substrate were cleaned and treated with one of two ammonium sulfide, (NH₄)₂S, wet chemistries: (NH₄)₂S/H₂O (1:100 v/v) or (NH₄)₂S/HCl/HF/H₂O (1:0.15:0.15:100 v/v). The surfaces of control MOSCaps were cleaned only. The contact area on each device was 12.6 μm^2 .

Average capacitance in accumulation for SiGe_x MOSCaps (x = 0.25, 0.5) was 199 ± 5.4 and 205 ± 22 pF, with a DC bias sweep from -2 to +2 V at 1 MHz. The same capacitance was 42 ± 1.3 pF for SiGe_x (x = 0.75) and 457 ± 12 pF for the Ge MOSCaps. Both (NH₄)₂S treatments increased the accumulation capacitance by 6% and 34%, on average, for SiGe_x (x = 0.25, 0.5), 8% for SiGe_x (x = 0.75), and 8% for Ge MOSCaps. Similarly, V_{FB} shifted -2 V (SiGe_x (x = 0.25, 0.5)) and -14 V (SiGe_x (x = 0.75) and Ge) with respect to the controls. While flatband shifting is at least due to reduction of oxide defects in the Al₂O₃ layer, the low magnitude of accumulation capacitance (according to oxide thickness calculations) suggests that there are other oxide layers present.

Half of the SiGe_x MOSCaps (x = 0.25, 0.75) were annealed in forming gas. V_{FB} shifted +3 V for SiGe_x MOSCaps (x = 0.25) with respect to non-annealed results, which is indicative of a reduction in negatively charged bulk oxide defects. SiGe_x (x = 0.75), and Ge MOSCaps possibly had less bulk oxide defects because their V_{FB} were within ± 0.5 V before and after annealing.

Thursday Afternoon Poster Sessions, November 10, 2016

Less bulk oxide defects in these MOSCaps suggest that nucleation and growth of the Al_2O_3 layer on these surfaces may differ from that of the SiGe_x ($x = 0.25$) surface. Among all three SiGe_x ($x = 0.25$) MOSCaps, the one treated with $(\text{NH}_4)_2\text{S}$ and acid and annealed resulted in the flatband voltage closest to 0 V, as well as the lowest capacitance.

EM-ThP8 Investigating U_3O_8 for Solid-State Direct-Conversion Neutron Detection Applications, *Shailesh Dhungana, G. Bhattarai*, University of Missouri-Kansas City; *B.C. Shaver, S. Lawson, B. Musicó, T. Meek*, The University of Tennessee Knoxville; *M.M. Paquette, A.N. Caruso*, University of Missouri-Kansas City

Solid-state direct-conversion neutron detectors, wherein a semiconductor detector heterostructure is made up of a neutron absorbing material, are capable in principle of very high neutron detection efficiencies. High-efficiency direct-conversion detectors have not yet been achieved in practice, however, because of challenges in finding suitable materials that simultaneously meet the necessary criteria, including high neutron absorption, high mobility-lifetime product, and low leakage current. Uranium-oxide-based semiconductors make up a promising class of neutron detection materials as uranium undergoes neutron-induced fission to yield very high energy primary reaction products, which can in turn create a large number of electron-hole pairs—two-to-four orders of magnitude higher than in the case of boron and lithium, the materials commonly studied for direct-conversion detectors. This additional charge can help to overcome limitations in charge transport properties, such as high leakage current and low charge carrier mobility, typically seen in candidate neutron-absorbing semiconductor materials. Of the uranium oxides, UO_2 has been studied the most, and literature reports show that its resistivity and charge carrier mobility vary widely with stoichiometry and microstructure. Very few studies on the electrical transport properties of U_3O_8 exist, with one reporting values of $10^4 \text{ } \Omega \text{ cm}$ for resistivity and $1 \text{ cm}^2/\text{V s}$ for mobility (George & Karkhanavala, 1963). Like for UO_2 and other semiconductors, however, these properties would be expected to vary widely. To determine the range of the possible charge transport properties in U_3O_8 , as well as how they vary with material composition and microstructure, a rigorous study is necessary. We report the results of charge transport measurements using a range of techniques, including four-point van der Pauw resistivity and DC Hall, on sintered U_3O_8 pellets of varying stoichiometry and grain size. Additionally, we report results from ultraviolet and x-ray photoelectron spectroscopy toward probing the electronic structure of the U_3O_8 surface toward the development of suitable electrical contacts for this material.

George, A. M., & Karkhanavala, M. D. (1963). Studies on the electrical properties of uranium oxides I. Electrical conductivity of alpha U_3O_8 . *J. Phys. Chem. Solids*, 24, 1207–1212. doi:10.1103/PhysRevB.81.205324

EM-ThP9 Investigation of Electro-Optical and Chemical properties InN epilayer grown on Ga-face GaN by RF-MOMBE, *W.-C. Chen, Chien-Nan Hsiao*, Instrument Technology Research Center, National Applied Research Laboratories, Taiwan, Republic of China

Epitaxial indium nitride layers were grown on gallium nitride/c-sapphire by radio frequency metal-organic molecular beam epitaxy. We discussed the effect of V/III flow ratios on the Electro-Optical and Chemical properties of epitaxial indium nitride. The chemical properties of the indium nitride films were characterized in detail using Secondary ion mass spectrometry and X-ray photoelectron spectroscopy, and the electrical and optical properties were studied by Hall Effect and photoluminescence measurements. Secondary ion mass spectrometry and X-ray photoelectron spectroscopy results showed that carbon and hydrogen of average concentration were measured about 10^{20} cm^{-3} in InN films and O concentration in the InN film is about 10^{19} cm^{-3} . Also, the C and O concentrations decrease with increasing trimethylindium flow rate. A relatively high C, H and O concentration exists near the surface of the InN film. After etching, the etched InN film exhibited a decreased carrier concentration of $3.31 \times 10^{19} \text{ cm}^{-3}$, increased electron mobility of $335 \text{ cm}^2/\text{V-s}$. Optical properties showed that the PL spectra exhibited NBE peak in the range of $0.692 \sim 0.735 \text{ eV}$. Also, the peaks showed blue-shift with increasing V/III flow ratio.

EM-ThP12 Temperature-Resistance Effect of Carbon Black / Polydimethylsiloxane Composite, *Jing Xu, L.Z. Ouyang*, Tennessee State University

In the present work, temperature-resistance effect is found in carbon black/Polydimethylsiloxane composites. The composites were made by mixing the carbon black, aluminium oxide power and polydimethylsiloxane (PDMS). Interdigitated copper electrodes were obtained using chemical etching method on the flexible polyimide substrate in order to determine the resistance change of the composites at different temperatures. The resistances of as-fabricated composites at different temperatures are measured using multimeter. From the results, we found out that the resistance increases dramatically with temperature increasing, and the fitting result shows that it's an exponential increase. This composite has the potential to fabricate the flexible and high-precision temperature sensor.

EM-ThP13 Dependence of Electrical Conductivity on Observed Microstructure of Sintered U_3O_8 , *Seth Lawson, B.C. Shaver, B. Musicó*, The University of Tennessee Knoxville; *S. Dhungana, G. Bhattarai, M.M. Paquette, A.N. Caruso*, University of Missouri-Kansas City; *T. Meek*, The University of Tennessee Knoxville

Actinide compounds, such as uranium oxides, have been shown to have band gaps similar to conventional semiconducting materials such as Si, Ge, and GaAs but with significantly higher operating temperatures as well as higher resistance to radiation damage, allowing for possible use as a detector material in environments and conditions that would otherwise be impractical. Under standard atmosphere and pressure, U_3O_8 is the most stable form of uranium oxide. This work will focus on the stoichiometric composition and will detail the methods used to develop green pellets of U_3O_8 from natural uranium in the form of uranyl acetate. Understanding the microstructure morphology of these pellets as a function of sintering conditions is an important step toward elucidating the activation energy of sintering and grain growth kinetics of this material. The morphology and grain size can then be correlated to changes of measured electrical properties. Optical microscopy was used to determine the grain characteristics for each sintering condition in order to evaluate the influence on sintering on grain growth. Electrical property studies were conducted with measurements including four-point van der Pauw resistivity and DC Hall measurements. These studies will contribute to a larger effort aimed at exploring the electrical properties of uranium oxides to determine whether the properties of U_3O_8 can be optimized to fabricate a competitive direct conversion solid-state neutron detector.

Advanced Ion Microscopy Focus Topic Room Hall D - Session HI-ThP

Aspects of Advanced Ion Microscopy Poster Session

HI-ThP1 Gas Field Ion Sources from Single-Atom Tips, *W.T. Chang, C.Y. Lin, W.C. Lai, Y.F. Yu*, Institute of Physics, Academia Sinica, Taipei, Taiwan, Republic of China; *T.Y. Fu*, National Taiwan Normal University, Taipei, Taiwan, Taiwan, Republic of China; *T.T. Tsong, I.S. Hwang*, Institute of Physics, Academia Sinica, Taipei, Taiwan, Taiwan, Republic of China

Focused ion beams (FIBs) have been widely used in a large number of applications, such as high-resolution scanning ion microscopy, lithography, nanofabrication, secondary ion mass spectroscopy (SIMS), serial sectioning tomography, etc. Current FIB systems have relied on the high brightness, moderate energy spread, ease-of-use, and robustness of the gallium liquid metal ion source (LMIS). One of the main drawbacks of LMIS-FIB system is the inevitable contamination of liquid metal in materials. To extend the applications of FIB technology, it is essential to develop high-brightness ion sources of various species because different ion beams serve different purposes. It has been well recognized that the brightest ion sources are gas field ion sources (GFISs). The virtual source size ($\sim 1 \text{ nm}$ or smaller) and the energy spread ($< 1 \text{ eV}$) of GFISs are at least one order of magnitude smaller than those of LMISs. This implies GFIS-FIB systems can achieve a much better resolution than the current Ga-FIB systems. Another important advantage of GFIS-FIB systems is that the same emitter is capable of producing different ion beams simply by changing the gas species.

Since 2006, Zeiss Orion helium ion microscope (HIM) [1] successfully demonstrated a spatial resolution better than 0.5 nm . The HIM uses a pure tungsten trimer tip as the emitter and two ion species, He^+ and Ne^+ , can be stably emitted. Here we present another type of GFIS emitters, noble

Thursday Afternoon Poster Sessions, November 10, 2016

metal covered tungsten single-atom tips (SATs), which can reliably produce a wider variety of ion species. These SATs are thermally stable and chemically inert, and thus can be generated and regenerated through annealing [2]. Helium, neon, argon, hydrogen, oxygen, nitrogen, and recently xenon ions have been emitted from this type of SATs. Light ions have the lowest sputtering rates and are beneficial for scanning ion microscopy. Heavy ions can provide a high sputtering rate, suitable for ion milling. Due to the high secondary ion yields, oxygen and xenon ion beams can be applied to SIMS. These SAT-GFISs have a half opening angle $\sim 0.5^\circ$ and a brightness several orders of magnitude higher than that of Ga-LIMS. The ion current of these SAT-GFISs are very stable (instability $<5\%$). Since these SATs can be regenerated for more than 50 times, therefore their lifetimes are sufficiently long for most practical applications.

References

Scanning 28, 63 (2006); Photonics Spectra 41, 68 (2007); J.Vac. Sci. & Technol.B 24, 2871 (2006).

Phys Rev B 64 113401(2001); Nano Letters 4 2379 (2004); Jap. J. Appl. Phys. 45 8972 (2006); Appl. Phys. Lett. 92 063106 (2008).

In-Situ and Operando Spectroscopy and Microscopy for Catalysts, Surfaces, & Materials Focus Topic Room Hall D - Session IS-ThP

In-Situ and Operando Spectroscopy and Microscopy for Catalysts, Surfaces, & Materials Poster Session

IS-ThP3 Challenges and Current Progress in Characterizing the Solid Electrolyte Interface in Lithium-Sulfur Batteries, *Manjula Nandasiri*, A.M. Schwarz, V. Shutthanandan, Pacific Northwest National Laboratory; P. Kandasamy, Pusan National University, Republic of Korea; S.A. Thevuthasan, Qatar Environment and Energy Research Institute; V. Murugesan, Pacific Northwest National Laboratory

Lithium-sulfur (Li-S) battery is a promising candidate to replace Li-ion battery due to their high theoretical specific capacity and energy density. However, there are some challenges to overcome to realize the practical applications of Li-S batteries. One of the most critical challenges to overcome is the shuttling of long chain lithium polysulfides (LiPS), which results in the formation of solid-electrolyte interface (SEI) layer on the electrodes and fading of the battery capacity. The constituents and properties of the SEI layers are dependent on the electrolyte and not very well-understood. It was suggested that the application of *in-situ* or *in-operando* techniques can capture the dynamic changes in the SEI layer during the battery cycling. Thus, our aim was to study the fundamental properties of SEI layer of various electrode-electrolyte systems in their working environment using *in-situ* XPS and imaging XPS. In order to do that, we developed an *in-situ* XPS capability at Environmental Molecular Sciences Laboratory located in Pacific Northwest National Laboratory.

Analyzing the SEI layers *in-situ* using XPS techniques is very challenging task due to the nature of the electrolytes and their behavior in vacuum systems. Therefore, a vacuum friendly ionic liquid (1-butyl-1-methylpyrrolidinium bis(trifluoromethyl-sulfonyl)imide) was selected as the electrolyte along with Li and graphite electrodes for the *in-situ* XPS characterization of SEI layers. Using this *in-situ* configuration, we were able to determine the composition of SEI layers formed on Li anode and graphite cathode in Li/ionic liquid/graphite battery system. These XPS results show the gradual formation of LiPS compounds and the decomposition of electrolyte on Li anode with the formation of LiF during the charging and discharging process. Moreover, the elemental and chemical state distributions of SEI layer were mapped using *in-situ* imaging XPS. In addition, we continued the SEI layer characterization of electrodes cycled in the electrolytes which cannot be handled in vacuum using a glove box attached to the XPS system. The XPS and imaging XPS results of these studies will be extensively discussed.

IS-ThP4 Traceable Calibration of High-Quality Pitch Standards Based on an Atomic Force Microscopy System Combined with a Piezo-Actuated Flexure Stage, *Chien-ying Su*, N.N. Chu, M.H. Shiao, C.N. Hsiao, F.Z. Chen, J.A. Yeh, Instrument Technology Research Center, National Applied Research Laboratories, Taiwan, Republic of China

A high-precision atomic force microscope (AFM) metrology system has been established for traceable calibration of transfer standards based on a commercial AFM system and a piezo-actuated flexure stage. By adopting a DSP-based controller, this system is capable of providing high-level nanomotion control. The piezo-actuated flexure stage includes capacitive position sensors in all three axes for highly linear motions over 110 mm scan size and as low as one nanometer out-of-plane motion. And the capability of subnanometer resolution with linearity error as less as 0.05% is achievable. For measuring periodical structures such as pitch standards, two operation modes are applicable: (a) Combined scanning mode, where the position of the closed-loop displacement stage is controlled point by point while the AFM scanner head measures and records the height variations simultaneously; (b) Direct scanning mode, where the closed-loop displacement stage actuates three axes offsets which are multiples of the pitch length according to the feedback signal of the AFM scanner head in order to locate edge profiles.

In addition, inductively coupled plasma reactive ion etching (ICP-RIE) process has been applied for high-quality pitch standard fabrication. System details, characteristics and results for pitch standard calibrations are presented. System calibrations through transfer standards such as 99.999 nm pitch standard with expanded uncertainties of 0.014 nm establish traceability to the national metrology institute Physikalisch-Technische Bundesanstalt (PTB). The estimated combined uncertainties of this system for pitch standard calibration are in accordance with the Guide to the Expression of Uncertainty in Measurement (ISO GUM).

Keywords: high-precision, transfer standards, nanomotion, flexure stage, feedback, ICP-RIE, combined uncertainties, metrology

IS-ThP5 XPS Enables Visualization of Charge Screening in Metal-ionic Liquid Interfaces with Temporal- and Lateral-resolution, *M.T. Camci*, Mrs, Turkey; P. Aydogan, B. Ulgut, C. Kocabas, *Sefik Suzer*, Bilkent University, Turkey

X-ray photoelectron spectroscopic (XPS) investigation of charge screening across two gold electrodes fabricated on a porous polymer surface which is impregnated with an ionic liquid (IL) will be presented. The IL provides a sheet of conducting layer to the insulating polymer film, and allows monitoring charging and screening dynamics at the polymer + IL / vacuum interface in a laterally resolved fashion across the electrodes. Time-resolved measurements are also implemented by recording F1s peak of the IL, while imposing 10 mHz square-wave-pulses (SQW) across the two electrodes in source-drain geometry. Variations in the F1s binding energy reflects directly the transient local electrical potential, and allow us visualize screening of the otherwise built-in local voltage drop on and across the metal electrodes in the range of millimeters. Accordingly, the device is partitioned into two oppositely polarized regions, each following polarization of one electrode through the IL medium. On the other extreme, upon imposing a relatively fast 1 kHz square-wave pulses the charge screening is prevented and the device is brought to assume a simple resistor role. The presented structure and variants of XPS measurements, enabling to record voltage transients in unexpectedly large lateral distances away from the interface(s), can impact on understanding of various electrochemical concepts.

IS-ThP6 Ambient Pressure Photoemission Instrumental Development and Applications within the Field of Energy Related Research, *John Åhlund*, Scienta Omicron, Sweden

Ambient pressure photoelectron spectroscopy (APPEs) is a rapidly developing technique, suitable for studies in the field of energy harvesting, e.g. solar cells and energy storage, e.g. batteries. We have developed two analysers, capable of measuring samples with a surrounding gas pressure in the mbar range.

Here we present the design and performance of these two new hemispherical electron energy analyzers, the Scienta Omicron HiPP-2 analyser, designed for energies ranging from x-ray photoelectron spectroscopy (XPS) to hard x-ray photoelectron spectroscopy (HAXPES) and the Scienta Omicron HiPP-3 analyser, designed for XPS energies. Where the latter also having imaging capabilities.

For laboratories both analyzers can be equipped with an Al K α X-ray anode, as demonstrated in Eriksson et al RSI 85(2014)075119 and Edwards et al,

Thursday Afternoon Poster Sessions, November 10, 2016

NIMA, 785(2015)191. Firstly the performance of the analysers in combination with Al K α X-rays is demonstrated using standard test samples and procedures, including a demonstration of the HiPP-3 spatial performance under ambient pressure conditions. Secondly the performance is linked to a general discussion about sample to first aperture distance (Kahk et al, JEPEC, 205(2015)57).

Finally we will demonstrate the performance of the HiPP-2 analyzer with applications examples from a dye-sensitized solar cell interacting with water (Eriksson et al Top. Cal. 59(2016)583) and a method to study the battery solid/liquid interface. For the first time the presence of a liquid electrolyte was realized during photoemission measurements (Maibach et al RSI 86(2015)044101).

IS-ThP7 Highly Sensitive Ion Trap Mass Spectrometer for Inline Process Control, G. Fedosenko, H.-Y. Chung, M. Aliman, A. Laue, R. Reuter, V. Derpmann, M. Antoni, L. Gorkhover, **Tina Graber**, Carl Zeiss SMT GmbH, Germany

Real-time inline control of process gas compositions with high sensitivity has been of particular importance in recent years in the semiconductor industry and beyond. Most of the real-time process gas analysis was carried out with differentially pumped Residual Gas Analyzer (RGA) which are based on a linear quadrupole mass filtering technique. To generate a complete mass spectrum, a RGA usually needs a few minutes which is often too slow for real-time inline process control. A new process control mass spectrometer, based on Fourier-Transform 3D-Quadrupole Ion Trap technology, is more appropriate for real-time inline process and will be presented in this work.

The 3D-Quadrupole Ion Trap mass spectrometer (*iTrap*[®]) by ZEISS is installed in a vacuum chamber (120mm x 120mm x ~ 500mm) with an ALD valve for pulsed gas sample injection (pulse duration ~ 50ms). An electron gun is used for ionization of the gas pules. The Ion Trap achieves ion trapping and accumulation by means of a radio frequency applied to the ring electrode of the trap. With the aid of advanced electronic amplifiers and selective ion excitation technique the ion oscillations can be measured electrically without using any separate particle detector. The mass spectrum is finally obtained by a Fourier Transform of the recorded electrode current signal in less than one second.

Real-time measurements of the hydrogen plasma cleaning process of Sn contaminated samples were performed with the *iTrap*[®] mass spectrometer. The working pressure of the plasma cleaning process was 0.5 mbar. Decreasing signal of SnH₄ and other contaminations from the samples which are directly correlated to the cleaning process were observed with *iTrap*[®]. This result is extremely useful for the process control of Plasma processes and inline real-time contaminations control for high-end applications such as the EUV Lithography manufacturing.

MOCVD process for GaN growth was also investigated with *iTrap*[®]. The result shows that gas species related to wafer holder contamination, gas phase reaction products and dopant memory effects due to Cp₂Mg could be observed clearly. These information will help the user to recognize process drift and/or minimize chamber cleaning intervals.

The new mass spectrometer of ZEISS (*iTrap*[®]) has successfully detected real-time SnH₄ signal in the hydrogen plasma cleaning process. Inline measurement at a MOCVD chamber showed that *iTrap*[®] is capable to detect reaction products, contaminations on the wafer holder and dopant memory in real-time. These results demonstrate that *iTrap*[®] is a very sensitive and fast process mass spectrometer suitable for real-time inline process monitoring.

IS-ThP8 Real-time State-resolved Reactivity Measurements as a Probe of Carbon Dissolution Kinetics on Ni(111), Eric Dombrowski, E.H. High, A.L. Utz, Tufts University

The steam reforming of methane to produce hydrogen occurs on an industrial scale at catalyst temperatures exceeding 1000 K, but most of the published sticking data on the methane / nickel system focuses on low surface coverages and surface temperatures, T_s, below 650K. At higher T_s, the carbon products of methane dissociation dissolve into the nickel bulk, which prevents post-dose measurements of reactivity.

To address this limitation, we couple King & Wells molecular beam reflectivity measurements with modulated infrared laser excitation to quantify methane's dissociative chemisorption probability, S_{over}, over a wide range of incident fluxes and T_s. This new method simultaneously measures ground state and eigenstate resolved reactivities in real time. Each dose produces upwards of 20 independent reactivity measurements, increasing our precision greatly. Our ability to quantify S in real time reveals the

coverage-dependent reaction probability, S(q,T_s). Measuring the full adsorption isotherm further constrains our measured value of the initial sticking probability, S₀.

We measure S(0,T_s) for methane on Ni(111) over a wide range of T_s (500 - 1000 K) and reactive flux (from 0.004 to 0.40 ML/s). Under these conditions, methane initially dissociates into H and methyl fragments. The surface-bound methyls then dehydrogenate to C + 3H, and recombinative desorption of H at these surface temperatures is prompt. Initial measurements of S(0=0, T_s) show how elevated surface temperatures promote methane dissociation. As the dose proceeds, we observe coverage-dependent changes in S(0,T_s) that arise from the accumulation of C on and beneath the surface. These effects reveal the kinetics of carbon dissolution into bulk nickel starting with the initial CH bond cleavage event. We observe a sharp transition for the onset of observed site blocking. At all investigated reactive fluxes no site blocking occurs above T_s = 900 K. Below 900K, we observed a reactive flux dependent induction period as the carbon dissolution kinetics approach steady state. Observing how these kinetics change with reactive flux shows how the presence of surface and subsurface C can enhance or inhibit methane activation under the high temperature conditions present in a steam reforming reactor.

IS-ThP9 Design and Performance of Large Surface Area Graphene Liquid Cell for in Situ Electron Spectroscopy and Microscopy, Hongxuan Guo, National Institute of Standards and Technology (NIST); A. Yulaev, A. Kolmakov, National Institute of Standards and Technology

For applications such as electrochemistry, environmental science or (photo-) catalysis it is important to characterize materials and interfaces in reactive liquid or aquatic environments. However, interface sensitive characterization techniques, such as X-ray photoelectron spectroscopy (XPS), XAS, Auger electron spectroscopy (AES), SEM, electron microscopies require high or ultrahigh vacuum environments for their operation. To circumvent these pressure gap challenges, the graphene membrane based environmental cells have been recently developed ^{1, 2, 3} Graphene is the strongest materials with one molecularly impermeable atomic layer thick and it is transparent to electrons and x-rays in a wide energy range. Therefore, it is the best separating membrane material so far for fabrication of liquid cell for *thein-situ* studies of liquid samples in high or ultra-high vacuum environments.

We report on high yield fabrication of double layer graphene capped multichannel matrix which can be impregnated with a large variety of liquids and electrolytes for in-situ SEM, EDS, SAM, XPS. The liquid life time inside a cell can reach many hours and is limited by the defects density in the graphene and interfacial diffusion between the graphene membrane and MCA matrix. Using SEM, in combination with EDS and XAS spectroscopies we analyzed the electronic structure and dynamics of water-graphene interface. Auger spectroscopy was used to analyzed the attenuation of the water generated Auger electrons by double layer graphene. Electrochemical graphene liquid cells have been fabricated via Pt electrodes atomic layer deposition deep in to the MCA matrix. , We performed first feasibility tests via electroplating and stripping of Cu on the surface of double layer graphene from CuSO₄ solution. This new sample platform provides a new experimental ground for characterization of liquid materials for energy, catalysis, biomedical and environmental research.

1. J. Kraus, R. Reichelt, S. Guenther, L. Gregoratti, M. Amati, M. Kiskinova, A. Yulaev, I. Vlasiokiv and A. Kolmakov, Nanoscale, 2014. 6, 14394-14403

2. J. D. Stoll and A. Kolmakov, Nanotechnology, 2012, 23, 505704.

3. Andrei Kolmakov, Luca Gregoratti, Maya Kiskinova, Sebastian Günther, Topics in Catalysis, 2016, 59, 448–468

MEMS and NEMS

Room Hall D - Session MN-ThP

MEMS/NEMS Poster Session

MN-ThP1 Method for Patterning Poly-Acrylic Acid Sacrificial Layers for Use in Solder Based Self-Assembly for 3D Integration, Connor Smith, Y. Feng, S.L. Burkett, The University of Alabama

Poly-acrylic acid (PAA) has been shown to be a useful material for both sacrificial layers and patterning in micro-fabrication. This usefulness stems from various critical properties of PAA—particularly its high solubility in water. Due to this, PAA results in a much safer environment as opposed to other materials, such as silicon dioxide, which are traditionally etched using hazardous etchants, such as hydrofluoric acid. However, in certain

Thursday Afternoon Poster Sessions, November 10, 2016

processes, such as solder based self-assembly for 3D integration, a patterned sacrificial layer is highly desirable. Unfortunately, PAA is not a conductive material for this due to the fact that water is so prevalent in many processes' post-patterning and pre-sacrificial layer removal steps and, thus, could result in damage to the PAA layer. This research focuses on providing a technique by which PAA can be used as a patterned sacrificial layer in such processes by taking advantage of the ease with which the substance can be thermally cross-linked and the ability to etch such cross-linked PAA using a solution with a significantly high pH level.

MN-ThP2 An Application of Aligned Electrospun PVDF Nanofibers, Akira Ueda, O. Ali, Fisk University; Y. Zhang, Vanderbilt University; B. Storr, A. Byrne, C.S. Carson, Fisk University; C. Marvinney, A.L. Cook, Vanderbilt University; S. Avanesyan, W.E. Collins, R. Mu, Fisk University

We report an application of the aligned electrospun nanofibers of PVDF, poly(vinylidene fluoride). Although the electrospinning is a quite old technique, recently it has been paid attentions in order to fabricate nano-sized materials. PVDF is a piezoelectric and pyroelectric material, and it is recently found to be aligned nanofibers by using a set of grounded electrodes during electrospinning. By using this delicate material, an application to the molecular sensors will be reported.

Plasma Science and Technology

Room Hall D - Session PS-ThP

Plasma Science and Technology Division Poster Session

PS-ThP1 RF Assisted Reactive High Power Impulse Magnetron Sputtering Deposition of Titanium Nitride Thin Film for Plasmonic Applications, Ru-Jing Sun, National Tsing Hua University, Taiwan, Republic of China; B.H. Liao, C.-N. Hsiao, Instrument Technology Research Center, Taiwan, Republic of China; K.C. Leou, National Tsing Hua University, Taiwan, Republic of China

Titanium nitride (TiN) films have attracted a great deal of interests recently for applications in plasmonic devices in near-infrared wavelengths range. Here we report the optical properties of the TiN films prepared by using radio frequency power assisted reactive high power impulse magnetron sputtering (HIPMS) deposition technique. The TiN films were grown on either Si or glass substrates for a thickness up to 400 nm. A spectroscopic ellipsometer was used to measure the refraction index (n) and extinction coefficient (k) of the films. Measurements results show that, depending on the deposition conditions, the optical properties of the TiN films vary over a wide range, from those of typical TiN film as deposited by conventional magnetron sputtering, to those of metallic copper or gold. Sheet resistance of the film was also measured by hall-effect method and strong correlation between the optical and the electrical properties are demonstrated. Results from XRD analysis also reveal that the lowest film resistivity occurs for TiNx film with a stoichiometric composition, as expected. These results demonstrate that one can fine tune the optical property of TiN film by simply controlling the deposition conditions to meet the requirements of optical devices.

PS-ThP2 Transport Line for Laser Multicharged Ion Implantation and Deposition System, MdHaider Shaim, M.M. Rahman, O. Balki, Old Dominion University; A. Sarkissian, Plasmionic Technologies; M.L. Korwin-Pawlowski, University Du Quebec en outaouais, Canada; H.E. Elsayed-Ali, Old Dominion University

Components of a transport line for a laser multicharged ion (MCI) source are constructed and tested. These components are an einzel lens for ion focusing, parallel deflection plates for multicharged ion selection, electrostatic cylindrical ion energy analyzers for MCI energy-to-charge E/z selection, three-grid energy analyzer, and Faraday cup for time-of-flight ion detection. Aluminum and carbon MCIs are generated by a nanosecond Nd:YAG laser (wavelength 1064 nm, pulse width 7.4 ns) ablation of a target in a vacuum chamber. Time-of-flight and a three-grid retarding ion energy analyzers are used to determine the velocity and the charge state of the MCIs. A three-electrode cylindrical einzel lens is used to focus the MCIs. At a distance of 30 cm from the center of the focusing electrode of the einzel lens, Al^{1+} and Al^{2+} has a minimum beam diameter of ~ 1.5 mm, while for Al^{3+} and Al^{4+} the minimum beam diameter is ~ 2.5 mm. Simulation of the ion trajectories was done using SIMION 8.1. A high voltage pulse applied to a set of two parallel deflecting plates is used for the pickup of ions with different charge states according to their time-of-flight. The electrostatic ion energy analyzer combined with the time-of-flight measurement are used to resolve both E/z and z and obtain the energy distribution of each

charge. The Overall energy resolution of the electrostatic ion energy analyzer for carbon MCI is 7 – 9%.

PS-ThP5 Optimizing Process Parameters for Plasma Assisted Atomic Layer Epitaxy (PA-ALE) of Nitrides, Virginia Anderson, D.R. Boris, N. Nepal, S.D. Johnson, A.C. Kozen, Naval Research Laboratory; Z. Robinson, Boston University; S.C. Hernandez, C.R. Eddy, Jr., S.G. Walton, Naval Research Laboratory

III-Nitride (III-N) binary compounds (InN GaN and AlN) are attractive semiconductor materials for a wide range of device applications. Plasma assisted atomic layer epitaxy (PA-ALE) is a low temperature conformal layer-by-layer deposition technique that is based on a pair of self-terminating and self-limiting gas-surface half-reactions, in which at least one half-reaction involves species from a plasma. In this work we employ optical emission spectroscopy and charged particle collectors to characterize an inductively coupled plasma on a commercial atomic layer epitaxy tool. In particular, we assess the total ion flux reaching the substrate surface and the relative fractions of atomic and molecular species generated in the plasma under a variety of pressures and gas input flow fractions of argon and nitrogen. The objective is to diagnose optimum conditions for the production of N^* radicals in the plasma source, believed to be most useful for the growth of III-N films, and correlate these changes in N^* production with changes in film characteristics.

PS-ThP6 Plasma Treatment of Plated Surfaces, Christopher Fields, M.J. Buie, Coherent Inc

Plasma treatment is used increasingly in vacuum applications to ensure removal of surface level micro-contamination which may prevent or inhibit bonding or joining applications. [1-4] We have characterized via a designed experiment the changes to the surface after plasma treatment. Stainless steel 304L was chosen as the flange material for the study. One surface was milled to provide at a minimum surface finish of 16 m in. A thorough characterization of the material was performed prior to plating including surface roughness measurements using an optical profilometer. Pre-plating results show a surface with 'race track' grooves around the sealing surface. The optical profilometer measured a surface roughness of 12 m in and a total roughness profile height of 105 m in. The flanges were plated with a decorative bright nickel, nickel sulfamate and a combination of the two films. The plating thickness varied from 0.5 mil to 1.5 mil. Samples were treated with either an ultrasonic aqueous clean, a plasma clean or a combination of the two. The flanges were then measured for ionic contamination via ultra-pure water extraction ion chromatography. Elemental analysis was performed using x-ray photoelectron spectroscopy (XPS). The data reveals an effective plasma treatment which removes all traces of carbon and minimizes Na. Additionally, plasma parameters were optimized in order to minimize surface roughening during processing.

References:

- [1] D. Korzec, J. Rapp, D. Theirich and J. Engemann, J. Vac. Sci. Technol. A 12, 369 (1994).
- [2] P. Ponath, A. B. Posadas, R. C. Hatch and A. A. Demkov, J. Vac. Sci. Technol. B 31, 031201 (2013).
- [3] R. A. DiFelice, "An Investigation of Plasma Pretreatments and Plasma Polymerized Thin Films for Titanium / Polyimide Adhesion, Ph.D. Thesis, Virginia Polytechnic Institute and State University, 2001.
- [4] T. S. Williams, "Surface Modification by Atmospheric Pressure Plasma for Improved Bonding", Ph.D. Thesis, University of California at Los Angeles, 2013.

PS-ThP7 Customizing Arrays of Microplasmas for Controlling Properties of Electromagnetic Waves, Chenhui Qu, P. Tian, M.J. Kushner, University of Michigan

Arrays of microplasmas are being investigated to manipulate electromagnetic waves. Such applications require control of the electromagnetic properties of individual plasma cells. Motivated by the tradeoff between fast response and high plasma density, the optimum operating range for the plasma includes pressures from 10s to 100s Torr, and so the scale of each cell shrinks to 100s μm due to pd scaling. Controlling cross-talk is a major challenge in design of microplasma arrays since plasma cells are not separated by physical barriers as in conventional plasma-display-panels. This lack of physical barriers is necessary in order to reduce the loss or scattering of incident electromagnetic waves.

Small 2-dimensional arrays of microplasmas are being computationally investigated with the goals of maximizing electron densities while minimizing cross-talk between plasma cells. The microplasma arrays are

Thursday Afternoon Poster Sessions, November 10, 2016

sustained in 10s to 100s Torr of rare gas mixtures excited by dc-unipolar pulses. The small arrays contain 4 to 9 plasma cells.

The base case geometry contains four plasma cells operating in 60 Torr Ar powered by 300 V peak value unipolar pulses having a 10 MHz pulse repetition frequency and 30% duty cycle. The width of the array is 320 μm and the length is 830 μm , conditions which produce maximum electron densities up to $2 \times 10^{14} \text{ cm}^{-3}$ with a cathode fall region forming near the exposed cathodes. Beam ionization by secondary electrons contributes $\approx 65\%$ of the total ionization during the pulse on period. Cross-talk between plasma cells does not significantly affect the performance of individual plasma cells even though they are not physically isolated. The predicted plasma properties are used to evaluate the potential for controlling electromagnetic wave properties when propagating through large arrays of such microplasmas. The electromagnetic simulator HFSS was used to investigate microwave propagation through the microplasma array, including control of the magnitude and polarization of the electric field.

Work was supported by Air Force Office of Scientific Research, Department of Energy Office of Fusion Energy Science and the National Science Foundation.

PS-ThP8 Optical Emission Diagnostics of a Non-equilibrium Helium Plasma Jet at 1 Atm in Ambient Air, Tam Nguyen, E. Hernández, D.J. Economou, V.M. Donnelly, University of Houston

Non-thermal atmospheric pressure plasmas are of interest for their potential use in surface treatment and biomedical applications. Even though considerable progress has been made, less is known about the species generated in close proximity to a surface. A novel approach using optical emission spectroscopy (OES) has been developed to probe emissions close to the surface. The plasma jet splays along the flat face of a hemispherical quartz prism. Emission was observed through the prism as a function of the angle of incidence. In this manner, emission integrated from a line-of-sight across the jet was obtained. Emission was also recorded as a function of angle through a MgF_2 window coupled to a VUV spectrometer. At normal incidence (0°), light was detected mainly from the discharge within the plasma source, which consisted of a quartz tube surrounded by two electrodes, powered by a 200 kHz AC source. He emission at 706 nm peaked twice per cycle, near the positive and negative voltage maxima. Conversely, VUV-UV-visible emissions from H, O, N, OH, NO and N_2^+ impurities contained in the He feed gas within the discharge were hardly modulated. The only exception was $\text{N}_2(\text{C-B})$ emission, which peaked strongly near the maximum positive voltage and weakly near the maximum negative voltage. When the angle of incidence was reduced to just below the critical angle (43.4°) to observe the region within $\sim 1 \text{ mm}$ of the surface, all emissions were strongly modulated and peaked near (lead or lag) the maximum positive voltage; no emission was detected at the maximum negative voltage. All of these observations are consistent with excitation of O, N, OH, H, and NO being predominantly due to dissociative excitation of precursors O_2 , N_2 , H_2O and NO_2 resulting from collisions with He metastables (He^*). Similarly, N_2^+ emission was attributed to He^* Penning ionization and formation of excited N_2^* . Only He 706 nm and $\text{N}_2(\text{C-B})$ emissions were due to electron impact excitation. Inside the discharge tube, He^* is long lived because it is quenched very slowly by diffusion to the walls or by collisions with He or electrons, hence He^* -induced emission are only weakly modulated. Near the surface, air diffuses into the He and leads to rapid He^* quenching and hence a strong modulation of the emissions.

PS-ThP9 Etching Capability of Silicon Nitride using a Low Electron Temperature Plasma Source, Hiroyuki Miyazoe, A.V. Jagtiani, S.U. Engelmann, IBM T.J. Watson Research Center; D.R. Boris, S.C. Hernández, E.H. Lock, S.G. Walton, Naval Research Laboratory; E.A. Joseph, IBM T.J. Watson Research Center

The ability to achieve atomic layer precision is among the ultimate goals envisioned for plasma etching technology. Electron beam generated plasma (Large Area Plasma Processing System: LAPPS) as developed in the Naval Research Laboratory (NRL) is one such candidate to realize these process goals [1]. We have been demonstrating process feasibility for single layer graphitic carbon films such as graphene and carbon nanotubes (CNTs), which have unique properties, making them well-suited for studying the ability to process with atomic layer precision and assess impact of plasma damage. [2] In this work, we explore SiN etching using pulsed, electron beam generated plasmas produced in Ar/SF_6 and Ar/O_2 mixtures. The impact of process parameters such as relative gas concentration, duty factor, and substrate bias on the etch rates and selectivity (vs. carbon films, silicon and silicon oxide) has been investigated.

The results indicate the ability to achieve etch rates lower than 50 nm/min, depending on material, suggesting the potential for surface engineering with monolayer precision. We also investigated tight pitch patterning of SiN films using LAPPS. Etching of $\approx 10\text{nm}$ -thick SiN at 60 nm pitch with minimized line roughness was demonstrated. Taken together, this work suggests electron beam generated plasmas are a promising route toward atomic layer processing. This work is partially supported by the Naval Research Laboratory base program.

Reference: [1] S.G. Walton, et al., ECS J. Solid State Sci. Technol. 4 (2015) N5033. [2] A. Jagtiani et al., J. Vac. Sci. Technol A 34 (2016) 01B103.

PS-ThP10 Deep GaAs Etching with V-shaped Trench Profile Using Inductively Coupled Plasma Technology, T. Sugahara, SAMCO Inc., Japan; Shogo Uehara, SAMCO Inc.; M. Hiramoto, SAMCO Inc., Japan

There is an ongoing demand for device miniaturization, and at the same time, improvement of the die yields per wafer. For die separation with brittle wafer materials such as Gallium Arsenide (GaAs), Indium Phosphide (InP), and Gallium Nitride (GaN), a diamond tipped tool is widely used for the scribe and break process. Using a diamond tipped tool provides deep V-shaped scribe lines with a sharpened point profile on the bottom. However, this scribing method may cause die chipping, and also limits the minimum width of the streets between die. Wet etching can fabricate a V-shaped scribe line with a sharpened point profile on the bottom, but its depth is limited to just a few hundred nanometers [1], and is not deep enough to break substrates that are a few hundred micrometers thick. As an alternative to scribing with the diamond tipped tool or wet etching, plasma scribing technology offers a chipping-free process solution with deep scribe lines and narrow street widths for higher die yields. Additionally, batch processing of multiple wafers by the plasma scribing technology enables higher throughput than other techniques. However, conventional GaAs deep plasma etching processes yield scribe lines with a rounded bottom profile, and the rounded bottom makes the die separation irreproducible. In order to make die separation more precise and reliable for plasma scribing, the trench profile of scribe lines needs to be a V-shape with a sharp bottom profile.

In this research, an Inductively Coupled Plasma (ICP) etching technology suitable for GaAs die separation was developed to achieve a V-shaped trench with sharp bottom profile. Scribing and breaking of GaAs depend on the orientation of the scribe lines on the GaAs surface. The GaAs wafers used for this experiment had a $\langle 100 \rangle$ crystal orientation, and were 350 μm thick. A 10 μm wide photoresist mask and chlorine chemistry were used to etch 50 μm deep trenches with a sharp point profile at the bottom. The GaAs etch rate was 9.6 $\mu\text{m}/\text{min}$ and the etch selectivity of GaAs over photoresist was approximately 10:1. In the investigation of the relationship between the etch depth and the trench profile, it was found that the bottom flat of the trench shrinks in size from the initial trench width, as the trench depth increases.

The V-shape with the sharp point profile on the trench bottom enables reproducible plasma scribing of GaAs wafers, minimal street widths between die and minimal damage to the die upon die separation.

References

[1] A. Turala, A. Jaouad, D.P. Masson, S. Fafard, R.Arès, and V. Aimez. International Journal of Photoenergy **2013**, 583867 (2013)

PS-ThP12 Ion Beam Etch Process Optimization for the Patterning of High Density STTRAM Pillars, Vincent Ip, Veeco; S. Huang, Lam Research Corporation; S.D. Carnevale, Veeco; I.L. Berry, Lam Research Corporation; K. Rook, Veeco; T.B. Lill, Lam Research Corporation; A.P. Paranjpe, F. Cerio, Veeco

STTRAM device patterning has been demonstrated via either: reactive ion etch followed by ion beam etch (IBE); or by a full IBE strategy.[1],[2] The patterning of high density STTRAM structures requires detailed process optimization, due to multiple requirements including: high aspect ratio; avoidance of shorting across the MTJ barrier; and minimization of damage to the active layers of the structure. We discuss methods to address each of these challenges under a full IBE patterning scheme. For large CD structures, with wide pitch, a single-step IBE recipe may be sufficient, but for small CD or tight pitch features, a multi-step IBE process appears to be necessary.

The primary consideration during the first etch step(s) is to effectively open up the pattern, while minimizing re-deposition across the tunnel junction. We present experimental IBE etch rates for typical STTRAM stack and hard mask materials versus: incidence angle; ion species (Neon, Argon, Xenon); and ion energy. We utilize these etch rates combined with 2-D etch

Thursday Afternoon Poster Sessions, November 10, 2016

simulations, to present guidelines for etching of STTRAM pillars with mask height ~ 150 nm, and pitch varying from 80 – 800 nm. The simulations capture etched feature shapes and spatial distribution of redeposited material. We show that re-deposition can be minimized by: etch angle further from normal incidence; using lower mass ion; and/or higher ion energy.

The primary consideration during the final etch step(s) is to remove any sidewall damaged layer resulting from the earlier step(s), while minimizing further damage.[3] We present 3-D etch calculations and SRIM simulations to provide guidelines for the damage cleanup steps, in terms of optimal etch angle, and optimal ion species and energy.[4] We show that sidewall damage cleanup is maximized by etch angle further from normal, while further damage generation is minimized primarily by lower ion energy. In particular, we present minimum ion energies required to maintain specified damaged layer thicknesses from <1nm upwards.

We simulate optimized combinations of multiple etch steps, and demonstrate effective patterning of pillars of 80 nm pitch, resulting in feature sidewalls with ~ 85° sidewall angle and no metal re-deposition across the tunnel junction.

[1] M. Gajek et al, Applied Physics Letters 100, 2012.

[2] Shigeki Takahashi *et al*, IEEE Transactions on Magnetics 42 (10), October 2006.

[3] Yuichi Ohsawa *et al*, International Magnetism Conference 2016, to be published IEEE Transactions on Magnetism.

[4] J. Ziegler, 1998, available at <http://www.srim.org/>

PS-ThP13 Down Stream Plasma Ash Process Impact on Metal Electrode Oxidation and Nitridation for 10nm and Below Logic Technology, B. Elliston, G. Kishko, V. Vaniapura, V.P. Nagorny, *Shawming Ma*, Mattson Technology

For the semiconductor process flow with advanced nodes below 10nm, it is desired to remove the photoresist on top of metal electrodes, such as TiN, with minimum oxidation and nitridation. In general, the resist is typically removed by plasma strip followed by wet clean or by plasma strip or wet strip only. To minimize and control the oxidation, it is desired to use a non-oxygen chemistry. In this paper, detailed surface characterization methods including surface sheet resistance (Rs), optical ellipsometry, X-ray Photoelectron Spectroscopy (XPS), Transmission Electron Microscopy (TEM) and Electron Energy Loss Spectroscopy (EELS) are used to evaluate the surface oxidation and nitridation under various hardware and process conditions. It is identified that the grounded Faraday shield is critical to reducing tube erosion from the Inductive Coupled Plasma (ICP) coil's strong electric field which may contribute to less wafer surface oxidation. Current modeling suggests the tube's erosion from high electric fields inside the source may contribute small amounts of oxygen that induces more wafer oxidation on wafers, even when a non-oxygen chemistry is used. In addition, extended gate times can affect the post oxidation measurements. Possible hardware and process solution are also discussed to minimize metal oxidation and nitridation.

PS-ThP14 Atomic Layer Etching of Conventional and 2D Materials, Mike Cooke, A.L. Goodyear, R. Sundaram, B. Halsall, Oxford Instruments Plasma Technology, UK

How close can a real plasma etcher come to delivering ideal atomic layer etch (ALE)? We describe hardware studies into the limits of using conventional plasma etch tools to perform cyclical self-limiting etch processes, especially the chemical stability of the chamber and the electrical reproducibility of short RF plasmas. Self-limiting behaviour is not in itself evidence of single layer etching: silicon ALE etch rates are shown to depend strongly on chamber history.

The promise of ALE to etch single atomic layers is tested by using an optimised etch tool to etch 2D materials, grown by CVD. Raman spectroscopy of MoS₂ few-layer films before and after a cyclical etch process are presented.

PS-ThP15 Rapid In Situ H Plasma Carbon and Oxygen Cleaning of In_{0.53}Ga_{0.47}As(001) and Si_{0.5}Ge_{0.5}(110), S. Wolf, M. Edmonds, University of California at San Diego; X. Jiang, PIE Scientific; R. Droopad, Texas State University; N. Yoshida, L. Dong, Applied Materials; R. Galatage, S. Siddiqui, B. Sahu, GLOBALFOUNDRIES; A.C. Kummel, University of California at San Diego; *Mahmut Kavrik*, University of California San Diego

InGaAs and SiGe have demonstrated good potential to replace silicon in MOS devices due to their intrinsically high mobilities. In order to implement these compound semiconductors into devices, the surfaces of

these materials must be atomically flat and void of surface defects, which can be accomplished by performing one of several surface cleaning techniques available: RCA standard cleaning procedure consisting of various treatments with NH₄OH, H₂O₂, HF, HCl, and H₂O to remove the native oxide and organic and ionic contaminants, UV/ozone treatments, and cleaning via thermal gas crackers and plasma sources. However, wet processing can leave organic residues and a thin layer of native oxide on the surface due to exposure to ambient conditions, while the vacuum/dry processing steps can take over 30 minutes to perform. A technique that overcomes these issues involves the use of in-situ hydrogen plasma to remove carbon and oxygen present on the surface. In this study, X-ray photoelectron spectroscopy (XPS) was employed to characterize the chemical composition of the In_{0.53}Ga_{0.47}As(001) and Si_{0.5}Ge_{0.5}(110) surfaces before and after plasma exposures. To optimize the conditions for cleaning with a plasma source, the effect of plasma power and pressure on carbon cleaning and oxygen contamination were determined. In addition, the effect of pure H₂ versus an H₂/Ar mixture was investigated in relation to the removal of carbon and oxygen contaminants. Using the described approach, a two second H plasma clean removed all carbon and oxygen from the In_{0.53}Ga_{0.47}As(001) surface while minimally etching the surface, and nearly all carbon and some oxygen were removed on the Si_{0.5}Ge_{0.5}(110) surface. The SiGe surface is more difficult to clean because it is more sensitive to oxygen than the InGaAs surface and can easily be explained by the high heat of formation of SiO₂. In effect, the high heat of formation for SiO₂ poses two challenges for cleaning of the surface: (1) trace O₂ or H₂O in the plasma gas are likely to form more Si-O bonds and (2) breaking Si-O bonds by atomic H will be unlikely. By incorporating the in-situ downstream plasma source and optimized experimental conditions, the efficacy of ion-less plasma treatment for the rapid cleaning of the In_{0.53}Ga_{0.47}As(001) and Si_{0.5}Ge_{0.5}(110) surfaces has been demonstrated.

PS-ThP17 Backside Via Last Process Technologies for Wafer Level 3D Stacking, Toshiyuki Sakuishi, T. Murayama, Y. Morikawa, ULVAC Inc., Japan

The number of devices connected to the internet has been increasing year by year. Not only Smartphone and Tablet PC, Devices for IoT (Internet of Things) are expected to increase rapidly. Data traffic is increasing exponentially and the data centers are required to be high speed data processing and low power consumption. Required performances are high bandwidth/bandwidth density, low latency, increased data processing speed, expanded data storage. These are desired to achieve without increasing cost. For multifunctionality and downsizing, heterogeneous integration is essential technology. To achieve these requirements, the backside via-last process is very important. We have been developing Si deep RIE technique and process integration that are optimized for via-last TSV formation. Our etching process is mainly non-Bosch etching using SF₆/O₂ based gas. To realize high rate etching, high density F radical is necessary. In addition, the Non-Bosch etching performs etching and sidewall protection simultaneously, so proportion of F and O radical is important. Key technology to achieve a uniform proportion of F and O radical is multi-ICP (Inductively Coupled Plasma) source. Our etching source newly developed shows excellent performance in Non-Bosch etching, but also adapts to Bosch etching. Our Non-Bosch etching is better to taper angle controllability. Tapered shape and smooth sidewall improve the deposition coverage and reduce the TSV formation cost. New Si deep RIE technique using multi-ICP source opens the way to new 3D packaging technology.

PS-ThP18 New Deep SiO₂ Etching Process Issues for Silicon Photonics Device Fabrications, Keizo Kinoshita, PETRA, Japan; M. Noguchi, PETRA; T. Horikawa, AIST; T. Nakamura, T. Mogami, PETRA

Silicon Photonics (SiPh) is a promising technology for wide-band and large-capacity data communications. The SiPh chip needs to embed laser diodes (LD's) for optical communication. In our approach, LD's have to be mounted on a pedestal structure [1, 2]. To fabricate the pedestal structure, 5 μm deep SiO₂ hole should be patterned by a deep etching process.

A 300 mm CCP etch system was applied to etch the SiO₂ layer. Photoresist (PR) patterns with 4.6 μm thick were developed by a KrF lithography system. Ar diluted fluorocarbon gas chemistries were adopted. Three etch-selectivity conditions for the SiO₂ against the PR were examined. Significant etch residues over the etched surface were observed under a relatively high etch selectivity condition. In contrast, the sample etched under a relatively low etch selectivity condition showed no etch residues, but showed conspicuous striations at the sidewalls of SiO₂ which can cause

Thursday Afternoon Poster Sessions, November 10, 2016

optical coupling loss of the SiPh devices. These deep SiO₂ etching issues as a function of the etch selectivity can be discussed qualitatively.

Under the high etch selectivity condition, deposited fluorocarbon polymer and etch by-products over the chamber walls increase generally. They can re-deposit over the wafer surface during etching, and cause the etch residue. The amount of the deposition (*DP*) can be expressed as follows,

$$DP = f(t),$$

where *t* is total etching time, and *f* is a function which reflect the etch selectivity. Higher the etch selectivity is, larger the *DP* is. The etch residue issue will happen when the *DP* value exceeds some threshold. This is a common issue in fabricating both CMOS and SiPh chips.

On the other hand, the etching under the lower etching selectivity condition brings about larger damages on PR polymer by bond breaking and desorption of functional groups, and causes the large line edge roughness (*LER*) of the PR pattern which will be transferred to the striation during etching. The *LER* can be expressed as follows,

$$LER = g(t),$$

where *g* is a function related to the etch selectivity reflecting protective ability for the PR. Higher the etch selectivity is, smaller the *LER* is at the same *t*. This issue is apparent for the SiPh chip fabrication.

Therefore, it is important to minimize *DP-LER* products within some threshold in the deep SiO₂ etching process developments for the SiPh devices. And, we succeeded in the deep SiO₂ etching by the *DP-LER* products minimization approach.

This work was supported by NEDO. The authors thank staff members of SCR station in AIST for their technical support. [1] T. Shimizu, et al., Photon. Res., 2, A19 (2014). [2] K. Kinoshita, et al., AVS 62th Int. Symp., PS-ThP8, p. 51, (2015).

PS-ThP20 Modeling of Remote Plasma Sources using CFD-ACE+, Abhra Roy, P. Shukla, K. Jain, A.N. Bhoj, ESI US R&D Inc.

Remote plasma processing typically involves plasma generation in a main chamber and the substrate activation (or etching or deposition) by plasma activated species outside the plasma zone to reduce damage to the substrate. The remote substrate location also enables control of plasma properties to a sufficient degree to preferentially result in a desired flux of species to the substrate. The CFD-ACE+ modeling platform can be used for simulations of remote plasma sources to address gas flow, heat transfer, plasma physics and chemistry and electromagnetics in a coupled fashion. In this paper, we report on computational modeling studies of plasmas sustained in Ar/N₂ and Ar/NF₃ mixtures using global and 2D simulations. The Kinetic Module of CFD-ACE+ is used to generate the electron energy distribution function (EEDF) and compute electron impact reaction rates and transport coefficients. The fast global models help isolate the major reaction pathways and help reduce the number of reaction steps of the volumetric mechanism for multidimensional simulations. At these pressures of interest, the back diffusion of injected Ar into the plasma zone results in activation of reaction pathways that result in feedstock dissociation. The effect of mixture ratios, power, frequency and pressure on the resulting plasma, ion and radical densities in the main reactor chamber, and fluxes of plasma species at the remote substrate are discussed.

PS-ThP21 Controllable Deposition of TiO₂ Films by Atmospheric Pressure Dielectric Barrier Discharge: Gas Composition Effect and Mechanism, Qianqian Chen, A. Ozkan, S. Collette, J. Mertens, J. Baneton, M.P. Delplancke, F. Reniers, Université Libre de Bruxelles, Belgium

In this work, various controlled morphologies of TiO₂ films are synthesized by atmospheric pressure argon/oxygen dielectric barrier discharge (DBD) using titanium tetraisopropoxide (TTIP) as precursor. The gas compositions for the formation of TiO₂ films are optimized by adjusting the flow rate of plasmagen gas from 0 to 9.5 L/min, while keeping the flow rate of TTIP and O₂ as constant. The morphology of the deposited films is observed by Scanning Electron Microscopy (SEM). It is found that the morphologies change from columnar film to dense film as the flow rate of plasmagen gas increases. The chemical structures and properties of the deposited films are characterized by means of Infrared Reflection-Absorption Spectroscopy (IRRAS), Raman spectroscopy and X-ray Photoelectron Spectroscopy (XPS). The results show that the films are amorphous with similar chemical compositions. The plasma properties are investigated using Optical Emission Spectroscopy (OES) and Mass Spectrometry (MS). The intensity of Ar* species increase as the flow rate of plasmagen gas increases, which indicates that the concentration of Ar* species have a strong effect on the

morphology of the TiO₂ films. The MS measurements show that H⁺, O⁺, H₂O⁺, CO₂⁺, C₃H₆O⁺ and a weak signal of TiO₂⁺ are produced in the plasma. The mechanisms of the TiO₂ films formation from TTIP by DBD are discussed.

PS-ThP22 Synthesis of Acrylate Coatings with Tunable and Permanent Wettability by Atmospheric Plasma, B. Nisol, J. Guesquière, Delphine Merche, N. Vandecasteele, F. Reniers, Université Libre de Bruxelles, Belgium

Plasma polymerization is an eco-friendly route (low temperature, solvent-free process) used to prepare functional thin films with desired properties (e.g aesthetics coatings, protective coatings against corrosion and abrasion, coatings for adhesion and barrier properties...) on any kinds of substrates. In this study, transparent acrylate coatings were synthesized by PECVD under atmospheric pressure, from the simultaneous injection of acrylic acid (AA) and propargyl methacrylate (propaMA) into a dynamic DBD, using argon as the carrier gas.

The influence of the ratio AA/propaMA and the power on the physical and chemical properties of the coatings deposited onto various substrates (Si wafers, polyolefins films and thick gold films) was highlighted by WCA (wettability), mechanical profilometry (thickness), XPS and FTIR-IRRAS (chemical composition).

The addition of propaMA to AA allows reaching high deposition rates (up to 11 nm/sec) thanks to its highly unsaturated (and reactive) nature.

WCA results evidenced the possibility to tune the surface wettability from highly hydrophobic (140° for the pure propaMA coatings) to highly hydrophilic (15° for the pure AA coatings). Moreover, the coatings were very stable over time and were seen not to suffer from hydrophobic recovery. Indeed, the WCA remained constant for at least a period of 2 months.

The highly hydrophobic character of pure propaMA coatings is due to an important texturization of its surface, as revealed by scanning electron micrographs (SEM); the high reactivity of propaMA is thought to induce gas-phase polymerization, and to the subsequent formation of globular features. Also, in the explored conditions, smooth coatings could only be obtained for high AA proportions in the gas mixture.

XPS and FTIR results revealed the presence of alcohol and ketones groups in addition to the carboxylic/esters functions of the monomer precursors. The COOR groups related to the presence of carboxylic acid increase with the proportion of AA in the AA/propaMA mixture while the C-O and C=O groups decrease.

Thanks to excellent ageing properties, such thin and transparent coatings represent a promising alternative to polymer surface plasma functionalization.

We would like to thank the Belgian Federal Government IAP-(interuniversity program) "Physical Chemistry of Plasma Surface Interactions" P7/34, and the Walloon Region.

PS-ThP23 A High-flux Low-energy Hydrogen Ion Beam Using an end-Hall Ion Source, Jacqueline van Veldhoven, E. te Sligte, J.P.B. Janssen, TNO Technical Sciences, Netherlands; I. Ament, Carl Zeiss SMT GmbH, Germany

Most ion sources that produce high-flux hydrogen ion beams, particularly gridded sources, perform best in the high energy range (keV) [1]. Alternatively, some plasma sources produce very-low-energy ions (<< 10 eV). However, in an intermediate energy range of 10-200 eV, to our knowledge, there are no hydrogen ion sources that produce high-flux beams.

Despite this absence, we believe such a source would be of interest to a variety of fields, such as surface passivation and treatment [1-3], solar winds [4], fusion reactors [5], and EUV sources [6].

A typical ion source that is known for its high fluxes at the relevant ion energy range is the end-Hall ion source. This source produces good results with argon and oxygen [7], but no report of it being used with hydrogen was found. This contribution shows the use of an end-Hall ion source with hydrogen. Both the flux and the ion energy distribution of the ion beam were measured using a Retarding Field Energy Analyzer (RFEA) for different settings of the source and at different positions.

At the lowest discharge voltage and highest discharge current where the signal is still stable (100 V, 4A), a maximum hydrogen ion flux of $8.2 \cdot 10^{19}$ ions/m²/s was measured at an energy range of ~0-130 eV and at a distance of 11 cm.

References

Thursday Afternoon Poster Sessions, November 10, 2016

[1] N. Oudini, G.J.M. Hagelaar, J.-P. Boeuf and L. Garrigues, *Journal of Applied Physics* 109 (2011) 073310.

[1] J.C. Muller, Y. Ababou, A. Barhdadi, E. Courcelle, S. Unamuno, D. Salles and P. Siffert, *Solar cells* 17 (1986) 201-231.

[2] K. Srikanth, J. Shenai and S. Ashok, *Nuclear Instruments and Methods in Physics Research B* 88 (1994) 401-406.

[3] A. Slaoui, A. Barhdadi, J.C. Muller and P. Siffert, *Applied Physics A* 39(1986), 159-162.

[4] F.W. Meyer, P.R. Harris, C.N. Taylor, H.M. Meyer III, A.F. Barghouty, J.H. Adams, *Nuclear Instruments and Methods in Physics Research B* 269 (2011) 1316-1320.

[5] T. Ito, Y. Yamauchi, T. Hino, T. Shibayama, Y. Nobuta, K. Ezato, S. Suzuki, M. Akiba, *Journal of Nuclear Materials* 417 (2011) 1147-1149.

[6] A.N. Bykanov, N. Bowering, I.V. Fomenkov, D.C. Brandt, A.I. Ershov, O. Khodykin, W.N. Partlo, *US 7,671,649 B2* (2010).

[7] L. Mahoney, D. Burtner and D. Siegfried, *Society of Vacuum Coaters 49th Annual Technical Conference Proceedings* (2006) 706.

PS-ThP24 A System of Radical Probes for Plasma Characterization, Dren Qerimi, University of Illinois at Urbana-Champaign; *I.A. Shchelkanov*, University of Illinois at Urbana Champaign; *D.N. Ruzic*, University of Illinois at Urbana-Champaign

The current state-of-the-art methods to identify presence of radical species in vacuum chambers are optical methods, which suffer from the lack of spatial resolution and require expensive optical equipment. Center for Plasma Material Interactions (CPMI) at the University of Illinois aims to develop a probe array (catalytic probe) to measure concentration of reactive gas species in low temperature plasma with high temporal and spatial resolution. Radical probes as plasma diagnostic device will be used to determine plasma parameters in helicon plasma source. The basic principle and advantage of a probe array is that it has several sensitive elements capable to distinguish between different gas species. The sensitive element has a size of several millimetres with a nanostructured chemically sensitive to specific reactive gas species surface. The nanostructured surface is positioned right on top of a thermocouple [1]. The nanostructured probe surface provides efficient recombination of active species with subsequent energy release as a heat. The system consists of additional two probes, first to obtain the overall heat flux on probe array, and the second is a reference probe with surface chemically active to all gases. The thermocouple detects the heat released after recombination and gives immediate voltage signal output. The array of several probes is capable to distinguish between different gas species with sub centimeter spatial resolution. The probes give accurate results in a broad range of reactive species concentrations from about 10^{19} to 10^{22} m⁻³.

Reference:

[1] M. Mozetič, M. Drobnič, A. Pregelj, K. Zupan, *Determination of density of hydrogen atoms in the ground state*, *Vacuum*, Volume 47, Issues 6–8, June–August 1996, Pages 943-945, ISSN 0042-207X

PS-ThP25 Using Optical Emission and Broadband Absorption Spectroscopy to Elucidate Energy Partitioning Trends Within Inductively Coupled Plasma Systems, Angela Hanna, J.M. Blechle, E.R. Fisher, Colorado State University

A fundamental understanding of interactions between plasma species is essential to characterizing complex plasma chemistry phenomena. By utilizing various optical spectroscopy techniques to probe internal energetics within nitrogen and oxygen-containing plasmas, we have elucidated energy partitioning information for both ground and excited state plasma species. Our approach focused initially on characterizing internal energies of N₂ within a simple homonuclear diatomic system (N₂). We then broadened our study to include the slightly more complex N₂O system and also a mixed gas plasma system (N₂ and O₂). In these systems, both N₂ and NO molecules can be studied. Optical emission spectroscopy (OES) and broadband absorption spectroscopy (BAS) techniques were employed to study internal energies of both excited and ground state species in all of these systems. Characteristic plasma energies (e.g. electron temperatures (T_e) and small molecule vibrational and rotational temperatures [T_v and T_r , respectively] were determined for species formed within each system. In most cases, T_e is significantly higher than T_r for molecules such as N₂ and NO, with T_v ranging from ~2000 K to >3000K and T_r having values between ~300 K and 1000 K. In general, vibrational and rotational temperatures show a strong positive correlation with applied rf power and often display a negative correlation with system pressure for

the precursors studied. Deviations from these trends have also been investigated. Additional data from more complex systems used to modify a range of materials such as catalyst particles will also be presented. Collectively, these data enable insight into the properties of various plasma systems and the role energy partitioning plays in the assessment of plasma chemistry.

PS-ThP27 Modeling of Electron Kinetics in rf Discharges at Low and High Pressures, Ananth Bhoj, Z.A. Xiong, ESI US R&D Inc.; *V.I. Kolobov*, CFD Research Corporation

Low temperature plasmas (LTPs) are used for numerous applications over a wide range of gas pressures from a few mTorr up to ambient pressures (760 Torr). Simulations of LTPs involve the multiphysics coupling of gas flow, heat transfer, plasma physics, volumetric and surface chemistry and electromagnetics. For CAE models like CFD-ACE+, to accurately capture the plasma physics, a kinetic treatment is often important for different plasma species. In particular, while the mean free paths and the energy relaxation lengths for ions and neutrals are similar, they differ vastly for electrons. This memory effect for elastic collisions of electrons with neutrals has a profound influence to electron kinetics. The kinetic treatment for electrons assumes significance because the electron energy distribution function (EEDF) in highly non-Maxwellian in most cases, and the electron-induced reaction rates are sensitive to the tail of the EEDF. At very low pressures, global models that assume diffusion dominated electron transport with conservation of total energy are useful to quickly estimate plasma characteristics and trends in RF systems. In this approach, the EEDF depends on the total electron energy and energy dependence is obtained by spatially averaging the Fokker-Planck (FP) equation for the EEDF. At intermediate pressures, the tail of the EEDF becomes local, whereas the rest of the EEDF remains non-local. In this regime, the isotropic part of the EEDF depends both on energy and space, so nonlocal effects must be explicitly accounted for by solving the FP equation. Such EEDF nonlocality behavior has been shown to extend up to pL = 10 Torr-cm. Beyond this range, fluid models with non-Maxwellian EEDFs based on lookup tables are computationally more efficient and capture the physics well. We show examples of simulations in these various regimes using CFD-ACE+.

PS-ThP29 Nanoparticle Synthesis via a High Voltage Pulsed DC Atmospheric-Pressure Microplasma Jet, Steven Doyle, K.G. Xu, University of Alabama in Huntsville

A high voltage pulsed DC microplasma jet operating at atmospheric pressure has been developed for nanoparticle synthesis applications. The configuration consists of a high voltage center pin electrode inserted in a quartz tube, running between 5kv – 10kv. The plasma forming gas, being argon, is fed into the tube along with a small concentration of methane, which serves as the working gas. Flow rates and methane ratios vary between 2 – 5 slm and 0.01/Ar – 0.05/Ar, respectively. Nanoparticles of interest include both metal oxides and carbon. Metal oxide nanoparticle formation comes from the oxidation of the center pin electrode, while carbon nanoparticles are a product of the decomposition of the methane working gas. The impact of the center pin electrode chemical composition on the resulting nanoparticles has been tested. The main properties of interest for the nanoparticles are the size, shape, and population density. Copper, tungsten, and mechanical pencil graphite were chosen as the three most desirable electrodes based on the literature. Finally, the flow rates and voltages of the system have been adjusted to further demonstrate their impact on the nanoparticles formed. The nanoparticles are imaged with an SEM and the chemical compositions are confirmed via EDS analysis. The system generates a “cold” microplasma with a gas temperature of just over 300 K. This property makes the microplasma system design of great interest for applications where low temperature limits exist.

PS-ThP30 Extending the Volume and Processing Area of Atmospheric Pressure Plasma Jets, Eric Gillman, D.R. Boris, M.H. Helle, S.C. Hernández, Tz.B. Petrova, G.M. Petrov, S.G. Walton, Naval Research Laboratory

Atmospheric pressure plasmas have certain advantage in materials synthesis and processing that are not available with other approaches including low-pressure plasmas. In particular, the breadth of reactions afforded by non-equilibrium, low temperature plasmas is unique; plasmas produced in full density air allows one to extend the application space to systems and materials that are not vacuum compatible. Non-equilibrium, atmospheric pressure plasma jet devices are well-suited for such applications given their relatively simple design and modest power requirements. However, their size tends to limit their utility to small scale processes and treatments. In this work, we describe approaches to extend the volume of non-equilibrium, atmospheric pressure plasma jets and thus,

Thursday Afternoon Poster Sessions, November 10, 2016

surface area that can be treated. In particular, we consider geometric and gas flow solutions to increase volume without increasing power requirements. We use high-speed cameras, optical emission spectroscopy (OES), current and voltage measurements, and simulations to characterize the results and understand the potential for and/or limitations to scale-up. This work is supported by the Naval Research Laboratory base program.

PS-ThP31 Characteristics of Cutoff Probe for Magnetized Plasma Measurement, Jung-Hyung Kim, Korea Research Institute of Standards and Science, Republic of Korea; *K.H. You*, Korea Research Institute of Standards and Science; *S.J. You*, Chungnam National University; *H.C. Lee*, *D.J. Seong*, Korea Research Institute of Standards and Science

We investigate the transmission spectrum of a cutoff probe in magnetized plasma using a circuit simulation and experiment. The circuit simulation was calculated using a permittivity tensor that can be changed depending on the direction of the magnetic field and electric field which is generated by radiating antenna of the cutoff probe instead of a permittivity of non-magnetized plasma. The experiment was performed at various probe directions and magnetic field strength while maintaining the plasma density constant. When the magnetic field and electric field are same directions, the measured cutoff frequency can be used for the plasma frequency (f_{pe}) same as non-magnetized plasma results. However, electric field is perpendicular with the magnetic field, the measured cutoff frequency can be considered for upper hybrid frequency ($f_{uh} = (f_{pe}^2 + f_{ce}^2)^{1/2}$). All results are consistent with a circuit simulation results.

PS-ThP32 Development of the Gas Cherenkov Detector (GCD-3) and the Unique Engineering Challenges Associated with the ASME Boiler and Pressure Vessel Code, Frank Lopez, H.W. Herrmann, J.A. Oertel, S.H. Batha, Y.H. Kim, J.R. Griego, T.N. Archuleta, R.J. Aragon, V.E. Fatherley, C.S. Young, A. Hsu, R.M. Malone, Los Alamos National Laboratory

The development of the LANL Gas Cherenkov Detector (GCD-3) fielded at the Laboratory for Laser Energetics OMEGA laser facility generated significant engineering challenges. The GCD-3 is a third-generation gas Cherenkov diagnostic that provides important information about Inertial Confinement Fusion (ICF) implosions including fusion burn and imploded capsule conditions. The GCD-3 utilizes CO_2 , SF_6 and C_2F_6 gases separately pressurized at 400psig to provide the scintillation media. Unique experimental objectives contrasted with the requirements of the ASME Boiler and Pressure Vessel (B&PV) Code resulted in diverging pressure vessel concepts throughout the design process. In addition, a facility-specific weight limitation and stringent fluorinated gas leak rate requirements added to the complexity of the diagnostic's development. Specifically, achieving a vessel/detector weight limit of 100 pounds in conjunction with a maximum fluorinated gas leak rate of 1×10^{-9} STD cc/second (helium) at 1 atmosphere differential pressure proved to be challenging. As such, Conflat knife-edge crushed-metal seals were an essential aspect of the design. The LANL Pressure Safety Program in compliance with DOE Order 10CFR851 invokes the ASME Boiler and Pressure Vessel Code, Section VIII, Division I and II for the design of all pressure vessels. As the B&PV Code can be characterized as a "one size fits all" standard, the tendency toward conservatism is typical. Vessel wall and flange thicknesses are routinely substantial, although inconsequential to refineries, are atypical of pressurized ICF diagnostics. A detailed summary of these design challenges correlated with the resulting experimental results bring emphasis to the successful collaborative mix of engineering and physics expertise within the ICF diagnostic development arena.

PS-ThP33 Magnetic Tunnel Junctions Etch and Encapsulation Process Optimization for High-Density STT-MRAM Applications, Laurent Souriau, D. Radisic, S. Kundu, V. Paraschiv, imec, Belgium; *F. Yamashita*, *K. Fujimoto*, *S. Tahara*, *K. Maeda*, TEL, Japan; *W. Kim*, *S. Rao*, *G. Donadio*, *D. Crotti*, *D. Tsvetanova*, *J. Swerts*, *S. Mertens*, *T. Lin*, *S. Couet*, *D. Piumi*, *G.S. Kar*, A. Furnemont, imec, Belgium

STT-MRAM is being extensively developed as a potential candidate to replace conventional memories due to its unique characteristics: fast speed, non-volatility and excellent endurance. One of the major challenge for high-volume, high density STT-MRAM fabrication remains the patterning of the Magnetic Tunnel Junction (MTJ). Practically, the metals used in the MTJ stack hardly form any volatile compounds with conventional etching plasmas often resulting in strong re-deposition of metals on the sidewall (SW) of the junction and hence shorting of the device. Moreover, MTJs manifest strong sensitivity to any form of chemical or physical damage caused by plasma processing leading to degradation of the electrical/magnetic performance of the fabricated memory cell. The focus of this work is to develop a Reactive Ion Etching based patterning

process in combination with SW engineering by oxidation and in-situ encapsulation to mitigate those issues. We demonstrated patterning of MTJ down to 30nm, in pitch down to 200nm with excellent electrical yield and very limited performance degradation.

The MTJ patterning process has been developed on a TACTRAS platform from Tokyo Electron Limited using a dual-frequency capacitive coupled plasma reactor specially customized for STT-MRAM application as well as a microwave plasma CVD reactor to deposit Si_3N_4 . A TiN metallic hard mask has been used to pattern the CoPt or CoNi based MTJs with perpendicular magnetic anisotropy. The patterning consisted of a 2-step sputtering based etch process. The first etch was carried out with Ar to define the MTJ pillar while the second etch used Kr to efficiently remove metallic residues from the MTJ SWs. Noble gases were used in order to avoid chemical damage. The patterning was followed by an in-situ mild oxidation of the MTJ SWs to passivate metallic residues as well as the peripheral damaged zone caused by ion bombardment. Finally, a Si_3N_4 encapsulation was applied in-situ to protect the MTJ from air exposure.

We demonstrated isolated pillar size down to 30nm as well as 45nm pillars at a 200nm pitch. Tight RP distribution ($\sigma \sim 4\%$) was achieved demonstrating that pillar size was uniform across the wafer surface and the MTJ short were efficiently circumvented. Limited degradation ($<10\%$) of the TMR as function of pillar size was achieved. A yield of more than 97% was achieved in Mbit array with less than 0.5% cells exhibiting electrically shorted behavior and the 2.5% remainder of the cell being not switchable. The optimization of the Si_3N_4 encapsulation process to improve the thermal stability of the device post processing will be discussed at the conference.

PS-ThP34 Effect of High DC Bias on Silicon Oxide Coatings Deposited by Plasma Enhanced Chemical Vapor Deposition, Norihiro Jiko, Kobe Steel, Ltd., Japan; *A. Narai*, Kobe Steel, Ltd.; *N. Kawakami*, *T. Okimoto*, Kobe Steel, Ltd., Japan

It is well known that electronic devices such as organic light emitting diode and electronic paper are degenerated by water vapor and oxygen that penetrate from air. Therefore polymer substrates, which are expected to replace glass substrates for their flexibility and light weight but are permeable to water vapor and oxygen, are required to be coated with gas-barrier layers such as Silicon oxide (SiO_x). In addition to the high barrier property, it is necessary for practical use to suppress curl of the polymer substrates caused by the coating with high stress.

Plasma enhanced chemical vapor deposition (PECVD) is one of the industrial-scale coating techniques of the SiO_x layers with high barrier performance (see, for example, ref. 1). It has been reported that for the deposition of the SiO_x layers using PECVD, ion bombardment plays an important role to densify the layers and improve the barrier performance, through experiments in which SiO_x layers are deposited with DC bias applied at the substrate [2]. However curl of the polymer substrates tends to be enhanced by a high compressive stress of the SiO_x layers caused by a strong ion bombardment and is required to be controlled.

The objective of this study is to explore the possibility of compatible high density and low stress through experiments in which SiO_x layers were deposited with a wide range of DC bias. SiO_x layers were deposited using a PECVD system. The substrate silicon wafers (4 inch in diameter) were mounted on a 400kHz RF applied electrode (6 inch in diameter). The power was varied to yield DC bias from 0 to -1.2kV. 13.56MHz RF was inductively coupled into the chamber with a planar-coiled RF antenna through a quartz window with an applied power kept at 300W. Hexamethyldisiloxane and oxygen were introduced into the chamber at a pressure of 4Pa.

The density of the SiO_x layers examined with a X-ray reflectometer increased with enhancing DC bias from 0 to -360V, and it remained almost constant for higher DC bias. On the other hand, compressive stress measured with a profilometer steeply increased from DC bias of 0 to -200V and then reduced gradually to the highest DC bias investigated, which is in contrast to the above-mentioned constant density for high DC bias. These results suggest that the high bias enables a desirable polymer substrate with a SiO_x barrier layer. Detailed analysis of the SiO_x layers to comprehend these bias dependent phenomena will be reported at the presentation.

[1] T. Okimoto et al., The 21th International Display Workshops Proceedings, 1448-1451 (2014)

[2] L. Martinu et al., Journal of Vacuum Science & Technology A 12, 1360-1364 (1994)

Thursday Afternoon Poster Sessions, November 10, 2016

Thin Film

Room Hall D - Session TF-ThP

Thin Films Poster Session

TF-ThP2 Interfaces in Hybrid Structures: A 'non'-Destructive, In Situ Insight in Bonds and Failure, *Tom Hauffman*, S. Pletinckx, K. Marcoen, Vrije Universiteit Brussel, Belgium; *P. Kerger*, Max Planck Institut für Eisenforschung GmbH (Düsseldorf- Germany), Germany; *L.I. Fockaert*, Technical University of Delft, Netherlands; *M. Rohwerder*, Max Planck Institut für Eisenforschung GmbH (Düsseldorf- Germany), Germany; *J.M.C. Mol*, Technical University of Delft, Netherlands; *H. Terryn*, Vrije Universiteit Brussel, Belgium

Polymer/(hydr)oxide/metal systems play an important role in engineering. In aerospace, microelectronics, automotive, packaging and even biomedical industry engineering metals are adhesively bonded by a polymer adhesive. Next to adhesive joints, organic coatings are used in these industries and in construction in order to protect the underlying substrate against atmospheric influences. The interface between the organic layer and the oxide of these hybrid systems is very important as it determines largely the performance of the entire system. However, in which sense this interface is of extreme importance is the topic of a large debate. Although mechanical interlocking has always been put forward as the main force holding hybrid structures, it becomes increasingly clear that interfacial chemical interactions are the key players in hybrid structure durability. Furthermore, the access to the interface of hybrid structures is challenging as it is mostly covered by μm range thick polymer overlayers. The so-called buried interface can only be accessed by using monomeric model compounds or by removing (e.g. by argon sputtering or stripping) the polymeric layer partially [1-5]. However, monomers do not fully represent the interphases to be expected in polymer – metal oxide structures and sputtering alters the interface itself. In this presentation, we will present an innovative approach to study interfacial interactions between metallic oxide layers and polymeric films in a non-destructive, in situ manner. This will be done using ultrathin polymeric films deposited on well-tuned oxides. The interactions will be probed using X-ray Photoelectron Spectroscopy, AFM-TOF-SIMS, Infrared Spectroscopy in a Kretschmann geometry and Near Ambient Pressure X-Ray Photoelectron Spectroscopy.

1. Hauffman, T. Van Lokeren, L. Willem, R. Hubin, A. and Terryn, H. *Langmuir* 28 (2012) 3167-3173.
2. Bekir, S. Özkanat, Ö. Mol, J. Terryn, H. and Rohwerder, M., *Journ. Phys. Chem. C* 117 (2013) 4480-4487.
3. Taheri, P. Ghaffari, M. Flores, J. Hannour, F. de Wit, J. Mol, J. and Terryn, H. *Journ. Phys. Chem. C* 117 (2013) 27480-2792.
4. Wielant, J. Hauffman, T. Blajiev, O. Hausbrand, R. and Terryn, H. *Journ. Phys. Chem. C* 111 (2007) 13177-13184.
5. Taheri, P. Terryn, H., and Mol, J., *Appl. Surf. Sci.* 354 (2015) 242-249.

TF-ThP5 Valence Band Investigation of Cu(In,Ga)Se₂ Semiconductor: Improvements by Ag Alloying, *Kevin Jones*, R.L. Opila, F. Fang, University of Delaware; *L. Chen*, W. Shafaraman, University of Delaware and Institute of Energy Conversion at University of Delaware

The surface valence band-edge energy lies below the Fermi level by about 1.1eV for CuInSe₂. This energy is larger than the bulk band gap energy of 1.04eV, therefore was indicated that the surface of CuInSe₂ has a wider bandgap than its bulk. It was later found that the surface band gap of polycrystalline CuInSe₂ is 1.4eV, more than 0.3eV larger than its bulk band gap. This led to many experimental observations of what may be the cause of this surface widening effect, in which most progress has been computational. Empirical data suggest that preferential formations of electrical neutral defect pairs are created naturally in Cu-chalcopyrites, in which forms a so called "surface defect layer" on the surface and between the interfaces of the buffer and back contact layer of Cu-based solar devices. The need for an efficient wide band gap absorber has been established for a monolithic tandem solar cell design of the Cu(In,Ga)Se₂ thin-film system, therefore, understanding related surface electronic properties is a necessity for band gap tuning. This work investigates the surfaces of the proposed Ag-alloyed wide band gap system of Cu(In,Ga)Se₂, by way of ultra-violet photoemission spectroscopy. In these efforts, we relate the valence band spectra of certain Ag and Ga ratios of Cu-In-Se system to reported empirical data of CuInSe₂ and CuInSe₈ (ODC) stoichiometry, and how these ratios effect surface electronic properties.

TF-ThP7 Internal Charge Transfer at the MBE-Grown Complex Oxide Interface, *Peng Xu*, University of Minnesota; *T.C. Droubay*, Pacific Northwest National Laboratory; *J.S. Jeong*, K.A. Mkhoyan, University of Minnesota; *P.V. Sushko*, S.A. Chambers, Pacific Northwest National Laboratory; *B. Jalan*, University of Minnesota

Two-dimensional (2D) ultra-high carrier densities are of significant interest for novel plasmonic and high charge-gain devices. The highest 2D electron density obtained is thus far limited to $3 \times 10^{14} \text{ cm}^{-2}$ ($\frac{1}{2}$ electron/unit cell/interface) at GdTiO₃/SrTiO₃ interfaces, and is typically an order of magnitude lower at LaAlO₃/SrTiO₃ interfaces. In this work, we will present detailed study from experiments and modeling to show that carrier densities much higher than $3 \times 10^{14} \text{ cm}^{-2}$ /interface can be achieved via band engineering at MBE-grown NdTiO₃/SrTiO₃ interfaces. The SrTiO₃ (8 u.c.) / NdTiO₃ (2 u.c.) / SrTiO₃ (8 u.c.) / LSAT(001) heterostructure shows the expected 0.5 electron/unit cell/interface starting at $t = 2$ u.c., but then exhibits a higher carrier density regime at $t \geq 6$ u.c. due to additional charge transfer from broken gap band alignment between NdTiO₃ and SrTiO₃. The thickness dependence of electronic transport behavior will also be discussed.

TF-ThP9 Preparation of a Transparent Conductive Multilayer Consists of MoO₃/Ag/MoO₃ and its Application in OLEDs, *Midori Kawamura*, T. Chiba, T. Kiba, Y. Abe, K.H. Kim, Kitami Institute of Technology, Japan

Transparent conductive films are widely used as electrodes in solar cells and display devices. As a material, indium tin oxide (ITO) has been most popular. However, development of indium-free or indium-saving materials is also demanded. As one of the solutions, a multilayer structure with oxide/metal/oxide layers has been developed. Previously, we have prepared indium zinc oxide (IZO)/Ag/IZO multilayer as an anode of an OLED, and obtained an excellent properties. In the present paper, we prepared an indium-free multilayer consists of molybdenum oxide (MoO₃) and Ag. We report a properties of the multilayer as a transparent conductive film and as an anode of OLED.

Film deposition was conducted on a glass substrate at room temperature by vacuum evaporation method. The thicknesses of the Ag layer and the MoO₃ layer were varied from 10 to 14 nm and 5 to 30 nm, respectively. The figure of merit (FOM) was calculated based on the sheet resistance and transmittance at a wavelength of 550 nm to estimate the performance of the transparent conductive films. The OLEDs consists of anode/MoO₃(1nm)/ α -NPD(60,70nm)/Alq₃(65, 75nm)/LiF(1nm)/Al(150nm) were fabricated and the current [http://ejje.weblio.jp/content/current+of+electricity] and the luminance of the devices as a function of applied voltage were measured.

Sheet resistance of the multilayer was mainly governed by thickness of the Ag layer, therefore multilayer where the thickness of Ag layer was 14 nm showed low values. However, optical transmittance at a wavelength of 550nm changed depending on the thickness of oxide layer, and the highest FOM value was obtained in a multilayer consists of MoO₃(30nm)/Ag(14nm)/MoO₃(30nm). By AFM observation, it was found that hillocks were formed on the multilayer surface and this caused a short-circuit of an OLED device. Finally, we obtained a good OLED properties by increasing thicknesses of organic layers. It is found that efforts to reduce surface roughness of the multilayer is needed to improve OLED properties further.

TF-ThP11 X-Ray Analysis of Metamorphic In_xGa_{1-x}As/In_yGa_{1-y}As Superlattices on GaAs (001) Substrates, *Fahad Althowibi*, J.E. Ayers, University of Connecticut

Strained-layer superlattices have been used in metamorphic device structures for the control of the threading dislocation density. If placed below a graded layer, the superlattice can modify the misfit dislocation length, and if placed above a metamorphic buffer, the superlattice can promote annihilation and coalescence reactions between threading dislocations. In either application, the superlattice is metamorphic, or partly lattice relaxed, and it is of interest to be able to determine the threading dislocation density within the superlattice by means of non-destructive characterization. In this paper we report a study of the dynamical x-ray diffraction from In_xGa_{1-x}As/In_yGa_{1-y}As superlattices grown epitaxially on GaAs (001) substrates. We show that the threading dislocation density in the superlattice may be estimated from non-destructive x-ray rocking curve measurements. This approach may also be extended to complex device structures containing metamorphic superlattices.

Thursday Afternoon Poster Sessions, November 10, 2016

TF-ThP12 Synthesis of Novel Ta Precursor and its Application in Atomic Layer Deposition of TaN Film, J.H. Han, Korea Research Institute of Chemical Technology, Republic of Korea; S.C. Lee, H.Y. Kim, T.M. Chung, Korea Research Institute of Chemical Technology; **ChangGyun Kim**, Korea Research Institute of Chemical Technology, Republic of Korea

Tantalum nitride (TaN) film has received considerable attention for the application in the Cu diffusion barrier owing to its promising properties including high electrical conductivity, high chemical stability, and high resistivity against Cu diffusion [1,2]. Although physical vapor deposition method such as sputtering is being mainly used for TaN coating in semiconductor industry, the use of atomic layer deposition (ALD) is expected to be essential to fabricate highly scaled semiconductor devices. A variety of Ta precursors have been reported for TaN ALD films. Although tantalum halides such as TaCl₅, TaF₅ and TaI₅ were most widely performed with NH₃ and ¹BuNH₂, the halide precursors are solid with relatively low vapor pressure [3]. In addition, ALD with halide sources resulted in formation of corrosive by-products and required relatively high growth temperature to obtain pure TaN film.

We successfully synthesized novel Ta precursor which is thermally stable and volatile liquid at room temperature. Thermal decomposition test for novel Ta precursor revealed that it starts to decompose approximately at 350 °C. Self-limiting growth of TaN ALD film was observed with co-reactant either NH₃ or NH₃ plasma at the temperatures of 150-300 °C. Deposition rate of TaN using NH₃ plasma at 200 °C is 0.06 nm/cycle, and AES depth profile showed that PEALD TaN film contains carbon and oxygen levels below 5 %. In this presentation, chemical/physical characteristics and Cu diffusion barrier property of TaN film will be covered.

Figure. AES depth profile of PEALD TaN film grown at 200 °C

[1] T. Chakraborty and E. T. Eisenbraun, J. Vac. Sci. Technol. A 30, 020604 (2012).

[2] H. Kim, C. Detavernier, O. van der Straten, S. M. Rosnagel, A. J. Kellock and D.-G. Park, J. Appl. Phys. 98, 014308 (2005).

[3] J.-D. Kwon, J. Yun, and S.-W. Kang, Jpn. J. Appl. Phys., 8, 025504 (2009).

TF-ThP13 Transmission of Plasma-Generated Free Radicals through Silicon Nitride Dielectric Films, F.A. Choudhury, G. Sabat, M. Sussman, University of Wisconsin-Madison; Y. Nishi, Stanford University; J.L. Shohet, University of Wisconsin-Madison

A high concentration of free-radicals is present in many processing plasmas, which affects the processing conditions and the properties of materials exposed to the plasma. Determining the types and concentrations of these free radicals is critical in order to determine their effects on the materials being processed. Previous work utilized simulations[1] to determine the free-radical density and doses from the processing plasma. Several techniques have been developed and tested over the years for radical measurements[2], but the methods do not provide a direct measurement of the free radical concentrations at the location of the sample during processing. A new technique, using fluorophore dyes, that can detect free radicals in a processing plasma and determine their fluence at the surface of a sample during processing is investigated. The fluorophores used in this work is Alexa Fluor® 488. After reaction with reactive oxygen species (ROS), the bright green fluorescence (excitation/emission maxima ~490/515 nm) of the dye is significantly degraded. This degradation is measured using a fluorometer. The change in intensity of the fluorescence is used to measure the free radical fluence incident on the sample holder under various plasma conditions. This technique is also used to determine the number of free radicals that can penetrate through a layer of Silicon Nitride (SiN) film as follows. Alexa 488 is placed under free-standing SiN films of various thicknesses and exposed to oxygen plasma to determine the absorption coefficient and penetration depth of the free radicals. Using this method, the absorption length was found to be about 30 nm. Using X-ray Reflection (XRR) spectroscopy, it was found that the top 25 nm of the plasma-exposed film is modified which corresponds to the depth of free radical induced damage.

This work has been supported by the Semiconductor Research Corporation under Contract No. 2008-KJ-1871 and the National Science Foundation under Grant No. CBET-1066231.

1 Shi, H. and Huang, H., Bao, J., Liu, J., Ho, P. S., Zhou, Y., Pender, J.T., Armacost, M. D. and Kyser, D., Journal of Vacuum Science & Technology B, 30, 011206 (2012)

2 Moon, C.S., Takeda, K., Takashima, S., Sekine, M., Setsuhara, Y., Shiratani, M., and Hori, M., Journal of Applied Physics, 107, 103310 (2010)

TF-ThP16 PEALD BSG PSG Doping Diffusion Characterization, Jeff Shu, Y. Zhang, H. Sheng, J. Liu, GLOBALFOUNDRIES U.S. Inc.

Continuous CMOS scaling becomes more and more difficult due to the extreme process challenges. After FIN FET device architectures were introduced into the industry at end of 2011, they have been widely adopted by the industry to continue device scaling with improved short channel control and performance at lower supply voltages. Compared to SOI substrate, careful punch-through stopper junction design and STI are required for FINs formed on bulk substrate [1]. A novel subfin doping technique had been reported at the 14nm node, which is achieved through solid-source doping to enable better optimization of punch-through stopper dopants [2]. High dopant concentration below the channel to suppress leakage and low dopant concentration in the channel for high performance & less variability can be achieved by solid-source doping techniques while high impurity concentration in the channel and silicon damage could be caused if ion implantation is used for this subfin doping. In this paper, thorough diffusion characterizations were performed at both BSG (Boron Doped Silicate Glass) and PSG (Phosphorus Doped Silicate Glass) on silicon substrates with different drive-in anneal conditions and different insulator cap options. A novel solid-source doping scheme with BSG for NFET subfin doping and PSG for PFET subfin doping is proposed due to the fact that no enough space exists to continue the traditional dual doped liner (BSG/PSG) scheme on 7nm node and beyond.

[1] K. -I. Seo et al., "A 10nm Platform Technology for Low Power and High Performance Application Featuring FINFET Devices with Multi Workfunction Gate Stack on Bulk and SOI" Symp. VLSI Tech. Dig., p.14 – 15, 2014

[2] S. Natarajan et al., "A 14nm Logic Technology Featuring 2nd-Generation FinFET, Air-Gapped Interconnects, Self-Aligned Double Patterning and a 0.0588 m2 SRAM cell size" IEDM. Tech. Dig, p.71 – 73, 2014

TF-ThP17 Low Temperature Deposition of nc-Silicon Thin Films using SiH₄/H₂ mixture, Moniruzzaman Syed, Lemoyne Owen College; Tong. Goh, University of Malaya, Malaysia; N.F.F.B. Nazarudin, University of Malaya, Kuala Lumpur; A. Jahangir, University of Memphis; Y. Hamada, Lemoyne Owen College; A.M. Ali, King Khalid University, Saudi Arabia

Nanocrystalline-silicon (nc-Si) films were simultaneously deposited on glass and single-crystal Si substrates that were exposed to H₂ plasma excited using RF power = 80 W prior to the film deposition, under 250°C by plasma enhanced chemical vapor deposition using a SiH₄/H₂ mixture. Structural changes of the nc-Si films were investigated by X-ray diffraction, Raman spectroscopy, infrared absorption, UV-VIS and AFM measurements. All nc-Si films were deposited as a function of RF power conditions. <110> preferentially oriented nc-Si films were observed to grow suddenly with RF power of 80 W resulted in improved crystalline qualities. These results were examined on the basis of the effect of various mechanisms on the crystalline properties, although these mechanisms may jointly determine the properties.

KEYWORDS: polycrystalline Si, plasma-enhanced chemical vapor deposition, surface morphology of substrates, growth mechanism, crystalline qualities

TF-ThP19 Low Energy Ion Scattering (LEIS) Analysis of ALD Deposited GaSb Films on SiO₂, Thomas Grehl, P. Brünner, ION-TOF GmbH, Germany; R. ter Veen, M. Fartmann, Tascon GmbH, Germany; T. Blomberg, M. Tuominen, ASM Microchemistry Ltd., Finland

GaSb is a promising candidate as a III-V channel material for p-channel for future metal-oxide-semiconductor field-effect transistors (p-MOSFETs) due to its high hole mobility. Also other applications like thin film solar cells or other optoelectronic applications are being discussed. In many of these applications, a well-controlled deposition of GaSb thin films is required.

During deposition process development, characterization of the early stages of film growth is essential to optimize the deposition conditions and possible pre-treatments of the substrate. Low Energy Ion Scattering (LEIS) is a valuable tool for this: Its key feature is the ability to quantitatively determine the composition of the outermost atomic layer. In addition, it non-destructively obtains information about the composition of the first few nm of the sample. These features make it the ideal technique to follow the nucleation of the film and its development until the film is closed. This includes information about the initial growth per cycle as a function of the cycle number, the accurate determination of film closure, and monitoring of unexpected contamination.

The instrument in this study is equipped with a high-sensitivity and high-resolution energy analyzer to record the energy spectrum of noble gas ions

Thursday Afternoon Poster Sessions, November 10, 2016

scattered back from the sample surface. The 3 – 8 keV ions undergo binary collisions with surface atoms, leading to a characteristic energy loss depending on the mass of the scattering partner. The energy loss is used for identification, while the intensity is used for quantifying the surface coverage per element. Ions which were scattered at sub-surface atoms are detected with a lower probability due to specific neutralization and reionization effects. At the same time they exhibit a depth-dependent energy loss by traveling through the solid. This explains why on the one hand the surface composition can be quantified with ultimate surface sensitivity of one atomic layer, and at the same time the composition of the first few nm can be determined without sputtering.

The GaSb films in this study were deposited on SiO₂, using a GaCl₃ + Sb(SiMe₃)₃ chemistry at 110 °C in a Pulsar 2000 reactor. Samples were taken out after 1 – 20 ALD cycles and analyzed using LEIS. As the analysis involved transport of the samples through air, an appropriate method to remove atmospheric hydrocarbons from the surface had to be applied. For this purpose, different treatments were tested for their ability to remove the adsorbents while minimizing the effect on the composition of the surface.

TF-ThP21 Characterization and Use of Porous Materials for Solid Phase Microextraction by Sputtering and CVD, Massoud Kaykhaii, T. Roychowdhury, A. Diwan, B. Singh, M.R. Linford, Brigham Young University
This presentation will focus on both the characterization of new materials for SPME and their use in extracting analytes of interest from complex matrices. Solid phase microextraction (SPME) is an important sampling tool. It consists of placing a coated fiber above a sample (headspace mode) or immersing it in a liquid such that molecules (analytes) of interest can be selectively extracted and concentrated. The captured species are then released by heating or dissolution into a chromatograph for separation and identification. It is a 'green' method because no additional solvent is used in this process. We have developed a new class of SPME fibers that offer extraordinary capacity and speed. They are prepared by sputtering a material under conditions that lead to a nanoporous coating on the fiber. When silicon is sputtered under these conditions, its outermost surface can be additionally oxidized, leading to a high density of silanol groups than can be subsequently silanized. For example, the fibers can be derivatized with octadecyldimethylmethoxysilane by chemical vapor deposition (CVD), which creates a hydrophobic extraction medium. The performance of our 2 micron sputtered coatings has been compared to that of thicker (7 micron) commercial coatings. Our fiber consistently outperforms the commercial fiber, showing significantly higher capacity for alcohols, amines, aldehydes, and esters. Real world samples, e.g., hops and PAH from water, have also been analyzed. Different coating thicknesses have been prepared and evaluated. Sputtered coatings have been characterized by X-ray photoelectron spectroscopy (XPS), scanning electron microscopy (SEM), and wetting.

TF-ThP22 Simulation and Characterization of Short Channel Organic Thin Film Transistors Fabricated Using Ink-jet Printing and Imprint Process, Juhyun Bae, Sungkyunkwan University, Republic of Korea; *K.H. Kim, N.Y. Kwon,* Samsung Electronics Co., LTD., South Korea; *I.S. Chung,* Sungkyunkwan University, Republic of Korea

Printable Organic Thin Film Transistors (OTFTs) are of increasing interest for low cost electronic applications. Among those, inkjet-printing has attracted attention in flexible and light-weight electronic products based on OTFTs due to its advantages like non-contact patterning and good local registration without wasting material. In addition, To use inkjet-printed TFTs for commercial productions, it is required to reduce channel length below 10µm because TFTs with channel lengths of 5 and 10 µm are typically used in active-matrix display applications.

In this work, We fabricated short channel OTFTs on a polyethersulphone substrate using inkjet printing combined with an imprint method. 6,13-bis(triisopropylsilyl)ethynyl) TIPS pentacene and polyvinyl alcohol were used for an active material and a gate insulator, respectively. We utilized schematic of bottom contact OTFTs with silver electrode. Imprint method was attempted to precisely separate printing of S/D electrodes has difficulties in controlling the short channel lengths. Thereby we obtain the 2.5µm, 3.8nm and 6.4µm channel length. This confined structure could dominant big grains instead of dendrite grains. Because confined structure is to reduce the solvent evaporation at the edge of droplet since boundary is blocked. Physical analysis of confined structure was investigated using scanning probe microscopy (SPM). Furthermore, we clearly obtained big grains in SEM images. We found that crystallization of TIPS pentacene is confirmed from big grains and dendrite grains plays an important role in

determining the electrical properties. To compare the electrical properties of the two types of grain, we measured the transfer and family curve from OTFTs having big grains and dendrite grains TIPS pentacene for three channel lengths by Keithley-4200.

The mobility and on/off ratio of case of big grains are better than case of dendrite grains. And as the channel length decrease, the on current slightly increases and the off current decreases. However, the threshold voltages and field-effect mobility of OTFTs appeared a small fluctuations in the different channel length.

The experimental I_{DS}-V_{DS} family curves and I_{DS}-V_{GS} transfer curves were numerically well simulated by SILVACO. The simulation is applied the same schematic structure of experiment. Simulation results also obtained that as the channel length decrease, the on current increases and the off current decreases. And threshold voltages and mobility were rarely fluctuations in the difference in the channel length. Therefore, we could admit the simulation results support for the experiment results.

TF-ThP24 Toward Reliable Production of Well-Structured, Self-Assembled Thin Films of Quantum Dots for Surface Coatings, Cuong Nguyen, J.J. Weimer, The University of Alabama in Huntsville

The goal of this study is to deposit Langmuir films of quantum dots (QDs) as reliably well-structured, self-assembled, monolayer films. Such films will be increasingly important as pre-cursors to coat thin-film light-emitting devices, solar cells, transistors, and diode lasers where the uniformity of the film plays a key role in the consistency of its properties. The structure of the Langmuir films is imaged at macroscopic to microscopic scales using optical and Brewster angle microscopy. Image processing and analysis are done to characterize the patterns. Corresponding image analysis is also done on Langmuir-Schaefer (LS) films that have been templated from the Langmuir films, and comparisons are made to the film quality in the two cases. The topography and thickness of the LS films are subsequently measured by scanning probe microscopy. The structure of the Langmuir films is controlled to first order by the concentration and volume used during deposition. Common patterns seen include agglomerates, sheets, and streaks. The structure can be refined by adding an organic co-additive at different molar concentration ratios. Above a certain ratio, the QDs and co-additive show phase separation. Systematic characterization of the relationships between deposition parameters and film structure will bring the Langmuir deposition process from being just a laboratory-scale experiment to being a reliable production-level tool to produce well-structured, self-assembled thin films of QDs for surface coatings.

TF-ThP25 IN SITU Spectroscopic Analysis of Perovskite/Graphene Hybrid Films for Graphene-Based Perovskite Solar Cells, Seth B. Darling, Argonne National Laboratory, University of Chicago; *M.A. Acik,* Argonne National Laboratory

Power conversion efficiency in perovskite-based solar cells has improved to ≥20%, however, there is insufficient understanding of the underlying optoelectronic device function. Organolead halide perovskites, MAPbX₃ (X=I, Br, Cl), have stood out with their long electron-hole diffusion length and high electron/hole mobility. Replacement of ETL/HTL with graphene-derived materials (graphene oxide, reduced graphene oxide, n/p-doped graphene, etc.) has emerged recently as a pathway to improved device performance. Nevertheless, graphene/perovskite structure-property relationships are not well understood due to unclear chemistry/poor characterization at the interfaces of ETL/perovskite/HTL hybrids (1). To explore interfacial working mechanisms and perovskite film formation, we performed variable temperature (≤600°C) *in situ* spectroscopy (infrared absorption, micro-Raman, UV-vis-NIR, x-ray photoelectron and luminescence). Our studies targeted perovskite/graphene interfaces and perovskite growth mechanisms to overcome detrimental effects of incomplete lead precursor conversion, inconsistent crystallite formation/film uniformity, weak cation-anion-solvent coordination. Effect of film thickness, lead content, stoichiometry control, underlayer/overlayer composition, and growth temperature were optimized for better film efficiency and charge transport (2). To address film scalability and stability, we studied opto-thermal changes in reduced graphene/graphite oxide (RGO) upon halide-based (CH₃NH₃PbI₃, CH₃NH₃PbBr₃, CH₃NH₃PbCl₃) perovskite deposition, and performed spectroscopic analysis derived from the intensity and peak areas of perovskite vibrational normal modes of C-H (~2800-3200 cm⁻¹) and N-H (~2000-2800 cm⁻¹) and their interfacial reactions with oxygen functional groups in RGO (3). Controlled perovskite formation was achieved at room temperature for bromide/chloride-based perovskites resulting improved chemical stability with heat (vs. iodide derivative) that were decomposed at ≥150°C. Poor perovskite formation

Thursday Afternoon Poster Sessions, November 10, 2016

was monitored on RGO resulting in film degradation in air (O_2 , H_2O) by *in situ* characterization (4); additional insights were derived from defect analysis from I_b/I_g ratio variation at perovskite/RGO interfaces. Film morphology and composition was examined by *ex situ* XRD, SEM, TEM, and AFM.

(1) M Acik, SB Darling. J. Mater. Chem. A (2016) Advance Article. Doi: 10.1039/C5TA09911K (2) J Gong, SB Darling, F You, Energy Environ. Sci. (2015) 8, 1953-1968 (3) M Acik, G Lee, C Mattevi, M Chhowalla, K Cho, YJ Chabal. Nature Mater. (2010) 9 (10), 840-845 (4) M Acik, C Mattevi, C Gong, G Lee, K Cho, M Chhowalla, YJ Chabal. ACS Nano (2010) 4 (10), 5861-5868.

Use of the Center for Nanoscale Materials was supported by the U.S. Department of Energy, Office of Science, Office of Basic Energy Sciences, under Contract No. DE-AC02-06CH11357. The abstract has been created by UChicago Argonne, LLC, Operator of Argonne National Laboratory ("Argonne"). Argonne, a U.S. Department of Energy Office of Science Laboratory, is operated under Contract No. DE-AC02-06CH11357. The U.S. Government retains for itself, and others acting on its behalf, a paid-up nonexclusive, irrevocable worldwide license in said article to reproduce, prepare derivative works, distribute copies to the public, and perform publicly and display publicly, by or on behalf of the Government. Office of Science User Facility under Contract No. DE-AC02-06CH11357. M.A. also acknowledges support from the Joseph Katz Named Fellowship at Argonne National Laboratory.

TF-Thp26 Synergetic Effect of Nitrogen and Fluorine on the Total Dose Radiation Hardness of the Buried Oxide Layer in SOI Wafers, Zhongshan Zheng, Institute of Microelectronics of Chinese Academy of Sciences, China
In order to improve the total dose radiation hardness of the buried oxide layer in silicon-on-insulator (SOI) wafers, the buried oxide was modified by a combined implantation of nitrogen and fluorine ions and subsequent anneal processing. The samples were irradiated using Co-60 gamma rays with various doses, and the radiation responses of the buried oxide layers were characterized using the capacitance-voltage (C-V) technique. The experimental results show the considerably increased radiation hardness of the modified buried oxide layers which received a proper post-implantation annealing with the nitrogen- and fluorine-related electron traps introduced. It is also found that the anneal time is a very important variable affecting the radiation hardness for the modified buried oxide layers, and the depth profiles of nitrogen and fluorine in the buried oxide, which are obtained by secondary ion mass spectrometry (SIMS) analysis, each are nearly identical for all the implanted wafers although there are the obvious differences in the buried oxide radiation hardness between the different samples. Additionally, the rebound and fluctuation phenomena of the buried oxide radiation responses have been observed, which can be attributed to the charge trapping and de-trapping in the buried oxide due to irradiation.

TF-Thp27 The Effect of Vacuum Ultraviolet Irradiation on the Dielectric Constant, Leakage Currents and Time-Dependent Dielectric Breakdown of Low-k Dielectric Films, Dongfei Pei, W. Li, P. Xue, University of Wisconsin-Madison; S.W. King, Intel Corp; Y. Nishi, Stanford University; J.L. Shohet, University of Wisconsin-Madison

Plasma-induced damage is a major concern of the application of low-k dielectric materials in the backend of the line (BOEL) of integrated circuits. Plasma processing, which involves reactive radicals, ion bombardment and vacuum ultraviolet (VUV) irradiation, can cause serious effects on the electrical properties of low-k dielectric materials. The contribution of VUV photons to the damage process was studied in this work. Synchrotron irradiation was used to simulate VUV photon irradiation from processing plasmas without any particle flux. The photon flux varies with the wavelength so the irradiation time was chosen to produce the similar amount of photon fluence at each photon energy. The time dependent dielectric breakdown (TDDb), leakage current, k-value, bandgap and mobile charge of the VUV irradiated low-k dielectric films were measured and compared. FTIR, XPS and ESR analysis were applied to the films. An energy threshold for the VUV photons to induce damage of low-k dielectrics was found. TDDb degradation, leakage current increase and mobile charge generation were observed in low-k dielectric films irradiated by the VUV photon with energy above the threshold.

This work was supported by the Semiconductor Research Corporation under Contract 2012-KJ-2359

TF-Thp28 Fabrication of and Photovoltaic Characterization of SnS Solar Cell, YoungKuk Lee, S.G. Kang, C.G. Kim, Korea Research Institute of Chemical Technology, Republic of Korea

Tin (II) sulfide (SnS) is a promising candidate to replace current thin film light absorbing materials in photovoltaics. SnS has a moderate band-gap (1.1-1.3 eV) and high absorption coefficient. SnS thin films have been prepared by metal organic chemical vapor deposition (MOCVD) from the reaction of $Sn(dmamp)_2$ and H_2S gas as the source materials. The molecular structure of $Sn(dmamp)_2$ is shown in fig. 1. SnS films were deposited on Si and glass substrates at the deposition temperature of 200-400 °C. Post annealing of SnS thin films was carried out at 400 °C for 1 h under the H_2S ambient. Hall measurement using van der Pauw method indicate that the film has a p-type conductivity with a hole mobility of $13 \text{ cm}^2/\text{V}\cdot\text{s}$. Raman spectroscopy and x-ray photoelectron spectroscopy results show that SnS thin film has no impurities or other binary phase detected inside the films

TF-Thp29 Solution Deposition of Pentacene Thin Films for Solar Cells and Organic Electronics, Michael Lee, R. Mendoza, R.T. Rodriguez, B.F. Kunzler, Northern Arizona University

Since bulk conductivity in organic crystals was discovered in the 1960s,[1] high mobilities for single-crystal organic semiconductors have been reported with $35 \text{ cm}^2 \text{ V}^{-1} \text{ s}^{-1}$ for pentacene,[2] and even $40 \text{ cm}^2 \text{ V}^{-1} \text{ s}^{-1}$ for rubrene.[3], [4] However, these large aromatic molecules are generally insoluble for solution-processing.[5] Optimized films have been prepared by solution-processing derivatized molecules, such as TIPS-pentacene. In TIPS-pentacene, the derivitized groups comprise over half of the mass. Optimized devices using modified pentacene can reach a carrier mobility of only $6 \text{ cm}^2 \text{ V}^{-1} \text{ s}^{-1}$. [6]

While much of the decrease is due to the polycrystalline nature of the films, the added functional groups also play a direct role. Their effect has been tested to some extent by synthesizing pentacene with removable functional groups. Preparing a film and removing of the functional groups gave nearly 50% increased mobility, or $8.8 \text{ cm}^2 \text{ V}^{-1} \text{ s}^{-1}$. [7]

We present our recent results on using an alternative strategy to directly solution-process unmodified pentacene and other large organic semiconductors into thin films that can be used for organic field-effect transistors and solar cells. This strategy can be extended to other large semiconductors without requiring organic synthesis of new molecules.

[1] H. Kallmann and M. Pope, "Bulk Conductivity in Organic Crystals," *Nature*, vol. 186, no. 4718, pp. 31–33, Apr. 1960.

[2] O. D. Jurchescu, J. Baas, and T. T. M. Palstra, "Effect of impurities on the mobility of single crystal pentacene," *Appl. Phys. Lett.*, vol. 84, no. 16, pp. 3061–3063, Apr. 2004.

[3] V. Podzorov, S. E. Sysoev, E. Loginova, V. M. Pudalov, and M. E. Gershenson, "Single-crystal organic field effect transistors with the hole mobility $\sim 8 \text{ cm}^2/\text{V s}$," *Appl. Phys. Lett.*, vol. 83, no. 17, pp. 3504–3506, Oct. 2003.

[4] T. Hasegawa and J. Takeya, "Organic field-effect transistors using single crystals," *Sci. Technol. Adv. Mater.*, vol. 10, no. 2, p. 24314, Apr. 2009.

[5] R. S. Ruoff, D. S. Tse, R. Malhotra, and D. C. Lorents, "Solubility of fullerene (C60) in a variety of solvents," *J. Phys. Chem.*, vol. 97, no. 13, pp. 3379–3383, Apr. 1993.

[6] Y. Xu, M. Benwadih, R. Gwoziecki, R. Coppard, T. Minari, C. Liu, K. Tsukagoshi, J. Chroboczek, F. Balestra, and G. Ghibaudo, "Carrier mobility in organic field-effect transistors," *J. Appl. Phys.*, vol. 110, no. 10, pp. 104513-104513–9, Nov. 2011.

[7] K.-Y. Chen, H.-H. Hsieh, C.-C. Wu, J.-J. Hwang, and T. J. Chow, "A new type of soluble pentacene precursor for organic thin-film transistors," *Chem. Commun.*, no. 10, pp. 1065–1067, Feb. 2007.

TF-Thp30 Protected Aluminum Mirrors in the DUV Spectral Range for Astronomical applications, Hung-Pin Chen, W.H. Cho, C.-N. Hsiao, Instrument Technology Research Center, National Applied Research Laboratories, Taiwan, Republic of China; C.C. Lee, National Central University, Taiwan, Republic of China

Protected or enhanced aluminum is widely used for the preparation of highly reflective coatings in the DUV spectral range. For astronomical applications, the DUV reflector demand high quality on these coatings, not only with regard to their optical performance but also to their environmental stability, their thermal properties, and their radiation resistance. In this article, we prepare the protected aluminum mirrors by electron-beam evaporation with ion beam assisted, and optimize the beam voltage and beam current of ion source to improving film quality. Explore

Thursday Afternoon Poster Sessions, November 10, 2016

the refractive index, absorption and the microstructure by difference ion source parameters. The corresponding optical and mechanical properties of multilayer optical thin film were investigated by in-situ optical monitoring, spectrometer, ellipsometry, and Atomic Force Microscope (AFM). Space environment was partially simulated through the employment of a Co60 gamma (γ) radiation source (Nuclear Science and Technology Development Center), to determinate the optical stability of optical thin films for aerospace applications. The reflectance results were measured at the BL04B Beamline of National Synchrotron Radiation Research Center (Taiwan) in DUV spectral region.

TF-ThP31 Physical Characteristics of TiO_x Thin Films Obtained by DC Reactive Sputtering, *Victor Lima, I. Doi, J.A. Diniz, R.R. César*, State University of Campinas, Brazil

This work presents the results of the physical characterization of TiO_x thin films obtained under different deposition conditions such as O₂/Ar ratio and deposition plasma power using dc reactive sputtering process. Two sets of the films were prepared, one set varying the sputtering discharge power ranging from 600 W to 1500 W, at constant gas flow ratio of Ar = 60 sccm and O₂ = 40 sccm, and 10 minutes deposition time. Other set of the TiO_x films were prepared with constant 1000 W deposition power for 10 minutes and gas flow O₂/Ar ratio ranging from 0.166 to 0.5. The obtained samples of both sets were all characterized by different techniques, ellipsometry, Raman spectroscopy, Atomic Force Microscopy (AFM) and Scanning Electron Microscopy (SEM) to determine thickness and refractive index of the films, crystalline structure, roughness and surface morphology, respectively. The ellipsometry results show that deposition rate of the samples increases linearly as the power increases, and that the refractive index slightly decreases with the power increment, remaining however between 2.44 and 2.47, therefore close to the typical value of titanium oxide. As for the crystalline structure, the results of the Raman spectroscopy showed Raman shift peaks at 150, 230, 420, 600, 670 and 810 cm⁻¹, corresponding to anatase and rutile form of TiO_x thin films, which agree to those results observed by different researchers. The obtained spectra demonstrate also that the brookite structure was not found on the studied TiO_x samples. AFM images showed rms roughness ranging from 0.150 nm for the samples obtained at 600 W deposition power to 0.872 nm for those obtained at 1500 W deposition power, that may explained considering increase of temperature at the sample surface and sputtered materials from the target. The characterization of the second set of the TiO_x samples, showed that deposition rates increases as more Ar is provided to the sputtering atmosphere, as well as the refractive index, this one exhibiting a small increment as O₂ ratio is increased, with low standard deviation values, showing deposition of the films with quite homogeneous surface. AFM and Raman results showed very small variations in rms roughness of the samples and crystalline structure when gas flow ratio were varied, remaining around the values of 0.441 nm roughness and Raman peaks of anatase and rutile crystalline structure, similar results as those observed for the first set of the samples. These exhibited properties of TiO_x obtained by dc reactive magnetron sputtering technique, make it a interesting material for several applications, for instances for dielectric in semiconducting FETs.

TF-ThP32 Modification of the Vacuum-ultraviolet Absorption Spectrum during Plasma Exposure of Low-k Dielectrics: A Time-dependent Density Functional Theory Analysis, *Ha Nguyen, F.A. Choudhury, J.L. Shohet*, University of Wisconsin - Madison

Methyl depletion of organosilicate (SiOCH) films due solely to the absorption of plasma vacuum-ultraviolet (VUV) photons has been a crucial concern in plasma processing of interconnects. Research on determining VUV photon penetration into SiOCH films is still of great interest. Several systematic studies [1,2] have been published on how parameters such as absorption coefficient, penetration depth, and quantum yield of methyl depletion chemical processes depend on film porosity, VUV dose, and particularly VUV wavelength. These studies contributed significantly to the advance of this research field. However, these studies did not address an important question of how VUV photoabsorption changes during the course of VUV irradiation. This results in the concentration of Si-CH₃ bonds being reduced with time. This in turn affects how the VUV-penetration depth varies with time. In this work, we aim at addressing this question by using time-dependent density functional theory (TDDFT) to model the absorption spectrum in a continuous photon energy range of 0 to 20 eV for an octamethylsilsequioxane, (CH₃)₈Si₈O₁₂, molecule, which is chosen from among siloxane-based molecular precursors of low-k films as a benchmark case as the first step to understand VUV photoabsorption of SiOCH films. Our calculated results show that for the whole range of VUV

photoabsorption energies, the absorption cross-section decreases substantially as the number of Si-CH₃ broken bonds increases. This decrease of the absorption cross-section, however, occurs at different rates, which depend strongly on VUV photon energy (e.g., the highest and lowest rates are in the ranges of 10-15 eV and 7-10 eV, respectively). These interesting results suggest that the modification of VUV photoabsorption during plasma processing is a paramount factor to determine the penetration of VUV photons into low-k dielectric films.

This work was supported by the Semiconductor Research Corporation under Contract 2012-KJ-2359.

References:

- [1] T. V. Rakhimova et al, Appl. Phys. Lett. **102** (2013) 111902.
- [2] T. V. Rakhimova et al, J. Phys. D: Appl. Phys. **47** (2014) 025102

TF-ThP33 High Moisture-Barrier Films using Roll-to-Roll-Plasma CVD grown SiO_x on Room-Temperature ALD treated PEN Substrates, *Nobuyuki Kawakami, N. Jiko, T. Okimoto*, Kobe Steel, Ltd., Japan; *K. Kanomata, F. Hirose*, Yamagata University, Japan

Flexible electronic devices are expected to extend its commercial applicability for the bendable applications. Barrier coating depositions on plastic substrates, such as, polyethylene terephthalate (PET) and polyethylene naphthalate (PEN), are essential, because water vapor passes through the plastic films, which might degenerate the performance of electronics devices. It is also essential to enhance the productivity of the barrier coating while minimizing its process costs, where the roll-to-roll process is expected to be a candidate. So far, the roll-to-roll type plasma enhanced chemical vapor deposition (PECVD) system for the SiO_x coating was developed where its barrier ability of water vapor transmission rate (WVTR), was at as low as 5×10⁻⁴ g/m²/day with the 500 nm thick coating on PEN [1]. However, further improvement of WVTR down to below 10⁻⁶ g/m²/day is still demanded for organic light emitting diodes (OLEDs).

In this study, the SiO_x coating is deposited by the roll-to-roll PECVD, combined with room temperature atomic layer deposition (ALD) of AlO_x to form a stacked structure on the PEN substrate. The SiO_x coating was processed by a PECVD roll coating system (Kobe Steel, Ltd., W35-350CS), where hexamethyldisiloxane (HMDSO) was used as precursor mixed with oxygen. The ALD of AlO_x was performed using trimethylaluminum (TMA) and remote-plasma-excited water vapor, where the plasma was generated with a mixture of water vapor and argon by an induction coil with a frequency of 13.56 MHz [2]. In order to simplify the whole process, the single ALD layer was inserted for the barrier film formation. The stacked structure consisting of CVD-SiO_x/ALD-AlO_x/PEN substrates was used for the experiment. The barrier performance was measured by AquatranTM produced by MOCON Inc. with a temperature of 40 °C and a relative humidity of 90 %.

The stacked structure of 300 nm thick CVD-SiO_x on 10 nm thick ALD-AlO_x exhibited the WVTR below 5×10⁻⁴ g/m²/day (This is the detection limit of AquatranTM), whereas the film with a single layer of 300 nm thick CVD-SiO_x deposited directly on PEN had a WVTR of 3.38×10⁻³ g/m²/day. As a view point of productivity, it is notable that the thin inserting ALD layer drastically effects on the barrier performance. We consider that the present layer-stacking approach is used for the high moisture-barrier films since this technique goes well with the roll-to-roll production.

- [1] T. Okimoto *et al.*, The 21th International Display Workshops Proceedings (2014) 1448-1451.
- [2] K. Kanomata *et al.*, 15th International Conference on Atomic Layer Deposition Technical Program & Abstracts (2015) 442.

TF-ThP34 Determination of the Characteristic Times of Surface Coverage of HfO₂ in Si Substrates by ALD, *Pierre Giovanni Mani-Gonzalez*, UACJ, Mexico; *M.M.M. Contreras-Turrubiates*, UASLP, Mexico; *P.E. Garcia-Casillas*, *H. Leos-Mendez*, UACJ, Mexico; *H. Hernandez-Arriaga*, UASLP, Mexico; *J.A. Hernandez-Marquez*, *J.L. Enriquez-Carrejo*, UACJ, Mexico; *M. Melendez-Lira*, CINVESTAV-IPN, Mexico; *E. Lopez-Luna*, UASLP, Mexico

Actually atomic layer deposition has been used for electronic devices ensemble. The high quality at the interface allows the use of this technique as a deposition method. But when growing any material it is important to think in three important points: the aperture-times of each precursor, the number of ALD cycles and the time of surface saturation. The present work shows the process of surface saturation as function of pressure and physical models. This way of obtaining films is innovative because it has not been considered in every ALD equipment. Also, increasing the superficial area, stoichiometric control and thickness. Those features can be

Thursday Afternoon Poster Sessions, November 10, 2016

controlled using variables such temperature. In previous research it was found that an interface is formed and some defects in film when it is grown by ALD. Those works do not consider this proposed model.

TF-ThP37 Linear Scanning Magnetron for Solar Cell PVD Applications, *Vladimir Kudriavtsev, A. Riposan, L. Mandrell, C.W. Smith, T.M. Bluck,* Intevac

In this presentation we discuss Linear Scanning Magnetic Array (LSMA) technology for magnetron sputtering in

conjunction with in-line substrate processing. In this approach, the magnet array (pole) scans over planar target

spreading the erosion pattern in a controlled fashion. Thus, high quality, dense metal films with good uniformity can be

produced at significant advantages over static magnetrons, such as significantly higher target utilization, longer

uptime, and prevention/removal of target defects related to re-deposition.

We review the influence of magnet motion acceleration/deceleration, the influence of endpoint motion offset

(stagger), and the influence of magnet - to - substrate velocity ratio, on target utilization and lead-to-trail edge film

uniformity. Trade-offs between uniformity and target utilization were established and characterized.

The optimization method we use employs a combination of theoretical simulations and experimental

measurements. Theoretical analysis utilizes ANSYS static magnetic field simulations, erosion profile calculations

including motion integration effects, and ray tracing method for sputtering film thickness calculations

(MATLAB). The structure and uniformity of LSMA-deposited thin films was characterized experimentally by

XRF, 4 point probe and SEM, and the target erosion measured by weight and erosion profiles of spent targets.

We have demonstrated that, with a judicious design approach, an optimal range of operating parameters can be

defined and target utilizations in 60-70% range can be reached, while maintaining deposition uniformity below 2% with

excellent film properties. This makes the LSMA plasma source (using planar targets) more economically

competitive than static and rotatable magnetrons.

TF-ThP39 Chemical Vapor Deposition of Manganese Nitride from bis(2,2,6,6 tetramethylpiperidido) Manganese (II), Mn(tmp)₂, and Ammonia, *E. Mohimi, B. Trinh, Shaista Babar, G.S. Girolami, J.R. Abelson,* University of Illinois at Urbana Champaign

Manganese nitride can be synthesized in numerous phases whose solid-state properties are attractive for spintronic, magnetic or microelectronic applications. It is desirable to develop chemical vapor deposition (CVD) routes for manganese nitride films compared to physical vapor deposition (PVD) paths, since CVD can conformally coat high aspect ratio (deep) features, which are increasingly used in the architecture of nanoscale devices. However, lack of suitable precursors for deposition of manganese nitride hindered its development in novel applications where a conformal thin film is required.

Here, we report CVD growth of amorphous manganese nitride films, from a novel and practical precursor, bis(2,2,6,6 tetramethylpiperidido)Manganese (II) Mn(tmp)₂ and ammonia as co-reactant. Growths are done in a high vacuum chamber at substrate temperature of 50-350 °C. Precursor container is heated at 60 °C and Ar carrier gas passes through the container at flow rates of 5-40 sccm to deliver precursor to the chamber. Ammonia is delivered through a separate line at pressures from 0-13 mTorr.

XPS reveals a bulk Mn:N ratio of 2.6:1 to 2.8:1 for films grown in the temperature range examined, with no carbon contamination within the detection limits of instrument. All films show a nodular microstructure in cross-section SEM, with rms roughness of 0.4 and 0.5 nm for films grown at 50 and 150 °C, respectively. We propose a transamination reaction between precursor and ammonia to be responsible for the nitride growth, as no reaction is observed in the absence of ammonia. Films are conformal in micro-trenches of aspect ratio 3, while having a directional growth component which led to higher thickness at the opening of the features.

Copper diffusion barrier properties of a 12nm manganese nitride film is investigated by deposition on 300 nm thermal silicon oxide/Si substrate, and e-beam evaporation of 200 nm copper on top of manganese nitride film, followed by annealing at 500 °C under Ar for 1 hour. Samples were analyzed by Auger electron spectroscopy for depth profile composition, and compared with a reference sample of no diffusion barrier. Results show that manganese nitride performs well as copper diffusion barrier for microelectronic applications.

TF-ThP40 Effect of Substrate Temperature and Pulse Frequency on the Properties of SiC Film on Si (111) Deposited by Pulsed dc Magnetron Sputtering, *H.-P. Chen, C.-T. Lee, P.-K. Chiu, D. Chiang, Wei-Chun Chen,* ITRC, National Applied Research Laboratories, Taiwan, Republic of China; S.-L. Ou, Da-Yeh University, Taiwan, Republic of China

In this work, the SiC thin film was deposited on Si(111) substrate by a pulsed dc magnetron sputtering deposition for developing the suitable buffer-layer between GaN film and Si substrate. The SiC thin film was prepared from a high purity (99.999%) SiC target and deposited on Si(111) at conditions with various substrate temperatures (600~900 °C) and pulse frequencies (10~100 kHz) by a pulsed-dc magnetron sputtering. Effects of process parameters on the film composition, microstructure, surface roughness, and electrical properties were investigated by field emission scanning electron microscopy with energy dispersive X-ray spectroscopy (FESEM-EDX), X-ray diffraction (XRD), high resolution transmission electron microscopy (HRTEM), atomic force microscopy (AFM), Raman spectrometer, and Hall-effect measurement, respectively. The research goal is to obtain preferred orientation along SiC (111) and root-mean-square surface roughness below 0.5 nm. It is expected that the high quality GaN layer can be epitaxial grown on Si substrate with SiC interface layer.

TF-ThP41 Reactive Magnetron Sputtering of Epitaxial Scandium Nitride for High Performance Electronics, *Amber Reed,* Air Force Research Laboratory, Wright Patterson Air Force Base; *D.C. Look, V. Vasilyev,* Air Force Research Laboratory, Wright-Patterson Air Force Base; *H.M. Jeon, H.A. Smith, M.R. Schmitt,* Air Force Research Laboratory, Wright Patterson Air Force Base; *J.S. Cetnar,* Air Force Research Laboratory, Wright-Patterson Air Force Base; *B.M. Howe,* Air Force Research Laboratory, Wright Patterson Air Force Base

With technological advances in electronics increasing the need for high performance devices (i.e. high power-high speed), there has recently been a surge in research in transition metal nitrides. The inherent mechanical, chemical and high temperature stability of transition metal nitrides make them ideal candidates for high-performance high-temperature electronics. Scandium nitride (ScN) is of particular interest for incorporation into gallium nitride (GaN) based electronics. Stoichiometric ScN is an n-type III-V semiconductor with a moderate band-gap (2.1-2.4 eV) and high reported carrier concentrations (up to 10²¹ cm⁻³). With its rock salt structure and lattice constant of 4.51 nm, ScN has great potential for hetero-epitaxial growth on sapphire (Al₂O₃) and magnesium oxide (MgO). In addition, its close lattice match with GaN (<0.1% mismatch) makes ScN a good candidate for use as a buffer layer for hetero-epitaxial GaN on silicon (Si), in ScN-GaN heterostructures, or as an ohmic contact for GaN devices. Incorporation of ScN films into GaN devices requires high quality (i.e. low surface roughness, large grain-oriented crystals, low oxygen contamination) films.

In this work we investigate hetero-epitaxial growth of ScN films on GaN, Al₂O₃ <0001>, and MgO <100> substrates using unbalanced reactive magnetron sputtering with external electro-magnetic coils. The effect of coil current, target power and nitrogen gas fraction on film stoichiometry, microstructure and surface morphology was investigated by correlating film properties, determined through x-ray photoelectron spectroscopy, x-ray diffraction, transmission electron microscopy and atomic force microscopy, with the deposition parameters and plasma conditions during film growth. Hall measurements of the films showed that resistivity and mobility were strongly dependent on crystalline quality and ScN crystal orientation. The Hall mobility of (111)-oriented ScN films on (0001) sapphire increased from 0.95 cm²/(V*s) to 7.8 cm²/(V*s) and the resistivity decreased from 1.57x10⁻³ W cm⁻¹ to 6.52x10⁻⁴ W cm⁻¹ as the full width half maximum of the ScN (001) x-ray diffraction peak decreased. The transport properties of the (100)-oriented ScN were significantly better than those of the (111)-oriented films with mobilities > 80 cm²/(V*s) and resistivities < 1.77 x10⁻⁵ W cm⁻¹.

Thursday Afternoon Poster Sessions, November 10, 2016

TF-ThP42 Amorphous Phase Content Determination in TiO₂ Thin Films on Glass Substrates using the PONKCS Approach, *T. Malek, Stanislav Danis*, Charles University in Prague, Czech Republic; *L. Matejova*, Technical University of Ostrava, Czech Republic; *M. Cerhova*, Czech Academy of Sciences, Czech Republic

Polycrystalline titania oxide are of great interest recently namely for their photocatalytic properties. Samples of TiO₂ could be prepared as polycrystalline powder (nano-powder) and/or in the form of polycrystalline thin films. In our contribution we will present structural studies of thin layers prepared on different substrates (amorphous glass and crystalline silicon) by dip-coating method. A set of layers were analysed all of them synthesized via sol-gel process controlled within reverse micelles of nonionic surfactant Triton X-114 in cyclohexane combined with pressurized water extraction and/or supercritical/pressurized methanol drying. Obtained thin films were heated up to 400°C for 4 hours in order to obtain crystalline phase. However, some amount of non-crystalline phase of TiO₂ could be expected due to preparation procedure. In case of powder the amount of the non-crystalline part can be determined using internal standard, for example. Unfortunately, this technique cannot be used in the case of thin layer. We show how to apply PONKCS method [1] in order to at least estimate the amorphous phase concentration within prepared samples on the glass substrate.

The presented work is supported by the Grant Agency of the Czech Republic by the project No.14-23274S.

[1] Scarlett, N.V.Y., Madsen, I.C. (2006), *Powder Diffraction*, 2006,21(4), 278-284

Keywords: thin films , quantitative phase analysis, amorphous phase

TF-ThP43 The Atomic Layer Deposited SrTiO₃ Films using Thin Seed Layer and their Improvement of Dielectric Properties for DRAM Capacitor, *Sang Hyeon Kim*, Samsung Electronics, Republic of Korea; *C.S. Hwang*, Seoul National University, Republic of Korea

Dynamic random access memory (DRAM) plays the role as main memory in computers and mobile electronic devices. Further evolution of DRAM requires increase in change density of capacitors. However, the currently using ZrO₂/Al₂O₃/ZrO₂ stacked dielectric layer is facing its limitation for further scaling due to the increased leakage current. Thus, perovskite structured SrTiO₃ (STO) material is attracting great attention as a future dielectric material in DRAM capacitors. Atomic layer Deposition (ALD) is the most suitable method for DRAM capacitor application which requires excellent conformality on complicated three-dimensional structure with an aspect ratio of 100:1.

ALD of STO films has been researched at a high growth temperature of 370 °C in a series of investigations by the authors' group in order to achieve in-situ crystallization.^{(1),(2)} However, abnormally too high growth rate at initial stage of film growth on Ru electrode, which is the most probable electrode material, was observed,⁽²⁾ due to the involvement of CVD-like growth behavior. In this study, therefore, 1.5-nm very thin seed layers were deposited under low temperature to make dense seed layers. As a result, the dielectric constant was improved from ~160 to ~270 which was one of the best results of the STO dielectric material. STO films were deposited in a traveling-wave-type ALD reactor (CN-1 Co, Plus-100) for a 4-in.-diameter single wafer. Sr(iPr₃Cp)₂ and Ti(Me₃Cp)(OMe)₃ (synthesized by Air Liquide) were employed as the Sr and Ti precursors, respectively. H₂O and high density (250g/m³) O₃ were employed as oxygen source for SrO and TiO₂ sublayers, respectively. The ALD saturation curve was confirmed in SrO and TiO₂ deposition, and the deposition showed a linear growth behavior with respect to the number of deposition cycle with no indication of abnormal growth at the initial stage. In STO deposition, cation composition (Sr/(Sr+Ti)) was evaluated from 50% - 70%. Electrical properties of the (top) RuO₂ / STO / Ru (bottom) planar capacitor were estimated to confirm the feasibility of the next generation DRAM capacitor applications.

(1) Woongkyu Lee et al., *Chem. Mater.* **2015**, 27, 3881-3891.

(2) Woongkyu Lee et al., *Chem. Mater.* **2013**, 25, 953-961.

TF-ThP44 Water Cooled Low Temperature Evaporation (LTE) Source for Thin Film Organic Semiconducting Materials, *Salahud Din*, Kurt J. Lesker Company, UK

Rapid advances in research and development in organic electronics have resulted in many exciting discoveries and applications, including organic light-emitting devices for information display and illumination, solar cells, photodetectors, chemosensors, and logic devices. Organic semiconducting materials are broadly classified as polymeric or small molecular. For the latter category, solvent-free thin film deposition techniques are generally

preferred to form well-defined interfaces and improve device performance. Controlled deposition of organic semiconductor materials has become more and more important. Due to lower process temperatures (up to ~500°C), the manufacturing of organic electronic devices such as light emitting diodes (OLEDs) and other electronic devices is less energy consuming than conventional silicon based electronics. Additionally, these low temperatures also make it possible to use flexible substrates, e.g. plastic films, which can serve as a basis for elastic electronic devices. The crucial part of the fabrication is the deposition of the active organic layers (films) with a layer thickness between 10 and 100 nanometres. It is mostly done by thermal evaporation in a high vacuum environment. The mobility of the charge carriers within the layers and the layer morphology strongly depend on the deposition rates, i.e. the increase in layer thickness with time during the deposition process. The desired deposition rates range between 0.01 and 5 Angstrom per second.

Kurt J. Lesker Company has developed thin film LTE deposition sources which can deposit a wide range of organic materials with precise deposition rates and thickness control. These sources can be coupled with quartz crystal monitors (QCM) and closed loop PID control systems to ensure consistent high-quality results. The process can be performed at very high levels of vacuum allowing for a long mean free path and therefore lower tendency to introduce film impurities. High deposition rates can be achieved and lower energy particles can reduce substrate damage. Low temperature evaporation sources can take hours to cool in a vacuum system before venting is possible to replenish. This increases device fabrication tact times, reduces throughput and creates the need for more sources in larger platforms. Kurt Lesker's water cooled LTE source has the ability to cool down 3.7x times faster against the standard LTE source, saving precious time while maintaining precise thin film growth during deposition process.

TF-ThP45 Reactive RF Magnetron Sputtering of Vanadium Oxides: Substrate Bias Issues, *Sergey Jr. Maklakov, V.I. Polozov, I.A. Ryzhikov, V.N. Kisel*, Institute for Theoretical and Applied Electromagnetics RAS, Russian Federation

Thin films of vanadium oxides are widely applied functional coatings for electronics. Non-stoichiometric nanocrystalline VO_x films possess low thermal activation energy (~ 0.1 eV). These films serve as infrared detectors in uncooled bolometers. Under certain annealing conditions, VO_x films undergo recrystallization, and stoichiometric VO₂ oxide may be formed. Crystalline VO₂ films possess metal-insulator transition at 68°C. These VO₂ films works as switches for transmission lines for terahertz and microwave range. All these VO_x coatings are frequently deposited through magnetron sputtering.

Although reactive sputtering of vanadium in oxygen-containing atmosphere has been studied since 1960's, there are several points that still not clear. It is well known, that when a negative DC bias are applied to substrate, it provides additional energetic treatment of a growing film. It causes re-sputtering of a surface layer and increases effective surface temperature of a growing coating. As a result, films, grown under the bias conditions, are depleted with light elements and show decreased concentration of admixtures. These effects are studied well for biases more than -20 V (*J. Phys. D: Appl. Phys.* **39** (2006) 2220-2223). We present experiment which shows that substrate bias of low value may influence chemical reactivity of reactive components, giving similar results to large biases.

Series of VO_x thin films was deposited by means of unbalanced RF magnetron source in Ar + O₂ gas mixture. Oxygen-depleted films appear as black coatings with metal conductivity. Oxygen-rich films are yellow dielectrics. Oxygen content may be easily controlled through gas composition, which is a common knowledge. Gas mixture (13.6 % O₂ for a vacuum facility applied) which gives transient VO_x films between oxygen depleted and oxygen rich compositions, was applied for the experiment. Negative bias of a few volts (starting from -1 V), which is comparable to a floating potential, reduces vanadium oxidation state from V⁺⁵ down to V⁺². No biased substrate, under designated conditions, results in VO_x films, substantially consisting of V⁺⁵. Observed effect cannot be explained by resputtering process. Resistivity of VO_x films in the series varies by 5 orders in magnitude. Reduction of vanadium oxidation state also changes the Meyer-Neldel rule type from conventional to inverse. This phenomenon may be caused by changes in oxygen reactivity associated with variations in RF discharge characteristics.

The study was financially supported by the Russian Foundation for Basic Research under grant No. 16-33-01089.

Thursday Afternoon Poster Sessions, November 10, 2016

Tribology Focus Topic

Room Hall D - Session TR-ThP

Tribology Poster Session

TR-ThP1 Wear Behavior of Nitrided Cast Iron D6510 and Cast Steel S0050A under Normal Sliding and Inclined Sliding Conditions, *Chen Zhao, J. Zhang, X. Nie*, University of Windsor, Canada

Four different nitriding technologies, called plasma nitriding (A), fluidized bed nitriding (B), pulsed plasma diffusion process (C) and gas nitriding (D), were used for surface modification of cast iron D6510 and cast steel S0050A, respectively. Microhardness tester and EDX spectroscopy were used to measure the cross-sectional hardness and nitrogen concentration along the depth of the treated cast iron and steel samples. A pin-on-disk sliding test and inclined-sliding test were applied to evaluate the tribological properties of the treated samples under dry condition. Scanning electron microscopy and surface profilometry were also employed to study their wear behaviors. It was found that all cast iron samples had lower wear rates than cast steel samples during both the pin-on-disk sliding test and inclined-sliding test. While the cast iron samples behaved uniformly during these two different tests, the treated steel samples appeared to have a reversal trend in wear resistance. This phenomenon could be attributed to the formation of fatigue cracks on cast steel samples under ultra-high contact stresses during the inclined-sliding tests.

Acknowledgement: The research was also supported by Stamping Tooling Optimization (STO) team, Auto/Steel Partnership, Southfield, MI, USA.

Keywords: wear; nitriding; plasma nitriding; inclined sliding;

2D Materials Focus Topic

Room 103B - Session 2D+NS-FrM

2D Materials: Device Physics and Applications

Moderator: Miguel M. Ugeda, CIC nanoGUNE, Spain

8:20am **2D+NS-FrM1 Direct Writing of 2D Flexible Electronic Devices via Illumination-based Techniques**, M.E. McConney, N.R. Glavin, A.T. Juhl, Air Force Research Laboratory; J.E. Bultman, J.J. Hu, University of Dayton Research Institute/Air Force Research Laboratory; M.F. Durstock, Air Force Research Laboratory; A.A. Voevodin, University of North Texas; **Christopher Muratore**, University of Dayton

Ultra-thin two-dimensional (2D) semiconducting materials possess a combination of large, tunable electronic bandgaps, optical transparency, and mechanical flexibility, and will likely revolutionize electronic devices such as wearable sensors and flexible displays. A primary step in the development of such devices with integrated 2D materials is the development of scalable, transfer-free synthesis over large areas at low temperatures. Electrically insulating amorphous transition metal dichalcogenide (TMD) films can be deposited via physical vapor deposition on large area flexible substrates at room temperature, and crystallized with subsequent illumination with light. Focused laser light with a power density of $\sim 1 \text{ kW cm}^{-2}$ is suitable for writing micron scale features in semiconducting transition metal dichalcogenides on polymer substrates. Broad band illumination from a xenon lamp can also be used over the large substrate areas ($> 100 \text{ cm}^2$), or passed through a physical mask to print features only in desired locations. The semiconducting properties of 2D MoS_2 and WS_2 materials synthesized in this way have been characterized using conductive atomic force microscopy, and other techniques to observe the expected temperature dependence on electrical conductivity. Structure and composition of the materials can be controlled by altering the incident fluence as well as by controlling the ambient environment during illumination, as verified by Raman spectroscopy, X-ray photoelectron spectroscopy, cross-sectional and plan view transmission electron spectroscopy, and other techniques. Multiple layers of 2D materials can also be treated in this way. For example, both layers in a MoS_2/WS_2 heterostructure of 10 nm total thickness on a polymer (PDMS) substrate were crystallized upon laser illumination. Diverse 2D architectures and devices built from illumination-based crystallization techniques will be highlighted.

8:40am **2D+NS-FrM2 Resolving and Tuning Mechanical Anisotropy in Black Phosphorus Nanoelectromechanical Resonators**, Zenghui Wang, H. Jia, P.X.-L. Feng, Case Western Reserve University

Black phosphorus (P) has emerged as a layered semiconductor with unique crystal structure featuring corrugated atomic layers and strong in-plane anisotropy in its physical properties. In particular, it is predicted to exhibit strong in-plane mechanical anisotropy, which shall lead to previously inaccessible dynamic responses in resonant 2D nanostructures [1], and new opportunities for studying carrier-lattice interaction in atomic layers. It is therefore of both practical and fundamental importance to systematically investigate the mechanical anisotropy in black P crystal and NEMS devices.

Enabled by the first demonstration of black P resonant nanostructures [2] with multimode responses, we show that the spatial mapping of the multimode resonance mode shapes [3] creates a new means for precise determination of black P crystal orientation (*i.e.*, the anisotropic zigzag and armchair axes) [4]. Further, the multimode technique enables simultaneous quantification of the anisotropic mechanical properties (*i.e.*, elastic moduli along both major crystal axes): combined with finite element method (FEM) modeling, we determine the Young's moduli of multilayer black P to be 116.1 GPa and 46.5 GPa in zigzag and armchair directions, respectively. In addition, we demonstrate that electrostatic gating induced straining can continuously tune the mechanical anisotropic effects on multimode resonances in black P electromechanical devices. Our results show that multimode resonant response manifests the unique mechanical anisotropy effect in black P nanodevices, and provides a new method for determine the material's crystal orientation and elastic properties *in situ*, independent from conventional optical, electrical, and nanoindentation calibration techniques.

[1] Wang, Z. & Feng, P. X.-L. Design of Black Phosphorus 2D Nanomechanical Resonators by Exploiting the Intrinsic Mechanical Anisotropy. *2D Materials* **2**, 021001 (2015).

[2] Wang, Z., Jia, H., Zheng, X.-Q., Yang, R., Wang, Z., Ye, G.J., Chen, X.H., Shan, J., & Feng, P. X.-L. Black Phosphorus Nanoelectromechanical Resonators Vibrating at Very High Frequencies. *Nanoscale* **7**, 877 (2015).

[3] Wang, Z., Lee, J., & Feng, P. X.-L. Spatial Mapping of Multimode Brownian Motions in High Frequency Silicon Carbide (SiC) Microdisk Resonators. *Nature Communications* **5**, 5158 (2014).

[4] Wang, Z., Jia, H., Zheng, X.-Q., Yang, R., Ye, G.J., Chen, X.H., & Feng, P. X.-L. Resolving and Tuning Mechanical Anisotropy in Black Phosphorus via Nanomechanical Multimode Resonance Spectromicroscopy. *under review*. (2016).

9:00am **2D+NS-FrM3 2D Devices for Flexible and Topological Nanoelectronics**, Li Tao, W. Zhu, D. Akinwande, The University of Texas at Austin

INVITED

Two-dimensional (2D) buckled atomic sheets, such as silicene and phosphorene, yield collective properties of mechanical flexibility and tunable bandgap, which hold promise for advanced flexible and topological nanoelectronics. Silicene is the 2D silicon equivalent of graphene, and is predicted to offer a host of exotic electrical properties, such as quantum spin Hall effect, subjected to external fields. Despite great theoretical expectations on silicene, air-stability had prevented experimental device studies. Recently, our research progress debuts silicene transistors corroborating theoretically predicted ambipolar transport with Dirac band structure. Electrostatic characterization on non-optimized silicene transistors exhibited carrier mobility $\sim 100 \text{ cm}^2/\text{V-s}$ and $10\times$ gate modulation in ambient condition. Without non-ideal limiting factors, *e.g.* phase boundary scattering and electron-phonon coupling, pristine free-standing silicene is predicted to offer intrinsic mobility $\sim 1200 \text{ cm}^2/\text{V-s}$. Further optimization is on-going to shed light on the mobility upper bound achievable and aging evolution of silicene devices. It is likely with further experimental study that monolayer or multilayer silicene can be a platform for realizing advanced device concepts, *e.g.* topological bits, on flexible substrates. The unique allotropic affinity of silicene with crystalline bulk silicon suggests a more direct integration with ubiquitous semiconductor technology.

Phosphorene, few-layer black phosphorus (BP), is another promising candidate for flexible nanoelectronics. Phosphorene exhibits high carrier mobility (100 to $1000 \text{ cm}^2/\text{Vs}$) and tunable direct bandgap (0.3 to 2 eV) even on plastic substrates, making it the most suitable contemporary 2D semiconductor that combines the merits of graphene and transitional metal dichalcogenides. We reported the first BP based flexible RF transistors with intrinsic $f_1=20 \text{ GHz}$ and $f_{\text{Max}}=14.5 \text{ GHz}$, and such performance sustained under ex-situ bending test with tensile strain up to 1.5%. Raman spectroscopy analysis of few-layer BP under tensile strain up to 7% was carried out for the first time to reveal the strain effect on BP. Significant orientation dependence was observed while applying tensile strain along armchair (AC) and zigzag (ZZ) directions, exhibiting the trend of Raman peak shift well agreed with theoretical projections. This recent progress on silicene and phosphorene represent a renewed opportunity for future nanoscale flexible and topological electronics beyond what is available in graphene.

9:40am **2D+NS-FrM5 Optical Detectors Based on Bismuth Telluride Nanowire Arrays Capped by Graphene**, Tito Huber, T. Brower, O. Abana, Howard University

Recently, research on graphene based photodetectors has drawn substantial attention. The gapless nature of graphene and low light absorption can cause low responsivity. The synergetic integration of graphene with other materials is a promising approach to overcome these shortcomings. There have been reports of broadband photodetectors based on heterostructures of few-layer $\text{Bi}(2)\text{Te}(3)/\text{graphene}$ devices that are very encouraging. Here we discuss a different approach, where single layer graphene caps the top of a bismuth telluride nanowire array

(where the wire axis are perpendicular to the graphene surface). Partially, our motivation was to test the exceptional thermoelectric properties of the interface. The room-temperature thermoelectric efficiencies of bismuth telluride compounds are the highest reported for any material, and, therefore, Bi(2)Te(3) nanowires are interesting as building blocks of nanoscale thermoelectric devices, as in this case. Graphene strong photothermoelectric response is also very well known. We employed devices composed of bismuth telluride nanowire arrays which are capped with single layer graphene. Dense arrays of 200-nm nanowires have been prepared by a nonlithographic fabrication technique consisting of the pressure injection of an alumina template with molten Bi₂Te₃, a method that can be successfully employed with 100- μ m thick templates of pore diameters in the range of 2 to 200 nm. Bismuth telluride is a semiconductor with a small gap. The nanowire arrays electronic properties including magnetotransport and thermopower were characterized in separate experiments. The single layer graphene layer was fabricated by transfer by Graphene. Graphene on the device was characterized using Raman spectroscopy. We observed the D, G and 2D peaks and broadening indicating that graphene is nearly intact. We also observed the Raman peaks of bismuth telluride. The incident surface features very low optical reflectivity and enhanced light trapping. Light trapping causes strong light absorption at the interface, an effect that counteracts the weak absorption of graphene and has not been mentioned in the literature before. The unique attributes of the thermoelectric arrays are the combination of strong temporal and optical wavelength dependences of the photocurrent. Under infrared illumination, the signal can be completely described by thermoelectric effects considering cooling rates given by heat diffusion through the array. We will discuss that, in addition, under visible illumination we observe a photovoltaic response. This work was supported by the National Science Foundation through PRDM 1205608 and STC 1231319

10:00am 2D+NS-FrM6 Graphene Nanoelectromechanical Resonators with Electrothermal Excitation and Tuning, F. Ye, Jaesung Lee, P.X.-L. Feng, Case Western Reserve University

Graphene, a hallmark of two-dimensional (2D) materials, has been employed as an atomically thin building block for highly miniaturized nanoelectromechanical system (NEMS) and shown attractive potential for nanoscale actuators and sensors. Thanks to its exceptional elastic modulus ($E_f \sim 1$ TPa), ultralow mass density ($\rho \sim 2200$ kg/m³), and superior strain limits ($\epsilon_{\text{limit}} \sim 25\%$) [1], high performance and frequency tunable graphene resonators have been demonstrated using photothermal [2] and electrostatic actuation [3] schemes. In addition to excellent mechanical properties, graphene possesses high temperature stability [4] and negative thermal expansion coefficient [5], hence graphene resonators may inherently exhibit better performance under high temperature. In existing reports, graphene resonators are exposed in high temperature using annealing or Joule heating (e.g., applying up to 1.8V from drain to source) only for thermal annealing [3], high temperature operation of graphene resonators has not been demonstrated yet.

In this work, we fabricate mono- and bi-layer (1L and 2L) graphene resonators and investigate their resonance characteristics at high temperature up to ~ 500 K using Joule heating. We conveniently use DC voltage to heat graphene resonators, and apply AC voltage to excite resonance motion. Then, we simultaneously measure temperature and resonance characteristic of graphene resonators using a home-built, integrated Raman spectroscopy and laser interferometry measurement system. We first test electrothermal frequency tuning and find that frequency of graphene resonators upshift from ~ 80 MHz to ~ 86 MHz as DC voltage increases from 0.5V to 2.5V. Unlike electrostatic force resonance tuning and excitation [3], we do not observe capacitive softening or loaded Q effects which may compromise performance of resonators. We then investigate mechanical nonlinearity of graphene resonators in high temperature by changing both DC and AC voltage. This study opens new capabilities for engineering tunable graphene NEMS resonators and oscillators for a number of emerging applications.

[1] C. Lee, *et al.*, *Science***321**, 385-388 (2008).

[2] J. S. Bunch, *et al.*, *Science***315**, 490-493 (2007).

[3] C. Chen, *et al.*, *Nat. Nanotech.***4**, 861-867 (2009).

[4] K. Kim, *et al.*, *Phys. Status Solidi RRL***4** 302-304 (2010).

[5] M. Pozzo, *et al.*, *Phys. Rev.Lett.***106** 135501 (2011).

10:20am 2D+NS-FrM7 Pushing the Performance Limit of 2D Semiconductor Transistors, Xiangfeng Duan, California Nanosystems Institute, University of California, Los Angeles

INVITED

Two-dimensional semiconductors (2DSCs) such as MoS₂ have attracted intense interest as an alternative electronic material in the post-silicon era. However, the on-current density achieved in 2DSC transistors to date is considerably lower than that of silicon devices. It remains an open question whether 2DSC transistors can offer competitive performance. To achieve a high performance (high on-current) device requires (1) a pristine channel with high carrier mobility, (2) an optimized contact with low contact resistance and (3) a short channel length. The simultaneous optimization of these parameters is of considerable challenge for atomically thin 2DSCs since the typical low contact resistance approaches either degrade the electronic properties of the channel or are incompatible with the fabrication of short channel devices. Here I will first review different strategies that have been developed to optimize these factors, and discuss how we can combine these strategies together to achieve high performance 2DSC semiconductor transistors. In particular, we will discuss a unique approach towards high-performance MoS₂ transistors using a physically assembled nanowire as a lift-off mask for creating ultra-short channel devices with pristine MoS₂ channel and self-aligned low resistance metal/graphene hybrid contact. With the optimized contact in short channel devices, we demonstrate that a sub-100 nm MoS₂ transistor can deliver a record a high on-current density comparing well with that of silicon devices, demonstrating the exciting potential of 2DSCs for future electronic applications.

11:00am 2D+NS-FrM9 Low Temperature Al₂O₃ ALD on 2D Semiconductors, Il Jo Kwak, J.H. Park, A.C. Kummel, University of California at San Diego

2D semiconductors have attracted attention for future electronic devices due to their excellent electronic and optoelectronic properties. These devices require few nanometer thick and pin hole-free dielectric layers as gate insulators. However, due to the inert nature of 2D semiconductors such as graphene and Transition Metal Chalcogenides (TMDs), the dielectric layer selectively nucleates on defect sites or step edges. In the conventional atomic layer deposition (ALD) process on graphene or other 2D semiconductors, such non-uniform oxides result in large leakage currents in 2D semiconductor based device. Therefore, for successful integration into device, uniform and insulating gate oxides on 2D semiconductors should be prepared.

In this work, Al₂O₃ was directly deposited on HOPG and MoS₂ surface by low temperature ALD with trimethylaluminum(TMA) and H₂O or O₃ without any seeding layer or surface treatments. Using short purge time between two precursor pulses at 50C, a CVD growth component was intentionally induced to provide more nucleation sites on the surface. The CVD growth component induces deposition of 1 nm Al₂O₃x particles on the surface which provide a uniform layer of nucleation centers. Before ALD, HOPG and MoS₂ samples were cleaned by mechanical exfoliation method. For HOPG substrate, 50 cycles of ALD Al₂O₃ was deposited at 50C using 600ms of TMA and 50 ms of H₂O pulse time with 500ms purge time between two pulses. In the case of MoS₂, 300ms of O₃ pulse was employed instead of H₂O pulse. The same ALD recipes were performed on SiGe substrates in order to compared the quality of the oxide. After ALD process, MOSCAP devices were fabricated to measure the capacitance and leakage current of the oxide. Non-contact mode AFM was performed to check the topography of the oxide and the results showed that uniform and pin hole-free oxide layer was formed on the surface. The leakage current of the oxide on HOPG and MoS₂ was as low as 10⁻⁵ A/cm² which was comparable to the oxide on SiGe substrates.

11:20am 2D+NS-FrM10 Atomic Layer Deposition of High-k Dielectrics on WSe₂ for High Performance Electronic Devices, Pushpa Raj Pudasingi, M.G. Stanford, A. Hoffman, The University of Tennessee Knoxville; T.Z. Ward, Oak Ridge National Laboratory; D.G. Mandrus, P.D. Rack, The University of Tennessee Knoxville

The performance of electronic and optoelectronic devices based on two-dimensional (2D) transition metal dichalcogenides (TMDs), such as tungsten diselenide (WSe₂) is significantly affected by the quality of the various interfaces present in the device. Historically, the performance of bottom-gate SiO₂ 2D TMDs field effect transistor (FET) devices has been greatly limited by the carrier scattering due to the oxide trapped charges, surface roughness, and surface optical phonons, among others. One approach to mitigate this issue is to explore alternatives to SiO₂ which ideally would involve high-k dielectrics, in which Coulombic impurity scattering is confirmed to be strongly shielded by the dielectric screening.

However, depositing high quality high-k dielectric film onto the surfaces of TMDs is very challenging due to the chemical inertness of the TMD basal planes. Here, we present an aluminum oxide and hafnium oxide top-gate on WSe₂, deposited using atomic layer deposition (ALD) both with and without hydrogen/oxygen plasma treatments and titanium seed layers. The top gated WSe₂ FET devices are fabricated by employing ALD deposited high k-dielectrics, with promising device characteristics having large current on-off ratio ($\sim 10^8$), small threshold voltage (~ 5 V) and relatively large field effect mobility (~ 70 cm²/V.s) at room temperature. A high performance logic inverter device is also demonstrated.

11:40am 2D+NS-FrM11 Layer-dependent Measurements of Electronic Band Alignment for Individual MoS₂ Flakes Supported on SiO₂ using Photoemission Electron Microscopy (PEEM) with Deep Ultraviolet Illumination, Morgann Berg, Sandia National Laboratories; **K. Keyshar,** Rice University; **I. Bilgin, F. Liu,** Northeastern University, Los Alamos National Laboratory; **H. Yamaguchi,** Los Alamos National Laboratories; **R. Vajtai,** Rice University; **C. Chan,** Sandia National Laboratories; **G. Gupta,** Los Alamos National Laboratories; **S. Kar,** Northeastern University; **P. Ajayan,** Rice University; **T. Ohta,** Sandia National Laboratories; **A. Mohite,** Los Alamos National Laboratories

Tailoring band alignment layer-by-layer using heterojunctions of two-dimensional (2D) semiconductors is an attractive prospect for producing next-generation electronic and optoelectronic devices that are ultra-thin, flexible, and efficient. 2D layers of transition metal dichalcogenides (TMDs) in laboratory devices have already demonstrated properties favorable for electronic and optoelectronic applications. Despite these strides, a systematic understanding of how band alignment evolves from monolayer to multilayer for MoS₂, a model TMD system, is still missing owing to the lack of a suitable experimental approach. Quantitative determination of the electronic band alignment necessitates that measurements be performed in a controlled environment (such as vacuum) using a substrate that interacts minimally with the overlying TMDs (preferably insulating) to suppress the electronic influence of supporting substrates and prevent chemical modification of TMDs due to adsorbates (primarily water).

Here we report on the local band alignment of monolayer, bilayer, and trilayer MoS₂ on a 285-nm-thick SiO₂ substrate, measured using a new approach to probe the occupied electronic states based on photoemission electron microscopy with deep ultraviolet excitation. The spatially-resolved, simultaneous measurements of the vacuum level and the valence band edge at the Brillouin zone center show that the addition of layers to monolayer MoS₂ increases the relative work function, and pushes the valence band edge toward the vacuum level. We also find n-type doping of few-layer MoS₂ and type-I band alignment across monolayer-to-bilayer and bilayer-to-trilayer lateral junctions. Our results differ from some earlier reports based on Kelvin probe and scanning photocurrent microscopies [Sci. Reports, 5, 10990 (2015), Nano Lett., 15, 2278 (2015)], and highlight the strong influence of environmental effects on the band alignment in MoS₂ homojunctions. We are now applying this exciting new metrology to systematically examine the ionization energies of a series of TMDs. The results will provide fundamental information necessary to assess the band alignments of TMD heterojunction devices, and to validate or refine existing theoretical predictions [APL, 103, 053513 (2013), J. Phys. Chem. C, 119, 13169 (2015)].

This work was performed at CINT (DE-AC04-94AL85000), and is supported by Sandia LDRD, US DOE EERE SunShot Initiative BRIDGE (DE-FOA-0000654 CPS25859), and Army Research Office MURI (W911NF-11-1-0362). SNL is a multi-program laboratory managed and operated by Sandia Corporation, a wholly owned subsidiary of Lockheed Martin Co., for the US DOE NNSA (DE-AC04-94AL85000).

12:00pm 2D+NS-FrM12 Visualizing Light Scattering in Silicon Waveguides with few-layer Black Phosphorous Photodetectors, Tianjiao Wang, S. Hu, Vanderbilt University; **B. Chamlagain, Z. Zhou,** Wayne State University; **S.M. Weiss, Y. Xu,** Vanderbilt University

We investigate the light scattering properties of a silicon nanobeam waveguide through wavelength- and polarization-dependent scanning photocurrent measurements of a black phosphorus (BP) photodetector on top of the silicon waveguide. The measured photocurrent responses exhibit similar patterns as the light intensity distribution calculated by finite-difference time-domain simulations, suggesting that the light scattering properties of the waveguide can be detected as photocurrent signals by the BP photodetector. Interestingly, no photocurrent signals are observed

when the incident photon energy is below the bandgap of silicon, indicating that the photocurrent response generated in the BP photodetector is mainly attributed to the photo-excited electron-hole pairs in the silicon waveguide which can be injected into the BP and dominate its photocurrent generation. Our experimental results suggest that two dimensional (2D) material based photodetectors can offer an effective approach to visualize the light scattering properties of photonic structures by photocurrent mapping, which not only opens up avenues for learning about light matter interaction of photonic structures but also provides a way of engineering future 2D material based optoelectronic devices with integrated photonic structures.

Spectroscopic Ellipsometry Focus Topic Room 104C - Session EL+AS+EM+MI+TF-FrM

Spectroscopic Ellipsometry: Novel Applications and Theoretical Approaches

Moderators: Morten Kildemo, Norwegian University of Science and Technology, Nikolas Podraza, University of Toledo

8:20am EL+AS+EM+MI+TF-FrM1 Magneto-optical properties of Metals, Half-Metals, and Garnets Probed by Vector-Magneto-Optical Generalized Ellipsometry, Heidemarie Schmidt, Technische Universität Chemnitz, Nano-Spintronics Group, Germany **INVITED**

Magnetotransport measurements are a standard technique for the electrical characterization of single layers on insulating substrates. However, magnetotransport measurements require electrical contacts and known current paths, which excludes application to multilayer stacks. Motivated by the recent development of fast Mueller matrix ellipsometers, we have set-up a vector magneto-optical generalized ellipsometer (VMOGE) with an 0.4 T octupole magnet [1] and have investigated magneto-optical response of a single layers and multilayer stacks in a magnetic field of arbitrary orientation and magnitude up to 0.4 T at room temperature. We assume that the off-diagonal element of the magneto-optical dielectric tensor of every magnetizable layer in the multilayer stack is a product of the magnetic field independent and wavelength dependent complex magneto-optical coupling constant and the magnetic field dependent and wavelength independent magnetization of the layer. As an example, the complex magneto-optical coupling constant of nominally 10, 20, and 30 nm thick ferromagnetic Ni films obtained from modelling corresponding VMOGE data is discussed. It was challenging to identify the magnetization direction of Ni films from different sets of magnetic field dependent Mueller matrix elements [2]. In the future knowledge of complex magneto-optical coupling constant of all magnetizable materials in a multilayer stack will allow for modelling and optimizing the magneto-optical response of given stack. As a second example, the modelled complex magneto-optical coupling constant of capped, ferromagnetic Fe, Ni₂₀Fe₈₀, Co, Ni₈₀Fe₂₀, and Ni thin films on ZnO substrates is discussed and related with the spin-dependent electronic bandstructure of given weakly correlated, magnetizable materials [3]. For this comparison the experimental complex off-diagonal elements of the magneto-optical dielectric tensor have been converted into theoretical complex off-diagonal elements of magneto-optical conductivity tensor. Finally, the experimental magneto-optical response of strongly correlated, magnetizable materials [4], e.g. half-metals and garnets, is presented and as an outlook development of new theoretical frameworks for calculating the bandstructure of such strongly correlated, magnetizable materials for a comparison with experiment is motivated. [1] K. M. Mok, N. Du, H. Schmidt, Rev. Sci. Instrum. 82 (2011) 033112; [2] K.M. Mok, C. Scarlat, G. J. Kovács, L. Li, V. Zviagin, J. McCord, M. Helm, H. Schmidt, J. Appl. Phys. 110 (2011)123110; [3] K.M. Mok, G. J. Kovács, J. McCord, L. Li, M. Helm, H. Schmidt, Phys. Rev. B 84 (2011) 094413; [4] G. Kotliar and D. Vollhardt, Physics Today 57 (2004) 53

9:00am EL+AS+EM+MI+TF-FrM3 In Situ Terahertz Optical Hall Effect Measurements of Ambient Doping Effects in Epitaxial Graphene, S. Knight, University of Nebraska-Lincoln; **C. Bouhafs, N. Armakavicius, P. Kühne, V. Stanishev, R. Yakimova,** Linköping University, Sweden; **S. Wimer, M. Schubert,** University of Nebraska-Lincoln; **V. Darakchieva,** Linköping University, Sweden; **Tino Hofmann,** University of North Carolina at Charlotte

Recently, the cavity-enhanced THz optical Hall effect (THz-OHE) has been demonstrated as non-contact method to obtain free charge carrier properties using low-field permanent magnets [1,2]. A tunable, externally-

coupled cavity is used to enhance the THz-OHE signal which allows the accurate determination of a sample's free charge carrier properties even at low magnetic fields. In this work we take advantage of this approach by integrating the permanent magnet into a gas flow cell. We demonstrate for the first time the application of the cavity-enhanced THz-OHE for the *in-situ* characterization of free charge carrier properties of monolayer graphene on Si-face 4H-SiC as a function of ambient conditions. The experiments were performed using a new rotating-analyzer THz ellipsometer at Linköping University. Upon changing the CO₂, H₂O, and O₂ concentration in the cell, large variations in both free charge carrier sheet density N_s and mobility μ are observed for the *n*-type graphene. The lowest N_s was found for the as-grown sample with $N_s = 5.9(1) \times 10^{11} \text{ cm}^{-2}$ where $\mu = 2507(57) \text{ cm}^2/\text{Vs}$. The highest N_s was found after purging the sample with nitrogen for 6 hours with $N_s = 2.43(4) \times 10^{12} \text{ cm}^{-2}$ where $\mu = 1604(23) \text{ cm}^2/\text{Vs}$. These significant changes are attributed to a redox-reaction of oxygen and water at the graphene surface which results in the extraction of electrons from graphene [3]. This will be discussed in detail in our presentation. We further observe that this doping mechanism is only partially reversible at room temperature upon removal of oxygen, carbon dioxide, and water by purging the cell with nitrogen. In conclusion, we demonstrate *in-situ* THz-OHE as a new and powerful technique to determine ambient-dependent doping mechanisms which is illustrated here using monolayer epitaxial graphene on Si-face 4H-SiC.

[1] S. Knight, S. Schöche, V. Darakchieva, P. Kühne, J.-F. Carlin, N. Grandjean, C. M. Herzinger, M. Schubert, and T. Hofmann, *Opt. Lett.* **40**, 2688 (2015).

[2] P. Kühne, C.M. Herzinger, M. Schubert, J.A. Woollam, and T. Hofmann, *Rev. Sci. Instrum.* **85**, 071301 (2014).

[3] A.N. Sidorov, K. Gaskill, M.B. Nardelli, J.L. Tedesco, R.L. Myers-Ward, C.R. Eddy Jr., T. Jayasekera, K.W. Kim, R. Jayasingha, A. Sherehiy, R. Stallard, and G.U. Sumanasekera, *J. Appl. Phys.* **111**, 113706 (2012).

9:20am EL+AS+EM+MI+TF-FrM4 Excitons at Interfaces in Ellipsometric Spectra, Nuwanjula Samarasingha, C. Rodriguez, J.M. Moya, N.S. Fernando, S. Zollner, New Mexico State University; P. Ponath, K. Kormondy, A. Demkov, University of Texas at Austin; D. Pal, A. Mathur, A. Singh, S. Dutta, J. Singhal, S. Chattopadhyay, Indian Institute of Technology Indore, India

The presence of excitonic features in the optical constants and ellipsometry spectra of bulk semiconductors and insulators has been known for many years. In Si, Ge, and GaAs, the E_1 critical points are strongly enhanced by two-dimensional excitons, even at room temperature. Three-dimensional excitons have been seen in ellipsometry spectra for GaP and Ge. Excitons also influence the dielectric function of SrTiO₃. An exciton is an electron-hole pair bound by the Coulomb interaction, with properties similar to a hydrogen atom. The influence of excitonic absorption on the dielectric function was described by Tanguy.

In a thin epitaxial layer (with a thickness below or near the Bohr radius) on a substrate with a different band gap, the wave functions of the electron and hole are strongly modified. In a thin type-I quantum well, consisting of a narrow-gap semiconductor grown on a large-gap substrate, both the electron and the hole are confined, which leads to an increase in the dipole overlap matrix element. Therefore, the dominant absorption peak at 4.2 eV is larger in a 20 nm thick SrTiO₃ layer on a LaAlO₃ substrate than in bulk SrTiO₃. (The band gap of LaAlO₃ is larger than that of SrTiO₃.)

On the other hand, in a staggered type-II quantum well, either the electron is confined, or the hole, but not both. Therefore, the overlap dipole matrix element (and thus the excitonic absorption) is strongly reduced, because one quasiparticle resides in the quantum well and the other one in the substrate. If a SrTiO₃ layer is grown on Si or Ge, the valence band maximum occurs in the substrate, while the conduction band offset is very small. Therefore, the exciton wave function is delocalized (deconfined), which reduces the dipole overlap matrix element. Therefore, the real and imaginary part of ϵ of thin SrTiO₃ layers on Si or Ge are much smaller than in the bulk and decrease monotonically with decreasing thickness. A similar effect can be seen for thin ZnO layers on Si as a function of thickness.

The dielectric function of SrTiO₃ is not only affected by layer thickness. A very thick polycrystalline SrTiO₃ layer on Si has a much lower dielectric function than a single-crystalline SrTiO₃ substrate. In this case, we speculate that the magnitude of the dielectric function is related to other Tanguy parameters, perhaps the excitonic binding energy or the exciton decay rate (broadening). To investigate this further, we will perform temperature-dependent ellipsometry measurements on bulk zinc blende

GaP, which has a much simpler band structure than wurtzite ZnO or the correlated metal oxide SrTiO₃, but shows similar excitonic effects.

9:40am EL+AS+EM+MI+TF-FrM5 Infrared and Visible Dielectric Properties of (LaAlO₃)_{0.3}(Sr₂AlTaO₆)_{0.35}, Jacqueline Cooke, N.T. Nunley, T. Willett-Gies, S. Zollner, New Mexico State University

Using spectroscopic ellipsometry, we determined the dielectric function of LSAT, from the mid-IR to the deep UV (0.03 to 6.5 eV). LSAT is an acronym for the chemical formula (LaAlO₃)_{0.3}(Sr₂AlTaO₆)_{0.35}, equivalent to (La_{0.3}Sr_{0.7})(Al_{0.65}Ta_{0.35})O₃. LSAT is a common substrate for epitaxial growth of complex metal oxides. Precise knowledge of the optical constants is useful to investigate the properties of epitaxial films grown on LSAT. We also investigated the band gap and the infrared-active phonons. Czochralski-grown LSAT wafers with (001) surface orientation were obtained commercially (MTI Corp., Richmond, CA). Single-side polished wafers were used for spectroscopic ellipsometry and two-side polished wafers with 0.5 mm thickness for transmission. Between 0.8 and 6.5 eV, we measured the normal-incidence transmission and the ellipsometric angles from 60° to 80° incidence in 2° steps on a J.A. Woollam variable angle of incidence ellipsometer with a computer-controlled Berek waveplate compensator. We also measured in the mid-IR on a rotating compensator FTIR ellipsometer. Transmission measurements show a steep rise of the absorption coefficient (α) between 4.6 and 4.8 eV, where LSAT becomes opaque. Fitting the ellipsometry data with a model containing two Tauc-Lorentz oscillators and 19 Å surface roughness thickness yields an excellent fit to the data. The Tauc gap is 4.9 eV and the high-frequency dielectric constant $\epsilon_\infty = 4.0$. Plotting α^2 versus photon energy yields a direct band gap of 5.8 eV. An Urbach tail extends towards lower energies. The resulting dielectric function is in agreement with previous ellipsometry and minimum-deviation prism measurements. The mid-IR dielectric function shows four ϵ_2 peaks due to TO phonon absorption. The loss function shows four LO peaks. A fifth TO phonon was seen at 155 cm⁻¹ in far-IR ellipsometry. An ideal ABO₃ perovskite has only three IR-active TO phonons. FCC ordering on the B-site as in (Sr₂AlTaO₆) adds a fourth phonon. We argue that the TO phonons at 155 and 283 cm⁻¹ are vibrations of the tetrahedra against the La/Sr sublattices, respectively (mode splitting due to disorder). On the other hand, the 397 and 442 cm⁻¹ modes are B-O bending modes due ordering in the Al/Ta sublattice. Finally, a B-O stretch mode at 664 cm⁻¹ and broad two-phonon absorption at 765 cm⁻¹ are also found. Fitting the spectra with a factorized TO/LO model yields better results than a sum of Lorentzians, because the individual TO/LO pairs are not well separated. The presence of FCC ordering was also confirmed with x-ray diffraction. We will also discuss temperature dependent ellipsometry and transmission measurements.

10:00am EL+AS+EM+MI+TF-FrM6 A New Constant of Product of Electronic Scattering Time and Resistivity in Thin Silver Refractive Index Calculation from Ellipsometry and Resistivity Measurements, Guowen Ding, C. Clavero, D. Schweigert, M. Le, Intermolecular, Inc.

The optical and electrical response of metal thin films is highly affected by electronic scattering with the interfaces and defects. We are able to successfully model the electrical resistivity and near infrared (IR) optical response using a thickness dependent electronic scattering time. We investigated Ag films thickness in the range of 3 nm to 74 nm and determined that the product of electronic scattering time (τ) and resistivity (ρ) remains constant regardless of the thickness ($\tau \times \rho = C$), with a value of $59 \pm 2 \text{ } \mu\Omega \text{ cm-fs}$ for Ag films. As a result, determining the constant C for a given thin film will allow to calculate the properties of the film over a large range of wavelengths while limiting the number of measurements. Our findings enable us to develop a theoretical framework to determine the optical response of metal thin films in the near IR by using single wavelength ellipsometer measurements. An excellent agreement is found between experimental measurements and predicted values. We first reported this constant $\tau \times \rho = C$ for silver, and we posit that such constant concept could be applied for other conducting films. Application of the model presented here will allow rapid characterization of the IR optical response of metal thin films, with important application in a broad spectrum of fundamental and industrial applications, including optical coatings, low-emissivity windows and semiconductor industry.

10:20am **EL+AS+EM+MI+TF-FrM7 Realization of an *In Situ* Mueller-matrix Imaging Ellipsometer for the Real Time Observation of Surface Properties in an Ultra-high Vacuum EUV Facility**, *Pim Mulwijk*, N.B. Koster, F.T. Molkenboer, E. Sligte, te, A.F. Deutz, P. Walle, van der, TNO Technical Sciences, Netherlands

TNO is realizing EUV Beamline 2 (EBL2), a facility to investigate the effects of Extreme Ultra-Violet (EUV) radiation on surfaces to enable future EUV High Volume Manufacturing (HVM) production. In this facility, samples with sizes up to 152x152x20 mm (6" EUV reticles) can be exposed to EUV radiation of up to 500W equivalent at intermediate focus (IF) under realistic environmental conditions and analyzed by in-situ ellipsometry and XPS. EBL2 consists of EUV source, automated handling system, beam line and an exposure chamber with an in-situ dual wavelength Mueller-matrix imaging ellipsometer.

Light from the dual wavelength light source (405 & 640nm) enters the exposure chamber through a polarizer, configurable retarder and a vacuum window producing a defined polarization state. After reflecting off of the sample, the light exits the exposure chamber through a vacuum window, configurable retarder and polarizer. The sample position is imaged on two camera's, one for each wavelength. By combining all combinations of 4 polarization illumination states with 4 analyser states the full Mueller matrix of the sample can be recovered.

Calibration is performed in-situ with two insertable polarizers and two different calibration samples. The calibration procedure does not require prior knowledge of the polarizer orientation nor of the calibration samples.

This presentation will focus on the design and realization of the ellipsometer and will also touch upon the process of interpreting the data.

EBL2 will be publicly accessible as a test facility for EUV lithography related research after qualification, which is expected to be finished end of Q1 2017.

10:40am **EL+AS+EM+MI+TF-FrM8 Conducting, Semi-Conducting and Insulating 2D-Materials Characterized by Spectroscopic Imaging Ellipsometry**, *Matthias Duwe*, S. Funke, Accurion GmbH, Germany; U. Wurstbauer, Technical University of Munich, Germany; A. Matkovic, University of Belgrade, Serbia; A. Green, SUNY College of Nanoscale Science and Engineering; A. Molina-Mendoza, Universidad Autonoma de Madrid, Spain; A. Castellanos-Gomez, IMDEA Nanoscience, Spain; P.H. Thiesen, Accurion GmbH, Germany

Finding thin-film flakes of 2D-materials after the fabrication and identifying their layer thicknesses often is a challenging and time-consuming task. Here, we present various applications of spectroscopic imaging ellipsometry (SIE) to a variety of conducting, semi-conducting, and insulating 2D-Materials such as graphene, molybdenum disulfide (MoS₂), hexagonal boron nitride, and black phosphorus. As a combination of polarization-contrast microscopy and spectroscopic ellipsometry, SIE measurements localize microscopic flakes of the 2D-materials, yield the samples' optical dispersion functions, and determine the layer thicknesses.

Matkovic et al. [1] characterized monolayers of graphene by SIE, and they obtained the optical dispersion by Fano-resonance modelling. Using this dispersion, SIE offers a straightforward search for and identification of few-layer graphene flakes on various opaque or transparent substrates. As this flake search uses ellipsometric measurements, it depends far less on the used substrate compared to e.g. conventional light-microscopy. In a similar procedure, SIE identified monolayers of insulating hexagonal boron nitride, and it yielded the material's optical properties.

SIE measurements on MoS₂ revealed the repercussion of the used substrate [2]. Ellipsometric contrast micrographs showed the lateral variation of the optical parameters for a structured flake. Spectroscopic measurements of the ellipsometric values (Ψ & Δ) obtained from selected regions of interest on the flake yielded the optical dispersion for the in-plane and out-of-plane components of the dielectric function in the visible spectral range.

Finally, we will present imaging Mueller-matrix ellipsometry (IMME) for the characterization of thin-film flakes of the semi-conducting 2D-material black phosphorus. In contrast to MoS₂, black phosphorus also features an optical in-plane anisotropy. IMME-micrographs easily reveal this anisotropy as the Mueller matrix's off-diagonal blocks deviate from zero. By performing spectroscopic Mueller-Matrix mapping and rotational Mueller-matrix measurements combined with atomic force microscopy, we obtained the flake's layer thickness, the orientations of the optical axes, and the material's optical properties in the visible spectral range.

[1] A. Matković, A. Beltaos, M. Miličević, U. Ralević, B. Vasić, D. Jovanović, and R. Gajić, *Spectroscopic imaging ellipsometry and Fano resonance modeling of graphene*, *J. Appl. Phys.*, **112** 123523, (2012)

[2] S.Funke, E. Parzinger, B. Miller, P. H. Thiesen, A.W. Holleitner, U. Wurstbauer, *Imaging Ellipsometry of Mono- to Multilayer of MoS₂ on Transparent Sapphire Substrate*, Manuscript in preparation

Electronic Materials and Photonics Room 102A - Session EM-FrM

Late Breaking News on Electronic Materials and Devices

Moderator: Nikolaus Dietz, Georgia State University

8:40am **EM-FrM2 Pulsed Laser Deposition of In₂O₃-SnO₂: From Films to Nanowires**, *Davide Del Gaudio*, C. Reese, C. Boone, S. Yarlagadda, J.T. Heron, University of Michigan, Ann Arbor; I. Shalish, Ben-Gurion University of the Negev, Beersheba, Israel; R.S. Goldman, University of Michigan, Ann Arbor

As micrometer sized device structures approach their limits in performance, nano-structures, such as nano-wires (NW) are being considered for next-generation high efficiency energy conversion and storage devices.^[1] For example, metal oxides have been identified as promising materials for lithium ion batteries^[2] and UV lasers.^[3] Furthermore, metal-oxide NWs have been embedded in field-effect transistors, lasers, solar cells, and various chemical sensors.^[4] Typically, metal-oxide NW are prepared by vapor deposition^[4] or thermal evaporation.^[5] Recently, pulsed-laser deposition (PLD)^{[6][7][8]} has emerged as a promising approach for the fabrication of tin-doped indium oxide (ITO), with film or NW growth often determined by the choice of a reactive (O₂) or inert (N₂) atmosphere.^[6] To date, cubic NW with up to 5 atomic % Sn incorporated into In₂O₃ have been reported. However, a mechanistic understanding of the influence of growth parameters and substrates on the morphology, composition, and crystal structure of the deposited film is needed. Additionally, PLD of various In₂O₃-SnO₂ mixtures has yet to be considered. Therefore, we report on PLD of various In₂O₃-SnO₂ mixtures, onto c-plane sapphire and Inconel substrates. Using an inert atmosphere, we have identified parameters to obtain smooth films; pyramid-shaped nano-scale clusters; sparse, tapered nano-rods; and high density, vertically oriented NWs, with and without catalyst spheres. We will present high-resolution transmission electron microscopy (HRTEM) images and selective-area electron diffraction (SAED) patterns illustrating the structure and composition of the films, nanowires, and catalyst spheres. The photoluminescence emission from NWs and films, as well as the electronic transport properties of individual NWs will also be discussed.

References

[1] Guo, Y.-G., Hu, J.-S., & Wan, L.-J. (2008) *Advanced Materials*, **20**(15), 2878–2887

[2] Poizot, P., Laruelle, S., Grugeon, S., Dupont, L., & Tarascon, J.-M. (2000) *Nature*, **407**(6803), 496–499

[3] Kong, Y. C. and Yu, D. P. and Zhang, B. and Fang, W. and Feng, S. Q. (2001) *Applied Physics Letters*, **78**, 407–409

[4] Shen, G., Chen, P.-C., Ryu, K., & Zhou, C. (2009) *Journal of Materials Chemistry*, **19**(7), 828–839

[5] Yao, B. D. and Chan, Y. F. and Wang, N. (2002) *Applied Physics Letters*, **81**, 757–759

[6] Khan, G. G., Ghosh, S., Sarkar, A., et. al. (2015) *Journal of Applied Physics*, **118**(7), 074303

[7] Kee, Y. Y., Tan, S. S., Yong, T. K., et. al. (2012) *Nanotechnology*, **23**(2), 025706

[8] Savu, R., & Joanni, E. (2006) *Scripta Materialia*, **55**(11), 979–981

9:00am **EM-FrM3 ZnSnN₂: Band Gap Engineering Through Cation Disorder**, R. Makin, Western Michigan University; N. Senabulya, J.P. Mathis, R. Clarke, University of Michigan; T. Veal, University of Liverpool; **Steven Durbin**, Western Michigan University

Chalcopyrite heterovalent ternary compounds can undergo an order-disorder transition between an ordered chalcopyrite structure and a disordered zinc-blende-like phase. Unlike in adamantine alloys, the disorder results in a band gap reduction in the disordered phase relative to the band gap of the ordered lattice. ZnSnN₂ represents an interesting member of the chalcopyrite family of materials, due to its earth abundant element constituents and a band gap of use for solar cells. It is also part of

the Zn-IV-N₂ family of materials, whose band gaps span from the infrared to the UV. Density functional theory (DFT) calculations predict the ordered ZnSnN₂ phase to have an orthorhombic lattice and a direct band gap of 2.0 eV. Using special quasirandom structures (SQS) to model the disordered Zn and Sn cation sub-lattice, DFT simulations predict that the band gap for the disordered ZnSnN₂ phase will be close to 1.0 eV and will have a hexagonal lattice. This almost 1.0 eV reduction of the band gap of ZnSnN₂ presents an opportunity for band gap engineering by controlling the disorder on the cation sublattice. Recently, however, an alternative theory of disorder for ZnSnN₂ has been proposed that does not depend on cation lattice disorder. This alternate disorder, unlike the cation disorder model, does not violate the octet rule locally and results in a band gap that is independent of the order. If either model is accurate is presently unknown.

A series of films have been grown by plasma assisted molecular beam epitaxy in order to investigate the possibility of controlled cation disorder as well as its effects on physical and electronic properties of the material. By varying the growth conditions, specifically either the metal flux to the nitrogen pressure or the substrate, we have confirmed the existence of both the hexagonal and orthorhombic phases of the crystal via synchrotron x-ray diffraction (performed at Argonne National Laboratory). All of the films at present have a high free carrier concentration (in excess of 10^{19} cm^{-3}). Taking into account the Burstein-Moss shift caused by the high carrier concentration and calculating the effective masses of the carriers from parabolic fits to the density results, the optically measured band gaps appear to be consistent with the DFT calculations; the band gaps show a clear dependence on cation disorder.

9:20am EM-FrM4 Role of Single Dopants in Inter-Band Current Enhancement of Nano-*pn* Tunnel Diodes: An Atomistic Study, Manoharan Muruganathan, Japan Advanced Institute of Science and Technology, Japan; *D. Moraru, M. Tabe*, Research Institute of Electronics, Shizuoka University; *H. Mizuta*, Japan Advanced Institute of Science and Technology, Japan

As the Tunnelling Field Effect Transistor (TFET) overcomes the subthreshold slope thermal limitation of MOSFETs, they are a potential successor of MOSFETs [1]. Moreover silicon-based TFETs are the most attractive because of the well-established silicon technology. However, a large bandgap in silicon results in a small band-to-band-tunnelling efficiency, hence low on-current. In order to improve the on-current, fundamental study of atomistic *pn* tunnel diode is an imperative step. Here, we report that inter-band tunnelling current can be enhanced by the resonance of deepened energy levels of discrete dopants. Number and position of dopants at the *pn* junction interface play a crucial role in enhancing the inter-band tunnelling current. These results are based on the first-principles simulations in comparison with our experimental results for nano-*pn* tunnel diodes [2].

Our simulated atomistic structure consists of *p*- and *n*-type electrodes, which are highly doped with doping concentration similar to the experimental levels and a thin central intrinsic Si channel that corresponds to the depletion region. As realized in the fabricated devices, single P and B dopants are placed in the intrinsic Si channel the depletion region. The uniform bulk doping in the regions away from the depletion region was realized by using the atomic compensation technique [3-4]. We noticed a remarkable current increase by four orders of magnitude for the device with a P-B pair placed 1.3 nm apart as compared to no discrete dopants in the depletion region. This is due to the energy levels created by the P-B pair in the depletion region and their matching to the electrode energy levels when the bias voltage is changed. Moreover, these devices exhibit typical Esaki-diode negative differential conductance (NDC) behaviours as well. When the single dopants were placed nearer to the uniformly doped bulk regions then well aligned energy levels were formed in the depletion region. This leads to an increase in the inter-band tunnelling current. If the number of single dopants in the depletion region is increased then we have more induced states in the depletion region, which also helps to increase the inter-band tunnelling current. These results illustrate the impact of individual dopants in the depletion region and provide pathways to increase the inter-band tunnelling in nano-*pn* tunnel diodes.

References:

- [1] A. M. Ionescu *et al.*, Nature 479.7373 (2011): 329-337.
- [2] M. Tabe *et al.*, Applied Physics Letters 108.9 (2016): 093502.
- [3] M. Brandbyge *et al.*, Physical Review B 65.16 (2002): 165401.

[4] Atomistix ToolKit version 2015.1, QuantumWise A/S www.quantumwise.com.

9:40am EM-FrM5 CVD growth of Hexagonal Boron Nitride Films on Cu-Ni Alloys, Karthik Sridhara, Texas A&M University; *B.N. Feigelson, J.K. Hite, V. Anderson, A. Nath, F. Kub*, US Naval Research Laboratory; *L.O. Nyakiti*, Texas A&M University Galveston

Chemical vapor deposition (CVD) method of growth of hexagonal boron nitride (h-BN) has been demonstrated on various transition metal substrates such as Ni, Pt, Au and Ag. Of these metals, polycrystalline Cu is by far the most frequently used substrate for CVD growth of h-BN. Despite being extensively studied, issues still persist with Cu, including a high density of nucleation sites where the imperfections in surface morphology act as potential nucleation sites. Recently, Cu-Ni alloys have been reported for the growth of controllable monolayer h-BN with fewer nucleation sites [1]. Despite the promise, there are still questions of optimal Ni concentration and the morphology of Cu-Ni alloys.

In this work, we prepare Cu-Ni alloys by electroplating Ni on high purity (99.98%) polycrystalline Cu foils (25 μm thickness). Four different weight percents of Ni (10, 15, 20 and 25 wt%) are electroplated onto Cu. The electroplated foils are then thermally annealed at 1030°C for 3 hours in an H₂ environment, during which time the Ni diffuses into the Cu foils. We then grow h-BN on these Cu-Ni alloys, with high purity (~99.98%) Cu foils acting as our control samples. The growth uses borazane as the precursor at 1030°C with H₂ and N₂ as carrier gases. FTIR and scanning electron microscope (SEM) are used to confirm and assess the growth of h-BN on the samples. Energy dispersive spectroscopy (EDS) mapping is employed to cross-check the Ni percentage in Cu. From the preliminary results, we observe that with increasing Ni concentration there is an increase in surface roughness with the existence of atomic step edges and various morphological irregularities. Initial FTIR results show that with increasing amount of Ni in the Cu foil, we see a gradual increase in the amount (proportional to the FTIR peak intensity) of h-BN grown where the amount is proportional to the h-BN film effective thickness on the substrate [2]. We see the lowest amount of h-BN is on Cu, while the highest is on Cu_{0.75}Ni_{0.25} foils. The growth kinetics of h-BN on Cu-Ni alloys will be discussed.

References:

- [1] G. Lu, T. Wu, Q. Yuan, H. Wang, H. Wang, F. Ding, "Synthesis of large single-crystal hexagonal boron nitride grains on Cu-Ni alloy," vol. 6, p. 6160, 2015.
- [2] B. N. Feigelson, V. M. Bermudez, J. K. Hite, Z. R. Robinson, V. D. Wheeler, K. Sridhara, "Growth and spectroscopic characterization of monolayer and few-layer hexagonal boron nitride on metal substrates," vol. 7, pp. 3694-3702, 2015.

10:00am EM-FrM6 p-GaAs/AlGaAs Heterostructures with a Current Blocking Barrier for Mid-infrared Detection, Dilip Chauhan, A.G.U. Perera, Georgia State University; *L.H. Li, L. Chen, E.H. Linfield*, University of Leeds, United Kingdom

p-GaAs/Al_xGa_{1-x}As heterojunction is an attractive material system due to its mature III-V material growth and processing technology. Infrared detection in the mid-infrared range is possible by exploiting the intra-valance band hole transitions in the light hole/heavy hole and spin-orbit split-off bands. The wavelength threshold can be tuned by varying the Al mole fraction (*x*), while graded Al_xGa_{1-x}As potential barriers create an asymmetry to allow a photovoltaic operation. The operation under photovoltaic mode is advantageous due to thermal noise limited performance. In a preliminary study in a 2 – 6 μm photovoltaic detector, we implemented a current blocking barrier, which improved the specific detectivity by two orders of magnitude, to 1.9×10^{11} Jones at 2.7 μm , at 77K. At zero bias, the resistance-area product (R_0A) had a value of $\sim 7.2 \times 10^8 \Omega \text{ cm}^2$, which is five orders higher in magnitude compared to the R_0A value without the blocking barrier. A photoresponse was observed up to 130K. Further work is in progress to optimize the detector at a higher operating temperature.

Acknowledgement: This work was supported in part by the U.S. Army Research Office under Grant No. W911 NF-15-1-0018, and in part by National Science Foundation (NSF) under Grant No. ECCS-1232184.

10:20am EM-FrM7 SSI-LEDs - 20,000 Hrs of Lifetime and Failure Mechanism Study, Yue Kuo, S. Zhang, Texas A&M University

Recently, a new type of solid state incandescent LED (SSI-LED) that emitted the broad band warm white light upon the application of a voltage was reported by our group [1-4]. This kind of device also has unique antifuse- and diode-like characteristics in the low voltage operation range [5,6]. The operation of this new device is based on the passing of current through

nano-sized conductive paths after the breakdown of an amorphous high-*k* thin film stack deposited on top of a silicon wafer. The principle of light emission of the SSI-LED is the black body effect, which is different from the electron-hole or exciton-exciton recombination in the conventional crystalline compound semiconductor structure. A lifetime of over 12,000 hours was obtained previously [4].

In this talk, authors will present the new result on the lifetime study of the SSI-LED. Without a passivation layer, the device has been successfully operated continuously for over 20,000 hours in air. Changes of electrical and optical characteristics of the device over the whole operation period have been monitored. In order to understand the failure mechanism within a short period of time, we further carried out accelerated voltage stress tests. The change of the surface morphology with the applied voltage has been systematically investigated. Based on these results, authors review the mechanisms of the device operation and failure.

[1] Y. Kuo and C.-C. Lin, *APL*, **102**, 031117 (2013).

[2] Y. Kuo and C.-C. Lin, *ECS SSL*, **2**, Q59 (2013)

[3] Y. Kuo, *IEEE TED*, **62**, 3536-3540 (2015).

[4] C.-C. Lin and Y. Kuo, *JVST B*, **32**, 011208 (2014).

[5] Y. Kuo, *ECST*, **67**, 183 (2015).

[6] Y. Kuo, *ECST*, **69**, 23 (2015).

In-Situ and Operando Spectroscopy and Microscopy for Catalysts, Surfaces, & Materials Focus Topic Room 101C - Session IS-FrM

In situ Characterization of Nanomaterials

Moderators: Stephen Nonnenmann, University of Massachusetts - Amherst, Xiao-Ying Yu, Pacific Northwest National Laboratory

8:20am IS-FrM1 In-situ High-Energy X-ray Scattering for Probing Colloidal Nanoparticles in Solution, Yugang Sun, Temple University INVITED
Growth and transformation of colloidal nanoparticles are important for synthesizing functional nanoparticles with tailored properties that represent the foundation for enabling nanotechnology. However, the involving chemical and physical processes are very complicated and barely understood, which limits the precise control over the properties of the nanoparticles. In this presentation, high-energy x-ray scattering techniques will be discussed to serve as unique in-situ approach to monitor these processes in real time. High-energy x-rays have strong penetration in reaction solutions, enabling the possibility to probe the solid colloidal nanoparticles with small volume fractions. In addition, the weak absorption of high-energy x-rays in materials can eliminate the possible side reactions. Reaction systems including the synthesis of colloidal silver nanocubes and microwave synthesis of silver nanoparticles have been successfully studied with the high-energy x-ray scattering at the beamline 1ID of Advanced Photon Source (APS)

9:00am IS-FrM3 Microfluidics Applied to Ultrafast Spectroscopy, Adrien Chauvet, University of Sheffield, UK INVITED

The use of ultrafast laser technologies became essential in the characterization of molecular complexes, as these techniques have opened new doors for the study of fundamental photo-chemical and photo-physical behaviour. However the application of laser-based spectroscopy for the study of biological samples came along with technical challenges: On one hand, purified biological samples are sensitive to their environment (e.g. oxygen) and are only available in small (sub-millilitres) quantities. On the other hand, the use of ultrafast laser systems primarily demands that the sample is refreshed at each laser shot, at a few kHz repetition rate. Consequently, there exists a pressing need to apply microfluidics systems in the field of ultrafast spectroscopy.

After a brief introduction on laser spectroscopy, I will describe some of the most common solutions that are currently in use in order respond to the constraints of both, the sample and the analytical system. I will then present our newly developed microfluidic flow cell: the cell, while it is convenient to set-up and to use, is suitable to most laser systems up to ~10 kHz repetition rate, and requires a minimal sample amount of ~ 250 microL. The benefits of such a microfluidic system will be illustrated through the analysis of multi-hemes cytochromes.

9:40am IS-FrM5 Adsorbate-Induced Structural Changes Precious Metal Nano Catalysts, Zheng Lu, Y. Lei, University of Alabama in Huntsville

Metal nanoparticles can exhibit dramatically different catalytic properties compared to their bulk counterparts. The structure of the supported metal nanoparticles can change dynamically under reaction condition such as when molecules adsorb on the surface. A fundamental understanding of the structure of supported nano catalysts under reaction conditions is an important step towards achieving precise structure-reactivity relationship in catalysis and will ultimately lead to better catalysts.

In this work, we combined X-ray absorption spectroscopy (XAS), pair distribution function (PDF) and small angle X-ray scattering (SAXS) measurements to reveal the lattice contraction and expansion of supported small platinum, palladium and Au nanoparticles as a function of the particle size and the adsorbates. X-ray absorption spectroscopy measurements were performed at the sector 10 beamline at the Advanced Photon Source (APS) at Argonne National Laboratory (ANL). Scattering data of PDF were collected at beamline 11-ID-B at the APS. High energy X-rays (58 keV) were used in combination with a large area detector. SAXS experiments were performed at the APS 12-ID-B station. The 2D SAXS data were collected on an area detector, a *q* range of 0.006–0.7 Å⁻¹ with an incident energy of 12 keV.

The support precious metal nano catalysts were studied under selective oxidation reaction conditions. These findings will help us to understand adsorbate-induced structural and chemical changes in precious metal nano catalysts and be useful for improving catalytic activity.

10:00am IS-FrM6 Understanding the Role of Atmospheric Surface Adsorbates on the Chemical Reactivity of Zirconium Hydroxide Nanopowders using Operando Vibrational Spectroscopy, Robert Balow, NRC/NRL Postdoctoral Fellow; W. Gordon, Edgewood Chemical Biological Center; D.E. Barlow, Naval Research Laboratory; I. Iordanov, C. Knox, Edgewood Chemical Biological Center; V. Bermudez, J. Lundin, J. Wynne, Naval Research Laboratory; G.W. Peterson, C. Karwacki, Edgewood Chemical Biological Center; P.E. Pehrsson, Naval Research Laboratory

Much effort has been focused on developing materials and sorbents for decontamination of chemical warfare agents (CWAs); however, CWAs can have different reactivity and decomposition pathways, making it difficult to find an all-in-one decontamination solution. Zirconium hydroxide (Zr(OH)₄) has excellent sorption properties and wide-ranging reactivity towards numerous types of CWA and simulants.¹ This reactivity has been attributed to a combination of diverse surface hydroxyl species (terminal, bridging, etc.) and under-coordinated Zr defects. Unfortunately, these promising preliminary results were often obtained under pristine and unrealistic operating conditions in which the potential impact of atmospheric components (e.g. H₂O and CO₂) and trace contaminants (e.g. NO_x, SO₂, H₂S and various hydrocarbons) was not a factor.

A more complete picture of the reactivity under *operando* conditions is necessary to evaluate the potential field use of Zr(OH)₄ for CWA decontamination. We couple insights from theory with a suite of *operando* infrared spectroscopy techniques to probe the Zr(OH)₄ surface, at ambient pressure, under atmospheric components such as humidity and CO₂. Contaminated surfaces are then exposed to a sarin CWA simulant, dimethyl methylphosphonate, to evaluate the impact of these adsorbed surface contaminants on the decomposition performance of Zr(OH)₄.

1. Bandosz, T. J., Laskoski, M., Mahle, J., Mogilevsky, G., Peterson, G. W., Rossin, J. A., & Wagner, G. W. (2012). Reactions of VX, GD, and HD with Zr(OH)₄: Near Instantaneous Decontamination of VX. *The Journal of Physical Chemistry C*, 116(21), 11606-11614. doi:10.1021/jp3028879

10:20am IS-FrM7 In Situ Molecular Characterization of the Solid-Electrolyte Interface on Lithium Metal Anode, Y. Zhou, Xiaofei Yu, R. Cao, W. Xu, M. Su, Z. Xu, D.R. Baer, C. Wang, Z. Zhu, Pacific Northwest National Laboratory

Currently, the main stream anode material in Li ion battery industry is graphite. Though it has been a great commercial success, the energy density of graphite-based Li-ion batteries will reach their limit soon. Li metal is an ideal anode material for next generation rechargeable Li batteries because of its extremely high theoretical specific capacity and very low negative electrochemical potential. It has been over 40 years since the first attempt of using Li metal as an anode; however, large-scale commercial applications are still not achieved due to a few challenges, such as dendritic Li growth and limited Coulombic efficiency. Recent years, it has been reported that highly concentrated electrolytes, such as 4.0 M lithium bis(fluorosulfonyl)imide (LiFSI) in 1,2-dimethoxyethane (DME), can result

in the dendrite-free plating of Li metal and with high Columbic efficiency. However, the detailed mechanism is not clear. In this research, *in situ* liquid SIMS was used to molecularly characterize the structure of the Solid-Electrolyte Interfaces (SEI) formed in 1.0 M and 4.0 M LiFSI in DME. The thickness of the SEI in 4.0 M electrolyte is thinner than that in 1.0 M electrolyte. More importantly, less solvent molecules (DME) and Li metal residuals were found in the SEI layer formed in 4.0 M electrolyte. In addition, more F was found in the SEI layer formed in 4.0 M electrolyte, indicating that more LiF stays in the SEI layer formed in 4.0 M electrolyte. Our data suggest that the residual solvent molecules (DME) in the SEI layer may play an important role in formation of dendrite and decreasing of Columbic efficiency.

10:40am **IS-FrM8 *In Situ* DRIFTS of TiO₂ Nanoparticles**, *Michelle Foster*, University of Massachusetts, Boston

This project describes recent work focused on the surface chemistry of TiO₂ nanoparticles. These materials are commonly used in photocatalytic systems, where light induced reactions take place at the interface between the nanoparticle and an adsorbed sensitizing molecule. There are two primary classes of photocatalytic reactions: an adsorbate is excited by the light and interacts with the substrate, or the substrate is excited by the light and transfers an electron to the molecule. In both types of catalysis, it is the interaction of the adsorbate with the nanoparticle that truly drives the entire system. To optimize these catalytic processes, a better understanding of the interactions between the nanoparticles and the adsorbate is needed. *In situ* Diffuse Reflectance Infrared Fourier Transform Spectroscopy (DRIFTS) is well suited for analyzing the surface reactions on TiO₂ nanoparticles. These powders are mostly transparent to the infrared and the multi-bounce nature of the diffuse reflectance helps to increase the signal from these low coverage reactions. This project explores, on a molecular level, the reactions between acetic acid and TiO₂ nanoparticles using *in situ* DRIFTS as a function of both temperature and relative humidity. To better understand the reactivity, different crystal structures of TiO₂, including anatase, rutile, and the commercially available P25 are investigated. Using DRIFTS and a high-temperature reaction chamber, we monitor surface changes when the TiO₂ is exposed to water and acetic acid. It is important to first understand how water alone reacts with the surface, creating a surface hydroxyl layer. After the reactivity between water and TiO₂ nanoparticles is clarified, the reaction of acetic acid with the surface of TiO₂ nanoparticles is investigated under a variety of different water coverages to better understand the role surface hydroxyls play in the reaction between acetic acid and TiO₂ nanoparticles.

11:00am **IS-FrM9 *In situ* Characterization of Green Rust Synthesized in Ionic Liquids by Liquid ToF-SIMS and SALVI**, *Juan Yao, X. Sui, D. Lao, J. Weisenfeld, Y. Zhou, S. Nune, D. Heldebrant, Z. Zhu, X.-Y. Yu*, Pacific Northwest National Laboratory

Ionic liquids as green solvents have wide applications in material synthesis, catalysis, and separation. A model switchable ionic liquids (SWILs) consisting of 1,8-diazabicycloundec-7-ene (DBU) and 1-hexanol with carbon dioxide (CO₂) gas was chosen to synthesize nanocrystalline green rust. Under anoxic conditions, a nanoparticulate green rust with carbonate (nano GR) was synthesized by the addition of methanol to the degassed switchable ionic liquid (SWIL) solution consisting of 1-hexanol, DBU, CO₂ and iron (II) acetate (Fe(C₂H₃O₂)₂). The structure and oxidation state of nanocrystalline green rust were confirmed using SEM, TEM and Mössbauer spectroscopy. More importantly, the molecular structure change of the ionic liquid leading to green rust formation was characterized using *in situ* liquid using time-of-flight secondary ion mass spectrometry (ToF-SIMS) coupled with a vacuum compatible microfluidic reactor, SALVI (System for Analysis at the Liquid Vacuum Interface). Principal component analysis (PCA) was conducted to identify the key components of the solvated iron acetate in methanol and the green rust synthesized in the SWILs. Our results show that liquid SIMS can be a useful tool to study complex liquids at the molecular level providing insights in predictive synthesis of nanomaterials using environmentally friendly solvents.

11:20am **IS-FrM10 Direct Observation of the Growth and Dissolution Process of SnO₂ Nanowires**, *Bethany Hudak, Y.-J. Chang*, University of Kentucky; *L.F. Allard*, Oak Ridge National Laboratory; *B.S. Guiton*, University of Kentucky

The vapor-liquid-solid (VLS) nanowire growth mechanism is a widely used synthesis technique known to produce high-quality, single crystalline nanowires. This method was first developed by Wagner and Ellis to grow silicon nanowires, and has evolved to utilize many different catalyst materials with facile control over nanowire length, diameter, and dopant

concentrations. While this method is prevalent for the growth of inorganic nanowires, the growth kinetics of the VLS mechanism are not well understood, especially for binary and ternary crystal systems. Theoretical predictions suggest that the VLS growth mechanism is governed by steady-state kinetics, and that the crystal chemistry of the reverse process may be different from that which governs nanowire growth. The use of *in situ* microscopy techniques has advanced the understanding of the VLS growth process and nanowire growth kinetics. Through the use of *in situ* heating and atmosphere control in the transmission electron microscope (TEM), we have developed a method to study the forward and reverse growth mechanism of Au-catalyzed SnO₂ nanowires, the reverse process being dubbed solid-liquid-vapor (SLV) nanowire dissolution. By controlling the total pressure of the sample environment, the forward and reverse growth mechanisms can be directed. This method of observing the growth and dissolution of SnO₂ nanowires should provide an experimental platform to explore features relevant to the VLS growth mechanism, such as saturation concentration of a reactant within a VLS catalyst droplet and the use of VLS catalyst metals for controlled etching of semiconducting materials.

11:40am **IS-FrM11 Probing Glyoxal Aqueous Surface Chemistry by *In Situ* Molecular Imaging**, *Fei Zhang, Y. Zhou, X. Sui*, Pacific Northwest National Laboratory; *J. Chen*, Shandong University; *Z. Zhu, X.-Y. Yu*, Pacific Northwest National Laboratory

Aqueous surfaces after photochemical and dark reactions of glyoxal and hydrogen peroxide (H₂O₂) have been studied by a microfluidic reactor coupled with *in situ* liquid Time-of-Flight Secondary Ion Mass Spectrometry (ToF-SIMS) for the first time. Both positive and negative ion mode mass spectra provided complementary information of the surface reactions. Compared with previous results using bulk solutions, our unique liquid surface molecular imaging approach made it possible to observe glyoxal hydrolysis (i.e., first and secondary products, hydrates), oxidation products (i.e., glyoxylic acid, oxalic acid, formic acid, malonic acid, tartaric acid), oligomers, and water clusters (i.e., (H₂O)_nH⁺, (H₂O)_nOH⁻) with sub-micrometer spatial resolution. Spectral principal component analysis was used to determine similarities and differences among various photochemical aging and dark reaction samples and controls. Observations of oxidation products give the physical foundation to deduce new reaction pathways at the aqueous surface. The first chemical mapping of water cluster changes between dark and photochemical aging provides the direct physical evidence that glyoxal oxidation affects the hydrophobicity and water microenvironment at the surface. SIMS three-dimensional chemical mapping enables visualization of the surface mixing state at the molecular level. We potentially provide a new way to investigate complex surface reaction mechanisms as an important source of aqueous secondary organic aerosol (SOA) formation in atmospheric chemistry.

MEMS and NEMS

Room 102B - Session MN+MS-FrM

Radiation Effect in Emerging Micro/Nano Structures, Devices, and Systems

Moderators: Michael Alles, Vanderbilt University, Philip Feng, Case Western Reserve University

8:20am **MN+MS-FrM1 Radiation Effects in Emerging MEMS/NEMS Devices**, *Jacob Calkins*, Defense Threat Reduction Agency

Recent advance in MEMS based computing, signal filtering, and sensing offer significant opportunities for reducing the size, weight, cost, and power requirements of Department of Defense (DoD) systems while improving reliability in extreme environments. Natural and manmade high radiation environments are one of the most extreme environments where DoD systems must both survive and continue to function. This high radiation environment includes satellites in Earth orbit and robots or unmanned vehicles responding to nuclear disasters. This Defense Threat Reduction Agency (DTRA) basic research program seeks to investigate, understand, and model the fundamental effects of radiation on MEMS/NEMS devices.

Gamma rays, x-rays, as well electrons and ions are expected to deposit charge in dielectrics and may also charge the sealed gas environment in which the devices operates. Neutrons, protons, and ions may change the underlying mechanical properties, optical properties, and ferroelectric or piezoelectric properties of MEMS materials. All types of radiation may alter the surface chemistry and morphology causing changes in the performance of physical and electrical contacts. It is expected that MEMS devices will be

resistant to upsets or changes in state due to individual strikes by high energy particles. However, nanoscale devices may be susceptible to either the physical impact or the associated charge deposition. It is important to understand these fundamental effects of radiation on MEMS/NEMS devices and materials before they are incorporated in critical DoD systems.

This talk introduces the DTRA basic research radiation effects program and the radiation effects in MEMS/NEMS topic.

8:40am **MN+MS-FrM2 Effect of Top Electrode Material on Radiation-Induced Degradation of Ferroelectric Thin Films, Nazanin Bassiri-Gharb, S.J. Brewer, C.Z. Deng, C.P. Callaway**, Georgia Institute of Technology; *M.K. Paul*, Woodward Academy; *K.J. Fisher*, Riverwood International Charter School; *J.E. Guerrier, J.L. Jones*, North Carolina State University; *R.Q. Rudy, R.G. Polcawich*, Army Research Laboratory; *E.R. Glaser, C.D. Cress*, Naval Research Laboratory

INVITED

The effects of gamma irradiation on the dielectric and piezoelectric responses of $\text{Pb}[\text{Zr}_{0.52}\text{Ti}_{0.48}]\text{O}_3$ (PZT) thin films were investigated for structures with conductive oxide (IrO_2) and metallic (Pt) top electrodes. All samples showed a general degradation of various key dielectric, ferroelectric, and electromechanical responses when exposed to 2.5 Mrad(Si) ^{60}Co gamma radiation. However, the low-field, relative dielectric permittivity, ϵ_r , remained largely unaffected by irradiation in samples with both types of electrodes. Samples with Pt top electrodes showed substantial degradation of the remanent polarization and overall piezoelectric response, as well as pinching of the polarization hysteresis curves and creation of multiple peaks in the permittivity-electric field curves post irradiation. The samples with oxide electrodes, however, were largely impervious to the same radiation dose, with less than 5% change in any of the functional characteristics. The results suggest a radiation-induced change in the defect population or defect energy in PZT with metallic top electrodes, which substantially affects motion of internal interfaces such as domain walls. Additionally, the differences observed for devices with different electrode materials implicates the ferroelectric-electrode interface as either the predominant source of radiation-induced effects (Pt electrodes) or the site of healing for radiation-induced defects (IrO_2 electrodes).

9:20am **MN+MS-FrM4 Radiation Survivability of MEMS Microelectronic Circuits with CNT Field Emitters, Jason Amsden, E.J. Radauscher, T. von Windheim**, Duke University; *K.H. Gilchrist*, RTI International; *S.T. Di Dona, Z.E. Russell*, Duke University; *L.Z. Scheick*, Jet Propulsion Laboratory, California Institute of Technology; *J.R. Piascik*, RTI International; *C.B. Parker*, Duke University; *B.R. Stoner*, RTI International; *J.T. Glass*, Duke University

INVITED

Radiation survivability of MEMS microelectronic circuits with carbon nanotube field emitters

Jason J. Amsden,^{†*} Erich J. Radauscher,[†] Tasso von Windheim,[†] Kristin H. Gilchrist,[§] Shane T. Di Dona,[†] Zach E. Russell,[†] Leif Z. Scheick,[^] Jeffrey R. Piascik,[§] Charles B. Parker,[†] Brian R. Stoner,^{§,†} Jeffrey T. Glass[†]

[†] Department of Electrical & Computer Engineering, Duke University, 130 Hudson Hall, Box 90291, Durham, NC 27708, USA

[§] Engineering and Applied Physics Division, RTI International, Research Triangle Park, NC 27709, USA

[^] Jet Propulsion Laboratory, California Institute of Technology, Pasadena, CA 91108

*e-mail: jason.amsden@duke.edu [mailto:jason.amsden@duke.edu]

INVITED ABSTRACT

Solid-state technology dominates the consumer electronics market because of the low cost associated with large-scale integration. However, there are numerous applications in which solid-state devices are unreliable or do not provide adequate performance, particularly applications with military systems operating in high radiation environments. In these applications, vacuum microelectronic devices present an attractive alternative. Despite the performance advantages, the use of vacuum electronics has been limited because there is no versatile and reliable microscale platform that enables integration of large numbers of vacuum circuit elements on a single substrate. To address this need, RTI International in collaboration with Duke University has been developing a Microelectromechanical systems (MEMS) platform that enables integration of high-performance microelectronic vacuum components into functional circuits on a single silicon substrate.¹ We have demonstrated a wide variety of vacuum electronic devices including vacuum triodes and ion sources using a freestanding panel approach fabricated with the Polysilicon Multi-

User MEMS Process (PolyMUMPS) with integrated carbon nanotube field emission cathodes. While these devices avoid the radiation-induced charge carrier problems in solid-state devices, other effects of radiation on this MEMS platform have not been studied. The presentation will present our preliminary findings on the radiation effects on this vacuum microelectronics platform.

1. Stoner, B. R.; Piascik, J. R.; Gilchrist, K. H.; Parker, C. B.; Glass, J. T., A Bipolar Vacuum Microelectronic Device. *Electron Devices, IEEE Transactions on* **2011**, *58*, 3189-3194.

Acknowledgements: This work was supported by the Defense Threat Reduction Agency, Basic Research Award # HDTRA1-15-1-0071, to Duke University. The contents does not necessarily reflect the position or the policy of the federal government, and no official endorsement should be inferred

10:00am **MN+MS-FrM6 Radiation Effects in Integrated Photonics and Nano-OptoMechanical Systems, Q. Du**, Massachusetts Institute of Technology; *B Li*, University of Minnesota; *D. Ma, A. Agarwal, Juejun Hu*, Massachusetts Institute of Technology; *M. Li*, University of Minnesota

INVITED

We present integrated photonic devices and Nano-OptoMechanical Systems (NOMS) as highly sensitive

and accurate platforms for quantifying radiation effects in optical materials and MEMS/NEMS systems.

Our approach benefits from the high precision of optical interrogation techniques. Further, compared to

traditional capacitive or piezoelectric actuated devices, NOMS are immune to extrinsic

degradation associated with driving circuit and metal contact failure or charge-trapping in dielectrics, and

are thus ideal test vehicles to measure radiation-induced, intrinsic optical and mechanical material

property modifications. In this talk, we will discuss design, fabrication and characterization of optical and

NOMS devices based on Si, SiN and SiC materials as well as gamma-ray radiation effects in these

devices. Defect identities responsible for the observed optical and mechanical property shifts are clarified

through spectroscopy and microscopy characterization techniques to unravel the radiation damage

mechanisms in these devices.

10:40am **MN+MS-FrM8 Radiation Effects in 2D Materials and Nano Electrical Mechanical Devices, Michael Alles, K.I. Bolotin**, Vanderbilt University; *A. Zettl*, University of California at Berkeley; *B. Homeijer*, Sandia National Laboratories; *J.L. Davidson, R.D. Schrimpf, R.A. Reed, R.A. Weller, D.M. Fleetwood, W. Liao, R.J. Nicholl*, Vanderbilt University

INVITED

The dramatic reduction in size and power consumption offered by micro- and nano-scale electromechanical systems (M&NEMS) offer compelling advantages for adoption in many areas, including space and military systems. Mission reliability and survivability of next-generation space-borne systems depends critically upon a detailed understanding of the radiation response and reliability of the constituent devices when exposed to the relevant radiation environment. M&NEMS may be employed for a variety of sensor and actuation applications, oscillators, and have potential to be incorporated as high-reliability solid-state (logic) switches.

While there has been considerable study of radiation effects on some of the common materials (single and poly crystalline silicon, and silicon-dioxide), the study in the context of MEMS has been more limited, and mainly experimental. The general indication is that depending on the operating principal, MEMS can be sensitive to radiation-induced charging of insulators, and to displacement damage at very high exposure doses of energetic particles.

More recently, fabrication process, namely the ability to create nano-scale structures, and the introduction of new materials (esp. 2D and CNTs), have expanded the opportunities for M&NEMS. The Defense Threat Reduction Agency (DTRA) has recently initiated multiple projects in the study of various aspects and configurations of M&NEMS. This talk will discuss a specific project which seeks to advance the understanding of the effect of radiation on the relevant electro-mechanical properties of the constituent

materials and structures, focusing on 2D materials and CNTs, and the implications for space and military applications.

The key question for this work is: *How does radiation damage to constituent materials impact the mechanical and electrical basis of operation of M&NEM structures?* In particular, cumulative damage by non-ionizing energy loss can, in principle, alter the mechanical properties of structures such as cantilever's and 2D membranes, and surface effects and trapped charge in insulators can impact electrical operating conditions. Presently, the extent to which such effects impact the operation of advanced M&NEM devices is unclear. This particular project combines expertise and experience in materials science, M&NEMS, and radiation effects of the University of California at Berkeley, Sandia National Laboratories, and Vanderbilt University to conduct a systematic study of the impact of relevant radiation types on the key operating properties of novel M&NEM structures, and to capture observed effects in finite element models.

11:20am MN+MS-FrM10 Influence of Radiation on MEMS Oscillators, Bruce Alphenaar, University of Louisville; *M.L. Alles, H. Gong*, Vanderbilt University; *P. Deb Shurva, J.T. Lin*, University of Louisville; *J.L. Davidson*, Vanderbilt University; *S. McNamara, K. Walsh*, University of Louisville; *W. Liao, R.A. Reed*, Vanderbilt University

INVITED

The beneficial size, weight, and power requirements provided by micro-electromechanical (MEMS) and nanoelectromechanical (NEMS) memory, logic and sensors for systems operating in extreme radiation environments make it essential that the effects of radiation on MEMS/NEMS devices be investigated. Here we report on the influence of radiation on a micro-scale oscillator consisting of a electrostatically driven silicon cantilever fabricated from a silicon-on-insulator wafer. The position of the cantilever is detected by the piezoresistive change in an asymmetric silicon beam supporting the cantilever. Prior to radiation exposure, the frequency response of the oscillator remains very stable, provided temperature and pressure are kept constant. Four different radiation sources are used, covering a range of excitation energies: 1) UV B (265 nm) photons 2) 10 keV X-rays 3) 0.8 MeV protons and 4) 2.0 MeV protons. Exposure to 10 keV X-rays at 10.5 krad/minute causes the resonant frequency to shift downwards by approximately 0.4 Hz (50 ppm change) following 2.1 Mrads irradiation. Once the X-ray exposure is removed, the device returns to its original state after an annealing time of 10 hours. The long annealing time and a correlation to the silicon resistance change shows that sample heating is not an important factor. A comparison to UV B results suggests that the frequency shift is related to charge accumulation in the silicon cantilever. Exposure to 0.8 MeV shows permanent change to the resonant frequency suggesting that displacement damage has occurred. This work was funded by the Defense Threat Reduction Agency under contract HDTRA-15-1-0027.

12:00pm MN+MS-FrM12 Radiation Effects on Silicon Carbide (SiC) Nanomechanical Devices, Philip Feng, Case Western Reserve University

We report on exploratory research effort on investigating fundamental radiation effects in resonant-mode and contact-mode microelectromechanical systems (MEMS/NEMS) enabled by silicon carbide (SiC) micro/nanostructures. We calibrate and compare the radiation effects in a few selected MEMS/NEMS resonators – namely, SiC microdisk resonators, SiC membrane resonators, SiC-on-insulator (SICOI) cantilever beam resonators, and resonant switches.

We focus on discovering fundamental effects of SiC MEMS/NEMS devices due to exposure to radiation sources representative of space and nuclear environments, and attaining comprehensive, in-depth understandings of how these radiations affect the key attributes and performance of the devices. The main properties and metrics include resonance frequency, quality (Q) factor, multimode responses, off-state leakage, on-current, on-voltage, switching speed, surface and nanocontact properties, reliability and lifetime, etc.

In this work, we have carefully performed experiments on extensive testing of multimode SiC MEMS/NEMS resonators and resonant switches, before and after controlled radiation exposure with designed dosage and energetic parameters of the radiation sources. Furthermore, we have done extensive computer simulation studies on the effects of implanting protons (hydrogen ions, H⁺) into SiC thin layers on silicon (Si) substrate and on SiO₂, and explore the ion implantation conditions that are relevant to experimental radiation of SiC device layers.

Surface Science

Room 104E - Session SS+HC-FrM

Deposition and Analysis of Complex Interfaces

Moderators: Bruce D. Kay, Pacific Northwest National Laboratory, Daniel Killelea, Loyola University Chicago

8:20am SS+HC-FrM1 A Quantitative, Experimentally Supported Model for Surface Energy (SE) as a Function of Surface Defect Density (DD): the SEDD Model - Comparison with Three Liquid Contact Angle Analysis and AFM, Abijith Krishnan, Arizona State University/BASIS HS Scottsdale/SiO₂ Innovates LLC; *N.X. Herbots*, Arizona State University/SiO₂ Innovates LLC; *Y.W. Pershad*, Arizona State University/BASIS HS Scottsdale/SiO₂ Innovates LLC; *S.D. Whaley*, SiO₂ Innovates LLC/Arizona State University; *R.J. Culbertson, R.B. Bennett-Kennett*, Arizona State University

Metal Oxide Semiconductor Field Emission Transistors (MOSFETs) have been key to micro- and nano-electronics for the past six decades, but electrically active defects resulting from dangling bonds (unbounded electrons) or mobile ions create parasitic charges, known as surface charges (Q_{ss} for dangling bonds and Q_o for mobile ions), that limit performance. Passivation via oxygen and hydrogen species can reduce surface defects. However, surface state charge analysis via capacitance-voltage (C-V) curves is used to evaluate the extent of passivation but does not accurately reflect the number of structural defects. On the other hand, surface characterization by Tapping Mode Atomic Force Microscopy (TMAFM) can be used for topographic observation and surface roughness measurements but has not been used to measure surface defect density. The new theoretical model proposed the Surface Energy Defect Density (SEDD) Model [1] aims to relate surface defect density to surface energy, a macroscopic quantity measured via high statistics Three Liquid Contact Angle Analysis (3LCAA) metrology [2,3]. Three Liquid Contact Angle Analysis (3LCAA) conducted in a class 100 clean-room using the Sessile Drop method and the Van Oss theory enables for accurate and reproducible contacts angles analysis within 1°, and a reproducible relative error lower than 2-3% for the total surface energy. These results have led to the conception a new theoretical model, the Surface Energy -Defect Density Model (SEDD) which relates the macroscopic surface energy density to the microscopic defect density. To test this model with experimental defect densities, this work uses PIXNANOVERT, a new algorithm to extract defect densities from high resolution large area (1 x10 μm²) TMAFM topographs taken on Si(100) passivated by the Herbots-Atluri process [5-7]. Analysis using surface effect density extracted. PIXNANOVERT shows that the SEDD Model predicts, within 5 the measured surface defect densities of oxidized Si surfaces with known surface energies. With this model, MOSFET manufacturers can determine the defect density in the oxide interface of their transistors by measuring the surface energy of the oxide. Testing transistor effectiveness for computers and other electronic devices would thus become more accurate than relying on C-V curves to quantify surface charge density. The SEDD Model would also allow us to determine the surface chemistry (e.g. hydrophobicity) of many other crystalline or amorphous materials, such as polymers and glasses, by measuring the surface energy.

[1] AS Krishnan, Senior Thesis (2016)

[2] Pat. pend., Herbots et al. (2011,2012,2016)

[3] SD Whaley, PhD, ASU (2013)

8:40am SS+HC-FrM2 Ab initio Analysis of Elementary Reactions during ALD Tungsten Nucleation on Selective Substrates, Mariah King, G.N. Parsons, North Carolina State University

In 1987, selective deposition of tungsten via silane reduction was confirmed with a high deposition rate at a low temperature. Despite the numerous studies that have been conducted in the following years, many chemical processes that control selective tungsten ALD growth are not yet sufficiently understood and the leading concern remains that, past the "selective window", uniform deposition is observed on silica, the non-reactive surface. This loss of selectivity is due to the ability of the non-selective surface to promote nucleation in time due to surface processes and chemical reactions. The primary cause of tungsten nucleation on silica is a long-standing problem in the semiconductor industry that will require new fundamental understanding and an accurate description of the reaction kinetics between reactants and substrates at the atomic level.

In this computational study, we use density functional theory to study the reaction energetics, structural stability, and electronic distribution to describe initial reactions during ALD tungsten nucleation on silicon, silica and tungsten substrates. The objective is to identify reactions that have a

lower probability of occurrence, but may lead to defects that enable nucleation on otherwise non-reactive surfaces. Understanding the probability at which a species reacts with a pristine non-reactive surface will enable designers to define the limits of process defect generation, thereby identifying viable process options. Additionally, these simulations are used to suggest alternative system conditions that could lead to improved selectivity.

As a first step towards understanding the kinetics of complex deposition reactions, we present the kinetics of the elementary reactions for silane and tungsten deposition on silica and fluorinated tungsten surfaces. Along with intensive experimental data on this specific system, we have used the calculated reaction energetics to suggest the most probable series of reactions that lead to loss of selectivity. Extending these results will allow us to define viable options and directions for highly selective processes that minimize defect creation and propagation in electronic device manufacturing.

9:00am SS+HC-FrM3 Design and Synthesis of Nanofence Cerium Oxide Coated Platinum Catalysts via Facet-selective Atomic Layer Deposition, Kun Cao, J.M. Cai, State Key Laboratory of Digital Manufacturing Equipment and Technology, Huazhong University of Science and Technology, China; R. Chen, State Key Laboratory of Digital Manufacturing Equipment and Technology, School of Mechanical Science and Engineering, School of Optical and Electronic Information, Huazhong University of Science and Technology, China

Sintering of Pt nanoparticles (NPs) catalysts at elevated working temperature is highly undesirable, as coalescence of NPs will cause significant decrease in the number of active sites and resulting catalytic performance degradation. Oxide overcoating techniques have been recently developed to minimize Pt sintering. However, certain trade-off has to be made between stabilization and reactivity. Stabilize metal nanoparticles and simultaneously enhance catalytic activity is still very challenging.

Here, we designed a cerium oxide nanofence coating structure to stabilize Pt NPs using facet selective atomic layer deposition. The facet selectivity is realized through differences in binding energy of Ce precursor fragments Pt surfaces. CeO_x prefers to selectively deposit on Pt (111) facets, while leaving the Pt (100) surface intact. CeO_x has synergy with metal as coating layer and creates highly active sites at Pt-CeO_x interfaces. From stability point of view, CeO_x anchors Pt NPs with a strong metal oxide interaction, and nanofence coating layer provide physical blocking that suppresses NP particle migration. Such nanofence CeO_x coated Pt catalysts show both enhanced CO conversion activity and improved sintering resistance up to 700 °C under oxidative atmospheric condition.

9:20am SS+HC-FrM4 Dehydrogenation and Rehybridization of ZnTPP on Ag(100) and Ag(111), C. Ruggieri, S. Rangan, Robert Bartynski, Rutgers, the State University of New Jersey; E. Galoppini, Rutgers - Newark

The interactions between zinc(II) tetraphenylporphyrin (ZnTPP) molecules and the Ag(100) and Ag(111) surfaces were investigated using a combination of scanning tunneling microscopy as a local probe of the molecular adsorption configuration and X-ray, ultraviolet, and inverse photoemission spectroscopies as probes of the electronic structure. When forming a molecular monolayer by desorption of a multilayer on the Ag(100) surface, an order molecular array in registry with the substrate and having a square unit cell results. A similar preparation on the Ag(111) surface produces an overlayer that is considerably less dense but is also commensurate with the substrate having a unit cell that is slightly rectangular. Subsequent annealing leads to a transition from intact molecular adsorption to dehydrogenation and subsequent intramolecular and intermolecular rehybridization. Upon annealing, the molecule flattens as the phenyl portions of the molecule form bonds with a neighboring pyrrole group. This leads to a measurable alteration of the electronic structure. In addition, we find evidence of bonding between neighboring rehybridized molecules, consistent with the formation of biphenylene-type structures, leading to the growth of extended two-dimensional covalently bound structures. Understanding basic rules for molecule-molecule hybridization, potentially templated by prior self-assembly, could enable the directed formation of large, complex, and ordered 2-dimensional arrays of organic or metalorganic units.

C. Ruggieri, S. Rangan, R.A. Bartynski, and E. Galoppini, J. Phys. Chem. C 120, 7575 (2016)

9:40am SS+HC-FrM5 A Case Study of the SMSI Effects: CO Oxidation on the TiO_x/Pt(111) Model Surfaces, Mingshu Chen, H. Li, X.F. Weng, H. Zhang, H.L. Wan, Xiamen University, China

Well-ordered ultrathin TiO_x films were grown on Pt(111) as model surfaces to probe the effects of the strong metal-support interaction (SMSI) on the catalytic performance. The model surfaces of TiO_x/Pt(111) were prepared under UHV and characterized by low-energy electron diffraction (LEED) and Auger electron spectroscopy (AES). CO oxidation was tested for the model surfaces in a batch reaction cell as a function of the TiO_x coverages and structures. And a home-built reflection adsorption infrared spectroscopy (IRAS) was used for *in-situ* studying the surface species and stability of the model surfaces under the reaction conditions. The results show that catalytic activity could be improved significantly on the monolayer z-TiO_x, while a maximum is achieved at 0.3~0.5 ML for the w-TiO_x. The TiO_x thin films were found to be stable under CO oxidation conditions. The activation energy for CO oxidation reaction on the 1 ML z-TiO_x/Pt(111) was found to be 46 kJ/mol, which is much lower than that of 87 kJ/mol on the clean Pt(111) surface.

10:00am SS+HC-FrM6 Toluene and Benzyl Radical Formation during Deoxygenation of Phenylmethanol on Rutile TiO₂(110), Long Chen, R.S. Smith, B.D. Kay, Z. Dohnalek, Pacific Northwest National Laboratory

Understanding the reaction pathways of lignin-derived molecules on catalyst surfaces is of great importance for the sustainable production of energy carriers. In this regard, the role of radicals in the reaction mechanisms leading to functionalized aromatics has been extensively argued. The involvement of radical species has been firmly established for a number of simpler reactions on high surface area oxide catalysts, such as oxidative coupling of methane and selective oxidation of propylene. However, the formation of free radicals is rarely demonstrated. In this work, the reaction pathways of simple lignin-derived aromatic alcohols, i.e. phenol, phenylmethanol, and 2-phenylethanol, on a prototypical model oxide surface, rutile TiO₂(110), are studied using a combination of molecular beam dosing and temperature programmed desorption (TPD). For phenylmethanol, the coverage dependent TPD data show that about 40% of molecules adsorbed on the surface at a saturation coverage are converted to reaction products indicating that the reactions proceed on regular five-fold coordinated Ti sites. This is in contrast to aliphatic alcohols where the reactions are shown to proceed exclusively on bridging oxygen vacancy defect sites. The studies of OD-labelled phenylmethanol demonstrate that a fraction of OD hydrogen is transferred to the benzyl group to form toluene that desorbs between 300 K and 480 K. In the competing reaction, the OD hydrogen is converted to water at ~350 K. Once the OD hydrogen is depleted above 480 K, the remaining phenylmethoxy surface species dissociate yielding benzyl radicals in the gas phase. Combined, these results show that the conversion of phenylmethanol on TiO₂(110) proceeds via a unique chemistry. In contrast, both phenol and 2-phenylethanol exhibit expected surface chemistry analogous to that of aliphatic alcohols. These findings reveal for the first time the formation of free radical species from the interaction of phenylmethanol with TiO₂(110) and demonstrate a new direct mechanism for deoxygenation of lignin-derived benzylic alcohols to aromatics on TiO₂.

Thin Film

Room 105A - Session TF-FrM

CVD, ALD and Film Characterization

Moderators: David Adams, Sandia National Laboratories, Halil Akyildiz, North Carolina State University

8:20am TF-FrM1 Assessing the Role of Temperature and Pressure on the Tungsten ALD Selectivity Window on Si/SiO₂ Substrates, Paul Lemaire, G.N. Parsons, North Carolina State University

Operating conditions such as temperature and pressure are critical variables for atomic layer deposition (ALD) processes. The ALD "temperature window" describes the temperature range in which the growth per cycle is relatively constant. Yet the temperature window typically is in reference to the growth surface and does not include deposition on less thermodynamically favored surfaces. Pressure is typically maintained at ~1 Torr in order to maintain a balance between gas interdiffusion and entrainment, but there has been little work investigating how pressure affects ALD nucleation. In this work we discuss how process temperature and pressure can be adjusted to improve an ALD "selectivity window" aka deposit more material on a growth surface over a non-growth surface. We specifically study a tungsten hexafluoride (WF₆) - silane (SiH₄)

Friday Morning, November 11, 2016

ALD process (W-ALD) to selectively deposit tungsten on silicon (Si) over silicon oxide (SiO_2). Ellipsometric and x-ray photoelectron spectroscopy (XPS) analysis shows that the W-ALD selectivity window increases at lower temperatures and at higher pressure. We suggest that this improved selectivity is due to the lowered probability of the WF_6 reacting with defect sites on the non-growth SiO_2 surface. In addition, we discuss how cyclic gas exposures during the ALD deposition can be used to rapidly change the operating pressure and temperature in order to improve the selectivity window. Results from ellipsometric, and XPS analysis show that dosing He , H_2 , and CH_4 immediately prior to the WF_6 exposure improves the selectivity window. We attribute the improved selectivity window to rapid substrate heating which assists in desorption of WF_x species from the SiO_2 surface and helps limit undesired tungsten nucleation.

8:40am TF-FrM2 X-ray Absorption Spectroscopy Study of Nanocomposite Thin Films Grown by Atomic Layer Deposition, Anil Mane, S. Babar, A. Yanguas-Gil, Argonne National Laboratory; A. O'Mahony, Incom, Inc.; T. Wu, J.W. Elam, Argonne National Laboratory

We have established an ALD approach to synthesize nanocomposite coatings comprised of conducting, metallic nanoparticles embedded in an amorphous dielectric matrix. These films are nominally composed of $\text{M:Al}_2\text{O}_3$ where (M= W and Mo) and are prepared using alternating exposures to trimethyl aluminum (TMA) and H_2O for the Al_2O_3 ALD and alternating $\text{MF}_6/\text{Si}_2\text{H}_6$ exposures for the metal ALD. By varying the ratio of ALD cycles for the metal and the Al_2O_3 components during material growth, we can tune precisely the various material properties such as microstructure, electrical, optical and chemical properties. We have exploited these nanocomposite coatings in several applications such as resistive coatings for large-area microchannel plates suitable for large area photodetectors, charge drain coatings for electron-optic MEMS devices (Digital Pattern Generation chips) for maskless reflection electron beam lithography, protective barrier coatings for Li-ion battery cathodes and solar selective absorber coating for high temperature concentrated solar power (CSP) components.

The ALD surface chemistry for these $\text{M:Al}_2\text{O}_3$ nanocomposite films is complex, particularly during the transitions between the Al_2O_3 and the metal ALD since the surface functional groups are completely different for these two types of processes. To better understand the relationship between the ALD surface chemistry and the resulting microstructure and composition of these nanocomposite materials, we used a suite of analytical methods including transmission electron microscopy (TEM), X-ray photoelectron spectroscopy (XPS) and synchrotron X-ray absorption spectroscopy (XAS) performed at the Argonne Advanced Photon Source to characterize $\text{W:Al}_2\text{O}_3$ films while varying the W cycle ratio, $\text{W}\% = (\text{W cycles})/(\text{total cycles}) \times 100$. A key result was that for $\text{W}\% < 50$, W is present in both metallic and sub-oxide states whereas for $\text{W}\% \geq 50$, only metallic W is seen. This transition from dielectric to metallic character at $\text{W}\% \sim 50$ is accompanied by an increase in the electrical conductivity and the disappearance of a clear bandgap in the absorption spectrum. TEM revealed that the conducting phase is composed of 1-2 nm metallic nanoparticles embedded in an amorphous matrix. We believe that these nanoparticles form spontaneously during the TMA exposure following a W ALD cycle, and that the TMA acts as a reducing agent.

9:00am TF-FrM3 A Fundamental Study of Thermal Conductivity in ALD-deposited Amorphous Oxide Thin Films of Varying Density, Brandon Piercy, Georgia Institute of Technology; K.E. Meyer, P.E. Hopkins, University of Virginia; M.D. Losego, Georgia Institute of Technology

Non-crystalline materials are believed to follow the minimum thermal conductivity model first proposed by Einstein in 1911. This model predicts that the thermal conductivity (Λ) of an amorphous solid is proportional to the atomic density (n) via a Λ proportional to $n^{2/3}$ relationship. This theory implies that the thermal conductivity of amorphous oxide materials can be controlled via their density. While processing conditions in the microelectronics industry often focus on optimizing the dielectric and electrical resistivity properties of amorphous oxide materials, less attention is given to these layers' thermal properties. However, in high-power applications, the thermal conductivity of these materials begins to have importance. In this presentation, we will report on our new fundamental understanding of two industrially important amorphous metal oxide thin films: Al_2O_3 and TiO_2 . ALD deposition of these materials—besides having industrial relevance—also enables direct control over atomic density of these amorphous materials via deposition temperature. In this study, amorphous thin films of Al_2O_3 and TiO_2 of varying density were deposited with ALD over a range of temperatures from 25 °C to 250 °C. The atomic

density of these films is assessed with multiple techniques including ellipsometry, x-ray reflectivity, and gravimetric measurements. Time-domain thermoreflectance (TDTR) is used to measure thermal conductivity. TDTR is an ultrafast optical pump-probe measurement that is particularly well-suited for evaluating the thermal conductivity of thin films and other nanostructures. In this study, the density of Al_2O_3 films was increased by 15%, leading to an increase in thermal conductivity from 1.2 W/m-K to 1.7 W/m-K, a 42% change. TiO_2 films saw an increase from 1.4 W/m-K to 1.9 W/m-K (36%) with a 12% increase in density. Thermal conductivities as a function of film densities were fit with the Einstein minimum effective limit model modified with a differential effective-medium approximation, affirming the applicability of the amorphous limit to metal oxide systems. For the case of TiO_2 , a discrete jump in thermal conductivity to 2.5 W/m-K was detected at the onset of film crystallization (125°C). This result suggests that TDTR can be more sensitive than XRD in detecting the onset of crystallization in amorphous thin films.

9:20am TF-FrM4 The Development of ALD Barrier Layers for Harsh Environment Applications, Ankit Singh, Georgia Institute of Technology; A. Perrotta, Eindhoven University of Technology, Netherlands; S. Graham, Georgia Institute of Technology

Encapsulation of electronic devices using vacuum deposited moisture barrier films is a critical step for their protection and enhancement of lifetime. Devices like implantable devices, OLEDs, OPVs, thin film transistors and thin film solar cells are prone to rapid degradation through chemical reactions with surrounding gas or liquid media. Barrier layers help in avoiding direct exposure of these devices to their surrounding environment thus enhancing their lifetime. Several deposition techniques can be used for preparation of such layers. Atomic layer deposition (ALD) is known to be able to produce ultra-barrier films with water vapor transmission rates lesser than 10⁻⁴ g/m²/day. However, performance and reliability of ALD based barrier films is governed by their stability in corresponding environments where resistance to corrosion and material stability will remain a key parameter to their durability.

In this work, we explore the use of TiO_2 , HfO_2 , ZrO_2 , and Al_2O_3 ALD based barrier films in harsh conditions like high temperature and a range of chemical exposure. The barrier layers were coated over ZnO sensors in order to test their ability to protect the ZnO in harsh environments and can be detected optically using photoluminescence. The exposure included DI water, salt water, phosphate buffer saline solution and low pH (HCl) solution. Degradation in ZnO films was monitored by photoluminescence testing in order to track the decrease in PL signal with time. To compliment the PL study, electron microscopy and a detailed EIS study was conducted in order to understand the mechanism of ALD barrier degradation in different environments. Several of ALD based metal oxides have shown enhanced corrosion resistance outperforming aluminum oxide which showed the least resistance. Finally, application of these barrier layers in protection of organic electronics and inorganic solar cells has been demonstrated.

9:40am TF-FrM5 Conformal CVD Growth of HfB_xC_y and HfB_xAl_y Hard Coatings with Low Coefficient of Friction and High Oxidation Resistance, Elham Mohimi, T. Ozkan, S. Babar, Z. Zhang, S. Liu, G.S. Girolami, A.A. Polycarpou, J.R. Abelson, University of Illinois at Urbana Champaign

Conformal hard coatings with low coefficient of friction, high oxidation resistance and chemical stability are desired for applications such as components with convoluted structures, cutting tools that sustain high temperature, thermal protection systems for extreme environments, and machines with relative motion of parts. We previously reported the conformal growth and excellent mechanical properties of HfB_2 and HfB_xN_y hard coatings by chemical vapor deposition (CVD) below 300°C using the high vapor pressure precursor hafnium borohydride, $\text{Hf}(\text{BH}_4)_4$. Here we report a further improvement in the properties of HfB_2 films by alloying with C to reduce the coefficient of sliding friction, and with Al to impart high temperature oxidation resistance.

All Depositions are performed in a high vacuum chamber using 0.1-0.5 mTorr of the hafnium borohydride precursor. Carbon-alloyed HfB_xC_y films are grown using a co-flow of 0.1-0.4 mTorr dimethylbutene (DMB) as the C source at substrate temperatures of 250-600°C. The resulting films contain 5-33 at. % C. DMB also acts as growth inhibitor that reduces the growth rate by a factor of 2-6 compared to growth using the precursor alone; this affords almost perfect conformality, e.g., a step coverage > 90% in a trench of aspect ratio 30:1. The nanoindentation hardness varies from 21 to 9 GPa for films with 5-21 at. % C grown at 300°C, and from 23-25 GPa for films with 28-35 at. % C grown at 600°C. The coefficient of sliding friction is

remarkably low, 0.05-0.08 for films with the highest and lowest carbon content, respectively. In addition, the elastic response is more compliant, which is expected to improve the tribological wear performance.

Al-alloyed HfB_2Al_x films are grown using a co-flow of 0.05-0.20 mTorr trimethyl amine alane (TMAA) as aluminum source at a temperature of 250-300°C. In the absence of alloying, HfB_2 films exposed to an oxygen ambient at 800°C will oxidize deeply because HfO_2 does not provide a protective layer and B_2O_3 evaporates rapidly. In sharp contrast, films containing 1-20 at. % Al form a protective aluminum oxide surface layer. Compositional depth profiles confirm the absence of oxidation below this surface layer. In addition these films are morphologically stable: whereas HfB_2 crystallizes, densifies and forms a network of cracks at temperatures above ~ 600°C, the HfB_2Al_x films do not crystallize or crack upon annealing to 800°C in inert or oxidizing atmospheres. Future work, including the co-alloying with C and Al, will explore property optimization in which both low friction and oxidation resistance are desired.

10:00am TF-FrM6 Chemical Vapor Deposition of Silanes for Surface Modification, Brian Johnson, M.R. Linford, Brigham Young University

Silanes are arguably the most important reagents for chemically modifying surfaces. They have the unique ability to attach to silanol (SiOH) groups while imparting desired functionality. Indeed, they are extensively used to modify silica for chromatography and silicon wafers to create attachment layers for biosensors and bioarrays. Of course, HMDS is an important silane that is widely used in the semiconductor industry. Interestingly, most of the reports in the literature on silane deposition describe their liquid phase deposition. The obvious drawbacks of this approach are its lack of reproducibility and the consumption of large amounts of solvent both in the deposition and rinsing of the surfaces. Clearly there are health/safety issues associated with this use of solvent. Its advantages are simplicity – only beakers/simple glassware are required. The gas phase deposition of silanes has exactly the opposite advantages. It offers greater reproducibility and control, but the equipment required is much more complex and expensive. Nevertheless, the semiconductor and related industries much prefer the latter chemical vapor deposition (CVD) direction. Here we describe the CVD of various silanes under the controlled conditions offered by a commercial deposition system. We describe the effect of reactive functionality in the silane on deposition. We show how varying the temperature substantially changes film growth (silane deposition). We describe system cleanliness issues and the means by which carry over between runs can be nearly eliminated. We discuss the deposition of both monofunctional and trifunctional silanes. Films are characterized by X-ray photoelectron spectroscopy, time-of-flight secondary ion mass spectrometry, and contact angle goniometry. Water contact angles and film thicknesses of hydrophobic silanes are strongly correlated. Best conditions for the gas phase deposition of some important silanes are presented.

10:20am TF-FrM7 Iron CVD from Iron Pentacarbonyl: Growth Inhibition by CO Dissociation and Use of Ammonia to Restore Constant Growth, P. Zhang, E. Mohimi, T. Talukdar, G.S. Girolami, John Abelson, University of Illinois at Urbana Champaign

The precursor $\text{Fe}(\text{CO})_5$ can be used to deposit Fe and Fe alloy thin films by CVD. However, at temperatures of 200-300°C this system exhibits undesirable behaviors – a reduction in growth rate with increasing temperature, a change in morphology from faceted to irregular, and a self-limiting film thickness – that make film growth very difficult to control and reproduce. We hypothesize that decomposition of CO ligands poisons the growth surface with graphitic carbon, on which further precursor reaction is suppressed.

Here, we report a novel solution based on surface chemistry: injection of NH_3 along with $\text{Fe}(\text{CO})_5$ eliminates the poisoning effect, i.e., Fe CVD becomes stable and reproducible in the temperature range of 200-300°C with little change in morphology or growth rate. We propose that NH_3 removes CO from the growth surface before it can decompose based on mechanisms that were previously investigated for CO on static Fe surfaces[1].

We report that co-flow of NH_3 entirely restores the growth rate and morphology of pure Fe and of $\text{Fe}_x\text{Co}_{1-x}$ films. The use of NH_3 may be applicable to other set carbonyl-based CVD precursors.

1. Johnston, Colin, Norman Jorgensen, and Colin H. Rochester. "Infrared study of ammonia-carbon monoxide reactions on silica-supported iron catalysts." *Journal of the Chemical Society, Faraday Transactions 1: Physical Chemistry in Condensed Phases* 84.10 (1988): 3605-3613.

10:40am TF-FrM8 New Insights on the Structure and Chemistry of the Tin Oxide-emitter Interface in CdTe Solar Cells as revealed by Thermomechanical Cleavage and Electron Spectroscopy, Craig Perkins, C. Beall, J.M. Burst, A. Kanevce, M.O. Reese, T.M. Barnes, National Renewable Energy Laboratory

CdTe solar cells having superstrate architectures have a poorly understood, complex front surface formed via interdiffusion of the CdS-based emitter and the CdTe absorber. Interfaces in this region of the cell are difficult to probe by standard surface analytical methods because they are bound by glass on one side and microns of CdTe on the other. Post-growth processing with CdCl_2 and for back contacting is likely to further change these buried interfaces, making the traditional scheme of interface analysis – interleaved depositions and analyses – impractical. Yet these front interfaces are important. Recent modeling shows that recombination at the cell front will be increasingly critical to cell efficiency as doping levels are improved from $\sim 10^{14}/\text{cm}^3$ to $10^{16}/\text{cm}^3$. In this study we make use of a LN2-based thermomechanical cleavage technique and a surface analysis cluster tool to probe in detail the tin oxide-emitter interface in completed CdTe solar cells. We show that this thermomechanical cleavage occurs within a few angstroms of the SnO_2 -emitter interface. An unexpectedly high concentration of chlorine, ~20%, was determined from a calculation that assumed a uniform chlorine distribution. Angle-resolved X-ray photoelectron spectroscopy was used to further probe the structure of the chlorine containing layer, revealing that both sides of the cleave location are covered by a single unit cell of CdCl_2 . Exposing these newly formed surfaces to water showed that CdTe solar cells made using CdCl_2 and CdS:O emitters contain water-soluble components at their front surfaces, raising questions pertinent to cell reliability. We show that the SnO_2 -emitter interface is also characterized by an extremely strong gradient in oxidation of the chalcogens present as well as a high fraction of oxidized tellurium. Selenium addition to the front of the device, done to improve carrier lifetimes, also affects the extent of chalcogen oxidation. Our work provides new and unanticipated details about the structure and chemistry of front surface interfaces and should prove vital to improving materials, processes, and reliability of next generation CdTe-based solar cells.

11:00am TF-FrM9 Defect Tolerance in Methylammonium Lead Triiodide Perovskite, Xerxes Steirer, P. Schulz, G. Teeter, V. Stevanovic, M. Yang, K. Zhu, J.J. Berry, National Renewable Energy Laboratory

X-ray photoelectron spectroscopy (XPS) is used to track dynamic chemical and electronic changes in hybrid perovskite ($\text{CH}_3\text{NH}_3\text{PbI}_3$) thin-films used in photovoltaic applications. We report in detail X-ray induced transformations with implications on theoretical predictions of hybrid perovskite defect tolerance. Large changes in perovskite composition are analyzed with simultaneously acquired valence band spectra. A clear and reproducible trend is found that provides evidence for vacancy-type defect formation upon X-ray irradiation as $\text{CH}_3\text{NH}_3\text{PbI}_3$ is continuously converting to PbI_2 . Remarkably, the position of the valence band edge with respect to the Fermi level (E_F) is invariant to significant losses of both CH_3NH_3 and I. It is not until the I/Pb ratio drops below 2.5 that E_F shifts toward the valence band edge indicating that the $\text{CH}_3\text{NH}_3\text{PbI}_3$ film becomes less *n*-type. This shift is correlated with the formation of PbI_2 as demonstrated in Pb 4f and I 3d core level spectra. Results gained from these XPS studies demonstrate that the electronic structure of the hybrid perovskite compound investigated is tolerant to defects (CH_3NH_3 and iodine vacancies) on the order of one defect pair per octahedron.

11:20am TF-FrM10 Non Uniform Deposition Rate Profile during the Growth of SiO_2 Films Deposited by Atmospheric Pressure PECVD, Anna Meshkova, FOM Institute DIFFER, Netherlands; F.M. Elam, S.A. Starostin, FUJIFILM Manufacturing Europe, Netherlands; M.C.M. van de Sanden, FOM Institute DIFFER, Netherlands; H.W. de Vries, FOM institute DIFFER, Netherlands

It was recently demonstrated that high quality dense inorganic oxide films can be synthesized on polymers utilizing the roll-to-roll Atmospheric Pressure PECVD process assisted by the diffuse dielectric barrier discharge (DBD) between cylindrical drum electrodes. In such a reactor configuration the local deposition rate as well as the local plasma chemistry is highly non-uniform along the gas flow due to the depletion of the precursor and spatial-temporal non uniformity of the discharge.

It is therefore expected that the properties of the film will vary depending on deposition location within the reactor. Hence the analysis of the spatially averaged layer deposited on the substrate roll-to-roll transported through the active reactor length is not sufficient for understanding the film growth process. The aim of the present contribution, therefore, is to

study the local kinetics, gas phase transport and film growth mechanisms by means of spatially resolved analysis of the film properties in the gas flow direction of the AP-PECVD reactor, by analysis of the deposition rate profile, morphology, chemical composition and microstructure.

The set of SiO₂ films was grown in an AP-PECVD reactor with parallel bi-axial cylindrical electrode geometry on PEN foil. TEOS was used as a precursor for silica-like thin films and the process gases were argon, nitrogen and oxygen. The variation of the deposition rate along the gas flow was accessed by measuring the film thickness profile by means of a focused beam SE with a beam size of 120 µm. The composition and microstructure was analysed by spatially resolved XPS and ATR-FTIR.

Surprisingly it was found that deposition rate profile along the gas flow has two distinct maxima. The presence of two maxima indicates a difference in the transport kinetics of the precursor fragments arriving to the surface. This coincides well with the observed variation in film microstructure in the downstream direction, assessed by ATR-FTIR analysis, with higher network porosity for lower gas residence time and denser films deposited in high residence time regions. This spatial non-uniformity within the reactor results in a depth gradient of the film properties synthesized on web-rolled substrate. One can conclude that, for the studied AP-PECVD process, the film density will increase from the silica/polymer interface towards silica/air interface when the polymer substrate is transported along gas flow. By controlling the gas flow speed the density of the layer can be modified. The last observation is especially relevant regarding the design of the gas diffusion barrier layers.

11:40am **TF-FrM11 X-Ray Diffraction from Pseudomorphic GaAs/In_{0.3}Ga_{0.7}As Superlattice High Electron Mobility Transistor Heterostructures on GaAs (001) Substrates, *Fahad Althowibi, J.E. Ayers*, University of Connecticut**

Pseudomorphic high-electron mobility transistors (HEMTs) are of great interest for high-frequency applications. One approach to pseudomorphic transistors involves a superlattice structure, thereby decreasing the individual active layer thicknesses and extending the range of composition for pseudomorphic realization. Generally, X-ray characterization of pseudomorphic HEMTs is difficult to implement due to the complexity of the resulting diffraction profiles. In this work we show for the first time that superlattice implementation of HEMTs aids in the characterization of the pseudomorphic/metamorphic transition by x-ray diffraction means.

Here we report a study of the dynamical x-ray diffraction from GaAs/In_{0.3}Ga_{0.7}As superlattice high electron mobility transistor heterostructures on GaAs (001) substrates both with (metamorphic) and without (pseudomorphic) dislocations. We show that the threading dislocation density may be estimated from non-destructive x-ray rocking curve measurements, using the rocking curve peak intensity ratios and widths for superlattice diffraction peaks. Here, the peak widths are obtained from the broadening of the individual rocking curve peaks, while the reduction in peak intensity values may be also used to serve as a sensitive tool for the characterization of threading dislocations. These approaches therefore allow characterization of HEMT structures as pseudomorphic or metamorphic.

12:00pm **TF-FrM12 Flexible CIGS Nanorod Array Photodetectors, *Emad Badraadeen, M. Brozak, K.M. Al-Mayalee, F. Keles, T. Karabacak*, University of Arkansas at Little Rock**

In this study, we fabricated core-shell nanostructured flexible photodetectors on flexible substrates of Kapton. For this purpose, p-type copper indium gallium selenide (CIGS) nanorod arrays (core) were coated with aluminum doped zinc oxide (AZO) films (shell) at relatively high Ar gas pressures. CIGS nanorods were prepared by glancing angle deposition (GLAD) technique using a RF magnetron sputtering unit at room temperature. AZO films were deposited by RF sputtering at Ar pressures of 1.0 x10⁻² mbar (high pressure sputtering, HIPS) for the shell and at 3.0 x10⁻³ mbar (low pressure sputtering, LPS) for top contact. The morphological characterization was carried out by field-emission scanning electron microscope. The photocurrent measurement was conducted under 1.5 AM sun under zero electrical bias. GLAD nanostructured flexible photodetectors were shown to demonstrate enhanced photoresponse with a photocurrent density value of 2.88 µA/cm². On the other hand, conventional planar thin film devices did not show any notable photoresponse. Improved photoresponse of CIGS nanorod devices are believed to be due to their enhanced light trapping property and the reduced inter-electrode distance as a result of core-shell structure, which allows the effective capture of the photo-generated carriers. This approach

can open up a new strategy to boost the performance of flexible photodetectors.

Bold page numbers indicate presenter

— A —

Abana, O.: 2D+NS-FrM5, 249
 Abate, Y.: EM+NS+PS+SS+TF-MoM5, 7;
 EM+NS+SP+SS-WeA9, 154; EM-ThP2, 230;
 SP+AS+MI+NS+SS-MoM8, **20**; SP-TuP4,
 115; SP-TuP5, 115; SP-TuP6, 115; SP-TuP7,
 115
 Abatecola, A.: VT-TuM3, **75**
 Abbas, A.: TF-TuA7, 99
 Abbott, J.: 2D+MI-ThM10, 175
 Abe, Y.: TF-ThP9, 241
 Abedzadeh, N.: NS+BI-ThA3, **215**
 Abel, M.L.: AS+SS-TuA8, **80**; AS+SS-WeM6,
 125; AS-WeA7, 152
 Abelson, J.R.: TF-FrM5, 260; TF-FrM7, **261**;
 TF-ThP39, 246
 Abere, M.: SE-TuP5, 114
 Abhilash, T.S.: MN+NS-WeA4, 159
 Ablett, J.M.: SA+AS+BI+MI-TuA12, 91
 Abudayyeh, O.K.: EM-MoM8, 9; SE+MS+TF-
 TuA7, **92**
 Abutan, A.: VT-TuA10, 101
 Acharya, S.R.: HC+SS-ThA11, 210
 Achenbach, J.: SE+TR-WeM1, 137
 Acik, M.A.: TF-ThP25, 243; TF-TuA3, **98**
 Ackerman, M.: 2D+MI+SA-MoM11, 3
 Adams, D.P.: SE+NS+TF+TR-TuM4, 65; SE-
 TuP5, 114; TF+EM+MI-WeA9, **170**
 Adams, H.L.: TR+BI+SE+TF-ThA1, 224
 Addou, R.: 2D+NS-WeA12, **150**; 2D-TuA12,
 78; SE+2D+EM-WeA10, 166
 Adelmini, L.: TF+MI-WeA9, 172
 Adhikari, D.: EL+AS+BI+EM+TF-ThA11, **206**
 Adusumilli, P.: TF+EM+MI-WeA10, 170
 Afanas'ev, V.: EM-ThP1, 230
 Africh, C.: SA+2D+AC+AS+TF-TuM3, 63
 Aga, R.S.: 2D-ThP5, 227
 Agarwal, A.: MN+MS-FrM6, 257; PS1-ThM4,
190; PS1-ThM6, 191; PS-TuM1, 61; PS-
 TuM3, 62
 Agarwal, S.: PS+TF-WeA8, 161; PS-WeA12,
 164; TF-MoM10, 23
 Agarwal, S.P.: TF+MI+NS-WeM11, 146
 Agasie, R.: EM+MI+MN-TuA11, 83; EM-ThP6,
 231
 Agüero, A.: SE+TR-WeM5, 138
 Aguileria, R.: BI+PB-TuP3, 108
 Aharonovich, I.: NS-TuM1, 58
 Ahles, C.F.: PS2-ThM12, **194**
 Åhlund, J.: IS-ThP6, **233**
 Ahmadi, E.: EM-MoA5, 30
 Ahmadi, M.: HC+NS+SS-WeA10, **156**
 Ahmed, W.: SS2+AS+HC+NS-TuM11, **70**
 Ahn, C.H.: TF+MI-WeA8, 172
 Ahyi, A.C.: EM+NS+PS+SS+TF-MoM6, 8
 Aizenberg, J.: BI+AS-MoM2, 6
 Ajayan, P.: 2D+NS-FrM11, 251
 Akabori, M.: HI+MI+NS-ThA11, 212
 Akarvardar, K.: PS-MoM4, 17
 Akhter, S.: SS-TuP10, **117**
 Akinwande, D.: 2D+MI+SA-MoM10, 3;
 2D+NS-FrM3, 249
 Aksu, C.: TF+MI+NS-WeM5, 145
 Aksyuk, V.: MN+NS-WeA7, 159; MN-WeM5,
 132
 Akylidiz, H.I.: TF2-ThM12, **200**
 Albrecht, M.: TR+AS+NS+SS-WeA7, 173
 Alden, D.: SP+AS+MI+NS+SS-MoM8, 20
 Alducin, M.: SS1+AS+HC+NS-TuM5, 68
 Alexander, M.R.: AS+BI-MoA8, 28; BI+AS-
 MoM5, **6**; NS+BI-ThA10, 217
 Alfrey, J.L.: VT-MoM1, **24**
 Ali, A.: AS+SS-WeM2, 124
 Ali, A.M.: TF-ThP17, 242

Ali, M.: TF+EM+MI-WeA10, 170
 Ali, O.: MN-ThP2, 235; MS-TuP5, **111**
 Alia, S.: AS-WeA10, 152; SA-TuP1, 113
 Aliman, M.: IS-ThP7, 234
 Allain, J.P.: BI+AS+SA-ThM3, **180**; BI+PB-
 TuP9, 109; SE-TuP4, 114
 Allard, L.F.: IS-FrM10, 256; IS-ThM13, **188**
 Allen, S.: BI+AS+SA-TuA3, 82
 Alles, M.: BI+AS-MoM6, 6
 Alles, M.L.: MN+MS-FrM10, 258; MN+MS-
 FrM8, **257**
 Allison, S.: BI+MI-WeM11, 128
 Allred, D.D.: TF+MI+NS-WeM6, 145; TF+MI-
 WeA12, **172**
 Almadori, Y.: SE+MS+TF-TuA12, 93
 Al-Mayalee, K.M.: TF-FrM12, 262
 Almyras, G.A.: SE+NS+TF+TR-TuM3, 65
 Alphenaar, B.: MN+MS-FrM10, **258**
 Al-Rubeai, M.: PB+BI+PS-TuM3, 60
 Alsharif, N.: NS-MoM9, 13
 Althowibi, F.: TF-FrM11, **262**; TF-ThP11, **241**
 Altieri, N.D.: PS+TF-WeM11, **135**; PS2-
 ThM13, 194
 Altman, A.B.: AC+AS+SA-ThM6, 177
 Altuntas, S.: EM+NS+PS+SS+TF-MoM3, 7
 Alvarez Barragan, A.: EM-ThP3, 230; PS+2D-
 TuA2, **88**
 Alvarez, H.: VT-TuP4, **119**
 Alvarez-Barragan, A.: EM+NS-WeM6, 129
 Amann, M.-C.: PS-TuM12, 62
 Amaty, J.: TF1-ThM1, 196
 Ambaye, H.: MI+2D+AC-MoM4, 10
 Ambrosio-Lázaro, R.C.: 2D-ThP4, 227
 Ament, I.: PS-ThP23, 238
 Amin, T.: MI-TuA9, 85
 Amiri, P.K.: SE+2D+EM-WeA12, 166
 Amsalem, E.: AS-ThA7, 203
 Amsden, J.J.: MN+MS-FrM4, **257**
 Amster, O.: MS+AS-TuM11, 58
 Andahazy, W.: HC+NS+SS-WeA9, 156
 Anders, A.: PS-TuM13, 63; SE-TuP7, 114
 Anders, M.A.: EM+AC+SS+TF-ThM13, 183
 Anderson, S.: SS2+AS+HC+NS-TuM1, **69**
 Anderson, T.J.: EM-MoA10, **31**; EM-MoA3,
 29
 Anderson, V.: EM-FrM5, 254; PS-ThP5, **235**;
 TF+SA+MI-TuM12, 73
 Anderton, C.R.: AS+BI-MoA2, 27; AS+BI-
 MoA3, **28**
 Andreasson, B.: VT-MoM11, 25
 Andriessen, R.: TF-TuA4, 98
 Angerer, T.B.: AS+BI-MoA6, **28**; NS+BI-
 ThA11, 217
 Anh, L.T.: HI+MI+NS-ThA11, 212
 Antipov, S.: NS-TuM5, 59
 Antoni, M.: IS-ThP7, 234
 Aoukar, M.: PS-WeM3, 136
 Appenzeller, J.: EM+MN-TuM10, **56**
 Aragonez, R.J.: PS-ThP32, 240
 Aramaki, F.: HI+MI+NS-ThA1, 210
 Arbiol, J.: SS2+AS+HC+NS-TuM12, 71
 Arble, C.: SS+AS-WeM4, 143
 Archiblad, R.K.: AS+SS-TuA2, 79
 Archuleta, T.N.: PS-ThP32, 240
 Arefi-Khonsari, F.: PB+BI+PS-MoA3, **36**
 Arehart, A.: EM-MoA5, 30
 Arghavani, R.: PS-WeA4, 163
 Argibay, N.: AS-WeA11, 153; SE+NS+TF+TR-
 TuM4, **65**; TR+BI+SE+TF-ThA10, 226;
 TR+BI+SE+TF-ThA11, 226; TR+BI+SE+TF-
 ThA12, 226
 Argoud, M.: TF-ThA1, **223**
 Arias Suarez, S.L.: BI+PB-TuP9, 109
 Arias, P.: 2D+TF-WeM13, **122**

Arias, S.: BI+AS+SA-ThM3, 180
 Aripova, N.: SP+SS+TF-WeM12, 140
 Aristov, V.Y.: EM-MoM11, 10;
 SA+2D+AC+AS+TF-TuM6, **64**
 Aristova, I.M.: EM-MoM11, 10
 Arlinghaus, H.F.: AS+BI-MoA8, 28; AS+SS-
 ThM12, 179; AS+SS-TuA12, 81; AS+SS-
 TuA9, **80**; BI+PB-TuP5, 108
 Armacost, M.D.: PS-TuM3, 62
 Armakavicius, N.: EL+AS+EM+MI+TF-FrM3,
 251
 Arnadottir, L.: HC+SS-ThA10, **210**;
 SS1+AS+HC+NS-TuM11, 69
 Arnarson, L.: SS+AS-TuA12, 96
 Arnaud, S.: PS2-ThM6, 193
 Arnold, J.: AC+AS+SA-ThM6, 177
 Arnold, J.C.: PS-MoA10, 41; PS-MoA2, 40
 Arpa-Sancet, M.P.: BI+AS-MoM6, 6
 Arrigo, R.: IS+HC-WeA1, 158; IS+HC-WeA9,
158
 Artyushkova, K.: AS+SS-WeM2, **124**
 Askew, L.: BI+AS+SA-ThM12, 182
 Aspinwall, C.A.: BI+AS+SA-ThM10, 181
 Asthagiri, A.: SS+AS-TuA3, 95; SS-TuP4, 116
 Atiganyanun, S.: EM-MoM6, **9**
 Attenkofer, K.: MS-TuA4, **86**
 Atzin-Mondragon, C.: NS-TuP7, 112
 Aube, A.: PS+SE-MoM6, 15
 Audi, M.: VT-TuM3, 75
 Audinet, J.-N.: HI-WeA11, 157
 Auerbach, D.J.: SS1+AS+HC+NS-TuM5, **68**
 Auras, S.V.: SS-TuP5, **116**
 Avanesyan, S.: MN-ThP2, 235; MS-TuP5, 111
 Avasaraia, S.: AS+SS-WeM2, 124
 Avila, J.R.: TF+EM-MoA3, 47
 Aydil, E.S.: NS-TuA12, 88
 Aydogan, P.: IS-ThP5, 233
 Ayers, J.E.: SS+AS+EM-WeA12, 168; TF-
 FrM11, 262; TF-ThP11, 241
 Azcatl, A.: 2D+MI-MoA1, **26**; 2D+MI-MoA2,
 26
 — B —
 Babar, S.: TF-FrM2, 260; TF-FrM5, 260; TF-
 ThP39, **246**
 Babenkov, S.V.: EM-MoM11, 10;
 SA+2D+AC+AS+TF-TuM6, 64
 Baber, A.E.: HC+NS+SS-WeA9, **156**
 Babicheva, V.E.: EM+NS+SP+SS-WeA9, **154**;
 SP+AS+MI+NS+SS-MoM8, 20; SP-TuP7, 115
 Babore, A.: SS+AS+HC-MoA9, **46**
 Babuska, T.: TR+BI+SE+TF-ThA10, 226;
 TR+BI+SE+TF-ThA11, **226**; TR+BI+SE+TF-
 ThA12, 226
 Bachman, J.N.: MN+NS-WeA3, 159
 Bachor, J.M.: SS-TuP9, 117
 Badan, C.: HC+SS-ThM3, 184
 Badano, G.: TF+MI-WeA9, 172
 Baddorf, A.P.: HC+NS+SS-WeA4, 155
 Badrudeen, E.O.: TF-FrM12, **262**
 Bae, J.H.: TF-ThP22, **243**
 Baer, D.R.: AS+SS-ThM6, 179; AS-MoM1, 3;
 AS-ThA3, **202**; IS-FrM7, 255; MS-TuA10, **87**
 Bagge-Hansen, M.: NS-TuM6, **59**; SA-TuP2,
 113; TF+SA+MI-TuM10, 72
 Bagley, J.: AS+SS-TuA7, 80
 Bagus, P.S.: AC+MI-WeM10, **123**
 Bahm, A.: NS-TuM1, 58
 Bai, S.: SS-ThM13, **196**
 Baik, K.: VT-TuP1, 118
 Baio, J.E.: BI+AS-MoM1, 5
 Baitukha, A.: PB+BI+PS-MoA3, 36
 Bajdich, M.: HC+SS-ThA7, 209
 Bakkers, E.P.A.M.: TF+MI+NS-WeM3, 144
 Baklanov, M.: EM-ThP1, 230

- Balci, S.: 2D+TF-WeM10, 122
 Balder, E.: TF-TuM6, 74
 Balijepalli, S.K.: 2D-ThP13, 229
 Balkanci, A.: TR+BI+SE+TF-ThA3, 225
 Balki, O.: PS-ThP2, 235
 Ballet, P.: TF+MI-WeA9, 172
 Balog, R.: 2D+MI-TuM6, 53
 Balow, R.: IS-FrM6, **255**
 Bandak, D.: 2D-TuA11, 78
 Bandophadyay, A.S.: 2D+TF-WeM1, **121**; 2D-ThP3, **227**
 Bandorf, R.: TF+PS+SE-MoA11, 51
 Banerjee, D.: SE+MS+TF-TuA2, 91
 Banerjee, P.: TF-TuA10, 99
 Banerjee, S.K.: 2D+MI+SA-MoM10, 3; 2D-ThA8, 201
 Baneton, J.: PS2-ThM10, **193**; PS-ThP21, 238
 Banis, G.: BI+PB-TuP2, **107**
 Banno, Y.: PS-WeA7, 163
 Bañuls Ciscar, J.: AS-WeA7, **152**
 Barati, Gh.: IS-ThA11, 213
 Barats-Damatov, D.: AS+SS-WeM10, 125
 Barbé, J.-C.: SE+MS+TF-TuA12, 93
 Barinov, A.V.: 2D-ThP13, 229
 Barkam, S.: AS-TuP27, **107**
 Barker, D.: VT-MoM5, 24; VT-MoM6, 24
 Barlow, A.J.: AS+SS-TuA11, 80; HI+NS-ThM12, **187**
 Barlow, D.E.: BI+PB-TuP7, **108**; IS-FrM6, 255
 Barnes, A.C.: MN-WeM10, 133
 Barnes, T.M.: TF-FrM8, 261
 Barnola, S.: PS2-ThM6, 193
 Barnwell, A.: BI+AS+SA-ThM3, 180
 Baron, A.: SA+AS+MI-MoM8, **19**
 Barral, A.: MI+2D+AC-MoA2, 31
 Barraza-Valdez, E.: VT-TuP3, **119**
 Barrett, N.: SA+2D+AC+AS+TF-TuM10, **64**
 Barroo, C.: HC+SS-ThM10, 185
 Barsoum, M.W.: 2D+MI-TuM3, 53
 Bartels, L.: 2D+MI-ThM6, **175**; 2D-ThP13, 229
 Bartha, A.: EM+SS+TF-ThA12, **208**
 Barton, A.T.: 2D-TuA12, 78; SE+2D+EM-WeA10, **166**
 Bartynski, R.A.: SS+HC-FrM4, **259**
 Baryshev, S.: NS-TuM5, 59
 Basavalingappa, A.: PS-MoM10, 18
 Bassiri-Gharb, N.: MN+MS-FrM2, **257**
 Bastea, S.: NS-TuM6, 59; SA-TuP2, 113
 Batha, S.H.: PS-ThP32, 240
 Batra, V.: MN-WeM3, 132; TF-TuA12, **100**
 Batson, T.: AS-TuP22, 106
 Batzill, M.: 2D+MI-MoA9, **27**
 Bauer, E.D.: AC+AS+SA-ThM6, 177
 Bauer, J.: AS+SS-WeM10, 125
 Bauer, R.: VT-TuA11, 101
 Baumberg, J.: NS+BI-ThA6, 216
 Baydin, A.: EM-MoA9, **31**
 Baykara, M.Z.: TR+BI+SE+TF-ThA3, **225**
 Baylet, J.: PS-ThA6, 218
 Beall, C.: TF-FrM8, 261
 Beam, J.B.: AS-TuP29, 107
 Beams, R.: 2D+TF-WeM12, 122
 Beardslee, L.: BI+PB-TuP2, 107
 Beebe, Jr., T.P.: AS+SS-ThM10, 179; AS+SS-ThM13, 180
 Beebe, M.R.: EM-MoM5, **9**
 Behafarid, F.: HC+NS+SS-WeA10, 156
 Beik Mohammadi, J.: TF+MI-WeA3, 171
 Beinik, I.: SS+AS-TuA12, 96
 Belianinov, A.: 2D+MI-MoA6, 26; AS+SS-TuA2, 79; HI+MI+NS-ThA4, 210; HI+MI+NS-ThA8, **211**; HI+NS-ThM10, 186; SP+AS+MI+NS+SS-MoM1, 19
 Bell, D.: 2D+TF-WeM5, 121
 Bellan, L.: EM+SS+TF-ThA9, 207
 Bellido-Gonzalez, V.: EW-WeL4, 148; VT-MoA10, 52
 Bello, N.: SS-TuP6, **117**
 Benck, E.: VT-WeM10, **147**
 Bendikov, T.: AS+SS-WeM10, **125**; AS-TuP6, 103
 Beniwal, S.: TF+SA+MI-TuM2, 71
 Benjamin, D.: TF+EM+MI-WeA11, 170
 Bennett, S.: MI-TuP2, 110
 Bennett-Kennett, R.B.: SS+HC-FrM1, 258
 Bennewitz, R.: TR+AS+NS+SS-WeA7, **173**
 Benoit, D.: EW-WeL4, 148
 Bent, S.F.: SS+2D-WeM4, 141; TF-MoM5, 23
 Bentley, W.E.: MN+BI-ThM12, 190
 Ben-Yoav, H.: NS+BI-ThA8, 216
 Berg, M.: 2D+NS-FrM11, **251**
 Bergbreiter, S.: MN-WeM1, **132**
 Berger, B.: PS-TuM10, 62
 Berggren, K.K.: NS+BI-ThA3, 215
 Bergner, U.: VT-TuA11, 101
 Bermudez, V.: IS-FrM6, 255
 Bernhardt, H.: VT-TuM1, 75
 Bernholc, J.: SP+AS+MI+NS+SS-TuM5, 67
 Berrio, L.F.: BI+AS+SA-ThM3, 180
 Berry, I.L.: PS-ThP12, 236
 Berry, J.J.: TF-FrM9, 261
 Berry, R.J.: 2D-ThP5, 227
 Bertran, F.: SA+2D+AC+AS+TF-TuM2, 63; SA+AS-MoA6, 42
 Beton, P.: 2D+NS-WeA11, 150
 Bettac, A.: SP+AS+MI+NS+SS-MoM3, **20**
 Betthausen, T.: EM+MI+MN-TuA11, 83; EM-ThP6, 231
 Beyer, A.: HI-WeA9, **157**
 Bhat, N.: 2D-ThA8, 201
 Bhattacharjee, S.: 2D-ThA8, 201
 Bhattacharya, P.: AS-MoM1, 3; EM+AC+SS+TF-ThM1, 182
 Bhattacharya, S.: AS-TuP17, 105; HC+SS-ThA1, **208**
 Bhattarai, G.: EM+AC+SS+TF-ThM12, 183; EM+AC+SS+TF-ThM4, **182**; EM-ThP13, 232; EM-ThP8, 232
 Bhoj, A.N.: PS-ThP20, 238; PS-ThP27, **239**
 Bhowmick, R.: PS-WeA12, 164
 Bi, Z.X.: PS-MoM10, 18
 Bielinski, A.: TF+MI+NS-WeM10, **145**
 Biewer, T.M.: PS-WeM10, 137
 Biffinger, J.C.: BI+PB-TuP7, 108
 Bigelow, T.S.: PS-WeM10, 137
 Bihlmayer, G.: MI+2D+AC-MoA1, 31
 Bilgin, I.: 2D+NS-FrM11, 251
 Binggeli, N.: SA+2D+AC+AS+TF-TuM3, 63
 Biolsi, P.: PS-MoA11, 41
 Birch, J.: TF+PS+SE-MoA4, 49
 Birchfield, C.: 2D-ThP8, 228; 2D-ThP9, **228**
 Bischoff, L.: HI+NS-ThM5, 186
 Bishal, A.K.: BI+AS+SA-ThM2, **180**
 Bishop, J.: NS-TuM1, 58
 Biswas, C.: 2D+TF-WeM1, 121; 2D-ThP2, 227; 2D-ThP3, 227
 Bittle, E.G.: TF-ThA7, 224
 Biyikli, N.: EM+NS+PS+SS+TF-MoM3, **7**
 Bizouerne, M.: PS-MoM11, **18**
 Black, L.E.: TF+MI+NS-WeM3, **144**
 Blajan, M.: PB+BI+PS-TuM2, 60
 Blake, J.: AS+SS-WeM2, 124
 Blake, M.: PS+AS+SS-MoA11, **39**
 Blanco-Rey, M.: SS1+AS+HC+NS-TuM5, 68
 Blank, K.G.: BP-SuA1, **1**
 Blasco, N.: TF-MoM1, **22**
 Blass, J.: TR+AS+NS+SS-WeA7, 173
 Blatnik, M.: SS+AS-TuA9, 95
 Blatz, J.: TF+EM+MI-WeA11, 170
 Blechle, J.M.: PS-ThP25, 239
 Blessing, J.E.: VT-MoA8, 52
 Bliem, R.: SS+AS+HC-MoA8, 46
 Blomberg, T.: TF-ThP19, 242
 Blomfield, C.J.: AS+SS-WeM13, 126; AS-MoM10, 5; AS-TuP4, 102; AS-TuP5, 103; AS-TuP6, 103; EW-TuL4, **77**
 Bluck, T.M.: TF-ThP37, 246
 Bluestein, B.M.: BI+AS+SA-TuA10, **82**; BI+MI-WeM12, 128
 Blügel, S.: MI+2D+AC-MoA1, 31
 Bluhm, H.: IS-ThA2, 212; SS+AS+HC-MoA10, 46; SS+AS+HC-MoM10, 22; TF-ThA6, 223
 Boban, M.: TF+MI+NS-WeM10, 145
 Boehme, C.: MI-TuA1, **84**
 Boettcher, S.W.: TF-TuA8, 99
 Bogaerts, A.: PS+SE-MoM4, 14; PS-ThA3, 218
 Bogan, J.: EM+SS+TF-ThA11, 208
 Bøggild, P.: 2D+MI-TuM6, 53
 Bohnheio, Ch.: SE+TR-WeM2, 137
 Boland, T.: BI+PB-TuP3, 108; NS-TuP2, 111
 Bolat, S.: EM+NS+PS+SS+TF-MoM3, 7
 Bolotin, I.L.: EM+NS-WeM1, 128
 Bolotin, K.I.: MN+MS-FrM8, 257
 Bolotnikov, A.E.: EM+AC+SS+TF-ThM10, 183
 Bolvardi, H.: SE+TR-WeM6, 138; TF1-ThM13, 198
 Bolvin, H.: AC+MI-WeA3, **150**
 Bongiorno, G.: VT-TuA9, 101
 Bonilla, J.E.: EM-MoM8, 9
 Bonnecaze, R.T.: PS-ThA12, 220
 Bonnell, D.: EM-MoM10, **9**; SS+2D-WeM5, 142
 Boone, C.: EM-FrM2, 253
 Booth, C.H.: AC+AS+SA-ThM6, 177; AC-TuP1, 102
 Booth, J.-P.: PS-TuM1, **61**; PS-TuM10, 62; PS-WeM1, 136
 Boris, D.R.: PS+SE-MoM11, 16; PS-ThP30, 239; PS-ThP5, 235; PS-ThP9, 236; PS-WeA3, **162**; TF+SA+MI-TuM12, 73
 Borowik, L.: SE+MS+TF-TuA12, **93**
 Borup, K.A.: TF-TuA8, 99
 Bosch, R.H.E.C.: PS+TF-WeA7, 161
 Boschen, J.S.: SS1+AS+HC+NS-TuM12, 69
 BOSCHER, N.: PS+2D-TuA7, **89**
 Bouanani, S.: TF-ThA1, 223
 Boufnichel, M.: PS1-ThM12, 191
 Bouhafs, C.: EL+AS+EM+MI+TF-FrM3, 251
 Boulard, F.: PS-ThA6, 218; TF+MI-WeA9, **172**; TF+PS+SE-MoA8, 50
 Boulet, P.: SS+AS-TuA1, 94
 Bouwstra, J.B.: SE+MS+TF-TuA8, 92
 Bowers, A.: HI+MI+NS-ThA7, 211
 Boxford, W.: AS-TuP6, 103
 Boyce, B.L.: AS-WeA11, 153; SE+NS+TF+TR-TuM4, 65
 Boyd, A.: TF1-ThM10, 197
 Boyd, R.D.: SE+NS+TF+TR-TuM3, 65
 Boyle, D.T.: HC+NS+SS-WeA9, 156
 Boyuk, D.S.: NS-MoA11, **35**
 Bozna, B.L.: TR+AS+NS+SS-WeA7, 173
 Bozorgzad Moghim, T.: AS+SS-WeM6, **125**
 Bradford, P.D.: TF+MI+NS-WeM5, 145; TF2-ThM12, 200
 Bradley, A.J.: 2D+MI-ThM12, 176
 Bradshaw, G.K.: SE+MS+TF-TuA7, 92
 Brady, M.P.: AS-TuP19, 105
 Brady, S.L.: NS+BI-ThA8, 216
 Brand, O.: MS-TuA1, 85
 Brandt, A.J.: HC+SS-WeM6, 131
 Brandt, S.: PS-TuM10, 62
 Bravo-Sanchez, M.: AS-MoM4, 4
 Brearley, A.: AS+SS-WeM2, 124
 Breen, A.: PB+BI+PS-TuM3, 60

Author Index

- Brems, S.: TF+EM+MI-WeA3, 169
 Brennan, C.: PS-WeA11, **164**
 Breton, M.: PS-MoM9, 18
 Breuer, L.: AS-ThA9, **203**; HI+NS-ThM11, 187
 Brewer, S.J.: MN+MS-FrM2, 257
 Brierley, M.: AC+AS+SA-ThM5, **177**
 Brihoum, M.: PS2-ThM6, 193
 Brindley, J.: EW-WeL4, **148**; VT-MoA10, **52**
 Broderick, A.: SS+AS-WeM4, 143
 Brower, T.: 2D+NS-FrM5, 249
 Brown, K.A.: NS-MoM9, **13**
 Brown, R.D.: HC+SS-WeM5, **130**
 Brown, T.M.: TF-TuA4, 98
 Browning, J.: MI-TuP2, 110
 Browning, N.: EM+NS-WeM10, 129
 Brozak, M.: TF-FrM12, 262
 Brozena, A.H.: TF-TuM13, 75
 Bruce, R.L.: PS-MoA2, **40**; PS-MoM2, 17
 Bruchhaus, L.: HI+NS-ThM5, 186
 Brucker, G.A.: VT-MoM8, **25**
 Bruener, P.: AS-TuP7, 103
 Bruinen, A.L.: AS+BI-MoA10, 29
 Bruix, A.: 2D+MI-TuM13, 54
 Brukman, M.: SS+2D-WeM5, 142
 Brumbach, M.: AS-WeA11, **153**
 Bruneau, B.: PS-TuM10, 62; PS-WeM2, 136
 Brunelle, L.D.: AS-TuP15, **104**; AS-TuP16, 104
 Brüner, P.: TF-ThP19, 242
 Bryan, I.: EM+NS+PS+SS+TF-MoM1, 7
 Bryan, S.R.: AS+BI-MoA10, 29; AS+SS-ThM11, 179; AS+SS-WeM3, 125; AS-WeA2, 151
 Bryan, Z.: EM+NS+PS+SS+TF-MoM1, 7
 Bsiesy, A.: PS-WeM3, 136
 Buck, E.C.: AC+MI-WeA7, 150
 Buck, J.: EM+SS+TF-ThA9, 207
 Budak, S.: 2D-ThP7, 228; 2D-ThP8, 228; 2D-ThP9, 228; NS-MoM1, 12; SE+2D+EM-WeA8, **165**
 Buditama, A.: TF+MI-WeA8, 172
 Buehler, M.J.: 2D+MI-ThM1, 175
 Buie, M.J.: PS-ThP6, 235; VT-TuM13, **76**
 Bullen, H.J.: SA+2D+AC+AS+TF-TuM5, **64**; TF+SA+MI-TuM11, 72
 Bultman, J.E.: 2D+NS-FrM1, 249
 Bünermann, O.: SS1+AS+HC+NS-TuM5, 68
 Burch, M.J.: HI+MI+NS-ThA4, **210**; HI+NS-ThM10, 186
 Burger, A.: BI+MI-WeM13, 128; EM+AC+SS+TF-ThM1, **182**
 Burkatovsky, A.: NS-MoM9, 13
 Burkes, D.: AS-ThA11, 204
 Burkett, S.L.: MN-ThP1, 234
 Burst, J.M.: SS+2D-WeM6, 142; TF-FrM8, 261
 Burtin, P.: PS-MoM11, 18
 Bussmann, E.: NS-MoM10, **14**
 Butler, J.: BI+MI-WeM13, 128
 Butorin, S.: AC+AS+SA-ThM11, 177
 Butschke, B.: AS+SS-WeM10, 125
 Buyukserin, F.: EM+NS+PS+SS+TF-MoM3, 7
 Byrne, A.: MN-ThP2, 235
 — C —
 Cabrera, G.: MI+2D+AC-MoM10, 11
 Cabrera-German, D.: AS-MoM4, 4
 Cadigan, C.: AS-TuP22, 106
 Cai, J.M.: SS+HC-FrM3, 259
 Caillard, A.: SS+AS-TuA1, 94
 Caldarella, G.: PS2-ThM10, 193
 Caldwell, J.: EM-MoM3, **8**; TF+EM+MI-WeA1, 169
 Calkins, J.: MN+MS-FrM1, **256**
 Callaway, C.P.: MN+MS-FrM2, 257
 Calzolari, L.: BI+AS+SA-TuA2, 81
 Camarda, G.S.: EM+AC+SS+TF-ThM10, 183
 Camci, M.T.: IS-ThP5, 233
 Camilli, L.: 2D+MI-TuM6, 53
 Camillone, N.: SS+AS+HC-MoA6, 45; SS1+AS+HC+NS-TuM2, 67
 Camillone, N.R.: SS+AS+HC-MoA6, 45; SS1+AS+HC+NS-TuM2, 67
 Campanini, D.: MN-WeM11, 133
 Campbell, C.T.: HC+SS-ThA10, 210; HC+SS-ThA7, 209; SS+AS+HC-MoA2, 45; SS1+AS+HC+NS-TuM11, 69; SS2+AS+HC+NS-TuM4, **70**
 Campbell, I.H.: PS-WeM10, 137
 Canaperi, D.: PS-MoM10, 18
 Canning, A.: AC+AS+SA-ThM11, 177
 Cant, D.J.H.: AS-MoM3, **4**
 Cao, C.: 2D+NS-WeA8, 149
 Cao, J.: IS-ThM5, 187
 Cao, K.: SS+HC-FrM3, **259**; TF-TuM5, **74**
 Cao, L.: MI-TuA9, 85
 Cao, R.: AS+SS-ThM6, 179; IS-FrM7, 255
 Capomaccio, R.: BI+AS+SA-TuA2, 81
 Carabelli, A.: BI+AS-MoM5, 6
 Cardinaud, C.: PS-ThA6, **218**
 Carette, M.: TF+PS+SE-MoA3, 49
 Carey, S.: HC+SS-ThA7, 209
 Carman, G.P.: MI-TuP1, 109; TF+MI-WeA1, 171
 Carnevale, S.D.: PS-ThP12, 236
 Carpick, R.W.: AS-MoM5, 4
 Carr, A.: PS-MoA3, 40
 Carr, D.M.: AS+SS-ThM11, **179**; AS+SS-WeM3, 125
 Carrizosa, S.B.: SE+2D+EM-WeA2, **164**
 Carroll, M.: NS-MoM10, 14
 Carson, C.S.: MN-ThP2, 235; MS-TuP5, 111; NS-TuP5, 112
 Carter, J.: VT-MoA1, **51**
 Carter, R.E.: EM+SS+TF-ThA1, 206; MS-MoM8, 12; SS+AS+HC-MoM8, 22; TF+EM-MoA2, 47; TF+EM-MoA8, **48**
 Cartron, M.: NS+BI-ThA6, 216
 Caruso, A.N.: EM+AC+SS+TF-ThM12, 183; EM+AC+SS+TF-ThM4, 182; EM-ThP13, 232; EM-ThP8, 232; PS-MoA1, 40
 Carvalho, I.: SE+TR-WeM12, 138
 Carvalho, S.: SE+TR-WeM12, 138
 Casey, S.M.: SS1+AS+HC+NS-TuM3, **68**
 Caspi, E.N.: 2D+MI-TuM3, 53
 Cassidy, A.: 2D+MI-TuM6, 53
 Castellanos-Gomez, A.: EL+AS+EM+MI+TF-FrM8, 253
 Castner, D.G.: AS+AC-TuM12, **55**; AS+BI-MoA1, 27; AS-MoM1, 3; AS-MoM3, 4; BI+AS+SA-TuA9, 82
 Castro, G.R.: SA+AS+BI+MI-TuA11, 91
 Catalan, J.: 2D-ThP2, **227**; MS-MoA4, **33**
 Caughman, J.B.O.: PS-WeM10, **137**
 Caulton, K.: SS-TuP11, 118
 Cavalli, A.: TF+MI+NS-WeM3, 144
 Cavanagh, A.S.: TF-TuM2, 73
 Ceccone, G.: BI+AS+SA-TuA2, **81**
 Celebioglu, A.: EM+NS+PS+SS+TF-MoM3, 7
 Cerhova, M.: TF-ThP42, 247
 Cerio, F.: PS-ThP12, 236
 Cerrato, J.M.: AS+SS-WeM2, 124
 César, R.R.: TF-ThP31, 245
 Cetnar, J.S.: TF-ThP41, 246
 Cha, M.H.: PS1-ThM3, 190
 Chabal, Y.J.: TF-MoM9, 23
 Chacon, E.: SP+AS+MI+NS+SS-MoM10, 20
 Chagarov, E.: SS+AS+EM-WeA7, 167; SS+AS+EM-WeA8, 168
 Chaika, A.N.: SA+2D+AC+AS+TF-TuM6, 64
 Chakrabartty, J.: SE+2D+EM-WeA7, **165**
 Chakraborty, S.A.: TF+SA+MI-TuM4, 72; TF-ThP7, 241
 Chambettaz, F.: PS-WeA2, **162**
 Chamiot-Maitrala, G.: TF-ThA1, 223
 Chamlagain, B.: 2D+NS-FrM12, 251
 Chan, C.: 2D+NS-FrM11, 251
 Chan, P.: PS+TF-WeM3, 134; PS-MoM1, 16
 Chandrasena, R.U.: SA+AS-MoA10, 43
 Chandross, M.: SE+NS+TF+TR-TuM4, 65; TR+BI+SE+TF-ThA10, 226; TR+BI+SE+TF-ThA11, 226; TR+BI+SE+TF-ThA12, 226
 Chang, D.: HI+MI+NS-ThA4, 210
 Chang, H.: SP+AS+MI+NS+SS-MoM2, 19
 Chang, J.: EM+MI+MN-TuA11, 83; EM-ThP6, 231; TF+MI-WeA2, 171; TF+MI-WeA8, **172**
 Chang, J.P.: MI-TuP1, **109**; PS+TF-WeM11, 135; PS2-ThM13, 194; SE+2D+EM-WeA12, 166; TF+MI-WeA1, 171; TF+MI-WeA8, 172
 Chang, M.: SS+AS+EM-WeA7, 167
 Chang, M.H.: SP+AS+MI+NS+SS-TuA8, **94**
 Chang, P.: BI+AS-MoM10, 7
 Chang, S.H.: BI+PB-TuP6, 108
 Chang, S.Q.: BI+PB-TuP9, **109**
 Chang, T.: EM+MI+MN-TuA11, 83; EM-ThP6, 231
 Chang, W.T.: HI+NS-ThM2, 186; HI-ThP1, **232**
 Chang, Y.H.: SP+AS+MI+NS+SS-TuA8, 94
 Chang, Y.-J.: IS-FrM10, 256
 Chatterjee, S.: AS+SS-ThM2, **178**
 Chattopadhyay, S.: EL+AS+EM+MI+TF-FrM4, 252
 Chauhan, D.: EM-FrM6, **254**
 Chauvet, A.: IS-FrM3, **255**
 Chave, T.: AC+AS+SA-ThM4, 176
 Chen, C.: MN-WeM6, 133; TF+EM+MI-WeA11, 170
 Chen, D.A.: HC+SS-WeM6, **131**
 Chen, E.L.: PS+TF-WeM11, 135; PS2-ThM13, 194
 Chen, F.Z.: IS-ThP4, 233
 Chen, G.H.: MN-WeM12, **133**
 Chen, H.-P.: TF-ThP30, **244**; TF-ThP40, 246
 Chen, J.: IS-FrM11, 256
 Chen, J.G.: IS-ThM10, 188; SS+AS-ThA11, **221**
 Chen, J.H.-C.: TF+EM+MI-WeA10, 170
 Chen, K.: MI+2D+AC-MoM5, 10
 Chen, L.: EM-FrM6, 254; SS+AS+HC-MoM2, **21**; SS+HC-FrM6, **259**; TF-ThP5, 241
 Chen, M.J.: BI+PB-TuP6, 108
 Chen, M.S.: SS+HC-FrM5, **259**
 Chen, N.: HC+SS-ThM4, 184
 Chen, Q.: PS-ThP21, **238**
 Chen, R.: SS+HC-FrM3, 259; TF-TuM5, 74
 Chen, T.: PS+2D-TuA3, 89
 Chen, W.-C.: EM-ThP9, 232; TF-ThP40, **246**
 Chen, X.: SP+AS+MI+NS+SS-TuM2, 66
 Chen, Y.: 2D+MI-ThM12, 176; SP+2D+AS+NS+SS-MoA3, 43
 Chen, Y.T.: SE+TR-WeM1, 137
 Cheng, L.: 2D+MI-MoA2, 26; 2D-TuA12, 78; SE+2D+EM-WeA10, 166
 Cheng, M.-K.: TF+EM+MI-WeA12, 170
 Cheng, T.S.: 2D+NS-WeA11, 150
 Cheon, S.: SP+2D+AS+NS+SS-MoA4, 43
 Cherepy, N.: EM+AC+SS+TF-ThM1, 182
 Cheung, P.L.: TF+MI-WeA2, **171**
 Cheung, W.S.: VT-TuP1, **118**
 Chevalier, N.: SE+MS+TF-TuA12, 93
 Chevalier, X.: TF-ThA1, 223
 Chew, H.B.: PS+2D-TuA9, **89**
 Chi, M.: IS-ThA6, **213**
 Chiang, D.: TF-ThP40, 246
 Chiang, N.: SP+AS+MI+NS+SS-TuM2, **66**; SP-TuP1, 115
 Chiang, Y.-M.: MS-MoM3, **11**
 Chiape, D.: TF+EM+MI-WeA3, 169
 Chiba, T.: TF-ThP9, 241
 Chien, M.-H.: IS-ThA11, 213

- Childs, K.: TF+EM+MI-WeA9, 170
 Chiu, P.-K.: TF-ThP40, 246
 Cho, B.: VT-TuP7, 119
 Cho, K.J.: 2D+NS-WeA12, 150; SE+2D+EM-WeA10, 166
 Cho, W.H.: TF-ThP30, 244
 Cho, Y.: 2D+NS-WeA11, 150; SP+AS+MI+NS+SS-TuA12, 94
 Choi, A.S.: AS-TuP28, 107
 Choi, H.: SS1+AS+HC+NS-TuM1, 67
 Choi, J.S.: TR+BI+SE+TF-ThA9, 226
 Choi, J.Y.: SS+AS+EM-WeA8, 168; TF+EM+MI-WeA8, **170**
 Choi, T.: SP+AS+MI+NS+SS-TuA3, **93**
 Choi, Y.C.: NS-TuP9, 112
 Chollon, G.: PS-MoA1, 40
 Chopra, H.D.: SA+AS-MoA10, 43
 Chopra, M.J.: PS-ThA12, **220**
 Chopra, S.: TF2-ThM3, 199
 Chorkendorff, I.: SS+AS-ThA10, **221**
 Chou, L.-W.: NS-MoA11, 35
 Choudhury, F.A.: EM+SS+TF-ThA8, **207**; TF-ThP13, 242; TF-ThP32, 245
 Choy, J.H.: 2D+MI-TuM5, 53
 Christ, J.: AS-TuP22, 106
 Christophis, C.: BI+AS-MoM6, 6
 Christou, A.: EM-MoA10, 31
 Chu, J.P.: BI+PB-TuP6, **108**
 Chu, N.N.: IS-ThP4, 233; SE-TuP3, 114
 Chu, Y.-H.: MI+2D+AC-MoM10, 11
 Chugh, S.: 2D-ThP3, 227
 Chulhai, D.: SP+AS+MI+NS+SS-TuM2, 66
 Chung, H.-Y.: IS-ThP7, 234
 Chung, I.S.: TF-ThP22, 243
 Chung, N.-K.: VT-TuP7, 119
 Chung, T.M.: TF-ThP12, 242
 Chung, Y.: EM-MoA8, 30
 Ciobanu, C.: 2D+TF-WeM13, 122
 Cioldin, F.H.: VT-TuP4, 119
 Clark, B.L.: SE+NS+TF+TR-TuM4, 65
 Clarke, R.: EM-FrM3, 253
 Claveau, G.: TF-ThA1, 223
 Clavero, C.: EL+AS+EM+MI+TF-FrM6, 252
 Cleland, A.N.: MN+NS-WeA1, **159**
 Clemons, M.S.: SE+2D+EM-WeA11, 166
 Clima, S.: EM+MI+MN-TuA9, **83**
 Cobet, C.: IS-ThA11, **213**
 Coenye, T.: PB+BI+PS-MoA2, 35
 Cohen, H.: AS-MoM11, 5; SP+SS+TF-WeM13, **141**
 Cohen, J.: SS2+AS+HC+NS-TuM5, **70**
 Cohen, S.: TF+EM+MI-WeA10, 170
 Cohen, S.R.: AS+AC-TuM13, **56**
 Cohn, A.P.: EM+SS+TF-ThA1, 206; EM+SS+TF-ThA7, **207**; MS-MoM8, 12; SS+AS+HC-MoM8, 22; TF+EM-MoA8, 48
 Cole, J.: 2D-ThP8, **228**; 2D-ThP9, 228; SE+2D+EM-WeA8, 165
 Cole, K.: TF+MI-WeA3, 171
 Coleman, D.: EM-MoM9, **9**
 Collazo, R.: EM+NS+PS+SS+TF-MoM1, 7; SP+AS+MI+NS+SS-MoM8, 20
 Collette, S.: PS+SE-MoM8, **15**; PS-ThP21, 238
 Collins, K.S.: PS+TF-WeM5, 134; PS1-ThM4, 190; PS1-ThM6, 191
 Collins, R.W.: EL+AS+BI+EM+TF-ThA6, 205
 Collins, W.E.: MN-ThP2, 235; MS-TuP5, 111
 Colombo, L.: 2D-TuA12, 78; SE+2D+EM-WeA10, 166
 Colpo, P.: BI+AS+SA-TuA2, 81
 Colvin, J.: EM+NS+SP+SS-WeA4, 153
 Comes, R.: TF+SA+MI-TuM4, **72**
 Conard, T.: SA+AS+BI+MI-TuA12, **91**
 Conley, Jr., J.F.: TF2-ThM1, **198**
 Connolly, A.: TF2-ThM10, 199
 Conroy, M.A.: AC+MI-WeA7, **150**
 Consiglio, S.: TF+EM+MI-WeA2, 169
 Conti, R.: PS-MoM10, 18
 Contreras-Turrubiarres, M.M.M.: TF-ThP34, 245
 Cook, A.L.: MN-ThP2, 235; NS-TuP5, **112**
 Cook, B.: SS-TuP11, 118
 Cook, C.J.: AS-TuP28, 107
 Cooke, I.R.: SS-TuP12, **118**
 Cooke, J.: EL+AS+EM+MI+TF-FrM5, **252**
 Cooke, M.J.: PS-ThP14, **237**
 Cornelissen, L.E.: PS+TF-WeA7, 161
 Cornil, D.: SS+AS-TuA1, 94
 Cornil, J.: SS+AS-TuA1, 94
 Corrion, A.L.: EM-MoA1, **29**
 Costa, P.S.: TF+SA+MI-TuM2, **71**
 Cottle, H.: PS-MoA11, **41**
 Cotton, N.: VT-TuM1, 75
 Couet, S.: PS-ThP33, 240
 Coultas, S.J.: AS+SS-WeM13, 126; AS-TuP4, **102**; AS-TuP5, 103; AS-TuP6, 103; EW-TuL4, 77
 Coumou, D.: PS-WeM6, 137
 Counsell, J.D.P.: AS+SS-WeM13, **126**; AS-MoM10, 5; AS-TuP4, 102; AS-TuP5, 103; AS-TuP6, 103; EW-TuL4, 77
 Coutts, T.: SS+2D-WeM6, 142
 Covington, C.L.: 2D-TuA3, **78**
 Craighead, H.G.: NS+BI-ThA7, 216
 Craver, B.: PS-TuM3, 62
 Creatore, M.: PS+TF-WeA7, 161; TF1-ThM12, 198; TF-TuA4, **98**
 Cremers, V.: AS+SS-ThM5, 178
 Cress, A.: VT-TuM13, 76
 Cress, C.D.: 2D+MI-ThM5, 175; MN+MS-FrM2, 257
 Crommie, M.F.: 2D+MI-ThM12, 176
 Cronin, S.: SP-TuP7, 115
 Crookes-Goodson, W.J.: BI+PB-TuP7, 108
 Cross, B.G.: SP-TuP4, 115; SP-TuP5, **115**
 Cross, N.: 2D+MI-MoA6, 26
 Crotti, D.: PS-ThP33, 240
 Crouch, A.L.: BI+PB-TuP7, 108
 Crow, A.M.: SS+2D-WeM4, 141
 Crow, J.A.: AS-TuP28, 107
 Crutcher, X.: 2D-ThP7, 228; NS-MoM1, 12
 Cui, Y.: EM+AC+SS+TF-ThM10, 183; TF+MI+NS-WeM3, 144
 Culbertson, E.J.: AS+SS-WeM1, 124; BI+PB-TuP11, 109
 Culbertson, R.J.: SS+HC-FrM1, 258
 Cullen, D.: HI+MI+NS-ThA10, 211
 Cullen, P.J.: PS+SE-MoM3, 14
 Culler, E.C.: EM-MoM8, 9
 Cummings, M.: SP+AS+MI+NS+SS-MoM2, 19
 Cumpson, P.J.: AS+SS-TuA11, **80**; HI+NS-ThM12, 187
 Cunge, G.: PS+AS+SS-MoA5, 38
 Curley, M.: 2D-ThP8, 228; 2D-ThP9, 228
 Currie, M.: 2D+MI+SA-MoM2, 2; 2D-ThA10, 201; TF+EM+MI-WeA1, 169
 Curry, J.: TR+BI+SE+TF-ThA10, 226; TR+BI+SE+TF-ThA11, 226; TR+BI+SE+TF-ThA12, **226**
 Curtis, J.E.: BI+AS-MoM10, **7**
 Custers, J.: EM+SS+TF-ThA12, 208
 Cutshall, D.B.: SS1+AS+HC+NS-TuM4, 68
 Cvelbar, U.: PB+BI+PS-MoA2, **35**
 Czaplewski, D.A.: MN-WeM6, **133**
 — **D** —
 Da Silva, S.: AS+BI-MoA5, 28
 Da, B.: IS-ThA8, 213
 Dadap, J.: 2D-ThP6, 227
 Dahal, A.: SS+AS+HC-MoA1, **45**
 Dahint, R.: BI+AS+SA-ThM11, 181
 Dahl, M.: AS-ThA11, 204
 Dahlqvist, M.: 2D+MI-TuM3, 53
 Dai, Z.: AC-TuP2, 102
 Dalbauer, V.: SE+TR-WeM13, **139**
 Dallorto, S.: PS+AS+SS-MoA9, 38
 Dalodière, E.: AC+AS+SA-ThM4, 176
 Daneshmand, M.: NS-MoA3, 34
 Daniel, B.: VT-MoA10, 52
 Daniels, K.M.: TF1-ThM10, 197
 Danis, S.: AC+MI-WeM5, 123; TF-ThP42, **247**
 Darakchieva, V.: EL+AS+EM+MI+TF-FrM3, 251
 Darling, S.B.D.: TF-ThP25, **243**; TF-TuA3, 98
 Das, D.: TF+MI+NS-WeM11, 146
 Das, K.K.: EM-MoA4, 30
 Das, L.: AS-TuP10, **104**
 Das, S.: AS-TuP27, 107; EM+NS+SP+SS-WeA1, **153**
 Dasgupta, N.P.: TF+EM-MoA5, **47**; TF+MI+NS-WeM10, 145; TF+MI+NS-WeM11, 146
 Dattelbaum, D.: NS-TuM6, 59
 Dave, K.: 2D+TF-WeM2, 121
 Davidson, J.L.: 2D-TuA8, 78; EM-MoA9, 31; MN+MS-FrM10, 258; MN+MS-FrM8, 257
 Davies, A.: 2D+NS-WeA11, 150
 Davis, R.F.: 2D+MI-ThM10, 175; EM-MoA4, 30; MN-WeM12, 133; NS-TuP4, 112
 Davis, T.: SE+2D+EM-WeA8, 165
 Davisson, M.: AC-TuP2, 102
 Davydov, A.V.: 2D+TF-WeM12, 122
 De Alba, R.: MN+NS-WeA4, **159**
 De Feyter, S.: TF+EM+MI-WeA3, 169
 de Gendt, S.: TF+EM+MI-WeA3, **169**
 De Geronimo, G.: EM+AC+SS+TF-ThM10, 183
 de Graaf, F.: VT-MoA4, 51
 de la Mata, M.: SS2+AS+HC+NS-TuM12, 71
 de los Arcos, T.: SS+AS+HC-MoA11, 46
 De Lucia, F.C.: PS-TuM3, 62
 de Marneffe, J.: EM-ThP1, 230
 de Miguel, M.T.: SE+TR-WeM5, 138
 De Vos, C.: PS+2D-TuA1, **88**; SE+MS+TF-TuA9, 92
 de Vries, H.W.: PS+SE-MoM10, **16**; SE+MS+TF-TuA8, 92; TF-FrM10, 261
 Deb Shurva, P.: MN+MS-FrM10, 258
 DeBenedetti, W.J.I.: SS+AS-WeM6, **143**; SS+HC-TuA2, 97
 Dechene, J.M.: PS-MoA3, 40
 DeCoste, J.: MS-TuP5, 111; NS-TuP5, 112
 Deeks, C.: AS-MoM6, 4; AS-TuP2, 102; AS-TuP3, 102; AS-WeA1, **151**
 DeGhetaldi, K.R.: AS+SS-ThM13, 180
 Deguns, E.W.: TF+PS+SE-MoA5, 49
 Deitz, N.: SP+AS+MI+NS+SS-MoM8, 20
 Del Gaudio, D.: EM-FrM2, **253**
 Delabie, A.: TF+EM+MI-WeA3, 169
 Delachat, F.: TF-ThA1, 223
 Delgado, A.: MS-MoA4, 33
 Deloach, A.: MI-TuA3, 84
 Delplancke, M.P.: PS-ThP21, 238
 Deluze, J.R.: VT-MoA8, 52
 Deminsky, P.: EM+NS+PS+SS+TF-MoM3, 7
 Demkov, A.: EL+AS+EM+MI+TF-FrM4, 252
 Demkowicz, M.: EM+AC+SS+TF-ThM6, 182
 Dendooven, J.: AS+SS-ThM5, 178
 Dendzik, M.: 2D+MI-TuM13, 54
 Deng, C.Z.: MN+MS-FrM2, 257
 Deng, T.: TF+MI+NS-WeM11, 146
 Deng, X.: SS+AS+HC-MoM6, **21**; SS+AS-WeM11, 144
 DePond, P.: TF+SA+MI-TuM10, **72**
 Derouin, J.: HC+SS-WeM13, 131
 Derpmann, V.: IS-ThP7, 234
 Derzsi, A.: PS-TuM10, 62

Author Index

- Desai, J.: 2D-ThP2, 227
 Deshmukh, P.: NS-MoA2, **34**
 DeSouza, R.: SP+AS+MI+NS+SS-TuM1, 66
 Despiau-Pujo, E.: PS+AS+SS-MoA10, **39**;
 PS+AS+SS-MoA6, 38
 Detavernier, C.: AS+SS-ThM5, 178
 Deutz, A.F.: EL+AS+EM+MI+TF-FrM7, 253;
 VT-TuA10, 101
 Devarajan, T.: PS-MoM10, 18
 Dewey, J.: TF1-ThM6, 197
 Dey, S.: TF+EM+MI-WeA2, **169**
 Dezelah, C.: TF-MoM9, 23
 Dhanunjaya, M.: EM-MoA9, 31
 Dhayal, M.: 2D+TF-WeM2, 121
 Dhowre, H.S.: BI+AS+SA-ThM4, **181**
 Dhuey, S.D.: PS+AS+SS-MoA9, 38
 Dhungana, S.: EM+AC+SS+TF-ThM12, 183;
 EM+AC+SS+TF-ThM4, 182; EM-ThP13, 232;
 EM-ThP8, **232**; PS-MoA1, 40
 di Carlo, A.: TF-TuA4, 98
 Di Dona, S.T.: MN+MS-FrM4, 257
 di Giacomo, F.: TF-TuA4, 98
 Diao, Y.: SS+AS-WeM10, **143**
 Diao, Z.: MN+NS-WeA3, 159; MN-WeM11,
133
 Diebold, A.C.: TF+EM+MI-WeA2, 169
 Diebold, U.: SS+AS+HC-MoA8, 46
 Diem, S.J.: PS-WeM10, 137
 Diercks, D.R.: AS+AC-TuM5, 55
 Diesveld, J.R.H.: VT-TuA10, 101
 Dietz, N.: EM+NS+PS+SS+TF-MoM5, 7; EM-
 ThP2, 230; SP-TuP6, 115
 Dietzel, D.: TR+AS+NS+SS-WeA12, **174**
 DiFonzo, L.G.: AS+SS-WeM5, 125
 Din, S.: TF-ThP44, **247**
 Dine, S.: PS-WeM1, 136
 Ding, G.: EL+AS+EM+MI+TF-FrM6, **252**
 Ding, H.: EM+AC+SS+TF-ThM6, **182**
 Diniz, J.A.: TF-ThP31, 245; VT-TuP4, 119
 Dippo, P.C.: TF-TuA8, 99
 Discher, D.E.: BP-SuA5, **1**
 Diviš, M.: EM+SS+TF-ThA12, 208
 Diwan, A.: SE+2D+EM-WeA4, 165; TF-ThP21,
 243
 Dobrosavljevic, V.: 2D+MI-MoA5, 26
 Dodson, G.: EM+NS+PS+SS+TF-MoM8, 8
 Doerwald, D.: SE+NS+TF+TR-TuM10, 65
 Dohnalek, Z.: HC+NS+SS-WeA1, **155**; SS+HC-
 FrM6, 259
 Dohnálek, Z.: SS+AS+HC-MoA1, 45;
 SS+AS+HC-MoM9, 22
 Doi, I.: TF-ThP31, 245
 Dollery, C.T.: AS+BI-MoA8, 28
 Dombrowski, E.K.: HC+SS-ThM11, 185; IS-
 ThP8, **234**
 Donadio, G.: PS-ThP33, 240
 Donald, S.: AC+MI-WeA12, 151; AC-TuP2,
102
 Donath, M.: MI+2D+AC-MoA3, 32;
 MI+2D+AC-MoA8, **32**
 Dong, B.: TF+PS+SE-MoA2, 49
 Dong, L.: PS-ThP15, 237; SE+2D+EM-WeA11,
 166
 Dong, R.: SP+SS+TF-WeM12, 140
 Dong, S.: MI+2D+AC-MoM10, 11
 Dong, Y.: SS-ThM5, 195
 Donko, Z.: PS-TuM10, 62
 Donnelly, V.M.: PS+AS+SS-MoA3, 37; PS-
 ThP8, 236; PS-TuM6, 62
 Dorenkamp, Y.: SS1+AS+HC+NS-TuM5, 68
 Dorf, L.: PS+TF-WeM5, 134
 Döring, S.: MI+2D+AC-MoA1, 31
 Douidin, N.: SS+AS-TuA9, 95
 Dougherty, D.B.: MI-TuA3, **84**
 Douglas, A.E.: TF+EM-MoA2, **47**; TF+EM-
 MoA8, 48
 Dowben, P.A.: 2D-ThP13, 229;
 EM+AC+SS+TF-ThM3, 182; TF+PS+SE-
 MoA2, 49; TF+SA+MI-TuM2, 71
 Dowling, D.: PB+BI+PS-TuM3, **60**
 Downey, B.P.: TF+EM+MI-WeA1, 169;
 TF+SA+MI-TuM12, 73
 Dowsett, D.M.F.: HI-WeA11, **157**
 Doyle, S.: PS-ThP29, **239**
 Drag, C.: PS-TuM1, 61
 Drahi, E.: PS-WeM2, 136
 Dreisewerd, K.: BI+PB-TuP5, 108
 Drezner, Y.: HI+MI+NS-ThA9, 211
 Droopad, R.: PS-ThP15, 237; SS+AS+EM-
 WeA7, 167
 Droubay, T.C.: TF-ThP7, 241
 Du, Q.: MN+MS-FrM6, 257
 Duan, C.L.: TF-TuM5, 74
 Duan, S.: IS-ThM13, 188
 Duan, X.: 2D+NS-FrM7, **250**
 Duan, Y.: SE+2D+EM-WeA1, **164**
 Dudley, N.J.: EM+SS+TF-ThA3, **207**
 Dufour, T.: PS+SE-MoM4, 14
 Dugger, M.T.: SE+NS+TF+TR-TuM4, 65;
 TR+BI+SE+TF-ThA11, 226; TR+BI+SE+TF-
 ThA12, 226
 Duke, A.S.: HC+SS-WeM6, 131
 Dumas, T.: AC+AS+SA-ThM4, **176**
 Dunn, A.C.: TR+BI+SE+TF-ThA6, **225**
 Dunn, D.: PS-MoM5, **17**
 Duperron, M.: TF+MI-WeA9, 172
 Durand, C.: SP+SS+TF-WeM5, **140**
 Durbin, S.M.: EM-FrM3, **253**
 Durr, M.: AS-TuP8, 103; SS+AS+EM-WeA2,
167
 Durrett, J.: PS2-ThM5, **193**
 Durstock, M.F.: 2D+NS-FrM1, 249; 2D-ThP5,
 227
 Duscher, G.: 2D+MI-MoA6, 26
 Dušek, M.: EM+SS+TF-ThA12, 208
 Duska, C.: TF1-ThM1, 196
 Dutta, S.: EL+AS+EM+MI+TF-FrM4, 252
 Dutton, P.L.: NS+BI-ThA6, 216
 Duwe, M.D.: EL+AS+EM+MI+TF-FrM8, **253**
 Dwyer, J.: NS-TuA12, 88
 Dykman, M.I.: MN-WeM6, 133
 Dylla, H.F.: VT-WeM3, **146**
 Dzara, M.J.: AS-TuP22, **106**
 — E —
 Eads, C.: 2D-TuA11, 78
 Eaves, L.: 2D+NS-WeA11, 150
 Ebnonnasir, A.: 2D+TF-WeM13, 122
 Echegoyen, L.: 2D-ThP3, 227
 Echeverria, E.M.: 2D-ThP13, 229; TF+PS+SE-
 MoA2, 49
 Echeverria, F.: BI+AS+SA-ThM3, 180
 Eckel, S.: VT-MoM5, 24; VT-MoM6, 24
 Economou, D.J.: PS-ThP8, 236; PS-TuM6, 62
 Eddy, Jr., C.R.: EM-MoA10, 31; EM-MoA3,
29; PS-ThP5, 235; TF+EM+MI-WeA1, 169;
 TF+SA+MI-TuM12, 73; TF+SA+MI-TuM3, 71
 Edmonds, M.: PS-ThP15, 237; SS+AS+EM-
 WeA7, 167
 Edmonds, M.T.: 2D+MI-ThM12, 176
 Edmondson, P.: AS-TuP24, 106
 Edwards, Jr., D.: AS-TuP12, **104**
 Egan, P.: VT-MoM3, 24; VT-MoM4, 24
 Ehasarian, A.P.: SE+TR-WeM5, 138;
 TF+PS+SE-MoA10, **50**
 Ehrenberg, S.: PS+2D-TuA3, 89
 Eibagi, N.: PS-ThA7, 218
 Eich, A.: 2D+MI-TuM13, 54
 Eichfeld, S.M.: 2D+MI+SA-MoM1, 2; 2D+NS-
 WeA12, 150
 Eickholt, P.: MI+2D+AC-MoA3, 32
 Einstein, T.L.: SS1+AS+HC+NS-TuM10, **68**
 Eisenbraun, E.T.: SS2+AS+HC+NS-TuM3, 69
 Ekerdt, J.G.: TF2-ThM3, **199**
 Eklund, P.: 2D+MI-TuM3, 53
 Ekuma, C.E.: 2D+MI-MoA5, **26**
 El Mokh, M.: SS+AS-TuA1, 94
 El Soda, M.: HC+NS+SS-WeA3, 155
 Elam, F.M.: SE+MS+TF-TuA8, **92**; TF-FrM10,
 261
 Elam, J.W.: TF+EM-MoA3, **47**; TF1-ThM11,
 197; TF-FrM2, 260
 Elder, L.F.: AS-TuP28, 107
 Elhadji, S.: TF+SA+MI-TuM10, 72
 Eliezer, S.: AC+MI-WeM6, 123
 Elisabeth, S.: TF+PS+SE-MoA3, 49
 Ellefson, R.E.: VT-MoA11, **52**
 Ellinger, C.R.: TF2-ThM2, **198**
 Ellingsworth, E.: MI-TuA4, 84
 Ellis, C.: TF+EM+MI-WeA1, 169
 Elliston, B.: PS-ThP13, 237
 Eloffson, V.: SE+NS+TF+TR-TuM3, 65
 Elsayed-Ali, H.E.: PS-ThP2, 235
 Elyaakoubi, M.: TF+PS+SE-MoA1, 48
 Enders, A.: TF+SA+MI-TuM2, 71
 Endeve, E.: AS+SS-TuA2, 79
 Endo, K.: PS-WeA9, 163
 Engelhard, M.H.: AS-MoM1, 3; EM+NS-
 WeM10, 129; MS-TuA10, 87
 Engelkamp, B.: MI+2D+AC-MoA8, 32
 Engelmann, S.U.: PS-MoA2, 40; PS-MoA9,
 41; PS-MoM2, **17**; PS-ThP9, 236
 Engler, M.: HI+MI+NS-ThA12, 212
 English, C.R.: EM-MoA3, 29
 Engstrom, J.R.: SA+2D+AC+AS+TF-TuM5, 64;
 TF+SA+MI-TuM11, **72**
 Enriquez-Carrejo, J.L.: TF-ThP34, 245
 Enyashin, A.: AS+AC-TuM13, 56
 Eom, C.-B.: SP+AS+MI+NS+SS-TuM1, 66
 Eren, B.: IS+HC-WeA3, 158; IS-ThA2, 212; IS-
 ThA9, **213**
 Eriguchi, K.: TR+BI+SE+TF-ThA8, 225
 Ernst, K.-H.: SS-ThM3, **195**
 Ernst, P.: SE+TR-WeM2, 137
 Esan, D.A.: HC+SS-ThM1, **183**
 Eschbach, M.: MI+2D+AC-MoA1, 31
 Escobedo-Alcaraz, R.: NS-TuP7, 112
 Escorihuela, J.: TF-ThA3, 223
 Espiau de Lamaestre, R.: TF+MI-WeA9, 172
 Espinosa-Marzal, R.M.: SS+AS-WeM10, 143;
 SS-ThM10, **195**
 Esposito, D.: AS-TuP26, 107
 Esquinazi, P.: MI+2D+AC-MoA9, 32
 Estevez, L.: AS-MoM1, 3
 Evans, J.W.: SS1+AS+HC+NS-TuM12, 69
 Evans, K.: EM+NS+PS+SS+TF-MoM8, 8
 Evans-Lutterodt, K.: MS-TuA4, 86
 Evoy, S.: BI+MI-WeM1, **126**
 Ewing, P.R.: PS-TuM3, 62
 Exarhos, S.A.: EM+NS-WeM6, **129**; EM-ThP3,
 230
 — F —
 Facsko, S.: HI+MI+NS-ThA12, 212
 Fadley, C.: TF+SA+MI-TuM4, 72
 Fadley, C.S.: SA+AS-MoA1, **41**
 Fadnek, A.: PS-WeM10, 137
 Fain, J.S.: EM+SS+TF-ThA6, **207**
 Fairley, N.: AS-MoM10, 5; SS+2D-WeM2, 141
 Fali, A.: EM+NS+PS+SS+TF-MoM5, 7; EM-
 ThP2, 230; SP+AS+MI+NS+SS-MoM8, 20;
 SP-TuP6, **115**
 Falk, M.L.: TR+AS+NS+SS-WeA1, **172**
 Falkenberg, G.: AS+SS-TuA1, 79
 Fang, F.: TF-ThP5, 241
 Fankhauser, F.: 2D+TF-WeM13, 122

Author Index

- Fantini, A.: EM+MI+MN-TuA9, 83
 Faraz, T.: PS+TF-WeA11, **161**; PS+TF-WeA7, 161
 Farber, R.G.: HC+SS-ThM3, **184**; HC+SS-WeM13, 131; SS-TuP3, 116
 Farewell, A.: NS+BI-ThA11, 217
 Farra, R.: IS-ThM5, 187
 Farrar, A.: TF+MI-WeA3, 171
 Farsinezhad, S.: NS-MoA3, 34
 Fartmann, M.: TF-ThP19, 242
 Farys, V.: TF-ThA1, 223
 Farzana, E.: EM-MoA5, 30
 Fatherley, V.E.: PS-ThP32, 240
 Fay, P.: MI-TuA9, **85**
 Fedchak, J.A.: VT-MoM5, **24**; VT-MoM6, **24**; VT-TuM12, 76
 Fedosenko, G.: IS-ThP7, 234
 Feeley, G.M.: SS2+AS+HC+NS-TuM4, 70
 Feenstra, R.: 2D+MI+SA-MoM1, 2
 Fehling, D.T.: PS-WeM10, 137
 Fei, X.: 2D+TF-WeM11, 122
 Feidenhans'l, R.: AS+SS-TuA1, 79
 Feigelson, B.N.: EM-FrM5, 254
 Feldman, L.C.: EM-MoA9, 31
 Feldmann, M.: TR+AS+NS+SS-WeA12, 174
 Felts, J.R.: 2D-ThA11, **202**
 Feltz, A.: SP+AS+MI+NS+SS-MoM3, 20
 Feng, P.X.-L.: 2D+NS-FrM2, 249; 2D+NS-FrM6, 250; 2D+NS-WeA1, 149; MN+2D+NS-ThA6, 214; MN+2D+NS-ThA8, 215; MN+BI-ThM4, 189; MN+MS-FrM12, **258**; PS+SE-MoM9, 16
 Feng, Y.: MN-ThP1, 234
 Fenton, J.: AS-WeA9, **152**
 Ferguson, I.T.: MS-MoA10, **34**
 Fernandez, V.: SS+2D-WeM2, **141**
 Fernando, N.S.: EL+AS+EM+MI+TF-FrM4, 252; EL+AS+EM+TF-ThP1, 229; SE+2D+EM-WeA9, **165**
 Ferrari, V.: MI+2D+AC-MoA2, 31
 Field, D.A.: SS1+AS+HC+NS-TuM4, 68
 Fields, C.: PS-ThP6, **235**; VT-TuM13, 76
 Filler, M.A.: EM+NS-WeM12, 129; NS-MoA11, 35; SS2+AS+HC+NS-TuM12, **71**
 Filleter, T.: 2D+NS-WeA8, **149**
 Fink, K.: PS-ThA8, 219
 Firestone, M.: NS-TuM6, 59
 Fischer, A.: AS-ThA10, 204
 Fischer, G.: PS-WeM2, **136**
 Fisher, E.R.: PB+BI+PS-MoA10, 36; PS+TF-WeA3, 160; PS-ThP25, 239
 Fisher, G.L.: AS+BI-MoA10, **29**; AS+SS-ThM11, 179; AS+SS-WeM3, 125; AS-WeA2, 151
 Fisher, K.J.: MN+MS-FrM2, 257
 Fishman, R.: MI+2D+AC-MoM4, 10
 Fitzell, K.: SE+2D+EM-WeA12, **166**
 Fitz-Gerald, J.M.: BI+PB-TuP8, 109; SE+MS+TF-TuA1, 91
 Flämmich, M.: VT-TuA11, **101**
 Flatoff, D.: AS+SS-ThM3, 178
 Fleetwood, D.M.: MN+MS-FrM8, 257
 Fletcher, I.W.: AS+SS-TuA11, 80
 Fletcher, J.S.: AS+BI-MoA6, 28; AS-TuP18, 105; NS+BI-ThA11, **217**
 Florian, D.C.: BI+PB-TuP8, **109**; SE+MS+TF-TuA1, 91
 Floro, J.A.: TF1-ThM1, **196**
 Fo, J.G.: VT-TuP4, 119
 Fockaert, L.I.: TF-ThA6, 223; TF-ThP2, 241
 Föhlisch, A.: SA+AS+MI-MoM10, **19**
 Foley, B.M.: EM+SS+TF-ThA11, 208; PS+SE-MoM11, 16
 Fong, D.: TF+SA+MI-TuM5, **72**
 Fonseca, N.M.: BI+AS+SA-ThM10, **181**
 Fornari, E.: BI+AS+SA-TuA3, 82
 Förster, T.: MI+2D+AC-MoA3, 32
 Fortuna, F.: SA+2D+AC+AS+TF-TuM2, 63
 Fortunelli, A.: SS+AS-TuA9, 95
 Foster, M.: IS-FrM8, **256**; SS-TuP10, 117; SS-TuP2, 116; SS-TuP6, 117
 Foucher, M.: PS-TuM1, 61
 Fourkas, J.T.: PS-ThA9, 219
 Fowler, D.: TF+MI-WeA9, 172
 Fowler, J.E.: BI+AS-MoM1, 5
 Fowlkes, J.D.: HI-WeA8, 157; NS-MoM5, 13
 Foxon, C.T.: 2D+NS-WeA11, 150
 Franchini, C.: SS+AS+HC-MoA8, 46
 Franke, A.: EM+NS+PS+SS+TF-MoM1, 7
 Frantzeskakis, E.: SA+2D+AC+AS+TF-TuM2, 63
 Franz, G.: PS-TuM12, **62**
 Franz, J.: BI+AS-MoM1, 5
 Franz, R.: SE+TR-WeM12, **138**; SE-TuP7, 114
 Freedy, K.M.: EM+SS+TF-ThA11, **208**
 Freeman, M.R.: MN+NS-WeA3, 159; MN+NS-WeA8, **160**
 Frenkel, A.I.: IS-ThM10, 188; IS-ThM12, **188**
 Frese, N.: HI+MI+NS-ThA7, **211**
 Freund, H.: SS+AS-ThA7, **220**
 Friddle, P.: PS-MoM4, 17
 Fried, J.: EM+AC+SS+TF-ThM10, 183
 Fried, L.: NS-TuM6, 59; SA-TuP2, 113
 Friederich, P.: PS-ThA8, 219
 Friedman, A.L.: 2D+MI+SA-MoM2, 2; 2D+MI-ThM5, **175**
 Friedman, S.L.: MS+AS-TuM11, **58**
 Frolet, N.: PS2-ThM5, 193
 Fu, C.: SS-TuP8, 117
 Fu, H.: PS+2D-TuA3, 89
 Fu, T.Y.: HI+NS-ThM2, 186; HI-ThP1, 232
 Fujimoto, K.: PS-ThP33, 240
 Fujita, T.: MI-TuA11, 85
 Fujitani, T.: SS-TuP1, 116
 Fujiwara, Y.: SE-TuP1, **113**
 Fukasawa, M.: PS-MoM3, 17; PS-ThA8, 219
 Fullerton-Shirey, S.K.: 2D+MI+SA-MoM1, 2
 Fung, H.: TF+EM+MI-WeA11, 170
 Funke, S.: EL+AS+EM+MI+TF-FrM8, 253
 Furchner, A.: 2D-ThA12, 202
 Furdyna, J.: 2D+MI+SA-MoM1, 2
 Furnemont, A.: PS-ThP33, 240
 Furnish, T.A.: SE+NS+TF+TR-TuM4, 65; TR+BI+SE+TF-ThA10, 226
 — **G** —
 Gadzuk, J.W.: SS+AS-ThA2, **220**
 Gage, S.: AS-TuP26, **107**
 Gai, Z.: SP+2D+AS+NS+SS-MoA10, 44; SP+2D+AS+NS+SS-MoA11, 44
 Gaidau, C.: SE+TR-WeM12, 138
 GAILLARD, F.G.: NS-MoM8, 13
 Galatage, R.: PS-ThP15, 237
 Galhenage, R.P.: IS-ThA12, **214**
 Gallagher, M.C.: SS-TuP8, 117
 Galoppini, E.: SS+HC-FrM4, 259
 Gamage, S.: EM+NS+SP+SS-WeA9, 154; SP+AS+MI+NS+SS-MoM8, 20; SP-TuP4, 115; SP-TuP5, 115; SP-TuP6, 115; SP-TuP7, **115**
 Gamalski, A.: IS-ThM10, 188
 Gamble, L.J.: BI+AS+SA-TuA10, 82; BI+AS+SA-TuA11, 83; BI+MI-WeM12, **128**
 Gan, L.: 2D+TF-WeM11, 122
 Ganapathi, K.: 2D-ThA8, 201
 Gangavarapu, P.: MN+2D+NS-ThA7, 215
 Gangireddy, R.: EM-MoA4, 30
 Ganguly, S.: NS-TuA12, 88
 Gans, T.: PS+AS+SS-MoA11, 39; PS-TuM10, 62
 Gao, F.: SS+AS+EM-WeA10, **168**
 Gao, H.J.: 2D+TF-WeM11, 122
 Gao, L.: 2D+TF-WeM11, **122**
 Gao, Z.N.: TF-TuA10, **99**
 Gapp, N.D.: SE+MS+TF-TuA7, 92
 Garces, N.Y.: EM-MoA3, 29
 Garcia, A.J.: BI+AS+SA-ThM5, **181**
 Garcia, B.: AS-ThA10, 204
 Garcia, R.: NS-TuA1, **87**; SP+AS+MI+NS+SS-MoM10, 20; SP+AS+MI+NS+SS-MoM4, 20
 Garcia-Casillas, P.E.: TF-ThP34, 245
 Garcia-Sotelo, A.: NS-TuP7, 112
 Garg, S.: 2D+TF-WeM10, 122; 2D-ThA4, **201**
 Garratt, E.: 2D+TF-WeM12, 122
 Gaskill, K.: TF1-ThM10, 197
 Gaspar, D.J.: AS-MoM1, **3**
 Gassilloud, R.: PS-WeM3, 136
 Gasvoda, R.J.: PS+TF-WeA8, 161; PS-WeA12, **164**; TF-MoM10, 23
 Gautier, N.: TF+PS+SE-MoA3, 49
 Gay, G.: PS2-ThM6, **193**
 Gebhardt, C.R.: AS-TuP8, **103**
 Gehlmann, M.: MI+2D+AC-MoA1, 31
 Geisler, H.: SS-TuP9, **117**
 Gelb, L.D.: AS-ThA8, 203
 Gellman, A.J.: SS-ThM4, **195**
 Geng, D.: EM+NS+SP+SS-WeA10, 154
 Gentry, K.: EM+NS+PS+SS+TF-MoM8, 8
 Geohagan, D.B.: 2D+NS-WeA3, 149; SS+AS+HC-MoM8, 22
 George, S.M.: PS+TF-WeM12, 135; PS+TF-WeM13, 135; TF-TuA9, 99; TF-TuM12, 74; TF-TuM2, 73
 Gerdes, H.: TF+PS+SE-MoA11, 51
 Gernold, Z.A.: AS-TuP15, 104
 Gerratt, A.: MN-WeM1, 132
 Gessert, T.A.: SS+2D-WeM6, 142
 Gharbi, A.: TF-ThA1, 223
 Ghesquiere, J.: SE+MS+TF-TuA9, 92
 Ghimire, K.: EL+AS+BI+EM+TF-ThA6, 205
 Ghiringhelli, L.M.: HC+SS-ThA1, 208
 Ghodssi, R.: BI+PB-TuP2, 107; MN+BI-ThM12, 190; NS+BI-ThA8, 216
 Ghosh, R.: 2D+MI+SA-MoM10, **3**
 Ghosh, S.: AS-TuP17, 105; EM-MoM8, 9; PS+SE-MoM6, 15; PS+SE-MoM9, **16**
 Giannuzzi, L.A.: HI+MI+NS-ThA6, **211**
 Gibson, A.R.: PS+AS+SS-MoA11, 39
 Gierak, J.: HI+NS-ThM5, **186**
 Gignac, L.: TF+EM+MI-WeA10, 170
 Gilbert, U.P.A.: SA+AS+BI+MI-TuA1, **90**
 Gilchrist, K.H.: MN+MS-FrM4, 257
 Giles, A.: TF+EM+MI-WeA1, 169
 Gilis, N.: HC+SS-ThM10, 185
 Gilliland, D.: BI+AS+SA-TuA2, 81
 Gillman, E.D.: PS+SE-MoM11, 16; PS-ThP30, **239**
 Gilmore, I.S.: AS+BI-MoA8, **28**; AS+BI-MoA9, 29; AS+SS-ThM12, 179; AS-MoM9, 5; AS-ThA6, 203
 Giolando, D.: EL+AS+BI+EM+TF-ThA9, 206
 Giorgio, T.D.: NS-TuP5, 112
 Giri, A.: EM+SS+TF-ThA11, 208; PS+SE-MoM11, 16
 Girolami, G.S.: TF-FrM5, 260; TF-FrM7, 261; TF-ThP39, 246
 Givon, A.: AS-MoM11, **5**; SP+SS+TF-WeM13, 141
 Gkogkou, D.: 2D-ThA12, 202
 Glam, B.: AC+MI-WeM6, 123
 Glaser, E.R.: MN+MS-FrM2, 257
 Glass, J.T.: MN+MS-FrM4, 257
 Glavin, N.R.: 2D+NS-FrM1, 249; 2D-ThP5, 227
 Glazyrina, P.: AS+AC-TuM13, 56
 GLEASON, K.: PS+2D-TuA7, 89

Author Index

Go, E.: NS-TuP9, 112
 Goacher, R.E.: AS+SS-WeM5, **125**; AS-TuP15, 104; AS-TuP16, 104
 Goeckner, M.J.: PS-TuM5, 62; PS-WeM6, 137
 Goh, Tong.: TF-ThP17, 242
 Golbek, T.W.: BI+AS-MoM1, **5**
 Goldbart, O.: AS+AC-TuM13, 56
 Goldman, R.S.: EM-FrM2, 253
 Götzhäuser, A.: HI+MI+NS-ThA7, 211
 Gomez, M.: 2D+MI-ThM6, 175; 2D-ThP13, 229
 Gong, H.: MN+MS-FrM10, 258
 Gonon, P.: PS-WeM3, 136
 Gonzales, J.M.: 2D+MI-ThM2, **175**
 González, D.L.: SS1+AS+HC+NS-TuM10, 68
 Goodwin, C.M.: AS+SS-ThM10, **179**; AS+SS-ThM13, 180
 Goodyear, A.L.: PS-ThP14, 237
 Gorai, P.: TF-TuA8, 99
 Gordon, M.J.: PS+2D-TuA1, 88; SP+AS+MI+NS+SS-MoM11, **20**
 Gordon, W.: IS-FrM6, 255
 Gorkhover, L.: IS-ThP7, 234
 Gospodarcic, P.: MI+2D+AC-MoA1, 31
 Goss, M.: PS-MoM10, 18
 Gosztola, D.J.: TF2-ThM10, 199
 Gotoh, K.: PB+BI+PS-MoA11, 37
 Gottfried, D.: MS-TuA1, 85
 Gottfries, J.: NS+BI-ThA11, 217
 Gottschall, S.: VT-TuA11, 101
 Goubert, G.: SP+AS+MI+NS+SS-TuM2, 66
 Gouder, T.: AC+MI-WeA11, 151
 Goulding, R.H.: PS-WeM10, 137
 Goulet, A.: TF+PS+SE-MoA3, 49
 Gourgon, C.: PS2-ThM5, 193
 Goux, L.: EM+MI+MN-TuA9, 83
 Goves, M.: SS-ThM5, 195
 Govoreanu, B.: EM+MI+MN-TuA9, 83
 Graber, T.: IS-ThP7, **234**; NS-TuM6, 59
 Gracias, D.: MN+BI-ThM10, **189**
 Graham, D.J.: BI+AS+SA-TuA11, **83**; BI+MI-WeM12, 128
 Graham, M.E.: TR+BI+SE+TF-ThA4, 225
 Graham, S.: TF+PS+SE-MoA6, 50; TF-FrM4, 260
 Granier, A.: TF+PS+SE-MoA3, **49**
 Grant, J.T.: EL+AS+BI+EM+TF-ThA3, 205; EL+AS+BI+EM+TF-ThA4, 205
 Gravrand, O.: TF+MI-WeA9, 172
 Gray, A.X.: SA+AS-MoA10, **43**
 Gray, J.: NS-MoM1, 12; SE+2D+EM-WeA8, 165
 Green, A.: EL+AS+EM+MI+TF-FrM8, 253
 Green, D.E.: MS-MoA3, **33**
 Green, D.L.: PS-WeM10, 137
 Greenaway, A.L.: TF-TuA8, 99
 Greenburg, M.J.: TF+MI-WeA12, 172
 Greenzweig, Y.: HI+MI+NS-ThA9, **211**; HI-WeA4, 157
 Gregar, K.C.: MS-TuA8, **86**
 Gregorczyk, K.: MS-MoM6, 12; MS-MoM9, 12
 Grehl, T.: AS-TuP7, 103; TF-ThP19, **242**
 Grenet, G.: SA+AS-MoA5, 42
 Greving, M.: TF+BI-ThA8, 222
 Grice, C.R.: EL+AS+BI+EM+TF-ThA10, 206
 Griego, J.R.: PS-ThP32, 240
 Grier, T.: MS-TuP5, 111
 Grierson, D.: TR+AS+NS+SS-WeA9, 173
 Griffin, J.: 2D+TF-WeM5, 121
 Groß, A.: HC+SS-ThA8, **209**
 Groza, M.: BI+MI-WeM13, 128; EM+AC+SS+TF-ThM1, 182
 Grozinger, C.M.: AS-ThA7, 203
 Grundmeier, G.: SS+AS+HC-MoA11, 46

Grunze, M.: SS+AS-ThA8, **221**
 Grutzik, S.J.: MN-WeM5, 132
 Grützmacher, D.: MI+2D+AC-MoA1, 31
 Gschneidner, K.A.: AC+MI-WeM12, 124
 Guaitella, O.Y.N.: PB+BI+PS-TuM12, 61; PS-TuM1, 61
 Gudmundsson, J.T.: PS1-ThM1, **190**
 Guenther, B.: SP+AS+MI+NS+SS-MoM3, 20
 Guerrier, J.E.: MN+MS-FrM2, 257
 Guesquière, J.: PS-ThP22, 238
 Guisinger, N.P.: 2D+MI-TuM4, 53; SP+SS+TF-WeM11, **140**
 Guiton, B.S.: IS-FrM10, 256
 Gujrati, A.: TR+AS+NS+SS-WeA11, 173
 Gunlycke, D.: 2D+MI-MoA5, 26; 2D+MI-ThM11, **176**
 Guo, D.: 2D+MI-MoA8, 27; PS-MoM10, 18
 Guo, G.: VT-MoA5, 51
 Guo, H.X.: IS-ThP9, **234**
 Guo, X.: TF+EM+MI-WeA11, 170; TF+EM+MI-WeA12, 170
 Gupta, G.: 2D+NS-FrM11, 251
 Gupta, P.: TR+BI+SE+TF-ThA4, **225**
 Gupta, S.: 2D+MI-TuM12, **54**; SE+2D+EM-WeA2, 164; TF+MI-WeA7, 171
 Gurrieri, T.: TF+EM+MI-WeA9, 170
 Gustavsen, R.: NS-TuM6, 59
 Gutierrez Razo, S.: PS-ThA9, 219
 Guzman, A.: AS-ThA11, 204
 — H —
 Hacker, C.A.: TF-ThA7, 224
 Hagen, J.: AS-TuP23, 106
 Haglund, R.F.: EL+AS+EM+TF-ThP3, 229; SP-TuP4, 115
 Hagmann, M.J.: SP-TuP8, **115**
 Haider, A.: EM+NS+PS+SS+TF-MoM3, 7
 Halevy, I.: AC+MI-WeM6, **123**
 Hallman, K.: EL+AS+EM+TF-ThP3, 229
 Hall-Wilton, R.: TF+PS+SE-MoA4, 49
 Halsall, B.: PS-ThP14, 237
 Hamada, Y.: TF-ThP17, 242
 Hamaguchi, S.: PB+BI+PS-MoA11, 37; PS+AS+SS-MoA1, **37**; PS1-ThM13, 192; PS-ThA11, 219; PS-ThA8, 219
 Hamers, R.J.: NS-TuM10, **59**
 Hamilton, M.C.: EM-MoA8, 30
 Hammer, B.: 2D+MI-TuM13, 54; SS-ThM5, 195
 Hammond, J.S.: AS+BI-MoA10, 29; AS+SS-WeM3, 125; AS-TuP9, 104; AS-WeA2, **151**
 Hammond, R.: 2D-ThP7, 228; NS-MoM1, 12
 Hammouti, S.: PS2-ThM11, 194; SE+MS+TF-TuA10, 93
 Han, J.H.: TF-ThP12, 242
 Han, L.: MN+2D+NS-ThA6, 214
 Han, S.E.: EM-MoM6, 9; EM-MoM8, 9
 Han, S.J.: EM-MoM8, **9**
 Han, S.M.: EM+NS+SP+SS-WeA3, 153; EM-MoM6, 9; EM-MoM8, 9; SE+MS+TF-TuA7, 92
 Hanaguri, T.: SP+2D+AS+NS+SS-MoA5, **44**
 Hanay, S.: MN+BI-ThM3, **189**
 Hanbicki, A.T.: 2D+MI+SA-MoM2, **2**; 2D-ThA10, 201
 Handa, H.: BI+AS-MoM3, **6**
 Hangarter, S.C.: 2D-ThA6, 201
 Hanley, L.: EM+NS-WeM1, **128**
 Hanna, A.R.: PS-ThP25, **239**
 Hannesdottir, H.: PS1-ThM1, 190
 Hansen, D.: NS-TuM6, 59; SA-TuP2, 113
 Hansen, R.P.: SS2+AS+HC+NS-TuM3, **69**
 Hao, Y.: IS-ThA2, 212
 Haran, B.: PS-MoM9, 18
 Harb, J.: NS-TuP4, 112
 Harpale, A.: PS+2D-TuA9, 89

Harrell, W.R.: SS1+AS+HC+NS-TuM4, 68
 Harris, G.L.: 2D+TF-WeM5, 121; MS-MoA3, 33
 Harrison, E.: AS+BI-MoA1, **27**
 Harrison, I.: SS+HC-TuA8, 97
 Harriss, J.E.: SS1+AS+HC+NS-TuM4, 68
 Hart, J.: SE+2D+EM-WeA9, 165
 Hase, W.L.: HC+SS-ThA12, **210**
 Hasegawa, S.: TR+BI+SE+TF-ThA8, 225
 Hasegawa, Y.: MS-TuP4, 111
 Hashizume, H.: PB+BI+PS-TuM11, 61
 Hauffman, T.: TF-ThA6, 223; TF-ThP2, **241**
 Hausmann, D.M.: PS+TF-WeA11, 161; PS+TF-WeA8, 161; TF-MoM10, 23
 Hävecker, M.: IS+HC-WeA1, 158
 Havela, L.: AC+MI-WeA11, **151**; AC+MI-WeM5, 123
 Havelund, R.: AS+BI-MoA8, 28; AS+SS-ThM12, 179; AS-MoM9, **5**
 Havercroft, N.J.: AS+SS-ThM12, 179; AS-TuP7, **103**; EW-WeM8, **130**; HI+MI+NS-ThA3, 210
 Hawtof, R.: PS+SE-MoM6, 15
 Hayashi, T.: PS-ThA10, 219
 Hazbun, R.: SE+2D+EM-WeA9, 165
 He, S.: 2D-TuA1, **78**
 He, Y.: TF+MI+NS-WeM10, 145
 Head, A.R.: SS+AS+HC-MoA10, **46**; TF-ThA6, 223
 Heben, M.: EL+AS+BI+EM+TF-ThA9, 206
 Heckman, E.M.: 2D-ThP5, 227
 Heeger, M.: BI+PB-TuP5, 108
 Heeren, R.M.A.: AS+BI-MoA10, 29; AS+BI-MoA2, 27
 Heffelfinger, J.: AS-WeA9, 152
 Heilman, A.L.: SP+AS+MI+NS+SS-MoM11, 20
 Heine, C.: IS+HC-WeA3, **158**
 Heinonen, O.: MI+2D+AC-MoM3, 10
 Heinrich, A.J.: SP+AS+MI+NS+SS-TuA3, 93
 Helal, Y.H.: PS-TuM3, **62**
 Heldebrandt, D.: IS-FrM9, 256
 Hellberg, C.S.: 2D+MI+SA-MoM2, 2
 Helle, M.H.: PS-ThP30, 239
 Hemminger, J.C.: IS-ThA12, 214; SS+AS+HC-MoA9, 46; SS+AS-TuA4, 95
 Hemmingson, S.L.: SS2+AS+HC+NS-TuM4, 70
 Henderson, M.A.: SS+HC-TuA7, 97
 Hendricks, J.: VT-MoM3, **24**; VT-MoM4, 24
 Henk, J.: MI+2D+AC-MoA8, 32
 Hennig, C.: AC+AS+SA-ThM4, 176
 Henri, J.: PS+TF-WeA11, 161
 Hensgens, Toivo: MI-TuA11, **85**
 Herath, N.: MI-TuP2, **110**
 Herbots, N.X.: AS+SS-WeM1, 124; BI+PB-TuP11, **109**; SE+2D+EM-WeA3, 165; SS+HC-FrM1, 258
 Hercules, D.M.: SS+AS-ThA3, **220**
 Hermann, R.: SP+AS+MI+NS+SS-MoM11, 20
 Hernández, E.: PS-ThP8, 236
 Hernandez, S.C.: PS-ThP5, 235; PS-WeA3, 162
 Hernández, S.C.: PS+2D-TuA11, **89**; PS+SE-MoM11, 16; PS-ThP30, 239; PS-ThP9, 236; TF+SA+MI-TuM12, 73
 Hernandez-Arriaga, H.: TF-ThP34, 245
 Hernandez-Hernandez, A.: NS-TuP7, 112
 Hernandez-Marquez, J.A.: TF-ThP34, 245
 Heron, J.T.: EM-FrM2, 253
 Herrera-Gomez, A.: AS+SS-TuA7, 80; AS-MoM4, **4**
 Herrmann, H.W.: PS-ThP32, 240
 Hersam, M.C.: 2D+MI-TuM4, 53; SP+AS+MI+NS+SS-TuM2, 66
 Heslop, S.L.: EM-ThP7, 231; SS+AS+EM-WeA11, **168**

Author Index

- Heyne, M.: TF+EM+MI-WeA3, 169
 Heyrich, H.: HC+SS-ThM3, 184
 Hibbard, N.: AS-WeA1, 151
 Hickey, R.: SE+2D+EM-WeA9, 165
 Hidaka, A.: MS+AS-TuM1, 57
 Hiebert, W.K.: BI+MI-WeM2, 127; MN+NS-WeA3, 159
 Higgs, J.: TF-TuM12, **74**
 High, E.H.: HC+SS-ThM4, 184; IS-ThP8, 234
 Higuchi, Y.: PS1-ThM3, 190
 Hilton, D.R.: VT-MoA8, 52
 Hilton, J.: SP+AS+MI+NS+SS-MoM3, 20
 Hines, M.A.: SS+AS-WeM6, 143; SS+HC-TuA2, 97
 Hingerl, K.: IS-ThA11, 213
 Hinkle, C.L.: 2D-TuA12, 78; SE+2D+EM-WeA10, 166
 Hinrichs, K.: 2D-ThA12, **202**
 Hinton, K.: TF+MI+NS-WeM6, 145
 Hirahara, T.: SP+2D+AS+NS+SS-MoA8, **44**
 Hiramoto, M.: PS-ThP10, 236
 Hirose, F.: TF-ThP33, 245
 Hisamatsu, H.: VT-TuA3, 100; VT-TuP2, 119
 Hisamatsu, T.: PS+AS+SS-MoA4, 37
 Hite, J.K.: EM-FrM5, 254; EM-MoA3, 29
 Hitz, E.: MS-MoM9, 12
 Hjort, M.: EM+NS+SP+SS-WeA4, 153
 Hla, S.W.: SP+AS+MI+NS+SS-MoM2, 19
 Hlawacek, G.: HI+MI+NS-ThA12, **212**
 Ho, W.: SP+AS+MI+NS+SS-TuM10, **67**
 Hoard, B.R.: EM-MoM8, 9
 Hobart, K.: EM-MoA10, 31
 Hobbs, R.G.: NS+BI-ThA3, 215
 Hockenbery, D.: BI+AS+SA-TuA10, 82; BI+MI-WeM12, 128
 Hodgins, R.: NS-TuM6, 59; SA-TuP2, 113
 Hofer, U.: SS+AS+EM-WeA2, 167
 Hoff, F.H.: AS-TuP29, 107
 Hoffman, A.: 2D+MI-MoA6, **26**; 2D+NS-FrM10, 250; 2D-ThP11, 228
 Hoffmann, A.: EM+NS+PS+SS+TF-MoM5, 7; MI+2D+AC-MoM3, **10**
 Hoffmann, M.: HC+SS-ThA7, 209
 Hoffmann, P.: TF-TuM3, 73
 Hofmann, P.: 2D+MI+SA-MoM8, **3**; 2D+MI-TuM13, 54
 Hofmann, T.: EL+AS+EM+MI+TF-FrM3, **251**
 Höglund, C.: TF+PS+SE-MoA4, 49
 Hojnik, N.: PB+BI+PS-MoA2, 35
 Holcomb, M.B.: MI+2D+AC-MoM10, **11**
 Holländer, B.: MI+2D+AC-MoA1, 31
 Hollemans, C.L.: VT-TuA10, 101
 Holliday, K.S.: AC-TuP1, 102
 Hollingworth, N.: TF+MI+NS-WeM6, 145
 Holybee, B.: SE-TuP4, 114
 Homeijer, B.: MN+MS-FrM8, 257
 Honda, M.: PS+AS+SS-MoA4, 37
 Hong, K.: HI+MI+NS-ThA4, 210; MI-TuP2, 110; SP+AS+MI+NS+SS-TuM5, 67
 Hong, S.: HC+SS-ThA11, 210; SS1+AS+HC+NS-TuM13, 69
 Hong, S.-Y.: SS+AS+HC-MoA6, 45; SS1+AS+HC+NS-TuM2, **67**
 Honnell, P.D.: VT-TuM6, 76
 Hoogstrate, A.M.: VT-TuA10, 101
 Hook, A.L.: BI+AS-MoM5, 6
 Hook, D.J.: AS-ThA12, 204
 Höök, F.: BI+MI-WeM5, **127**
 Hooper, D.: SS+AS+HC-MoM8, 22
 Hopkins, P.E.: EM+SS+TF-ThA11, 208; PS+SE-MoM11, 16; TF-FrM3, 260
 Hopstaken, M.J.P.: MS+AS-TuM5, **57**
 Hori, M.: PB+BI+PS-TuM11, 61; PS+TF-WeM1, 134; PS+TF-WeM10, 134; PS-ThA10, 219
 Horiike, Y.: PS-ThA10, 219
 Horikawa, T.: PS-ThP18, 237
 Horiuchi, K.: MS-TuP4, **111**
 Hornekær, L.: 2D+MI-TuM6, 53
 Hornicek, G.: TF+EM+MI-WeA10, 170
 Horning, S.: AS+BI-MoA8, 28; AS+SS-ThM12, 179
 Hossain, A.: EM+AC+SS+TF-ThM10, 183
 Hossain, R.: 2D-ThP2, 227
 Hou, J.: EM-MoM10, 9
 Hovsepian, P.Eh.: SE+TR-WeM5, **138**
 Howard, M.: 2D-ThP8, 228; 2D-ThP9, 228; SP-TuP5, 115
 Howe, B.M.: TF-ThP41, 246
 Howe, J.Y.: 2D+NS-WeA8, 149
 Howell, C.: BI+AS-MoM2, **6**
 Howell, L.: TF+BI-ThA8, 222
 Hrebik, J.: PS-WeM12, 137; TF+PS+SE-MoA11, **51**
 Hsiao, C.N.: IS-ThP4, 233
 Hsiao, C.-N.: EM-ThP9, **232**; SE-TuP3, 114
 Hsiao, C.-N.: PS-ThP1, 235
 Hsiao, C.-N.: TF-ThP30, 244
 Hsieh, C.H.: NS-TuP8, **112**
 Hsu, A.: PS-ThP32, 240
 Hsu, J.: 2D-TuA12, 78; SE+2D+EM-WeA10, 166
 Hsu, K.: EM+MI+MN-TuA11, **83**; EM-ThP6, 231; TF+EM+MI-WeA11, 170
 Hu, C.-K.: TF+EM+MI-WeA10, **170**
 Hu, E.: 2D+TF-WeM5, 121
 Hu, J.: 2D+NS-WeA1, 149; MN+MS-FrM6, **257**
 Hu, J.J.: 2D+NS-FrM1, 249
 Hu, J.N.: NS-TuP1, 111
 Hu, Q.: NS-TuA9, **87**
 Hu, S.: 2D+NS-FrM12, 251
 Hu, W.: EM+NS-WeM12, **129**
 Hua, X.: AS+SS-WeM12, 126
 Huang, C.-Y.: MI+2D+AC-MoM10, 11
 Huang, H.: EM+NS+SP+SS+TF-WeA10, 154; TF+EM+MI-WeA10, 170
 Huang, J.: MI-TuP2, 110
 Huang, M.J.: NS-TuP8, 112
 Huang, S.: PS-MoA4, **40**; PS-MoA8, 40; PS-ThP12, 236
 Huang, S.W.: NS-TuP1, 111
 Huang, W.J.: NS-TuP1, **111**; TF1-ThM3, 196
 Huang, Y.: TF2-ThM1, 198
 Huard, C.M.: PS+TF-WeM4, **134**; PS-MoA4, 40
 Huber, D.: MS-TuA9, **87**
 Huber, F.: AC+MI-WeA11, 151
 Huber, T.: 2D+NS-FrM5, **249**
 Hubert, J.: SE+MS+TF-TuA9, 92
 Hudak, B.M.: IS-FrM10, **256**
 Hudson, E.A.: PS-WeA1, 162; PS-WeA12, 164
 Huerta-Ruelas, J.A.: AS-MoM4, 4
 Hui, H.: SS2+AS+HC+NS-TuM12, 71
 Huiszoon, R.C.: MN+BI-ThM12, **190**
 Hultman, L.: 2D+MI-TuM3, 53
 Hulva, J.: SS+AS+HC-MoA8, **46**
 Hung, C.S.: BI+PB-TuP7, 108
 Hung, R.: TF+EM+MI-WeA8, 170
 Hunold, O.: SE+TR-WeM1, **137**
 Hunter, A.: NS-TuA12, 88
 Hunter, C.N.: NS+BI-ThA6, 216
 Hus, S.: SP+2D+AS+NS+SS-MoA3, **43**
 Hussain, Z.: 2D+MI-ThM12, 176
 Hussein, R.: BI+AS+SA-TuA2, 81
 Hutton, S.J.: AS-TuP6, **103**
 Huyghebaert, C.: TF+EM+MI-WeA3, 169
 Hwang, C.S.: TF-ThP43, 247
 Hwang, I.S.: HI+NS-ThM2, **186**; HI-ThP1, 232
 Hwang, J.H.: SP-TuP3, **115**; TR+BI+SE+TF-ThA9, 226
 Hwang, S.W.: SP+AS+MI+NS+SS-TuA12, 94
 Hysmith, H.: HI+MI+NS-ThA8, 211; HI+NS-ThM10, 186
 — I —
 Ibdah, A.A.: EL+AS+BI+EM+TF-ThA6, 205
 Iberi, V.: HI+MI+NS-ThA10, 211; HI+MI+NS-ThA8, 211; HI+NS-ThM10, 186
 Ichi, T.: SE-TuP2, 113
 Ichii, T.: 2D+MI+SA-MoM5, 2; 2D-ThP10, 228; PS-WeA10, 163; SE-TuP1, 113
 Ilevlev, A.: HI+MI+NS-ThA8, 211; HI+NS-ThM10, 186
 Iida, S.: AS+BI-MoA10, 29; AS+SS-ThM11, 179; AS-WeA2, 151
 Ikeda, K.: MS+AS-TuM1, 57
 Ikeda, M.: TF1-ThM13, 198
 Ikeda, Y.: PB+BI+PS-TuM1, 59; PB+BI+PS-TuM5, 60
 Ilatikhameneh, H.: MI-TuA9, 85
 Ilavsky, J.: NS-TuM6, 59
 Ilic, B.R.: MN+NS-WeA7, 159; MN-WeM4, 132; MN-WeM5, 132
 Illana, A.: SE+TR-WeM5, 138
 Imam (Yimamu), M.: TF+PS+SE-MoA4, **49**
 Imam, M.: SA+2D+AC+AS+TF-TuM3, 63
 Iniguez, E.: NS-TuP2, 111
 Inoue, K.: BI+MI-WeM4, 127
 Inoue, R.: AS+SS-WeM3, 125
 Inspektor, A.: SE+MS+TF-TuA2, **91**
 Interlandi, G.: AS+BI-MoA1, 27
 Iordanov, I.: IS-FrM6, 255
 Ip, V.: PS-ThP12, **236**
 Isbill, S.B.: SS-TuP19, **118**
 Ishibashi, T.: VT-TuA3, 100; VT-TuP2, 119
 Ishii, H.: MS+AS-TuM1, **57**
 Ishikawa, K.: PB+BI+PS-TuM11, 61; PS+TF-WeM1, 134; PS+TF-WeM10, 134; PS-ThA10, **219**
 Iski, E.V.: HC+SS-WeM12, **131**; HC+SS-WeM13, 131
 Islam, S.: MI-TuA9, 85
 Isobe, M.: PB+BI+PS-MoA11, 37; PS1-ThM13, 192
 Ito, T.: PB+BI+PS-MoA11, 37; PS1-ThM13, 192
 Ivanov, I.: 2D+MI-MoA6, 26; MI-TuP2, 110
 Ivanov, I.G.: TF+PS+SE-MoA4, 49
 Iwasa, Y.: 2D+MI-TuM10, **54**
 Iyer, S.: NS-MoA2, 34
 Izawa, M.: PS+TF-WeM1, 134; PS+TF-WeM10, 134
 — J —
 J. Podraza, N.: EL+AS+BI+EM+TF-ThA11, 206
 Jackson, L.: HC+SS-WeM12, 131
 Jacob, D.: PS-MoA1, 40
 Jacobs, R.: SE+NS+TF+TR-TuM10, 65
 Jacobs, T.D.B.: TR+AS+NS+SS-WeA1, 172; TR+AS+NS+SS-WeA11, **173**
 Jagtiani, A.V.: PS-ThP9, 236
 Jahangir, A.: TF-ThP17, 242
 Jahnke, R.: AS-WeA9, 152
 Jain, K.: PS-ThP20, 238
 Jakowski, J.: HI+NS-ThM10, 186; MI-TuP2, 110
 Jalan, B.: TF1-ThM6, **197**; TF-ThP7, 241
 James, R.B.: EM+AC+SS+TF-ThM10, **183**
 Janke, S.M.: SS1+AS+HC+NS-TuM5, 68
 Janlamool, J.: SS-TuP5, 116
 Janssen, J.P.B.: PS-ThP23, 238
 Jansson, U.J.: TF+PS+SE-MoA9, 50
 Jarrahi, Z.: 2D-TuA8, **78**
 Javani, M.: SP-TuP7, 115
 Jelinek, P.: SP+AS+MI+NS+SS-TuM12, **67**

Author Index

Jena, D.: 2D+MI+SA-MoM1, 2; MI-TuA9, 85
 Jennings, J.: AS+SS-ThM1, 178
 Jensen, B.J.: NS-TuM6, 59
 Jensen, J.: TF+PS+SE-MoA4, 49
 Jensen, L.: SP+AS+MI+NS+SS-TuM2, 66
 Jeon, H.: NS-TuP9, 112
 Jeon, H.M.: TF-ThP41, 246
 Jeon, S.: SP+SS+TF-WeM3, **139**
 Jeong, J.S.: TF-ThP7, 241
 Jeong, J.W.: NS-TuP9, 112
 Jesse, S.: AS+SS-TuA2, **79**; HI+MI+NS-ThA8, 211; SP+AS+MI+NS+SS-MoM1, 19
 Ji, Z.: VT-MoA5, 51
 Jia, H.: 2D+NS-FrM2, 249; MN+2D+NS-ThA8, 215; MN+BI-ThM4, **189**
 Jiang, G.H.: BI+PB-TuP6, 108
 Jiang, H.: AS+BI-MoA9, 29; SS1+AS+HC+NS-TuM5, 68
 Jiang, N.: SP+AS+MI+NS+SS-TuM2, 66; SP-TuP1, **115**
 Jiang, W.: MI+2D+AC-MoM3, 10
 Jiang, X.: PS-ThP15, 237
 Jiko, N.: PS-ThP34, **240**; TF-ThP33, 245
 Jin, K.L.: NS-TuP1, 111
 Jin, M.: EW-WeL3, 148
 Jing, C.: NS-TuM5, 59
 Jinno, M.: PB+BI+PS-TuM1, 59; PB+BI+PS-TuM5, **60**
 Joachim, C.: SP+SS+TF-WeM5, 140
 Job, N.: PS2-ThM10, 193
 Joghee, P.: AS-TuP22, 106
 Johansson, P.K.: BI+AS+SA-TuA9, **82**
 Johansson, U.: AS+SS-TuA1, 79
 Johnon, N.J.: PS+TF-WeM13, **135**
 Johnson, A.T.C.: 2D+TF-WeM3, **121**
 Johnson, B.I.: TF-FrM6, **261**
 Johnson, E.V.: PS-TuM10, 62; PS-WeM1, **136**; PS-WeM2, 136; TF+PS+SE-MoA1, 48
 Johnson, G.: EM+NS-WeM10, **129**
 Johnson, J.: NS-MoM1, 12
 Johnson, M.: MS-MoM10, **12**
 Johnson, S.D.: PS-ThP5, 235; TF+SA+MI-TuM12, 73
 Jones, G.: HC+SS-WeM12, 131
 Jones, J.G.: EL+AS+BI+EM+TF-ThA3, 205; EL+AS+BI+EM+TF-ThA4, 205
 Jones, J.L.: MN+MS-FrM2, 257
 Jones, K.: TF-ThP5, **241**
 Jones, T.E.: IS+HC-WeA1, 158
 Jonker, B.T.: 2D+MI+SA-MoM2, 2; 2D-ThA10, 201
 Jordan-Sweet, J.: TF+EM+MI-WeA2, 169
 Joress, H.: TF+SA+MI-TuM3, 71
 Jørgensen, J.: 2D+MI-TuM6, **53**
 Joseph, E.A.: PS-MoA2, 40; PS-MoA9, 41; PS-MoM2, 17; PS-ThP9, 236
 Joseph, P.: MS-TuA1, **85**
 Jouan, P.Y.: SS+2D-WeM2, 141
 Joubert, O.: PS+AS+SS-MoA10, 39; PS+AS+SS-MoA5, 38; PS+AS+SS-MoA6, 38; PS-WeA2, 162
 Jousten, K.: VT-TuM10, 76
 Joy, N.: PS-MoA9, 41
 Juez-Lorenzo, J.: SE+TR-WeM5, 138
 Juhl, A.T.: 2D+NS-FrM1, 249; 2D-ThP5, 227
 Jun, Y-S.: TF+PS+SE-MoA2, 49
 Junda, M.M.: EL+AS+BI+EM+TF-ThA10, **206**; EL+AS+BI+EM+TF-ThA9, 206
 Jung, G.S.: 2D+MI-ThM1, 175
 Junge, T.: TR+AS+NS+SS-WeA11, 173
 Jungfleisch, M.B.: MI+2D+AC-MoM3, 10
 Jupille, J.: SS+AS-TuA10, 96
 Jur, J.S.: TF+MI+NS-WeM5, **145**; TF2-ThM12, 200

Jurczak, M.: EM+MI+MN-TuA9, 83
 Jurczyk, B.: PS-WeM12, 137
 Juurlink, L.B.F.: HC+SS-ThM12, **185**; HC+SS-ThM3, 184
 — K —
 Kachian, J.: SS+AS+EM-WeA7, 167; SS+AS+EM-WeA8, 168
 Kaden, W.E.: SS+HC-TuA12, **98**
 Kagan, C.R.: EM+NS-WeM3, **128**
 Kahng, S.J.: SP+AS+MI+NS+SS-TuA8, 94
 Kalanyan, B.: 2D+TF-WeM12, **122**; TF-MoM4, 22
 Kaliakin, D.S.: SS1+AS+HC+NS-TuM3, 68
 Kalihari, V.: AS-WeA8, 152
 Kalinin, S.V.: AS+SS-TuA2, 79; HI+MI+NS-ThA8, 211; SP+AS+MI+NS+SS-MoM1, 19
 Kamada, K.: BI+MI-WeM4, **127**
 Kamarajugadda, M.: TF+BI-ThA6, **222**
 Kambham, A.: AS+SS-ThM3, **178**
 Kamineneni, V.M.: TF+EM+MI-WeA10, 170
 Kaminski, P.M.: TF-TuA7, 99
 Kammler, M.: SS1+AS+HC+NS-TuM5, 68
 Kanai, Y.: BI+MI-WeM4, 127
 Kanakabasapathy, S.: PS-MoM4, 17
 Kanakasabapathy, S.: PS-MoM10, 18; PS-MoM2, 17; PS-MoM8, 17; PS-MoM9, 18
 Kanarik, K.: PS-WeA4, 163
 Kanazawa, K.: VT-TuA3, 100; VT-TuP2, 119
 Kandasamy, P.: IS-ThP3, 233
 Kandel, S.A.: HC+SS-WeM5, 130
 Kandratsenka, A.: SS1+AS+HC+NS-TuM5, 68
 Kandyba, V.: 2D-ThP13, 229
 Kane, T.: TF+EM+MI-WeA10, 170
 Kanevce, A.: TF-FrM8, 261
 Kaneza, N.: EM+NS-WeM13, **130**
 Kang, H.M.: 2D+MI-TuM5, 53
 Kang, J.T.: NS-TuP9, **112**
 Kang, S.G.: TF-ThP28, 244
 Kanjolia, R.: TF-MoM9, 23; TF-TuA10, 99
 Kankanamge, I.: SP-TuP6, 115
 Kanomata, K.: TF-ThP33, 245
 Kant, C.: EM+MI+MN-TuA12, 84
 Kanzaki, T.: HI+MI+NS-ThA11, 212
 Kanzawa, T.: SE-TuP2, **113**
 Kaplan-Ashiri, I.: AS+AC-TuM13, 56
 Kapur, M.: AS-WeA8, 152
 Kar, G.S.: PS-ThP33, 240
 Kar, S.: 2D+NS-FrM11, 251
 Karabacak, T.: TF-FrM12, 262
 Karahashi, K.: PS+AS+SS-MoA1, 37; PS1-ThM13, 192; PS-ThA11, **219**; PS-ThA8, 219
 Karppinen, M.J.: TF+EM-MoA9, **48**
 Karslioglu, O.: SS+AS+HC-MoA10, 46; SS+AS+HC-MoM10, **22**
 Karslioglu, O.: TF-ThA6, 223
 Karve, G.: PS-MoM4, 17
 Karwacki, C.: IS-FrM6, 255
 Kasanaboina, P.: NS-MoA2, 34
 Kassu, A.: 2D-ThP7, **228**; NS-MoM1, 12; SE+2D+EM-WeA8, 165
 Kaul, A.B.: 2D+TF-WeM1, 121; 2D-ThP2, 227; 2D-ThP3, 227; MS-MoA4, 33
 Kavrik, M.: PS-ThP15, **237**
 Kawahara, T.: BI+MI-WeM4, 127
 Kawai, M.: SP+AS+MI+NS+SS-MoM5, **20**
 Kawakami, N.: PS-ThP34, 240; TF-ThP33, **245**
 Kawamura, T.: TF-ThP9, **241**
 Kawamura, T.: PS-MoM3, 17
 Kay, B.D.: SS+AS-WeM12, 144; SS+HC-FrM6, 259
 Kaykhaili, M.: SE+2D+EM-WeA4, 165; TF-ThP21, **243**
 Kazyak, E.: TF+MI+NS-WeM10, 145
 Kelber, J.A.: TF+PS+SE-MoA2, **49**

Kelchner, K.M.: PS+TF-WeA8, 161; TF-MoM10, 23
 Keles, F.: TF-FrM12, 262
 Keller, S.: MI-TuA9, 85
 Kelley, M.J.: AS-TuP10, 104
 Kellner, J.: MI+2D+AC-MoA1, 31
 Kelly, D.L.: NS+BI-ThA8, 216
 Kelly, J.: TF+EM+MI-WeA10, 170
 Kelly, T.F.: AS+AC-TuM1, **54**
 Kenney, J.A.: PS+TF-WeM5, 134
 Kent, T.: SS+AS+EM-WeA7, 167
 Kepaptsoglou, D.: TF+SA+MI-TuM4, 72
 Keraudy, J.: SS+2D-WeM2, 141
 Kercher, K.: EM+SS+TF-ThA3, 207
 Kerger, P.: IS-ThA10, **213**; TF-ThP2, 241
 Kerherve, G.: IS-ThA1, 212
 Kerkhof, P.J.: VT-TuA10, 101
 Kerlain, A.: TF+PS+SE-MoA8, 50
 Kessels, W.M.M.: PS+TF-WeA11, 161; PS+TF-WeA12, 162; PS+TF-WeA7, **161**; TF+MI+NS-WeM3, 144; TF1-ThM12, 198; TF-MoM5, 23; TF-MoM8, 23; TF-TuA4, 98
 Keszler, D.A.: TF2-ThM1, 198
 Keum, J.: MI-TuP2, 110
 Keuter, P.: SE+TR-WeM1, 137
 Keyshar, K.: 2D+NS-FrM11, 251
 Khajetoorians, A.A.: 2D+MI-TuM13, 54; SP+AS+MI+NS+SS-TuA1, **93**
 Khaled, K.: EM+NS+PS+SS+TF-MoM3, 7
 Khalifa, Y.: SS+AS-WeM4, 143
 Khan, S.: TF2-ThM13, 200
 Khanal, M.P.: EM+NS+PS+SS+TF-MoM6, **8**; EM-MoA11, 31; EM-MoA8, 30
 Khanal, R.: EL+AS+BI+EM+TF-ThA9, 206
 Khanal, S.R.: TR+AS+NS+SS-WeA11, 173
 Khlobystov, A.N.: 2D+NS-WeA11, 150
 Kiba, T.: TF-ThP9, 241
 Kidd, D.W.: 2D-TuA4, **78**
 Kido, Y.: PB+BI+PS-TuM1, **59**; PB+BI+PS-TuM5, 60
 Kiehlbauch, M.: PS-MoA5, **40**
 Kievit, O.: VT-MoA4, 51
 Kihara, Y.: PS+AS+SS-MoA4, **37**
 Kildemo, M.K.: EL+AS+BI+EM+TF-ThA1, **204**
 Killelea, D.R.: HC+SS-ThM3, 184; HC+SS-WeM13, **131**; SS-TuP3, 116
 Kim, C.G.: TF-ThP12, **242**; TF-ThP28, 244
 Kim, C.S.: NS+BI-ThA3, 215
 Kim, D.-J.: EM-MoA8, 30
 Kim, E.: NS+BI-ThA8, 216
 Kim, H.W.: SP+AS+MI+NS+SS-TuA12, 94; SP+AS+MI+NS+SS-TuA8, 94
 Kim, H.Y.: TF-ThP12, 242
 Kim, J.: 2D+MI-MoA2, 26; 2D-TuA12, 78; EM-MoA4, 30; SE+2D+EM-WeA10, 166; TR+BI+SE+TF-ThA6, **225**
 Kim, J.H.: PS-ThP31, **240**
 Kim, J.W.: NS-TuP9, 112
 Kim, K.: EM+NS+PS+SS+TF-MoM6, 8; TF+PS+SE-MoA6, **50**
 Kim, K.H.: TF-ThP22, 243; TF-ThP9, 241
 Kim, M.: 2D-TuA12, 78; SE+2D+EM-WeA10, 166; SS+AS-TuA3, 95; SS-TuP4, 116
 Kim, S.: 2D+TF-WeM10, 122; 2D-ThA4, 201; SS+HC-TuA11, 97
 Kim, S.H.: NS-TuP9, 112; TF-ThP43, **247**
 Kim, T.-H.: SP+2D+AS+NS+SS-MoA4, **43**
 Kim, W.: PS-ThP33, 240
 Kim, Y.: HC+NS+SS-WeA7, 155; SP+AS+MI+NS+SS-MoM5, 20
 Kim, Y.H.: PS-ThP32, 240
 Kim, Y.-H.: SP+AS+MI+NS+SS-TuA8, 94; TR+BI+SE+TF-ThA9, 226
 Kimes, W.A.: 2D+TF-WeM12, 122
 Kimmel, G.A.: SS+HC-TuA7, **97**

Author Index

- Kimmerle, K.S.: EW-WeL6, 148
Kimmerle, W.: EW-WeL6, **148**
Kimura, A.: MI+2D+AC-MoA8, 32
King, M.: SS+HC-FrM2, **258**
King, S.W.: EM+AC+SS+TF-ThM5, 182; NS-TuA9, 87; PS-MoA1, 40; TF+EM+MI-WeA12, 170; TF-ThP27, 244
Kinoshita, K.: PS-ThA11, 219; PS-ThP18, **237**
Kioseoglou, G.: 2D+MI+SA-MoM2, 2; 2D-ThA10, 201
Kipreos, M.: SS-TuP2, **116**
Király, B.: 2D+MI-TuM4, 53; SP+SS+TF-WeM11, 140
Kirnbauer, A.: SE+TR-WeM6, 138
Kirste, R.: EM+NS+PS+SS+TF-MoM1, **7**
Kisel, V.N.: TF-ThP45, 247
Kishko, G.: PS-ThP13, 237
Kisieliowski, C.: EM+NS+SP+SS-WeA11, **154**
Kittiwatanakul, S.: EM-MoM5, 9
Kizir, S.: EM+NS+PS+SS+TF-MoM3, 7
Kjoller, K.: NS-TuA9, 87
Klee, V.: 2D+MI-ThM6, 175
Klein, P.: TF1-ThM10, 197
Klimeck, G.: MI-TuA9, 85
Klopf, J.M.: EM-MoM5, 9
Klős, G.: BI+MI-WeM3, **127**
Knight, K.B.: AC-TuP1, 102
Knight, S.: EL+AS+EM+MI+TF-FrM3, 251
Knoops, H.C.M.: PS+TF-WeA11, 161; PS+TF-WeA7, 161
Knop-Gericke, A.: IS+HC-WeA1, **158**
Knowles, J.P.: AC+AS+SA-ThM5, 177
Knox, C.: IS-FrM6, 255
Knuffman, B.: HI+NS-ThM3, 186
Knutsson, J.: EM+NS+SP+SS-WeA4, 153
Ko, J.-H.: TR+BI+SE+TF-ThA9, 226
Ko, W.: SP+AS+MI+NS+SS-TuA12, **94**
Kobayashi, H.: PS+TF-WeM1, 134; PS+TF-WeM10, 134
Kocbas, C.: IS-ThP5, 233
Koch, R.D.: AS-TuP28, 107
Kodali, G.: NS+BI-ThA6, 216
Kodambaka, S.: 2D+TF-WeM13, 122; SE+MS+TF-TuA3, **92**
Koeck, F.A.: PS2-ThM1, 192
Koehler, A.D.: EM-MoA10, 31
Koehler, M.: 2D+MI-MoA6, 26
Koel, B.E.: SS+HC-TuA1, **96**
Koelsch, P.: BI+AS+SA-TuA9, 82
Koepke, J.: NS-MoM10, 14
Koepke, M.: PS-TuM10, 62
Koert, U.: SS+AS+EM-WeA2, 167
Koga, K.: PB+BI+PS-TuM10, **60**
Kohlhauser, B.: SE+NS+TF+TR-TuM12, 66
Koirala, P.: EL+AS+BI+EM+TF-ThA6, 205
Kojima, Y.: 2D-ThP13, 229
Koju, V.: TF+BI-ThA2, **222**
Kolev, I.: SE+NS+TF+TR-TuM10, 65
Koller, C.M.: SE+NS+TF+TR-TuM12, 66; SE+TR-WeM13, 139; SE+TR-WeM6, **138**
Kollmer, F.: HI+MI+NS-ThA3, 210
Kolmakov, A.: EM+SS+TF-ThA2, 207; IS-ThA3, **213**; IS-ThP9, 234; NS-TuA11, 88
Kolobov, V.I.: PS-ThP27, 239
Kolodzey, J.: SE+2D+EM-WeA9, 165
Koloszvári, S.: SE+NS+TF+TR-TuM12, 66; SE+TR-WeM13, 139; TF1-ThM13, 198
Komachi, J.: PS-MoM3, 17
Komesu, T.: 2D-ThP13, 229
Kondo, H.: PB+BI+PS-TuM11, 61
Kondo, T.: 2D+MI-MoA8, **27**; HC+SS-ThM2, 184
Konoshita, K.: BP-SuA3, 1
Konstantinidis, S.: SS+AS-TuA1, 94
Kooi, S.: NS-MoM2, **12**
Kormondy, K.: EL+AS+EM+MI+TF-FrM4, 252
Kornblum, L.: TF+MI-WeA8, 172
Korolkov, V.V.: 2D+NS-WeA11, 150
Korolov, I.: PS-TuM10, 62
Körsgen, M.: BI+PB-TuP5, **108**
Kortshagen, U.R.: PS+2D-TuA3, **89**
Korwin-Pawlowski, M.L.: PS-ThP2, 235
Koster, N.B.: EL+AS+EM+MI+TF-FrM7, 253; VT-MoA4, 51; VT-TuA10, 101
Kotru, S.: MN-WeM3, **132**; TF-TuA12, 100
Koust, S.: SS+AS-TuA12, **96**
Kovalenko, Y.: BI+AS-MoM2, 6
Kovarik, L.: AS-MoM1, 3
Kowalczyk, P.: PS-WeM3, 136
Koyn, Z.: SE-TuP4, **114**
Kozakai, T.: HI+MI+NS-ThA1, 210
Kozarashi, T.: HC+SS-ThM2, 184
Kozen, A.C.: MS-MoM6, 12; PS-ThP5, 235; TF+SA+MI-TuM12, 73; TF+SA+MI-TuM3, **71**
Kramer, N.J.: PS+2D-TuA3, 89
Krashennikov, A.V.: 2D+MI-MoA3, **26**
Kratochvilová, M.: EM+SS+TF-ThA12, 208
Kratz, C.: 2D-ThA12, 202
Kreit, E.B.: 2D-ThP5, 227
Kreuzer, H.J.: SS+AS-ThA8, 221
Krick, B.: TR+BI+SE+TF-ThA11, 226; TR+BI+SE+TF-ThA12, 226
Krishnan, A.S.: SS+HC-FrM1, **258**
Kristo, M.J.: AC-TuP1, 102
Kristof, J.: PB+BI+PS-TuM2, **60**
Kroes, G.-J.: SS1+AS+HC+NS-TuM5, 68
Kronawitter, C.X.: SS+HC-TuA1, 96
Krooswyk, J.D.: HC+SS-WeM2, 130
Kropman, D.: SS+AS+EM-WeA9, **168**
Krüger, P.: MI+2D+AC-MoA3, **32**
Kruppe, C.M.: HC+SS-WeM2, **130**
Kruse, N.: HC+SS-ThM10, 185
Krylov, S.: MN-WeM4, **132**; MN-WeM5, 132
Krzyzanowska, H.: EM-MoA9, 31
Kub, F.: EM-FrM5, 254; EM-MoA10, 31
Kuboi, N.: PS-MoM3, **17**
Kubotera, H.: PS1-ThM3, 190
Kuchakova, I.: PB+BI+PS-MoA2, 35
Kuciauskas, D.: TF-TuA8, 99
Kucukgok, B.: MS-MoA10, 34
Kudriavtsev, V.: TF-ThP37, **246**
Kühne, P.: EL+AS+EM+MI+TF-FrM3, 251
Kuhness, D.: SS+AS-TuA9, 95
Kujofsa, T.: SS+AS+EM-WeA12, **168**
Kuk, Y.: SP+AS+MI+NS+SS-TuA12, 94
Kuklja, M.M.: SS+AS+HC-MoA10, 46
Kuljanishvili, I.: SP+SS+TF-WeM12, **140**
Kulkarni, D.D.: SS1+AS+HC+NS-TuM4, **68**
Kumamoto, A.: PS1-ThM13, **192**
Kumar, P.: 2D+MI+SA-MoM11, 3
Kumar, Y.: MI+2D+AC-MoA9, 32
Kummel, A.C.: 2D+MI+SA-MoM1, **2**; 2D+NS-FrM9, 250; 2D-ThA8, 201; PS2-ThM12, 194; PS-ThP15, 237; SE+2D+EM-WeA11, 166; SS+AS+EM-WeA7, 167; SS+AS+EM-WeA8, 168
Kundu, S.: PS-ThP33, 240
Kung, P.: 2D+TF-WeM10, 122; 2D-ThA4, 201
Kunzler, B.F.: TF-ThP29, 244
Kuo, C.M.: NS-TuP8, 112
Kuo, C.T.: TF+SA+MI-TuM4, 72
Kuo, Y.: EM-FrM7, **254**
Kurake, N.: PB+BI+PS-TuM11, 61
Kurihara, M.: PS+TF-WeM10, 134
Kurokawa, K.: PB+BI+PS-TuM11, **61**
Kushner, M.J.: PS+TF-WeM4, 134; PS-MoA4, 40; PS-MoA8, 40; PS-ThP7, 235; PS-WeM5, 136
Kustas, A.: TR+BI+SE+TF-ThA10, **226**
Kuwahara, K.: PS+TF-WeM1, 134
Kuzminykh, Y.: TF-TuM3, 73
Kwak, I.J.: 2D+NS-FrM9, **250**; 2D-ThA8, 201
Kwon, J.Y.: SS+AS-TuA4, 95
Kwon, N.Y.: TF-ThP22, 243
— L —
Laas, T.: SS+AS+EM-WeA9, 168
Labau, S.: PS2-ThM6, 193; PS-MoM11, 18
Labonte, A.P.: PS-MoA10, 41; PS-MoA3, **40**
Ladd, P.: VT-TuA1, **100**
Lafleur, T.: PS-TuM10, 62
Lahneman, D.: EM-MoM5, 9
Lai, C.-C.: 2D+MI-TuM3, **53**
Lai, C.S.: PS-WeA1, 162
Lai, W.: 2D-ThP5, **227**
Lai, W.C.: HI+NS-ThM2, 186; HI-ThP1, 232
Lake, W.: AC+AS+SA-ThM3, 176
Lallo, J.: AS-TuP3, **102**
Lalor, J.: PS+SE-MoM3, 14
Lam, V.: HC+NS+SS-WeA9, 156
Lambeets, S.V.: HC+SS-ThM10, **185**
Lambright, K.: EL+AS+BI+EM+TF-ThA9, 206
Lancaster, D.K.: TF-TuA9, **99**
Landa, A.: AC+MI-WeM13, **124**
Landberg, G.: AS+BI-MoA6, 28
LANDIS, S.L.: NS-MoM8, 13
Landova, M.: PB+BI+PS-MoA8, 36
Landsbergen, J.: SE+NS+TF+TR-TuM10, 65
Lane, B.G.: PS-ThA7, **218**
Lanford, W.A.: PS-MoA1, 40
Lang, B.N.: TF+EM-MoA1, 47
Langer, C.: SS+AS+EM-WeA2, 167
Langford, J.M.: IS-ThA12, 214; SS+AS-TuA4, **95**
Langlois, G.G.: SS+AS-WeM13, **144**
Lanham, S.J.: PS-WeM5, **136**
Lanius, M.: MI+2D+AC-MoA1, 31
Lao, D.: IS-FrM9, 256
Lapeyre, C.: TF-ThA1, 223
Lara Saenz, G.A.: 2D+TF-WeM1, 121
Lara, G.: 2D-ThP3, 227
Larson, S.: TF1-ThM3, 196
Lasanta, M.I.: SE+TR-WeM5, 138
LaScala, N.A.: SS-TuP9, 117
Laskin, J.: EM+NS-WeM10, 129
Latu-Romain, E.: PS+AS+SS-MoA5, 38; PS-MoM11, 18
Lau, C.H.: PS-WeM10, 137
Lauderbach, L.: NS-TuM6, 59; SA-TuP2, 113
Laue, A.: IS-ThP7, 234
Laughlin, K.: AS-WeA8, 152; SE+NS+TF+TR-TuM6, **65**
Lauhon, L.: MN+2D+NS-ThA1, **214**
Lauritsen, J.V.: SS+AS-TuA12, 96
Lauter, H.: MI+2D+AC-MoM4, 10
Lauter, V.: MI+2D+AC-MoM4, 10; MI-TuP2, 110; TF+SA+MI-TuM1, **71**
LaVoie, A.: PS+TF-WeA9, **161**
Lavoie, C.: TF+EM+MI-WeA2, 169
Lavrik, N.: NS-MoM6, **13**
Law, T.J.: MS-TuA10, 87
Lawson, S.: EM+AC+SS+TF-ThM12, 183; EM-ThP13, **232**; EM-ThP8, 232
Lazzari, R.: SS+AS-TuA10, **96**
Le Brizoual, L.: PS-ThA6, 218
Le Dain, G.: PS1-ThM12, **191**
Le Fèvre, P.: SA+2D+AC+AS+TF-TuM2, **63**; SA+AS-MoA6, 42
Le Tarte, L.: AS-TuP11, 104
Le, M.: EL+AS+EM+MI+TF-FrM6, 252
Leach, J.: EM+NS+PS+SS+TF-MoM8, **8**
LeClair, P.: MI+2D+AC-MoM4, 10
Lecoeur, P.: SA+2D+AC+AS+TF-TuM2, 63; SA+AS-MoA6, 42
Lee, C.: SS1+AS+HC+NS-TuM1, 67
Lee, C.C.: TF-ThP30, 244

Author Index

- Lee, C.-T.: TF-ThP40, 246
 Lee, D.: 2D+MI-ThM12, 176
 Lee, E.T.: PS-WeA9, 163
 Lee, H.: SP+AS+MI+NS+SS-TuM1, 66; SP-TuP3, 115; SS1+AS+HC+NS-TuM1, **67**; TR+BI+SE+TF-ThA9, **226**
 Lee, H.C.: PS-ThP31, 240
 Lee, J.: 2D+NS-FrM6, **250**; 2D+NS-WeA1, 149; MN+2D+NS-ThA6, 214; PS-MoA2, 40; SS+AS+HC-MoM6, 21; SS+AS-WeM11, **144**; SS1+AS+HC+NS-TuM12, 69; TF+SA+MI-TuM10, 72
 Lee, J.W.: NS-TuP9, 112
 Lee, J.-W.: SP+AS+MI+NS+SS-TuM1, 66
 Lee, K.H.: PS1-ThM3, 190
 Lee, K.Y.: PS+AS+SS-MoA9, 38
 Lee, M.V.: TF-ThP29, **244**
 Lee, S.: PS-MoA4, 40; PS-MoA8, 40; TF+EM+MI-WeA12, 170
 Lee, S.B.: MS-MoM6, 12; MS-MoM9, 12
 Lee, S.C.: TF-ThP12, 242
 Lee, S.H.: SP+AS+MI+NS+SS-TuA8, 94
 Lee, T.L.: SA+AS-MoA4, 42
 Lee, W.K.: 2D-ThA6, 201
 Lee, Y.K.: SS1+AS+HC+NS-TuM1, 67; TF-ThP28, **244**
 Lee, Z.R.: 2D-ThP12, **229**
 Leggett, G.J.: NS+BI-ThA6, **216**
 Lei, Y.: IS-FrM5, 255
 Leick, N.: PS+TF-WeA8, 161; PS-WeA12, 164; TF-MoM10, **23**
 Leite, M.S.: EM+SS+TF-ThA2, 207
 Lelis, A.J.: EM+AC+SS+TF-ThM13, 183
 Lemaire, P.C.: TF-FrM1, **259**
 Lemay, J.-C.: SS-ThM5, 195
 Lenahan, P.M.: EM+AC+SS+TF-ThM13, 183; EM+AC+SS+TF-ThM5, 182
 Leng, C.Z.: TF2-ThM11, **199**
 Leonard, D.: AS-TuP19, 105
 Leos-Mendez, H.: TF-ThP34, 245
 Leou, K.C.: NS-TuP8, 112; PS-ThP1, 235
 Lerach, J.O.: AS-ThA7, **203**
 Lesko, K.C.: AS+SS-WeM5, 125
 Létard, J.-F.: TF+SA+MI-TuM2, 71
 Leusink, G.J.: TF+EM+MI-WeA2, 169
 Leuty, G.M.: 2D-ThP5, 227
 Levy, J.: TF1-ThM1, 196
 Lewin, E.L.: TF+PS+SE-MoA9, 50
 Lewis, B.B.: HI-WeA8, 157; NS-MoM5, **13**
 Leys, C.: PB+BI+PS-MoA2, 35
 Lézec, H.J.: NS-MoA8, **35**
 Li, A.: TR+AS+NS+SS-WeA9, 173
 Li, A.-P.: SP+2D+AS+NS+SS-MoA3, 43; SP+AS+MI+NS+SS-TuM5, 67
 Li, B.: MN+MS-FrM6, 257
 Li, C.: AS-TuP27, 107; PS-WeA1, **162**
 Li, C.L.: BI+PB-TuP6, 108
 Li, H.: PS1-ThM13, 192; PS-ThA8, **219**; SS+HC-FrM5, 259
 Li, J.: SS+AS-TuA10, 96
 Li, L.: SP+2D+AS+NS+SS-MoA1, **43**
 Li, L.H.: EM-FrM6, 254
 Li, M.: MN+MS-FrM6, 257
 Li, P.-C.: HI+NS-ThM2, 186
 Li, Q.: TF-ThA7, 224
 Li, T.: SS+AS-TuA3, 95; SS-TuP4, **116**; SS-TuP7, 117
 Li, W.: EM+SS+TF-ThA8, 207; EM-ThP1, 230; MI-TuA9, 85; TF+EM+MI-WeA11, 170; TF+EM+MI-WeA12, **170**; TF-ThP27, 244
 Li, X.: MS-MoM5, 11; SE+2D+EM-WeA12, 166
 Li, Y.: 2D-TuA1, 78; IS-ThM10, 188; VT-MoA3, **51**
 Li, Y.Z.: 2D-ThP6, 227
 Lian, G.: TF+EM+MI-WeA10, 170
 Lian, T.: SS+HC-TuA3, **97**
 Liang, B.: BI+AS+SA-ThM10, 181
 Liang, J.: SP-TuP4, 115
 Liang, L.: SP+AS+MI+NS+SS-TuM5, 67
 Liang, Z.: SS+AS-TuA3, 95; SS-TuP4, 116; SS-TuP7, **117**
 Liao, B.H.: PS-ThP1, 235
 Liao, W.: MN+MS-FrM10, 258; MN+MS-FrM8, 257
 Libera, J.A.: TF+EM-MoA3, 47
 Lie, F.L.: PS-MoM10, 18; PS-MoM4, **17**
 Liehr, M.: MS-MoA8, **33**
 Liénard, S.: TF+PS+SE-MoA8, **50**
 Lill, T.B.: PS-ThP12, 236; PS-WeA4, 163
 Lim, J.Y.: VT-TuP1, 118
 Lim, K.Y.: PS-MoM4, 17
 Lima, V.: TF-ThP31, **245**
 Lin, C.: MS-MoM6, **12**
 Lin, C.Y.: HI-ThP1, 232
 Lin, J.T.: MN+MS-FrM10, 258
 Lin, Q.: TF+EM+MI-WeA12, 170
 Lin, S.C.: TF+SA+MI-TuM4, 72
 Lin, T.: PS-ThP33, 240
 Lin, Y.: 2D-ThP6, **227**; TF+EM+MI-WeA11, 170
 Lin, Y.-C.: 2D+NS-WeA12, 150
 Lin, Y.-W.: SE-TuP3, **114**
 Lince, J.R.: TR+AS+NS+SS-WeA3, **173**
 Linderoth, T.: SS-ThM1, **194**
 Linfield, E.H.: EM-FrM6, 254
 Linford, M.R.: AS+SS-TuA7, **80**; SE+2D+EM-WeA4, 165; TF-FrM6, 261; TF-ThP21, 243
 Lingerfelt, E.J.: AS+SS-TuA2, 79
 Lippner, M.A.: SS+AS+EM-WeA2, 167
 Lissandrello, C.: NS-MoM9, 13
 List, T.: PS+AS+SS-MoA3, 37; PS-TuM6, **62**
 Liu, C.: MS-MoM9, 12
 Liu, D.: IS-ThM10, 188
 Liu, D.-J.: HC+NS+SS-WeA7, 155; SS1+AS+HC+NS-TuM12, **69**
 Liu, D.R.: EM-ThP4, **231**
 Liu, F.: 2D+NS-FrM11, 251
 Liu, G.: TF-MoM9, 23
 Liu, J.: IS-ThM13, 188; TF-ThP16, 242
 Liu, R.: SS-TuP8, **117**
 Liu, S.: AS+SS-WeM12, 126; SS+AS+HC-MoA6, 45; TF-FrM5, 260
 Liu, X.: 2D+MI+SA-MoM1, 2; PS-MoM9, 18; VT-MoA3, 51
 Liu, Y.: NS-MoA2, 34; PS-TuM10, 62
 Livengood, R.H.: HI-WeA4, 157; HI-WeA8, 157
 Lloyd, K.G.: AS-WeA3, **152**
 Locatelli, A.: SA+2D+AC+AS+TF-TuM3, **63**
 Loch, D.A.: TF+PS+SE-MoA10, 50
 Lock, E.H.: PS-ThP9, 236
 Lockhart de la Rosa, C.: TF+EM+MI-WeA3, 169
 Long, R.: TF+EM+MI-WeA10, 170
 Look, D.C.: TF-ThP41, 246
 Lopez, D.: MN-WeM6, 133
 Lopez, F.E.: PS-ThP32, **240**
 Lopez, V.: 2D+TF-WeM11, 122
 Lopez-Luna, E.: TF-ThP34, 245
 Lorenz, M.: AS-ThA6, **203**
 Lorite, I.: MI+2D+AC-MoA9, **32**
 Losago, M.D.: TF2-ThM11, 199; TF2-ThM5, **199**; TF-FrM3, 260
 Lott, D.: MI+2D+AC-MoM5, **10**
 Louwagie, N.: VT-WeM2, 146
 Lownsbury, J.: SS+AS+HC-MoA2, 45
 Lozano, P.: HI+NS-ThM5, 186
 Lü, B.: SE+NS+TF+TR-TuM3, 65
 Lu, J.: 2D+MI-TuM3, 53; EM-MoM5, 9
 Lu, N.: MS-MoA10, 34
 Lu, P.: SE+NS+TF+TR-TuM4, 65; TR+BI+SE+TF-ThA10, 226
 Lu, S.: PS-MoA4, 40; PS-MoA8, 40
 Lu, W.: SP+AS+MI+NS+SS-TuM5, 67
 Lu, Z.: IS-FrM5, **255**
 Lucas, J.M.: PS-MoA10, 41; PS-MoA3, 40
 Lucas, S.: SS+AS-TuA1, 94
 Lucci, F.R.: HC+NS+SS-WeA3, 155
 Luciani, V.K.: MS-TuA3, **86**
 Ludwig, K.F.: TF+SA+MI-TuM12, 73
 Lueders, M.: AC+MI-WeM12, 124
 Luethy, P.: SE+TR-WeM2, 137
 Luftman, H.: TR+BI+SE+TF-ThA12, 226
 Luican-Mayer, A.: 2D+MI+SA-MoM3, **2**
 Lukaszew, R.A.: EM-MoM5, 9
 Lukehart, C.M.L.: AS-TuP29, 107
 Lukens, W.W.: AC-TuP1, 102
 Lulinsky, S.: MN-WeM4, 132
 Luna-López, J.A.: 2D-ThP4, 227
 Lund, C.: MI-TuA9, 85
 Lundgren, E.: HC+SS-WeM3, **130**
 Lundin, J.: IS-FrM6, 255
 Luo, G.-N.: PS-WeM10, 137
 Luo, H.: TF+PS+SE-MoA6, 50
 Luo, M.: SP-TuP5, 115
 Luo, Y.: HI+MI+NS-ThA4, 210
 Luther, J.M.: NS-MoA5, **35**
 Lutz, C.P.: SP+AS+MI+NS+SS-TuA3, 93
 Luysberg, M.: MI+2D+AC-MoA1, 31
 Lynch, K.: BI+AS+SA-ThM1, **180**
 Lynn, K.G.: AS+SS-ThM1, 178
 Lyubinetzky, I.: SS+AS+HC-MoA1, 45
 — **M** —
 M. Junda, M.: EL+AS+BI+EM+TF-ThA11, 206
 M. Rouleau, C.: 2D+NS-WeA3, 149
 Ma, C.: SP+AS+MI+NS+SS-TuM5, **67**
 Ma, D.: MN+MS-FrM6, 257
 Ma, S.: PS-ThP13, **237**; SS+HC-TuA8, **97**
 Ma, T.: PS+AS+SS-MoA3, **37**
 Ma, Y.: EM+NS-WeM5, **129**
 Ma, Y.M.: MI+2D+AC-MoA2, **31**
 Ma, Z.: EM+MI+MN-TuA11, 83; EM-ThP6, 231
 Maas, D.J.: VT-MoA4, 51
 Maaß, S.: SS+AS+HC-MoA8, 46
 Macak, K.: AS-TuP6, 103
 Macaluso, R.T.: TF-TuA8, 99
 Maccallini, E.: VT-TuA9, 101
 MacIsaac, C.: TF-MoM5, 23
 Mack, P.: AS-MoM6, 4; AS-ThA4, **203**; AS-TuP2, 102; AS-TuP3, 102; AS-WeA1, 151
 Mackus, A.J.: PS+TF-WeA12, 162; TF-MoM5, **23**
 Madachik, M.: SS+AS+EM-WeA1, 167
 Madan, A.: PS+TF-WeA4, 160
 Maddumapatabandi, T.D.: HC+SS-WeM6, 131
 Madison, L.: SP+AS+MI+NS+SS-TuM2, 66
 Maeda, K.: PS-ThP33, 240
 Maehashi, K.: BI+MI-WeM4, 127
 Magnusson, Y.: AS+BI-MoA6, 28
 Magyari-Kope, B.: EM+MI+MN-TuA7, 83
 Mahadik, N.: TF1-ThM10, 197
 Mahady, K.: HI-WeA4, **157**
 Mahapatra, M.: SS-ThM6, **195**
 Mahjouri-Samani, M.: 2D+NS-WeA3, **149**
 Mahler, G.: EM+AC+SS+TF-ThM10, 183
 Mairena, A.: SP+SS+TF-WeM10, **140**; SS-ThM3, 195
 Majeski, M.W.: EM+NS-WeM1, 128
 Makarov, A.A.: AS+BI-MoA8, 28; AS+SS-ThM12, 179
 Makhneva, E.: PB+BI+PS-MoA8, 36
 Makin, R.: EM-FrM3, 253

Author Index

- Maklakov, S.A.: TF-ThP45, **247**
Makowski, M.J.: IS-ThA12, 214
Maksymovych, P.: HC+NS+SS-WeA4, 155;
SP+SS+TF-WeM3, 139; SS+AS-ThA12, **222**
Maldonado, R.: NS-TuP2, 111
Malek, T.: TF-ThP42, 247
Malinovskis, P.M.: TF+PS+SE-MoA9, **50**
Mallinson, C.F.: SP+AS+MI+NS+SS-TuA11, **94**
Mallouk, T.E.: SS+AS+HC-MoA2, 45
Malone, R.M.: PS-ThP32, 240
Manakhov, A.: PB+BI+PS-MoA8, 36
Manandhar, S.: TF1-ThM4, **196**
Mandrell, L.: TF-ThP37, 246
Mandrus, D.G.: 2D+MI-MoA6, 26; 2D+NS-FrM10, 250; 2D-ThP11, 228
Mane, A.: TF+EM-MoA3, 47; TF-FrM2, **260**
Mangolini, F.: AS-MoM5, **4**
Mangolini, L.: EM+NS-WeM6, 129; EM-MoM9, 9; EM-ThP3, **230**; PS+2D-TuA2, 88
Mani-Gonzalez, P.G.: TF-ThP34, **245**
Manini, P.: VT-TuA9, **101**
Maniura, K.: BI+AS+SA-TuA7, **82**
Mankey, G.: MI+2D+AC-MoM4, **10**
Mann, H.S.: TF+EM-MoA1, 47
Mann, J.E.: AS+SS-WeM3, 125; AS-TuP9, **104**
Mann, M.N.: PB+BI+PS-MoA10, **36**
Manning, C.: EM+SS+TF-ThA9, 207
Mannix, A.J.: 2D+MI-TuM4, **53**
Mansergh, R.H.: TF2-ThM1, 198
Mao, Z.-Q.: 2D+NS-WeA1, 149
Marchack, N.P.: PS-MoA2, 40; PS-MoA9, **41**; PS-MoM2, 17
Marcinkowski, M.D.: HC+NS+SS-WeA3, **155**
Marcoen, K.: TF-ThP2, 241
Mares, J.W.: EM+SS+TF-ThA6, 207
Maria, J.-P.: TF2-ThM5, 199
Marinov, D.: PS-TuM1, 61
Marko, M.: AS-TuP11, 104
Marom, N.: HC+SS-ThA1, 208
Maroutian, T.: SA+2D+AC+AS+TF-TuM2, 63; SA+AS-MoA6, 42
Marquardt, A.E.: PS+TF-WeM12, **135**
Marshall, M.: NS-MoM10, 14
Marshall, P.: AS+BI-MoA8, 28
Marsillac, S.: EL+AS+BI+EM+TF-ThA6, 205
Martin, A.A.: NS-TuM1, **58**; TF+SA+MI-TuM10, 72
Martin, E.H.: PS-WeM10, 137
Martin, I.T.: TF-TuA11, **100**
Martin, M.: PS-MoM11, 18
Martin, M.C.: SA+AS+BI+MI-TuA3, **90**
Martinez, A.D.: TF-TuA8, **99**
Martinez, E.: SA+AS-MoA5, 42
Martinez, G.: SE+NS+TF+TR-TuM5, **65**
Martinez, J.: 2D+MI-ThM6, 175
Martinez-Criado, G.: SA+AS+MI-MoM3, **18**
Martini, A.: TR+BI+SE+TF-ThA1, 224; TR+BI+SE+TF-ThA3, 225
Martin-Jimenez, D.: SP+AS+MI+NS+SS-MoM10, **20**
Martin-Martinez, F.J.: 2D+MI-ThM1, 175
Martins, I.P.O.: BI+PB-TuP11, 109
Martirosyan, V.: PS+AS+SS-MoA10, 39; PS+AS+SS-MoA6, **38**
Maruyama, B.: SS+AS+HC-MoM8, 22
Marvel, R.E.: SP-TuP4, 115
Marvinney, C.: MN-ThP2, 235; MS-TuP5, 111
Mascareno, A.: SE+2D+EM-WeA3, **165**
Maskova, S.: AC+MI-WeM5, **123**; AC+MI-WeM6, 123
Maslar, J.E.: 2D+TF-WeM12, 122; TF-MoM4, 22
Mass, J.L.: AS+SS-ThM13, 180
Mastro, M.A.: EM-MoA3, 29
Matei, L.: EM+AC+SS+TF-ThM1, 182
Matejova, L.: TF-ThP42, 247
Mathis, J.P.: EM-FrM3, 253
Mathur, A.: EL+AS+EM+MI+TF-FrM4, 252
Matkovic, A.: EL+AS+EM+MI+TF-FrM8, 253
Matsuda, O.: HI+MI+NS-ThA1, 210
Matsumoto, K.: BI+MI-WeM4, 127
Matsumuro, A.: MS-TuP2, 110; MS-TuP3, 110; MS-TuP4, 111
Matsuo, J.: PS-ThA11, 219
Matthews, M.: TF+SA+MI-TuM10, 72
Matthews, R.: TF-TuA11, 100
Mauchamp, N.: PS1-ThM13, 192
Mauger, S.: SA-TuP1, 113
May, C.: NS-TuM6, 59; SA-TuP2, 113
Maynard, M.R.: PB+BI+PS-MoA10, 36
Mayrhofer, P.H.: SE+NS+TF+TR-TuM12, 66; SE+TR-WeM13, 139; SE+TR-WeM6, 138; TF1-ThM13, 198
Mazarov, P.: HI+NS-ThM5, 186
McArthur, S.L.: BI+AS+SA-ThM12, **182**
McBreen, P.H.: SS-ThM5, **195**
McBride, J.R.: NS+BI-ThA2, **215**
McCann, J.P.: SS+AS+HC-MoM2, 21
McClelland, J.J.: HI+NS-ThM3, 186
McClimon, J.B.: AS-MoM5, 4; SS2+AS+HC+NS-TuM10, 70
McConney, M.E.: 2D+NS-FrM1, 249
McCreary, K.M.: 2D+MI+SA-MoM2, 2; 2D-ThA10, **201**
McDermott, S.: PS-MoM9, 18
McDonald, B.: SE+2D+EM-WeA2, 164
McDonald, C.: BI+AS+SA-TuA9, 82
McDonnell, S.: EM+SS+TF-ThA11, 208
McEntee, M.: HC+NS+SS-WeA4, 155
McEuen, P.: 2D+NS-WeA9, **149**
McGahan, C.L.: SP-TuP4, **115**
McGugan, J.D.: PS1-ThM2, **190**
McGuire, G.: NS-TuM2, **58**
McGuire, M.: HI+MI+NS-ThA8, 211
McInerney, E.J.: TF-TuM1, **73**
McIntyre, P.C.: SE+2D+EM-WeA11, 166
McKibbin, S.: EM+NS+SP+SS-WeA4, 153
McKown, C.: NS-MoM6, 13
McLain, J.T.: PS-WeM12, **137**
McLane, L.T.: BI+AS-MoM10, 7
McMurtry, G.M.: VT-MoA8, **52**
McNamara, S.: MN+MS-FrM10, 258
McNerny, C.: SE+MS+TF-TuA2, 91
Medalova, J.: PB+BI+PS-MoA8, 36
Meek, T.: EM+AC+SS+TF-ThM12, 183; EM-ThP13, 232; EM-ThP8, 232
Mehrotra, P.: SE+MS+TF-TuA2, 91
Mehta, S.: PS-MoM10, 18; PS-MoM9, 18
Meier, M.: SS+AS+HC-MoA8, 46
Melendez-Lira, M.: NS-TuP7, **112**; TF-ThP34, 245
Melia, M.A.: BI+PB-TuP8, 109; SE+MS+TF-TuA1, **91**
Mellor, C.J.: 2D+NS-WeA11, 150
Mendoza, R.: TF-ThP29, 244
Mennell, P.: PS+TF-WeA4, 160
Mente, T.-O.: SA+2D+AC+AS+TF-TuM3, 63
Merche, D.: PS2-ThM10, 193; PS-ThP22, **238**; SE+MS+TF-TuA9, 92
Merida, C.: 2D+MI-ThM6, 175
Mersey, B.: SA+2D+AC+AS+TF-TuM2, 63
Mershon, J.S.: VT-MoA3, 51
Mertens, J.: PS+SE-MoM5, **15**; PS-ThP21, 238
Mertens, S.: PS-ThP33, 240
Meshkian, R.: 2D+MI-TuM3, 53
Meshkova, A.S.: SE+MS+TF-TuA8, 92; TF-FrM10, **261**
Messer, B.: PS-MoA3, 40
Metz, A.: PS-MoA10, 41; PS-MoA11, 41; PS-MoA3, 40
Metzler, D.: PS-WeA1, 162
Mewes, C.: TF+MI-WeA3, **171**
Mewes, T.: TF+MI-WeA3, 171
Meyer, D.J.: TF+EM+MI-WeA1, 169; TF+SA+MI-TuM12, 73
Meyer, H.M.: AS-TuP19, **105**
Meyer, K.E.: TF-FrM3, 260
Meyer, M.: AS-WeA1, 151
Meyer, R.: PS-TuM12, 62
Michael, K.: NS-TuP2, 111
Michaud, R.: TF+PS+SE-MoA3, 49
Michel, M.: 2D-ThP2, 227
Michels, T.: MN+NS-WeA7, **159**
Michienzi, M.R.: AS-TuP16, 104
Mikkelsen, A.: AS+SS-TuA1, **79**; EM+NS+SP+SS-WeA4, 153
Miles, M.: TF+MI-WeA12, 172
MILES, F.M.: NS-MoM8, 13
Miliyanchuk, K.: AC+MI-WeM5, 123
Miller, E.: PS-MoM2, 17; PS-MoM4, 17
Milosavljevic, V.: PS+SE-MoM3, **14**
Milson, G.: BI+AS+SA-TuA3, 82
Milstein, D.: AS+SS-WeM10, 125
Minardi, L.: PS+TF-WeM11, 135; PS2-ThM13, **194**
Minari, H.: PS-MoM3, 17
Minasian, S.G.: AC+AS+SA-ThM11, 177; AC+AS+SA-ThM6, **177**; AC-TuP1, 102
Minelli, C.: AS-ThA1, **202**
Miralidharan, N.: TF+EM-MoA8, 48
Mirhosseini, H.: MI+2D+AC-MoA8, 32
Mirkhani, V.: EM+NS+PS+SS+TF-MoM6, 8; EM-MoA11, 31; EM-MoA8, 30
Mishra, D.: BI+PB-TuP4, 108
Mishra, R.: TF-TuA10, 99
Misra, A.: AS-TuP29, 107
Misra, S.: NS-MoM10, 14
Mita, S.: EM+NS+PS+SS+TF-MoM1, 7
Mitchell, S.T.: HI+MI+NS-ThA7, 211
Mitterer, C.: SE+TR-WeM3, **138**
Miwa, J.A.: 2D+MI-TuM13, 54
Miyamoto, K.: MI+2D+AC-MoA8, 32
Miyayama, T.: AS+BI-MoA10, 29; AS+SS-ThM11, 179; AS+SS-WeM3, 125; AS-WeA2, 151
Miyazoe, H.: PS-MoA2, 40; PS-MoM2, 17; PS-ThP9, **236**
Miyoshi, N.: PS+TF-WeM1, 134; PS+TF-WeM10, 134
Mizotani, K.: PS1-ThM13, 192; PS-ThA11, 219
Mizubayashi, W.: PS-WeA9, 163
Mizuta, H.: EM-FrM4, 254; HI+MI+NS-ThA11, 212
Mkhoyan, K.A.: TF-ThP7, 241
Mlynczak, E.: MI+2D+AC-MoA1, 31
Mo, S.K.: 2D+MI-ThM12, 176
Modic, M.: PB+BI+PS-MoA2, 35
Modin, A.: AC+AS+SA-ThM11, 177
Mody, J.: PS+TF-WeA4, 160
Moellers, R.: AS+BI-MoA8, 28; AS+SS-ThM12, 179; EW-WeM8, 130; HI+MI+NS-ThA3, 210
Moffitt, C.: AS+SS-WeM13, 126; AS-TuP4, 102; AS-TuP5, **103**; EW-TuL4, 77
Mogami, T.: PS-ThP18, 237
Mohimi, E.: TF-FrM5, **260**; TF-FrM7, 261; TF-ThP39, 246
Mohite, A.: 2D+NS-FrM11, 251
Moiseev, A.G.: SS-TuP8, 117
Moisy, P.: AC+AS+SA-ThM4, 176
Mol, J.M.C.: TF-ThA6, 223; TF-ThP2, 241
Moler, K.A.: TF+MI-WeA8, 172
Molina-Mendoza, A.: EL+AS+EM+MI+TF-FrM8, 253
Molinari, V.: AS-TuP26, 107

Author Index

- Molis, S.: PS+TF-WeA4, 160
Molkenboer, F.T.: EL+AS+EM+MI+TF-FrM7, 253; VT-TuA10, **101**
Molodtsov, S.: SA+AS-MoA8, **43**
Molodtsova, O.V.: EM-MoM11, **10**;
SA+2D+AC+AS+TF-TuM6, 64
Monazami, E.: SS2+AS+HC+NS-TuM10, **70**
Monfil-Leyva, K.: 2D-ThP4, **227**
Monget, C.: TF-ThA1, 223
Mont, F.: TF+EM+MI-WeA10, 170
Montanini, P.: PS-MoM9, 18
Monti, O.L.A.: 2D-TuA11, **78**
Monzami, E.: 2D+MI+SA-MoM6, 2
Moore, G.: SS+AS+EM-WeA1, 167
Moore, L.: SP+SS+TF-WeM12, 140
Moraes, V.: TF1-ThM13, **198**
Morales, E.: SS+2D-WeM5, **142**
Morales-Cifuentes, J.R.: SS1+AS+HC+NS-TuM10, 68
Moraru, D.: EM-FrM4, 254
More, K.: IS-ThA6, 213
Moreno, D.: AC+MI-WeM6, 123
Morgan, H.: HC+SS-WeM12, 131
Morgenstern, M.: MI+2D+AC-MoA1, 31
Morikawa, Y.: PS-ThP17, 237
Morishita, T.: 2D-ThP1, **227**
Morosini, V.: AC+AS+SA-ThM4, 176
Moroz, D.J.: SS+2D-WeM13, 142
Moroz, P.: SS+2D-WeM13, **142**
Morris, T.: SS-TuP11, 118
Morrish, F.: BI+AS+SA-TuA10, 82; BI+MI-WeM12, 128
Moser, T.: EM+NS-WeM10, 129
Moses, P.G.: SS+AS-TuA12, 96
Moten, R.: NS-MoM1, 12
Motobayashi, K.: SP+AS+MI+NS+SS-MoM5, 20
Motomura, H.: PB+BI+PS-TuM1, 59;
PB+BI+PS-TuM5, 60
Moulder, J.F.: AS+SS-WeM3, 125; AS-TuP9, 104
Mowll, T.R.: 2D+TF-WeM6, **121**
Moya, J.M.: EL+AS+EM+MI+TF-FrM4, 252;
EL+AS+EM+TF-ThP1, **229**
Mu, R.: MN-ThP2, 235; MS-TuP5, 111; NS-TuP5, 112; SS+AS+HC-MoA1, 45
Mu, T.: PS-TuM6, 62
Mudryk, Y.: AC+MI-WeM12, 124
Mueller, M.: SA+2D+AC+AS+TF-TuM12, **64**
Mugnaini, V.: NS+BI-ThA9, 217
Mulhewijk, P.M.: EL+AS+EM+MI+TF-FrM7, **253**; VT-MoA4, 51; VT-TuA10, 101
Mulckhuysen, W.F.W.: VT-TuA10, 101
Mulhern, E.: VT-WeM10, 147
Müller, B.: EL+AS+BI+EM+TF-ThA8, **205**
Muller, R.: NS-MoM10, 14
Mullins, D.R.: IS+HC-WeA4, **158**
Mulvaney, S.P.: 2D-ThA6, 201
Mundy, J.Z.: AS-TuP7, 103
Munem, M.: AS-TuP18, **105**
Muñoz-Zurita, A.L.: 2D-ThP4, 227
Munster, N.: SS+AS+EM-WeA2, 167
Muralidharan, N.: EM+SS+TF-ThA1, **206**;
TF+EM-MoA2, 47
Murari, N.: TF2-ThM1, 198
Muratore, C.: 2D+NS-FrM1, **249**; 2D-ThP5, 227
Murayama, T.: PS-ThP17, 237
Murday, J.S.: MS+AS-TuM12, **58**
Murdoch, R.: NS+BI-ThA4, **216**
Murphy, N.R.: EL+AS+BI+EM+TF-ThA3, **205**;
EL+AS+BI+EM+TF-ThA4, 205
Muruganathan, M.: EM-FrM4, **254**;
HI+MI+NS-ThA11, 212
Murugesan, V.: IS-ThP3, 233
Muscat, A.J.: EM-ThP7, 231; SS+AS+EM-WeA11, 168
Music, D.: SE+TR-WeM1, 137
Musicó, B.: EM+AC+SS+TF-ThM12, 183; EM-ThP13, 232; EM-ThP8, 232
Mussenbrock, T.: PS-TuM10, 62
Mussler, G.: MI+2D+AC-MoA1, 31
Mutch, M.J.: EM+AC+SS+TF-ThM5, **182**
Myers-Ward, R.L.: TF1-ThM10, **197**
Myoui, A.: PB+BI+PS-MoA11, 37
Myung, Y.: TF-TuA10, 99
— N —
Na, L.: SE+MS+TF-TuA10, 93
Naaman, R.: BI+PB-TuP4, 108; TF+SA+MI-TuM13, 73
Naciri, M.: PB+BI+PS-TuM3, 60
Nadeau, L.: BI+PB-TuP7, 108
Naes, B.: AS-ThA10, 204; AS-ThA11, 204
Nagabhirava, B.: PS-MoM10, 18
Nagahata, K.: PS-ThA8, 219
Nagase, M.: MS+AS-TuM1, 57
Nageswara Rao, S.V.S.: EM-MoA9, 31
Nagorny, V.P.: PS1-ThM5, **191**; PS-ThP13, 237
Nahm, R.K.: SA+2D+AC+AS+TF-TuM5, 64;
TF+SA+MI-TuM11, 72
Naik, A.K.: MN+2D+NS-ThA3, **214**;
MN+2D+NS-ThA7, 215
Naik, R.R.: 2D-ThP5, 227
Nakakita, S.: BI+MI-WeM4, 127
Nakamura, I.: SS-TuP1, **116**
Nakamura, J.: 2D+MI-MoA8, 27; HC+SS-ThM2, **184**
Nakamura, K.: PS-WeA7, 163
Nakamura, T.: PS-ThP18, 237
Nakano, Y.: PS-WeA7, 163
Nakayama, K.S.: SS2+AS+HC+NS-TuM13, **71**
Nallan, H.: TF2-ThM3, 199
Nanayakkara, C.E.: TF-MoM9, **23**
Nandasiri, M.I.: IS-ThP3, **233**
Narai, A.: PS-ThP34, 240
Narimannezhad, A.: AS+SS-ThM1, **178**
Narwankar, P.: AS+SS-ThM2, 178
Näslund, L.-Å.: 2D+MI-TuM3, 53
Nastasi, M.: EM+AC+SS+TF-ThM3, 182
Nath, A.: EM-FrM5, 254; EM-MoA3, 29
Natoli, S.N.: TF-ThA7, 224
Navarro, C.: TF-ThA1, 223
Nazarudin, N.F.F.B.: TF-ThP17, 242
N'Diaye, A.T.: TF+SA+MI-TuM2, 71
Necas, D.: PB+BI+PS-MoA8, 36
Nedrygailov, I.: SS1+AS+HC+NS-TuM1, 67
Needham, D.: BP-SuA3, **1**
Neek-Amal, M.: 2D+MI+SA-MoM11, 3
Neese, C.F.: PS-TuM3, 62
Negrea, G.: SE+NS+TF+TR-TuM10, 65
Neilson, J.: 2D+TF-WeM11, 122
Nelson Weker, J.: AS-WeA10, 152; SA-TuP1, 113
Nelson, A.J.: AC+MI-WeA12, **151**; AC-TuP2, 102
Nelson, C.: MS-TuA4, 86
Nelson, S.F.: TF2-ThM2, 198
Nemanich, R.J.: PS2-ThM1, **192**
Nemsak, S.: TF+SA+MI-TuM4, 72
Nepal, N.: PS-ThP5, 235; TF+SA+MI-TuM12, **73**
Netzer, F.P.: HC+NS+SS-WeA1, 155;
SS+AS+HC-MoM9, 22; SS+AS-TuA2, **95**;
SS+AS-TuA9, 95
Neumann, C.: PS-WeA11, 164
Neumann, E.: MI+2D+AC-MoA1, 31
Neumann, R.: AS+SS-WeM10, 125
Neupane, M.: 2D-TuA11, 78
Neurock, M.: HC+NS+SS-WeA4, 155
Newberg, J.: SS+AS-WeM4, **143**
Newman, J.: AS+SS-WeM3, **125**; EW-TuL5, **77**
Neyerlin, K.C.: SA-TuP1, 113
Nganheu, A.S.: 2D+MI-TuM13, 54
Ngo, C.: AS+AC-TuM5, **55**; AS-TuP22, 106;
AS-TuP23, 106; AS-WeA10, 152; SA-TuP1, 113
Ngunjiri, J.: AS-WeA8, 152
Nguyen, C.V.: TF-ThP24, **243**
Nguyen, H.M.: EM+SS+TF-ThA8, 207; TF-ThP32, **245**
Nguyen, S.D.: TF-TuA8, 99
Nguyen, T.: PS-ThP8, **236**
Nguyen, T.D.: EM+AC+SS+TF-ThM4, 182
Nguyen, Y.N.: PB+BI+PS-TuM12, 61
Nicholl, R.J.: MN+MS-FrM8, 257
Nickels, M.: EM+SS+TF-ThA9, 207
Nickles, J.: EM+MI+MN-TuA11, 83; EM-ThP6, 231
Nicolet, C.: TF-ThA1, 223
Nicotera, E.: HC+SS-ThM11, 185
Nie, X.: TR-ThP1, 248
Niehuis, E.: AS+BI-MoA8, 28; AS+SS-ThM12, 179; HI+MI+NS-ThA3, 210
Nielsen, M.: NS-TuM6, 59; SA-TuP2, 113
Nieuwkoop, E.: VT-MoA4, 51
Nijland, B.A.H.: VT-TuA10, 101
Nikiforov, A.: PB+BI+PS-MoA2, 35
Nikitenko, I.: AC+AS+SA-ThM4, 176
Nikolaev, P.: SS+AS+HC-MoM8, 22
Nikoobakht, B.: 2D+TF-WeM12, 122
Nishi, Y.: EM+MI+MN-TuA11, 83;
EM+MI+MN-TuA7, **83**; EM+SS+TF-ThA8, 207; EM-ThP1, 230; EM-ThP6, 231;
TF+EM+MI-WeA11, 170; TF-ThP13, 242;
TF-ThP27, 244
Nishiyama, K.: PB+BI+PS-MoA11, **37**
Nishizawa, Y.: PS1-ThM3, 190
Nisol, B.: PS-ThP22, 238; SE+MS+TF-TuA9, 92
Niu, C.: MI+2D+AC-MoA1, 31
Niu, X.: EM+NS+SP+SS-WeA10, 154
Noda, S.: PS-WeA9, **163**
Noé, P.: PS-WeM3, 136
Noguchi, M.: PS-ThP18, 237
Noh, J.: 2D+NS-WeA12, 150
Noh, J.H.: 2D+MI-MoA6, 26
Noked, M.: MS-MoM6, 12
Nolte, K.: BI+AS-MoM6, 6
Noma, M.: TR+BI+SE+TF-ThA8, **225**
Nonnenmann, S.S.: SP+AS+MI+NS+SS-TuM1, **66**
Nordeen, P.: MI-TuP1, 109; TF+MI-WeA1, 171
Nordell, B.J.: PS-MoA1, 40
Nordgren, J.: AC+AS+SA-ThM11, 177
Nordlund, D.: 2D-TuA11, 78
Norman, A.G.: TF-TuA8, 99
Nørskov, J.: HC+SS-ThA7, 209
Notte, J.A.: HI-WeA3, **156**
Nouri, L.N.: NS-MoM8, **13**
Nova, K.: HI+NS-ThM1, 185
Novikov, S.V.: 2D+NS-WeA11, 150
Novotny, Z.: HC+NS+SS-WeA1, 155;
SS+AS+HC-MoM9, **22**
Nozaki, T.: PS-ThA1, **217**
Nune, S.: IS-FrM9, 256
Nunley, N.T.: EL+AS+EM+MI+TF-FrM5, 252
Nunley, T.N.: EL+AS+EM+TF-ThP1, 229
Nunn, N.J.: NS-TuM2, 58
Nunney, T.S.: AS-MoM6, 4; AS-TuP2, **102**;
AS-TuP3, 102; AS-WeA1, 151
Nuzzo, R.: IS-ThM10, 188
Nyakiti, L.O.: EM-FrM5, 254
Nygren, L.: AS-WeA9, 152
Nyns, L.: SA+AS+BI+MI-TuA12, 91

— O —

- O'Donnell, K.: SS+AS+EM-WeA1, 167
 Oakes, L.: EM+SS+TF-ThA1, 206; MS-MoM8, **12**; SS+AS+HC-MoM8, 22; TF+EM-MoA8, 48
 Oates, T.: 2D-ThA12, 202
 Öberg, K.I.: SS-TuP12, 118
 Obermüller, T.: SS+AS-TuA2, 95
 Obrusnik, A.: PB+BI+PS-MoA8, 36; PB+BI+PS-TuM12, 61
 Ochoa, M.: MN+BI-ThM5, 189
 Ocola, L.E.: SP+SS+TF-WeM12, 140; TF2-ThM10, **199**
 O'Connell, D.: PS+AS+SS-MoA11, 39; PS-TuM10, 62
 O'Conner, R.: EM+SS+TF-ThA11, 208
 O'Donoghue, J.: PB+BI+PS-MoA5, 36
 Oehrein, G.S.: PS-ThA9, 219; PS-WeA1, 162
 Oertel, J.A.: PS-ThP32, 240
 Ogawa, D.: PS-WeA7, **163**
 Ogawa, S.: HI-WeA7, **157**; PS+AS+SS-MoA4, 37
 Ogawa, T.: HC+SS-ThM2, 184
 Ogrinc Potocnik, N.: AS+BI-MoA10, 29; AS+BI-MoA2, **27**
 Oguro, Y.: MS-TuP2, **110**
 Oh, J.: HC+NS+SS-WeA7, 155
 Ohashi, T.: HI-WeA7, 157
 O'Hayre, R.: AS-TuP22, 106
 Ohldag, H.: MI+2D+AC-MoM11, **11**
 Ohlhausen, J.A.: AS-TuP20, **105**
 Ohno, Y.: BI+MI-WeM4, 127
 Ohta, T.: 2D+NS-FrM11, 251
 Oishi, T.: PS+AS+SS-MoA4, 37
 Ojeda, I.: BI+AS+SA-TuA2, 81
 Ojeda-Aristizabal, C.: 2D+MI-ThM12, 176
 Okamoto, M.: PB+BI+PS-MoA11, 37
 Okimoto, T.: PS-ThP34, 240; TF-ThP33, 245
 Oktyabrysky, S.: SE+2D+EM-WeA11, 166
 Okuda, T.: MI+2D+AC-MoA8, 32
 Okyay, A.K.: EM+NS+PS+SS+TF-MoM3, 7
 Oldham, C.J.: TF-TuM13, 75
 Oleynik, I.I.: 2D+MI-ThM2, 175
 Olson, N.: AS+BI-MoA5, 28
 Olynick, D.L.: PS+AS+SS-MoA9, 38
 O'Mahony, A.: TF-FrM2, 260
 O'Neill, L.: PB+BI+PS-MoA5, **36**
 Onishi, S.: 2D+MI-ThM12, 176
 Ono, T.: BI+MI-WeM4, 127
 Oostdijck, B.W.: VT-TuA10, 101
 Openshaw, M.: AS-TuP4, 102
 Opila, R.L.: TF-ThP5, 241
 Oppeneer, P.: AC+AS+SA-ThM11, 177
 Ornleas, A.: NS-TuP2, 111
 Orosz, K.S.: BI+AS+SA-ThM10, 181
 Ortiz, B.R.: TF-TuA8, 99
 Ortoll-Bloch, A.: SS+AS-WeM6, 143; SS+HC-TuA2, 97
 Osano, Y.: PS1-ThM3, **190**
 Osgood, R.: 2D-ThP6, 227
 Oshima, Y.: EM-MoA5, 30; HI+MI+NS-ThA11, 212
 Osmani, B.: EL+AS+BI+EM+TF-ThA8, 205
 Ostrovski, Y.: TF+EM+MI-WeA10, 170
 O'Toole, R.: PS+SE-MoM6, 15
 Ou, S.-L.: TF-ThP40, 246
 Oura, M.: SA+AS-MoA4, 42
 Ouyang, L.Z.: AS-TuP29, 107; EM-ThP12, 232
 Ovanessian, R.A.: PS+TF-WeA8, **161**; PS-WeA12, 164; TF-MoM10, 23
 Ovchinnikova, O.S.: HI+MI+NS-ThA4, 210
 Ovchinnikov, O.S.: AS+SS-TuA2, 79
 Ovchinnikova, O.S.: HI+MI+NS-ThA8, 211; HI+NS-ThM10, **186**
 Overbury, S.H.: IS+HC-WeA4, 158
 Overton, J.: BI+AS-MoM2, 6
 Overzet, L.J.: PS-TuM5, 62; PS-WeM6, **137**
 Owczarek, S.: HC+SS-ThM10, 185
 Owen, A.G.: TF+MI-WeA7, **171**
 Owen, J.: NS-MoM10, 14
 Oyama, S.: HI-WeA7, 157
 Oyefeso, A.: BI+AS+SA-TuA3, 82
 Oyelade, A.: TF+PS+SE-MoA2, 49
 Ozden, B.: EM+NS+PS+SS+TF-MoM6, 8; EM-MoA11, **31**; EM-MoA8, 30
 Ozeri, O.: 2D+MI-TuM3, 53
 Ozkan, A.: PS+SE-MoM4, **14**; PS-ThP21, 238
 Ozkan, T.: TF-FrM5, 260
 — P —
 Pacholski, M.L.: AS-WeA8, **152**
 Pacold, J.I.: AC+AS+SA-ThM6, 177; AC-TuP1, **102**
 Page, S.C.: AS-TuP6, 103; EW-TuL4, 77
 Pageau, A.: PS-ThA6, 218
 Paisley, E.A.: TF2-ThM5, 199
 Pal, D.: EL+AS+EM+MI+TF-FrM4, 252
 Palisaitis, J.P.: TF+PS+SE-MoA9, 50
 Pallier, C.: PS-MoA1, 40
 Palmes, E.: EM+NS-WeM6, 129
 Paltiel, Y.: TF+SA+MI-TuM13, **73**
 Pan, S.: EM+NS-WeM11, 129; EM+NS-WeM13, 130; EM+NS-WeM5, 129
 Pan, Y.: PS-WeA4, 163
 Panaccione, G.: SA+AS-MoA4, 42
 Pandey, R.R.: EM+MI+MN-TuA12, 84
 Paneta, V.: SE+NS+TF+TR-TuM12, 66
 Panici, G.A.: PS2-ThM11, 194
 Panjan, M.P.: PS-TuM13, **63**
 Pankin, A.Y.: PS1-ThM2, 190
 Papa, F.: VT-MoA10, 52
 Papalia, J.M.: PS-MoA2, 40
 Paprotny, I.: NS-MoM3, **13**
 Paquette, M.M.: EM+AC+SS+TF-ThM12, 183; EM+AC+SS+TF-ThM4, 182; EM-ThP13, 232; EM-ThP8, 232; PS-MoA1, **40**
 Parajuli, P.: BI+MI-WeM11, 128
 Paranjpe, A.P.: PS-ThP12, 236
 Paraschiv, V.: PS-ThP33, 240
 Pargon, E.: PS2-ThM6, 193; PS-MoM11, 18
 Parish, C.: AS-TuP24, 106
 Park, I.-Y.: VT-TuP7, **119**
 Park, J.: TF-TuA10, 99
 Park, J.H.: 2D+MI+SA-MoM1, 2; 2D+NS-FrM9, 250; 2D-ThA8, **201**
 Park, J.Y.: SP-TuP3, 115; SS1+AS+HC+NS-TuM1, 67; TR+BI+SE+TF-ThA9, 226
 Park, K.H.: 2D+TF-WeM2, **121**
 Park, K.T.: SS+HC-TuA9, 97
 Park, M.: EM+NS+PS+SS+TF-MoM6, 8; EM-MoA11, 31; EM-MoA8, 30
 Park, S.: 2D+MI-TuM5, **53**; NS-TuP9, 112
 Park, S.W.: SS+AS+EM-WeA8, **168**; TF+EM+MI-WeA8, 170
 Parker, C.B.: MN+MS-FrM4, 257
 Parker, D.S.: SP+2D+AS+NS+SS-MoA10, 44
 Parkinson, G.S.: SS+AS+HC-MoA3, **45**; SS+AS+HC-MoA8, 46
 Parpia, J.M.: MN+NS-WeA4, 159
 Parra, E.: BP-SuA3, 1
 Parschau, M.: SS-ThM3, 195
 Parsons, G.N.: AS-TuP7, 103; SS+HC-FrM2, 258; TF2-ThM13, 200; TF-FrM1, 259; TF-TuM13, **75**
 Parthasarathy, R.: AS-TuP29, **107**
 Pasa-Tolic, L.: AS+BI-MoA2, 27
 Paschen, S.: TF1-ThM13, 198
 Passarelli, M.K.: AS+BI-MoA8, 28; AS+SS-ThM12, 179
 Pastewka, L.: TR+AS+NS+SS-WeA11, 173
 Patera, L.: SA+2D+AC+AS+TF-TuM3, 63
 Paterson, A.: PS+TF-WeM4, 134
 Patlolla, R.: TF+EM+MI-WeA10, 170
 Paudyal, D.: AC+MI-WeM12, 124
 Paukov, M.: AC+MI-WeA11, 151
 Paul, D.: AS+SS-WeM3, 125
 Paul, M.K.: MN+MS-FrM2, 257
 Paul, W.: HI+MI+NS-ThA3, 210; SP+AS+MI+NS+SS-TuA3, 93
 Pavelec, J.: SS+AS+HC-MoA8, 46
 Pavenelo, M.: SS1+AS+HC+NS-TuM5, 68
 Payne, D.J.: IS-ThA1, **212**
 Payne, G.F.: NS+BI-ThA8, 216
 Payne, S.: EM+AC+SS+TF-ThM1, 182
 Pearce, A.J.: MS-MoM6, 12
 Pearson, J.E.: MI+2D+AC-MoM3, 10
 Pecharsky, V.K.: AC+MI-WeM12, 124
 Peck, J.A.: PS2-ThM11, **194**
 Peckler, L.: EM-ThP7, **231**
 Pedersen, H.: TF+PS+SE-MoA4, 49
 Peeters, F.: 2D+MI+SA-MoM11, 3
 Peethala, B.: TF+EM+MI-WeA10, 170
 Pehrsson, P.E.: IS-FrM6, 255
 Pei, D.: TF+EM+MI-WeA11, 170; TF+EM+MI-WeA12, 170; TF-ThP27, **244**
 Pellegrino Morono, J.: AS+SS-WeM10, 125
 Pelster, A.: BI+PB-TuP5, 108
 Pemmaraju, C.: AC+AS+SA-ThM11, 177
 Pemmaraju, C.D.: AC+AS+SA-ThM6, 177
 Peng, Q.: SS+AS-WeM5, 143; SS-TuP17, 118; TF2-ThM6, **199**
 Penn, D.R.: IS-ThA8, 213
 Pentzer, E.B.: TF-TuA11, 100
 Peppler, M.: AS-TuP27, 107
 Percy, C.: VT-MoM10, 25; VT-MoM8, 25; VT-MoM9, **25**
 Perepichka, D.F.: SS-TuP8, 117
 Perera, A.G.U.: EM-FrM6, 254
 Perez Martinez, C.: HI+NS-ThM5, 186
 Perez, C.: SS+2D-WeM5, 142
 Perez, F.J.: SE+TR-WeM5, 138
 Perez, S.: MI+2D+AC-MoA9, 32
 Perkins, C.L.: TF-FrM8, **261**
 Perovic, D.: 2D+NS-WeA8, 149
 Perrino, A.: SP+AS+MI+NS+SS-MoM4, **20**
 Perrotta, A.: TF1-ThM12, **198**; TF-FrM4, 260
 Pershad, Y.W.: AS+SS-WeM1, **124**; SS+HC-FrM1, 258
 Persson, O.: EM+NS+SP+SS-WeA4, 153
 Persson, P.O.A.: SE+TR-WeM1, 137; TF+PS+SE-MoA9, 50
 Pesavento, P.V.: PS-WeM10, 137
 Peshek, T.J.: SS+2D-WeM6, **142**; TF-TuA11, 100
 Peterson, E.: AS+SS-WeM2, 124; HC+SS-ThM11, **185**
 Peterson, E.W.: SS+AS+HC-MoA5, 45
 Peterson, G.G.: EM+AC+SS+TF-ThM3, **182**
 Peterson, G.W.: IS-FrM6, 255
 Peterson, T.: BI+MI-WeM13, 128
 Petit, L.: AC+MI-WeM12, **124**
 Petit-Etienne, C.: PS2-ThM6, 193; PS-MoM11, 18
 Petrik, N.G.: SS+HC-TuA7, 97
 Petrov, A.Yu.: SA+AS-MoA4, 42
 Petrov, G.M.: PS+SE-MoM11, 16; PS-ThP30, 239; PS-WeA3, 162
 Petrova, Tz.B.: PS+SE-MoM11, 16; PS-ThP30, 239; PS-WeA3, 162
 Petrovykh, D.Y.: NS+BI-ThA9, **217**
 Petz, C.W.: TF1-ThM1, 196
 Pfeifer, V.: IS+HC-WeA1, 158
 Philipson, R.: TF+EM+MI-WeA3, 169
 Phillips, A.: EL+AS+BI+EM+TF-ThA9, 206; HC+SS-WeM12, 131
 Phillips, R.S.: SS2+AS+HC+NS-TuM3, 69
 Piallat, F.: PS-WeM3, 136

Author Index

- Piao, H.: AS-TuP11, 104
Piascik, J.R.: MN+MS-FrM4, 257
Piercy, B.D.: TF-FrM3, **260**
Pierron, O.: TF+PS+SE-MoA6, 50
Pierson, J.F.: SS+AS-TuA1, 94
Pimenta Barros, P.: TF-ThA1, 223
Pimpinelli, A.: SS1+AS+HC+NS-TuM10, 68
Pincelli, T.: SA+AS-MoA4, **42**
Pint, C.L.: EM+SS+TF-ThA1, 206; EM+SS+TF-ThA7, 207; MS-MoM8, 12; SS+AS+HC-MoM8, 22; TF+EM-MoA2, 47; TF+EM-MoA8, 48
Piotrowicz, P.: PS-WeM10, 137
Pirkil, A.: AS+BI-MoA8, 28; AS+SS-ThM12, **179**; EW-WeM8, 130
Pitters, J.L.: HI+NS-ThM1, 185
Piumi, D.: PS-ThP33, 240
Pivovar, B.: AS-WeA10, 152; SA-TuP1, 113
Plank, H.: NS-MoM5, 13
Pletincx, S.: TF-ThA6, **223**; TF-ThP2, 241
Plucinski, L.: MI+2D+AC-MoA1, **31**; TF+SA+MI-TuM4, 72
Podraza, N.J.: EL+AS+BI+EM+TF-ThA10, 206; EL+AS+BI+EM+TF-ThA6, **205**; EL+AS+BI+EM+TF-ThA9, 206
Pohlman, A.J.: SS1+AS+HC+NS-TuM3, 68
Polcawich, R.G.: MN+MS-FrM2, 257
Polcik, P.: SE+TR-WeM6, 138
Polezhaev, A.: SS-TuP11, 118
Polozov, V.I.: TF-ThP45, 247
Polunin, P.M.: MN-WeM6, 133
Polycarpou, A.A.: TF-FrM5, 260
Ponath, P.: EL+AS+EM+MI+TF-FrM4, 252
Pond, T.A.: AS-TuP28, 107
Poedt, P.: TF-TuM6, **74**
Pookpanratana, S.: TF-ThA7, **224**
Popczun, N.J.: AS-ThA9, 203; HI+NS-ThM11, **187**
Porach, Z.: SP-TuP1, 115
Porcelli, T.: VT-TuA9, 101
Porter, L.M.: EM-MoA4, 30
Portoles, J.F.: HI+NS-ThM12, 187
Portz, A.: AS-TuP8, 103
Posen, S.: VT-TuA7, **100**
Posseme, N.P.: NS-MoM8, 13
Poulain, G.: PS-WeM2, 136
Poulouse, J.: PS-TuM5, **62**; PS-WeM6, 137
Pourang, K.: MI-TuA9, 85
Pourtois, G.: EM+MI+MN-TuA9, 83
Powell, C.J.: IS-ThA8, **213**
Pozzi, E.: SP+AS+MI+NS+SS-TuM2, 66
Prabhakaran, V.: EM+NS-WeM10, 129
Prakash, A.: TF1-ThM6, 197
Pranda, A.: PS-ThA9, **219**
Prasad, D.K.: EW-TuM8, **57**
Pratihari, S.: HC+SS-ThA12, 210
Preciado, E.: 2D+MI-ThM6, 175
Prendergast, D.G.: AC+AS+SA-ThM11, 177; AC+AS+SA-ThM6, 177
Price, D.: SE+2D+EM-WeA8, 165
Primetzhofer, D.: SE+NS+TF+TR-TuM12, 66; SE+TR-WeM1, 137
Prindle, C.: PS-MoM9, 18
Prinz, F.: TF+PS+SE-MoA5, 49
Prochaska, L.: TF1-ThM13, 198
Provine, J.: TF+PS+SE-MoA5, 49
Provo, J.L.: VT-WeM12, **147**
Prusnick, T.: EW-WeL5, **148**
Pudasaini, P.R.: 2D+MI-MoA6, 26; 2D+NS-FrM10, **250**; 2D-ThP11, 228
Pulpytel, J.: PB+BI+PS-MoA3, 36
Purandare, Y.: SE+TR-WeM5, 138
Puretzky, A.A.: 2D+NS-WeA3, 149; SS+AS+HC-MoM8, 22
Puro, M.: VT-TuA9, 101
Puurunen, R.L.: AS+SS-ThM5, **178**
Pylypenko, S.: AS+AC-TuM5, 55; AS-TuP22, 106; AS-TuP23, 106; AS-TuP26, 107; AS-WeA10, **152**; SA-TuP1, 113
— Q —
Qazilbash, M.M.: EM-MoM5, 9
Qerimi, D.Q.: PS-ThP24, **239**
Qi, J.: TF+MI+NS-WeM4, **145**
Qin, X.: 2D+MI-MoA2, 26
Qin, Z.: 2D+MI-ThM1, **175**
Qiu, X.H.: SP+AS+MI+NS+SS-TuM3, **67**
Qu, C.: PS-ThP7, **235**
Quan, J.: HC+SS-ThM2, 184
Quayle, P.: EM+NS+PS+SS+TF-MoM8, 8
— R —
Race, A.M.: AS+BI-MoA8, 28
Rack, P.D.: 2D+MI-MoA6, 26; 2D+NS-FrM10, 250; 2D-ThP11, 228; HI-WeA4, 157; HI-WeA8, **157**; NS-MoM5, 13
Radauscher, E.J.: MN+MS-FrM4, 257
Rading, D.: HI+MI+NS-ThA3, 210
Radisic, D.: PS-ThP33, 240
Rafique, S.: MN+2D+NS-ThA6, 214
Raghuraman, S.: 2D-ThA11, 202
Rahimi, R.: MN+BI-ThM5, 189
Rahman, M.M.: PS-ThP2, 235
Rahman, R.: MI-TuA9, 85
Rahman, T.S.: HC+SS-ThA11, 210; SS1+AS+HC+NS-TuM13, **69**
Rai, A.: 2D-ThA8, 201
Rai, R.: SS+AS-TuA3, **95**; SS-TuP4, 116; SS-TuP7, 117
Raimondi, S.: VT-TuA9, 101
Rajput, S.: SP+2D+AS+NS+SS-MoA11, **44**
Rajput, S.: SP+2D+AS+NS+SS-MoA10, 44
Rakowska, P.D.: AS+BI-MoA8, 28; AS+BI-MoA9, **29**
Ramalingam, G.: 2D+MI+SA-MoM6, 2; SP+SS+TF-WeM4, **139**
Raman, P.: PS-WeM12, 137
Ramana, C.V.: SE+NS+TF+TR-TuM5, 65; TF1-ThM4, 196
Ramasse, Q.: TF+SA+MI-TuM4, 72
Ramm, J.: SE+TR-WeM13, 139; SE+TR-WeM2, **137**
Rand, R.H.: MN+NS-WeA4, 159; MN-WeM5, 132
Rangan, S.: SS+HC-FrM4, 259
Rangelow, I.W.: MN+NS-WeA7, 159; PS+AS+SS-MoA9, 38
Rani, S.: SS+AS-WeM4, 143
Ranjan, A.: PS+TF-WeM3, 134; PS2-ThM4, 193; PS-MoA9, 41; PS-MoM1, 16; PS-MoM8, 17; PS-ThA7, 218
Rankin, R.: SP+SS+TF-WeM11, 140
Rao, R.: SS+AS+HC-MoM8, 22
Rao, S.: PS-ThP33, 240
Rapp, J.: PS-WeM10, 137
Rappich, J.: 2D-ThA12, 202
Rastogi, V.: PS2-ThM4, **193**; PS-ThA7, 218
Rauf, S.: PS+TF-WeM5, 134; PS1-ThM4, 190; PS1-ThM6, 191; PS-TuM1, 61
Rault, J.E.: SA+AS-MoA3, **42**; SA+AS-MoA6, **42**; TF+SA+MI-TuM4, 72
Raveh, A.: HI+MI+NS-ThA9, 211; HI-WeA4, 157
Rawal, T.B.: HC+SS-ThA11, **210**
Ray, H.B.: PS-WeM10, 137
Raza, M.: SS+AS-TuA1, **94**
Rebellato, J.: SA+AS-MoA6, 42
Rebello de Figueiredo, M.: SE+TR-WeM12, 138
Reed, A.N.: TF-ThP41, **246**
Reed, R.A.: MN+MS-FrM10, 258; MN+MS-FrM8, 257
Reese, C.: EM-FrM2, 253
Reese, M.O.: TF-FrM8, 261
Reeves, R.V.: SE-TuP5, 114
Regoutz, A.: IS-ThA1, 212
Reich, J.: AS-WeA11, 153
Reich, K.: PS+2D-TuA3, 89
Reid, K.R.: NS+BI-ThA2, 215
Reinholt, S.J.: NS+BI-ThA7, **216**
Reinke, M.: TF-TuM3, **73**
Reinke, P.: 2D+MI+SA-MoM6, 2; SP+SS+TF-WeM4, 139; SS2+AS+HC+NS-TuM10, 70
Reish, M.: SS+HC-TuA8, 97
Rementer, C.R.: MI-TuP1, 109; TF+MI-WeA1, **171**
Ren, T.: TF-ThA7, 224
Ren, Y.D.: HC+SS-ThM1, 183
Renault, O.J.: AS+AC-TuM6, **55**; SA+AS-MoA3, 42; SA+AS-MoA5, 42
Reniers, F.: PS+2D-TuA1, 88; PS+SE-MoM4, 14; PS+SE-MoM5, 15; PS+SE-MoM8, 15; PS2-ThM10, 193; PS-ThP21, 238; PS-ThP22, 238; SE+MS+TF-TuA9, **92**
Reuter, R.: IS-ThP7, 234
Reutzel, M.: SS+AS+EM-WeA2, 167
Reynolds Jr., C.: NS-MoA2, 34
Reynolds, A.: NS-MoM1, 12
Rezaee, M.: 2D+TF-WeM5, **121**
Rhallabi, A.: PS1-ThM12, 191
Rhodes, M.: AS-ThA11, 204
Rice, W.: TF+EM+MI-WeA9, 170
Richard Plouet, M.: TF+PS+SE-MoA3, 49
Richards, R.: AS-TuP22, 106
Richter, C.A.: TF-ThA7, 224
Ricker, J.: VT-MoM3, 24; VT-MoM4, **24**
Riedl, H.: SE+NS+TF+TR-TuM12, **66**; TF1-ThM13, 198
Rincon, J.: BI+PB-TuP3, 108
Ringel, S.A.: EM-MoA5, **30**
Riposan, A.: TF-ThP37, 246
Riss, A.: 2D+MI-ThM12, 176
Risse, T.: SS+AS-TuA7, **95**
Rivin, O.: 2D+MI-TuM3, 53
Roach, A.: AS-WeA11, 153
Roark, C.M.: PS1-ThM2, 190
Robbennolt, S.: SE+2D+EM-WeA12, 166
Roberts, A.J.: AS-MoM10, **5**
Robertson, J.L.: MI+2D+AC-MoM4, 10
Robertson, J.W.F.: TF-ThA7, 224
Robertson, W.M.: TF+BI-ThA2, 222
Robey, S.W.: SS+HC-TuA10, **97**
Robinson, J.A.: 2D+MI+SA-MoM1, 2; 2D+NS-WeA12, 150
Robinson, J.T.: 2D+MI-ThM5, 175; 2D-ThA6, 201
Robinson, Z.: PS-ThP5, 235
Robinson, Z.R.: 2D+TF-WeM6, 121; TF+SA+MI-TuM12, 73
Rödel, T.C.: SA+2D+AC+AS+TF-TuM2, 63
Rodelas, J.: AS-WeA11, 153
Rodgers, B.: 2D-ThP8, 228; 2D-ThP9, 228
Rodriguez, C.: EL+AS+EM+MI+TF-FrM4, 252; MI+2D+AC-MoA9, 32
Rodriguez, J.: HC+SS-WeM10, **131**
Rodriguez, M.A.: SE+NS+TF+TR-TuM4, 65
Rodriguez, R.E.: TF+MI+NS-WeM11, **146**
Rodriguez, R.T.: TF-ThP29, 244
Rodriguez-Freire, L.: AS+SS-WeM2, 124
Rogalev, A.: AC+MI-WeM1, 122
Rogers, B.R.: MS+AS-TuM12, 58
Rohlfing, M.: MI+2D+AC-MoA3, 32
Rohrer, G.S.: SE+NS+TF+TR-TuM1, **65**
Rohwerder, M.: IS-ThA10, 213; TF-ThP2, 241
Rojas, O.J.: TF2-ThM13, 200
Roldan Cuenya, B.: HC+NS+SS-WeA10, 156; IS+HC-WeA11, **159**

Author Index

- Rondinelli, J.M.: SS2+AS+HC+NS-TuM10, 70
Rondinone, A.J.: 2D+MI-MoA6, 26;
HI+MI+NS-ThA10, **211**
Rook, K.: PS-ThP12, 236
Roozeboom, F.: TF-TuM6, 74
Roqueta, F.: PS1-ThM12, 191
Rose, V.: NS-TuA3, **87**; SP+AS+MI+NS+SS-MoM2, 19
Rosen, J.: 2D+MI-TuM3, 53
Rosenberg, A.: TF+MI-WeA8, 172
Rosenberg, R.A.: BI+PB-TuP4, **108**
Rosenhahn, A.: BI+AS-MoM6, 6
Rosenthal, S.J.: NS+BI-ThA2, 215
Rösicke, F.: 2D-ThA12, 202
Rosner, F.: SS+AS-TuA4, 95
Rossi, G.: SA+AS-MoA4, 42
Rouleau, C.: MI-TuP2, 110
Roussel, P.: AC+AS+SA-ThM3, **176**
Roussos, J.: TF+EM+MI-WeA1, 169
Rowe, E.: BI+MI-WeM13, 128;
EM+AC+SS+TF-ThM1, 182
Rowe, M.: SE+MS+TF-TuA2, 91
Rowley, J.T.: 2D+MI-ThM10, **175**
Roy, A.: PS-ThP20, **238**
Roy, S.: HC+SS-ThA2, **209**; SS-TuP19, 118
Roy, S.K.: BI+MI-WeM2, 127
Roy, U.: EM+AC+SS+TF-ThM10, 183
Roychowdhury, T.: SE+2D+EM-WeA4, **165**;
TF-ThP21, 243
Rozhkova, E.A.: NS-TuM12, **59**
Ruan, W.: 2D+MI-ThM12, 176
Rubio, E.: TF1-ThM4, 196
Rubio-Zuazo, J.: SA+AS+BI+MI-TuA11, **91**
Rubloff, G.: MS-MoM6, 12; MS-MoM9, **12**
Rudy, R.Q.: MN+MS-FrM2, 257
Ruggieri, C.: SS+HC-FrM4, 259
Rummel, B.: EM+NS+SP+SS-WeA3, **153**
Russakoff, A.: 2D-TuA1, 78
Russell, J.N.: BI+PB-TuP7, 108; SS+AS-ThA1, **220**
Russell, N.A.: BI+AS+SA-ThM4, 181; BI+AS-MoM5, 6
Russell, Z.E.: MN+MS-FrM4, 257
Ruzic, D.N.: PS2-ThM11, 194; PS-ThP24, 239;
PS-WeM10, 137; PS-WeM12, 137;
SE+MS+TF-TuA10, **93**
Rydh, A.: MN-WeM11, 133
Ryu, H.: 2D+MI-ThM12, 176
Ryzhikov, I.A.: TF-ThP45, 247
— S —
Saavedra, S.S.: BI+AS+SA-ThM10, 181
Sabat, G.: TF-ThP13, **242**
Sabri, F.: BI+AS+SA-ThM1, 180; BI+MI-WeM11, **128**
Sadowski, J.: 2D+MI-TuM6, 53
Sahaf, H.: BI+AS+SA-ThM4, 181
Sahu, B.: PS-ThP15, 237; SS+AS+EM-WeA8, 168
Saif, M.T.: MN+BI-ThM1, **188**
Saini, G.: TF+BI-ThA8, **222**
Saini, K.: EM+MI+MN-TuA12, 84
Sakaguchi, H.: MS-TuP3, **110**
Sakai, S.: PS+TF-WeM10, 134
Sakar, B.: EM+NS+PS+SS+TF-MoM1, 7
Sakuishi, T.: PS-ThP17, **237**
Sala, A.: SA+2D+AC+AS+TF-TuM3, 63
Salagaj, T.: EM-MoA4, 30
Salahuddin, S.: EM+MN-TuM12, **57**
Salas, J.A.: 2D-TuA7, **78**
Salmeron, M.B.: IS+HC-WeA3, 158; IS-ThA2, 212; IS-ThA9, 213; TR+BI+SE+TF-ThA9, 226
Salomons, M.: HI+NS-ThM1, 185
Salvador, P.A.: SE+MS+TF-TuA2, 91;
SE+NS+TF+TR-TuM1, 65
Samanta, C.: MN+2D+NS-ThA7, **215**
Samarasingha, N.: EL+AS+EM+MI+TF-FrM4, **252**; EL+AS+EM+TF-ThP1, 229
Sam-Giao, D.: TF+PS+SE-MoA8, 50
Samuelson, L.: AS+SS-TuA1, 79
Samukawa, S.: PS-WeA9, 163
Sanders, C.E.: 2D+MI-TuM13, **54**
Sandoval, T.E.: SS+2D-WeM4, **141**
Sankaran, R.M.: PS+2D-TuA1, 88; PS+SE-MoM6, **15**; PS+SE-MoM9, 16
Sankarapandian, M.: PS-MoM10, 18; PS-MoM4, 17; PS-MoM9, 18
Sano, N.: AS+SS-TuA11, 80; HI+NS-ThM12, 187
Santander-Syro, A.F.: SA+2D+AC+AS+TF-TuM2, 63
Santiago Cordoba, M.A.: AC+AS+SA-ThM10, **177**
Santos, A.R.: VT-TuP4, 119
Saraf, I.: PS-MoA11, 41
Saraf, S.: AS-TuP27, 107
Sarakinis, K.: SE+NS+TF+TR-TuM3, **65**
Sardashti, K.: SE+2D+EM-WeA11, **166**;
SS+AS+EM-WeA7, 167
Sarinont, T.: PB+BI+PS-TuM10, 60
Sarker, D.: AS-TuP17, **105**
Sarkissian, A.: PS-ThP2, 235
Sartin, B.C.: AS-TuP28, 107
Sassolini, S.: PS+AS+SS-MoA9, 38
Satake, M.: PS2-ThM3, 192
Satoh, S.: PB+BI+PS-TuM1, 59; PB+BI+PS-TuM5, 60
Sattler, K.: HI+MI+NS-ThA7, 211
Sauer, V.T.K.: BI+MI-WeM2, 127; MN+NS-WeA3, **159**
Sbrockey, N.: EM-MoA4, 30
Scace, G.: VT-MoM3, 24
Scally, L.: PS+SE-MoM3, 14
Scarel, G.: TF+EM-MoA1, **47**
Schall, J.D.: SE+TR-WeM10, **138**
Scharfenberger, K.: PS-MoA1, 40
Schatz, G.: HC+SS-ThA3, **209**;
SP+AS+MI+NS+SS-TuM2, 66
Schauermann, S.: HC+SS-ThM5, **184**
Scheick, L.Z.: MN+MS-FrM4, 257
Scherschligt, J.: VT-MoM5, 24; VT-MoM6, **24**; VT-TuM12, 76
Schilke, K.F.: BI+AS-MoM1, 5
Schirmeisen, A.: TR+AS+NS+SS-WeA12, 174
Schlögl, R.: IS+HC-WeA1, 158; IS-ThM5, 187
Schlosser, D.: HC+NS+SS-WeA9, 156
Schmeling, M.: EM+NS-WeM1, 128
Schmid, M.: SS+AS+HC-MoA8, 46
Schmidt, A.B.: MI+2D+AC-MoA3, 32;
MI+2D+AC-MoA8, 32
Schmidt, B.: AS+SS-WeM3, 125; AS-TuP9, 104
Schmidt, H.: EL+AS+EM+MI+TF-FrM1, **251**
Schmidt, M.E.: HI+MI+NS-ThA11, **212**
Schmidt, S.: TF+PS+SE-MoA4, 49
Schmitt, M.R.: TF-ThP41, 246
Schmitz, S.: PS-MoM4, 17
Schmucker, S.W.: 2D+MI-ThM5, 175
Schneider, M.: MI+2D+AC-MoA1, 31
Schneider, J.M.: SE+TR-WeM1, 137
Schneider, T.: EM+NS+PS+SS+TF-MoM8, 8
Schöeche, S.: EL+AS+EM+TF-ThP2, **229**
Schofield, S.: SS+AS+EM-WeA1, 167
Schramke, K.: PS+2D-TuA3, 89
Schrimpf, R.D.: MN+MS-FrM8, 257
Schubert, M.: EL+AS+EM+MI+TF-FrM3, 251
Schuck, P.J.: EM+NS+SP+SS-WeA7, **154**
Schuengel, E.: PS-TuM10, 62
Schüfflegen, P.: MI+2D+AC-MoA1, 31
Schulz, P.: TF-FrM9, 261
Schulze, J.: PS-TuM10, **62**
Schurz, R.: SP+SS+TF-WeM12, 140
Schwarz, A.M.: IS-ThP3, 233
Schwarzkopf, A.: HI+NS-ThM3, 186
Schweigert, D.: EL+AS+EM+MI+TF-FrM6, 252
Schwier, E.F.: 2D-ThP13, 229
Schwoerer, F.: BI+AS+SA-ThM11, **181**
Scott, S.L.: SS+AS+HC-MoM3, **21**
Scrimgeour, J.: BI+AS-MoM10, 7
Scrymgeour, D.: NS-MoM10, 14
Scudder, L.: AS+SS-ThM2, 178
Scully, J.R.: BI+PB-TuP8, 109; SE+MS+TF-TuA1, 91
Seah, M.P.: AS-MoM9, 5
Seal, S.: AS-TuP27, 107
Sechovský, V.: EM+SS+TF-ThA12, 208
Sefa, M.S.: VT-MoM5, 24; VT-MoM6, 24; VT-TuM12, **76**
Sefat, A.S.: SP+2D+AS+NS+SS-MoA10, 44;
SP+2D+AS+NS+SS-MoA11, 44
Seibert, F.: SE+TR-WeM2, 137
Seibert, R.: 2D+NS-WeA7, 149; 2D-ThP12, 229; AS-TuP24, **106**; SS+2D-WeM1, 141
Seideman, T.: SP+AS+MI+NS+SS-TuM2, 66
Seidlitz, D.: EM+NS+PS+SS+TF-MoM5, **7**; EM-ThP2, 230; SP+AS+MI+NS+SS-MoM8, 20;
SP-TuP6, 115
Seki, T.: PS-ThA11, 219
Sekine, M.: PB+BI+PS-TuM11, 61; PS-ThA10, 219
Sen, R.: TF-ThA3, **223**
Senabulya, N.: EM-FrM3, 253
Senevirathna, I.: EM+NS+PS+SS+TF-MoM5, **7**; EM-ThP2, **230**
Seo, S.: PS-MoM9, 18
Seong, D.J.: PS-ThP31, 240
Serege, M.: PS+AS+SS-MoA5, **38**
Serna, C.: NS-TuP2, **111**
Sethian, J.A.: AS+SS-TuA3, **79**
Setina, J.: VT-TuM10, **76**
Shafaraman, W.: TF-ThP5, 241
Shahab, A.: 2D-ThA4, 201
Shahin, D.I.: EM-MoA10, 31; EM-MoA3, 29
Shaim, M.H.: PS-ThP2, **235**
Shalish, I.: EM-FrM2, 253
Shang, W.: TF+MI+NS-WeM11, 146
Shankar, K.: NS-MoA3, **34**
Shannon, S.: PS-WeM6, 137
Shao, Y.: TR+AS+NS+SS-WeA1, 172
Shard, A.G.: AS+BI-MoA8, 28; AS+SS-ThM12, 179; AS-MoM3, 4; AS-ThA6, 203
Share, K.: SS+AS+HC-MoM8, **22**; TF+EM-MoA2, 47; TF+EM-MoA8, 48
Sharif, R.: IS-ThA11, 213
Sharma, A.: 2D-ThP7, 228
Sharma, J.: EM+MI+MN-TuA12, **84**
Sharma, K.: PS+TF-WeM13, 135
Sharma, P.: TF+BI-ThA10, **223**
Sharma, R.: AS-WeA8, 152
Shaver, B.C.: EM+AC+SS+TF-ThM12, **183**;
EM-ThP13, 232; EM-ThP8, 232
Shaw, G.C.: PS-WeM10, 137
Shaw, S.W.: MN-WeM6, 133
Shaykhutdinov, T.: 2D-ThA12, 202
Shchelkanov, I.A.: PS2-ThM11, 194; PS-ThP24, 239; PS-WeM12, 137; SE+MS+TF-TuA10, 93
Shearer, J.C.: PS-MoA10, **41**; PS-MoA2, 40;
PS-MoA3, 40
Sheehan, P.E.: 2D-ThA6, **201**
Shen, L.: EM+NS+PS+SS+TF-MoM6, 8; EM-MoA11, 31
Shen, M.: SS+HC-TuA7, 97
Shen, Z.X.: 2D+MI-ThM12, 176
Shenderova, O.A.: NS-TuM2, 58
Sheng, H.: TF-ThP16, 242

Author Index

- Shepard Jr, J.: PS+TF-WeA4, 160
 Sherpa, S.D.: PS-MoM1, **16**
 Shetty, A.R.: BI+AS+SA-ThM3, 180; BI+PB-TuP9, 109
 Shi, J.: EM+NS+SP+SS-WeA10, 154
 Shiao, M.H.: IS-ThP4, 233
 Shiba, Y.: MS+AS-TuM1, 57
 Shibata, K.: VT-TuA3, 100; VT-TuP2, **119**
 Shibuya, R.: 2D+MI-MoA8, 27
 Shim, S.: PS-MoA4, 40; PS-MoA8, 40
 Shimada, K.: 2D-ThP13, 229
 Shimizu, K.: PB+BI+PS-TuM2, 60
 Shimoda, T.: HI+MI+NS-ThA11, 212
 Shin, M.S.: NS-TuP9, 112
 Shinault, D.R.: AS-TuP28, 107
 Shinoda, K.: PS+TF-WeM1, **134**; PS+TF-WeM10, **134**
 Shinotsuka, H.: IS-ThA8, 213
 Shirai, M.: VT-TuA3, 100; VT-TuP2, 119
 Shirai, Y.: MS+AS-TuM1, 57
 Shiratani, M.: PB+BI+PS-TuM10, 60
 Shirato, N.: SP+AS+MI+NS+SS-MoM2, **19**
 Shklovskii, B.: PS+2D-TuA3, 89
 Shmilovich, T.: MN-WeM4, 132
 Shohet, J.L.: EM+MI+MN-TuA11, 83; EM+SS+TF-ThA8, 207; EM-ThP1, 230; EM-ThP6, **231**; TF+EM+MI-WeA11, 170; TF+EM+MI-WeA12, 170; TF-ThP13, 242; TF-ThP27, 244; TF-ThP32, 245
 Shoshani, O.: MN-WeM6, 133
 Showers, M.A.: PS-WeM10, 137
 Shu, J.: PS+TF-WeA4, 160; TF-ThP16, **242**
 Shuh, D.K.: AC+AS+SA-ThM11, **177**; AC+AS+SA-ThM4, 176; AC+AS+SA-ThM6, 177; AC-TuP1, 102
 Shukla, P.: PS-ThP20, 238
 Shulda, S.: AS-WeA10, 152; SA-TuP1, **113**
 Shutthanandan, V.: IS-ThP3, 233
 Sibener, S.J.: SS+AS-WeM13, 144
 Siddiqui, S.: PS-ThP15, 237; SS+AS+EM-WeA8, 168; TF+EM+MI-WeA10, 170
 Sieg, S.: PS-MoM4, 17
 Siekhaus, J.: AC+MI-WeA12, 151
 Sikorski, E.M.: PS-MoM2, 17
 Siligardi, G.: BI+AS+SA-TuA2, 81
 Simonson, R.J.: NS-MoM10, 14
 Simpson, M.L.: MS-TuA7, **86**
 Simpson, R.: AS-TuP2, 102
 Simsek, E.: 2D+MI-ThM11, 176
 Singh, A.: EL+AS+EM+MI+TF-FrM4, 252; TF+PS+SE-MoA6, 50; TF-FrM4, **260**
 Singh, B.: AS+SS-TuA7, 80; SE+2D+EM-WeA4, 165; TF-ThP21, 243
 Singh, S.: 2D+MI+SA-MoM11, 3
 Singhal, J.: EL+AS+EM+MI+TF-FrM4, 252
 Singla, M.: 2D-ThA4, 201
 Sintim, H.O.: MN+BI-ThM12, 190
 Sioncke, S.: SA+AS+BI+MI-TuA12, 91
 Sitar, Z.: EM+NS+PS+SS+TF-MoM1, 7
 Sivaram, S.V.: SS2+AS+HC+NS-TuM12, 71
 Siviero, F.: VT-TuA9, 101
 Sk, M.H.: EM-MoA8, 30
 Skalli, O.: BI+AS+SA-ThM1, 180
 Skibinski, E.S.: SS+AS-WeM6, 143; SS+HC-TuA2, **97**
 Skomski, D.: SS-TuP11, 118
 Skvarla, M.: MS-TuA2, **85**
 Sligte, te, E.: EL+AS+EM+MI+TF-FrM7, 253
 Slikboer, ET.: PB+BI+PS-TuM12, 61
 Slotwinski, J.: MS-MoA1, **33**
 Smentkowski, V.: AS-TuP11, **104**; SS+AS-ThA1, 220
 Smith, A.R.: MI+2D+AC-MoA2, 31; SP+AS+MI+NS+SS-TuA9, **94**
 Smith, C.: MN-ThP1, **234**
 Smith, C.W.: TF-ThP37, 246
 Smith, D.: TF+BI-ThA8, 222; VT-WeM2, **146**
 Smith, E.F.: 2D+NS-WeA11, 150
 Smith, H.A.: TF-ThP41, 246
 Smith, J.D.: PS1-ThM2, 190
 Smith, K.: SS-TuP11, 118
 Smith, R.S.: SS+AS-WeM12, 144; SS+HC-FrM6, 259
 Smulders, M.M.J.: TF-ThA3, 223
 Smyth, C.M.: 2D+NS-WeA12, 150; SE+2D+EM-WeA10, 166
 Snoeckx, PS-ThA3, **218**
 Snyders, R.: SS+AS-TuA1, 94
 Sobczak, C.: SE-TuP5, **114**
 Sobota, A.: PB+BI+PS-TuM12, **61**
 Söderlind, A.: AC+MI-WeM13, 124
 Soga, M.: 2D-ThP10, **228**
 Sokolov, I.: NS-TuA7, **87**
 Soliman, A.I.A.: PS-WeA10, **163**
 Solis, L.: BI+PB-TuP3, **108**
 Solokha, V.: IS-ThA11, 213
 Soltis, J.A.: AC+MI-WeA7, 150
 Somaratne, D.: SS+HC-TuA11, 97
 Somnath, S.: AS+SS-TuA2, 79; SP+AS+MI+NS+SS-MoM1, **19**
 Somorjai, G.A.: IS+HC-WeA3, 158; IS-ThA9, 213
 Song, A.: SS+AS-WeM6, 143; SS+HC-TuA2, 97
 Song, B.: NS-MoA10, **35**
 Song, I.-C.: PS-MoA4, 40; PS-MoA8, 40
 Song, Y.H.: NS-TuP9, 112
 Song, Y.L.: 2D+MI-TuM5, 53
 Sonoda, Y.: PS+TF-WeM1, 134
 Sordes, D.: SP+SS+TF-WeM5, 140
 Sorescu, D.C.: SS+AS+HC-MoM6, 21; SS+AS-WeM11, 144
 Sosolik, C.E.: SS1+AS+HC+NS-TuM4, 68
 Sotiri, I.: BI+AS-MoM2, 6
 Sottili, L.: HI+MI+NS-ThA12, 212
 Souriau, L.: PS-ThP33, **240**
 Sowa, M.J.: TF+PS+SE-MoA5, **49**
 Spampinato, V.: SA+AS+BI+MI-TuA12, 91
 Specht, P.: EM+NS+SP+SS-WeA11, 154
 Speck, J.: EM-MoA5, 30
 Spentzouris, L.: 2D+NS-WeA7, 149; 2D-ThP12, 229
 Sperling, B.A.: 2D+TF-WeM12, 122; TF-MoM4, **22**
 Spinner, G.: MS-TuA1, 85
 Splawn, H.: EM+NS+PS+SS+TF-MoM8, 8
 Spooner, T.: TF+EM+MI-WeA10, 170
 Sporre, J.R.: PS-MoM8, 17; PS-MoM9, **18**
 Spreemann, D.: TF+PS+SE-MoA11, 51
 Sprenger, J.K.: TF-TuM2, **73**
 Sprowl, L.H.: HC+SS-ThA10, 210; SS1+AS+HC+NS-TuM11, **69**
 Spurgeon, S.: TF+SA+MI-TuM4, 72
 Sretenović, G.: PB+BI+PS-TuM12, 61
 Sridhara, K.: EM-FrM5, **254**
 Sriraman, S.: PS+TF-WeM4, 134
 Srivastava, A.: 2D+MI-ThM3, **175**
 Srivastava, P.: AS-TuP17, 105
 St. Pierre, R.: MN-WeM1, 132
 Staaks, D.: PS+AS+SS-MoA9, **38**
 Stach, E.: IS-ThM10, **188**
 Stahlbush, R.: TF1-ThM10, 197
 Stan, G.: NS-TuA9, 87
 Stanford, M.G.: 2D+MI-MoA6, 26; 2D+NS-FrM10, 250; 2D-ThP11, **228**; HI-WeA8, 157
 Stanishev, V.: EL+AS+EM+MI+TF-FrM3, 251
 Stanke, F.: MS+AS-TuM11, 58
 Stankevic, T.: AS+SS-TuA1, 79
 Starostin, S.A.: PS+SE-MoM10, 16; SE+MS+TF-TuA8, 92; TF-FrM10, 261
 Stassun, G.: EM+AC+SS+TF-ThM1, 182
 Staunton, J.B.: AC+MI-WeM12, 124
 Stavitski, E.: MS-TuA4, 86
 Steele, A.V.: HI+NS-ThM3, **186**
 Steeves Lloyd, K.: EM+NS-WeM1, 128
 Steirer, K.X.: TF-FrM9, **261**
 Steitz, R.: BI+AS+SA-ThM11, 181
 Stelmakhovich, O.: AC+MI-WeM5, 123
 Stempel Pereira, T.: EW-TuL2, **77**
 Steuer, W.: BI+PB-TuP8, 109
 Stevanovic, V.: TF-FrM9, 261; TF-TuA8, 99
 Stock, P.: BI+AS+SA-TuA1, 81
 Stockman, M.I.: EM+NS+SP+SS-WeA9, 154; SP+AS+MI+NS+SS-MoM8, 20
 Stoddard, M.: NS-TuP4, 112
 Stojić, N.: SA+2D+AC+AS+TF-TuM3, 63
 Stoltz, P.H.: PS1-ThM2, 190
 Stone, J.: VT-MoM3, 24; VT-MoM4, 24
 Stoner, B.R.: MN+MS-FrM4, 257
 Stoot, A.: 2D+MI-TuM6, 53
 Storr, B.: MN-ThP2, 235
 Stotz, E.: IS+HC-WeA1, 158
 Stout, P.J.: PS-TuM3, 62
 Stowe, A.: EM+AC+SS+TF-ThM1, 182
 Strand, M.B.: AS+AC-TuM5, 55; AS-TuP23, **106**
 Strandwitz, N.C.: TR+BI+SE+TF-ThA12, 226
 Strane, J.: PS-MoM10, 18; PS-MoM4, 17
 Stranick, S.J.: 2D+TF-WeM12, 122
 Straube, B.: MI+2D+AC-MoA9, 32
 Strbkova, L.: PB+BI+PS-MoA8, 36
 Strietzel, C.: VT-MoM11, 25
 Strong, T.: 2D-ThP8, 228; 2D-ThP9, 228; NS-MoM1, 12; SE+2D+EM-WeA8, 165
 Strouse, G.F.: VT-MoM3, 24; VT-WeM5, **146**
 Stubbers, R.: PS-WeM12, 137
 Stucky, G.D.: TF+PS+SE-MoA2, 49
 Stutzman, M.L.: VT-TuM11, **76**
 Su, C.Y.: IS-ThP4, **233**
 Su, M.: IS-FrM7, 255
 Su, Q.: EM+AC+SS+TF-ThM3, 182
 Subramanian, S.: MN+BI-ThM12, 190
 Suetsugu, Y.: VT-TuA3, **100**; VT-TuP2, 119
 Sugahara, T.: PS-ThP10, 236
 Sugawa, S.: MS+AS-TuM1, 57
 Sugimoto, S.: PB+BI+PS-MoA11, 37
 Sugimura, H.: 2D+MI+SA-ThM5, 2; 2D-ThP10, 228; PS-WeA10, 163; SE-TuP1, 113; SE-TuP2, 113
 Suh, T.: TF+SA+MI-TuM11, 72
 Sui, X.: IS-FrM11, 256; IS-FrM9, 256
 Sukotjo, C.: BI+AS+SA-ThM2, 180
 Sultan, M.: EM-MoA8, 30
 Sumant, A.V.: NS-TuM5, **59**
 Summerfield, A.: 2D+NS-WeA11, **150**
 Sumpter, B.G.: SP+AS+MI+NS+SS-TuM5, 67
 Sun, H.: PS+TF-WeM12, 135; PS+TF-WeM13, 135; TF-TuA9, 99; TF-TuM2, 73
 Sun, L.: EL+AS+BI+EM+TF-ThA3, 205; EL+AS+BI+EM+TF-ThA4, **205**
 Sun, R.J.: NS-TuP8, 112; PS-ThP1, **235**
 Sun, Y.: 2D+NS-WeA8, 149; IS-FrM1, **255**
 Sun, Z.: PS+TF-WeA4, **160**
 Sundaram, R.: PS-ThP14, 237
 Sung, M.G.: PS-MoM4, 17
 Sung, M.M.: TF-ThA8, **224**
 Surnev, S.: SS+AS-TuA2, 95; SS+AS-TuA9, **95**
 Susan, D.: AS-WeA11, 153
 Sushko, P.V.: TF+SA+MI-TuM4, 72; TF-ThP7, 241
 Susner, M.A.: HI+MI+NS-ThA8, 211
 Sussman, M.: TF-ThP13, 242
 Sutherland, D.S.: BI+MI-WeM3, 127
 Sutter, E.: SS+AS-WeM1, **143**
 Suzer, S.: IS-ThP5, **233**
 Suzuki, Y.: BI+MI-WeM4, 127

Svedberg, E.B.: MS+AS-TuM12, 58
 Swagler, C.S.: AS-TuP15, 104; AS-TuP16, **104**
 Swerts, J.: PS-ThP33, 240
 Swett, J.: HI+MI+NS-ThA10, 211
 Swinney, T.R.: VT-MoM10, **25**; VT-MoM8, 25
 Syed, M.: TF-ThP17, **242**
 Sykes, E.C.H.: HC+NS+SS-WeA11, **156**;
 HC+NS+SS-WeA3, 155; HC+SS-ThA6, 209
 Szakal, C.: AS+BI-MoA5, **28**
 Szkutnik, P.D.: PS-WeM3, 136
 Szlufarska, I.: TR+AS+NS+SS-WeA9, **173**
 Szotek, Z.: AC+MI-WeM12, 124
 Szulczewski, G.J.: MI-TuA4, **84**
 — T —
 Tabe, M.: EM-FrM4, 254
 Tadjer, M.J.: EM-MoA10, 31
 Tahara, S.: PS-ThP33, 240
 Tait, S.L.: SS+AS+HC-MoM1, 21; SS+AS+HC-
 MoM2, 21; SS-TuP11, 118
 Takagi, S.: EM+MN-TuM3, **56**
 Takeda, K.: PB+BI+PS-TuM11, 61
 Takenaka, M.: EM+MN-TuM3, 56
 Takoudis, C.G.: BI+AS+SA-ThM2, 180
 Talin, A.A.: EM+SS+TF-ThA2, 207
 Talukdar, T.: TF-FrM7, 261
 Tamboli, A.C.: TF-TuA8, 99
 Tan, S.: HI-WeA4, 157; HI-WeA8, 157; PS-
 WeA4, 163
 Tanabe, I.: 2D-ThP13, **229**
 Tanaka, H.: PB+BI+PS-TuM11, 61
 Tanaka, M.: PS+TF-WeM1, 134
 Tanatsugu, Y.: BI+PB-TuP6, 108
 Tang, H.: MN+BI-ThM4, 189
 Tang, K.: SE+2D+EM-WeA11, 166
 Tang, W.: HC+NS+SS-WeA4, 155
 Tangpatjaroen, C.: TR+AS+NS+SS-WeA9, 173
 Taniguchi, T.: 2D+NS-WeA11, 150
 Tanuma, S.: IS-ThA8, 213
 Tao, C.: SP+SS+TF-WeM1, **139**
 Tao, L.: 2D+NS-FrM3, **249**
 Tapily, K.: TF+EM+MI-WeA2, 169
 Tarazona, P.: SP+AS+MI+NS+SS-MoM10, 20
 Tarnavich, V.: MI+2D+AC-MoM5, 10
 Tarolli, J.: AS-ThA10, **204**; AS-ThA11, 204
 Tassi, N.G.: AS-TuP21, 106
 Tatsumi, T.: PS-MoM3, 17; PS-ThA8, 219
 Taylor, C.: 2D+TF-WeM5, 121
 Taylor, M.: NS+BI-ThA10, **217**
 te Sligte, E.: PS-ThP23, 238; VT-TuA10, 101
 te Velthuis, S.G.E.: MI+2D+AC-MoM3, 10
 Teeter, G.: TF-FrM9, 261
 Tempas, C.: SS-TuP11, 118
 Tenne, R.: AS+AC-TuM13, 56
 Teplyakov, A.V.: SE+2D+EM-WeA1, 164;
 SS+2D-WeM3, **141**; SS+AS+EM-WeA1, 167;
 SS+AS+EM-WeA10, 168; SS2+AS+HC+NS-
 TuM6, 70
 ter Veen, R.: TF-ThP19, 242
 Teramoto, A.: PS+TF-WeA1, **160**
 Terrani, K.: AS-TuP24, 106
 Terrell, J.R.: SP-TuP5, 115
 Terry, J.: 2D+NS-WeA7, **149**; 2D-ThP12, 229;
 AS+SS-TuA7, 80; AS-TuP24, 106; SS+2D-
 WeM1, 141
 Terryn, H.: TF-ThA6, 223; TF-ThP2, 241
 Terui, S.: VT-TuA3, 100; VT-TuP2, 119
 Tevis, I.: SS-TuP10, 117; SS-TuP6, 117
 Teyssandier, F.: PS-MoA1, 40
 Theodosiou, A.: AS-TuP5, 103
 Therrien, A.J.: HC+SS-ThA6, **209**
 Thevuthasan, S.A.: IS-ThP3, 233
 Thibado, P.: 2D+MI+SA-MoM11, **3**
 Thiel, P.A.: HC+NS+SS-WeA7, **155**; SS+AS-
 ThA6, **220**; SS1+AS+HC+NS-TuM12, 69
 Thiesen, P.H.: EL+AS+EM+MI+TF-FrM8, 253

Thilmany, P.R.: BI+PB-TuP11, 109
 Thissen, A.: SS+AS-WeM3, **143**
 Thissen, N.F.W.: PS+TF-WeA12, 162
 Thomann, A.L.: SS+AS-TuA1, 94
 Thomas, J.: AS-TuP27, 107
 Thomas, S.: TF+MI-WeA12, 172
 Thomsen, L.: SS+AS+EM-WeA1, 167
 Thuening, T.D.: HC+SS-WeM1, **130**
 Thuo, M.: SS-TuP10, 117; SS-TuP6, 117
 Thygesen, K.S.: 2D+MI-TuM1, **53**
 Tian, H.: AS-ThA9, 203
 Tian, P.: PS-MoA8, **40**; PS-ThP7, 235
 Tian, W.: PS1-ThM6, **191**
 Tietema, R.: SE+NS+TF+TR-TuM10, **65**
 Timm, R.: EM+NS+SP+SS-WeA4, **153**
 Tiron, R.: TF-ThA1, 223
 Tischendorf, B.: AS-WeA9, 152
 Tischler, J.: TF+EM+MI-WeA1, 169
 to Baben, M.: SE+TR-WeM1, 137
 Toberer, E.S.: TF-TuA8, 99
 Tobin, J.G.: AC+AS+SA-ThM1, **176**
 Tobin, R.G.: SS2+AS+HC+NS-TuM5, 70
 Tokunaga, M.: SS-TuP1, 116
 Tolbert, S.H.: SE+2D+EM-WeA12, 166;
 TF+MI-WeA8, 172
 Tolk, N.H.: 2D-TuA8, 78; EM-MoA9, 31
 Tomova, Z.: PS-ThA9, 219
 Tompa, G.S.: EM-MoA4, 30
 Töpper, T.: EL+AS+BI+EM+TF-ThA8, 205
 Torelli, M.: NS-TuM2, 58
 Torma, P.: NS+BI-ThA6, 216
 Torres, A.: SA+AS-MoA5, 42
 Tosti, N.: HC+NS+SS-WeA9, 156
 Toth, M.: NS-TuM1, 58
 Tougard, S.: SA+AS-MoA5, 42
 Towlson, C.: BI+AS+SA-ThM4, 181
 Tran, N.: PB+BI+PS-TuM2, 60
 Trapp, M.: BI+AS+SA-ThM11, 181
 Trappen, R.: MI+2D+AC-MoM10, 11
 Treacy, J.P.W.: AS-MoM6, **4**; AS-TuP2, 102;
 AS-TuP3, 102; AS-WeA1, 151
 Trejo, N.: NS-TuA12, **88**
 Trelles, J.P.: PS1-ThM10, **191**
 Trenary, M.: HC+SS-ThM1, 183; HC+SS-
 WeM2, 130; SS+AS-ThA9, **221**
 Trinh, B.: TF-ThP39, 246
 Troian, A.: EM+NS+SP+SS-WeA4, 153
 Trotochaud, L.: SS+AS+HC-MoA10, 46;
 SS+AS+HC-MoM10, 22; TF-ThA6, 223
 Tsai, H.Z.: 2D+MI-ThM12, 176
 Tsargorodska, A.: NS+BI-ThA6, 216
 Tselev, A.: NS-TuA11, **88**
 Tseng, F.: 2D+MI-ThM11, 176
 Tsoi, S.D.: 2D-ThA6, 201
 Tsong, T.T.: HI+NS-ThM2, 186; HI-ThP1, 232
 Tsuji, A.: PS+AS+SS-MoA4, 37
 Tsutsumi, T.: PS-ThA10, 219
 Tsvetanova, D.: PS-ThP33, 240
 Tsyshkevsky, R.: SS+AS+HC-MoA10, 46
 Tu, Y.: 2D+MI+SA-MoM5, **2**; 2D-ThP10, 228
 Tuominen, M.: TF-ThP19, 242
 Turano, M.E.: HC+SS-WeM13, 131; SS-TuP3,
116
 Turchi, E.A.: AC+MI-WeM13, 124
 Turley, R.S.: TF+MI-WeA12, 172
 Tusche, C.: MI+2D+AC-MoA5, **32**
 Tuteja, A.: TF+MI+NS-WeM10, 145
 Tweedie, J.: EM+NS+PS+SS+TF-MoM1, 7
 Tyler, B.J.: AS+SS-TuA12, **81**; BI+PB-TuP5,
 108
 Tylliszcaak, T.: AC+AS+SA-ThM4, 176
 Tylliszczak, T.: AC+AS+SA-ThM11, 177;
 AC+AS+SA-ThM6, 177; AC-TuP1, 102
 Tysoe, W.T.: SS-ThM6, 195; TR+BI+SE+TF-
 ThA1, **224**

— U —
 Udworthy, K.: EM+NS+PS+SS+TF-MoM8, 8
 Ueba, H.: SP+AS+MI+NS+SS-MoM5, 20
 Ueda, A.: MN-ThP2, **235**; MS-TuP5, 111
 Uehara, S.: PS-ThP10, **236**
 Ugeda, M.M.: 2D+MI-ThM12, **176**
 Ulgut, B.: IS-ThP5, 233
 Unocic, R.R.: HI+NS-ThM10, 186
 Uppuluri, R.: SS+AS+HC-MoA2, 45
 Upreti, P.: EL+AS+BI+EM+TF-ThA9, **206**
 Upreti, S.: EM+NS+PS+SS+TF-MoM6, 8; EM-
 MoA8, 30
 Uptrey, B.: NS-TuP4, 112
 Urban, R.A.: HI+NS-ThM1, **185**
 Utsunomiya, T.: 2D+MI+SA-MoM5, 2; 2D-
 ThP10, 228; PS-WeA10, 163; SE-TuP1, 113;
 SE-TuP2, 113
 Utter, B.C.: TF+EM-MoA1, 47
 Utz, A.L.: HC+SS-ThM11, 185; HC+SS-ThM4,
184; IS-ThP8, 234
 Utzig, T.: BI+AS+SA-TuA1, 81
 Uyar, T.: EM+NS+PS+SS+TF-MoM3, 7
 — V —
 Vaganova, E.: EM-ThP5, **231**
 Vajtai, R.: 2D+NS-FrM11, 251
 Valentin, M.: 2D+MI-ThM6, 175
 Valinaj Omran, A.: PB+BI+PS-MoA3, 36
 vallon, R.: PS-WeM3, 136
 Vallee, C.: PS-WeM3, **136**
 Vallée, C.: TF+PS+SE-MoA8, 50
 Vallier, L.: PS+AS+SS-MoA5, 38; PS-WeA2,
 162
 Valtiner, M.: BI+AS+SA-TuA1, **81**
 van Baak, W.: PS+SE-MoM10, 16
 van Buuren, T.: NS-TuM6, 59; SA-TuP2, 113;
 TF+SA+MI-TuM10, 72
 van de Sanden, M.C.M.: PS+SE-MoM10, 16;
 SE+MS+TF-TuA8, 92; TF-FrM10, 261
 van de Steeg, A.: PS-WeA12, 164
 van der Heide, P.A.W.: AS+SS-ThM3, 178;
 MS+AS-TuM3, **57**
 van der Walle, P.: VT-TuA10, 101
 Van Drie, A.D.: VT-TuM4, **75**
 van Drunen, M.: PS+TF-WeA7, 161
 Van Duyne, R.P.: SP+AS+MI+NS+SS-TuM2, 66
 van Ommen, J.R.: TF+MI+NS-WeM1, **144**
 van Putten, M.: VT-MoA4, **51**; VT-TuA10, 101
 van Ruitenbeek, J.M.: SS2+AS+HC+NS-
 TuM11, 70
 Van Schravendijk, B.: EM+MI+MN-TuA1, **83**
 Van Slyke, S.E.: AS-TuP28, 107
 Van Surksom, T.L.: PS+TF-WeA3, **160**
 van 't Erve, O.M.J.: 2D+MI-ThM5, 175
 van Veldhoven, J.: PS-ThP23, **238**
 Vance, A.: TF+MI-WeA12, 172
 Vandalon, V.: TF-MoM5, 23; TF-MoM8, **23**
 Vandencastele, N.: PS-ThP22, 238;
 SE+MS+TF-TuA9, 92
 VanDerslice, J.: EL+AS+EM+TF-ThP2, 229
 Vandersypen, L.M.K.: MI-TuA11, 85
 Vandervorst, W.: AS+AC-TuM10, **55**;
 SA+AS+BI+MI-TuA12, 91
 Vanfleet, R.R.: 2D+MI-ThM10, 175; MN-
 WeM12, 133; TF+MI+NS-WeM6, **145**
 Vaniapura, V.: PS-ThP13, 237
 Varela-Ramirez, A.: BI+PB-TuP3, 108
 Varga, K.: 2D-TuA1, 78; 2D-TuA3, 78; 2D-
 TuA4, 78
 Varganov, S.A.: SS1+AS+HC+NS-TuM3, 68
 Vasilev, C.: NS+BI-ThA6, 216
 Vasilyev, V.: TF-ThP41, 246
 Veal, T.: EM-FrM3, 253
 Vega, A.: TF-MoM9, 23
 Veith, M.: EM+SS+TF-ThA3, 207
 Velasco-Velez, J.J.: IS+HC-WeA1, 158

Author Index

- Velazquez, D.: 2D+NS-WeA7, 149
Velázquez, D.: 2D-ThP12, 229; SS+2D-WeM1, **141**
Velmurugan, J.: NS-TuA11, 88
Venkatasubramanian, A.: BI+MI-WeM2, **127**
Ventrice, Jr., C.A.: 2D+TF-WeM6, 121; SS2+AS+HC+NS-TuM3, 69
Ventzek, P.: PS+TF-WeM3, 134; PS-ThA7, 218
Verguts, K.: TF+EM+MI-WeA3, 169
Verheijen, M.A.: TF+MI+NS-WeM3, 144
Vernon, E.: EM+AC+SS+TF-ThM10, 183
Veryovkin, I.V.: EM+NS-WeM1, 128
Vianco, P.: AS-TuP20, 105
Vilde, V.: AS+SS-TuA8, 80
Villar-Garcia, I.: IS-ThA1, 212
Virost, M.: AC+AS+SA-ThM4, 176
Visart de Bocarmé, T.: HC+SS-ThM10, 185
Vishwanath, S.: 2D+MI+SA-MoM1, 2; SA+2D+AC+AS+TF-TuM5, 64
Vispute, R.D.: MS-MoA3, 33
Vitale, S.: PS-WeA11, 164
Viville, P.: PS+SE-MoM8, 15
Voevodin, A.A.: 2D+NS-FrM1, 249
Vogel, D.: IS-ThA10, 213
Vogtmann, D.: MN-WeM1, 132
Vojvodic, A.: HC+SS-ThA7, 209
Volders, C.: 2D+MI+SA-MoM6, **2**
Volk, A.: SS-TuP17, **118**
Vollnhals, F.: HI-WeA11, 157
von Bergmann, K.: MI+2D+AC-MoM1, **10**
von Windheim, T.: MN+MS-FrM4, 257
Vondrackova, B.: AC+MI-WeM5, 123
Voras, Z.E.: AS+SS-ThM10, 179; AS+SS-ThM13, **180**
Vorng, J.-L.: AS-ThA6, 203
Voronin, S.: PS-MoM8, **17**
Vos, M.F.J.: PS+TF-WeA12, **162**
— **W** —
Wagner, H.D.: AS+AC-TuM13, 56
Wagstaffe, M.: SS-ThM12, **195**
Wahl, P.: MI-TuA7, **84**
Wajda, C.S.: TF+EM+MI-WeA2, 169
Walczak, L.: EW-TuL3, **77**
Walén, H.: HC+NS+SS-WeA7, 155
Walker, A.V.: AS-ThA8, **203**
Walker, H.C.: AC+MI-WeM3, **123**
Walker, P.: TF-MoM10, 23
Wallace, R.M.: 2D+MI-MoA1, 26; 2D+MI-MoA2, 26; 2D+NS-WeA12, 150; 2D-TuA12, 78; SE+2D+EM-WeA10, 166
Walle, van der, P.: EL+AS+EM+MI+TF-FrM7, 253
Wallin, C.B.: MN-WeM5, **132**
Walls, D.: AS-TuP21, 106
Walls, J.M.: TF-TuA7, **99**
Walsh, K.: MN+MS-FrM10, 258
Walsh, L.A.: 2D-TuA12, **78**
Walsh, P.: TF+BI-ThA8, 222
Walton, S.G.: PS+SE-MoM11, **16**; PS-ThP30, 239; PS-ThP5, 235; PS-ThP9, 236; PS-WeA3, 162; TF+SA+MI-TuM12, 73
Waluyo, I.B.: HC+SS-ThM1, 183
Wan, H.L.: SS+HC-FrM5, 259
Wang, C.: AS+SS-ThM6, 179; IS-FrM7, 255; IS-ThA6, 213; TF+MI+NS-WeM10, 145
Wang, H.: SP-TuP7, 115
Wang, J.: EM+NS-WeM11, **129**; HC+NS+SS-WeA4, **155**; MI-TuA3, 84; TF+PS+SE-MoA1, **48**
Wang, J.C.: PS+TF-WeM5, **134**
Wang, K.L.: MI+2D+AC-MoM3, 10; SE+2D+EM-WeA12, 166
Wang, L.L.: VT-TuM6, **76**
Wang, M.: PS+TF-WeM3, **134**; SS+AS+HC-MoM1, **21**
WANG, M.: PS+2D-TuA7, 89
Wang, P.: PS-MoM10, 18
Wang, S.: 2D+MI-ThM1, 175; EM-MoA8, 30
Wang, T.: 2D+NS-FrM12, **251**
Wang, X.D.: EM+NS+SP+SS-WeA10, 154; TF+EM-MoA4, 47
Wang, Y.: EM+AC+SS+TF-ThM3, 182; EM-MoM5, 9; MI-TuP1, 109; TF+MI-WeA1, 171
Wang, Y.C.: AS-MoM3, 4
Wang, Y.-C.: AS-MoM1, 3
Wang, Y.-C.: AS+AC-TuM12, 55
Wang, Y.-C.: BI+AS+SA-TuA9, 82
Wang, Y.N.: PS-TuM10, 62
Wang, Z.: 2D+NS-FrM2, **249**; EM+MI+MN-TuA11, 83; EM-ThP6, 231; TF+BI-ThA1, **222**
Wang, Z.-J.: IS-ThM5, 187
Ward, B.: HI-WeA1, **156**
Ward, D.: NS-MoM10, 14
Ward, T.Z.: 2D+MI-MoA6, 26; 2D+NS-FrM10, 250; IS+HC-WeA4, 158
Warner, J.H.: 2D+MI-ThM1, 175
Warren, E.L.: TF-TuA8, 99
Warschkow, O.: SS+AS+EM-WeA1, 167
Waskiewicz, R.J.: EM+AC+SS+TF-ThM13, **183**
Wasserman, D.: EM-MoM1, **8**
Watanabe, H.: PS+AS+SS-MoA4, 37
Watanabe, K.: 2D+NS-WeA11, 150
Watanabe, Y.: BI+MI-WeM4, 127
Waters, J.: 2D+TF-WeM10, **122**; 2D-ThA4, 201
Watkins, E.: NS-TuM6, 59
Watson, C.F.: AS+SS-WeM1, 124; BI+PB-TuP11, 109; SE+2D+EM-WeA3, 165
Watts, J.F.: AS+SS-TuA8, 80; AS+SS-WeM6, 125; AS-WeA7, 152; SP+AS+MI+NS+SS-TuA11, 94
Weatherup, R.S.: IS-ThA2, **212**
Weaver, J.F.: SS+AS-TuA3, 95; SS-TuP4, 116; SS-TuP7, 117
Weber, M.H.: AS+SS-ThM1, 178
Weckhuysen, B.M.: IS-ThM3, **187**
Wehrli, P.: NS+BI-ThA11, 217
Wei, J.: 2D+NS-WeA1, 149
Wei, W.: BI+AS-MoM10, 7
Weidner, T.: BI+AS-MoM1, 5; BI+AS-MoM8, **6**
Weierstall, U.: SA+AS+BI+MI-TuA7, **90**
Weimer, J.J.: TF1-ThM5, 197; TF-ThP24, 243
Weisenfeld, J.: IS-FrM9, 256
Weiss, F.M.: EL+AS+BI+EM+TF-ThA8, 205
Weiss, S.M.: 2D+NS-FrM12, 251; EM+SS+TF-ThA6, 207
Weller, R.A.: MN+MS-FrM8, 257
Welton, E.R.: AS-TuP15, 104; AS-TuP16, 104
Wendt, S.: SS+AS-TuA12, 96
Weng, C.J.: EM-ThP4, 231
Weng, X.F.: SS+HC-FrM5, 259
Wenz, G.: TR+AS+NS+SS-WeA7, 173
Wenzel, W.: PS-ThA8, 219
Werme, L.: AC+AS+SA-ThM11, 177
West, A.: AS+BI-MoA8, 28
Westerhout, J.: VT-TuA10, 101
Westly, D.A.: MN-WeM5, 132
Westover, T.: NS-TuP4, **112**
Whaley, S.D.: SS+HC-FrM1, 258
Wheeler, V.D.: EM-MoA10, 31; EM-MoA3, 29; TF+EM+MI-WeA1, **169**; TF+EM-MoA1, 47; TF+SA+MI-TuM3, 71
White, A.: AS-TuP23, 106
White, A.E.: NS-MoM9, 13
White, M.G.: SS+AS+HC-MoA6, 45; SS1+AS+HC+NS-TuM2, 67
White, S.T.: EL+AS+EM+TF-ThP3, **229**
Whiteman, P.: SP-TuP1, 115
Whitener, K.E.: 2D-ThA6, 201
Whitfield, Z.: TF1-ThM5, **197**
Whitten, J.E.: SS+HC-TuA11, **97**
Widrig, B.: SE+TR-WeM2, 137
Wieliczka, D.M.: AS-TuP28, **107**
Wiesing, M.: SS+AS+HC-MoA11, **46**
Wilhelm, F.: AC+MI-WeM1, **122**
Wilke, J.: HC+NS+SS-WeA9, 156
Willers, T.: EW-WeL3, **148**
Willett, S.: TF+MI-WeA12, 172
Willett-Gies, T.: EL+AS+EM+MI+TF-FrM5, 252
Willey, T.M.: NS-TuM6, 59; SA-TuP2, **113**
Williams, B.: MN+BI-ThM1, 188
Williams, C.: SS+AS+HC-MoM1, 21
Williams, C.K.: IS-ThA1, 212
Williams, E.D.: SS+AS-ThA4, **220**
Williams, L.W.: BI+MI-WeM13, **128**
Williams, M.G.: SS2+AS+HC+NS-TuM6, **70**
Williams, P.: BI+AS-MoM5, 6
Williams, P.M.: BI+AS+SA-TuA3, **82**
Williams, T.: VT-MoA10, 52
Williamson, C.: SP+SS+TF-WeM12, 140
Willingham, M.G.: IS-ThM5, **187**
Willingham, D.: AS-ThA10, 204; AS-ThA11, **204**
Willis, B.G.: TF+MI+NS-WeM4, 145
Wilt, D.M.: SE+MS+TF-TuA7, 92
Wimer, S.: EL+AS+EM+MI+TF-FrM3, 251
Windus, T.L.: SS1+AS+HC+NS-TuM12, 69
Winkler, R.: NS-MoM5, 13
Winkler, T.E.: MN+BI-ThM12, 190; NS+BI-ThA8, **216**
Winograd, N.: AS-ThA9, 203; HI+NS-ThM11, 187
Wirth, A.: VT-TuM1, **75**
Wirtz, T.: HI-WeA11, 157
Wishart, D.: BI+MI-WeM2, 127
Wisman, D.: SS-TuP11, **118**
Wiss, T.: AC+AS+SA-ThM4, 176
Wolden, C.A.: MS-MoM5, **11**
Wolf, S.: PS-ThP15, 237; SS+AS+EM-WeA7, **167**
Wolf, S.A.: EM-MoM5, 9
Wolkow, R.A.: HI+NS-ThM1, 185
Wong, A.T.: 2D-ThP11, 228
Wong, K.: SE+2D+EM-WeA12, 166
Wood, J.D.: 2D+MI-TuM4, 53
Woollam, J.A.: EL+AS+EM+TF-ThP2, 229
Woolley, A.: NS-TuP4, 112
Worsch, C.: VT-TuA11, 101
Wortelen, H.: MI+2D+AC-MoA8, 32
Wrasman, C.: NS-TuA12, 88
Wu, H.-C.: SA+2D+AC+AS+TF-TuM6, 64
Wu, R.: MI+2D+AC-MoA10, **33**
Wu, T.: TF-FrM2, 260
Wu, W.: AS-TuP21, 106; NS-MoA10, 35
Wu, Y.L.: SE+MS+TF-TuA10, 93
Wu, Z.: SP+2D+AS+NS+SS-MoA10, 44
Wucher, A.: AS-ThA9, 203; HI+NS-ThM11, 187
Wüest, M.P.: VT-MoM11, **25**
Wurstbauer, U.: EL+AS+EM+MI+TF-FrM8, 253
Wygladacz, K.A.: AS-ThA12, **204**
Wynne, J.: IS-FrM6, 255
— **X** —
Xia, Y.: IS-ThA6, 213; SS+HC-TuA9, 97
Xiao, G.: EM+MN-TuM5, **56**
Xiao, X.D.: SS+AS+EM-WeA3, **167**
Xiao, Z.: 2D-ThP7, 228; 2D-ThP8, 228; 2D-ThP9, 228; NS-MoM1, **12**; SE+2D+EM-WeA8, 165; SP+AS+MI+NS+SS-TuM5, 67
Xie, K.: HC+SS-WeM6, 131
Xie, R.: PS-MoM9, 18

Author Index

- Xie, W.: TF2-ThM13, **200**
Xing, H.G.: 2D+MI+SA-MoM1, 2;
SA+2D+AC+AS+TF-TuM5, 64
Xing, Z.: EM-MoM5, 9
Xiong, Z.A.: PS-ThP27, 239
Xu, J.: EM-ThP12, **232**
Xu, K.G.: PS-ThP29, 239
Xu, P.: PS-MoM10, **18**; PS-MoM4, 17;
SS+AS+HC-MoA6, **45**; SS1+AS+HC+NS-
TuM2, 67; TF1-ThM6, 197; TF-ThP7, **241**
Xu, Q.: MI-TuP1, 109; TF+MI-WeA1, 171
Xu, W.: AS+SS-ThM6, 179; IS-FrM7, 255
Xu, Y.: 2D+NS-FrM12, 251
Xu, Z.: IS-FrM7, 255
Xue, P.: EM-ThP1, **230**; TF-ThP27, 244
Xue, Q.-K.: MI+2D+AC-MoM8, **11**
— Y —
Yakimov, M.: SE+2D+EM-WeA11, 166
Yakimova, R.: EL+AS+EM+MI+TF-FrM3, 251
Yakovlev, V.S.: EM+NS+SP+SS-WeA9, 154;
SP+AS+MI+NS+SS-MoM8, 20; SP-TuP7, 115
Yamada, M.: PS2-ThM3, **192**
Yamaguchi, H.: 2D+NS-FrM11, 251
Yamashita, F.: PS-ThP33, 240
Yamashita, M.: TR+BI+SE+TF-ThA8, 225
Yamashita, S.: MS+AS-TuM1, 57
Yamashita, Y.: SA+AS-MoA5, 42
Yamazaki, M.: PS-MoA9, 41
Yan, P.: AS+SS-ThM6, 179
Yan, Y.: EL+AS+BI+EM+TF-ThA10, 206;
EL+AS+BI+EM+TF-ThA6, 205
Yang, C.: EM-MoA11, 31
Yang, D.: TF1-ThM1, 196
Yang, G.: EM+AC+SS+TF-ThM10, 183
Yang, H.J.: HC+NS+SS-WeA7, 155
Yang, J.H.: 2D+MI-TuM5, 53
Yang, M.: TF-FrM9, 261
Yang, Q.: PS-MoA9, 41
Yang, R.: MN+2D+NS-ThA8, **215**
Yang, W.: PS-WeA4, **163**
Yang, X.: PS+AS+SS-MoA9, 38
Yang, Y.: MS+AS-TuM11, 58; MS-MoM5, 11
Yanguas-Gil, A.: TF+EM-MoA3, 47; TF1-
ThM11, **197**; TF2-ThM10, 199; TF-FrM2,
260
Yao, J.: IS-FrM9, **256**
Yao, Y.: EM-MoA4, **30**
Yapabandara, K.: EM+NS+PS+SS+TF-MoM6,
8; EM-MoA11, 31; EM-MoA8, **30**
Yarlagadda, S.: EM-FrM2, 253
Yarmoff, J.A.: SS+2D-WeM10, **142**; SS+2D-
WeM12, 142
Yasaka, A.: HI+MI+NS-ThA1, **210**; HI+MI+NS-
ThA11, 212
Yasui, N.: PS+TF-WeM1, 134
Yates, Jr., J.T.: HC+NS+SS-WeA4, 155; SS+HC-
TuA8, 97
Ye, F.: 2D+NS-FrM6, 250; 2D+NS-WeA1, **149**
Ye, Z.: TR+BI+SE+TF-ThA3, 225
Yeh, J.A.: IS-ThP4, 233
Yemane, Y.: TF+PS+SE-MoA5, 49
Yeom, H.W.: SP+2D+AS+NS+SS-MoA4, 43
Yeon, J.H.: NS-TuP9, 112
Yilmaz, I.: EM+NS+PS+SS+TF-MoM3, 7
Yilmaz, M.: EM+NS+PS+SS+TF-MoM3, 7
Yilmaz, S.: TF-TuA7, 99
Yin, X.: EM+NS+SP+SS-WeA10, **154**
Yngman, S.: EM+NS+SP+SS-WeA4, 153
Yoo, J.H.: TF+SA+MI-TuM10, 72
Yoshida, N.: PS-ThP15, 237; SE+2D+EM-
WeA11, 166; SS+AS+EM-WeA8, 168
Yoshikawa, H.: IS-ThA8, 213; PB+BI+PS-
MoA11, 37
Yoshinobu, J.: SS+AS+HC-MoM5, **21**
You, K.H.: PS-ThP31, 240
You, S.J.: PS-ThP31, 240
Young, C.S.: PS-ThP32, 240
Yu, C.C.: BI+PB-TuP6, 108
Yu, G.: MI+2D+AC-MoM3, 10; SE+2D+EM-
WeA12, 166
Yu, J.: AS+SS-WeM12, **126**; MI+2D+AC-
MoM4, 10
Yu, K.-H.: TF+EM+MI-WeA2, 169
Yu, W.: MN+BI-ThM5, 189
Yu, X.: AS+SS-ThM6, 179; IS-FrM7, **255**;
SS+AS-WeM5, **143**; SS-TuP17, 118
Yu, X.-Y.: AS+SS-WeM11, **126**; AS+SS-
WeM12, 126; IS-FrM11, 256; IS-FrM9, 256
Yu, Y.F.: HI-ThP1, 232
Yu, Y.Y.: TF+EM-MoA4, **47**
Yuan, C.: SS+AS-WeM12, **144**
Yuan, H.: SA+AS+BI+MI-TuA9, **90**
Yuan, Q.: PS+TF-WeA4, 160
Yudovsky, J.Y.: TF-TuM10, **74**
Yue, R.: 2D-TuA12, 78; SE+2D+EM-WeA10,
166
Yulaev, A.: EM+SS+TF-ThA2, **207**; IS-ThP9,
234
Yun, Y.: SS-ThM4, 195
— Z —
Zaera, F.: IS-ThM1, **187**
Zaizen, Y.: PS-MoM3, 17
Zajickova, L.: PB+BI+PS-MoA8, **36**
Zakel, J.: HI+MI+NS-ThA3, **210**
Zamborlini, G.: SA+2D+AC+AS+TF-TuM3, 63
Zardetto, V.: TF-TuA4, 98
Zarifi, M.H.: NS-MoA3, 34
Zborowski, C.: SA+AS-MoA5, **42**
Zegkinoglou, I.: SS+AS+HC-MoM10, 22
Zell, T.: AS+SS-WeM10, 125
Zelzer, M.: BI+AS+SA-ThM4, 181; NS+BI-
ThA10, 217
Zenhnder, A.T.: MN-WeM5, 132
Zettl, A.: 2D+MI-ThM12, 176; MN+MS-FrM8,
257
Zhang, B.: VT-MoA5, **51**
Zhang, D.: 2D-TuA4, 78; SE+2D+EM-WeA9,
165
Zhang, F.: IS-FrM11, **256**
Zhang, H.: MI-TuP2, 110; SS+HC-FrM5, 259
Zhang, J.: TR-ThP1, 248
Zhang, L.: AS-TuP21, **106**
Zhang, P.: TF-FrM7, 261
Zhang, S.: EM-FrM7, 254
Zhang, W.: SS+AS+HC-MoA2, **45**
Zhang, X.: EM+SS+TF-ThA9, **207**; HI+MI+NS-
ThA11, 212; MI+2D+AC-MoM3, 10;
TF+SA+MI-TuM2, 71
Zhang, Y.: 2D+MI-ThM12, 176; 2D-TuA9, **78**;
MN-ThP2, 235; PS+TF-WeA4, 160; PS+TF-
WeM4, 134; PS-ThA10, 219; SS-TuP20, **118**;
TF-ThP16, 242
Zhang, Z.: EM-MoA5, 30; SS+HC-TuA8, 97;
SS+HC-TuA9, **97**; TF2-ThM3, 199; TF-FrM5,
260
Zhao, C.: TR-ThP1, **248**
Zhao, H.: MN+2D+NS-ThA6, 214
Zhao, J.: SS+AS+EM-WeA1, **167**
Zhao, L.: EM+MI+MN-TuA11, 83; EM-ThP6,
231; TR+AS+NS+SS-WeA9, 173
Zhao, R.: AS+SS-ThM6, 179
Zhao, S.: IS-ThM10, 188
Zhao, W.: HC+SS-ThA7, **209**
Zhao, Y.P.: NS-TuP1, 111; TF1-ThM3, **196**
Zhen, L.: SP-TuP7, 115
Zheng, H.: TF+EM+MI-WeA11, **170**
Zheng, M.: 2D-ThP13, 229
Zheng, Q.: SP+2D+AS+NS+SS-MoA10, 44
Zheng, X.-Q.: MN+2D+NS-ThA6, **214**
Zheng, Z.: TF-ThP26, **244**
Zhong, J.: MN-WeM3, 132
Zhong, L.: PS+2D-TuA2, 88
Zhong, Z.: 2D-ThA1, **201**
Zhou, C.D.: PS1-ThM2, 190
Zhou, H.: 2D+MI+SA-MoM1, 2
Zhou, J.: MI+2D+AC-MoM10, 11; SS+AS+HC-
MoA5, **45**
Zhou, W.: SS+2D-WeM10, 142; SS+2D-
WeM12, **142**
Zhou, Y.: AS+SS-ThM6, 179; AS+SS-WeM12,
126; IS-FrM11, 256; IS-FrM7, 255; IS-FrM9,
256; MI+2D+AC-MoM3, 10
Zhou, Z.: 2D+NS-FrM12, 251
Zhu, C.: VT-MoA5, 51
Zhu, H.: 2D+MI-MoA2, **26**; 2D-TuA12, 78;
SS+2D-WeM10, 142; SS+2D-WeM12, 142;
TF-ThA7, 224
Zhu, J.: SE+NS+TF+TR-TuM10, 65;
SP+AS+MI+NS+SS-TuM1, 66
Zhu, K.: SS+HC-TuA9, 97; TF-FrM9, 261; TF-
TuA1, **98**
Zhu, T.: TF+PS+SE-MoA6, 50
Zhu, W.: 2D+NS-FrM3, 249
Zhu, Z.: AS+SS-ThM6, **179**; AS+SS-WeM12,
126; IS-FrM11, 256; IS-FrM7, 255; IS-FrM9,
256
Ziaie, B.: MN+BI-ThM5, **189**
Zoehrer, S.: SE-TuP7, **114**
Zollner, S.: EL+AS+EM+MI+TF-FrM4, 252;
EL+AS+EM+MI+TF-FrM5, 252;
EL+AS+EM+TF-ThP1, 229; SE+2D+EM-
WeA9, 165
Zorman, C.A.: MN+2D+NS-ThA6, 214; MN-
WeM10, **133**; PS+SE-MoM9, 16
Zou, Q.: SP+2D+AS+NS+SS-MoA10, **44**;
SP+2D+AS+NS+SS-MoA11, 44
Zuithof, H.: AS-WeA12, **153**; TF+BI-ThA1,
222; TF-ThA3, 223